S-N/99205--096

Phase I Contaminant Transport Parameters for the Groundwater Flow and Contaminant Transport Model of Corrective Action Unit 97: Yucca Flat/Climax Mine, Nevada Test Site, Nye County, Nevada

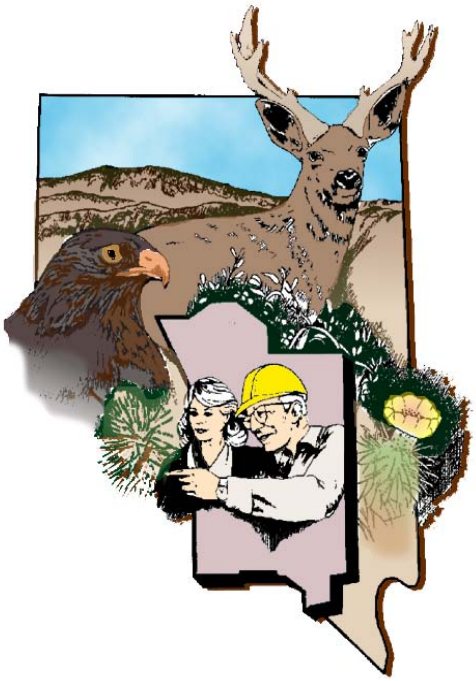

Revision No.: 0

September 2007

Prepared for U.S. Department of Energy under Contract No. DE-AC52-03NA99205.

Approved for public release; further dissemination unlimited.

S-N/99205--096

PHASE I CONTAMINANT TRANSPORT PARAMETERS FOR THE GROUNDWATER FLOW AND CONTAMINANT TRANSPORT MODEL OF CORRECTIVE ACTION UNIT 97: YUCCA FLAT/CLIMAX MINE, NEVADA TEST SITE, NYE COUNTY, NEVADA

Contributors:

Stoller-Navarro Joint Venture
Irene Farnham
William Fryer
John Pickens
Toya Jones
Chrissi Brown-King
John Hand
John Londergan
Nathan Bryant

National Securities Technologies, LLC
Sigmund L. Drellack

Lawrence Livermore National Laboratory
Mavrik Zavarin

Revision No.: 0

September 2007

Stoller-Navarro Joint Venture
7710 W. Cheyenne, Building 3
Las Vegas, NV 89129

Prepared for U.S. Department of Energy under Contract No. DE-AC52-03NA99205.

Approved for public release; further dissemination unlimited.

PHASE I CONTAMINANT TRANSPORT PARAMETERS FOR THE GROUNDWATER FLOW AND CONTAMINANT TRANSPORT MODEL OF CORRECTIVE ACTION UNIT 97: YUCCA FLAT/CLIMAX MINE, NEVADA TEST SITE, NYE COUNTY, NEVADA

Approved by: /s/ John McCord Date: 09/25/2007

John McCord, UGTA Project Manager
Stoller-Navarro Joint Venture

ACKNOWLEDGEMENT

We thank the many individuals who assisted us in creating this report. In particular, the Stoller-Navarro Joint Venture team acknowledges the previous work of Shaw Environmental, Inc., and Los Alamos National Laboratory for their preparation of the report titled *Contaminant Transport Parameters for the Groundwater Flow and Contaminant Transport Model of Corrective Action Units 101 and 102: Central and Western Pahute Mesa, Nye County, Nevada* (Shaw, 2003), which established the pattern and provided example methodologies for portions of this report. We greatly appreciate the efforts of Christie Miller, Christy Morris, Ellen Cook, and the document production staff for their support and dedication in preparing this document for publication. We also thank the following individuals for their contributions and review of sections of this report: Rick Warren, Paul Reimus, Greg Ruskauff, and John McCord.

TABLE OF CONTENTS

List of Figures . . . xii
List of Plates . . . xxiii
List of Tables . . . xxiv
List of Acronyms and Abbreviations . . . xxix
List of Symbols for Elements and Compounds . . . xxxiv
List of Hydrostratigraphic Unit Abbreviations and Symbols . . . xxxvi

1.0 Introduction . . . 1-1
- 1.1 Purpose, Objectives, and Scope . . . 1-1
- 1.2 Yucca Flat/Climax Mine CAU Background . . . 1-2
- 1.3 Corrective Action Strategy . . . 1-4
- 1.4 Planning Documents . . . 1-7
- 1.5 Data Collection Activities . . . 1-8
- 1.6 Project Participants . . . 1-8
- 1.7 Document Organization . . . 1-8

2.0 Corrective Action Unit Modeling Approach . . . 2-1
- 2.1 Overview of the CAU Modeling Approach . . . 2-1
  - 2.1.1 Integrated Three-Dimensional Model Development . . . 2-1
- 2.2 Transport Modeling Approach and Data Requirements . . . 2-2
  - 2.2.1 Transport Modeling Approach . . . 2-2
  - 2.2.2 Data Requirements . . . 2-3
    - 2.2.2.1 Hydrologic Source Term . . . 2-3
    - 2.2.2.2 Transport Parameters . . . 2-5
    - 2.2.2.3 Radionuclide Concentration Data . . . 2-5
    - 2.2.2.4 Groundwater Chemistry Data . . . 2-5

3.0 Data Analysis . . . 3-1
- 3.1 Data Compilation . . . 3-1
  - 3.1.1 Transport Data Types . . . 3-1
    - 3.1.1.1 Porosity . . . 3-2
    - 3.1.1.2 Dispersivity . . . 3-2
    - 3.1.1.3 Matrix Diffusion Coefficient . . . 3-3
    - 3.1.1.4 Matrix and Fracture Sorption Parameters . . . 3-3
    - 3.1.1.5 Colloid-Facilitated Transport Parameters . . . 3-4
  - 3.1.2 Supporting Information . . . 3-4
  - 3.1.3 Data Sources . . . 3-5
    - 3.1.3.1 Nevada Test Site Data . . . 3-6
    - 3.1.3.2 Yucca Mountain Project Data . . . 3-6
    - 3.1.3.3 Other Data . . . 3-6
- 3.2 Data Transfer Methodology . . . 3-6
  - 3.2.1 General Transferability Approach . . . 3-6

TABLE OF CONTENTS (CONTINUED)

3.2.2 Similarity Criteria 3-7
3.2.2.1 Geologic History 3-7
3.2.2.2 Lithology 3-8
3.2.2.3 Alteration 3-8
3.2.2.4 Groundwater Chemistry 3-8
3.3 Quality Assurance of Data and Data Documentation 3-8
3.3.1 Data Documentation Evaluation 3-9
3.3.2 Data Quality Evaluation 3-10
3.3.3 Checking Procedures 3-10
3.3.4 Standard Methodologies 3-10
3.3.5 Technical and Peer Reviews 3-11
3.3.6 Corroboration of Data Through Models 3-11
3.3.7 Data Analysis Limitations 3-11

4.0 Yucca Flat/Climax Mine Hydrostratigraphic Framework 4-1

4.1 Yucca Flat/Climax Mine Hydrostratigraphic Framework Model 4-1
4.1.1 Model Development 4-1
4.1.2 Hydrogeologic and Hydrostratigraphic Units of the Yucca Flat/Climax Mine HFM 4-4
4.1.2.1 Hydrogeologic Units of the Yucca Flat/Climax Mine HFM 4-4
4.1.2.2 Hydrostratigraphic Units of the Yucca Flat/Climax Mine HFM 4-6
4.2 Mineralogy of Hydrostratigraphic Units in the Yucca Flat/Climax Mine HFM 4-21
4.2.1 Data Compilation and Data Transfer 4-28
4.2.2 Playa Confining Unit 4-28
4.2.3 Alluvial Aquifer 4-36
4.2.4 Basalt Lava-Flow Aquifer 4-37
4.2.5 Timber Mountain Upper Vitric-Tuff Aquifer 4-38
4.2.6 Timber Mountain Welded-Tuff Aquifer 4-40
4.2.7 Timber Mountain Lower Vitric-Tuff Aquifer 4-41
4.2.8 Upper Tuff Confining Unit 4-42
4.2.9 Topopah Spring Aquifer 4-42
4.2.10 Lower Vitric-Tuff Aquifer 4-43
4.2.11 Lower Tuff Confining Units 4-44
4.2.11.1 Lower Tuff Confining Unit 4-45
4.2.11.2 Oak Spring Butte Confining Unit 4-46
4.2.11.3 Argillic Tuff Confining Unit 4-46
4.2.12 Belted Range Aquifer 4-47
4.2.13 Belted Range Confining Unit 4-49
4.2.14 Pre-Grouse Canyon Tuff Lava-Flow Aquifer (PRETBG and PRETBG1) 4-49

TABLE OF CONTENTS (CONTINUED)

4.2.15 Tub Spring Aquifer 4-50
4.2.16 Mesozoic Granite Confining Unit 4-50
4.2.17 Upper Carbonate Aquifer 4-51
4.2.18 Upper Clastic Confining Unit 4-51
4.2.19 Lower Carbonate Aquifer 4-52
4.2.20 Lower Clastic Confining Unit 4-53

5.0 Yucca Flat/Climax Mine Geochemistry 5-1

5.1 Summary of the FY 2006 Geochemical Evaluation of the Yucca Flat/Climax Mine Groundwater Flow System 5-1
5.2 Data Compilation and Data Transfer 5-5
5.2.1 Data Compilation 5-5
5.2.2 Data Transfer 5-7
5.2.3 Data Analysis 5-7
5.2.3.1 Groundwater Chemistry Representative of Hydrostratigraphic Units 5-8
5.2.3.1.1 Alluvial Aquifer 5-9
5.2.3.1.2 Volcanic-Rock Aquifers and Tuff Confining Units 5-11
5.2.3.1.3 Carbonate Aquifers 5-15
5.2.4 Clastic Confining Units 5-25
5.2.5 Granite Confining Unit 5-28
5.2.6 Perched Springs 5-31
5.3 Limitations 5-31
5.4 Summary 5-33

6.0 Contamination Sources and Extent 6-1

6.1 Data Compilation and Data Transfer 6-2
6.2 The Yucca Flat/Climax Mine Radiologic Source Term 6-2
6.3 Groundwater Sampling Locations in the Yucca Flat/Climax Mine CAU 6-6
6.4 Alluvium and Tuff Tests 6-11
6.4.1 DALHART 6-11
6.4.2 GASCON 6-13
6.4.3 BILBY 6-13
6.4.4 BASEBALL 6-15
6.4.5 INGOT 6-18
6.4.6 ALEMAN 6-20
6.4.7 Other Alluvium and Tuff Tests 6-20
6.5 Carbonate Tests 6-21
6.5.1 NASH 6-21
6.5.2 BOURBON 6-25
6.5.3 HANDCAR 6-29
6.6 Granite Tests 6-31
6.6.1 HARD HAT 6-31

TABLE OF CONTENTS (CONTINUED)

6.6.2 PILE DRIVER 6-35
6.6.3 Tritium Observations in Granite. 6-36
6.6.4 Tuff Pile/High-Pressure Area 6-40
6.7 Prompt Injection Phenomena 6-42

7.0 Matrix Porosity 7-1

7.1 Role of Matrix Porosity in Contaminant Transport 7-1
7.2 Data Compilation and Data Transfer 7-2
7.2.1 Data Types 7-2
7.2.2 Data Sources. 7-3
7.3 Data Evaluation. 7-3
7.3.1 Variability of Porosity with Depth 7-6
7.4 Development of Parameter Distributions 7-7
7.4.1 Porosity Distributions by HGU and HSU 7-7
7.5 Scaling Considerations 7-9

8.0 Effective Porosity 8-1

8.1 The Role of Effective Porosity in Contaminant Transport. 8-3
8.2 Data Compilation and Data Transfer 8-4
8.3 Data Evaluation Procedures 8-4
8.4 Data Documentation Qualification. 8-6
8.5 Effective Porosity for the Aquifer Hydrogeologic Units 8-6
8.5.1 The Alluvial Aquifer Hydrogeologic Unit. 8-7
8.5.2 The Welded-Tuff Aquifer Hydrogeologic Unit 8-7
8.5.2.1 Groundwater Tracer Tests 8-9
8.5.2.2 Gas Tracer Tests 8-17
8.5.2.3 Infiltration Tests 8-20
8.5.2.4 Seepage Tests 8-20
8.5.2.5 Calculations of Fracture Porosity from Fracture and Producing Zone Data in Test Well USW H-4 8-22
8.5.2.6 Hydraulic Conductivity and Fracture Spacing Calculations 8-23
8.5.2.7 Fracture Aperture, Density, Orientation, and Percent Open Area Calculations 8-29
8.5.2.8 Literature Review of Basin and Range Province Rocks 8-30
8.5.2.9 Values Used in Previous NTS Modeling Studies 8-30
8.5.2.10 Recommended Ranges in Previous NTS Data Document Reports 8-31
8.5.2.11 Summary and Recommended Distribution 8-32
8.5.3 The Vitric-Tuff Aquifer Hydrogeologic Unit. 8-35
8.5.4 The Lava-Flow Aquifer Hydrogeologic Unit. 8-36
8.5.4.1 Tracer Tests 8-37

TABLE OF CONTENTS (CONTINUED)

8.5.4.2 Hydraulic Conductivity and Fracture Spacing Calculations 8-40
8.5.4.3 Values Used in Previous NTS Modeling Studies 8-47
8.5.4.4 Recommended Ranges in Previous NTS Data Document Reports 8-48
8.5.4.5 Summary and Recommended Distribution 8-49
8.5.5 The Carbonate Aquifer Hydrogeologic Unit 8-52
8.5.5.1 Tracer Tests 8-53
8.5.5.2 Hydraulic Conductivity and Fracture Spacing Calculations 8-62
8.5.5.3 Fracture Spacing and Aperture Calculations 8-63
8.5.5.4 Geophysical Logging 8-66
8.5.5.5 Literature Review of Basin and Range Province Rocks 8-67
8.5.5.6 Values Used in Previous NTS Modeling Studies 8-68
8.5.5.7 Recommended Ranges in Previous NTS Data Document Reports 8-69
8.5.5.8 Summary and Recommended Distribution 8-69
8.6 Effective Porosity of the Confining Unit Hydrogeologic Units 8-72
8.6.1 The Playa Confining Unit. 8-72
8.6.2 The Tuff Confining Unit 8-72
8.6.3 The Granite Confining Unit 8-73
8.6.4 The Clastic Confining Unit 8-73
8.7 Data Scaling Considerations. 8-74
8.8 Limitations 8-75
8.9 Summary of Effective Porosity for the HGUs at the Yucca Flat/Climax Mine CAU 8-77

9.0 Dispersivity. 9-1

9.1 Role of Dispersion in Contaminant Transport 9-1
9.2 Data Compilation and Data Transfer 9-4
9.2.1 Data Types 9-4
9.2.2 Data Sources. 9-4
9.2.3 Data Documentation Evaluation. 9-6
9.3 Data Evaluation. 9-6
9.3.1 NTS and Vicinity Dispersivity Data. 9-7
9.3.1.1 Nye County Early Warning Drilling Program Site 22 9-11
9.3.1.2 ER-6-1 Well Cluster Tracer Test 9-13
9.3.2 Non-NTS Dispersivity Data 9-14
9.3.3 Data Quality Evaluation 9-16
9.3.4 General Description of Dispersivity-Scale Dataset 9-16
9.3.4.1 Longitudinal Dispersivity 9-16

TABLE OF CONTENTS (CONTINUED)

9.3.4.2 Transverse Dispersivities 9-18
9.3.4.3 Summary of Observations from Dispersivity Dataset Assessment 9-24
9.3.5 Evaluation of Scale Dependency of Dispersivity 9-24
9.3.5.1 Background and Previous Investigations of Scale Dependency 9-24
9.3.5.2 Determination of Dispersivity-Scale Relationships 9-27
9.4 Data Limitations 9-28
9.5 Summary 9-28

10.0 Matrix Diffusion Parameters 10-1

10.1 Role of Matrix Diffusion in Contaminant Transport 10-1
10.1.1 Diffusion Process 10-2
10.2 Data Compilation and Data Transfer 10-3
10.3 Data Types and Sources for Matrix Diffusion Coefficient 10-4
10.3.1 Laboratory Tracer Diffusion Experiments 10-4
10.3.2 Field Tracer Diffusion Experiments 10-15
10.3.3 Formation Factor-Porosity Approach 10-18
10.4 Data Analysis 10-20
10.4.1 Data Evaluation Approach 10-20
10.4.2 Data Quality/Transferability Protocol 10-21
10.4.3 Data Review and Statistics 10-23
10.4.4 Free Water Diffusion Coefficients 10-25
10.4.5 Effects of Temperature and Ionic Strength 10-29
10.4.6 Tortuosity-Porosity Correlations from Laboratory Diffusion Experimental Data 10-31
10.5 Scaling Considerations 10-34
10.6 Data Limitations 10-37
10.7 Summary 10-37

11.0 Matrix Sorption Parameters 11-1

11.1 The Role of Matrix Sorption in Contaminant Transport Models 11-1
11.2 Data Compilation and Data Transfer 11-1
11.3 Radionuclides of Potential Concern 11-2
11.4 The K_d Parameter 11-2
11.5 Direct Measurement of K_d 11-3
11.5.1 Alluvium 11-4
11.5.1.1 Americium and Samarium 11-7
11.5.1.2 Cesium and Strontium 11-9
11.5.1.3 Neptunium 11-9
11.5.1.4 Uranium 11-10
11.5.1.5 Europium 11-11
11.5.1.6 Plutonium 11-11

TABLE OF CONTENTS (CONTINUED)

11.5.1.7 Nickel 11-12
11.5.1.8 Iodine and Technetium 11-12
11.5.2 Volcanic Rocks. 11-12
11.5.2.1 YMP Sorption Data 11-13
11.5.2.1.1 YMP Sorption Data History 11-14
11.5.2.1.2 YMP Sorption Data Transfer 11-14
11.5.2.2 Americium 11-16
11.5.2.3 Cesium and Strontium 11-18
11.5.2.4 Neptunium 11-21
11.5.2.5 Uranium 11-23
11.5.2.6 Plutonium 11-25
11.5.3 Carbonate Rocks. 11-28
11.5.3.1 Carbon-14 11-29
11.5.3.2 Strontium and Cesium 11-29
11.5.3.3 Uranium 11-29
11.5.3.4 Neptunium 11-29
11.5.3.5 Plutonium 11-30
11.5.4 K_d Derived from Upscaled Mechanistic Sorption Models 11-31
11.6 K_d Derived from Scaled Mechanistic Models 11-33
11.6.1 Calculation of Distribution Coefficients Using Yucca Flat/Climax Mine Mineralogy and Water Chemistry Data 11-36
11.7 Summary of K_d Data. 11-36
11.8 Scaling Considerations 11-40

12.0 Fracture Sorption Parameter 12-1

12.1 The Role of Fracture Sorption in Contaminant Transport 12-1
12.2 Data Types and Sources for Fracture Sorption. 12-1
12.2.1 Data Types 12-2
12.2.2 Data Sources. 12-2
12.2.3 Data Transfer 12-3
12.3 Data Evaluation. 12-3
12.3.1 Derivation by Wolfsberg et al. (2002) 12-4
12.3.2 Derivation by Zavarin et al. (2004) 12-5
12.3.3 Reactive Transport Experiments by Zavarin et al. (2007) 12-5
12.3.4 Fracture Retardation Factor Summary and Integration 12-9

13.0 Colloid-Facilitated Transport Parameters. 13-1

13.1 Data Compilation and Data Transfer 13-2
13.2 Role of Colloids in Contaminant Transport 13-2
13.3 Summary of Colloid Studies. 13-3
13.4 Colloid Mineralogy. 13-7
13.5 Colloid Concentrations and Size Distributions. 13-8
13.5.1 Colloid Concentration and Size Data 13-9

TABLE OF CONTENTS (CONTINUED)

13.5.2 Colloid Concentration Distribution 13-10
13.5.3 Colloid Concentration Relationship to Water Chemistry. 13-16
13.5.4 Colloid Size Distributions 13-17
13.5.5 Data Limitations 13-19
13.5.6 Representativeness and Scaling Considerations. 13-21
13.6 Colloid Transport Parameters 13-22
13.6.1 Basis for Transport Parameter Values 13-22
13.6.2 Data Evaluation 13-24
13.6.2.1 Colloid Filtration Rate Constants 13-24
13.6.2.2 Colloid Retardation Factors 13-32
13.6.2.3 Additional Filtration and Retardation Analyses 13-34
13.6.3 Limitations of the Colloid Transport Parameter Data and Analysis. 13-36
13.6.3.1 Data Quality Limitations 13-36
13.6.3.2 Scaling Considerations 13-37
13.6.3.3 Colloid Retardation Transport Modeling Approach 13-37
13.7 Radionuclide Associations with Colloids. 13-38
13.8 Actinide Distribution Coefficients and Sorption Rates onto Colloids 13-39
13.8.1 Development of Parameter Distributions. 13-41
13.8.1.1 Distribution Coefficients 13-41
13.8.1.2 Radionuclide Sorption Rates onto Colloids 13-46
13.8.1.3 Radionuclide Desorption Rates from Colloids 13-47
13.8.2 Data Limitations 13-51
13.8.3 Scaling Considerations 13-51
13.9 Summary 13-52

14.0 References. 14-1

Appendix A - Underground Nuclear Tests in the Yucca Flat/Climax Mine Corrective Action Unit

A.1.0 Underground Nuclear Tests in the Yucca Flat/Climax Mine Corrective Action Unit A-1

A.2.0 References. A-27

Appendix B - Data Collection Activities

B.1.0 Summary of Data Collection for the Yucca Flat/Climax Mine Corrective Action Unit B-1

B.2.0 Yucca Flat/Climax Mine CAU-Specific Well Drilling and Testing. B-2

B.3.0 Yucca Flat/Climax Mine CAIP-Identified Characterization Activities B-8

B.3.1 Tuff Confining Unit Mineralogical Studies B-8

TABLE OF CONTENTS (CONTINUED)

B.3.2 Geophysical Interpretation of the Paleozoic Framework B-10
B.3.2.1 Natural-Source Magnetotelluric Survey B-10
B.3.2.2 Gravity and Aeromagnetic Data Interpretation B-10
B.3.2.3 Analysis of Existing Seismic Data B-11
B.3.3 Hydrologic Investigation of Wells ER-6-1 and ER-6-2 . . . . . B-11
B.3.4 Isotope/Geochemistry Mass-Balance Studies B-12
B.3.5 Analysis of Existing Tracer Test Data B-12
B.3.6 Laboratory Radionuclide Transport Studies B-13
B.3.7 Rainier Mesa Colloid Transport Studies B-14
B.3.8 Analysis of Data for Phenomenological Models B-15

B.4.0 Other Studies B-16

B.5.0 References B-18

Appendix C - Yucca Flat/Climax Mine Alternative Hydrostratigraphic Framework Models

C.1.0 Introduction C-1

C.2.0 Process of Addressing Alternatives to the Base Model C-2

C.3.0 Alternative Models C-3

C.3.1 CP Thrust Alternative C-3
C.3.2 Hydrologic Barrier in Northern Yucca Flat C-6
C.3.3 Contiguous UCCU in Southwestern Yucca Flat C-6
C.3.4 Fault Juxtaposition C-6
C.3.5 Partial Zeolitization C-11

C.4.0 References C-14

Appendix D - Compilation of Mineralogy Data

D.1.0 Compilation of X-ray Diffraction Analyses and Formal Definitions for Alteration . . . D-1

D.2.0 Dataset Summary D-3

D.3.0 Histograms of Reactive Minerals for Hydrostratigraphic Units D-19

D.4.0 Access to Dataset D-34

D.5.0 References D-35

Appendix E - Description of Geochemistry Dataset

E.1.0 Introduction E-1

E.2.0 Summary of Datasets E-2

E.3.0 Access to Dataset E-4

E.4.0 References E-11

TABLE OF CONTENTS (CONTINUED)

Appendix F - Description of Matrix Porosity Data

F.1.0 Introduction F-1
F.2.0 Dataset Summary F-2
F.2.1 Table Structures F-2
F.2.2 Access to Datasets F-3
F.3.0 Geophysically Derived Matrix Porosity Data Analysis F-4
F.4.0 References F-16

Appendix G - Description of Dispersivity Dataset

G.1.0 Introduction G-1
G.2.0 Dataset Summary G-2
G.3.0 Table Structure G-3
G.4.0 Access to Dataset G-4

Appendix H - Description of Matrix Diffusion Dataset

H.1.0 Introduction H-1
H.2.0 Dataset Summary H-2
H.3.0 Table Structure H-3
H.4.0 Access to Dataset H-5
H.5.0 References H-6

Appendix I - Description of Matrix Sorption Dataset

I.1.0 Introduction I-1
I.2.0 Dataset Summary I-2
I.2.1 Matrix Distribution Coefficients from Yucca Flat/Climax Mine Mineralogy and Water Chemistry Data I-2
I.2.1.1 Table Structure I-2
I.2.2 Matrix Sorption Parameters from Laboratory Studies I-3
I.2.2.1 Table Structure I-3
I.3.0 Data Transfer and Data Quality Protocol for Laboratory Distribution Coefficients I-6
I.3.1 Weights I-6
I.3.2 Rock Type I-6
I.3.2.1 Alluvium I-6

TABLE OF CONTENTS (CONTINUED)

I.3.2.2 Volcanic Rocks I-7
I.3.2.3 Scores I-7
I.3.3 Deposition and Alteration History I-8
I.3.4 Water Chemistry, Especially pH and Major Cation Concentrations I-8
I.3.5 Multipliers I-8
I.3.6 Measurement Method Considerations I-8
I.3.7 Data Reduction and Analysis Method I-9
I.3.8 Quality Documentation I-9
I.3.9 Overall Scores I-9

I.4.0 References I-10

Appendix J - Description of Colloid Parameter Datasets

J.1.0 Introduction J-1

J.2.0 Colloid Size, Concentration Data J-2

J.3.0 Alluvium Transport Parameter Data J-3

J.4.0 Volcanics, Carbonates Transport Parameter Data J-4

J.5.0 Colloid K_d Range Data J-5

J.6.0 Colloid Sorption, Desorption Data J-6

J.7.0 Access to Datasets J-7

J.8.0 References J-8

Appendix K - Nevada Division of Environmental Protection Comment Responses

LIST OF FIGURES

NUMBER	TITLE	PAGE
1-1	Nevada Test Site-Scale Boundaries	1-3
1-2	Underground Test Area Corrective Action Units Process Flow Diagram	1-6
2-1	Data Types and Utilization in the Contaminant Transport Model	2-4
4-1	Generalized Geologic Map of the Yucca Flat/Climax Mine Region	4-2
4-2	Correlation of Stratigraphic and Hydrostratigraphic Units of the Yucca Flat/Climax Mine HFM Area	4-11
4-3	Block Model View Showing Hydrostratigraphic Units at the Surface Within the Yucca Flat/Climax Mine Model Area	4-13
4-4	Hydrostratigraphic Units at the Water Table in the Yucca Flat/Climax Mine Model Area	4-14
4-5	Block Model View Showing Extent of the Playa Confining Unit and the Basalt Lava-Flow Aquifer Within the Yucca Flat/Climax Mine Model Area with the Upper Alluvial HSU (AA3) Removed	4-15
4-6	Block Model View Showing the Distribution of Hydrostratigraphic Units Within the Yucca Flat/Climax Mine HFM Area with Alluvium Removed	4-16
4-7	Block Model View Showing the Distribution of the Volcanic Confining Units in the Yucca Flat/Climax Mine HFM Area with Alluvium and Upper Volcanic Aquifers Removed	4-17
4-8	Block Model View Showing the Distribution of the Pre-Tertiary Hydrostratigraphic Units in the Yucca Flat/Climax Mine HFM Area with Alluvium and Volcanic Aquifers Removed	4-18
4-9	Schematic Cross Section Showing Relationships Among the Hydrostratigraphic Units and Reactive Mineral Categories for the Alluvium, Playa, and Basalt in Southern Yucca Flat	4-29
4-10	Schematic North-South Cross Section Showing Relationships of Hydrostratigraphic Units and Reactive Mineral Categories for the Volcanic Rocks in the Yucca Flat/Climax Mine HFM	4-39

LIST OF FIGURES (CONTINUED)

NUMBER	TITLE	PAGE
4-11	Schematic West-East Cross Section Showing Relationships of Hydrostratigraphic Units and Reactive Mineral Categories for the Belted Range and Older Volcanic Rocks in Northern Yucca Flat	4-48
5-1	Conceptual Flow Paths Evaluated in the Yucca Flat/Climax Mine Geochemistry Study	5-2
5-2	Yucca Flat/Climax Mine Geochemistry Study Area	5-6
5-3	Piper Diagram for Samples Collected from the Alluvial Aquifer	5-10
5-4	Bar Plot for Samples Collected from the Alluvial Aquifer	5-10
5-5	Piper Diagram for Samples Collected from the Volcanic Hydrostratigraphic Units	5-12
5-6	Bar Plot for Samples Collected from the Volcanic Hydrostratigraphic Units	5-12
5-7	Piper Diagram for Samples from the LCA of Northern and Western Yucca Flat	5-16
5-8	Bar Plot for Samples from the LCA of Northern and Western Yucca Flat	5-16
5-9	Piper Diagram for Samples Collected from the LCA of Eastern and Southwestern Yucca Flat	5-20
5-10	Bar Plot for Samples Collected from the LCA of Eastern and Southwestern Yucca Flat	5-20
5-11	Piper Diagram for Samples Collected from the LCA3 and UCA	5-24
5-12	Bar Plot for Samples Collected from the LCA3 and UCA	5-24
5-13	Concentration of Select Major Ions in Groundwater of UE-2ce	5-25
5-14	Piper Diagram for Samples Collected from the Clastic Confining Units	5-26
5-15	Bar Plot for Samples Collected from the Clastic Confining Units	5-26
5-16	Schematic for the U15 Shaft	5-29
5-17	Piper Diagram for Samples Collected from the Granite Confining Unit	5-30

LIST OF FIGURES (CONTINUED)

NUMBER	TITLE	PAGE
5-18	Bar Plot for Samples Collected from the Granite Confining Unit	5-30
5-19	Piper Diagram for Samples Collected from the Perched Springs of Yucca Flat	5-32
5-20	Bar Plot for Samples Collected from the Perched Springs of Yucca Flat	5-32
6-1	Locations of the 828 Underground Nuclear Tests at the Nevada Test Site Between 1951 and 1992	6-3
6-2	Map of the Nevada Test Site Showing the Near-field Sampling Sites	6-7
6-3	The DALHART Near-field	6-12
6-4	Plan View Location of Post-test and Exploratory Holes in the GASCON Near-field	6-14
6-5	The BILBY Near-field	6-16
6-6	The BASEBALL Near-field	6-17
6-7	The INGOT Slant Drilled Groundwater Sampling Well	6-19
6-8	Activity in the INGOT Drillback	6-19
6-9	Location of Four Tests Detonated in Carbonate Rock	6-22
6-10	The NASH Near-field	6-23
6-11	Tritium Concentrations in Pumped Groundwater from the NASH Satellite Well as a Function of (a) Time and (b) Total Volume of Water Pumped	6-25
6-12	Tritium Concentrations and Volume Pumped from the NASH Satellite Well as a Function of Time (10 to 11 Years, 11 to 12 Years, and 15 to 18 Years from Time of Detonation)	6-26
6-13	Tritium Concentrations in Pumped Groundwater from the NASH Satellite Well	6-27
6-14	BOURBON Near-field	6-28
6-15	Measured Tritium Concentrations in BOURBON Satellite Well	6-29

LIST OF FIGURES (CONTINUED)

NUMBER	TITLE	PAGE
6-16	Schematic of the HANDCAR Cavity and Distribution of Radioactivity	6-30
6-17	Location of Three Tests Detonated in Granite	6-32
6-18	Diagram of HARD HAT Near-field and Post-test Drilling Operations	6-33
6-19	Re-entry Drift at the HARD HAT Chimney Edge	6-34
6-20	Location and Measured Permeability of Rocks in the Vicinity of the HARD HAT Test	6-37
6-21	Summary of Permeability Measurements	6-38
6-22	Diagram of PILE DRIVER Near-field and Post-test Drilling Operations	6-39
6-23	PILE DRIVER Chimney Edge	6-40
6-24	Distribution of Tritium (pCi/L) in Waters Located Near the HARD HAT and PILE DRIVER Tests (red), Regional Water Table Identified in Blue	6-41
6-25	Location of Tuff Pile 1	6-42
7-1	Yucca Flat/Climax Mine Borehole Locations with Matrix Porosity Values	7-4
7-2	Linear Regression Analysis of HGU Porosity (%) as a Function of Depth (m bgs)	7-8
7-3	Yucca Flat HGU Porosity Values	7-10
7-4	Yucca Flat HSU Porosity Values	7-11
7-5	AA HGU Matrix Porosity Histogram and CDF	7-13
7-6	WTA HGU Matrix Porosity Histogram and CDF	7-14
7-7	VTA HGU Matrix Porosity Histogram and CDF	7-15
7-8	TCU HGU Matrix Porosity Histogram and CDF	7-16
7-9	GCU HGU Matrix Porosity Histogram and CDF	7-17
7-10	CCU HGU Matrix Porosity Histogram and CDF	7-18

LIST OF FIGURES (CONTINUED)

NUMBER	TITLE	PAGE
7-11	CA HGU Matrix Porosity Histogram and CDF	7-19
7-12	AA HSU Matrix Porosity Histogram and CDF	7-20
7-13	ATCU HSU Matrix Porosity Histogram and CDF	7-21
7-14	LCA HSU Matrix Porosity Histogram and CDF	7-22
7-15	LCCU HSU Matrix Porosity Histogram and CDF	7-23
7-16	LTCU HSU Matrix Porosity Histogram and CDF	7-24
7-17	MGCU HSU Matrix Porosity Histogram and CDF	7-25
7-18	OSBCU HSU Matrix Porosity Histogram and CDF	7-26
7-19	TM-LVTA HSU Matrix Porosity Histogram and CDF	7-27
7-20	TM-UVTA HSU Matrix Porosity Histogram and CDF	7-28
7-21	TM-WTA HSU Matrix Porosity Histogram and CDF	7-29
7-22	TSA HSU Matrix Porosity Histogram and CDF	7-30
7-23	TUBA HSU Matrix Porosity Histogram and CDF	7-31
7-24	UTCU HSU Matrix Porosity Histogram and CDF	7-32
8-1	Spatial Distribution of Effective Porosity Data	8-5
8-2	Function for Recirculating Tracer Tests	8-15
8-3	Estimated Effective Porosity Ranges for the Welded-Tuff Aquifer Hydrogeologic Unit	8-34
8-4	Estimated Effective Porosity Ranges for the Lava-Flow Aquifer Hydrogeologic Unit	8-51
8-5	Estimated Effective Porosity Ranges for the Carbonate Aquifer Hydrogeologic Unit	8-71
8-6	Recommended Effective Porosity Distributions for the Fractured Hydrogeologic Units	8-79

LIST OF FIGURES (CONTINUED)

NUMBER	TITLE	PAGE
9-1	Locations of CAMBRIC Radionuclide Migration Experiment and Tracer Tests at NTS and Vicinity	9-5
9-2	Schematic of Tracer Breakthrough Curve at the Pumping Well of a Convergent-Flow Tracer Test	9-10
9-3	Log-Log Plot of Longitudinal Dispersivity as a Function of Measurement Scale for All Rock Types	9-18
9-4	Comparison of NTS and Non-NTS Dispersivity-Scale Data	9-19
9-5	Cumulative Distribution Function for Scale for the Dispersivity-Scale Dataset	9-20
9-6	Cumulative Distribution Function for Longitudinal Dispersivity for the Dispersivity-Scale Dataset	9-21
9-7	(a) Transverse Horizontal Dispersivity versus Transport Scale and (b) Ratio of Longitudinal to Transverse Horizontal Dispersivity versus Transport Scale	9-22
9-8	(a) Transverse Vertical Dispersivity versus Transport Scale and (b) Ratio of Longitudinal to Transverse Vertical Dispersivity versus Transport Scale	9-23
9-9	Dispersivity-Scale Relationships Determined from Regression Analyses: (a) Log-Log Linear, (b) Log-Log Piecewise Linear, (c) Log-Log Quadratic, and (d) Log-Log Asymptotic	9-29
10-1	Typical Design for a Diffusion Cell Experiment	10-5
10-2	Log Tortuosity versus Linear Porosity from Different Reference Sources	10-9
10-3	Log Tortuosity versus Log Porosity from Different Reference Sources	10-9
10-4	Tortuosity Data by Rock Type	10-24
10-5	Tortuosity Data by Rock Type, Including Data Quality Score	10-24
10-6	Tortuosity Data by Sample Depth and Rock Type	10-26
10-7	Tortuosity versus Permeability	10-26

LIST OF FIGURES (CONTINUED)

NUMBER	TITLE	PAGE
10-8	Cumulative Distribution Function for Porosities of the Matrix Diffusion Samples	10-27
10-9	Cumulative Distribution Function for Tortuosities of the Matrix Diffusion Samples	10-27
10-10	Cumulative Distribution Function for Permeabilities of the Matrix Diffusion Samples	10-28
10-11	Free Water Diffusion Adjustment (Multiplier) for Increasing Temperature	10-30
10-12	Log-Log Relationships Between Tortuosity and Porosity from Various Published Studies Compared with the NTS Database Measurements	10-33
10-13	Comparison of Log-Log and Log-Linear Relationships Between Tortuosity and Porosity	10-34
10-14	Correlation of Tortuosity and Porosity (Log-Log Axes) for the Matrix Diffusion Dataset	10-35
10-15	Correlation of Tortuosity and Porosity (Log-Log Axes) for the Matrix Diffusion Dataset, Including the 95% Confidence Interval (Log Scale for Porosity)	10-35
10-16	Correlation of Tortuosity and Porosity (Log-Linear Axes) for the Matrix Diffusion Dataset, Including the 95% Confidence Interval (Linear Scale for Porosity)	10-36
11-1	Laboratory Measured Distribution Coefficients for Alluvium Samples	11-6
11-2	Samarium K_d as a Function of pH for Alluvium Samples Collected at Yucca Flat	11-8
11-3	Laboratory Measured Distribution Coefficients for Vitric-Tuff Samples	11-17
11-4	Laboratory Measured Distribution Coefficients for Devitrified-Tuff Samples	11-18
11-5	Laboratory Measured Distribution Coefficients for Zeolitic-Tuff Samples	11-19
11-6	Strontium Sorption as a Function of Temperature (°C) Measured During YMP Distribution Coefficient Experiments	11-22

LIST OF FIGURES (CONTINUED)

NUMBER	TITLE	PAGE
11-7	Distribution Coefficient (mL/g) for Plutonium Sorption onto Devitrified Tuff as a Function of Experiment Duration	11-27
11-8	Comparison of Distribution Coefficients for Laboratory Studies and Mechanistic Model Calculations for the Alluvium	11-37
11-9	Comparison of Distribution Coefficients for Laboratory Studies and Mechanistic Model Calculations for Vitric Tuffs	11-38
11-10	Comparison of Distribution Coefficients for Laboratory Studies and Mechanistic Model Calculations for Devitrified Tuffs	11-38
11-11	Comparison of Distribution Coefficients for Laboratory Studies and Mechanistic Model Calculations for Zeolitic Tuffs	11-39
13-1	Location Map for Colloid Samples	13-13
13-2	Cumulative Distribution Function of Log_{10} Colloid Concentrations for All NTS Data	13-14
13-3	Normalized Size Distributions of Colloids for Samples Selected for Each Well	13-18
13-4	Normalized Size Distributions of Colloids in the 50- to 200-nm Range	13-18
13-5	Cumulative Distribution Function of Colloid Diameter for All NTS Data and HGU Groups	13-20
13-6	Colloid Filtration Rate Constants as a Function of Mean Residence Time in Alluvium	13-26
13-7	Cumulative Probability Distribution of Colloid Filtration Rate Constants for Alluvium	13-28
13-8	CML Microsphere and Colloid Filtration Rate Constants as a Function of Mean Residence Time in Fractured Volcanics	13-29
13-9	Cumulative Probability Distribution of Colloid Filtration Rate Constants for Fractured Volcanics	13-30
13-10	Cumulative Probability Distribution of Colloid Retardation Factors for Alluvium	13-33

LIST OF FIGURES (CONTINUED)

NUMBER	TITLE	PAGE
13-11	Cumulative Probability Distribution of Colloid Retardation Factors for Fractured Volcanic Rocks	13-33
13-12	Ranges of K_d Values Measured for Actinide Sorption onto Colloids (Kersting and Reimus, 2003)	13-42
13-13	Distribution Coefficient Calculated for Pu^{+5} Sorbed onto Various Mineral Colloids (Kersting and Reimus, 2003)	13-45
13-14	Yucca Mountain Project Pu Desorption Experiments Using Smectite and Silica Colloids (Lu et al., 1998b)	13-50
B.2-1	Yucca Flat/Climax Mine CAU-Specific Investigation and Recompletion Well Locations	B-5
C.3-1	Comparison of the UCCU Extent and CP Thrust Location in the Base Model with the CP Thrust Alternative (Tertiary HSUs Removed for These Views)	C-4
C.3-2	West-East Profiles Through Central and Northern Yucca Flat Comparing the Base Model with the CP Thrust (CPT) Alternative	C-5
C.3-3	Comparison of the LCCU Geometry in the Base Model with the Hydrologic Barrier Alternative	C-7
C.3-4	West-East Profiles Through Climax Stock Comparing the Base Model with the Hydrologic Barrier Alternative	C-8
C.3-5	Comparison of the UCCU Extent in the Base Model with the Contiguous UCCU Alternative (Tertiary HSUs Removed)	C-9
C.3-6	West-East Profile Through the Southwestern Corner of the Yucca Flat/Climax Mine HFM Comparing the Base Model with Contiguous UCCU Alternative	C-10
C.3-7	West-East Profiles Through Central Yucca Flat Comparing the Base Model with Fault Juxtaposition Alternative	C-12
C.3-8	View of the Base Model Showing Area Affected in the Partial Zeolitization Alternative (Alluvium and Volcanic Aquifer HSUs Removed)	C-13
D.2-1	Sampling Locations in the Northern Areas of Yucca Flat Formally Used for Testing by Lawrence Livermore National Laboratory	D-4

LIST OF FIGURES (CONTINUED)

NUMBER	TITLE	PAGE
D.2-2	Sampling Locations in the Southern Areas of Yucca Flat Formally Used for Testing by Los Alamos National Laboratory	D-5
D.2-3	Schematic Diagram Illustrating Eruption and Subsequent Alteration of Volcanic Rocks Within SWNVF	D-7
D.4-1	Histograms and Percent Cumulative Probability Distributions for Zeolite Abundances in Yucca Flat/Climax Mine HSUs (Part 1 of 3)	D-20
D.4-1	Histograms and Percent Cumulative Probability Distributions for Zeolite Abundances in Yucca Flat/Climax Mine HSUs (Part 2 of 3)	D-21
D.4-1	Histograms and Percent Cumulative Probability Distributions for Zeolite Abundances in Yucca Flat/Climax Mine HSUs (Part 3 of 3)	D-22
D.4-2	Histograms and Percent Cumulative Probability Distributions for Smectite Abundances in Yucca Flat/Climax Mine HSUs (Part 1 of 3)	D-23
D.4-2	Histograms and Percent Cumulative Probability Distributions for Smectite Abundances in Yucca Flat/Climax Mine HSUs (Part 2 of 3)	D-24
D.4-2	Histograms and Percent Cumulative Probability Distributions for Smectite Abundances in Yucca Flat/Climax Mine HSUs (Part 3 of 3)	D-25
D.4-3	Histograms and Percent Cumulative Probability Distributions for Carbonate (Calcite plus Dolomite) Abundances in Yucca Flat/Climax Mine HSUs (Part 1 of 3)	D-26
D.4-3	Histograms and Percent Cumulative Probability Distributions for Carbonate (Calcite plus Dolomite) Abundances in Yucca Flat/Climax Mine HSUs (Part 2 of 3)	D-27
D.4-3	Histograms and Percent Cumulative Probability Distributions for Carbonate (Calcite plus Dolomite) Abundances in Yucca Flat/Climax Mine HSUs (Part 3 of 3)	D-28
D.4-4	Histograms and Percent Cumulative Probability Distributions for Mica Abundances in Yucca Flat/Climax Mine HSUs (Part 1 of 3)	D-29
D.4-4	Histograms and Percent Cumulative Probability Distributions for Mica Abundances in Yucca Flat/Climax Mine HSUs (Part 2 of 3)	D-30

LIST OF FIGURES (CONTINUED)

NUMBER	TITLE	PAGE
D.4-4	Histograms and Percent Cumulative Probability Distributions for Mica Abundances in Yucca Flat/Climax Mine HSUs (Part 3 of 3)	D-31
D.4-5	Histograms and Percent Cumulative Probability Distributions for Hematite Abundances in Yucca Flat/Climax Mine HSUs (Part 1 of 2)	D-32
D.4-5	Histograms and Percent Cumulative Probability Distributions for Hematite Abundances in Yucca Flat/Climax Mine HSUs (Part 2 of 2)	D-33
F.3-1	AA HGU ENP Matrix Porosity Histogram and CDF	F-6
F.3-2	CA HGU ENP Matrix Porosity Histogram and CDF	F-7
F.3-3	CCU HGU ENP Matrix Porosity Histogram and CDF	F-8
F.3-4	GCU HGU ENP Matrix Porosity Histogram and CDF	F-9
F.3-5	TCU HGU ENP Matrix Porosity Histogram and CDF	F-10
F.3-6	VTA HGU ENP Matrix Porosity Histogram and CDF	F-11
F.3-7	WTA HGU ENP Matrix Porosity Histogram and CDF	F-12
F.3-8	CA HGU Sonic Matrix Porosity Histogram and CDF	F-13
F.3-9	CCU HGU Sonic Matrix Porosity Histogram and CDF	F-14
F.3-10	TCU HGU Sonic Matrix Porosity Histogram and CDF	F-15

LIST OF PLATES

NUMBER **TITLE**

Plate 1 Map of Yucca Flat/Climax Mine Area Showing UGTA Corrective Action Sites, UGTA Well Locations, Test-Related Surface Effects, and Selected Basin-Forming Faults . . . . . Pocket

Plate 2 Select Profiles of Hydrostratigraphic Units for the Yucca Flat/Climax Mine Model Area . . . . . Pocket

LIST OF TABLES

NUMBER	TITLE	PAGE
1-1	Yucca Flat/Climax Mine CAU Corrective Action Investigation Planning Documents	1-7
4-1	Hydrogeologic Units of the Yucca Flat/Climax Mine HFM Area	4-5
4-2	Hydrostratigraphic Units of the Yucca Flat/Climax Mine HFM	4-7
4-3	Correlation of Hydrostratigraphic Units of the Yucca Flat/Climax Mine CAU Model and Earlier Models	4-19
4-4	Reactive Mineral Categories for the Yucca Flat/Climax Mine HFM Area	4-24
4-5	Reactive Mineral Category Assignments for the Hydrostratigraphic Units in the Yucca Flat/Climax Mine HFM	4-26
4-6	Summary of XRD Analyses of Whole Rocks for Hydrostratigraphic Units in the Yucca Flat/Climax Mine HFM Area	4-30
6-1	Radionuclide Inventory for Yucca Flat/Climax Mine	6-4
6-2	Underground Nuclear Tests Associated with Near-field Sampling Wells in the Yucca Flat/Climax Mine CAU	6-8
6-3	Compilation of Groundwater Sample Collection Methods and Dates	6-9
7-1	Yucca Flat Matrix Porosity Values from Laboratory Transport Experiments	7-5
7-2	HSU to HGU Assignment	7-6
7-3	Sample Summary Statistics for Matrix Porosity	7-12
7-4	Matrix Porosity Distribution Summary	7-33
8-1	Effective Porosities Determined from Tracer Testing at the C-holes Complex	8-17
8-2	Effective Porosities from Welded-Tuff Air-Permeability and Gas Tracer Tests (after Freifeld, 2001)	8-19
8-3	Estimate of Fracture Porosity of the Tuffs Penetrated by Test Well USW H-4 (from Erickson and Waddell, 1985)	8-23

LIST OF TABLES (CONTINUED)

NUMBER	TITLE	PAGE
8-4	Fracture Porosities Calculated for the Welded-Tuff Aquifers from Hydraulic Conductivity and Fracture Spacing Using Equation (8-10)	8-28
8-5	Calculated Fracture Porosities for the Welded-Tuff Aquifer (after DOE/NV, 1997a)	8-30
8-6	Effective Porosity Estimates for Welded Tuff in the Basin and Range Province (after Bedinger et al., 1989)	8-31
8-7	Fracture Porosities Used by Wolfsberg et al. (2002) for the Welded-Tuff Aquifer	8-32
8-8	Summary of Estimated Effective Porosity Ranges for the WTA HGU and Recommended Range for the Yucca Flat/Climax Mine CAU-Scale Model	8-33
8-9	Estimate of Effective Porosity for the BULLION Forced-Gradient Experiment Based on Plug Flow Calculations (after IT, 1998)	8-38
8-10	Effective Porosities from the IT (1998) Numerical Model Calibration to Tracer Recovery During the BULLION Forced-Gradient Experiment	8-39
8-11	Effective Porosities from the Reimus and Haga (1999) Analysis of the BULLION Forced-Gradient Experiment	8-41
8-12	Fracture Porosities Calculated for Lava-Flow Aquifers from Hydraulic Conductivity and Fracture Spacing Using Equation (8-10)	8-42
8-13	Fracture Porosities Used by Wolfsberg et al. (2002) for a Lava-Flow Aquifer	8-48
8-14	Summary of Estimated Effective Porosity Ranges for the Lava-Flow Aquifer and Recommended Range for the Yucca Flat/Climax Mine CAU-Scale Model	8-50
8-15	Summary of Effective Porosities Determined Using the Breakthrough Curves from the ER-6-1 Well Cluster Tracer Test	8-55
8-16	Calculated Porosities for the Two-Well Recirculating Tracer Tests Conducted at the Amargosa Tracer Site Assuming Plug Flow	8-59
8-17	Summary of Fracture Porosities Determined for the Culebra Dolomite at the Waste Isolation Pilot Plant Site	8-62

LIST OF TABLES (CONTINUED)

NUMBER	TITLE	PAGE
8-18	Fracture Porosities Calculated for Wells ER-6-1#2 and ER-7-1 Using Hydraulic Conductivity and Fracture Spacing (Equation [8-10])	8-64
8-19	Calculated Fracture Porosities for Boreholes ER-6-1#2 and ER-7-1 Using Fracture Spacing and Aperture Calculations	8-66
8-20	Effective Porosity Estimates for Carbonate Rocks in the Basin and Range Province (after Bedinger et al., 1989)	8-68
8-21	Summary of Estimated Effective Porosity Ranges for the Carbonate Aquifer and Recommended Range for the Yucca Flat/Climax Mine CAU-Scale Model	8-70
8-22	Summary of Recommended Distributions for the Effective Porosity of the Fractured Aquifer HGUs for the Yucca Flat/Climax Mine CAU-Scale Model	8-78
9-1	Dispersivity Information Summary from Studies at the Nevada Test Site and Vicinity	9-8
9-2	Dispersivity-Scale Relationships Determined from Regression Analyses	9-27
10-1	Summary of Data Transfer Protocol for Yucca Flat Matrix Diffusion Coefficient Dataset	10-22
10-2	Factor by Which Free Water Diffusion Coefficients Change as a Function of Water Temperature	10-29
11-1	Whole Rock Mineralogy from Alluvium K_d Experiments	11-5
11-2	Log K_ds (mL/g) Calculated from Flowthrough Experiments Reported in Zavarin, 2002	11-7
11-3	Class Definition for Volcanic Rocks Used by the Yucca Mountain Project	11-15
11-4	Chemical Composition (mg/L) of Groundwater in J-13, UE-25 p#1, and Three Locations in Yucca Flat	11-16
11-5	Carbonate Sorption K_d (mL/g) Ranges	11-30
11-6	Predicted Average Radionuclide Distribution Coefficients (Log K_d , mL/g) for Frenchman Flat Alluvium Using Reported Radionuclide Sorbing Mineral Abundances	11-34

LIST OF TABLES (CONTINUED)

NUMBER	TITLE	PAGE
11-7	Predicted Average Log K_d (mL/g) for Selected Regional Hydrostratigraphic Units from Zavarin et al. (2004)	11-35
12-1	Fracture Retardation Factors from Wolfsberg et al. (2002)	12-4
12-2	Fracture Retardation Factors, Log (R), from Zavarin et al. (2004)	12-6
12-3	Summary of Fracture Retardation Factors Developed Through LLNL and LANL Fracture Retardation Experiments	12-7
12-4	Summary of Fracture Retardation Factors for Yucca Flat HSUs	12-11
13-1	Representative Colloid Samples and Concentrations	13-11
13-2	Summary of Colloid Concentrations (Log_{10}) for HGU Groups	13-15
13-3	Lognormal CDF Shape Parameters for Colloid Concentration	13-15
13-4	Shape Parameters for Colloid Size Lognormal Distributions	13-19
13-5	Results of the Field-Scale Alluvial Tracer Test	13-25
13-6	ER-6-1 MWAT-TT Transport Analysis Results (Reimus, 2007c) for the LCA	13-31
13-7	Results of LCA Core Fracture Experiments (Reimus et al., 2006b)	13-32
13-8	Retardation Factors and Transport Parameters for Fracture Flowthrough Experiments	13-35
13-9	Ranges of Rate Constants for Sorption and Desorption of Actinides onto Colloids (Assuming Only a Single Type of Sorption Site) from UGTA and YMP Experiments	13-40
A.1-1	Shaft and Tunnel Nuclear Detonations in the Yucca Flat/Climax Mine Corrective Action Unit	A-3
B.2-1	Yucca Flat/Climax Mine Phase I Well Drilling and Testing	B-3
B.2-2	Yucca Flat/Climax Mine Phase I Well Recompletions and Testing	B-6
B.2-3	Near-field Well Activities UGTA Has Supported	B-7

LIST OF TABLES (CONTINUED)

NUMBER	TITLE	PAGE
B.2-4	Reports of Rainier Mesa Tunnel Sampling	B-7
B.3-1	Reports of TCU Studies	B-9
B.3-2	Reports of Gravity and Aeromagnetic Studies	B-10
B.3-3	Reports of Laboratory Radionuclide Transport Studies	B-13
B.3-4	Reports of Rainier Mesa Colloid Transport Studies	B-15
B.4-1	Reports of Other Studies Conducted for the Yucca Flat/Climax Mine Phase I Characterization	B-16
D.2-1	Definitions for Alteration	D-8
D.2-2	Description of Sample Type Codes	D-11
D.2-3	Methods of XRD Analysis for Splits from the SWNVF	D-13
D.2-4	Translation of Symbols Used During the Early 1970s by LLNL To Represent Semiquantitative XRD Analyses	D-13
D.2-5	Percentages of XRD Splits Within NTS Areas in Yucca Flat that Contain Moderate to High Abundances of Clay Minerals	D-15
E.3-1	Groundwater Chemistry Related Parameters for the Yucca Flat/Climax Mine CAU (Part a)	E-5
E.3-1	Groundwater Chemistry Related Parameters for the Yucca Flat/Climax Mine CAU (Part b)	E-8
F.3-1	Average HGU ENP Porosity by Well	F-4
F.3-2	Average HSU ENP Porosity by Well	F-5
F.3-3	Average HGU Sonic Porosity by Well	F-5

LIST OF ACRONYMS AND ABBREVIATIONS

2-D	Two-dimensional
3-D	Three-dimensional
A-D	Anderson-Darling
A&E	Architect and engineer
amsl	Above mean sea level
API	American Petroleum Institute
ASTM	American Society for Testing and Materials
bgs	Below ground surface
BN	Bechtel Nevada
CADD	Corrective Action Decision Document
CAI	Corrective Action Investigation
CAIP	Corrective Action Investigation Plan
CAP	Corrective Action Plan
CAS	Corrective Action Site
CAU	Corrective Action Unit
CD-ROM	Compact disc-read-only memory
CDF	Cumulative distribution function
CDR	Common Data Repository
CI	Confidence interval
cm	Centimeter
cm^2	Square centimeter
CML	Carboxylate-modified latex
CR	Closure Report
CTT	Conservative tracer test
CV	Coefficient of variation
DCE	Diffusion Cell Experiment
DDE_F	Data documentation evaluation flag
DEM	Digital elevation model
DOB	Depth of burial
DOE	U.S. Department of Energy
DQE_F	Data quality evaluation flag
DRI	Desert Research Institute
DTN	Data tracking number

LIST OF ACRONYMS AND ABBREVIATIONS (CONTINUED)

DTRA	Defense Threat Reduction Agency
ECDF	Empirical Cumulative Distribution Function
ENP	Epithermal Neutron Porosity
EPA	U.S. Environmental Protection Agency
ERP	Environmental Restoration Project
ESF	Exploratory Studies Facility
EV®	Earth Vision®
FAI	Formation access interval
FEHM	Finite element heat and mass transfer code
FFACO	*Federal Facility Agreement and Consent Order*
FGE	Forced-Gradient Experiment
ft	Foot
ft^2/d	Square foot per day
FY	Fiscal year
g/cm^3	Grams per cubic centimeter
GCP	Groundwater Characterization Project
gpd/ft	Gallons per day per foot
gpm	Gallons per minute
HFM	Hydrostratigraphic framework model
HGU	Hydrogeologic unit
HRMP	Hydrologic Resources Management Program
HST	Hydrologic source term
HSU	Hydrostratigraphic unit
in.	Inch
IT	IT Corporation
K-S	Kolmogorov-Smirnov
K	Hydraulic conductivity
K_d	Distribution coefficient
km^2	Square kilometer
km	Kilometer
kt	Kiloton
L/min	Liters per minute
L/s	Liters per second

LIST OF ACRONYMS AND ABBREVIATIONS (CONTINUED)

LANL	Los Alamos National Laboratory
LLNL	Lawrence Livermore National Laboratory
m	Meter
m^2	Square meter
M	Molar
mD	Millidarcy
M&O	Management and operating
m^2/d	Square meters per day
m^2/s	Square meters per second
m^3	Cubic meter
mg/L	Milligrams per liter
min	Minute
mL	Milliliter
mL/g	Milliliters per gram
mm	Millimeter
m/s	Meters per second
mS/cm	MilliSiemens per centimeter
MT	Magnetotelluric
mV	Millivolt
MWAT-TT	Multiple-well aquifer test-tracer test
m/yr	Meters per year
N/A	Not applicable
NA	Not available
NAD	North American Datum
NC	Not calculated
NC-EWDP	Nye County Early Warning Drilling Program
ND	Not determined
NDEP	Nevada Division of Environmental Protection
nm	Nanometer
NNSA/NSO	U.S. Department of Energy, National Nuclear Security Administration Nevada Site Office
NQA	Nuclear Quality Assurance
NR	Not reported
nSIGHTS	n-Dimensional Statistical Inverse Graphical Hydraulic Test Simulator

LIST OF ACRONYMS AND ABBREVIATIONS (CONTINUED)

NSTec	National Security Technologies, LLC
NTS	Nevada Test Site
NV	No value
NWIS	National Water Information System
ORP	Oxidation-reduction potential
pCi/kg	Picocuries per kilogram
pCi/L	Picocuries per liter
PDF	Probability distribution function
PGG	Petrographic, Geochemical, and Geophysical
ppm	Parts per million
QA	Quality assurance
QAPP	Quality Assurance Project Plan
REECo	Reynolds Electrical & Engineering Co., Inc.
RELAP	Reactive Transport LaPlace Inversion code
RETRAN	A transient version of RELAP
RMC	Reactive mineral category
RMU	Reactive mineral unit
RNM	Radionuclide Migration
RST	Radiologic source term
RTT	Reactive tracer test
SD	Standard deviation
SDWA	*Safe Drinking Water Act*
SFT	Spent Fuel Test
SI	Saturation index
SNJV	Stoller-Navarro Joint Venture
SWL	Static water level
t_0	Time zero
TDMS	Technical Data Management System
TWG	Technical Working Group
UGTA	Underground Test Area
USGS	U.S. Geological Survey
UTM	Universal Transverse Mercator
VOIA	Value of Information Analysis

LIST OF ACRONYMS AND ABBREVIATIONS (CONTINUED)

WIPP	Waste Isolation Pilot Plant
XRD	X-ray diffraction
XRF	X-ray fluorescence
YMP	Yucca Mountain Project
°C	Degrees Celsius
µm	Micrometer
µsec/ft	Microseconds per foot

LIST OF SYMBOLS FOR ELEMENTS AND COMPOUNDS

Al	Aluminum
Am	Americium
Ar	Argon
Br	Bromide
C	Carbon
Ca	Calcium
Cd	Cadmium
Cl^-	Chloride
Cl	Chlorine
Cm	Curium
Co	Cobalt
CO_2	Carbon dioxide
CO_3^{2-}	Carbonate
Cs	Cesium
DFBA	Difluorobenzoic acid
Eu	Europium
F	Fluoride
FBA	Fluorinated benzoate
Gd	Gadolinium
^3H	Tritium
HCO_3^-	Bicarbonate
Ho	Holmium
HTO	Tritiated water
I	Iodine
Ir	Iridium
K	Potassium
Kr	Krypton
Li	Lithium
LiBr	Lithium bromide
LiCl	Lithium chloride
Mg	Magnesium
MnO_2	Manganese oxide
N_2	Nitrogen gas

LIST OF SYMBOLS FOR ELEMENTS AND COMPOUNDS (CONTINUED)

Na	Sodium
NaI	Sodium iodine
Nb	Niobium
NH_4	Ammonia
Ni	Nickel
NO_2^-	Nitrite
NO_3^-	Nitrate
Np	Neptunium
O_2	Oxygen gas
Pb	Lead
Pd	Palladium
PFBA	Pentafluorobenzoic acid
PO_4^{3-}	Phosphate
Pu	Plutonium
Ra	Radium
S	Sulfur
SiO_2	Silica
Sm	Samarium
Sn	Tin
SO_4^{2-}	Sulfate
Sr	Strontium
Tc	Technetium
TcO^-_4	Pertechnetate
TFBA	Trifluorobenzoic acid
Th	Thorium
TNT	Trinitrotoluene
U	Uranium
Xe	Xenon
Zr	Zirconium

LIST OF HYDROSTRATIGRAPHIC UNIT ABBREVIATIONS AND SYMBOLS

AA	Alluvial aquifer
ARG	Argillic
ATCU	Argillic tuff confining unit
BA	Benham aquifer
BAQ	Basal aquifer
BFCU	Bullfrog confining unit
BLFA	Basalt lava-flow aquifer
BRA	Belted Range aquifer
BRCU	Belted Range confining unit
CA	Carbonate aquifer
CC	Reactive mineral category for carbonate rocks
CCU	Clastic confining unit
CFCM	Crater Flat composite unit
CHCU	Calico Hills composite unit
CHVTA	Calico Hills vitric-tuff aquifer
CHZCM	Calico Hills zeolitized composite unit
CPT	CP thrust
DMP	Devitrified mafic-poor
DMR	Devitrified mafic-rich
DVRFS	Death Valley Regional Ground-Water Flow System
FCCM	Fortymile Canyon composite unit
GCU	Granite confining unit
IDP	Interbedded playa unit
LCA	Lower carbonate aquifer
LCA3	Lower carbonate aquifer-thrust plate
LCCU	Lower clastic confining unit
LCCU1	Lower clastic confining unit 1-thrust plate
LFA	Lava-flow aquifer
LPCU	Lower Paintbrush confining unit
LTCU	Lower tuff confining unit
LVTA	Lower vitric-tuff aquifer
MGCU	Mesozoic granite confining unit
ML	Mafic lava

LIST OF HYDROSTRATIGRAPHIC UNIT ABBREVIATIONS AND SYMBOLS (CONTINUED)

OSBCU	Oak Spring Butte confining unit
PBRCM	Pre-Belted Range composite unit
PCM	Paintbrush composite unit
PCU	Playa confining unit
PCUT	Playa confining unit
PCU1C	Playa confining unit, upper
PLFA	Paintbrush lava-flow aquifer
PRETBG	Pre-Grouse Canyon Tuff lava-flow aquifer
SC	Reactive mineral category for silicic rocks
SWNVF	Southwestern Nevada Volcanic Field
TBA	Welded-tuff aquifer (also Belted Range aquifer)
Tbg	Grouse Canyon Tuff
Tc	Crater Flat Group
TC	Tuff cone
TCA	Tiva Canyon aquifer
TCB	Bullfrog confining unit
TCU	Tuff confining unit
TCVA	Thirsty Canyon volcanic aquifer
Th	Calico Hills Formation
Tm	Timber Mountain Group
Tma	Ammonia Tanks Tuff
TMA	Timber Mountain aquifer
Tmab	Bedded Ammonia Tanks Tuff
Tmap	Mafic-poor Ammonia Tanks Tuff
Tmar	Mafic-rich Ammonia Tanks Tuff
TMCM	Timber Mountain composite unit
TM-LVTA	Timber Mountain lower vitric-tuff aquifer
Tmr	Rainier Mesa Tuff
Tmrp	Mafic-poor portion of Rainier Mesa Tuff
Tmrr	Mafic-rich portion of Rainier Mesa Tuff
TM-UVTA	Timber Mountain upper vitric-tuff aquifer
TM-WTA	Timber Mountain welded-tuff aquifer
Tn	Tunnel Formation

LIST OF HYDROSTRATIGRAPHIC UNIT ABBREVIATIONS AND SYMBOLS (CONTINUED)

Tor	Redrock Valley Tuff
Tot	Tuff of Twin Peaks
Toy	Yucca Flat Tuff
Tp	Paintbrush Group
Tpt	Topopah Spring Tuff
TSA	Topopah Spring aquifer
Tub	Tub Spring Tuff
TUBA	Tub Spring aquifer
Tw	Wahmonie Formation
UCA	Upper carbonate aquifer
UCCU	Upper clastic confining unit
UPCU	Upper Paintbrush confining unit
UTCU	Upper tuff confining unit
VA	Volcanic aquifer
VCU	Volcaniclastic confining unit
VMP	Vitric mafic-poor
VMR	Vitric mafic-rich
VTA	Vitric-tuff aquifer
WTA	Welded-tuff aquifer
YMCFCM	Yucca Mountain Crater Flat composite unit
ZEOL	Zeolitic

1.0 INTRODUCTION

The U.S. Department of Energy (DOE), National Nuclear Security Administration Nevada Site Office (NNSA/NSO) initiated the Underground Test Area (UGTA) Project to assess and evaluate the effects of the underground nuclear tests on groundwater beneath the Nevada Test Site (NTS) and vicinity and to ensure the protection of the public and the environment. Since 1996, the Nevada Division of Environmental Protection (NDEP) has regulated the NNSA/NSO corrective action program for the NTS through the *Federal Facility Agreement and Consent Order* (FFACO) that was agreed to by the State of Nevada; DOE, Environmental Management; U.S. Department of Defense; and DOE, Legacy Management (FFACO, 1996; as amended, August 2006).

The objective of the corrective action strategy for UGTA, as described in Appendix VI, Revision No. 1 (December 7, 2000) of the FFACO (1996; as amended, August 2006), is to define contaminant boundaries for each UGTA corrective action unit (CAU) where groundwater may have become contaminated by underground nuclear weapons tests. This strategy requires the development of a CAU-scale flow and transport model that uses CAU-specific hydrogeologic and transport parameter data to estimate movement of contaminants and to define boundaries that encompass the extent of contamination.

1.1 Purpose, Objectives, and Scope

This report documents transport data and data analyses for Yucca Flat/Climax Mine CAU 97. The purpose of the data compilation and related analyses is to provide the primary reference to support parameterization of the Yucca Flat/Climax Mine CAU transport model.

Specific task objectives were as follows:

- Identify and compile currently available transport parameter data and supporting information that may be relevant to the Yucca Flat/Climax Mine CAU.

- Assess the level of quality of the data and associated documentation.
- Analyze the data to derive expected values and estimates of the associated uncertainty and variability.

The scope of this document includes the compilation and assessment of data and information relevant to transport parameters for the Yucca Flat/Climax Mine CAU subsurface within the context of unclassified source-term contamination. Data types of interest include mineralogy, aqueous chemistry, matrix and effective porosity, dispersivity, matrix diffusion, matrix and fracture sorption, and colloid-facilitated transport parameters. Data type descriptions are provided in Section 3.1.1.

Data analysis includes literature searches, data/information compilation, data documentation, data documentation qualification, data quality evaluation, and data assessment and interpretation activities. Scientific software is used to assist in estimating and visualizing each of the hydrogeologic data types.

The study area, as described in the Yucca Flat/Climax Mine Corrective Action Investigation Plan (CAIP) (DOE/NV, 2000a) and shown in Figure 1-1, was selected to encompass the Yucca Flat/Climax Mine corrective action sites (CASs) and downgradient areas that may be impacted by these CASs. The focus of data compilation for this investigation was on the area within the boundaries of the Yucca Flat/Climax Mine Hydrostratigraphic Framework Model (HFM) (Figure 1-1), although information considered to be relevant to this task may be obtained from other sites. These sites include other UGTA CAUs, the Yucca Mountain Site, other sites located within the NTS region, and similar sites from other locations when only limited data are available within the vicinity of the NTS. Data transferred from other sites have been documented and justified using methodologies consistent with the *Transferability of Data Related to Underground Test Area Project, Nevada Test Site, Nye County, Nevada* (SNJV, 2004e). A discussion of parameter-specific data transfer techniques is included in each data analysis section where data transfer was used.

1.2 Yucca Flat/Climax Mine CAU Background

The Yucca Flat/Climax Mine CAU area is a large (approximately 19 kilometers [km] east-west by 35 km north-south [11 by 21 miles]) structural valley located in the northeastern part of the NTS. The Yucca Flat/Climax Mine CAU constitutes the largest of five CAUs within the NTS previously used

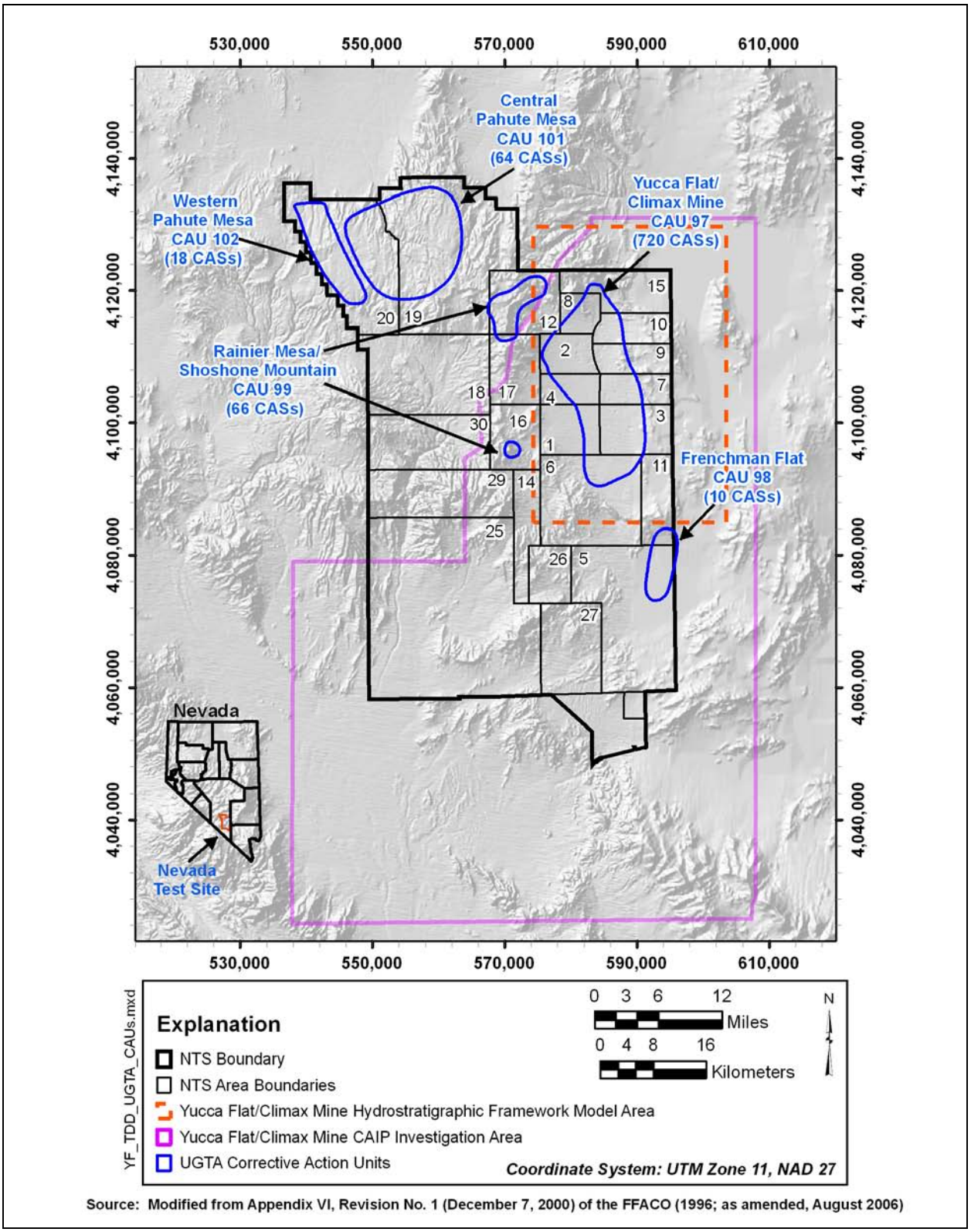

Source: Modified from Appendix VI, Revision No. 1 (December 7, 2000) of the FFACO (1996; as amended, August 2006)

Figure 1-1
Nevada Test Site-Scale Boundaries

for underground nuclear testing. This CAU includes portions of NTS Areas 1 through 4, 6 through 12, and 15 (Figure 1-1).

A total of 747 underground nuclear detonations were conducted in shafts and tunnels in this CAU between 1957 and 1992. These tests included 744 detonations in Yucca Flat proper and three in the Climax Mine tunnel complex (DOE/NV, 2000b). Underground nuclear tests are designated (either individually or as groups) as CASs in the FFACO (1996; as amended, August 2006). The tests comprise 720 CASs; the reduced number of CASs is the result of multiple (two or three) detonations for some CASs. Appendix A contains a complete list of the underground nuclear tests and related information. The location of the CASs and UGTA wells in the Yucca Flat/Climax Mine CAU, along with test-related surface effects, are shown in Plate 1.

Announced test yields for the Yucca Flat/Climax Mine CAU range from 0 to 500 kilotons (kt), and the depth of burial ranges from 58 to 780 meters (m) below ground surface (bgs). Nuclear devices were emplaced in one of four types of geologic media: alluvial deposits, Tertiary volcanics, carbonates, or intrusives (DOE/NV, 2000a). Approximately 23 percent of these detonations were conducted near or below the water table, with potential for groundwater contamination in the vicinity and possibly downgradient of the underground test locations. Transport in groundwater and gas phase transport are the primary long-term mechanisms for subsurface migration of contamination from underground testing.

1.3 Corrective Action Strategy

The focus of the UGTA corrective action strategy is to determine contaminant boundaries for each CAU in compliance with future monitoring requirements (FFACO, 1996; as amended, August 2006). The contaminant boundary is defined to encompass the predicted aggregate maximum extent of radionuclide contamination from underground testing exceeding the *Safe Drinking Water Act* (SDWA) standards. As such, it will be composed of both a perimeter boundary and a lower hydrostratigraphic unit (HSU) boundary. Groundwater flow and contaminant transport models will be used to predict the location of this boundary during a future period of 1,000 years at a 95 percent level of confidence. Monitoring of the contaminant boundaries will determine long-term compliance.

For the UGTA Project, the corrective action strategy includes two major phases: a regional evaluation addressing all CAUs and CAU-specific evaluations addressing each of the individual CAUs. The first major phase was completed with the document *Regional Groundwater Flow and Tritium Transport Modeling and Risk Assessment of the Underground Test Area, Nevada Test Site, Nevada* (DOE/NV, 1997a). The flow and transport model provided the initial basis for determining the magnitude of risk from the source areas on the NTS to potential receptors and a regional context for future individual CAU investigations. The second major phase focuses on refining the results of the regional-scale modeling through acquisition and analysis of CAU-specific data, and development of CAU-scale flow and transport models.

The process flow diagram for implementing the corrective action strategy for the UGTA CAUs, as required by the FFACO (1996; as amended, August 2006), is shown in Figure 1-2. The CAU-specific corrective action process includes six major elements:

1. Corrective Action Investigation Plan – This plan provides or references all specific information for planning investigation activities associated with CAUs or CASs.

2. Corrective Action Investigation (CAI) – This investigation includes the collection of new data, the evaluation of new and existing data, and the development and use of CAU-specific groundwater flow and transport model(s). The CAI process may be iterative, resulting in several phases of data collection, analysis, and modeling, with assessment of confidence in the results at the completion of each phase (Figure 1-2). If further data collection, analysis, and modeling are required, an addendum to the CAIP will be issued to direct the new phase of activities.

3. Corrective Action Decision Document (CADD) – This document describes the results of the CAI, the selected corrective action, and the selection rationale. The selection rationale will consist of an analysis of possible corrective action alternatives.

4. Corrective Action Plan (CAP) – This plan describes how the selected remedial alternative is to be implemented. The CAP will contain the engineering design and necessary specifications to implement the selected remedial alternative.

5. Closure Report (CR) – This report details closure activities, including the preparation of a CR, NDEP review of the CR, and long-term closure monitoring by DOE.

6. Long-term monitoring – Long-term, post-closure monitoring is designed to ensure the compliance boundary is not violated.

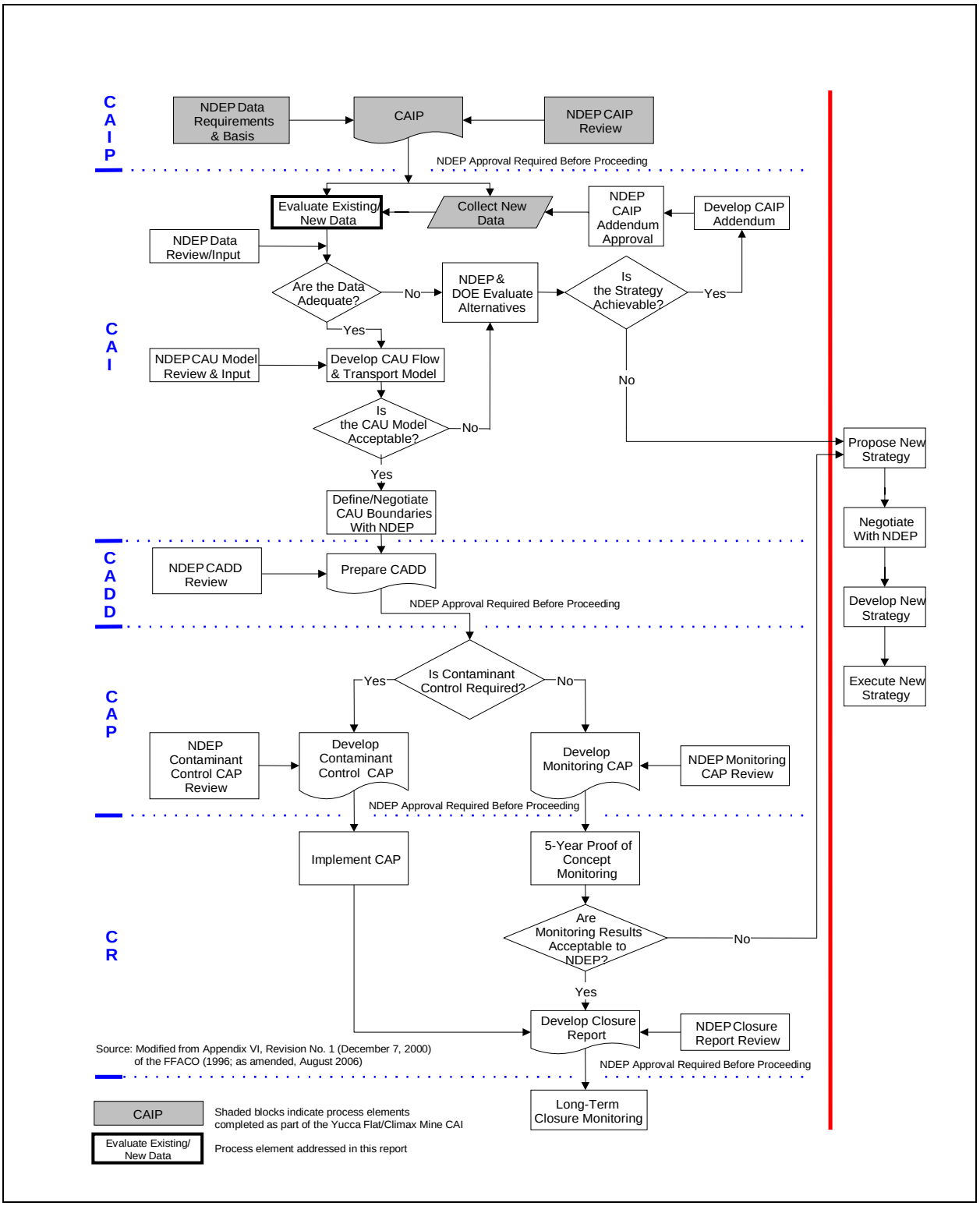

Figure 1-2
Underground Test Area Corrective Action Units Process Flow Diagram

The uppermost Yucca Flat/Climax Mine CAIP-level components (DOE/NV, 2000a) in Figure 1-2 (shaded) denote the steps completed in the regulatory framework for the Yucca Flat/Climax Mine CAU. The CAI-level "Collect New Data" component has been accomplished for Phase I (Appendix B). This report documents the completion of the next component, "Evaluate Existing/New Data," which consists of surveying available data, presenting a compilation and summarization of relevant data, and providing data analyses in support of groundwater transport model development.

1.4 Planning Documents

The Yucca Flat/Climax Mine CAI planning documents and descriptions are listed in Table 1-1. The Yucca Flat/Climax Mine Value of Information Analysis (VOIA) report (IT, 1999) assessed the value of different possible data collection activities with respect to reduction in uncertainty of the contaminant boundary, and provided the basis for identifying the data collection activities specified in the Yucca Flat/Climax Mine CAIP (DOE/NV, 2000a). The strategy for development of the groundwater flow and transport model was documented in the Yucca Flat/Climax Mine modeling strategy report (Shaw, 2003b), which specifies the modeling data requirements.

Table 1-1
Yucca Flat/Climax Mine CAU Corrective Action Investigation Planning Documents

Title	Description
Value of Information Analysis for Corrective Action Unit 97: Yucca Flat, Nevada Test Site, Nevada (IT, 1999)	Describes the evaluation of the sufficiency of existing information to support the CAI and identifies the major problems anticipated in developing the geologic, flow, and transport models. Potential data collection activities to improve characterization data are evaluated for potential benefit and prioritization.
Corrective Action Investigation Plan for Corrective Action Unit 97: Yucca Flat/Climax Mine, Nevada Test Site, Nevada (DOE/NV, 2000a)	An FFACO (1996; as amended, August 2006) requirement that summarizes the historical data for the Yucca Flat/Climax Mine CAU. Describes the characterization activities that will be implemented to evaluate the extent of contamination in groundwater due to underground nuclear testing and support the development of groundwater flow and transport models to predict the contaminant boundary.
Modeling Approach/Strategy for Corrective Action Unit 97, Yucca Flat and Climax Mine (Shaw, 2003b)	Describes approaches to modeling flow and transport through the hydrogeologic system over time. One approach is the development of numerical process models to represent the processes that control flow and transport. The other approach uses simplified representations of the process models to assess the interactions between model and parameter uncertainty.

Source: Modified from SNJV, 2006c

1.5 Data Collection Activities

A variety of data collection activities have been conducted to supply information for Phase I data analysis and modeling, including those activities specifically directed in the Yucca Flat/Climax Mine CAIP (DOE/NV, 2000a). Appendix B contains an overview of the major Yucca Flat/Climax Mine-specific data collection activities and studies, and lists the major reports produced.

1.6 Project Participants

The UGTA Project is a component of the NNSA/NSO Environmental Restoration Project (ERP) and is managed by the NNSA/NSO UGTA Federal Sub-Project Director. The following organizations participate in the UGTA Project: Desert Research Institute (DRI), Lawrence Livermore National Laboratory (LLNL), Los Alamos National Laboratory (LANL), National Security Technologies, LLC (NSTec), Stoller-Navarro Joint Venture (SNJV), and the U.S. Geological Survey (USGS). A Technical Working Group (TWG) has been established to assist the NNSA/NSO UGTA Federal Sub-Project Director with technical management issues. Assigned TWG tasks include providing expert technical support to plan, guide, and monitor UGTA technical work; and serving as internal peer reviewers of UGTA products. The TWG consists of representatives from the above-named agencies.

1.7 Document Organization

Content summaries of each section and appendix are as follows:

- Section 1.0 introduces the document, defines the scope and objectives, provides background information on the FFACO (1996; as amended, August 2006) corrective action strategy and the Yucca Flat/Climax Mine CAIP, and explains the document structure.
- Section 2.0 provides a brief overview of the modeling strategy proposed for the Yucca Flat/Climax Mine CAU and the associated data requirements.
- Section 3.0 presents the general data compilation and analysis approach used to assess the available transport data.
- Section 4.0 describes the HFM and detailed descriptions of HSU mineralogy. These descriptions are presented to support the analysis of the contaminant transport data presented in this document.

- Section 5.0 summarizes the results of a comprehensive geochemical flow-path analysis that was performed in collaboration between multiple UGTA organizations. In addition, an evaluation of the aqueous chemistry data used to support matrix sorption is presented.
- Section 6.0 provides source term information and describes contaminant data from near-field groundwater sampling events.
- Section 7.0 defines a stationary probability distribution of matrix porosity per HSU and hydrogeologic unit (HGU).
- Section 8.0 presents a brief explanation of the role of effective porosity in contaminant transport, outlines available sources of effective porosity, and recommends ranges for effective porosity estimates.
- Section 9.0 provides a description of dispersivity data collected at the NTS and sites around the world. Two methods are presented that characterize the uncertainty associated with longitudinal dispersivity values.
- Section 10.0 presents a description of matrix diffusion data applicable to Yucca Flat/Climax Mine HSUs.
- Section 11.0 provides an extensive review and analysis of matrix sorption data that are applicable to rocks within the Yucca Flat/Climax Mine CAU.
- Section 12.0 provides a basic overview of fracture sorption parameters that are applicable to fractured rocks within the Yucca Flat/Climax Mine CAU.
- Section 13.0 defines the colloid-facilitated transport parameters necessary for incorporation of colloid transport in the CAU model.
- Section 14.0 contains the reference list.
- Appendix A contains a listing of underground nuclear tests in the Yucca Flat/Climax Mine CAU with general information on each test — including name, location, depth, and yield — as well as a test location map.
- Appendix B presents an overview of Yucca Flat/Climax Mine CAIP data collection activities that were accomplished for the Yucca Flat/Climax Mine CAU during Phase I and lists the major reports produced to document the data collection activities.
- Appendix C contains information in support of the HFM described in Section 4.0.
- Appendices D through J contain dataset descriptions and supporting information for various analyses.
- Appendix K contains NDEP comments on the draft version of this document.

2.0 CORRECTIVE ACTION UNIT MODELING APPROACH

The process for achieving the UGTA corrective action strategy includes modeling to define the extent of contaminant transport within a 1,000-year time frame. The use of groundwater flow and transport models used to achieve the objectives of the corrective action strategy is specified in Appendix VI, Revision No. 1 (December 7, 2000) of the FFACO (1996; as amended, August 2006). This section presents an overview of the CAU groundwater flow and transport modeling approach, and a discussion of the transport modeling approach and data requirements for the Yucca Flat/Climax Mine CAU. Additional discussion of the modeling approach for the Yucca Flat/Climax Mine CAU is included in Shaw (2003b).

2.1 Overview of the CAU Modeling Approach

In areas of NTS underground nuclear testing, groundwater flow occurs through diverse and structurally complex rocks (Laczniak et al., 1996). Given the complexity of the hydrogeologic system, contaminant sources, and processes controlling transport, computer models are required to meet the objectives of the FFACO (1996; as amended, August 2006) corrective action strategy. The modeling approach used to develop an integrated three-dimensional (3-D) model for flow and transport begins with system characterization and is followed by the conceptual model development based on evaluations and assumptions of system processes, and mathematical representation of these processes. Mathematical models representing the system are then developed and implemented.

2.1.1 Integrated Three-Dimensional Model Development

The CAU flow and transport models consist of an integrated set of models. Some of these models focus on a small-scale process (relative to the CAU) such as radionuclide release from source regions. Others simplify CAU-scale processes such as reactive transport in fractures to an abstraction for system sensitivity analysis. Combined, the models (referred to as component models) constitute the CAU predictive model. Essential aspects of the processes described by the detailed mechanistic models must be represented accurately in the CAU model. This representation must include the uncertainty associated with the process or parameters.

The integrating numerical model will be a 3-D, finite-element flow and transport simulator that captures the complex geologic structure — including units of variable thickness, faults, and offsets — as well as complex transport processes associated with reactive solutes and fractured rock. The CAU groundwater flow model component requires two other component models: the Death Valley Regional Ground-Water Flow System (DVRFS) groundwater flow model (Belcher et al., 2004) and the precipitation recharge model(s) (SNJV, 2006c). The CAU contaminant transport model component requires the CAU groundwater flow model and the hydrologic source term (HST) model(s).

2.2 Transport Modeling Approach and Data Requirements

The approach and data requirements for the Yucca Flat/Climax Mine flow model are described in Shaw (2003b) and summarized in SNJV (2006c). The focus of this report is data compilation, analysis, and documentation for the Yucca Flat/Climax Mine transport model; therefore, the approach used for modeling transport of contaminants, along with the associated data requirements for the Yucca Flat/Climax Mine area, are described briefly.

2.2.1 Transport Modeling Approach

The CAU transport model will be built upon the groundwater flow model using the contaminant transport capabilities of the finite element heat and mass transfer code (FEHM) (Zyvoloski et al., 1997a and b). The CAU transport model will be used to simulate the transport of radionuclides in the hydrogeologic system of the Yucca Flat/Climax Mine area for the 1,000-year regulatory time frame.

Using the CAU transport model, concentrations of radionuclides will be calculated for specified points downgradient from the underground nuclear tests of the Yucca Flat/Climax Mine CAU. Simulated concentrations will then be used to estimate the location of the contaminant boundary as defined in Appendix VI, Revision No. 1 (December 7, 2000) of the FFACO (1996; as amended, August 2006).

The Climax Stock model developed by DRI will be used to estimate radionuclide fluxes resulting from the three tests in Climax Mine. Simulated flow across the southern boundary of the Climax Stock model can be used to define boundary conditions for the Yucca Flat flow and transport model.

2.2.2 Data Requirements

A variety of data types are required to simulate radionuclide transport in the groundwater system (Figure 2-1). The data types needed for the contaminant transport model include the HST, transport parameters, radionuclide concentration data, and groundwater chemistry data.

2.2.2.1 Hydrologic Source Term

The HST of an underground nuclear test is the portion of the total inventory of radionuclides that is released over time into the groundwater following the test. The total residual inventory of radionuclides associated with one or more tests is known as the radiologic source term (RST). The RST is comprised of radionuclides that are distributed within water, glass, or other phases within the test cavity and vicinity. The total unclassified radionuclide inventory (i.e., the RST) for all tests within the Yucca Flat/Climax Mine CAU is published in Bowen et al. (2001). The inventory is subdivided for the Yucca Flat/Climax Mine CAU by tests where the working point depth is more than 100 m above the water table and tests that were detonated below that level (Bowen et al., 2001).

Two HST datasets will be defined for the Yucca Flat/Climax Mine CAU. One source term will be based on unclassified data and extrapolated to all underground tests within the CAU. Later, a classified dataset (based on information from individual tests) will be used to calculate the final contaminant boundary location.

The unclassified HST for the CAU transport model will be comprised of abstracted release functions from the underground nuclear tests, or groups of underground nuclear tests, based on the RST published in Bowen et al. (2001). The release functions will capture the important hydrological and chemical processes that govern the migration of radionuclides in groundwater away from underground test cavities. The release functions associated with the three tests in Climax Mine will be provided by the DRI sub-CAU model for the Climax Stock. The unclassified HST for the Yucca Flat/Climax Mine CAU will be the subject of a future report: *Unclassified Source Term and Radionuclide Data for Corrective Action Unit 97: Yucca Flat/Climax Mine*.

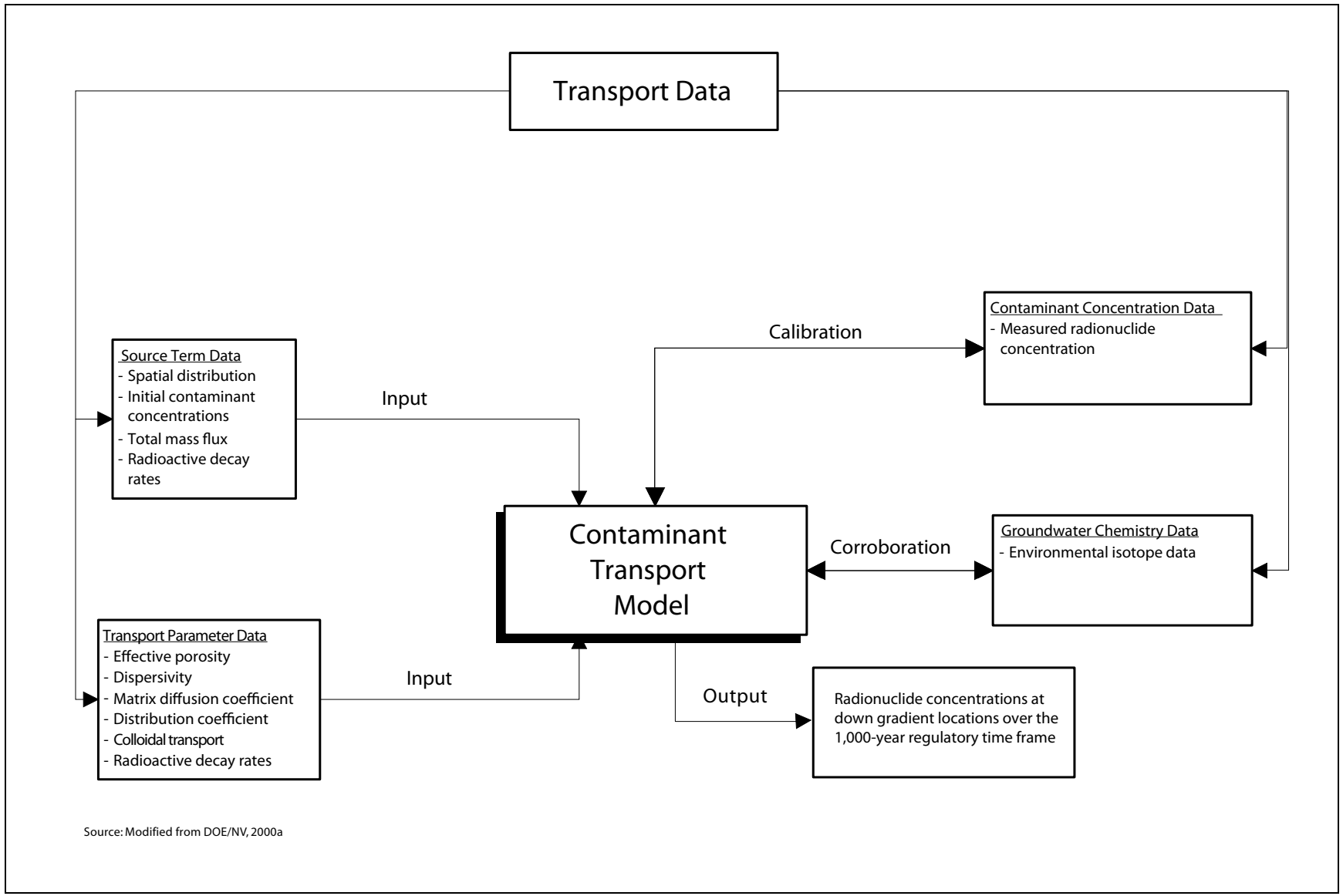

Figure 2-1
Data Types and Utilization in the Contaminant Transport Model

2.2.2.2 Transport Parameters

Parameters needed to simulate the radionuclide transport processes at work in the Yucca Flat/Climax Mine flow system include effective porosity, dispersivity, radioactive decay constants, distribution coefficients, matrix diffusion coefficients, matrix porosity, description of the fracture geometry, and colloid-facilitated transport parameters. A general description of the various transport parameters and the approach to developing parameter distributions is presented in Section 3.0. Compilation and analysis of these parameters for the Yucca Flat/Climax Mine CAU are described within subsequent sections of this report.

2.2.2.3 Radionuclide Concentration Data

Measurements of radionuclide concentrations in groundwater samples are useful in evaluating the CAU-model predictions. These data may be used to calibrate the transport model and/or provide further confidence in the simulations. Evidence of radionuclide migration away from underground nuclear test locations, such as that observed during the long-term pumping near the NASH location (see Section 6.0), could be compared with simulated results of the HST models.

Available data for the near-field environment of the underground nuclear tests are presented in Section 6.0. Further evaluation of the concentration of radionuclides within the Yucca Flat/Climax Mine CAU are the subject of a future report.

2.2.2.4 Groundwater Chemistry Data

Groundwater chemistry data are not directly used as input in the transport model; rather, representative groundwater chemistries are determined from the data and are used for a variety of analyses. Interpretations of groundwater flow paths and consequent geochemical mixing of characteristic groundwater chemistries are used to evaluate and verify groundwater flow and transport models. These interpretations provide independent information on potential groundwater flow paths and travel times that may be used in developing and calibrating the groundwater flow model for the Yucca Flat/Climax Mine CAU.

3.0 DATA ANALYSIS

Data analysis is the process of compiling, assessing, and interpreting available data in preparation for CAU groundwater flow and transport modeling. The data needed for CAU modeling include a broad variety of types, from numerous sources, that represent a wide variety of measurements and scales of measurement. The process of analyzing the data includes the following seven steps: (1) compilation of existing data for the Yucca Flat/Climax Mine investigation area, (2) transfer of applicable data from outside the Yucca Flat/Climax Mine area, (3) assignment of data quality indicators, (4) assessment of data representativeness and appropriateness for use in CAU modeling, (5) data reduction and analysis, (6) graphical and tabular presentation of results, and (7) discussion of data limitations and the possible impacts to the CAU groundwater flow and transport model. This document presents data analysis and results used to support the development of the Yucca Flat/Climax Mine transport model.

3.1 Data Compilation

The compilation of existing data is a multiple-step process of determining necessary data, identifying and acquiring available data, and compiling the data into structured databases. As discussed in later sections of this document, certain data types required for CAU modeling are derivative; these are determined by processing more basic data using models specifically developed for the purpose (e.g., sorption models used to develop sorption coefficients). Data types of interest and data sources are discussed in the following sections.

3.1.1 Transport Data Types

General descriptions of the various types of information needed for modeling are provided in the following sections. The descriptions are followed by explanations pertinent to the different transport parameters of interest to the Yucca Flat/Climax Mine CAU model. Information needed to support CAU contaminant transport modeling include porosity (matrix and effective), dispersivity, matrix

diffusion parameters, contaminant-rock sorption parameters, and colloid-facilitated transport parameters.

3.1.1.1 Porosity

As stated previously, effective porosity and matrix porosity are required parameters in the CAU models. Porosity, however, can be defined in several ways depending on the application (Freeze and Cherry, 1979; de Marsily, 1986). These include:

- Total Porosity - The total volume of void space divided by the total volume of rock. No other porosity measure can exceed the total porosity.

- Bulk Porosity - The bulk porosity is a total porosity measurement and for the purposes of the CAU model can be treated as total porosity. In fractured units, for example, bulk porosity is a sum of matrix and fracture porosity.

- Effective Porosity - Also called kinematic porosity by de Marsily (1986), effective porosity is defined as the volume of voids transmitting water (interconnected voids) per total volume of rock. From the perspective of transport, adhesive water, dead-end pores, isolated pores, or any other water that does not actively move should be excluded from the effective porosity. As a result, the effective porosity is always smaller than the total porosity. Effective porosity is a modeling parameter that is used to calculate particle velocity from Darcy velocity.

- Fracture Porosity (Secondary Porosity) - In fractured geologic units, the faults, fissures, cracks, joints, and bedding planes form a complicated network of interconnected planar features through which groundwater flows. Often, the majority of groundwater flow is through the fracture network and not through the matrix material separating the fractures.

- Matrix Porosity (Primary Porosity) - The matrix material between fractures is porous. In many cases, the porosity of the matrix is several orders of magnitude larger than the fracture porosity. Although the flow through the matrix is often much smaller than through the fractures, the vast majority of the water volume is in the matrix. In unfractured media, matrix porosity is comprised of effective flow porosity, transport storage porosity, and disconnected storage porosity. In many instances, the total porosity is a good approximation of the matrix porosity.

3.1.1.2 Dispersivity

The hydrodynamic dispersion of solutes (or particles) in groundwater describes the spreading phenomenon at a macroscopic level through the combined action of mechanical dispersion and molecular diffusion. With modeling approaches that do not account for heterogeneity, dispersion is

used to account for the variability in velocity and results in greater simulated transport distances than would be calculated using average velocity only.

3.1.1.3 Matrix Diffusion Coefficient

In fractured rock systems, where the primary pathway for groundwater flow is through the fractures, the matrix material is saturated with groundwater that is considered immobile for the purposes of modeling. A double-porosity conceptual model is typically assumed, with matrix diffusion between the fractures and the adjacent matrix attenuating both the concentration and travel velocity of aqueous-phase contaminants moving through fractures. The amount of immobile water in the matrix is governed primarily by the matrix porosity. In many fractured aquifers, the matrix porosity may be 10 or more times larger than the fracture porosity. Thus, although the bulk of the water travels through the fractures, a large reservoir of water in the matrix can act to store contaminants temporarily via the matrix diffusion process. If a contaminant diffuses into the matrix for a period of time, it effectively stops moving relative to the water in the fracture. Therefore, matrix porosity and the matrix diffusion process are necessary for successful modeling of contaminant transport in fractured aquifers of the CAU model.

Matrix diffusion is one of the processes that governs the transport of contaminants in fractured aquifer systems. It represents the rate of diffusion of solutes from flowing water (generally in fractures) into stagnant or nearly stagnant water contained in the pores of consolidated rock matrices (Neretnieks, 1980). Matrix diffusion coefficients for solutes in a porous medium are smaller in magnitude than free water diffusion coefficients because of the tortuous nature of the pathways that solutes must follow when they diffuse through the media; thus, matrix diffusion coefficients can be directly related to the solute free water diffusion coefficient by the tortuosity of the porous media. In natural systems, the matrix diffusion process may be further complicated by the presence of fracture coatings, which may have different physical (e.g., porosity and tortuosity) and sorptive properties than those for the matrix.

3.1.1.4 Matrix and Fracture Sorption Parameters

Contaminant sorption is a general term to describe a variety of chemical processes that bind (temporarily or permanently) contaminants to solids, either matrix or fracture minerals. Sorption

along the fracture surface and in the matrix acts to temporarily store contaminants and slow contaminant migration with respect to the flowing groundwater. Sorption is treated mathematically in the contaminant transport model through an equilibrium distribution coefficient (K_d) approach where the amount of contaminant stored on or in the rock is a function of its concentration in the groundwater. The transfer of the radionuclide from the water to the rock is assumed to occur instantaneously and be completely reversible. Sorption is represented by the K_d, or the retardation factor (R_f parameter) in the solute transport equation. The K_d is based upon a volumetric sample of material and is used to represent sorption to the matrix material. The retardation factor represents solute retardation per unit length, rather than per unit volume of rock, and thus better reflects sorption along a fracture. These two terms are related to each other by the bulk density (p_b) and porosity (ϕ) of the solid as $R_f = 1 + \frac{p_b}{\phi} K_d$.

3.1.1.5 Colloid-Facilitated Transport Parameters

Colloids are defined as small particles (less than 1 micrometer [μm]) comprised of organic material or inorganic minerals that are suspended in solution. Oxides and hydroxides of actinide elements (e.g., plutonium [Pu]) can also form colloids (Kersting et al., 1998). Migration of a given radionuclide sorbed onto colloids in flowing groundwater is often more rapid than that of the same radionuclide in solution. This is primarily the case when the radionuclide is transported due to sorption onto the colloid but would otherwise be retarded by sorption onto the immobile rock. Radionuclide transport on colloids could also be slower if there is low sorption to the immobile rock when compared to sorption onto the colloid. Parameters needed to represent colloid-facilitated transport include colloid types, concentrations, and size distribution; radionuclide sorption/desorption rates onto colloids; and colloid filtration rate constants.

3.1.2 Supporting Information

The following types of supporting information for each data type and/or data entry are recorded in the documentation, where applicable and available:

- Identification and location information
- Physical information on the location
- Sample information
- Chemical constituents

- Method of data collection or type of test
- Scale of measurement
- Date of data collection
- Stratigraphic unit
- Lithology
- Alteration
- Hydrostratigraphic unit
- Method of data analysis
- Observed parameter value
- Parameter spatial distribution
- Uncertainties
- References relating to the data records
- Noted deficiencies

References to the specific sources of information are provided along with the data. A general description of the data sources is provided in Section 3.1.3.

3.1.3 Data Sources

In general, data have been gathered by several organizations that include NSTec, LLNL, LANL, DRI, USGS, and the SNJV. A large amount of historic data had also been gathered under the auspices of previous NTS management and operating (M&O) contractors (Bechtel Nevada [BN] and Reynolds Electrical & Engineering Co., Inc. [REECo]), architect and engineer (A&E) contractors (Fenix & Scisson and Raytheon Services Nevada), and Environmental Restoration contractors (IT Corporation and Shaw Environmental, Inc.). Many data sources for the Yucca Flat/Climax Mine CAU exist from various scientific and engineering studies conducted by these organizations and, where applicable, are referenced in this document. Additional, unpublished data have also been obtained from project files of some of these organizations.

Data collected from within the Yucca Flat/Climax Mine HFM area (see Figure 1-1) are classified as Yucca Flat/Climax Mine-specific data. These data are directly applicable to the Yucca Flat/Climax Mine CAU. Data from within the larger Yucca Flat/Climax Mine CAIP investigation area (DOE/NV, 2000a) are also compiled for use in the Yucca Flat/Climax Mine CAU to support modeling that may extend further downgradient from this CAU. Use of data from sites outside the Yucca Flat/Climax Mine CAU may be appropriate to reduce parameter uncertainty when particular data types are sparse (Freeze et al., 1990). Parameter data for similar environments may therefore be used to establish parameter distributions to be used in modeling the study area. Sites considered as

additional data sources for the Yucca Flat/Climax Mine CAU are adjacent CAUs, sites associated with the YMP, and, in some cases, similar sites from distant locations.

3.1.3.1 Nevada Test Site Data

Data have been compiled from other CAUs and adjacent areas in the vicinity of the NTS, where applicable, to provide additional input to reduce parameter uncertainty.

3.1.3.2 Yucca Mountain Project Data

The Yucca Mountain Project (YMP) is the proposed geologic storage location for commercial high-level radioactive waste in the United States. High-quality data have been collected and analyzed during investigations of the Yucca Mountain site, including several parameters relevant to Yucca Flat/Climax Mine CAU modeling. Yucca Mountain is located adjacent to the southeastern part of the NTS. The proximity and similar hydrogeologic environment of the Yucca Mountain Site to Yucca Flat make it particularly relevant as a source of data for hydraulic and transport properties for similar HSUs and HGUs.

3.1.3.3 Other Data

Data from other distant locations may be incorporated in the analysis for select purposes. The use of such data is explained and justified in the data analysis discussion for the particular data type.

3.2 Data Transfer Methodology

A process was developed specifically to assess the transferability of data (SNJV, 2004e). The technical basis document for data transferability provides a comprehensive discussion of requirements and methodology for data transfer, which were considered for the analyses described in this document.

3.2.1 General Transferability Approach

The use of data from other study areas to develop parameter distributions for flow and transport modeling of UGTA CAUs can be justified by examining specific similarities that may exist between various investigation areas. It must be shown that there is a sufficient similarity that exists between

the two areas. The general approach for the transfer of data from one area to another is based on the following strategy:

- For each parameter of interest, sites are identified that contain data of the same type. In an ideal situation, sites could be found in the same general area that have roughly the same geologic setting. More likely, sites will be identified that are located farther away but have similar rock types. In the least desirable situation, data may be transferred from locations that are less similar to the original study area but otherwise can be justified as appropriate.

- Once the source of the flow and transport parameter data are identified, the factors affecting the specific parameter need to be clarified. If it can be shown that only one factor influences a given parameter, it may make the transfer of data easier to justify. For example, if it can be shown that a parameter is only influenced by lithology, then a comparison of the lithologies between the two investigation areas would suffice to make a decision.

- Finally, if sufficient data are present in the original study area, a statistical data comparison can be made from the other area to determine whether the two datasets are comparable.

- The relative emphasis assigned to the transferred data is established using a weight and multiplier system. Weights are assigned based on the similarity between the investigation areas, and multipliers are assigned based on the measurement method, the quality of data reduction and analyses, and documentation quality. The overall score for a given dataset is the sum of the weights multiplied by the product of the multipliers. Datasets from investigation areas that are less similar may be transferred but are assigned lower weights, so they ultimately "count less" in determining the final parameter distribution used in CAU-scale modeling. Likewise, datasets associated with measurement methods having large uncertainties or inappropriate scales, or datasets of low-quality or having poor documentation, are assigned lower multipliers, so they count less in the final CAU-scale application.

3.2.2 Similarity Criteria

Similarity criteria focus on rock genesis and evolution factors that influence rock characteristics and, therefore, flow and transport parameters. These factors include the geologic history of the area, lithology, alteration, and groundwater chemistry.

3.2.2.1 Geologic History

The geologic history of an area has a significant impact on the flow and transport of groundwater. For example, the depositional environment of a rock can influence things such as the porosity of sedimentary rocks or the texture of volcanic rocks. In addition, subsequent structural episodes may increase faulting in a given area, which could lead to increased groundwater flow.

3.2.2.2 Lithology

The specific rock type of a study area has an important impact on the flow and transport of groundwater. For instance, the type of rock (metamorphic, igneous, sedimentary, alluvium/valley fill deposits) is an important factor to be considered in the transferability of porosity data (SNJV, 2004e) and is also important to sorption processes. Fracture density varies depending on the lithology.

3.2.2.3 Alteration

Alteration (e.g., devitrification, zeolitization, and argillization) can significantly impact not only hydraulic properties but also the reactivity of the rocks with respect to radionuclide transport. For example, the formation of zeolitic material in volcanic tuffs can greatly increase sorption of certain radionuclides. Argillic alteration commonly is characterized by the presence of the clays smectite and kaolinite; these secondary alteration minerals are reactive with respect to sorption of some radionuclides. Devitrification results in the conversion of glass to microcrystalline quartz and feldspar, and thus yields a rock that is composed almost entirely of quartz and feldspar and is unreactive with respect to contaminant sorption reactions.

3.2.2.4 Groundwater Chemistry

Groundwater chemistry can play an important role in the flow and transport characteristics of a groundwater flow system. It can have a large impact on everything from mineral dissolution and precipitation reactions to fracture geometry. Groundwater chemistry controls radionuclide complexation reactions, which can affect the rate and extent of radionuclide sorption.

3.3 Quality Assurance of Data and Data Documentation

Quality assurance (QA) measures consistent with the UGTA Project Quality Assurance Project Plan (QAPP) (NNSA/NSO, 2003) have been used to control quality during the performance of all UGTA data analysis tasks. These measures include data documentation qualification, data quality assessment, checking procedures, software QA, use of standard methodologies, technical and peer reviews, and corroboration through models.

3.3.1 Data Documentation Evaluation

Data documentation flags provide information on the traceability (or pedigree) of the data. Typically, data collected in the recent past has much better documentation than data collected and reported many years ago. Qualification of the documentation of the data makes it easier to investigate and evaluate the quality of the data used in modeling.

Each data record for a given dataset is assigned a data documentation evaluation flag (DDE_F) value to indicate the level of documentation available for that data record. The process of data qualification ensures that the pedigree of the data is retained for database users. However, it is important to note that the data documentation quality does not neccessarily indicate the quality or the usefulness of the data for Yucca Flat/Climax Mine CAU modeling. Historic data may not meet current standards for documentation but are often of high quality and can be extremely useful in the CAU investigations. In some cases, historic data are invaluable, and new data cannot be acquired to serve the purpose.

The five levels of DDE_Fs are as follows:

Level 1 - Data are collected in accordance with the NNSA/NSO ERP QAPP, approved State of Nevada procedures, and/or participant-specific procedures. This ranking indicates that all supporting data documentation is on file and available to data users for review.

Level 2 - Data are collected in accordance with approved plans and procedures as required for Level 1, with the exception that one or more documentation requirements may be deficient in some way. Examples of data documentation deficiencies may include lost or destroyed field data collection forms or data acquired using interim or draft procedures.

Level 3 - Data are collected using accepted scientific methodology (e.g., American Society for Testing and Materials [ASTM], U.S. Environmental Protection Agency [EPA] methods, USGS procedures) and accompanied by supporting and corroborative documentation such as testing apparatus diagrams, field or laboratory notes, and procedures.

Level 4 - Data are collected by a participating NNSA/NSO ERP organization, or another organization not associated with the NNSA/NSO ERP, before the issuance and implementation of project-approved standard policies, procedures, or practices governing data acquisition and

qualification. The methods of data collection are documented and traceable; however, the validity of data use or compliance with reference procedures is indeterminate. Supporting documentation may or may not exist.

Level 5 - Data are obtained under unknown, undesirable, or uncertain conditions. When data documentation is unknown, any available supporting or helpful descriptions of the intended use and conditions of data capture should be described.

3.3.2 Data Quality Evaluation

The data qualification process varies depending on the type of parameter. The criteria used to evaluate the quality of different types of data are dependent on the data type and the intended use. Thus, various criteria are used to assess data quality. The general procedure includes assigning one or more data quality evaluation flags (DQE_F) to each record, or group of records compiled in the dataset, indicating the data quality or suitability of the individual data record for the intended usage. The DQE_F and their definitions depend on the data type. Specific quality evaluation procedures are described in the different sections of this document for each data type.

3.3.3 Checking Procedures

Various checking procedures were designed for quality control purposes. Checking procedures applicable to the UGTA data analysis include those developed for transcription of data and generation of figures, tables, logs, and calculations. Data compiled by project personnel are subjected to the checking procedures before inclusion in the appropriate dataset. However, the bulk of the available data are comprised of data gathered and compiled by agencies external to the UGTA Project. Internal procedures do not govern other UGTA participants; therefore, their data were subject only to the data transcription checking procedure described.

3.3.4 Standard Methodologies

Only standard and widely accepted methodologies are used in the development of the interpretive products. The various methodologies used are too numerous to list; however, they are described and referenced in this document where their use in the data analysis process is discussed.

3.3.5 Technical and Peer Reviews

The review process constitutes an important measure of product quality and is used throughout the performance of the data analysis activities. The review process may include internal and external technical reviews. The internal reviews are performed by individuals from organizations involved in performing UGTA Project work (see Section 1.6). External reviews may be conducted as directed by NNSA/NSO.

3.3.6 Corroboration of Data Through Models

This step is completed during the development of the groundwater flow and transport model. For example, during the contaminant transport modeling, observations of contaminant movement will be used to help assist and refine the contaminant transport model results. This may be accomplished by modifying the sorption coefficient or porosity in areas where no data are available.

3.3.7 Data Analysis Limitations

Data limitations need to be identified. These limitations may be related to the level of data documentation, data collection method, data analysis method, or other factors that may limit the confidence in the values. Within the discussion of each dataset, data limitations will be noted.

4.0 YUCCA FLAT/CLIMAX MINE HYDROSTRATIGRAPHIC FRAMEWORK

A 3-D HFM (base model and alternative models) for the Yucca Flat/Climax Mine CAU is fully documented in the report *A Hydrostratigraphic Framework Model and Alternatives for the Groundwater Flow and Contaminant Transport Model of Corrective Action Unit 97: Yucca Flat/Climax Mine, Lincoln and Nye Counties, Nevada* (BN, 2006). An overview of the Yucca Flat/Climax Mine HFM is provided in this section as background for the analyses presented in the later sections of this report. This overview also includes a summary of the available mineralogy data and introduces a new classification scheme for the rocks of the Yucca Flat/Climax Mine CAU based on these data, referred to as reactive mineral categories (RMCs).

4.1 Yucca Flat/Climax Mine Hydrostratigraphic Framework Model

The general hydrogeologic framework for the NTS and vicinity, established by USGS geoscientists in the 1970s (e.g., Winograd and Thordarson, 1975), provided the foundation for most subsequent hydrogeologic studies at the NTS, including the Yucca Flat/Climax Mine HFM. The HFM for the Yucca Flat/Climax Mine area documented in BN (2006) was further enhanced by many field and analytical studies supported by the UGTA Project and conducted over several years. As a result of these studies and the contributions of many experts and organizations associated with the NTS, the hydrogeologic understanding of the model area has become increasingly detailed and refined.

A generalized geologic map identifying the Yucca Flat/Climax Mine HFM boundaries and important geologic features present in the vicinity is presented in Figure 4-1.

4.1.1 Model Development

Construction of the digital Yucca Flat/Climax Mine HFM involved developing a structural model of the area that included the locations and orientations of all the relevant faults in the model area. The structural model of the base HFM incorporates many aspects of structural models of Yucca Flat

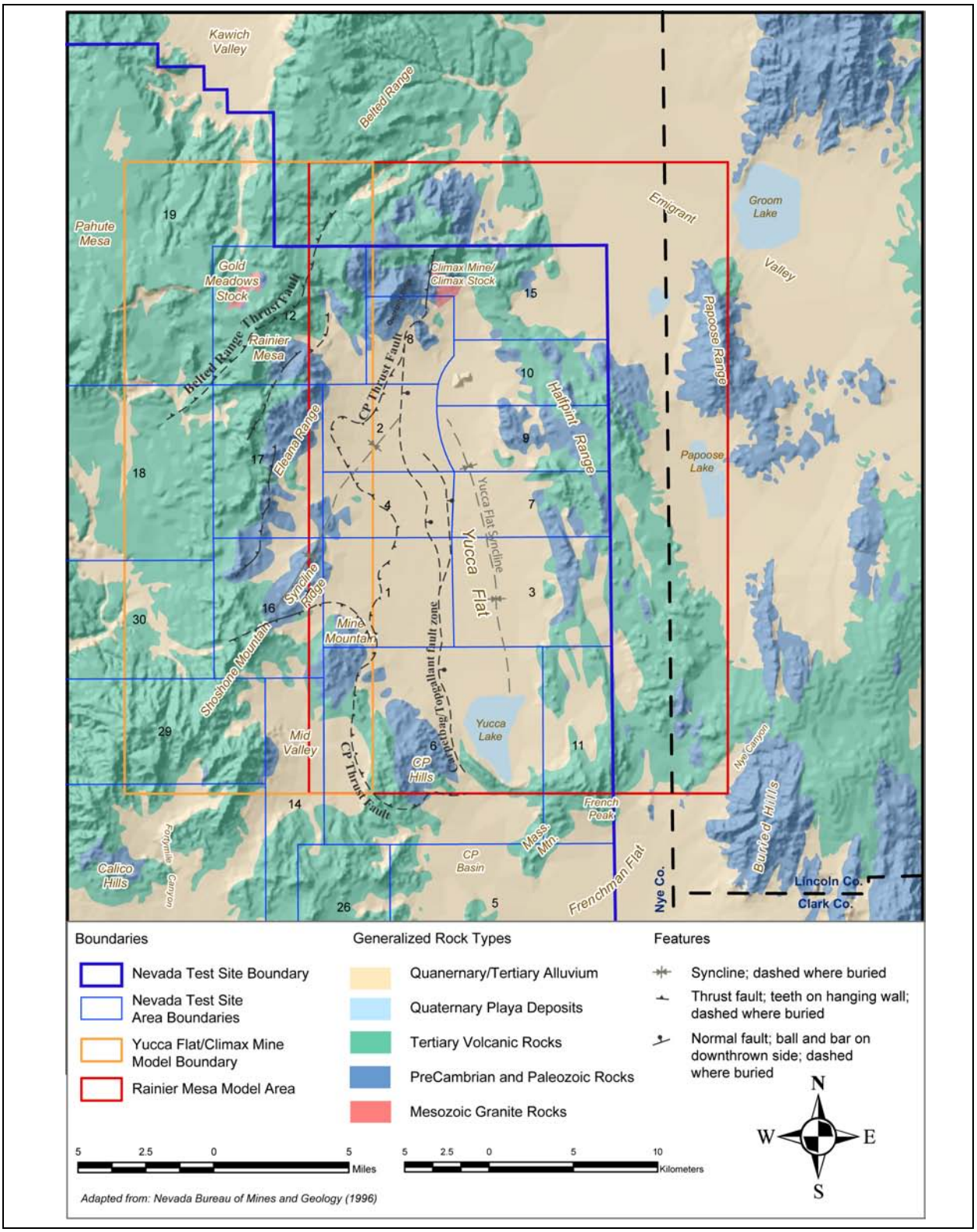

Figure 4-1
Generalized Geologic Map of the Yucca Flat/Climax Mine Region

developed over the years for the weapons testing program at the NTS. These models integrated various two-dimensional (2-D) datasets, including reflection seismic, gravity, aerial and surface magnetic, magnetotelluric (MT) survey, post-test surface effects, surface geology, and drill hole data (refer to Section 2.0 in BN, 2006 for more information and specific references). The structural model for the Yucca Flat base HFM is a refinement of these earlier models and incorporates new data collected by the UGTA Project including MT (Appendix D in BN, 2006), drill hole (NNSA/NSO, 2004b, c, d, e, and f; DOE/NV 1995a and b; BN, 1997b), and reprocessed gravity data (Phelps et al., 1999 and 2000). In addition, Phelps et al. (2000 and 2005) augmented the reprocessed gravity data with Paleozoic contact depth information from new drill holes.

The base HFM includes 180 structural elements, most of which are basin-and-range normal faults. Several older thrust faults, such as the CP and Belted Range thrust faults and associated imbricate thrust faults and folds, are also included. However, because the thrust faults are low angle, they are represented as an HSU contact in the model. Fault information was imported into the EarthVision® (EV®) modeling software (Dynamic Graphics, 2002) to form a fault-tree model that depicts all the model faults in 3-D space. The fault-tree model formed the framework on which the HFM was built. Only known faults that were considered to be hydrogeologically significant were included in the model. These include faults with apparent displacement typically greater than about 60 m (200 feet [ft]) and those that are thought to form significant structural boundaries. Based on observational data, the main surface faults controlling structural fabric typically have greater than 60 m of offset.

Although the structural framework of the Yucca Flat/Climax Mine HFM is the fault-tree, the foundation of the model is the HSU classification system, which is discussed in Section 4.1.2.2.

To address non-unique aspects of some interpretations within the base model, five alternative interpretations were considered in addition to the base HFM:

- Alternative #1 - CP thrust
- Alternative #2 - Hydrologic barrier in northern Yucca Flat
- Alternative #3 - Contiguous upper clastic confining unit (UCCU) in southwestern Yucca Flat
- Alternative #4 - Fault juxtaposition
- Alternative #5 - Partial zeolitization

These alternatives are summarized in Appendix C and described in detail in BN (2006).

4.1.2 Hydrogeologic and Hydrostratigraphic Units of the Yucca Flat/Climax Mine HFM

The rocks of the NTS have been classified hydrologically using a two-level classification scheme: HGUs and HSUs (IT, 1996b; BN, 2002, 2005, and 2006; NSTec, 2007). The HGUs categorize rocks according to their ability to transmit groundwater (i.e., aquifers or confining units), which is mainly a function of the primary lithologic properties of the rock, degree of fracturing, and secondary mineral alteration. The HSUs are larger, more regional mapping units that group contiguous stratigraphic intervals that have similar hydrogeologic characteristics (i.e., composed of similar HGUs).

4.1.2.1 Hydrogeologic Units of the Yucca Flat/Climax Mine HFM

The rocks of the Yucca Flat/Climax Mine HFM area are classified as one of the following nine HGUs: playa confining unit (PCU), alluvial aquifer (AA), welded-tuff aquifer (WTA), vitric-tuff aquifer (VTA), lava-flow aquifer (LFA), tuff confining unit (TCU), granite confining unit (GCU), clastic confining unit (CCU), and carbonate aquifer (CA) (Table 4-1). These HGUs are described in more detail below.

Alluvial Hydrogeologic Units

Two alluvial HGUs are present in the Yucca Flat/Climax Mine model area: the AA, which is also an HSU, and the PCU. The AA consists mainly of gravelly sand and sandy gravel eroded from the surrounding mountains during basin development and deposited on alluvial fans by debris flow and sheetflood processes. Deposits of finer-grained eolian sand are intercalated within the coarser alluvial deposits. The PCU consists of fine-grained sand, silt, and clay deposited as playa lake sediments in the topographic low point of the basin at the southern end of Yucca Flat.

Volcanic Hydrogeologic Units

The volcanic rocks within the model area are categorized into four HGUs (LFA, TCU, VTA, and WTA) based on primary lithologic properties, degree of fracturing, and secondary mineral alteration. In general, the altered volcanic rocks, which are typically zeolitized and support few fractures (Prothro, 1998), act as confining units, and the unaltered rocks form aquifers. The aquifer units are further divided into WTAs and VTAs, depending on degree of welding, and LFAs. Denser rocks,

Table 4-1
Hydrogeologic Units of the Yucca Flat/Climax Mine HFM Area

Hydrogeologic Unit	Typical Lithologies	Hydrologic Significance
Playa confining unit (PCU)	Argillic-silt, sandy-silt	Surface and near-surface confining unit at Yucca Lake. May also limit, or redirect, recharge where present at surface.
Alluvial aquifer (AA) [a]	Unconsolidated to partially consolidated gravelly sand, eolian sand, and colluvium	Has characteristics of a highly conductive aquifer, but less so where lenses of clay-rich paleocolluvium, zeolitic alteration, or playa deposits are present.
Welded-tuff aquifer (WTA)	Welded ash-flow tuff; vitric to devitrified	Degree of welding greatly affects interstitial porosity (i.e., less porosity as degree of welding increases) and permeability (i.e., greater fracture permeability as degree of welding increases).
Vitric-tuff aquifer (VTA)	Bedded tuff; ash-fall and reworked tuff; vitric	Constitutes a volumetrically minor HGU. Generally does not extend far below the static water level due to tendency of tuffs to become zeolitic under saturated conditions, which drastically reduces permeability. Significant interstitial porosity (i.e., 20 to 40 percent). Generally insignificant fracture permeability.
Lava-flow aquifer (LFA)	Rhyolite, basalt and dacite lava flows; includes flow breccia (commonly at base)	Generally occurs as small, moderately thick (rhyolite) to thin (basalt) local flows. Hydrologically complex, showing a wide range of transmissivity values; fracture density and interstitial porosity differ with lithologic variations.
Tuff confining unit (TCU)	Zeolitic bedded tuff with interbedded, but less significant, zeolitic, nonwelded to partially welded ash-flow tuff	May be saturated, but measured transmissivities are very low. May cause semi-perched conditions.
Granite confining unit (GCU)	Granodiorite and quartz monzonite	Saturated at depth but because of low intergranular porosity and permeability, plus the lack of interconnecting fractures, is considered a confining unit.
Clastic confining unit (CCU)	Argillite, siltstone, quartzite	Siliciclastic rocks are relatively impermeable; coarser-grained siliciclastic rocks are fractured, but with fracture porosity generally sealed due to secondary mineralization.
Carbonate aquifer (CA)	Dolomite, limestone	Transmissivity values differ greatly and are directly dependent on fracture frequency.

Source: BN, 2006 (Adapted from Winograd and Thordarson, 1975; IT, 1996b; and Laczniak et al., 1996)

[a] The AA is also an HSU in the Yucca Flat/Climax Mine HFM.

such as welded ash-flow tuff and lava flows, tend to fracture more readily, and therefore have relatively high fracture permeability (Blankennagel and Weir, 1973; Winograd and Thordarson, 1975; Laczniak et al., 1996; IT, 1996b; Prothro and Drellack, 1997a and b).

Pre-Tertiary Hydrogeologic Units

The hydrogeology of the pre-Tertiary sedimentary rocks at the NTS follows the framework developed by Winograd and Thordarson (1975), and used in the UGTA Phase I regional modeling effort (IT, 1996a and b) and subsequent CAU-scale HFMs (BN, 2002, 2005, and 2006; NSTec, 2007). Within the model area, pre-Tertiary rocks are categorized as aquifer or confining unit HGUs based on lithology. Siliciclastic rocks, such as quartzite, siltstone, and shale, are classified as CCUs. Carbonate rocks, such as limestone and dolomite, are classified as CAs (Winograd and Thordarson, 1975; Laczniak et al., 1996). The granitic intrusive rocks are classified as confining units (BN, 2002).

4.1.2.2 Hydrostratigraphic Units of the Yucca Flat/Climax Mine HFM

The hydrostratigraphic classification system is the foundation of the Yucca Flat/Climax Mine HFM (Table 4-2). This system was developed by first grouping the rocks within the model area into HGUs based on lithologic character, propensity to fracture, and the degree of secondary alteration. The HGUs of similar character were then grouped into larger HSUs to facilitate mapping and 3-D model construction. A critical component of this step was the careful integration of Yucca Flat stratigraphy. The integration of stratigraphic concepts is important to assure that individual HGUs grouped within HSUs, and the HSUs themselves, properly correlate within the model. The correlation of stratigraphic units and HSUs of the Yucca Flat/Climax Mine HFM area is depicted graphically in Figure 4-2.

Hydrostratigraphic units can be thought of as groupings of contiguous stratigraphic units that have a particular hydrogeologic character, such as aquifer or confining unit. For the Yucca Flat/Climax Mine model, most HSUs consist of a single HGU (e.g., the TM-LVTA essentially is 100 percent VTA). There are four exceptions (the TM-UVTA, TM-WTA, TSA, and VCU) that may consist of several HGUs but are defined so that a single general type of HGU dominates (e.g., mostly WTA). These exceptions are noted in the “Dominant Hydrogeologic Units” column of Table 4-2.

Table 4-2
Hydrostratigraphic Units of the Yucca Flat/Climax Mine HFM
(Page 1 of 4)

Hydrostratigraphic Unit	Dominant Hydrogeologic Units [a]	Typical Lithologies	Stratigraphic Unit Map Symbol(s) [b]	Hydrologic Significance
Alluvial aquifer (AA1, AA2, AA3)	AA	Alluvium: Gravelly sand; also includes one or more thin basalt flows, playa deposits (differentiated as separate HSUs) and eolian sands	Qay, QTc, Qai, QTa	Generally unsaturated except in deepest basins.
Playa confining unit (PCUT)	PCU	Argillic silt and sandy silt.	Qp	Playa units occur well above local water table, but could impede downward recharge, or could intermittently concentrate local recharge through large surface cracks. Forms surface and near-surface playas at Yucca Lake and Papoose Lake and southern West Emigrant Valley.
Basalt lava-flow aquifer (BLFA)	LFA	Basalt lava flows	Tyby, Ttb	Several (possibly dissected) basalt flows recognized in the middle of the alluvial section of southwestern Yucca Flat, at the surface as dikes and sills in the Half Pint Range, and as a dike in the subsurface of eastern Yucca Flat. Generally unsaturated, but deep feeder dikes could possibly affect groundwater flow.
Timber Mountain upper vitric-tuff aquifer (TM-UVTA)	VTA, minor (< 15%) WTA	Includes vitric nonwelded to partially welded ash-flow and bedded tuff	Tma, Tmab	Typically saturated only in the deepest structural basins. This HSU comprises only the Ammonia Tanks Tuff, which stratigraphically overlies the TM-WTA.
Timber Mountain welded-tuff aquifer (TM-WTA)	WTA, minor (< 20%) VTA	Partially to densely welded ash-flow tuff; vitric to devitrified	Tma, Tmab, Tmr	Typically saturated only in deep structural basins. Welded zones typically sandwiched between nonwelded zones.
Timber Mountain lower vitric-tuff aquifer (TM-LVTA)	VTA	Nonwelded ash-flow and bedded tuff; vitric	Tma, Tmab, Tmr, Tmrh, Tp, Th, Tw, Tc (in N. Yucca Flat may also include Tbgb, and Tn)	Typically includes the unaltered (i.e., vitric), nonwelded welded lower portion of the Rainier Mesa Tuff. However, this HSU can encompass all unaltered, nonwelded and bedded units below the welded Rainier Mesa Tuff and above the level of pervasive zeolitization. Unaltered nonwelded and ash-fall tuffs generally not found at depths much below the static water level due to tendency to become zeolitized (which drastically reduces permeability) under saturated conditions.

Table 4-2
Hydrostratigraphic Units of the Yucca Flat/Climax Mine HFM
(Page 2 of 4)

Hydrostratigraphic Unit	Dominant Hydrogeologic Units [a]	Typical Lithologies	Stratigraphic Unit Map Symbol(s) [b]	Hydrologic Significance
Upper tuff confining unit (UTCU)	TCU	Zeolitized bedded tuff	Tmr (lower most), Tmrh, Tp	Defined to encompass the zeolitized bedded tuffs which stratigraphically overlie the Topopah Spring aquifer (TSA). Although some geologic units of the UTCU are laterally continuous with those of the LTCU, the UTCU is limited areally to extreme southern Yucca Flat where the welded Topopah Spring Tuff is an important aquifer present between the two tuff confining units (UTCU and LTCU).
Topopah Spring aquifer (TSA)	WTA, minor (< 15%) VTA	Welded ash-flow tuff	Tpt	Distribution in Yucca Flat is limited to extreme southern portion, south of the N 828,000 (NTS) grid line. Hydrogeologic properties similar to those of the TM-WTA.
Lower vitric-tuff aquifer (LVTA)	VTA	Nonwelded and bedded ash-flow tuff; vitric	Th	Relatively thin VTA unit below the TSA. Grouped with the TM-LVTA where TSA is not present.
Belted Range aquifer (BRA)	WTA	Welded ash-flow tuff	Tbg	Typically saturated (perched water) only in the Rainier Mesa area. This HSU comprises only welded Grouse Canyon Tuff and is limited to the northern portion of the Yucca Flat/Climax Mine model area.
Belted Range confining unit (BRCU)	TCU	Zeolitized bedded tuffs	Tn, Tn4, Tn3	Generally includes all zeolitized tuffs between the (welded) Grouse Canyon Tuff and the (welded) Tub Spring Tuff. Limited to the northern portion of the Yucca Flat/Climax Mine model area.
Pre-Grouse Canyon Tuff lava-flow aquifer (PRETBG)	LFA	Lava flow	Tbq, Tuo	Defined to include all the comendite lava-flows emplaced before the Grouse Canyon Tuff but after the Tub Spring Tuff. Limited to the northern portion of the Yucca Flat/Climax Mine model area.
Tub Spring aquifer (TUBA)	WTA	Welded ash-flow tuff	Tub	Comprises only the welded Tub Spring Tuff and is thus limited to the northern portion of the Yucca Flat/Climax Mine model area.
Pre-Grouse Canyon Tuff lava-flow aquifer 1 (PRETBG1)	LFA	Lava flow	Tue	Defined to include all the comendite lava-flows emplaced before the Tub Spring Tuff but after the older Tunnel beds. Limited to the northern portion of the Yucca Flat/Climax Mine model area. . Hydrogeologically equivalent to the PRETBG.

Table 4-2
Hydrostratigraphic Units of the Yucca Flat/Climax Mine HFM
(Page 3 of 4)

Hydrostratigraphic Unit	Dominant Hydrogeologic Units [a]	Typical Lithologies	Stratigraphic Unit Map Symbol(s) [b]	Hydrologic Significance
Lower tuff confining unit (LTCU)	TCU	Zeolitized bedded tuffs with interbedded but less significant zeolitized, nonwelded to partially welded ash-flow tuffs	Tmrh, Tp, Th, Tw, Tc, Tn, Tub, Ton2, To, Tlt	Generally includes all zeolitized tuffs in the Yucca Flat area. Stratigraphically the LTCU may include all units from the base of the welded Rainier Mesa Tuff to the top of the Paleozoic rocks. The strongly argillized older tuffs and paleocolluvium that immediately overlie the pre-Tertiary rocks may also be included in areas with poor drill hole control. The uppermost zeolitized bedded tuffs overlying the TSA in southern Yucca Flat form a separate HSU, the UTCU.
Oak Spring Butte confining unit (OSBCU)	TCU	Devitrified to zeolitic nonwelded to partially welded tuffs and intervening bedded tuffs	Ton, To, Toy, Tor, Tot	Includes altered, older ash-flow tuff units and Tunnel beds 1 and 2. Welding in the older ash-flow units may increase hydraulic conductivity. Devitrification of the ash-flow units may have limited zeolitization. Differentiated only in the main Yucca Flat basin.
Argillic tuff confining unit (ATCU)	TCU	Argillic bedded tuffs, minor paleocolluvium	To, Tlt	Includes the argillic, lowermost Tertiary volcanic units and paleocolluvium that immediately overlie the pre-Tertiary rocks. Differentiated in the Yucca Flat basin.
Volcaniclastic confining unit (VCU)	In Yucca Flat/Climax Mine model: 80% AA, 20% TCU	Sandy gravels, siltstones, and tuffaceous sandstones	Tgp, Tgw	Older Tertiary-age sedimentary rocks of variable lithologies. Present in the southeastern corner of the model area. A significant HSU in the Frenchman Flat model (BN, 2005), but less so in Yucca Flat.
Mesozoic granite confining unit (MGCU)	GCU	Granodiorite and quartz monzonite	Kgc, Kgg	Includes two intrusives: Climax at the north end of Yucca Flat and Gold Meadows located west of the model area. The granite has very low permeability and is considered to be a confining unit. Locally may have perched water contained within fractures. The two stocks may be connected at depth and are believed to be part of the hydrogeologic barrier at the north end of Yucca Flat.
Lower carbonate aquifer - Yucca Flat upper plate (LCA3)	CA	Limestone and dolomite	Dg through upper Cc	Includes the Cambrian through Ordovician units that have been thrust over the Eleana Formation and the Chainman Shale.

Table 4-2
Hydrostratigraphic Units of the Yucca Flat/Climax Mine HFM
(Page 4 of 4)

Hydrostratigraphic Unit	Dominant Hydrogeologic Units [a]	Typical Lithologies	Stratigraphic Unit Map Symbol(s) [b]	Hydrologic Significance
Lower clastic confining unit - Yucca Flat upper plate (LCCU1 and 2)	CCU	Quartzite and siltstone	Lower Cc, Cz, Czw, Zs, Zj	Includes upper Proterozoic through lower Cambrian units that have been thrust over younger units.
Upper carbonate aquifer (UCA)	CA	Limestone	PPt	Includes the Tippipah Limestone, which stratigraphically overlies the Chainman Shale at Syncline Ridge and thus may contain perched water.
Upper clastic confining unit (UCCU)	CCU	Argillite and quartzite	Mc, MDe	As much as 2,745 m (9,000 ft) thick. Typically forms the footwall of Mesozoic thrust faults in NTS region. Areal extent limited to western Yucca Flat and portions of CP basin.
Lower carbonate aquifer (LCA)	CA	Dolomite and limestone	Dg through upper Cc	Important regional aquifer underlying most of southern Nevada. Composite thickness up to 4,430 m (14,500 ft). Transmissivity values differ greatly and are directly dependent on fracture and fault frequency.
Lower clastic confining unit (LCCU)	CCU	Quartzite and siltstone	Lower Cc, Cz, Czw, Zs, Zj	Significant regional confining unit. Composite thickness about 2,870 m (9,400 ft). May present barrier to deep regional groundwater flow where structurally high. (e.g., northeastern Yucca Flat).

Source: Table 4-4 in BN, 2006

[a] See Table 4-1 for definition of hydrogeologic units.
[b] See Appendix D for definition of stratigraphic unit map symbols.

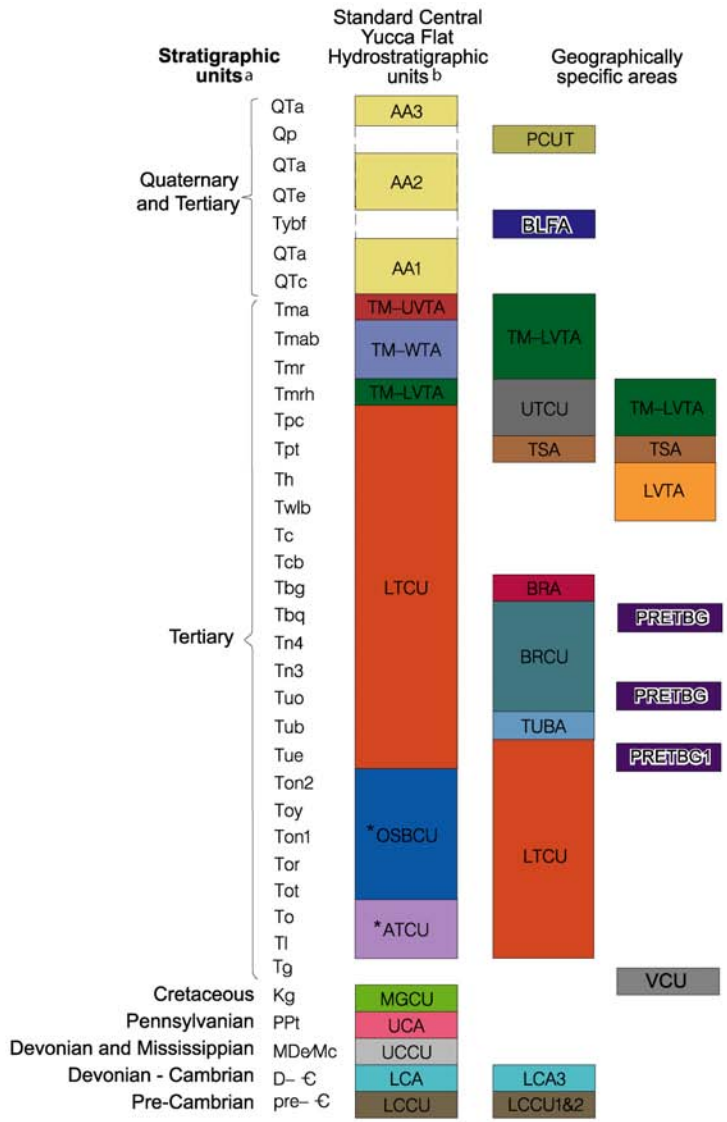

Definitions of Hydrostratigraphic Symbols

AA3	Alluvial aquifer 3
PCUT	Playa confining unit
AA2	Alluvial aquifer 2
BLFA	Basalt lava-flow aquifer
AA1	Alluvial aquifer 1
TM-UVTA	Timber Mountain upper vitric-tuff aquifer
TM-WTA	Timber Mountain welded-tuff aquifer
TM-LVTA	Timber Mountain lower vitric-tuff aquifer
UTCU	Upper tuff confining unit
TSA	Topopah Spring aquifer
LVTA	Lower vitric-tuff aquifer
BRA	Belted Range aquifer
BRCU	Belted Range confining unit
PRETBG	Pre-Grouse Canyon Tuff lava-flow aquifer
TUBA	Tub Spring aquifer
PRETBG1	Pre-Grouse Canyon Tuff lava-flow aquifer
LTCU	Lower tuff confining unit
*OSBCU	Oak Spring Butte confining unit
*ATCU	Argillic tuff confining unit
VCU	Volcaniclastic confining unit
MGCU	Mesozoic granite confining unit
LCCU1	Lower clastic confining unit 1-thrust plate
LCA3	Lower carbonate aquifer-thrust plate
LCCU2	Lower clastic confining unit 2-thrust plate
UCA	Upper carbonate aquifer
UCCU	Upper clastic confining unit
LCA	Lower carbonate aquifer
LCCU	Lower clastic confining unit

a Ferguson et al., 1994; Slate et al., 1999

b See Table 4-3

* The OSBCU and the ATCU are differentiated in the Yucca Flat basin and not in the surrounding highlands.

Source: Figure 4-2 in BN, 2006

Figure 4-2
Correlation of Stratigraphic and Hydrostratigraphic Units of the Yucca Flat/Climax Mine HFM Area

Brief descriptions of all HSUs in the Yucca Flat/Climax Mine HFM are provided in Table 4-2. They are generally listed in descending order from the top of the model to the bottom, although some are laterally rather than vertically contiguous, and not all units are present in all parts of the model area. A more detailed description of each HSU can be found in BN (2006).

The distribution of HSUs at the surface within the Yucca Flat/Climax Mine HFM area is shown in a block model view in Figure 4-3. The distribution of HSUs at the water table is presented in Figure 4-4. Figure 4-5 is a block model view with the upper alluvial HSU, AA3, removed. The figure shows the extent of the PCUT (the term used in the EV® model to represent the PCU), the BLFA, and intermediate alluvium (AA2 and AA1) within the Yucca Flat/Climax Mine HFM area. Figure 4-6 is a block model view with all the alluvial HSUs removed and thus shows the distribution of HSUs that directly underlie the alluvium in Yucca Flat. The distribution of volcanic confining HSUs (alluvial and upper volcanic aquifer units removed) within the Yucca Flat/Climax Mine HFM area is shown in Figure 4-7. The distribution of pre-Tertiary HSUs (alluvium and volcanic HSUs removed) is shown in Figure 4-8.

A north-south hydrostratigraphic profile along the general direction of groundwater flow is provided in Profile A-A' along with west-east hydrostratigraphic profiles B-B' and C-C' through central Yucca Flat that are normal to basin structure (see Plate 2). The profiles illustrate the relationships of the HSUs and structures in various vertical planes. The locations of these profile lines are shown on Figure 4-4. These model profiles are from the Yucca Flat 3-D framework documentation package (BN, 2006), where additional cross sections and detailed information regarding this CAU-scale model can be found.

Table 4-3 shows the correlation of Yucca Flat/Climax Mine HSUs with HSUs of earlier and nearby hydrostratigraphic models for the NTS area. As can be seen from the information presented in this section, the Yucca Flat/Climax Mine HFM includes considerable structural detail and stratigraphic enhancement over both of the preceding regional HFM models included in the UGTA regional model (IT, 1996b) and the DVRFS model (Belcher et al., 2004). Except for geometric details, the pre-Tertiary HSUs remain as initially defined, with the addition of the UCA and the LCCU2 thrust sheet.

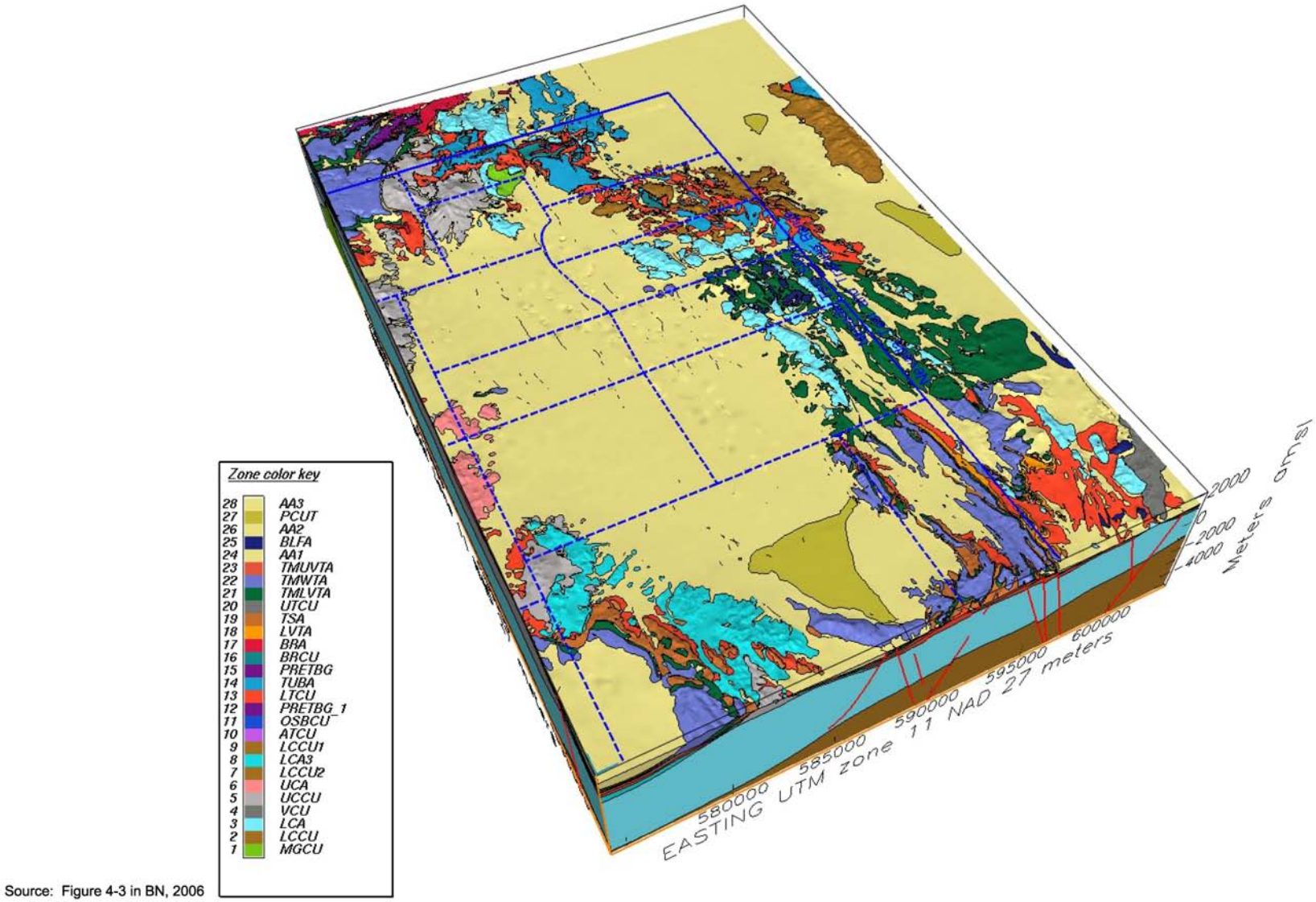

Source: Figure 4-3 in BN, 2006

Figure 4-3
Block Model View Showing Hydrostratigraphic Units at the Surface Within the Yucca Flat/Climax Mine Model Area

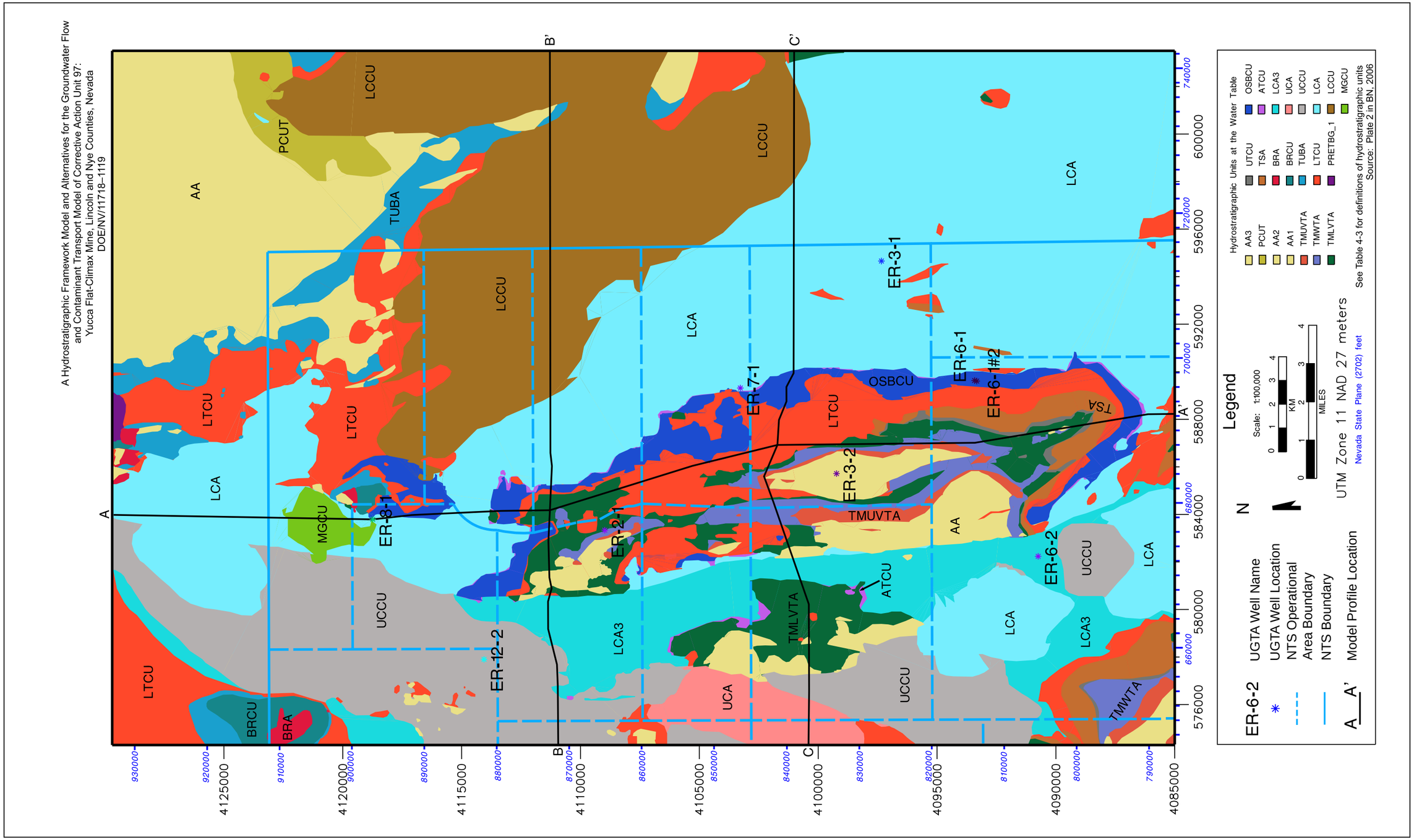

Figure 4-4
Hydrostratigraphic Units at the Water Table in the Yucca Flat/Climax Mine Model Area

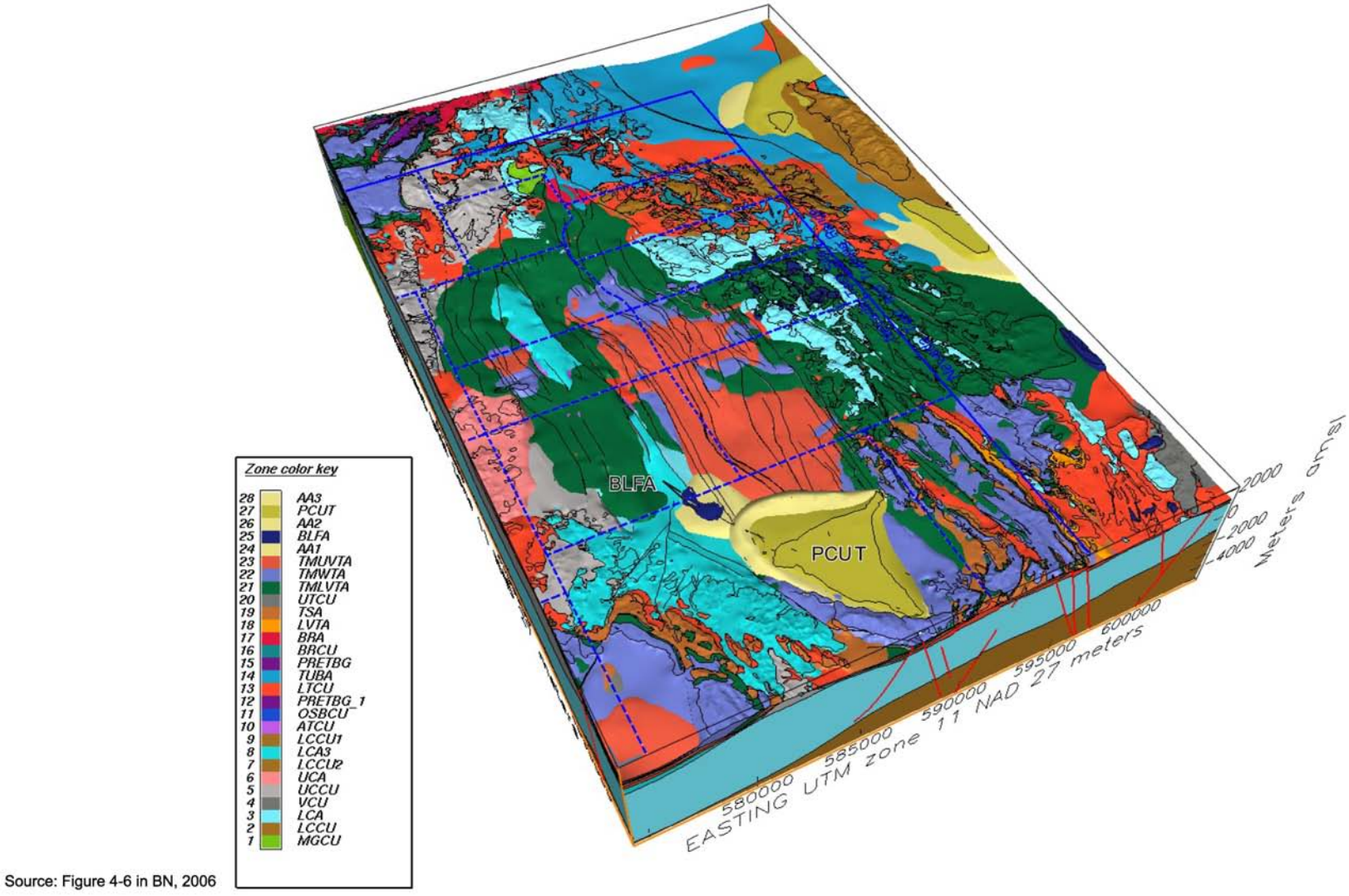

Source: Figure 4-6 in BN, 2006

Figure 4-5
Block Model View Showing Extent of the Playa Confining Unit and the Basalt Lava-Flow Aquifer Within the Yucca Flat/Climax Mine Model Area with the Upper Alluvial HSU (AA3) Removed

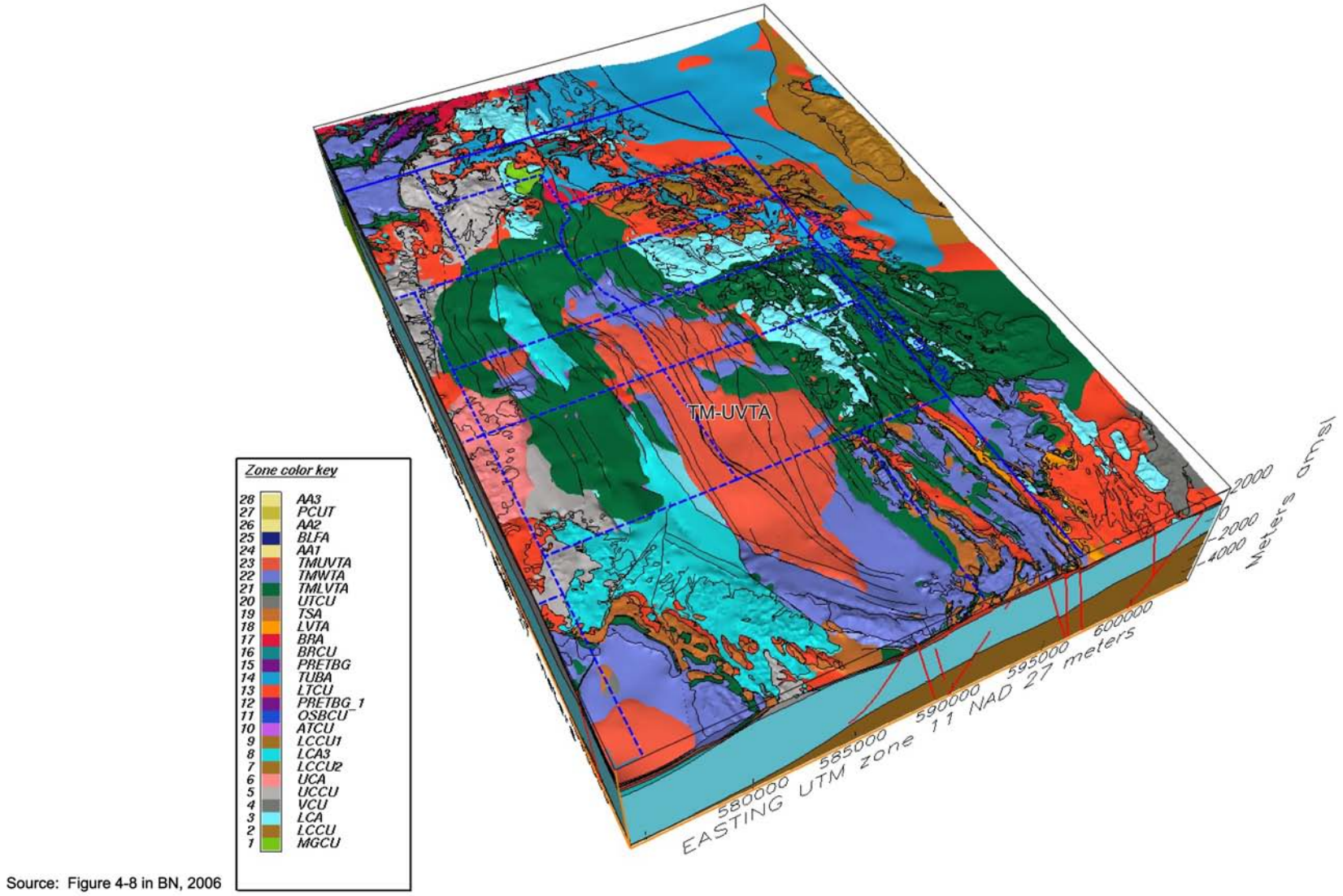

Source: Figure 4-8 in BN, 2006

Figure 4-6
Block Model View Showing the Distribution of Hydrostratigraphic Units Within the Yucca Flat/Climax Mine HFM Area with Alluvium Removed

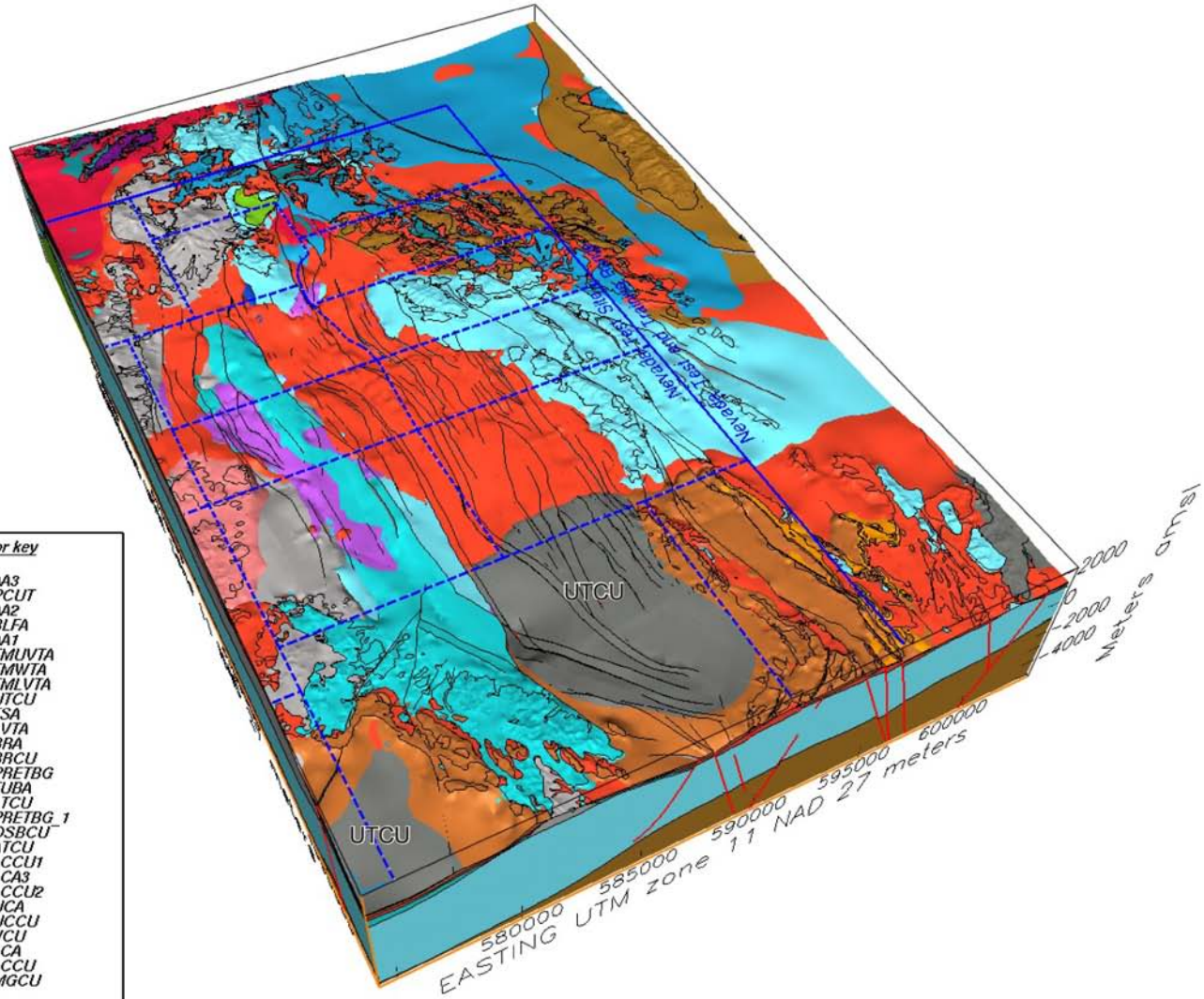

Source: Figure 4-16 in BN, 2006

Figure 4-7
Block Model View Showing the Distribution of the Volcanic Confining Units in the Yucca Flat/Climax Mine HFM Area with Alluvium and Upper Volcanic Aquifers Removed

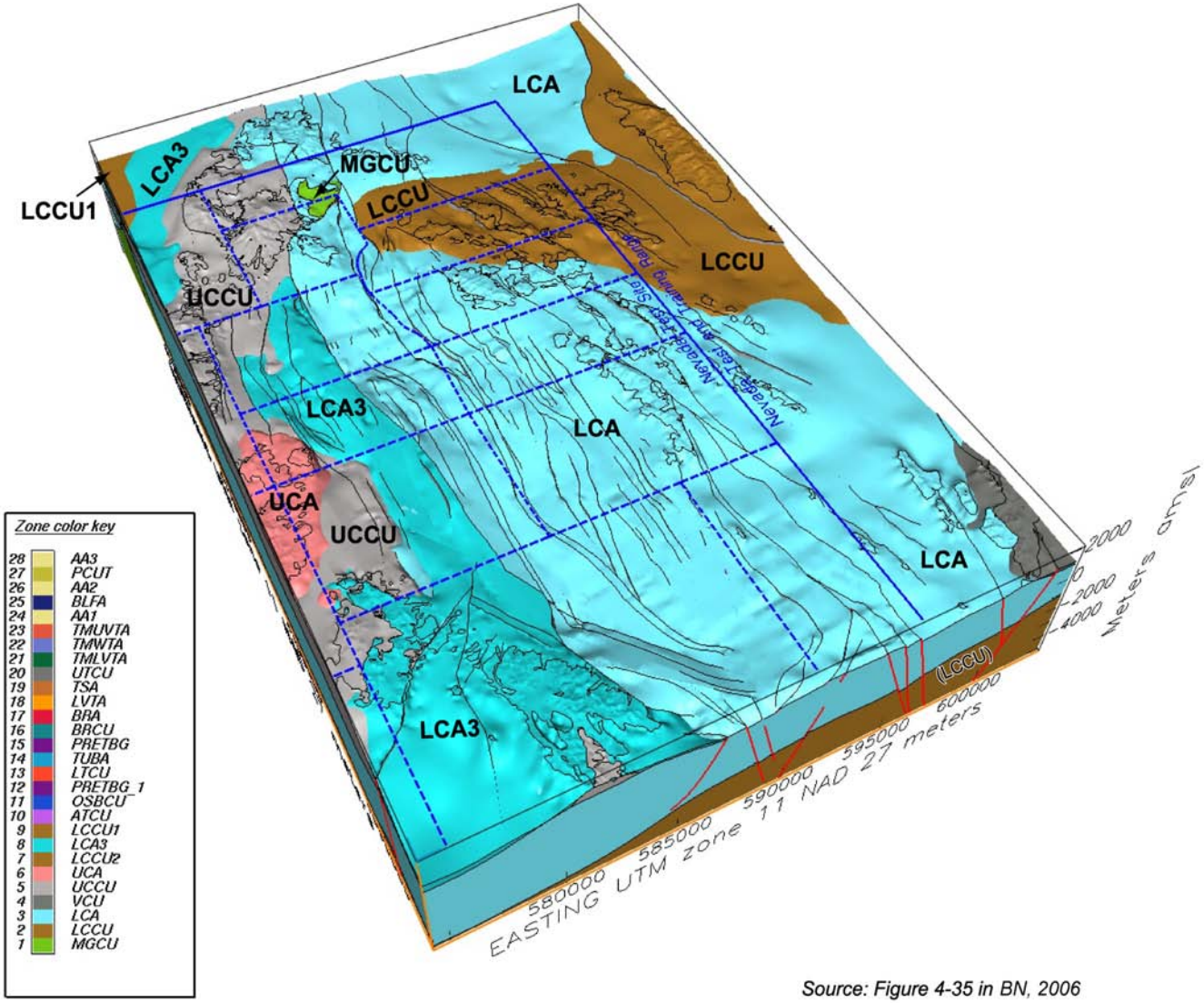

Source: Figure 4-35 in BN, 2006

Figure 4-8
Block Model View Showing the Distribution of the Pre-Tertiary Hydrostratigraphic Units in the Yucca Flat/Climax Mine HFM Area with Alluvium and Volcanic Aquifers Removed

Table 4-3
Correlation of Hydrostratigraphic Units of the Yucca Flat/Climax Mine CAU Model and Earlier Models
(Page 1 of 2)

Hydrostratigraphic Unit	Symbol This Report	Correlation with Phase II Frenchman Flat Model [a, b]	Correlation with Pahute Mesa Model [c]	Correlation with UGTA Phase 1 [d]	Correlation with DVRFS Model [e]
Alluvial aquifer	AA3, AA2, AA1 [f]	AA3, AA2, AA1 [f]	AA	AA [g]	YAA
Playa confining unit	PCUT	PCU2T, PCU1U, PCU1L	NP		YACU
Basalt lava-flow aquifer	BLFA	BLFA	YVCM		LFU
Timber Mountain upper vitric-tuff aquifer	TM-UVTA	NP	TMA [g]	TMA, VA [g], TC [g] TBA [h]	TMVA [g]
Timber Mountain welded-tuff aquifer	TM-WTA	TM-WTA			
Timber Mountain lower vitric-tuff aquifer	TM-LVTA	TM-LVTA	PVTA		TMVA, PVA
Upper tuff confining unit	UTCU	UTCU	UPCU, LPCU		PVA [g]
Topopah Spring aquifer	TSA	TSA	TSA		
Lower vitric-tuff aquifer	LVTA	LVTA	PVTA		CHVU
Belted Range aquifer	BRA	NP	BRA		BRU [g]
Belted Range confining unit	BRCU	NP (LTCU)	NP (PBRCM [g])		
Pre-Grouse Canyon Tuff lava-flow aquifer	PRETBG	NP	NP (PBRCM [g])		
Tub Spring aquifer	TUBA	NP	NP		OVU [g]
Pre-Grouse Canyon Tuff lava-flow aquifer 1	PRETBG1 [f]	NP	NP (PBRCM [g])		
Lower tuff confining unit	LTCU	LTCU [g], LTCU1 [f]	CFCU, BFCU, PBRCM [i]	VCU [g], BCU [g]	OVU [g]
Oak Spring Butte confining unit	OSBCU		PBRCM [f, i]		
Argillic tuff confining unit	ATCU				
Volcaniclastic confining unit	VCU	VCU	NP	BCU [g]	Lower VSU

Table 4-3
Correlation of Hydrostratigraphic Units of the Yucca Flat/Climax Mine CAU Model and Earlier Models
(Page 2 of 2)

Hydrostratigraphic Unit	Symbol This Report	Correlation with Phase II Frenchman Flat Model [a, b]	Correlation with Pahute Mesa Model [c]	Correlation with UGTA Phase 1 [d]	Correlation with DVRFS Model [e]
Mesozoic granite confining unit	MGCU	NP	MGCU	I	ICU
Lower clastic confining unit 1 - thrust plate	LCCU1	NP	LCCU1	LCCU1	LCCU_T1
Lower carbonate aquifer - thrust plate	LCA3	LCA3	LCA3	LCA3	LCA_T1
Lower clastic confining unit 2 - thrust plate	LCCU2	NP	NP	NP	LCCU_T1
Upper carbonate aquifer	UCA	NP	NP	LCA3	UCA
Upper clastic confining unit	UCCU	UCCU	UCCU	UCCU	UCCU
Lower carbonate aquifer	LCA	LCA	LCA	LCA	LCA
Lower clastic confining unit	LCCU	LCCU	LCCU	LCCU	LCCU

Source: Table 4-5 in BN, 2006

[a] If correlative to more than one HSU, all HSUs are listed.
[b] See BN (2005) for explanation of Frenchman Flat HSU nomenclature.
[c] See BN (2002) for explanation of Pahute Mesa HSU nomenclature.
[d] See IT (1996b) for explanation of the UGTA Phase I HSU nomenclature.
[e] See Belcher et al. (2004) for explanation of the Death Valley Regional Ground-Water Flow System (DVRFS) nomenclature.
[f] Subdivisions, although hydrogeologically equivalent, are necessary to satisfy operational requirements of the EarthVision® modeling software (Dynamic Graphics, 2002).
[g] Not subdivided.
[h] TBA correlates best to the BRA and PRETBG(1) HSUs.
[i] Pre-Belted Range Composite Unit (PBRCM) may include minor embedded ash-flow tuffs.

NP - Not present

4.2 Mineralogy of Hydrostratigraphic Units in the Yucca Flat/Climax Mine HFM

The HSUs developed for the HFM tend to emphasize the physical hydrologic significance of a unit, as opposed to the mineralogy. Because some transport parameters are closely related to the mineralogical environment in which transport occurs, distributions for these parameters will be associated with specific mineralogic units rather the HSUs. For instance, the nature and distribution of mineral phases in groundwater systems can exert a significant influence on the mobility of contaminants of concern. Distributions, representing matrix sorption as a function of the reactive minerals present within a given unit, are therefore established and used for contaminant transport modeling.

Minerals described as reactive within this document include those that are known to impact radionuclide transport via sorption processes (e.g., those minerals included in the mechanistic model approach described by Zavarin et al., 2004). Reactive minerals are expected to occur in four distinct settings within the Yucca Flat/Climax Mine CAU. These are (1) minerals in alluvial deposits, volcanic rocks, and carbonate rocks; (2) minerals occurring as coatings on fracture surfaces in fractured volcanic and carbonate rocks; and (3) colloids (fine-grained mineral particles) mobile in groundwater.

Most of the volcanic rocks in the vicinity of Yucca Flat are pyroclastic rocks composed of ash-flow tuffs and ash-fall deposits of generally rhyolitic composition. These silica-rich rocks can be composed of more than 80 percent glass when originally deposited (the remainder is a mixture of original phenocrysts and lithic fragments). Reactive minerals such as zeolite, clay, carbonate, mica, and hematite are rare in these vitric rocks. However, post-depositional processes such as welding, devitrification, zeolitization, and argillization can significantly alter not only the hydraulic properties but also the mineralogy of volcanic rocks. On average, volcanic units in the Southwestern Nevada Volcanic Field (SWNVF) show fairly consistent mineralogy that tends to vary only as a function of style and intensity of alteration (Warren et al., 2003).

Devitrification, which is typically associated with welded ash-flow tuffs and the interior portions of lava flows, occurs during cooling of ash-flow tuffs and lavas shortly after emplacement. This post-depositional process results in the conversion of the original glass to microcrystalline quartz and feldspar, and thus yields a rock composed almost entirely of quartz and feldspar that is resistant to

other post-depositional processes, such as zeolitization and argillization. Devitrified welded ash-flow tuffs form important aquifers beneath Yucca Flat (e.g., the TM-WTA).

Volcanic rocks that remain vitric after emplacement — such as nonwelded ash-flow tuffs, ash-fall deposits, and the outer portions of lavas — are susceptible to diagenetic alteration processes. Zeolitization is common in volcanic rocks in the Yucca Flat area and results in the original glass being converted to the zeolite mineral clinoptilolite, with lesser amounts of other zeolite minerals, such as mordenite and analcime, at the deeper levels. Because of the high percentage of glass in the original rocks, zeolitization results in volcanic rocks composed predominantly of zeolite. Other reactive minerals such as carbonate, mica, and hematite are typically rare in zeolitic rocks. Clay in the form of mainly smectite is usually a minor constituent. Large portions of the volcanic section beneath Yucca Flat are pervasively zeolitic, and form important confining units (e.g., the LTCU).

Unaltered volcanic rocks are also susceptible to argillization. In this post-depositional process, the original glass is converted to clay minerals, such as smectite and lesser kaolinite. In the Yucca Flat vicinity, the basal portion of the volcanic section is commonly pervasively argillic and forms a confining unit that directly overlies the regional CA (e.g., the ATCU).

Zeolitic and argillic alteration is commonly observed in the volcanic rocks at the NTS (Hoover, 1968; Prothro, 2005). Argillic alteration commonly is characterized by the presence of the clays smectite and kaolinite. In addition to decreasing the hydraulic conductivity of the rock, these secondary alteration minerals are reactive with respect to radionuclide transport (Tompson et al., 1999). Clinoptilolite and smectite, for example, have a strong sorptive affinity for certain radionuclides (Zavarin et al., 2004). The confining unit HSUs in the Yucca Flat model (e.g., the upper and lower tuff confining units) contain a significant amount of zeolite minerals, typically more than 30 percent (Prothro, 2005). The ATCU contains a significant percentage of clays, generally more than 30 percent. In addition to the zeolite and clay minerals mentioned above, reactive minerals of interest with respect to radionuclide transport modeling include iron oxides (hematite); certain mafic minerals, such as biotite; and calcite. These reactive minerals are found in the rock matrix, in lithic fragments, as phenocrysts, or in the fracture fillings and coatings.

After evaluating the occurrence of these reactive minerals, with respect to geologic processes relevant to the rocks at the NTS, several natural categories emerge. The RMCs for NTS volcanic rocks are

vitric mafic-poor (VMP), vitric mafic-rich (VMR), devitrified mafic-poor (DMP), devitrified mafic-rich (DMR), mafic lava (ML), zeolitic (ZEOL), and argillic (ARG). The RMCs for Paleozoic sedimentary rocks are calcic (CC) for the carbonate rocks, and silicic (SC) or ARG for the siliciclastic rocks. In general, the volcanic confining units are classified as the ZEOL RMC, the welded-tuff aquifers are classified as the DMR or DMP, the vitric-tuff aquifers are classified as VMR or VMP, and the argillic tuff confining unit is classified as the ARG RMC. Granite falls into the DMR RMC. The carbonate aquifers are classified as the CC RMC and the siliciclastic confining units are classified as the SC RMC if mostly quartzite or the ARG RMC if mostly shale. Mineralogical criteria used to establish RMCs for the Yucca Flat/Climax Mine HFM are provided in Table 4-4. Table 4-5 provides the RMC assignments for each HSU in the Yucca Flat/Climax Mine HFM. A large effort was placed on compiling the available x-ray diffraction (XRD) data for the Yucca Flat/Climax Mine CAU. The XRD data and a description of the compilation process are presented in Appendix D. A description of each HSU in the Yucca Flat/Climax Mine HFM is provided in the following sections. Each description includes a discussion of the mineralogy of the HSU.

Evaluation of mineralogy data must take into account sampling bias. These include different sampling objectives; operational limitations, such as the difficulty in sampling hard units (i.e., WTAs and LFAs) using percussion or Hunt sidewall sampling tools, and incompetent zones susceptible to erosion and borehole enlargement; and opportunity to sample certain units, or lack thereof, based on the location and distribution of boreholes. The majority of the data in Appendix D were collected for the specific objectives of the weapons testing program, with downhole sampling programs tending to sample and analyze anomalous zones. For example, of particular concern to the weapons testing program in Yucca Flat were intervals of argillic alteration within zeolitic rocks that may indicate the presence of a fault in the vicinity of the testing depth. Although these samples provide information on the heterogeneity within the zeolitic section, they will result in an overestimation of the amount of clay. Other studies producing XRD data were performed following weapons testing that focused on determining the zeolite content, and also the characterization of the TCU (Prothro, 2005), thus providing more representative sampling of the Yucca Flat/Climax Mine HSUs.

Table 4-4
Reactive Mineral Categories for the Yucca Flat/Climax Mine HFM Area
(Page 1 of 2)

Reactive Mineral Category (RMC)	**Typical Lithologies**	**Major Alteration**	**Reactive Minerals Present in Significant Quantities**	**Categorization Criteria** [a]
Zeolitic (ZEOL)	Bedded tuffs, nonwelded tuffs, pumiceous lavas, alluvium	Zeolitic, lesser argillic	Clinoptilolite, lesser mordenite and analcine; if argillic includes smectite, kaolinite	>30% zeolite and clay; zeolite > clay <10% glass
Vitric mafic-rich (VMR)	Ash-flow tuffs including nonwelded to partially welded tuffs and vitrophyres, bedded ash-fall tuffs (unaltered), vitrophyric and pumiceous lavas	None (vitric/glassy)	Biotite, hematite/iron oxide, hornblende, glass	vitric >30% glass <10% clay <20% zeolite mafic-rich >1.0% biotite or >1.5% biotite and hornblende
Vitric mafic-poor (VMP)	Ash-flow tuffs including nonwelded to partially welded tuffs and vitrophyres, bedded/ash-fall tuffs (unaltered), vitrophyric and pumiceous lavas	None (vitric/glassy)	Glass	vitric >30% glass <10% clay <20% zeolite mafic-poor <1.0% biotite or <1.5% biotite and hornblende
Devitrified mafic-rich (DMR)	Ash-flow tuffs including moderately to densely welded tuffs, dense/stony lavas	Devitrification, vapor-phase mineralization, quartzo-feldspathic, albitic	Biotite, hematite/iron oxide, hornblende	devitrified <20% glass >60% quartz and feldspars mafic-rich >1.0% biotite or >1.5% biotite and hornblende
Devitrified mafic-poor (DMP)	Ash-flow tuffs including moderately to densely welded tuffs, stony lavas	Devitrification, vapor-phase mineralization, quartzo-feldspathic, albitic	None	devitrified <20% glass >60% quartz and feldspars mafic-poor <1.0% biotite or <1.5% biotite and hornblende

Table 4-4
Reactive Mineral Categories for the Yucca Flat/Climax Mine HFM Area
(Page 2 of 2)

Reactive Mineral Category (RMC)	Typical Lithologies	Major Alteration	Reactive Minerals Present in Significant Quantities	Categorization Criteria [a]
Mafic lava (ML)	Lava flows; basalt, andesite, dacite	None (vitric) to devitrified	Olivine, clinopyroxene, hematite/iron oxide, magnetite, pyroxene, hornblende	>1.5% mafic minerals <20% zeolite <25% clay
Argillic (ARG)	Bedded tuffs, colluvium, shale, argillite, playa deposits	Argillic	Smectite, kaolinite, illite	>30% clay Clay > zeolite
Carbonate rocks (CC)	Limestone and dolomite	None, recrystallization	calcite, dolomite	>50% carbonate
Silicic rocks (SC)	Sandstone, siltstone, some argillite and conglomerate	None, silica	None	>50% silica/quartz

[a] Modifiers may be appended to the RMC name to denote specific instances of elevated abundances of some minerals (e.g., DMP-Z or DMR-C).
A if > 5% (but < 20%) clay
Z if > 5% (but < 30%) zeolite
C if > 3% (but < 50%) calcite/dolomite

Table 4-5
Reactive Mineral Category Assignments for the Hydrostratigraphic Units in the Yucca Flat/Climax Mine HFM
(Page 1 of 2)

HSU Layer No [a]	HSU [b]	HSU Symbol	Dominant HGUs [c]	Dominant RMCs [d]	Typical Stratigraphic Units [e]
28	Alluvial aquifer 3	AA3	AA	**VMP**	Qay, Qai,
27	Playa confining unit	PCUT	PCU	**ARG**, Lesser DMP-Z, A	Qp
NA [f]	Interbedded playa unit	IDP	PCU	**ARG**, Lesser DMP-Z, A	Qp, Qay
26	Alluvial aquifer 2	AA2	AA	**VMP**	Qay, Qai, QTc, QTa
25	Basalt lava-flow aquifer	BLFA	LFA	**ML**	Tyby
24	Alluvial aquifer 1	AA1	AA	**VMP**, minor VMP-Z	QTc, Qai, QTa
			ZEOL, minor AA	**ZEOL**, minor VMP-Z	QTc, Qai, QTa
23	Timber Mountain upper vitric-tuff aquifer	TM-UVTA	VTA	**VMR**, minor VMP-Z, ZEOL	Tmar, Tmap
			WTA, lesser VTA	**DMP**	Tma
			VTA	**VMP**, minor DMP	Tmap, Tma
			VTA	**VMP**, lesser VMR & DMR	Tmap, Tmab, Tmrb, Tmrr
22	Timber Mountain welded-tuff aquifer	TM-WTA	**WTA**, minor VTA	**DMR**	Tmrr, Tmr
			WTA, minor VTA	**DMP**	Tmrp, Tmr
21	Timber Mountain lower vitric-tuff aquifer	TM-LVTA	VTA	**VMP**, minor VMR, VMP-Z	Tma, Tmab, Tmr, Tmrh, Tp, Th, (in northern YF may also include Tw, Tc, Tbgb, and Tn)
20	Upper tuff confining unit	UTCU	TCU	**ZEOL**	Tmr (lower most), Tmrh, Tp
NA	Tiva Canyon aquifer	TCA	**WTA,** lesser VTA	**DMP**	Tpc
19	Topopah Spring aquifer	TSA	**WTA**, minor VTA	**DMP**	Tpt
			TCU	**ZEOL**	Tpt
18	Lower vitric-tuff aquifer	LVTA	VTA	**VMP**, minor VMP-Z, DMP, ZEOL	Th, Tw, Tc
NA	Upper tuff confining unit 1	UTCU1	TCU	**ZEOL**	Tmr (lower most), Tmrh, Tp
17	Belted Range aquifer	BRA	**WTA**, minor LFA	**DMP**	Tbg
NA	Lower vitric-tuff aquifer 1	LVTA1	VTA	**VMP**, minor VMP-Z, DMP, ZEOL	Th, Tw, Tc
16	Belted Range confining unit	BRCU	TCU	**ZEOL**	Tb, Tn, Tn4, Tn3
15	Pre-Tbg lava-flow aquifer	PRETBG	LFA	**DMP**	Tbq, Tuo, Tue

Table 4-5
Reactive Mineral Category Assignments for the Hydrostratigraphic Units in the Yucca Flat/Climax Mine HFM
(Page 2 of 2)

HSU Layer No [a]	HSU [b]	HSU Symbol	Dominant HGUs [c]	Dominant RMCs [d]	Typical Stratigraphic Units [e]
14	Tub Spring aquifer	TUBA	WTA	**DMP**	Tub
13	Lower tuff confining unit	LTCU	TCU	**ZEOL**	Tmrh, Tp, Th, Tw, Tc, Tn, Tub, Ton2, Ton1, To, Tlt
			TCU	**DMP**	Tcb
			TCU	**ZEOL**	Tc,Tbg,Tn4,Tn3
12	Pre-Tbg lava-flow aquifer 1	PRETBG_1	LFA	**DMP**	Tue
11	Oak Spring Butte confining unit	OSBCU	TCU	**ZEOL**	Ton2
			TCU	**DMR**	Toy
			TCU	**ZEOL**	Ton1
			TCU, lesser WTA	**DMP**	Tor
			TCU	**ZEOL**	To
			TCU	**DMP** minor ZEOL	Tot
			TCU	**ZEOL**	To, Tlt
10	Argillic tuff confining unit	ATCU	TCU	**ARG**	To, Tlt
4	Volcaniclastic confining unit	VCU	**AA,** minor TCU	**DMP**, minor ZEOL, SC, DMP-C	Tgp, Tgw
1	Mesozoic granite confining unit	MGCU	GCU	**DMR**	Kgc, Kgg
9	Lower clastic confining unit - thrust plate 1	LCCU1	CCU	**SC**	Cc, CZ, CZw, Zs
8	Lower carbonate aquifer - thrust plate	LCA3	CA	**CC**	Dg through Cc
7	Lower clastic confining unit - thrust plate 2	LCCU2	CCU	**SC**	Cc, CZ, CZw, Zs
6	Upper carbonate aquifer	UCA	CA	**CC,** lesser SC	PPt
5	Upper clastic confining unit	UCCU	CCU	**ARG**, minor SC	MDc
			CCU	**SC**	MDe
3	Lower carbonate aquifer	LCA	CA	**CC**	Dg through Cc
2	Lower clastic confining unit	LCCU	CCU	**SC,** lesserCC	Cc, CZ, Czw, Zs, Zj

[a] Layer in the EV® HFM. Refer to BN (2006) for description of the Yucca Flat 3-D HFM.
[b] See Table 4-2 for explanation of HSU nomenclature.
[c] Dominant HGU in bold. See Table 4-3 in BN (2006) for explanation of HGU nomenclature.
[d] Dominant RMC in bold. See Table 4-4 for explanation of RMC nomenclature.
[e] See Tables 4-1 and 4-2 in BN (2006) for explanation of stratigraphic nomenclature.

NA - Unit not differentiated as a separate HSU in the EV® HFM.

4.2.1 Data Compilation and Data Transfer

All data used in the quantitative analyses are from the Yucca Flat/Climax Mine HFM area; see Appendix D and the associated dataset referenced in Section D.4.0.

4.2.2 Playa Confining Unit

As shown in Figure 4-1, there are three playa deposits within the Yucca Flat model area: Yucca Lake, at the south end of Yucca Flat; Papoose Lake, on the east side of the Halfpint Range; and an unnamed playa located in the southern part of west Emigrant Valley (Slate et al., 1999). The playa deposits are mainly argillic silt but also contain interbeds of sand and pumice. The playa deposits behave as confining units because of the abundance of silt and clay (Winograd and Thordarson, 1975). Because the playa deposits all have surficial exposures and are separated areally by typical alluvium, they have the same designation (PCUT in Table 4-2) in the HFM. The spatial relationship of the PCUT and the AA is shown in Figure 4-9.

Polygonal desiccation cracks are commonly found on dry surfaces of the playas, indicating significant amounts of clay are present. This is consistent with mineralogic analyses from Yucca Lake playa deposits, which typically include more than 30 percent clay in the form of smectite and lesser kaolinite (PCUT in Table 4-6). Other reactive mineral constituents include calcite, mica, and zeolite. The bedded nature of playa deposits is reflected in the occurrence of intervals with only minor amounts of clay (Appendix D). These intervals probably represent cleaner deposits of silt and fine-grained sand.

A local occurrence of playa deposits is intercalated within alluvium in the subsurface of southern Yucca Flat just north of Yucca Lake (interbedded playa unit [IDP] in Table 4-6). Although these deposits are included within the AA, they are probably related to Yucca Lake playa deposition. They are generally less clay-rich, which may indicate more interbeds of cleaner silt and sand at this location. Although the mineralogic data presented in Table 4-6 and Appendix D are from Yucca Flat, reactive mineral characteristics of all three PCUTs are assumed to be similar.

Overall, the PCUT is categorized as an ARG RMC because of the high amounts of clay present. However, intervals of cleaner sands and silts are present within playa deposits. Such deposits represent intercalated intervals of DMP with lesser amounts of ZEOL and ARG.

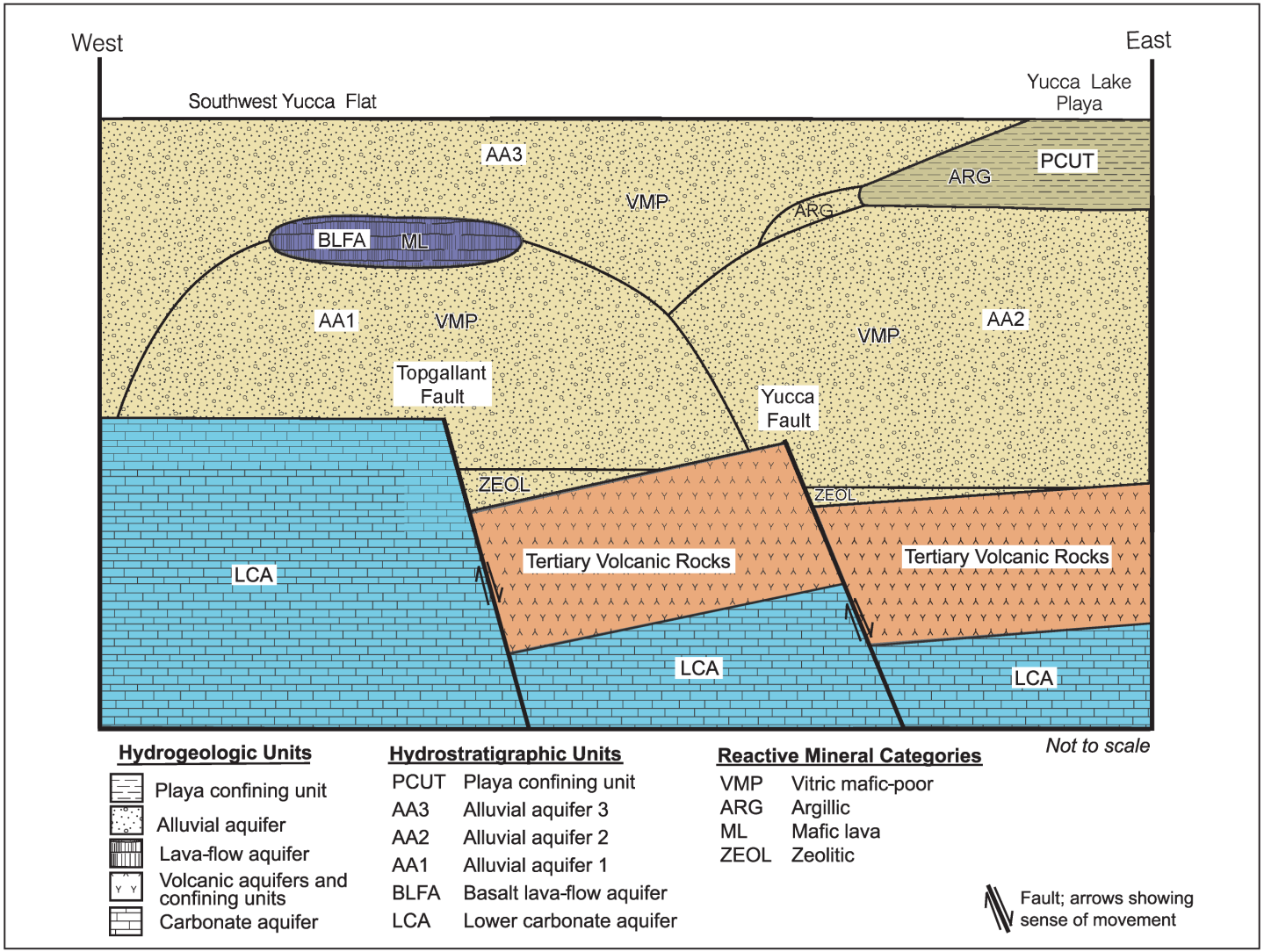

Source: Modified from Figure 4-4 in BN, 2006

Figure 4-9
Schematic Cross Section Showing Relationships Among the Hydrostratigraphic Units and Reactive Mineral Categories for the Alluvium, Playa, and Basalt in Southern Yucca Flat

Table 4-6
Summary of XRD Analyses of Whole Rocks for Hydrostratigraphic Units in the Yucca Flat/Climax Mine HFM Area
(Page 1 of 6)

HSU	Reactive Minerals					Other Minerals							
AA - Typical													
	Zeolite	SM	CC+DM	MI	HM	GL	OP	CR	TR	QZ	HN	FS	KA
Mean	9.9	7.3	7.1	6.2	0.3	15.6	7.3	4.0	0.1	23.2	1.0	26.2	1.1
SD	13.4	10.1	8.0	9.3	0.6	18.9	3.7	6.0	0.8	18.0	1.6	14.0	1.7
Minimum	0.0	0.0	0.0	0.0	0.0	0.0	2.5	0.0	0.0	1.7	0.0	0.0	0.0
Maximum	65.5	89.0	45.0	39.0	2.5	71.0	21.6	35.0	4.6	80.0	10.0	80.0	7.0
Count	164	160	154	157	16	142	57	102	32	160	111	160	101
AA - Altered													
	Zeolite	SM	CC+DM	MI	HM	GL	OP	CR	TR	QZ	HN	FS	KA
Mean	27.1	19.2	8.1	0.9	0.0	4.6	6.6	4.7	2.1	15.4	0.7	27.5	0.0
SD	26.0	24.4	14.1	1.2	0.0	10.5	6.0	3.7	2.9	11.3	1.2	13.9	0.0
Minimum	0.0	0.0	0.0	0.0	0.0	0.0	2.5	0.0	0.0	2.5	0.0	9.0	0.0
Maximum	92.5	87.5	60.0	3.0	0.0	45.0	25.0	16.0	4.1	46.0	5.0	58.0	0.0
Count	72	72	69	62	2	47	16	34	2	48	43	48	27
PCUT (Playa)													
	Zeolite	SM	CC+DM	MI	HM	GL	OP	CR	TR	QZ	HN	FS	KA
Mean	2.8	20.6	12.6	6.9	NM	8.3	4.8	4.4	NM	20.5	NM	17.8	14.5
SD	5.5	20.4	13.8	4.6	N/A	8.8	3.2	9.8	N/A	11.8	N/A	11.9	6.9
Minimum	0.0	0.0	2.5	0.0	N/A	0.0	2.5	0.0	N/A	0.0	N/A	2.5	7.0
Maximum	19.0	60.0	46.0	15.0	N/A	25.0	7.0	22.0	N/A	35.0	N/A	40.0	25.0
Count	12	12	12	12	0	12	2	5	0	12	0	12	6
IDP (Interbedded playa)													
	Zeolite	SM	CC+DM	MI	HM	GL	OP	CR	TR	QZ	HN	FS	KA
Mean	7.3	17.6	6.0	5.8	2.5	22.5	8.5	NM	0.0	17.0	2.5	10.7	3.7
SD	3.2	4.6	2.1	3.3	N/A	7.2	5.1	N/A	0.0	5.5	0.0	4.0	2.4
Minimum	2.5	10.0	2.5	2.5	2.5	10.0	2.5	N/A	0.0	10.0	2.5	2.5	2.5
Maximum	15.0	25.0	9.5	15.0	2.5	40.0	15.0	N/A	0.0	30.0	2.5	15.0	10.0
Count	20	20	20	20	1	20	20	0	4	20	3	20	17

Table 4-6
Summary of XRD Analyses of Whole Rocks for Hydrostratigraphic Units in the Yucca Flat/Climax Mine HFM Area
(Page 2 of 6)

HSU	Reactive Minerals					Other Minerals							
TM-UVTA													
	Zeolite	SM	CC+DM	MI	HM	GL	OP	CR	TR	QZ	HN	FS	KA
Mean	8.9	10.9	11.5	2.2	0.2	26.8	0.6	3.4	1.6	13.0	0.2	32.8	0.4
SD	16.6	17.3	19.9	5.0	0.2	25.8	1.1	5.4	3.2	10.4	0.3	23.6	1.2
Minimum	0.0	0.0	0.0	0.0	0.0	0.0	0.0	0.0	0.0	1.6	0.0	3.0	0.0
Maximum	61.0	61.3	68.0	21.0	0.4	76.1	2.5	19.5	6.4	41.0	1.0	80.0	4.0
Count	18	18	13	17	4	14	7	13	4	16	9	16	11
TM-WTA - Typical													
	Zeolite	SM	CC+DM	MI	HM	GL	OP	CR	TR	QZ	HN	FS	KA
Mean	2.2	4.9	0.7	1.5	0.1	15.4	3.1	28.8	NM	12.2	0.2	38.6	0.0
SD	6.2	8.1	2.3	2.5	0.1	21.2	5.4	27.5	N/A	9.8	0.4	19.3	0.0
Minimum	0.0	0.0	0.0	0.0	0.0	0.0	0.0	0.0	N/A	0.0	0.0	14.0	0.0
Maximum	25.0	35.0	12.5	10.0	0.3	70.0	15.0	81.0	N/A	37.5	1.0	75.0	0.0
Count	40	38	33	38	5	36	8	35	0	39	19	39	19
TM-WTA - Altered													
	Zeolite	SM	CC+DM	MI	HM	GL	OP	CR	TR	QZ	HN	FS	KA
Mean	11.9	28.9	0.0	0.0	NM	44.2	3.0	5.9	0.0	6.0	0.0	11.9	0.0
SD	25.7	18.1	0.0	0.1	N/A	25.4	N/A	7.1	N/A	3.3	0.0	7.8	0.0
Minimum	0.0	0.0	0.0	0.0	N/A	0.0	3.0	1.0	0.0	0.0	0.0	5.5	0.0
Maximum	69.5	53.0	0.0	0.3	N/A	62.0	3.0	17.5	0.0	9.0	0.0	25.0	0.0
Count	7	7	5	7	0	5	1	5	1	6	4	6	4
TM-LVTA - Typical													
	Zeolite	SM	CC+DM	MI	HM	GL	OP	CR	TR	QZ	HN	FS	KA
Mean	3.7	6.8	0.7	1.6	0.1	50.0	5.5	3.5	0.0	11.4	0.9	25.4	0.1
SD	11.6	11.5	3.2	3.8	0.3	29.4	9.8	7.9	0.2	14.5	2.0	19.3	0.8
Minimum	0.0	0.0	0.0	0.0	0.0	0.0	0.0	0.0	0.0	0.0	0.0	0.0	0.0
Maximum	75.0	90.0	39.1	30.0	1.0	100.0	57.0	52.0	1.7	100.0	12.5	90.0	5.0
Count	312	307	277	291	37	294	59	223	51	287	222	301	208

Table 4-6
Summary of XRD Analyses of Whole Rocks for Hydrostratigraphic Units in the Yucca Flat/Climax Mine HFM Area
(Page 3 of 6)

HSU	Reactive Minerals					Other Minerals							
TM-LVTA - Argillic (Area 8)													
	Zeolite	SM	CC+DM	MI	HM	GL	OP	CR	TR	QZ	HN	FS	KA
Mean	1.0	62.2	4.7	1.3	0.0	12.0	1.3	1.3	0.0	4.7	0.9	18.1	3.2
SD	3.9	21.2	6.5	1.3	N/A	16.2	1.8	1.9	N/A	3.3	1.2	13.3	2.6
Minimum	0.0	25.0	0.0	0.0	0.0	0.0	0.0	0.0	0.0	0.9	0.0	2.5	0.0
Maximum	15.0	92.0	20.0	2.5	0.0	42.0	2.5	4.0	0.0	10.0	2.5	40.0	7.0
Count	15	15	9	10	1	8	2	4	1	7	4	7	5
UTCU													
	Zeolite	SM	CC+DM	MI	HM	GL	OP	CR	TR	QZ	HN	FS	KA
Mean	65.1	1.8	0.0	1.7	NM	1.4	7.4	0.4	0.0	11.4	0.0	18.5	0.0
SD	28.7	2.1	0.0	2.2	N/A	1.3	3.5	0.9	N/A	19.1	N/A	23.4	N/A
Minimum	9.0	0.0	0.0	0.0	N/A	0.0	2.5	0.0	0.0	2.0	0.0	2.5	0.0
Maximum	92.0	7.0	0.0	7.0	N/A	2.5	10.0	2.0	0.0	58.0	0.0	84.0	0.0
Count	11	11	5	10	0	11	4	5	1	8	1	11	1
TSA - Typical													
	Zeolite	SM	CC+DM	MI	HM	GL	OP	CR	TR	QZ	HN	FS	KA
Mean	7.3	0.0	0.0	1.9	NM	0.0	NM	26.7	0.0	34.3	0.0	29.3	2.0
SD	9.3	0.0	0.0	4.9	N/A	0.0	N/A	13.6	N/A	16.7	0.0	12.0	3.5
Minimum	0.0	0.0	0.0	0.0	N/A	0.0	N/A	9.0	0.0	15.0	0.0	10.0	0.0
Maximum	20.0	0.0	0.0	13.0	N/A	0.0	N/A	45.0	0.0	55.0	0.0	42.0	6.0
Count	7	7	7	7	0	6	0	7	1	7	3	7	3
TSA - Zeolitic													
	Zeolite	SM	CC+DM	MI	HM	GL	OP	CR	TR	QZ	HN	FS	KA
Mean	64.8	1.7	0.0	1.5	NM	1.9	9.0	11.0	0.0	20.0	0.0	17.8	0.0
SD	17.0	1.4	N/A	1.5	N/A	1.3	1.7	7.8	N/A	N/A	N/A	13.9	N/A
Minimum	39.0	0.0	0.0	0.0	N/A	0.0	7.0	2.0	0.0	20.0	0.0	2.5	0.0
Maximum	80.0	2.5	0.0	3.0	N/A	2.5	10.0	16.0	0.0	20.0	0.0	35.0	0.0
Count	6	3	1	4	0	4	3	3	1	1	1	6	1

Table 4-6
Summary of XRD Analyses of Whole Rocks for Hydrostratigraphic Units in the Yucca Flat/Climax Mine HFM Area
(Page 4 of 6)

HSU	Reactive Minerals					Other Minerals							
TUBA													
	Zeolite	SM	CC+DM	MI	HM	GL	OP	CR	TR	QZ	HN	FS	KA
Mean	0.0	2.4	0.0	0.0	0.0	11.9	0.0	13.8	0.0	24.2	0.0	49.5	0.0
SD	0.0	3.4	N/A	0.0	N/A	N/A	N/A	5.3	N/A	18.9	N/A	17.0	0.0
Minimum	0.0	0.0	0.0	0.0	0.0	11.9	0.0	10.0	0.0	10.8	0.0	37.5	0.0
Maximum	0.0	4.8	0.0	0.0	0.0	11.9	0.0	17.5	0.0	37.5	0.0	61.5	0.0
Count	2	2	1	2	1	1	1	2	1	2	1	2	2
LTCU													
	Zeolite	SM	CC+DM	MI	HM	GL	OP	CR	TR	QZ	HN	FS	KA
Mean	55.1	6.5	0.8	2.3	0.3	7.6	8.4	1.8	1.0	6.8	0.7	21.0	0.0
SD	21.3	7.6	3.3	3.0	0.8	15.6	5.7	3.5	2.6	6.6	1.4	12.3	0.1
Minimum	0.0	0.0	0.0	0.0	0.0	0.0	0.0	0.0	0.0	0.0	0.0	0.0	0.0
Maximum	95.0	67.0	43.0	30.0	2.5	95.0	42.3	30.0	11.2	60.0	11.0	76.0	0.7
Count	626	610	415	550	121	321	300	234	34	486	252	479	175
OSBCU													
	Zeolite	SM	CC+DM	MI	HM	GL	OP	CR	TR	QZ	HN	FS	KA
Mean	39.1	10.7	0.3	2.5	0.1	4.2	8.4	3.0	0.2	11.2	0.4	27.9	0.2
SD	26.1	14.7	1.0	3.8	0.5	10.4	5.5	6.0	1.4	12.1	1.2	16.3	1.6
Minimum	0.0	0.0	0.0	0.0	0.0	0.0	0.0	0.0	0.0	0.0	0.0	0.0	0.0
Maximum	93.0	100.0	11.3	35.0	2.5	55.0	26.3	62.0	9.0	62.5	9.0	81.0	15.0
Count	373	371	283	351	74	238	143	268	40	347	215	348	203
OSBCU - Zeolitic tuffs													
	Zeolite	SM	CC+DM	MI	HM	GL	OP	CR	TR	QZ	HN	FS	KA
Mean	42.8	11.3	0.2	2.5	0.1	4.6	8.7	2.3	0.3	9.1	0.4	25.6	0.3
SD	24.8	15.3	0.8	3.9	0.5	10.9	5.4	4.0	1.5	10.1	1.1	14.7	1.7
Minimum	0.0	0.0	0.0	0.0	0.0	0.0	0.0	0.0	0.0	0.0	0.0	0.0	0.0
Maximum	93.0	100.0	5.0	35.0	2.5	55.0	26.3	37.5	9.0	50.0	9.0	71.0	15.0
Count	333	331	246	311	69	209	137	231	36	307	186	308	180

Table 4-6
Summary of XRD Analyses of Whole Rocks for Hydrostratigraphic Units in the Yucca Flat/Climax Mine HFM Area
(Page 5 of 6)

HSU	Reactive Minerals					Other Minerals							
OSBCU - Ash-flow tuffs													
	Zeolite	SM	CC+DM	MI	HM	GL	OP	CR	TR	QZ	HN	FS	KA
Mean	7.9	5.0	0.3	2.2	0.3	1.2	1.2	7.3	0.0	27.4	0.7	45.8	0.0
SD	12.0	5.4	1.9	3.0	0.3	4.1	2.9	11.9	0.0	14.0	1.8	16.9	0.0
Minimum	0.0	0.0	0.0	0.0	0.0	0.0	0.0	0.0	0.0	1.0	0.0	17.5	0.0
Maximum	43.0	17.5	11.3	13.0	0.7	17.0	7.0	62.0	0.0	62.5	7.0	81.0	0.0
Count	40	40	37	40	5	29	6	37	4	40	29	40	23
ATCU													
	Zeolite	SM	CC+DM	MI	HM	GL	OP	CR	TR	QZ	HN	FS	KA
Mean	5.0	40.4	3.6	1.3	0.9	2.7	0.6	0.6	2.0	27.0	0.1	19.2	4.1
SD	13.6	24.2	9.9	1.6	1.7	10.8	2.0	1.5	4.5	23.5	0.5	12.9	11.7
Minimum	0.0	0.0	0.0	0.0	0.0	0.0	0.0	0.0	0.0	2.0	0.0	0.0	0.0
Maximum	80.0	91.4	62.5	6.0	7.0	49.0	7.0	8.0	12.0	98.0	2.0	68.0	60.0
Count	56	56	50	55	17	40	23	50	11	52	27	51	28
MGCU													
	Zeolite	SM	CC+DM	MI	HM	GL	OP	CR	TR	QZ	HN	FS	KA
Mean	0.3	9.8	1.0	11.7	0.1	0.0	0.0	0.1	0.0	19.6	0.8	54.3	0.0
SD	0.5	5.3	1.4	5.9	0.2	0.0	0.0	0.0	0.0	11.2	1.2	8.1	0.0
Minimum	0.0	2.5	0.0	5.9	0.0	0.0	0.0	0.1	0.0	2.9	0.0	49.6	0.0
Maximum	1.0	15.2	2.6	20.0	0.3	0.0	0.0	0.1	0.0	26.7	2.5	66.5	0.0
Count	4	4	3	4	3	3	3	3	3	4	4	4	3
UCCU													
	Zeolite	SM	CC+DM	MI	HM	GL	OP	CR	TR	QZ	HN	FS	KA
Mean	0.0	13.0	2.7	11.7	0.0	0.0	0.0	0.0	0.0	53.8	0.2	7.9	6.8
SD	0.0	20.2	2.3	13.5	0.0	0.0	0.0	0.0	0.0	19.2	0.7	5.3	6.7
Minimum	0.0	0.0	0.0	0.0	0.0	0.0	0.0	0.0	0.0	25.0	0.0	0.0	0.7
Maximum	0.0	48.2	7.3	35.0	0.0	0.0	0.0	0.0	0.0	79.0	2.5	17.4	21.0
Count	13	13	12	13	10	12	10	12	10	13	13	12	13

Table 4-6
Summary of XRD Analyses of Whole Rocks for Hydrostratigraphic Units in the Yucca Flat/Climax Mine HFM Area
(Page 6 of 6)

HSU	Reactive Minerals					Other Minerals							
UCCU - Eleana Fm.													
	Zeolite	SM	CC+DM	MI	HM	GL	OP	CR	TR	QZ	HN	FS	KA
Mean	0.0	3.7	3.7	16.6	0.0	0.0	0.0	0.0	0.0	59.7	0.0	11.1	1.7
SD	0.0	8.2	2.0	11.5	0.0	0.0	0.0	0.0	0.0	14.3	0.0	3.9	1.1
Minimum	0.0	0.0	1.5	4.3	0.0	0.0	0.0	0.0	0.0	42.8	0.0	7.2	0.7
Maximum	0.0	22.2	7.3	30.1	0.0	0.0	0.0	0.0	0.0	76.0	0.0	17.4	3.1
Count	7	7	7	7	7	7	7	7	7	7	7	7	7
UCCU - Chainman Shale													
	Zeolite	SM	CC+DM	MI	HM	GL	OP	CR	TR	QZ	HN	FS	KA
Mean	0.0	23.8	1.4	5.9	0.0	0.0	0.0	0.0	0.0	47.0	0.4	3.5	12.6
SD	0.0	25.2	2.1	14.3	0.0	0.0	0.0	0.0	0.0	23.2	1.0	3.4	5.6
Minimum	0.0	0.0	0.0	0.0	0.0	0.0	0.0	0.0	0.0	25.0	0.0	0.0	7.3
Maximum	0.0	48.2	5.0	35.0	0.0	0.0	0.0	0.0	0.0	79.0	2.5	9.0	21.0
Count	6	6	5	6	3	5	3	5	3	6	6	5	6
LCA													
	Zeolite	SM	CC+DM	MI	HM	GL	OP	CR	TR	QZ	HN	FS	KA
Mean	0.0	0.0	98.9	0.0	0.0	NM	0.0	0.0	0.0	1.6	0.0	0.0	0.0
SD	0.0	0.0	3.5	0.0	N/A	N/A	N/A	0.0	N/A	5.0	N/A	0.0	N/A
Minimum	0.0	0.0	88.8	0.0	0.0	N/A	0.0	0.0	0.0	0.0	0.0	0.0	0.0
Maximum	0.0	0.0	100.0	0.0	0.0	N/A	0.0	0.0	0.0	15.8	0.0	0.0	0.0
Count	10	10	10	10	1	0	1	10	1	10	1	10	1

Notes
Refer to Table 4-2 for explanation of HSUs.
See Appendix D for entire XRD dataset and an explanation of the XRD measurement process.
No XRD data are available for the LVTA BRA, BRCU, PRETBG1, VCU, LCA3, LCCU, LCCU1, LCCU2 and UCA HSUs.
Only two samples that may not be representative are available for the BRCU HSU.

Abbreviations
CC+DM - Calcite and dolomite combined
CR - Cristobalite
FS - Feldspars (combined)
GL - Glass
HM - Hematite
HN - Hornblende
KA - Kaolinite
MI - Mica (includes biotite and illite)
N/A - Not applicable
NM - Not measured
OP - Opal
QZ - Quartz
SD - Standard deviation
SM - Smectite clay
TR - Tridymite

4.2.3 Alluvial Aquifer

The alluvium in Yucca Flat is a poorly consolidated mixture of debris eroded from the surrounding highlands of Tertiary-age silicic volcanic and Paleozoic-age sedimentary rocks, and ranging in particle size from clay to boulders. Sediment deposition is largely in the form of alluvial fans formed from debris flows, sheetwash, and braided streams that coalesce to form discontinuous, gradational, and poorly sorted deposits. Eolian sands, rare basalt flows, and playa deposits are also present within the alluvium section. The playa and basalt flows are addressed as separate HSUs in the model. The alluvium thickness in the Yucca Flat model area generally ranges from about 50 m (164 ft) to more than 800 m (2,625 ft) in south-central Yucca Flat (BN, 2006; Drellack and Thompson, 1990; Wagoner and Richardson, 1986).

Because the water table in the study area is typically greater than 500 m (1,640 ft) deep, the alluvium is generally unsaturated, except in the deep subbasins of central and southern Yucca Flat. However, the water level in West Emigrant Valley is relatively shallow, at approximately 76 m (250 ft) below the ground surface; therefore, the alluvium in the northeastern corner of the HFM is mostly saturated.

The mineralogy of the alluvium mainly reflects the lithologic composition of the constituent clasts. Although typically tuffaceous, it may also contain a significant percentage of carbonate clasts (e.g., limestone and dolomite). Volcanic clasts will contribute feldspars, quartz, and mafic minerals of biotite, hornblende, and magnetite, which may be oxidized to hematite. The mafic minerals are generally present in very small amounts, approximately on the order of 1 percent. The volcanic fragments may also contribute significantly, but usually less than 10 to 20 percent of zeolite and clay minerals are present, although some clay minerals may be of sedimentary origin. Disseminated calcite from alluvial, eolian, and diagenic processes is also common.

Mineralogy of the alluvium varies laterally and vertically reflecting the lithologic composition of the source rocks and depositional processes. In general, the older (i.e., deeper) alluvium in Yucca Flat tends to be more tuffaceous, while the upper portion of the alluvium may be relatively carbonate-rich with up to 25 percent limestone and/or dolomite. Alluvium east of the Topgallant fault in southern Yucca Flat is also more carbonate rich. Rayburn et al. (1989) mapped out these areas of more carbonate-rich alluvium for southern Yucca Flat, and Wagoner and McKague (1984) subdivided the alluvium in northern Yucca Flat into a lower tuffaceous alluvium and an upper mixed alluvium. The

alluvium in Area 8 around the BANEBERRY underground test is more argillic than alluvium in other areas of Yucca Flat. Also, in portions of Areas 2, 4, and 9, the lower portion of the alluvium is partially zeolitized (see the "Partial Zeolitization" alternative in Appendix C of this document, or Section 5.0 in BN, 2006).

Reactive minerals within typical Yucca Flat alluvium include zeolite, clay, carbonate, and mica in mean percentages ranging from 6 to 10 percent (AA in Table 4-6). In Area 8, where the alluvium is more argillic, and in Areas 2, 4, and 9, where the base of the alluvium is partially zeolitized, zeolite and clay are considerably more abundant and mica is substantially less abundant than typical Yucca Flat alluvium (AA-Altered in Table 4-6).

Overall, the three AA HSUs (AA1, AA2, and AA3) can be classified as a VMP RMC reflecting relatively low mean percentages of the reactive minerals zeolite, clay and mica. In portions of Areas 2, 4, 8, and 9, where percentages of zeolite and clay are greater, the alluvium can be locally categorized as an ARG RMC (part of Area 8) or a ZEOL RMC (portions of Areas 2, 4, and 9).

4.2.4 Basalt Lava-Flow Aquifer

At least two basalt flows have been identified within the alluvium section in southwestern Yucca Flat in drill holes UE-1h and UE-1j (Fernald et al., 1975). The flows are apparently limited in areal extent. The thickness of basalt ranges from 12.2 m (40 ft) at drill hole UE-1j to 76.2 m (250 ft) at UE-1h. These basalt flows are above the water table.

Several basalt flows and dikes are mapped in the northern Halfpint Range on the east side of Yucca Flat (Byers and Barnes, 1967; Barnes et al., 1965). These are generally above the water table as well. A mafic-rich intrusive rock in the form of a diabase dike was encountered within saturated pre-Tertiary carbonate rocks between the depths of 743.7 to 765.0 m (2,440 to 2,510 ft) in exploratory hole UE-7h on the east side of Yucca Flat (Drellack and Thompson, 1990; Gonzales et al., 1982). Consequently, some interaction between the groundwater and mafic-rich intrusive rocks in this area is presumed. The basalt flow(s) are modeled as a separate HSU designated BLFA (Table 4-2). The relationship of the BLFA to other alluvial HSUs is shown in Figure 4-9.

Clinopyroxene and olivine can be relatively abundant, with lesser clinopyrene in basalts around Yucca Flat; while biotite, hematite, and orthopyroxene occur in lesser amounts (Warren et al., 2003). Smectite may be present in weathered portions of basalt, while calcite, opal, and zeolite may be present in vesicles (SNJV, 2005b). There are no XRD data specific to the BLFA. However, based on detailed lithologic descriptions and petrographic data, the RMC for the BLFA is ML (Tables 4-4 and 4-5).

4.2.5 Timber Mountain Upper Vitric-Tuff Aquifer

The upper portion of the volcanic section directly below the alluvium in much of Yucca Flat is composed of the Timber Mountain Group. The TM-UVTA is defined to include the nonwelded to partially welded, nonzeolitized ash-flow and bedded tuff of the younger Ammonia Tanks Tuff (Tma), which lie above the TM-WTA (see Section 4.2.6). These rocks are included in the laterally more extensive TM-LVTA (see Section 4.2.7) where the TM-WTA is not present; that is, where the Rainier Mesa Tuff (Tmr) is less than 76 m (250 ft) thick, and thus no welded horizon has developed (see Figure 4-7 in BN, 2006, for an example of this configuration). The TM-UVTA may locally include devitrified moderately welded Tma. The spatial relationships of the three Timber Mountain HSUs and other volcanic HSUs are shown in Figure 4-10. The TM-UVTA is of minor importance hydrogeologically because it is limited in lateral extent and generally unsaturated. It is saturated only in the deepest subbasins of central and southern Yucca Flat. The mineralogy of the TM-UVTA reflects the lithology of the Tma in Yucca Flat, which consists of nonwelded to moderately welded, rhyolitic ash-flow tuff. These rocks contain abundant phenocrysts of sanidine, quartz, and sodic plagioclase, with much less abundant biotite and clinopyroxene, and accessory sphene, zircon, and apatite (Warren et al., 2003).

The reactive minerals zeolite, clay, carbonate, and mica (i.e., biotite) typically occur in relatively low percentages in the TM-UVTA, reflecting the unaltered and mafic-poor character of these volcanic rocks (Table 4-6). In many places at the NTS, the Tma can be divided into a mafic-rich (Tmar) upper part and a mafic-poor (Tmap) lower part based on the abundance of mafic minerals such as biotite and clinopyroxene. Within most of Yucca Flat, however, Tmar is rare.

Based on the low percentages of the reactive minerals zeolite, clay, carbonate, and mica, and the abundance of glass, the TM-UVTA is categorized as a VMP RMC. But, as shown in Table 4-5, the

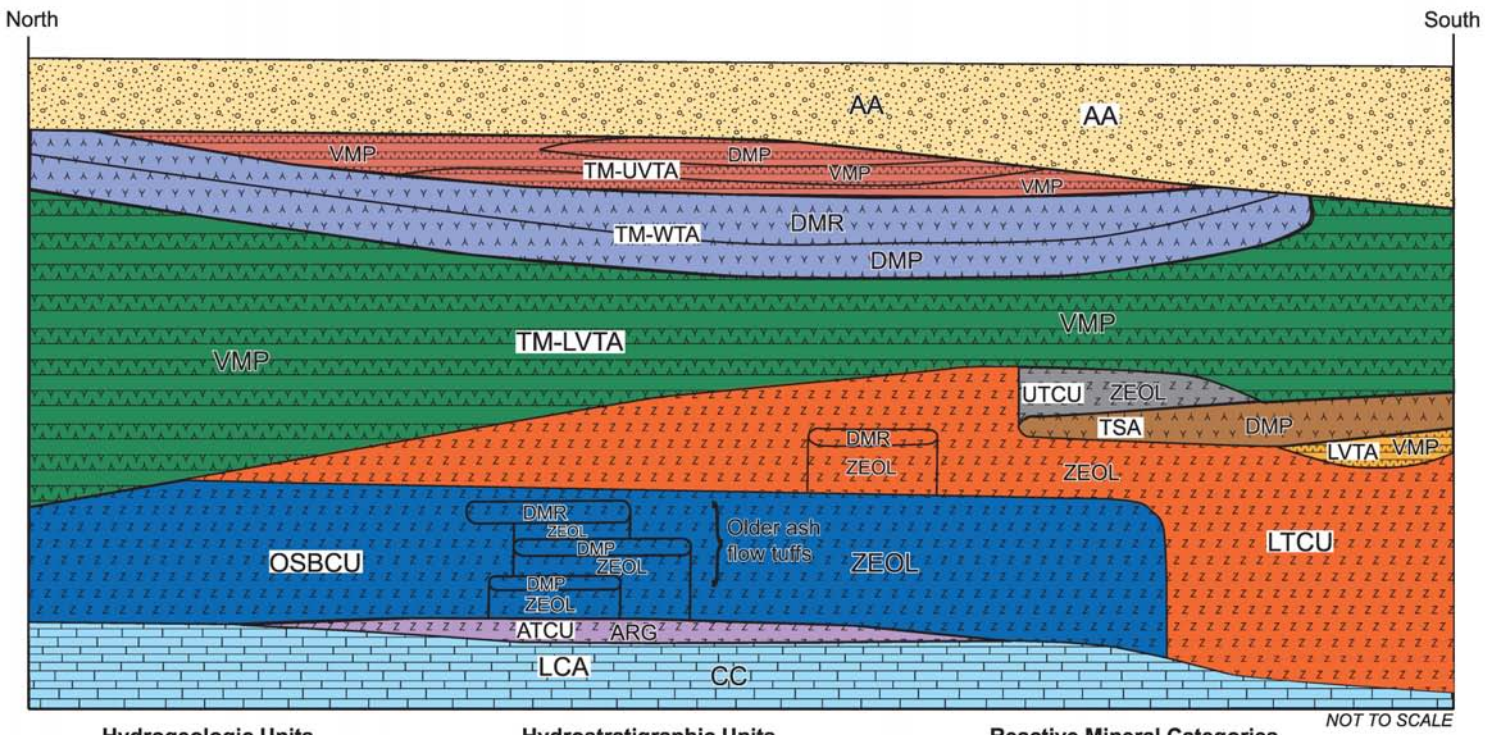

Hydrogeologic Units

- Alluvial aquifer
- Welded-tuff aquifer
- Vitric-tuff aquifer
- Tuff confining unit
- Carbonate aquifer

Hydrostratigraphic Units

AA	Alluvial aquifer
TM-UVTA	Timber Mountain upper vitric-tuff aquifer
TM-WTA	Timber Mountain welded-tuff aquifer
TM-LVTA	Timber Mountain lower vitric-tuff aquifer
UTCU	Upper tuff confining unit
TSA	Topopah Spring aquifer
LVTA	Lower vitric-tuff aquifer
LTCU	Lower tuff confining unit
OSBCU	Oak Spring Butte confining unit
ATCU	Argillic tuff confining unit
LCA	Lower carbonate aquifer

Reactive Mineral Categories

AA	Alluvium
VMR	Vitric mafic-rich
DMP	Devitrified mafic-poor
VMP	Vitric mafic-poor
DMR	Devitrified mafic-rich
ZEOL	Zeolitic
ARG	Argillic
CC	Carbonate

Figure 4-10
Schematic North-South Cross Section Showing Relationships of Hydrostratigraphic Units and Reactive Mineral Categories for the Volcanic Rocks in the Yucca Flat/Climax Mine HFM

welded Tmap would be classified as a DMP, and the less common Tmar would be classified as a VMR RMC.

4.2.6 Timber Mountain Welded-Tuff Aquifer

The TM-WTA consists mostly of devitrified welded ash-flow tuff and lesser amounts of vitric (i.e., unaltered) nonwelded ash-flow tuff, bedded tuff, and vitrophyre. Stratigraphically, this HSU typically includes only the Tmr, but may also include the Tma, where the Tma consists of a significant thickness of welded tuff. In most places, the Tma is separated from the underlying Tmr by a 1.5- to 9.1-m (5- to 30-ft)-thick bedded tuff member, called the bedded Ammonia Tanks Tuff (Tmab). The Tmab is typically vitric and slightly calcareous, although a couple of samples are argillic. Like the Tma, the Tmr can usually be divided into a mafic-rich upper member (Tmrr) and a mafic-poor lower member (Tmrp).

The TM-WTA is not an extensive HSU, being generally confined to the south-central portion of the basin east of the Topgallant fault, where Tmr is thickest. In Yucca Flat, TM-WTA is saturated only in the deeper subbasins.

Reactive minerals within the TM-WTA are typically rare, reflecting the devitrified welded tuff lithology that results in a rock composed mostly of microcrystalline quartz and feldspar (Table 4-6). Consequently, the TM-WTA is categorized as a DMR RMC where the Tmrr is present and a DMP RMC where the Tmrp occurs.

Fracture-filling minerals in the TM-WTA, as reported in various lithologic log, include silica, calcite, clay, and possibly zeolite (e.g., Davies et al., 1982; Prothro et al., 1999; Cavazos et al., 1987). Whole rock mineralogy (XRD data) is summarized in Table 4-6. The XRD dataset for the TM-WTA is not large because its welded character is too hard to be easily sampled using typical sidewall sampling tools. Because of the small sample population, the averages may be skewed due to several anomalous samples. The samples identified as anomalous are typically from altered zones (ZEOL or ARG) often related to faults or near formation contacts (TM WTA-Altered in Table 4-6) as determined from cuttings, boring and geophysical logs, and display mineralogic characteristics related to alteration not representative of welded tuffs in general. Sampling bias in the database was discussed in Section 4.2.

4.2.7 Timber Mountain Lower Vitric-Tuff Aquifer

The TM-LVTA includes all unaltered ash-fall tuff, reworked tuff, and nonwelded ash-flow tuff present above the level of pervasive zeolitization in Frenchman and Yucca Flats. Where welded Topopah Spring Tuff (Tpt) is present (Tpt is a formation within the Tp and forms the TSA), unaltered nonwelded tuffs below the TSA are grouped within a separate HSU called the LVTA (see Section 4.2.10). Stratigraphically, the TM-LVTA may include formations and members of the Timber Mountain Group (Tm), Paintbrush Group (Tp), Calico Hills Formation (Th), Wahmonie Formation (Tw), Crater Flat Group (Tc), Grouse Canyon Tuff (Tbg), and Tunnel Formation (Tn). Older volcanic units are typically zeolitized or argillized, and are therefore categorized as confining units and placed within the LTCU, OBSCU, or ATCU (see Section 4.2.11). Welded tuffs of the Tm are included in the TM-WTA, as described in Section 4.2.6.

The TM-LVTA has a much wider distribution than the TM-WTA. Some TM-LVTA rocks are present beneath the alluvium throughout the eastern two-thirds of Yucca Flat, although this unit is absent in areas where it has been removed by erosion over major structural highs. These include the area west of the Topgallant fault in southern Yucca Flat, the Buried Ridge in west-central Yucca Flat (Figure 4-4), and the margins of the valley in northern Yucca Flat. The relationship of the TM-LVTA with other volcanic HSUs is shown in Figure 4-10.

In Yucca Flat, the TM-LVTA units are saturated in the deep central portion of the basin. The TM-LVTA exhibits significant interstitial porosity, ranging from about 20 to 40 percent (Wagoner and McKague, 1984; Burkhard, 1989; App and Marusak, 1997). However, because these lithologies tend to be poorly to moderately indurated, fractures are not common. So, even though interstitial porosity may be high, transmissivities are not great.

Reactive minerals are typically rare in the TM-LVTA owing to its unaltered character (Table 4-6). Therefore, the TM-LVTA is categorized as a VMP RMC (Table 4-5). In the southern portion of Area 8, however, the TM-LVTA is argillic (Appendix D and TM-LVTA Argillic in Table 4-6). At this location, the TM-LVTA is categorized as ARG. The XRD dataset for the TM-LVTA is fairly representative of the natural variability in the mineralogy of this unit, but it also contains several anomalous samples. These anomalous samples are typically altered horizons and are often related to

weathered zones, contacts, or faults. Anomalous samples are identified in the XRD dataset (Appendix D) and were not included in the analysis.

4.2.8 Upper Tuff Confining Unit

The zeolitized nonwelded tuffs that overlie the Tpt in southern Yucca Flat are designated as the UTCU (Table 4-2). Stratigraphically, the UTCU may include units from the top of the welded Tpt (i.e., TSA) to the base of the welded Tmr (i.e., TM-WTA). The areal extent of the UTCU is limited in the Yucca Flat basin, occurring only beneath the southern portion of the basin (BN, 2006). Where the TSA is not present but zeolitic rocks stratigraphically equivalent to the UTCU are present, the zeolitic rocks are assigned to the LTCU, (see Section 4.2.11.1). The spatial relationships of the UTCU and other volcanic HSUs are shown in Figures 4-7 and 4-10. The UTCU is mostly saturated in the Yucca Flat/Climax Mine HFM.

The UTCU averages 65 percent zeolite (Table 4-6). Other reactive minerals are relatively low in abundance. Because of the dominance of zeolite minerals in the UTCU, the RMC is ZEOL. The hydrogeologic and mineralogic properties of the two tuff confining units (UTCU and LTCU) are considered to be essentially identical.

Prothro (1998) conducted an analysis of fractures in core from the tuff confining units in Yucca Flat. Prothro (1998) noted that almost all natural fractures observed were either coated or filled with some type of secondary mineral, and that zeolite and metallic oxides (e.g., iron and manganese oxides) were the two most common minerals. Typical fracture-filling and fracture coating minerals for the UTCU and LTCU in Yucca Flat include zeolite, metallic oxides, crystalline quartz and chalcedony, calcite, and clay.

4.2.9 Topopah Spring Aquifer

The TSA consists of a single welded-tuff aquifer composed of welded ash-flow tuff of the Yucca/Frenchman Flat lobe of the Topopah Spring Tuff (Tpt in Table 4-2). The Tpt in Yucca Flat is a devitrified densely to moderately welded ash-flow tuff. There is a characteristic 5-m-thick black, glassy vitrophyre near the top. A lithophysal zone below the vitrophyre is also common. The lithophysal cavities are generally lined with euhedral cristobalite, tridymite, and feldspar crystals.

The TSA is highly transmissive but is limited in areal extent. The TSA can be more than 100 m (332 ft) thick in southern Yucca Flat, but the unit thins to the north, to the east in the Halfpint Range, and to the south in CP basin and northern Frenchman Flat. The TSA is absent west of the Topgallant fault where the volcanic strata have been either eroded away or were never deposited (i.e., over the Buried Ridge). The unit is saturated in the deeper south-central portion of Yucca Flat (BN, 2006). The relationship of the TSA to other volcanic HSUs is shown in Figure 4-10.

Reactive minerals are rare in the TSA (Table 4-6). This reflects the high degree of devitrification characteristic of the Tpt in Yucca Flat, which yields a rock that is predominantly composed of felsic minerals. Therefore, the TSA is categorized as a DMP RMC. At some locations in southern Yucca Flat, however, the relatively thin nonwelded to partially welded basal portion of the TSA may be zeolitic. For these minor occurrences, the basal zeolitic portion is categorized as a ZEOL RMC (TSA Zeolitic in Table 4-6). The XRD dataset for the welded portion of the TSA is not large (Appendix D) because, like the TM-WTA, its highly welded character is not easily sampled using sidewall sampling tools. Therefore, in order to obtain accurate mineralogy for the TSA, averages for minerals were calculated separately for the welded TSA (i.e., TSA-Typical) and the basal zeolitic portion (i.e., TSA Zeolitic).

Fracture-filling minerals in the TSA, as reported in various lithologic logs include quartz, calcite, clay and possibly zeolite (e.g., Cavazos et al., 1987). Whole rock mineralogy (XRD data) for the TSA is given in Table 4-6.

4.2.10 Lower Vitric-Tuff Aquifer

The LVTA includes all unaltered ash-fall, reworked, and nonwelded ash-flow tuffs below the TSA and above the level of pervasive zeolitization in Frenchman and Yucca Flats (Table 4-2; BN, 2004 and 2006). The LVTA is only differentiated where the TSA is present; these rocks would otherwise be included in the TM-LVTA (Figure 4-10). Stratigraphically, the LVTA may include formations and members of the Calico Hills Formation (Th), Wahmonie Formation (Tw), and Crater Flat Group (Tc). Older volcanic units are generally zeolitized, and are therefore categorized as confining units and assigned to the LTCU.

The LVTA has a distribution similar to the TSA. However, the LVTA is not present beneath portions of south-central Yucca Flat because stratigraphically equivalent units are zeolitic, and thus assigned to confining unit HSUs. The LVTA is unsaturated.

There are no XRD analyses specifically of the LVTA rocks in the Yucca Flat dataset. However, a portion of the TM-LVTA contains similar unaltered stratigraphic units. Given the known mineralogy for the stratigraphic ash-fall tuff units in this HSU, the dominant RMC is the VMP. Chemistry and mineralogy attributes for the TM-LVTA (as presented in Appendix D and summarized in Table 4-6) may be used as a first approximation for the LVTA.

4.2.11 Lower Tuff Confining Units

Altered volcanic rocks that compose the lower portion of the volcanic section beneath Yucca Flat form an important hydrogeologic unit that separates the alluvial and volcanic aquifer units from the underlying regional LCA. Stratigraphically, these altered volcanic rocks may include all the Tertiary volcanic strata from the top of the Paleozoic rocks to the base of the welded portions of the Tmr (i.e., TM-WTA). In Yucca Flat, these altered tuff units are subdivided into three tuff confining unit HSUs based on the relative abundances of major mineral assemblages (Prothro, 2005). These HSUs are: (1) an upper zone characterized by the abundance of the zeolite mineral clinoptilolite with lesser amounts of felsic minerals and clay, designated the LTCU; (2) a middle zone with felsic minerals greater than zeolites and much greater than clay, designated the OSBCU; and (3) a basal argillic zone where clay is dominant over felsic minerals and clinoptilolite, designated the ATCU.

These confining units are generally present in the eastern two-thirds of Yucca Flat, east of the Carpetbag and Topgallant faults. They are absent over the major structural highs, where the volcanic rocks have been removed by erosion, or were never deposited. Areas where the volcanic confining units are absent include the “Paleozoic bench” west of the Topgallant fault in southern Yucca Flat, and over the Buried Ridge in the west-central portion of the basin. In northern Yucca Flat, the volcanic confining units tend to be confined to the deeper structural subbasins. Outside the subbasins and around the edges of Yucca Flat the volcanic rocks are thinner and are not always zeolitized, and thus are grouped within the TM-LVTA. Outside the Yucca Flat basin, where subsurface data are scarce to absent, the altered volcanic rocks are not subdivided but are simply designated as the LTCU.

The LTCU, OSBCU, and ATCU are typically saturated; however, measured transmissivities are very low (SNJV, 2006c).

Prothro (1998) conducted an analysis of fractures in core from altered volcanic rocks beneath Yucca Flat, and noted that almost all natural fractures were coated or filled with some type of secondary mineral, with many fractures containing more than one type of secondary mineral. Typical fracture-filling and coating minerals include zeolite, metallic oxides, crystalline quartz and chalcedony, calcite, and clay. Prothro (1998) reported that zeolite was observed in 48 percent of the fractures examined, and metallic oxides were observed in 37 percent of the fractures. Of the metallic oxides, iron oxides appeared to be the most common, with manganese oxide being less common.

Additional mineralogical and isotopic details for altered tuffs beneath Yucca Flat are available in Dickerson et al. (2004). These investigators used micrographic (SEM-EDS) and isotope ratio analytical methods to characterize secondary minerals occurring in both the rock matrix and fractures. The secondary minerals identified, in approximate order of decreasing abundance, are clinoptilolite, illite/smectite, erionite/mordenite, alkali feldspar, silica, calcite, analcime, and secondary manganese and iron oxides.

Whole rock mineralogy for the LTCU, OSBCU, and ATCU is summarized in Table 4-6. It is useful to note that the sampling protocols in place during the weapons testing program preferentially sampled the more altered horizons. Consequently, the dataset for these HSUs may be skewed toward higher clay values.

4.2.11.1 Lower Tuff Confining Unit

The uppermost of the three tuff confining units in Yucca Flat is the LTCU. Beneath Yucca Flat, the LTCU includes all zeolitic tuffs from the base of the Tub Spring Tuff (Tub) to the base of the welded Tmr (i.e., TM-WTA), outside the lateral extent of the welded Tpt (i.e., TSA). As mentioned previously, all zeolitic volcanic rocks around the margins of Yucca Flat that are generally outside the area of drill-hole control and are typically unsaturated, are grouped within the LTCU. The LTCU is thick and extensive beneath Yucca Flat east of the Carpetbag and Topgallant faults, where it is typically saturated. The LTCU generally correlates to the ZC zone (dominated by the zeolite mineral clinoptilolite with lesser amounts of felsic minerals and clay minerals) of Prothro (2005).

Zeolite is the major mineral component of the LTCU (Table 4-6). Other reactive minerals are typically rare. Because of the high zeolite content, the LTCU is categorized as a ZEOL RMC.

4.2.11.2 Oak Spring Butte Confining Unit

The OSBCU consists of all volcanic units from the base of the Tub (i.e., base of the LTCU) down to the top of pervasive argillization (i.e., top of the ATCU). Most of the volcanic units within this section are assigned to the Volcanics of Oak Spring Butte and consist mostly of zeolitic nonwelded tuff, but also include several intercalated devitrified to weakly zeolitized, nonwelded to partially welded, ash-flow tuff deposits. Stratigraphically, these older ash-flow tuffs are assigned to the Yucca Flat Tuff (Toy), Redrock Valley Tuff (Tor), and Tuff of Twin Peaks (Tot), all formations of the Volcanics of Oak Spring Butte. Because these ash-flow tuff units were devitrified soon after deposition, there was little glass to be converted to zeolite. The OSBCU was created to address the hydrogeologic and mineralogic variability these older, devitrified ash-flows impart to an otherwise zeolitic interval. The OSBCU generally correlates to the FS zone (felsic minerals are dominant over clinoptilolite and clay minerals) of Prothro (2005). The lateral extent of the OSBCU is similar to that of the LTCU. The OSBCU is typically saturated.

The OSBCU has a relatively high zeolite content, with an average abundance of 39 percent (Table 4-6), and is therefore categorized, like the LTCU, as a ZEOL RMC. However, the presence of several weakly zeolitized to devitrified ash-flow tuffs within the OSBCU, results in a zeolite content lower than the LTCU. Other reactive minerals are generally rare, although clay is present with an average abundance of 11 percent and mica 2.5 percent. The intercalated ash-flow tuffs consist predominately of felsic minerals (OSBCU Ash-flow tuffs in Table 4-6) and thus are categorized as DMP or DMR depending on the mafic content of each ash-flow tuff unit. In summary, the diverse lithologies included in the OSBCU are manifested by the presence of several RMCs in the dataset; primarily ZEOL with lesser DMR, and DMP representing the older ash-flow tuffs, Toy, Tor, and Tot (Figure 4-10).

4.2.11.3 Argillic Tuff Confining Unit

The ATCU includes pervasively argillized volcanic and volcaniclastic deposits that typically occur at the base of the volcanic section in Yucca Flat. The ATCU is characterized by an abundance of clay,

moderate amounts of felsic minerals, and a general absence of zeolites (Prothro, 2005). The ATCU directly overlies pre-Tertiary sedimentary rocks, and includes the stratigraphically distinct paleocolluvium.

The ATCU is present beneath Yucca Flat east of the Carpetbag and Topgallant faults and in the western subbasin of Areas 2 and 4. The HSU is typically saturated. The ATCU correlates to the AR zone (clay minerals are dominant over felsic minerals and clinoptilolite) of Prothro (2005).

The ATCU is characterized by high clay and low zeolite content (Table 4-6). Thus, the ATCU is categorized as an ARG RMC. In some areas, the paleocolluvium, typically included within the ATCU, contains abundant carbonate clasts. Several analyses in Appendix D have high carbonate content and likely represent samples of paleocolluvium.

4.2.12 Belted Range Aquifer

The BRA consists of a single WTA composed of peralkaline, welded ash-flow tuff of the Tbg. Beneath Yucca Flat, the Tbg is an ash-fall tuff. In northern Yucca Flat, where the Tbg is vitric, it is included in the TM-LVTA. In southern Yucca Flat, where the Tbg is zeolitized, it is included with the LTCU. However, in the Belted Range just north of Yucca Flat, the Tbg is a highly welded ash-flow tuff (i.e., a WTA HGU). The BRA HSU was established to address this mappable HGU. The relationship of the BRA with other units is shown in Figure 4-11. The unit is typically unsaturated. The BRA is a peralkaline ash-flow tuff and is mineralogically classified as a DMP RMC because of the characteristic high felsic mineral content of devitrified ash-flow tuffs and the absence of biotite in the Tbg. The Yucca Flat XRD dataset does not contain any samples specifically from the BRA. However, the BRA in the Rainier Mesa and Pahute Mesa HFMs is the same extra-caldera ash-flow sheet; thus, XRD data from these CAUs would be applicable for the Yucca Flat/Climax HFM. Fracture-filling minerals in the BRA, as reported in various lithologic logs, include quartz, calcite, clay, and possibly zeolite (e.g., Maldonado et al., 1979).

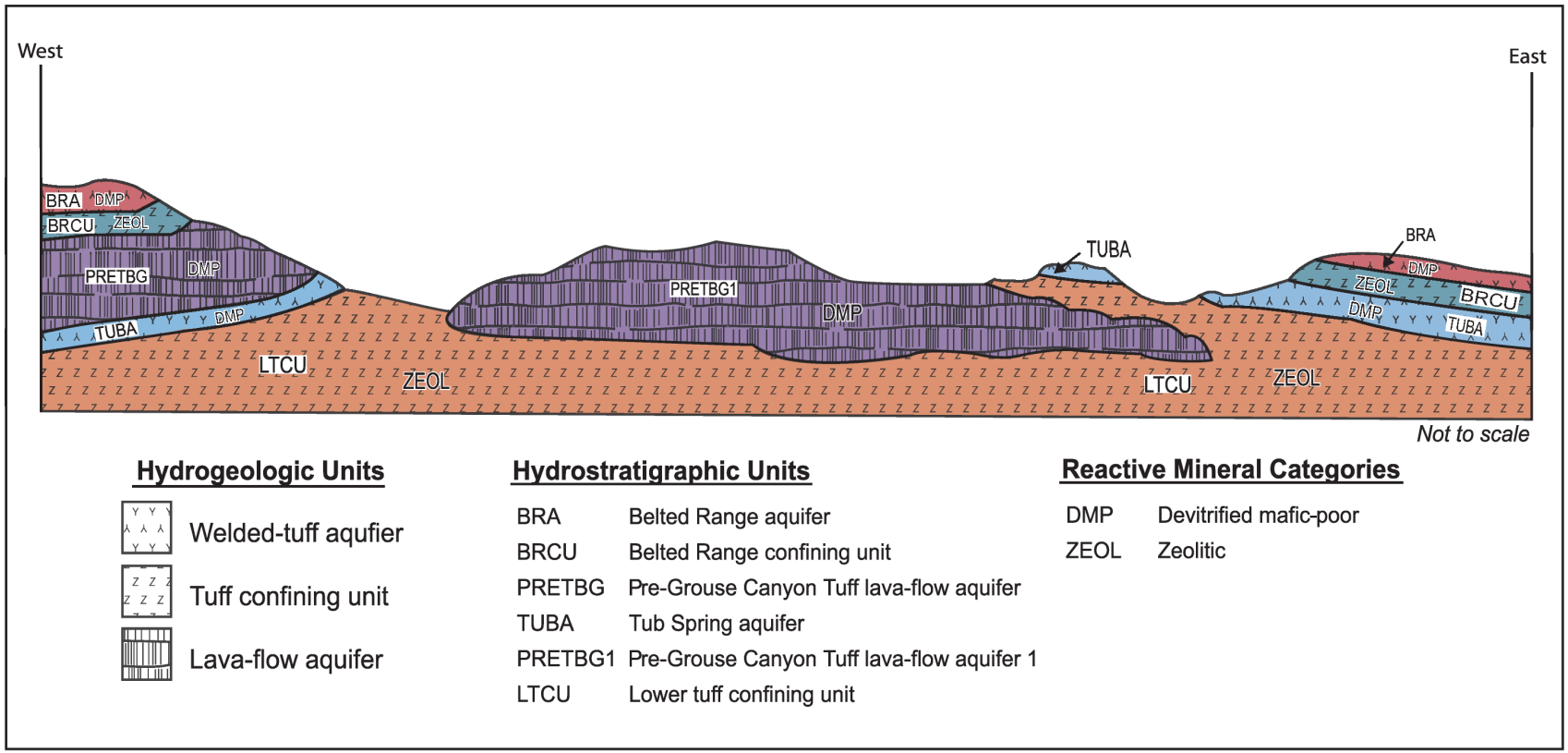

Source: Modified from Figure 4-23 in BN, 2006

Figure 4-11
Schematic West-East Cross Section Showing Relationships of Hydrostratigraphic Units and Reactive Mineral Categories for the Belted Range and Older Volcanic Rocks in Northern Yucca Flat

4.2.13 Belted Range Confining Unit

The BRCU generally consists of zeolitized bedded and nonwelded tuffs that occur between the welded ash-flow tuff lithofacies of the Tbg (i.e., BRA) and the underlying Tub (i.e., TUBA), or above the pre-Tbg LFA (PRETBG in Section 4.2.14) where the Tub is absent. The upper part of this unit is locally vitric, but the unit is usually unsaturated. Beyond the extents of the PRETBG, BRA, and TUBA, the rocks that compose the BRCU are grouped with the LTCU. Hydrologically, this TCU would behave similarly to the UTCU and the LTCU. The relationship of the BRCU with other HSUs in the northern portion of the model area is shown in Figure 4-11.

The mineralogic dataset for the Yucca Flat/Climax Mine HFM includes two BRCU samples, and both of these are of questionable quality (Appendix D). Consequently, statistical analysis of BRCU reactive mineralogy is impossible. The BRCU, however, is composed of zeolitic tuffs similar to the LTCU and thus is categorized as a ZEOL RMC. Any mineralogic data for the BRCU from the Rainier Mesa/Shoshone Mountain HFM area would also be applicable to the Yucca Flat/Climax Mine area. Mineralogic data from the approximate stratigraphic interval (i.e., Tn4 and Tn3) within the larger LTCU dataset from Yucca Flat could also be used to approximate the BRCU.

4.2.14 Pre-Grouse Canyon Tuff Lava-Flow Aquifer (PRETBG and PRETBG1)

The PRETBG and PRETBG1 consist of peralkaline lava flows extruded in the area north of Yucca Flat before the eruption of the Tbg ash-flow tuff. These HSUs consist of several separate local lava flows. The PRETBG and PRETBG1 are not extensive HSUs, being generally confined to the northwestern portion of the model area (Figure 4-26 in BN, 2006). Stratigraphically, the PRETBG is between the Tbg and the Tub (i.e., BRA and TUBA). The PRETBG1 is below the Tub (i.e., TUBA in Figure 4-11). Based on lithologic characteristics, these units are believed to be equivalent hydrogeologically except for position relative to the other HSUs. These subdivisions are necessary to satisfy operational requirements of the EV® software (Dynamic Graphics, 2002). Only a small portion of this HSU is saturated along the northern boundary of the Yucca Flat/Climax Mine model area (Figure 4-4).

The PRETBG is not represented in the Yucca Flat/Climax Mine XRD dataset. Mineralogy from the Pahute Mesa or Rainier Mesa/Shoshone Mountain datasets would be applicable, however.

4.2.15 Tub Spring Aquifer

The TUBA consists only of the devitrified, welded portion of the Tub and is limited to the northern Yucca Flat area, where it can be up to 90 m (300 ft) thick. The TUBA is a fairly extensive HSU in West Emigrant Valley and in the northwestern corner of the model area (Figure 4-27 and Profile B-B' in BN, 2006), but it is saturated only in the deeper basins of the area. Based on its welded tuff lithology, its hydraulic properties are similar to those of the BRA and the TM-WTA.

The TUBA is a devitrified, welded ash-flow tuff, and thus is mineralogically categorized as a DMP RMC. Although only two analyses of TUBA are available, they indicate a very high felsic mineral content characteristic of devitrified ash-flow tuffs (Table 4-6). Reactive mineral abundances are low, reflecting the devitrification and absence of mafic minerals characteristic of welded Tub. Any mineralogic data for the TUBA from the nearby Rainier Mesa/Shoshone Mountain HFM area would be applicable also to the Yucca Flat/Climax Mine area.

4.2.16 Mesozoic Granite Confining Unit

The Climax granitic stock is located at the north end of Yucca Flat and just south of Oak Spring Butte (Slate et al., 1999). This granitic body has intruded through Paleozoic-age carbonate rocks now exposed around the stock. The granite intrusion constitutes the MGCU in the hydrostratigraphic model for the area (Table 4-2). The Climax Stock is related in chemistry and age with the Gold Meadows Stock located further west and just north of Rainier Mesa.

This unit is an intrusive stock of quartz monzonite and granodiorite. Primary phenocrysts include plagioclase, potassium feldspar, quartz, and biotite, with a trace of pyrite, sphene, zircon, apatite, and iron oxides (Maldonado, 1977). Based on this mineralogy, the MGCU is classified as a DMR RMC (Table 4-5). Whole rock mineralogy (XRD data) for the MGCU is given in Table 4-6.

Fracture-filling minerals in the MGCU, as reported in various lithologic logs, include calcite, quartz, secondary feldspars, clay, chlorite, pyrite, epidote and iron oxides (Maldonado, 1977).

In addition to the bulk granite mineralogy, a variety of secondary alteration minerals due to hydrothermal alteration and contact metamorphism have been reported (Houser and Poole, 1961; Maldonado, 1977; Orkild et al., 1983). The intrusives have altered the surrounding carbonate rock to

form marble and tactite out to several hundred meters from the edge of the stock. Tactite mineralogy includes garnet, quartz, epidote, chlorite, limonite, hematite, calcite, idocrase, and lesser amounts of the pyrite copper carbonate minerals, scheclite and powellite. Historical mining at the Climax stock has yielded small amounts of tungsten, molybdenum, lead zinc, copper, and silver ore (Quade and Tingley, 1983).

Hydrothermal alteration within the stock is generally associated with deposition of veinlets and joint fillings (Orkild et al., 1983). This group of secondary minerals includes clays, chlorite, secondary feldspar, sericite, quartz, epdiote, pyrite, chalcopyrite, limonite, and manganese (Houser and Poole, 1959).

The location, mineralogy, and intensity of the secondary alteration is quite variable, although some of the complete characterization was not undertaken for this effort.

4.2.17 Upper Carbonate Aquifer

The Tippipah Limestone in western Yucca Flat is designated the UCA. This unit is found at the surface only at Syncline Ridge, although it is believed to underlie a slightly larger area in the subsurface of the western part of Yucca Flat (BN, 2006). Surface exposures are highly deformed and fractured. This unit consists of thick limestone layers interbedded with mudstone and siltstone beds (largely silica [SiO_2]). There are no XRD data for the UCA in the Yucca Flat/Climax Mine HFM area. However, based on detailed lithologic descriptions, the UCA is predominately a CC RMC, and as noted here, there could be rare SC due to the presence of mudstone and siltstone interbeds.

Fracture-filling minerals in the UCA, as reported in various lithologic logs include mostly calcite and iron-staining, and lesser clay (Hodson and Hoover, 1978; Metcalf et al., 1999).

4.2.18 Upper Clastic Confining Unit

Upper Devonian and Mississippian siliciclastic rocks at the NTS and vicinity are assigned to the Eleana Formation and the Chainman Shale (Cashman and Trexler, 1991; Trexler et al., 1996). The Eleana Formation as originally defined by Poole et al. (1961) was partitioned by Cashman and Trexler (1991) on the basis of lithofacies variations and sediment source. The shaley lithofacies in western Yucca Flat have been assigned to the Chainman Shale, while the section bearing the

non-shaley quartzite, sandstone, and conglomeratic lithofacies retains the original formation name. Both formations are grouped into the UCCU. The UCCU is present only in the western portion of the Yucca Flat model, generally west of the Carpetbag/Topgallant fault system (BN, 2006).

The mineralogy of the UCCU varies with lithology. Rocks associated with the Eleana Formation are generally siltstone and sandstones of quartz and chert grains (SiO_2). The Eleana Formation also contains several bioclastic limestones. The Chainman Shale contains significant quartz and smectite/illite, minor feldspar and mica, lesser chlorite, and trace amounts of hematite, limonite, calcite and manganese oxide (MnO_2). The XRD dataset for the UCCU is not large; however, it does show two distinct RMCs (Appendix D). The dominant RMC for the Eleana Formation is SC. The dominant RMC for the Chainman Shale is ARG, with minor SC representing the interbedded quartzite lithologies. Whole rock mineralogy (XRD data) for the UCCU is given in Table 4-6.

Fracture-filling minerals in the UCCU, as reported in various lithologic logs (BN, 2004; Russell et al., 1996; Fernald et al., 1975) include quartz, calcite, clay and rare pyrite, and trace MnO_2.

4.2.19 Lower Carbonate Aquifer

The LCA consists of thick sequences of Middle Cambrian-age through Upper Devonian-age carbonate rocks (Table 4-2; Winograd and Thordarson, 1975; BN, 2004 and 2006). This HSU serves as the regional aquifer for most of southern Nevada, and locally may be as thick as 5,000 m (16,400 ft) (Winograd and Thordarson, 1975; Cole, 1992 and 1997).

This thick carbonate section consists mostly of limestone and dolomite, with minor chert, quartzite, and shale. Virtually all of the LCA is classified as a CC RMC, with only a few percent of the total thickness being an SC (e.g., Eureka Quartzite) and an ARG (e.g., Dunderberg Shale). Whole rock mineralogy (XRD data) for the LCA is given in Table 4-6.

Detailed information about fracture geometry and fracture-filling minerals in LCA core samples from Wells ER-6-1 and ER-6-2 in southern Yucca Flat is presented in IT (1996c). IT (1996c) found that the fractures in the LCA rocks were generally filled or lined with three types of minerals: iron oxides (limonite and hematite) including scarce MnO_2, carbonaceous clays, and carbonate minerals generally consisting of calcite with rare occurrences of dolomite. They also noted that silica cements are rare and restricted to fractures in quartzite lithologies. Another observation was that most of the

fractures are lined or filled with a combination of two or more of these materials. Many of the fractures within the upper 15 m (50 ft) of the LCA are typically filled with tuffaceous, argillic mud (e.g., BN, 2004; Davies et al., 1982).

Deformation related to the west-vergent CP thrust fault has placed older LCA rocks over younger rocks of the UCCU and LCA west of the Carpetbag/Topgallant fault system and in the northwest corner of the HFM. The position of these rocks above the UCCU requires that they be distinguishable (in the model) from the regional aquifer (LCA). These thrusted carbonate rocks, designated LCA3 (Table 4-2), are stratigraphically equivalent, and hydrogeologically and mineralogically similar to the LCA.

4.2.20 Lower Clastic Confining Unit

The Proterozoic to Middle-Cambrian rocks in the vicinity of the NTS are largely quartzite (SiO_2) and silica-cemented siltstone. Although these rocks are brittle and commonly fractured, secondary silica mineralization seems to have greatly reduced formation permeability (Winograd and Thordarson, 1975). These units make up the LCCU, which is considered to be the regional hydrogeologic basement (IT, 1996c). Where it is in a structurally high position, the LCCU may act as a barrier to deep regional groundwater flow. The present structural interpretation for Yucca Flat depicts the LCCU at great depth, except in the northeast corner of the study area. The Zabriskie Quartzite and Wood Canyon Formation, which are both classified as clastic confining units, are exposed in the northern portion of the Halfpint Range. The high structural position of the LCCU in the northern Halfpint Range may be at least partially responsible for the steep hydraulic gradient observed between western Emigrant Valley and Yucca Flat (BN, 2006).

The upper plate of both the Belted Range and CP thrust faults include these same Precambrian clastic rocks. Although these HSUs, designated LCCU1 and LCCU2, include some of the same units as the LCCU (Table 4-2; BN, 2006), their position above the younger LCA and LCA3 requires that they be distinguished from the LCCU.

As reported from outcrop descriptions and a few lithologic logs, fracture-filling minerals in the LCCU, LCCU1, and LCCU2 include quartz, calcite, and rare clay. Whole rock mineralogy (XRD data) for the LCCU is given in Table 4-6. Nearly all of the LCCU is an SC RMC, with lesser CC representing carbonate interbeds and the Noonday Dolomite.

5.0 YUCCA FLAT/CLIMAX MINE GEOCHEMISTRY

The dissolved constituents in groundwater may influence the rate and extent of molecular-level reactions between contaminants and aquifer materials. Knowledge of the groundwater chemistry is therefore important to the prediction of contaminant sorption onto rock surfaces and thus to the prediction of contaminant transport. Groundwater chemistry also provides a means for determining the origin, flow paths, and time scale of groundwater flow and transport that is independent of estimates based on hydraulic flow analysis.

This section provides a summary of a comprehensive geochemical evaluation of the groundwater flow system in the Yucca Flat/Climax Mine CAU that was performed in fiscal year (FY) 2005 and published in FY 2006 (SNJV, 2006b). An evaluation of the major and minor solute chemistry of groundwaters in this CAU is also provided. A dataset is presented that provides the supporting geochemistry data necessary for calculating K_ds using the mechanistic model approach described in Section 11.6.1. The goal is to provide data that are representative of the natural variability in water chemistry within the Yucca Flat/Climax Mine CAU. Limitations to these geochemical analyses are presented at the end of this section.

5.1 Summary of the FY 2006 Geochemical Evaluation of the Yucca Flat/Climax Mine Groundwater Flow System

The geochemical evaluation of the Yucca Flat/Climax Mine groundwater flow system described in SNJV (2006b) was a collaborative effort between LANL, LLNL, DRI, USGS, and the SNJV. The data used for the evaluation, as well as a description of all groundwater chemistry data available for this CAU in the UGTA groundwater quality database, GEOCHEM06.mdb (SNJV, 2006a) are provided in SNJV (2006c). The extent of the area included in the study is shown in Figure 5-1.

The approach for the flow path and travel time evaluations included compilation and examination of all currently available geochemical and isotopic data, construction of mixing models using conservative tracers, evaluation of the mixing models with strontium (Sr) concentration and isotopic

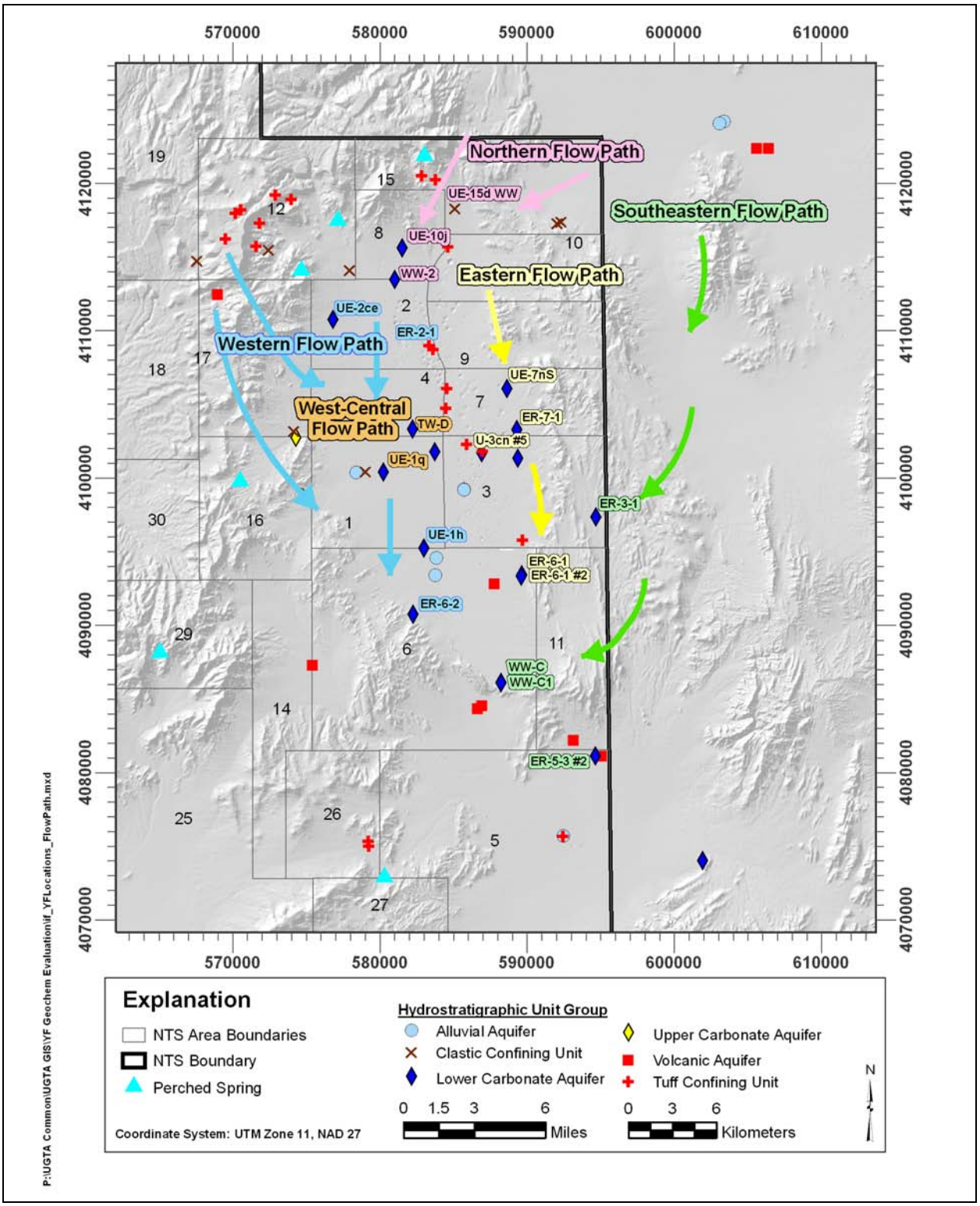

Figure 5-1
Conceptual Flow Paths Evaluated in the Yucca Flat/Climax Mine Geochemistry Study
Source: SNJV, 2006b

data, and modeling of geochemical reactions using the geochemical modeling programs PHREEQC and NETPATH. The geochemical modeling codes were also used for estimating groundwater travel times based on carbon isotope data. The basis for the geochemical modeling approach is described in the UGTA Project *Geochemistry Technical Basis Document* (Benedict et al., 2003).

The main objectives of the evaluation were to identify probable pathways for groundwater flow within the LCA and develop constraints on groundwater transit times between selected data collection sites. Although few underground tests were actually conducted in the LCA (see Section 6.5), it is considered the most important aquifer within the study area because of its hydraulic continuity with the larger regional flow system, and thus represents the most likely pathway for contaminant transport beyond the boundaries of the NTS.

The investigation began with an evaluation of the geochemical characteristics of groundwater in northern Yucca Flat and specifically addressed the proportion of groundwater inflow to Yucca Flat from outlying areas versus local recharge from the surrounding highlands. The study then investigated three conceptual groundwater flow paths within the LCA: flow from north to south along the eastern side of the Yucca Flat basin, flow from north to south along the western side of the basin, and flow entering Yucca Flat along the southeastern basin margin and moving through southern Yucca Flat to Frenchman Flat. Conceptual flow-path development was guided by previous hydrogeologic studies of the groundwater flow system together with observed trends in geochemical parameters. The separation of flow paths in the eastern and western parts of the basin is strongly inferred on the basis of observed hydraulic head relationships, the presence of major geologic structures near the center of the basin, and differences in geochemical parameters in these two areas. The isotopic and geochemical characteristics of the LCA groundwater in the west-central part of the basin were also identified as unique relative to all other LCA groundwaters within the basin. These groundwaters were therefore evaluated as a separate west-central flow path. The conceptual flow paths evaluated and the specific wells modeled for each flow path are presented in Figure 5-1.

Geochemical modeling results indicated that groundwater originating from recharge within the Yucca Flat basin is a prominent feature of the groundwater system, particularly in western Yucca Flat, where high-elevation recharge areas at Rainier Mesa, the Eleana Range, and Shoshone Mountain lie adjacent to the basin (see Figure 4-1). Locally derived recharge is also prominent in the northeastern

part of the basin, but geochemical models indicate an additional groundwater component possibly entering the basin from Emigrant Valley through low-permeability siliciclastic rocks in the Halfpint Range. Groundwater also appears to enter northern Yucca Flat along an LCA flow path near the margin of the Climax Stock; however, a lack of data for LCA groundwater north of the NTS precluded a rigorous evaluation.

Modeling results indicated that the groundwater in northern Yucca Flat moves southward along independent flow paths on the eastern and western sides of the basin. However, the models for these north-to-south flow paths were frequently non-unique, and the composition of groundwater at a given well could often be explained by mixing groundwater from more than one combination of wells. Nevertheless, the models consistently indicated that the groundwater transit times are extremely long. For example, transit times based on carbon-14 (^{14}C) of approximately 16,000 to 24,000 years were predicted for flow in the LCA from UE-10j in northern Yucca Flat to WW-C in southern Yucca Flat, resulting in estimated linear groundwater velocities of approximately 1.3 to 1.9 meters per year (m/yr) over this 30-km distance. Along a shorter path length between wells ER-7-1 and ER-6-1#2, ^{14}C derived transit times were estimated to be approximately 6,500 years, yielding a similar flow velocity of 1.7 m/yr. It is notable that recent hydraulic tests have indicated a high degree of hydraulic continuity between ER-7-1 and ER-6-1#2 (SNJV, 2005a). Hence, the long transit times suggest the groundwater flux through the LCA in Yucca Flat may be relatively small. This feature is attributed to the small inflow of groundwater into the basin from the north and the low hydraulic gradient from the north to the south within the basin (SNJV, 2006c).

Geochemical models also indicated that influx of LCA groundwater from east of Yucca Flat is not a prominent part of the groundwater system except in the southeastern part of the basin. In this area, ^{14}C derived transit times are on the order of 1,000 to 3,000 years between ER-3-1 and WW-C, and predicted groundwater flow velocities show a corresponding increase (4.3 to 13 m/yr). The increased flux of groundwater from east of the basin into the southeastern part of Yucca Flat is consistent with the absence of the LCCU in the southeast portion of the basin. Flow conditions in this part of the system appear to be more dynamic when compared to the relatively stagnant flow conditions within the upgradient parts of the Yucca Flat basin.

Wells completed in the LCA near the west-central part of the basin (e.g., TW-D and UE-1q) show potential evidence of groundwater leakage from overlying volcanic units. Although it was not possible to uniquely ascribe the observed geochemical signatures to locally derived vertical transport, it is possible that nearby faults have created localized flow paths between the volcanic and carbonate HSUs in this area.

5.2 Data Compilation and Data Transfer

5.2.1 Data Compilation

Groundwater major and minor chemistry data from wells and springs within the Yucca Flat/Climax Mine HFM boundaries (Figure 5-2) were compiled from GEOCHEM06.mdb (SNJV, 2006a). The resulting Yucca Flat/Climax Mine chemistry dataset includes samples collected over a large period of time (1957 to 2006) that were analyzed using a variety of techniques (SNJV, 2006c). The variation in sampling and analytical techniques over this time period resulted in significant variations in some measurements. The goal of the data compilation described within this section is to acquire a dataset that contains representative major and minor solute data for groundwaters of the Yucca Flat/Climax Mine HSUs, primarily for use in calculating K_ds as described in Section 11.0. The first step in the analysis was therefore to reduce the dataset so that it excludes as much of the variability due to poor sampling conditions and analysis as possible. The dataset used for the analyses is described as follows:

1. The chemical constituents included are calcium (Ca^{2+}), magnesium (Mg^{2+}), sodium (Na^{+}), potassium (K^{+}), chloride (Cl^{-}), sulfate (SO_4^{2-}), bicarbonate (HCO_3^{-}), carbonate (CO_3^{2-}), silica (SiO_2), nitrate (NO_3^{-}), bromide (Br^{-}), phosphate (PO_4^{3-}), and fluoride (F^{-}). Also included are pH and water temperature.

2. Samples with a full suite of the above parameters and a charge balance within ±5 percent are included. This criterion was relaxed if the charge balance exceeded 5 percent for all samples collected from a given location or when anomalous (or inconsistent) water chemistry is observed in the sample with a 5 percent charge balance.

3. Samples were removed if multiple outliers (outliers for multiple parameters) were present.

In addition to the parameters described above, this compilation includes the results of *in situ* measurements performed by LANL for a select number of wells within Yucca Flat. The *in situ*

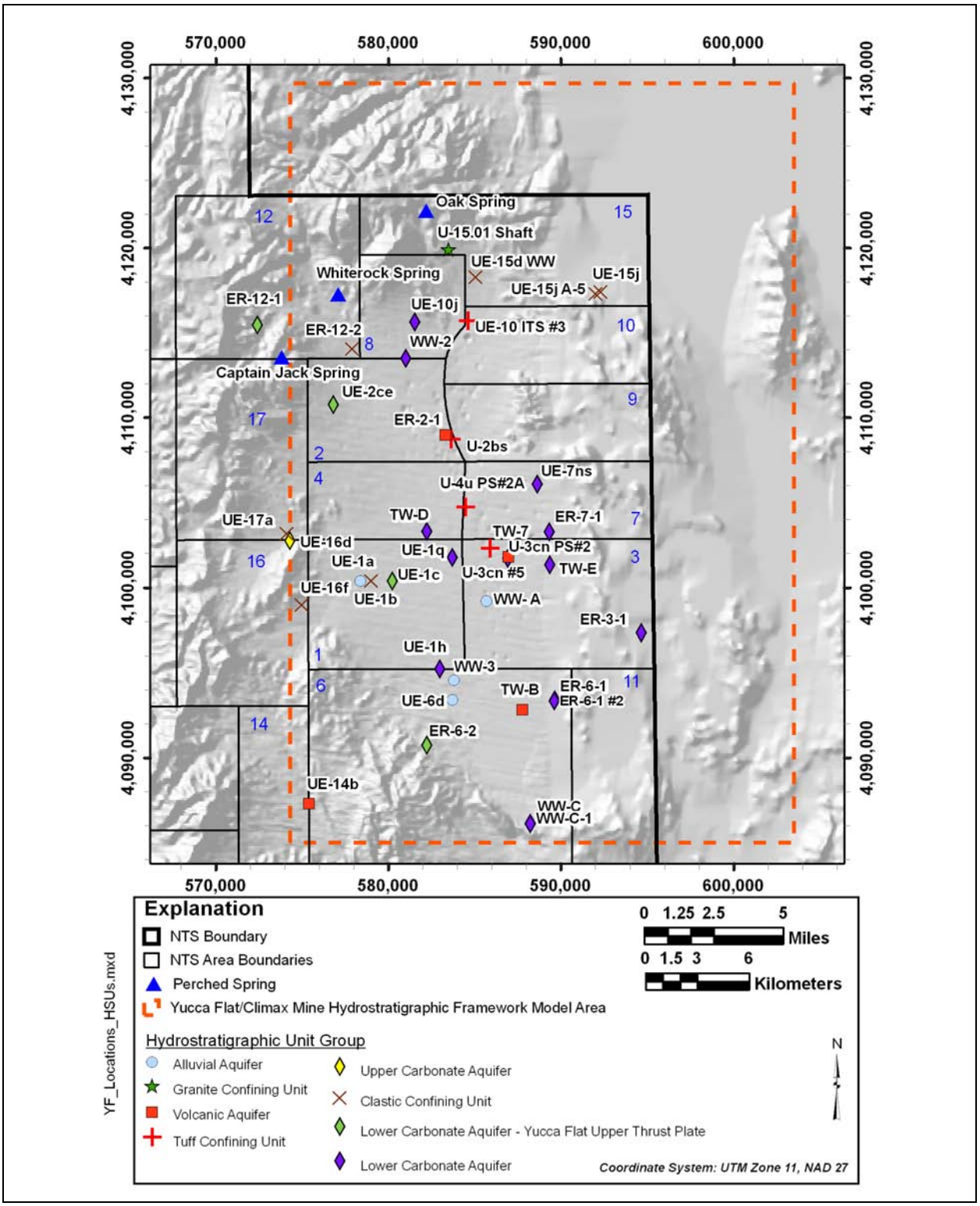

Figure 5-2
Yucca Flat/Climax Mine Geochemistry Study Area

measurements include oxidation-reduction potential (ORP), water temperature, specific conductance, and pH. These results are compiled from a series of LANL annual reports (Finnegan et al., 2004 and 2005; Finnegan and Thompson, 2002 and 2003). The calcite and dolomite saturation indices as presented in SNJV (2006b) are also presented. A positive saturation index indicates that the mineral is oversaturated, and a negative saturation index indicates undersaturation. The final dataset is presented in Appendix E.

Data documentation evaluation flags (DDE_Fs) are also provided for these data; these data documentation evaluation indicators are also reported within GEOCHEM06.mdb (SNJV, 2006a). Data quality evaluation flags (DQE_Fs) for the data used in this analysis are reported as "Level C." This indicates that the analytical result is consistent with historical or regional trends for the reported location(s); or, for a given sample, there are no anomalous results within the suite of parameters that would indicate sample contamination due to improper sample collection or erroneous laboratory procedures. This data quality indicator is included in the GEOCHEM06.mdb database as well.

5.2.2 Data Transfer

All data used in the quantitative analyses in this section are from the Yucca Flat/Climax Mine HFM area or surrounding springs; see Figure 5-2, Appendix E, and the associated dataset referenced in Section E.3.0.

5.2.3 Data Analysis

Using the dissolved constituents in groundwater, Schoff and Moore (1964), Blankennagel and Weir (1973), and Winograd and Thordarson (1975) identified three main hydrochemical water types, or facies, in NTS groundwaters. These include a Na-K-HCO_3 groundwater facies (Na^+ plus K^+ constitute at least 60 percent of the total cation concentration) commonly found in volcanic-rock aquifers, a Ca-Mg-HCO_3 facies (Ca^{2+} plus Mg^{2+} constitute at least 60 percent of the total cation concentration) commonly occurring in carbonate aquifers, and a Ca-Mg-Na-HCO_3 facies assumed to be a mixture of the Na-K-HCO_3 and Ca-Mg-HCO_3 facies (Schoff and Moore, 1964). The source of Ca^{2+} and Mg^{2+} in the groundwater of carbonate aquifers is dissolution of calcite and dolomite. Groundwater in volcanic HSUs gains Na^+ from reaction with volcanic glass and feldspar minerals.

Bicarbonate is the predominant anionic constituent in the majority of the groundwater and is derived primarily from the dissolution of soil carbon dioxide (CO_2) gas and reaction with carbonate minerals.

Piper diagrams are used within this section to classify the groundwater as a hydrochemical type; ion concentrations are expressed in percent milliequivalents per liter. A Piper diagram consists of three different component representations of major-ion chemistry. Cation (i.e., Ca^{2+}, K^+, Mg^{2+}, Na^+) and anion (i.e., Cl^-, SO_4^{2-}, HCO_3^-, and CO_3^{2-}) data are plotted in separate triangles. Both cation and anion data are then projected on to a central diamond-shaped area so that compositional relationships (such as mixing or evolutionary trends) within or between a group or groups of groundwater samples are visually presented. In addition, bar plots are used to illustrate the total concentrations of each chemical constituent; chemical concentrations are reported in units of milligram per liter (mg/L). Because of the high relative concentration of HCO_3^- compared to the other constituents in some of the groundwaters, HCO_3^- is plotted on a separate right axis for some bar plots. Error bars (mean ± 1 standard deviation [SD]) are presented on the bar plots when multiple samples have been collected from the same location.

5.2.3.1 Groundwater Chemistry Representative of Hydrostratigraphic Units

The primary HSU is assigned to each groundwater sample based on the HSU associated with either the formation access interval (FAI) or with the depth from which the discrete bailed samples were collected. Well samples included in the dataset were often collected as composites, either from wells with single completions that transect multiple HSU boundaries, or from wells with multiple completions that were all pumped simultaneously. Generally, the HSU that spans the largest portion of the formation access interval is assigned to a water sample. For those cases with large relative proportions of multiple HSUs encountered, the most transmissive unit is generally assigned.

Groundwater samples have been collected using several different techniques. Recent samples collected for the UGTA Project include both depth-discrete bailed samples and composite groundwater characterization samples. Depth-discrete bailed samples are typically collected using a wireline run discrete bailer, under pumping conditions, after flow logging is complete. The depths at which discrete bailer samples are collected are determined using flow log and temperature data, and are generally above each screened completion interval that is productive. Composite groundwater characterization samples are collected from the well-head during pumping. The sample is a

composite representative of the proportional contribution from the water-producing zone(s) in the well. During drilling operations, makeup water is tagged with lithium bromide (LiBr) as a tracer to evaluate the progress and completeness of development. A low Br^- concentration likely indicates that the well was sufficiently developed to restore groundwater quality back to its natural condition. Water discharged during well development is monitored for pH, electrical conductivity, dissolved oxygen, temperature, turbidity, and Br^- concentration. Groundwater samples are collected after these parameters have stabilized. Earlier groundwater sampling included depth-discrete bailed samples and pumped composite samples, although the sampling technique is not always reported with the GEOCHEM06.mdb database (SNJV, 2006a).

5.2.3.1.1 Alluvial Aquifer

Four wells (UE-1a, UE-6d, WW-A, and WW-3) are completed in the AA in southern Yucca Flat (Figure 5-2). The chemistry of these groundwaters range from a borderline Ca-Mg-HCO_3 type (UE-1a) to the Ca-Mg-Na-HCO_3 mixed type (WW-3) to a borderline Na-K-HCO_3 type (UE-6d and WW-A). The more recent samples from WW-A (collected between 2003 and 2005) were collected from a depth of approximately 550 m using a bailer; the earlier samples from this well (collected between 1961 and 1988) were collected during pumping while it was used as a supply well. The three bailed samples are distinguishable from all others in the Piper diagram as having a slightly greater relative proportion of Cl^- (Figure 5-3). The difference in the chemistry of the bailed versus pumped samples may reflect differences in groundwater of the deeper zone of the alluvium (sample collected using the discrete bailer) relative to the composite samples that combine groundwater from the entire length of the FAI (approximately 80-m thickness).

The groundwater chemistry of the samples of the AA are further evaluated in the bar plot presented in Figure 5-4. The concentration of the major and minor solutes are shown to be quite similar for the AA groundwaters with the exception of UE-1a. Groundwater of UE-1a has a higher concentration of HCO_3^-, Ca^{2+}, Mg^{2+}, and Cl^- and a lower concentration of SO_4^{2-} and SiO_2 more typical of water that has interacted with carbonate rocks. The pH of the AA groundwater samples (mean ± SD) are 7.8 ± 0.2, 7.9 ± 0.1, 8.0, and 8.3 for WW-A, WW-3, UE-1a, and UE-6d, respectively.

The ORP was measured *in situ* for WW-3 at depths ranging from 1,550 ft to 1,750 ft (472 m to 533 m). The groundwaters were determined to be in an oxidizing environment with the ORP ranging

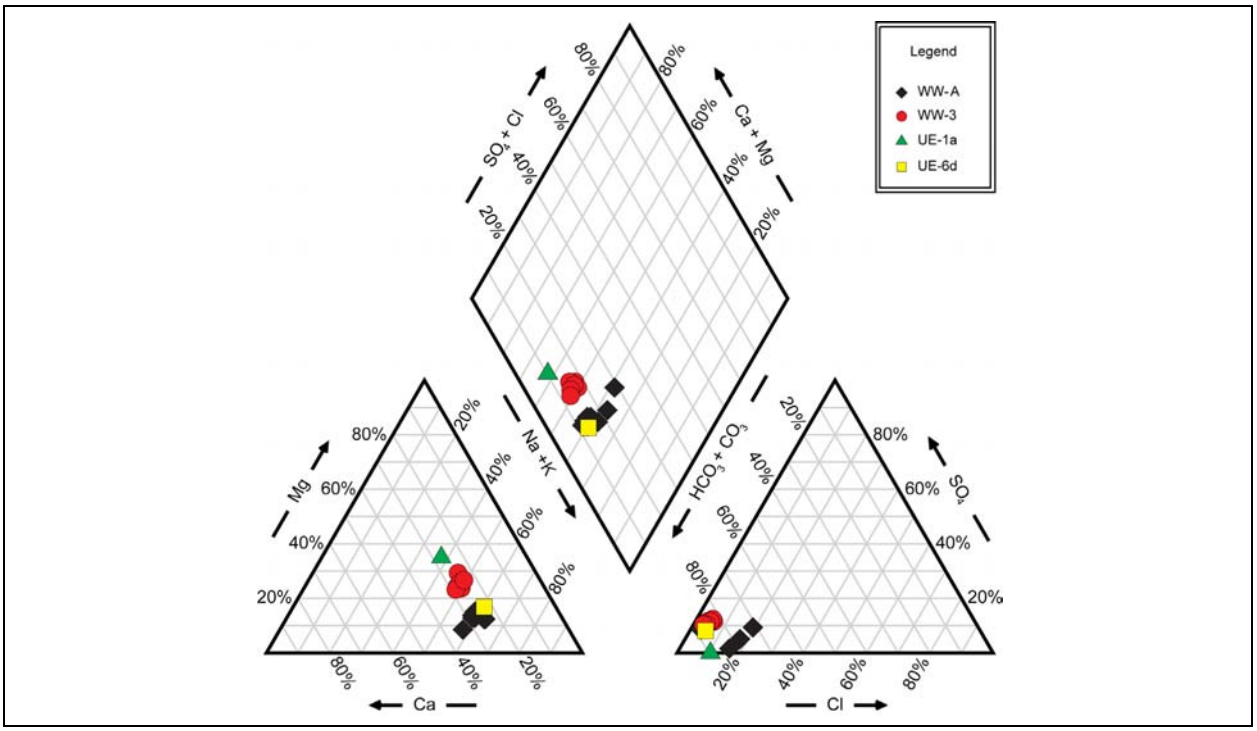

Figure 5-3
Piper Diagram for Samples Collected from the Alluvial Aquifer

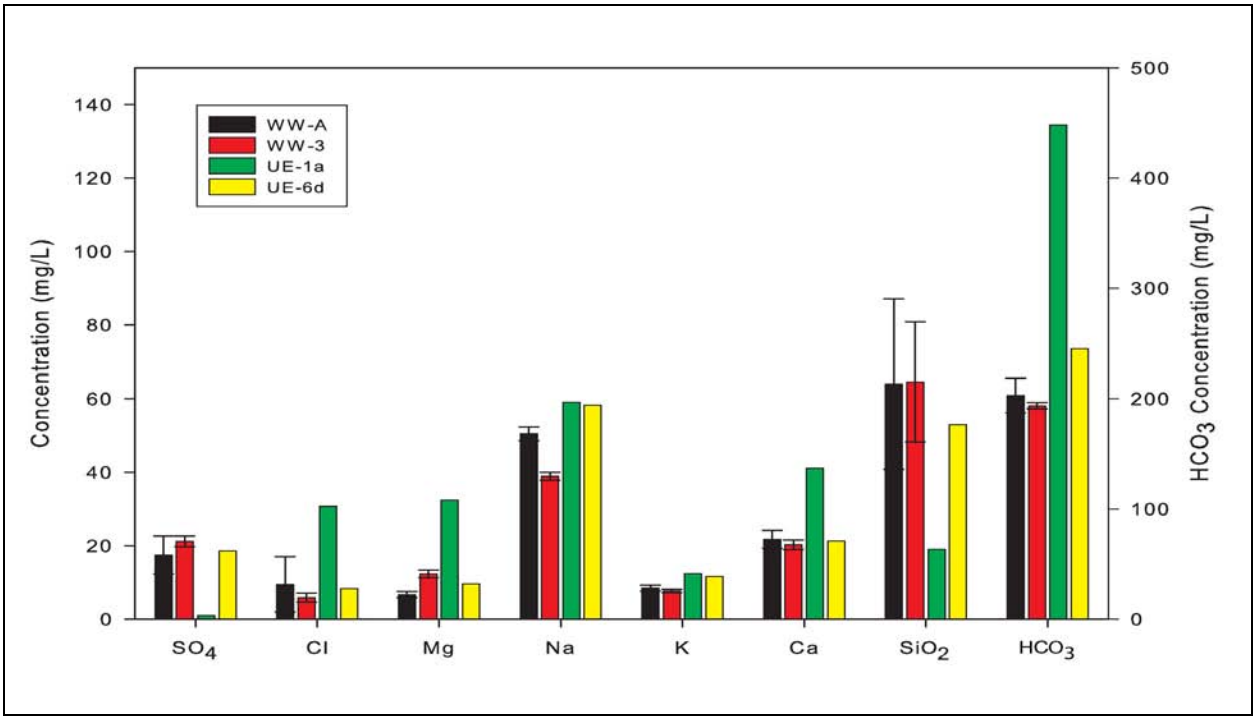

Figure 5-4
Bar Plot for Samples Collected from the Alluvial Aquifer

from 52 to 169 millivolts (mV). No correlation between ORP and well depth was observed; the range in ORP was thought to be a result of measurement variability (Finnegan et al., 2004). The *in situ* water temperatures ranged from 19.3 to 19.9 degrees Celsius (°C) and the specific conductance ranged from 0.41 to 0.42 milliSiemens per centimeter (mS/cm). No *in situ* measurements of pH were made (Finnegan et al., 2004).

The RMC associated with the AA is the VMP (see Table 4-5). As shown in Table 4-4, this RMC represents a high glass content (greater than 30 percent), low clay (less than 10 percent) and zeolite (less than 10 percent), and low biotite plus hornblende (less than 1.5 percent).

5.2.3.1.2 Volcanic-Rock Aquifers and Tuff Confining Units

The dataset is limited with respect to the number of groundwater samples from the volcanic-rock aquifers and the tuff confining units of the Yucca Flat/Climax Mine CAU. Two wells sample groundwater of the TSA (UE-14b and TW-B), four wells sample the LTCU (TW-7, U-2bs, U-3cn PS#2, and U-4u PS#2A), and one well samples the OSBCU (UE-10 ITS #3). The FAI for ER-2-1 includes a large section of both the TM-LVTA (53-m thickness) and the LTCU (80-m thickness). The groundwater of these volcanic HSUs are all the Na-K-HCO_3 type; Na^+ is the dominant cation, and HCO_3^- is the dominant anion (Figure 5-5). Relatively tight clusters are formed in the Piper diagram for most samples collected from the same well, indicating consistent sampling and analysis for the majority of the groundwaters.

The groundwater chemistry of the well, J-13, is also presented in Figures 5-5 and 5-6. Groundwater from this well, or synthetic water similar in chemical composition to this well, was used in the laboratory sorptions studies performed in support of the YMP (see Section 11.0). These data are therefore presented to allow for comparison between waters used for the sorption studies and those of the Yucca Flat/Climax Mine CAU.

Groundwater of the TSA HSU

Three samples from UE-14b and five samples from TW-B were collected between 1988 and 1991. A larger proportion of SO_4^{2-} is present in the groundwaters of UE-14b relative to all others in the volcanic HSUs (Figures 5-5 and 5-6). The concentration of Ca^{2+} is lower in one sample (7.5 mg/L

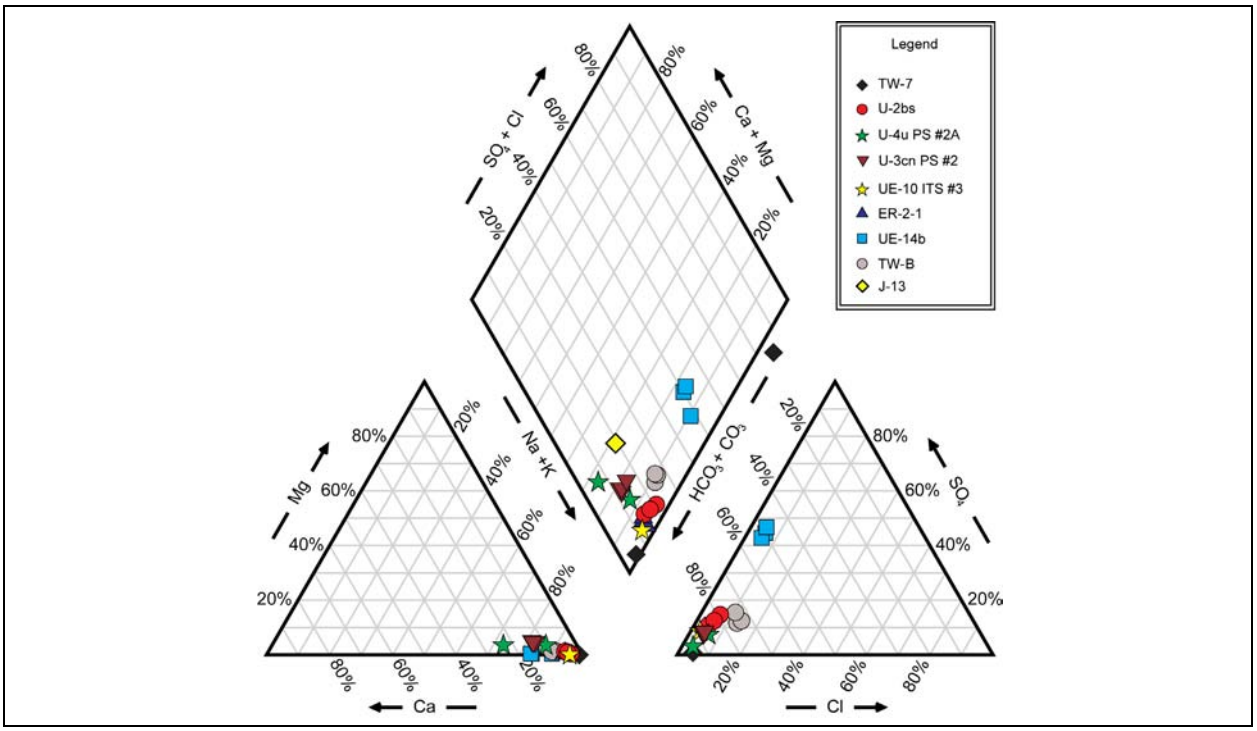

Figure 5-5
Piper Diagram for Samples Collected from the Volcanic Hydrostratigraphic Units

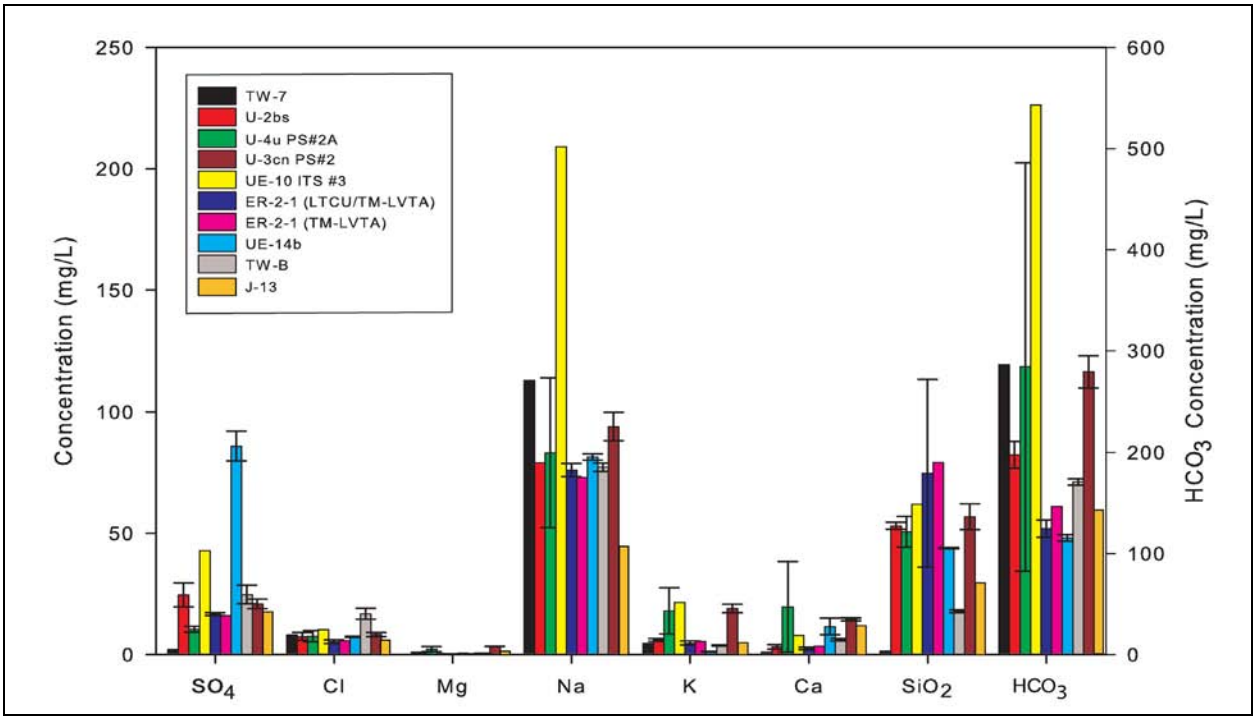

Figure 5-6
Bar Plot for Samples Collected from the Volcanic Hydrostratigraphic Units

compared to 13.4 and 13.5 mg/L) probably due to analytical variability. The major-ion composition of groundwater sampled at TW-B is consistent between samples and with other groundwaters of the volcanic HSUs (Figures 5-5 and 5-6). The pH of these groundwater samples were 8.4 ± 0.1 for UE-14b and 8.31 ± 0.02 for TW-B. No water temperature data were reported for either of these groundwaters.

The RMC associated with the TSA in the vicinity of UE-14b and TW-B is the DMP (see Table 4-5). As presented in Table 4-4, this RMC represents a high content of quartz and feldspar (greater than 60 percent), low glass (less than 20 percent), and low biotite plus hornblende (less than 1.5 percent).

Groundwater of the LTCU HSU

Groundwater sampling of TW-7 and U-2bs is limited to one sample collected in 1958 from TW-7 and two samples collected in 1972 from U-2bs. These groundwaters are strongly dominated by Na^+ (Figures 5-5 and 5-6) consistent with cation exchange of Ca^{2+} with Na^+ in the highly zeolitic rocks of the TCU. A near neutral pH of 7.3 (TW-7) and 7.1 ± 0.4 (U-2bs) is observed for these groundwaters.

Finnegan and Thompson (2002) report the results of *in situ* ORP measurements made for TW-7 at depths ranging from 500 to 672 m. The ORP indicates that the groundwaters may be slightly reducing; the ORP ranged from 206 mV to -59 mV. Reducing waters, with an ORP of -8 mV, were observed beginning at a depth of 565 m. The ORP slightly decreased for each subsequent measurement even though measurements were made both while proceeding down the hole as well as back up again. The last measured value was -59 mV at a depth of 581 m, whereas a value of -20 mV was observed earlier at a depth of 596 m. The results suggest that some of the variability in the ORP may have been due to instrument drift. The *in situ* water temperatures ranged from 22.1 to 23.1°C and the specific conductance ranged from 0.54 to 0.57 mS/cm (Finnegan and Thompson, 2002).

Two wells, U-3cn PS#2 and U-4u PS#2A, are post-test holes and will be discussed further in Sections 6.4.3 and 6.4.1, respectively. Well U-3cn PS#2 was drilled into the chimney of the BILBY test. Five groundwater samples have been collected from this well over the period of 1969 to 2004. With the exception of a slightly greater Cl^- and SiO_2 concentration in the most recent sample, the major-ion composition is relatively consistent between all samples (Figure 5-6). The concentrations in the recent sample were 17.3 and 100 mg/L for Cl^- and SiO_2, respectively, compared to ranges of

7.2 to 8.8 mg/L for Cl^-, and 51 to 61 mg/L for SiO_2 in the earlier samples. The pH values were reported as 7.8 ± 0.2.

Five samples have been collected from U-4u PS#2A over the period of 1993 to 2003. Only one sample, collected in 1993, has a charge balance within ±5 percent (Appendix E). The concentrations of most major solutes in this early sample are greater than in all subsequent samples collected from this well. This may be attributed to the impact of drilling fluids. Although all samples from this well are the Na-K-HCO_3 type, a high degree of variability is observed in the major-ion concentrations (Figure 5-6). The pH reported for these samples was 7.6 ± 0.7.

The RMC associated with the LTCU for the above described wells is ZEOL. For this RMC, zeolites and clays are abundant (greater than 30 percent) with zeolites more abundant than clays, and the abundance of glass is low (less than 10 percent).

Groundwater of the TM-LVTA/LTCU HSU

Well ER-2-1 is located just west of the Yucca Fault and is completed in the TCU near a cluster of underground nuclear tests. During well development and testing, the water level in ER-2-1 declined substantially at low pumping rates, implying very low hydraulic conductivity (SNJV, 2004c). Despite the close proximity of this well to several underground test cavities, a low-level tritium (^3H) activity (228 picocuries per liter [pCi/L]) was measured in the water, suggesting very slow groundwater flow in the vicinity of ER-2-1. The FAI of this well contains large sections of both the TM-LVTA (53-m thickness) and the LVTA (80-m thickness) HSUs. Water produced during development and testing entered the borehole above a depth of about 610 m (SNJV, 2004c and 2005d). The temperature log suggests specific inflows of water through fractures in the upper 22 m of the LTCU. Additional inflow probably occurs above these fractures within the TM-LVTA; there are additional fractures in the vicinity of 580 m and above. Water production during drilling primarily occurred within the TM-LVTA, with no water production in the LTCU below the fractures mentioned above. The chemical composition of the groundwaters collected both as the composite samples (sampled from the interval spanning both the LTCU and the TM-LVTA) and the depth-discrete bailed sample (sampled from the TM-LVTA) are quite similar suggesting the source of this groundwater may be the TM-LVTA. The RMC associated with the TM-LVTA, VMP, is the same as that assigned to the AA (Table 4-5). A relatively high pH, ranging from 8.8 to 9.3, is observed for all groundwater samples

collected from ER-2-1. The high pH may result from the inability to adequately develop this well (SNJV, 2004c).

Groundwater of the OSBCU HSU

Only a single sample has been collected from UE-10 ITS #3. Although the major-ion composition of the groundwater of UE-10 ITS#3 is similar to the other samples as shown in the Piper diagram, the bar plot (Figure 5-6) shows that these groundwaters have a much higher concentration of most major ions than in all other samples collected from the volcanic HSUs. A pH of 8.3 was measured for this sample, and no water temperature was reported. The OSBCU is assigned as the ZEOL RMC, consistent with that of the LTCU.

5.2.3.1.3 Carbonate Aquifers

A significant number of samples have been collected from the carbonate aquifers of the Yucca Flat/Climax Mine CAU (Figure 5-2). Groundwaters of the LCA are separated into the northern, western, eastern, and southeastern sections of the Yucca Flat basin for this analysis. In addition, several wells were completed within the LCA3, and one was completed within the UCA. These groundwaters are also described within this section. The RMC associated with all of the carbonate aquifers, characterized by greater than 50 percent carbonates, is CC.

Lower Carbonate Aquifer of Northern Yucca Flat

Well UE-10j is the northernmost Yucca Flat well completed in the LCA (Figure 5-2). This well was constructed with three sliding sleeves so that discrete groundwater samples could be collected at three depth intervals: 765.0 to 773.0 m (UE-10j-1), 732.3 to 740.1 m (UE-10j-2), and 691.1 to 699.0 m (UE-10j-3). All three zones are completed within the Banded Mountain Member of the Cambrian Bonanza King Formation (IT, 1995). The groundwaters are the Ca-Mg-HCO_3 type with a consistent major-ion composition for all three zones (Figures 5-7 and 5-8). It was concluded by SNJV (2006b), that groundwater of the deeper zone of UE-10j (UE-10j-1) is linked to a regional LCA flow path north of Yucca Flat and the more shallow LCA groundwater of UE-10j (UE-10j-3) contains a dominant component of local recharge (groundwater entering the LCA from overlying units) that has mixed with a much smaller percentage of deeper LCA groundwater. The geochemical and stable

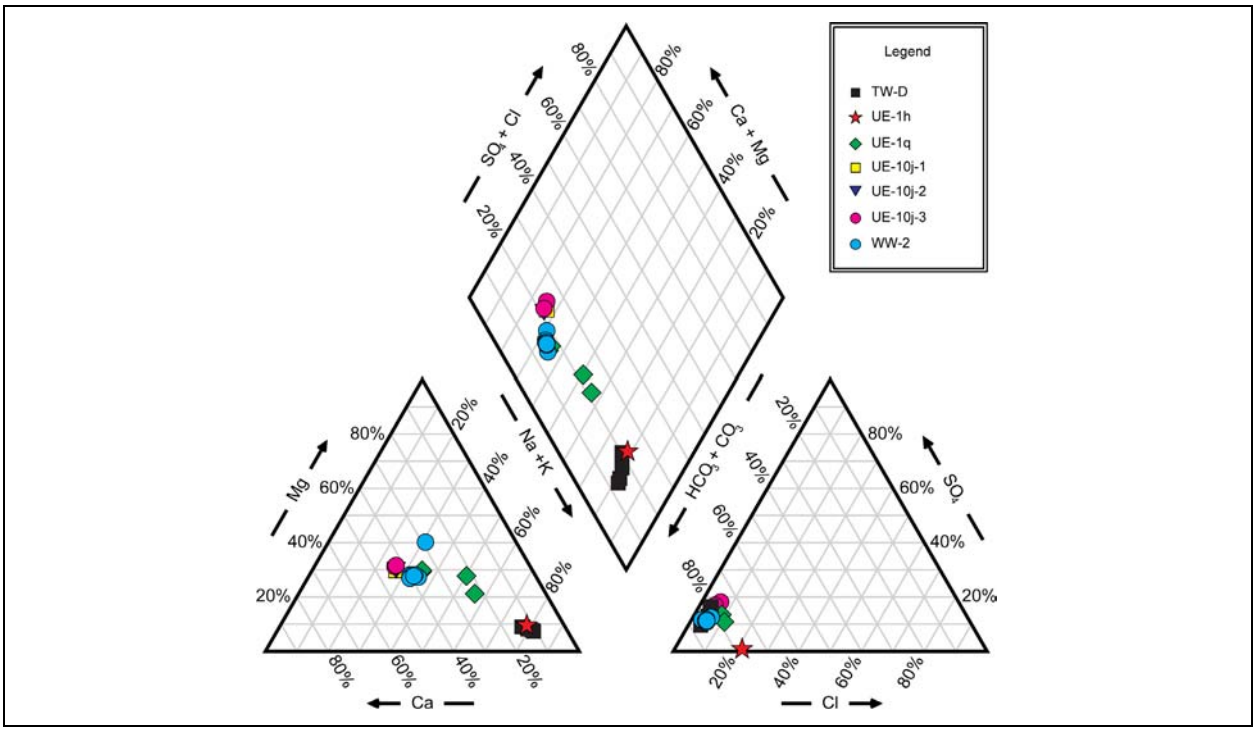

Figure 5-7
Piper Diagram for Samples from the LCA of Northern and Western Yucca Flat

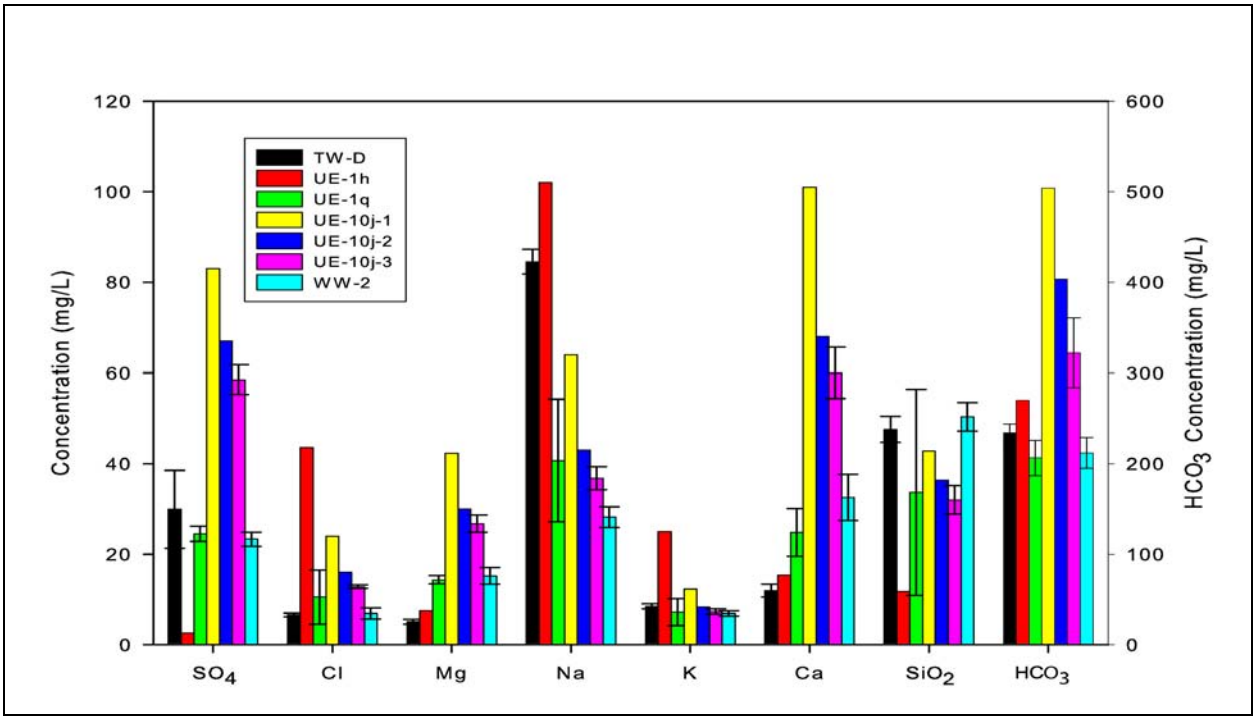

Figure 5-8
Bar Plot for Samples from the LCA of Northern and Western Yucca Flat

isotope compositions of groundwaters from the middle zone of UE-10j (UE-10j-2) are intermediate between those of UE-10j-1 and UE-10j-3. The pH and water temperature of groundwaters of UE-10j range from 6.4 to 7.2 and 32.1 to 32.7 °C, respectively.

The ORP was measured for groundwaters of UE-10j in 2003 for depths ranging from 2,170 ft (661 m) to 2,330 ft (710 m) and the results ranged from -342 to -439 mV, indicating a reducing environment. Although variability in the measurements is rather large, a trend of increasing ORP with depth is reported (Finnegan et al., 2004). The *in situ* water temperatures ranged from 32.0 to 32.5 °C. The specific conductance (and pH) ranged from 0.22 to 0.24 mS/cm (pH of 8.9 to 9.2) at depths of 661 to 689 m, and from 0.59 to 0.60 mS/cm (pH of 8.0 to 8.1) at depths of 698 to 710 m (Finnegan et al., 2004). Only the uppermost sleeve has been left open since March 1997 (Fenelon, 2005), restricting circulation of groundwater in this well.

The groundwaters of WW-2, another well in northern Yucca Flat completed in the LCA, are also the Ca-Mg-HCO_3 type (Figure 5-7). These groundwaters are thought to contain little deep LCA groundwater but are instead composed predominantly of local recharge with a component of groundwater with a volcanic geochemical signature (SNJV, 2006b). The Ca^{2+} concentration was slightly lower and the Mg^{2+} concentration slightly greater in the earliest sample (collected in 1963) from WW-2. Water Well 2 was pumped as a water-supply well between 1962 and 1990 (Fenelon, 2005). This well was resampled in 2006, and the major-ion compositions were consistent with that of the pumped samples as well as the bailed sample that was collected in 1991. The pH of the water samples from WW-2 were reported as 7.9 ± 0.2, and the water temperature was reported as 34.4 ± 0.4 °C.

The ORP was measured *in situ* for WW-2 in 2001 and again in 2006 by LANL. The more recent measurements were made under pumping conditions. The first measurements, made in 2001, were made at depths ranging from 633 to 749 m (Finnegan and Thompson, 2002). The reported values range from -97 to -149 mV, indicating a reducing environment. An increasing trend in water temperature, ranging from 27.3 to 30.0 °C, was observed with depth. The *in situ* measurements of pH and specific conductance ranged from 7.9 to 8.4 and 0.317 to 0.324 mS/cm, respectively. Interestingly, the ORP measured more recently for WW-2, 33 mV relative to the standard hydrogen electrode, indicated an oxidizing environment. In addition to the directly measured ORP, some

measurements of redox couples were performed in 2006. For instance, the concentration of the oxidized form of nitrogen, NO_3^-, was measured along with the reduced forms, nitrite (NO_2^-) and ammonia (NH_4). The reported concentrations of NO_3^-, NO_2^-, and NH_4 were 5.5, 0.000, and 0.1 mg/L, respectively. In addition, the concentrations of total iron and ferrous iron (the reduced form of iron) were measured to be 0.32 and 0.03 mg/L, respectively. The presence of both ferrous iron and ammonia, along with the relatively high concentration of manganese, 0.134 mg/L, in the groundwater of WW-2 indicates that, although the groundwaters are oxidizing, reduced species are present possibly resulting from mixing of reducing and oxidizing groundwaters from different producing zones in the wellbore. The water temperature, specific conductance, and pH were reported to be 33.6 °C, 452, and 7.56, respectively, for the 2006 *in situ* measurements.

Lower Carbonate Aquifer of Western Yucca Flat

Samples were collected from three wells (UE-1q, TW-D, and UE-1h) completed in the LCA in west central Yucca Flat. The groundwater chemistry of these groundwaters varies considerably, ranging from the Ca-Mg-HCO_3 type, which is typical of groundwater of a carbonate aquifer, to the Na-K-HCO_3 type, which is typical of groundwater of a volcanic-rock aquifer (Figure 5-7).

Two samples were collected from UE-1q in 1992 toward the end of a long-term aquifer test (DOE/NV, 1996). The water chemistry for these samples was considerably different than that of the samples collected more recently using a discrete bailer (Figure 5-7). The 1992 samples plot similarly to those of WW-2 on the Piper diagram and are a Ca-Mg-HCO_3 type, whereas the more recent depth-discrete bailed samples are the Ca-Mg-Na-HCO_3 mixed type (Figure 5-7). The top of the FAI for UE-1q, defined by a fully cemented casing, is 33.4 m below the top of the LCA. There is approximately 31-m head difference between the overlying volcanic formation and the LCA, based on pre-recompletion water levels (Fenelon, 2005), with the gradient downward. It is reasonable to assume that there is vertical flow from the overlying volcanic formation into the LCA driven by the head gradient, and further, there may be downward flow in the open hole completion within the LCA. During prolonged pumping, the production from the LCA, which is typically a much more productive formation than the overlying volcanic tuff, would probably contribute a high proportion of the total production. Lower carbonate aquifer water chemistry would predominate in a water sample of the produced water. However, in the ambient flow condition, vertical flow from the overlying volcanic

formation may be a larger component of the water in the completion. A groundwater sample collected downhole from the completion in an equilibrium condition would have a volcanic component proportional to the ratio of the vertical flow to ambient lateral flow in the LCA; lateral flow in the LCA within Yucca Flat is presumed to be low as a function of the low horizontal gradient.

Groundwater at UE-1h in western Yucca Flat has a unique geochemical signature relative to other LCA groundwater in Yucca Flat. These groundwaters are the Na-K-HCO_3 type (Figure 5-7) and have relatively high Cl^- and low SO_4^{2-} concentrations (Figure 5-8). Geochemical models presented in SNJV (2006b) indicated that UE-1h groundwater could originate from mixtures of groundwater of a volcanic aquifer and groundwater from the UCCU in western Yucca Flat.

Groundwater at TW-D, the final well located in west-central Yucca Flat, is the Na-K-HCO_3 type, indicating a large component of groundwater from a volcanic-rock HSU. Geochemical mixing models developed for the groundwater of these wells indicates a maximum of 18 percent of an LCA component in the groundwaters of TW-D. Within the TW-D completion, there is about 1.4 m of ATCU at the top, above the LCA contact. This overlying formation is described as brecciated in the original drilling report. There is approximately 30-m head difference between the overlying volcanic formation(s) and the LCA, with the gradient downward. It is reasonable to assume that there is vertical flow from the overlying volcanic formation into the LCA driven by the head gradient, and further, there may be downward flow in the open hole completion in the LCA. This downward flow (recharge) could result in a volcanic component in groundwater samples from the LCA completion.

Lower Carbonate Aquifer of Eastern Yucca Flat

A series of wells have been completed in the LCA along a north-south trend on the eastern side of Yucca Flat. These include UE-7nS, ER-7-1, U-3cn #5, TW-E, ER-6-1, and ER-6-1 #2. The major-ion compositions of the majority of these LCA groundwaters are the Ca-Mg-Na-HCO_3 mixed type (Figure 5-9). Their compositions are quite similar, as indicated by the relatively tight clustering of most samples within the Piper diagram.

The geochemical compositions of groundwaters of ER-7-1, ER-6-1, and ER-6-1 #2 are nearly identical (Figures 5-9 and 5-10). A near neutral pH was observed: 7.62 ± 0.04 (ER-7-1), 7.3 ± 0.1 (ER-6-1), and 7.6 ± 0.1 (ER-6-1 #2). Water temperatures for these samples were reported as 49.0 ± 1.1 °C (ER-7-1), 38.1 ± 4.2 °C (ER-6-1), and 36.9 ± 5.4 °C (ER-6-1 #2). The ORP, measured for

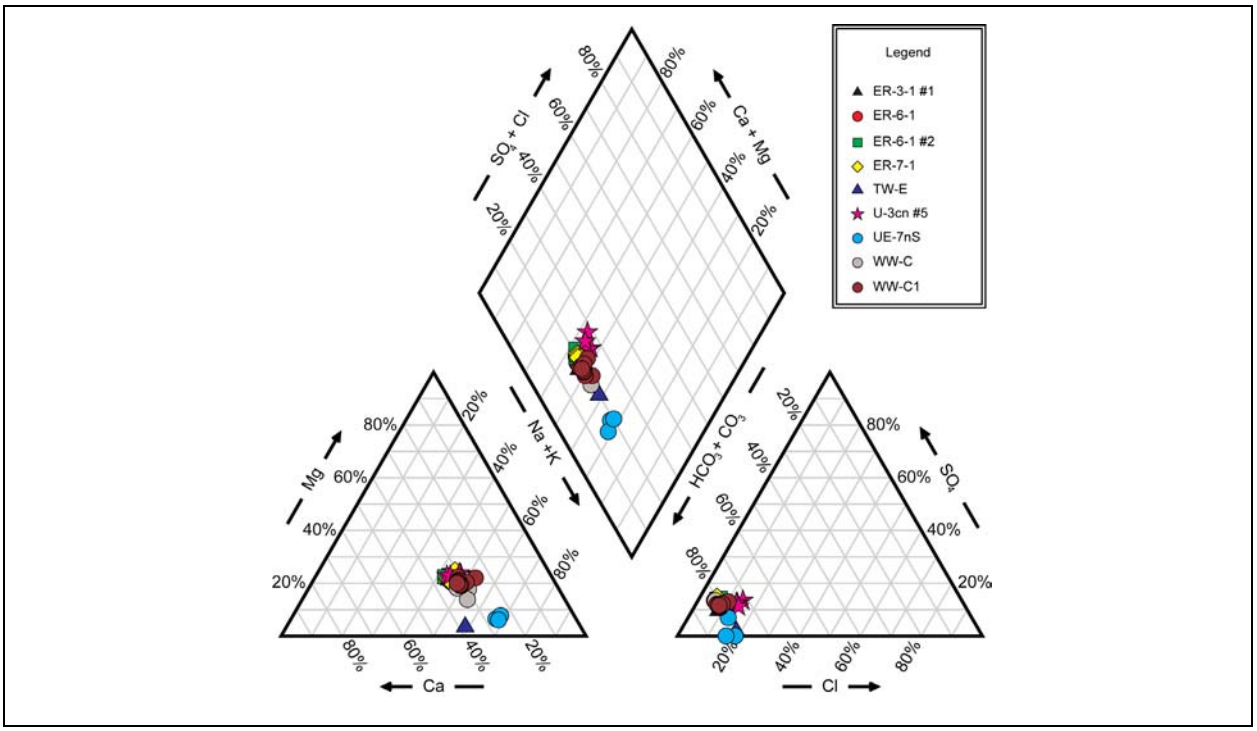

Figure 5-9
Piper Diagram for Samples Collected from the LCA of Eastern and Southwestern Yucca Flat

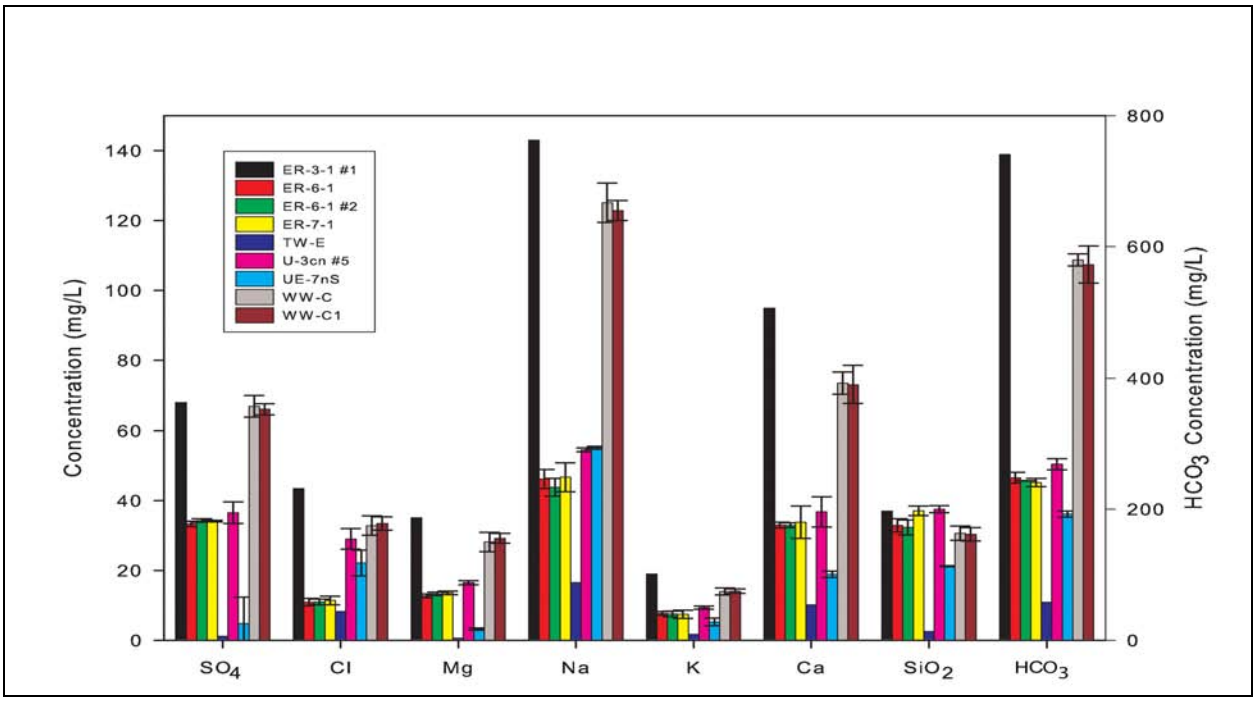

Figure 5-10
Bar Plot for Samples Collected from the LCA of Eastern and Southwestern Yucca Flat

ER-6-1 in 2001, ranged from 134 mV (504-m depth) to 143 mV (489-m depth) to 266-276 mV (473-m depth), indicating that the groundwaters are oxidizing (Finnegan and Thompson, 2002). An increasing trend in water temperature with depth was observed with temperatures ranging from 38.2 (473-m depth) to 39.1 °C (504-m depth). The *in situ* measurements of pH were consistently 7.9, and the specific conductance ranged from 0.637 to 0.638 mS/cm.

Well TW-E is located approximately 2 km southeast of ER-7-1, and both wells appear to be completed in the same LCA structural block. Fenelon (2005) states that the recently measured water levels in TW-E are assumed to be a composite of water levels in volcanic tuffs and the LCA. It is also stated that this well was never properly developed and that significant amounts of mud were observed in the groundwaters in 2003. The water chemistry of TW-E is unusually dilute compared with other LCA water samples (Figure 5-10), which raises concerns that this sample may reflect water that leaked into the well from an overlying (possibly perched) zone. Groundwater of this well is therefore not considered to be representative of the LCA.

Well UE-7nS is a satellite well that is located 137 m southeast of the emplacement hole (U-7n) used for the BOURBON test and will be discussed further in Section 6.5.2. The major-ion composition of groundwater of UE-7nS is unique when compared to that of the other wells in its vicinity (Figure 5-9). The groundwaters of UE-7nS are the Na-K-HCO_3 type and have significantly greater concentrations of Cl^- and lower concentrations of SO_4^{2-} (Figure 5-10). The pH of the samples collected from UE-7nS were 7.6 ± 0.1, and the water temperatures were 36.2 ± 1.3 °C.

Well U-3cn #5 is a satellite well that is located 122 m laterally from the BILBY working point location and is discussed further in Section 6.4.3. Samples have been collected from this well over the period of 1967 to 1997. The groundwater is a Ca-Mg-Na-HCO_3 mixed type similar to that observed in the other wells within its vicinity although the relative concentration of Cl^- is greater in the U-3cn #5 groundwaters (Figures 5-9 and 5-10).

Lower Carbonate Aquifer of Southeastern Yucca Flat

Three wells in southeastern Yucca Flat (ER-3-1, WW-C, and WW-C1) produce LCA groundwater with a distinct set of geochemical characteristics. Although the relative major-ion compositions of these groundwaters are quite similar to those previously described (Figure 5-9), these groundwaters have high solute concentrations, including Cl^- concentrations that range from 35 to 42 mg/L (Figure 5-10).

Water-level contours for the LCA in Yucca Flat (SNJV, 2006c) indicate that groundwater in the eastern, northern, and western parts of the Yucca Flat basin converges toward faults in the center of the basin and probably exits the basin in the vicinity of WW-C and WW-C1. Well ER-3-1 penetrates the LCA just east of Yucca Flat in the southern portion of the Halfpint Range. Wells WW-C and WW-C1 are located at the southernmost margin of Yucca Flat, approximately 12 km southwest of ER-3-1. The two wells are only about 30 m apart, and both are completed to nearly the same depth in Cambrian limestone of the Carrera Formation (Winograd and Thordarson, 1975). Hence, both wells should produce groundwater that is essentially identical in composition. Small differences in the average stable isotope and Cl^- values are observed, but these differences are within the range of analytical uncertainty. A near neutral pH was observed: 6.7 (ER-3-1), 7.4 ± 0.3 (WW-C), and 7.4 ± 0.4 (WW-C1). Water temperatures were reported as 37.8 °C (ER-3-1), 36.7 ± 0.3 °C (WW-C), and 36.2 ± 1.3 °C (WW-C1).

Lower Carbonate Aquifer - Thrusts

Four wells within the Yucca Flat/Climax Mine geochemistry study area (ER-6-2, UE-1c, UE-2ce, and ER-12-1) are completed within the LCA3 (Figure 5-2). The first three (ER-6-2, UE-1c, and UE-2ce) are completed in the Yucca Flat upper thrust plate of the CP thrust. Well ER-12-1 is completed in a thrust block of the Belted Range thrust. These groundwaters range from borderline mixed (ER-6-2 and UE-1c) to the Ca-Mg-HCO_3 type (UE-2ce) to a Ca-Mg-SO_4 type (ER-12-1).

Well UE-2ce is completed in the LCA3 near the NASH (U2ce) underground nuclear test. Well UE-2ce groundwater appears to contain a large fraction of locally derived perched water represented in the geochemical models of SNJV (2006b) by the Oak, Whiterock, and Captain Jack Springs. The major-ion compositions of these groundwaters, Ca-Mg-HCO_3 type, are highly variable over the time

period sampled (Figure 5-11). The time trend for the concentrations of four chemical parameters in groundwaters of UE-2ce is presented in Figure 5-13. As shown in this figure, a significant increase in the concentration of the major ions, especially Ca^{2+} and Cl^{-} (possibly due to increased calcite dissolution), was observed during the period of 1977 to 1978. This time period coincides with the pumping experiments performed at this well. The pumping experiments are discussed further in Section 6.5.1. Although the concentrations appear to have stabilized by 2005 (the most recent sampling of this well), the Cl^{-} concentration is still high relative to other groundwaters of the LCA3 (Figure 5-12). It is likely that the satellite wells associated with underground tests in the LCA would have signatures of high calcite dissolution.

Wells ER-6-2 and UE-1c are LCA3 wells in southwestern Yucca Flat that produces groundwater chemically similar to other Yucca Flat LCA groundwater and are the Ca-Mg-Na-HCO_3 mixed type (Figure 5-11). The pH of the groundwater samples are 7.3 ± 0.2 for ER-6-2 and 7.5 ± 0.6 for UE-1c. A water temperature of 35.2 ± 0.5 °C was reported for the ER-6-2 samples, and temperature was not reported for the UE-1c samples. The ORP measured for UE-1c indicates that the groundwaters are oxidizing with very small variability observed (179 to 183 mV) between depths ranging from 1,310 to 1,700 ft (400 m to 518 m) (Finnegan and Thompson, 2003). The *in situ* measurements performed on groundwaters of UE-1c reported a range in pH of 7.2 to 7.4 and a range in water temperature of 25.8 to 27.7 °C. A trend of increasing water temperature with groundwater depth was observed (Finnegan and Thompson, 2003).

The monitored zone in ER-12-1 is between depths of 518 and 555 m and consists of a thin sliver of Upper Simonson or Lower Guilmette Formation dolostone that is tectonically sandwiched within Eleana Formation clastic rocks. Groundwater of ER-12-1 is unique relative to all others within the carbonate aquifers. The dominant cation and anion are Ca^{2+} and SO_4^{2-}, respectively, and the groundwaters are a Ca-Mg-SO_4 type (Figures 5-11 and 5-12). The *in situ* measurements of ORP (-113 to 13 mV) indicate that the groundwaters of ER-12-1 are slightly reducing at most depths 1,540 to 2,500 ft (469 to 762 m) measured (Finnegan and Thompson, 2003). Both the completion casing string and the production string for this well are carbon steel. Although five sliding sleeves exist in this well (Russell et al., 1996), only the upper sleeve (535.5 to 536.7 m) was open during all sampling, including *in situ* measurements, for this well. Stagnant water would therefore be expected to exist below the sliding sleeve opening, and reducing conditions may have resulted from oxidation

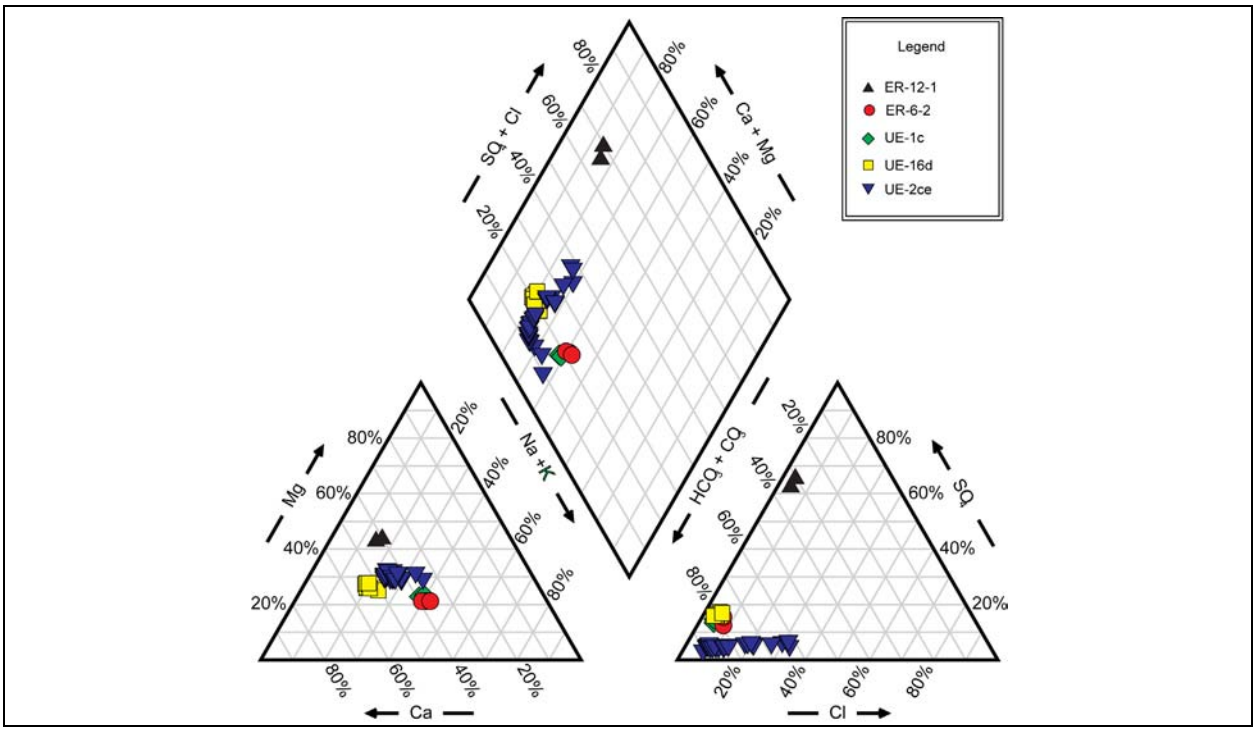

Figure 5-11
Piper Diagram for Samples Collected from the LCA3 and UCA

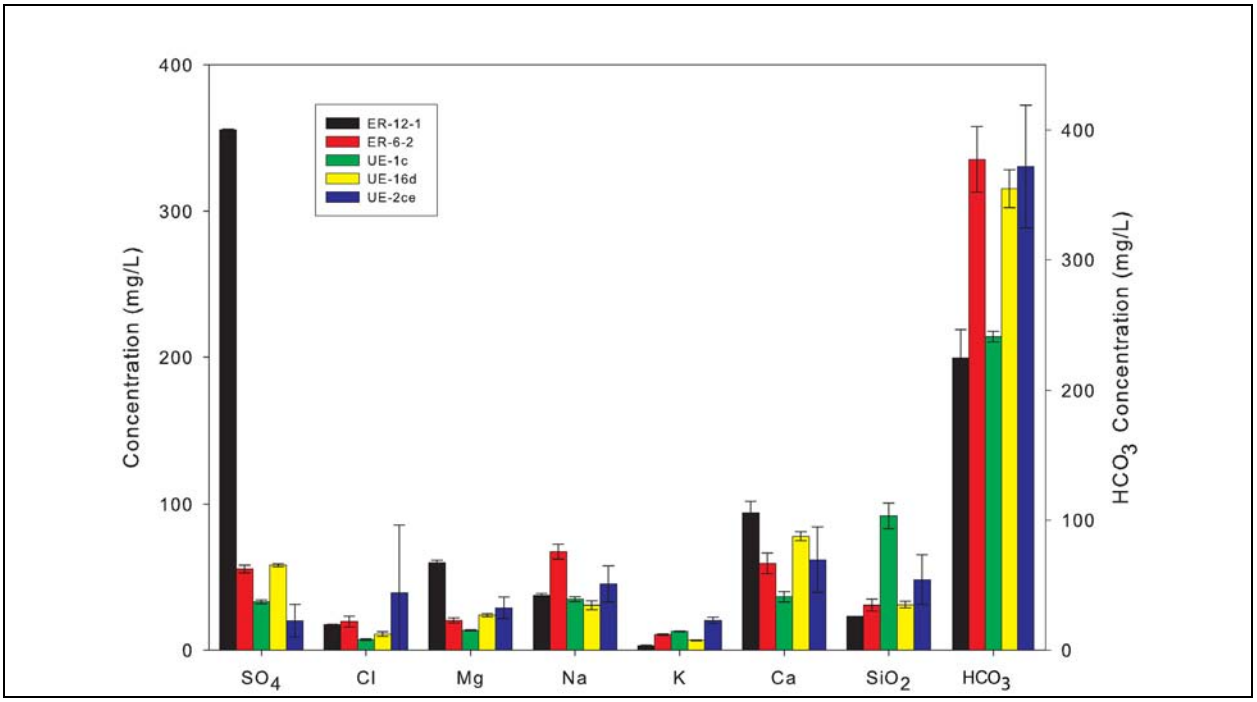

Figure 5-12
Bar Plot for Samples Collected from the LCA3 and UCA

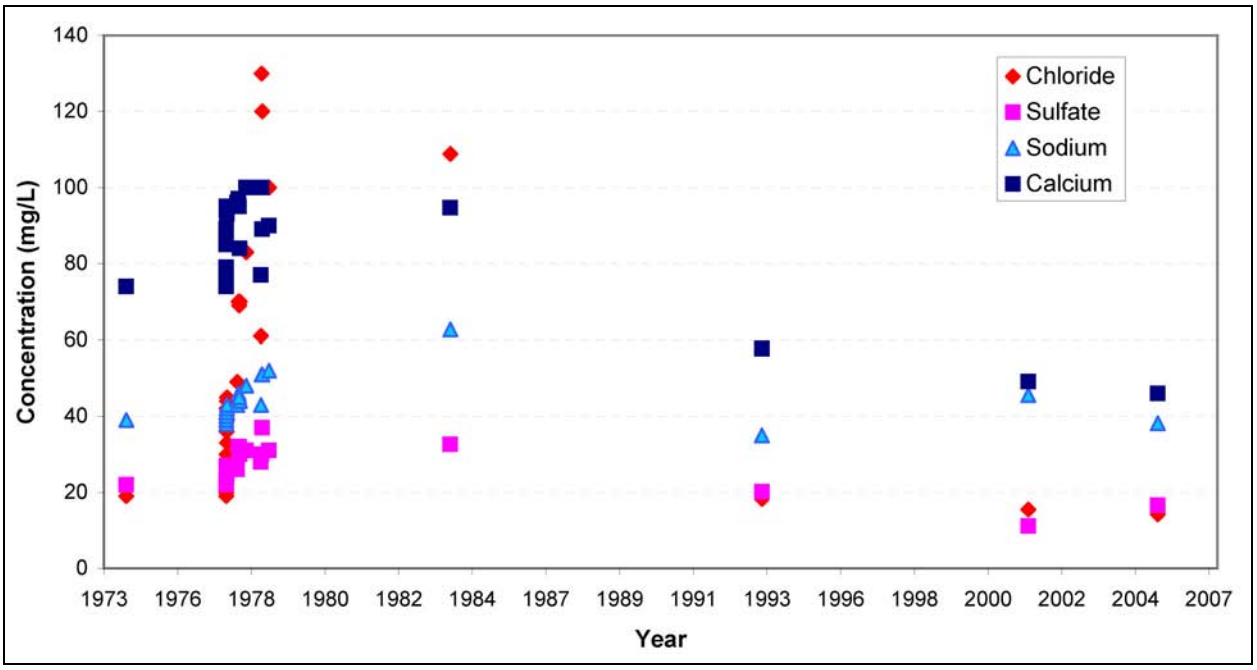

Figure 5-13
Concentration of Select Major Ions in Groundwater of UE-2ce

of the carbon-steel casing of this well. A trend of decreasing pH (8.9 to 6.4) and increasing temperature (22.8 to 28.3 °C) with depth was observed. The pH and water temperature measured at a depth closest to the sliding sleeve (549-m depth) were 8.8 and 24.2 °C, respectively (Finnegan and Thompson, 2003).

Upper Carbonate Aquifer

A single well, UE-16d, is completed in the UCA within the Yucca Flat/Climax Mine CAU. The groundwaters of UE-16d are a Ca-Mg-HCO_3 type (Figure 5-11), similar to the LCA groundwaters of northern Yucca Flat. The pH and water temperature reported for the samples collected from UE-16d were 7.6 ± 0.2 and 23.1 ± 1.8 °C, respectively.

5.2.4 Clastic Confining Units

Four wells within the Yucca Flat/Climax Mine geochemistry study area are completed in the UCCU (ER-12-2, UE-16f, UE-17a, and UE-1b), and three are completed within the LCCU (UE-15d WW, UE-15j, and UE-15j A-5). A relatively variable chemical composition of these groundwaters is observed (Figures 5-14 and 5-15).

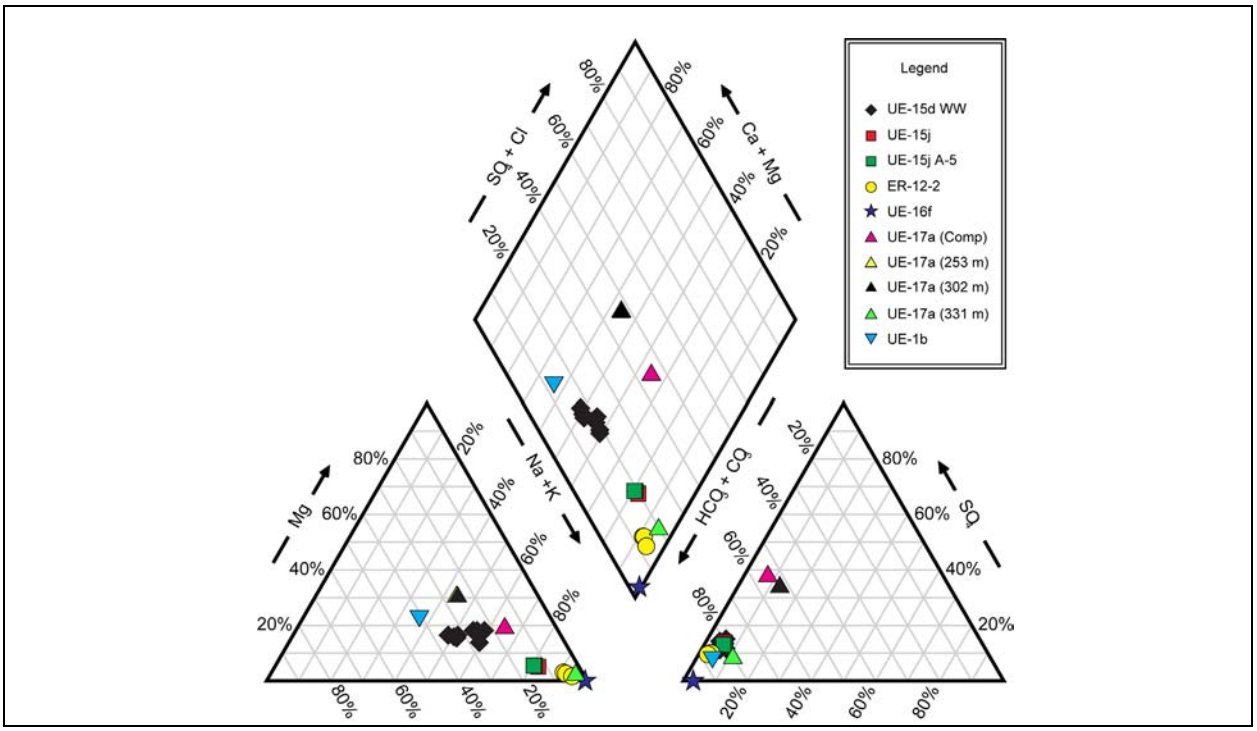

Figure 5-14
Piper Diagram for Samples Collected from the Clastic Confining Units

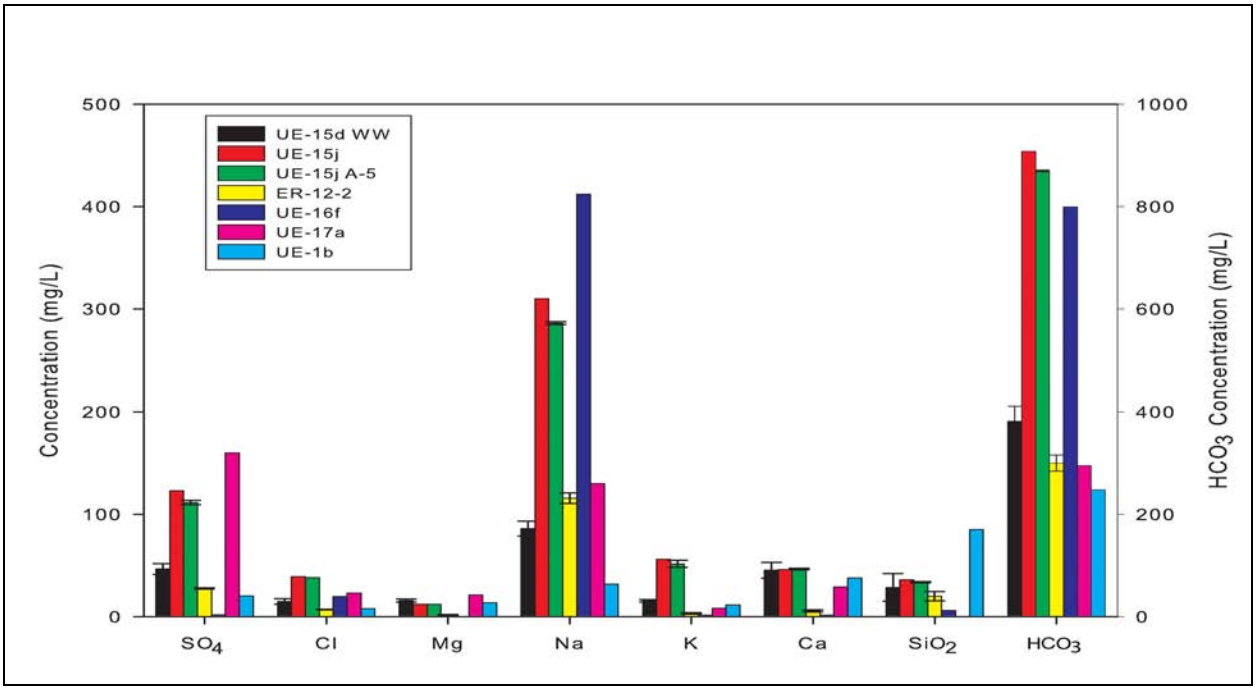

Figure 5-15
Bar Plot for Samples Collected from the Clastic Confining Units

Note: All samples (composite and discrete-depth) are combined for UE-17a.

Upper Clastic Confining Unit

A discrete bailer sample and a composite sample were collected from ER-12-2. The composite sample was collected after approximately 350,000 gallons of groundwater had been pumped from the well during development and testing activities. The groundwaters are the Na-K-HCO_3 type with relatively consistent chemistry between the composite and bailed samples (Figures 5-14 and 5-15). The groundwater of ER-12-2 is thought to be derived from local recharge sources in the Rainier Mesa area (SNJV, 2006b). The pH and water temperature reported for the samples collected from ER-12-2 were 8.3 ± 0.2 °C and 35.0 ± 1.1 °C, respectively.

Only a single sample, collected in 1988, is available from UE-16f. This well is open to about 180 ft (55 m) of quartzite and argillite, and the groundwaters are the Na-K-HCO_3 type. The Na^+ concentration for this groundwater sample exceeds that of any other samples within the Yucca Flat/Climax Mine CAU (Figure 5-15). The pH reported for this sample was 9.4. This relatively high pH possibly is a result of the inability to adequately purge this well of residual drilling fluid. The ORP measurements for groundwater of UE-16f (depths between 380 to 1,350 ft [116 m to 411 m]) ranged from -51 to -367 mV, indicating a reducing environment. The *in situ* measurements of water temperature, ranging from 19.6 to 26.2 °C, indicate an increasing trend with depth (Finnegan et al., 2004).

Samples were collected from UE-17a during two sampling events. The first sample was collected at the end of well construction (Fenelon, 2005). This sample is the only one with a charge balance within ± 5 percent. During the second sampling event bailed samples were collected from depths of 253, 302, and 331 m bgs. The groundwater major-ion chemistry for all four samples are presented in the Piper diagram (Figure 5-14). The two samples collected at depths of 253 and 302 m are the Ca-Mg-Na-HCO_3 mixed type and plot identically on the Piper diagram. The sample collected at a depth of 331 m is the Na-K-HCO_3 type and plots next to the ER-12-2 samples (Figure 5-14). The concentration of Na^+ is significantly greater in this sample (298 mg/L) when compared to that of the other depths of this well (79 and 80 mg/L). The composite sample for UE-17a, collected in 1976, lies between the depth discrete samples and is the Na-K-HCO_3 type, which indicates mixing of groundwaters with significantly different water chemistry within the borehole. This variability in groundwater chemical parameters with depth is consistent with the *in situ* measurements made at this well (Finnegan and Thompson, 2003). The specific conductance increased from 0.760 mS/cm at a depth of 640 ft (195 m) to 1.530 mS/cm at 1,175 ft (358 m). The water temperature (22.3 to 25.3 °C) showed an increase with increasing depth. The ORP measured for this groundwater ranged from -144

to -349 mV, indicating a reducing environment. The pH reported for the groundwater samples was 7.58 (253-m depth), 7.63 (302-m depth), and 8.3 (331-m depth). The pH was not measured for the composite sample.

The saturated part of UE-1b is open to about 75 ft (23 m) of bedded and reworked tuff overlying about 500 ft (152 m) of primarily argillite of the Eleana Formation (Fenelon, 2005). A single sample collected from UE-1b in 1988 meets the charge balance criteria set for these analyses. An additional sample was collected in 1992 from a depth of 207 m bgs, but SO_4^{2-} was not measured for this sample and the HCO_3 appears to be low. The groundwater of this sample is the Ca-Mg-HCO_3 type. The pH of this sample was 8.08.

The primary RMC associated with the UCCU of these wells is the ARG (see Table 4-5). As shown in Table 4-4, this RMC represents a high clay content (greater than 30 percent) with the abundance of clay exceeding that of zeolite.

Lower Clastic Confining Unit

Well UE-15d WW was completed as a supply well in April 1962 and is open to about 600 ft (183 m) of dolomite of the Precambrian Noonday Dolomite within the LCCU (Fenelon, 2005). The groundwater of UE-15d WW is the mixed Ca-Mg-Na-HCO_3 type. The pH and water temperature reported for the samples collected from this well were 7.4 ± 0.5 and 35.0 ± 1.4 °C, respectively.

The saturated part of UE-15j is open to about 800 ft (244 m) of Precambrian Stirling Quartzite, and the saturated part of well UE-15j A-5 is open to about 280 ft (85 m) of zeolitized tuff (Fenelon, 2005). The major-ion composition of these groundwaters are quite similar and are the Na-K-HCO_3 type (Figure 5-14). The similarities between these groundwaters are further demonstrated in Figure 5-15. The pH and water temperature of the groundwater samples were 6.6 and 45 °C, respectively, for UE-15j and 6.7 and 44 °C, respectively, for UE-15j A-5.

The RMC associated with the LCCU of these wells is the SC (see Table 4-5). As shown in Table 4-4, this RMC represents a high silica/quartz content (greater than 50 percent).

5.2.5 Granite Confining Unit

The available groundwater chemistry data for the Climax Stock (MGCU HSU) are limited to that reported in Isherwood et al. (1982). Groundwater samples were collected from five sites in the fractured climax granite at the Spent Fuel Test facility (Shaft U-15.01) at depths ranging from 64 to

565 m bgs (Figure 5-16). Four of the samples were collected from groundwater seeps out of isolated fractures, and one was collected from a borehole believed to intersect with the local water table (UG-02, see Figure 5-16). The major-ion composition of the Climax waters are highly variable (Figure 5-17). In addition, the Climax Stock samples are relatively unique when compared to all samples within the study area in that the total solute concentrations are much greater in general (Figure 5-18), and the dominant anion is SO_4^{2-} rather than HCO_3^-. The high SO_4^{2-} in these samples is inferred to reflect oxidation of the abundant pyrite present along the fractures in the hydrothermally altered granite. One sample from the Climax Stock, C30, is somewhat similar to samples of ER-12-1 groundwater shown in Figure 5-11. The dominant anion and cation in both samples are SO_4^{2-} (343 mg/L in ER-12-1 and 325 mg/L in C30) and Ca^{2+} (94 mg/L in ER-12-1 and 126 mg/L in C30), respectively. The total dissolved solids in the C30 sample (1,150 mg/L) is greater than that of the ER-12-1 sample (760 mg/L) because of the higher relative concentrations of most major ions (Appendix E). The differences in composition between the five samples suggest the samples are from different independent fracture systems. However, an apparent trend of Na^+ with depth at the expense of Ca^{2+}, and Mg^{2+} suggests a common evolutionary chemical process, and possibly an interconnected system (Isherwood et al., 1982).

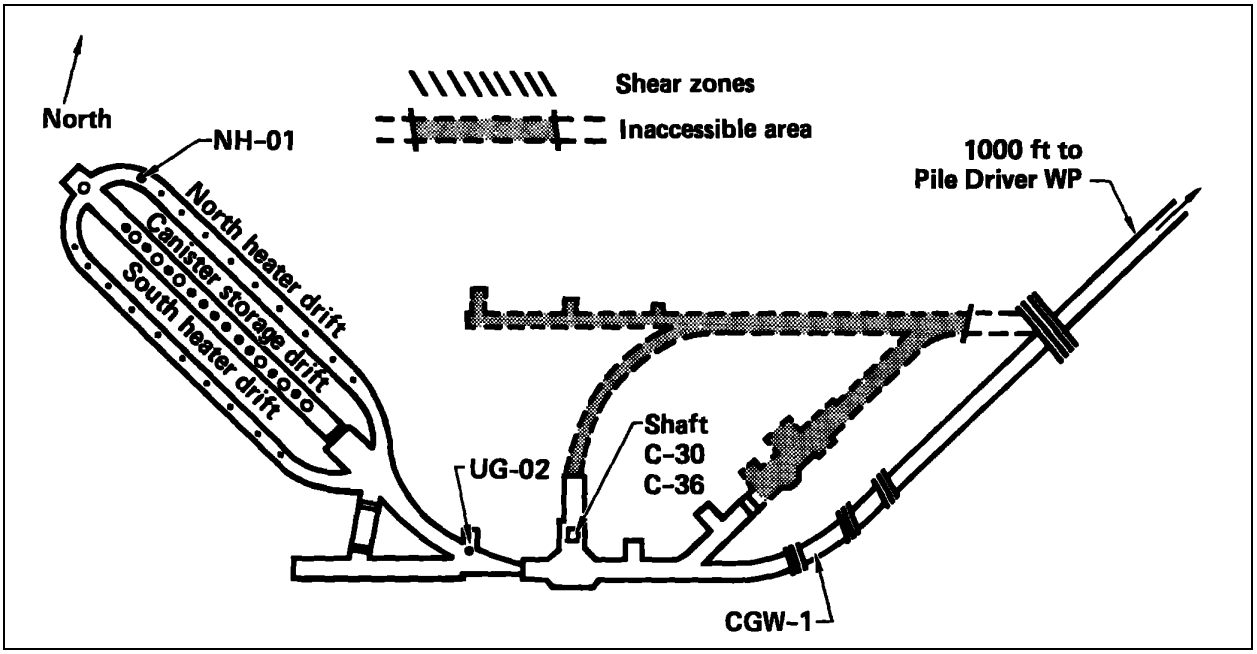

Figure 5-16
Schematic for the U15 Shaft
Source: Isherwood et al., 1982

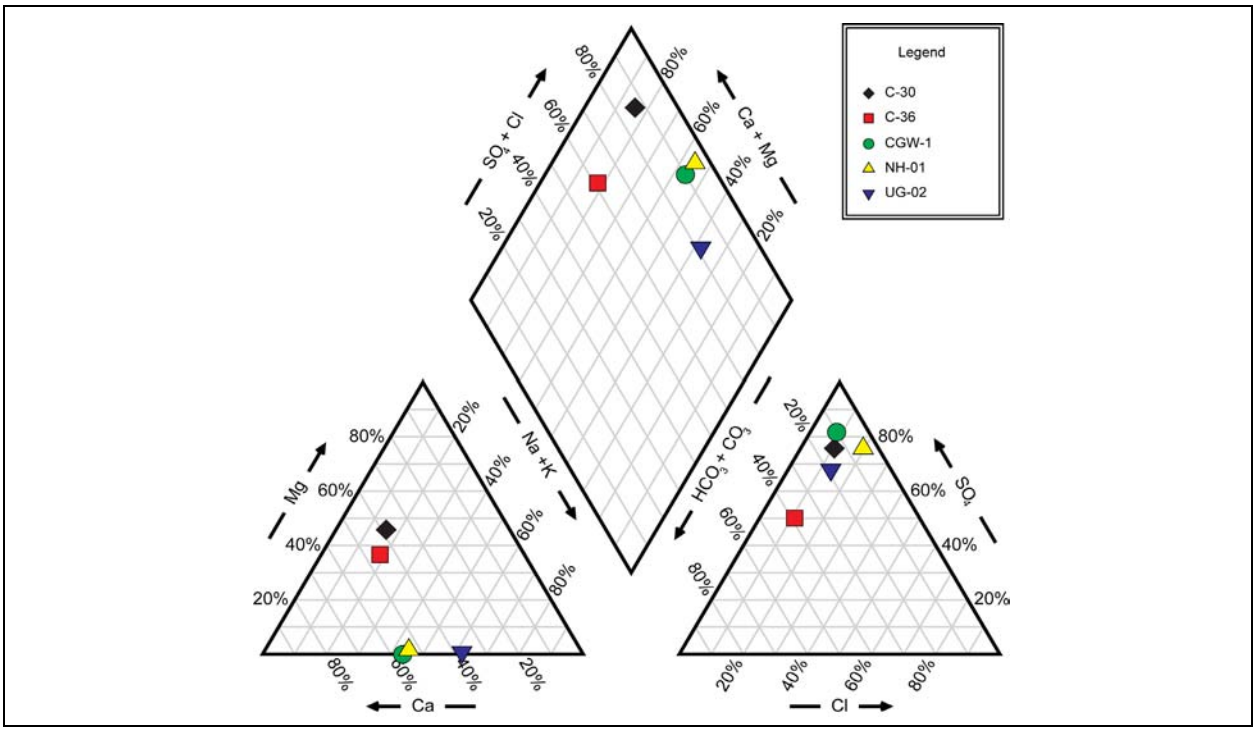

Figure 5-17
Piper Diagram for Samples Collected from the Granite Confining Unit

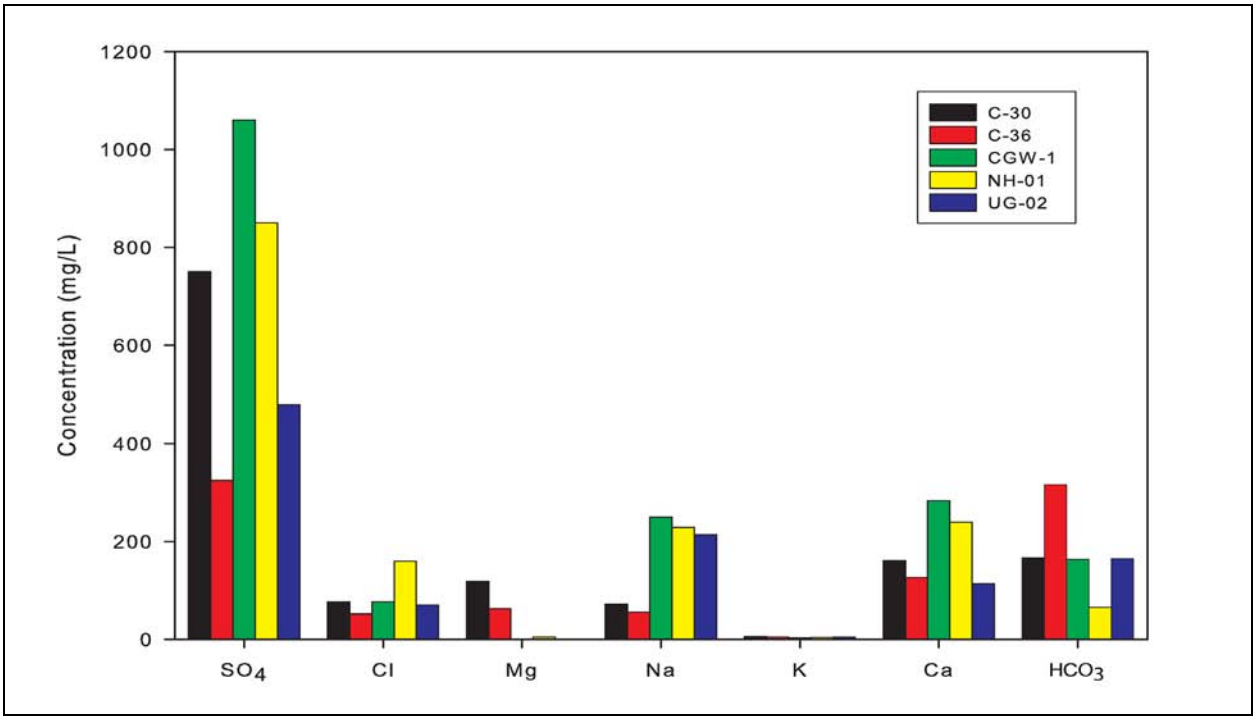

Figure 5-18
Bar Plot for Samples Collected from the Granite Confining Unit

The RMC associated with the MGCU is the DMR (see Table 4-5). As shown in Table 4-4, this RMC represents a high content of quartz and feldspars (greater than 60 percent), and a biotite and hornblende content exceeding 1.5 percent.

5.2.6 Perched Springs

Three small springs — Captain Jack Spring, Whiterock Spring, and Oak Spring — are located in the Yucca Flat/Climax Mine geochemistry study area. The springs emanate from the OSBCU HSU. Captain Jack Spring discharges from the base of a narrow rocky box canyon where a shallow pool of water (20 centimeters [cm] deep) forms (Hansen et al., 1997). Whiterock Spring has been developed with two shallow adits, and water is transmitted approximately 50 m to a weir box through a plastic pipe with a 4-cm diameter (Lyles et al., 1990). Oak Spring, which is the smallest of the these springs, is only a small depression in the soil about 2.5 cm deep with a surface area of less than 1 square meter (m^2) (Hansen et al., 1997). These springs have discharge rates ranging from as little as 0.4 liters per minute (L/min) at Oak Spring (Hansen et al., 1997) to an average flow rate at one of the two adits at Whiterock Spring of 1.2 L/min, over a seven-year period (Lyles et al., 1990). Groundwater sources of the springs are perched above the regional saturated groundwater flow system. The major-ion chemistry is of two types, an Na-K-HCO_3 type water and a Ca-Na-K-HCO_3 type water. These chemical differentiations are shown on Figures 5-19 and 5-20.

5.3 Limitations

Groundwater data included in this study represent a time period from the late 1950s to 2005, and in many cases, data for a given well or spring are limited to samples collected more than 20 years ago. These older datasets are limited in that the entire parameter suite used for the geochemical investigations is lacking. Geochemical evaluations depend on adequate data coverage, both laterally and vertically, within the study region. Within the Yucca Flat/Climax Mine CAU, the wells with the parameter suite necessary to support geochemical flow-path analysis and characterization are irregularly distributed. This is compounded by sparse groundwater samples from most HSUs, particularly the alluvial and volcanic aquifers. Well samples included in the dataset were often collected as composites, either from wells with single completions that transect multiple HSU boundaries, or from wells with multiple completions that were all pumped simultaneously. Many wells draw from a large vertical cross section of saturated media, possibly resulting in

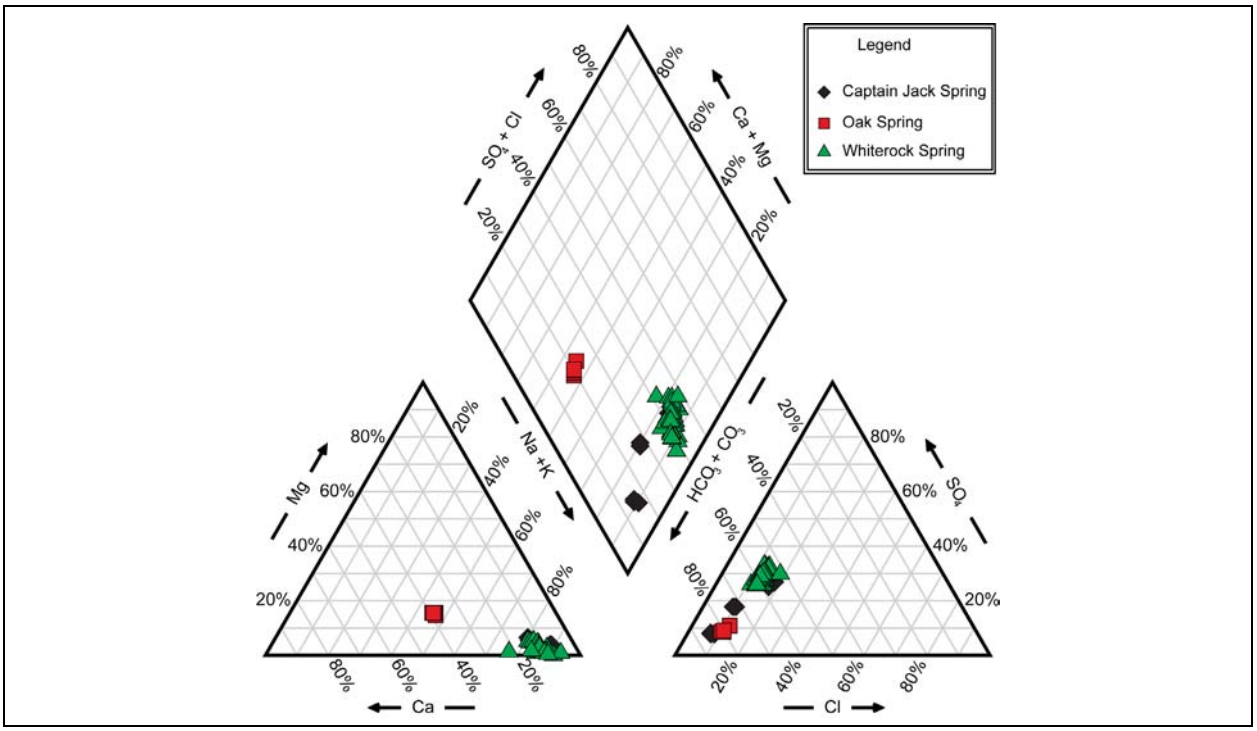

Figure 5-19
Piper Diagram for Samples Collected from the Perched Springs of Yucca Flat

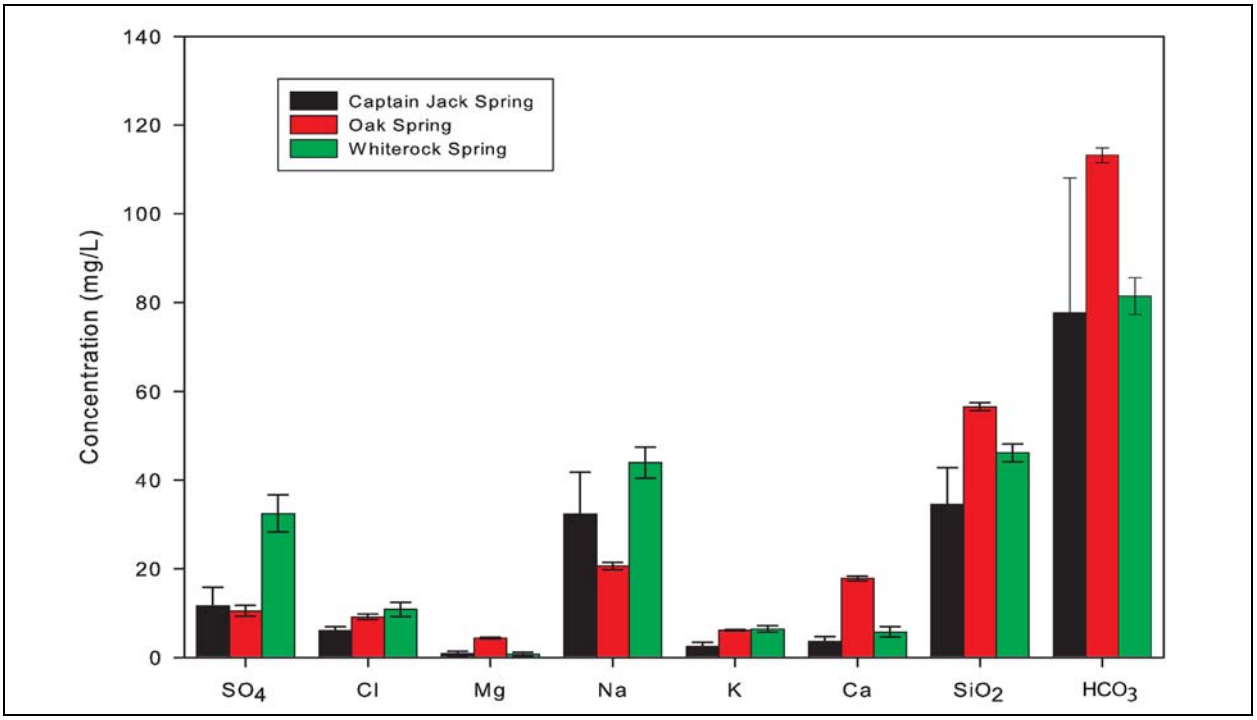

Figure 5-20
Bar Plot for Samples Collected from the Perched Springs of Yucca Flat

homogenization of the water composition within the borehole (Fenelon, 2005). This limits the ability to uniquely define the geochemical characteristics of groundwater within a specific HSU, either locally or regionally, and may have resulted in some of the groundwater mixing that is inferred to have taken place through hydrodynamic processes. Additional limitations associated with the geochemical flow-path evaluation are described in SNJV (2006b).

Oxidation-reduction potentials were made *in situ* for groundwaters of several wells within the Yucca Flat/Climax Mine CAU. It is important to note that these measurements are not always straightforward to make, and the resulting values of ORP are often significantly different than those calculated based on redox couples (Lindberg and Runnells, 1984). As stated in Langmuir (1997), several reasons for these differences include (1) malfunction of the indicator electrode, (2) disequilibrium between and among different redox couples resulting from irreversible or slow kinetics of most redox couple reactions, and (3) existence of mixed potentials in natural waters. More recently (2006 sampling of WW-2), measurements of several different redox couples have been made to reduce uncertainty of the redox state of the groundwater.

5.4 Summary

Recent geochemical evaluations of groundwater flow paths focused on flow in the LCA. Based on previous hydrogeologic studies of the groundwater flow system along with observed trends in geochemical parameters, five conceptual flow paths were identified and thus evaluated. The flow paths were (1) a northern flow path that addressed the proportion of groundwater inflow to Yucca Flat, (2) a flow path from north to south along the eastern side of the Yucca Flat basin, (3) a flow path from north to south along the western side of the basin, (4) a flow path from the southeastern basin margin and moving through southern Yucca Flat to Frenchman Flat, and (5) a west-central flow path addressing the possible source of the strong volcanic-rock signature of the LCA groundwaters. Possible mixing components for individual wells along these groundwater flow paths were identified, and groundwater transit times were estimated. The details of these evaluations are presented within a report, SNJV (2006b), that was prepared in collaboration between multiple UGTA organizations. An important finding of this investigation was the large predicted ^{14}C derived transit times, approximately 16,000 to 24,000 years, for flow in the LCA from UE-10j in northern Yucca Flat to WW-C in southern Yucca Flat.

Further geochemical analysis described within this section focused on compiling and describing a geochemistry dataset that is representative of the HSUs of the Yucca Flat/Climax Mine CAU. This analysis was preformed primarily to support the estimates of distribution coefficients described in Section 11.0. Included in the compilation were major and minor chemistry data, along with *in situ* measurements of ORP, water temperature, pH, and specific conductance. A summary of the data for the HSU groups is as follows.

Alluvial Aquifer

Four wells are completed in the AA in southern Yucca Flat (Figure 5-2). The chemistry of these groundwaters range from a borderline Ca-Mg-HCO_3 type to a borderline Na-K-HCO_3 type. *In situ* measurements were performed for only a single well, WW-3, within the AA. The groundwaters were determined to be in an oxidizing environment with the ORP ranging from 52 to 169 mV. The pH of groundwaters within the AA ranged from 7.8 to 8.3. The RMC associated with the AA is the VMP, which represents a high glass content (greater than 30 percent), low clay (less than 10 percent) and zeolite (less than 10 percent), and low biotite and hornblende (less than 1.5 percent).

Volcanic Units

The dataset is limited with respect to the number of groundwater samples from the volcanic-rock aquifers and the tuff confining units of the Yucca Flat/Climax Mine CAU. Two wells sample groundwater of the TSA, four wells sample the LTCU, and one well samples the OSBCU. The formation access interval for one well, ER-2-1, includes a large section of both the TM-LVTA and the LTCU. Although quite variable, the groundwater of these HSUs are all the Na-K-HCO_3 type. Strong correlations between water chemistry and the specific HSU were not observed. *In situ* measurements were performed for only a single well within the LTCU, TW-7. The groundwaters were determined to be slightly reducing at some depths with the ORP ranging from 206 to -59 mV. This series of *in situ* measurements was performed in 2001, and the results suggest possible instrument drift. Further measurements are required to determine whether these groundwaters are truly within a reducing environment. The mean pH of these groundwaters ranges from 7.1 to 8.4. The anomalously high pH observed for the groundwater of ER-2-1 (mean pH of 9.1) is not included in this range.

The RMC associated with the LTCU and OSBCU for the well locations described within this dataset is ZEOL. For this RMC, zeolites and clays are abundant (greater than 30 percent) with zeolites more abundant than clays, and the abundance of glass is low (less than 10 percent). The RMC associated with the TM-LVTA, VMP, is the same as that assigned to the AA. The RMC associated with the TSA in the vicinity of the well locations described within this dataset is the DMP; this RMC represents a high content of quartz and feldspar (greater than 60 percent), low glass (less than 20 percent), and low biotite and hornblende (less than 1.5 percent).

Clastic Confining Units

Four wells within the Yucca Flat/Climax Mine geochemistry study area are completed in the UCCU, and three are completed within the LCCU. A relatively variable chemical composition of the groundwaters is observed within these units. The groundwater of the UCCU ranges from the Ca-Mg-Na-HCO_3 mixed to the Na-K-HCO_3 type, and that of the LCCU ranges from the Ca-Mg-HCO_3 to the Na-K-HCO_3 type. *In situ* ORP measurements for groundwater of two wells completed in the UCCU indicate a reducing environment (ORP ranges from -51 to -349 mV). No *in situ* measurements were performed on groundwater of the LCCU. The mean pH of groundwater samples ranged from 6.6 to 7.4 and 8.1 to 8.3 for the LCCU and UCCU, respectively. An anomalously high pH observed for the UCCU Well (9.4), UE-16f, is not included in this range.

The primary RMC associated with the UCCU of these wells is the ARG; this RMC represents a high clay content (greater than 30 percent) with the abundance of clay exceeding that of zeolite. The RMC associated with the LCCU is the SC, which represents a high silica/quartz content (greater than 50 percent).

Granite Confining Unit

The available groundwater chemistry data for the Climax Stock (MGCU HSU) are limited to samples collected from five sites in the fractured climax granite from Shaft U-15.01. Four of the samples were collected from groundwater seeps out of isolated fractures, and one was collected from a borehole believed to intersect with the local water table. The major-ion composition of the Climax waters is highly variable. In addition, the Climax Stock samples are relatively unique when compared to all samples within the study area in that the total solute concentrations are much greater in general,

and the dominant anion is SO_4^{2-} rather than HCO_3^-. The high SO_4^{2-} in these samples is inferred to reflect oxidation of the abundant pyrite present along the fractures in the hydrothermally altered granite.

The RMC associated with the MGCU is the DMR. This RMC represents a high content of quartz and feldspars (greater than 60 percent), and a biotite and hornblende content exceeding 1.5 percent.

Carbonate Aquifers

A significant number of samples have been collected from the carbonate aquifers (LCA, LCA3, and UCA) of the Yucca Flat/Climax Mine CAU. Groundwaters of the LCA are separated into the northern, west-central, eastern, and southeastern sections of the Yucca Flat basin for the analysis. The RMC associated with all of the carbonate aquifers is CC, which is characterized by the presence of greater than 50 percent carbonates.

The LCA groundwaters of northern Yucca Flat are the Ca-Mg-HCO_3 type. The other LCA groundwaters within Yucca Flat range from the mixed Ca-Mg-Na-HCO_3 to the Na-K-HCO_3 type. The mean pH for these samples range from 6.4 to 8.4. Measurements of ORP (-97 to -439 mV) indicate a reducing environment for the LCA groundwaters within northern Yucca Flat. The reducing conditions in two of the wells, UE-10j and ER-12-1, (and possibly others) may be attributed to the presence of stagnant water reacting with well casing or sliding sleeve material. A single series of *in situ* measurements of ORP (134 to 276 mV) for the groundwater of a well located within eastern Yucca Flat (ER-6-1) indicates an oxidizing environment.

Groundwaters of the single well completed within the UCA are the Ca-Mg-HCO_3 type. Groundwaters of the LCA3 range from borderline mixed (Ca-Mg-Na-HCO_3) to the Ca-Mg-HCO_3 to a Ca-Mg-SO_4 type. A large variability in groundwater chemistry for the near-field well, UE-2ce, is observed over the time period sampled. A significant increase in the concentration of the major ions was observed during the pumping experiments performed at this well. This variability may be attributed to nuclear test-related effects. The ORP measured for one well completed within the LCA3, UE-1c, indicates that the groundwaters are oxidizing (179 to 183 mV).

6.0 CONTAMINATION SOURCES AND EXTENT

A total of 828 underground nuclear tests were conducted at the NTS between 1951 and 1992 (DOE/NV, 2000b). The Yucca Flat/Climax Mine CAU is particularly important because of the large number of tests (747 detonations) and the variability of geological settings (including both saturated and unsaturated alluvium, vitric tuff, welded tuff, zeolitized tuff, carbonate rock, and granite). In the FFACO (1996; as amended, August 2006), tests are subdivided into CASs, which are either individual tests or small groups of tests. Thus, the number of CASs (720) in the Yucca Flat/Climax Mine CAU is less than the number of detonations.

Unclassified information related to the underground nuclear tests conducted within the Yucca Flat/Climax Mine CAU is compiled primarily in two reports, *United States Nuclear Tests, July 1945 through September 1992* (DOE/NV, 2000b) and *Shaft and Tunnel Nuclear Detonations at the Nevada Test Site: Development of a Primary Database for the Estimation of Potential Interactions with the Regional Groundwater System* (DOE/NV, 1997b). These data — including the name and date of each detonation, name and location of the emplacement holes, announced yields, depths of burial (i.e., the working point), estimated depths to the water table, and the HSU associated with the working point — are summarized in Appendix A.

The term "yield" refers to the total effective energy released in a nuclear explosion and is usually expressed in terms of equivalent tonnage of trinitrotoluene (TNT) required to produce the same energy release in an explosion (1 kt = 10^{15} calories). Announced yield ranges are reported in DOE/NV (2000b); the specific yields for many tests remain classified. The announced yields for some tests were termed low, intermediate, or slight (see Appendix A). Between 1945 and 1963, a less-than-20-kt yield was defined as "low," while a 20- to 200-kt-yield range was referred to as "intermediate." In a few cases, the term "slight" was used without amplification (DOE/NV, 2000b). The maximum upper limit of the announced yield range for Yucca Flat is 500 kt, whereas that of the Climax Mine tests is 62 kt. A zero yield was reported for three tests, SAN JUAN (Operation Hardtack II), COURSER (Operation Whetstone), and TRANSOM (Operation Cresset).

The TRANSOM nuclear device did not detonate and was later destroyed, as planned, by the HEARTS detonation (Operation Quicksilver) approximately 16 months later (DOE/NV, 2000b).

The total inventory (or quantity) of radionuclides associated with each individual test, regardless of form and distribution, is referred to as the radiologic source term (RST) of that test. Radionuclides listed in Bowen et al. (2001) are the most relevant radionuclides for consideration. These should not be considered an exhaustive list of all possible test-related radionuclides but, rather, those with sufficiently long half-lives and abundance to be of regulatory concern over the next 1,000 years. It should be noted that the reported inventories of ^{40}K, ^{232}Th, ^{234}U, ^{235}U, and ^{238}U include estimates of their natural (non test-related) abundance that was incorporated in melt glass. With the exception of ^{40}K, the amount of these radionuclides that is either natural or test-related in origin has not been determined. Note that ^{40}K is entirely of natural origin (Tompson et al, 2004).

The hydrologic source term (HST), which is the amount of radionuclide available for transport in groundwater, is a subset of the RST, both as the specific radionuclides and the amounts of radionuclide. The "exchange volume" is the initially contaminated region for each test. Inventory fractions described as located in the "rubble," "gas," and "water" phases are assigned to the exchange volume, where they are distributed among aqueous and sorbed states in alluvium as described below. The melt glass comprises a storage component for radionuclides from which the radionuclides are slowly released with dissolution of the glass. Some radionuclides are in forms that are almost completely mobile in groundwater, and these are sometimes referred to as "conservative tracers" because they do not interact with the rock through which they move.

6.1 Data Compilation and Data Transfer

All data used in the quantitative analyses in this section are from the Yucca Flat/Climax Mine HFM area; see Appendix A.

6.2 The Yucca Flat/Climax Mine Radiologic Source Term

The RST for the Yucca Flat/Climax Mine CAU was reported in an unclassified report (Bowen et al., 2001), wherein the RST associated with underground nuclear tests at the NTS was subdivided into five principal geographic test centers (Figure 6-1). For each geographic test center, a total

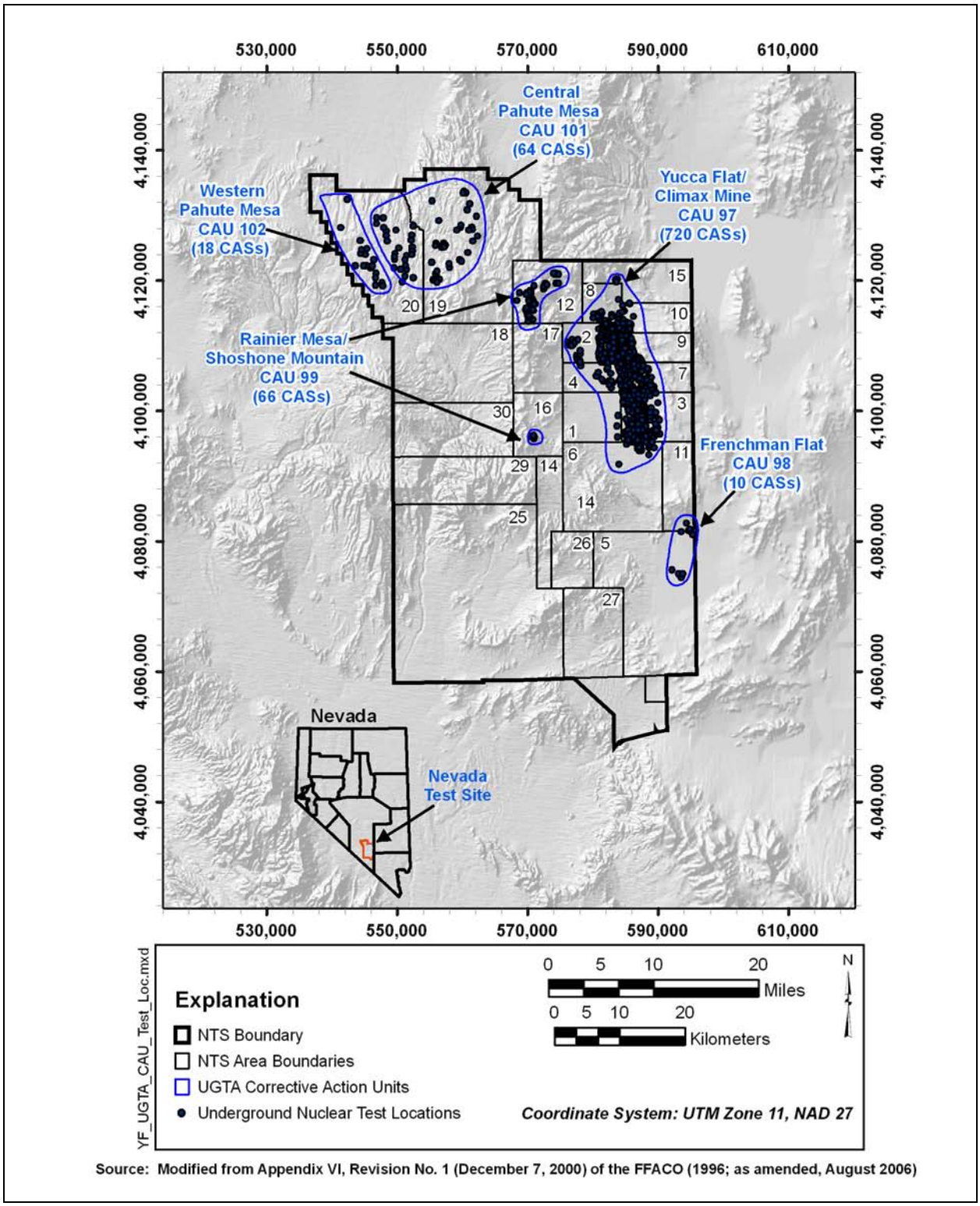

Source: Modified from Appendix VI, Revision No. 1 (December 7, 2000) of the FFACO (1996; as amended, August 2006)

Figure 6-1
Locations of the 828 Underground Nuclear Tests at the Nevada Test Site Between 1951 and 1992

unclassified RST was calculated based on the sum of the classified inventories of individual tests. The list of radionuclides included in Bowen et al. (2001), with Yucca Flat/Climax Mine CAU inventories corrected to September 23, 1992, is presented in Table 6-1. For the Yucca Flat/Climax Mine CAU, Bowen et al. (2001) subdivided tests detonated greater than 100 m above the water table (a total of 577 nuclear tests), and below or within 100 m of the water table (170 tests). Of these, four tests consisted of multiple detonations conducted simultaneously over a depth interval both above and below the static water level (SWL) plus 100 m (Smith et al., 2003). The locations of the water table and the test were taken from DOE/NV (1997b). Importantly, the water table position reported in DOE/NV (1997b) may be less reliable than the most recent regional water table estimates completed for the Yucca Flat/Climax Mine CAU. As a result, tests considered saturated or unsaturated in Bowen et al. (2001) may not be so in future Yucca Flat/Climax Mine CAU flow and transport models.

Table 6-1
Radionuclide Inventory for Yucca Flat/Climax Mine
(Page 1 of 2)

Radionuclide	Symbol	Half-Life (Years)	Atoms		Curies			
			Yucca Flat - Above [a]	Yucca Flat- Below [b]	Yucca Flat - Above [a]	Yucca Flat - Below [b]	Total Yucca Flat	Ratio of Yucca Flat to NTS (%)
Tritium	^{3}H	12.32	3.055E+26	6.881E+26	1.472E+07	3.316E+07	4.79E+07	38.1
Carbon-14	^{14}C	5715	1.094E+25	8.076E+24	1.137E+03	8.389E+02	1.98E+03	69.5
Aluminum-26	^{26}Al	7.1×10^{5}	6.665E+22	4.300E+22	5.573E-02	3.595E-02	9.17E-02	84.6
Chlorine-36	^{36}Cl	3.01×10^{5}	5.899E+25	1.171E+26	1.163E+02	2.309E+02	3.47E+02	56.4
Argon-39	^{39}Ar	269	1.452E+23	4.328E+23	3.204E+02	9.551E+02	1.28E+03	39.8
Potassium-40	^{40}K	1.27×10^{9}	1.758E+29	5.181E+29	8.219E+01	2.422E+02	3.24E+02	40.0
Calcium-41	^{41}Ca	1.03×10^{5}	1.483E+26	2.882E+26	8.545E+02	1.661E+03	2.52E+03	56.8
Nickel-59	^{59}Ni	7.6×10^{4}	2.738E+24	5.460E+24	2.139E+01	4.265E+01	6.40E+01	56.5
Nickel-63	^{63}Ni	100	3.932E+23	8.808E+23	2.334E+03	5.229E+03	7.56E+03	59.1
Krypton-85	^{85}Kr	10.76	2.06E+23	1.052E+24	1.137E+04	5.805E+04	6.94E+04	39.0
Strontium-90	^{90}Sr	28.78	7.265E+24	3.626E+25	1.499E+05	7.479E+05	8.98E+05	41.2
Zirconium-93	^{93}Zr	1.5×10^{6}	1.731E+25	6.587E+25	6.852E+00	2.607E+01	3.29E+01	43.1
Niobium-93m	^{93m}Nb	16.1	1.694E+22	1.825E+23	6.246E+02	6.730E+03	7.35E+03	47.7
Niobium-94	^{94}Nb	2.0×10^{4}	7.734E+23	6.652E+24	2.296E+01	1.975E+02	2.20E+02	55.1
Technetium-99	^{99}Tc	2.13×10^{5}	2.208E+25	6.727E+25	6.153E+01	1.875E+02	2.49E+02	43.6
Palladium-107	^{107}Pd	6.5×10^{6}	8.359E+24	1.010E+25	7.634E-01	9.226E-01	1.69E+00	49.3
Cadmium-113m	^{113m}Cd	14.1	3.719E+21	1.186E+22	1.566E+02	4.994E+02	6.56E+02	33.9
Tin-121m	^{121m}Sn	~55	6.243E+22	1.777E+23	6.738E+02	1.918E+03	2.59E+03	36.2

Table 6-1
Radionuclide Inventory for Yucca Flat/Climax Mine
(Page 2 of 2)

Radionuclide	Symbol	Half-Life (Years)	Atoms		Curies			
			Yucca Flat - Above [a]	Yucca Flat- Below [b]	Yucca Flat - Above [a]	Yucca Flat - Below [b]	Total Yucca Flat	Ratio of Yucca Flat to NTS (%)
Tin-126	^{126}Sn	2.5×10^{5}	1.433E+24	3.858E+24	3.402E+00	9.161E+00	1.26E+01	37.9
Iodine-129	^{129}I	1.57×10^{7}	5.498E+24	1.434E+25	2.079E-01	5.422E-01	7.50E-01	42.6
Cesium-135	^{135}Cs	2.3×10^{6}	2.683E+25	7.633E+25	6.926E+00	1.970E+01	2.66E+01	44.4
Cesium-137	^{137}Cs	30.07	1.478E+25	4.710E+25	2.919E+05	9.299E+05	1.22E+06	42.8
Samarium-151	^{151}Sm	90	2.105E+24	4.835E+24	1.388E+04	3.189E+04	4.58E+04	42.9
Europium-150	^{150}Eu	36	8.209E+23	6.664E+21	1.354E+04	1.099E+02	1.36E+04	92.3
Europium-152	^{152}Eu	13.54	8.288E+23	1.615E+24	3.634E+04	7.083E+04	1.07E+05	71.1
Europium-154	^{154}Eu	8.593	4.297E+23	7.932E+23	2.968E+04	5.480E+04	8.45E+04	79.7
Holmium-166m	^{166m}Ho	1.2×10^{3}	5.387E+22	1.115E+23	2.665E+01	5.514E+01	8.18E+01	55.7
Thorium-232	^{232}Th	1.40×10^{10}	1.408E+29	4.133E+29	5.969E+00	1.752E+01	2.35E+01	39.8
Uranium-232	^{232}U	69.8	1.059E+22	4.338E+22	9.004E+01	3.690E+02	4.59E+02	63.7
Uranium-233	^{233}U	1.592×10^{5}	3.223E+25	4.090E+25	1.202E+02	1.525E+02	2.73E+02	58.5
Uranium-234	^{234}U	2.46×10^{5}	3.534E+25	6.194E+25	8.528E+01	1.495E+02	2.35E+02	60.6
Uranium-235	^{235}U	7.04×10^{8}	3.032E+27	3.819E+27	2.557E+00	3.220E+00	5.78E+00	67.2
Uranium-236	^{236}U	2.342×10^{7}	3.599E+25	1.364E+26	9.123E-01	3.458E+00	4.37E+00	46.6
Uranium-238	^{238}U	4.47×10^{9}	6.531E+28	1.182E+29	8.674E+00	1.570E+01	2.44E+01	54.8
Neptunium-237	^{237}Np	2.14×10^{6}	4.108E+24	3.863E+25	1.140E+00	1.072E+01	1.19E+01	24.4
Plutonium-238	^{238}Pu	87.7	2.621E+24	1.647E+24	1.774E+04	1.115E+04	2.89E+04	73.1
Plutonium-239	^{239}Pu	2.410×10^{4}	4.058E+27	1.115E+27	9.997E+04	2.746E+04	1.27E+05	79.6
Plutonium-240	^{240}Pu	6.56×10^{3}	2.798E+26	7.785E+25	2.523E+04	7.045E+03	3.24E+04	77.2
Plutonium-241	^{241}Pu	14.4	8.284E+24	2.508E+24	3.415E+05	1.034E+05	4.45E+05	75.2
Plutonium-242	^{242}Pu	3.75×10^{5}	4.728E+24	2.919E+24	7.485E+00	4.621E+00	1.21E+01	74.8
Americium-241	^{241}Am	432.7	1.683E+25	4.437E+24	2.309E+04	6.088E+03	2.92E+04	78.6
Americium-243	^{243}Am	7.37×10^{3}	3.33E+22	4.241E+22	2.682E+00	3.416E+00	6.10E+00	86.2
Curium-244	^{244}Cm	18.1	4.836E+22	7.641E+22	1.586E+03	2.506E+03	4.09E+03	54.3
Total			3.899E+29	1.057E+30	1.578E+07	3.523E+07	5.10E+07	38.6

Source: Modified from Bowen et al., 2001
[a] Total inventory for tests detonated more than 100 m above the water table
[b] Total inventory for tests detonated below or within 100 m of the water table

Note: Data are decay corrected to September 23, 1992 (date of last underground nuclear test).

Bowen et al. (2001) also report an estimation of the accuracy of the radionuclide inventory. Radionuclides measured directly are more accurately reported than those for which estimates had to be made based on device characteristics and performance. There are also tests in the inventory for which little or no post-test information exists; estimates of radionuclide content for these tests are considerably more uncertain and increase the overall uncertainty for a given nuclide. The accuracy of the estimate of the radionuclide content is highly dependent on the source(s) of the radionuclide. Bowen et al. (2001) therefore report the accuracy of the reported inventory as a function of radionuclide groups depending on their source: fission products (approximately 10 to 30 percent), unspent fuel materials (less than or equal to 20 percent), fuel activation products (less than or equal to 50 percent), residual ^{3}H (less than or equal to 300 percent), and activation products (approximately a factor of 10).

6.3 Groundwater Sampling Locations in the Yucca Flat/Climax Mine CAU

Of the 828 underground nuclear detonations at the NTS, 259 are located near or below the regional water table. Few of these sites have wells that can be used for groundwater sampling. The paucity of sampling locations reflects the logistical complexities associated with accessing the underground testing environment. Most of the nuclear tests were conducted between 300 and 1,400 m bgs. Well construction and development at these sites is difficult and expensive (Smith, 2002). Approximately half of the near-field wells (wells with radionuclide contamination located nearby nuclear tests) used for groundwater sampling were completed opportunistically in post-test, re-entry holes. These boreholes were originally drilled into test cavities to return solid samples for the diagnosis of device performance. The remaining wells were drilled specifically for near-field groundwater characterization purposes by the Hydrologic Resources Management Program (HRMP), the Radionuclide Migration (RNM) Program, or the UGTA Project.

Groundwater samples from near-field or post-test wells have been collected at 15 test locations, shown on Figure 6-2. Of these, eight are located in the Yucca Flat/Climax Mine CAU. Details regarding the sampling wells located in Yucca Flat are compiled in Table 6-2. The table includes information on the associated nuclear test name. Several of the sites have (or had) more than one sampling well, providing data at different locations or depth intervals relative to the test working point, so radionuclide transport information could be inferred. Many of the sampling wells were

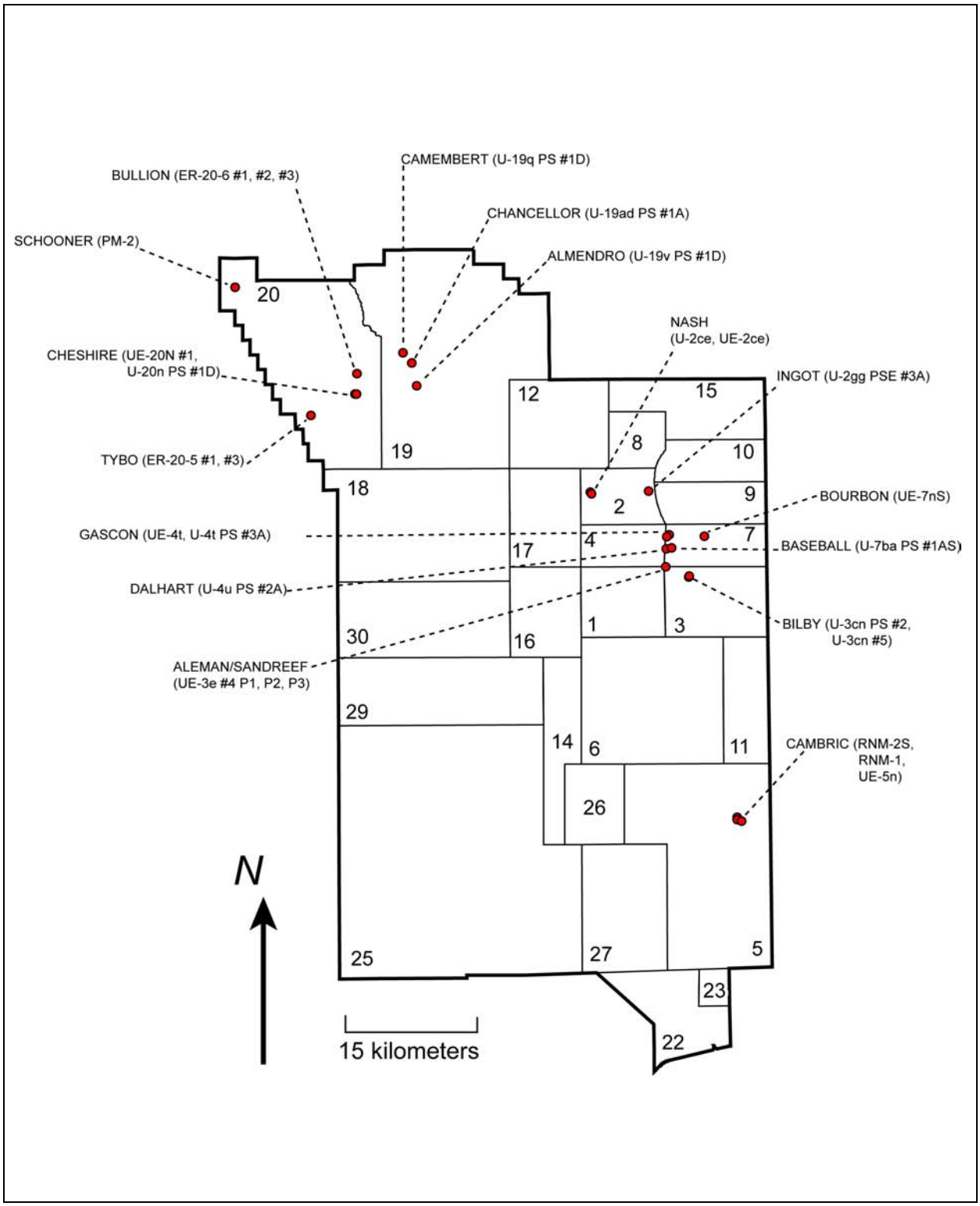

Figure 6-2
Map of the Nevada Test Site Showing the Near-field Sampling Sites

Test name and affiliated near-field well (in parentheses) are provided.

Table 6-2
Underground Nuclear Tests Associated with Near-field Sampling Wells in the Yucca Flat/Climax Mine CAU

Test Name	Emplacement Hole	Test Date	Working Point (m)	Test Yield (kt) [a]	Working Point HGU/HSU	Sampling Well	Sampled HGU/HSU	Sampling Location with Respect to the Emplacement Hole
ALEMAN	U-3kz	09/11/1986	503	<20	VTA	UE-3e #4 (slant hole)	VTA	58 m north
BASEBALL	U-7ba	01/15/1981	564	20-150	TCU	U-7ba PS #1AS (slant hole)	TCU	Cavity/chimney region
BILBY	U-3cn	09/13/1963	715	249	TCU	U-3cn PS #2	TCU	Chimney region
						U-3cn #5	LCA	129 m southeast
BOURBON	U-7n	01/20/1967	560	20-200	LCA	UE-7nS	LCA	137 m from working point
DALHART	U-4u	10/13/1988	640	<150	TCU	U-4u PS #2A (slant hole)	TCU	Chimney region
GASCON	U-4t	11/14/1986	593	20-150	TCU	UE-4t	TCU	~170 m to the south
						U-4t PS #3A (slant hole)		~54 m from cavity wall
INGOT	U-2gg	03/09/1989	500	20-150	VTA	U-2gg PSE #3A (slant hole)	VTA	65 m below working point in saturated zone
NASH	U-2ce	01/19/1967	364	39	LCA3	UE-2ce	LCA3	183 m from working point

[a] Announced yields are from DOE/NV, 2000b.

drilled at a slant to access the cavity from a surface location outside of the collapse crater. True vertical depth is provided unless otherwise specified. The "working point" refers to the depth of burial of the nuclear device in meters below the local ground surface. Reported test yields (in kilotons of TNT equivalent) are taken from an unclassified data compilation prepared by the DOE (DOE/NV, 2000b). The HGUs or HSUs at the working point and at the sampling point are specified; the LCA and LCA3 are distinguished at the HSU-level to indicate significant differences. Hydrogeologic units are used to categorize rocks according to their ability to transmit groundwater, which is a function of their lithologic properties, degree of fracturing, and secondary mineral alteration (Section 4.0).

Table 6-3 provides a historical summary of the groundwater sampling events — including the collection method, dates, and number of sampling events — for each of the near-field wells located within the Yucca Flat/Climax Mine CAU. A comprehensive database, recently compiled by LLNL and LANL, contains radionuclide data for 22 monitoring wells associated with 15 underground

Table 6-3
Compilation of Groundwater Sample Collection Methods and Dates

Test Name	Sampling Well Name(s)	Sample Collection Method	Sample Collection Dates
ALEMAN	UE-3e #4 (P1, P2, P3)	Pump/Pressure tube	1990 - 1998
BASEBALL	U-7ba PS #1AS	Pressure tube	1995
BILBY	U-3cn PS #2	Pump	1964 - 2004
	U-3cn #5		1965 - 1997
BOURBON	UE-7nS	Pump/Bailer	1983 - 2005
DALHART	U-4u PS #2A	Bailer (1992 - 1997); Pump (after 1997)	1992 - 2003
GASCON	U-4t PS #3A	Pressure tube	1993
	UE-4t		1990 - 1992
INGOT	U-2gg PSE #3A	Bailer	1993 - 1994
NASH	UE-2ce	Pump/Bailer	1977 - 2005

nuclear tests at the NTS (Figure 6-2), with a total of nearly 1,300 sampling events. However, approximately 950 of these sampling events were at RNM-2S in Frenchman Flat during the CAMBRIC RNM experiment. The near-field well database has been incorporated, and is updated annually, in the *Comprehensive Water Quality Database for Groundwater in the Vicinity of the Nevada Test Site, Geochem06.mdb* (SNJV, 2006a).

Each near-field well is unique, and the set of wells with radionuclide contamination presents a wide range of geologic and hydrogeologic conditions, RSTs, and groundwater sample quality. There also have been significant differences in sampling protocols over the years; hence, caution should be used when comparing data from different wells (Kersting, 1996). Samples collected using downhole submersible pumps are more likely to be representative of the bulk fluid composition in the near-field environment. Several of the wells, particularly those that have been converted from post-test re-entry holes, consist of a small diameter (7.3-cm) carbon-steel piezometer tube (Smith, 2002). In most cases, these wells have only been sampled using wireline bailers, although there have been recent attempts to develop pumps that would fit into the small diameter tubing. Given that the standing fluid in these piezometers does not circulate freely with the sampled formation and that thorough purging could not be accomplished, samples collected from these wells tend to be of lower quality than those

from pumped wells. Sample collection methods for wells within Yucca Flat are compiled in Table 6-3.

Hu et al. (2003) assessed the migration behavior of mobile radionuclides (^{3}H, ^{14}C, ^{36}Cl, ^{85}Kr, ^{99}Tc, and ^{129}I) at the NTS and concluded that understanding the speciation and partitioning of radionuclides (e.g., long-lived ^{99}Tc and ^{129}I) is important for understanding their transport behavior. For example, the interaction of ^{3}H with a solid surface via isotopic exchange with clay lattice hydroxyls may cause a slight delay in the transport of ^{3}H. The transport of ^{14}C is likely retarded by its isotopic exchange with carbonate minerals, and the exchange may be more pronounced in the vadose zone. Without a detailed examination of rock properties (e.g., mineralogy), the role of processes such as anion exclusion cannot be adequately evaluated.

Based on available groundwater radiochemical analyses, it appears that actinides (one class of radionuclides, the remainder from unburned fuel) are only present at very low concentrations in NTS groundwater (Hu et al., 2006). The majority of the actinide source term is immobilized in the melt glass or on rubble surfaces. Actinide release rates are dependent on glass dissolution rates as well as the rate of water-rock reactions with sorbed species. Their mobility in groundwater is strongly dependent on ambient reduction-oxidation (redox) conditions because the most prominent actinides (U, Np, Pu) occur in multiple valence states. Low-solubility (low valence state) actinides may also be transported as real colloids or pseudo-colloids (actinide sorbed to mineral colloids).

In addition to the sites discussed above, where groundwater samples have been collected and analyzed, there are several sites (e.g., BASEBALL, INGOT, HYRAX, HANDCAR) where information is available on the physical distribution of radionuclides in the near-field, but data for radionuclide concentrations in groundwater are either absent or extremely limited. Drillbacks into nuclear test cavities have been conducted for many tests to obtain melt glass for diagnostic purposes. Other drillbacks were specifically performed with the objective of acquiring data on the distribution of radionuclides, and useful information on vertical distributions of ^{3}H and fission products at the NTS has been obtained (Thompson, 1996b; Smith, 1998). Tests associated with the Plowshare program were often examined in great detail. Furthermore, due to the nature of the Plowshare program, much of this information is unclassified. Unclassified data used to characterize the

near-field environment of tests detonated in the Yucca Flat/Climax Mine CAU are summarized in the following sections.

In addition to information on radionuclides in the test cavity, there is some information on radionuclides distributed by prompt injection and by convection in the chimney. Prompt injection refers to dynamic, early-time movement of radionuclides as plasma or high-temperature gas along zones of weakness in rock adjoining the test cavity (Smith, 2002). Convection in the chimney driven by residual heat from the test can move radionuclides upwards to permeable rock layers. The extent of convection from the cavity up the chimney is dependent upon the saturated height within the chimney, sufficient increase of permeability in the chimney, and the residual heat to drive buoyancy effects.

6.4 Alluvium and Tuff Tests

6.4.1 DALHART

The DALHART test was conducted in 1988 with an announced yield of less than 150 kt (DOE/NV, 2000b). The test working point was at a depth of 640 m bgs in zeolitized tuff (Figure 6-3). The water level was at a depth of 508 m bgs. Mathews et al. (1994) estimated a cavity radius of 61 m based on a yield of 150 kt. In 1990, the post-test drillback U-4u PS #2A was completed with a slotted interval between 472 and 501 m; the water level had risen to 477 m by 1993 and to 455 m by 1998 (Thompson, 1995; Fenelon, 2005). The slotted interval is 139 to 168 m above the working point (2.25 to 2.75 cavity radii). Radioactivity in drilling fluids was first encountered at 532 m bgs. The radionuclide, ^{137}Cs, was detected in core from 525 m bgs, 115 m above the working point (1.9 cavity radii). Importantly, no radioactivity was observed in the vadose zone (Figure 6-3).

Water samples have been collected intermittently at this site since 1992. Early samples had a significant particulate load resulting from drilling muds (Thompson, 1995 and 1999). The well had never been thoroughly cleaned out. However, the most recent set of samples were collected in 2003 using a low-flow coil pump. At that time, a total of 7,058 gallons (26.7 cubic meters [m^3]) of water was purged from the well before sampling. Samples contained 6.17 x 10^7 pCi/L ^{3}H decay corrected to time zero (t_0) for the DALHART test. This represents a modest increase compared to the previous sampling event in August 1999, when the decay-corrected activity for ^{3}H was 1.6 x 10^7 pCi/L. The

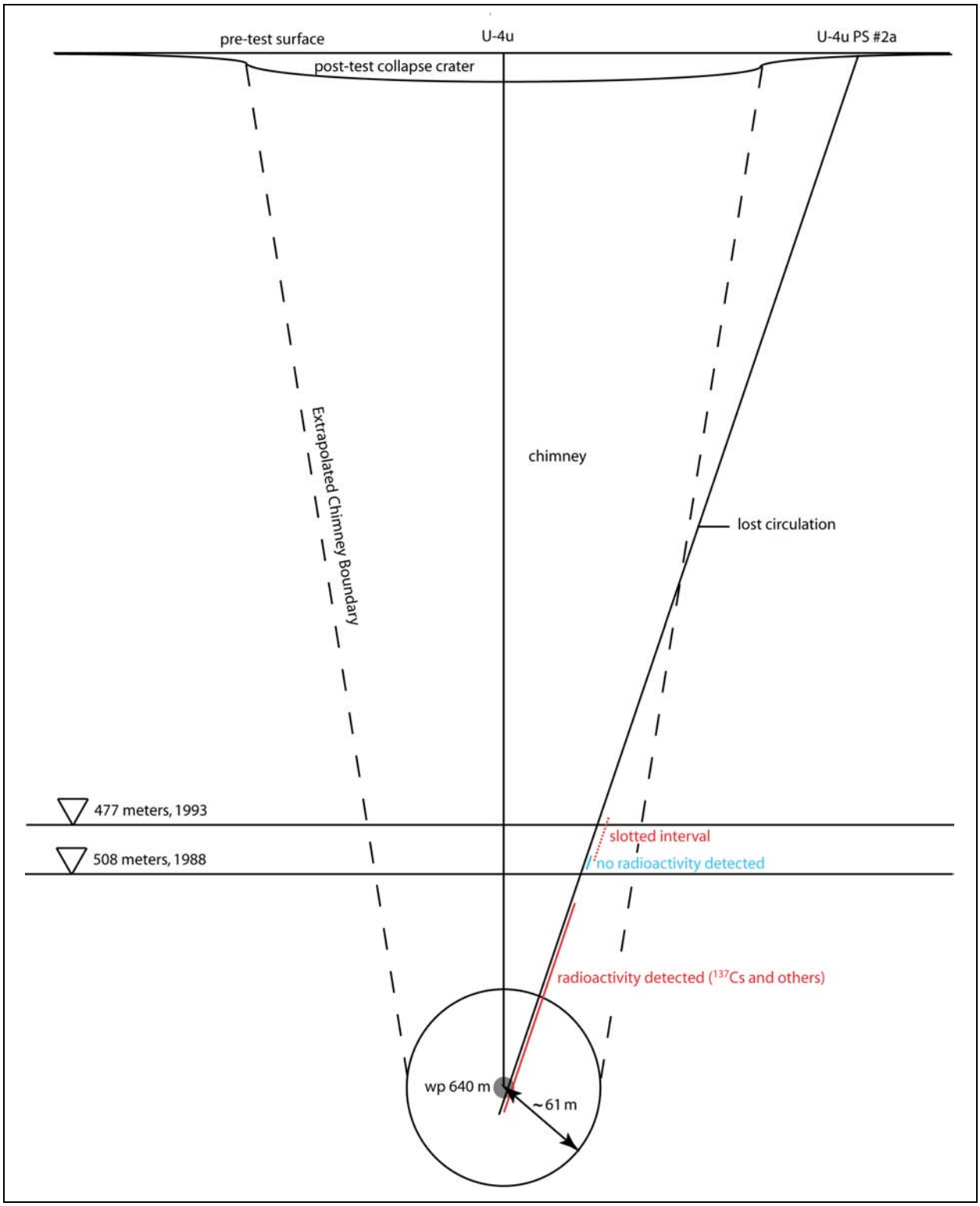

Figure 6-3
The DALHART Near-field
Drillback location is approximate.

^{14}C activity in the 2003 samples (326 pCi/L) increased by 30 percent relative to the 1999 samples (229 pCi/L). The ^{36}Cl activity showed a more dramatic change over the same time period, increasing from 8.52 pCi/L to 29.3 pCi/L. Between 1999 and 2003, the ^{99}Tc activity rose by almost a factor of three (13.1 to 35.1 pCi/L), and the ^{129}I activity increased by more than a factor of four (0.029 to 0.13 pCi/L). Although only modest amounts of groundwater have been pumped from the U-4u PS #2A borehole throughout its history, the pumping process may be drawing in water with higher levels of activity from the test cavity. However, the rocks associated with the working point and chimney (TCU versus LFA) are much different, and the expected vertical hydraulic conductivity of the chimney would be much lower than that of the DALHART cavity. Alternatively, test-derived heat may be driving radionuclides higher into the chimney, as predicted at CHESHIRE and other sites (Pawloski et al., 2001). The 2003 samples also contained readily detectable amounts of Pu, with a total concentration of 5.0 picograms per liter and a $^{239,240}Pu$ activity of 0.32 pCi/L. Filtration experiments showed that essentially all of the Pu is associated with colloids. It appears that both non-sorbing and colloid-associated radionuclides (e.g., Pu) migrated at least 2 to 3 cavity radii vertically in the DALHART chimney over the 15-year period following detonation.

6.4.2 GASCON

GASCON was a 20- to 150-kt test detonated in 1986 (DOE/NV, 2000b). The working point was at a depth of 593 m bgs, and a confined aquifer was penetrated during drilling (Thompson, 1994; DOE/NV, 1997b). In May 1993, post-test hole (U-4t PS #3A) was drilled to within 54 m of the cavity wall and extended underneath the cavity (Figure 6-4). Tritium was encountered during drilling, indicating some radionuclide transport occurred beyond the GASCON cavity. Sampling at GASCON was attempted in 1993 from U-4t PS #3A and UE-4t in 1990, 1992, and 2000. However, samples appeared to be highly contaminated with drilling fluids. Thus, radionuclide concentrations measured in GASCON at U-4t PS #3A may be unrepresentative of formation waters, and little information can be gleaned from these measurements (Thompson, 1994).

6.4.3 BILBY

The BILBY test (249 kt, 87-m cavity radius) was emplaced in zeolitized tuff very close to the underlying regional carbonate aquifer (within approximately 150 m). The bottom of the BILBY cavity is estimated to be approximately 60 m from the tuff-carbonate contact. Both a post-test

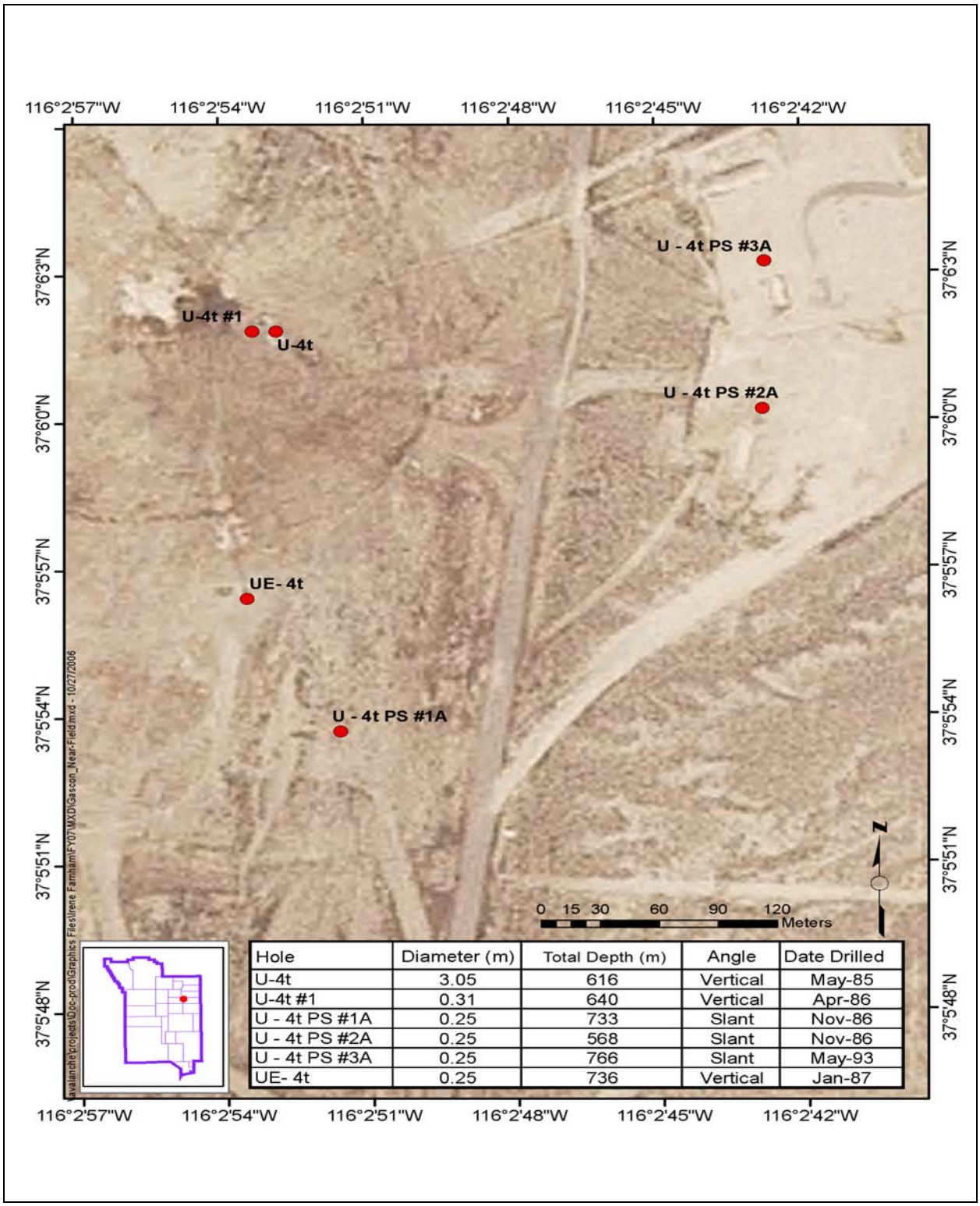

Hole	Diameter (m)	Total Depth (m)	Angle	Date Drilled
U-4t	3.05	616	Vertical	May-85
U-4t #1	0.31	640	Vertical	Apr-86
U - 4t PS #1A	0.25	733	Slant	Nov-86
U - 4t PS #2A	0.25	568	Slant	Nov-86
U - 4t PS #3A	0.25	766	Slant	May-93
UE- 4t	0.25	736	Vertical	Jan-87

Figure 6-4
Plan View Location of Post-test and Exploratory Holes in the GASCON Near-field
Source: Modified from Thompson, 1994

drillback access hole (U-3cn PS #2), and a satellite well (U-3cn #5), 122 m laterally from the working point and completed in carbonate rock, have been sampled over many years (Figure 6-5). The drillback has both perforations approximately 200 m above the working point and is open to the cavity, but crimping below the perforations prevented sampling at a lower level. The satellite well was drilled to evaluate the connectivity between the TCU and carbonate aquifer (Buddemeier and Isherwood, 1985). Water levels in the satellite well completed in the carbonate aquifer are 15.8 m lower than the post-test hole. Thus, the groundwater gradient is from the tuff to the carbonate, but the permeability of the zeolitized unit may prevent significant downward transport (Carle et al., 2007). Note that water levels in the BILBY post-test hole took approximately five years to recover. No significant radioactivity has been detected in the satellite well. However, some indication of prompt injection was reported (Buddemeier and Isherwood, 1985). It appears from these analyses that upward migration of radionuclides into the chimney (possibly as a result of test-induced heat) is more likely than downward migration and contamination of the carbonate aquifer. However, as noted in Buddemeier and Isherwood (1985), due to the spatially heterogeneous nature of fracture flow in the carbonate aquifer, contamination of the carbonate aquifer cannot be ruled out based on sampling of U-3cn #5 alone. Pumping rates of 50 gallons per minute (gpm) were used in the satellite well. This is significantly lower than the CAMBRIC pumping rate (600 gpm) and may not have provided a sufficient gradient to draw the BILBY cavity water to the satellite well.

6.4.4 BASEBALL

The BASEBALL test was detonated in 1981 in Yucca Flat with an announced yield of 20 to 150 kt (DOE/NV, 2000b). The BASEBALL test was located at a depth of 564 m bgs in tuff and with a water table measured at 458 m (DOE/NV, 1997b). Smith (1997) and Thompson (1996a and b) report the water table at 512 m (Figure 6-6). Smith (2002) reports the water table at both 458 and 512 m, suggesting that pre-test and post-test water levels may have changed. In 1994, two post-test holes were drilled into the cavity of BASEBALL (Thompson, 1996a and b). During post-test drilling, radiation levels in the upper part of the cavity were measured using a high-sensitivity gamma detector. The results showed extremely heterogeneous radionuclide deposition in the underground environment of the cavity region. An extreme variability of radionuclide content exists in samples taken from locations close to one another even at the same depth. Even ^{3}H preserves a distribution pattern such that large concentration differences exist over narrow intervals both vertically and

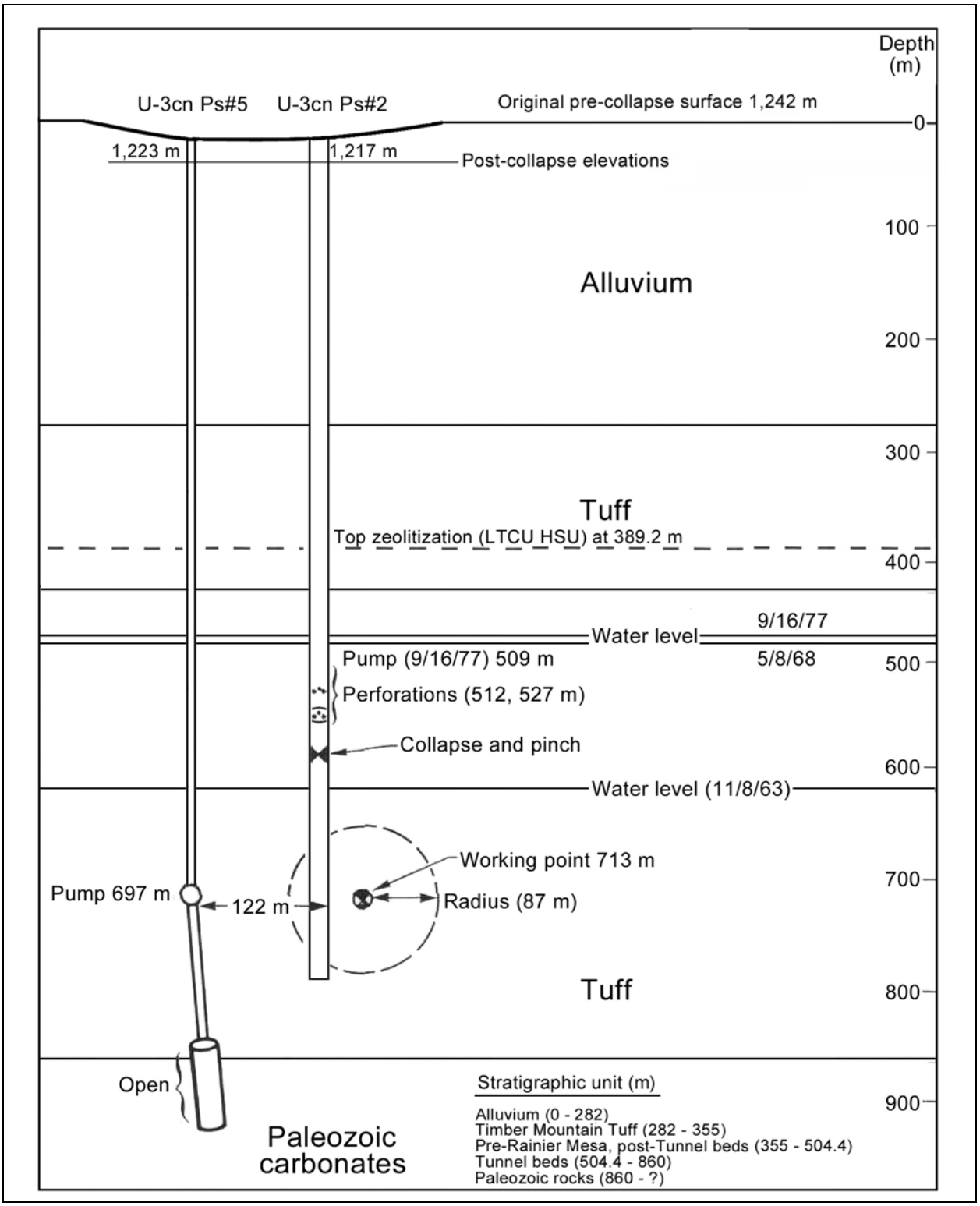

Figure 6-5
The BILBY Near-field

Source: Modified from Buddemeier and Isherwood, 1985

Note: Cavity radius reported in original figure, 64 m, was changed to be consistent with Buddemeier and Isherwood (1985) text and information reported in DOE/NV (1997b).

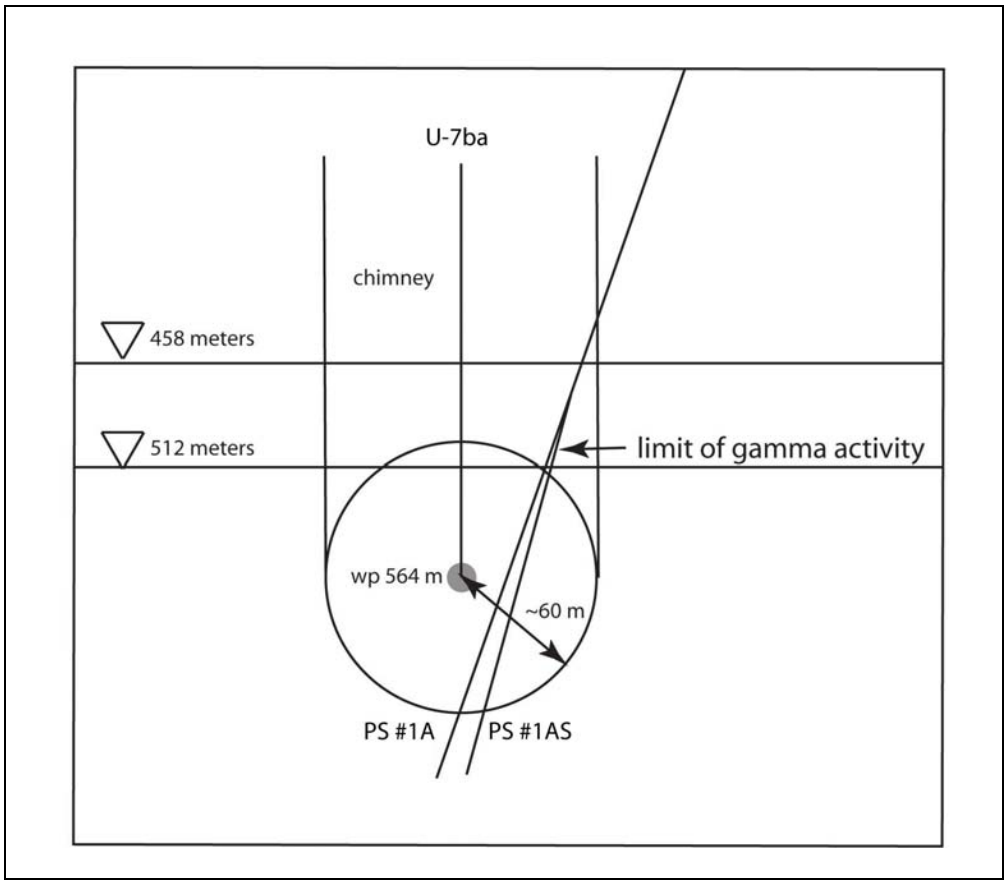

Figure 6-6
The BASEBALL Near-field
Source: Modified from Figure 3 of Thompson, 1996b

horizontally. Radionuclides appear to have remained where they were originally deposited during the formation of the cavity and chimney (Thompson, 1996a and b). During a 13-year span from the detonation and drillbacks, there seems to have been little vertical or horizontal migration of ^{3}H. It is likely that the lack of vertical migration is in part due to the very shallow location of this test relative to the water table. Unlike the DALHART test, a water column above the working point, which could provide vertical transport as a result of test-derived heat, is not present. Gamma activity was not detected above the water table or significantly outside the estimated cavity radius of approximately 60 m based on a yield of 150 kt. A similar lack of vertical migration was simulated at the CAMBRIC test due to the proximity of the water table to the working point.

In July 1995, bailed samples were taken at several intervals in the BASEBALL post-test hole (U7ba PS#1AS). Unfortunately, the hole was never successfully cleaned out. Thompson (1996a

and b) concluded that little or no communication occurred between the water in the casing and the formation water since the time the hole had been drilled. Interestingly, the ^{3}H concentration in the bailed samples (approximately 2 x 10^{7} pCi/L) is consistent with the ^{3}H concentrations found in water from earlier core samples (10^{6} to 10^{8} pCi/L).

6.4.5 INGOT

The INGOT test was detonated in emplacement hole U-2gg in 1989, in Yucca Flat, with an announced yield of 20 to 150 kt (DOE/NV, 2000b). The INGOT test was located at a depth of 500 m bgs in tuff and 300 m above the Paleozoic carbonates (Hudson and Stubbs, 1990). The water table was reported at 564 m (DOE/NV, 1997b). As discussed in Smith (1998) and Smith et al. (1996a and b), the 1994 INGOT drillback targeted fractured media adjacent to the edge of the cavity and emphasized the extent of gaseous transport in discrete intervals of enhanced permeability (Figure 6-7). The drillback hole, U-2gg PSE #3A, was slant-drilled to pass within 10 m of the edge of the cavity, at the level of the working point, at a total depth 46 m below SWL. The results show that in addition to ^{3}H, gaseous fission daughter products, including ^{137}Cs, are abundant and may be encountered 10 m or more from the cavity edge (Figure 6-8). Over 90 percent of the ^{137}Cs is produced from beta-decay of a gaseous ^{137}Xe parent with a 3.84-minute (min) half-life. Overall, the late-time gaseous transport of ^{137}Xe and ^{90}Kr is responsible for the dispersion and subsequent deposition of ^{137}Cs and ^{90}Sr. Importantly, the INGOT cavity is located in the unsaturated zone, with a working point that is 65 m above the SWL. Bailed groundwater samples collected from below the cavity suggests that very little radioactivity reached the water table. For example, measured ^{3}H concentrations are on the order of 10,000 pCi/L, below the EPA limit for drinking water (EPA, 2000). The ^{137}Cs and ^{85}Kr concentrations in groundwater were less than 10 pCi/L and less than 20 pCi/L, respectively. This can be compared to the 1 x 10^{3} to 3 x 10^{6} picocuries per kilogram (pCi/kg) measured in rubble material located approximately 10 m away from the INGOT cavity. The ^{14}C activity in these waters was reported to be as high as 20,000 pCi/L in these waters; however, the value was reported only once (Smith et al., 1998; Thompson, 1995). Thus, the reported groundwater chemistry may not be representative of formation waters. The observed poor connectivity between the unsaturated cavity and saturated groundwater is not conclusive.

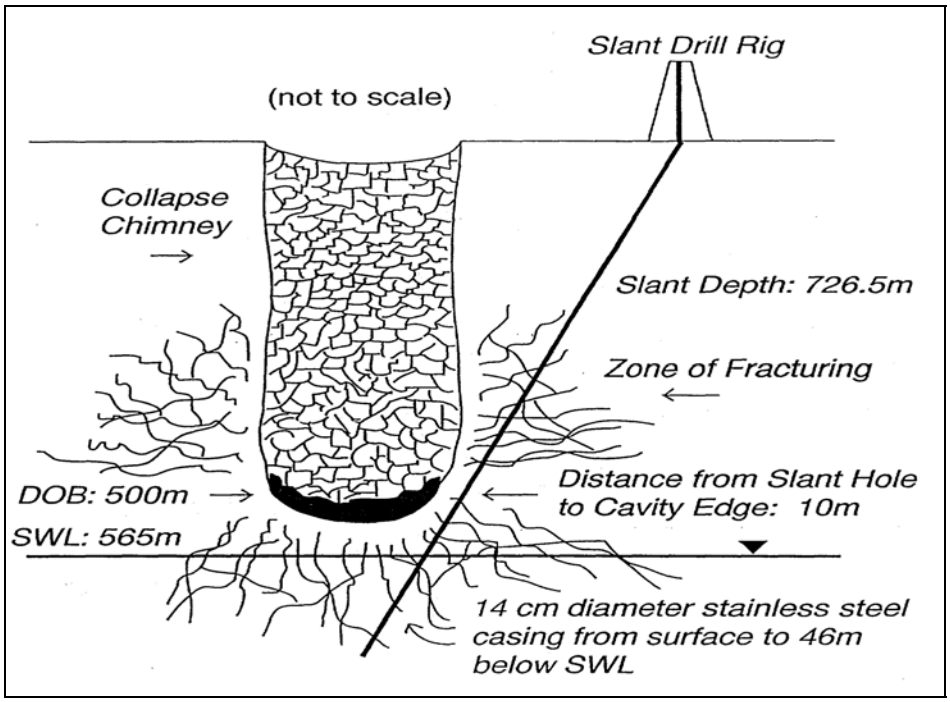

Figure 6-7
The INGOT Slant Drilled Groundwater Sampling Well
Source: Smith et al., 1996b

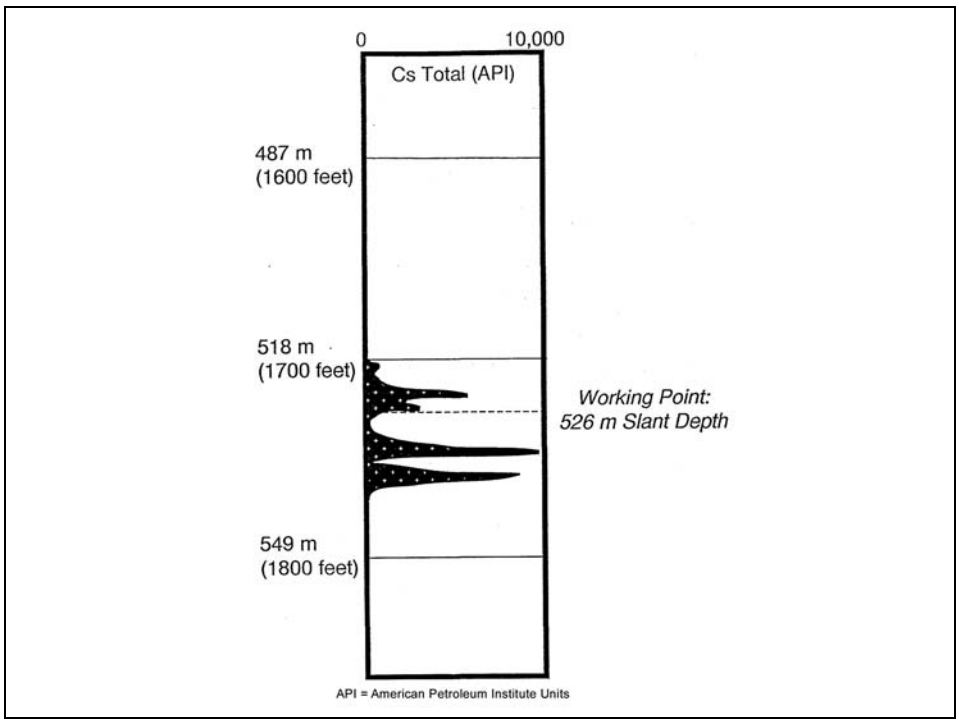

Figure 6-8
Activity in the INGOT Drillback
Source: Smith et al., 1996b

6.4.6 ALEMAN

The ALEMAN test was detonated in 1986 with an announced yield of less than 20 kt (DOE/NV, 2000b). The ALEMAN test was located at a depth of 503 m bgs in tuff; the water table was reported to be 474 m (DOE/NV, 1997b). Hole UE-3e #4 was completed 57 m from the working point with three piezometer tubes accessing depths 655 to 662 m (tube 1), 575 to 582 m (tube 2), and 493 to 500 m (tube 3) (Thompson, 1999). The tubes were swabbed in an attempt to clean them out. Nevertheless, groundwater samples had significant quantities of cement and corresponding very high pHs. Samples from the deepest interval consistently had higher ^{3}H concentrations than in the other two tubes. Thompson (1992a) suggested that ^{137}Cs found at approximately 650 m in sidewall samples in this hole is likely to be coming from the SANDREEF test (701 m depth of burial; 20 to 150 kt yield) that is located 350 m laterally from the ALEMAN test. It is possible that measured ^{3}H is also influenced by SANDREEF. This would be an example of prompt injection of volatile radionuclides along fractures.

6.4.7 Other Alluvium and Tuff Tests

Early-time ^{137}Cs transport due to the volatility of its precursors has been observed at HYRAX (hole U-3bh). HYRAX was detonated in unconsolidated alluvium of Area 3 in 1962 at a working point 272 m above the static water table (Smith, 1998). Two vertical boreholes (U-3bh #1 and #2), separated by 15 m, were drilled in the bottom of the subsidence crater. Drill cores indicate the presence of ^{137}Cs in the collapse chimney at 152 m above the working point (about 5 cavity radii based on a yield of 20 kt) in the unsaturated zone. This ^{137}Cs was probably produced from the beta-decay of a gaseous ^{137}Xe parent due to gas movement at the time the cavity and chimney formed (cavity collapse time was 7.9 min). This suggests that significant radionuclide transport can occur in the distributed chimney region of a nuclear test conducted in the vadose zone. A significant amount of carbonate existed at the HYRAX working point, and the vaporization and melting of the carbonate produced an abundance of noncondensible CO_2 gas (based on 5.9 weight percent calcite for Yucca Flat alluvium, approximately 106 liters of CO_2 gas are produced per kt of nuclear explosive yield) that entrained the radioactive gases (Thompson, 1997). While ^{137}Cs abundances are nearly the same in the two boreholes, the ^{3}H abundances vary by two orders of magnitude; other causes for the observed ^{3}H distribution were suspected (Thompson, 1997).

Two neighboring tests, BOBAC and JERBOA, were conducted at similar depths as HYRAX in the same carbonate-rich alluvium with similar phenomenology, but these tests showed no evidence of significant ^{137}Cs ascent through the chimney (Thompson, 1999; Smith, 2002). This implies that differences in radionuclide production, transport mechanisms, or collapse phenomena produced significantly different radionuclide distributions at BOBAC and JERBOA compared to HYRAX (Smith, 2002). The BOBAC test (U-3bl) was conducted in 1962 at a depth of 195 m bgs. Cavity collapse occurred 8.2 min after the test (similar to HYRAX); the collapse zone extended to the surface and formed a crater about 14 m deep. The slant hole (U-3bl-D2), drilled in 1996, passed under the collapse zone and through the rubble chimney below the zone. The hole terminated at a vertical depth of approximately 97 m. Twenty-nine cores were collected at 3-m intervals throughout the chimney region. No ^{137}Cs was detected, even in cores taken from about 3.5 to 4.5 cavity radii above the working point; the ^{3}H content in all cores was also quite low.

The JERBOA test was conducted in 1963 at a depth of 310 m bgs in Emplacement Hole, U-3at. The cavity collapsed 35.3 min after detonation (long enough for the precursor to ^{137}Cs to have decayed to its nongaseous radionuclide); the collapse zone extended to the surface and formed a crater about 32 m deep. In 1996, a slant hole (U-3at-D1) was drilled under the collapse crater at U-3at, and core samples were obtained from vertical depths as deep as 147 m. No ^{137}Cs was detected in any cores, although there was a slight increase in ^{3}H levels over the ambient levels in the very deepest samples (at about 4 cavity radii above the working point).

6.5 Carbonate Tests

Only four tests have been detonated in carbonate rock at the NTS (Figure 6-9). Of these, satellite wells were installed at the NASH and BOURBON locations to evaluate radionuclide transport (Table 6-2). The HANDCAR test was the site of significant post-test characterization efforts as part of the Plowshare program. Few data are available regarding the KANKAKEE test.

6.5.1 NASH

The NASH test was detonated in 1967 at a depth of 368 m and a yield of 39 kt in carbonate rock (Buddemeier and Isherwood, 1985). In this location, the carbonates are LCA3 in the HFM model. The tuff-carbonate contact is located at 340 m (Figure 6-10). A satellite well, UE-2ce, was completed in 1977 to a total depth of 503 m with the bottom 73 m slotted. The satellite well is located

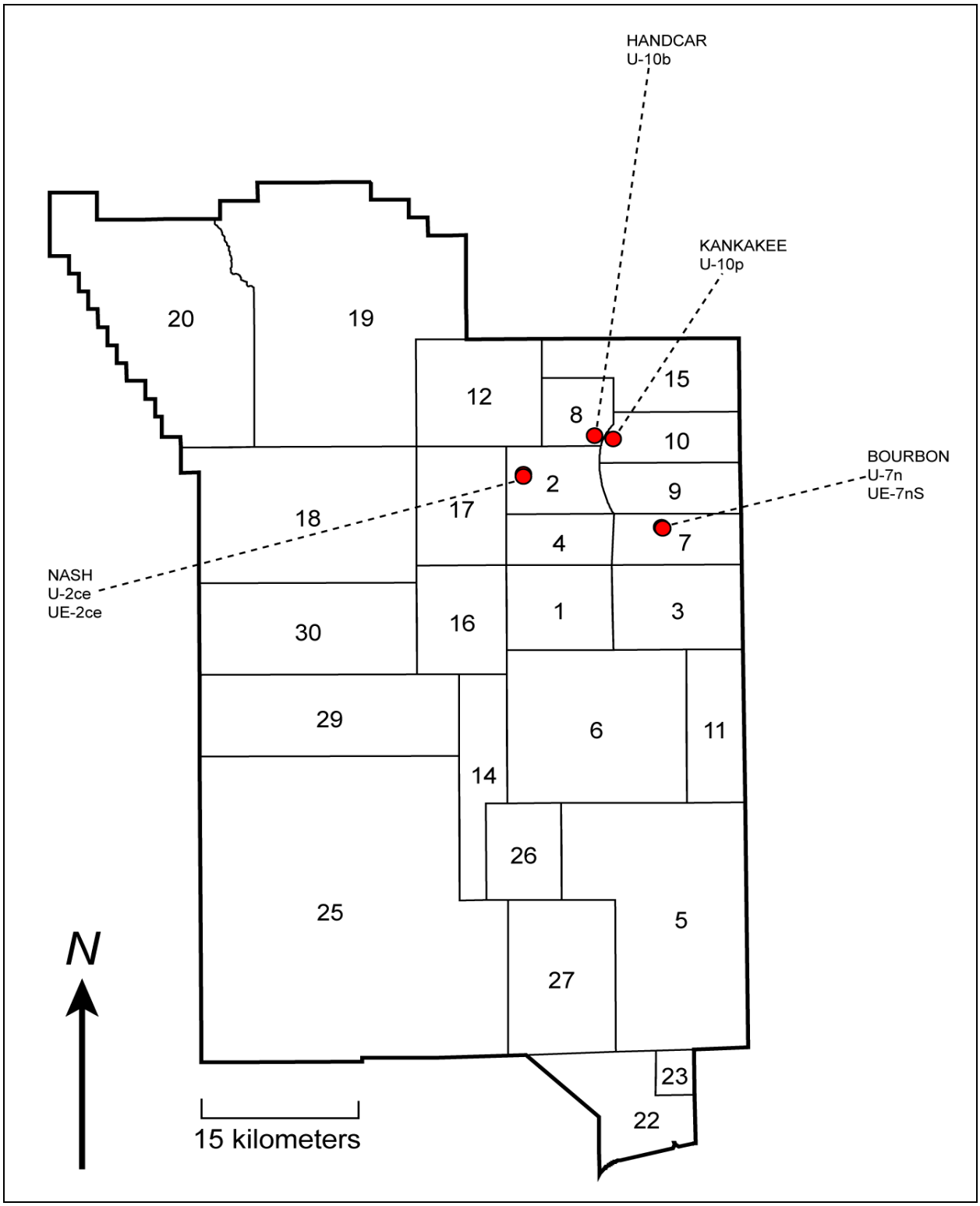

Figure 6-9
Location of Four Tests Detonated in Carbonate Rock

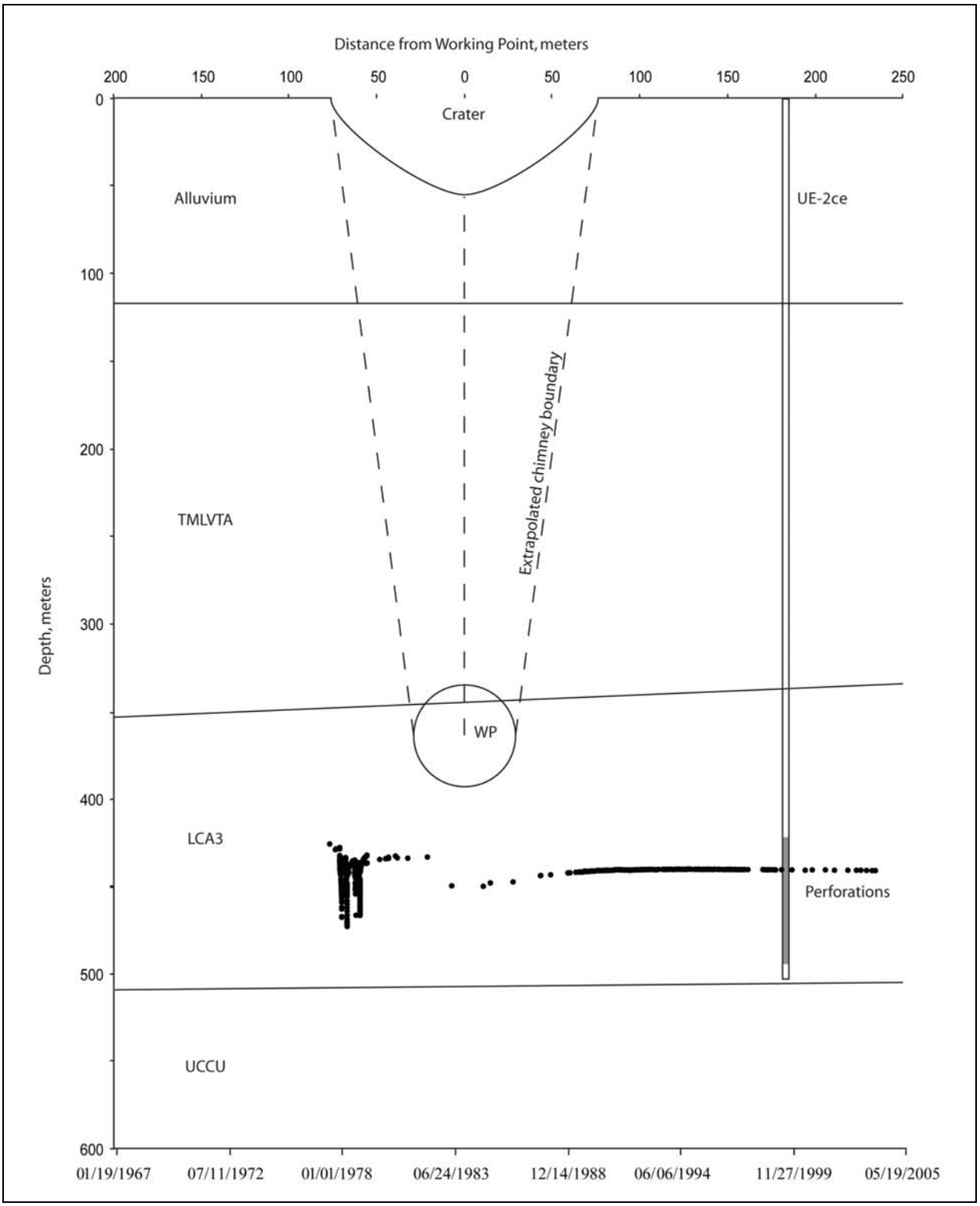

Figure 6-10
The NASH Near-field

approximately 183 m south of the NASH working point (Figure 6-10). Water levels measured at UE-2ce are shown in Figure 6-10. The water level was drawn down during different pumping episodes from 1977 to 1984. After pumping ended in 1984, water levels recovered through 1994 and have since declined about 2 ft (0.6 m) from 1995 to 2003 (Fenelon, 2005). The DOE/NV (1997b) reports a water level at NASH of 527 m.

The NASH site is the only location in Yucca Flat where a long-term pumping experiment was performed. It was meant to be analogous to the radionuclide migration pumping experiment performed at the CAMBRIC site in Frenchman Flat. Pumping at the satellite well began in 1977. The ^{3}H concentrations rose with the cumulative volume of water pumped from the well. By late 1977, a few thousand cubic meters of water had been pumped, and the ^{3}H concentration had begun to level off at approximately 10^{7} to 10^{8} pCi/L, decay corrected to t_0 (Figure 6-11). The pump in the NASH satellite well (UE-2ce) failed in 1984, after pumping approximately 42,000 m^3. Since then, periodic samples have been collected from the satellite well by bailing. In the bailed samples, ^{3}H concentrations are approximately two orders of magnitude lower than in the earlier pumped samples. Other radionuclides that have been detected in the satellite well include ^{14}C, ^{22}Na, ^{36}Cl, ^{85}Kr, ^{90}Sr, ^{129}I, ^{137}Cs, and ^{155}Eu. The results indicate that non-sorbing and some sorbing radionuclides have been transported downgradient in the carbonate aquifer. Well UE-2ce is an important site because it is the only case in which it is clear that radionuclides from a nuclear test at the NTS are present in the carbonate aquifer.

Three separate pumping experiments were performed at UE-2ce between 1977 and 1978 (Figure 6-12). An injection exercise was also performed. The pumping rate was typically around 28 gpm (Figures 6-11 through 6-13), but it was estimated that only 50 days of constant pumping were sustainable. Archived data at LLNL include an unclassified source term estimate for ^{3}H and ^{85}Kr at NASH. Discussions with the LLNL classification office deemed these data unclassified. The ^{3}H source term was estimated to be 3 to 6 moles. The ^{85}Kr source term was estimated to be 0.016 to 0.033 moles. These source term data, combined with the radionuclide breakthrough results at UE-2ce, can be used to calibrate radionuclide transport models at NASH. Based on pumping data, it is estimated that only 0.7 to 1.3 percent of the ^{3}H source term has reached the NASH satellite well. It is not known whether this fraction represents prompt injection, intersection of the exchange volume

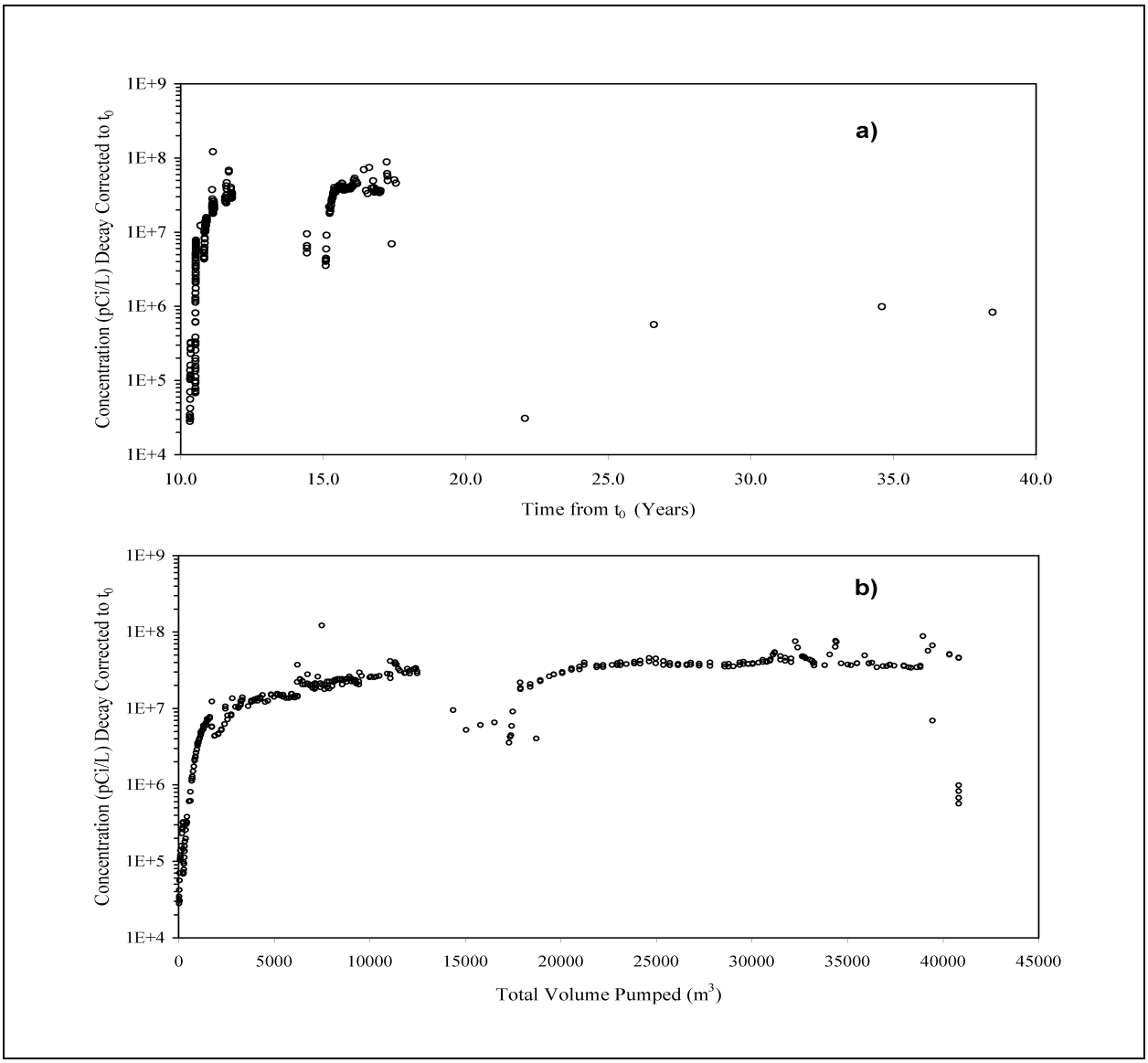

Figure 6-11
Tritium Concentrations in Pumped Groundwater from the NASH Satellite Well as a Function of (a) Time and (b) Total Volume of Water Pumped

with the water table, recharge through the vadose zone cavity, or a combination of these processes. Detailed HST modeling will be necessary to further evaluate each of these transport pathways.

6.5.2 BOURBON

The BOURBON test (U-7n) was detonated in 1967 at a depth of 560 m, with an announced yield of 20 to 200 kt (DOE/NV, 2000b). The rock at the working point was a silty limestone and located very close to the tuff-Paleozoic carbonate boundary. The water table depth is reported as 601 m

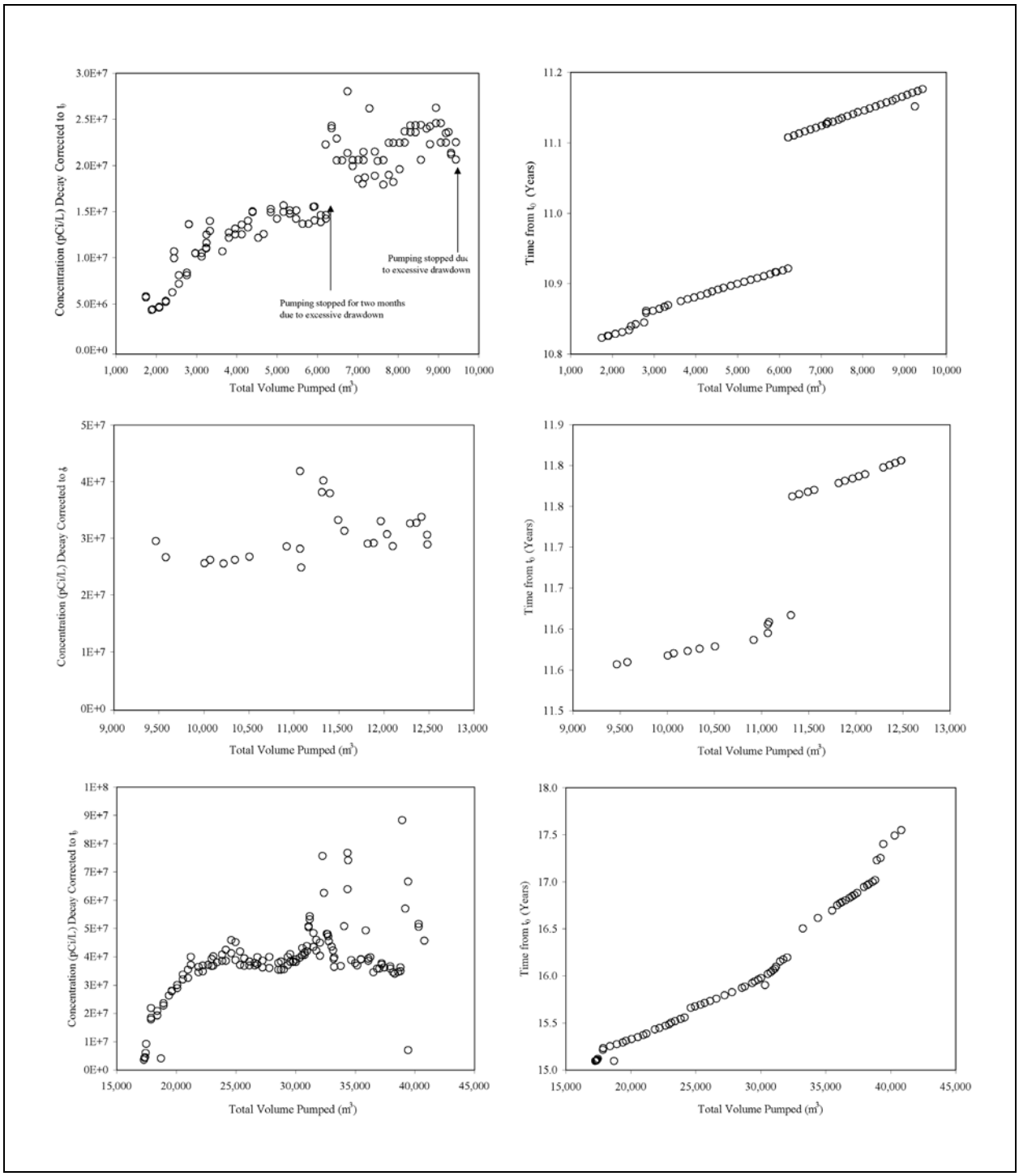

Figure 6-12
Tritium Concentrations and Volume Pumped from the NASH Satellite Well as a Function of Time (10 to 11 Years, 11 to 12 Years, and 15 to 18 Years from Time of Detonation)

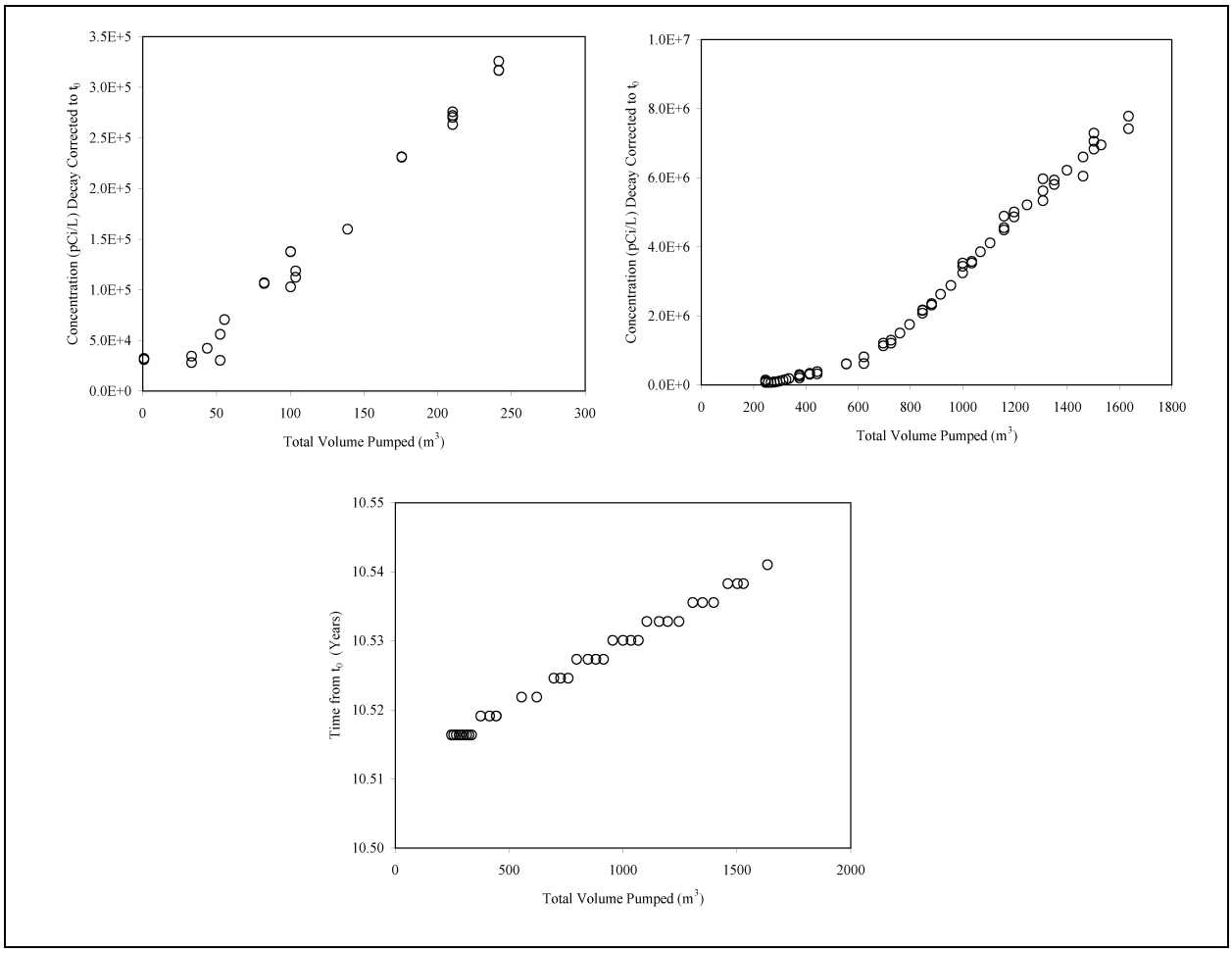

Figure 6-13
Tritium Concentrations in Pumped Groundwater from the NASH Satellite Well

(DOE/NV, 1997b). Thus, the bottom of the BOURBON cavity is likely to be located in the saturated zone.

A satellite well, UE-7nS, was drilled in 1976 to a depth of 672 m with the bottom 62 m slotted. The satellite well is located 137 m southeast of the emplacement hole (Figure 6-14). A fault was identified at 594 m, very close to the water table. A pump was installed in the satellite well, but the yield was too low to adequately clean out the well. Groundwater has been sampled at this well periodically. However, only very low ^3H concentrations have been measured (Figure 6-15). Measured concentrations have consistently been near 10^4 pCi/L, which is several orders of magnitude lower than those measured at NASH.

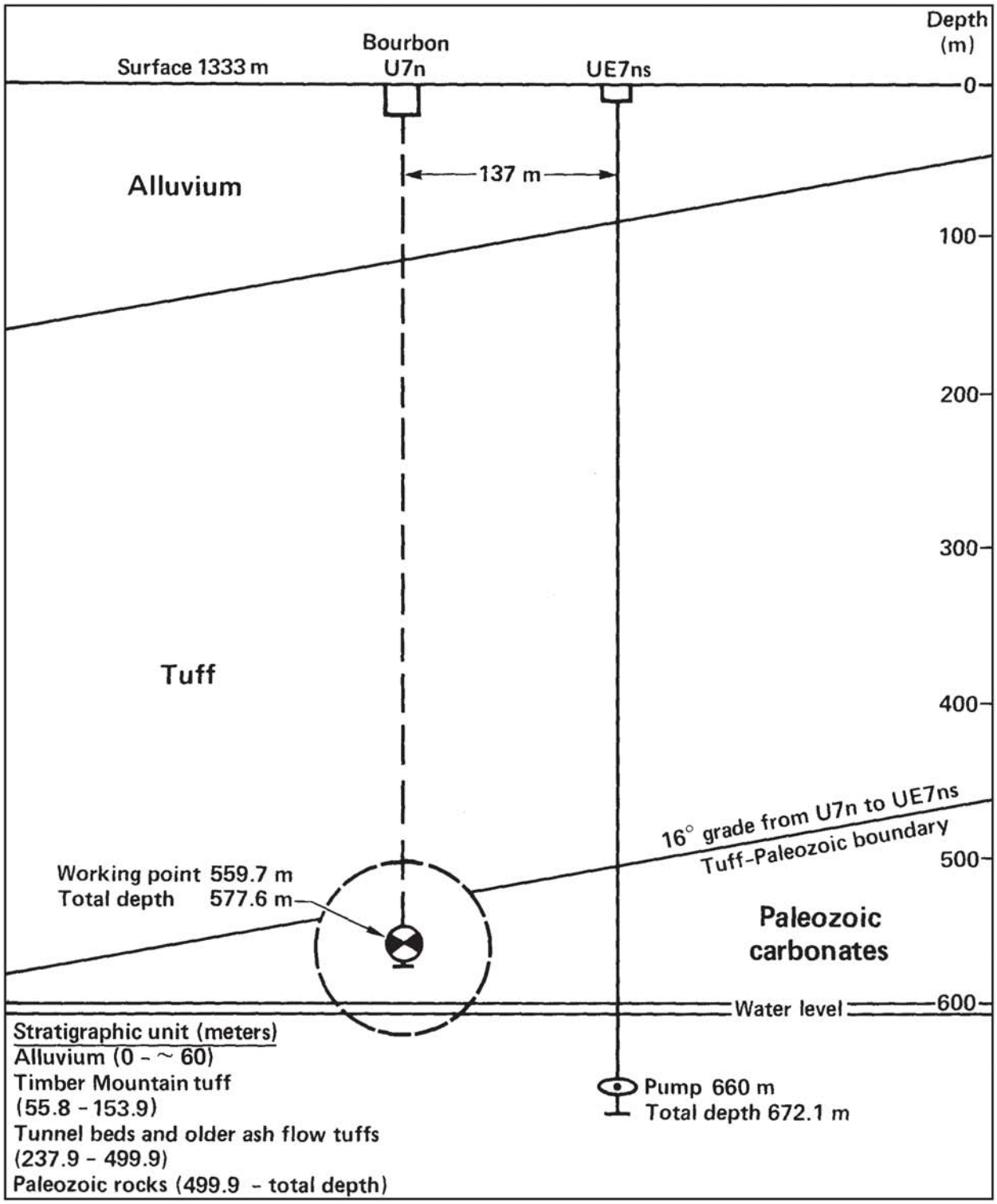

Figure 6-14
BOURBON Near-field

Source: Modified from Buddemeier and Isherwood, 1985

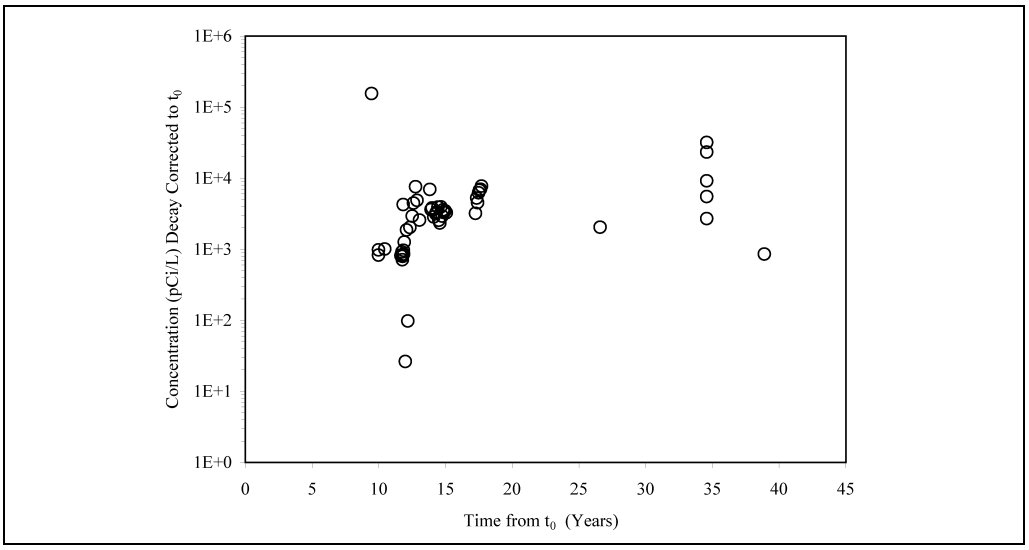

Figure 6-15
Measured Tritium Concentrations in BOURBON Satellite Well

6.5.3 HANDCAR

The HANDCAR test (U-10b) was detonated in 1964 in the Bonanza King dolomite at a depth of 403 m, with an announced yield of 12 kt (DOE/NV, 2000b). The water table depth is reported at 598 m (DOE/NV, 1997b). Thus, the HANDCAR cavity is unsaturated and located far above the water table. Importantly, this test was part of the Plowshare program and underwent significant post-test characterization. It is the only carbonate test to have received a detailed post-test investigation. Werth (1970) and others provide a detailed summary of the HANDCAR test and the characterization of radionuclide distribution (Figure 6-16). Importantly, the liberation of large quantities of CO_2 as a gas phase is distinctly different from tests detonated in silicate materials. Werth (1970) estimates that $(9 \pm 7) \times 10^8$ liters of CO_2 (at standard temperature and pressure) were generated by the HANDCAR detonation. Generation of this large quantity of CO_2 could drastically increase the distribution of radionuclides external to the cavity region as a result of cavity gas expansion. Also, the formation of puddle glass does not occur due to the nature of the surrounding medium. Refractory radionuclides are deposited in a rubblized material composed of limestone, dolomite, calcium oxide, magnesium oxide, and other trace minerals. The dissolution of this material and subsequent release of radionuclides will differ drastically from what is expected for silicate glass.

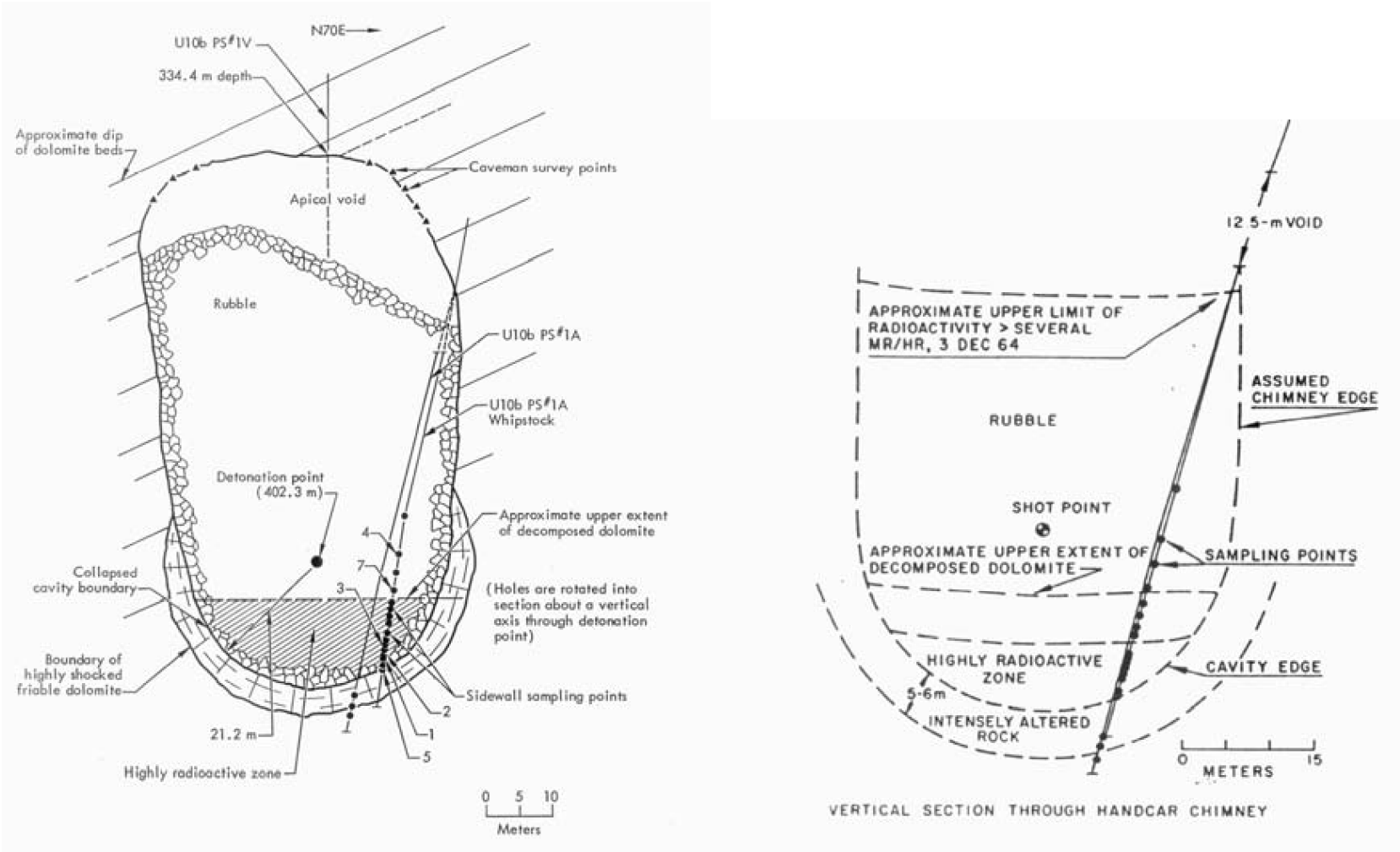

Figure 6-16
Schematic of the HANDCAR Cavity and Distribution of Radioactivity
Source: Nervik, 1970; Boardman and Meyer, 1970

6.6 Granite Tests

Only three tests were detonated in granite (Figure 6-17) at the NTS. Of these, the HARD HAT and PILE DRIVER tests were characterized with a large number of post-test drill holes. Little information is available regarding the TINY TOT test.

6.6.1 HARD HAT

The HARD HAT test was conducted on February 15, 1962, in U15a with an announced yield of 5.7 kt. The surface elevation at that location is 1,532 m (DOE/NV, 2000b). A surface elevation of 1,559 m and a device depth of burial of 287.4 m bgs is reported in DOE/NV (1997b). The water table depth was reported at 222 m (DOE/NV, 1997b). This is likely to be a perched water zone and not representative of the regional water table depth. In addition to the emplacement hole (U15a), pre-test underground workings included a vertical shaft and one main tunnel that reached within 180 ft horizontally and 89 ft vertically of the working point. The underground workings also included a number of drifts normal to the main tunnel (Figure 6-18).

The HARD HAT test was emplaced in the Climax Stock granite. The stock varies from a quartz monzonite to a granodiorite; the HARD HAT event took place within the granodiorite (McArthur, 1963). As part of post-test operations, the original tunnel was reopened and extended into the chimney. A post-test drillback (U15a PS or U15a 28s) was also completed. Additional drilling occurred approximately 1.5 or more years after the test; those results are discussed later in this section. Test fractures were evident in the extended tunnel and significant movement along a near-vertical shear zone was observed. At 21 ft (6.4 m) from the chimney edge, the intensity of shock fractures increased and vertical sheers parallel to the chimney occurred at 3- to 4-ft intervals. Within the chimney, rock was severely damaged and was not competent (Figure 6-19).

The combined cavity-collapse chimney was 347 ft (106 m) high and 43 to 35.4 m in diameter. The cavity radius was estimated at 63 ft (19.2 m). A 34-ft (10-m) void existed at the top of the chimney (McArthur, 1962), and based on volume calculations, it is estimated that 27 percent of the chimney is void space. If the void at the top of the chimney is excluded, that void space is reduced to 22 percent (Boardman, 1965 and 1966). Beyond the lower hemisphere of the cavity, a zone of extreme alteration (greater than 15 ft) was observed in which quartz and feldspar were minutely fractured so as to appear

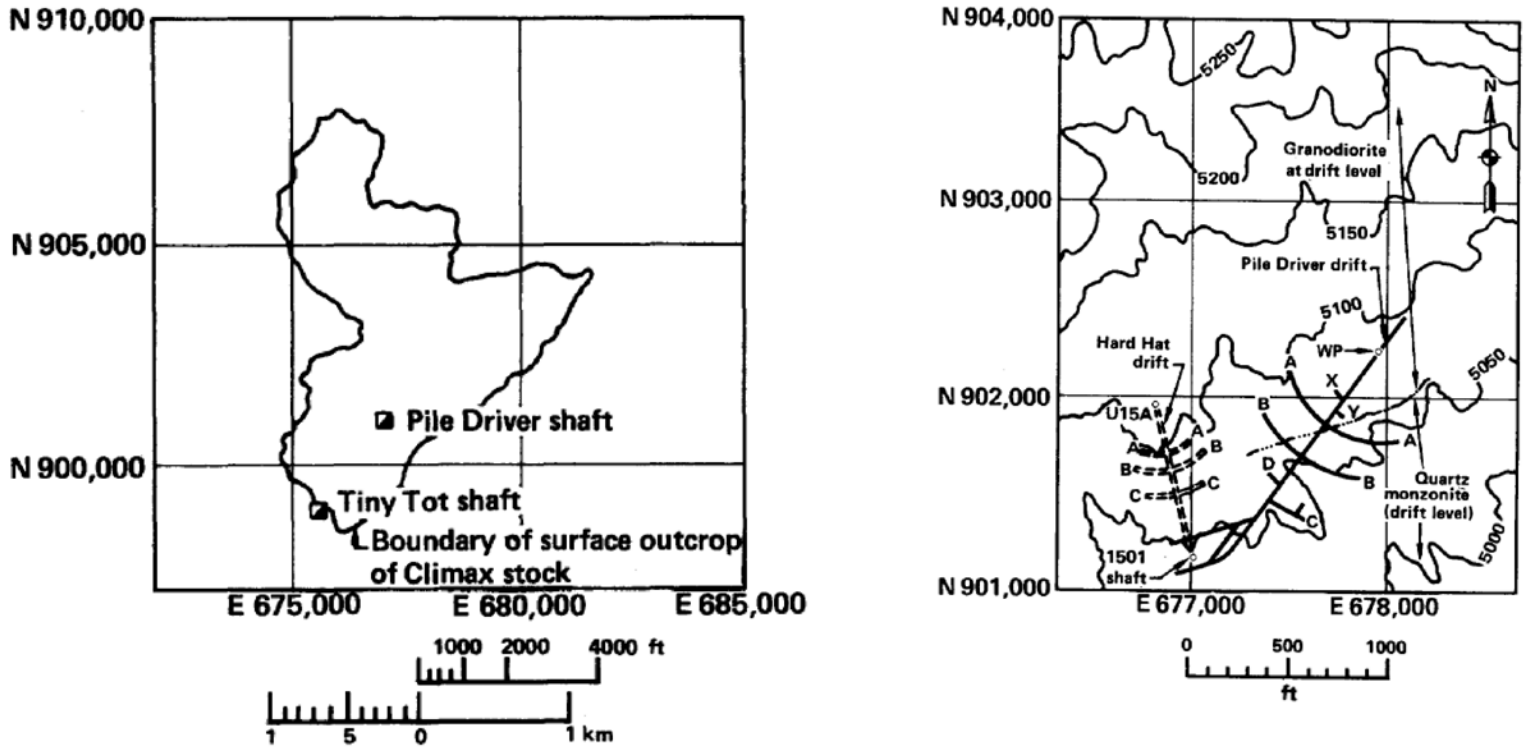

Figure 6-17
Location of Three Tests Detonated in Granite
Source: Modified from Murray, 1981

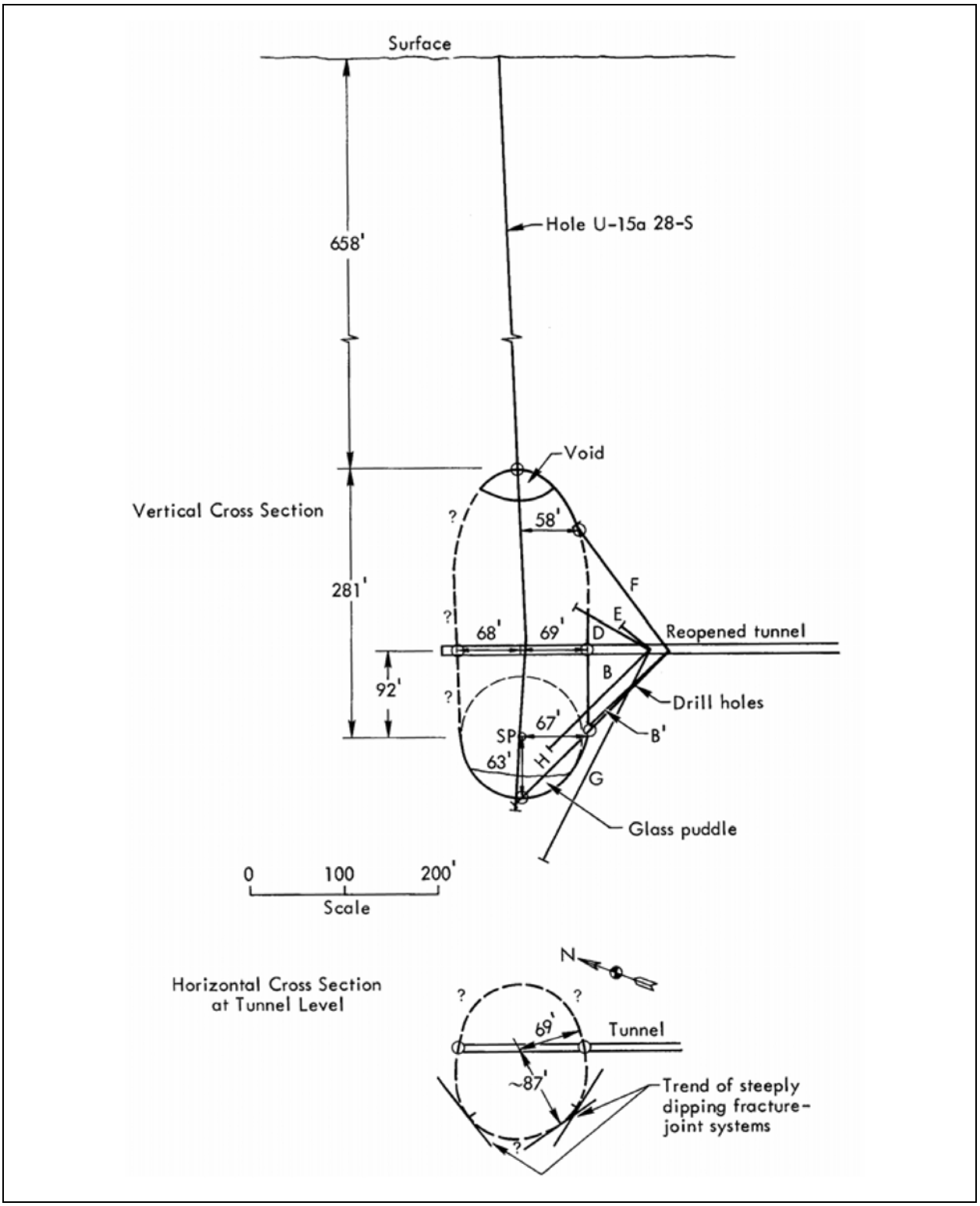

Figure 6-18
Diagram of HARD HAT Near-field and Post-test Drilling Operations
Source: Borg, 1970

Figure 6-19
Re-entry Drift at the HARD HAT Chimney Edge
Source: McArthur, 1963

chalky. Bulk densities in this zone decreased from 2.67 to 2.36 grams per cubic centimeter (g/cm^3), resulting in a porosity of 11 percent (Boardman, 1965 and 1966).

Fluid losses during drilling occurred at 483 ft (147 m) above the working point. This is equivalent to 7.7 cavity radii and is consistent with observations of shock fractures out to 520 ft (158 m, 8.25 cavity radii) (McArthur, 1963). In the summer of 1964, nearly 1.5 years after the HARD HAT test, three holes were continuously cored from the original exploratory tunnel into or close to the cavity/chimney (Boardman, 1966). For the two holes that entered the cavity/chimney, loss of drilling fluid circulation occurred only when drilling reached to within a few meters of the cavity/chimney. For the hole that was drilled through the cavity edge and past the glass zone, rock out to 4 m beyond the cavity had a chalky appearance and was friable. A similar chalky appearance was observed in the third hole up to 7 m beyond the cavity edge, which was meant to approach but not reach the cavity

boundary. The permeability of small core samples from this zone was measured to be 7 to 15 millidarcies (mD) (Boardman, 1966). However, fracture permeability is said to be much higher. Permeability of native rock is on the order of 0.01 mD (Mehta et al., 1964). Cavity/chimney pressurization measurements suggested that wall rock permeabilities are on the order of 1.2 to 1.4 darcies (1,200 to 1,400 mD) (Boardman, 1965). More direct measurements of rock permeability near the cavity/chimney were reported to be 0.2 to 2 darcies and decaying exponentially with distance from the working point to less than 1 mD (Figure 6-20) (Boardman and Skrove, 1966). It is apparent that field-scale permeabilities are likely driven by large-scale fracture flow phenomena that cannot be captured with small laboratory measurements (Figure 6-21).

Interestingly, melt glass was found as far as 23.8 m from the working point (1.2 cavity radii) and is likely the result of a prompt injection. Similar injection phenomena were observed in the PILE DRIVER test. Importantly, the HARD HAT cavity did not collapse until 11 hours after detonation. As a result, sufficient time was available for much of the melt glass to flow and pool at the bottom of the cavity and begin to solidify. This led to an unusually high fraction of glass in the glass puddle (73 percent by volume). Cavities that collapse quickly typically have glass fractions of 20 to 30 percent in the glass puddle due to the incorporation of infallen rock (Boardman, 1966).

6.6.2 PILE DRIVER

The PILE DRIVER test was conducted in 1966 in U15a.01 with an announced yield of 62 kt (DOE/NV, 2000b). Accidental release of radioactivity detected onsite only is reported in DOE/NV (2000b) for the PILE DRIVER test. The surface elevation is reported to be 5,090 ft (1,551 m), and the depth of burial is reported as 1,518 ft (463 m) (DOE/NV, 1997b). The water table depth is reported as 185 m; however, this is likely to be perched water and not the regional water level. A number of drillback operations were conducted in the years following the PILE DRIVER test. These are shown in Figure 6-22.

From July 21 to August 2, 1966, a chimney exploration program was conducted (Boardman, 1967). Hole U15.01 PS#1V was drilled into the top of the PILE DRIVER chimney (Figure 6-22). The top of the chimney was found to be at 277.3 m from the working point. Based on air pressurization experiments, it was found that the void volume in the chimney was 367,900 ± 20,000 m^3. This is equivalent to an open cavity radius of 44.5 ± 1 m and a chimney void porosity of 19 percent. Field

permeability measurements above the chimney suggest that increased permeabilities extend out to 7.1 ± 0.2 cavity radii and approach 1 darcy. The field permeability of the chimney wall rock was found to be 1.5 ± 0.3 darcies.

In September/October 1967, a drift was extended into the chimney of the PILE DRIVER test from the emplacement drift (Rabb, 1968). This drift extended 67 ft into the chimney. The chimney edge was clearly discernible (Figure 6-23) with relatively solid rock outside the chimney and highly rubblized material within it. Particle sieving found that about 40 percent of the chimney rubble is greater that 6 inches (in.) (greater than 0.15 m) and 20 percent is less than 1 in. (less than 0.025 m). Interestingly, radioactivity correlated with particle surface area, with most of the radioactivity found in the smaller particle-size fractions.

In June to August 1969, three holes were drilled into the lower part of the PILE DRIVER cavity and below the access drift (Sterrett, 1969). Distribution of radioactive material was found to be very heterogeneous near the cavity. In one drilling operation, drilling fluid circulation was lost at 1.5 cavity radii. In another drilling operation, fluid circulation was never lost even though drilling was as close as 1.2 cavity radii from the working point. Seams of glass were encountered outside the cavity sporadically during these drilling operations. Thin section examination of core samples from these hole identified radial distances of intense to low test-induced micro-fracturing (Borg, 1971). These results were compared with an analysis of HARD HAT core material. PILE DRIVER and HARD HAT limits of intense fracturing were 1.3 ± 0.1 and 1.3 ± 0.2 cavity radii, respectively. Detectable microfracturing was observed out to 2.7 ± 0.2 and 2.9 ± 0.4 cavity radii, respectively. Field scale permeability measurement at HARD HAT indicated that test-induced high permeabilities (greater than 0.1 darcy) were observed at these distances as well. Interestingly, the observed distance for intense and detectable fracturing in granite from French tests conducted in Algeria showed similar behavior (Borg, 1973).

6.6.3 Tritium Observations in Granite

Observations of ^{3}H distribution in the Climax Stock provide important information with regard to tracer transport in the near field. Figure 6-24 is a plot of the measured ^{3}H concentrations relative to the locations of the HARD HAT and PILE DRIVER tests. The location of the pre-test tunnel complex and Spent Fuel Test (SFT) drift is also included. Samples in the tunnel complex were

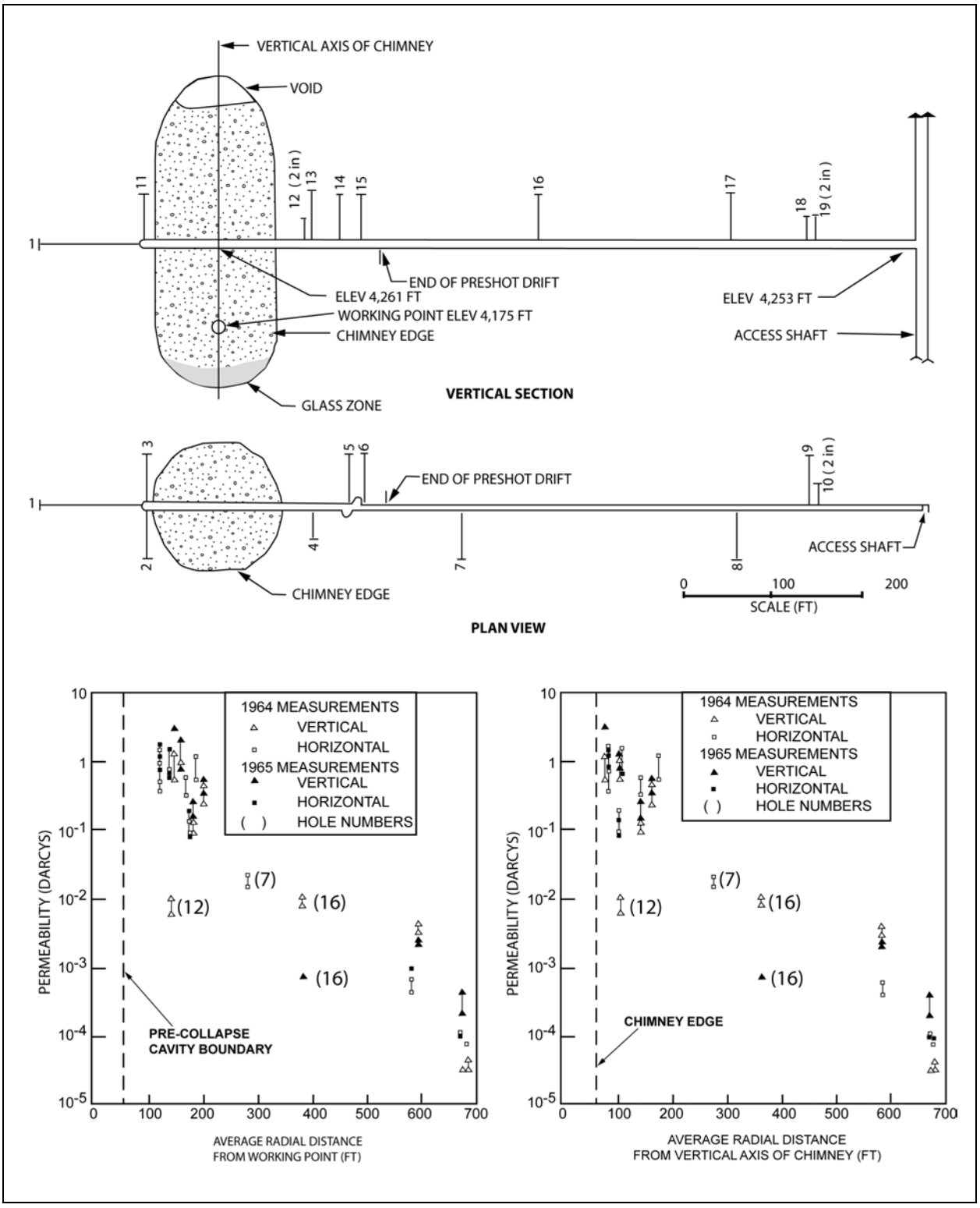

Figure 6-20
Location and Measured Permeability of Rocks in the Vicinity of the HARD HAT Test

Source: Modified from Boardman and Skrove, 1966

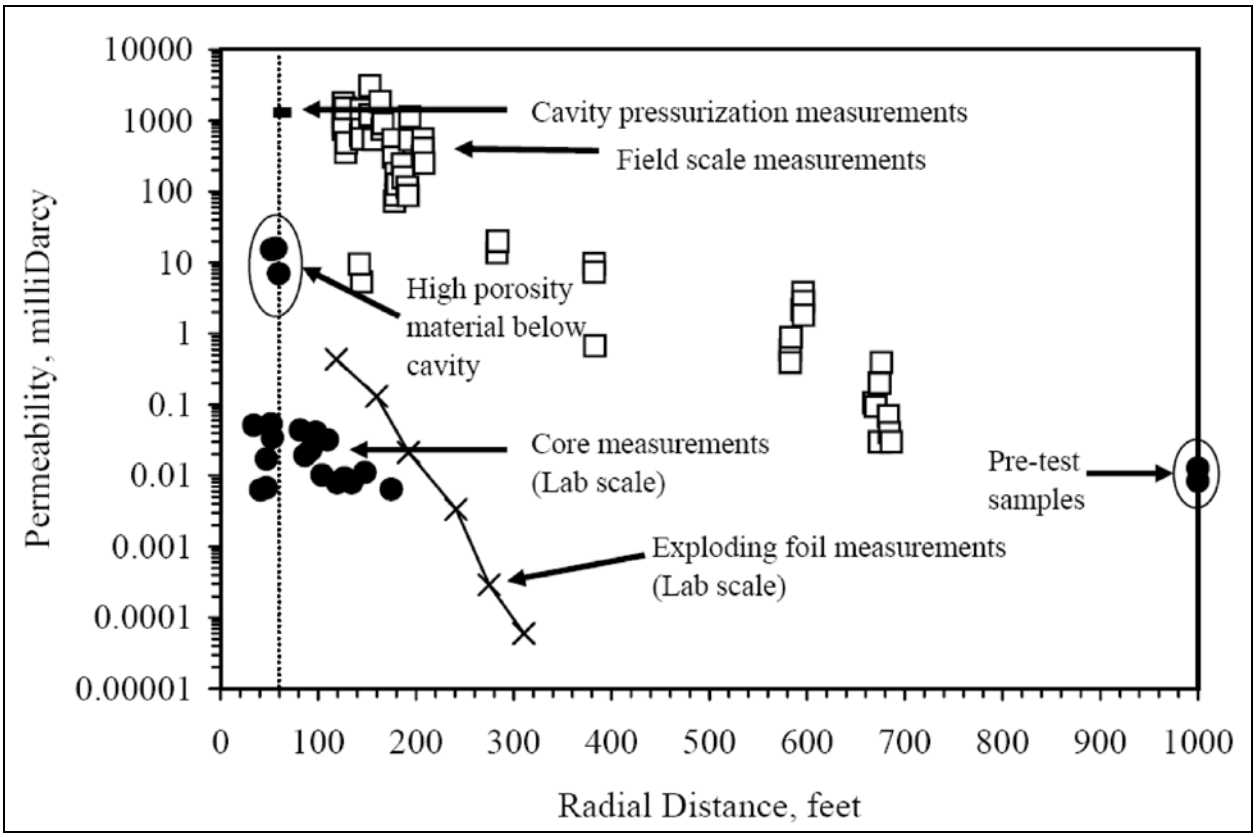

Figure 6-21
Summary of Permeability Measurements
Source: Quong, 1969; Boardman and Skrove, 1966; Short, 1964; Mehta et al., 1964; and Boardman, 1965

analyzed for ^{3}H in 1981 and 1982 (Isherwood et al., 1982). The ^{3}H concentration in the PILE DRIVER cavity was estimated from ^{3}H concentrations in water trapped in nuclear melt glass measured by Borg (1974). Importantly, these data suggest that (1) a significant quantity of ^{3}H has escaped well beyond the exchange volume of the two tests, (2) the observed concentrations outside the exchange volume are significantly lower than those observed in the cavity glass, and (3) ^{3}H has migrated down to the regional groundwater and contaminated it well above the drinking water standards (20,000 pCi/L). This indicates that tests conducted above the water table may still provide a significant RST below the regional groundwater table.

In the original evaluation of ^{3}H data, Isherwood et al. (1982) suggested that ^{3}H observed in the shafts and tunnels were likely deposited as a result of the PILE DRIVER test, soon after the detonation, without elaboration on how the conclusion was reached. Although it may be true that observed ^{3}H concentration were the result of the PILE DRIVER test, the potential role of the HARD HAT test

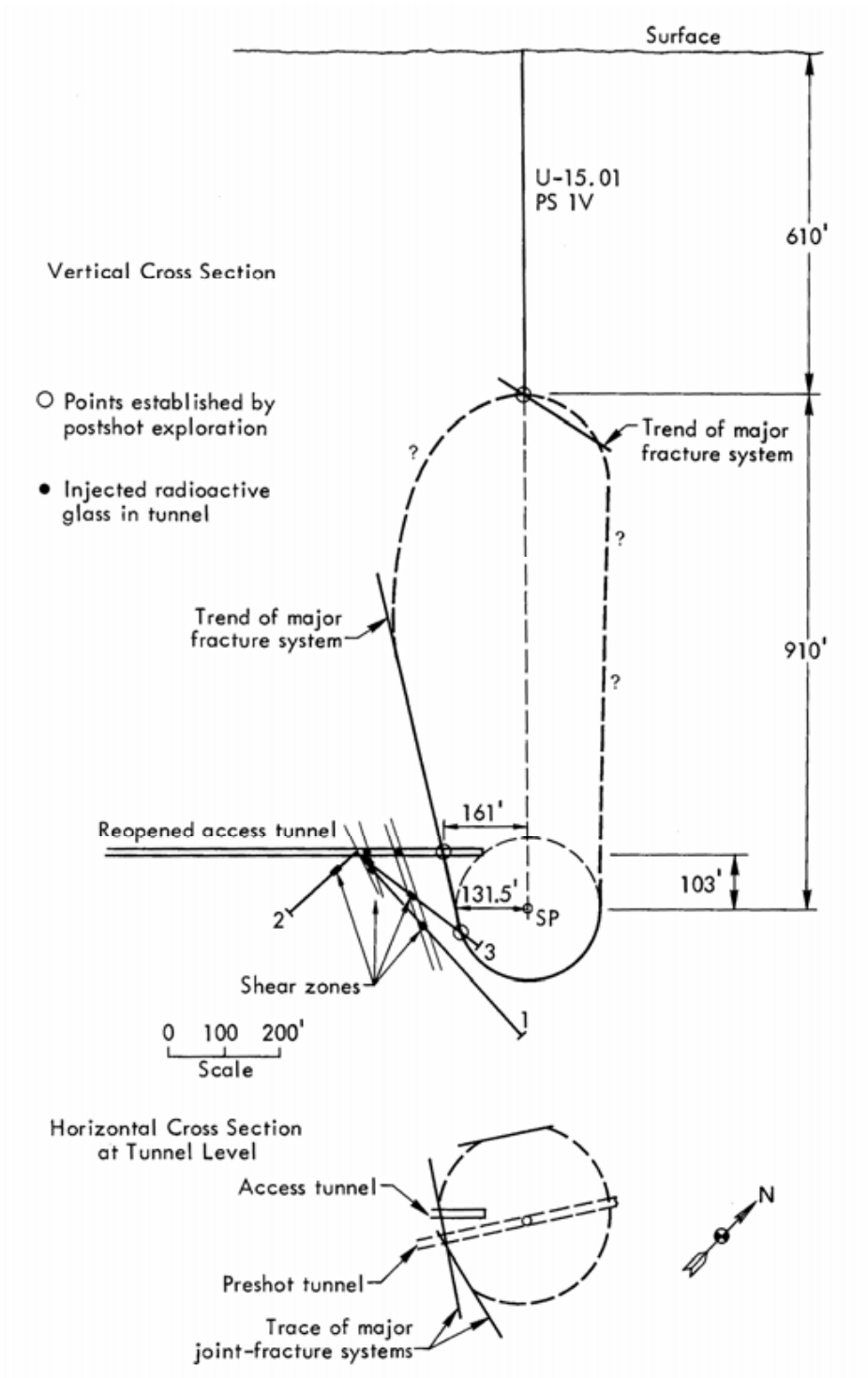

Figure 6-22
Diagram of PILE DRIVER Near-field and Post-test Drilling Operations
Source: Borg, 1970

Figure 6-23
PILE DRIVER Chimney Edge
Source: Rabb, 1968

should not be ignored. Because all samples but one were derived from seeps located in the shafts and tunnels, and that the highest ^{3}H concentration were found in vertical fractures, it should be expected that the source of the ^{3}H should have a significant vertical component. In fact, it was suggested in several reports that the seepage rates in the tunnels increased markedly during heavy rainfall. This would suggest fast water transport rates in the vadose zone when an underground excavation at atmospheric pressure exists. The HARD HAT test is laterally closer to the locations of measured ^{3}H and is also located vertically above the areas where high ^{3}H concentrations were measured. The PILE DRIVER test is located vertically well below all ^{3}H measurement locations except the sample located at the water table. Importantly, Wilder (1987) indicated that significant seepage in the Climax Stock tunnels appears to occur only near fault and sheer zones, but not in joints. Based on the location of the seepage points and direction of prominent sheer and fault zones, it is not clear whether PILE DRIVER is the source of the ^{3}H found in the Climax Stock tunnels. The HARD HAT test seems to be as likely of a source.

6.6.4 Tuff Pile/High-Pressure Area

The Tuff Pile is an area in west-central Yucca Flat, situated between the Yucca Fault to the east and the Topgallant Fault to the west, with a thick sequence of buried air-fall tuffs that has been used extensively for underground nuclear tests. The Tuff Pile area encompasses about 8 square kilometers

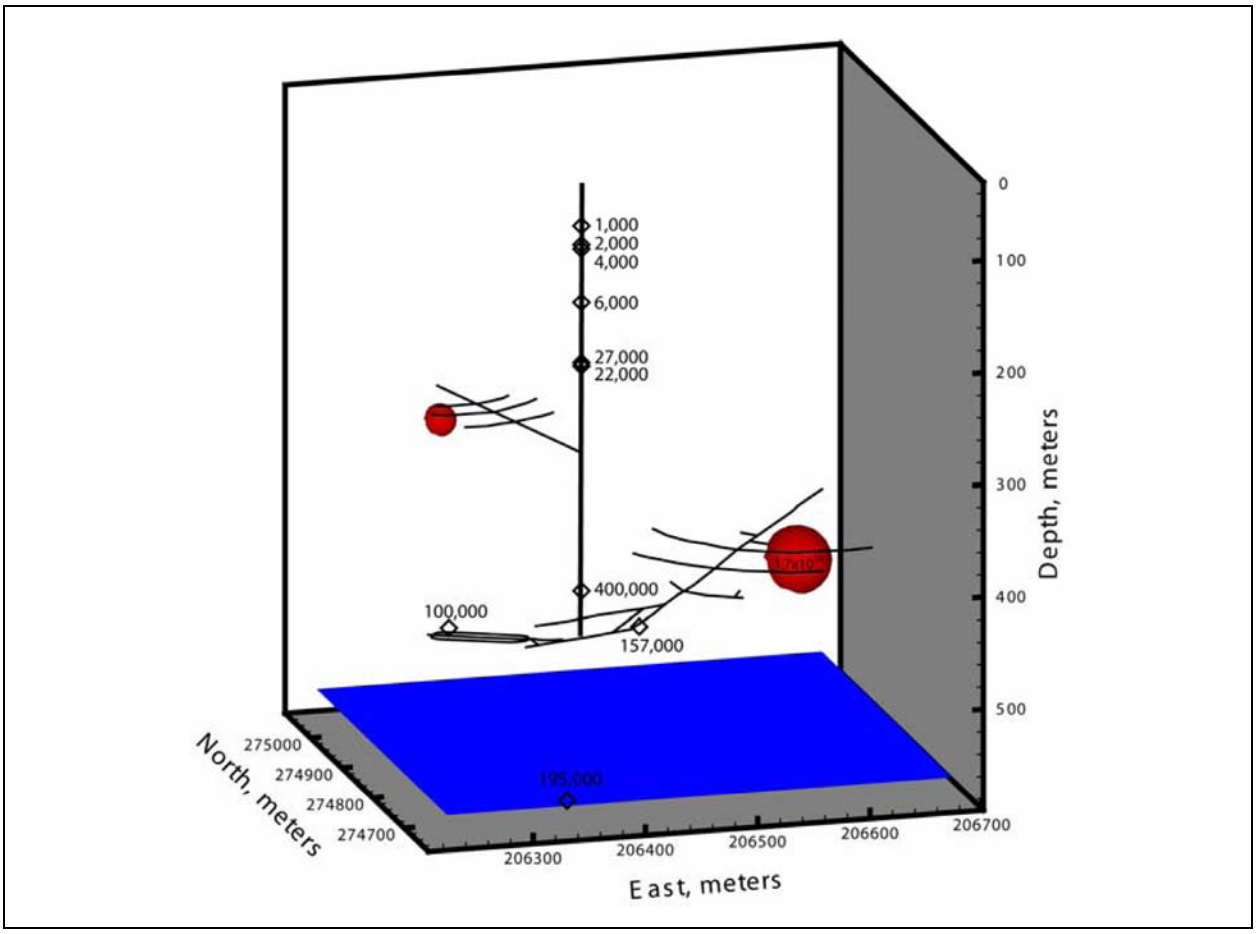

Figure 6-24
Distribution of Tritium (pCi/L) in Waters Located Near the HARD HAT and PILE DRIVER Tests (red), Regional Water Table Identified in Blue
Pre-test shafts and tunnels identified along with the SFT drifts.

(km^2), including parts of Areas 1, 3, 4, and 7 (Figure 6-25). Numerous observations of water levels in drill holes in the vicinity of the Tuff Pile that are elevated by up to hundreds of meters (hence also referred to as the high-pressure area) are coupled to measurements of radionuclide contamination in groundwater sampled from areas nearby (Wohletz et al., 1999). Changes in the groundwater levels within the tuffs and changes in the rate and distribution of land-surface subsidence above the tuffs indicate that pore-fluid pressures have been slowly depressurizing since the cessation of nuclear testing in 1992 (Halford et al., 2005). Recently, analyses of groundwater flow and transport in the high-pressure areas have been conducted by the USGS and LANL. The USGS study results are reported in Halford et al. (2005). The LANL study is in progress, and a report will be published following completion of the study. These reports address the mechanisms for generating high pore

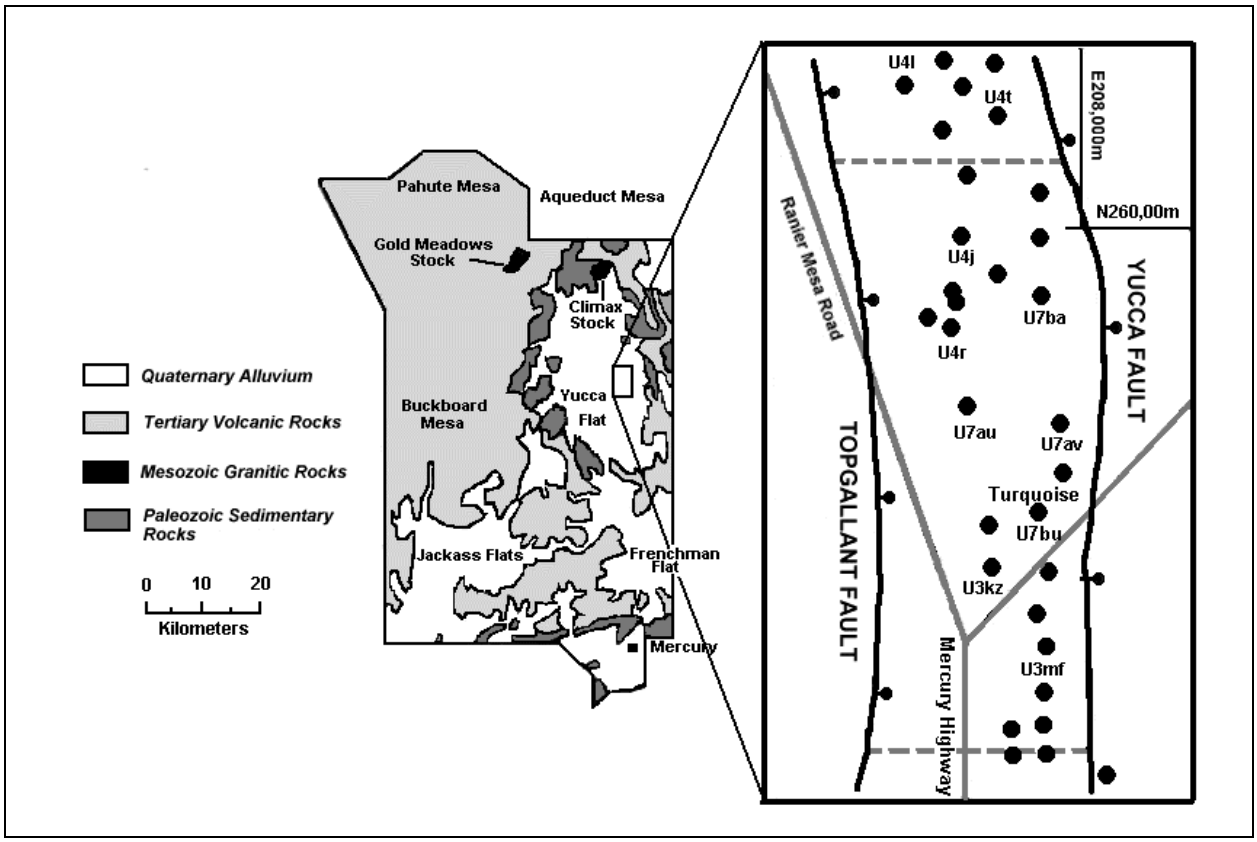

Figure 6-25
Location of Tuff Pile 1
Source: Wohletz et al., 1999

pressures and evaluate the persistence of the high pressures. The LANL study considers the effect of the high pressure on groundwater flow, specifically regarding potential transport of contaminants from the high-pressure tuffs (host to nuclear tests) to the LCA. In general, the reports conclude that the high pressures occur locally within very low-permeability formations and do not result in substantially increased groundwater flow to the LCA from the high-pressure areas. The high-pressure areas do not appear to represent integral features of the hydrologic system, but rather localized and compartmentalized pore pressure.

6.7 Prompt Injection Phenomena

A number of investigations at the NTS have suggested “prompt fracture injection” as a mechanism for transporting radionuclides away from the working point. In this conceptual model, a high-temperature and high-pressure plasma produced by the detonation is injected along newly created and reactivated fractures/fault zones surrounding the working point. The DOE/NV (1992)

attributed radionuclide migration in the unsaturated zone at U-3 cn#5 (BILBY satellite well), UE-4g #2, U-9 ITS U-29, U-3kz (ALEMAN), and UE-2ce (NASH) to prompt injection. Thompson (1992b) reported that ^{192}Ir and fission products were found in fractures in an emplacement hole 170 m from a nuclear test (detonated two months earlier) in which ^{192}Ir was loaded as a tracer. The fractures were well above the water table, so water transport was not a possibility. Other examples of prompt injection have also been described in this section.

7.0 MATRIX POROSITY

The matrix porosity of a geologic medium is a component of the medium's total porosity. The total porosity is the proportion of void space within the total unit volume of the medium at a representative elementary scale. The porosity of geologic material can be of two types: primary (or interstitial) and secondary. Primary porosity is due to the soil or rock matrix (i.e., matrix porosity), and secondary porosity is due to secondary changes to the rock, such as solution or fracture development (i.e., fracture porosity). If the medium is porous, the matrix porosity can be considered to be approximately equivalent to the total porosity of the medium. In fractured rock, fracture porosity and matrix porosity differ, and matrix porosity becomes a distinct component of the total porosity. Definitions of the various porosity types are presented and further discussed in Section 3.1.1.1.

The objective of this section is to evaluate matrix porosity data and assign a probability distribution of matrix porosity to each Yucca Flat HGU for use in a CAU-scale flow and contaminant transport model.

7.1 Role of Matrix Porosity in Contaminant Transport

In unfractured rock, flow is through the rock matrix. In a fractured rock, a double-porosity conceptualization is typically assumed, with flow and transport through the fractures and the matrix acting as storage for solutes diffusing from the fractures into the matrix or from the matrix into the fractures. For most fractured geologic systems, the volume of rock that comprises fractures is a small percentage of the total rock volume; the matrix comprises the majority of the rock volume. In this case, the total porosity and matrix porosity are nearly equivalent. The large reservoir of water in the matrix can be extremely important to radionuclide migration. When matrix pores are well connected through diffusive pathways, a higher radionuclide concentration in fracture water causes the migration of the radionuclide into the matrix, effectively slowing the rate of transport relative to groundwater flow. The matrix porosity, coupled with the matrix diffusion coefficient, controls the rate of diffusion into and out of the matrix.

7.2 Data Compilation and Data Transfer

Matrix porosity data are widely available from boreholes in Yucca Flat. This section discusses the types of measurements and sources from which the porosity data are derived and their evaluation and analysis. All data used in the quantitative analyses are from the Yucca Flat/Climax Mine HFM area; see Appendix F and associated dataset referenced in Section F.2.2.

7.2.1 Data Types

Matrix porosity data are available from the analysis of borehole geophysical logs and borehole core samples. Almost all of the matrix porosity data used in this study are from 13,832 borehole core samples (USGS, 2006). Appendix F contains additional data and analyses from the ER wells geophysical logs. In addition, matrix porosity values have been recently measured by LANL, LLNL, and DRI for the LCA and TCU using laboratory transport experiments (Ware et al., 2005; Reimus et al., 2006c; Zavarin et al., 2005).

Porosity measurement methods for core data typically involve the measurement of dry bulk density, grain density, and saturated water content in the laboratory. A discussion of laboratory core measurement is also in Attachment A, Section 2.0, of SNJV (2004e). In general, core-derived measurements provide the best estimates of matrix porosity in both porous and fractured media if the sample is at least as large as the matrix representative elementary volume. However, in unconsolidated media (e.g., alluvium), grain radii can range in size from microns to meters, and the sample volume will be, in general, too small to accurately measure matrix porosity. Accordingly, estimates of matrix porosity in unconsolidated media may be highly spatially variable depending on the degree of grain size heterogeneity and anisotropy. Other sources of uncertainty related to core laboratory measurement are incomplete saturation of the sample (underestimate of matrix porosity), and unconsolidation of the sample resulting from both physical disturbance and reduced lithostatic confining pressure in the laboratory (overestimate of matrix porosity).

A large portion of the data used to determine matrix porosity is total porosity. In most fractured rock aquifers, the total porosity is the sum of matrix porosity and effective or fracture porosity. Fracture porosities are typically less than 1 percent, whereas matrix porosity may be 25 percent or more. The total porosity is, therefore, a good estimator of the matrix porosity of fractured rocks in most cases. In

the case of unfractured rocks, matrix porosity can be reasonably assumed to be equivalent to total porosity.

7.2.2 Data Sources

The porosity dataset is primarily from the USGS Rock-Property Database generated as part of the FY 2006 data integration task for the UGTA Project (USGS, 2006). The data are therefore current to the end of FY 2006. The USGS compiled interval-specific rock-property data for nearly 600 holes drilled or mined on and around the NTS. Rock-property data were taken from reports and historical paper files located at the USGS Las Vegas office and the USGS Core Library and Data Center in Mercury, NV. Records were compiled from a combination of sources, including field notes and forms, memorandums and other internal correspondence, unpublished draft manuscripts and tables, and published reports. Because record reviews ranged from cursory to thorough, some data are preliminary and may be subject to revision. Figure 7-1 is a map of the 281 borehole locations used in the porosity study for Yucca Flat. Matrix porosity values for the LCA and TCU, which were measured during recent laboratory transport studies (Table 7-1), are also included in this analysis. In addition, geophysical logs from nine ER wells were analyzed and are included in Appendix F. The complete matrix porosity datasets are described in Appendix F.

7.3 Data Evaluation

Because the matrix porosity data are primarily from a single source (i.e., the USGS Rock-Property Database [USGS, 2006]) they were not weighted before analysis. The data consist of laboratory measurements of porosity collected since the early 1970s as part of the underground testing containment program. Hydrostratigraphic units were assigned to each porosity value using a query of the Yucca Flat/Climax Mine HFM. This dataset was supplemented with porosity values from the recent laboratory studies for the LCA and TCU presented in Table 7-1 (Ware et al., 2005; Reimus et al., 2006c; Zavarin et al., 2005). Although not discussed within this section, the geophysical data analysis of ER wells is summarized in Appendix F. The basis of the HGU assignments for each porosity value is provided in Table 7-2.

Several high porosity values for the carbonate aquifers, ranging from approximately 9 to 44 percent, were identified and subsequently removed from the dataset. The high porosities are inconsistent with

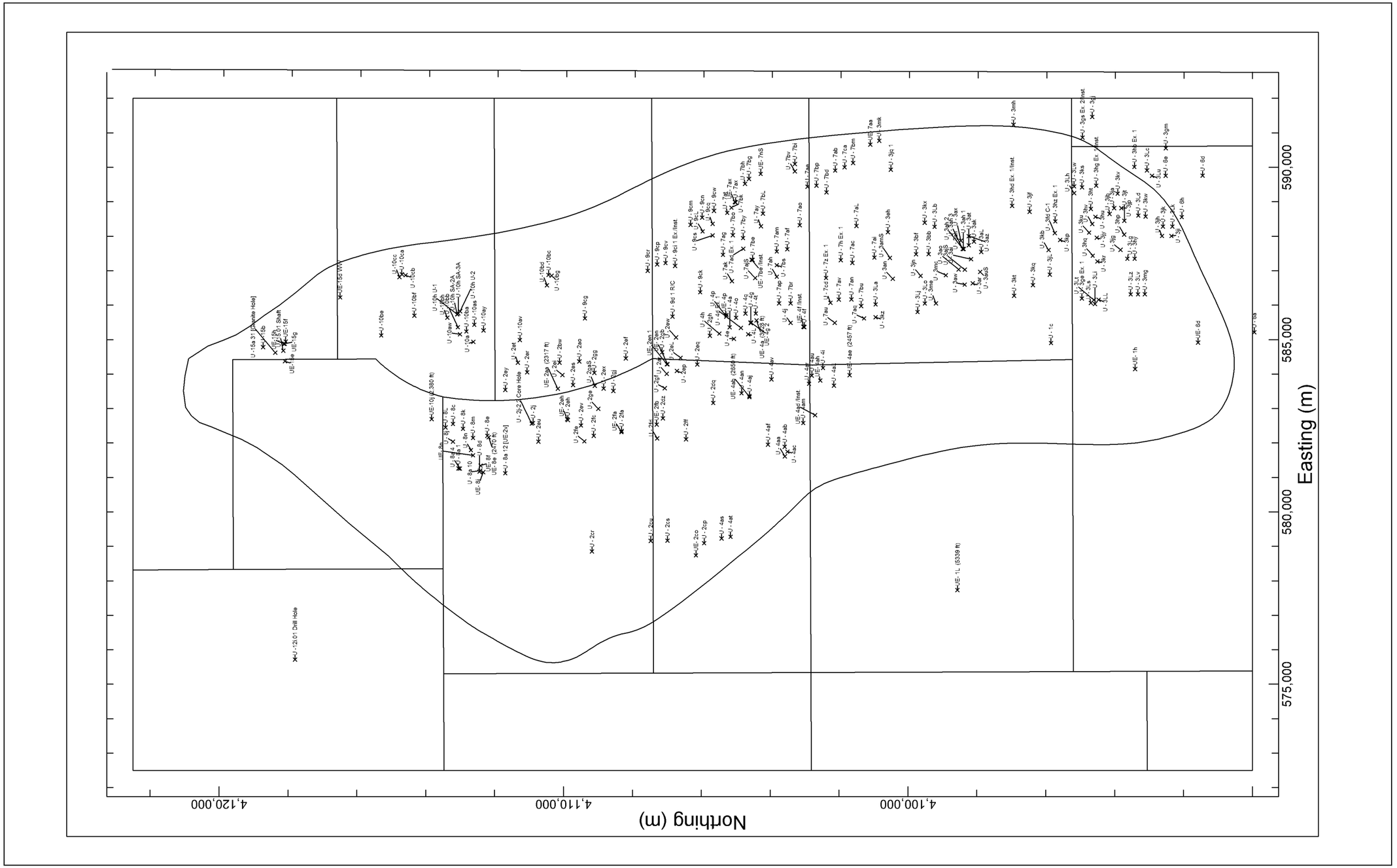

Figure 7-1
Yucca Flat/Climax Mine Borehole Locations with Matrix Porosity Values

Table 7-1
Yucca Flat Matrix Porosity Values from Laboratory Transport Experiments

Borehole	Sample ID	Interval (ft)	Matrix Porosity	Range	Mean	Source	Source Table	Method
Lower Carbonate Aquifer								
ER-6-1	LCA	2,240 - 2,240.8	0.031 & 0.035	0.004	0.0330	B	3	wafer
ER-6-1	LCA	2,399.4 - 2,400.1	0.003 - 0.015	0.012	0.0090	A	3	weight
ER-6-1	LCA	2,400.2 - 2,400.7	0.009 & 0.01	0.001	0.0095	B	3	wafer
ER-6-1	LCA	2,512 - 2,512.8	0.011 - 0.038	0.027	0.0250	A	3	weight
ER-6-1	LCA-3	2,552.1 - 2,553.1	0.0170	N/A	0.0170	C	2.1	helium
ER-6-1	LCA-1	2,604.7 - 2,605.7	0.0220	N/A	0.0220	C	2.1	helium
ER-6-1	LCA	2,675 - 2,675.7	0.014 - 0.028	0.014	0.0210	A	3	weight
ER-6-1	LCA-2	2,732.2 - 2,733.1	0.0160	N/A	0.0160	C	2.1	helium
ER-6-1	LCA	2,846.5 - 2,847.3	0.013 - 0.027	0.014	0.0200	A	3	weight
ER-6-1	LCA	2,915 - 2,915.8	0.017 - 0.042	0.025	0.0300	A	3	weight
ER-6-1	LCA	2,943.8 - 2,944.2	0.059 & 0.06	0.001	0.0595	B	3	wafer
ER-6-1	LCA	3,028 - 3,029	0.016 - 0.031	0.015	0.0240	A	3	weight
ER-6-1	LCA	3,047.5 - 3,048.2	0.013 & 0.013	0	0.0130	B	3	wafer
ER-6-2	LCA	2,730.2 - 2,730.7	0.002 - 0.015	0.013	0.0090	A	3	weight
ER-6-2	LCA	2,749.9 - 2,750.9	0.0026 - 0.0058	0.0032	0.0040	A	3	weight
Tuff Confining Unit								
UE-4a	TCU	2,028.9 - 2,031.1	0.36 - 0.38	0.02	0.3700	A	4	weight
UE-7az	TCU-6	1,678.2 - 1,679	0.3370	N/A	0.3370	C	2.1	helium
UE-7az	TCU	1,769.1 - 1,771.1	0.36 - 0.37	0.01	0.3650	A	4	weight
UE-7az	TCU-4	1,779.9 - 1,780.2	0.3080	N/A	0.3080	C	2.1	helium
UE-7az	TCU-2	1,798.8 - 1,799.5	0.2910	N/A	0.2910	C	2.1	helium
UE-7ba	TCU-5	1,626.2 - 1,627	0.3090	N/A	0.3090	C	2.1	helium
UE-7ba	TCU	1,822.3 - 1,823.7	0.27 - 0.28	0.01	0.2750	A	4	weight
UE-7ba	TCU	1,862.5 - 1,863.3	0.26 - 0.28	0.02	0.2700	A	4	weight

A - Ware et al., 2005
B - Reimus et al., 2006c
C - Zavarin et al., 2005

N/A - Not applicable (only a single measurement is reported)

Table 7-2
HSU to HGU Assignment

HSU [a]	HGU [b]
AA VCU	AA
LCA3 UCA LCA	CA
LCCU1 LCCU2 UCCU LCCU	CCU
MGCU	GCU
BLFA PRETBG PRETBG1	LFA
PCUT	PCU
UTCU BRCU LTCU OSBCU ATCU	TCU
TM-LVTA LVTA TM-UVTA	VTA
TSA BRA TM-WTA TUBA	WTA

[a] See Table 4-2 for definitions of hydrostratigraphic units.
[b] See Table 4-1 for definitions of hydrogeologic units.

the ranges of 0 to 9 percent reported by Winograd and Thordarson (1975) for the LCA as well as those of the laboratory studies (Table 7-1). These samples were collected from the contact zone between the carbonate aquifer and the overlying unit.

7.3.1 Variability of Porosity with Depth

The intent of this section is to assign a matrix porosity probability distribution to each Yucca Flat HGU. A probability distribution does not include spatial components of the measured data (i.e., the distribution and its descriptive parameters do not contain any information describing the spatial variability of first- or higher-order statistics of the measured porosity). It is important to confirm spatial trends do not exist within an HSU that would act to both bias and increase the apparent

variability of the measured and estimated probability distribution. The spatial features of the porosity data are considered in the vertical direction only due to the spatial orientation of porosity measurements in boreholes.

Figure 7-2 presents the porosity data for each HGU as a function of depth. Although a trend of decreasing porosity with depth is often observed due to compaction, high stresses, closing fractures and circulating groundwater, no significant correlation between porosity and depth is observed for any of the HGUs. Subtle trends that may exist cannot be identified due to the large scatter in the measured data. A trend is inherently difficult to identify in the alluvium due to the variability resulting from the unconsolidated, complex poorly sorted nature of alluvial deposits and limitations with the techniques used to collect and analyze them.

7.4 Development of Parameter Distributions

Part of the Yucca Flat CAU-scale flow and transport model input parameter selection involves the assignment of the matrix porosity parameters from a probability distribution. To derive the HGU and HSU porosity data probability distributions, cumulative distribution functions (CDFs) were fit to the sample data. The fitting algorithm uses Maximum Likelihood Estimation, a statistical method used to make inferences about parameters of the underlying probability distribution of a given dataset (Fisher, 1922). The fitted distribution parameters do not always exactly reproduce the measured data statistics so the fitted distributions are ranked based on either their chi-squared statistic, Anderson-Darling (A-D) statistic, or Kolmogorov-Smirnov (K-S) statistic. A CDF for the data is chosen based on the most suitable fit statistic for the fitted distribution.

7.4.1 Porosity Distributions by HGU and HSU

Box and whisker plots of the HGU and HSU values are presented in Figures 7-3 and 7-4, and the sample summary statistics are contained in Table 7-3. (Figures and tables are presented at the end of this section.) Plots are not presented for HSUs with sample population sizes of less than 10. Figures 7-5 through 7-24 show histograms and CDFs of matrix porosity for the Yucca Flat HGUs and HSUs. Table 7-4 lists the fitted distribution, descriptive statistics, and fit statistics for the matrix porosities for the Yucca Flat HGUs and HSUs, respectively. The distribution parameters in Table 7-4 may be used for populating the model hydrogeologic flow domain with matrix porosity values.

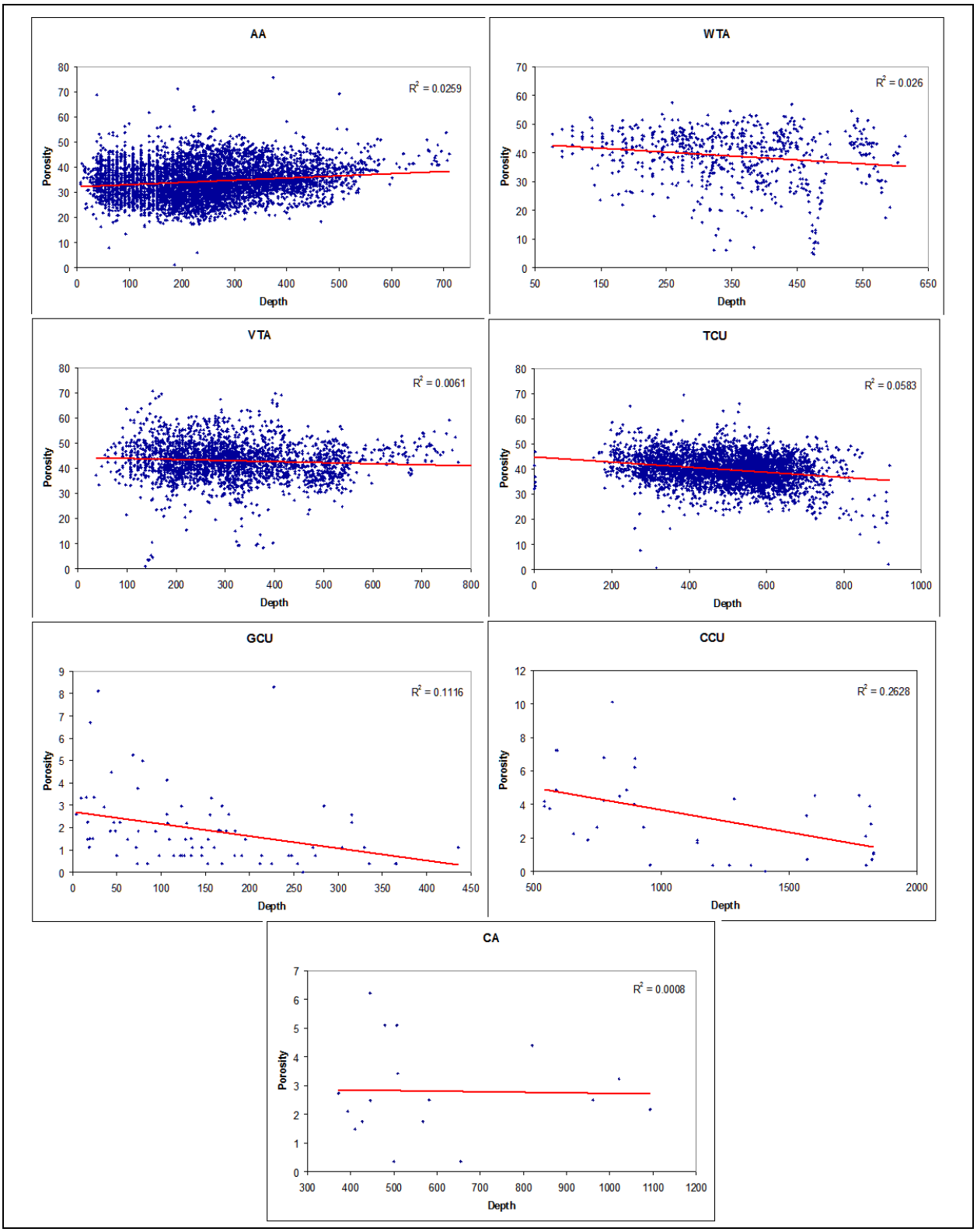

Figure 7-2
Linear Regression Analysis of HGU Porosity (%) as a Function of Depth (m bgs)

7.5 Scaling Considerations

The matrix porosity data are small-scale (sub-meter) measurements that, in most cases, do not correspond with the larger (tens-of-meters to km) scale at which flow and transport modeling are completed. As noted by McKenna and Rautman (1996), porosity can be effectively upscaled by the volume variance method, which is also presented in several textbooks including Journel and Huijbregts (1978) and Vanmarcke (1983). The method preserves the sample mean, and the upscaled variance reduction (due to sample averaging) is a function of the ratio of the correlation length of the point process to the averaging interval. The point process correlation length is unknown and cannot be sufficiently estimated (with respect to the sample number) in any orientation but the vertical; therefore, the method is impractical for application with this dataset.

In general, the spatial sampling of matrix porosity (and related hydrogeologic rock properties) is sparse in the horizontal plane, primarily because the majority of data are collected from vertical boreholes. Limited lateral porosity data have been collected at Yucca Mountain from surface outcrops (e.g., Flint et al. [1996]) and from tunnels (e.g., Freifeld [2001]); however, these data are from the unsaturated zone and do not represent the full suite of HGUs at Yucca Flat. To circumvent the problem of limited data for estimation of a spatial statistic (e.g., the correlation length) in the horizontal plane, it is common to assume a ratio of anisotropy in the principal directions and then scale the statistic relative to the known orientation. Lateral spatial statistics may be inferred if the relationship is known between matrix porosity and a secondary variable with known directional spatial statistics. For example, in the alluvium, porosity strongly correlates with the sample grain size distribution, which itself depends on depositional features. In other words, laterally varying deposits could define the scale at which matrix porosity varies.

Additional complications to spatial averaging are related to heterogeneity due to contributions from different lithologies within a single HGU. Consider, for example, a stratum of welded tuffs situated between nonwelded tuffs in a single (composite) HGU. Because the welded tuff is likely to transmit most of the flow, the upscaled matrix porosity should reflect the welded unit (through vertical thickness weighting) rather than corresponding to the arithmetic mean of all lithologies in the unit.

In summary, the variance reduction for each HGU cannot be calculated at this time, although the HGU sample means (Table 7-4) can be as they are unaffected by the scaling process. Before applying the data at the larger CAU scale, it may be important to resolve the quantity of variance reduction per HGU. For example, high porosities will result in either unrealistically slow groundwater flow rates, large amounts of matrix diffusion, or both. Alternatively, the quantity of variance reduction may be addressed via a parameter sensitivity analysis during the numerical simulation of transport.

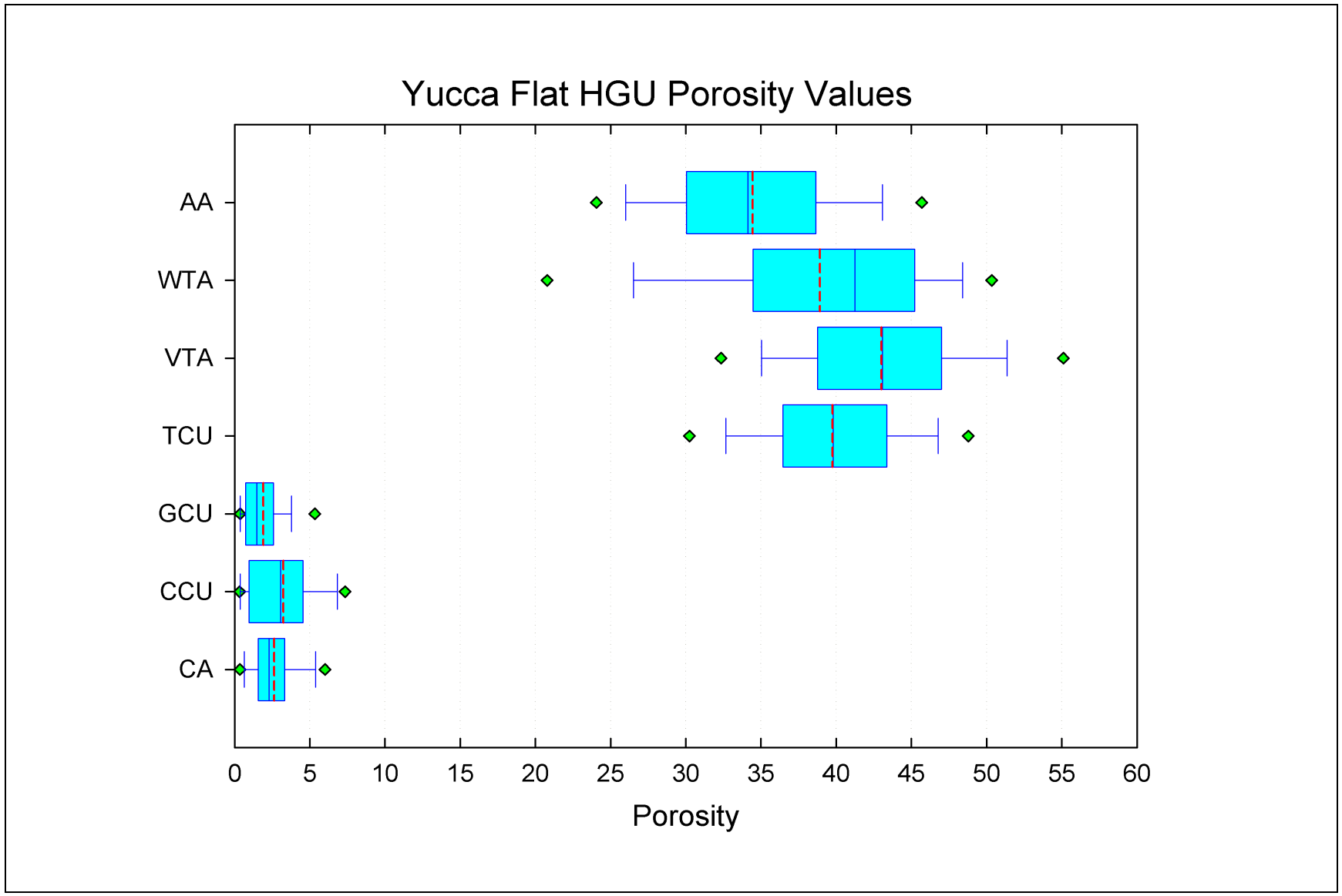

Figure 7-3
Yucca Flat HGU Porosity Values

Note: Mean – Red vertical dashed line in box; Median – Blue vertical line in box; 25th Percentile – Left box side; 75th Percentile – Right box side; 10th Percentile – Left whisker; 90th Percentile – Right whisker; 5th Percentile – Left green diamond; 95th Percentile – Right green diamond

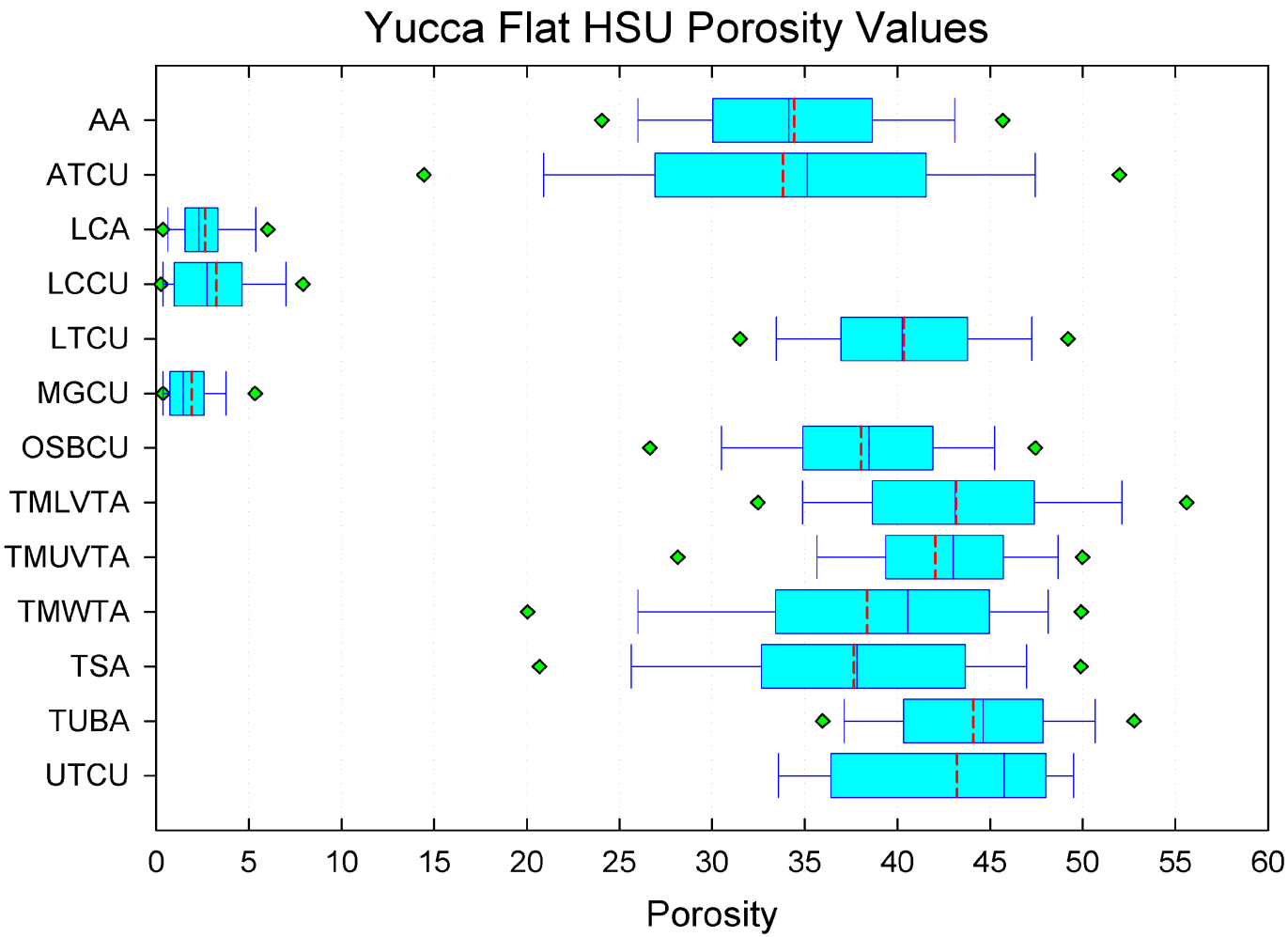

Figure 7-4
Yucca Flat HSU Porosity Values

Note: Mean – Red vertical dashed line in box; Median – Blue vertical line in box; 25th Percentile – Left box side; 75th Percentile – Right box side; 10th Percentile – Left whisker; 90th Percentile – Right whisker; 5th Percentile – Left green diamond; 95th Percentile – Right green diamond

Table 7-3
Sample Summary Statistics for Matrix Porosity

Unit	N	Range	Min	Max	Mean	Median	SD	CV
Hydrogeologic Units								
AA	6203	95.73	1.30	97.03	34.44	34.13	6.65	19.30%
CA	34	5.85	0.35	6.20	2.63	2.44	1.63	61.98%
CCU	38	10.11	0.00	10.11	3.24	3.06	2.42	74.72%
GCU	78	8.30	0.00	8.30	1.91	1.48	1.64	85.65%
LFA	1	0.00	4.12	4.12	4.12	N/A	N/A	N/A
PCU	1	0.00	36.72	36.72	36.72	N/A	N/A	N/A
TCU	3839	68.72	0.70	69.42	39.75	39.80	5.87	14.78%
VTA	2718	69.92	0.85	70.76	43.00	43.08	7.32	17.02%
WTA	693	52.85	4.61	57.47	38.91	41.24	9.09	23.37%
Hydrostratigraphic Units								
AA2	113	20.49	29.80	50.29	40.90	42.67	5.97	14.59%
AA3	6090	95.73	1.30	97.03	37.33	34.08	6.61	19.25%
ATCU	34	52.52	2.11	54.63	33.83	35.14	10.71	31.65%
BLFA	1	0.00	4.12	4.12	4.12	N/A	N/A	N/A
BRCU	1	0.00	46.15	46.15	46.15	N/A	N/A	N/A
LCA	26	5.60	0.35	5.95	2.23	2.10	1.40	62.78%
LCA3	8	4.46	1.75	6.20	3.94	3.92	1.74	44.02%
LCCU	34	10.11	0.00	10.11	3.26	2.73	2.52	77.20%
LTCU	2828	61.85	7.57	69.42	40.36	40.27	5.52	13.68%
MGCU	78	8.30	0.00	8.30	1.91	1.48	1.64	85.65%
OSBCU	958	57.25	0.70	57.95	38.06	38.47	6.19	16.25%
PCUT	1	0.00	36.72	36.72	36.72	N/A	N/A	N/A
TMLVTA	2290	69.92	0.85	70.76	43.18	43.10	7.47	17.29%
TMUVTA	428	54.78	8.34	63.12	42.05	43.00	6.39	15.21%
TMWTA	592	52.85	4.61	57.47	38.36	40.55	9.32	24.29%
TSA	31	33.18	17.83	51.01	37.64	37.80	8.36	22.20%
TUBA	70	21.70	32.90	54.60	44.11	44.63	4.98	11.28%
UCCU	4	3.60	0.73	4.33	3.09	3.65	1.63	52.79%
UTCU	18	17.73	33.29	51.02	43.22	45.76	6.06	14.02%

CV - Coefficient of variation
Max - Maximum
Min - Minimum
N - Population size
N/A - Not applicable (only a single measurement is reported)
SD - Standard deviation

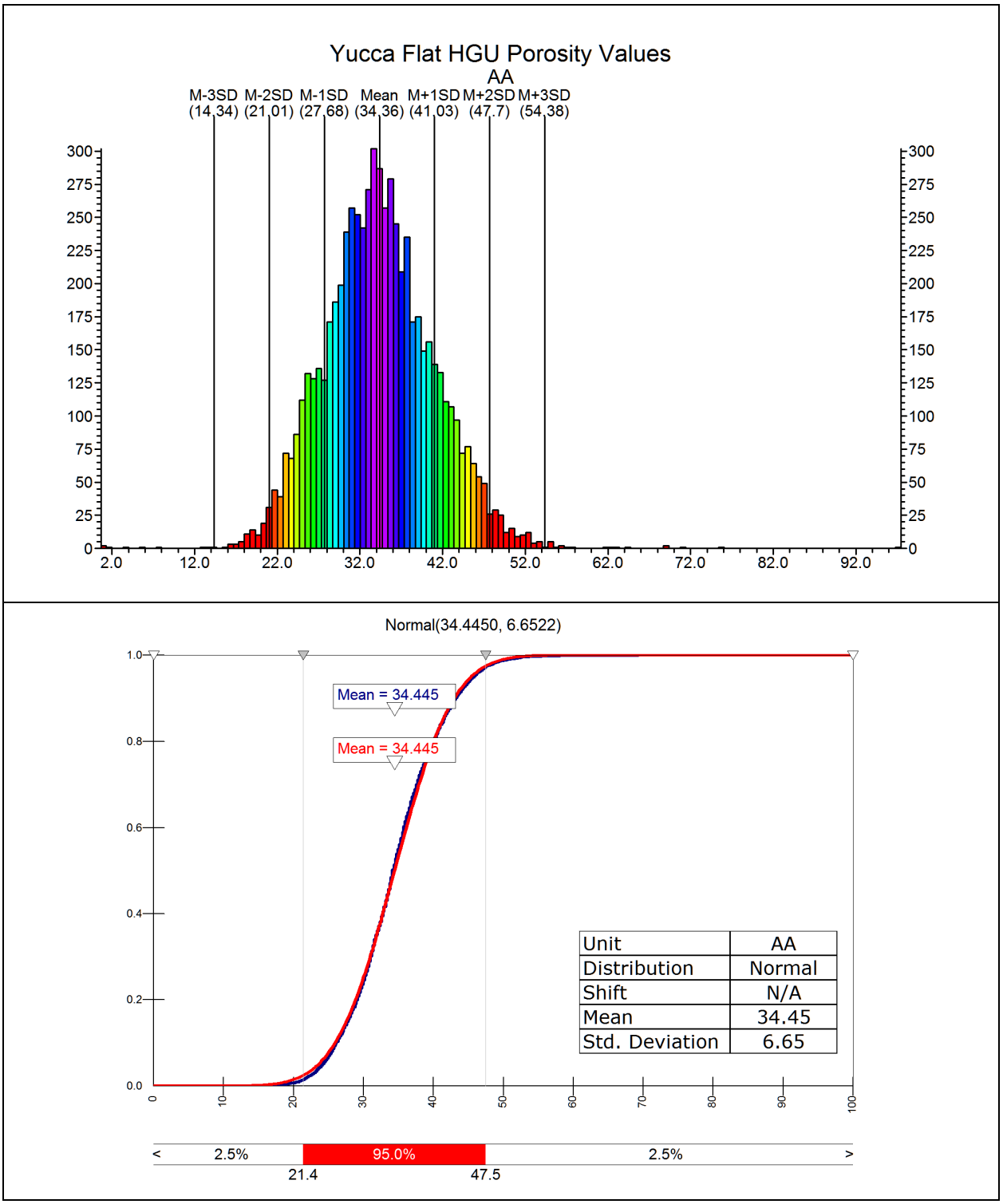

Figure 7-5
AA HGU Matrix Porosity Histogram and CDF

Note: M + 2SD – Mean plus two standard deviations; Blue curve (darker line) and annotations – Sample data CDF; Red curve (lighter line) and annotations – Fitted PDF

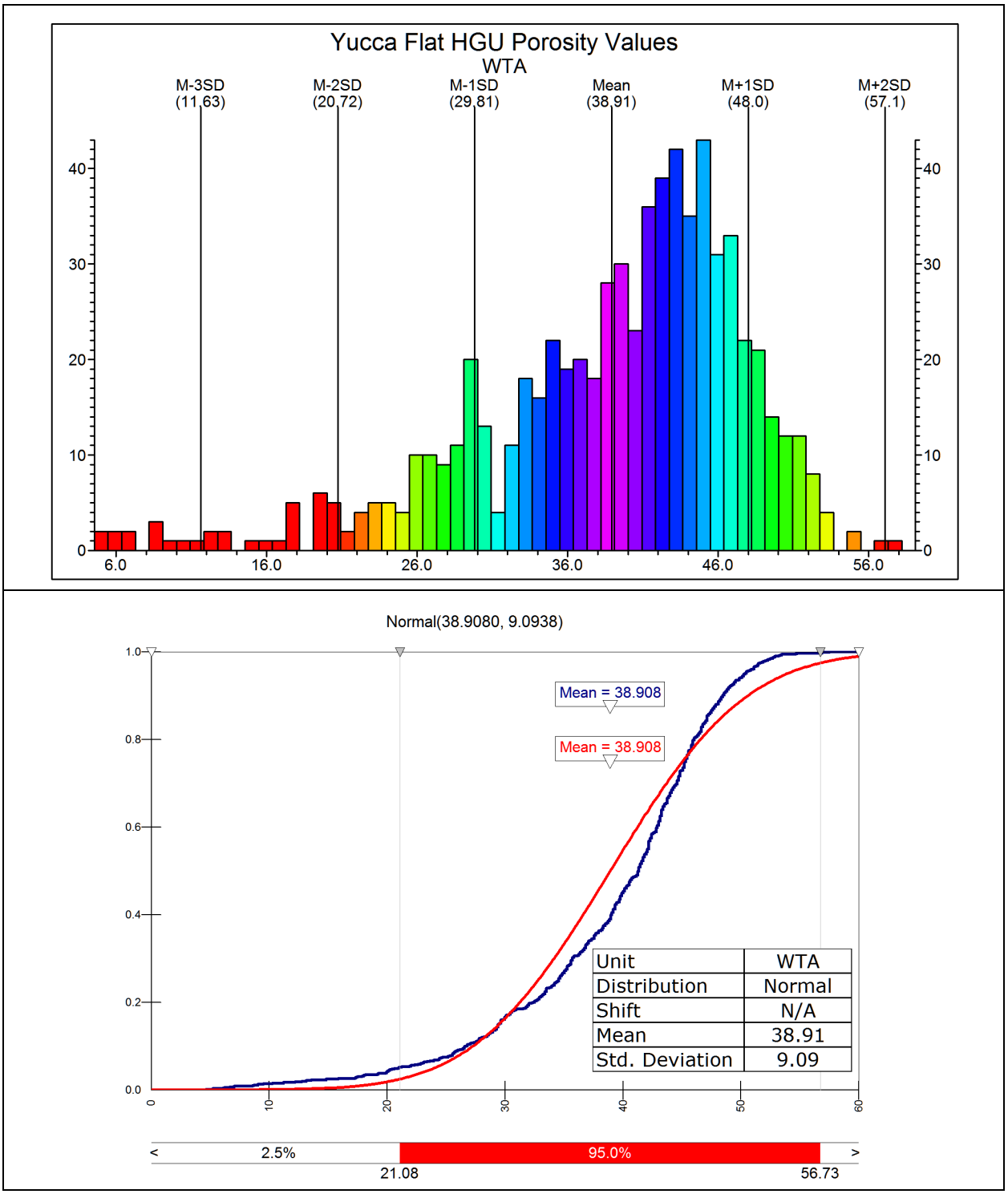

Figure 7-6
WTA HGU Matrix Porosity Histogram and CDF

Note: M + 2SD – Mean plus two standard deviations; Blue curve (darker line) and annotations – Sample data CDF; Red curve (lighter line) and annotations – Fitted PDF

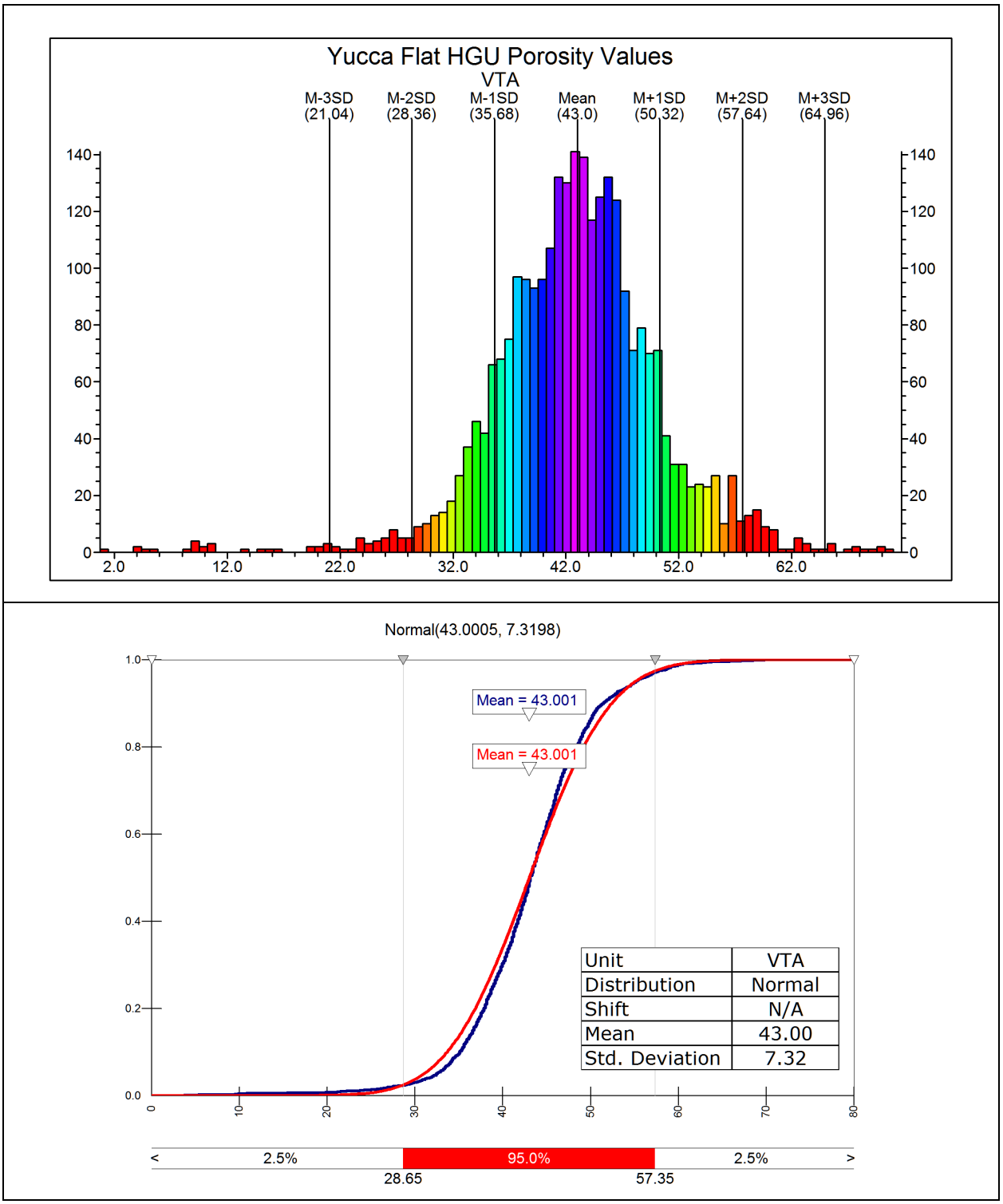

Figure 7-7
VTA HGU Matrix Porosity Histogram and CDF

Note: M + 2SD – Mean plus two standard deviations; Blue curve (darker line) and annotations – Sample data CDF; Red curve (lighter line) and annotations – Fitted PDF

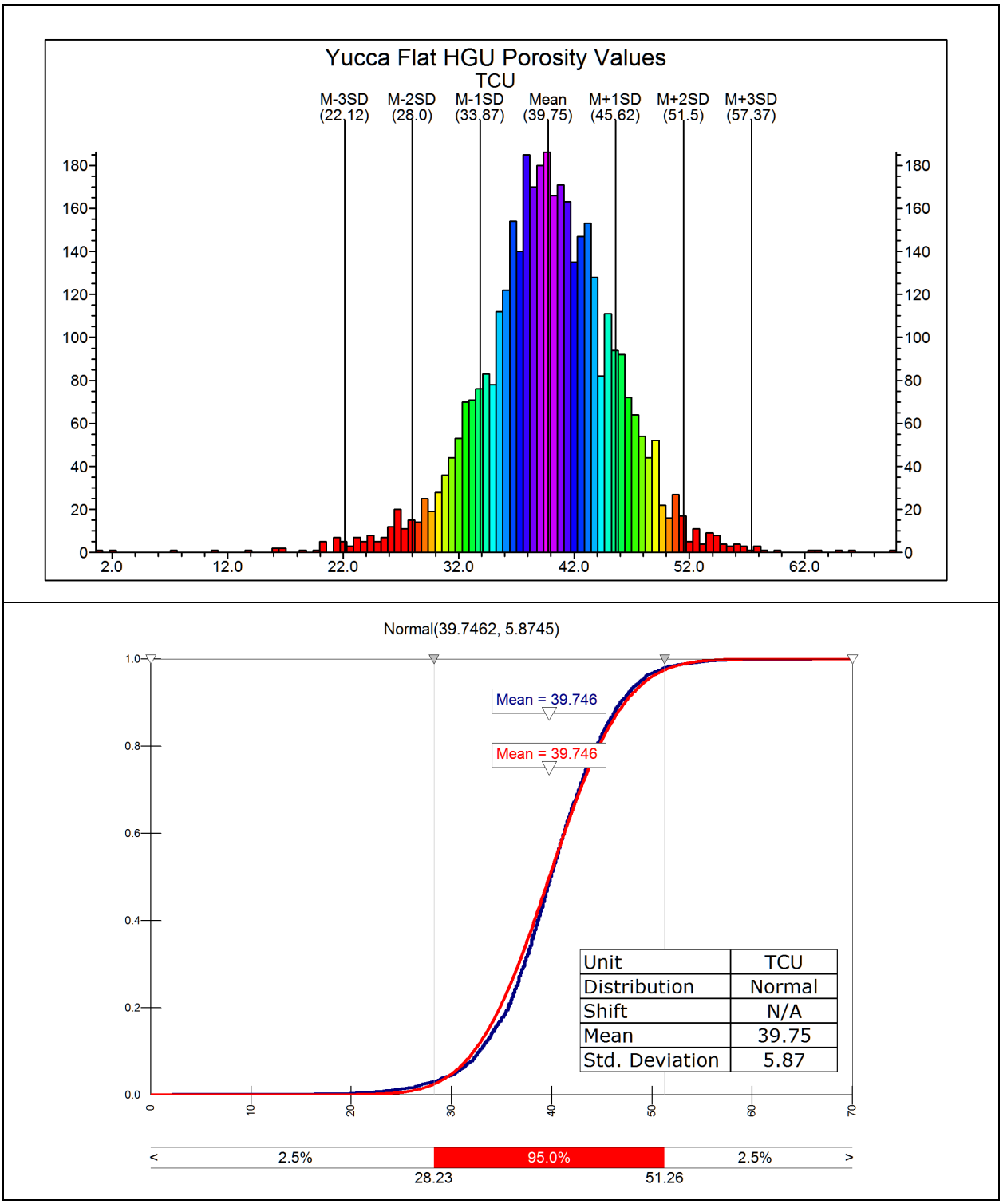

Figure 7-8
TCU HGU Matrix Porosity Histogram and CDF

Note: M + 2SD – Mean plus two standard deviations; Blue curve (darker line) and annotations – Sample data CDF; Red curve (lighter line) and annotations – Fitted PDF

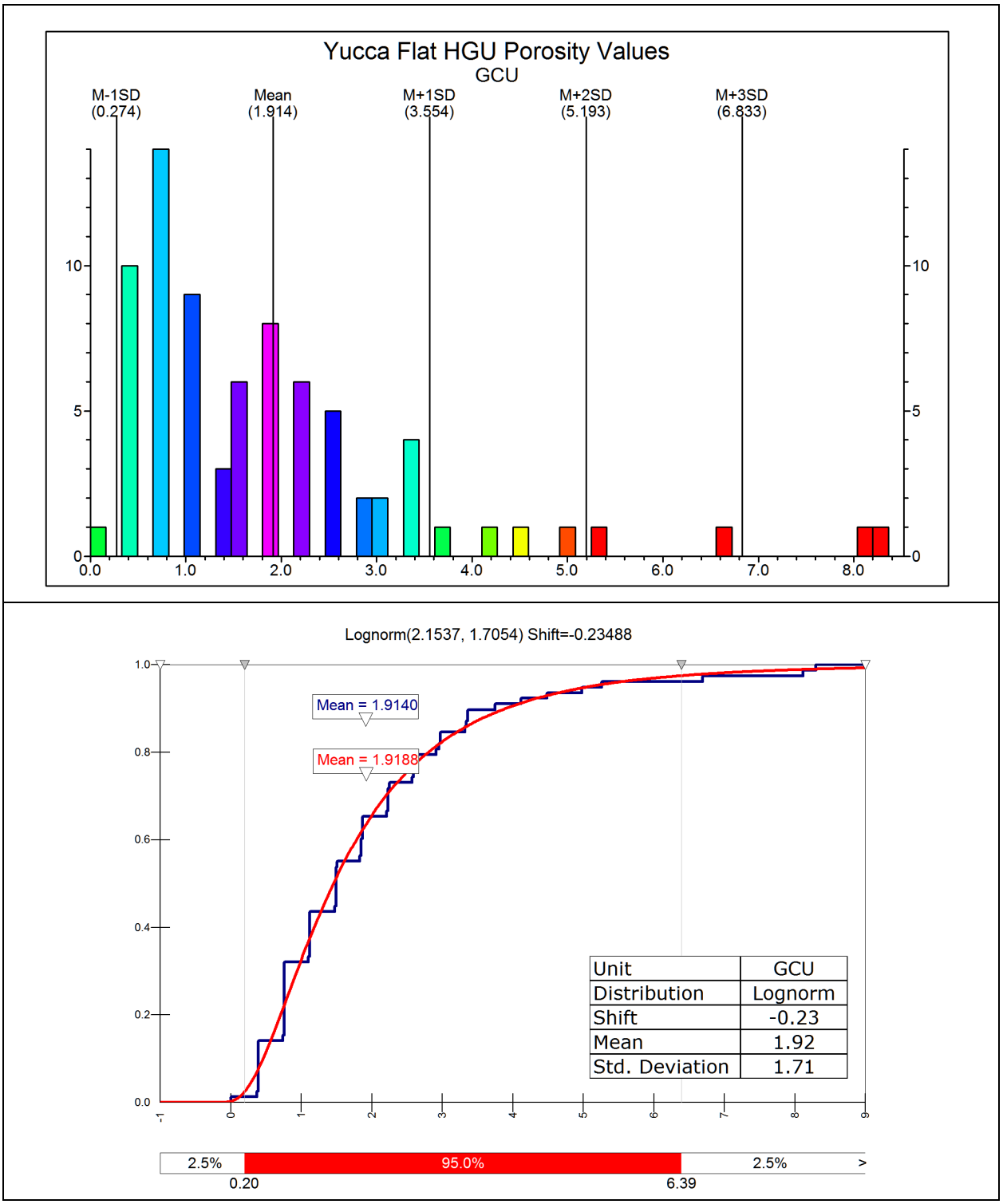

Figure 7-9
GCU HGU Matrix Porosity Histogram and CDF

Note: M + 2SD – Mean plus two standard deviations; Blue curve (darker line) and annotations – Sample data CDF; Red curve (lighter line) and annotations – Fitted PDF

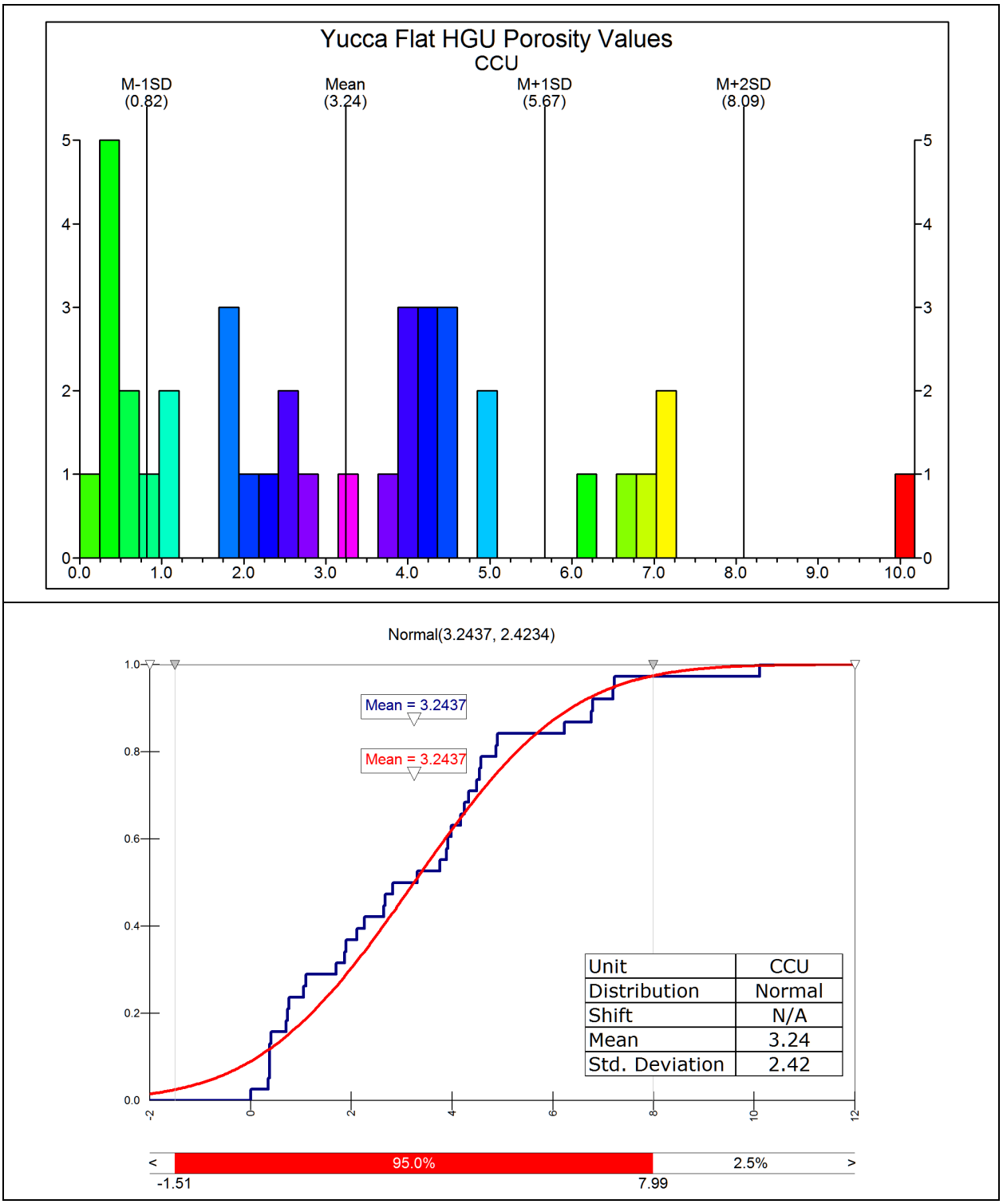

Figure 7-10
CCU HGU Matrix Porosity Histogram and CDF

Note: M + 2SD – Mean plus two standard deviations; Blue curve (darker line) and annotations – Sample data CDF; Red curve (lighter line) and annotations – Fitted PDF

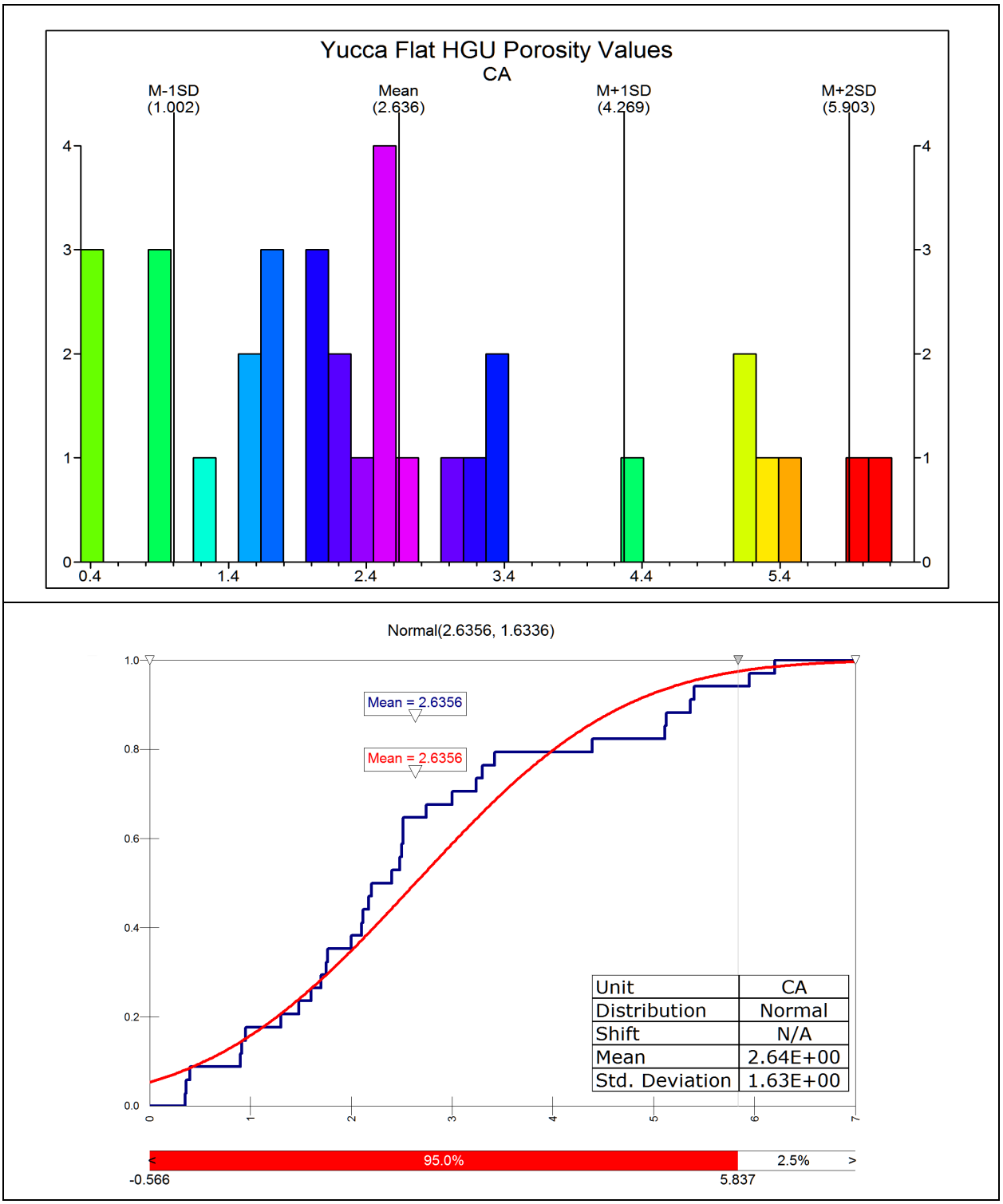

Figure 7-11
CA HGU Matrix Porosity Histogram and CDF

Note: M + 2SD – Mean plus two standard deviations; Blue curve (darker line) and annotations – Sample data CDF; Red curve (lighter line) and annotations – Fitted PDF

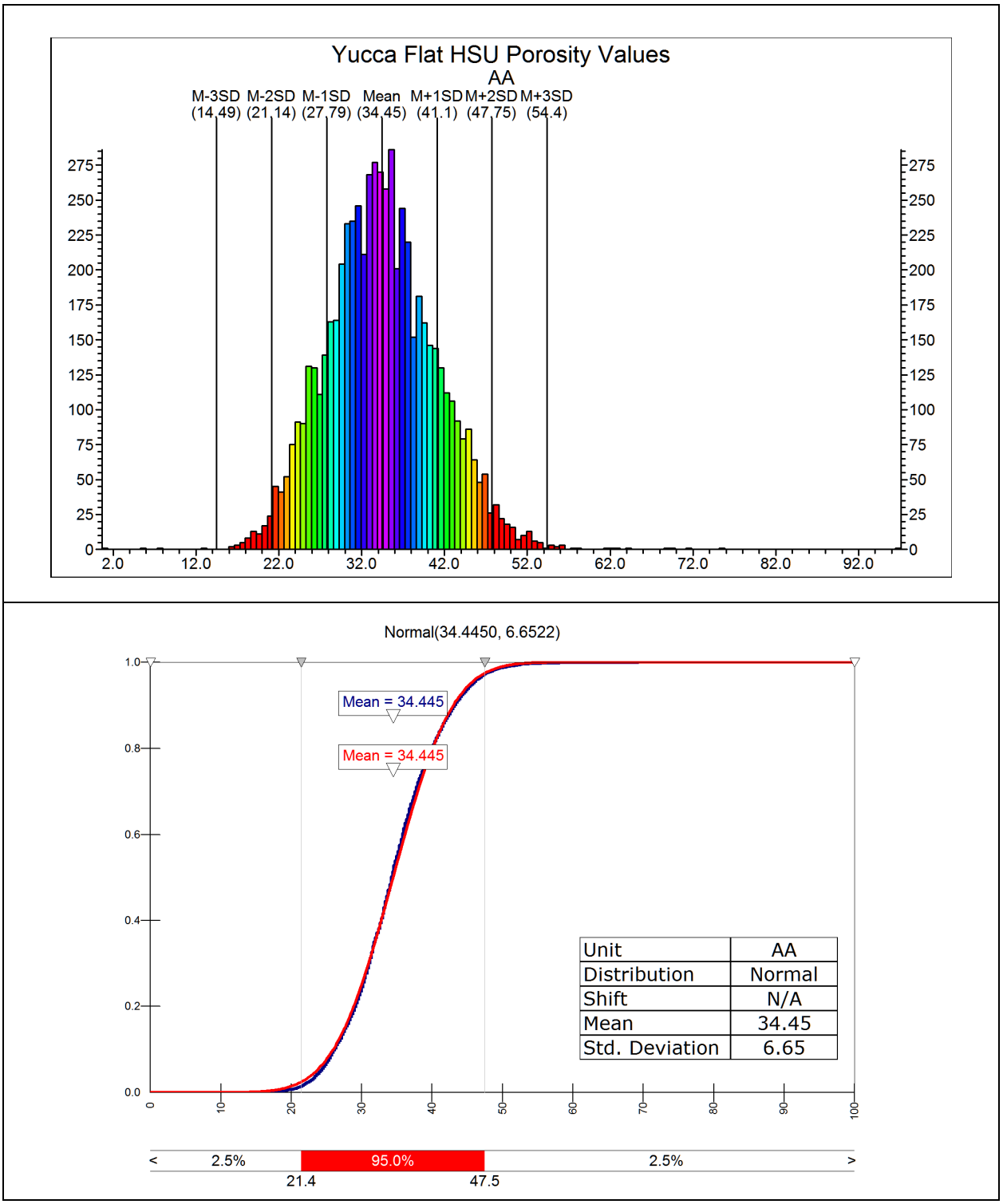

Figure 7-12
AA HSU Matrix Porosity Histogram and CDF

Note: M + 2SD – Mean plus two standard deviations; Blue curve (darker line) and annotations – Sample data CDF; Red curve (lighter line) and annotations – Fitted PDF

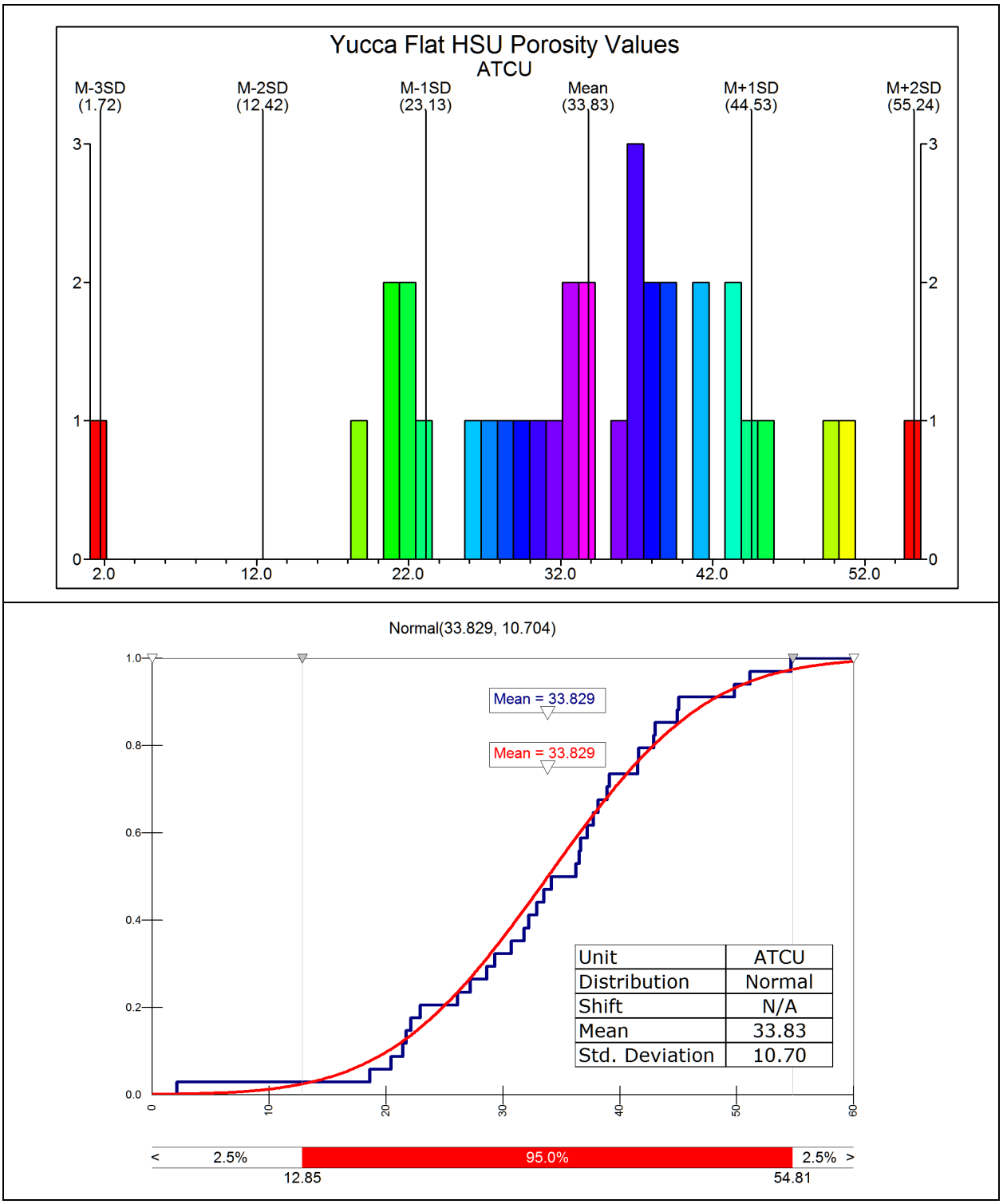

Figure 7-13
ATCU HSU Matrix Porosity Histogram and CDF

Note: M + 2SD – Mean plus two standard deviations; Blue curve (darker line) and annotations – Sample data CDF; Red curve (lighter line) and annotations – Fitted PDF

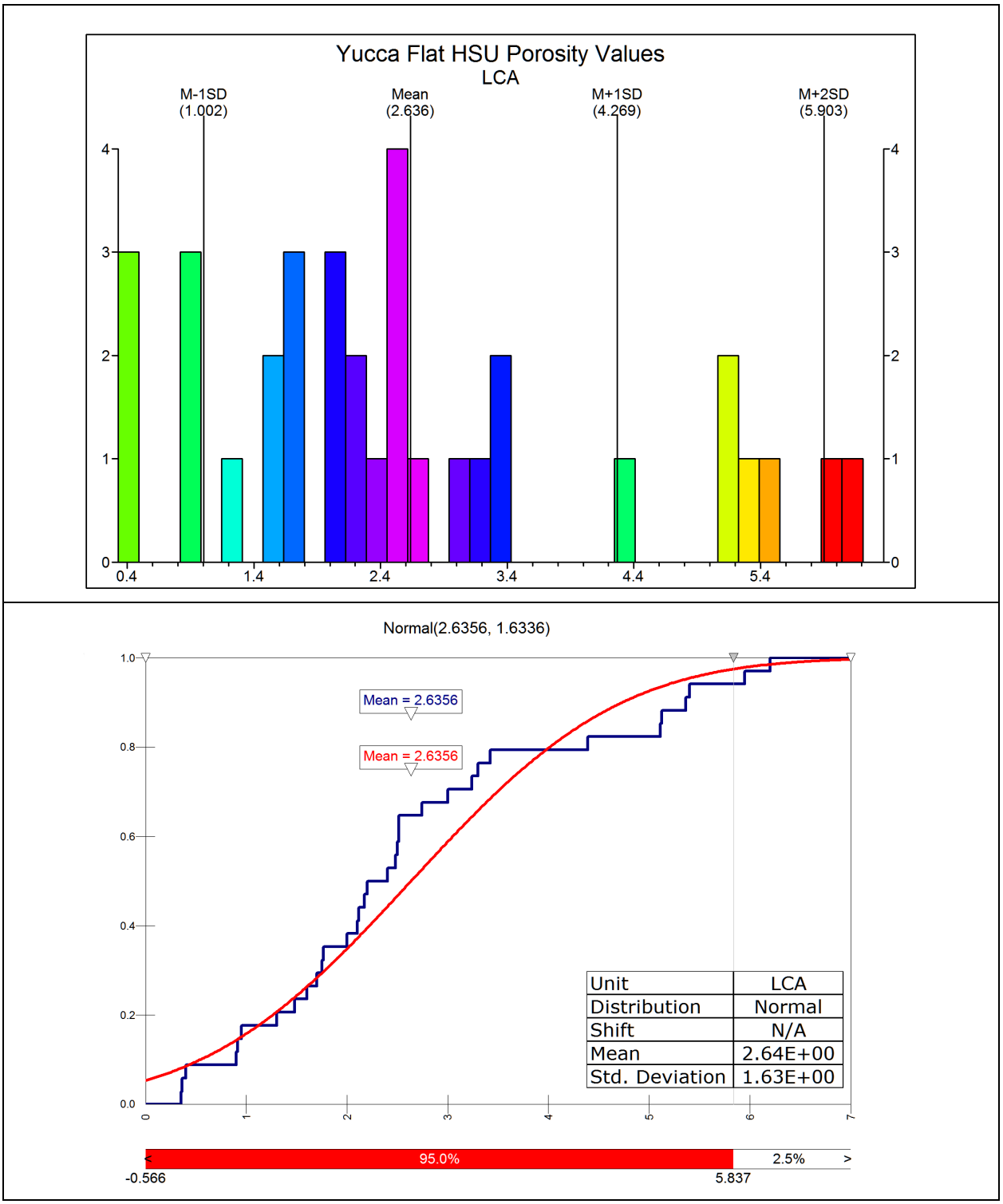

Figure 7-14
LCA HSU Matrix Porosity Histogram and CDF

Note: M + 2SD – Mean plus two standard deviations; Blue curve (darker line) and annotations – Sample data CDF; Red curve (lighter line) and annotations – Fitted PDF

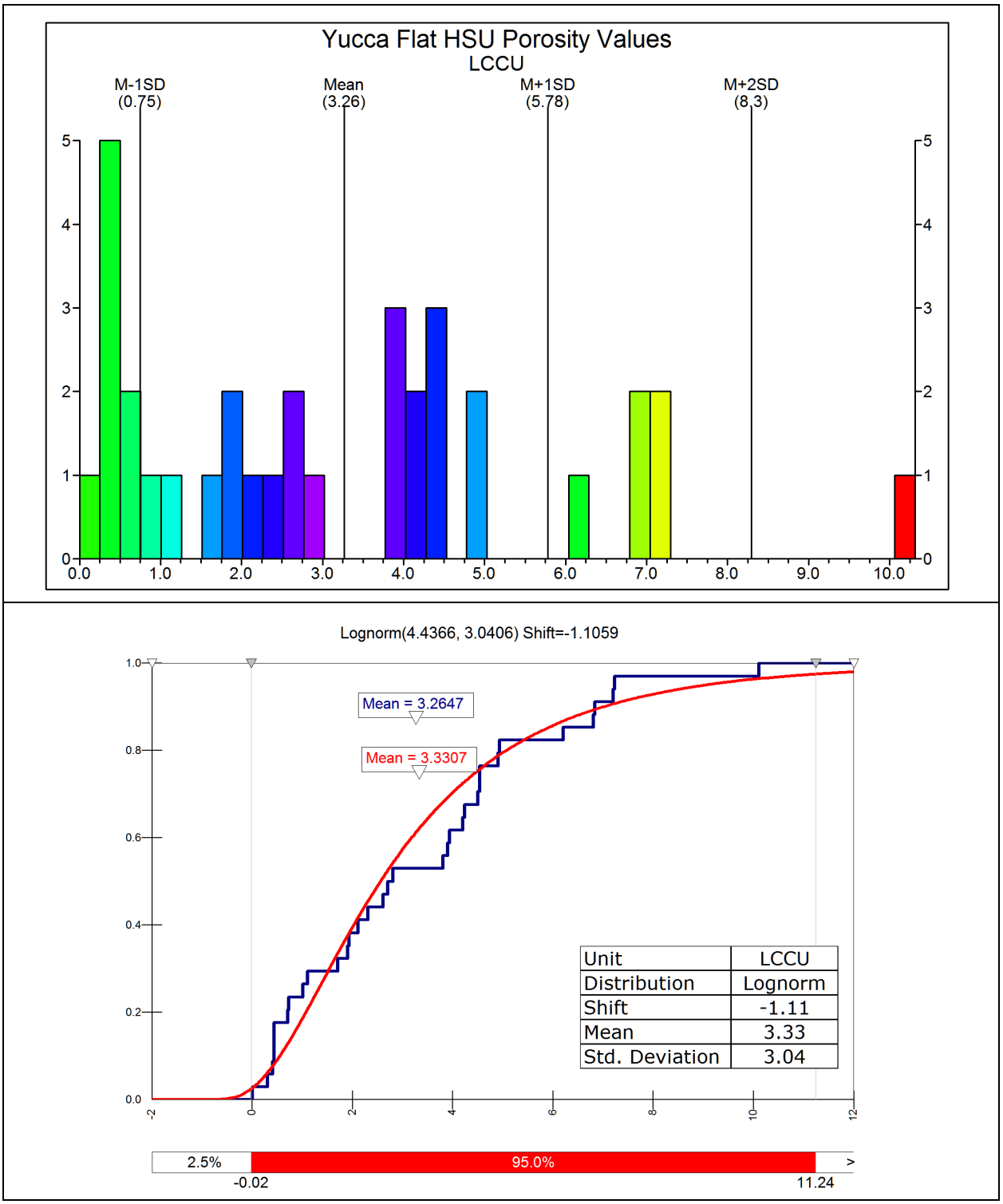

Figure 7-15
LCCU HSU Matrix Porosity Histogram and CDF

Note: M + 2SD – Mean plus two standard deviations; Blue curve (darker line) and annotations – Sample data CDF; Red curve (lighter line) and annotations – Fitted PDF

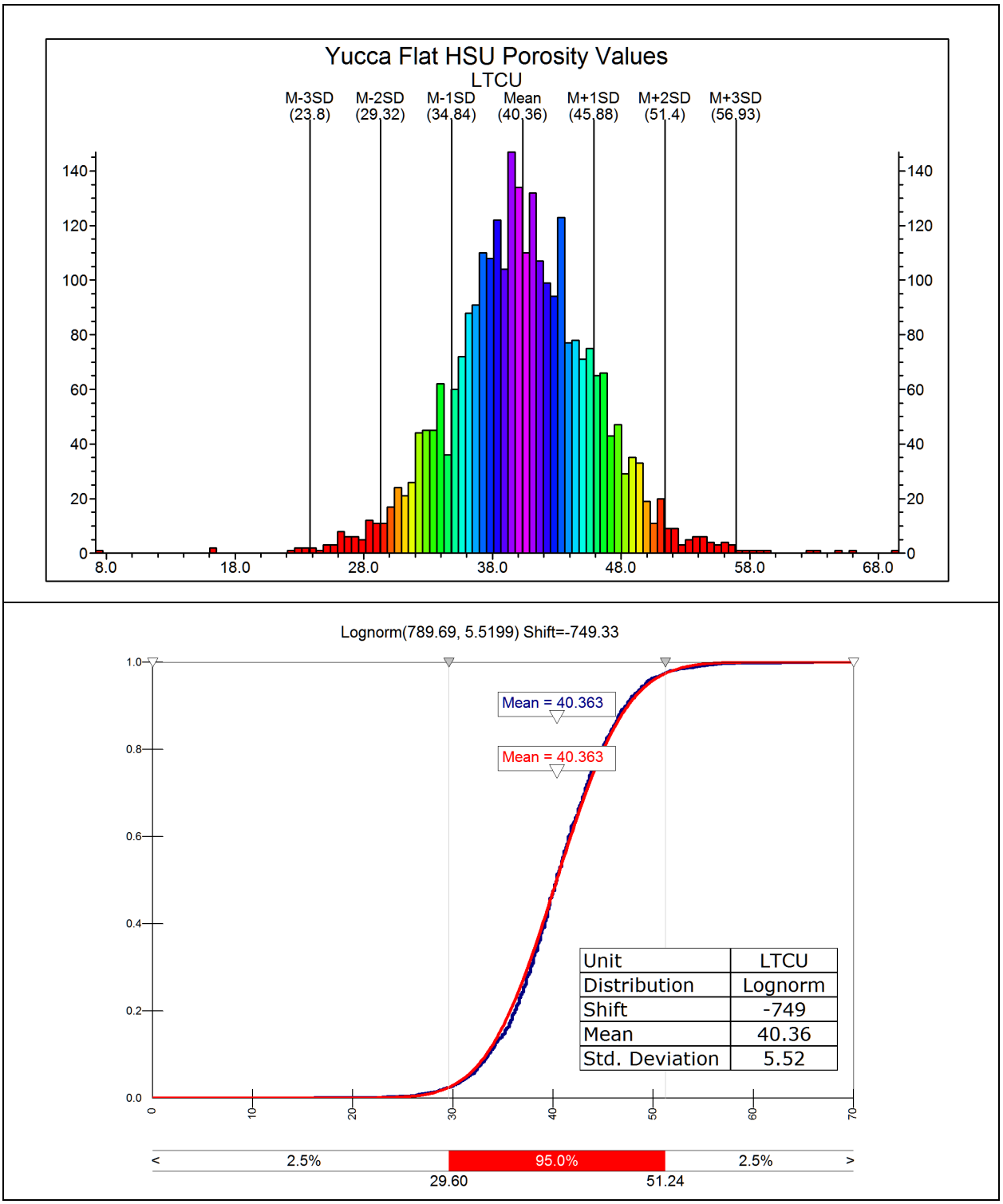

Figure 7-16
LTCU HSU Matrix Porosity Histogram and CDF

Note: M + 2SD – Mean plus two standard deviations; Blue curve (darker line) and annotations – Sample data CDF; Red curve (lighter line) and annotations – Fitted PDF

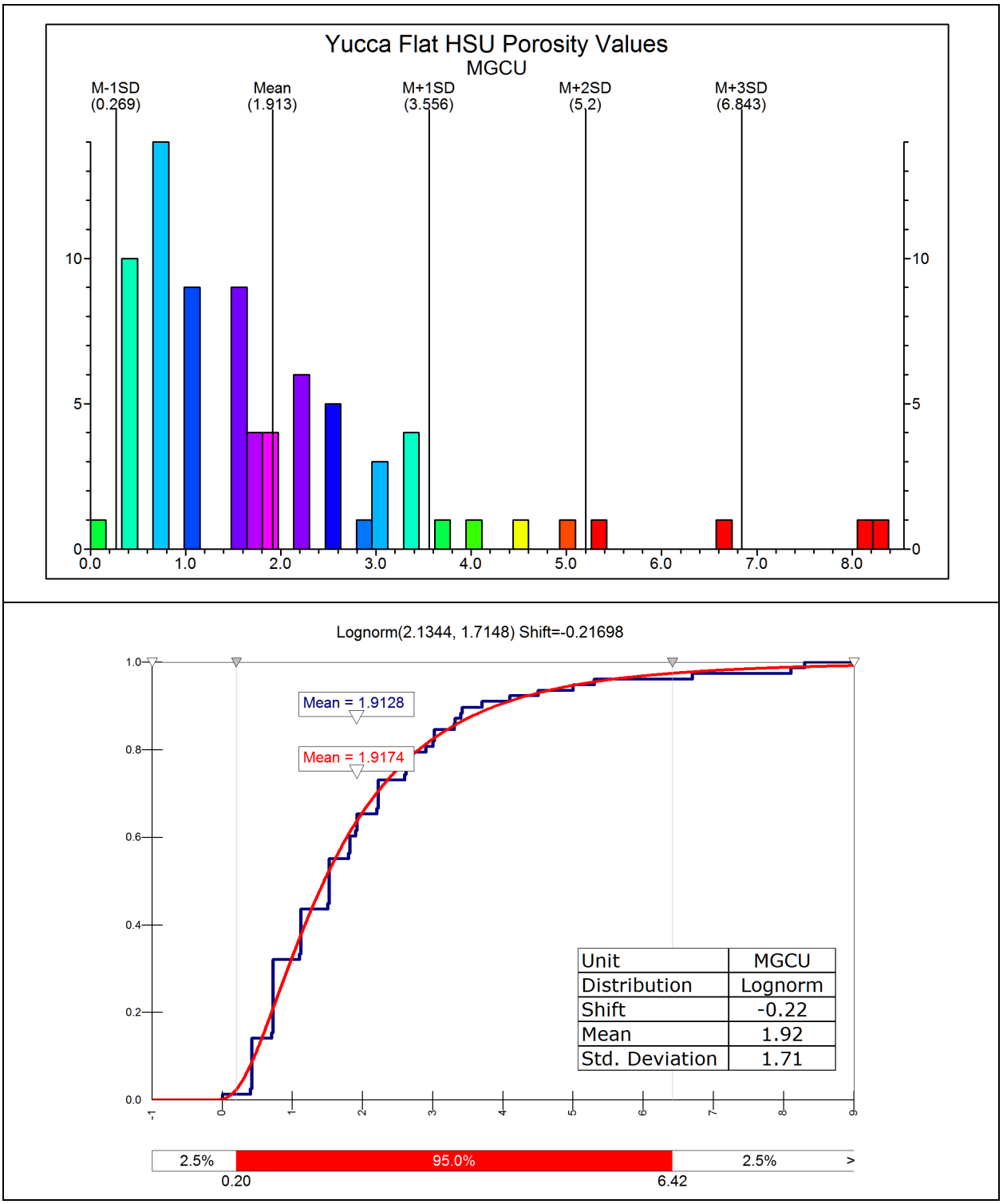

Figure 7-17
MGCU HSU Matrix Porosity Histogram and CDF

Note: M + 2SD – Mean plus two standard deviations; Blue curve (darker line) and annotations – Sample data CDF; Red curve (lighter line) and annotations – Fitted PDF

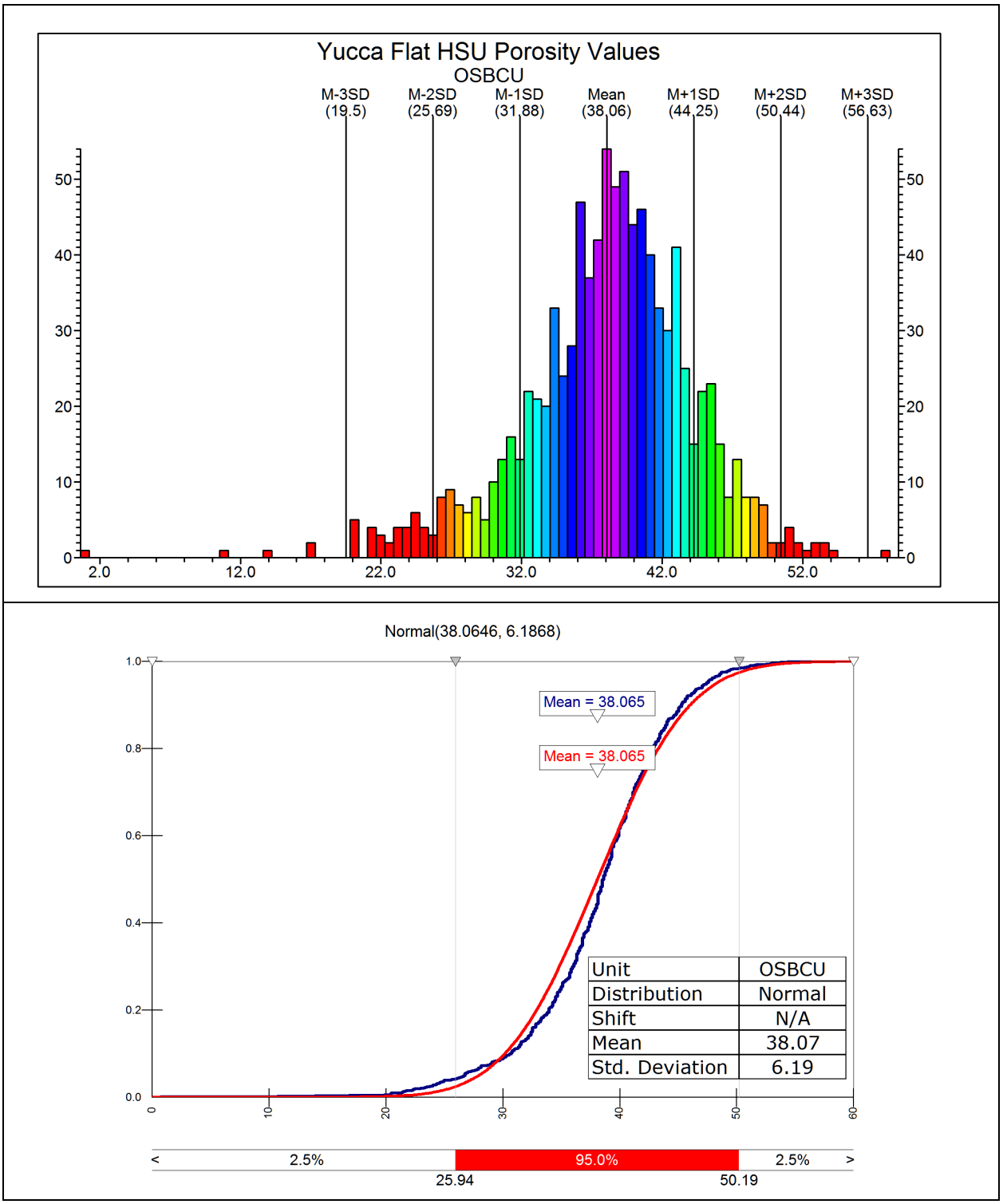

Figure 7-18
OSBCU HSU Matrix Porosity Histogram and CDF

Note: M + 2SD – Mean plus two standard deviations; Blue curve (darker line) and annotations – Sample data CDF; Red curve (lighter line) and annotations – Fitted PDF

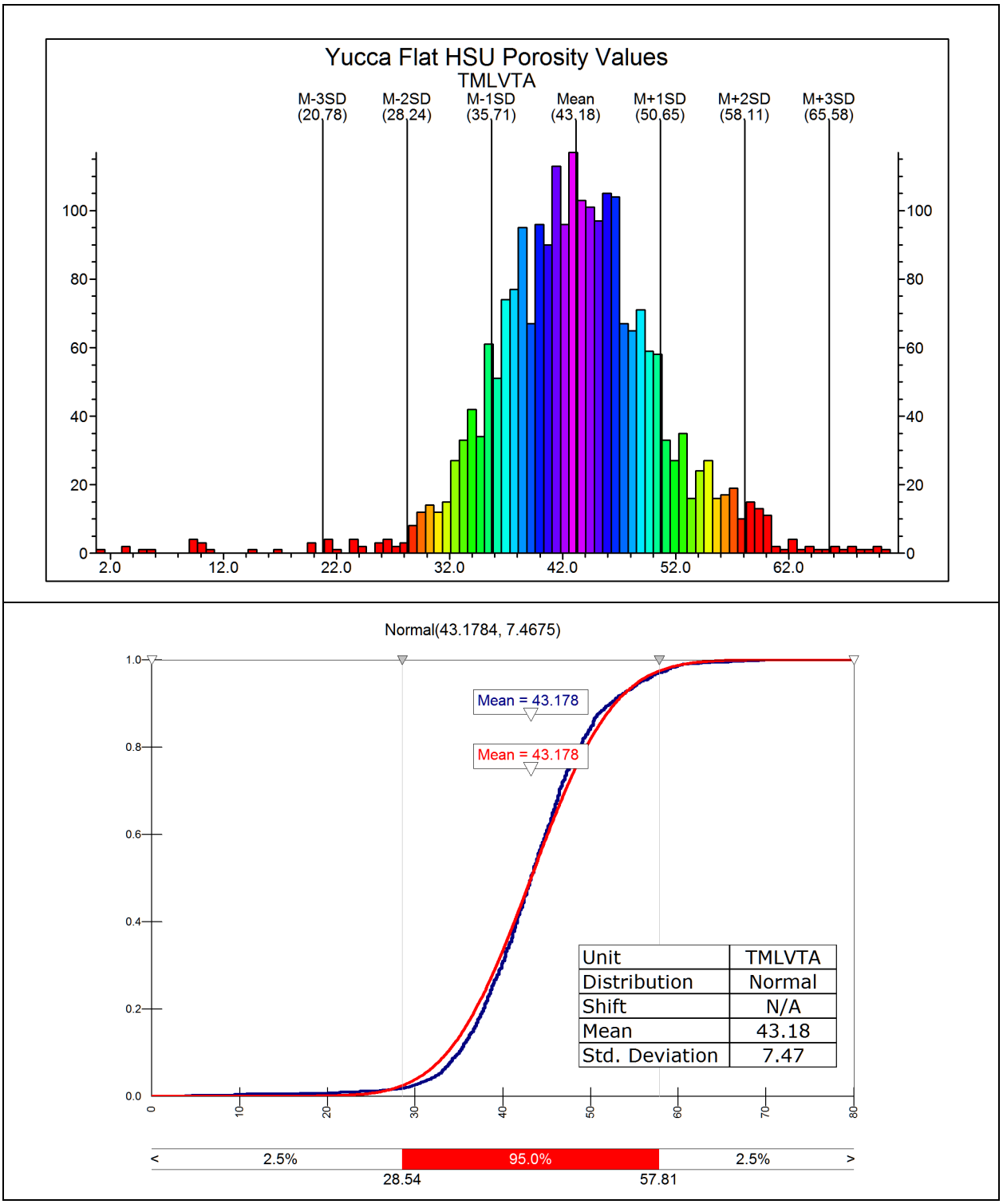

Figure 7-19
TM-LVTA HSU Matrix Porosity Histogram and CDF

Note: M + 2SD – Mean plus two standard deviations; Blue curve (darker line) and annotations – Sample data CDF; Red curve (lighter line) and annotations – Fitted PDF

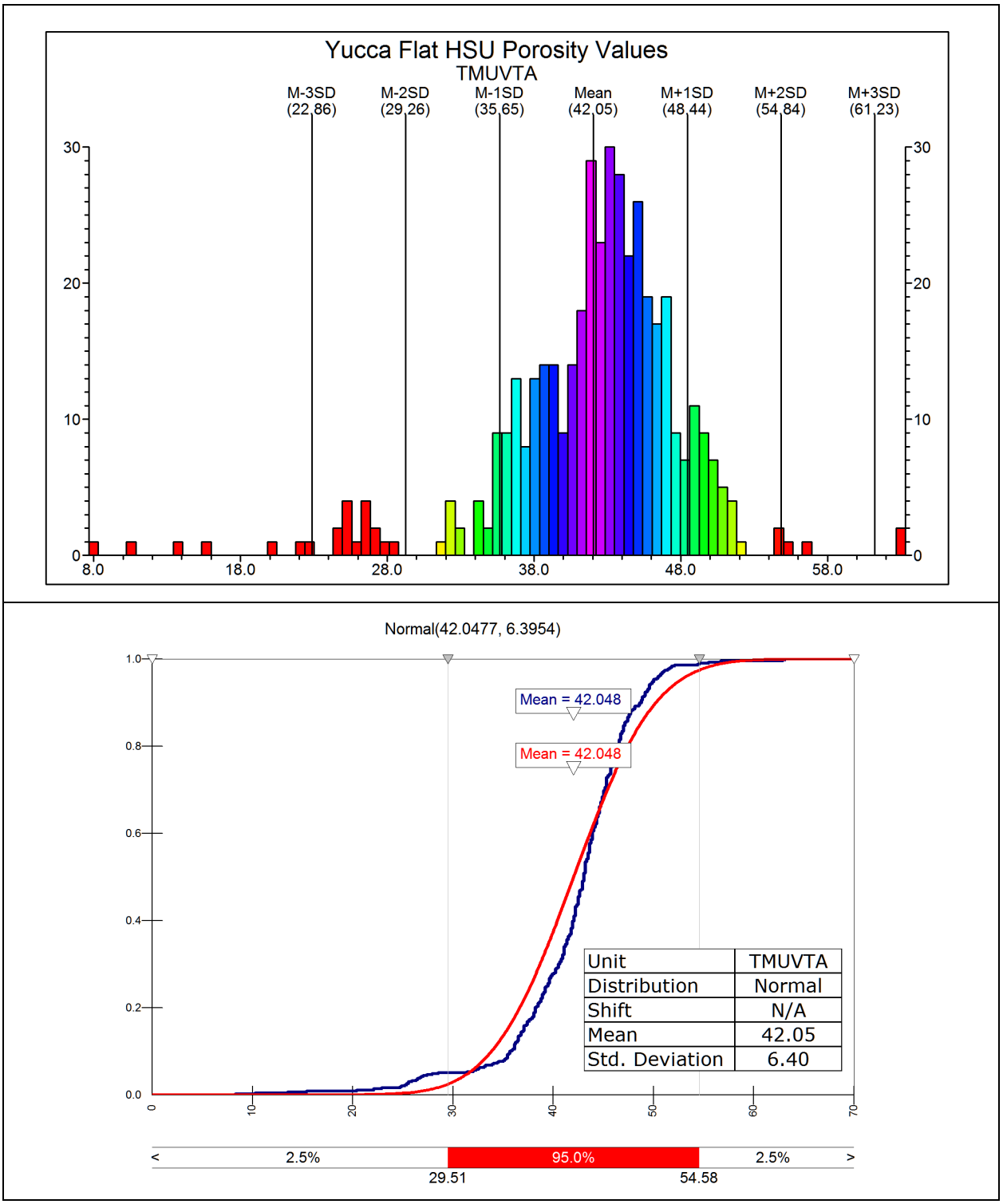

Figure 7-20
TM-UVTA HSU Matrix Porosity Histogram and CDF

Note: M + 2SD – Mean plus two standard deviations; Blue curve (darker line) and annotations – Sample data CDF; Red curve (lighter line) and annotations – Fitted PDF

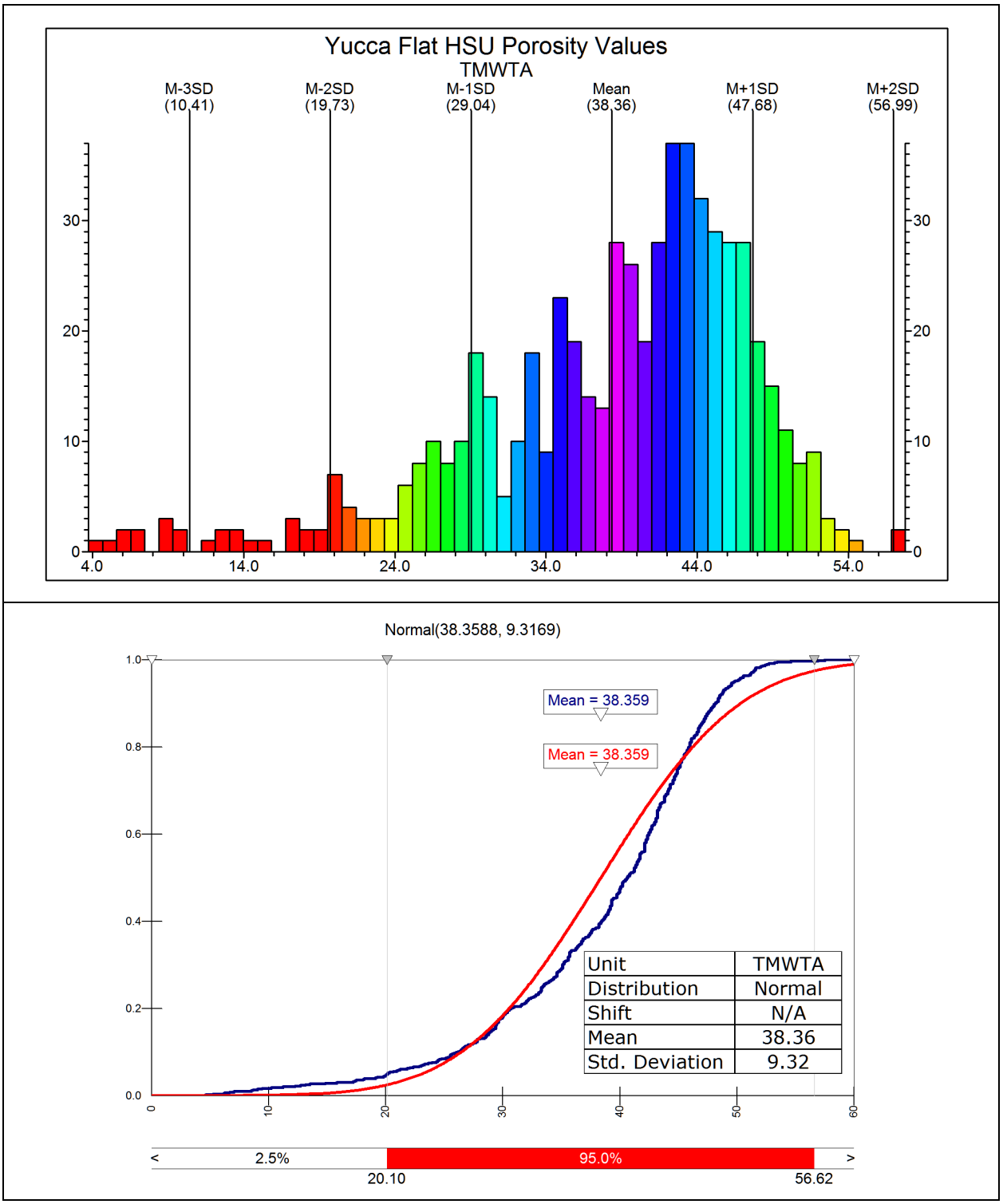

Figure 7-21
TM-WTA HSU Matrix Porosity Histogram and CDF

Note: M + 2SD – Mean plus two standard deviations; Blue curve (darker line) and annotations – Sample data CDF; Red curve (lighter line) and annotations – Fitted PDF

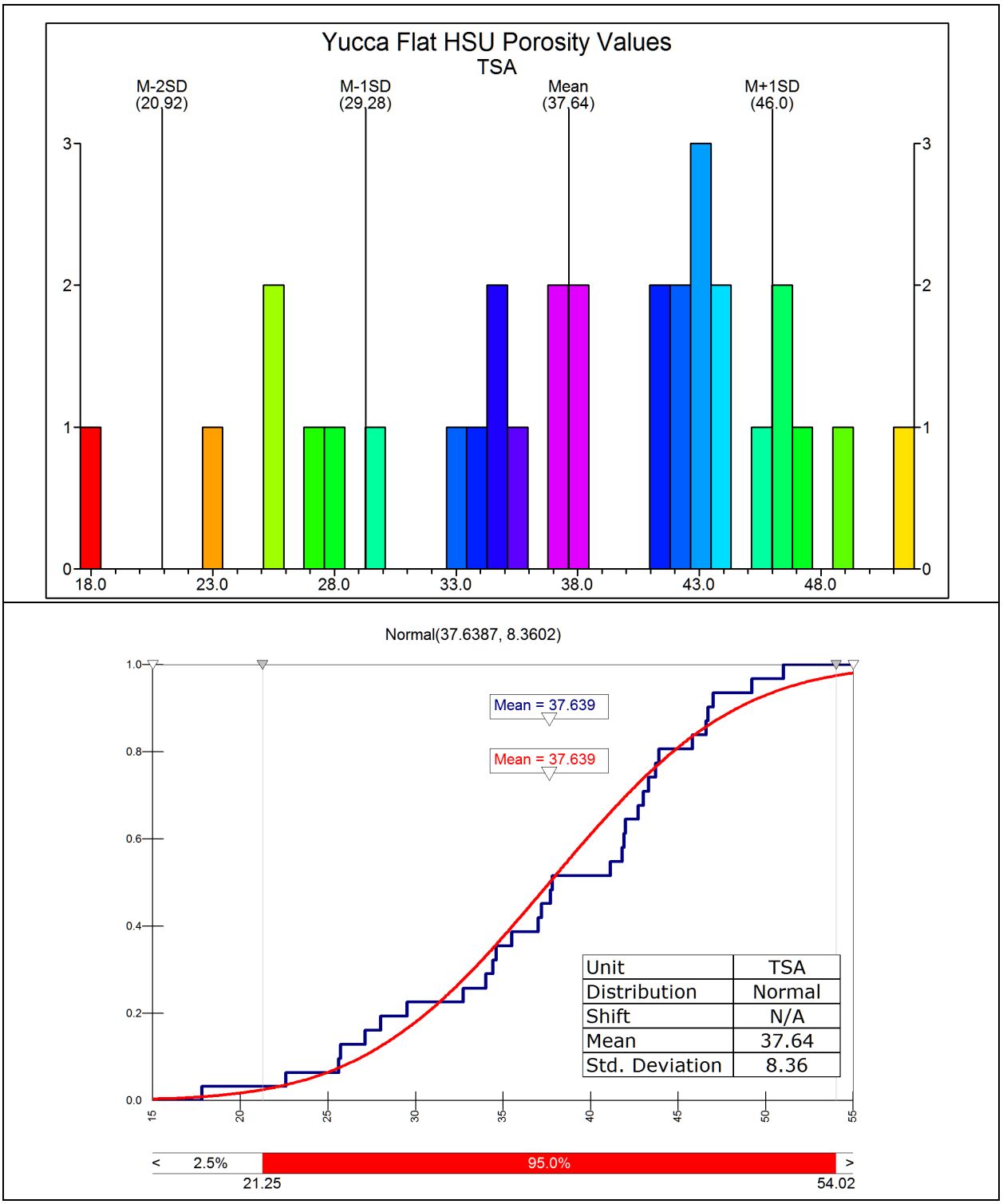

Figure 7-22
TSA HSU Matrix Porosity Histogram and CDF

Note: M + 2SD – Mean plus two standard deviations; Blue curve (darker line) and annotations – Sample data CDF; Red curve (lighter line) and annotations – Fitted PDF

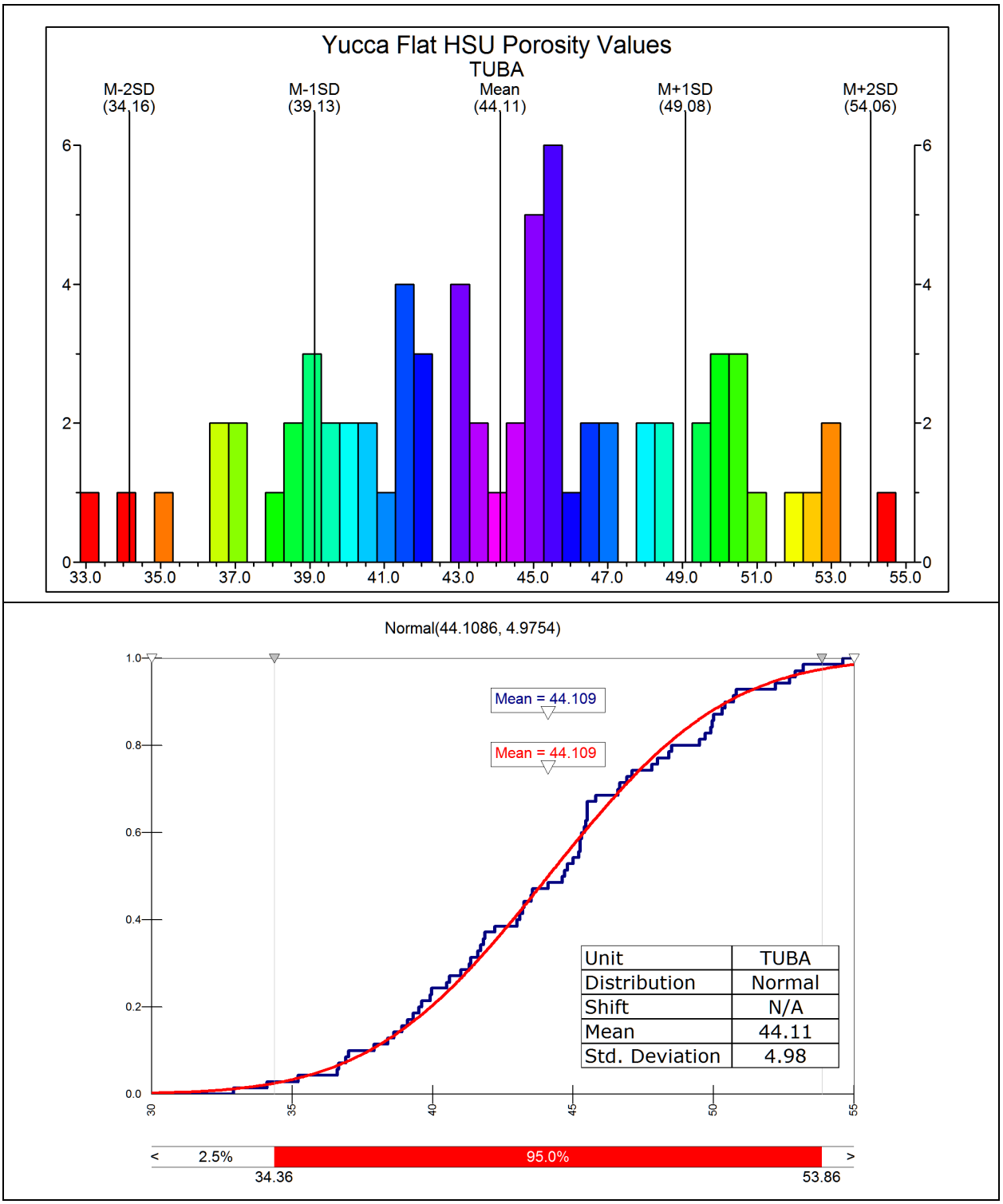

Figure 7-23
TUBA HSU Matrix Porosity Histogram and CDF

Note: M + 2SD – Mean plus two standard deviations; Blue curve (darker line) and annotations – Sample data CDF; Red curve (lighter line) and annotations – Fitted PDF

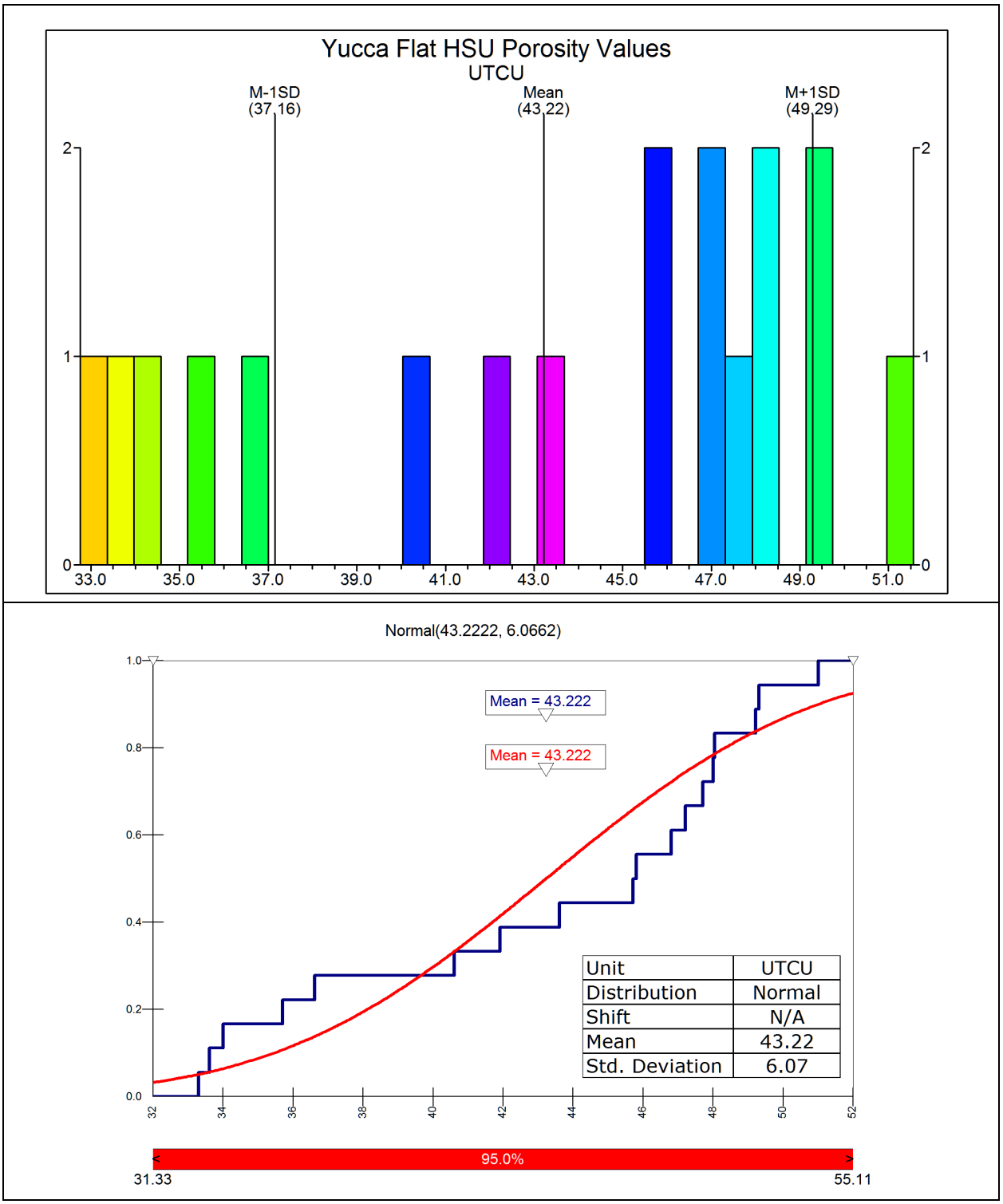

Figure 7-24
UTCU HSU Matrix Porosity Histogram and CDF

Note: M + 2SD – Mean plus two standard deviations; Blue curve (darker line) and annotations – Sample data CDF; Red curve (lighter line) and annotations – Fitted PDF

Table 7-4
Matrix Porosity Distribution Summary

HGU	Distribution	Shift	Mean	SD	A-D Test Value	A-D Rank	K-S Test Value	K-S Rank	Chi-Sq Test Value	Chi-Sq Rank
Hydrogeologic Units										
AA	Normal	N/A	34.45	6.65	+Infinity	10	0.03	6	137.70	4
WTA	Normal	N/A	38.91	9.09	13.65	2	0.11	2	136.40	2
VTA	Normal	N/A	43.00	7.32	14.44	2	0.05	2	154.70	2
TCU	Normal	N/A	39.75	5.87	9.11	2	0.04	2	136.60	2
GCU	Log Normal	-0.23	1.92	1.71	0.61	2	0.10	4	23.79	6
CCU	Normal	N/A	3.24	2.42	0.68	3	0.10	2	8.32	5
CA	Normal	N/A	2.64	1.63	1.03	7	0.18	8	8.82	7
Hydrostratigraphic Units										
AA	Normal	N/A	34.45	6.65	+Infinity	10	0.03	6	137.70	4
ATCU	Normal	N/A	33.83	10.70	0.26	3	0.09	3	4.29	2
LCA	Normal	N/A	2.64	1.63	1.03	7	0.18	8	8.82	7
LCCU	Log Normal	-1.11	3.33	3.04	0.70	6	0.15	9	5.94	6
LTCU	Log Normal	-749	40.36	5.52	2.55	3	0.03	5	74.40	1
MGCU	Log Normal	-0.22	1.92	1.71	0.71	2	0.12	4	23.79	6
OSBCU	Normal	N/A	38.07	6.19	6.48	3	0.07	3	106.20	3
TMLVTA	Normal	N/A	43.18	7.47	8.99	2	0.04	2	111.50	2
TMUVTA	Normal	N/A	42.05	6.40	10.36	3	0.12	3	88.07	3
TMWTA	Normal	N/A	38.36	9.32	11.53	3	0.11	3	119.70	3
TSA	Normal	N/A	37.64	8.36	0.51	4	0.14	4	5.19	3
TUBA	Normal	N/A	44.11	4.98	0.24	3	0.06	1	4.57	3
UTCU	Normal	N/A	43.22	6.07	0.90	3	0.21	4	2.00	4

N/A - Not applicable

8.0 EFFECTIVE POROSITY

This section presents the development of effective porosity estimates for the Yucca Flat/Climax Mine CAU groundwater flow and transport model. Porosity is defined as the total volume of voids per total volume of rock. In geologic material, not all voids transmit water. Therefore, the appropriate porosity for transport modeling is the effective porosity, which is defined as the volume of voids transmitting water (interconnected voids) per total volume of rock.

Effective porosity is always less than or equal to total porosity due to the adhesion of water to solids, unconnected pores, and dead-end pores. The difference between the total and effective porosity increases as the size of the grains in the rock decreases (de Marsily, 1986) and as the amount of cementation increases (Bradley, 1992). Thus, for small-grained, well-cemented sediments, the effective porosity could be significantly lower than the total porosity but for unconsolidated, large-grained sediments, the effective porosity could be about equal to the total porosity. De Marsily (1986), citing Castany (1967), presents a comparison of effective and total porosity as a function of grain size. That comparison shows an effective to total porosity ratio ranging from about 0.5 for fine-grained clay (grain size of 0.0003 millimeter [mm]) to 0.9 for fine gravel (grain size of 30 mm). Using a radial diffusion method on core samples, van der Kamp et al. (1996) found a ratio of effective to total porosity of 0.43 to 1 for a low-permeability aquitard. In a controlled experiment using clean, coarse silica sand, van der Kamp et al. (1996) found that the effective porosity was close to the total porosity. Hudak (1994) measured effective and total porosity on unconsolidated sand samples and found that the two closely match. In summary, the effective porosity for systems that behave as a porous media can be estimated as 50 to 100 percent of the total porosity depending on the characteristics of the media (e.g., grain size, consolidated or unconsolidated).

An issue that should be evaluated from a feasibility standpoint during regional transport model implementation is the conceptualization adopted for the solute transport simulations. Typically, flow through the matrix is ignored, and all flow is assumed to be in the fractures (with diffusive interaction with the matrix) when modeling a double-porosity transport system. However, as fracture spacing

becomes large and/or the aperture size becomes very small (and/or fracture continuity becomes limited), the assumption of flow in fractures only may become invalid and a greater proportion of the solutes will be transported in the matrix system.

Van Golf-Racht (1982) provides a comprehensive presentation of the origin of fractures, fracture detection and evaluation, case studies, and flow to wells in fractured formations. Van Golf-Racht (1982) presents ranges of fracture porosities: macrofracture network (10^{-4} to 5×10^{-3}), isolated fissures or microfractures (10^{-5} to 10^{-4}), and fissure network (10^{-4} to 2×10^{-2}). He states that macrofractures are extended fractures with wider openings that develop through various geologic layers and fissures, and microfractures are fractures with narrower openings and limited extent. Freeze and Cherry (1979) report similar effective fracture porosities for fractured rock. They report that typical values range from 10^{-5} to 10^{-2}. The fracture opening or aperture is dependent on depth, pressure, lithologic-petrographic characteristics of the rock, structural unit thickness, nature of *in situ* stresses, and geologic history of the formation. Van Golf-Racht (1982) presents a frequency plot of fracture opening data and a fitted curve. The asymmetrical curve through the data has a rising limb starting at about 4 microns, peaks at about 23 microns with a frequency of about 30 percent, and ends at about 150 microns with a frequency of about 3 percent.

Effective or fracture porosity estimates determined for fractured geologic systems must have magnitudes consistent with the conceptualization of the site-specific fractured system. For example, there are cases with reported porosities that have large magnitudes beyond that expected for fractured systems and are also inconsistent with the interpreted hydraulic properties for the site. These reported porosities are uncertain and are not considered representative. The problem with using these questionable values is further amplified in cases where the parameter distribution for effective porosity is sampled in conjunction with fracture spacing distribution and may yield extremely unrealistic fracture apertures. In the evaluations presented in this section, there has been an attempt to eliminate the more uncertain reported fracture porosities.

Several field methods are available for determining the porosity of a geologic material. These include, but are not limited to:

- Determined through interpretations of field tracer tests
- Calculated from borehole fracture data
- Calculated from density and moisture content measurements with geophysical logs

Some of these methods, however, typically determine the matrix or fracture porosity but not the effective porosity. The method that yields the best estimate of the effective porosity is through interpretation of field tracer tests. Unfortunately, it is impractical to perform tracer tests in all geologic materials of interest at all locations of interest. Therefore, the available information on effective porosity is limited and is often assumed to be equivalent to the matrix or fracture porosity, which are more easily determined.

This section is divided into multiple subsections that discuss (1) the role of effective porosity in contaminant transport, (2) the procedures used to determine estimates of effective porosity, (3) the effective porosity estimates for each HGU, (4) the limitations in the estimated effective porosities, and (5) a summary of the effective porosity distribution recommended for each HGU.

8.1 The Role of Effective Porosity in Contaminant Transport

The nature of fluid flux through a porous system was first outlined by French engineer Henri Darcy in 1856. Darcy's law states that the volumetric discharge of a porous flow system is equal to the hydraulic conductivity of the media multiplied by the hydraulic gradient and the cross-sectional flow area. The law is described by the equation (Domenico and Schwartz, 1990):

$$q = \frac{Q}{A} = -Ki \qquad (8\text{-}1)$$

where:

q = specific discharge (L/t),
Q = volumetric flow rate (L^3/t),
A = cross-sectional area perpendicular to flow (L^2),
K = hydraulic conductivity (L/t), and
i = hydraulic gradient (dimensionless).

In Equation (8-1), the cross-sectional area is the entire surface area not the surface area of the pore openings. Therefore, the specific discharge in Darcy's law must be divided by the effective porosity in order to obtain the actual groundwater velocity. The interstitial groundwater velocity is given by the equation (Domenico and Schwartz, 1990):

$$v = \frac{q}{\phi_e} = \frac{Q}{\phi_e A} = -\frac{K}{\phi_e} i \qquad (8\text{-}2)$$

where:

v = interstitial groundwater velocity (L/t), and
ϕ_e = effective porosity (dimensionless)

The interstitial velocity is always larger than the specific discharge and decreases with increasing effective porosity. The groundwater velocity, and thus velocity of contaminant migration, in a porous media is governed by Equation (8-2). Therefore, knowledge of the effective porosity of a porous media is essential for contaminant transport modeling.

8.2 Data Compilation and Data Transfer

Data from the Yucca Flat/Climax Mine HFM area and data from other NTS CAUs and YMP were used for this analysis due to the unavailability of comprehensive data from the Yucca Flat/Climax Mine HFM area for all HGUs. Figure 8-1 shows the source locations for the data used in the analysis. Individual discussions of the applicability of the transferred data are provided for each HGU. The data were used to determine a distribution appropriate for the Yucca Flat/Climax Mine CAU based on professional judgment. A quantitative assessment of the sensitivity of transport modeling to the uncertainty in this parameter cannot be provided before the transport model development. The parameter description discusses the importance of this parameter.

8.3 Data Evaluation Procedures

The hydrogeologic framework for Yucca Flat and vicinity uses two classification systems for the geologic material (BN, 2006). The first is HGUs, which categorize lithologic types by their ability to transmit water. The second is HSUs, which are groupings of contiguous stratigraphic units that have a particular hydrogeologic character, such as an aquifer or confining unit. A detailed description of the HGUs and HSUs in the Yucca Flat/Climax Mine CAU is provided in Section 4.0.

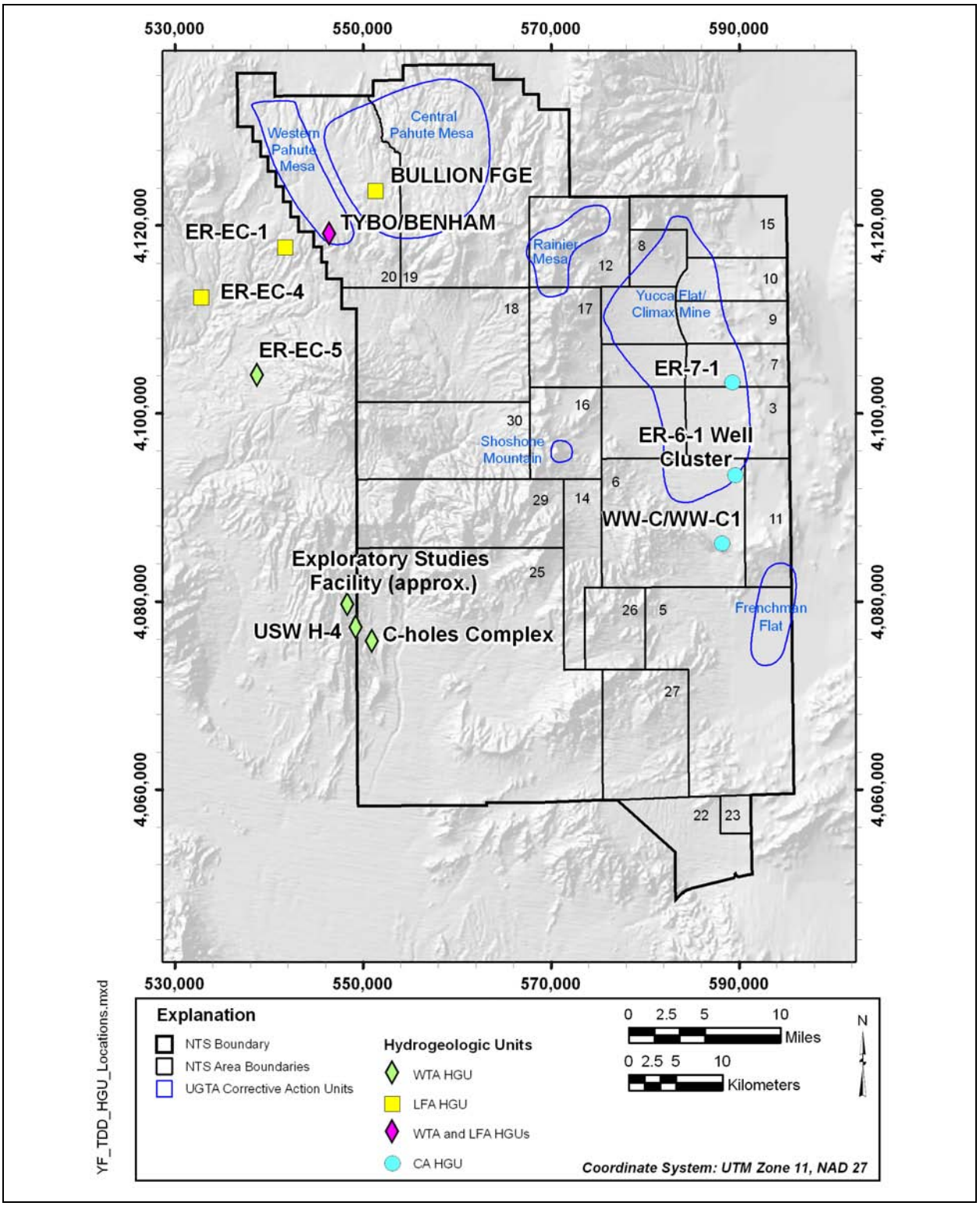

Figure 8-1
Spatial Distribution of Effective Porosity Data

The effective porosities for Yucca Flat were evaluated by HGU. The HGUs classified as aquifers are discussed first, followed by the HGUs classified as confining units. The first step in investigating the effective porosity for an HGU was assessing whether it behaves as porous media or fractured media. If it behaves as porous media, the effective porosity for the HGU was assumed to be represented by a fraction of the matrix porosity discussed in Section 7.0. The value of the fraction varied depending on the type of sediments, grain size, and cementation or welding. If it behaves as fractured media, fracture porosities from available sources were compiled and evaluated, and a distribution was developed. For fractured media, the effective porosity was assumed to be the same as the fracture porosity.

To assign an effective porosity to an HGU, the quality and suitability of the data sources for the unit must be evaluated. Where multiple data sources exist for a given HGU, they must be compared and condensed to define an estimate and account for uncertainty. Each measurement and analysis method is discussed, and an estimate is recommended based on their associated strengths and weaknesses.

8.4 Data Documentation Qualification

Data documentation provides information on the traceability (or pedigree) of the data. Typically, data collected in recent years have better documentation than that collected and reported years ago. Qualification of the data documentation provides a mechanism for investigating and evaluating the quality of the data used in modeling. The data used to develop recommended ranges of the effective porosity for the Yucca Flat/Climax Mine CAU have been assigned a DDE_F value to indicate the level of documentation available for the data (see Section 3.3.1 for discussion of DDE_F values). It is important to note that the data documentation qualification does not indicate the usefulness of the data for modeling. Historical data, which may be poorly documented by current standards, are often of high quality and extremely useful in the CAU investigations.

8.5 Effective Porosity for the Aquifer Hydrogeologic Units

The hydrostratigraphic model of Yucca Flat comprises five HGUs (AA, WTA, VTA, LFA, and CA) classified as aquifers.

8.5.1 The Alluvial Aquifer Hydrogeologic Unit

The AA consists of unconsolidated to partially consolidated sandy gravel and gravelly sand. The source of these sediments is erosion of the surrounding mountains during basin development. Interspersed within these coarser-grained alluvial deposits are finer-grained eolian sands. The AA HSU corresponds to the AA HGU in Yucca Flat. Although the AA HGU is thick and extends over much of the Yucca Flat basin, significant sections of it are saturated only in the central portion of the basin (BN, 2006).

This loosely consolidated aquifer is not fractured; therefore, flow through it is diffuse and the effective porosity is assumed to be a fraction of the matrix porosity. The recommended matrix porosity distribution for the AA HGU is discussed in Section 7.0. Based on the loosely consolidated sediments making up this HGU, it is estimated that the effective porosity ranges from 80 to 100 percent of the matrix porosity. Therefore, the recommended distribution for the effective porosity is 80 to 100 percent of the recommended matrix porosity distribution.

8.5.2 The Welded-Tuff Aquifer Hydrogeologic Unit

The WTA consists of ash-flow tuffs welded to varying degrees. The initial primary components of the ash-flow tuffs are glass shards and pumice fragments. After emplacement, devitrification of the glass and pumice commonly occurs. The material in these tuffs is not sorted and does not show signs of bedding. The thickness of ash-flow tuffs can range from tens to hundreds of meters (Winograd, 1971).

Welding of the ash-flow tuffs occurs after emplacement and involves bonding of the hot glass shards and pumice. The degree of welding is affected by the temperature, the amount and composition of volatiles, the composition of the ash, the lithostatic load, the rate of cooling, and the rate of crystallization (Winograd, 1971). Within a single ash flow, welding is variable. In general, welding is most dense near the middle of the ash flow and decreases both above and below. As described in Winograd (1971), “the zone of dense welding is commonly underlain and overlain by zones of partial welding that, in turn, are sandwiched between zones of no welding.” Ash flows can occur as a single emplacement, multiple flows that are emplaced in rapid succession and cool as a single unit, and multiple flows that are emplaced such that they cool separately. For the first two occurrences

(referred to as a simple cooling unit), a single zone of densely welded tuff is typical. For the latter occurrence (referred to as a compound cooling unit), multiple zones of dense welding may be present.

The degree of welding of the ash-flow tuffs is a primary factor controlling its porosity and permeability. Welding bonds the glass and pumice fragments together and causes them to flatten and become subparallel, which results in a decrease in the interstitial (matrix) porosity and permeability. Therefore, the interstitial porosity and permeability decrease as the degree of welding increases. Winograd (1971) reports that densely welded tuff may have an interstitial porosity less than 5 percent, and nonwelded tuff may have an interstitial porosity greater than 50 percent.

Columnar fractures caused by tensional forces active during cooling characterize the zones of dense and partial welding in the ash-flow tuffs. The spacing of these fractures ranges from a few tenths of an inch to several feet (Winograd, 1971). The smallest spacings are usually associated with the most densely welded zones. These cooling fractures are uncommon in nonwelded tuff.

Regional stresses may induce secondary fracturing in ash-flow tuffs. Although densely welded tuffs have very low interstitial porosity and permeability, they can transmit groundwater due to the presence of fractures. Because the degree of fracturing and its continuity is variable due to the variable degrees of welding, the hydraulic conductivity of these tuffs is also variable.

The WTA HGU is characterized by aquifers consisting predominately of welded tuffs. In Yucca Flat, the WTA HGU is defined by four HSUs (TM-WTA, TSA, BRA, and TUBA). The TM-WTA is located east of the faults that form the Yucca Flat basin and is saturated only in the deeper portions of the basin. Up to 20 percent vitric-tuff aquifer may by contained in the TM-WTA. At some locations, intervening nonwelded tuff and bedded tuff are incorporated into the TM-WTA. Wells completed in the TM-WTA generally have high production as observed in well ER-5-3 in Frenchman Flat and wells WW-4 and WW-4a in CP basin. Bechtel Nevada (2006) states that this HSU “is a fracture-controlled aquifer.”

The TSA HSU, which is composed of welded ash-flow tuff, is located only in the extreme southern portion of Yucca Flat. This HSU is saturated, typically well fractured, and typically highly transmissive. Although this ash-flow tuff is generally welded, up to 15 percent may consist of nonwelded portions overlying and underlying the welded portion. The BRA HSU is composed of

peralkaline, welded ash-flow tuff; is located in the Belted Range just north of Yucca Flat; and is typically unsaturated in the Yucca Flat/Climax Mine CAU model area. The welded portion of the Tub Spring tuff makes up the TUBA HSU. This HSU is found only in the northern portion of Yucca Flat, is saturated only in the deeper portions of West Emigrant Valley, and is typically fractured and has high productivity.

The WTA HGU will be conceptualized as a double-porosity medium in the Yucca Flat/Climax Mine CAU flow and transport model due to its fractured nature. A double-porosity conceptualization consists of fractures and matrix. Advective and diffusive flow and transport are assumed to occur exclusively in the fractures. Interaction between the fractures and matrix is restricted to molecular diffusion from the fractures to the matrix and vice versa. It is generally assumed that no advective flow or transport occurs in the matrix. In order to appropriately represent the WTA HGU in the CAU-scale model, the recommended distribution for the effective porosity must be consistent with this conceptualization. Data sources relevant for estimating the effective porosity of the WTA HGU are described below.

8.5.2.1 Groundwater Tracer Tests

Cross-hole, forced-gradient tracer tests were conducted at the C-holes Complex in fractured volcanic tuffs for the YMP (Bechtel SAIC, 2004c). The fractured volcanic tuffs tested with these tracer tests are assumed to be representative of the WTA HGU. The C-holes Complex consists of three wells (UE-25 c#1, UE-25 c#2, and UE-25 c#3) located about 2 km southeast of the footprint of the potential repository (Figure 8-1). Tracers were injected into two horizons. The upper horizon consisted of the lower Prow Pass Tuff, and the lower horizon consisted of the lower Bullfrog Tuff.

Bechtel SAIC (2004c) states that the completion interval in both the Prow Pass Tuff and the Bullfrog Tuff consists of variably welded tuffaceous rocks. The tuff at the completion in the Prow Pass Tuff is described as partially welded and partially to moderately welded. The tuff at the completion in the Bullfrog Tuff is described as partially welded, partially to moderately welded, and moderately to densely welded.

Tracer Test in the Bullfrog Tuff

Two tracer tests were conducted in the Bullfrog Tuff at the C-holes Complex. The first was a pilot test with injection into wells c#1 and c#2 and pumping of well c#3. The purpose of the pilot test was to determine the fastest flow path at the complex. The test results indicate that the most rapid transport occurs between wells c#2 and c#3. That path was then used for a subsequent multi-tracer test involving the injection of two conservative tracers (pentafluorobenzoic acid [PFBA] and Br), one reactive tracer (lithium [Li]), and one microsphere tracer.

For the multi-tracer test, tracer was injected over a period of 10 hours into well c#2, and well c#3 was pumped at a rate of about 9.5 liters per second (L/s). About 3.3 percent of the fluid pumped from well c#3 was recirculated into tracer-injection well c#2. This recirculation was initiated about 36 hours before tracer injection and continued for 40 days after injection. The volume of the tracer solution injected into well c#2 was about 2.8 times larger than the packed-off injection interval volume. The thickness of the Bullfrog Tuff interval tested was about 100 m. At the depth of the completion intervals, the distance between the wells is about 30 m.

The breakthrough curves observed in the pumping well show a bimodal behavior for all tracers (Bechtel SAIC, 2004c). The first peak occurred at about 31 hours for PFBA, Br, and Li, and at about 23 hours for the microspheres. The arrival time for the second peak varied from about 210 hours to more than 1,000 hours and was different for each of the tracers. The magnitude of the second peak for Li was very small. The tracer responses in the Bullfrog Tuff are consistent with double-porosity transport behavior. This is evidenced by the different first peak concentrations for the conservative tracers consistent with their different molecular diffusion coefficients.

Bechtel SAIC (2004c) attributes the bimodal behavior of the breakthrough curves to tracer transport through two different flow paths within the tested interval. An open-hole flow survey of the Bullfrog Tuff interval in injection well c#2 indicates that the majority of flow (about 75 percent) enters the formation near the top (Bechtel SAIC, 2004c). The tracer-injection solution was about 2 percent more dense than the groundwater. Bechtel SAIC (2004c) speculate that some of the tracer entered the formation near the top of the interval but that most of the tracer solution sank rapidly to the bottom of the interval, due to its higher density, and then entered the formation.

Due to the quick arrival and higher normalized concentrations of the first peaks, those peaks are assumed to be representative of fracture flow through the moderately to densely welded tuffs in the upper portion of the interval. The long time of arrival and lower normalized concentrations of the second peaks is assumed to be the result of transport through fractures and matrix in the partially welded tuff at the bottom of the interval. This conclusion assumes that the densely welded tuff is more fractured than the partially welded tuff. This assumption is consistent with the known characteristics of welded tuffs.

The semi-analytical, dual-porosity transport model Reactive Transport LaPlace Inversion code (RELAP) was used to analyze the results from the tracer test conducted in the Bullfrog Tuff (Bechtel SAIC, 2004c). In order to account for the two peaks observed in the breakthrough curves, each of the first peaks were fit first, the response for the first peak was subtracted from the entire curve, and then each of the second peaks were fitted (Bechtel SAIC, 2004c). The fitting parameters were the mean fluid residence times, the Peclet number (equal to the distance between the injection and withdrawal wells divided by the longitudinal dispersivity), the tracer mass fraction participating in the test, and the mass transfer coefficient for matrix diffusion (equal to the matrix porosity divided by the fracture half aperture times the square root of the matrix diffusion coefficient). The breakthrough curves for PFBA and Br, which have different molecular diffusion coefficients, were analyzed simultaneously. The breakthrough curves were interpreted assuming both radial and linear flow.

Effective porosity was calculated using the equation of Welty and Gelhar (1989), which assumes plug flow in a cylindrical homogeneous isotropic volume of the tested stratigraphic interval centered on the production well with outer radius equivalent to the distance to the tracer-addition well:

$$t = \frac{\phi \pi b R^2}{Q} \quad \Rightarrow \quad \phi = \frac{Qt}{\pi b R^2} \qquad (8\text{-}3)$$

where:

t = travel time (t),
ϕ = effective porosity (fraction),
b = interval thickness or length (L),
R = distance between tracer-injection and withdrawal wells (L), and
Q = production rate (L^3/t).

Travel time, *t*, in Equation (8-3) for convergent-flow tracer tests, is defined in two different ways in the literature. Some researchers define it as the time of arrival of the peak tracer concentration at the pumped well (e.g., Halevy and Nir, 1962; Welty and Gelhar, 1989; Jones et al., 1992; IT, 1998, Section 5.1). Other researchers (e.g., Lenda and Zuber 1970; Zuber, 1974) define *t* in Equation (8-3) as the mean transit time found principally through simultaneous fitting of mean transit time and a dispersion parameter. Similar to Lenda and Zuber (1970) and Zuber (1974), the documents by IT (1998, Section 5.2), Reimus and Haga (1999), and Reimus (2003) define *t* as the mean fluid residence time and perform a least squared fit of the simulated to observed breakthrough curves by simultaneously fitting mean fluid residence time, mass injected, Peclet number, and mass transfer coefficient (function of matrix porosity, fracture half aperture, and matrix diffusion coefficient for double-porosity cases). Either approach (peak-concentration arrival time or mean residence time) has been shown in the literature to be suitable for calibration of the breakthrough curves from convergent-flow tracer tests.

The tracer breakthrough at the pumping well will be dominated by the most transmissive interconnected zone(s) between the tracer-injection well and the pumping well. The effective thickness of the test interval should be incorporated in the choice of interval thickness, *b*, in Equation (8-3). The rate of transport between the wells is dependent on the variability (in three dimensions) of both hydraulic conductivity and effective porosity. One may expect that the difference between the time of arrival of the peak concentration and the mean residence time may increase with increasing heterogeneity. The effective porosities calculated using Equation (8-3) and the time of arrival of the peak tracer concentration tend to be smaller than those calculated using the fitted mean transit or mean residence time. Also, the dispersivities determined using the fitting approach with mean transit or mean residence time are typically much greater than those determined using the time of arrival of peak concentration. In some cases, the interpreted dispersivities can be extremely large (indicating an overwhelmingly dispersion-dominated transport system) and inconsistent with dispersivity values generally reported in the literature for similar scales. For this reason, this report favors the use of effective porosities calculated using travel time equal to the time of arrival of the peak concentration.

The effect of recirculated flow (3.3 percent of the pumped flow for the tracer test in the Bullfrog Tuff) is assumed to have a negligible effect on the calculation of effective porosity using Equation (8-3).

Bechtel SAIC (2004c) calculated effective porosities with Equation (8-3) using the mean residence times from RELAP fits to both the first and second peaks. They report a minimum effective porosity of 3×10^{-3} using the shortest residence time (radial fit to first peaks) and a maximum effective porosity of 3.1×10^{-2} using the longest residence time (linear fit to second peaks). These calculations assumed that 75 percent of the production flow was associated with the flowpaths that resulted in the first peaks and 25 percent was associated with the flowpaths that resulted in the second peaks based on flow survey results (Bechtel SAIC, 2004c). The mean residence times determined with RELAP were 36 and 30 hours for assumptions of linear and radial flow, respectively. For comparison, these times are similar to the peak-concentration arrival times for the two conservative tracers (about 30 and 31 hours) and the reactive tracer (about 32 hours). Because the first peaks are assumed to represent the effects of fracture flow through the densely welded tuff at the top of the injection interval, these values were used in developing the effective porosity distribution for the WTA HGU.

The maximum effective porosity reported by Bechtel SAIC (2004c) based on fitting to the second peaks is on the order of 3 percent. This value was not considered when developing the effective porosity distribution for the WTA HGU at Yucca Flat because it (1) is likely not representative of purely fracture flow; (2) the conceptualization for the WTA HGU for the CAU-scale transport model is that of a double-porosity medium with advective flow and transport through the fractures only; and (3) the interpreted value is affected by the likely heterogeneous, nonradial character of flow through the fractured tuffs (principal fracture strikes at the C-holes Complex are approximately perpendicular to the direct path between tracer-injection and pumping wells). Examples of simulations of the effect of heterogeneity and fracture orientations on interpreted effective porosity are presented in Reimus (2003).

Fracture porosity can also be calculated using Equation (8-3) and the peak-concentration arrival time. Equation (8-3) assumes a homogeneous, isotropic volume and plug flow. In application, the total fracture volume is treated as homogeneous and isotropic, with no flow in the matrix. While actual field conditions, whether in fractured or porous media, are generally more complex, initial estimates of fracture porosity using this equation have been demonstrated to be consistent with final calibrated values from calibration of numeric transport models to field tracer tests (Jones et al., 1992). This time is considered to be representative of the time for tracer to travel through the fractures from the tracer-injection well to the pumping well. Because the mean residence times determined by Bechtel

SAIC (2004c) are relatively similar to the peak-concentration arrival times (see above), fracture porosity was not calculated using the peak-concentration arrival times.

Tracer Tests in the Prow Pass Tuff

Two phases of tracer testing were conducted in the Prow Pass Tuff at the C-holes Complex. The first phase (the conservative tracer test) consisted of the injection of two conservative tracers (trifluorobenzoic acid [TFBA] and iodide [I]). The second phase (the reactive tracer test) consisted of the injection of three conservative tracers (PFBA, Br, and Cl), one sorbing tracer (Li), and three microsphere tracers. The testing procedure for the two phases was similar. Well c#3 was the tracer-injection well, and well c#2 was the pumping well. The pumping rate during the tests was 0.33 L/s. Of the 0.33 L/s of fluid pumped from c#2, 0.095 L/s (about 29 percent) was recirculated into injection well c#3. The time to flush the tracer from the injection well was about 8.5 hours for the conservative tracer test. Wells c#2 and c#3 are located 29 m apart at the depth of the completion interval. The tracer responses for both phases of testing in the Prow Pass Tuff are consistent with double-porosity transport behavior. This is evidenced by the different peak concentrations for the conservative tracers consistent with their different molecular diffusion coefficients.

The fracture porosity for the portion of the Prow Pass Tuff tested during the conservative and reactive tracer tests can also be estimated from the arrival time of the peak concentration of the conservative tracers in both tests. For a recirculating tracer test, the plug flow travel time is defined as (Gelhar, 1982):

$$t = \frac{2\phi\pi b R^2}{Q} F \qquad (8\text{-}4)$$

where F is a nonlinear expression that varies from one half for a test with no recirculation to one sixth for a test with 100 percent recirculation. For no recirculation, Equation (8-4) is identical to Equation (8-3). The values of F at various recirculation percentages are illustrated in Figure 8-2 (calculated using Equation E21 from Gelhar [1982]). For the 29 percent recirculation in the Prow Pass Tuff tracer tests, F is equal to 0.277 and Equation (8-4) becomes:

$$t = \frac{\phi\pi b R^2}{1.81Q} \quad \Rightarrow \quad \phi = \frac{1.81Qt}{\pi b R^2} \qquad (8\text{-}5)$$

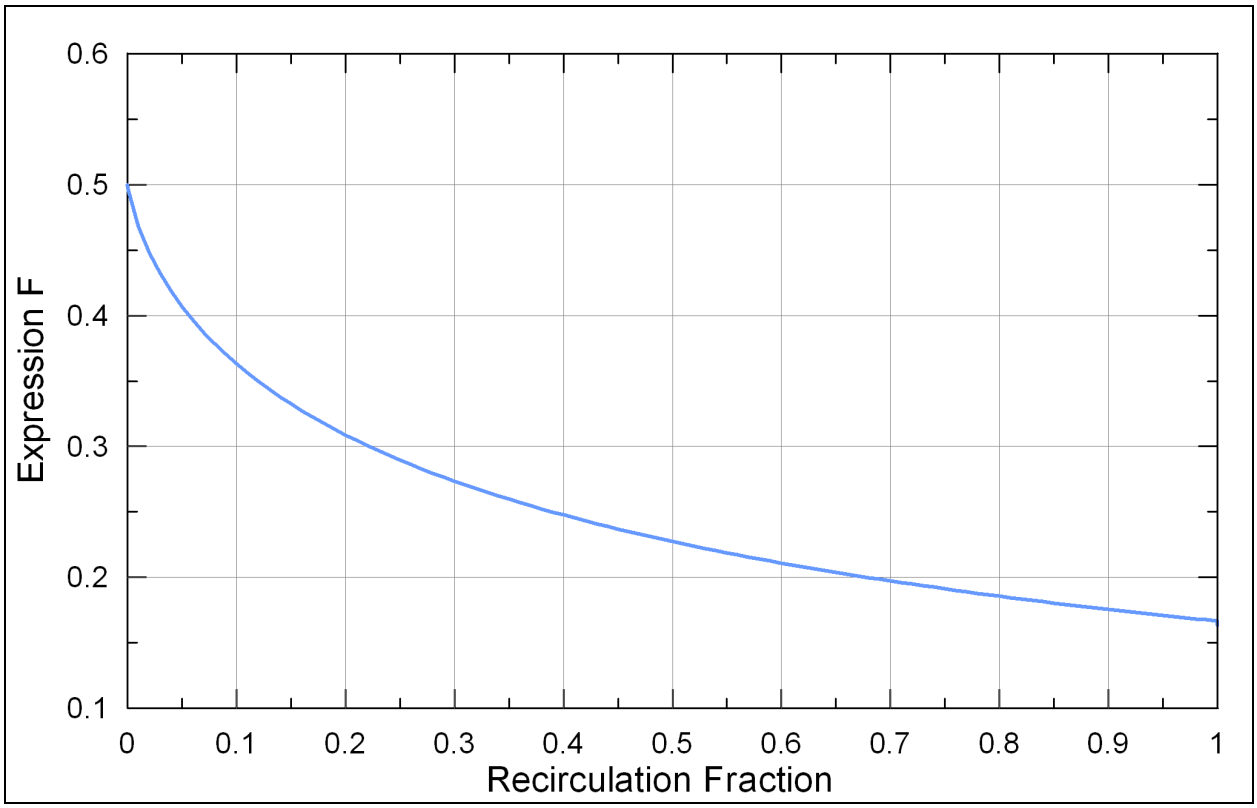

Figure 8-2
Function for Recirculating Tracer Tests

The peak tracer concentrations arrived at about 7 days in the conservative tracer test and at about 10.4 days in the reactive tracer test. Recall that the pumping rate for both tests was 0.33 L/s, and the distance between wells at the location of the Prow Pass is about 29 m. The interval thickness used in the calculations was taken as the distance from the top of the uppermost packer in the two wells to the bottom of the lowermost packer in the two wells. This thickness was about 74 m for the conservative tracer test and about 80 m for the reactive tracer test. Fracture porosities were also calculated using the thickness of the transmissive zone in well c#3 (33.8 m) as reported in Geldon et al. (1998). Using Equation (8-5), the calculated fracture porosities are 1.8×10^{-3} for the conservative tracer test and 2.4×10^{-3} for the reactive tracer test using the full thickness, and 4.0×10^{-3} for the conservative tracer test and 5.8×10^{-3} for the reactive tracer test using the thickness of the transmissive zone.

Bechtel SAIC (2004c) analyzed the results of the conservative tracer test using the single-porosity Moench (1989) solution to the advection-dispersion equation assuming both purely convergent flow and partial recirculation. Their interpretation for the purely convergent flow field assumed two

values for the mixing length, which is the length within the boreholes through which tracer enters or exits the aquifer. These two values were 30.5 m and 0.3 m. All of their interpretations assumed an aquifer thickness of 61 m. The flow porosities determined assuming a purely convergent flow field and a single-porosity conceptualization were 7×10^{-4} and 1.6×10^{-3} for mixing lengths of 30.5 and 0.3 m, respectively. Their analysis using the Moench (1989) single-porosity solution and incorporating a partially recirculating flow field yielded a flow porosity of 4.5×10^{-4}. The range in flow porosity due to uncertainties in the method used to incorporate recirculation was 2×10^{-4} to 5×10^{-4}. Although Bechtel SAIC (2004c) interpreted the conservative tracer test using a double-porosity conceptualization and partial recirculation, that interpretation used the same fracture porosity as determined for the single-porosity conceptualization. The effective porosities determined using the Moench (1989) single-porosity solution were not used in developing the effective porosity distribution for the WTA HGU at Yucca Flat. The single-porosity conceptualization used in the analysis is inconsistent with the double-porosity conceptualization of the WTA HGU selected for the CAU-scale model.

Bechtel SAIC (2004c) analyzed the results of the reactive tracer test using the semi-analytical, dual-porosity transport model RELAP. Their analysis included the recirculation and simultaneously fit responses for tracers with different molecular diffusion coefficients. The parameters adjusted in RELAP to obtain fits to the observed breakthrough curves were the mean residence time, the Peclet number, the fraction of injected mass participating in the test, and the matrix diffusion mass transfer parameter. The RELAP analyses were conducted assuming both linear and radial flow. The breakthrough curves for PFBA and Br were analyzed simultaneously, and the curves for PFBA and Cl were analyzed simultaneously. The flow porosity interpreted from the tracer test was calculated by using the mean residence time yielded by RELAP and the equation for plug flow (Equation [8-3]). The flow porosities calculated by Bechtel SAIC (2004c) range from 3×10^{-3} to 6×10^{-3} for mean residence times of 610 and 1,210 hours (25.4 and 50.4 days), respectively.

The effective porosities determined from tracer testing at the C-holes Complex by all methods are summarized in Table 8-1. The porosities considered as representative range from 1.8×10^{-3} to 6×10^{-3}.

Table 8-1
Effective Porosities Determined from Tracer Testing at the C-holes Complex

Method	Effective Thickness (m)	Travel Time (hours)	Fracture Porosity (fraction)
Bullfrog Tuff			
Mean residence time from RELAP fit to first peak - radial flow (Bechtel SAIC, 2004c)	100	30	3×10^{-3}
Mean residence time from RELAP fit to second peak - linear flow (Bechtel SAIC, 2004c)	100	1,020	$3 \times 10^{--2}$
Prow Pass Tuff			
CTT - Peak-concentration arrival time and Equation (8-5)	74	168	1.8×10^{-3}
CTT - Peak-concentration arrival time and Equation (8-5)	33.8	168	4.0×10^{-3}
RTT - Peak-concentration arrival time Equation (8-5)	80	250	2.4×10^{-3}
RTT - Peak-concentration arrival time Equation (8-5)	33.8	250	5.8×10^{-3}
RTT - Moench single-porosity solution - no recirculation - 30.5 m mixing length (Bechtel SAIC, 2004c)	61	N/A	7×10^{-4}
RTT - Moench single-porosity solution - no recirculation - 0.3 m mixing length (Bechtel SAIC, 2004c)	61	N/A	1.6×10^{-3}
RTT - Moench single-porosity solution - partial recirculation - 30.5 m mixing length (Bechtel SAIC, 2004c)	61	N/A	4.5×10^{-4}
RTT - Moench single-porosity solution - investigation of uncertainty (Bechtel SAIC, 2004c)	61	N/A	2×10^{-4} to 5×10^{-4}
RTT - Minimum mean residence time from RELAP fit PFBA and Br - radial flow (Bechtel SAIC, 2004c)	80	1,210	6×10^{-3}
RTT - Maximum residence time from RELAP fit to PFBA and Br - linear flow (Bechtel SAIC, 2004c)	80	610	3×10^{-3}

Note: Shaded values were not used in developing the effective porosity distribution for the WTA HGU (see discussion in text).

CTT - Conservative tracer test
N/A - Not applicable
RTT - Reactive tracer test

8.5.2.2 Gas Tracer Tests

Freifeld (2001) discusses fracture porosities estimated from air-permeability tests and gas tracer tests conducted in the unsaturated portion of the Topopah Spring welded-tuff aquifer in the Exploratory Studies Facility (ESF) at the Yucca Mountain site. Estimation of fracture porosity from the air-permeability tests used the air-injection pressure transients for tests conducted in four boreholes

drilled from a drift in the ESF. Freifeld (2001) first developed a transient flow model that incorporated the geometry of the borehole and the injection flowrate of the testing gas. He then performed inverse modeling of the measured pressure and flowrate data using iTOUGH2. The purpose of this inversion was to develop a best estimate of both porosity and permeability as a function of distance from the injection borehole to an outer-boundary condition. A range for the radius of the assumed outer boundary was determined using cross-hole pressure data. Using that range, the porosity was estimated. Error bounds were placed on the porosity based on the uncertainty in the radius of the outer boundary.

Matrix diffusion was not included in the iTOUGH simulations. As a result, the estimated fracture porosities are considered to be upper bounding estimates (Freifeld, 2001). Pressure responses at nearby boreholes were reviewed in order to identify a distance at which no discernible pressure response was observed based on injection into the test borehole. Table 8-2 summarizes the fracture porosities estimated using this method, which are 0.01 ± 0.003 for one borehole and 0.001 ± 0.0001 for the other borehole. Freifeld (2001) states that the pore space measured with the air-injection tests will be that for all connected fractures, including dead-end fractures that do not participate in advective transport. As a result, the fracture porosities estimated using the results of this test are likely overestimates. Therefore, these porosities were not used in developing the effective porosity for the WTA HGU.

Freifeld (2001) also estimated fracture porosity from the results of two gas tracer tests conducted in the unsaturated portion of the Topopah Spring welded-tuff aquifer in the ESF at the Yucca Mountain site. These tests consisted of injecting sulfur hexafluoride (SF6) gas into one borehole and withdrawing it from another borehole. For both tests, the flow rate for tracer injection was much smaller than the flow rate for withdrawal. For one test, the ratio of withdrawal flow rate to injection flow rate was 10:1, and for the other test, ratios of both 10:1 and 30:1 were used. The injection and withdrawal boreholes for both tests were the same, with each test conducted in a different packed off zone. The distance between the boreholes was 7.93 m for one zone and 9.12 m for the other zone.

Fracture porosities were estimated by two methods using breakthrough curves from the gas tracer tests (Freifeld, 2001). The first method involved estimating the fracture porosity assuming plug flow and using Equation (8-3). The travel time entered into the equation was the average travel time for

Table 8-2
Effective Porosities from Welded-Tuff Air-Permeability and Gas Tracer Tests (after Freifeld, 2001)

Borehole(s)	Withdrawal Rate to Injection Rate Ratio	Estimated Fracture Porosity (fraction)
58-3	N/A	$1 \times 10^{-2} \pm 3 \times 10^{-3}$ [a]
74-2	N/A	$1 \times 10^{-3} \pm 1 \times 10^{-4}$ [a]
76-2 to 75-2	10:1	1×10^{-2} [b]
76-2 to 75-2	30:1	6×10^{-3} [b]
76-4 to 75-4	10:1	9×10^{-3} [b]
76-2 to 75-2	10:1	2×10^{-3} [c]
76-2 to 75-2	30:1	4×10^{-3} [c]
76-4 to 75-4	10:1	3×10^{-3} [c]

Note: Shaded values were not used in developing the effective porosity distribution for the WTA HGU (see discussion in text).
[a] Estimated from air-injection pressure transients resulting from air-permeability testing.
[b] Estimated from gas tracer tests using the plug flow method.
[c] Estimated from gas tracer tests using random-walk particle method simulations.

N/A - Not applicable

the tracer calculated as the integrated time weighted cumulative mass recovery divided by the integrated actual mass recovery (Freifeld, 2001). This method to calculate the average travel time was used to account for the fact that tracer recovery is frequently less than 100 percent. The calculated fracture porosities ranged from 6×10^{-3} to 1×10^{-2} (Table 8-2). Freifeld (2001) states that these porosities should be taken as an upper bound because they were determined neglecting retardation of tracer arrival due to diffusion and dispersion. Therefore, these estimates may not be representative in developing the effective porosity distribution for the WTA HGU.

The gas tracer tests were also analyzed using a random-walk particle method incorporating Fickian transport. The tests were analyzed in two dimensions and included the effect of dispersion and diffusion. The results of the random-walk particle method simulations were matched to the observed breakthrough curves using fracture porosity and dispersivity as fitting parameters. The best-fit fracture porosities ranged from 2×10^{-3} to 4×10^{-3}. Freifeld (2001) places a high degree of confidence in the fracture porosities determined using this method based on the results of an uncertainty analysis. An advantage of the gas tracer tests over the air-permeability tests is that the tracer tests involve only fractures that are hydraulically connected between the injection and withdrawal boreholes. The

fracture porosities determined from the interpreting gas tracer tests using the random-walk particle method are considered to be representative of fracture porosities in the WTA HGU and were, therefore, used in developing the effective porosity distribution.

8.5.2.3 Infiltration Tests

An infiltration test was conducted at the Yucca Mountain site in Alcove 1 near the North Portal of the ESF (Liu et al., 2003; CRWMS M&O, 2004). The predominant lithology tested was welded tuff of the Tiva Canyon Tuff. This tuff is assumed to be representative of the WTA HGU. Alcove 1 is located about 30 m bgs. The infiltration test consisted of applying water at the ground surface and collecting water that seeped into the alcove. Two phases of infiltration were performed with the infiltration rate for the first phase higher than that for the second phase. Bromide tracer was added to the infiltrating water during the late portion of the second phase. A numerical model was used to calibrate to the seepage data collected in Alcove 1 during the infiltration test. The model was calibrated to both phases by adjusting the hydraulic rock-properties fracture porosity, vertical fracture and matrix permeabilities, horizontal fracture and matrix permeabilities, the van Genuchten parameter, α, and a factor describing the reduction in interface area between the fractures and matrix. The calibrated fracture porosity was 2.8×10^{-2} for the first phase and 3×10^{-2} for the second phase (Liu et al., 2003; CRWMS M&O, 2004). These porosities were not used in developing the distribution for the effective porosity of the WTA HGU for two reasons. First, this test was conducted in near-surface (ground-surface to alcove-depth) rocks that are likely to be more fractured and exhibit a larger fracture porosity than the buried welded-tuff aquifers in Yucca Flat. Second, many of the properties of the tested rock were unknown, resulting in a large number of fitting parameters, which results in large uncertainty in the calibrated parameters.

8.5.2.4 Seepage Tests

Seepage tests were conducted in the fractured middle nonlithophysal zone of the unsaturated Topopah Spring welded tuff at Niches 2, 3, and 4 in the ESF at the Yucca Mountain site (Bechtel SAIC, 2004a). This tuff is assumed to be representative of the WTA HGU. Water was pumped into three boreholes above each niche. Different tests were conducted using different test intervals within the boreholes. The distance from the borehole test intervals to the top of the niches ranged from 0.58 to 1.23 m. The general purpose of the tests was to evaluate how much water seeps into the drift from a

localized water source of known intensity and duration. A liquid-return, or overflow, line was used in each of the test intervals. The rate of liquid release from the test intervals to the formation was calculated as the injection flow rate into the borehole minus the return flow rate. Water that migrated from the boreholes to the niches was captured and weighed. The seepage tests at Niche 2 were of short duration and the seepage tests at Niches 3 and 4 were of long duration.

Seepage data from the Niche 2 and 4 tests were used to estimate the change in volumetric water content (Bechtel SAIC, 2004a). The saturated fracture volumetric water content, which is defined as the volume of water in the fractures divided by the bulk volume of the fractured material, was assumed to provide an approximation of the fracture porosity, which is defined as the fracture volume divided by the total volume, under saturated conditions. Bechtel SAIC (2004a) used the wetting-front arrival times from the seepage tests to indirectly determine the average volumetric water contents using the relationship:

$$z_p = \frac{q_s t}{\left(\theta_{ave} - \theta_n\right)} \qquad (8\text{-}6)$$

where:

z_p = depth from the water source to the leading edge of the wetting front (L),
q_s = flow rate of water supplied at the source (L/t),
t = arrival time of the front at depth z_p (t),
θ_{ave} = average water content, and
θ_n = initial or antecedent or residual water content.

The change in volumetric water content change (i.e., the change in θ_{ave} - θ_n) was calculated for zones where three or more seepage tests were conducted. This change becomes the average volumetric water content assuming θ_n is negligible compared to θ_{ave}. This average volumetric water content approximates the fracture porosity. The average volumetric water contents, or fracture porosities, calculated by Bechtel SAIC (2004a) range from 9×10^{-4} to 5.03×10^{-2}, and average 1.2×10^{-2} for 20 tests at Niche 2 and 11 tests at Niche 4. These fracture porosities are not considered to be representative for estimating the effective porosity distribution for the WTA HGU at Yucca Flat. The seepage tests were conducted in fractured tuff likely to have been altered due to construction of the niches and boreholes, resulting in estimates that are large compared to zones of undisturbed fracture tuff.

8.5.2.5 Calculations of Fracture Porosity from Fracture and Producing Zone Data in Test Well USW H-4

Erickson and Waddell (1985) calculated the fracture porosity for fractured volcanic tuffs in test well USW H-4 located near the western boundary of the NTS (Figure 8-1). This tuff is assumed to be representative of the WTA HGU. In their calculation, they assumed that each production zone in the well, as determined by a temperature log, was due to a single fracture. These fractures were assumed to all have the same aperture and permeability. They divided the estimated transmissivity for the well by the number of producing zones and then used the cubic law for flow between parallel plates to calculate the equivalent fracture aperture. They then determined a correction factor to account for error in the sampling frequency due to the high dip angle of the fractures relative to the borehole. The inverses of the cosines of the dip angle for the fractures determined from the acoustic-televiewer log were summed and then divided by the total number of fractures. This calculation yielded a correction factor of 5.17, which was multiplied by the number of producing zones to estimate the number of fractures that would have been intersected by the borehole if all of the fractures had been oriented perpendicular to the borehole. The fracture porosity was then calculated as the equivalent aperture of the fractures times the corrected number of fractures divided by the length of the production zone in the borehole.

The cubic law assumes flow between two smooth plates. Erickson and Waddell (1985) used an empirical roughness coefficient to account for changes in flow rate through fractures due to deviation from smooth plates. They arbitrarily selected roughness factors of 1.0 (corresponding to smooth plates), 0.1, and 0.01. For each roughness factor, they calculated the fracture porosity for the estimated minimum and maximum transmissivity for the test well. Table 8-3 summarizes the fracture porosities calculated by Erickson and Waddell (1985) for test well USW H-4. The calculated values range from 1.1×10^{-4} to 8.4×10^{-4}. They state that the effective porosity for the tuffs at the location of this test well is the same or less than their calculated fracture porosities. These fracture porosity estimates are relatively uncertain as a result of all of the assumptions used in their determination as discussed above.

Table 8-3
Estimate of Fracture Porosity of the Tuffs Penetrated by Test Well USW H-4 (from Erickson and Waddell, 1985)

Roughness Coefficient	Assumed Transmissivity (ft^2/d)	
	2,152	8,500
	Fracture Porosity (fraction)	
1.0 (smooth plate)	1.1×10^{-4}	1.8×10^{-4}
0.1	2.5×10^{-4}	3.9×10^{-4}
0.01	5.3×10^{-4}	8.4×10^{-4}

ft^2/d - Square feet per day

8.5.2.6 Hydraulic Conductivity and Fracture Spacing Calculations

Rehfeldt et al. (2003) calculated fracture porosities for the volcanic rocks at the NTS based on interpreted hydraulic conductivities derived from pumping tests and fracture spacings determined from borehole logs and core surveys. The fracture porosity was calculated using an equation that combines the cubic law, Darcy's law, and the definition of fracture porosity. The cubic law describing the volumetric flow rate in the direction of flow between parallel, smooth plates is given by Domenico and Schwartz (1990) as:

$$Q = \frac{\rho_w g b^2}{12\mu}(bw)\frac{\partial h}{\partial L} \qquad (8\text{-}7)$$

where:

Q = volumetric flow rate (L^3/t),
ρ_w = density of water (M/L^3),
g = gravitational acceleration (L/t^2)
b = fracture aperture (L),
μ = viscosity of water (M/Lt),
w = fracture width perpendicular to the flow direction (L), and
$\frac{\partial h}{\partial L}$ = hydraulic gradient (L/L).

Darcy's law, which calculates the water discharge or flow rate through a porous medium in the direction of flow, is given by Domenico and Schwartz (1990) as:

$$Q = KA\frac{\partial h}{\partial L} \tag{8-8}$$

where:
K = hydraulic conductivity (L/t), and
A = discharge area perpendicular to the flow direction (L^2).

The fracture porosity is defined as:

$$\phi_e = \phi_f = \frac{v_f}{v_t} \tag{8-9}$$

where:
ϕ_e = effective porosity (dimensionless),
ϕ_f = fracture porosity (dimensionless),
v_f = fracture volume (L^3), and
v_t = total volume (L^3).

Development of the equation to calculate fracture porosity requires the assumption of the equivalent porous media model. This assumption is necessary to assign an estimation of hydraulic conductivity to an interval containing fractures within a geologic media. With some algebraic manipulation, the equivalent porous media model shows that the product of the fracture spacing (e) and fracture width perpendicular to the flow direction (w) can be substituted for discharge area (A) in Equation (8-8); and the fracture aperture (b) can be substituted for the fracture volume (v_f), and the fracture spacing (e) can be substituted for the total volume (v_t) in Equation (8-9). After making these substitutions, Equations (8-7) and (8-8) are solved for the volumetric flow rate (Q) and then set equal to solve for the fracture aperture (b). The solution for the fracture aperture (b) is then substituted into Equation (8-9) to yield the following equation for calculation of the effective porosity (SNJV, 2005b):

$$\phi_e = \left(\frac{12K\mu}{\rho_w g}\right)^{1/3} e^{-2/3} \tag{8-10}$$

where *e* is the fracture spacing. The two independent variables in Equation (8-10) are the fracture spacing and the hydraulic conductivity.

Rehfeldt et al. (2003) used hydraulic conductivities derived from pumping tests, and fracture spacings derived from borehole logs and core surveys. Of these two variables, fracture spacing is the most uncertain and has the largest effect on the calculated effective porosity. The estimates of fracture spacing used for these calculations are uncertain and probably biased low because the surveys count fractures that are open at the borehole, and these fractures may have limited lateral extent or have been infilled before drilling but opened up as a consequence of drilling and well development operations. The calculations by Rehfeldt et al. (2003) used a water density of 998.2 kilograms per cubic meter, a water viscosity of 1.002 grams per meter per second, and an acceleration of gravity of 9.80665 meters per square second. The water density and viscosity values correspond to water at a temperature of 20 °C.

The frequency of fractures determined by the borehole image logs is biased due to a vertical borehole intersecting non-horizontal fractures. Therefore, the fracture spacing observed in the borehole is not the same as the true fracture spacing, which is defined as the distance between two parallel fractures measured perpendicular to the fracture plane (Rehfeldt et al., 2003). Rehfeldt et al. (2003) calculated a correction to account for the difference between the observed and true fracture spacing. They first grouped the observed fractures according to their dip angle. They considered three groups: fractures with a dip angle between 0 and 30 degrees, those with a dip angle between 30 and 60 degrees, and those with a dip angle between 60 and 90 degrees. For each of these groups, they calculated the observed fracture frequency as the number of fractures in the group divided by the total length of the interval of interest and they calculated the average dip angle. The corrected fracture frequency was calculated as (Rehfeldt et al., 2003):

$$N_c = \frac{N_r}{cos(f)} \qquad (8\text{-}11)$$

where:

N_c = corrected fracture frequency (L^{-1}),
N_r = observed fracture frequency (L^{-1}), and
f = average fracture dip angle (degrees).

A corrected fracture frequency was calculated for each of the three groups. The total corrected fracture frequency was calculated as the sum of the corrected fracture frequency of each group. The

total corrected fracture spacing, S_f, was calculated as the inverse of the total corrected fracture frequency:

$$S_f = \frac{1}{N_c} \tag{8-12}$$

The total corrected fracture spacing was then used in Equation (8-10) to calculate the fracture porosity.

Using this method, Rehfeldt et al. (2003) reported calculated fracture porosities for four boreholes completed to the WTA HGU: ER-18-2, ER-EC-5, ER-EC-8, and UE-18r. Fracture porosity calculations for these boreholes were repeated, where meaningful, using available underlying borehole logging and testing information. Additional data for these wells are provided in SNJV (2004b).

ER-18-2

The following completion information for well ER-18-2 was taken from BN (2003). Well ER-18-2 consists of uncemented casing from depths of 408.1 to 653.2 m. The casing is slotted in three about 9-m-long intervals between the depths of 588.4 to 640.3 m. The total length of the slotted intervals is 51.9 m. Below this casing, the well is completed open hole from a depth of 653.2 m to total depth at 762.0 m. The length of the portion of the formation not isolated from the borehole, that is the length adjacent to either uncemented casing or open hole, is about 353.9 m (from total depth at 762.0 m to depth of bottom of cemented casing at 408.1 m). Information on the portion of the formation producing fluid is not available for ER-18-2 because flow logging was not conducted in this well (IT, 2002a). Although estimates of transmissivity are available for ER-18-2 (IT, 2002a), the appropriate thickness for calculation of hydraulic conductivity for use in Equation (8-10) is unknown. Therefore, porosity values were not calculated for ER-18-2.

ER-EC-5

IT (2002d) reports hydraulic conductivities for eight of the nine screened intervals in well ER-EC-5 determined from analysis of flow logging data. The flow rate was too low in one of the screened intervals to determine a hydraulic conductivity. The screens are configured into three groups consisting of three screens each. A filter pack is adjacent to each group. The filter packs are

separated by cement plugs. The length of the filter packs is longer than that of the screened intervals. This leads to some uncertainty in the appropriate thickness to use in calculating hydraulic conductivity from interpreted transmissivity values. IT (2002d) calculated hydraulic conductivities using both the length of the screen interval and the length of the filter pack to obtain maximum and minimum values, respectively. They calculated a hydraulic conductivity for each logging run using three interpretation methods. In determining the hydraulic conductivity for use in calculating the fracture porosity, all hydraulic conductivities reported by IT (2002d) assuming the screen length were averaged to get a maximum value and all of the hydraulic conductivities assuming the filter pack length were averaged to get a minimum value.

Fracture density and dip data are available for well ER-EC-5 in IT (2001) based on interpretation of ultrasonic borehole imager and micro-resistivity electronic scanner logs. Fracturing in the borehole at the location of the upper filter pack/screen group is not available because the portion of the image log across this interval was of poor quality and was not analyzed (IT, 2001). Therefore, fracture porosities could not be calculated for the upper three screen intervals. IT (2001) identified fractures as either conductive or resistive. A fracture was identified as conductive if it was a dark feature and if its topography produced by low acoustic response was negative. A fracture was identified as resistive if it was a white feature and had a positive topography. A total of 35 conductive fractures were observed in ER-EC-5 across the logged thickness of 188.7 m (IT, 2001). Twenty-five of the fractures dipped at an angle between 0 and 30 degrees, and 10 dipped at an angle between 30 and 60 degrees. Assuming the average dip angle is the average of the dip for each group (e.g., average dip angle is 15 degrees for fractures with a dip angle between 0 and 30 degrees), the fracture spacing calculated using Equations (8-11) and (8-12) is 4.7 m. This spacing is an average spacing across the entire logged interval having good image quality. The fracture density plot in IT (2001) indicates that the density of fractures is higher across screen intervals 4 through 6 than across intervals 7 through 9. This difference could not be incorporated into the calculation of fracture spacing, however, because individual fracture locations and dips are not reported in IT (2001). The calculated spacing of 4.7 m is about twice that used by Rehfeldt et al. (2003). The difference between the two spacings could not be reconciled because the specific fracture data used by Rehfeldt et al. (2003) was not available. The calculated fracture porosities for well ER-EC-5, which are summarized in Table 8-4, range from 1.3×10^{-4} to 3.7×10^{-4}.

Table 8-4
Fracture Porosities Calculated for the Welded-Tuff Aquifers from Hydraulic Conductivity and Fracture Spacing Using Equation (8-10)

Well	Interval Name	Hydraulic Conductivity (m/s)		Fracture Spacing (m)	Calculated Fracture Porosity (fraction)		HGU
		Minimum	Maximum		Minimum	Maximum	
ER-18-2	Value not calculated due to large uncertainty in effective interval thickness						WTA
ER-EC-5	Screen Interval 1	4.24×10^{-5}	6.93×10^{-5}	NA [a]	N/A	N/A	WTA
ER-EC-5	Screen Interval 2	4.35×10^{-5}	1.23×10^{-4}	NA [a]	N/A	N/A	WTA
ER-EC-5	Screen Interval 3	NC [b]	NC [b]	NA [a]	N/A	N/A	WTA
ER-EC-5	Screen Interval 4	1.58×10^{-4}	3.37×10^{-4}	4.7	2.1×10^{-4}	2.7×10^{-4}	WTA
ER-EC-5	Screen Interval 5	3.18×10^{-4}	8.85×10^{-4}	4.7	2.6×10^{-4}	3.7×10^{-4}	WTA
ER-EC-5	Screen Interval 6	1.05×10^{-4}	4.22×10^{-4}	4.7	1.8×10^{-4}	2.9×10^{-4}	WTA
ER-EC-5	Screen Interval 7	4.92×10^{-5}	1.42×10^{-4}	4.7	1.4×10^{-4}	2.0×10^{-4}	WTA
ER-EC-5	Screen Interval 8	5.48×10^{-5}	1.52×10^{-4}	4.7	1.4×10^{-4}	2.0×10^{-4}	WTA
ER-EC-5	Screen Interval 9	4.09×10^{-5}	1.82×10^{-4}	4.7	1.3×10^{-4}	2.2×10^{-4}	WTA
ER-EC-8	Values not calculated due to borehole characteristics inconsistent with WTA HGU conceptualization						WTA
UE-18-r	Completion interval	3.22×10^{-6}		0.76	1.9×10^{-4}		WTA

Note: Shaded value was not used in developing the effective porosity distribution for the WTA HGU (see discussion in text).
[a] Not available due to poor image log quality (IT, 2001).
[b] Not calculated due to low flow rate (IT, 2002d).

m/s - Meters per second
N/A - Not applicable

ER-EC-8

IT (2002g) reports hydraulic conductivities for 6 of the 10 screened intervals in well ER-EC-8 determined from analysis of flow logging data. Two of the screens are completed across partially

welded tuff, one is completed across moderately welded tuff, and seven are completed across the tuff confining unit. Interpretation of flow logging results yields higher hydraulic conductivities for the tuff confining unit than for the partially and moderately welded tuff (IT, 2002g). Fracture density and dip data are available for well ER-EC-8 in IT (2001) based on interpretation of ultrasonic borehole imager logs. They report no fractures in the partially welded tuff and only a few fractures in the moderately welded tuff. The lack of fracturing and low hydraulic conductivities, relative to the tuff confining unit, for the welded tuff at this borehole is inconsistent with the conceptualization of the WTA HGU as a transmissive, fractured unit. Therefore, fracture porosities were not calculated from the hydraulic conductivity and fracture spacing for this well.

UE-18r

Blankennagel and Weir (1973) report a transmissivity for well UE-18r of 23,000 gallons per day per foot (gpd/ft), which converts to 3.31 x 10^{-3} square meters per second (m^2/s). The length from the top of the uppermost screen in this well to the bottom of the lowermost screen is 1,028.7 m. For this length, the calculated hydraulic conductivity is 3.22 x 10^{-6} m/s. Well UE-18r is completed across welded-tuff and lava-flow aquifers. Analysis of 35.7 m of core from this well yielded 42 fractures, 26 percent of which were high-dip open fractures (60 to 90 degrees) and 7 percent of which were medium-dip open fractures (30 to 60 degrees) (Drellack et al., 1997). All other fractures were identified as closed and were not used in the calculation of fracture spacing. The fracture spacing calculated using Equations (8-11) and (8-12) for open fractures is 0.76 m. This spacing is highly uncertain as representative of the tested formation interval because it is based on only 35.7 m of core, but the completion interval is 1,028.7 m thick. The fracture porosity calculated from the fracture spacing and hydraulic conductivity is 1.9 x 10^{-4}. This porosity is highly uncertain because of the uncertainty in the fracture spacing. Therefore, this fracture porosity was not used in developing the effective porosity distribution for the WTA HGU at Yucca Flat.

8.5.2.7 Fracture Aperture, Density, Orientation, and Percent Open Area Calculations

Regional groundwater flow and ^3H transport models used to evaluate migration from the underground testing areas of the NTS are presented in DOE/NV (1997a). They compiled existing and new hydrogeologic data for a large portion of southern Nevada and California, including the NTS. Using the fracture aperture, density, orientation, and percent open area data from seven wells in Pahute Mesa, they calculated fracture porosities for the welded-tuff aquifer ranging from 6.1 x 10^{-6} to

2.3×10^{-4} (Table 8-5). Using these data, DOE/NV (1997a) selected a range of 2×10^{-6} to 5×10^{-4} for the effective porosity of fractured volcanic rock for their modeling of ^{3}H transport at the NTS. The specific data and method used by DOE/NV (1997a) to calculate these fracture porosities were not reported. Therefore, these values are considered to be uncertain and were not used in developing the effective porosity distribution for the WTA HGU at Yucca Flat.

Table 8-5
Calculated Fracture Porosities for the Welded-Tuff Aquifer (after DOE/NV, 1997a)

Unit	Description	Calculated Fracture Porosity Range (fraction)
Timber Mountain Aquifer (TMA)	Uppermost welded tuffs	2.2×10^{-5} to 2.1×10^{-4}
Belted Range Aquifer (TBA)	Welded tuffs above the basal confining unit	1.2×10^{-5} to 4.4×10^{-5}
Basal Aquifer (BAQ)	Welded tuffs	6.1×10^{-6} to 2.3×10^{-4}

Note: Shaded values were not used in developing the effective porosity distribution for the WTA HGU (see discussion in text).

8.5.2.8 Literature Review of Basin and Range Province Rocks

Bedinger et al. (1989) developed distributions for hydraulic properties of rocks in the Basin and Range Province in the southwestern United States. They conducted a literature review of hydraulic conductivity and effective porosity for rocks in the Basin and Range Province and for rocks of similar types in other areas. The collected data were then synthesized, and the mean and 16.5 and 93.5 percentiles were determined for each rock type. Table 8-6 summarizes their findings of effective porosity for welded tuff. Because the degree to which the characteristics of the rocks found in the review by Bedinger et al. (1989) match the characteristics of the WTA HGU at Yucca Flat is unknown, these effective porosities were not used in developing the effective porosity distribution for the WTA HGU at Yucca Flat.

8.5.2.9 Values Used in Previous NTS Modeling Studies

Wolfsberg et al. (2002) simulated the migration of radionuclides from the BENHAM and TYBO underground nuclear tests at Pahute Mesa in response to the observation of radionuclides in groundwater wells ER-20-5#1 and ER-20-5#3 located downgradient of the cavities. These wells are located about 1.3 km and 300 m from the BENHAM and TYBO cavities, respectively. The working

Table 8-6
Effective Porosity Estimates for Welded Tuff in the Basin and Range Province (after Bedinger et al., 1989)

Rock Type	Description	Effective Porosity (fraction)		
		16.5 Percentile	Mean	83.5 Percentile
Tuff	Welded and fractured	2×10^{-2}	3×10^{-2}	4×10^{-2}
	Welded and moderately fractured to dense	4×10^{-4}	1×10^{-3}	3×10^{-3}

Note: Shaded values were not used in developing the effective porosity distribution for the WTA HGU (see discussion in text).

point of BENHAM and the sampling location in a lava formation of well ER-20-5#3 are at about the same elevation. Well ER-20-5#1 samples a welded-tuff aquifer that is just above the working point of TYBO and more than 500 m above the working point of BENHAM. Wolfsberg et al. (2002) used a reactive, dual-porosity transport model to simulate contaminant migration from BENHAM to the observations wells and the NTS boundary in a 3-D, heterogeneous flow field. For these simulations, they calculated low and high fracture porosity estimates for the welded-tuff aquifer and then calculated a base case value as the log average of the high and low values. The low and high values were calculated using fracture spacing and fracture aperture data from Drellack et al. (1997) assuming a parallel-plate model. The low value was determined assuming a single set of parallel fractures, and the high value was determined assuming three orthogonal fracture sets. Table 8-7 summarizes the fracture porosity values given in Wolfsberg et al. (2002). In their simulation of 30 equally likely realizations of the heterogeneous flow field using the base case parameter values, they found that one of the realizations generated transport results consistent with field observations. This supports that the base case fracture porosity determined by Wolfsberg et al. (2002) may be an appropriate effective porosity at larger scales. However, this interpreted value is uncertain because it represents just one realization that provided a match of simulated versus field transport results.

8.5.2.10 Recommended Ranges in Previous NTS Data Document Reports

Distributions and ranges of effective porosity for the WTA HGU for use in groundwater flow and contaminant transport models have been estimated and reported for Pahute Mesa (Rehfeldt et al., 2003) and Frenchman Flat (SNJV, 2005b). Rehfeldt et al. (2003) recommended a range from 1×10^{-5}

Table 8-7
Fracture Porosities Used by Wolfsberg et al. (2002) for the Welded-Tuff Aquifer

Value	Fracture Porosity (fraction)
Low Value	7.00×10^{-5}
Base Case Value	4.98×10^{-4}
High Value	3.54×10^{-3}

Note: Shaded values were not used in developing the effective porosity distribution for the WTA HGU.

to 0.1 for Pahute Mesa. The SNJV (2005b) report recommended a range of 1.4×10^{-5} to 5.2×10^{-4} for the CAU-scale modeling for Frenchman Flat. These ranges are superseded by the range developed from the more recent analyses presented above.

8.5.2.11 Summary and Recommended Distribution

The previous sections discussed fracture porosity data for the WTA HGU determined by several methods and used or recommended in previous NTS modeling studies. The values used in developing the distribution for the effective porosity must be consistent with the conceptual model that will be used for the WTA HGU in the CAU-scale flow and transport model. That conceptualization is one of a double-porosity system with advective flow and transport through fractures only and matrix participation only through molecular diffusion from and to the fractures. The fracture porosities considered to be consistent with this conceptualization are summarized in Table 8-8 and graphically illustrated in Figure 8-3.

The fracture porosities calculated from hydraulic conductivities and fractures spacings are consistently lower, by about one order of magnitude, than those calculated using peak-concentration arrival times from convergent-flow tracer tests. The cause of this discrepancy has been addressed by Tsang (1984 and 1992). This difference is a function of the portion of the aperture distribution within the fracture that participates during hydraulic and tracer tests. For hydraulic tests, the effective aperture will be most impacted by the smaller aperture regions because those are the areas that offer the most resistance to flow (Tsang, 1992). The influence of fracture roughness and contact area, resulting in tortuous flow and reduction in flow rate, is largest when there is a larger fraction of small

Table 8-8
Summary of Estimated Effective Porosity Ranges for the WTA HGU and Recommended Range for the Yucca Flat/Climax Mine CAU-Scale Model

Source	Effective Porosity (fraction)		Location	Method	DDE_F
	Minimum	Maximum			
Groundwater Tracer Tests					
Bechtel SAIC, 2004c	3×10^{-3}		Bullfrog Tuff at C-holes Complex at Yucca Mountain	Plug flow method (Equation [8-3]) using mean residence time from RELAP analysis	3
Bechtel SAIC, 2004c	3×10^{-3}	6×10^{-3}	Prow Pass Tuff at C-holes Complex at Yucca Mountain	Plug flow method (Equation [8-3]) using mean residence time from RELAP analysis	3
Current Report	1.8×10^{-3}	5.8×10^{-3}	Prow Pass Tuff at C-holes Complex at Yucca Mountain	Plug flow method (Equation [8-5]) using peak-concentration arrival time	1
Gas Tracer Tests					
Freifeld, 2001	2×10^{-3}	4×10^{-3}	Exploratory Studies Facility at Yucca Mountain	Random-walk particle method analysis of breakthrough curves	3
Calculated from Producing Zone and Fracture Data					
Erickson & Waddell, 1985	1.1×10^{-4}	8.4×10^{-4}	Test well USW H-4	Calculated using fracture orientation, fracture frequency, and production zone data	3
Calculated from Hydraulic Conductivity and Fracture Spacing Data					
Current Report	1.3×10^{-4}	3.7×10^{-4}	Well ER-EC-5 at Pahute Mesa	K from hydraulic tests; fracture spacing calculated using Equations (8-11) and (8-12); porosity calculated using Equation (8-10)	1
Used in Previous NTS Modeling Studies					
Wolfsberg et al., 2002	4.98×10^{-4}		TYBO/BENHAM	Base case value; one of 30 flow field realizations fitted	1
Recommended Range for the Yucca Flat/Climax Mine CAU-Scale Flow and Transport Model					
Current Report	1×10^{-4}	6×10^{-3}	Yucca Flat	Recommended range based on review and analyses	N/A

K - Hydraulic conductivity
N/A - Not applicable

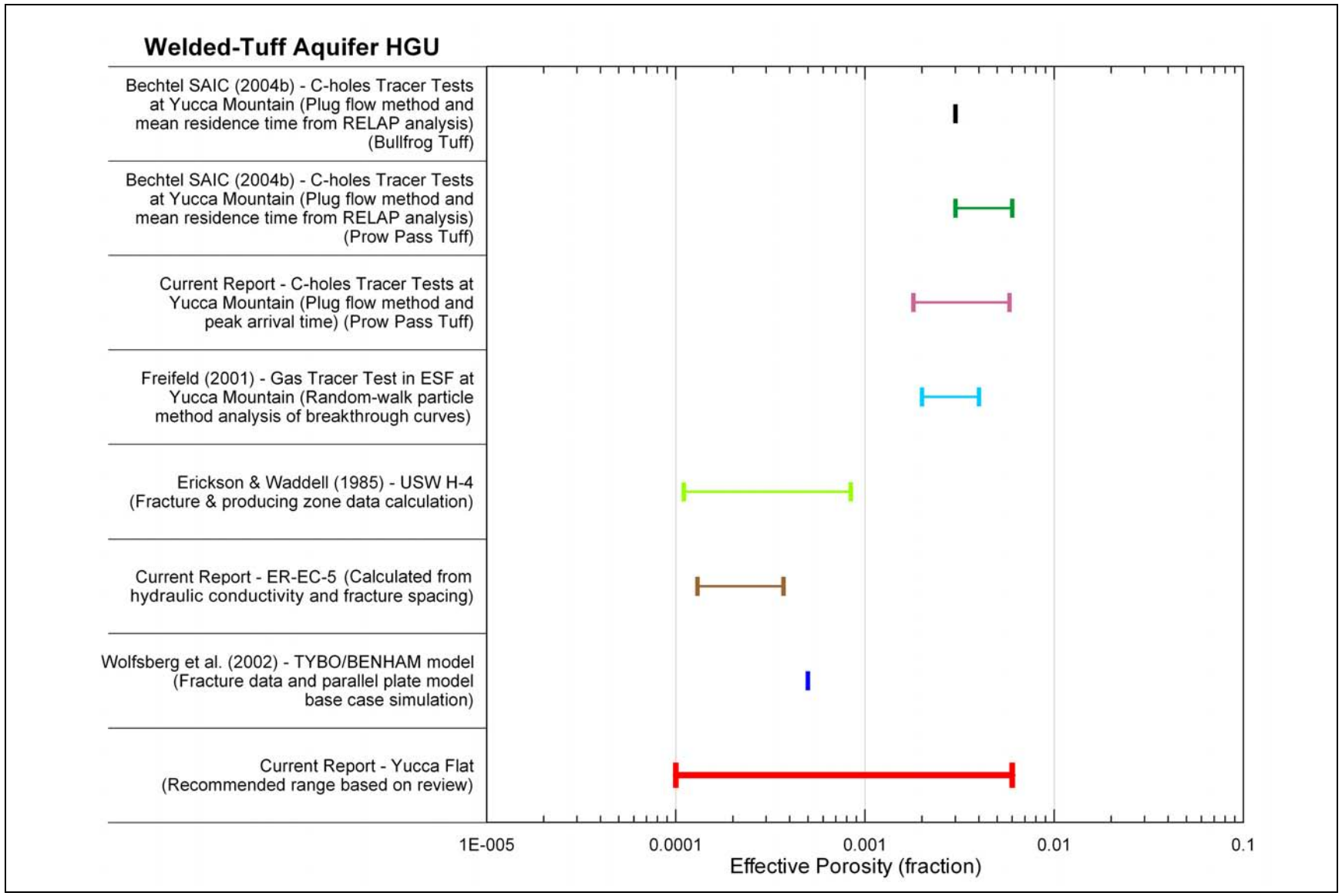

Figure 8-3
Estimated Effective Porosity Ranges for the Welded-Tuff Aquifer Hydrogeologic Unit

aperture regions (Tsang, 1984). The parallel-plate conceptualization is based on the assumption that roughness and tortuous flow caused by the aperture variation with the fracture have no effect on fluid flow. Moreover, tracer tests measure a volumetric flow rate that is not affected by the tortuous flow resulting from aperture variation. Therefore, the migration during tracer tests is controlled by the arithmetic mean of the fracture apertures (Tsang, 1992). Hydraulic conductivities from hydraulic tests will be controlled by the small aperture regions in the fracture system, and they will yield smaller fracture porosities calculated using the cubic law than will fracture porosities calculated from tracer tests that are controlled by the mean fracture aperture. Thus, the fracture porosities calculated from hydraulic conductivity and fracture spacing will likely be consistently biased lower than those calculated from tracer test results. This conclusion suggests that the fracture porosities determined from hydraulic conductivities and fracture spacings are too low to be representative for modeling transport at the CAU scale. This consideration should be included in developing the effective porosity distribution for the Yucca Flat/Climax Mine CAU flow and transport model.

Although the arrival time of the peak concentration from a convergent-flow tracer test provides a good estimate of the fracture porosity assuming plug flow, it yields a value that is biased slightly high for double-porosity media. This occurs because the plug flow calculation neglects the effects of matrix diffusion, which acts to retard the tracer.

Based on the results of the evaluation of fracture porosities for the WTA HGU, a range in effective porosity of 1×10^{-4} to 6×10^{-3} (interpreted values are rounded to one significant figure) is recommended for the WTA HGU at Yucca Flat (Table 8-8 and Figure 8-3). The recommended distribution for sampling this range is skewed log triangular with a peak at 3×10^{-3}. This distribution reflects the fact that fracture porosities determined from tracer tests are considered more representative and less uncertain than those determined from hydraulic conductivities and fracture spacings.

8.5.3 The Vitric-Tuff Aquifer Hydrogeologic Unit

The VTA HGU consist of nonzeolitized, nonwelded ash-flow and bedded tuff units and, in general, is saturated only in the deepest portion of the basin and does not extend much below the water table (BN, 2006). The VTA HGU is defined by three HSUs: the TM-UVTA, TM-LVTA, and LVTA (BN, 2006). Fractures are not common in the VTA HGU because it tends to be poorly to moderately

indurated (BN, 2006). Winograd and Thordarson (1975), Borg et al. (1976), and Blankennagel and Weir (1973) indicate that the formation and maintenance of open fractures is rare in ash-fall and nonwelded or slightly welded ash-flow tuffs due to their soft, friable nature. Winograd and Thordarson (1975) state that the bedded-tuff aquifers (assumed to be equivalent to the VTA HGU) "store and transmit ground water chiefly through primary or interstitial openings." Bechtel Nevada (2006) states that the interstitial porosity for the VTA HGU ranges from about 20 to 40 percent and its transmissivity is low.

Due to the lack of open fractures and the high interstitial porosity in the VTA HGU, flow through it is considered to be diffuse rather than fracture dominated. As a result, the effective porosity is considered to be a fraction of the matrix porosity for this HGU. Details regarding the recommended matrix porosity distribution for the VTA HGU at Yucca Flat are provided in Section 7.0. The effective porosity of this HGU is estimated to range from 80 to 100 percent of the matrix porosity because the VTA HGU is only slightly welded and has a soft, friable nature.

8.5.4 The Lava-Flow Aquifer Hydrogeologic Unit

The LFA HGU at Yucca Flat is defined by two HSUs: the BLFA and PRETBG. All occurrences of basalt beneath Yucca Flat are included in the BLFA HSU. Basalt has been identified in drill holes UE-1h and UE-1j in western Yucca Flat (Drellack and Thompson, 1990) and along the eastern side of Yucca Flat in the northern portion of Halfpint Range (Byers and Barnes, 1967). The BLFA is unsaturated within the Yucca Flat model area (BN, 2006). Separate local peralkaline lava flows that erupted before the Grouse Canyon Tuff make up the PRETBG HSU. These lava flows are located north of Yucca Flat in the northwest corner of the model area. Only small portions of this HSU are saturated (BN, 2006). In general, the lava-flow aquifers are dense and, as a result, tend to be fractured (BN, 2006). Blankennagel and Weir (1973) state that most groundwater flow in the rhyolitic lava flows in Pahute Mesa "occurs along faults and interconnected vertical and horizontal fracture systems that developed during cooling and shrinkage of the lava flow."

The LFA HGU will be conceptualized as a double-porosity medium in the flow and transport model of the Yucca Flat/Climax Mine CAU due to its fractured nature. A double-porosity conceptualization consists of fractures and matrix. Advective and diffusive flow and transport are assumed to occur exclusively in the fractures. Interaction between the fractures and matrix is restricted to molecular

diffusion from the fractures to the matrix and vice versa. It is assumed that no advective flow or transport occurs in the matrix. In order to appropriately represent the LFA HGU in the CAU-scale model, the recommended distribution for the effective porosity must be consistent with this model conceptualization. Data sources relevant for estimating the effective porosity of the LFA HGU are described below.

8.5.4.1 Tracer Tests

The most extensive information regarding lava-flow aquifers at the NTS was obtained from the BULLION Forced-Gradient Experiment (FGE) conducted at Pahute Mesa. The following general description of this experiment was taken from IT (1998). The BULLION FGE consisted of the injection of solute and microsphere tracers into a fractured lava-flow aquifer at a location downgradient of the BULLION nuclear test. Three wells were installed in an approximate line oriented consistent with the major fracture system. Tracers were injected into two wells (ER-20-6#1 and ER-20-6#2), while the third well (ER-20-6#3) was pumped at an average rate of 7.3 L/s. Within about three days of injection, pumping of both tracer-injection wells at a rate of about 0.3 L/s began. The purpose of this pumping was (1) to provide tracer pumpback data, (2) to sample for radionuclides migrating from the BULLION cavity due to the flow field induced by the pumping well, and (3) to provide data regarding transport of tracers from tracer-injection well ER-20-6#1 to tracer-injection well ER-20-6#2. The tracer-injection wells are located approximately 89 and 132 m from the pumping well (ER-20-6#3).

Tracer recovery was observed in the pumping well and in the tracer-injection well located closest to the pumping well for a total of three flow paths for data analysis. Two of the flow paths were from the tracer-injection wells (ER-20-6#1 and ER-20-6#2) to the pumping well (ER-20-6#3), and the third flow path was from the tracer-injection well located 130 m from the pumping well (ER-20-6#1) to the tracer-injection well located 89 m from the pumping well (ER-20-6#2). Samples were analyzed for the injected tracers as well as for radionuclides originating from the BULLION test. Well characterized breakthrough curves were observed for the tracers injected during the experiment, but little information regarding migration of radionuclides from the BULLION cavity was obtained.

IT (1998) interpreted the breakthrough curves from the BULLION FGE using two methods. First, they used a plug flow method (Equation [8-3]) assuming the average groundwater travel time is

approximated as the time of arrival of the peak concentration. The parameters and calculated porosities obtained by IT (1998) are summarized in Table 8-9. They performed this analysis only on the solute breakthrough curves observed at the pumping well and obtained calculated effective porosities of 6.8×10^{-3} and 4.9×10^{-3}.

Table 8-9
Estimate of Effective Porosity for the BULLION Forced-Gradient Experiment Based on Plug Flow Calculations (after IT, 1998)

Parameter	Transport from Tracer-Injection Well ER-20-6#1 to Pumping Well ER-20-6#3	Transport from Tracer-Injection Well ER-20-6#2 to Pumping Well ER-20-6#3
Peak-Concentration Arrival Time	41 days	26 days
Discharge Rate	7.6 L/s	7.6 L/s
Aquifer Thickness	100 m	100 m
Radial Distance	131.5 m	89.16 m
Calculated Effective Porosity	6.8×10^{-3}	4.9×10^{-3}

IT (1998) also interpreted the results from the BULLION FGE using the numerical model MODFLOWT, which they modified to add matrix diffusion capabilities. After calibrating the model to the flow data, they calibrated it to the tracer data observed in the pumping well. Their primary fitting parameters for the calibration were effective porosity, matrix porosity, longitudinal dispersivity, and effective matrix diffusion coefficient. If needed to obtain a better fit between the simulated and observed data, they also adjusted the fracture spacing, hydraulic anisotropy ratios, and the amount of water injected or withdrawn from the upper and lower portions of the tested interval. Table 8-10 summarizes their model parameters and transport calibration results for the solute tracer breakthrough curves observed at the pumping well. Based on calibration to the tracer breakthrough curves observed in the pumping well, the analyses by IT (1998) yielded effective porosities of 1.8×10^{-2} and 2.3×10^{-2}.

IT (1998) also conducted nine alternative calibrations to the breakthrough curves for tracers injected into ER-20-6#1 and recovered in the pumping well. These alternatives showed that the calibration is non-unique and the calibrated parameter values are uncertain. A factor of two is estimated for uncertainty for effective porosity because any change greater than a factor of two would make

Table 8-10
Effective Porosities from the IT (1998) Numerical Model Calibration to Tracer Recovery During the BULLION Forced-Gradient Experiment

Parameter	DFBA Transport from Injection Well ER-20-6#1 to Pumping Well ER-20-6#3	Iodide Transport from Injection Well ER-20-6#1 to Pumping Well ER-20-6#3	PFBA Transport from Injection Well ER-20-6#2 to Pumping Well ER-20-6#3
Fracture Spacing	0.25 m	0.25 m	0.25 m
Matrix Porosity	0.35	0.35	0.35
Effective Matrix Diffusion Coefficient	1.2×10^{-6} m²/d	1.6×10^{-6} m²/d	1.35×10^{-6} m²/d
Dispersivity			
longitudinal transverse vertical	10 m 3 m 2 m	10 m 3 m 2 m	10 m 3 m 2 m
Portion of Mass Injected into Tested Interval			
upper interval lower interval	35% 65%	35% 65%	75% 25%
Effective Porosity	1.8×10^{-2}	1.8×10^{-2}	2.3×10^{-2}

DFBA - Difluorobenzoic acid

calibration to the observed data extremely difficult. The effective porosities obtained with the alternative calibrations were 1.8×10^{-2}, 3.6×10^{-2}, and 9×10^{-3}.

The results of the MODFLOWT calibration to the BULLION FGE are considered to be uncertain because of the large number of parameters varied to obtain a match between measured and simulated breakthrough curves. The model consisted of six layers, and the amount of water injected into or withdrawn from two of those layers was varied during the calibration. For the calibrated transient flow model, which was used for calibration of the transport model, the amount of flow into and out of these two layers in the model was different for all three wells. Hydraulic conductivity zones were incorporated into the model in each of the six layers, and the amount of data available to support the zone locations and values was limited. Two of the fitting parameters for the transport calibration are matrix porosity and effective matrix diffusion coefficients. Both of these parameters have a large impact on the tracer travel time in the formation, and thus on the interpreted effective porosity. For these reasons, the effective porosities determined with the MODFLOWT model are considered to be

somewhat uncertain but were included in developing the effective porosity distribution for the LFA HGU at Yucca Flat.

The BULLION FGE was also analyzed by Reimus and Haga (1999). They used the semi-analytical model RELAP to interpret the solute and microsphere data from the cross-hole breakthrough curves. They did not interpret the breakthrough curves from pumpback of the injection wells. As a sensitivity analysis, Reimus and Haga (1999) evaluated the effects of radial versus linear flow, a finite rather than infinite matrix, and rate limited versus equilibrium sorption. The fitting parameters for model calibration were the tracer mass fraction participating in the test, the mean fluid residence time, the Peclet number (equal to the distance between the injection and withdrawal wells divided by the longitudinal dispersivity), and an effective mass transfer coefficient for diffusion into the matrix (equal to the matrix porosity divided by the fracture half aperture times the square root of the matrix diffusion coefficient). The fitting parameters were manually adjusted to achieve a least squared fit of the simulated data to the observed data. The effective porosities for the calibrated results were determined directly from the fitted mean residence time using the equation for plug flow (Equation [8-3]).

The effective porosities obtained by Reimus and Haga (1999) for their model fits to the various cross-hole breakthrough curves are summarized in Table 8-11. In their analysis of the breakthrough curve for tracer travel from injection well ER-20-6#1 to injection well ER-20-6#2, they considered two scenarios for the source of tracer movement. The first scenario assumed movement between these two wells was due solely to the pumping in injection well ER-20-6#2 and the second scenario assumed the movement was due solely to the pumping in pumping well ER-20-6#3. Their analyses for the various transport paths yielded effective porosities ranging from 3.6×10^{-4} to 2.1×10^{-2}. Note that the mean residence times (66.7 to 81.3 days) that Reimus and Haga (1999) obtained with RELAP are significantly larger than the peak-concentration arrival time of 41 days for the pathway from well #1 to well #3. For the pathways from well #2 to well #3, the peak-concentration arrival time is 26 days, and the mean residence times from Reimus and Haga (1999) range from 53.1 to 96.9 days.

8.5.4.2 Hydraulic Conductivity and Fracture Spacing Calculations

Rehfeldt et al. (2003) calculated fracture porosities for the volcanic rocks at the NTS based on hydraulic conductivities derived from pumping tests and on fracture spacings determined from

Table 8-11
Effective Porosities from the Reimus and Haga (1999) Analysis of the BULLION Forced-Gradient Experiment

Travel Path [a]	Source of Tracer Migration	Mean Residence Time (hr)		Effective Porosity (fraction)	
		Linear Flow	Radial Flow	Linear Flow	Radial Flow
Injection Well #1 to Pumping Well #3	Well #3 Pumping	1,950	1,600	8.0×10^{-3}	6.6×10^{-3}
Injection Well #1 to Injection Well #2	Well #2 Pumping	300	210	5×10^{-4}	3.6×10^{-4}
Injection Well #1 to Injection Well #2	Well #3 Pumping	300	210	2.3×10^{-3}	1.6×10^{-3}
Injection Well #2 to Pumping Well #3	Well #3 Pumping	2,325	1,675	2.1×10^{-2} [b]	1.5×10^{-2} [b]
Injection Well #2 to Pumping Well #3	Well #3 Pumping	1,825	1,275	1.6×10^{-2} [c]	1.1×10^{-2} [c]

[a] Well #1 is ER-20-6#1, well #2 is ER-20-6#2, and well #3 is ER-20-6#3.
[b] Assumes smallest value of effective mass transfer coefficient as determined for well #1 to well #3 travel path.
[c] Assumes largest value of effective mass transfer coefficient as determined for well #1 to well #3 travel path.

borehole logs and core surveys. The fracture porosity was calculated using an equation that combines the cubic law, Darcy's law, and the definition of fracture porosity. This method for estimating fracture porosity is described in detail in Section 8.5.2.6. Rehfeldt et al. (2003) reported calculated fracture porosities, using this method, for seven boreholes completed to the LFA HGU: ER-20-6#1, ER-20-6#2, ER-EC-1, ER-EC-4, ER-EC-6, ER-EC-7, and UE-18r. Fracture porosity calculations for these boreholes were repeated using available underlying borehole logging and testing information. Those calculations are described below and the calculated porosities are summarized in Table 8-12.

ER-20-6#1

IT (1998) reports transmissivities for well ER-20-6#1 based on analysis of hydraulic responses during the BULLION FGE. The drawdown data were analyzed using both the Theis equation for a confined aquifer and using a dual-porosity model for a fractured formation. The recovery data were also analyzed using the Theis equation. Well ER-20-6#1 is completed with a gravel or sand pack adjacent to the lava-flow aquifer, which is 132.6 m thick at the location of this well (BN, 1997a). The transmissivities reported in IT (1998) were converted to hydraulic conductivities using this thickness.

Table 8-12
Fracture Porosities Calculated for Lava-Flow Aquifers from Hydraulic Conductivity and Fracture Spacing Using Equation (8-10)

Well	Interval Name	Hydraulic Conductivity (m/s)		Fracture Spacing (m)	Calculated Fracture Porosity (fraction)		HGU
		Minimum	Maximum		Minimum	Maximum	
ER-20-6#1	Completion Interval	2.06×10^{-5}	3.07×10^{-5}	0.59	4.2×10^{-4}	4.8×10^{-4}	LFA
ER-20-6#2	Completion Interval	1.23×10^{-5}	1.82×10^{-5}	1.7	1.7×10^{-4}	2.0×10^{-4}	LFA
ER-EC-1	Screen Interval 1	1.98×10^{-4}	6.11×10^{-4}	3.9	2.5×10^{-4}	3.7×10^{-4}	LFA
ER-EC-1	Screen Interval 2	4.46×10^{-5}	1.24×10^{-4}	3.9	1.5×10^{-4}	2.2×10^{-4}	LFA
ER-EC-1	Screen Interval 3	1.19×10^{-4}	3.30×10^{-4}	3.9	2.1×10^{-4}	3.0×10^{-4}	LFA
ER-EC-1	Screen Interval 4	1.26×10^{-5}	3.57×10^{-5}	3.9	1.0×10^{-4}	1.4×10^{-4}	LFA
ER-EC-4	Screen Interval 1	3.42×10^{-4}	6.63×10^{-4}	8.0	1.9×10^{-4}	2.3×10^{-4}	LFA
ER-EC-4	Screen Interval 2	3.23×10^{-4}	9.14×10^{-4}	8.0	1.8×10^{-4}	2.6×10^{-4}	LFA
ER-EC-4	Screen Interval 3-1	3.27×10^{-4}	5.66×10^{-3}	8.0	1.8×10^{-4}	4.8×10^{-4}	LFA
ER-EC-6	Values not calculated due to borehole characteristics inconsistent with LFA HGU conceptualization						LFA
ER-EC-7	Screen Interval 1	1.51×10^{-5}	3.11×10^{-5}	6.8	7.4×10^{-5}	9.4×10^{-5}	LFA
ER-EC-7	Screen Interval 2	1.31×10^{-4}	1.97×10^{-4}	4.8	1.9×10^{-4}	2.2×10^{-4}	LFA
UE-18r	Completion Interval	3.22×10^{-6}		0.76	1.9×10^{-4}		LFA

Note: Shaded values were not used in developing the effective porosity distribution for the LFA HGU (see discussion in text).

Fracture location and dip data for ER-20-6#1 are available in Data Tracking Number (DTN) 1161 of the Common Data Repository (CDR). A corrected fracture spacing of 0.59 m was calculated from these data for the lava-flow aquifer using Equations (8-11) and (8-12). The minimum and maximum fracture porosities calculated for this well from the minimum and maximum reported transmissivities using Equation (8-10) are 4.2×10^{-4} and 4.8×10^{-4}, respectively.

ER-20-6#2

IT (1998) reports transmissivities for well ER-20-6#2 based on analysis of hydraulic responses during the BULLION FGE. The drawdown data were analyzed using both the Theis equation for a confined aquifer and using a dual-porosity model for a fractured formation. The recovery data were also analyzed using the Theis equation. Well ER-20-6#2 is completed with a gravel or sand pack adjacent to the upper 139 m of the 195.4-m-thick lava-flow aquifer at the location of this well (DOE/NV, 1998). The transmissivities reported in IT (1998) were converted to hydraulic conductivities using a thickness of 139 m. Fracture location and dip data for ER-20-6#2 are available in DTN 1161 of the CDR. A corrected fracture spacing of 1.7 m was calculated from these data for the lava-flow aquifer using Equations (8-11) and (8-12). The minimum and maximum fracture porosities calculated for this well from the minimum and maximum reported transmissivities using Equation (8-10) are 1.7×10^{-4} and 2.0×10^{-4}, respectively.

ER-EC-1

IT (2002b) reports hydraulic conductivities for the upper four screen intervals in well ER-EC-1 based on analysis of flow logging data. These intervals are screened across a lava-flow aquifer. A filter pack extends from above the top of the uppermost screen to below the base of the fourth screen. IT (2002b) calculated hydraulic conductivities from the interpreted transmissivity values using both the length of the screened interval and the length of the filter pack. They calculated a hydraulic conductivity for each logging run using three interpretation methods. In determining the hydraulic

conductivity for use in calculating the fracture porosity, all of the hydraulic conductivities reported by IT (2002b) using the screen length were averaged to get a maximum value, and all of the hydraulic conductivities calculated using the filter pack length were averaged to get a minimum value for each screen.

Fracture density and dip data are available for well ER-EC-1 in IT (2001). These data are based on interpretation of formation microimager and ultrasonic borehole imager logs. The upper four screened intervals are located in the top 90 m of the 835-m-thick logged interval. The density of fractures is much higher at the top of the logged interval than in the middle and at the bottom. Therefore, an average fracture spacing for the entire logged interval calculated using Equations (8-11) and (8-12) would yield a value that is not representative of fracturing at the location of the upper four screened intervals. It is not possible to calculate a corrected fracture spacing at the locations of the upper four screened intervals based on the information provided in IT (2001) because the fracture location and fracture dip data are not correlated. That is, the provided fracture locations and fracture dips do not indicate which dip goes with which fracture. As a result, an uncorrected fracture spacing was calculated. Twenty-three fractures are located in the 90-m section that includes the upper four screen intervals. This corresponds to a fracture spacing of 3.9 m. Using this spacing and the hydraulic conductivities provided in IT (2002b), fracture porosities ranging from 1.0×10^{-4} to 3.7×10^{-4} were calculated using Equation (8-10).

ER-EC-4

IT (2002c) reports hydraulic conductivities for the three upper screened intervals in well ER-EC-4 based on analysis of flow logging data. These intervals are screened across a lava-flow aquifer. A filter pack extends from above the top of the uppermost screen to below the base of the third screen. IT (2002c) calculated hydraulic conductivities from the interpreted transmissivity values using both the length of the screened interval and the length of the filter pack. A hydraulic conductivity for each logging run that produced measurable flow using three interpretation methods was calculated. In determining the hydraulic conductivity for use in calculating the fracture porosity, all of the hydraulic conductivities reported by IT (2002c) assuming the screen length were averaged to get a maximum value and all of the hydraulic conductivities calculated assuming the filter pack length were averaged to get a minimum value for each screen.

Fracture density and dip data are available for well ER-EC-4 in IT (2001). These data are based on interpretation of formation microimager and ultrasonic borehole imager logs. The upper three screened intervals are located in the top about 64 m of the 780-m-thick logged interval. The density of fractures is variable across the logged interval. Therefore, an average fracture spacing for the entire logged interval calculated using Equations (8-11) and (8-12) would yield a value that is not representative of fracturing at the location of the upper three screened intervals. It is not possible to calculate a corrected fracture spacing at the locations of the upper three screened intervals based on the information provided in IT (2001) because the fracture location and fracture dip data are not correlated. As a result, an uncorrected fracture spacing was calculated. Eight fractures are located in the 64-m section that includes the upper three screen intervals. This corresponds to a fracture spacing of 8.0 m. Using this spacing and the hydraulic conductivities provided in IT (2002c), fracture porosities ranging from 1.8×10^{-4} to 4.8×10^{-4} were calculated using Equation (8-10).

ER-EC-6

IT (2002e) reports hydraulic conductivities for the two uppermost screened intervals in well ER-EC-6 determined from analysis of flow logging data. These screens are completed across a lava-flow aquifer. Interpretation of flow logging results yields lower hydraulic conductivities for the lava-flow aquifer in this well (from 10^{-6} to 10^{-5} m/s) than was interpreted for the lava-flow aquifer in wells ER-EC-1, ER-EC-4, and ER-EC-7 (from 10^{-5} to greater than 10^{-3} m/s). Fracture density and dip data are available for well ER-EC-6 in IT (2001) based on interpretation of ultrasonic borehole imager logs. Nondense fracturing in the lava-flow aquifer adjacent to the two uppermost screened intervals was reported. The lack of fracturing and low hydraulic conductivities for the lava-flow aquifer at this borehole is inconsistent with the conceptualization of the LFA HGU as a transmissive, fractured unit. Therefore, fracture porosities were not calculated from hydraulic conductivity and fracture spacing for this well.

ER-EC-7

IT (2002f) reports hydraulic conductivities for the two screened intervals in well ER-EC-7 based on analysis of flow logging data. These intervals are screened across a lava-flow aquifer. A filter pack extends from above the top to below the bottom of each screen. The filter packs are separated by cement. IT (2002f) calculated hydraulic conductivities from the interpreted transmissivity values

using both the length of the screened interval and the length of the filter pack. They calculated a hydraulic conductivity for each logging run that produced measurable flow using three interpretation methods. In determining the hydraulic conductivity for use in calculating the fracture porosity, all of the hydraulic conductivities reported by IT (2002f) using the screen length were averaged to get a maximum value and all of the hydraulic conductivities calculated using the filter pack length were averaged to get a minimum value for each screen.

Fracture density and dip data are available for well ER-EC-7 in IT (2001). These data are based on interpretation of ultrasonic borehole imager logs. The screened intervals are located near the top and bottom of the logged interval and are separated by an interval of tuff-confining unit that is basically unfractured. The density of fractures is different across the two screened intervals and is extremely low in the tuff-confining unit interval that was also logged. Therefore, an average fracture spacing for the entire logged interval calculated using Equations (8-11) and (8-12) would yield a value that is not representative of fracturing at the location of the screened intervals. It is not possible to calculate a corrected fracture spacing at the location of the two screened intervals based on the information provided in IT (2001) because the fracture location and fracture dip data are not correlated. As a result, an uncorrected fracture spacing was calculated. Five fractures are located in the 34-m section that includes the upper screen interval and filter pack. This corresponds to a fracture spacing of 6.8 m. Eight fractures are located in the 38-m section that includes the lower screen interval and filter pack. This corresponds to a fracture spacing of 4.8 m. Using these spacings and the hydraulic conductivities provided in IT (2002f), fracture porosities ranging from 7.4×10^{-5} to 2.2×10^{-4} were calculated using Equation (8-10). IT (2001) indicates that the quality of the image log in well ER-EC-7 is only fair due to missing fractures in washout zones. Adjacent to both screened intervals, washouts probably concealed fractures (IT, 2001). Therefore, the fracture porosities given above are most likely low estimates because the fracture spacings used in the calculations are most likely too large due to the missed fractures as a result of the only fair quality of the log. As a result, these fracture porosities were not used in developing the effective porosity distribution for the LFA HGU at Yucca Flat.

UE-18r

Blankennagel and Weir (1973) report a transmissivity for well UE-18r of 23,000 gpd/ft, which converts to 3.31 x 10^{-3} m^2/s. The length from the top of the uppermost screen in this well to the bottom of the lowermost screen is 1,028.7 m. For this length, the calculated hydraulic conductivity is 3.22 x 10^{-6} m/s. Well UE-18r is completed across the welded-tuff and lava-flow aquifers. Analysis of 35.7 m of core from this well yielded 42 fractures, 26 percent of which were high-dip open fractures (60 to 90 degrees) and 7 percent of which were medium-dip open fractures (30 to 60 degrees) (Drellack et al., 1997). All other fractures were identified as closed and were not used in the calculation of fracture spacing. The fracture spacing calculated using Equations (8-11) and (8-12) for open fractures is 0.76 m. This spacing is highly uncertain as representative of the tested formation interval because it is based on only 35.7 m of core but the completion interval is 1,028.7 m thick. The fracture porosity calculated from the fracture spacing and hydraulic conductivity is 1.9 x 10^{-4}. This porosity is also highly uncertain because of the uncertainty in the fracture spacing. Therefore, this fracture porosity was not used in developing the effective porosity distribution for the LFA HGU at Yucca Flat.

8.5.4.3 Values Used in Previous NTS Modeling Studies

Wolfsberg et al. (2002) simulated the migration of radionuclides from the BENHAM and TYBO underground nuclear tests at Pahute Mesa in response to the observation of radionuclides in groundwater wells ER-20-5#1 and ER-20-5#3 located downgradient of the cavities. These wells are located about 1.3 km and 300 m from the BENHAM and TYBO cavities, respectively. The working point of BENHAM and the sampling location in a lava formation of well ER-20-5#3 are at about the same elevation. Well ER-20-5#1 samples a welded-tuff aquifer that is just above the working point of TYBO and more than 500 m above the working point of BENHAM. Wolfsberg et al. (2002) used a reactive, dual-porosity transport model to simulate contaminant migration from BENHAM to the observations wells and the NTS boundary in a 3-D, heterogeneous flow field. For these simulations, they estimated a low and high fracture porosity for the lava-flow aquifer and then calculated a base case value as the log average of the high and low values. The low fracture porosity was calculated using fracture spacing and fracture aperture data from Drellack et al. (1997) assuming parallel plates. The high fracture porosity was taken as the highest value determined by the IT (1998) analysis of the BULLION FGE. Table 8-13 summarizes the fracture porosity values given in Wolfsberg et al.

(2002). In their simulation of 30 equally likely realizations of the heterogeneous flow field using the base case parameter values, they found that one of the realizations generated transport results consistent with field observations. This suggests that the base case fracture porosity determined by Wolfsberg et al. (2002) may be an appropriate effective porosity at larger scales. However, this interpreted value is uncertain because it represents just one realization that provided a match of simulated versus field transport results.

Table 8-13
Fracture Porosities Used by Wolfsberg et al. (2002) for a Lava-Flow Aquifer

Values	Fracture Porosity (fraction)
Low Value	2.19×10^{-4}
Base Case Value	2.09×10^{-3}
High Value	2.00×10^{-2}

Pawloski et al. (2001) simulated radionuclide release and migration in the groundwater from the CHESHIRE cavity, located in Pahute Mesa, over a time period of 1,000 years. The CHESHIRE cavity is located within fractured rhyolite lava flows. They calculated a fracture porosity for the lava of 2×10^{-4} using average fracture density and aperture data from Drellack et al. (1997). They then multiplied this fracture porosity by a factor of 45 to obtain an effective porosity of 9×10^{-3}. The factor of 45 applied to the effective porosity over fracture porosity was obtained from Knox et al. (1965) from tracer tests in fractured dolomite at the GNOME site in New Mexico. The factor is obtained from the conversion of fracture porosity to effective porosities for a homogeneous porous media model. Based on their calculations, Pawloski et al. (2001) selected an effective porosity of 1×10^{-2} for the portions of the lava assigned high and moderate permeabilities in their model. Considering the purpose and use of the effective porosity determined using this approach, it is not used in developing the effective porosity distribution for the LFA HGU.

8.5.4.4 Recommended Ranges in Previous NTS Data Document Reports

Distributions and ranges of effective porosity for the LFA HGU for use in groundwater flow and contaminant transport models have been estimated and reported for Pahute Mesa (Rehfeldt et al., 2003) and Frenchman Flat (SNJV, 2005b). Rehfeldt et al. (2003) selected a log triangular distribution

with a minimum of 1 x 10^{-5}, a maximum of 0.1, and a mean of 1 x 10^{-3} for Pahute Mesa. The SNJV (2005b) report recommended a range of 2.4 x 10^{-5} to 0.1 for the CAU-scale modeling of Frenchman Flat.

8.5.4.5 Summary and Recommended Distribution

The previous sections discussed fracture porosity data for the LFA HGU determined by several methods and used or summarized in previous NTS modeling studies. The values used in developing the distribution for the effective porosity must be consistent with the conceptual model that will be used for the LFA HGU in the CAU-scale flow and transport model. That conceptualization is one of a double-porosity system with advective flow and transport through fractures only and matrix participation only through molecular diffusion from and to the fractures. The fracture porosities considered to be consistent with this conceptualization are summarized in Table 8-14 and are graphically illustrated in Figure 8-4.

The fracture porosities calculated from hydraulic conductivity and fracture spacing will likely be consistently biased lower than those determined from tracer test results because hydraulic tests are controlled by small aperture regions in the fractures and tracer tests are controlled by the average fracture aperture (see discussion in Section 8.5.2.11). This consideration should be included in developing the effective porosity distribution for the Yucca Flat/Climax Mine CAU flow and transport model. Although the arrival time of the peak concentration from a tracer test provides a good estimate of the fracture porosity assuming plug flow, it yields a value that is biased slightly high for double-porosity media. This occurs because the plug flow calculation neglects the effects of matrix diffusion, which acts to retard the tracer.

Based on the results of the evaluation of fracture porosities for the LFA HGU, a range in effective porosity of 1 x 10^{-4} to 2 x 10^{-2} (interpreted value is rounded to one significant figure) is recommended for the LFA HGU at Yucca Flat (Table 8-14 and Figure 8-4). The recommended distribution for sampling this range is skewed log triangular with a peak at 6 x 10^{-3}. This distribution reflects the fact that fracture porosities determined from tracer tests are considered more representative and less uncertain than those determined from hydraulic conductivities and fracture spacings.

Table 8-14
Summary of Estimated Effective Porosity Ranges for the Lava-Flow Aquifer and Recommended Range for the Yucca Flat/Climax Mine CAU-Scale Model

Source	Effective Porosity (fraction)		Location	Method	DDE_F
	Minimum	Maximum			
Tracer Tests					
IT, 1998	4.9×10^{-3}	6.8×10^{-3}	BULLION FGE	Plug flow method (Equation [8-3]) using peak-concentration arrival time	1
IT, 1998	1.8×10^{-2}	2.3×10^{-2}	BULLION FGE	Numerical model calibration (six-layer model)	1
Reimus and Haga, 1999	3.6×10^{-4}	2.1×10^{-2}	BULLION FGE	Plug flow method (Equation [8-3]) using mean residence time from RELAP analysis	1
Calculated from Hydraulic Conductivity and Fracture Spacing Data					
Current Report	1.0×10^{-4}	4.8×10^{-4}	Wells ER-20-6#1, ER-20-6#2, ER-EC-1, and ER-EC-4 at Pahute Mesa	K from hydraulic tests; fracture spacings calculated using Equations (8-11) and (8-12); porosity calculated using Equation (8-10)	1
Used in Previous NTS Modeling Studies					
Wolfsberg et al., 2002	2.09×10^{-3}		TYBO/BENHAM	Base case value; one of 30 flow field realizations fitted	1
Recommended Range for the Yucca Flat/Climax Mine CAU-Scale Flow and Transport Model					
Current Report	1×10^{-4}	2×10^{-2}	Yucca Flat	Recommended range based on review and analyses	N/A

K - Hydraulic conductivity
N/A - Not applicable

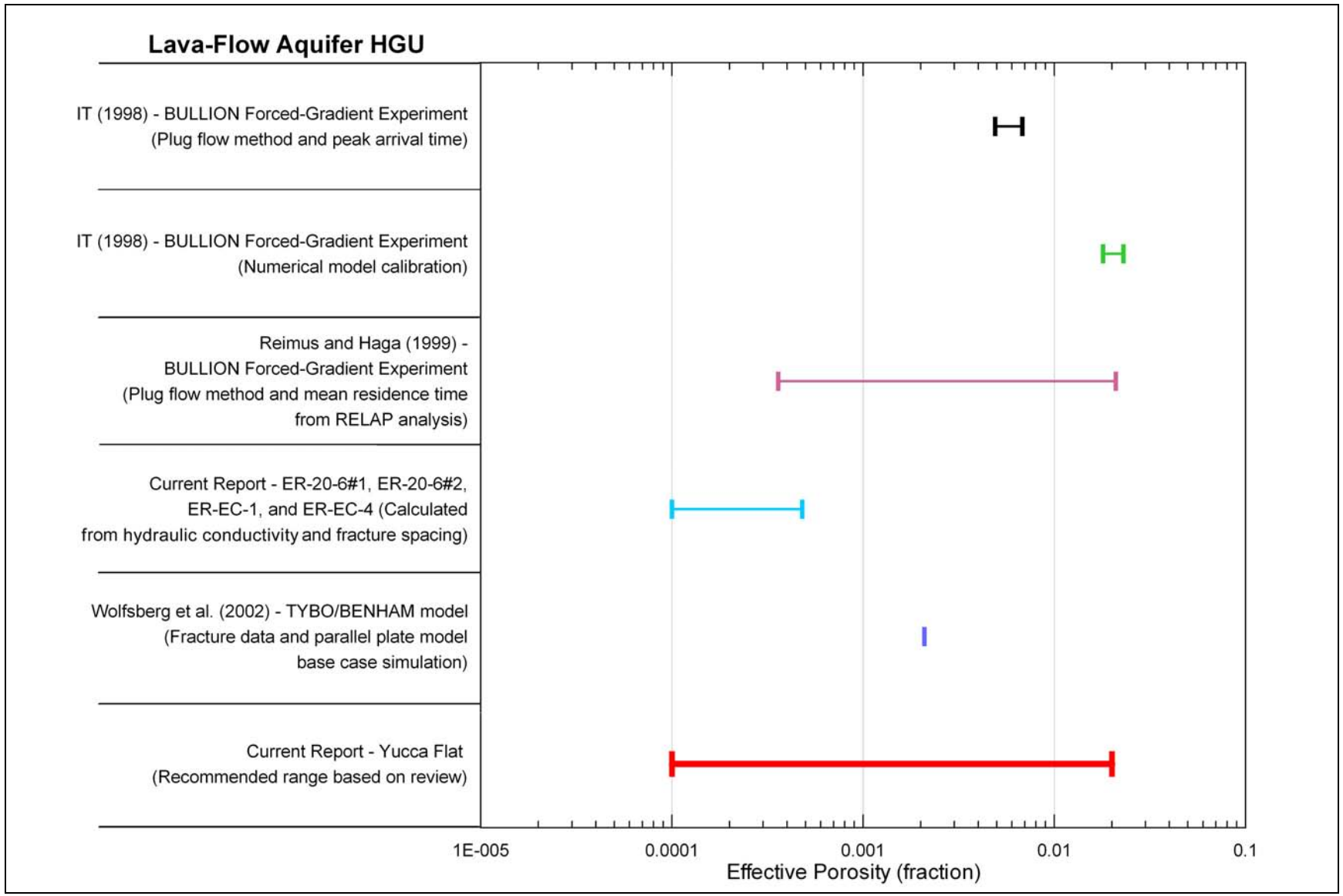

Figure 8-4
Estimated Effective Porosity Ranges for the Lava-Flow Aquifer Hydrogeologic Unit

8.5.5 The Carbonate Aquifer Hydrogeologic Unit

The following discussion of the CA HGU is taken from BN (2006). This HGU consists of Proterozoic and Paleozoic stratigraphic units of predominately limestone and dolomite lithology. Two HSUs are defined within the CA HGU: the UCA and LCA. The UCA HSU consists of thick limestone layers with interbedded mudstones and siltstones and is present only in the central portion of western Yucca Flat. Perched water is produced from this HSU by water well UE-16d. The LCA HSU consists of thick sequences of carbonate rock with thin layers of shale, quartzite, and calcareous clastic units. The LCA is a major regional aquifer underlying the NTS and most of southern Nevada.

Winograd and Thordarson (1975) state that the lower and upper carbonate aquifers "store and transmit ground water chiefly through secondary openings developed along fractures." They also report that the matrix porosity and permeability, determined from cores, is extremely low in the LCA. Results of pumping tests in 10 wells penetrating the LCA "may suggest that the water-bearing fractures are reasonably well connected and that fractures of differing transmissibility, if present, are randomly distributed" (Winograd and Thordarson, 1975). This conclusion is based on the fact that the portion of the drawdown curves representative of formation conditions do not show any change in slope. This information indicates that fracture flow dominates the movement of water in the LCA.

The CA HGU will be conceptualized as a double-porosity medium in the flow and transport model of the Yucca Flat/Climax Mine CAU due to its fractured nature. A double-porosity conceptualization consists of fractures and matrix. Advective and diffusive flow and transport are assumed to occur exclusively in the fractures. Interaction between the fractures and matrix is restricted to molecular diffusion from the fractures to the matrix and vice versa. It is assumed that no advective flow or transport occurs in the matrix. In order to appropriately represent the CA HGU in the CAU-scale model, the recommended distribution for the effective porosity must be consistent with this model conceptualization. The fracture porosity will be used as the effective porosity for the CA HGU. Data sources relevant for estimating the effective porosity of the CA HGU are described below.

8.5.5.1 Tracer Tests

Convergent Flow Tracer Test Between Water Wells C and C-1 in Yucca Flat

Winograd and West (1962) report on a convergent-flow tracer test conducted in the LCA between WW-C and C-1 in Yucca Flat. These two wells are about 29.3 m apart at the water table. The slotted interval is 32.9 m thick in WW-C. Water Well C-1 is completed open hole across 239 m of the LCA. Initial tracer breakthrough occurred after about 4.2 hours, and peak tracer concentration was observed between 3 and 4 hours later. The discharge rate at the withdrawal well was 13.9 L/s. For a radial flow field, the time for plug flow between the pumping and injection wells can be estimated Equation (8-3).

Using the parameter values from Winograd and West (1962) given above and peak-concentration arrival of about 3.5 hours after first tracer breakthrough, (7.7 hours after tracer injection), a porosity-thickness product of 0.14 m is calculated using Equation (8-3). A maximum effective porosity of 4.3×10^{-3} is calculated assuming a thickness equivalent to the slotted interval length of 32.9 m in WW-C. A minimum effective porosity of 5.9×10^{-4} is calculated assuming a thickness equivalent to the open interval length of 239 m in WW-C-1.

Convergent Flow Tracer Test at the ER-6-1 Well Cluster in Yucca Flat

A multiple-well aquifer test-tracer test (MWAT-TT) was conducted in the LCA at the ER-6-1 Well Cluster located in Yucca Flat from late April to late July 2004. The test details discussed here were taken from SNJV (2005e and f). Well ER-6-1#2 was the pumping well and tracers were injected into upper and lower completion intervals in ER-6-1, located 64 m from the pumping well, and ER-6-1#1, located 50.8 m from the pumping well. The direction of tracer migration from the injection wells to the pumping well is approximately aligned with the dominant local fracture orientation. The pumping rate in well ER-6-1#2 averaged 33.0 L/s over a 434.3-m-thick interval during the MWAT-TT. Tracer injection occurred in four stages. The first stage consisted of the injection of microspheres into the upper zone in well ER-6-1; the second stage consisted of the injection of 2,5-DFBA into well ER-6-1#1; the third stage consisted of the injection of NaI and 2,4,5-TFBA into the lower zone in well ER-6-1; and the fourth stage consisted of the injection of LiBr, LiCl, and PFBA into the upper zone in well ER-6-1. For each stage, tracer injection was followed by the

injection of chase water to flush the tracer from the borehole. A complete description of tracer breakthrough for this test can be found in SNJV (2005f).

Fracture porosities for the LCA were estimated using the breakthrough curves for the tracers injected into well ER-6-1 during the ER-6-1 MWAT-TT based on peak-concentration arrival time and the theoretical plug flow method (Equation [8-3]). Both of the breakthrough curves for tracers injected into the lower zone of well ER-6-1 show peak arrival at about nine days. Although the total pumping rate during the test averaged 33.0 L/s, the relative amounts of flow through the upper and lower zones of the LCA at the ER-6-1 complex were determined based on the flow logging results. Flow logging indicated that flow in the lower portion of well ER-6-1 is about 31 percent of the total flow and flow in the lower portion of well ER-6-1#2 is about 39 percent of the total flow. Using the average of these two percentages (35 percent) and multiplying by the total flow rate yields an adjusted flow rate of 11.6 L/s for the lower zone. An interval thickness of 148.1 m for the lower zone was used in the calculation. This thickness corresponds to the length between the top of the lower zone in ER-6-1 at a depth of 792.5 m and the top of the Eureka Quartzite at a depth of 940.6 m. Flow into and out of the borehole was assumed to be negligible in the Eureka Quartzite. Substituting these values in Equation (8-3) yields a fracture porosity of 4.7×10^{-3} based on the breakthrough of tracers injected into the lower zone in well ER-6-1 (Table 8-15).

This same method was also used to estimate a fracture porosity based on the breakthrough curves for tracers injected into the upper zone in well ER-6-1. Peak arrival for these tracers occurred at about 29 days. Flow into the upper zone in well ER-6-1 is about 69 percent of the total flow, and flow into the upper portion of well ER-6-1#2 is about 61 percent based on flow logging results. Using the average of these two values (65 percent) and multiplying it by the total flow rate yields an adjusted flow rate of 21.5 L/s. An interval thickness of 252.7 m was used. This thickness corresponds to the length between the top of the LCA at a depth of 539.5 m and the bottom of the upper zone at a depth of 792.2 m. Substituting these values into Equation (8-3) yields a fracture porosity of 1.7×10^{-2} (Table 8-15).

Observed tracer breakthrough curves from the tracer tests at the ER-6-1 cluster were analyzed by SNJV (2006d) using the semi-analytical model RELAP. Based on interpretations of hydraulic data at the cluster, analysis of the tracer test results assumed a linear flow regime. This analysis assumed

Table 8-15
Summary of Effective Porosities Determined Using the Breakthrough Curves from the ER-6-1 Well Cluster Tracer Test

Injection Well/Zone	ER-6-1 Lower			ER-6-1 Upper			ER-6-1#1	
	Current Report	SNJV, 2006d		Current Report	SNJV, 2006d		Current Report	SNJV, 2006d
		Single Porosity	Double Porosity		Pathway 1 Double Porosity	Pathway 2 Double Porosity		
Time	9 days [a]	34.4 days [b]	32.5 days [b]	29 days [a]	54.2 days [b]	145.8 days [b]	N/A [c]	137.5 days [b]
Flow rate	11.6 L/s [d]	Q_T x 0.4 [e]	Q_T x 0.4 [e]	21.5 L/s [f]	Q_T x 0.4 [e]	Q_T x 0.1 [g]	N/A	Q_T x 0.4 [e]
Thickness	148.1 m	125 m	125 m	252.7 m	300 m	300 m	N/A	300 m
Distance	64 m	NR	NR	64 m	NR	NR	N/A	64 m
Effective Porosity	4.7×10^{-3}	2×10^{-2}	1.8×10^{-2}	1.7×10^{-2}	1.6×10^{-2}	1.1×10^{-2}	N/A	2.0×10^{-2}

Note: Shaded values were not used in developing the effective porosity distribution for the CA HGU (see discussion in text).
[a] Time to peak arrival.
[b] Mean residence time as determined by RELAP analysis.
[c] No peak concentration identifiable in tracer breakthrough curve.
[d] 35 percent of total production rate of 33.0 L/s.
[e] Total production rate times 40 percent; actual value used not reported.
[f] 65 percent of total production rate of 33.0 L/s.
[g] Total production rate times 10 percent; actual value used not reported.

N/A - Not applicable
NR - Not reported

diffusion into a matrix with a 3 percent porosity. The breakthrough curves for I and 2,4,5-TFBA, injected into the lower zone in ER-6-1 and recovered in pumping well ER-6-1#2, were analyzed using both single- and double-porosity conceptualizations. The RELAP analyses yield a mean residence time for the tracers. The SNJV (2006d) then used this mean residence time and the assumption of plug flow to calculate the flow (or effective) porosity using Equation (8-3). The interpreted mean residence times were 825 hours (34.4 days) for the single-porosity conceptualization and 780 hours (32.5 days) for the double-porosity conceptualization (SNJV, 2006d). Note that these mean residence times are significantly larger than the peak-concentration arrival time of nine days discussed above. In their calculation of the flow porosity, they used a production rate equal to 40 percent of the total rate and an interval thickness of 125 m. Both of these values are slightly different from those used in the calculations discussed in the previous paragraph. For the RELAP interpretation of transport of tracers injected into ER-6-1 lower zone, the flow porosities reported by SNJV (2006d) are 2×10^{-2} for the single-porosity conceptualization and 1.8×10^{-2} for the double-porosity conceptualization (Table 8-15). The two interpreted values are similar, indicating a minimal effect of matrix diffusion; however, the effective porosity from the double-porosity interpretation is considered more representative for comparison purposes (Table 8-15).

The SNJV (2006d) report states that two inflow zones were identified by flow logging in pumping well ER-6-1#2 that correspond to the upper injection zone in ER-6-1. The analysis of the PFBA breakthrough in the upper zone considered these inflow locations as individual pathways. Spinner log results indicate that flow in the lower of these two inflow zones is less than 10 percent of the total flow rate. The RELAP analysis of the PFBA breakthrough curve yielded a mean residence time of 1,300 hours (54.2 days) for pathway 1 (the upper inflow zone in the upper injection zone) and 3,500 hours (145.8 days) for pathway 2 (the lower inflow zone in the upper injection zone) for a single-porosity conceptualization. The estimated mean residence times are much larger than the tracer peak-concentration arrival time of 29 days. They calculated the flow porosity with Equation (8-3) using mean residence times determined with RELAP. For the upper injections into ER-6-1, they assumed an interval thickness of 300 m and production rates of 40 and 10 percent of the total rate for pathways 1 and 2, respectively. Their calculated flow (effective) porosities are 1.6×10^{-2} for pathway 1 and 1.1×10^{-2} for pathway 2 (Table 8-15).

A single-porosity interpretation of the breakthrough of 2,5-DFBA, which was injected into ER-6-1#1, using RELAP yielded a mean residence time of 3,300 hours (137.5 days). Using this time, an interval thickness of 300 m, a production rate 40 percent of the total rate, and a distance of 92 m, SNJV (2006d) calculated a flow porosity of 2.0 x 10^{-2} (Table 8-15). The breakthrough curve for 2,5-DFBA for the ER-6-1#1 to ER-6-1#2 flow path exhibited a large amount of noise because measured concentrations were near the detection limit; thus any interpretation of the breakthrough curve is uncertain. The effective porosity from the RELAP single-porosity interpretation for this flow path is not recommended for inclusion in determining a representative range from the ER-6-1 tracer test.

Two-Well Recirculating Tracer Tests at the Amargosa Tracer Site

Johnston (1968) discusses the tracer well construction program for a two-well recirculating tracer test performed in the carbonate aquifer at the Amargosa tracer site. This site is located about 31.5 km southwest of Mercury, Nevada. The injection well is completed in the lower 20.7 m of the 22.9-m-thick Bonanza King Formation and in 41.8 m of the underlying Carrara Formations. The pumping well is completed in the lower 45.4 m of the 48.5-m-thick Bonanza King Formation and in the upper 6.4 m of the underlying Carrara Formation. The Bonanza King Formation consists primarily of brecciated dolomite while the Carrara Formation consists primarily of coarsely crystalline limestone. The Bonanza King Formation is highly permeable compared to the low permeability of the Carrara Formation. The injection and withdrawal wells are located 122.7 m apart at ground surface and were considered to be aligned approximately parallel to the direction of regional groundwater flow. Both wells were completed open hole in the carbonate portion except for a section of perforated casing across a fault zone in both wells that caused extensive caving of the holes. The fault zone was located between the dolomite of the Bonanza King Formation and the limestone of the Carrara Formation in the injection well, and in the Bonanza King Formation in the withdrawal well. A tracejector survey in the injection well identified two zones of greatest permeability: an upper zone approximately 1.5 m thick at the top of the carbonate section below the casing shoe, and a lower zone in the 14.9-m-thick fault zone. The rate of inflow in the upper zone was a factor of 11 greater than the rate of inflow in the lower zone. For the pumping well, the 9.8-m-thick fault zone was shown by a tracejector survey to be the most permeable interval in the well. The tracer for the recirculating tracer test consisted of tritiated water injected into the injection well.

Claassen and Cordes (1975) analyzed the breakthrough of the tritiated water at the pumping well for the two-well recirculating tracer test conducted at the Amargosa tracer site as described by Johnston (1968) above. They used the dispersion model method of analysis described in Grove and Beetem (1971) and Grove (1971) to analyze the test. This method involves developing theoretical breakthrough curves for various assumed longitudinal dispersion-porosity combinations, and then comparing those curves to the observed data. The theoretical curve that best matches the observed data gives the longitudinal dispersion and porosity for the tracer test. The analysis by Claassen and Cordes (1975) yielded a dispersivity of 15 m and a porosity-thickness product of 0.88 m. The active thickness for the tracer test at the Amargosa tracer site is unknown. Tracejector survey data (Johnston, 1968) suggest a range of 16.5 m (thickness of upper and lower permeable zones in the injection well) to 1.5 m (thickness of upper permeable zone only in the injection well). Using this range for thickness (16.5 to 1.5 m) and the porosity-thickness product from Claassen and Cordes (1975) yields a porosity range of 5.3×10^{-2} to 0.59, respectively. Claassen and Cordes (1975) found that the analysis results were more sensitive to changes in the porosity-thickness product than to changes in the dispersivity.

Leap and Belmonte (1992) discuss three two-well recirculating tracer tests conducted at the Amargosa tracer site. The first test is the same as that reported in Claassen and Cordes (1975). Leap and Belmonte (1992) do not present a reanalysis of this first test, but rather report the results from Claassen and Cordes (1975). The second and third tests used the same injection and withdrawal wells as did the first test. Sulfur-35 was the tracer for the second test, and ^{3}H and Br were the tracers for the third test. Leap and Belmonte (1992) also analyzed these tests using the method of Grove (1971) and obtained a porosity-thickness product of 0.84 m for all three breakthrough curves. They report a thickness for the Bonanza King Formation of 3.0 m at the injection well and 14.6 m at the withdrawal well. Using the average of these two thicknesses (8.8 m), Leap and Belmonte (1992) interpreted a porosity of 10 percent based on the analysis of the ^{35}S, ^{3}H, and Br breakthrough curves. Their analyses also yielded apparent dispersivities of 22.9, 27.4, and 30.5 m based on analysis of the ^{35}S, ^{3}H, and Br breakthrough curves, respectively. Note that the focus of the analyses by Leap and Belmonte (1992) was determination of dispersivity not determination of porosity.

The plug flow time for tracer to travel from the injection well to the withdrawal well in a two-well recirculating tracer test is given by Equation (8-4). For 100 percent recirculation, the function F has a value of one sixth and Equation (8-4) becomes:

$$t = \frac{\phi \pi b R^2}{3Q} \quad \Rightarrow \quad \phi = \frac{3Qt}{\pi b R^2} \tag{8-13}$$

Table 8-16 summarizes the approximate time to reach peak concentration, the pumping rate, the porosity-thickness product calculated using Equation (8-13), and the calculated porosity for several assumed effective thicknesses for each of the three two-well recirculating tracer tests conducted at the Amargosa tracer site. Assuming an average thickness of 9.0 m, the calculated effective porosity ranges from about 5.7 x 10^{-2} to 8.4 x 10^{-2}.

Table 8-16
Calculated Porosities for the Two-Well Recirculating Tracer Tests Conducted at the Amargosa Tracer Site Assuming Plug Flow

Tracer Test	Approx. Time to Peak Arrival (days) [a]	Pumping Rate (L/s)	Porosity-Thickness Product (m) [b]	Porosity (fraction)		
				1.5-m Thickness [c]	9.0-m Thickness [d]	16.5-m Thickness [e]
Test 1	6.2	22.5 [f]	0.764	0.51	8.4 x 10^{-2}	4.6 x 10^{-2}
Test 2	6.9	13.7 [g]	0.517	0.34	5.7 x 10^{-2}	3.1 x 10^{-2}
Test 3 ^{3}H Br	 7.4 7.8	15.5 [g]	 0.628 0.662	 0.42 0.44	 6.9 x 10^{-2} 7.3 x 10^{-2}	 3.8 x 10^{-2} 4.0 x 10^{-2}

Note: Shaded values were not used in developing the effective porosity distribution for the CA HGU (see discussion in text).
[a] Estimated from breakthrough curves given in Leap and Belmonte, 1992
[b] Calculated using Equation (8-13)
[c] Minimum estimated effective thickness
[d] Average estimated effective thickness
[e] Maximum estimated effective thickness
[f] Claassen and Cordes, 1975
[g] Leap and Belmonte, 1992

Johnston (1968) describes the carbonate aquifer at the Amargosa tracer site as having a few zones of very high permeability separated by rock of comparatively lower permeability. He states that "the zones of high permeability occur in faulted, highly brecciated intervals in the dolomite (Bonanza King Formation)." The estimated porosities of 3 to 10 percent determined from the tracer tests at the

Amargosa tracer site appear large if the tracer transport was controlled by a direct pathway in the fractures between the injection and pumping wells. Tracer tests conducted in fractured dolomite at the Waste Isolation Pilot Plant (WIPP) near Carlsbad, New Mexico, indicate that the direction of the tracer transport path relative to the primary fracture direction has a significant impact on the fracture porosities calculated using the peak-concentration arrival time (see discussion below). For three tracer test locations at the WIPP site, the fracture porosity calculated for the path aligned with the fractures (the fast path) were about 10^{-3}, while the apparent effective porosities calculated for paths not aligned with the fractures (the slow paths) were an order of magnitude or more higher (Jones et al., 1992). Travel along pathways not aligned with the predominate fracture direction will be more tortuous and undergo more molecular diffusion than pathways aligned with the fractures. Both of these factors may result in slower transport times, which result in the calculated fracture porosity being an overestimate.

The large porosities calculated for the tracer tests at the Amargosa tracer site suggest the possibility that the tracer flow path for the tests was not aligned with the predominate fracture direction. Therefore, the porosities determined from the tests may not be representative of the fracture porosity. In addition, fracture flow only in a geologic medium with a 10 percent fracture porosity would yield extremely large transmissivities (not consistent with those interpreted for the site). Because of these uncertainties, the porosities determined from these tests were not used in developing the effective porosity distribution for the CA HGU at Yucca Flat.

Tracer Test in the Culebra Dolomite at the Gnome Site, New Mexico

Grove and Beetem (1971) analyzed a two-well recirculating tracer test conducted in the Culebra Dolomite at the Gnome site in Eddy County, New Mexico. The Culebra Dolomite is similar to the LCA at the NTS in that it is a fractured dolomite aquifer. The two wells were originally designed to be parallel to the direction of regional flow in the aquifer. However, due to drilling problems, one of the wells deviated from vertical and the flow direction between the two wells is estimated to be about 35 degrees from the regional flow direction. The distance between the wells at the depth of the Culebra is 54.9 m, the Culebra thickness is 10.4 m, the withdrawal-injection rate was 2.8 L/s, and the time to peak concentration was about 12.8 days. Using their analysis method, Grove and Beetem (1971) obtained an estimated porosity of 0.12. Assuming plug flow and using Equation (8-3), a

porosity of 9.4 x 10^{-2} is calculated for this tracer test. For comparison, tracer tests conducted in the Culebra Dolomite at the WIPP site near Carlsbad, New Mexico, yielded estimated fracture porosities of about 10^{-3} (Jones et al., 1992). The high porosities determined for the test at the Gnome site are considered to be the result of the tracer travel path not being aligned with the predominate fracture direction. If that is the case, these porosities do not reflect the fracture porosity of the Culebra Dolomite at this site. Therefore, these porosities were not used in developing the effective porosity distribution for the CA HGU at Yucca Flat.

Tracer Tests in the Culebra Dolomite at the Waste Isolation Pilot Plant, New Mexico

Fracture porosities have been determined by analysis of three convergent-flow tracer tests conducted in the Culebra Dolomite at three different hydropad locations (H-3, H-6, and H-11) at the WIPP site near Carlsbad, New Mexico (Jones et al., 1992). At the H-3 and H-6 hydropads, tracer was injected into two wells and recovered in a third well. At the H-11 hydropad, tracer was injected into three wells and recovered in a fourth well. At all three locations, tracer transport during the test was rapid along one path and much slower along the other path(s). The rapid transport path was considered to be aligned approximately parallel to the dominate direction of fracture orientation. As a result, transport along the rapid path was assumed to be dominated by fracture flow. Numerical analysis of the tracer breakthrough curves for the rapid transport path for these three convergent-flow tracer tests yielded fracture porosities for the Culebra Dolomite ranging from 5.0 x 10^{-4} to 1.5 x 10^{-3} (Jones et al., 1992) (Table 8-17).

The porosities determined by Jones et al. (1992) are much lower than the value of 0.12 interpreted by Grove and Beetem (1971) for the Culebra at the Gnome site. This is likely the result of the transport direction for the recirculating tracer test at the Gnome site not being aligned parallel to the dominant fracture direction. Fracture porosities for the convergent-flow tracer tests discussed in Jones et al. (1992) were initially calculated using the peak-concentration arrival time and assuming plug flow (Equation [8-3]). Those calculated porosities are also given in Table 8-17. Notice that the calculated fracture porosities are higher than those determined through model calibration. As expected, fracture porosities calculated using Equation (8-3) are an overestimate even when determined from pathways with fracture-dominated transport because the delayed response resulting from matrix diffusion and dispersion is ignored. Also notice that the fracture porosities calculated for the fast transport paths,

Table 8-17
Summary of Fracture Porosities Determined for the Culebra Dolomite at the Waste Isolation Pilot Plant Site

Test Location	Path [a]/Tracer	Injection Well to Pumping Well Distance (m)	Fracture Porosity Determined from Model Calibration [b] (fraction)	Porosity Calculated Assuming Plug Flow [c] (fraction)
H-3 Hydropad	fast (m-TFMB)	30.7	1.2×10^{-3}	1.9×10^{-3}
	slow (PFBA)	26.8		2.3×10^{-2}
H-6 Hydropad	fast (PFBA)	29.9	1.5×10^{-3}	3.1×10^{-3}
	slow (m-TFMB)	29.9		5.6×10^{-2}
H-11 Hydropad	fast (m-TFMB)	20.9	5.0×10^{-4}	1.0×10^{-3}
	slow (PFBA)	21.4		1.8×10^{-2}
	slow (o-TFMB)	43.1		1.8×10^{-2}

Note: Shaded values were not used in developing the effective porosity distribution for the CA HGU (see discussion in text).
[a] Fast path means travel path with the most rapid tracer breakthrough; slow path means travel path with slower tracer breakthrough.
[b] Model calibration only to breakthrough curve from fast travel path (Jones et al.,1992).
[c] Calculated for this report assuming plug flow using Equation (8-3).

the paths assumed to be aligned approximately parallel with the fracture orientation, are more than one order of magnitude lower than those for the slow transport paths, which are not aligned with the fractures. This indicates that if the tracer transport path is not aligned with the major fracture direction, the calculated fracture porosity will likely be greatly overestimated.

8.5.5.2 Hydraulic Conductivity and Fracture Spacing Calculations

Section 8.5.2.6 discusses the methodology for calculation of fracture porosity using hydraulic conductivity data from hydraulic tests and fracture spacings from borehole fracture data. This method was used to calculate fracture porosities for wells ER-6-1#2 and ER-7-1 located in Yucca Flat and completed to the LCA. Well ER-5-3#2, located in Frenchman Flat, is also completed to the LCA. Analysis of the formation microimager log conducted in well ER-5-3#2 is provided in SNJV (2005c). The quality of this log is poor due to numerous washouts and breakouts in the well (SNJV, 2005c). These features cause intermittent contact between the logging tool pad and the borehole well. Because of the poor quality of the log, the fracture density in well ER-5-3#2 was considered to be uncertain, and no fracture porosity was calculated using hydraulic conductivity and fracture spacing.

ER-6-1#2

Hydraulic conductivity data for well ER-6-1#2 are reported in SNJV (2005a). A hydraulic conductivity value of 1.3 x 10^{-4} m/s was determined for the entire completion interval through analysis of a 90-day pumping test with ER-6-1#2 as the pumping well. Hydraulic conductivities determined through analysis of data from the spinner flow meter log conducted in the well were also reported. Fracture data from analysis of an electric microimager log conducted in well ER-6-1#2 is provided in SNJV (2005d). This report provides general information regarding fractures in the borehole. Specific locations and dip angles for the individual fractures were obtained from SNJV (2005d). Using these data and Equations (8-11) and (8-12), a fracture spacing was calculated for the entire completion interval and for each of the intervals associated with the reported hydraulic conductivities from analysis of the spinner flow log data. Table 8-18 summarizes the fracture porosities calculated for well ER-6-1#2 using hydraulic conductivity and fracture spacing (Equation [8-10]). These porosities range from 2.0 x 10^{-4} to 8.3 x 10^{-4}.

ER-7-1

Hydraulic conductivity data for well ER-7-1 are reported in SNJV (2004a). The nSIGHTS (n-Dimensional Statistical Inverse Graphical Hydraulic Test Simulator) code and a 50-simulation perturbation analysis were used to simulate 50 hydraulic conductivity solutions. They defined the range in hydraulic conductivity values as the central 90 percent of the solution distribution. This yielded hydraulic conductivities of 8.1 x 10^{-4} and 4.9 x 10^{-3} m/s. Fracture data from analysis of an electric microimager log conducted in well ER-6-1#2 are provided in SNJV (2005d). This report provides general information regarding fractures in the borehole. Specific locations and dip angles for the individual fractures were obtained from SNJV (2005d). Using these data and Equations (8-11) and (8-12), a fracture spacing of 1.0 m was calculated for the effective interval as determined with an impeller flowmeter. Table 8-18 summarizes the minimum and maximum fracture porosities calculated for well ER-7-1 using the minimum and maximum hydraulic conductivities and the fracture spacing. These porosities are 1.0 x 10^{-3} to 1.8 x 10^{-3}.

8.5.5.3 Fracture Spacing and Aperture Calculations

The SNJV (2005d) report provides a fracture analysis for four boreholes in Yucca Flat based predominately on the results from borehole electric microimager logs. These four boreholes are

Table 8-18
Fracture Porosities Calculated for Wells ER-6-1#2 and ER-7-1 Using Hydraulic Conductivity and Fracture Spacing (Equation [8-10])

Well	Interval (m bgs)		Hydraulic Conductivity (m/s)		Fracture Spacing (m)	Calculated Fracture Porosity (fraction)	
	Top	Bottom	Minimum	Maximum		Minimum	Maximum
ER-6-1#2	541.0	941.8	1.3×10^{-4} [a]		2.5	2.9×10^{-4}	
ER-6-1#2	563.9	593.1	ND [b]		1.4	N/A	
ER-6-1#2	593.1	619.0	2.8×10^{-4} [c]		1.0	7.0×10^{-4}	
ER-6-1#2	619.0	629.7	1.01×10^{-3} [c]		4.6	3.9×10^{-4}	
ER-6-1#2	629.7	645.0	ND [b]		4.4	N/A	
ER-6-1#2	645.0	649.5	3.93×10^{-3} [c]		0.8	2.0×10^{-3}	
ER-6-1#2	649.5	655.6	ND [b]		No fractures	N/A	
ER-6-1#2	655.6	678.5	5.66×10^{-3} [c]		16.5	2.9×10^{-4}	
ER-6-1#2	678.5	710.5	ND [b]		3.4	N/A	
ER-6-1#2	710.5	733.3	1.10×10^{-3} [c]		1.9	7.2×10^{-4}	
ER-6-1#2	733.3	750.1	ND [b]		1.4	N/A	
ER-6-1#2	750.1	776.0	1.11×10^{-3} [c]		2.4	6.2×10^{-4}	
ER-6-1#2	776.0	858.3	1.5×10^{-4} [c]		4.9	2.0×10^{-4}	
ER-6-1#2	858.3	869.0	3.54×10^{-3} [c]		7.6	4.2×10^{-4}	
ER-6-1#2	869.0	899.5	2.95×10^{-3} [c]		2.5	8.3×10^{-4}	
ER-7-1	664.9	722.4	8.1×10^{-4} [d]	4.9×10^{-3} [e]	1.0	1.0×10^{-3}	1.8×10^{-3}

[a] Value determined from analysis of pumping test.
[b] ND - No value determined because normalized flow rate was zero.
[c] Value determined from analysis of spinner flow log.
[d] 5th empirical percentile of K distribution determined through analysis of constant-rate test.
[e] 95th empirical percentile of K distribution determined through analysis of constant-rate test.

K - Hydraulic conductivity
N/A - Not applicable

ER-2-1 located in north-central Yucca Flat, ER-6-1#2 located in the southeastern corner of Yucca Flat, ER-7-1 located in eastern Yucca Flat, and ER-12-2 located in northwestern Yucca Flat. Two of these boreholes, ER-6-1#2 and ER-7-1, are completed in the LCA. The results from the borehole image logs were processed (enhanced) and then manually interpreted and statistically analyzed for fractures, bedding, and borehole washouts/breakouts. The analysis provided fracture aperture,

fracture dip, fracture orientation, and fraction of fracture infilling. Mineral infilling was considered to be 0 to 50 percent for fractures identified as open, 50 to 80 percent for fractures identified as mineral filled, and 80 to 100 percent for fractures identified as closed (SNJV, 2005d).

Estimates of the fracture porosity for the lower carbonate interval in boreholes ER-6-1#2 and ER-7-1 based on fracture data from the borehole image logs were determined using the following relationship given in Bryant (2005):

$$\phi_f = \frac{\left[{b_1 \cdot o_1}/{\cos(\theta_1)} + {b_2 \cdot o_2}/{\cos(\theta_2)} + \ldots + {b_n \cdot o_n}/{\cos(\theta_n)} \right]}{t_T} \qquad (8\text{-}14)$$

where:

ϕ_f is the fracture porosity (unitless),
b is the fracture aperture (L),
o is the fraction of the fracture that is open (unitless),
θ is the fracture dip angle,
t_T is the total interval thickness (L), and
n is the number of fractures.

The data for fracture aperture, fracture dip, and fraction of fracture infilling were obtained from SNJV (2005d). Two fracture porosities were calculated for each borehole. The first corresponds to the LCA interval, and the second corresponds to the interval within the LCA that is most productive. The depths for LCA intervals in each borehole were taken from BN (2006). The depths for the most productive interval or the water producing zone based on fluid logging were taken from SNJV (2005d) for borehole ER-6-1#2 and from SNJV (2004a) for borehole ER-7-1. The fracture porosity for the perforated interval in ER-7-1, taken from SNJV (2004a), was also calculated. In some instances, the top or bottom of the interval used in the calculation was defined by the depth range of the borehole image logging. Table 8-19 summarizes the fracture porosities for boreholes ER-6-1#2 and ER-7-1 calculated using Equation (8-14). For each interval, a minimum and maximum fracture porosity was calculated using the minimum and maximum from the range of infilling for the fracture. The calculated fracture porosities range from 1.9×10^{-3} to 9.4×10^{-3}. Some of the limitations involved with these calculations include:

- The manual interpretation used to estimate fracture data from the image logs is subject to human bias/error.

- Undersampling of vertical fractures is possible because the boreholes are vertical.
- The three ranges of mineral infilling used in the calculations most likely do not adequately characterize the nature of infilling in the fractures; also, the infilling may be removed locally by the drilling action, and therefore the degree of openness is likely overestimated.
- Each fracture aperture is assumed to be constant in thickness, although this is highly unlikely.
- The fractures are assumed to be continuous in lateral extent, although this is highly unlikely.

Table 8-19
Calculated Fracture Porosities for Boreholes ER-6-1#2 and ER-7-1 Using Fracture Spacing and Aperture Calculations

Interval	Depth to Interval Top (m)	Depth to Interval Bottom (m)	Minimum Fracture Porosity (fraction)	Maximum Fracture Porosity (fraction)
ER-6-1#2				
LCA	545.59 [a]	975.4 [b]	2.5×10^{-3}	5.6×10^{-3}
Producing Zone	883.92 [c]	975.4 [b]	1.9×10^{-3}	4.3×10^{-3}
ER-7-1				
LCA	539.50 [a]	758.65 [d]	3.8×10^{-3}	9.4×10^{-3}
Most Conductive Interval	665.07 [c]	722.38 [e]	2.4×10^{-3}	5.9×10^{-3}
Slotted Casing Interval	655.07 [f]	755.9 [g]	2.7×10^{-3}	6.8×10^{-3}

[a] Depth to the top of the borehole image log (SNJV, 2005d)
[b] Total depth of the borehole (BN, 2006)
[c] Depth to the top of producing zone (SNJV, 2005d)
[d] Depth to the bottom of the borehole image log (SNJV, 2005d)
[e] Depth to the bottom of the producing zone (SNJV, 2004a)
[f] Depth to the top of the slotted interval in the borehole (SNJV, 2004a)
[g] Depth to the bottom of the slotted interval in the borehole (SNJV, 2004a)

8.5.5.4 Geophysical Logging

Berger (1992) reports porosities for carbonate-rock aquifers in the Coyote Spring Valley Area determined from geophysical logging. These aquifers were investigated as part of the Nevada Carbonate Aquifers Program as potential sources for water supply and correlate to the CA HGU at the NTS. Coyote Spring Valley is located about 100 km due west of Frenchman Flat. Berger (1992) "describes the application and results of borehole geophysical log analyses from five test wells that penetrated the carbonate-rock aquifers." He used litho-porosity plots (*M-N* plots) to detect secondary

(fracture) porosity in the test wells. The porosity-independent parameters *M* and *N* are calculated from responses of neutron, gamma-gamma, and acoustic logs by (Berger, 1992):

$$M = \frac{\Delta t_f - \Delta t}{\rho_b - \rho_f} \tag{8-15}$$

and

$$N = \frac{\phi_f - \phi_{LS}}{\rho_b - \rho_f} \tag{8-16}$$

where:

Δt_f = transit time of the fluid (200 microseconds per foot [µsec/ft]),
Δt = transit time recorded by the acoustic log (µsec/ft),
ρ_b = bulk density recorded by the gamma-gamma log (grams per cubic centimeter [g/cm^3]),
ρ_f = fluid density (1g/cm^3),
ϕ_f = neutron porosity of fluid (100 percent as decimal), and
ϕ_{LS} = neutron porosity recorded by the neutron log (percent as decimal).

Values for *M* and *N* are calculated for pure lithologies of silica, calcite, and dolomite and for the lithologies in the test wells. Values of *M* are plotted versus *N* values. Well test zones with values that plot above the lithology triangle created by the pure mineral endpoints (which represents a shale-free carbonate zone) are considered to have secondary porosity. The magnitude of the secondary porosity is determined by the distance from the lithology triangle to the plotted point. Using this method, Berger (1992) identified secondary porosity in only one of the test wells (CE-DT-4). He determined secondary (fracture) porosity values for this well ranging from 6 x 10^{-3} to 9.6 x 10^{-2}. Due to the fact that only one of the five wells showed secondary porosity using this method and the method calculates secondary porosity indirectly, these values were not used in developing the effective porosity distribution for the CA HGU at Yucca Flat.

8.5.5.5 Literature Review of Basin and Range Province Rocks

Bedinger et al. (1989) developed distributions for hydraulic properties of rocks in the Basin and Range Province in the southwestern United States. They conducted a literature review of hydraulic conductivity and effective porosity for rocks in the Basin and Range Province and for rocks of similar types in other areas. The collected data were then synthesized, and the mean and 16.5 and 93.5 percentiles were determined for each rock type. Table 8-20 summarizes their findings of

effective porosity for carbonate rocks, including limestone, dolomite, and marble. Because the degree to which the characteristics of the carbonate rocks found in the review by Bedinger et al. (1989) match the characteristics of the CA HGU at Yucca Flat is unknown and the methods used to determine the porosities are unknown, these effective porosities were not used in developing the effective porosity distribution for the CA HGU at Yucca Flat.

Table 8-20
Effective Porosity Estimates for Carbonate Rocks in the Basin and Range Province (after Bedinger et al., 1989)

Rock Type	Description	Effective Porosity (fraction)		
		16.5 Percentile	Mean	83.5 Percentile
Carbonate Rocks, including limestone, dolomite, and marble	Fractured, karstic, cavernous	0.09	0.12	0.16
	Dense to moderately dense	0.005	0.01	0.02

Note: Shaded values were not used in developing the effective porosity distribution for the CA HGU (see discussion in text).

8.5.5.6 Values Used in Previous NTS Modeling Studies

The DOE/NV (1997a) report presents regional groundwater flow and ^{3}H transport models to evaluate migration from the underground testing areas of the NTS. They compiled hydrogeologic data for a large portion of southern Nevada and California, including the NTS. They looked at porosities for the LCA based on the tracer tests at the Amargosa tracer site (Leap and Belmonte, 1992) and the tracer test between wells C and C-1 in Yucca Flat (Winograd and West, 1962) analyzed using the method of Welty and Gelhar (1989). They also looked at the fracture analysis of core from ER-6-2 (IT, 1996c). For ER-6-2, they calculated a true fracture spacing of 0.22 m from the mean of the reported fracture dip angle (81 degrees) and fracture aperture (0.9 mm). They then divided the mean fracture aperture by the calculated true fracture spacing to determine a fracture porosity of 4×10^{-3}. They conducted a literature review and found fracture porosities ranging from 2×10^{-4} to 2×10^{-2} reported as representative for the Culebra Dolomite at the WIPP site (Tomasko et al., 1989). For their modeling of ^{3}H transport, DOE/NV (1997a) assumed a log-normal distribution having a $\log_{10}$ mean value of -2.46 and a $\log_{10}$ SD of 0.25 for the effective porosity of the LCA. This translates to a mean effective porosity of 3.47×10^{-3}. The effective porosity range, defined by two SDs, is 1.1×10^{-3} to 1.1×10^{-2}.

8.5.5.7 Recommended Ranges in Previous NTS Data Document Reports

Distributions and ranges of effective porosity for the CA HGU for use in groundwater flow and contaminant transport models have been estimated and reported for Pahute Mesa CAU (Rehfeldt et al., 2003) and Frenchman Flat CAU (SNJV, 2005b). The distribution selected by Rehfeldt et al. (2003) for Pahute Mesa is the distribution used by DOE/NV (1997a) for their regional ^{3}H model (see previous section). The SNJV (2005b) report selected a log-uniform distribution for the effective porosity of the CA HGU with a range of 6.4×10^{-4} to 1.6×10^{-2} for Frenchman Flat.

8.5.5.8 Summary and Recommended Distribution

The previous sections discussed fracture porosity data for the CA HGU determined by several methods and used or recommended in previous NTS modeling studies. The values used in developing the distribution for the effective porosity must be consistent with the conceptual model that will be used for this HGU in the CAU-scale flow and transport model. That conceptualization is a double-porosity system with advective flow and transport through fractures only, and matrix participation only through molecular diffusion from and to the fractures. The fracture porosities considered to be consistent with this conceptualization are summarized in Table 8-21 and graphically illustrated in Figure 8-5.

The fracture porosities calculated from hydraulic conductivity and fracture spacing will likely be consistently biased lower than those determined from tracer test results because hydraulic tests are controlled by small aperture regions in the fractures, and tracer tests are controlled by the average fracture aperture (see discussion in Section 8.5.2.11). Both hydraulic and tracer tests are impacted by the range and distribution of fracture apertures. This consideration should be included in developing the effective porosity distribution for the Yucca Flat/Climax Mine CAU flow and transport model. Although the arrival time of the peak concentration from a tracer test provides a good estimate of the fracture porosity assuming plug flow, it yields a value that is biased slightly high for double-porosity media. This occurs because the plug flow calculation neglects the effects of matrix diffusion, which acts to retard the tracer.

Based on the results of the evaluation of fracture porosities for the CA HGU, a range in effective porosity of 2×10^{-4} to 2×10^{-2} (interpreted values are rounded to one significant figure) is

Table 8-21
Summary of Estimated Effective Porosity Ranges for the Carbonate Aquifer and Recommended Range for the Yucca Flat/Climax Mine CAU-Scale Model

Source	Effective Porosity (fraction)		Location	Method	DDE_F
	Minimum	Maximum			
Tracer Tests					
Current Report (based on test data from Winograd and West, 1962)	5.9×10^{-4}	4.3×10^{-3}	WW-C and WW-C1 in Yucca Flat	Plug flow method (Equation [8-3]) using peak-concentration arrival time	5
Current Report	4.7×10^{-3}	1.7×10^{-2}	ER-6-1 Well Cluster in Yucca Flat	Plug flow method (Equation [8-3]) using peak-concentration arrival time	1
SNJV, 2006d	1.1×10^{-2}	1.8×10^{-2}	ER-6-1 Well Cluster in Yucca Flat	Plug flow method (Equation [8-3]) using mean residence time from RELAP analysis	1
Jones et al., 1992	5.0×10^{-4}	1.5×10^{-3}	Culebra Dolomite at the WIPP site in New Mexico	Model calibration to tracer breakthrough curves	3
Current Report	1.0×10^{-3}	3.1×10^{-3}	Culebra Dolomite at the WIPP site in New Mexico	Plug flow method (Equation [8-3]) using peak-concentration arrival time	1
Calculated from Hydraulic Conductivity and Fracture Spacing Data					
Current Report	2.0×10^{-4}	2.0×10^{-3}	ER-6-1#2 and ER-7-1 in Yucca Flat	K from hydraulic tests; fracture spacing calculated using Equations (8-11) and (8-12); porosity calculated using Equation (8-10)	1
Calculated from Fracture Spacing and Fracture Aperture Data					
Current Report	1.9×10^{-3}	9.4×10^{-3}	ER-6-1#2 and ER-7-1 in Yucca Flat	Calculated from fracture aperture and spacing using Equation (8-14)	1
Recommend Range for the Yucca Flat/Climax Mine CAU-Scale Flow and Transport Model					
Current Report	2×10^{-4}	2×10^{-2}	Yucca Flat	Recommended range based on review and analyses	N/A

K - Hydraulic conductivity N/A - Not applicable

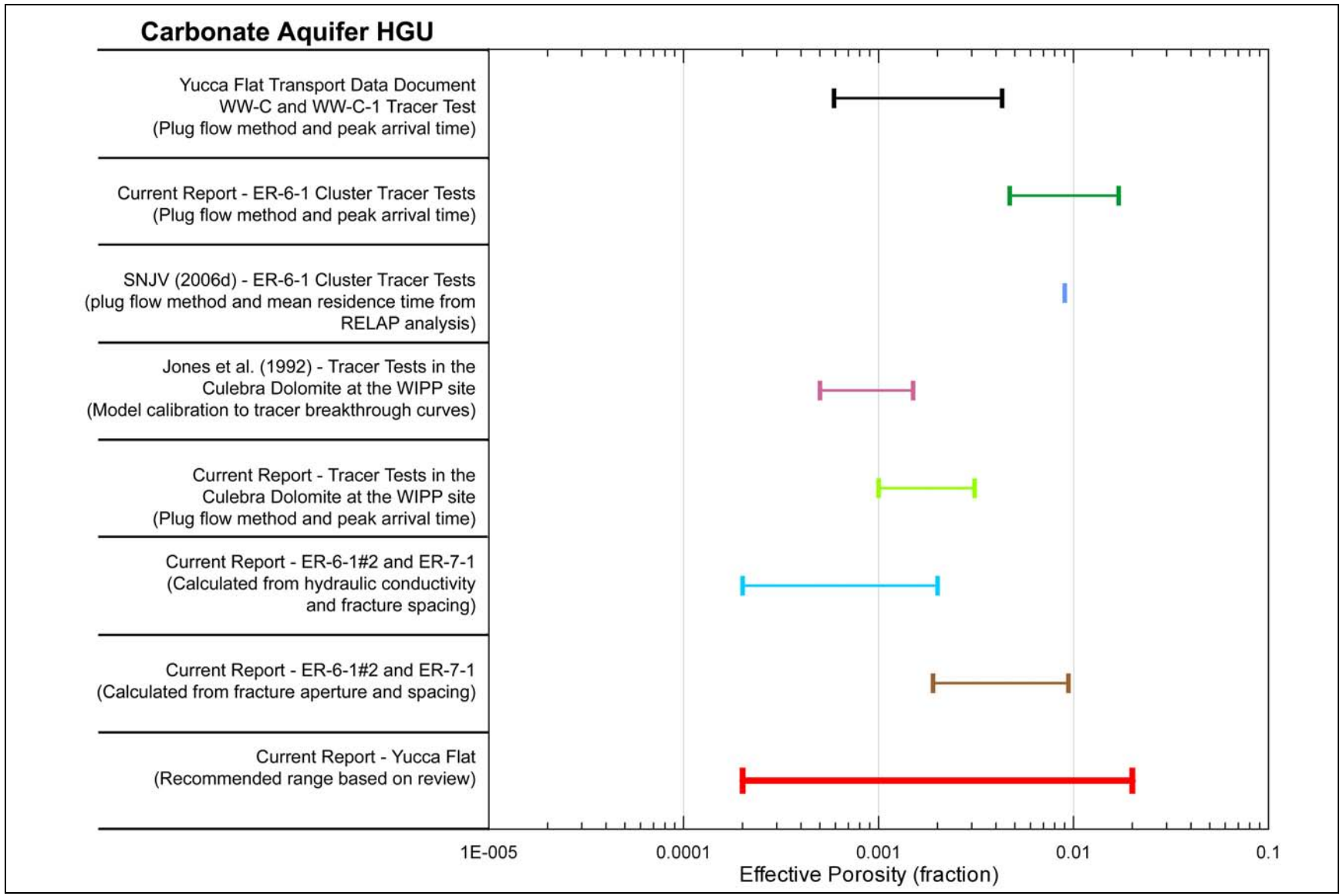

Figure 8-5
Estimated Effective Porosity Ranges for the Carbonate Aquifer Hydrogeologic Unit

recommended for the CA HGU at Yucca Flat (see Table 8-21 and Figure 8-5). The recommended distribution for sampling this range is skewed log triangular with a peak at 5×10^{-3}. This distribution reflects the fact that fracture porosities determined from tracer tests are considered more representative and less uncertain than those determined from hydraulic conductivities and fracture spacings.

8.6 Effective Porosity of the Confining Unit Hydrogeologic Units

There are four confining unit HGUs (PCU, TCU, GCU, and CCU) in the Yucca Flat model area.

8.6.1 The Playa Confining Unit

The PCU HGU consists predominately of clayey silt and is located at the Yucca Lake playa, the Papoose Lake playa, and an unnamed playa. There is no evidence of fracturing in the PCU. However, large cracks have historically opened in the dry bed of Yucca Lake. Water accumulating in the playa due to precipitation has rapidly drained into the cracks potentially providing a means of recharge to the regional groundwater system. Doty and Rush (1985) indicate that the cracks have naturally formed probably due to the combination of natural desiccation of playa deposits and fault movement.

The PGU HGU is unsaturated in Yucca Flat. Therefore, an effective porosity distribution is not provided since this HGU will not be included in the CAU-scale model.

8.6.2 The Tuff Confining Unit

The TCU HGU consists predominately of zeolitized nonwelded tuffs but also includes zeolitized bedded tuff, devitrified ash-flow tuff, tuffaceous sandstone, tuffaceous paleocolluvium, argillized bedded tuff, ash-fall tuff, and reworked tuff. A distinguishing characteristic of the TCU HGU is the extensive zeolitization that substantially decreases the permeability of the unit. Zeolitization diagenesis also tends to decrease the overall porosity of the TCU HGU (Moncure et al., 1981). The TCU HGU is defined by five HSUs (UTCU, BRCU, LTCU, OSBCU, and ATCU).

Although there are some fractures in the TCU HGU, they tend to be clogged with clay or zeolites and tend to be poorly hydraulically connected. Pumping tests in the unit indicate that fractured zones

initially yield more water than the surrounding matrix, but the yield of these zones generally decreases rapidly as fractures are depressurized. Flow through the unit is probably controlled by interstitial permeability rather than fracture transmissibility (Winograd and Thordarson, 1975).

Due to the lack of fracture flow within the TCU HGU, the effective porosity for this HGU is assumed to be represented by a fraction of the matrix porosity. The recommended matrix porosity distribution for the TCU HGU is discussed in Section 7.0. Based on the types of material found in this HGU, it is estimated that the effective porosity ranges from 50 to 80 percent of the matrix porosity. Therefore, the recommended distribution for the effective porosity of the TCU HGU is 50 to 80 percent of the recommended matrix porosity distribution.

8.6.3 The Granite Confining Unit

The following discussion of the granite confining unit HGU is taken from BN (2006). This HGU consists of the intrusive Climax Stock composed of granodiorite and quartz monzonite. The Climax Stock is located at the north end of Yucca Flat. The GCU HGU is saturated at depth, has low intergranular porosity, and has a low permeability. The GCU HGU is defined by a single HSU, the MGCU.

The GCU HGU will not be directly included in the Yucca Flat/Climax Mine CAU flow and transport model. Rather, it will be incorporated into the Climax Stock model. Simulated flow across the southern boundary of the Climax Stock model will then be used as a boundary condition for the Yucca Flat model. Therefore, an effective porosity distribution for the GCU HGU is not presented here.

8.6.4 The Clastic Confining Unit

The CCU HGU consists of siliciclastic sedimentary rocks, quartzite, and shale. Although some fractures are found within the CCU, they tend to be either healed or sealed, and little groundwater is produced from this HGU (BN, 2006). The CCU yields very little groundwater and is saturated only in parts of western Yucca Flat (BN, 2006). Winograd and Thordarson (1975) report that fractures observed in core from this HGU in a Yucca Flat well were “tightly sealed either by selvage minerals or by quartz or calcite veinlets, or by virtue of their never having been opened.” They also state that

the porous, fine-grained rock found in the CCU typically deform plastically, which limits development of open fractures. These porous, fine-grained rocks will also tend to seal or isolate fractures developed in the dense quartzite (Winograd and Thardarson, 1975). Regional flow in this HGU is most likely controlled by interstitial permeability rather than fracture transmissibility (Winograd and Thordarson, 1975).

Due to the lack of interconnected fractures, the effective porosity of the CCU HGU is considered to be a fraction of the matrix porosity. A detailed discussion of the matrix porosity for this HGU is provided in Section 7.0 along with the distribution recommended for the CAU-scale model. Based on the types of sediments found in this HGU, the effective porosity is estimated to be 50 to 90 percent of the matrix porosity. Therefore, the recommended effective porosity distribution for the CCU HGU is 50 to 90 percent recommended of the matrix porosity distribution.

8.7 Data Scaling Considerations

For proper representation of a double-porosity media in regional flow and transport models, characteristics of the fracture system at the scale of the model must be developed. The most common scales at which fracture data are available are the borehole scale through observations of fractures in core and with borehole image logs, and at the scale of tens of meters through interpretations of breakthrough curves from tracer tests. Both of these scales are significantly smaller than the scale of the Yucca Flat/Climax Mine CAU flow and transport model, which is tens of kilometers.

Scale and measurement uncertainty must be considered when determining ranges for fracture parameters. While the apertures (above a threshold minimum thickness) of fractures may be measured at various depths in a borehole based on borehole or core logging, observations of open or partially open fractures may be uncertain because the openness of the fracture may have resulted from physical erosion during drilling and may not be representative at even short distances beyond the nominal borehole diameter. In addition, fractures that are truly open may have limited lateral extent and continuity, and thus would not provide a fracture transport pathway important for the distance and time scales of interest in a regional transport evaluation.

In fractured media, the effective porosity is a measure of the interconnectedness of open fractures available for flow. Many fractures may dead end and not participate in flow at any scale, whereas

other fractures may participate at the scale of tens of meters but not at hundreds of meters or several kilometers. The percentage of fractures interconnected at the CAU scale will be much smaller than those interconnected at the scale of tens of meters and those observed in boreholes. From observations at the borehole scale, it is not possible to determine the interconnectedness of fractures beyond the borehole scale. In addition, the degree to which fractures interconnected at the tracer test scale (tens of meters) are also interconnected at the CAU scale is unknown. Adding to this complication are the assumptions of the fracture geometry and characteristics in the double-porosity conceptual model used in the CAU-scale modeling. This conceptualization typically assumes that fractures in a fractured HSU are equally spaced and hydraulically connected with a constant aperture across the entire domain of the HSU in the model.

In fractured media, the lateral extent and aperture of fractures is not constant. As a result, open fractures observed at one location may not be found at other locations, and dense fracturing at one location may diminish laterally or become sparse. This difference in scales is important because fracture characteristics determined at the measurement scale should not be expected to be representative to the much larger model scale, in particular if the fracture property is implemented as uniform for the entire HGU or HSU. The presence of a few fractures in a HGU at the local scale, which may indicate a fractured media conceptualization, may, in some cases, be more appropriately modeled as porous media conceptualized at the CAU scale when one considers the limited number and lateral extent of the fractures (e.g., in a situation where the HGU generally appears to be predominantly unfractured). When a double-porosity conceptualization is appropriate for an HGU, it is necessary to scale the fracture porosities obtained from borehole observations and tracer test interpretations to the CAU scale to appropriately incorporate the fractures in the CAU-scale models (see discussion below). Methods must be developed to address translating ranges determined at the measurement scale to ranges for implementation in the transport model.

8.8 Limitations

The major limitations associated with the effective porosity distributions developed for the Yucca Flat/Climax Mine CAU model are the sparse data environment, the uncertainty in the data inputs and methods used to estimate effective porosity, and the issue of scaling borehole and tracer test values to values representative at the CAU scale. Effective porosity distributions were developed in this section for the three fractured aquifer HGUs. The scale of these aquifers within the Yucca

Flat/Climax Mine CAU model is up to hundreds of square kilometers. The actual effective porosity in such a large area will be heterogeneous, varying both in the lateral and vertical directions. Determining values for effective porosity that capture this heterogeneity would require extensive data collection at time and spatial scales that are impractical. The limitation due to the sparse data environment results in an inability to capture the heterogeneous nature of the effective porosity and its effect on contaminant movement. The use of a distribution and multiple simulations using different values from the distribution is the method implemented to try to bound the effects of heterogeneity in effective porosity.

Fracture porosity must be estimated from fracture data or tracer tests because it cannot be measured directly *in situ*. Estimation of fracture porosity from fracture data uses the parallel-plate model and cubic law. A limitation to this approach is its assumption that the fractures are parallel yielding constant-thickness apertures, are infinite in extent, have the same properties everywhere, and are equally spaced. Because of these assumptions, estimates of fracture porosity based on this approach are considered to provide lower bound values (see discussion in Section 8.5.2.11). Effective porosities determined from tracer tests are dependent upon knowledge of the matrix diffusion process and on transport direction relative to the predominant fracture direction. If parameters related to matrix diffusion are uncertain, the effective porosities determined through numerical modeling will also be uncertain. If tracer migration in a tracer test occurs along a pathway that is near parallel with the primary interconnected fracture direction, transport times will predominantly be a function of advection and dispersion through the fractures with less influence of matrix diffusion as compared to other pathways. If, however, tracer migration occurs along a pathway at an angle to the primary fracture direction, transport will be retarded due to increased matrix diffusion along a more tortuous travel path (increased travel time and fracture surface area for diffusion). Therefore, use of time to peak arrival to estimate fracture porosity will yield different values depending on the geometry between the tracer travel path and the fracture direction. The closer the travel path is to the direction of fracturing, the smaller the estimated porosity and the closer the estimated value may reflect the actual fracture porosity.

Data scaling considerations are discussed in Section 8.7. These considerations are important because fracture characteristics determined at the measurement scale should not be expected to be representative at the scale of a regional model, where a single value is being implemented for the entire CAU for an individual model realization. If sufficient data were available, determination of an effective porosity distribution for an HGU on the regional scale should use the variance of the mean

values observed at various locations in the HGU at local scales rather than the variance of the entire distribution from all measurements in the HGU. This approach results in a reduction of the variance in the parameter at the regional scale. The extreme large and small values obtained from local measurements reflect local features. On a regional basis, these local features are not likely to be significant in controlling migration and the full range of parameter values from those features should not be used. Scaling of measurement data to the CAU scale needs to be considered in the final application of the effective porosity distributions to the Yucca Flat/Climax Mine CAU flow and transport model and sensitivity and uncertainty analyses.

8.9 Summary of Effective Porosity for the HGUs at the Yucca Flat/Climax Mine CAU

Effective porosity is defined as the volume of rock voids transmitting fluid (interconnected voids) per total volume of rock. All geologic material has primary (or interstitial) porosity due to the soil or rock matrix. Fractured geologic material also has secondary porosity as a result of the introduction of additional voids associated with the fractures. Flow and transport occurs through the rock matrix in an unfractured rock and through fractures, and sometimes also through the matrix, in a fractured rock. The two conceptualizations most often used for fractured rock are the double-porosity conceptualization or the dual-permeability conceptualization. For the former, advective and dispersive flow and transport occurs through the fractures only, and the matrix acts as a storage for solutes diffusing from the fractures into the matrix or from the matrix into the fractures. For the latter, advective and dispersive flow and transport occurs through both the fractures and the matrix. The double-porosity conceptualization will be used for the fractured HGUs in the Yucca Flat/Climax Mine CAU model.

The effective porosities for Yucca Flat were evaluated by HGU. The first step in the evaluation assessed whether the HGU behaves as a porous or fractured medium. Those HGUs determined to behave as a porous medium are the AA, VTA, PCU, TCU, and CCU HGUs. The effective porosity for these porous media HGUs was assumed to be represented by a fraction of the matrix porosity, which is discussed in Section 7.0. The value of the fraction varied depending on the type of sediments, grain size, and cementation or welding.

The HGUs determined to behave as fractured media are the WTA, LFA, and CA HGUs. For these HGUs, the fracture porosities from available sources were compiled and evaluated, and a distribution was developed. For fractured media, the effective porosity was assumed to be the same as the fracture porosity. Fracture porosity data were determined predominately from interpretations of

tracer tests and borehole fracture data. The spatial locations of the fracture porosity data used in developing the effective porosity distributions are shown in Figure 8-5.

The recommended effective porosity range and distribution for the WTA, LFA, and CA HGUs are summarized in Table 8-22 and shown graphically in Figure 8-6. The recommended range and distribution for each of these HGUs is similar with the lower bound at about 10^{-4} and the upper bound at about 2×10^{-2}. A skewed log triangular distribution is recommended for these HGUs, thus allowing a stronger weighting to the tracer test data. The modes, or most likely values, for the recommended distributions are slightly different for the three HGUs, with the value being highest for the LFA HGU and lowest for the WTA HGU (see Table 8-22). Because the distributions developed for these three HGUs are similar, a single distribution could be used for all of the fractured HGUs if needed (i.e., the data available for each HGU is sufficiently sparse that the three distributions could not be considered as distinctly different).

Table 8-22
Summary of Recommended Distributions for the Effective Porosity of the Fractured Aquifer HGUs for the Yucca Flat/Climax Mine CAU-Scale Model

HGU	Lower Bound	Upper Bound	Mode (Peak)	Distribution
WTA	1×10^{-4}	6×10^{-3}	3×10^{-3}	Skewed log triangular
LFA	1×10^{-4}	2×10^{-2}	6×10^{-3}	Skewed log triangular
CA	2×10^{-4}	2×10^{-2}	5×10^{-3}	Skewed log triangular

A skewed log triangular distribution is recommended because it reflects the fact that higher fracture porosities determined from tracer tests are considered more representative and less uncertain than the lower values determined from hydraulic conductivities, fracture spacings, and fracture apertures. The difference between the fracture porosities determined by the tracer test and hydraulic conductivity methods is a function of the portion of the fracture aperture effective during hydraulic and tracer testing. Hydraulic conductivity measurements are controlled by smaller apertures while migration during tracer tests is controlled by the mean fracture aperture (Tsang, 1992). Therefore, fracture porosities determined using hydraulic conductivity will be biased low, and thus they were given a lower probability in the distribution.

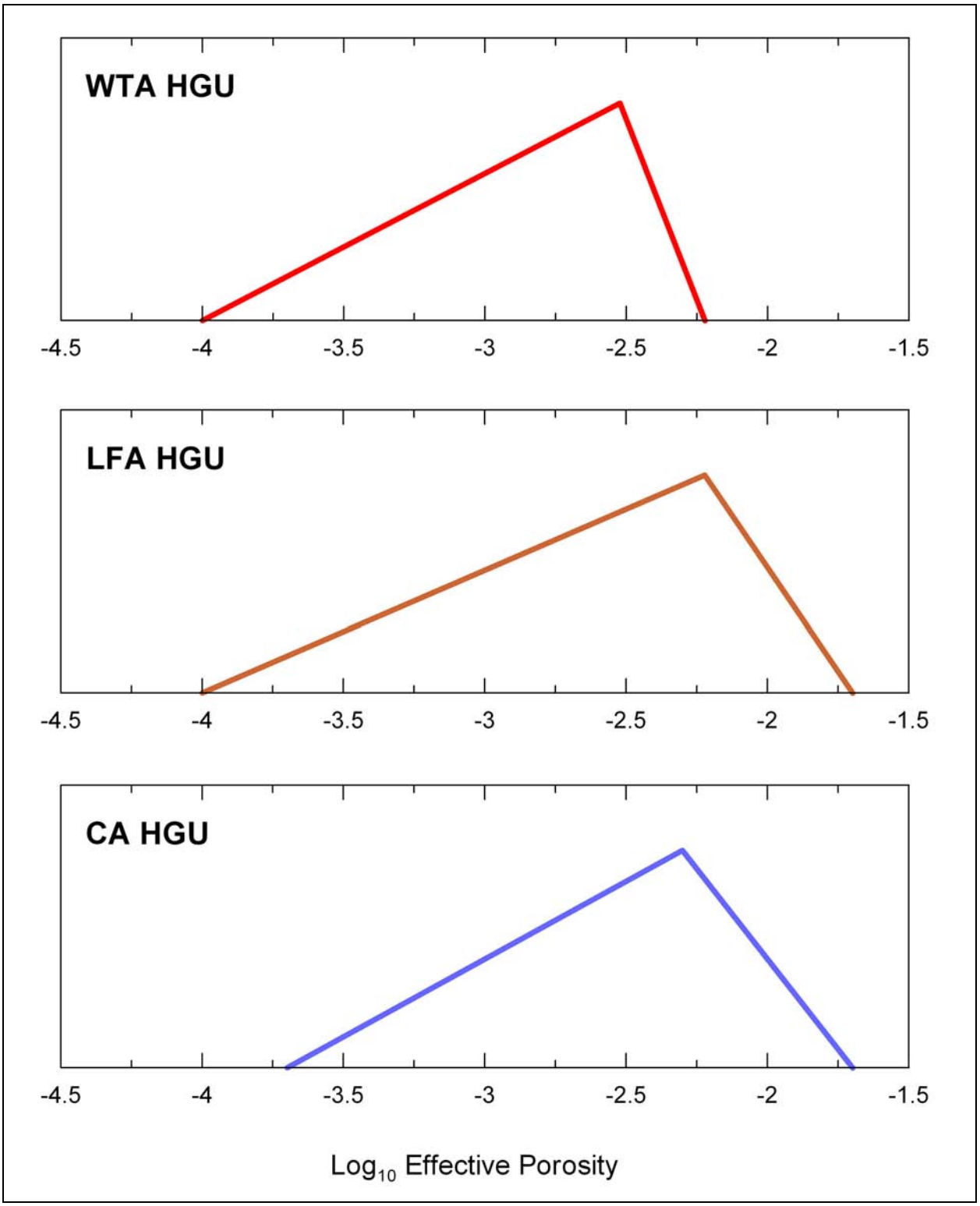

Figure 8-6
Recommended Effective Porosity Distributions for the Fractured Hydrogeologic Units

9.0 DISPERSIVITY

This section describes the role of dispersion in contaminant transport in groundwater, the available dispersivity data, analysis of these data, and the associated results. The objective is to use the data from the NTS and the scientific literature to develop an approach for selecting appropriate dispersivity values for use in the Yucca Flat/Climax Mine CAU groundwater flow and transport model. Conceptually, dispersivity is not a characteristic property of the geologic system but rather is a modeling parameter that accounts for the unmeasured and/or unspecified variability in the hydraulic properties within the flow and transport model domain. Dispersivity is often observed to be scale-dependent (i.e., a function of mean travel distance of solutes). Representative dispersivity values (at specific transport scales) are typically derived from data collected during tracer tests, and from model calibration of contaminant plumes and geochemical or environmental isotope distributions in regional flow systems. For additional discussion on the role of dispersion in contaminant transport, refer to the technical basis document entitled, *The Role of Dispersion in Radionuclide Transport - Data and Modeling Requirements* (SNJV, 2004d).

9.1 Role of Dispersion in Contaminant Transport

Unlike molecular diffusion, an inherent property of a solute in water, mechanical dispersion arises from the complex and heterogeneous movement of water and solute particles through an intricate network of pores and fractures. In the simplest terms, dispersion is the process of spreading a solute over a volume that is larger than it would be predicted based on estimates of the mean groundwater velocity. Because, in practice, the results of mechanical dispersion and molecular diffusion are not easily separable, hydrodynamic dispersion is defined as a combined effect of both processes. Freeze and Cherry (1979) write the following relationship for the hydrodynamic dispersion coefficient:

$$D = \alpha V + D_d \qquad (9\text{-}1)$$

where D is the hydrodynamic dispersion coefficient (L^2/t), α is dispersivity (L), V is the average groundwater flow velocity (L/t), and D_d is the coefficient of molecular diffusion (L^2/t) for the solute in the porous medium.

A conceptual understanding of mechanical dispersion along individual conduits can enhance the understanding of the processes involved. At relatively small scales in porous media, mechanical dispersion is the result of the velocity distribution in the pore spaces, changes in direction of flow, and variation in mean velocity as fluid moves from one pore space to the next. Mechanical dispersion in fractured networks can grow complicated as mixing occurs in preferential pathways. One might visualize the complicated system of fractures where fractures with varying dip and strike, aperture thickness, and aperture surface roughness are encountered in geologic systems such as that of the Yucca Flat/Climax Mine CAU. At larger scales, dispersion is controlled by the spreading caused by the heterogeneous nature of the geologic system.

The effect of dispersion during transport of solutes in geologic systems is commonly quantified in terms of longitudinal and transverse dispersivities. Longitudinal dispersivity is defined relative to the direction of flow, whereas transverse dispersivity is defined relative to directions normal to the flow direction. Determination of appropriate values for these dispersivities is important for predicting contaminant concentrations in groundwater flow systems. These parameters affect the spreading of contaminants at a macroscopic scale. Theoretically, hydrodynamic dispersion is independent of the scale of measurement as long as the measurement is made within a representative elementary volume (Bear, 1972; Bear and Verruijt, 1990). However, in reality, the representative elementary volume changes with the size of the measurement scale because the heterogeneity introduced in the expanded domain results in larger overall dispersivity values.

Dispersivities estimated from laboratory experiments are found to be much smaller that those determined for field conditions. Dispersivity values representative of field conditions are derived from data collected during tracer experiments or observations of plume migration, geochemical data, or environmental isotope data. Field-scale dispersion observed in large-scale plumes or geochemical/isotope data is generally accepted to be the result of the heterogeneous velocity field at scales smaller than the plume or scale of investigation. Heterogeneity at scales larger than the plume causes changes in the mean position of the plume; however, if the plume encompasses several

heterogeneous domains, the result may appear as a larger dispersivity. The nature of heterogeneity differs from site to site. Dispersivity values may vary by orders of magnitude depending on the nature of the site and the transport scale of interest. Unless the transport properties of each of the domains are characterized in detail, a lumped dispersivity value may be used to simulate the plume.

Based on data from studies in a variety of geologic settings, dispersivity appears to be scale-dependent (Lallemand-Barres and Peaudecerf, 1978; Pickens and Grisak, 1981a and b; Gelhar et al., 1992; Neuman, 1990 and 1995; Neuman and Di Federico, 2003; Schulze-Makuch, 2005). In the dispersivity-scale analyses presented in SNJV (2005b), it was noted that the scale/dispersivity relationship is not linear.

Field-scale tracer tests are typically limited to a few hundred meters in scale, so experimentally derived dispersivity values are available only for relatively short transport distances as compared to the transport distances of interest for predictions of long-term contaminant transport. Dispersivity data for larger scales have been determined at some sites through transport model calibration to observations of concentration distribution within contamination plumes. With a site as large and as varied as the Yucca Flat/Climax Mine CAU, it is impractical to conduct tracer tests in enough locations to accurately estimate dispersivity, particularly at a physical scale representative of transport for the 1,000-year period of interest. Tracer tests conducted at scales of a few tens to hundreds of meters will not yield dispersivity values appropriate at the CAU scale because of the apparent trends in dispersivity with scale. Time and budget constraints make it nearly impossible to perform a tracer test at the CAU scale. Thus, the appropriate dispersivity values to use for the CAU-scale modeling will depend on the expected distance of transport. As a result, it is helpful to know the expected distances of contaminant transport *a priori* to best assess the range of dispersivity values most appropriate for modeling efforts. Future Yucca Flat/Climax Mine CAU modeling activities will provide information about expected radionuclide transport paths and distances from source locations of interest. Based on the estimated distances, expected values and bounds of dispersivities may be estimated using the statistical relationships developed from this study. These bounds and statistical parameters will also be useful in uncertainty analysis for transport of contaminants.

This section is intended to document the available dispersivity data from the NTS region and the general literature and to provide relationships for use in estimating appropriate values for the Yucca Flat/Climax Mine CAU contaminant transport model and for performing uncertainty analyses.

9.2 Data Compilation and Data Transfer

The dispersivity data types, data sources, and data documentation evaluation process are described in this section. Data from the Yucca Flat/Climax Mine HFM area and data from other NTS CAUs, YMP, and Nye County were used for this analysis due to the unavailability of comprehensive data from the Yucca Flat/Climax Mine HFM area for all HGUs. Figure 9-1 shows the source locations for the NTS-area data used in the analysis. All data locations used in quantitative analyses are identified in Appendix G and the associated dataset referenced in Section G.4.0. Individual discussions of the applicability of the transferred data are provided for each HGU. There are limited data from the NTS area to determine a Yucca Flat/Climax Mine specific distribution for the parameter values. Data from literature for locations worldwide were used to evaluate the NTS area data with respect to the general distribution of dispersivity and scale dependence. A quantitative assessment of the sensitivity of transport modeling to the uncertainty in this parameter cannot be provided before the transport model development. The parameter description discusses the importance of this parameter.

9.2.1 Data Types

Dispersivity values are derived from interpretation of tracer tests or studies of contaminant plume migration. The types of data used to document dispersivity include the location of the site, primary lithology of the rocks, identity of the tracer or contaminant that migrated, transport scale, data analysis method, dispersivity interpretation results, and data source.

9.2.2 Data Sources

Dispersivity data have been determined from one RNM investigation (CAMBRIC) and several tracer tests conducted at or near the NTS. These studies were conducted at the following sites (Figure 9-1):

- CAMBRIC site, Frenchman Flat, NTS
- BULLION FGE, Pahute Mesa, NTS
- C-holes Complex, Yucca Mountain
- Amargosa Tracer Calibration Site, Amargosa Desert, NV

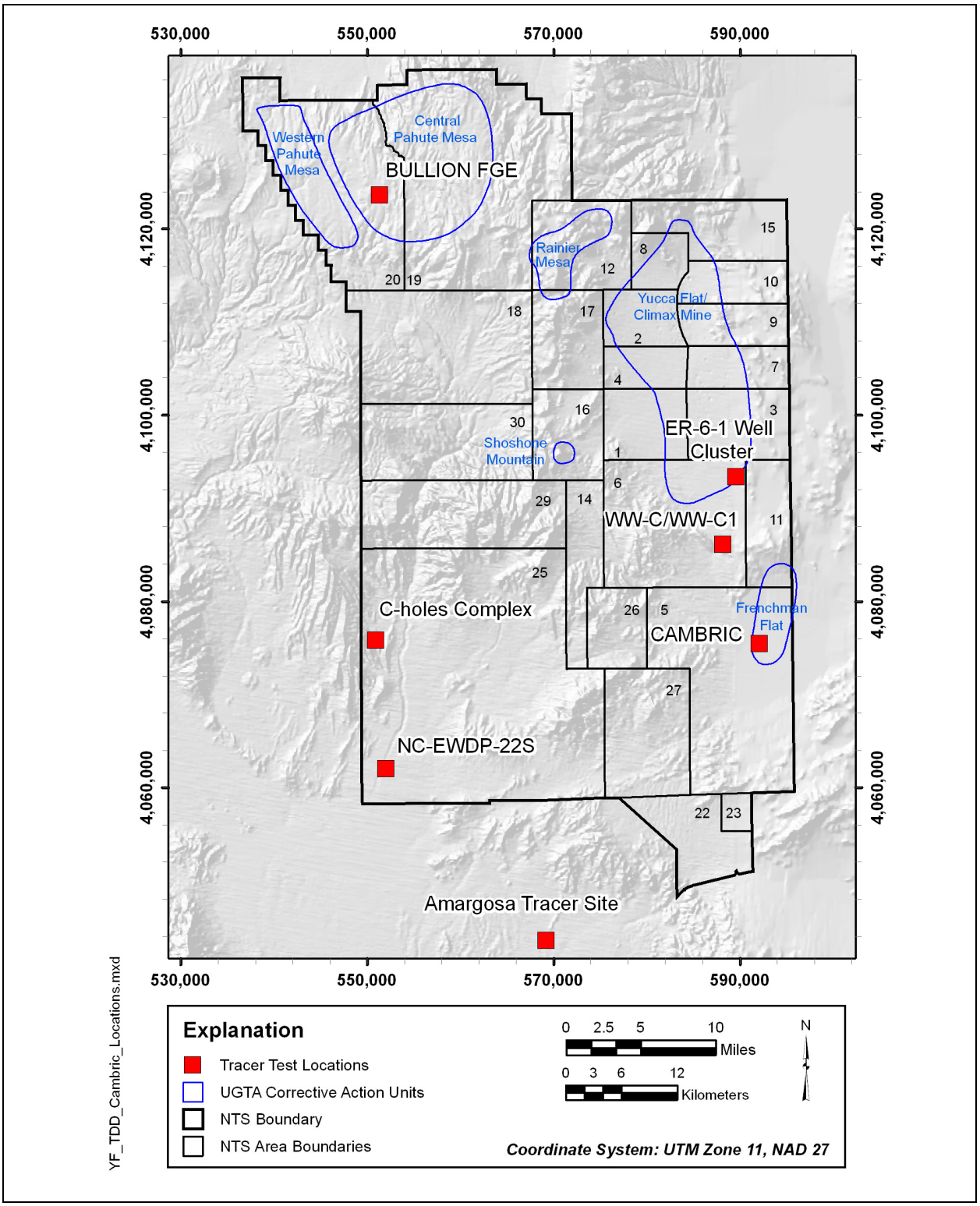

Figure 9-1
Locations of CAMBRIC Radionuclide Migration Experiment and Tracer Tests at NTS and Vicinity

- C-Well Site, Yucca Flat, NTS
- ER-6-1 Well Cluster, Yucca Flat, NTS
- Nye County Early Warning Drilling Program (NC-EWDP) Site 22, Fortymile Wash, NTS

Additional data available from non-NTS sites were obtained from the scientific literature. Gelhar et al. (1992) published a critical review of data on field-scale dispersion in aquifers reporting data from 59 different field sites. The most recent summary of laboratory and field dispersivity data is presented in Schulze-Makuch (2005). He states that he has summarized data from 109 authors, including those summarized in Gelhar et al. (1992). Dispersivity data from Gelhar et al. (1992), selected sources of values representative of field values cited by Schulze-Makuch (2005), and other investigations reported in the scientific literature were used to supplement the tracer test data from the NTS and vicinity to develop a dataset of dispersivity versus scale.

9.2.3 Data Documentation Evaluation

The DDE_F in the database was assigned to the records based on the level of reliability and the amount of documentation available (see Section 5.0). The BULLION FGE and the ER-6-1 Well Cluster multiple-well tracer tests are the only tracer tests conducted under the Environmental Restoration Project (ERP). These tests were conducted following an established QA program, and the data were assigned a DDE_F of 1 because adequate documentation is available. Documentation of the experiments conducted at the CAMBRIC site and the C-holes Complex of Yucca Mountain were assigned a DDE_F of 1. At the WIPP site, the data were assigned a level of 3 as these tests were conducted outside of the ERP but are well documented under a Nuclear Quality Assurance (NQA)-1 program. The DDE_F for the tracer tests conducted at the C-Well Site in Yucca Flat and at Amargosa Desert was assigned a level of 4 as the data were not documented under an NQA-1 program. All other data were assigned a DDE_F of 5 as sufficient documentation of the procedures and their application during field data collection and analysis are not readily available.

9.3 Data Evaluation

The data evaluation approach consisted of summarizing the existing NTS and vicinity studies, including the range of dispersivity values obtained by different investigators. Data from dispersivity studies available in the scientific literature were also incorporated to determine a range of values appropriate for the scales of interest for the Yucca Flat/Climax Mine CAU transport modeling effort.

This section provides descriptions of the available data, data quality evaluation, dataset analysis approach, and derived dispersivity-scale relationship results.

The dispersivity data derived from tracer tests and observations of plume migration, geochemical data, or environmental isotope data were compiled into a comprehensive dataset described in Appendix G. The dataset includes 208 records for longitudinal dispersivity. A subset of the data sources reporting longitudinal dispersivity also provides transverse dispersivity data. Summary descriptions of the dispersivity data and observations from an initial examination of the data are provided in the following sections.

9.3.1 NTS and Vicinity Dispersivity Data

This subsection describes dispersivities obtained from the RNM experiment and tracer tests conducted to date at the NTS and vicinity. Results derived from the migration and tracer tests data using different interpretation approaches are included. The data for these experiments are summarized in Table 9-1 with regard to the aquifer types and geology, test method, tracer type, analytical method, and the derived longitudinal dispersivities. Further information and discussion on the test sites, experimental methods, interpretation approaches, and interpreted dispersivity results for the CAMBRIC site, BULLION FGE, C-holes Complex, Amargosa Tracer Calibration Site, and C-Well Site are presented and discussed in detail in *Phase II Contaminant Transport Parameters for the Groundwater Flow and Contaminant Transport Model for Corrective Action Unit 98: Frenchman Flat, Nye County, Nevada* (SNJV, 2005b) and are not repeated here. Summary descriptions and discussions for the tracer tests conducted more recently at the NC-EWDP Site 22 and ER-6-1 Well Cluster and their interpreted dispersivities are presented in the following subsections.

Additional estimates of longitudinal dispersivity were obtained from evaluating the breakthrough curves from convergent-flow tracer tests at the NTS and vicinity using equations derived by Welty and Gelhar (1989). For convergent-flow tracer tests with a pulse input of tracer introduced at the tracer-addition well, Welty and Gelhar (1989) provide an expression for calculating longitudinal dispersivity (α) based on the distance between wells (R), time t_m to peak concentration (C_m), and change in time (Δt) between the times t_1 and t_2 to reach concentration $e^{-1}C_m$ on the rising and falling limbs, respectively, of the breakthrough curve (see Figure 9-2 for an illustration of these terms). Under the assumption that longitudinal dispersivity divided by the distance between the production

Table 9-1
Dispersivity Information Summary from Studies at the Nevada Test Site and Vicinity
(Page 1 of 2)

Site Location	Test Site Geology	Scale of Test (m)	Test Method	Tracers	Analysis Method	Longitudinal Dispersivity (m)	References
CAMBRIC Test, Frenchman Flat, Nevada	Tuffaceous Alluvium	91	Radial converging	Nuclear test radionuclides: ^{3}H	Sauty, 1980	2.0	Burbey and Wheatcraft, 1986
				Nuclear test radionuclides: ^{3}H	Sauty, 1980	9.1	Travis et al., 1983
				Nuclear test radionuclides: ^{3}H	Sauty, 1980	15.1	Thompson, 1988; Ogard et al., 1988
				Nuclear test radionuclides: ^{36}Cl, ^{3}H	Welty and Gelhar, 1989	3.1 - 9.6	Current Analysis; Thompson, 1991
BULLION FGE, Pahute Mesa, Nevada	Fractured Lava-Flow Aquifer, Calico Hills Formation	130.2	Radial converging	PFBA, DFBA, I, CML, polystyrene microspheres	MODFLOWT calibration	10 (horizontal) 3 (horizontal transverse) 2 (vertical transverse)	IT, 1998
		41.5 - 130.2			RELAP (Reimus and Haga, 1999)	8.7 - 25.3	IT, 1998
		88.7 - 130.2			Welty and Gelhar, 1989	3.9 - NA [a]	Current Analysis
C-holes Complex, Yucca Mountain, Nevada	Prow Pass Tuff (fractured)	30	Unbalanced dipole	TFBA, I	Moench, 1989	0.27 [b]	Bechtel SAIC, 2004c
				PFBA, Br, Cl, Li	RELAP (Reimus and Haga, 1999)	13.0	Bechtel SAIC, 2004c
				TFBA, PFBA, Cl	Welty and Gelhar, 1989	1.7 - 8.6	Current Analysis
	Bullfrog Tuff (fractured)	30	Unbalanced dipole	PFBA, Br, Li	RELAP (Reimus and Haga, 1999)	3.2	Bechtel SAIC, 2004c
				PFBA	Welty and Gelhar, 1989	0.8 - 2.6	Current Analysis

Table 9-1
Dispersivity Information Summary from Studies at the Nevada Test Site and Vicinity
(Page 2 of 2)

Site Location	Test Site Geology	Scale of Test (m)	Test Method	Tracers	Analysis Method	Longitudinal Dispersivity (m)	References
Amargosa Tracer Calibration Site, Amargosa Desert, Nevada	Cambrian Bonanza King Dolomite (fractured)	122.8	Doublet recirculating	^{3}H, ^{25}S, Br	Grove, 1977	15 - 30.5	Leap and Belmonte, 1992
C-Well Site, Yucca Flat, Nevada	Fractured Limestone	29.3	Radial converging test at WW-C and WW-C1	Fluorescein dye	Welty and Gelhar, 1989	0.6 - 1.4	Winograd and West, 1962 - data; Shaw, 2003a - calculation
ER-6-1 Well Cluster	Fractured Limestone	64	Radial converging	2,4,5-TFBA, I (lower zone)	RELAP (Reimus and Haga, 1999)	27 - 29	SNJV, 2006d; Current Analysis
				2,4,5-TFBA, I (lower zone)	Welty and Gelhar, 1989	3.1 - 10.8	
				PFBA (upper zone)	RELAP (Reimus and Haga, 1999)	19 - 22	SNJV, 2006d
				PFBA (upper zone)	Welty and Gelhar, 1989	3.0 - NA [a]	Current Analysis
NC-EWDP Site 22	Alluvium	18	Radial converging	2,4,5-TFBA, DFBA	RELAP (Reimus and Haga, 1999)	2.7 - 5	Reimus, 2006
					Moench, 1989 and 1995	0.3 - 3	Umari et al., 2006
					Welty and Gelhar, 1989	0.8 - 3.6	Current Analysis

[a] NA refers to case where falling limb of breakthrough curve was insufficient to allow calculation of dispersivity estimate using the equation from Welty and Gelhar (1989) that requires both rising and falling limbs of the breakthrough curve.
[b] The interpretation accounted for plume spreading by assuming a long, slow release of tracer from the injection well and, therefore, it was not necessary to invoke strong dispersion in the aquifer.

CML - Carboxylate-modified latex

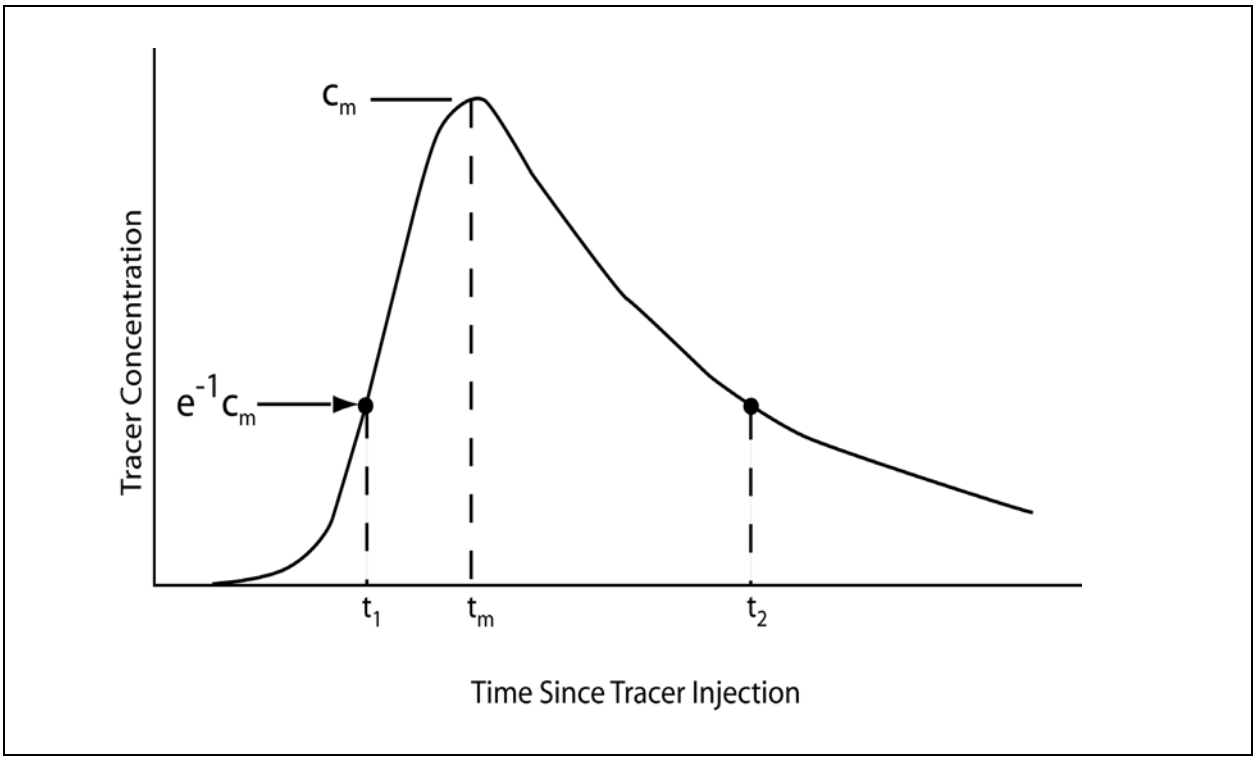

Figure 9-2
Schematic of Tracer Breakthrough Curve at the Pumping Well of a Convergent-Flow Tracer Test

and tracer-addition wells (α/R) is much less than unity, a simplified equation may be used to estimate dispersivity (Welty and Gelhar, 1989):

$$\alpha = \frac{3R}{(64)}\left(\frac{\Delta t}{t_m}\right)^2 \qquad (9\text{-}2)$$

In some cases, the falling limb of the breakthrough curve may exhibit a strong tailing behavior as a result of processes beyond that due to dispersion alone (e.g., matrix diffusion effects in double-porosity media as may occur at locations such as the BULLION site, ER-6-1, C-holes Complex, and C-Well Site; continued source release from the assumed tracer pulse input zone as may be the case at CAMBRIC; or tracer loss not available for capture because of drift caused by natural groundwater gradient). In such cases, it may be better to calculate the dispersivity based just on the rising limb of the breakthrough curve using Equation (9-2) where Δt is equal to twice the time period from concentration $e^{-1}C_m$ to peak concentration C_m. This approach was used successfully by Jones et al. (1992) for estimating dispersivity during double-porosity model calibration of breakthrough curves at three sites in the fractured Culebra Dolomite at the WIPP site in New Mexico. For the

convergent-flow tracer tests at the BULLION FGE, CAMBRIC site, ER-6-1, C-holes Complex, and C-Well Site, additional analyses were conducted to estimate a range for longitudinal dispersivity using both the rising and falling limbs of the breakthrough curve and using only the rising limb of the breakthrough curve. The dispersivities calculated using the rising limb may be slight underestimates because they do not take into account the asymmetrical nature of the breakthrough curve, whereas the dispersivities calculated using both the rising and falling limbs are overestimates because they include the effects of all processes that cause additional spreading such as matrix diffusion and continuing source release. Comparison of the results in Table 9-1 using different interpretation methods shows that longitudinal dispersivities estimated using the Welty and Gelhar (1989) method tend to be smaller than those using the Reimus and Haga (1999) RELAP method. A principal difference in interpretation approach is that the Welty and Gelhar (1989) method uses the time of arrival of peak concentration whereas the Reimus and Haga (1999) method uses the mean tracer arrival time.

In the dataset (see Appendix G) and for dispersivity-scale analysis purposes, a geometric average is calculated for cases where multiple dispersivities for a particular flow path at a site are available from different tests or different interpretation methods. For the data analysis reported by Schulze-Makuch (2005), he states: “If a range in longitudinal dispersivity was provided, the geometric mean was used (Table 1). The geometric mean was thought to represent a more suitable mean for dispersivity because the values varied commonly by an order of magnitude.” Where dispersivities were interpreted with RELAP using both radial and linear flow cases, only the values from the radial flow interpretation were used unless there was strong evidence of the possibility of linear flow.

9.3.1.1 Nye County Early Warning Drilling Program Site 22

Single-hole and cross-hole tracer tests have been conducted at Site 22 of the NC-EWDP, located in the southwestern corner of the NTS, to investigate transport characteristics of the alluvium. The complex consists of four wells arranged in an approximate square with 18-m sides. One of these wells (22S) is screened across multiple intervals and can be pumped at a high rate. The other three wells (22PA, 22PB, and 22PC) are essentially nested piezometers. A cross-hole tracer test was conducted at this site in early 2005, with well 22S as the pumping well and wells 22PA and 22PC as the tracer-injection wells. Injected tracers were TFBA, LiBr, and LiCl into well 22PA and DFBA into

well 22PC. A second cross-hole tracer test was conducted in the late summer/early fall 2005, with well 22S as the pumping well and well 22PA as the injection well.

The TFBA and DFBA breakthrough curves from the first cross-hole tracer test were interpreted by Umari et al. (2006) using the Moench (1989 and 1995) analytical solution to the advection-dispersion equation. The observed TFBA breakthrough (22PA to 22S pathway) exhibited three inflection points, suggesting three flow paths. Umari et al. (2006) separated this curve and analyzed each peak individually. They obtained longitudinal dispersivity values of 0.3, 3.0, and 2.4 m for matches to the first, second, and third peaks, respectively. They matched the single peak of the DFBA breakthrough curve (22PC to 22S pathway) using a longitudinal dispersivity of 3.0 m.

The breakthrough curves from the cross-hole tracer tests at Site 22 of the NC-EWDP were also analyzed by Reimus (2006) using the semi-analytical model RELAP. The fitting parameters for the RELAP analysis were the mean fluid residence time, the Peclet number (equal to the distance between the injection and withdrawal wells divided by the longitudinal dispersivity), the tracer mass fraction participating in the tracer test, and the mass transfer coefficient for matrix diffusion (equal to the square root of the matrix diffusion coefficient times the matrix porosity divided by the fracture half aperture).

Reimus (2006) also analyzed the three inflections observed in the TFBA breakthrough curve from the first test (22PA to 22S pathway) separately. These analyses yielded longitudinal dispersivities of 2.7, 5, and 3.4 m for the first, second, and third peaks, respectively. His analysis of the DFBA breakthrough curve from the first test (22PC to 22S pathway) yielded a longitudinal dispersivity of 3.1 m. Reimus (2006) also analyzed the results from the second cross-hole tracer test conducted at the site. For the second test (22PA to 22S pathway only), the breakthrough curve exhibited two inflection points. Reimus (2006) analyzed those two points separately and obtained dispersivities of 2.7 and 4.6 m for the first and second peaks, respectively.

The TFBA and DFBA breakthrough curves from the first cross-hole tracer test were also analyzed using the method of Welty and Gelhar (1989), as discussed in Section 9.3.1. Longitudinal dispersivities of 1.8 and 3.6 m were calculated based on the TFBA breakthrough curve, and values of 0.8 and 2.2 m were calculated based on the DFBA breakthrough curve.

9.3.1.2 ER-6-1 Well Cluster Tracer Test

An MWAT-TT was conducted in the LCA at the ER-6-1 Well Cluster located in Yucca Flat from late April to late July 2004. The test details discussed here were taken from SNJV (2005e and f). Well ER-6-1#2 was the pumping well, and tracers were injected into upper and lower completion intervals in ER-6-1, located 64 m from the pumping well, and into ER-6-1#1, located 51 m from the pumping well. The direction of tracer migration from the injection wells to the pumping well is approximately aligned with the dominant local fracture orientation. The pumping rate in ER-6-1#2 averaged 33.0 L/s over a 434.3-m-thick interval during the MWAT-TT. Tracer injection occurred in four stages. The first stage consisted of the injection of microspheres into the upper zone in ER-6-1; the second stage consisted of the injection of 2,5-DFBA into ER-6-1#1; the third stage consisted of the injection of NaI and 2,4,5-TFBA into the lower zone in ER-6-1; and the fourth stage consisted of the injection of LiBr, LiCl, and PFBA into the upper zone in well ER-6-1. For each stage, tracer injection was followed by the injection of chase water to flush the tracer from the borehole. A complete description of tracer breakthrough curves for this test can be found in SNJV (2005f).

The tracer breakthrough curves were analyzed to estimate longitudinal dispersivity using the method of Welty and Gelhar (1989), as discussed in Section 9.3.1. For the flow path that exhibited the most rapid breakthrough of tracer at the pumping well (ER-6-1 lower zone to ER-6-1#2), longitudinal dispersivities of about 3.1 and 10.8 m were calculated based on analysis of the I and TFBA breakthrough curves. For the flow path that exhibited the slower breakthrough of tracer from ER-6-1 to the pumping well (ER-6-1 upper zone to ER-6-1#2), a longitudinal dispersivity of about 3.0 m was calculated based on analysis of the rising limb of the PFBA breakthrough curve. The falling limb of the breakthrough curve was insufficient to estimate dispersivity using both rising and falling limbs of the breakthrough curve. Dispersivity was not estimated for the flow path from injection well ER-6-1#1 to the pumping well ER-6-1#2 because a peak concentration for the breakthrough curve was not attained, and measured concentrations at the pumping well were at or near the detection limit.

Observed tracer breakthrough curves from the tracer tests at the ER-6-1 Well Cluster were analyzed by SNJV (2006d) using the semi-analytical model RELAP. The fitting parameters for the RELAP analysis were the mean fluid residence times, the Peclet number (equal to the distance between the injection and withdrawal wells divided by the longitudinal dispersivity), the tracer mass fraction

participating in the tracer test, and the mass transfer coefficient (equal to the square root of the matrix diffusion coefficient times the matrix porosity divided by the fracture half aperture).

Analysis of I and TFBA, injected into the lower zone in ER-6-1, using RELAP was performed using both single- and double-porosity conceptualizations. This analysis yielded longitudinal dispersivities of 27 and 29 m for the single- and double-porosity conceptualizations, respectively. The SNJV (2006d) report states that two inflow zones were identified by flow logging in pumping well ER-6-1#2 that correspond to the upper injection zone in ER-6-1. The report analyzed the PFBA breakthrough in the upper zone, considering these inflow locations as individual pathways. Based on spinner log results, SNJV (2006d) assumed production rates of 40 and 10 percent of the total rate for pathways 1 and 2, respectively. The RELAP analysis of the PFBA breakthrough curve yielded a longitudinal dispersivity of 19 m for pathway 1 (the upper inflow zone), and a value of 22 m for pathway 2 (the lower inflow zone) assuming a single-porosity conceptualization.

The interpreted dispersivity for the pathway from injection well ER-6-1#1 to pumping well ER-6-1#2 using RELAP is very uncertain and has not been included in the dataset because all of the measured tracer concentration data at the pumping well were near the detection limit and a peak concentration for the breakthrough curve was not attained.

9.3.2 Non-NTS Dispersivity Data

Dispersivity data are available for many locations outside the NTS from the scientific literature with many cases summarized in Gelhar et al. (1992) and Schulze-Makuch (2005). These references provide detailed tables summarizing dispersivities, scale of transport, and other relevant information describing studies for both tracer tests and contaminant or environmental tracer transport modeling investigations. In addition, dispersivity data interpreted and published in the scientific literature from other tracer tests and modeling studies have been included in the dataset for use in developing a relationship between dispersivity and scale of transport for the Yucca Flat/Climax Mine CAU.

Gelhar et al. (1992) reviewed dispersivity observations from 59 different field sites worldwide. Their review included tabulated information on site location, description of aquifer material, average aquifer saturated thickness, hydraulic properties, effective porosity, mean pore velocity, flow configuration, dimensionality of monitoring network, tracer type, method of data interpretation,

overall scale of observation, and longitudinal and transverse dispersivities from original sources. Gelhar et al. (1992) classified the dispersivity data into three reliability classes corresponding to the data reliability evaluation flags described in Section 9.3.3. They found that, at a given scale, dispersivity varied over several orders of magnitude, with the higher-reliability data tending to be in the lower part of the dispersivity range. Neuman (1990) noted that part of the large scatter is due to experimental and interpretive errors. An example of an interpretation issue that can lead to apparent scaling of dispersivity is discussed by Domenico and Robbins (1985), where they present calculations showing that interpreted dispersivity will be scaled larger whenever an (n-1)-dimensional model is calibrated to describe transport in an n-dimensional system.

Analyses by various authors indicate a trend of systematic increase in the longitudinal dispersivity with increase in the observation scale. The longitudinal dispersivities reported by Gelhar et al. (1992) ranged from 10^{-2} to 10^{4} m for travel distances ranging from 10^{-1} to 10^{5} m; however, the largest distance with high-reliability data was only 250 m, and the largest high-reliability longitudinal dispersivity was only 4 m. Gelhar et al. (1992) also concluded from the data that, overall, dispersivity values tended to scatter over a similar range for both porous and fractured media.

Schulze-Makuch (2005) gathered data from additional sources and added the data to those presented by Gelhar et al. (1992). Schulze-Makuch (2005) presents 184 additional dispersivity values from 39 authors in a similar fashion to that of Gelhar et al. (1992). An evaluation of some of the data summarized by Schulze-Makuch (2005) has revealed a number of discrepancies such as:

1. Incorrectly reporting dispersivity (e.g., average dispersivity value referenced from Rivett et al. [1994] should be 49 cm, not 49 m; and transverse horizontal dispersivities from Lavenue and Domenico [1986] were reported as longitudinal dispersivities).
2. Using two to five dispersivity values for identical flow paths from some reference sources, which could lead to overrepresentation and bias if multiple values are included in the dataset for the same tested flow path (e.g., Ptak and Teutsch [1994]; D'Alessandro et al. [1997]; and Himmelsbach et al. [1998]).
3. Inappropriately selecting transport scale (e.g., use of the total model grid length rather than the mean travel distance for regional plumes presented in Avon and Bredehoeft [1989] and Chapelle [1986]).
4. Omitting dispersivities reported in sources (e.g., Chiang et al. [1989]; Engesgaard et al. [1996]; Mas-Pla et al. [1992]; and D'Alessandro et al. [1997]).

Because direct inclusion of all of the data reported in Schulze-Makuch (2005) could lead to undesirable uncertainty in the combined dataset constructed to support development of a dispersivity-scale relation, it was decided to only use data from those original sources that could be readily obtained and verified with emphasis on field studies with scales of interest (i.e., greater than 1 m). Where multiple dispersivity values where reported for the same flow path (e.g., from multiple tests and/or multiple analysis methods) in the original data sources, a geometric mean value was calculated for inclusion in the dataset.

9.3.3 Data Quality Evaluation

The dataset developed for the Yucca Flat/Climax Mine CAU includes a DQE_F that corresponds to the levels of reliability defined by Gelhar et al. (1992) and later adopted by Schulze-Makuch (2005). The reliability levels were defined using the following criteria:

- Level 1: Corresponds to "High Reliability," Level I of Gelhar et al. (1992). The tracer study meets the following criteria: (1) tracer test was either ambient flow, radial diverging flow, or two-well instantaneous pulse test without recirculation; (2) tracer input was well defined; (3) tracer was conservative; (4) spatial dimensionality of the tracer concentration measurements was appropriate; and (5) analysis of the tracer concentration data was appropriate and consistent with the measurements.
- Level 2: Corresponds to "Intermediate Reliability," Level II of Gelhar et al. (1992). The tracer study does not meet the criteria for high or low reliability.
- Level 3: Corresponds to "Low Reliability," Level III of Gelhar et al. (1992). The tracer study meets the following criteria: (1) two-well recirculating test with step input was used; (2) single-well, injection-withdrawal test where tracer monitoring at the single well was used; (3) tracer input was not clearly defined; (4) tracer breakthrough curve was assumed to be the superposition of breakthrough curves in separate layers; (5) measurement of tracer concentration in space was inadequate; and (6) equation used to obtain dispersivity was not appropriate for the data collected.

The "high-reliability" dispersivity values were considered to be accurate within a factor of two, and the "low-reliability" values were considered to be no more accurate than one to two orders of magnitude.

9.3.4 General Description of Dispersivity-Scale Dataset

9.3.4.1 Longitudinal Dispersivity

A log-log plot of the longitudinal dispersivity versus scale data developed from the NTS and non-NTS sources discussed above, including the reliability information (Levels 1, 2, or 3), is shown

in Figure 9-3. The longitudinal dispersivity values in the dataset range from 5×10^{-3} to 2.2×10^{4} m for field transport distances ranging from 1 to 9×10^{4} m. Longitudinal dispersivity varies from two to three orders of magnitude for a given scale of transport. The data show a systematic increase in longitudinal dispersivity with increasing transport scale which is consistent with findings by previous authors (e.g., Gelhar et al., 1992). The largest scale with high-reliability data (Level 1) was only 266 m, with a longitudinal dispersivity of 0.55 m. The high-reliability dispersivity data tend to be somewhat smaller in magnitude than other data at any particular scale. This was also observed by Gelhar et al. (1992), who noted that dispersivities in the lower half of the range are favored for a given scale. At the larger transport scales (e.g., greater than 300 m), only lower-reliability data are available, which could lead to greater uncertainty in longitudinal dispersivity for large plumes or longer transport distances.

The longitudinal dispersivity values determined from the NTS region are compared with the worldwide values in Figure 9-4. The longitudinal dispersivities from the NTS region range from 0.9 to 23.2 m (average values for individual flow paths) with transport scales ranging from 18 to 130 m. It can be seen that the longitudinal dispersivities determined from the contaminant migration experiment and the tracer tests conducted in the NTS and vicinity are consistent with those obtained from other studies in the literature at similar scales.

There are insufficient data across all transport scales for various rock types to allow for a meaningful assessment of whether the dispersivity-scale relationship is a function of rock type. Hence, the analysis to determine a dispersivity-scale relationship used the entire dataset lumped together using all rock types.

Cumulative probability distribution functions for scale and longitudinal dispersivity are shown in Figures 9-5 and 9-6, respectively. The median scale is about 30 m, and the median longitudinal dispersivity is 2 m. For the scale data, 95 percent of the data fall between 3 and 19,650 m, and 75 percent are less than 100 m. For the longitudinal dispersivity data, 95 percent of the data fall between 0.03 and about 174 m, and 75 percent is less than 8 m. These figures show that the majority of the data are at a scale much less than that for the Yucca Flat/Climax Mine CAU model and that the majority of the determined longitudinal dispersivities are less than 10 m.

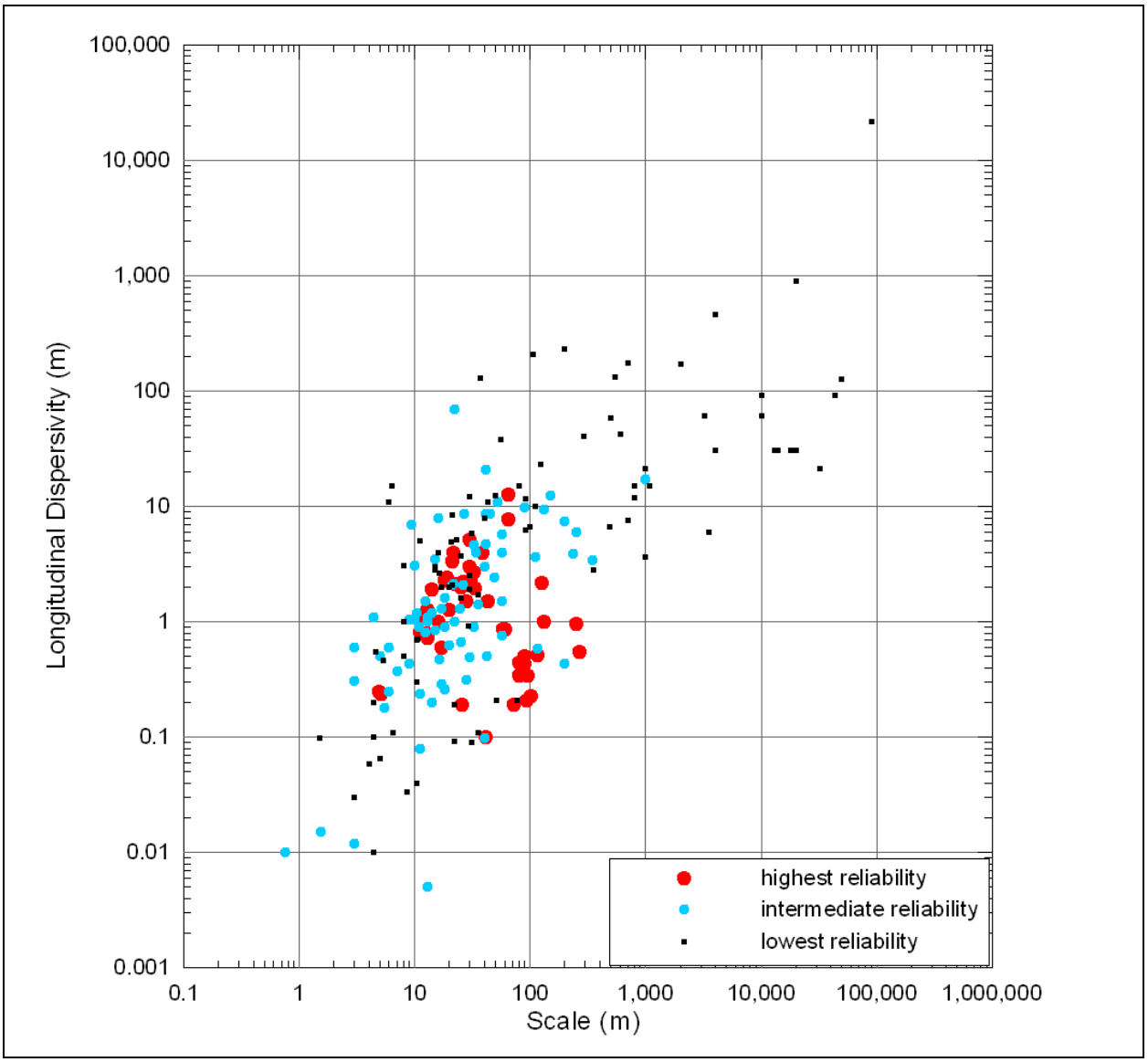

Figure 9-3
Log-Log Plot of Longitudinal Dispersivity as a Function of Measurement Scale for All Rock Types

9.3.4.2 Transverse Dispersivities

The data available for transverse horizontal dispersivity, or the spreading of solutes at right angles to the direction of horizontal groundwater flow, are shown in Figure 9-7(a). Transverse horizontal dispersivities up to 1,370 m have been reported. Although the data are much more sparse compared to that available for longitudinal dispersivity, the transverse horizontal dispersivity data exhibit the same pattern of increasing value with transport scale as does the longitudinal dispersivity. Although

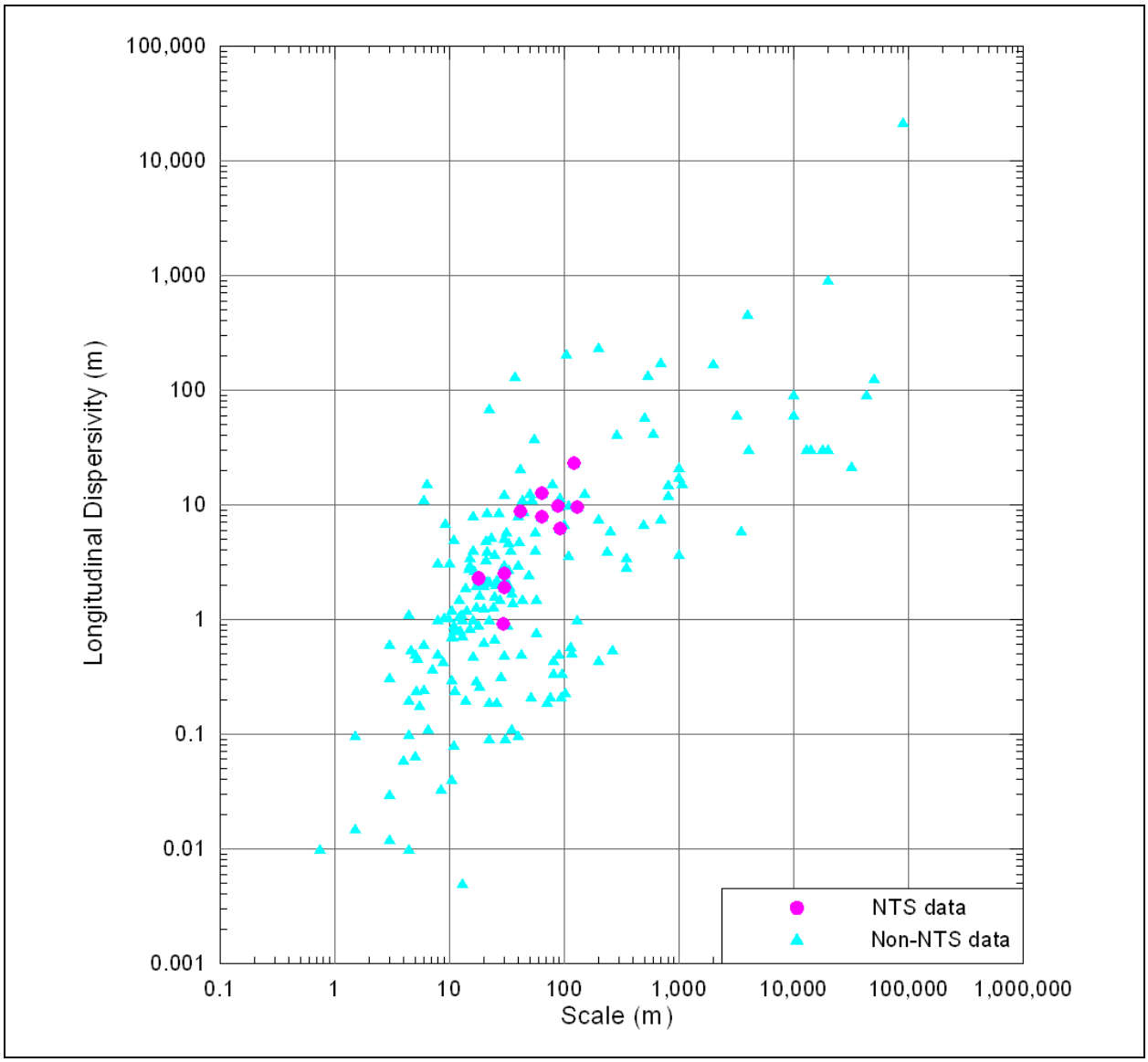

Figure 9-4
Comparison of NTS and Non-NTS Dispersivity-Scale Data

the low-reliability data show an increasing trend at larger scales, the intermediate- and high-reliability data show a trend of more constant transverse horizontal dispersivity values with scale. The ratio of longitudinal to transverse horizontal dispersivity is shown in Figure 9-7(b). The transverse horizontal dispersivity is, in general, a factor of 3 to 30 less than the longitudinal dispersivity. Gelhar et al. (1992) reported that, based on two high-reliability data points, transverse horizontal dispersivity is one order of magnitude less than longitudinal dispersivity. Ratios of longitudinal to transverse

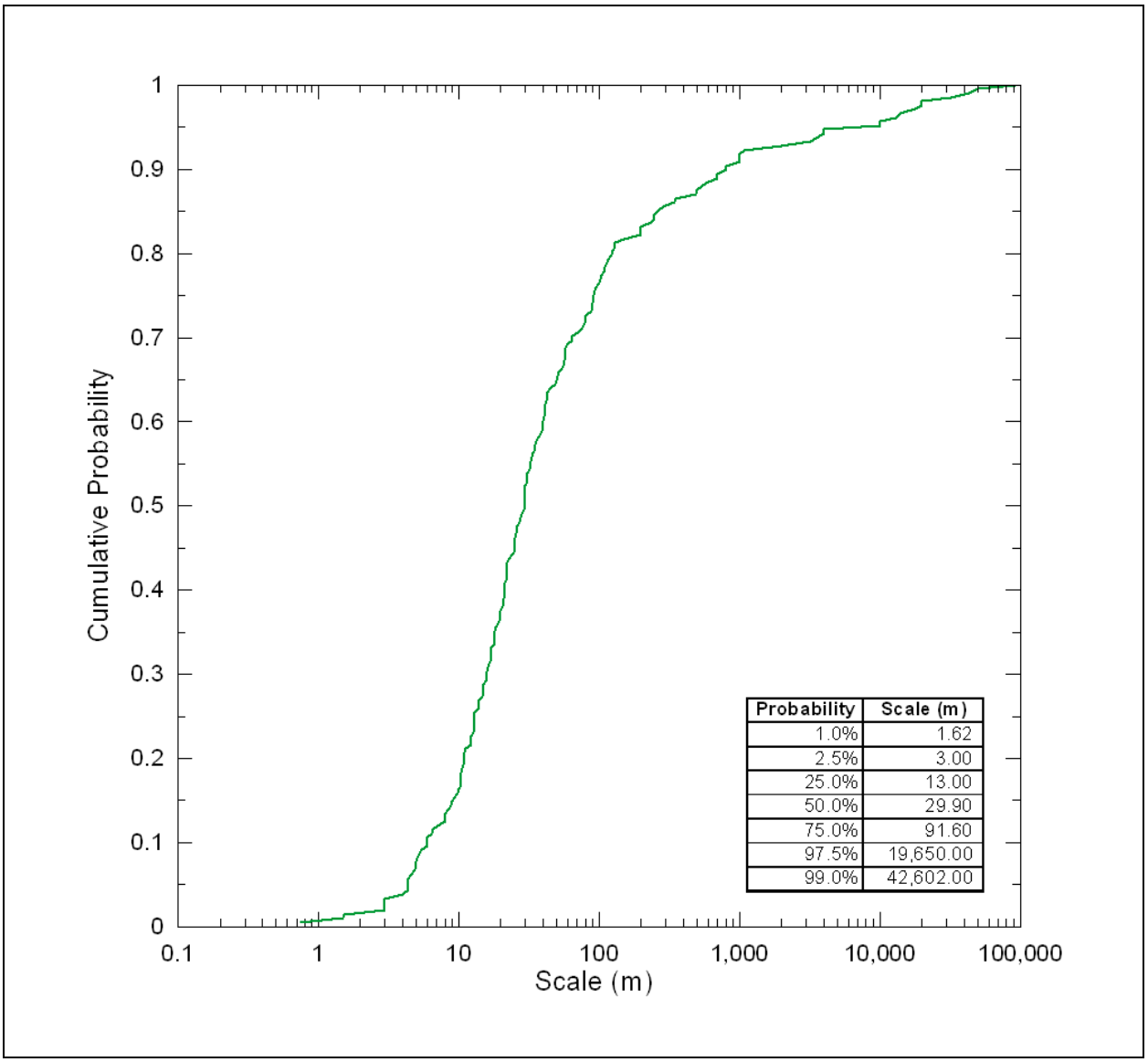

Figure 9-5
Cumulative Distribution Function for Scale for the Dispersivity-Scale Dataset

horizontal dispersivity of about 10 are typically chosen when developing appropriate values of horizontal transverse dispersivity for use in regional transport models.

Figure 9-8(a) depicts the sparse data for transverse vertical dispersivity. Transverse vertical dispersivities up to 2 m have been observed. No trend of transverse vertical dispersivity with transport scale is apparent. The ratio of longitudinal to transverse vertical dispersivity is shown in Figure 9-8(b). The only significant observation is that the transverse vertical dispersivity is much less than either the longitudinal or horizontal transverse dispersivity. Gelhar et al. (1992) found that in all

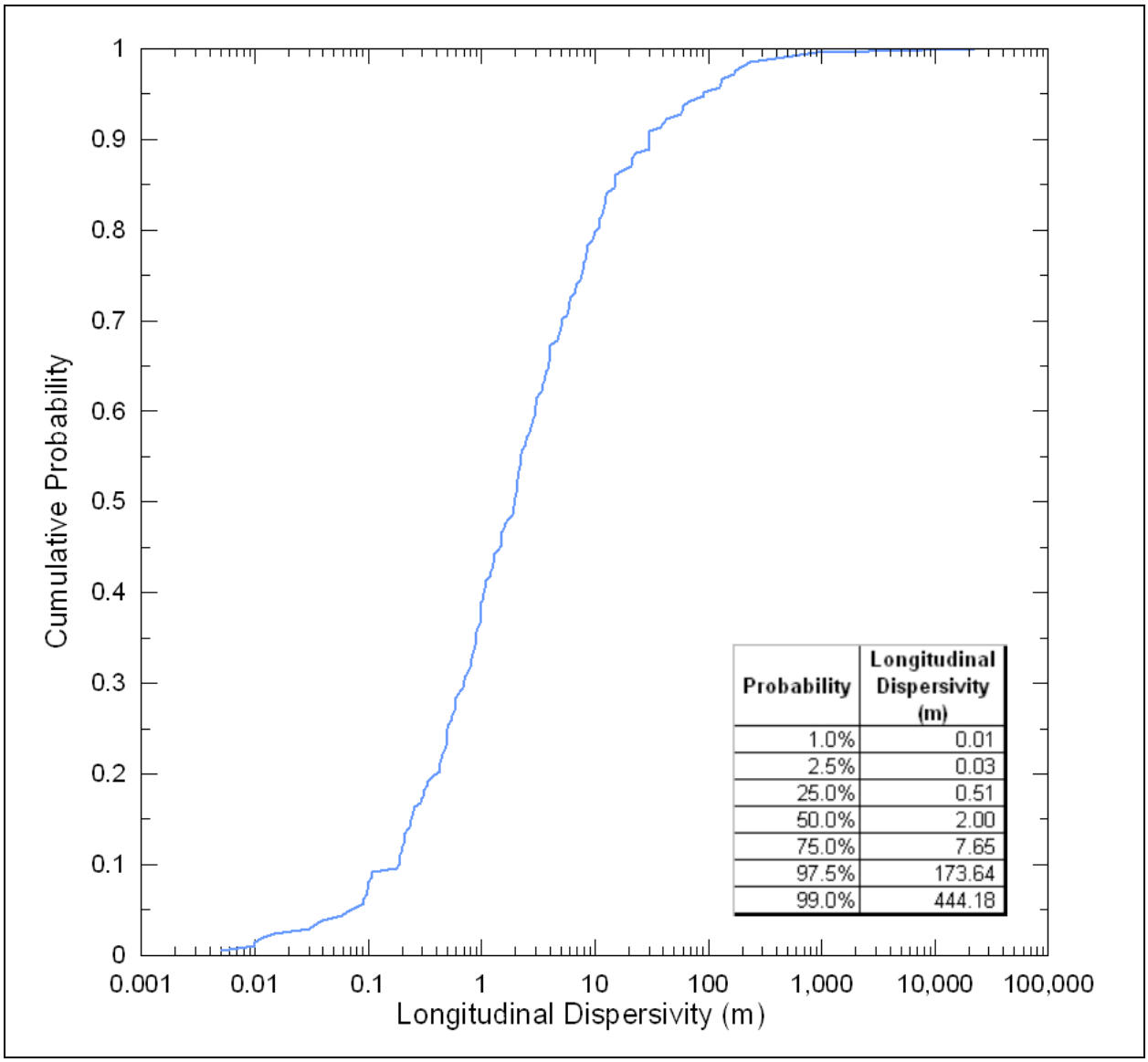

Probability	Longitudinal Dispersivity (m)
1.0%	0.01
2.5%	0.03
25.0%	0.51
50.0%	2.00
75.0%	7.65
97.5%	173.64
99.0%	444.18

Figure 9-6
Cumulative Distribution Function for Longitudinal Dispersivity for the Dispersivity-Scale Dataset

cases where both horizontal and vertical transverse dispersivities were measured, the values of vertical transverse dispersivity were one to two orders of magnitude less than those of the horizontal transverse dispersivity. This reduction in spreading may be controlled mainly by the layering of the geologic materials, where less permeable layers will significantly reduce the ability of the tracer to disperse upward or downward.

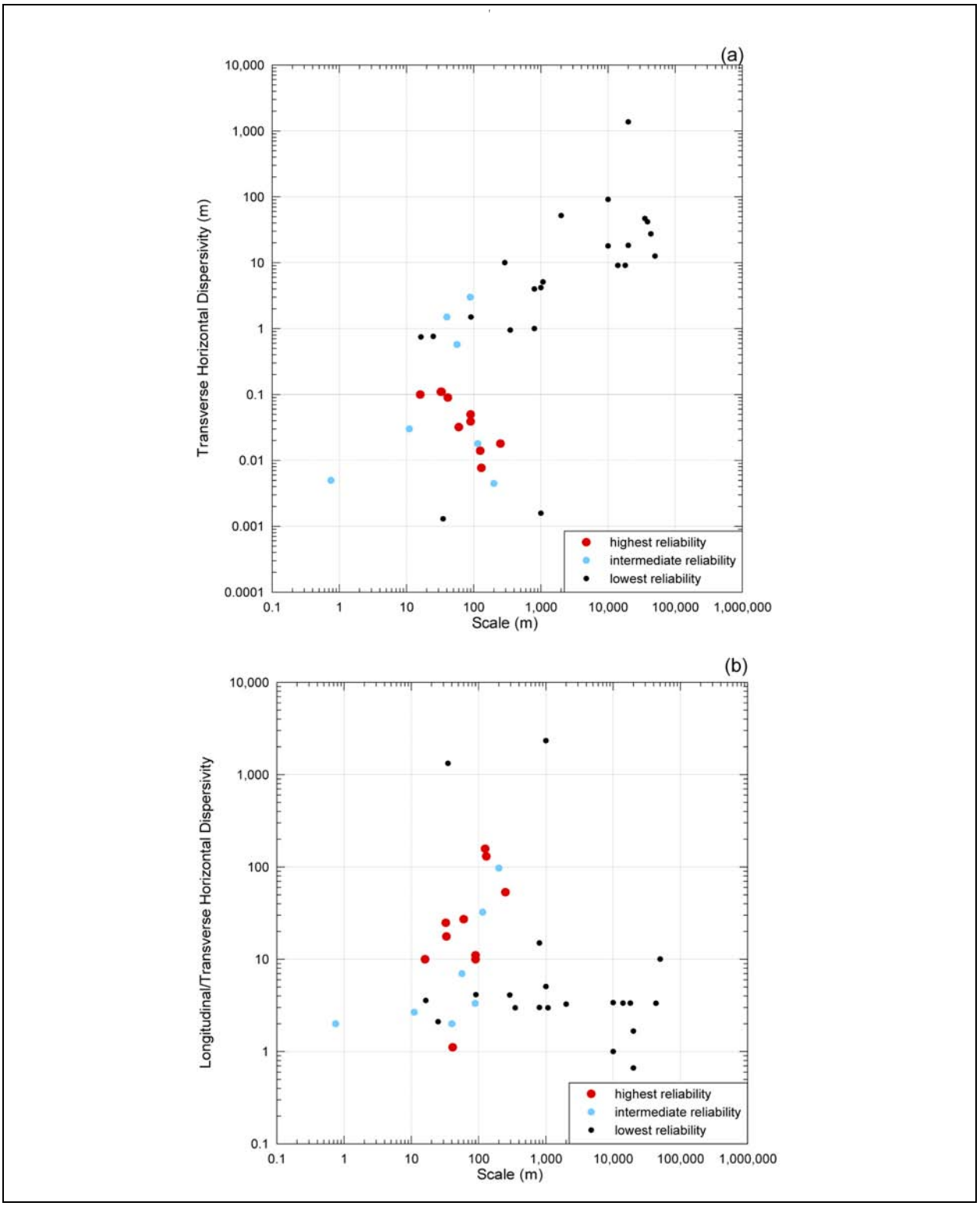

Figure 9-7
(a) Transverse Horizontal Dispersivity versus Transport Scale and (b) Ratio of Longitudinal to Transverse Horizontal Dispersivity versus Transport Scale

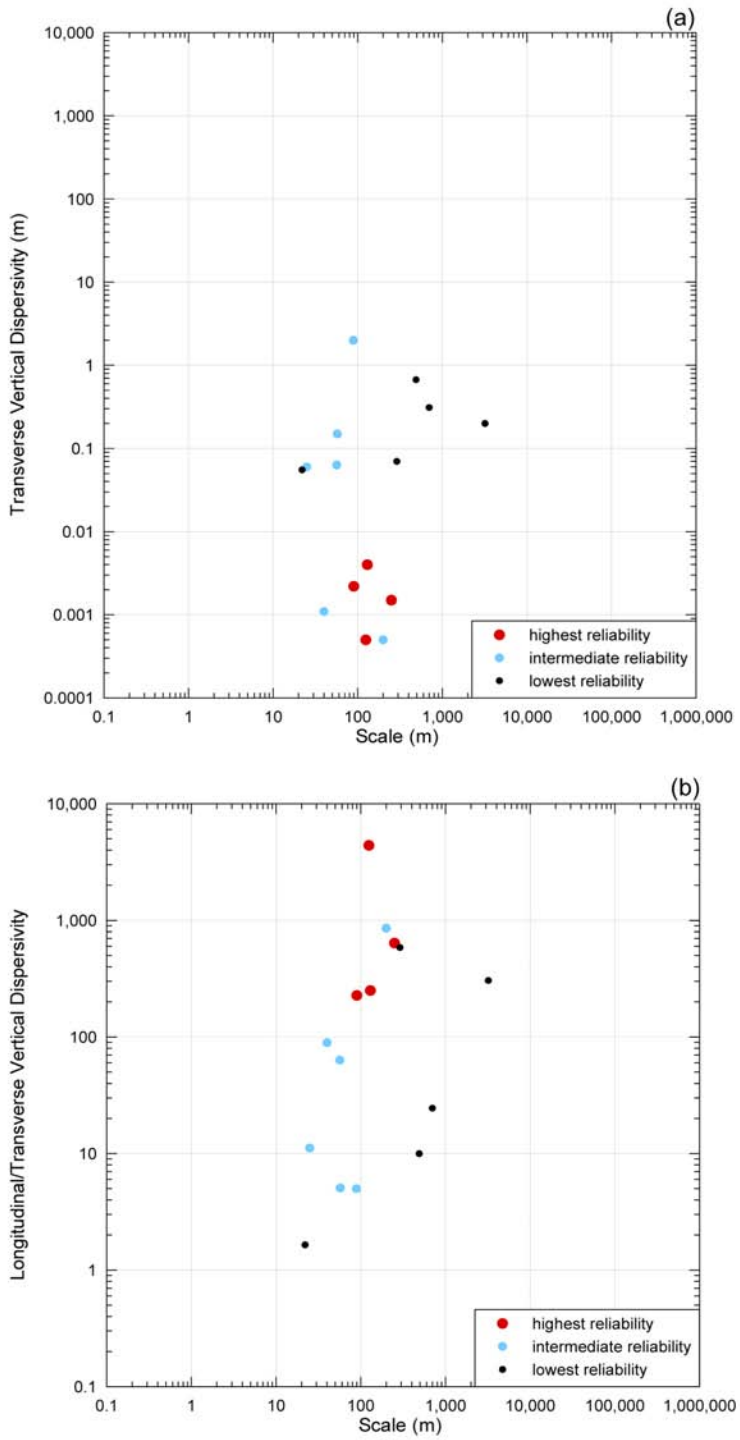

Figure 9-8
(a) Transverse Vertical Dispersivity versus Transport Scale and
(b) Ratio of Longitudinal to Transverse Vertical Dispersivity versus Transport Scale

9.3.4.3 Summary of Observations from Dispersivity Dataset Assessment

Several important observations related to the evaluation of dispersivity data in the literature were summarized in SNJV (2004d and 2005b) based on the available information. These observations generally are corroborated with the more recent data presented in this document and have been modified to reflect new information. The major observations are:

- Longitudinal dispersivity apparently increases with scale (distance from the contaminant source or the spacing between tracer-injection and monitoring wells).
- The ratio of longitudinal dispersivity to transverse horizontal dispersivity is generally in the range of 3 to 30, and the ratio of longitudinal dispersivity to transverse vertical dispersivity is generally in the range of 10 to 800. The transverse vertical dispersivity is typically one to two orders of magnitude smaller than the transverse horizontal dispersivity.
- As the density of information on hydraulic conductivity increases, the effect of dispersivity increasing with scale may be reduced. Dispersivity accounts for unmeasured and unspecified variability in the variations in hydraulic properties within the flow and transport model. As more of the variability is modeled explicitly, the appropriate dispersivity becomes smaller in magnitude.
- Whether the geologic media is porous or fractured appears to have no significant effect on dispersivity. In other words, dispersivities used for porous media can also be used in fractured media at similar scales.
- The longitudinal dispersivity data from NTS and vicinity studies fall within the range of values published in the scientific literature for other locations.

9.3.5 Evaluation of Scale Dependency of Dispersivity

9.3.5.1 Background and Previous Investigations of Scale Dependency

The scientific literature documents that longitudinal dispersivity representative of field conditions typically increases with the scale of measurement (Lallemand-Barres and Peaudecerf, 1978; Pickens and Grisak, 1981a and b; Gelhar et al., 1992; Neuman, 1990 and 1995; Neuman and Di Federico, 2003; and Schulze-Makuch, 2005).

Pickens and Grisak (1981a) developed a simple linear relationship between dispersivity and scale for transport in a stratified aquifer using a theoretical relationship based on the statistical properties of the aquifer. For a stratified sandy aquifer, they developed a simple linear relationship where dispersivity

equals 0.1 times the mean transport distance, and they found it to be consistent with results for a two-well tracer test conducted on a scale of 8 m. The authors recognized that dispersivity is unlikely to increase continually with scale but instead likely approaches some asymptotic value. They proposed a range of functional relationships between dispersivity and transport distance, including linear, exponential, and asymptotic.

Two studies (Neuman, 1990; Schulze-Makuch, 2005) graphically display large datasets of longitudinal dispersivity versus transport scale and fit dispersivity-scale power-law relationships (linear on a log-log graphical presentation of the dispersivity-scale data) of the form:

$$\alpha = cL^m \tag{9-3}$$

where α is the longitudinal dispersivity (L), c is a coefficient, L is the transport scale of interest or mean travel distance (L), and m is the scaling exponent (slope of the straight line fit on a log-log plot of the dispersivity-scale data). These authors fit this relationship to the databases they had assembled for longitudinal dispersivity versus transport scales.

Neuman (1990) developed expressions using Equation (9-3) from regression of the dispersivity-scale data excluding the large-scale contaminant-transport model calibration cases and determined two linear regions on the log-log plot corresponding to scales less than 100 m (c = 0.0169 and slope m = 1.53) and greater than 100 m (c = 0.32 and slope m = 0.83). When he included the dispersivity-scale data corresponding to the large-scale contaminant-transport model calibrations, he determined the slope m to be about 0.5. Gelhar et al. (1992) caution against routinely adopting dispersivities from a linear regression through the data because examination of the underlying data favors the use of dispersivities from the lower half of the dispersivity range at any given scale.

Neuman (1990) concluded that dispersivities interpreted from calibration of numerical models to both hydraulic and concentration data tend to increase more slowly with increasing scale than those that are calibrated to concentration data alone. This appears to occur because calibration often provides information about the spatial variation of hydraulic conductivities on scales exceeding the dimensions of model subregions (called “zones”) within which they are kept constant or allowed to vary at a relatively slow rate. The calibrated dispersivities are associated with a reduced length scale L_r that depends on the dimensions of the zones rather than on the mean travel distance L_s of the plume. The

regression analysis suggested that L_r increased with the mean travel distance at an average rate proportional to $L_s^{0.5}$. Neuman (1990) concluded that the scale parameter that controls dispersivity in a transport model diminishes as the amount of detail on hydraulic heterogeneity increases.

Xu and Eckstein (1995) developed dispersivity-scale relationships from the data presented in Gelhar et al. (1992) using a weighted least-squares method where weights could be assigned to data points in accordance with their reliability. They presented results for three weighting schemes (1:1:1, 1:1.5:2, and 1:2:3) that were assigned according to weight value for the lowest-reliability, intermediate-reliability, and highest-reliability data, respectively. They also presented a graphical presentation of the data that shows greater linearization when the data are plotted as log α versus log (log L) where α is longitudinal dispersivity and L is the transport scale of interest or mean travel distance. Using the Gelhar et al. (1992) data, Xu and Eckstein (1995) developed the following relationships for the three weighting schemes:

$$\alpha = 1.20\ (\log L)^{2.958} \qquad \textit{for 1:1:1 weighting scheme} \qquad (9\text{-}4)$$

$$\alpha = 0.94\ (\log L)^{2.693} \qquad \textit{for 1:1.5:2 weighting scheme} \qquad (9\text{-}5)$$

$$\alpha = 0.83\ (\log L)^{2.414} \qquad \textit{for 1:2:3 weighting scheme} \qquad (9\text{-}6)$$

As expected, these relationships exhibit a declining rate of change in dispersivity as transport scale increases.

Schulze-Makuch (2005) developed relationships for unconsolidated media and for various rock types (sandstones, carbonates, basalts, and granites) using Equation (9-3). The parameter c varied between approximately 0.01 and 0.8, and the scaling exponent m varied between 0.4 and 0.94. He obtained a mean scaling exponent of about 0.5 for his entire dataset, with no statistical difference between geologic media. This exponent of 0.5 is similar to that obtained by Neuman (1990) for his dataset when he included large scale plumes. Because of the limited amount of data for each rock type and the problems found when evaluating his summary table of dispersivity-scale data, the parameters from Schulze-Makuch (2005) are given here for comparison purposes only and should be considered with caution. The relationships that he developed for the various rock types should not be used because of the limited amount of data available across the range of scales for each rock type and the general large scatter in the data.

9.3.5.2 Determination of Dispersivity-Scale Relationships

For the dispersivity-scale analyses performed for the Frenchman Flat CAU (SNJV, 2005b), it was concluded that the nonweighted least squares analysis was deemed most appropriate for determining a dispersivity-scale relationship over the full range of transport scales because of the lack of any high-reliability data for scales greater than about 300 m. The dataset developed to support the Yucca Flat/Climax Mine CAU has the same limitation on data reliability at scales greater than 300 m. Therefore, a nonweighted least squares approach was adopted for the current analyses.

The log-log plot of longitudinal dispersivity versus scale for all rock types is shown in Figure 9-3 and demonstrates a consistent trend of increasing longitudinal dispersivity with transport scale. In addition, it is observed that the rate of increase in longitudinal dispersivity tends to decrease at larger transport scales (e.g., greater than 300 m). Regression analysis was performed using several types of dispersivity-scale relationships:

- Log-log linear (equivalent to relationship given in Equation [9-3])
- Log-log piecewise linear (1 line for less than 300-m scale and 1 line for greater than or equal to 300-m scale)
- Log-log quadratic
- Log-log asymptotic

The results of the regression analyses for the four dispersivity-scale relationships are summarized in Table 9-2.

Table 9-2
Dispersivity-Scale Relationships Determined from Regression Analyses

Relationship Type	Equation	Coefficient of Determination (R^2)	Equation Number
Log-log linear	$\log \alpha = 0.73 \log L - 0.91$	0.48	(9-7)
Log-log piecewise linear (1 line for <300 m scale and 1 line for ≥300 m scale)	$\log \alpha = 0.81 \log L - 1.02$ (for $L<300$ m) $\log \alpha = 0.61 \log L - 0.52$ (for $L \geq 300$ m)	0.49	(9-8)
Log-log quadratic	$\log \alpha = -0.065 (\log L)2 + 1.03 \log L - 1.18$	0.49	(9-9)
Log-log asymptotic	$\log \alpha = \log L - \log (L + 1710.32) + 1.95$	0.47	(9-10)

Note: α is longitudinal dispersivity and L is scale.

All four relationships provide reasonable and similar quality of fit with nearly identical coefficients of determination. The dispersivity-scale data and the fitted regression lines for each of the relationships are shown in Figure 9-9. Any of these relationships could be used to provide estimates of longitudinal dispersivity for expected transport scales within the Yucca Flat/Climax Mine CAU. The latter three types of relationships (log-log piecewise linear, log-log quadratic, and log-log asymptotic) offer the advantage of being able to capture the behavior of decreasing rate of dispersivity increase for larger transport scales.

The log-log linear relationship is equivalent to the power law shown in Equation (9-3), where coefficient *c* is 0.12 (inverse log of -0.91) and the scaling exponent m is 0.73. For the piecewise linear relationship, the scaling exponents are 0.81 and 0.61 for scales less than 300 m and greater than 300 m, respectively. The exponent of 0.61 for the scales greater than 300 m is relatively consistent with Neuman (1990), who obtained a scaling exponent of about 0.5 when he performed a regression on all data with scales greater than 100 m.

9.4 Data Limitations

Dispersivity is not an intrinsic property of the medium in the way that porosity and hydraulic conductivity are thought to be. In order to have a basis for predicting dispersivity from statistical distributions, its dependence on the scale of the measurement and on the type of test and method of analysis must be known. The data available from the NTS region are scarce and mostly consist of quantitative values only for longitudinal dispersivity. None of the NTS tracer tests produced good estimates of transverse dispersivities. The trends in dispersivity with transport distance are compiled from data obtained from locations around the world. As a result, the appropriate longitudinal dispersivity to apply at large scales for the Yucca Flat/Climax Mine CAU model has uncertainty associated with the range and distribution of data. This uncertainty should be addressed using sensitivity analyses during the application of the Yucca Flat/Climax Mine CAU flow and transport model.

9.5 Summary

As presented in Section 9.3, the dispersivity values tend to be scale dependent. As a result, it is helpful to know the expected distances of contaminant transport *a priori* to best assess the range of

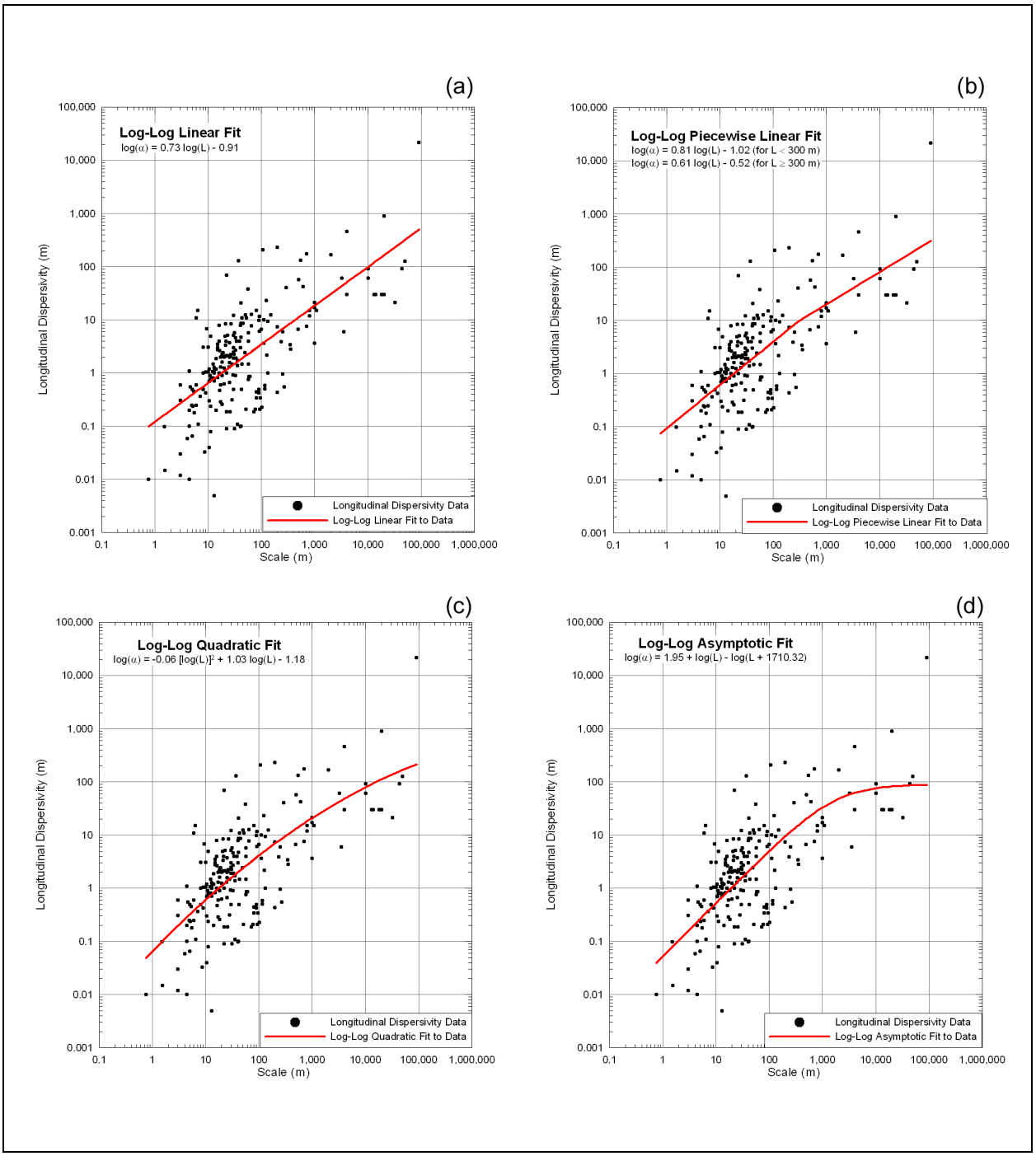

Figure 9-9
Dispersivity-Scale Relationships Determined from Regression Analyses: (a) Log-Log Linear, (b) Log-Log Piecewise Linear, (c) Log-Log Quadratic, and (d) Log-Log Asymptotic

dispersivity values that would be most appropriate for modeling efforts. For the Yucca Flat/Climax Mine CAU, flow modeling is required to enable assessment of the expected pathways and distances of contaminant transport. Flow model calibration and particle-tracking activities (using initial estimates of effective porosity) will be conducted in the future. These studies will provide insight into the expected advective transport distances for contaminants from the underground nuclear test locations.

The value selected for dispersivity is somewhat dependent on the degree to which the heterogeneity of the groundwater system is defined. Because of the large areal and vertical extent, the complex hydrostratigraphic and faulted nature, and the relatively sparse well data for heads and hydraulic properties for calibrating the groundwater flow model within the Yucca Flat/Climax Mine CAU, the calibrated groundwater flow model will likely only be moderately constrained. Dispersivity is a modeling parameter that accounts for unmeasured and unspecified variability in the hydraulic properties within the flow and transport model domain. As more of the variability of the groundwater flow regime is modeled explicitly, the appropriate dispersivity to use becomes smaller in magnitude. Longitudinal dispersivities estimated from the derived regression lines for ranges of transport scale (see Section 9.3.5.2) are considered reasonable.

An approach being used for transport modeling of the Pahute Mesa and Frenchman Flat CAUs is to select appropriate longitudinal dispersivities that will be representative for several transport scales of interest determined from groundwater flow modeling and particle tracking from locations of interest. As an example, using the log-log piecewise linear fit to the dispersivity-scale data (Equation [9-8] in Table 9-2), one could select a longitudinal dispersivity of about 4 m for scales of 30 to 300 m, 20 m for scales of 300 to 3,000 m, and 80 m for scales of 3,000 to 30,000 m. Uncertainty in the selected values can be addressed through sensitivity analyses.

It is recommended that transverse horizontal and vertical dispersivities should be selected based on a ratio of longitudinal to transverse horizontal dispersivity of about 3 to 30 and a ratio of longitudinal to transverse vertical dispersivity of about 10 to 800, respectively. The transverse vertical dispersivity is typically one to two orders of magnitude smaller than the transverse horizontal dispersivity.

10.0 MATRIX DIFFUSION PARAMETERS

This section includes descriptions of the role of matrix diffusion in contaminant transport in groundwater, the data available from matrix diffusion experiments, and the data analysis and associated results. The objective is to evaluate data from the NTS laboratory and field tracer experiments and from the literature to develop a matrix diffusion coefficient distribution for the HSUs in Yucca Flat. Matrix diffusion coefficients for solutes in a porous medium are smaller in magnitude than free water diffusion coefficients because of restriction due to the presence of the solid phase of the porous medium. It was found that a relationship could be developed between the ratio of matrix diffusion to free water diffusion coefficients (termed tortuosity) and porosity. The use of a tortuosity-porosity functional relationship is useful because porosity data are more readily available than experimentally derived matrix diffusion coefficient data.

10.1 Role of Matrix Diffusion in Contaminant Transport

Solute transport in high-permeability zones is typically dominated by advective-dispersive processes, while transport in low-permeability zones is dominated by diffusion. In fractured media, a double-porosity conceptualization is typically assumed with matrix diffusion between the fractures and the adjacent matrix having the effect of attenuating both the concentration and travel time of aqueous-phase contaminants moving through fractures. This process involves the diffusion of contaminants from groundwater flowing in rock fractures into and out of the relatively stagnant water in the pores of the surrounding rock matrix.

The importance of the diffusion of solutes from fractures into the adjacent matrix has been studied and reported extensively in the literature, and has been established as an important process for retarding the transport distance of solutes introduced into fractured geologic systems. Numerical models and analytical solutions presenting analyses of the effect of matrix diffusion during transport in fractured geologic media have been reported by Neretnieks (1980), Grisak and Pickens (1980 and 1981), Tang et al. (1981), Noorishad and Mehran (1982), Huyakorn et al. (1983a and b), Feenstra

et al. (1984), and others. Examples of investigation of double-porosity transport with matrix diffusion for laboratory experiments has been presented by Grisak et al. (1980), Grisak and Pickens (1981), Neretnieks et al. (1982), Moreno et al. (1985), Hershey et al. (2003), and Reimus et al. (2006a and b); and for field tracer tests by Jones et al. (1992), Novakowski and Lapcevic (1994), IT (1998), Reimus and Haga (1999), and Reimus et al. (1999 and 2003b).

As discussed in SNJV (2004c), mass transfer can also occur in unfractured media, including alluvium, by diffusion between the more permeable zones and lower-permeability zones. The low-permeability zones may consist of layers of fine-grained sediments. Diffusion, however, would be expected to be of less importance for alluvium, compared to fractured media, because the ratio of stagnant to flowing water volume in unconsolidated media is usually much smaller than in fractured media. Additionally, the contrast in permeability between the stagnant and flowing zones is typically much less for alluvium than for fractured rocks. For these reasons, matrix diffusion is not expected to be a significant source of reduction in transport distances for alluvium when compared to fractured media.

10.1.1 Diffusion Process

The molecular diffusion conceptualization is based on Fick's second law of diffusion (Crank, 1975) which, for a one-dimensional system in a porous medium, may be expressed as:

$$\frac{\partial C}{\partial t} = D_m \frac{\partial^2 C}{\partial z^2} \qquad (10\text{-}1)$$

where C is the species concentration (m/L^3), D_m is the effective matrix diffusion coefficient for solutes in the pores (L^2/T), z is the coordinate position (L), and t is time. This form of Fick's second law is seen in many standard hydrogeology texts, including Bear (1972) and Freeze and Cherry (1979). The diffusion in the porous medium is restricted because of the presence of the solid phase. The matrix diffusion coefficient in porous media, D_m, is directly related to the solute free water diffusion coefficient, D_o, by the tortuosity of the porous media, ω, using the relationship (Bear, 1972; Freeze and Cherry, 1979):

$$D_m = \omega D_o \qquad (10\text{-}2)$$

Tortuosity can be defined as a bulk measure of the constrictivity and tortuous nature of the interconnected pore space through which diffusion is occurring. These factors result in variation in pore channel diameters and path lengths as the diffusing solute migrates through the interconnected porosity. Tortuosity has a magnitude greater than zero and less than one when defined in the form presented in Equation (10-2). Smaller tortuosities are indicative of longer diffusional path lengths and greater resistance to diffusion through the medium. There are several alternate forms to Equation (10-2) in the scientific literature (e.g., $D_m = D_o \phi\kappa/\tau^2$ [Neretnieks, 1980]), so it is important to note which formulation was used for experimentally-derived or calculated parameters. In this alternative formulation, τ is the tortuosity factor (greater than one), ϕ is the porosity, and κ is the constrictivity factor. In this section, unless otherwise noted, tortuosity is of the "ω" form as expressed in Equation (10-2).

Tortuosity can be determined using Equation (10-2) with values for the matrix diffusion coefficient from experiments and free water diffusion coefficient from the literature. Its magnitude must be less than one because diffusion is restricted in the porous medium as compared to in water alone. Bear (1972) defines tortuosity as:

$$\omega = (L/L_e)^2 \qquad (10\text{-}3)$$

where L is the straight-line path length and L_e is the actual tortuous path length that a particle would take passing through a sample of length L. Freeze and Cherry (1979) state typical laboratory values for tortuosity range up to 0.5. De Marsily (1986) provides an upper limit of 0.7 for sands. Bear (1972) provides a review and gives an upper bounding value of 0.8 for L/L_e, which would correspond to ω equal to 0.64. Tortuosity values exceeding 0.7 reported from laboratory or field experiments are not considered to be representative and are likely the result of uncertainties from other factors such as sorption, precipitation, and inability to derive tortuosity from a tracer response that is represented by a lumped parameter.

10.2 Data Compilation and Data Transfer

Data from the Yucca Flat/Climax Mine HFM area and data from other NTS CAUs, YMP, and some literature values from other locations (specifically for granites, for which there were no NTS area data) were used for this analysis due to the unavailability of comprehensive data from the Yucca

Flat/Climax Mine HFM area for all HGUs. All data locations used in quantitative analyses are identified in Appendix H and the associated dataset referenced in Section H.4.0. Individual discussions of the applicability of the transferred data are provided for each HGU. There are limited data for the NTS area to determine a distribution for matrix diffusion values directly. The data were used to determine functional relationships with other parameters (see Section 10.4.6), for which there are more comprehensive data. A quantitative assessment of the sensitivity of transport modeling to the uncertainty in this parameter cannot be provided before the transport model development. The parameter description discusses the importance of this parameter.

10.3 Data Types and Sources for Matrix Diffusion Coefficient

Values of tortuosity or the matrix diffusion coefficient can be determined through several approaches including laboratory diffusion-cell experiments, field tracer tests, and rock-property measurements of formation factor and porosity.

10.3.1 Laboratory Tracer Diffusion Experiments

Laboratory Experimental Methods To Determine Matrix Diffusion

Matrix diffusion coefficients can be determined from several different types of laboratory experiments, including diffusion cell, rock beaker, and hollow core cylinder methods (SNJV, 2004c). The diffusion cell method, the most common method, has several variations, described as follows.

In the diffusion cell method, a disk or “wafer” is cut from the rock core, typically with the wafer thickness less than its diameter. In the diffusion cell apparatus, the groundwater saturated rock wafer is placed between two liquid reservoirs, as illustrated in Figure 10-1. One of these liquid reservoirs is the tracer reservoir and the other is the collection reservoir. The liquid levels of the reservoirs should be maintained as similar as possible to eliminate or minimize advective effects within the rock wafer. Initially, both reservoirs are filled with groundwater. Then tracer is introduced into the tracer reservoir, and matrix diffusion is determined by measuring over time the increasing tracer concentration in the collection reservoir, and/or the decreasing tracer concentration in the tracer reservoir. To achieve as high a concentration gradient as possible (to maximize diffusion), tracer may be added to the tracer reservoir over time to replace diffused tracer, and the collection reservoir may be flushed continually with “clean” groundwater.

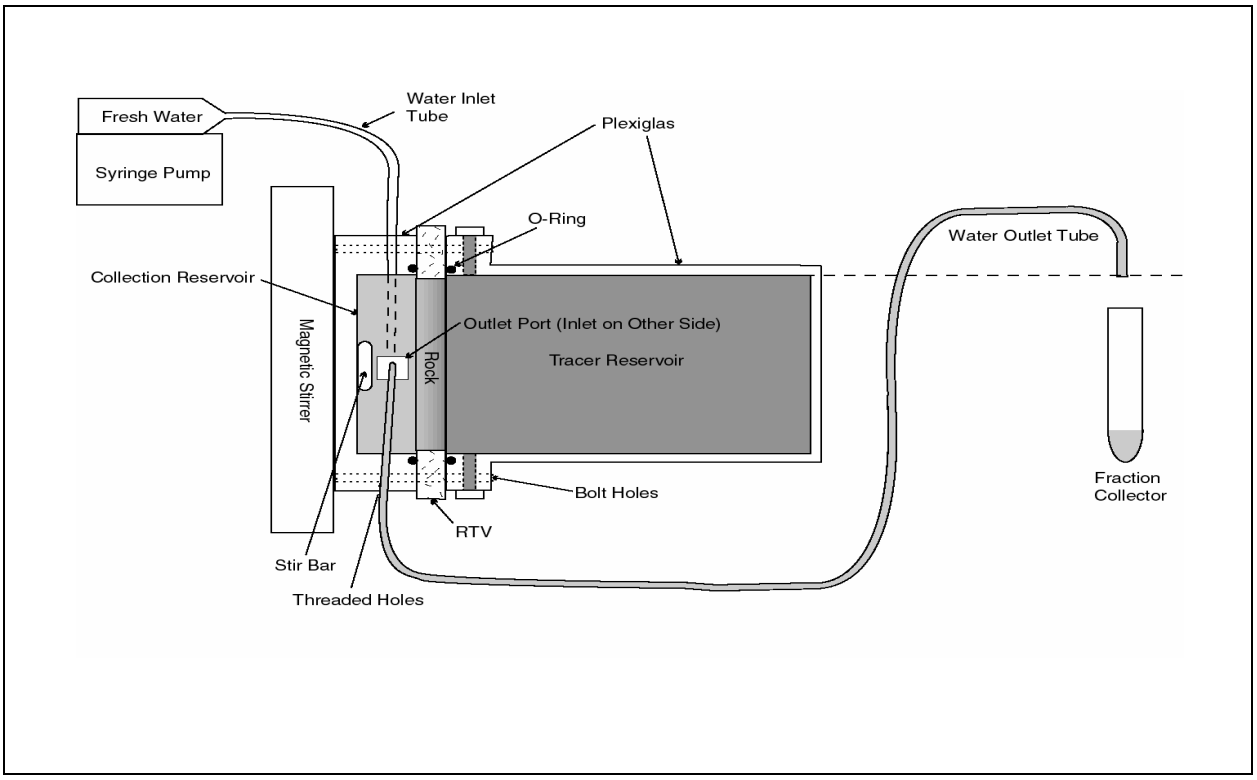

Figure 10-1
Typical Design for a Diffusion Cell Experiment
Source: SNJV, 2004c

A variation of the diffusion cell method is to use only one reservoir rather than two. For this approach, an impermeable boundary is placed on all but one face of the sample, and diffusion occurs only into the rock wafer, not through it.

Rather than one single tracer, a suite of tracers is typically used to increase the quality and quantity of data produced from each single experiment, and to allow for detection of nondiffusive processes that may also affect the reservoir tracer concentrations (e.g., adsorption, cation exchange).

The porosity can be determined directly on the diffusion cell wafer (the preferred method), before or after the experiment, or using a rock sample from an adjacent core. However, determining porosity on adjacent core wafers will introduce additional uncertainty due to rock heterogeneity. The permeability, likewise, can be measured directly from the wafer or from an adjacent core, which typically would introduce even more uncertainty than for porosity, due to higher expected variability in permeability compared to porosity. It is preferable to obtain porosity and permeability

measurements on the same wafers that are being used to perform the diffusion experiments. Obtaining porosity and permeability measurements on all samples facilitates evaluations to determine correlations between matrix diffusion coefficient or tortuosity and these parameters.

The "rock beaker" matrix diffusion method is a variation of the diffusion cell method. For this method, a hollow "cup" or cylinder is bored into the flat surface of a rock core. The outside of the core is made a no-flow boundary (typically with epoxy), and the core is then saturated with groundwater. A tracer solution is introduced in the "cup," and the decrease in tracer concentration (due to diffusion into the rock matrix over time) is measured.

A variation on the "rock beaker" method is the hollow core cylinder method, where a hollow inner cylinder is drilled through the core (and no-flow boundaries are established on the outside and top and bottom of the core) and diffusion takes place only through this inner cylindrical surface. Stirrers are typically used within the rock cavities and within the reservoirs to eliminate concentration variations within the free liquid volumes.

These different methodologies result in slightly different forms of the Fickian diffusion equation solution needed to analyze the change in tracer concentration over time for determining the matrix diffusion coefficient. Analyses can also be applied to more complicated geometries (e.g., core holes drilled into rectangular or irregular-shaped blocks), but a more complex set of boundary conditions and possibly a 3-D solution to the diffusion equation will be required. The diffusion cell method using two reservoirs is the conventional and most commonly used method because it allows for data acquisition in a shorter time period due to the greater concentration gradient achieved and maintained throughout the experiment.

Laboratory tracer diffusion experiments have been performed to support the UGTA and Yucca Mountain projects (denoted as NTS samples in the remaining discussion) using the above experimental methods. Data points from experiments that did not use rock core (e.g., Papelis and Um [2003a], which used pulverized and sieved rock particles) or where the calculated tortuosity is greater than 0.7 (see discussion on representative tortuosity values in Section 10.1.1) were eliminated as unrepresentative. The data sources for the laboratory diffusion coefficient experiments are discussed below.

Laboratory Data Sources

The matrix diffusion coefficients derived from laboratory experiments were obtained from 11 different references (listed below) plus the matrix diffusion coefficient databases developed for Pahute Mesa (Shaw, 2003a) and Frenchman Flat (SNJV, 2005b). A wide range of data and information from these experiments (e.g., sample location, lithology, temperature, depth, mineralogy, tracer species, matrix diffusion coefficient, tortuosity, author comments on experiment quality and results, porosity, permeability) were entered into one worksheet of a large Excel spreadsheet, with other worksheets containing analyses, original source data, graphics, and tables; this is referred to as the NTS matrix diffusion database. All of the reported results from the experiments were from NTS rock samples, with the exception of 10 granite/crystalline measurements from non-NTS rock. The latter were included because laboratory diffusion cell experimental measurements are not available for crystalline rock using NTS source rocks. Key data sources are listed in order of number of data points (n) in the NTS matrix diffusion database as follows:

1. Reimus et al. (2002c): *Diffusive and Advective Transport of ^{3}H, ^{14}C, and ^{99}Tc in Saturated, Fractured Volcanic Rocks from Pahute Mesa, Nevada*. n = 75

2. Reimus et al. (2006b): *Matrix Diffusion Coefficients in Volcanic Rocks at the Nevada Test Site: Influence of Matrix Porosity, Matrix Permeability, and Fracture Coating Minerals.* n = 64

3. Walter (1982): *Theoretical and Experimental Determination of Matrix Diffusion and Related Solute Transport Properties of Fractured Tuffs from the Nevada Test Site*. n = 24

4. Reimus et al. (2006c): *Tracer Transport Properties in the Lower Carbonate Aquifer of Yucca Flat*. n = 16

5. Triay et al. (1997): *Summary and Synthesis Report on Radionuclide Retardation for the Yucca Mountain Site Characterization Project: Yucca Mountain Site Characterization Program Milestone 3784M*. n = 11

6. Various sources of non-NTS data for granite rock type: Mazurek and Jakob (2002); Jakob (2004); Skagius and Neretnieks (1986); and Gustavsson and Gunnarsson (2005). n = 10

7. Papelis and Um (2003b): *Evaluation of Cesium, Strontium, and Lead Sorption, Desorption, and Diffusion in Cores from Western Pahute Mesa, Nevada Test Site, Based on Macroscopic and Spectroscopic Investigations.* n = 8

8. Zavarin et al. (2005): *Radionuclide Transport in Tuff and Carbonate Fractures from Yucca Flat, Nevada Test Site.* n = 5

9. Hershey et al. (2003): *Laboratory Experiments to Evaluate Diffusion of ^{14}C into Nevada Test Site Carbonate Aquifer Matrix.* n = 4

10. Callahan et al. (2000): "Using Multiple Experimental Methods to Determine Fracture/Matrix Interactions and Dispersion of Nonreactive Solutes in Saturated Volcanic Tuff." In *Water Resources Research.* n = 4

11. IT (1998): *Report and Analysis of the BULLION Forced-Gradient Experiment.* n = 3

For evaluation and discussion purposes, tortuosities were calculated using Equation (10-2) with matrix diffusion coefficients determined from the laboratory experiments and solute free water diffusion coefficients from the literature. The general trend of increasing tortuosity with increasing porosity in the data from the different sources may be seen in Figures 10-2 and 10-3 for log-linear and log-log tortuosity-porosity data presentations, respectively. The data trends and the experimental methods, rock types studied, and other information for the data sources are described below. Considerable scatter is shown for some of the data. The impact of the data scatter is reduced somewhat through the data quality analyses presented and discussed in Section 10.4.

Discussion of Laboratory Data Sources

Reimus et al. (2002c) derived matrix diffusion coefficients from diffusion cell experiments for a wide range of saturated volcanic rock samples from Pahute Mesa, including zeolitic tuff, basalt flow, and welded ash-flow tuff, many with mineral-coated fractures. The experimental setup was similar to that shown in Figure 10-1, with a synthetic groundwater saturated rock "wafer" separating two reservoirs. The larger reservoir contained tracer, and the smaller reservoir was flushed continuously with tracer-free water to maintain a concentration gradient. The fluid level was kept the same in the two reservoirs to minimize advective flow and maximize diffusive transport. Sixty-six matrix diffusion experiments were conducted on 23 different wafers from 8 different Pahute Mesa matrix lithologies. Up to 3 different tracers were used resulting in 111 reported data points (solid red squares plotted in Figure 10-2). Some of these experiments were "replicates," where wafers were cut in adjacent rock to assess the effect of near-scale heterogeneities, and some of the experiments were "repeats," where an experiment was repeated on the same wafer to assess experimental errors and repeatability. The surface area of the wafers varied from 19.9 to 62.1 square centimeters (cm^2), and the thickness varied

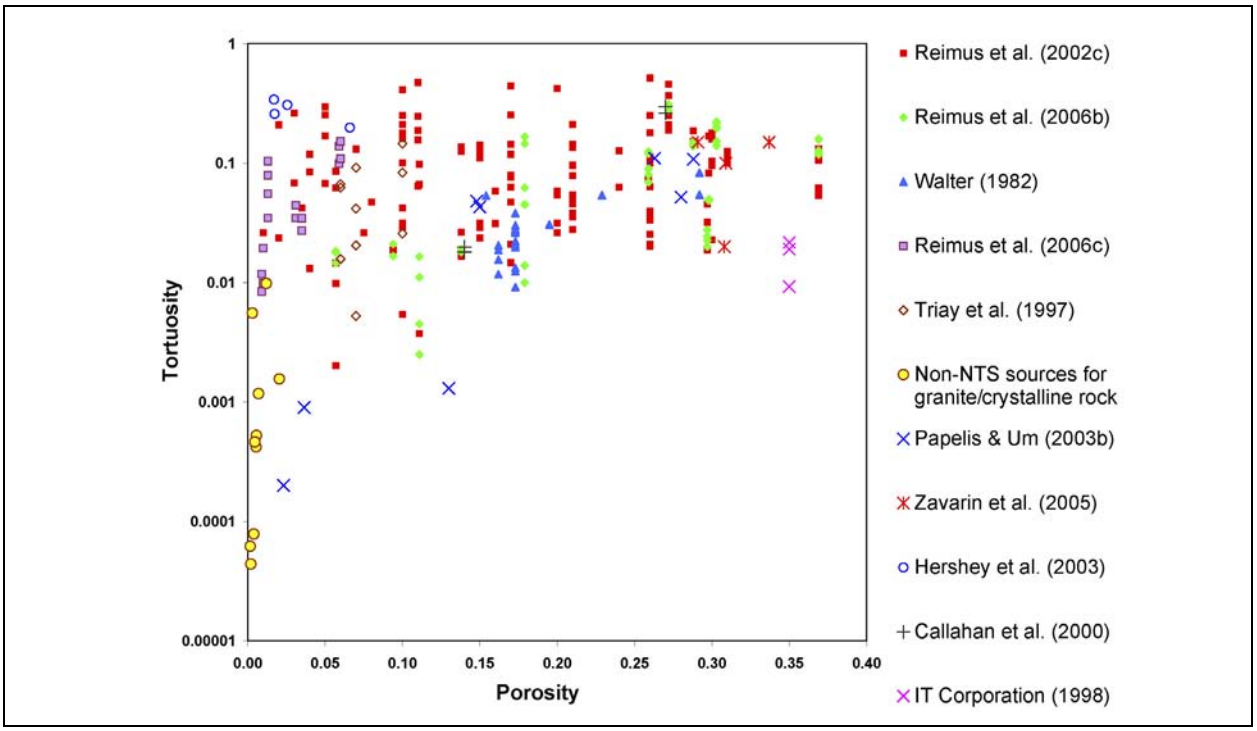

Figure 10-2
Log Tortuosity versus Linear Porosity from Different Reference Sources

The same graph plotted using the log scale for porosity is shown in Figure 10-3 for comparison purposes.

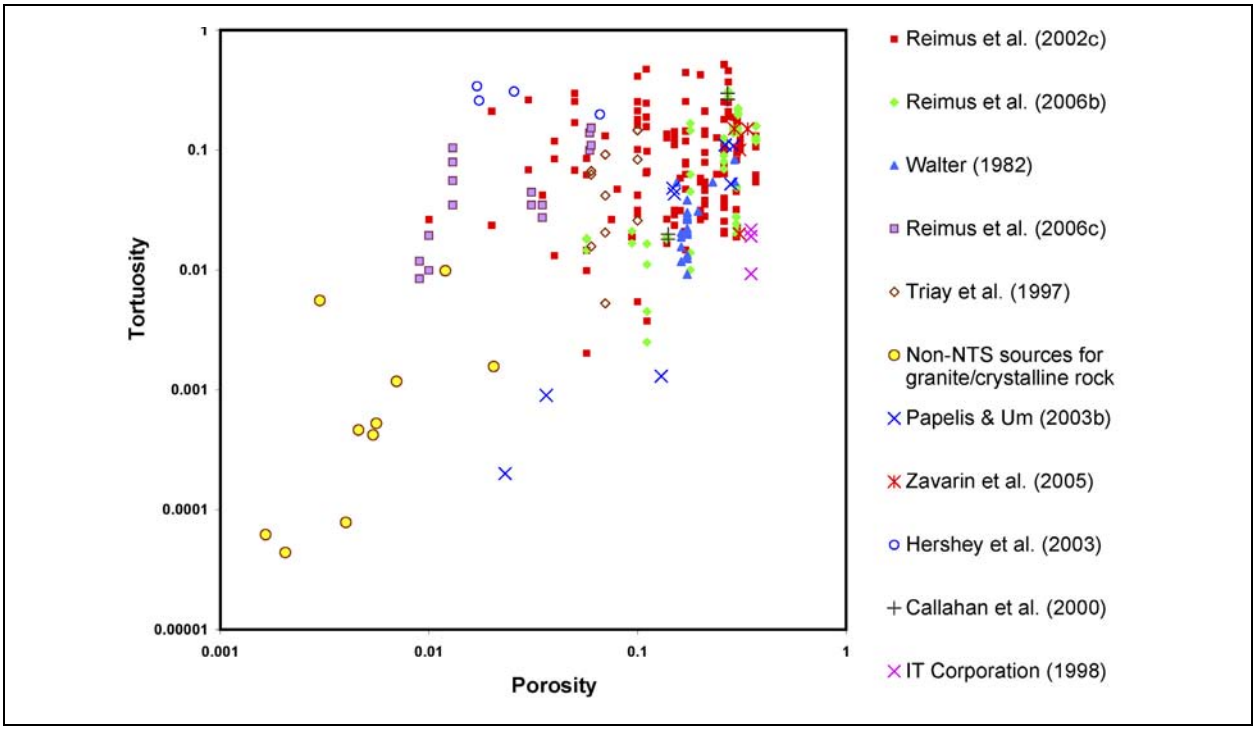

Figure 10-3
Log Tortuosity versus Log Porosity from Different Reference Sources

from 0.60 to 2.54 cm. Permeabilities were directly measured on each diffusion cell "wafer," but porosities were measured on an "intact rock sample" taken from the rock core adjacent to the diffusion cell wafer. Some uncertainty in developing a tortuosity-porosity relationship is introduced because porosities were not measured on the rock wafers used in the diffusion experiments. "Replicate" wafers were assigned the same porosity as the wafer adjacent to the sample for which the porosity was determined. This approach results in the "columns" of red squares seen in Figure 10-2 for the porosities corresponding to the samples that had porosity determinations. These columns of data points indicate several different tortuosities for a single measured porosity representing different wafers, different tracers, and "repeat" experiments. The three radioactive tracers used were tritiated water (HTO), $H^{14}CO^{-}_{3}$, and $^{99}TcO^{-}_{4}$. Matrix diffusion coefficients ranged from 5×10^{-12} to 2×10^{-9} m^2/s (equivalent tortuosity from 0.002 to 0.13). The porosities for cores used in these measurements ranged from 0.09 to 0.37, and the permeabilities ranged from 1.1×10^{-18} to 5.6×10^{-17} m^2. Experimental replicates were included in the study to gain insight into experimental errors, reproducibility, and variability. Documentation of the diffusion cell experiment in Reimus et al. (2002c) was clear, from experimental methodology to the discussion of results, including possible causes for anomalous results and suggestions for improving future measurements. The authors found that the matrix diffusion coefficients determined for the same wafer using three different tracers (HTO, $H^{14}CO^{-}_{3}$ and $^{99}TcO^{-}_{4}$) did not vary as expected. The matrix diffusion coefficients should have varied by the ratio of the solute free water diffusion coefficients of the three tracers (i.e., same tortuosity was not calculated for a rock sample using the three different tracers). This result suggests that both the $H^{14}CO^{-}_{3}$ and $^{99}TcO^{-}_{4}$ anions may have had access to less porosity than the HTO molecule, possibly due to anion exclusion or retardation by sorption or ion exchange. For this reason, matrix diffusion coefficients using the $H^{14}CO^{-}_{3}$ and $^{99}TcO^{-}_{4}$ tracers were assigned a lower quality score weighting (see Section 10.4.2).

Reimus et al. (2006a) conducted diffusion wafer and fracture transport experiments in 2004 and 2005 to determine solute matrix diffusion in the low-porosity LCA carbonate rocks, as an aid in the analysis of the multiple-well tracer tests conducted at the ER-6-1 Well Cluster in Yucca Flat. Diffusion wafer experiments were chosen instead of the generally preferable diffusion cell experiment type because some of these carbonate rocks had large voids that could have resulted in short circuiting and erroneously high apparent diffusion coefficients in a diffusion cell experiment, and because of the extremely low diffusion coefficients anticipated. The tracers in a diffusion cell

experiment must pass both into and out of a rock sample, but only into the sample during a diffusion wafer experiment. The diffusion wafer experiments indicated that solute matrix diffusion coefficients in the low-porosity LCA rocks are quite small, as expected for this low-porosity, low-permeability carbonate rock, ranging from 0.85 x 10^{-7} to 23 x 10^{-7} cm^2/s. A "loose positive correlation" was observed between the reported matrix diffusion coefficients and matrix porosities. A large suite of different types of tracers were used in the experiments, including fluorinated benzoate (FBA) tracers (PFBA, DFBA, TFBA), halide tracers (Br and I), ^{14}C, and Li. The ratio of halide to FBA matrix diffusion coefficients determined in LCA rocks was around two, which is smaller than the factor-of-three ratio expected (and encountered in previous matrix diffusion experiments with higher porosity rock), corresponding to the factor-of-three difference in the free water molecular diffusion coefficients for these different tracers. The reason for this unexpected result in this experiment could not be determined definitively, but the authors suggest it may be related to errors and uncertainties in the measurements and analysis. Batch experiments were also conducted to confirm non-sorption or to measure sorption for the tracers. These experiments indicated negligible sorption of the halides and FBAs, confirming their suitability for use as nonsorbing tracers in matrix diffusion experiments and in ER-6-1 field tracer tests. The ^{14}C tracer was somewhat retarded by an unidentified sorption mechanism or by isotopic exchange, with the authors considering the latter the most likely. Calculated tortuosities based on the ratio of matrix diffusion coefficients to free water diffusion coefficients (D_m/D_o) for the benzoate and halide tracers ranged from 0.008 to 0.153, and the measured porosities ranged from 0.009 to 0.060. In the fracture transport experiments, the normalized breakthrough curves of tracers with different diffusion coefficients showed little or no separation, suggesting an apparent lack of matrix diffusion occurring in these experiments. However, when the ratio of the two tracers' normalized concentrations versus time was plotted, rather than the concentrations themselves, these figures indicated that matrix diffusion was occurring in the fracture experiments. The authors conclude that "although matrix diffusion is much slower in the LCA than in fractured volcanic aquifers because of the much lower matrix porosities of the LCA, it is still a potentially important process over long time and distance scales" (Reimus et al., 2006a).

Reimus et al. (2006b) analyzed data obtained from laboratory diffusion cell experiments conducted over the past 10 years on NTS rock from four sources: Callahan et al. (2000), Reimus et al. (2002b), Reimus et al. (2002c), and Bechtel SAIC (2004c). The Reimus et al. (2006b) data were screened so that they were not duplicated in the database. These experiments used 47 different volcanic rock

samples from 8 different NTS locations, primarily from Pahute Mesa. Ten of the samples represented "parallel" samples where one sample consisted only of rock matrix and the other sample from the same interval contained a fracture surface with natural mineral coatings. Measured porosities ranged from 0.06 to 0.37 and measured permeabilities ranged from 7.8×10^{-19} to 4.7×10^{-15} m^2. Calculated tortuosities based on the ratio of matrix diffusion coefficients to free water diffusion coefficients (D_m/D_o) ranged from 0.002 to 0.31. Tracers used in the experiments included Br, I, and PFBA. Permeabilities were measured directly on the diffusion cell wafers but porosities were measured on other pieces of core assumed to be representative. For this reason, a number of experiments (different wafers, different tracers, and repeat experiments) have the same reported porosity, resulting in "columns" of green diamonds in Figures 10-2 and 10-3; exhibiting as much as an order of magnitude difference in the tortuosity for the same reported porosity. The authors found that, for this dataset, D_m/D_o (or tortuosity, ω, using Equation [10-2]) correlated to porosity, ϕ, by:

$$\log \omega = 3.068\ \phi - 1.979 \qquad (10\text{-}4)$$

with a coefficient of determination (R^2) value of 0.37; tortuosity correlated to permeability, k, by:

$$\log \omega = 0.254 \log k + 2.91 \qquad (10\text{-}5)$$

with an R^2 value of 0.49; and tortuosity correlated to permeability and porosity by:

$$\log \omega = (1.91 \pm 1.29)\phi + (0.19 \pm 0.089)\log k + (1.42 \pm 1.60) \qquad (10\text{-}6)$$

with an R^2 value of 0.54. The ranges in Equation (10-6) represent the 95 percent confidence interval (CI). The evaluations suggest that tortuosity correlates to permeability better than to porosity alone, and including both porosity and permeability improves the ability to predict tortuosity. A detailed presentation and discussion of the results for tortuosity as a function of porosity and permeability is presented in Reimus et al. (2006b). Including a correlation of tortuosity to permeability is not proposed for Yucca Flat/Climax Mine transport modeling because of the more limited data available for permeability as compared to the data available for porosity.

Walter (1982) derived matrix diffusion coefficients by diffusion cell experiments with fractured tuff samples from Yucca Mountain and also determined constrictivity and tortuosity from electrical

resistivity experiments (approach is discussed in Section 10.3.3). He found a high correlation between total porosity and matrix diffusion coefficient (correlation coefficient [r] = 0.9), and a "fair" correlation between tortuosity and median pore diameter (r = 0.75). Duplicate tracer samples were collected, and the mean concentration value was used in the data analysis. The concentration in the tracer cell was replaced every 24 hours to keep the concentration constant. This is one of the few experimental reports that documented experiment temperature and provided comments on the quality of each measurement. Walter (1982) also included calibration process information. Porosities of the tuff samples ranged from about 10 to 40 percent. Matrix diffusion coefficients ranged from 2×10^{-11} to 2×10^{-10} m^2/s. Tortuosities calculated using Equation (10-2) ranged from 0.009 to 0.083.

Papelis and Um (2003a) studied adsorption and diffusion and also conducted spectroscopic analysis of Frenchman Flat rock samples (welded ash-flow and zeolitic volcanic tuffs) using pulverized, sieved particles. The matrix diffusion values were determined by batch experiments, measuring the change in tracer concentration over time for a test tube containing spherical volcanic tuff particles, in a tracer solution, using three different tracers: Sr, Cs, and Pb. Matrix diffusion coefficients ranged from 2×10^{-14} to 9×10^{-9} m^2/s, corresponding to tortuosities of 0.0003 to 17. They studied adsorption and diffusion and also conducted spectroscopic analysis of Frenchman Flat rock samples using pulverized, sieved particles (welded ash-flow and zeolitic volcanic tuffs). The diffusion experiments ("rate of uptake") were conducted with batch experiments, measuring the change in tracer concentration over time for a test tube containing spherical volcanic tuff particles in a tracer solution. Three different tracers were used: Sr, Cs, and Pb. This batch type of experiment on substantially altered core fragments and using tracers that exhibited sorption effects resulted in the largest scatter for this dataset of any of the others reported here, with many tortuosities greater than one. As such, experimental difficulties and uncertainty in determining tortuosity are evident. For the above discussed reasons, the experimental data from this source were not included in the database for development of a tortuosity-porosity correlation.

Triay et al. (1997) derived matrix diffusion coefficients by diffusion cell experiments with volcanic tuff samples from Yucca Mountain, using two different tracers: HTO and $^{99}TcO^-_4$. The experimental results yielded matrix diffusion coefficients ranging from 1×10^{-11} to 3.5×10^{-10} m^2/s (equivalent tortuosities from 0.005 to 0.15). The porosities for cores used in these measurements ranged from 0.06 to 0.10. The permeability was not reported for the samples.

Papelis and Um (2003b) derived matrix diffusion coefficients by diffusion cell experiments using welded tuffs, nonwelded tuff, and devitrified lava samples from Pahute Mesa. The experiments used Br, Cs, Sr, and Pb as tracers. The Cs, Sr, and Pb all exhibited varying degrees of sorption. Thus, the matrix diffusion coefficients from the experiments using these tracers are more uncertain than those from experiments using Br. Therefore, only the matrix diffusion coefficients for Br are used for calculating tortuosity for each core sample reported. Both "matrix" and "fracture" slabs (2 cm x 2 cm x 0.5 cm thick) were used, where the "fracture" slabs had a natural fracture surface as one of the slab sides, to allow for study of diffusion through the surface coatings as well as the matrix, to see whether this resulted in substantially different matrix diffusion responses. No consistent trend was observed between "matrix" slabs and "fracture" slabs, with the diffusion coefficients determined for both types showing similar ranges.

Hershey et al. (2003) performed and evaluated laboratory diffusion experiments with Br and ^{14}C through three LCA cores obtained from two NTS wells. The diffusion experiments assessed diffusion from a core piece saturated with tracer solution into a reservoir in contact with one surface of the core sample. The diffusion cells were set on a vibrating platform that was operated daily for 15 min to keep the reservoir solution mixed. They determined tortuosities using the Br data only using a relation equivalent to Equation (10-2). The effective matrix diffusion coefficient for Br ranged from 5.2×10^{-10} to 6.9×10^{-10} m^2/s. The reported effective porosities ranged from 0.0170 to 0.0256, and the calculated tortuosities ranged from 0.25 to 0.33. These tortuosities appear to be uncharacteristically large for such low-porosity rock samples in comparison to other diffusion cell experiments on NTS samples and from other published diffusion experiments in the literature.

Laboratory diffusion data for NTS granite/crystalline rock were not available. Therefore, measurements for granite/crystalline rock were obtained from a number of sources around the world. These include samples from fractured granite rock in Sweden (Mazurek and Jakob, 2002; Jakob, 2004), crystalline rocks in Sweden (Skagius and Neretnieks, 1986), and a number of measurements on granite rock samples from the Swedish Askarshamn site investigation (Gustavsson and Gunnarsson, 2005). A wide variety of sample selection techniques, tracer types, and experimental methodologies were used in the experiments and will not be summarized here; these measurements are included for complete coverage of the lithologies that could be encountered in Yucca Flat transport modeling.

10.3.2 Field Tracer Diffusion Experiments

Field tracer experiments have been performed at several locations at or near the NTS to determine double-porosity transport parameters. Typically, data from the tracer tests are interpreted to evaluate transport conceptual models (e.g., single-porosity or double-porosity transport) and to yield transport parameters such as dispersivity, fracture spacing or aperture, effective porosity, and matrix diffusion coefficient. Because of the multiple parameters involved and the nonuniqueness of interpretations of field tracer tests, matrix diffusion coefficients determined from field tracer tests are more uncertain than those determined through laboratory experiments. Reimus and Haga (1999) recognized this uncertainty and defined a lumped parameter called the mass transfer coefficient, which is defined in terms of the matrix diffusion coefficient, matrix porosity, and fracture half aperture. Because the effects of the magnitude of each parameter are lumped together in the mass transfer coefficient, any estimate of matrix diffusion coefficient is quite uncertain. In fractured geologic media, tracer tests are most valuable for determining transport pathways, effective porosities, and mass transfer coefficients for matrix diffusion (the lumped parameter), and in confirming the presence or absence of matrix diffusion, but not for determining estimates of matrix diffusion coefficients.

Reimus et al. (2003a) determined diffusion coefficients from tracer experiments, conducted in alluvium at Well NC-EWDP-19D1, located 18 km south of Yucca Mountain. In the alluvium at this well, the diffusive mass transfer was found to be inconsequential. The field test involved several sets of two tracers with different free water molecular diffusion coefficients (pairs of halides and fluorinated benzoates) that were simultaneously injected. Each tracer in the pair had essentially an identical response, “consistent with little diffusive mass transfer between flowing and stagnant water in the aquifer over the time scales of the test” (Reimus et al., 2003a). The nearly identical responses of the tracers with different diffusion coefficients in the tests provided strong evidence that diffusion did not play an important role in solute transport in the AA (Reimus et al., 2003a).

The BULLION FGE (IT, 1998) was conducted within the lava-flow aquifer, composed of fractured Tertiary rhyolite lava flows, at Pahute Mesa. Three wells, aligned consistent with the orientation of the major fracture system and downgradient of the BULLION underground nuclear test, were used. Tracers 2,6-DFBA and I were injected into one well; PFBA was injected into a second well; and concentrations were measured from water samples from a third well, which was pumped. Maximum interwell distance was 131.5 m. The experiment duration was 87 days, at which point the peaks of all

tracer breakthrough curves had been captured. A range of alternative calibrations with different combinations of parameters (matrix diffusion coefficient, fracture spacing, matrix porosity, fracture porosity, dispersivity, and proportion of tracer mass injected) were developed that adequately matched these tracer breakthrough curves (IT, 1998). They concluded that these calibrations suggest that the uncertainty in the matrix diffusion coefficient is "at least one order of magnitude" (IT, 1998). It was concluded that the mechanism of matrix diffusion was demonstrated by the tracer test results because "the observed breakthrough curves cannot be explained without invoking matrix diffusion" (IT, 1998). Reimus and Haga (1999) presented an analysis of the BULLION tracer test, in which a mass transfer coefficient was determined that includes matrix porosity, fracture half aperture, and a matrix diffusion coefficient. The estimated matrix diffusion coefficients contain error because of uncertainty in the true value for matrix porosity and fracture half aperture.

Cross-hole, forced-gradient tracer tests were conducted at the C-holes Complex in fractured volcanic tuffs for the YMP (Reimus et al., 1999; Bechtel SAIC, 2004c). The C-holes consist of three wells with inter-well distances of about 30 to 80 m. Tracers were injected into two horizons. The upper horizon consisted of the lower Prow Pass Tuff and the lower horizon consisted of the lower Bullfrog Tuff. Reimus et al. (1999) state that the completion intervals for the Prow Pass Tuff and the Bullfrog Tuff consist of variably welded tuffaceous rocks. Two tracer tests were conducted in the Bullfrog Tuff at the C-holes Complex. The first was a pilot test to determine the fastest flow path at the complex. That path was then used for a subsequent tracer test involving the injection of two conservative tracers (PFBA and Br), one reactive tracer (Li), and one microsphere tracer. The experiment duration after initiation of tracer injection was about 40 days. The thickness of the Bullfrog Tuff interval tested was about 100 m. At the depth of the completion intervals, the distance between the wells is about 30 m. The breakthrough curves observed in the pumping well show a bimodal behavior for all tracers (Bechtel SAIC, 2004c). The tracer responses in the Bullfrog Tuff were consistent with double-porosity transport behavior. This is evidenced by the different first peak concentrations for the conservative tracers consistent with their different free water diffusion coefficients. Two phases of tracer testing (conservative and reactive) were conducted in the Prow Pass Tuff at the C-holes Complex. The first phase (the conservative tracer test) consisted of the injection of two conservative tracers (2,4,5-TFBA and I). The second phase (the reactive tracer test) consisted of the injection of three conservative tracers (PFBA, Br, and Cl), one sorbing tracer (Li), and three microsphere tracers. The wells are located 29 m apart at the depth of the completion

interval. The average thickness of the completion intervals in the Prow Pass Tuff at the two wells was 71 m for the conservative tracer test and 74 m for the reactive tracer test. The tracer responses for both phases of testing in the Prow Pass Tuff are consistent with double-porosity transport behavior. This is evidenced by the different peak concentrations for the conservative tracers consistent with their different molecular diffusion coefficients.

Reimus et al. (2003b) present the results of a multiwell tracer test using multiple tracers in a fractured granite formation at the SHOAL underground nuclear test site in west-central Nevada. Three tracers (PFBA, Br, and Li) were injected into one well and concentrations were measured in water samples from a second well which was pumped. Interwell distance was about 30 m, and screened intervals were about 35 m. A small recirculation/injection flow rate from the production well to the injection well was maintained during the test. There was a separation between the nonsorbing tracer breakthrough curves obtained for samples from the pumping well discharge, with the tracer with the higher free water diffusion coefficient exhibiting a lower peak concentration and a longer tail than the tracer with the lower free water diffusion coefficient. This tracer breakthrough curve response confirmed that a double-porosity fracture-matrix conceptualization was appropriate to describe transport in the fractured granite.

A tracer test was conducted in the LCA at the ER-6-1 Well Cluster in southern Yucca Flat in 2004 (SNJV, 2006d). Three wells were used with alignment consistent with the orientation of the major fracture system. Tracers 2,4,5-TFBA and I were injected in the lower interval of one well. Tracers PFBA, Li, and Br were injected into the upper interval of that same well. Tracer 2,5-DFBA was injected into a second well. Tracer concentrations were measured in water samples from a third well, which was pumped. Maximum interwell distance is about 64 m. The open vertical interval in the pumping well and the injection well with separate lower and upper interval injections was about 1,315 m. The experiment duration was 84 days, at which point the peaks of all tracer breakthrough curves had been captured with the exception of 2,5-DFBA. Identification of a double-porosity conceptualization for transport between injection and pumping wells in the LCA at the ER-6-1 Well Cluster was inconclusive. This can be attributed to the relatively low matrix porosity (some core samples show typical matrix porosity of about 0.01) and the similarity in magnitude of apparent fracture porosity and matrix porosity. Because of the relatively low matrix porosities, one would also expect corresponding lower tortuosities, which would further reduce the impact of matrix diffusion

(less solute transfer from fractures to matrix) at the spatial and temporal scales of the tracer test. It was concluded by SNJV (2006d) that the tracer test time scale, being much smaller than that required for deep diffusion into the matrix blocks coupled with the low solute storage capacity in the matrix, resulted in insignificant matrix diffusion effects during the tracer test.

10.3.3 Formation Factor-Porosity Approach

Matrix diffusion coefficients of dissolved species can be related to matrix porosity and formation factor of rock-core samples. Klinkenberg (1951a and b) concluded that the factors that impede electrical conductance through a porous medium are the same factors that impede diffusion of a conservative solute. Conca and Wright (1992) explain this as follows: "The reason that electrical conductivity can be related to ionic diffusion through the Nernst-Einstein equation is that the ease with which a species diffuses through a liquid is exactly analogous to the ease with which the water molecules can align their dipoles along the electric field vector." Thus, factors that affect the diffusive paths also affect the current paths. For this reason, electrical conductivity can be a useful surrogate for the more difficult to measure tortuosity from laboratory diffusion cell experiments.

The ratio of the resistivity of the formation sample, C_S, to the resistivity of the saturating fluid, C_W, is called the formation factor, f, expressed as (Archie, 1942; Bear, 1972):

$$f = C_S / C_W \qquad (10\text{-}7)$$

Porosity and tortuosity affect the electrical conductivity of a water-saturated geologic medium in almost the same way as they affect the diffusion coefficient. The tortuosity can be expressed in terms of porosity and formation factor using the relation (Bear, 1972):

$$\omega = 1 / f\phi \qquad (10\text{-}8)$$

Miller (1989) presents an evaluation of diffusion in aquitards used for long-term isolation for deep-well injection of liquid hazardous wastes. He developed expressions for the "geometric correction factor G," which is equivalent to the tortuosity, ω, in Equation (10-2). Miller (1989) states that the geometric correction factor is a function of the matrix porosity and the lithology. The geometric correction factor (or tortuosity) is a function of formation factor and porosity. In Miller

(1989), both graphical illustrations and equations demonstrate the relationship between formation factor and porosity for a range of geologic media (e.g., sands, sandstones, carbonates, and clays). A variety of literature sources are summarized that show relationships between formation factor and porosity. For example, Archie (1942) developed a relationship between formation factor and porosity of the form:

$$f = \phi^m \qquad (10\text{-}9)$$

where m is an exponent found to be about 1.3 for unconsolidated media and varies between 1.8 and 2.0 for consolidated sandstones. In some cases, Archie's equation includes a coefficient, commonly assumed to be at or near unity, on the right side of Equation (10-9). Substituting Equation (10-9) into Equation (10-8), tortuosity can be expressed as:

$$\omega = \phi^n \qquad (10\text{-}10)$$

where $n = m\text{-}1$. Based on well-defined trends from extensive experimental investigations, Miller (1989) concludes that the exponent n normally varies as a function of lithology with increases in magnitude based on increasing constrictions and tortuousness of the pore channels. The plotted relations between geometric correction factor and porosity presented in Miller (1989) went to porosities as low as 0.1, but it is expected that these relationships would be valid for even lower porosities. The summarized results from Miller (1989), for the exponent n for various geologic media, is as follows:

Geologic Media	Exponent n
Unconsolidated sand	0.5
Consolidated sandstone	0.9
Tight unfractured limestones and dolomites	1.0
Clays and shales	2.0

Keller and Ibrahim (1982) conducted electrical resistivity measurements on volcanic core samples (basalt to tuff). Values of the exponent m in Equation (10-9) ranging from 1.5 to 1.88 were obtained. Lower m values were reported in comparison to other studies for limestones and crystalline igneous

rocks. The range for *m* yields corresponding values of exponent *n* in Equation (10-10) for volcanics from 0.5 to 0.88.

Formation factors determined from resistivity measurements on 15 Culebra Dolomite core samples from the DOE WIPP site in New Mexico varied from 13 to 407, with porosity varying from 0.07 to 0.26, and calculated tortuosity varying from 0.03 to 0.33 (average = 0.141) (Jones et al., 1992). Laboratory diffusion cell experiments were also performed on Culebra core samples. The tortuosities determined by both the diffusion cell and formation factor-porosity methods were reasonably consistent. The formation factor-porosity data from the 15 core samples were analyzed to yield an exponent *m* of 2.1 in Equation (10-9) and an exponent *n* in Equation (10-10) of 1.1 with an R^2 of greater than 0.96. The exponent *n* of 1.1 from the Culebra Dolomite core samples is consistent with the value of 1.0 from Miller (1989) for limestones and dolomites.

Because formation factor and porosity are relatively straightforward and inexpensive to measure on core samples, this provides a simple approach to estimate tortuosity or matrix diffusion coefficients for a large number of core samples, and may be particularly useful for determining the range of variation in matrix diffusion coefficients for different locations and lithologies. Because porosity measurements are often more readily available than formation factor measurements, the use of simple relationships like Equation (10-10) to estimate tortuosities could be a useful approach to augment the limited data that may be available from laboratory diffusion cell and field tracer experiments.

The evaluation of NTS-specific data to examine the relationship between tortuosity from laboratory diffusion cell experiments as a function of porosity is presented in Section 10.4.6 as well as a discussion of the comparison to the literature values above based on the formation factor-porosity approach.

10.4 Data Analysis

10.4.1 Data Evaluation Approach

The matrix diffusion data quality evaluation, data review, and data analysis process is described in the remaining sections of this section. The process consisted of the following primary steps:

1. Update the matrix diffusion database from the previous Frenchman Flat matrix diffusion parameter analysis adding newly available NTS data and literature data for crystalline rocks that may be representative of the granite confining unit.

2. Determine the data quality of each matrix diffusion measurement using the data transfer protocol outlined in SNJV (2004c).

3. For those experiments where tortuosity is not reported, calculate the tortuosity from the free water diffusion coefficient and the reported matrix diffusion measurements.

4. Review and analyze the data and determine the most appropriate correlation between tortuosity and porosity.

5. Develop a recommended statistical model for tortuosity values, based on a correlation with porosity and the uncertainty range of the data.

These steps are discussed in detail in the following sections.

10.4.2 Data Quality/Transferability Protocol

A detailed explanation of the data documentation and data transfer protocol used for this analysis is included in Attachment B of SNJV (2004d). The scoring protocol used to assign weights and multipliers to the matrix diffusion data is reported in Table 10-1 and discussed in the following text. The overall multiplier factor is a product of the multiplier factors for the three criteria presented in Table 10-1. The overall "score" of the data is the product of the weight and multiplier factors.

Because no clear trends in the tortuosity-porosity data were found to be representative of individual HSUs, no benefit was found to group the data into HSU-specific subsets (Figure 10-4). For this analysis, the data were considered as a whole to capture the full range and variability of the matrix diffusion dataset. For this reason, the weight factors W1 and W2 discussed in Table 10-1, related to permeability and porosity similarity to the HSU of interest, were all set to 1.0 for this analysis. Therefore, the total quality score of the data is equal to the product of the multiplier factors M1, M2, and M3 for measurement method, quality of the analysis, and quality of the documentation, respectively. The scoring is calculated for each measurement in the matrix diffusion dataset. The total scores for the NTS matrix diffusion data points range from 0.05 to 2.8

Table 10-1
Summary of Data Transfer Protocol for Yucca Flat Matrix Diffusion Coefficient Dataset
(Page 1 of 2)

Total score = W x M (for both data quality and transferability) - see each dataset entry for specific values	
WEIGHT FACTORS	W = W1 x W2 for geologic similarity of the data to the HSU of interest
W1. Determine Weight Factor for Permeability Similarity	
1	If permeability of measured sample is within 1 order of magnitude of Yucca Flat HSU permeability
0.6	If permeability of measured sample is within 1-2 orders of magnitude of Yucca Flat HSU permeability
0.3	If permeability of measured sample is within 2-3 orders of magnitude of Yucca Flat HSU permeability
0	If permeability of measured sample is greater than 3 orders of magnitude different from Yucca Flat HSU permeability
0.5	If permeability of sample is not measured and reported
1	If mean permeability of Yucca Flat HSU is not yet available
W2. Adjust Weight Factor for Porosity Similarity by multiplying above by:	
1	If porosity of measured sample is less than 25% different from Yucca Flat HSU porosity
0.7	If porosity of larger value (between measured and Yucca Flat HSU) is within 25 to 90% of small value
0.4	If porosity of larger value (between measured and Yucca Flat HSU) is greater than 90% different than smaller value
0.5	If porosity of D_m sample is not measured and reported
MULTIPLIER FACTORS	M = M1 x M2 x M3 for measurement method and quality of the analysis and documentation
M1. Measurement Method: M1a x M1b x M1c	
1	Laboratory Diffusion Cell Experiments (DCEs) (M1a)
0.5	If D_m determined by a method other than DCE, such as x-ray or neutron imaging, electrical conductivity, batch experiments using pulverized particles, etc. (non-DCE) (M1a)
2	If sample includes natural fracture surface, which may have mineral coatings that affect diffusion (Frac) (M1b)
0.6	If sample thickness is 80% smaller than average and, therefore, less representative of field-scale diffusive path lengths: < 0.27 cm (M1c)
1.4	If sample thickness is 80% larger than average and, therefore, more representative of field-scale diffusive path lengths: > 2.5 cm (M1c) (1.4 cm, average sample thickness of all samples (arithmetic average of dataset sample thicknesses, “avg_sample_thickness”)
1.5	If both increasing and decreasing concentrations are measured (no such experiments were identified in study reports for this analysis)

Table 10-1
Summary of Data Transfer Protocol for Yucca Flat Matrix Diffusion Coefficient Dataset
(Page 2 of 2)

M2. Data Reduction and Analysis Method: = M2a x M2b	
1	Current
0.5	Good method, but calibration information is suspect or not possible to verify (M2a)
0.5	Based on older or less-widely accepted methods but calibration information is good (M2a)
0.2	Both method and calibration information are suspect (M2a)
0.1 - 2.0	Variable, author's evaluation of measurement's quality, fit of the data to the experimental model, etc., noted in the "Multiplier_Comments" column of the dataset (M2b)
M3. Quality of the Documentation	
1	Good (thorough, easy to follow, traceable)
0.6	Appearing in a reputable or peer-reviewed report, but otherwise lacking in thoroughness
0.3	Poor

10.4.3 Data Review and Statistics

Tortuosity, grouped by core lithology type, is shown in Figure 10-4. There were no clear divisions or patterns, except:

- The crystalline/granite rock type (the light blue squares) have low porosities, as expected, and the matrix diffusion coefficients trend lower than the low porosity values for all other rock types in the dataset.
- The four LCA data points from Hershey et al. (2003) show relatively high tortuosity for the relatively low porosity cores.
- Tuff data tend to be represented in the middle of the tortuosity dataset, with more outliers in the zeolitic tuff rock type, perhaps indicative of more variation in this more altered rock type.

Figure 10-5 shows the full matrix diffusion dataset with the data point size indicative of the total quality score for that data point. Higher quality data have a larger symbol size; lower quality data have smaller symbols.

There are no clear patterns or trends of data quality with tortuosity, porosity, or lithology. Also, there are no tortuosity data for many of the HSUs and there are generally no clear differences in tortuosities

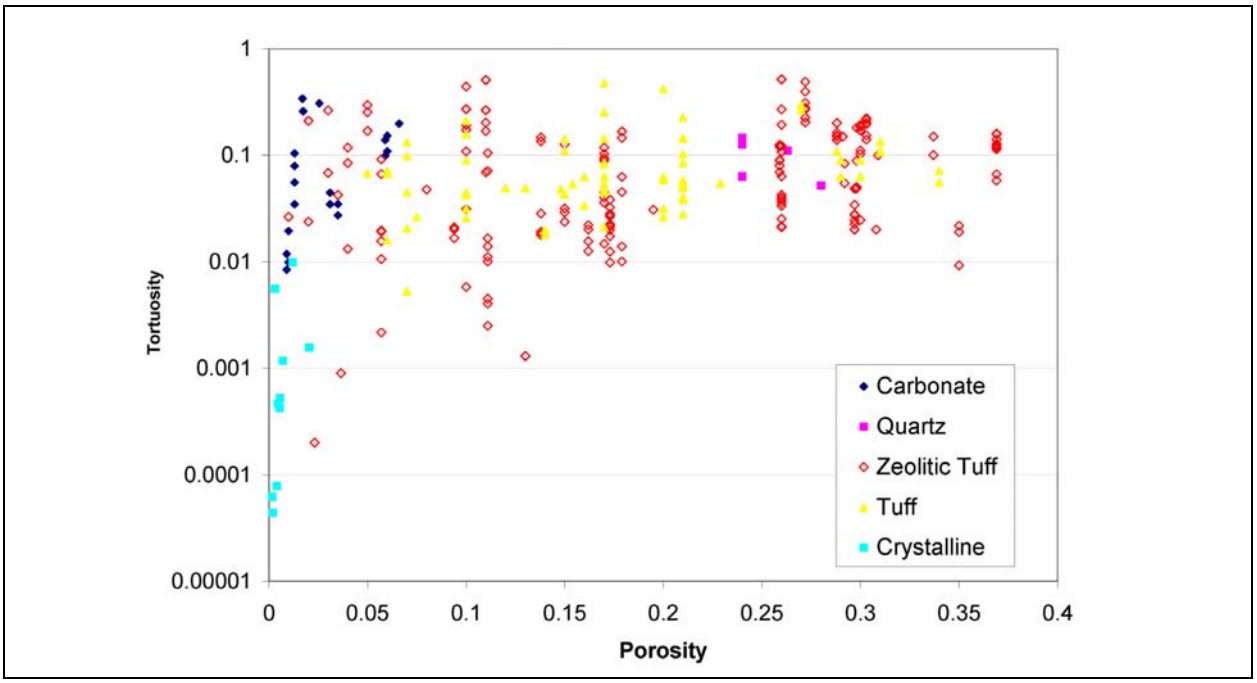

Figure 10-4
Tortuosity Data by Rock Type

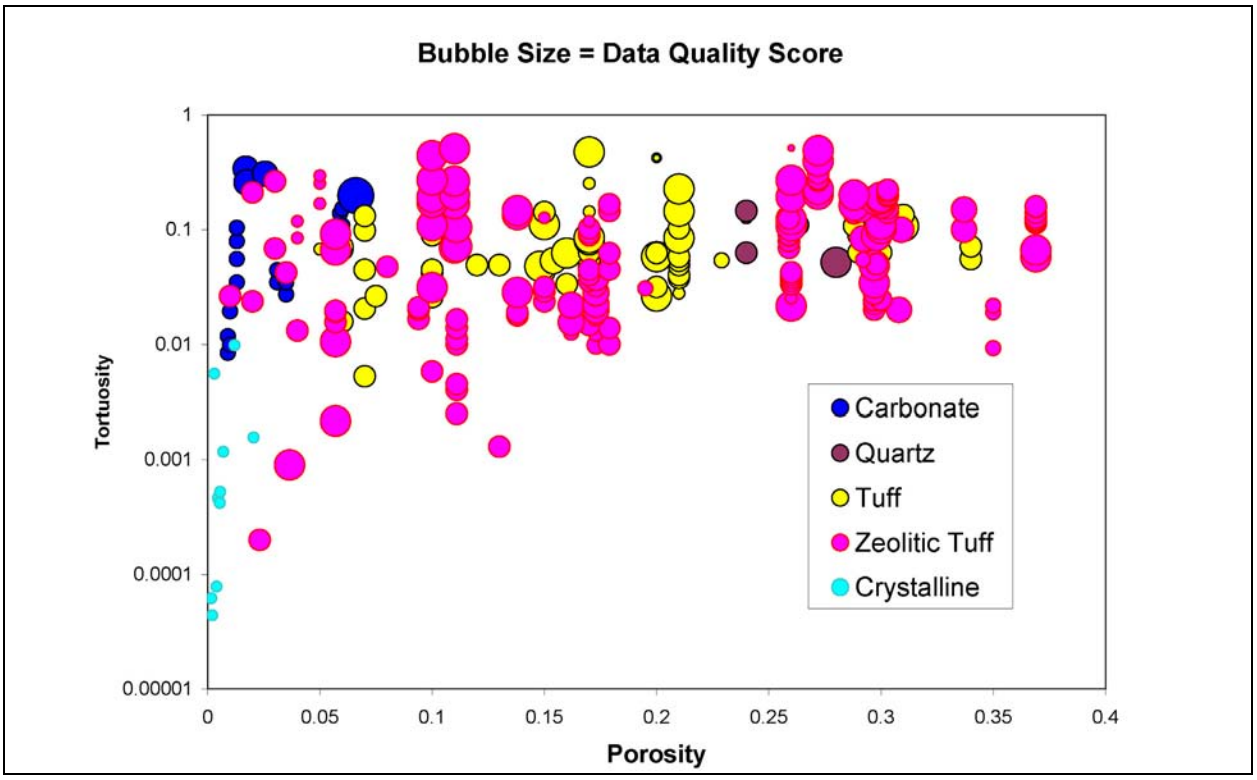

Figure 10-5
Tortuosity Data by Rock Type, Including Data Quality Score

for the individual HSUs with data. Therefore, the decision was made to not divide the data into HSU-specific subsets.

Figure 10-6 shows tortuosity versus depth of the core sample where depth was reported. There are no apparent trends of tortuosity with depth for this dataset.

Permeability data are unavailable for about half of the data points but, where measured and reported, show a general trend of increasing tortuosity with increasing permeability, as well as considerable variability in tortuosity for the lower-permeability cores (Figure 10-7).

Figures 10-8, 10-9, and 10-10 show the cumulative probability distribution functions for porosity, tortuosity, and permeability, respectively, for the matrix diffusion database. The median porosity is 0.173 and ranges from 0.002 to 0.369. For tortuosity (Figure 10-9), the entire database of tortuosities ranges over four orders of magnitude; it is important that any modeling recommendations capture this large variation appropriately. The median tortuosity is 0.072. Even the 75th percentile value is low, with 75 percent of all tortuosities less than 0.15. This suggests that even for rock with a relatively large porosity, the connectivity is low, and the rock pores are connected in a "tortuous" manner. This is supported by the generally low permeabilities, where they were measured and reported for the matrix diffusion experiments. The median permeability is only 2.4 x 10^{-17} m^2 (Figure 10-10). Ninety percent of the cores have permeabilities less than 1.0 x 10^{-15} m^2, indicating tight rock with poorly connected, very tortuous pore geometry. The highest permeability reported was less than 1.0 x 10^{-14} m^2.

10.4.4 Free Water Diffusion Coefficients

The free water diffusion coefficients (D_o) of most species range from 10^{-10} to 10^{-9} m^2/s (Drever, 1988). Free water diffusion coefficients are generally lower for larger molecules or ions with higher charges. A discussion of the various laboratory experimental methods for determining free water diffusion coefficients is presented in Mills and Lobo (1989). Because matrix diffusion coefficients (D_m) are a property of both the rock (through tortuosity ω) and the tracer species (through D_o), it is important that the best estimates of both are known, particularly when analyzing large sets of measurements from disparate sources. Calculated values of D_m (a property of the rock and the fluid) for any tracer may be determined by multiplying the tortuosity (a property of the rock alone) by the D_o value

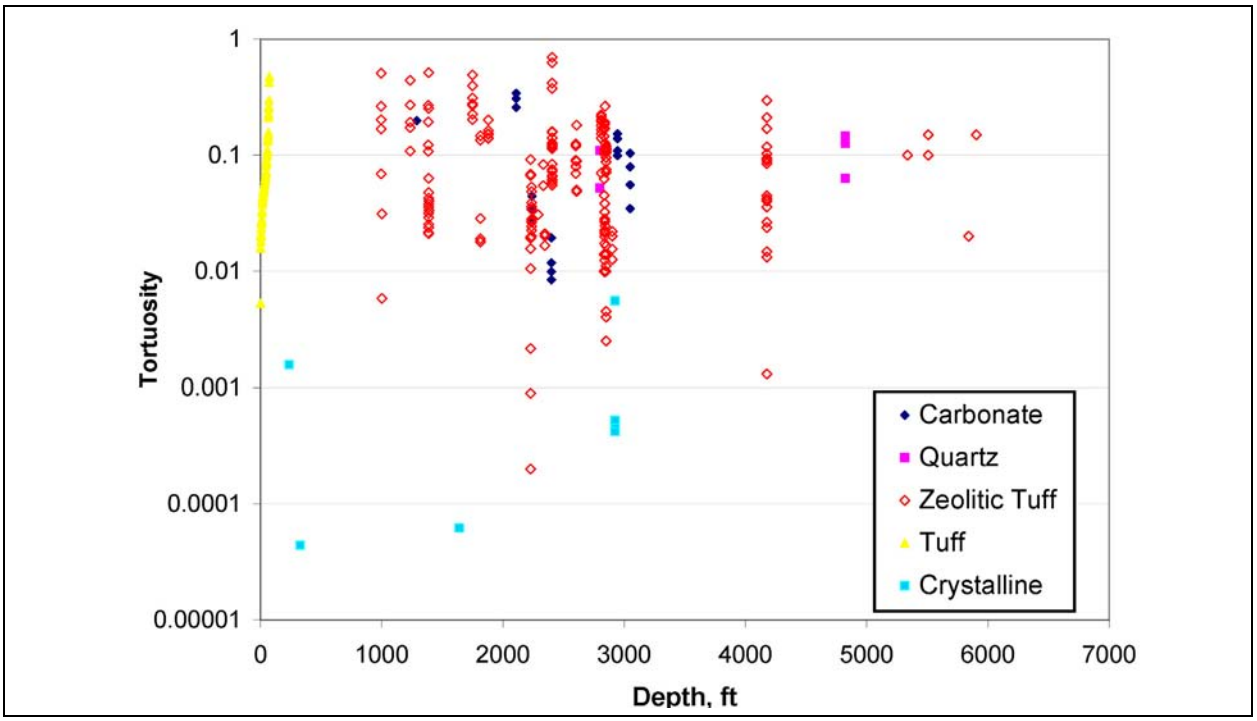

Figure 10-6
Tortuosity Data by Sample Depth and Rock Type

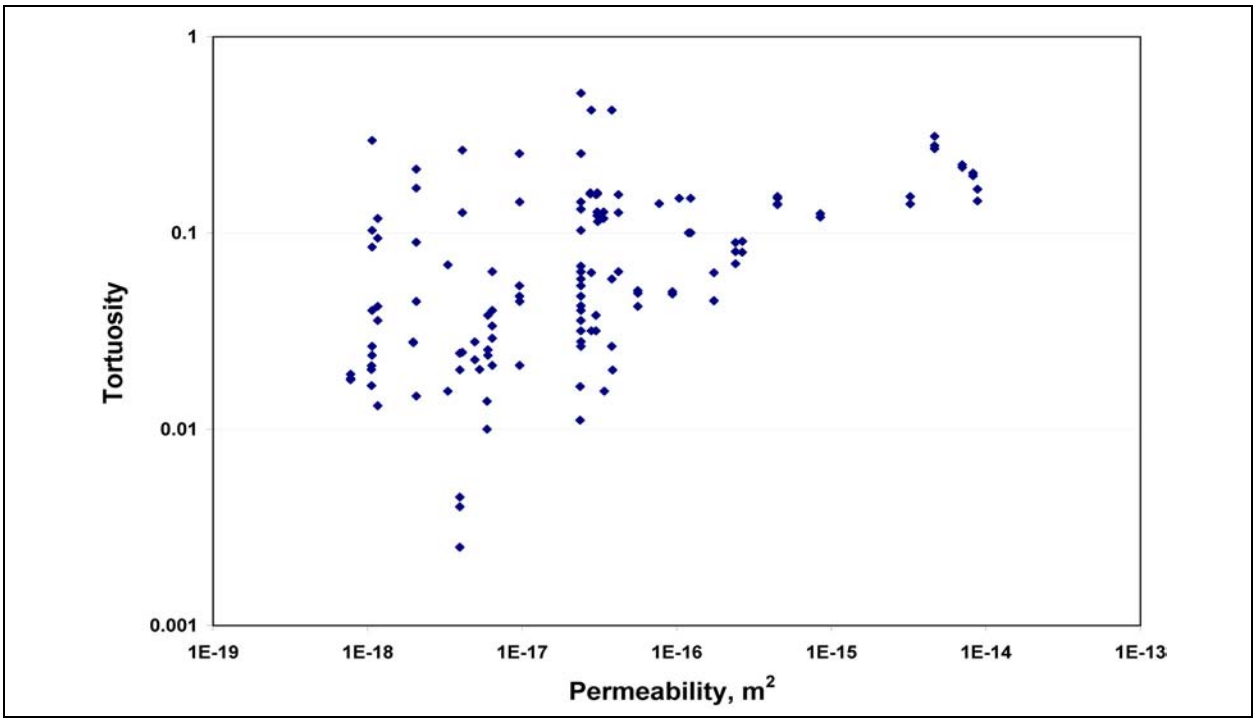

Figure 10-7
Tortuosity versus Permeability

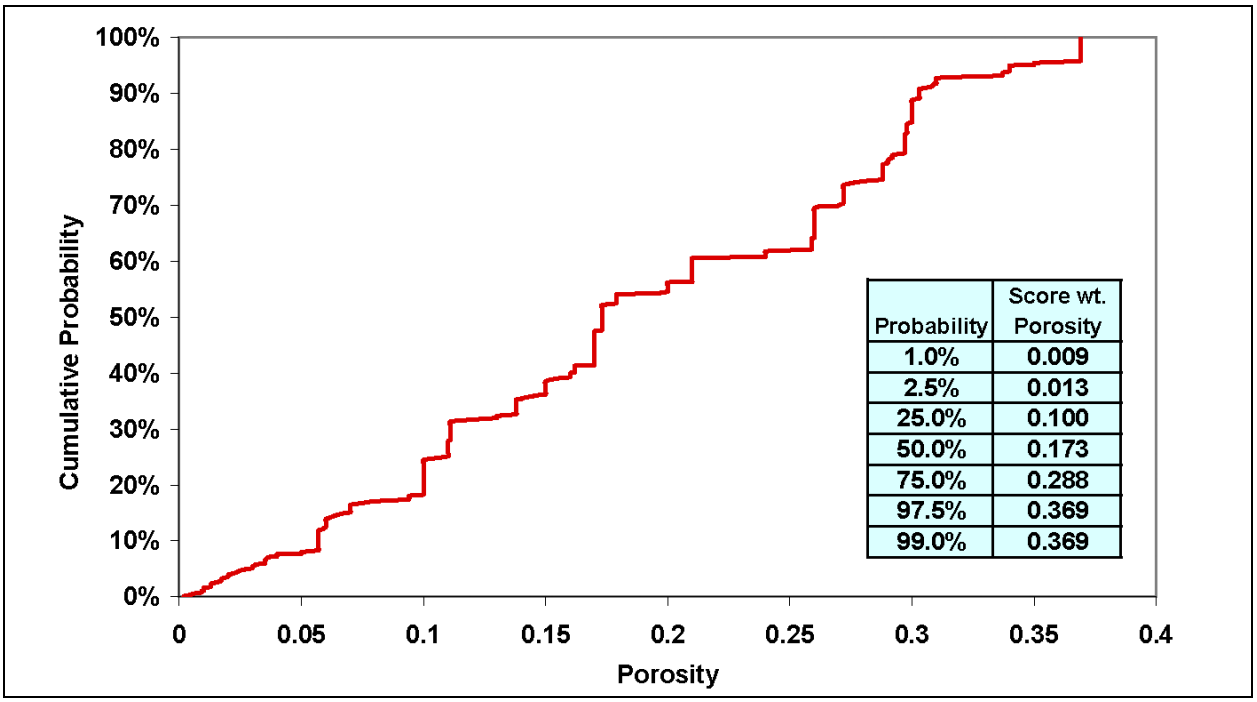

Probability	Score wt. Porosity
1.0%	0.009
2.5%	0.013
25.0%	0.100
50.0%	0.173
75.0%	0.288
97.5%	0.369
99.0%	0.369

Figure 10-8
Cumulative Distribution Function for Porosities of the Matrix Diffusion Samples

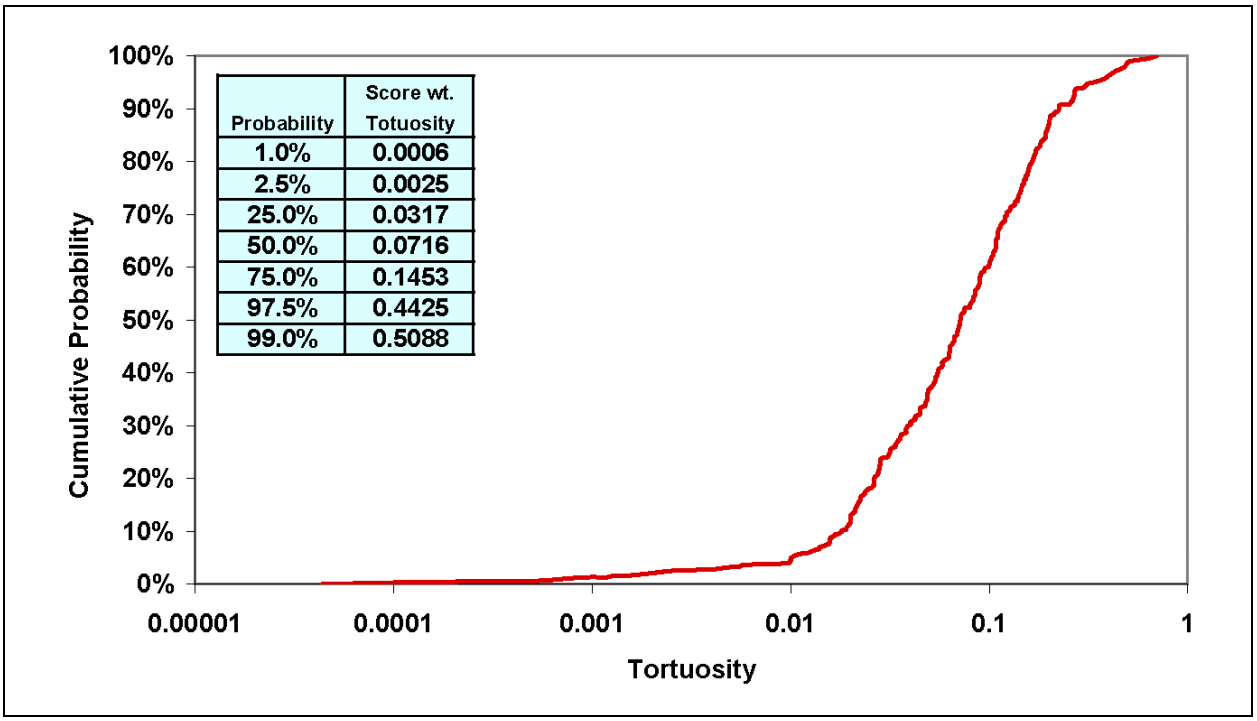

Probability	Score wt. Totuosity
1.0%	0.0006
2.5%	0.0025
25.0%	0.0317
50.0%	0.0716
75.0%	0.1453
97.5%	0.4425
99.0%	0.5088

Figure 10-9
Cumulative Distribution Function for Tortuosities of the Matrix Diffusion Samples

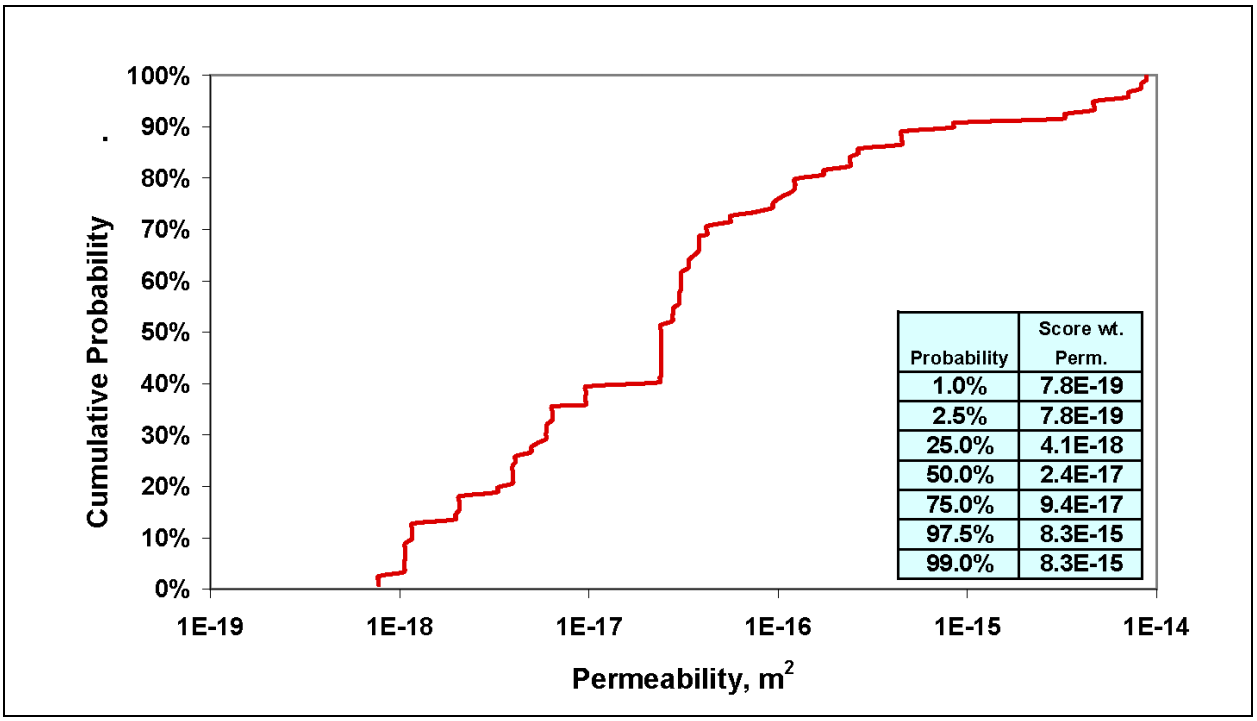

Figure 10-10
Cumulative Distribution Function for Permeabilities of the Matrix Diffusion Samples

(a property of the fluid alone). This relationship assumes that the only factor affecting the matrix diffusion coefficient other than porous media properties is the free water diffusion coefficient for the particular tracer species (i.e., no other processes other than diffusion are affecting the "apparent" diffusion coefficient [e.g., cation exchange, unaccounted sorption, complexation, anion exclusion, lowering of effective porosity for large molecules excluded from small pores]) and all tracer solutions are dilute (less than 1 molar [M]). Multi-component diffusion effects have also been excluded in this analysis.

A summary table of the unclassified radionuclide inventory relevant to the Yucca Flat/Climax Mine CAU is provided in Bowen et al. (2001). Tritium, as HTO, is the radionuclide with the largest free water diffusion coefficient (2.236×10^{-9} m^2/s at 25 °C [Mills, 1973]). The radionuclide with the lowest free water diffusion coefficient is Am (3×10^{-10} m^2/s [DOE/WIPP, 2004]). Thus, these two values bound the range for free water diffusion coefficient for species relevant to the NTS.

Various sources are available that provide free water diffusion coefficients for various species including Lerman (1979), Drever (1988), Mills and Lobo (1989), and Newman (1991). For

radionuclides where free water diffusion coefficients are not readily available in the literature, they can be calculated using the Nernst or Stokes-Einstein equations (Lerman, 1979; Mills and Lobo, 1989).

10.4.5 Effects of Temperature and Ionic Strength

The Stokes-Einstein equation predicts that free water diffusion coefficients (D_o) will be directly proportional to absolute temperature and inversely proportional to fluid viscosity, which decreases nonlinearly as temperature increases. Free water diffusion coefficient is directly related to temperature; therefore, temperature may be an important parameter if there is a large range in temperature in the laboratory diffusion experiments or throughout the groundwater flow system. If temperature is increased from 20 to 30 °C, the free water diffusion coefficient increases by 30 percent, as shown in Table 10-2. Temperatures are seldom reported for the matrix diffusion experiments discussed in Section 10.3.1, but those that were reported ranged from 25 to 30.5 °C. Because experimental temperatures are seldom reported, and when reported the range is small (typically laboratory ambient temperatures), laboratory matrix diffusion coefficient values were not corrected in this analysis for temperature. All laboratory measurements were assumed for the purposes of this analysis to be conducted at a temperature of 25 °C. The error introduced by this assumption is likely to be small, as the range of ambient indoor laboratory temperatures is small, especially compared to the range in temperatures expected in the HSUs over their lateral and vertical extent.

Table 10-2
Factor by Which Free Water Diffusion Coefficients Change as a Function of Water Temperature

Temperature (°C)	Free water diffusion coefficient should be multiplied by:
20	1
25	1.14
30	1.3
40	1.64
50	2.14
60	2.58

Source: Shaw, 2003a

The relationship between temperature and free water diffusion coefficients and the relative adjustment needed is presented in Shaw (2003a) and shown in Table 10-2 and Figure 10-11. These data, developed from the Stokes-Einstein equation, were fit to the polynomial shown in Figure 10-11 where the data in Table 10-2 are plotted as open circles and the polynomial relationship is shown as the red curve.

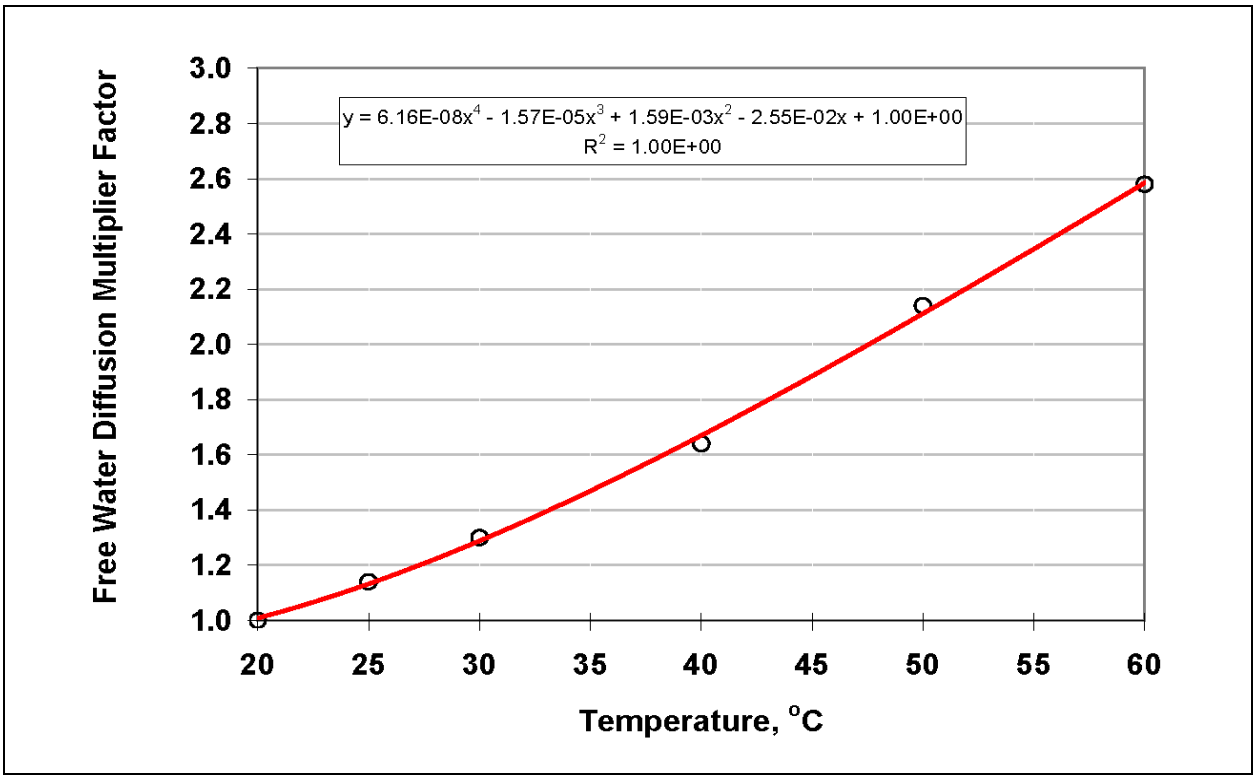

Figure 10-11
Free Water Diffusion Adjustment (Multiplier) for Increasing Temperature

Temperature conditions logged in the deeper HSUs in Yucca Flat are relevant if solutes should ever reach depths substantially below the ground surface. Temperatures measured from logging at the ER-6-1 Well Cluster and in wells ER-7-1 and ER-12-2 range up to 42, 53, and 63 °C, respectively. Correction of the free water diffusion coefficients for temperature effects is recommended for the CAU transport model as temperatures in the HSUs of Yucca Flat range from about 20 °C to more than 60 °C. The higher temperature ranges will result in about a factor of two increase in free water diffusion coefficient.

Alternatively, the value of the free water diffusion coefficient from one temperature to another can be estimated using a relation presented in Lerman (1979):

$$D_{T1} / D_{T2} = (\eta 1/T1) / (\eta 2/T2) \qquad (10\text{-}11)$$

where T is temperature in degrees Kelvin, D_{T1} and D_{T2} are the free water molecular diffusion coefficients at temperatures $T1$ and $T2$, respectively, and $\eta 1$ and $\eta 2$ are the water viscosities at temperatures $T1$ and $T2$, respectively. Thus, correcting for the change in the viscosity of water is sufficient to estimate the new free water diffusion coefficient. Lerman (1979) also presents expressions similar to Equation (10-11) for calculating free water diffusion coefficients as a function of modified water viscosity resulting from changes in total solutes concentration or pressure. Both of these effects are of minor importance in comparison to temperature for matrix diffusion in fractured media in Yucca Flat.

Diffusion coefficients are a relatively weak function of ionic strength until ionic strengths become greater than about 1 M (Newman, 1991). As ionic strengths greater than 1 M are unlikely to occur at the NTS (even in cavities), the effect of ionic strength on diffusion coefficients is considered to be relatively minor compared to the effect of rock properties and temperature (SNJV, 2004c). The concentration of the tracer species was not reported in all experiments discussed here; however, when reported, the concentrations were much less than 1 M.

10.4.6 Tortuosity-Porosity Correlations from Laboratory Diffusion Experimental Data

Various matrix diffusion formulations were considered in developing the tortuosity-porosity correlations for the NTS matrix diffusion database. The exponential type regression showed a better quality of fit (as measured by the R^2 value) compared to a log-linear type regression or a linear-linear type regression. An exponential formulation is of the type (same as Equation [10-10]):

$$\omega = \phi^n \qquad (10\text{-}12)$$

where n is an exponent determined by lithology or by the best fit to the dataset. This can also be rearranged to allow use of a linear regression:

$$\log \omega = n \log \phi \qquad (10\text{-}13)$$

where n is now the slope of the line and the intercept is set to zero.

Other laboratory diffusion investigations that develop tortuosity-porosity functional relationships are presented in the literature. For example, Boving and Grathwohl (2001) conducted laboratory tracer diffusion experiments on sandstone and limestone cores. The sandstone and limestone porosity ranges were 11.0 to 24.5 percent and 3.3 to 43.0 percent, respectively. They obtained tortuosities (using Equation [10-2]) for the sandstones and limestone samples that ranged from 9.1×10^{-3} to 3.8×10^{-2} and 3.6×10^{-4} to 0.16, respectively. The exponent n in Equation (10-10) that best fit both the sandstone and limestone data was 2.2. The larger exponent determined by Boving and Grathwohl (2001) as compared to Miller (1989) for sandstones (n = 0.9) and limestones (n = 1.04) indicates much smaller tortuosities for these authors even when investigating similar lithologies. These differences in exponent n for similar lithologies provide some measure of uncertainty and the need for site-specific data.

Zavarin (2002) adopts a similar relationship for relating matrix diffusion coefficients as a function of porosity expressed as:

$$D_m = D_o \, \phi^m \qquad (10\text{-}14)$$

where he defines m as the cementation factor, ranging from 1.3 to 2.5 (citing Dullien [1979] as the reference for the exponent m). (Note that this m is equivalent to n in Equation [10-2]). Rearranging with $D_m/D_o = \omega$, this equation is equivalent to the relation for tortuosity given in Equation (10-10). Zavarin (2002) analyzed the experimental data from 33 diffusion cell experiments using ^{3}H in a project report by Reimus and others (the data were later published as Reimus et al. [2002c]) with optimization of the value of m and minimization of the difference between experimentally determined and predicted D_m. He obtained a least squares fit with m = 1.7 but found the correlation to be weak noted by the spread in the data about the line representing the functional relationship. He also interpreted the best fit to the entire D_m dataset and determined m = 1.3 with the correlation between experimentally determined and predicted D_m being poor for the ^{14}C and ^{99}Tc tracers. It is likely that not performing porosity measurements on the same wafers used in the diffusion experiments (discussed further in Section 10.3.1) caused some of the scatter and thus the weaker correlation.

Lerman (1979) provides an extensive review of diffusion processes in sediments. He presented a log-log plot of matrix diffusion coefficient versus porosity and determined that matrix diffusion coefficient (or tortuosity) is approximately directly proportional to porosity raised to power of two (equivalent to n = 2 in Equation [10-10]).

Exponential type correlations (see Equation [10-12]) based upon lithology available from the literature are shown in Figure 10-12 in comparison to the NTS database measurements and regression line (n = 1.33).

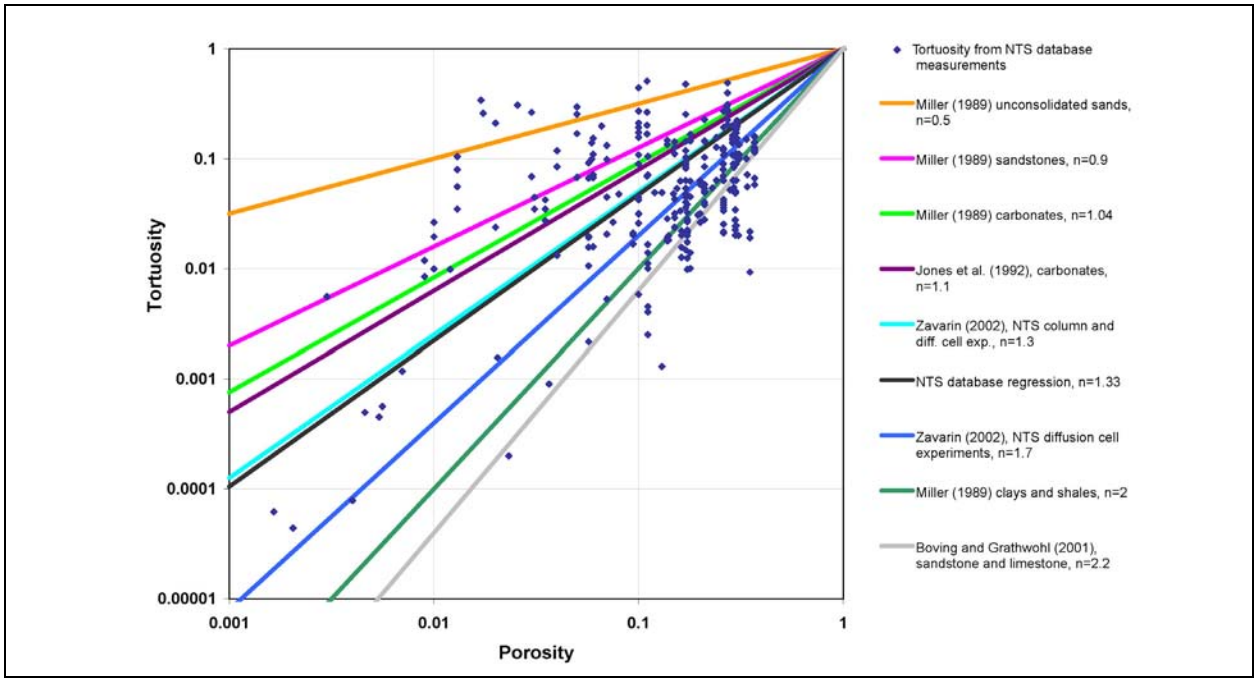

Figure 10-12
Log-Log Relationships Between Tortuosity and Porosity from Various Published Studies Compared with the NTS Database Measurements

Figure 10-13 shows a comparison of the exponential type formulations to the log-linear type correlation of Reimus et al. (2006b) given in Equation (10-4). The log-linear type correlation (the red curve in Figure 10-13) is much flatter at low porosities. Over the full range of porosities, the log-log or exponential type tortuosity correlations appear to track the general average trend of the data better than the log-linear type correlation.

The NTS database was fit to an exponential formulation by a least squares regression, as shown in Figures 10-14 through 10-16. The least squares regression-determined exponent is 1.33. The exponent for the upper limit of the 95 percent CI is 0.4. The exponent for the lower limit of the 95 percent CI is 3.2. The R^2 equals 0.82 for the exponential type equation regression for the NTS database.

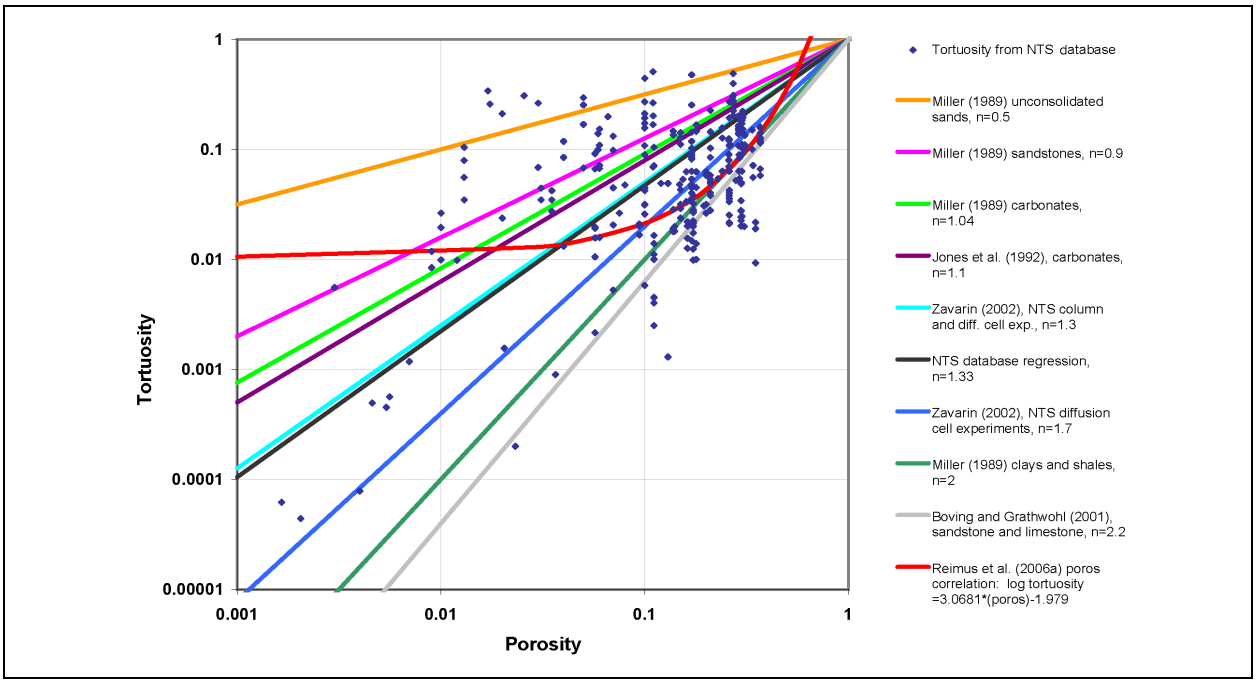

Figure 10-13
Comparison of Log-Log and Log-Linear Relationships Between Tortuosity and Porosity

The subset of measurements conducted upon carbonate samples within the NTS database consists of 20 datapoints, from Hershey et al. (2003) and Reimus et al. (2006a). The carbonate measurements appear to form a distinct subset in the measured data (the solid blue diamonds in Figure 10-4), with typically higher tortuosities at a given porosity than those observed for the database considered as a whole. The least squares regression-determined exponent for this carbonate subset is 0.7. This is in contrast with typical behavior for carbonates reported for Miller (1989) and Jones et al. (1992) where carbonate tortuosities are lower than other rock types considered, for a given porosity. These are shown in Figure 10-12, where the result from Miller (1989) is shown as the lime green line, with an exponent of 1.04, and the result from Jones et al. (1992) is shown as the purple line, with an exponent of 1.1. For the NTS carbonate subset, the exponent for the upper limit of the 95 percent CI is 0.3. The exponent for the lower limit of the 95 percent CI is 1.1.

10.5 Scaling Considerations

Liu et al. (2006) compiled values of effective matrix diffusion coefficients estimated from field tracer tests for a variety of different rock types. His analysis demonstrated that the effective matrix

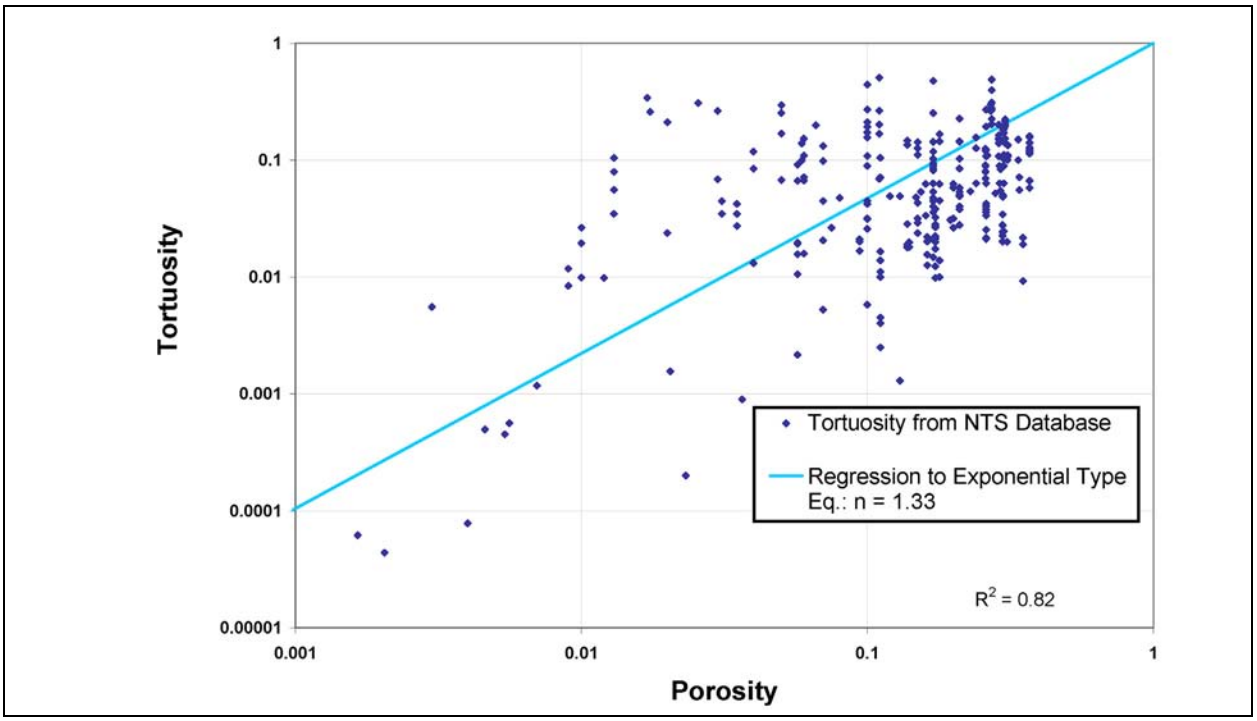

Figure 10-14
Correlation of Tortuosity and Porosity (Log-Log Axes) for the Matrix Diffusion Dataset

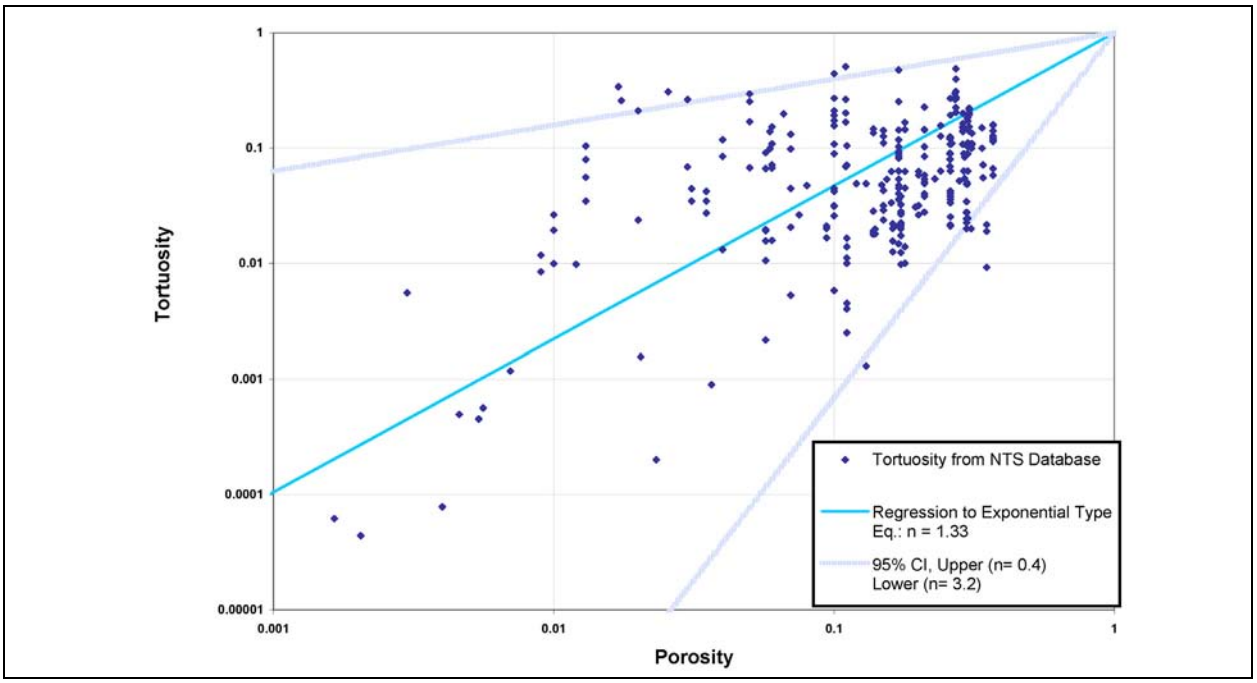

Figure 10-15
Correlation of Tortuosity and Porosity (Log-Log Axes) for the Matrix Diffusion Dataset, Including the 95% Confidence Interval (Log Scale for Porosity)

The same graph plotted using the linear scale for porosity is shown in Figure 10-16 for comparison purposes.

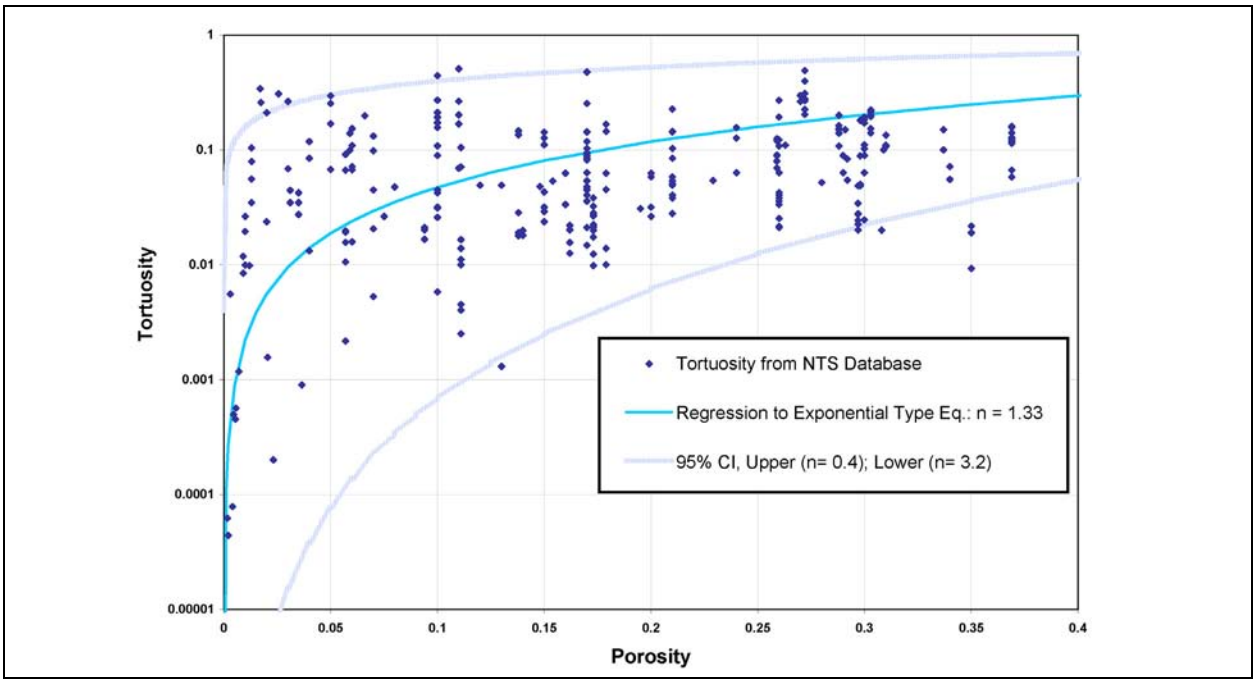

Figure 10-16
Correlation of Tortuosity and Porosity (Log-Linear Axes) for the Matrix Diffusion Dataset, Including the 95% Confidence Interval (Linear Scale for Porosity)

diffusion coefficient generally increases with test scale and concluded that simulated travel times may be significantly underestimated when this scale-dependent behavior is not considered. Reimus and Callahan (2006) evaluated scaling considerations in fractured volcanic rocks at the NTS from matrix diffusion studies from field tracer tests at two locations and laboratory experiments using core samples. The interpreted lumped parameter mass transfer coefficient (includes matrix diffusion coefficient, matrix porosity, and fracture half aperture) appeared to decrease as time and length scales of observation increased. They concluded that this is most likely the result of larger effective apertures as distance increases.

Interpretation of field tracer tests to determine matrix diffusion coefficients is inherently uncertain because of factors including non-ideal tracer test operating conditions, heterogeneity of the geologic media being investigated by the tracer test, simplifications in the tracer test interpretation approaches, and inability to isolate the effect of matrix diffusion alone in the tracer breakthrough response. For these reasons, inclusion of a scale effect in transport modeling for Yucca Flat/Climax Mine CAU would require further justification.

10.6 Data Limitations

This analysis assumes that all nondiffusive processes encountered during matrix diffusion experimental measurements can be neglected or are otherwise explicitly accounted for before matrix diffusion values are reported. Some of the nondiffusive processes that may have affected laboratory diffusion experiments include adsorption, cation exchange, complexation, anion exclusion, lowering of effective porosity for large molecules excluded from small pores, and inadvertent advective transport because of unintentional pressure gradients caused by barometric effects or tracer solution density contrasts. This analysis also assumes that all experimental tracer solutions are dilute (less than 1 M). Multi-component diffusion effects have not been included in this analysis.

The importance of the matrix diffusion coefficient is expected to be greater for transport in fractured media than in alluvial media. Therefore, it will be of more importance in transport model realizations where there is significant movement of contaminants in the volcanic aquifers or LCA.

10.7 Summary

Solute transport in high-permeability zones is typically dominated by advective-dispersive processes, while transport in low-permeability zones is dominated by diffusion. In fractured media, a double-porosity conceptualization is typically assumed with matrix diffusion between the fractures and the adjacent matrix having the effect of attenuating both the concentration and travel time of aqueous-phase contaminants moving through fractures. This process involves the diffusion of contaminants from groundwater flowing in rock fractures into and out of the relatively stagnant water in the pores of the surrounding rock matrix. The importance of diffusion of solutes from fractures into the adjacent matrix has been studied and reported extensively in the literature and has been established as an important process for retarding the transport distance of solutes introduced into fractured geologic systems.

Laboratory and field tracer experiments at NTS and additional experiments reported from the literature for other sites were synthesized to develop a matrix diffusion coefficient distribution for the HSUs in Yucca Flat. It was found that a relationship could be developed between tortuosity and porosity. Tortuosity is the ratio of the matrix diffusion coefficient to the free water diffusion coefficient. The use of a tortuosity-porosity functional relationship is useful because porosity data are

more often measured and more readily available than tortuosities or matrix diffusion coefficients. Using tortuosity rather than matrix diffusion in the analyses is useful because it allows for the separation of the effects of the individual tracer chemical from the effects intrinsic to the rock itself. The matrix diffusion value is always specific to a specific chemical tracer, whereas tortuosity is a rock property independent of the chemical tracer used to conduct the measurement. If matrix diffusion is needed for a specific chemical constituent, it can easily be calculated as the product of tortuosity for the rock and free water diffusion coefficient for that specific chemical.

Tortuosity can be defined as a bulk measure of the constrictivity and tortuous nature of the interconnected pore space through which diffusion is occurring. These factors result in variation in pore channel diameters and path lengths as the diffusing solute migrates through the interconnected porosity. Tortuosity has a magnitude $0 < \omega < 1$ when defined in the form presented here. Smaller tortuosities are indicative of longer diffusional path lengths and greater resistance to diffusion through the medium.

The entire dataset of tortuosities ranges over four orders of magnitude – it is important that any transport modeling approach captures this large variation appropriately. The score-weighted median tortuosity is 0.072. Even the 75th percentile tortuosity value is low, with 75 percent of all tortuosities less than 0.15. This suggests that, even for rock with a relatively large porosity, the connectivity is low – the rock pores are connected in a “tortuous” manner. This is supported by the generally low permeabilities, where they were measured and reported for the matrix diffusion experiments.

Permeability data were available for about half the datapoints, and these data indicated a general trend of increasing tortuosity with increasing permeability as well as more variation in tortuosity for the lower permeability cores. There were no apparent trends of tortuosity with lithology nor tortuosity with depth.

Because no clear trends in the tortuosity-porosity data by HSU were found, there is no benefit in grouping the data into HSU-specific subsets. Additionally, considering the dataset as a whole allows for the full range and variability of the matrix diffusion dataset to be captured, which would be difficult in a sparser subset of the data.

The exponential formulation recommended for developing tortuosities for the Yucca Flat/Climax Mine CAU is of the form:

$$\omega = \phi^n \qquad (10\text{-}15)$$

where ω = tortuosity, ϕ = porosity, and n = 1.33, an exponent determined by regression on the entire dataset of matrix diffusion coefficient experiments. The 95 percent upper CI is n = 0.4 and the 95 percent lower CI is n = 3.2.

This exponential correlation is recommended because it (1) honors the NTS data, (2) results in a realistically wide 95 percent CI, (3) has a theoretical basis, rather than a simple empirical correlation of the available data, and (4) shows a better quality of fit (as measured by the R^2 value) compared to log-linear type regression or linear-linear type regression correlations.

Matrix diffusion for any radionuclide can be simply calculated by multiplying the tortuosity determined from Equation (10-15) by the free water diffusion coefficient for that radionuclide:

$$D_m = \omega D_o \qquad (10\text{-}16)$$

where matrix diffusion, D_m, is a property of the rock and the radionuclide; tortuosity, ω, is a property of the rock alone; and the free water diffusion coefficient, D_o, is a property of the radionuclide alone (and temperature). This relationship assumes that no processes other than diffusion are affecting the "apparent" diffusion coefficient (e.g., cation exchange, unaccounted sorption, complexation, anion exclusion, lowering of effective porosity for large molecules excluded from small pores) and all tracer solutions are dilute (less than 1 M). Multi-component diffusion effects have also been excluded in this analysis.

The importance of the matrix diffusion coefficient is expected to be greater for transport in fractured media than in alluvial media. Therefore, it will be of more importance in transport model realizations where there is significant movement of contaminants in the volcanic aquifers or the LCA.

Free water diffusion coefficients are temperature dependent, and temperature conditions logged in the deeper HSUs in Yucca Flat are relevant if solutes should ever reach depths substantially below the

ground surface, on the order of 600 m bgs. Temperatures measured from logging at the ER-6-1 Well Cluster and in wells ER-7-1 and ER-12-2 range up to 42, 53, and 63 °C, respectively. Correction of the free water diffusion coefficients (and matrix diffusion coefficients) in the model for temperature effects is recommended as temperatures in the HSUs of Yucca Flat range from about 20 °C to more than 60 °C. The higher temperature ranges will result in about a factor of two increase in the free water diffusion coefficients. If temperature corrections are needed, they can be applied by the simple free water diffusion coefficient multiplier factor relationship shown in Figure 10-11 and Table 10-2.

11.0 MATRIX SORPTION PARAMETERS

11.1 The Role of Matrix Sorption in Contaminant Transport Models

Matrix sorption is a physiochemical process at mineral-water interfaces that controls solute mobility and solute retardation within the pore spaces of the immobile rock matrix. Similar physiochemical processes may occur on minerals coating fractures. Fracture sorption is treated separately in Section 12.0 because the conceptual and numerical models differentiate between the sorption process within the matrix pore space and along the surface of the fracture walls. There are multiple methods for mathematically representing the matrix sorption process in parameterized groundwater transport models. These methods include, but are not limited to: (a) mechanistic pore-scale models that represent the sorption process on each immobile mineral grain with thermodynamic relationships for each type of reactive surface; (b) mechanistic complexation and exchange models representing average processes on integrated volumes represented with discretized continuum models; and (c) isotherms that seek to describe or abstract, on a laboratory scale, the integrated behavior of the smaller-scale mechanistic processes.

The objective of this section is to compile and present the available, applicable, and representative data for matrix sorption that can be applied to transport modeling for the Yucca Flat/Climax Mine CAU. A reactive mineral model for the Yucca Flat/Climax Mine CAU will be developed to parameterize matrix sorption for the transport model, planned for FY 2008. The focus of this document is to compile and present the mineralogical and chemical data that will be needed for the mechanistic model that will be used for developing matrix sorption parameter values for the transport model.

11.2 Data Compilation and Data Transfer

Data from the Yucca Flat/Climax Mine HFM area and data from other NTS CAUs, YMP, and a nearby location (see note) were used for this analysis due to the unavailability of comprehensive data from the Yucca Flat/Climax Mine HFM area for all HGUs. (Note: The nearby location was the

low-level radioactive waste disposal facility in Beatty, Nevada. There were no NTS area data for some radionuclides for alluvium). All data locations used in quantitative analyses are identified in Appendix I and the associated dataset referenced in Section I.2.0. Individual discussions of the applicability of the transferred data are provided for each HGU. A quantitative assessment of the sensitivity of transport modeling to the uncertainty in this parameter cannot be provided before the transport model development. The parameter description discusses the importance of this parameter.

11.3 Radionuclides of Potential Concern

The unclassified radiologic inventory for the Yucca Flat/Climax Mine CAU is reported by Bowen et al. (2001) and summarized in Section 6.1. A total of 43 source-term radionuclides were included in the list prepared by Bowen et al. (2001). Available data for matrix sorption for these radionuclides are presented in this section. Laboratory sorption data are available for representative alluvium (Cs, Sr, Am, Eu, Sm, Np, U, Pu, Ni, Tc, and I), for volcanic rocks (Cs, Sr, Am, Np, U, and Pu), and for carbonate rocks (Cs, Sr, Eu, Pu, Am, U, Np). The matrix sorption parameter values can also be estimated based on data collected for other materials, elemental properties of the radionuclides, or mechanistic simulation estimates, and available data/estimates are also included.

11.4 The K_d Parameter

A commonly used isotherm is the linear distribution coefficient, K_d. In fact, most isotherms at low solute concentrations, or over a narrow range of concentrations, simplify to a linear model. Modeling solute transport using K_d is attractive due to the simplicity with which models are implemented and because the models represent an average behavior, thus decreasing the number of molecular-scale processes that need to be quantified and explicitly accounted for in transport models. For the purposes of this document, it is assumed that the K_d values will be used to parameterize radionuclide-rock interactions for use in the CAU transport model.

The K_d value is defined as:

$$K_d = \frac{\textit{Moles of solute per gram of solid phase}}{\textit{Moles of solute per milliliter of solution}} \qquad (11\text{-}1)$$

This approach assumes that the sorbent (radionuclide) has a uniform affinity for the rock surface that is independent of the mass of sorbent already adsorbed. Put simply, this means that there are many

more places for sorption to occur than radionuclides sorbing. Another assumption inherent in the use of this parameter is instantaneous equilibrium between the aqueous and sorbed phase. Although laboratory measurements rarely guarantee that experiments have reached equilibrium conditions, measurement of sorption and desorption frequently confirm that little error has been introduced by assuming these measurements are in equilibrium. The use of K_d values in the CAU-scale model requires the assumption of local equilibrium conditions because contact times between radionuclides and rocks may not be the same for the laboratory experiments as the rate of groundwater flow through the reactive rocks in the CAU model.

Grid cells in the Yucca Flat CAU transport model may be large relative to sub-block heterogeneities (non-uniform mineral distributions, fluctuations in aqueous chemistry) that affect water and solute flow and mineral-solute contact. Thus, averaging of the specific processes that occur at each mineral reaction site is necessary and appropriate for CAU-scale simulations. Although measured on a small sample, the K_d begins to provide such averaging. Additionally, modeling transport of sorbing solutes at the CAU scale presents a computational challenge when mechanistic-transport models are fully integrated. Distribution coefficients, however, are easy to include in large-scale transport models.

The K_d parameter may be developed either by direct measurement on aquifer material samples or computed by upscaling mechanistic processes. Both approaches are discussed in the following sections.

11.5 Direct Measurement of K_d

Laboratory sorption experiments measure K_d values directly. The experiments are generally designed with knowledge of the mechanistic processes that affect the K_d, but with the goal of simply measuring it given a set of environmental controls. Measurements of K_d values for several radionuclides on multiple types of minerals and rock material have been collected in support of UGTA and YMP transport studies. Such studies generally provide information on the rock type (rock mineralogy) and the conditions under which the experiment was performed. Such conditions include:

- Aqueous ion concentrations
- Temperature
- pH
- Eh (and/or other indicators of oxidation/reduction state such as oxygen fugacity)

- Solute concentration
- Rock characteristics
- Experimental atmospheric conditions (e.g., air, nitrogen gas [N_2], or CO_2 to control pH)

Thus, each measured K_d corresponds to a specific set of environmental conditions, albeit generally designed to represent *in situ* conditions.

Although the experiments used to obtain K_d parameters are relatively fast and simple, there are important limitations associated with the use of such parameters in transport models. Whereas transport processes are dynamic, the measurements from which the parameter values are obtained from tests with static conditions. Likewise, the contact time between the radionuclides and aquifer materials is considerably different between the laboratory experiments and the CAU-scale model. The representativeness of K_d batch experiments to *in situ* rocks may be hard to assess because these experiments are usually performed on freshly created surfaces from crushed or sieved rocks. Experimentally determined K_d values that are very small or very large contain the greatest uncertainties, even for the static conditions in which they are measured, due to the subtraction of two large numbers necessary for the calculation. The K_d simply represents the total mass of the element of interest and thus does not describe the behavior of any particular species. However, if more detailed mechanistic understanding is desired, it is possible to derive the speciation given the environmental conditions of the experiment. Finally, although the K_d parameter represents an integrated response of a sample brought in contact with the aqueous solute of interest, the sample size is still far smaller than the rock volume in the CAU-scale model that will be parameterized for flow and transport simulations.

The following sections provide a summary of the laboratory experiments used to measure K_d values for alluvium and volcanic rocks representative of those of the Yucca Flat/Climax Mine CAU. Because all of the data presented are for samples from Yucca Flat, these data will be labeled as Yucca Flat data.

11.5.1 Alluvium

Primary sources of alluvium sorption data included K_d values measured from Yucca Flat-specific experiments reported in Wolfsberg et al. (1983) and Zavarin et al. (2002). In addition, laboratory values for Frenchman Flat alluvial experiments are reported in Wolfsberg (1978a) and a

memorandum written by Wolfsberg (1978b); however, mineralogy of the rock samples and water chemistries used during these experiments were not included in the documentation, making these values difficult to interpret. Additional data were available from the Beatty low-level radioactive waste disposal facility (Wolfsberg et al., 1983), and from the YMP as described in Triay et al. (1997) and DOE/ORD (2001 and 2004) and stored in the YMP Technical Data Management System (TDMS) (YMP, 2004). The whole rock mineralogy and radionuclides tested for each series of samples are listed in Table 11-1. Note that the listed value for percent mass of smectite for location U-1a is significantly higher than for typical Yucca Flat alluvium. A summary of the K_d values for each of the locations described above is presented using box and whisker plots (Figure 11-1). Details for the specific radionuclides shown in this figure are provided in the following sections. Box and whisker plots provide an integrated presentation of parametric data including the 25th and 75th percentiles (upper and lower limits of the box), the median (interior crossbar of the box), the data range (upper and lower limits shown by the whiskers), and outliers (data points beyond the data range).

Table 11-1
Whole Rock Mineralogy from Alluvium K_d Experiments

Sample Location	Sample Site	Mass % Smectite	Mass % Mica	Mass % Zeolite	Mass % Hematite	Mass % Calcite	Radionuclides Tested
U-1a	Yucca Flat	30	3.4	1.3	NA	18.2	^{137}Cs, ^{152}Eu, Sm, ^{85}Sr, U, ^{237}Np
Trench 22	Beatty 1 low-level radioactive waste disposal facility, Nye County	3	1	3	NA	NA	^{241}Am, ^{137}Cs, ^{131}I, ^{63}Ni, ^{239}Pu, ^{85}Sr, ^{95m}Tc, ^{235}U
Trench 22	Beatty 5 low-level radioactive waste disposal facility, Nye County	5.5	1	3	NA	NA	^{241}Am, ^{137}Cs, ^{131}I, ^{63}Ni, ^{239}Pu, ^{85}Sr, ^{95m}Tc, ^{235}U
Trench 22	Beatty 2 low-level radioactive waste disposal facility, Nye County	3	1	3	NA	NA	^{241}Am, ^{137}Cs, ^{131}I, ^{63}Ni, ^{239}Pu, ^{85}Sr, ^{95m}Tc, ^{235}U
U-3hr	Yucca Flat	0	2.5	3	NA	NA	^{241}Am, ^{137}Cs, ^{131}I, ^{63}Ni, ^{239}Pu, ^{85}Sr, ^{95m}Tc, ^{235}U
Ue-5n	Frenchman Flat	11.6	3.3	19.7	0.3	2.6	^{137}Cs, Sm, ^{85}Sr, U, ^{237}Np

Source: Modified from SNJV, 2005b

NA - Not available

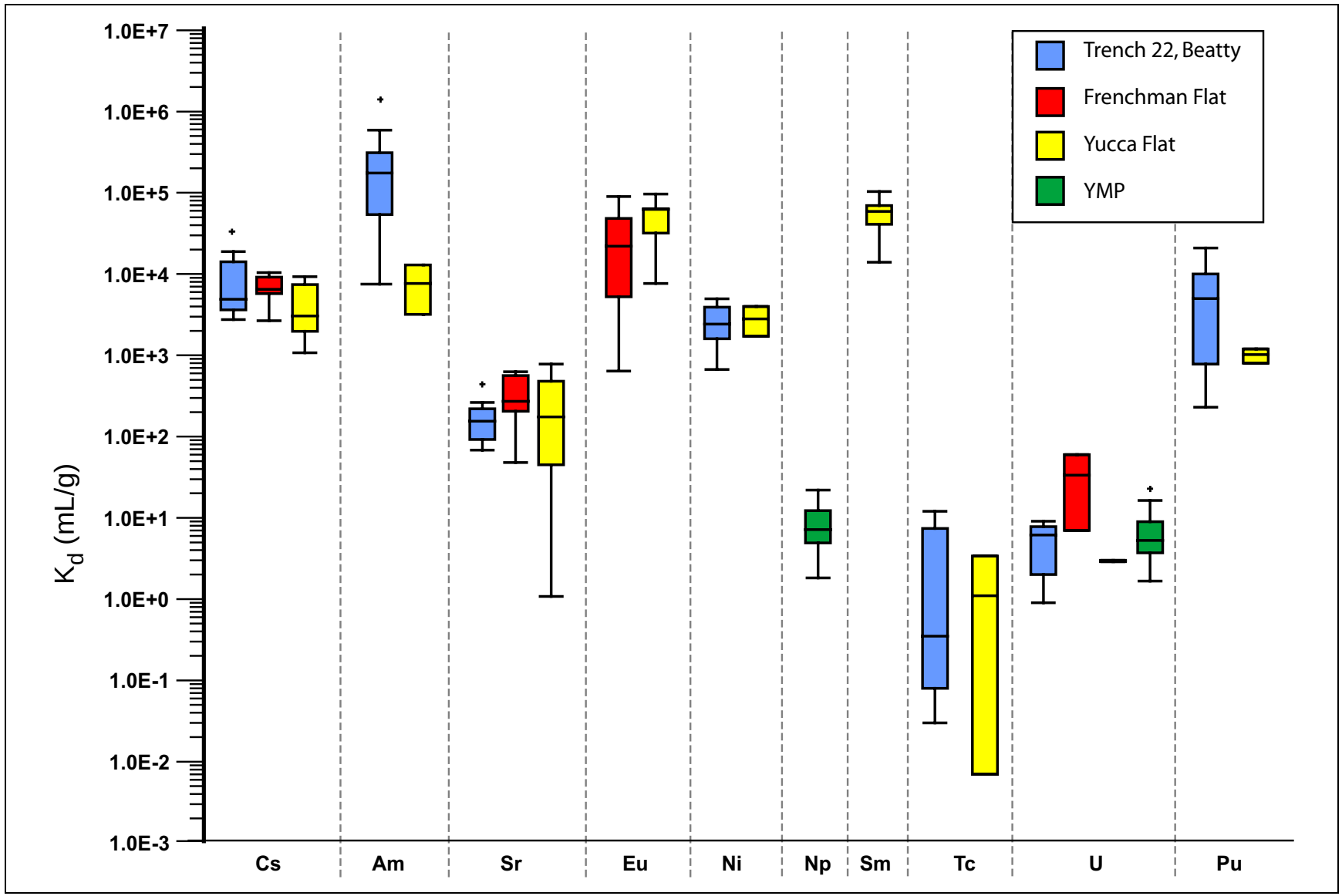

Figure 11-1
Laboratory Measured Distribution Coefficients for Alluvium Samples

Zavarin (2002) also conducted four flowthrough experiments using Frenchman Flat alluvium, and subsequently determined K_d values from the experimental results for two of the experiments. These K_d values are summarized in Table 11-2.

Table 11-2
Log K_ds (mL/g) Calculated from Flowthrough Experiments Reported in Zavarin, 2002

U-1a Flowthrough Experiments							
Element	**Breakthrough Front**	**Breakthrough Back**	**Breakthrough Peak**	**SIMS?**	**Effluent?**	**Underestimate?**	**Average**
U	0.4	0.2			X		0.3
Sr	1.9		2		X		1.9
Cs	2.4	2.7	2.4	X			2.5
Sm	2.8		3.3	X		X	3.1
Np	1.1	0.7	1.1		X		1.0
UE-5n Flowthrough Experiments							
Element	**Breakthrough Front**	**Breakthrough Back**	**Breakthrough Peak**	**SIMS?**	**Effluent?**	**Underestimate?**	**Average**
U	-0.3	-0.1			X		-0.2
Sr [a]	2.7		3.2	X		X	3.0
Cs	2.5		3.2	X		X	2.9
Sm	2.5		3.2	X		X	2.9
Np	0.7	0.3			X		0.5

[a] Sr data for UE-5n alluvium flowthrough is a best estimate of transport. However, unorthodox data manipulation was necessary to estimate K_d. Use result with caution.

Definitions:
Breakthrough Front - Based on 0.5*C/Cmax at the breakthrough front
Breakthrough Back - Based on 0.5*C/Cmax at the breakthrough back
Breakthrough Peak - Based on peak breakthrough
SIMS? - K_ds based on data from secondary ion mass spectrometry of sliced column after flowthrough experiment was completed
Effluent? - K_ds based on analysis of effluent
Underestimate? - K_ds likely to be somewhat underestimated due to resolution issues with the SIMS data

11.5.1.1 Americium and Samarium

Americium batch-sorption experiments were conducted on alluvium samples collected from U-3hr at Yucca Flat and from Trench 22 at the Beatty low-level radioactive waste disposal facility. The whole rock samples all had mineralogy within the range of observed values for Yucca Flat alluvium (see Appendix D); however, sieved fractions of the samples frequently altered the distribution of the sample mineralogy.

Samarium batch-sorption experiments were conducted by Zavarin et al. (2002) on alluvium samples collected from an exposed section of the C alcove of the U-1a.102 drift on Yucca Flat. Sorption experiments were conducted with pH values ranging from 7.41 to 9.42. A plot of Sm sorption coefficients as a function of pH reveals that Sm sorption is dependent on pH and has a maximum K_d at pH 8.4 under these experimental conditions (Figure 11-2). These changes in Sm sorption are likely to be the result of Sm-CO_3^{2-} complex formation, which tends to increase as pH increases. For the Yucca Flat basin, changes in pH within the alluvial aquifer may lead to considerable differences in Sm sorption, thus increasing the uncertainty in Sm transport predictions. The pH of groundwater of the Yucca Flat alluvial aquifer has been measured at values ranging from 7.4 to 8.3 (see Appendix E), values within the range of those examined in the Sm sorption experiments.

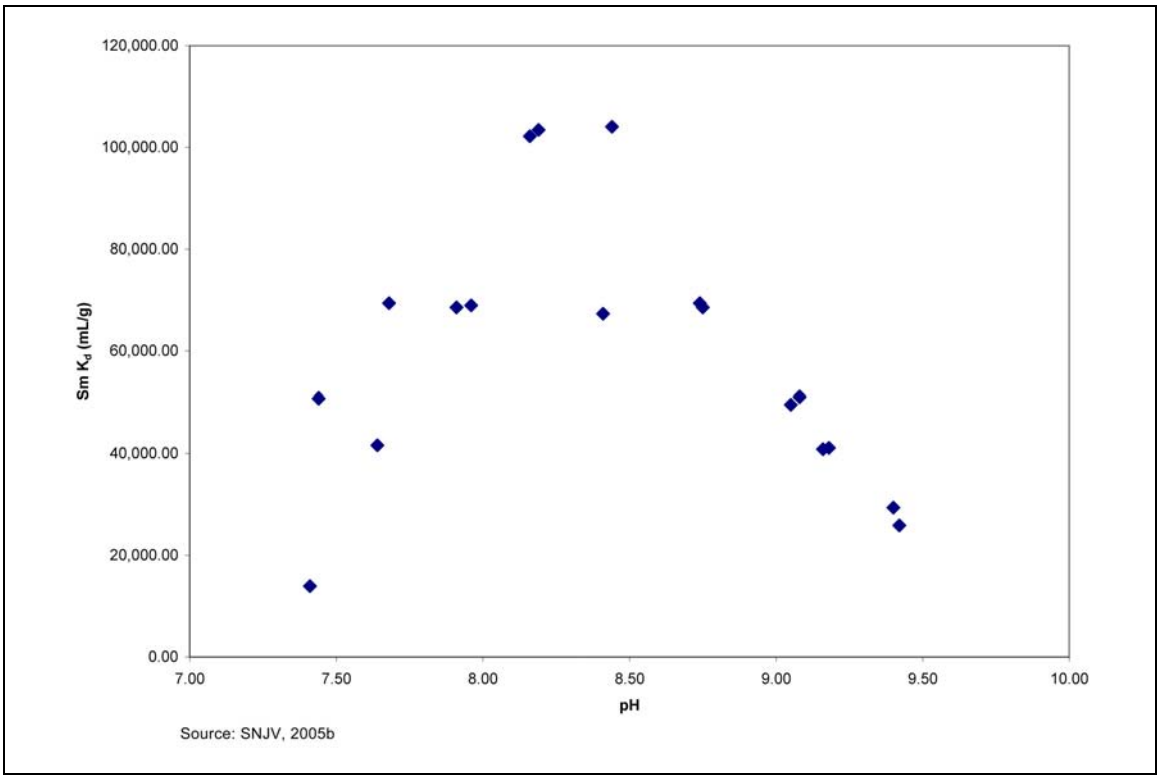

Figure 11-2
Samarium K_d as a Function of pH for Alluvium Samples Collected at Yucca Flat

Given the similar chemistry of Sm and Am, better agreement between the K_d values for these two radionuclides was expected. The K_d values ranged from 1.39 x 10^4 to 1.04 x 10^5 milliliters per gram (mL/g) for Sm compared to 3.20 x 10^3 to 1.30 x 10^4 mL/g for Am. Although the Sm sorption experiments included a greater variety of ion concentrations for the water chemistry used in the

experiments, there was considerably more variability in rock mineralogy of the samples in the Am experiments. This may indicate that Am and Sm sorption are more sensitive to rock chemistry than water chemistry (see Appendix I).

11.5.1.2 Cesium and Strontium

Fifty-six measurements of Cs sorption and 74 measurements of Sr sorption have been completed for alluvium collected from multiple Yucca Flat wells (U-1a, U-3hr, and U-3bu); the Frenchman Flat well RNM-1; and the Beatty low-level radioactive waste disposal facility. The K_d values for Cs ranged from 1,460 to 9,274 mL/g and from 1 to 781 mL/g for Sr for the alluvial materials represented in this dataset.

Neither Cs nor Sr changes oxidation states under the solution compositions expected for Yucca Flat groundwaters. Cesium and Sr should occur as cations with single and double positive charges, respectively. Behavior in the system will be predominantly ion exchange reactions with little dependence on pH but a large dependence on the concentration of competing ions in solution (e.g., Ca). Most ion exchange reactions will occur with clays and zeolites. Ion exchange reactions for Cs are dominated by illite and mica, while these reactions are dominated by zeolite and smectite for Sr.

11.5.1.3 Neptunium

Distribution coefficients for Np have been measured in batch experiments from core samples obtained from three wells drilled into the alluvium near Yucca Mountain (NC-EWDP-10SA, -22SA, and -19IM1A) (DOE/ORD, 2004). Samples were collected from below the water table at 5-ft intervals at two depths in wells NC-EWDP-19IM1A and -10SA, and at six depths in well NC-EWDP-22SA (DOE/ORD, 2004). For each core sample, batch experiments were run on three particle sizes: 500 to 2,000 μm, 75 to 500 μm, and less than 75 μm. The greatest K_d values were observed on the smallest particle size fraction, most likely due to one or more of the following reasons: mineral sorting effects (however, no sample mineralogy data were reported with these K_d values), increased surface areas of the particles, and increased cation-exchange capacity. The pH of the experiments (8.10 to 8.68) overlapped with the pH range observed within the groundwaters of the alluvium in Yucca Flat (7.4 to 8.3). The K_d values for Np ranged from 1.8 to 22.0 mL/g.

Under oxidizing conditions, Np tends to exhibit limited sorption on alluvium. Under reducing conditions, Np is expected to exhibit greater sorption and lower solubility. Yucca Flat groundwater in the alluvial aquifer is thought to be oxidizing (see Section 5.0); however, if pockets of reducing conditions are present, these may result in greater sorption and less transport in the subsurface.

11.5.1.4 Uranium

Forty-seven measurements of U sorption have been completed for alluvium collected from a Yucca Flat well (U-3hr); a Frenchman Flat well (RNM-1); the Beatty low-level radioactive waste disposal facility; and three wells near Yucca Mountain (NC-EWDP-10SA, -22SA, and -19IM1A). The K_d values for U ranged from 0.9 to 22.7 mL/g. Wolfsberg (1978a) reported K_d values of approximately 7 mL/g for alluvium samples collected at RNM-1 in the presence of RNM-2s groundwater. When Wolfsberg (1978a) measured sorption of U on Frenchman Flat alluvium in the presence of deionized water, the K_d was approximately 60 mL/g. Clearly, the presence of ions in the RNM-2s groundwater resulted in a net reduction in the total sorption of U.

Based on the expected redox potential of Yucca Flat alluvial groundwaters, U should be in the +6 oxidation state. In this oxidation state, U will occur as a variety of carbonate (CO_3^{2-} and HCO_3^-) complexes and, to a lesser extent, PO_4^{3-}, F^-, and SO_4^{2-} complexes because these anions have a relatively low abundance in Yucca Flat groundwaters (Triay et al., 1997). The complexation of U with carbonate species is dependent on the pH of the solution, where decreasing pH results in less complex formation, thus increasing U sorption (Triay et al., 1997; DOE/ORD, 2001).

Although U sorption is expected to be pH dependent, this was not apparent in the dataset (see Appendix I). It is likely that two competing processes are occurring: (1) pH changes resulting in changes in the net charge on the mineral surfaces, and (2) carbonate complex formation. Increasing pH will tend to increase sorption and carbonate complexation, while decreasing pH will tend to decrease sorption and carbonate complexation. Depending on the solution conditions (i.e., the balance between hydrogen ion availability and aqueous carbonate species), an increase or decrease in sorption may occur (however, at a very low pH, sorption will always decrease).

11.5.1.5 Europium

Thirty-four measurements of Eu sorption have been completed for alluvium collected from Yucca Flat wells U-1a (Zavarin et al., 2002) and U3bv (Wolfsberg, 1978a), and Frenchman Flat well RNM-1 (Wolfsberg, 1978a). Wolfsberg (1978b) reports a recommended K_d for alluvium of greater than 5,000 mL/g. Zavarin et al. (2002) report that the sorption of Eu on U-1a alluvium samples was dominated by sorption to calcite. As Zavarin et al. (2002) varied the pH of the solution, Eu sorption was reduced at low pH due to competition with Ca for calcite surfaces and at high pH due to Eu-carbonate complex formation in solution.

Europium is a member of the lanthanide series of transition metals and is expected to behave similarly to Sm by occurring in the +3 oxidation state in Yucca Flat groundwaters. The +2 oxidation state for Eu is more stable than the +2 oxidation state for Sm; however, the +2 oxidation state is limited to very reducing conditions at near neutral pH values (Krupka and Serne, 2002). Europium III tends to form strong aqueous complexes with dissolved hydroxide, CO_3^{2-}, HCO_3^-, PO_4^{3-}, F^-, and SO_4^{2-}, and weak complexes with Cl^-, and NO_3^- (Krupka and Serne, 2002). The majority of these ligands occur in low concentrations in the Yucca Flat alluvial aquifer.

Given the similar chemistry of Eu and Sm, better agreement between the K_d values are expected for these two radionuclides. The K_d values for Sm ranged from 1.39×10^4 to 1.04×10^5 mL/g compared to 2.52×10^3 to 9.59×10^4 mL/g for Eu. The Sm sorption experiments incorporated a greater variety of water and rock chemistries in the laboratory experiments, thus providing a greater range in measured K_d values. The sorption experiments for Eu, although more limited in number and scope, provide a more conservative estimate of transport.

11.5.1.6 Plutonium

In near neutral environments like Yucca Flat groundwater, the solution behavior of Pu is complicated (Triay et al., 1997). Plutonium may occur in many oxidation states in solution, and may also undergo complex formation with a variety of ligands. Plutonium sorption onto alluvium samples from U-3hr at Yucca Flat (Wolfsberg et al., 1983) and from Trench 22 at the Beatty low-level radioactive waste disposal facility were measured in the presence of an ambient air atmosphere and water collected from the alluvial aquifer at Frenchman Flat (U-5b) and the Waste Disposal Site, respectively.

Additional data such as the oxidation state of the Pu in the aqueous solution and the initial Pu concentration were not reported. The Pu K_d values ranged from 230 to 21,000 (Figure 11-1).

11.5.1.7 Nickel

Nickel batch-sorption experiments were conducted using 4 samples from Yucca Flat (U-3hr) and 20 samples collected from Trench 22 at the Beatty low-level radioactive waste disposal facility (Wolfsberg et al., 1983). The whole rock samples all had mineralogy within the range of observed values for Yucca Flat alluvium; however, sieved fractions of the samples frequently altered the distribution of the sample mineralogy. The Ni K_d values ranged from 672 to 4,960 mL/g. Wolfsberg et al. (1983) reports that Ni sorption occurs mostly on clays and zeolites (such as kaolinite, smectite, or clinoptilolite), which are minerals present in Yucca Flat alluvium in significant abundances (see Appendix D).

11.5.1.8 Iodine and Technetium

Wolfsberg et al. (1983) measured both I and Tc sorption onto alluvium collected from U-3hr at Yucca Flat and from Trench 22 at the Beatty low-level radioactive waste disposal facility. The reported K_d values for these experiments ranged from -9.1 to 24.5 mL/g for I, and from -2.5 to 12.0 mL/g for Tc. The negative values of K_d indicate the high variability associated with the measurements when low to zero sorption is observed.

For both of these radionuclides, Tompson et al. (2004) approximate sorption of zero, suggesting that they are modeled as conservative tracers. Given the very small measured K_d values, and the fact that neither of these radionuclides result in ingrowth of radioactive daughter products (Tompson et al., 2003), treating these radionuclides as non-reactive tracers is a reasonable and conservative simplification that should be considered during CAU transport modeling.

11.5.2 Volcanic Rocks

Zavarin et al. (2007) summarize two studies that investigated radionuclide transport in fractures of the TCU performed in support of the UGTA Project (Zavarin et al., 2005; Ware et al., 2005). The experiments included radionuclide transport through synthetic parallel-plate fractured tuff samples (Zavarin et al., 2007). These simplified fracture transport experiments isolated matrix diffusion and

sorption effects from all other fracture transport processes (e.g., fracture lining mineral sorption, heterogeneous flow). Additional fracture transport complexity was added by performing iron-oxide-coated parallel-plate TCU flowthrough experiments (effect of fracture lining minerals.) Finally, naturally fractured tuff and carbonate cores were examined. The models RELAP or RETRAN (a transient version of RELAP) were used to simulate the breakthroughs, and estimate retardation factors both in fractures (see Section 12.0) and for the matrix material. Zavarin et al. (2007) report the retardation factor, R, which is related to K_d as follows:

$$R = 1 + \frac{K_d \rho_b}{\phi} \qquad (11\text{-}2)$$

where bulk density for tuff [$\rho_b = 2.13*(1-\phi)$] is calculated using the rock porosity (ϕ) and mineral densities of zeolite. Porosity values are reported in Zavarin et al. (2007) and summarized in Section 7.0 of this report.

A limited number of studies have also been performed at DRI in support of the UGTA Project, primarily involving sorption of Pb, Sr, and Cs on a select number of rocks (tuff and devitrified lava) from Pahute Mesa and Rainier Mesa, and Frenchman Flat boreholes (Papelis and Um, 2003a and b; Decker et al., 2003). Based on sorption data with different solid and metal concentrations, linear sorption isotherms were derived for sorption at pH 8.3, representing a common NTS groundwater pH. Batch sorption experiments were conducted on crushed rock, and diffusion/sorption experiments were conducted on intact core.

11.5.2.1 YMP Sorption Data

The YMP has studied sorption of radionuclides (Pu, Np, U, Sr, and Cs) on minerals and volcanic rocks for more than two decades. The data are discussed by Triay et al. (1997) and DOE/ORD (2001 and 2004) and stored in the YMP TDMS (YMP, 2004). All of these reports provide reviews of the mechanistic processes governing sorption of radionuclides and describe the experiments that were conducted by YMP. As more data become available, one finds an evolving understanding and interpretation of sorption of radionuclides on minerals and volcanic rocks. Thus, DOE/ORD (2004) provides the most current data and interpretations for the YMP. However, Triay et al. (1997) provide greater detail for some experiments and background material not found in DOE/ORD (2004). As a result, the two reports provide complementary sets of information and analyses. Measurements of K_d,

maintained in the YMP TDMS (YMP, 2004), were collected under a stringent QA environment and are fully traceable with laboratory notebooks and data-tracking numbers. The analyses presented in this report incorporate data that meet all YMP QA requirements as of summer 2004.

11.5.2.1.1 YMP Sorption Data History

YMP Laboratory Sorption Data Obtained Before 1993. In 1993, the YMP conducted an expert elicitation regarding K_d values and distributions for various radionuclides and rock types (Wilson et al., 1994). The distributions developed in the elicitation are based substantially on the summary report by Thomas (1987), which summarizes sorption experiment results performed by the YMP before the QA procedures that were required for the analysis and model report by DOE/ORD (2004).

YMP Laboratory Sorption Data Obtained After 1993. With new data collected after 1993, Triay et al. (1997) developed improved K_d distributions for multiple radionuclides on devitrified, vitric, zeolitic, and iron-oxide rock types (iron oxides are important to YMP for assessing sorption in the vicinity of waste packages). These distributions were modified again by DOE/ORD (2004); during this modification, distributions of K_d values for vitric tuffs were eliminated. The data cited in DOE/ORD (2004) are available in the YMP TDMS (YMP, 2004), with appropriate data-tracking numbers and QA pedigrees linking to raw data and laboratory notebooks. These data provide most of the input to the distributions developed in the next sections.

11.5.2.1.2 YMP Sorption Data Transfer

Generally, volcanic rocks are classified by mineralogy and texture. The HSUs developed for CAU geologic models emphasize the stratigraphic and hydrologic significance of a unit as opposed to the mineralogy. To account for this, the Yucca Flat/Climax Mine CAU transport model will identify volcanic rocks based on mineralogy as defined by reactive mineral class (RMC) and reactive mineral units (RMUs). Class definitions for the volcanic rocks were selected to be consistent with the class definitions used for the YMP so that YMP data could be readily incorporated into the analysis for Yucca Flat, where appropriate. These classes are defined in Table 11-3.

Nearly all of the YMP K_d experiments involving rock samples taken from the field were conducted with water from, or similar in composition to, groundwaters of J-13 or UE-25 p#1. Well J-13 samples

Table 11-3
Class Definition for Volcanic Rocks Used by the Yucca Mountain Project

Class	Description	Glass	Clay	Zeolite
		Abundance (%)		
Vitric Tuff	High percentage of original glass in samples	>40	<10	<10
Devitrified Tuff	Composed primarily of quartz and feldspar	<40	<10	<10
Zeolitic Tuff	Dominated by alteration assemblages of zeolites	<10	<10	>20

the Topopah Spring aquifer, a volcanic hydrologic unit also present in parts of Yucca Flat. Well UE-25 p#1 samples the carbonate aquifer below the volcanic tuffs at Yucca Mountain. The groundwater compositions of these two wells are listed in Table 11-4. The mean groundwater compositions for three wells in Yucca Flat are also presented in Table 11-4. These groundwater samples were selected as the most similar to UE-25 p#1 (UE-10 ITS #3), and J-13 (U-2bs and TW-B) groundwaters (see Appendix E). Waters in the volcanic-rock aquifers and confining units of the Yucca Flat testing area tend to more calcium poor than J-13 well water. Well J-13 water is most similar to Yucca Flat water samples from TW-B (LTCU), but is more enriched in Ca and depleted in Na (Table 11-4). The pH of J-13 and UE-25 p#1 groundwaters is lower than those found in the majority of the Yucca Flat wells. Many YMP sorption experiments using water with J-13 and UE-25 p#1 compositions were conducted with atmospheric conditions (generally labeled as “air” or “bench” conditions) to obtain higher pH values between 8.5 and 9 (closer to the pH values observed in Yucca Flat groundwater samples). Some YMP sorption experiments were also conducted with CO_2 overpressure inside of glove boxes to obtain pH values of about 7 or using an N_2 atmosphere to stabilize pH during sorption experiments.

In the next several subsections, measured K_d data collected by LLNL, DRI, and the YMP are presented. For each of the radionuclides, sorption measurements were conducted on multiple pure-phase minerals as well as on tuffs classified as vitric, devitrified, and zeolitic. Whereas the pure-phase mineral studies could serve to inform future mechanistic modeling studies, in this analysis, only the tuffs are considered because they can be correlated with Yucca Flat HSUs.

Experiments on tuff samples were conducted with J-13 water and often with the higher ionic-strength UE-25 p#1 water (Table 11-4). Additionally, pH was often controlled by either conducting

Table 11-4
Chemical Composition (mg/L) of Groundwater in J-13, UE-25 p#1, and Three Locations in Yucca Flat

Constituent	J-13 [a, b]	UE-25 p#1 [a, b]	UE-10 ITS #3 [c, d]	U-2bs [c, d]	TW-B [c, e]
Na	45	171	209	79.0	74.9
K	5.3	13.4	21.5	6.0	3.3
Mg	1.8	31.9	0.4	0.5	0.5
Ca	11.5	87.8	7.8	3.1	5.5
SiO_2	30	30	62	53	18.6
F	2.1	3.5	N/A	1.3	N/A
Cl	6.4	37	10.2	7.5	17
SO_4^{2-}	18.1	129	42.8	24.5	23
HCO_3^-	143	698	543	198	164
pH	6.9	6.7	8.3	7.1	8.1

Source: Modified from SNJV, 2005b

[a] YMP, 1997 (DTN: LAIT831361AQ95.003 [SEP Table S98491.002])
[b] Ogard and Kerrisk,1984 (in Meijer, 1992)
[c] Concentrations are the mean concentration presented in Appendix E
[d] Example LTCU water chemistry
[e] Example TSA water chemistry

N/A - Not applicable

experiments with an air environment to achieve pH between 8 and 9, or with CO_2 overpressure to force the pH closer to 7. Finally, most experiments were conducted at 20 to 25 ^oC, but many were conducted at temperatures up to 90 ^oC. These different environmental conditions may or may not affect the K_d data. Therefore, in the discussion that follow, the roles of the different environmental conditions are highlighted when necessary.

11.5.2.2 Americium

Americium sorption data for vitric tuffs, devitrified tuffs, and zeolitic tuffs in the presence of J-13 water are reported in the YMP TDMS (YMP, 2004). Triay et al. (1997) report results from Am sorption in the presence of UE-25 p#1 water. These results suggest that all rocks in the presence of water saturated with calcite (like UE-25 p#1 water) showed very large distribution coefficients. Triay et al. (1997) conclude that Am coprecipitated with carbonates or formed solid solutions on the surfaces of existing carbonates. Given that UE-25 p#1 water is not similar to the water present in the

volcanic aquifers of Yucca Flat due to the high Ca content of this water, sorption experiments in this water would likely overpredict the sorption of Am onto Yucca Flat rocks. Therefore, only Am experiments conducted with J-13 water are considered here.

Vitric Tuff. Eight Am sorption experiments onto vitric-tuff rocks were reported in the YMP TDMS (YMP, 2004). All of these rocks were crushed and sieved before analysis, and the 75- to 500-µm sieve fraction was used for the experiments. The Am K_d values ranged from 860 to 2,050 mL/g (Figure 11-3).

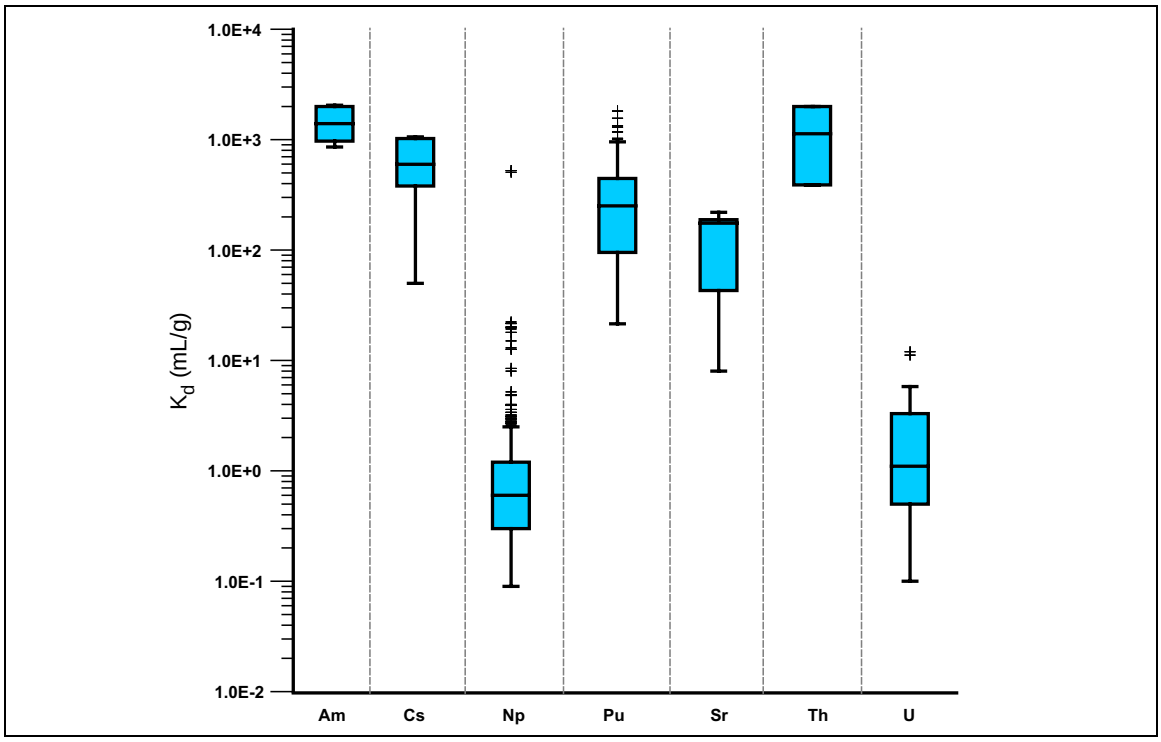

Figure 11-3
Laboratory Measured Distribution Coefficients for Vitric-Tuff Samples

Devitrified Tuff. Thirty-five Am sorption experiments onto devitrified-tuff rocks were reported in the YMP TDMS (YMP, 2004). All of these rocks were crushed and sieved before analysis, and four different sieve fractions were used for the experiments. Most experiments were conducted in the presence of an ambient air atmosphere; however, several experiments were conducted in an N_2 atmosphere with less than 0.2 parts per million (ppm) oxygen gas (O_2) and less than 20 ppm CO_2 to increase the pH from approximately 8.5 to 9.5 during the experiments. The measured K_d values

showed no trend with respect to pH. The Am K_d values ranged from 79 to 5,300 mL/g; one outlier (12,000 mL/g) is identified in the box and whisker plot (Figure 11-4).

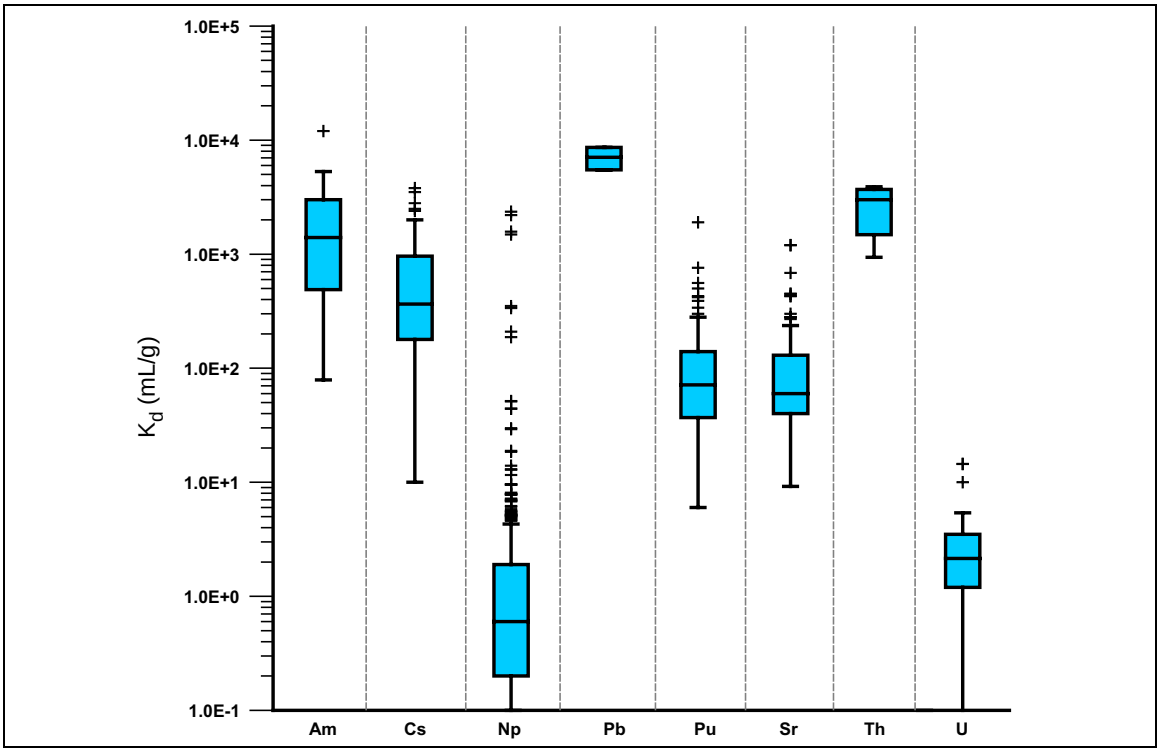

Figure 11-4
Laboratory Measured Distribution Coefficients for Devitrified-Tuff Samples

Zeolitic Tuff. Twenty-five Am sorption experiments onto zeolitic tuff rocks were reported in the YMP TDMS (YMP, 2004). All of these rocks were crushed and sieved before analysis, and the 75- to 500-µm and 106- to 250-µm sieve fractions were used for these experiments. The Am K_d values ranged from 470 to 15,000 mL/g; two outliers (31,000 and 33,000 mL/g) are identified in the box and whisker plot (Figure 11-5).

11.5.2.3 Cesium and Strontium

These two elements are grouped together, as in Triay et al. (1997) and DOE/ORD (2001 and 2004), because they show fairly simple solution behavior in typical groundwaters. Just as they are not subject to oxidation-state changes in the groundwater compositions of Yucca Mountain, one can expect the same simplicity in Yucca Flat groundwaters. Their sorption is primarily controlled by ion-exchange reactions, where the selectivity of most clays and zeolites for these elements should be

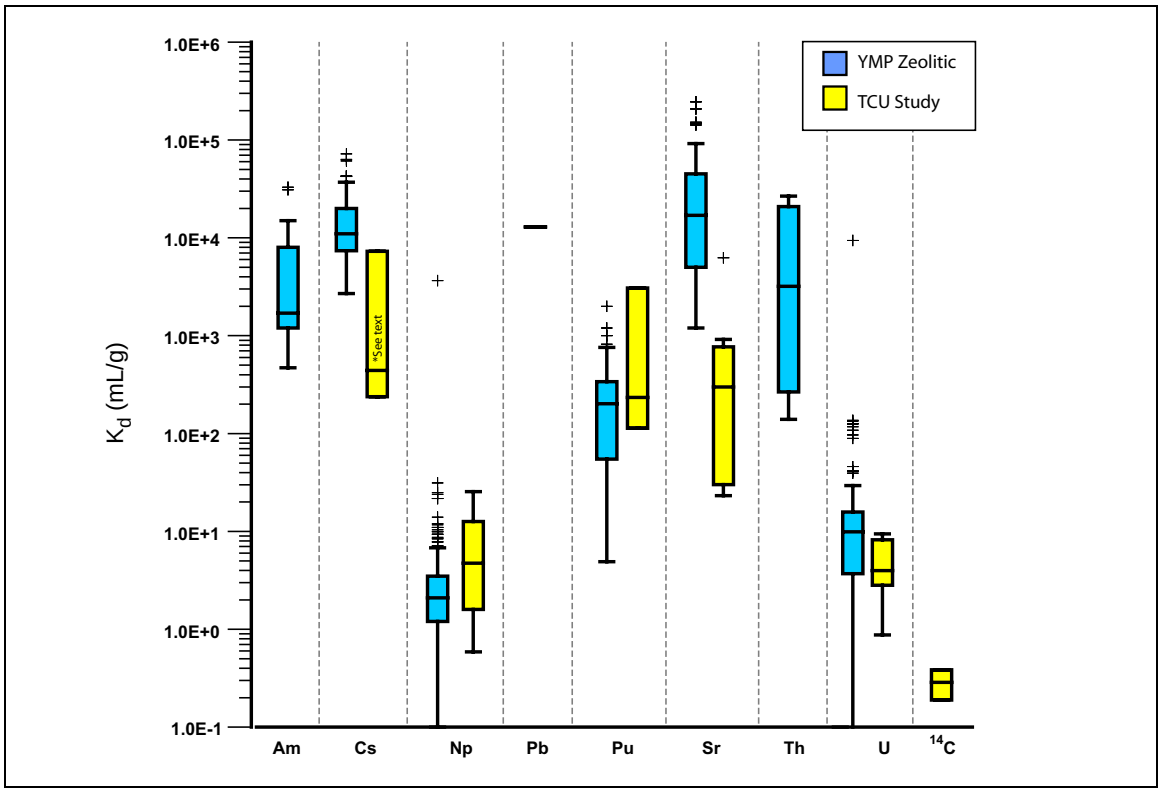

Figure 11-5
Laboratory Measured Distribution Coefficients for Zeolitic-Tuff Samples

larger than for major cations in solution. Distribution coefficients should be lower in higher ionic-strength water (e.g., UE-25 p#1) and should decrease with increasing solution concentrations. Sorption of these two elements has been extensively studied and reviewed by Daniels et al. (1983), Thomas (1987), and Meijer (1990), and summarized by Triay et al. (1997) and DOE/ORD (2001 and 2004). A limited number of DRI studies were conducted by Papelis and Um (2003a and 2003b) and Decker et al. (2003) to measure K_d values for Cs, and Sr on tuff and devitrified lava samples from Pahute Mesa, Rainier Mesa, and Frenchman Flat.

Cesium

Vitric Tuff. Sorption experiments using vitric-tuff samples and predominantly J-13 water were reported in the YMP TDMS (YMP, 2004). All rock samples were crushed and sieved before analysis, and the 75- to 500-µm and less-than-500-µm sieve fractions were used for the experiments. The Cs K_d values ranged from 50 to 1,061 mL/g (Figure 11-3).

Devitrified Tuff. Among all of the data sources, a total of 159 experiments measuring Cs sorption on devitrified tuff rocks are reported. All the rock samples were crushed and sieved before analysis, and several different sieve fractions were used for the experiments (see Appendix I). Most experiments were conducted in the presence of an ambient air atmosphere; however, several experiments were conducted in an N_2 atmosphere with less than 0.2 ppm O_2 and less than 20 ppm CO_2 to increase the pH during the experiments. The measured K_d values showed no trend with respect to pH. The Cs K_d values ranged from 10 to 2,000 mL/g; several outliers (ranging from 2,400 to 3,800 mL/g) are identified in the box and whisker plot (Figure 11-4). The K_d values were measured with essentially the same initial concentrations for all experiments. If field concentrations are greater than those used in the experiments, then Cs K_d values will likely be lower.

Zeolitic Tuff. Eighty-six Cs sorption experiments with zeolitic tuff rocks were reported in the YMP TDMS (YMP, 2004). All of these rocks were crushed and sieved before analysis. Particles sized from 75 to 500 μm were used for these experiments, but not necessarily all of the particles fell within this range. The Cs K_d values ranged from 2,700 to 37,000 mL/g; several outliers (ranging from 42,000 to 72,000 mL/g) are identified in the box and whisker plot (Figure 11-5). Retardation factors were reported for Cs (TCU study) as ranging from greater than or equal to 1,000, to greater than or equal to 35,000; no recovery of Cs was observed in the experiments (Zavarin et al., 2005). This corresponds to K_d values ranging from greater than or equal to 240 mL/g, to greater than or equal to 7,300 mL/g.

Strontium

Vitric Tuff. Distribution coefficient experiments using vitric-tuff samples and predominantly J-13 water were reported in the YMP TDMS (YMP, 2004). All of these rocks were crushed and sieved before analysis, and the 75- to 500-μm and less-than-500-μm sieve fractions were used for the experiments. The Sr K_d values ranged from 8 to 220 mL/g (Figure 11-3).

Devitrified Tuff. Experiments measuring the sorption of Sr onto devitrified tuffs are reported in the YMP TDMS (YMP, 2004) and by Papelis and Um (2003 a and b). All of these rocks were crushed and sieved before analysis, and several different sieve fractions were used for the experiments (see Appendix I). Most experiments were conducted in the presence of an ambient air atmosphere; however, several experiments were conducted in an N_2 atmosphere with less than 0.2 ppm O_2 and less

than 20 ppm CO_2 to increase the pH. Papelis and Um (2003a and b) leached the natural Sr out of the rock samples before their analyses; this procedure is likely to overestimate the sorption of Sr onto the devitrified rocks *in situ* at Yucca Flat. The Sr K_d values ranged from 9.2 to 237 mL/g; several outliers (ranging from 270 to 1,200 mL/g) are identified in the box and whisker plot (Figure 11-4).

Zeolitic Tuff. Eighty-three Sr sorption experiments onto zeolitic-tuff rocks were reported in the YMP TDMS (YMP, 2004). All of these rocks were crushed and sieved before analysis. Particles sized from 75 to 500 μm were used for these experiments, but not necessarily all of the particles fell within this range. The Sr K_d values ranged from 1,200 to 92,000 mL/g; several outliers (ranging from 142,000 to 246,000 mL/g) are identified in the box and whisker plot (Figure 11-5). Retardation factors were reported for Sr (TCU study) as ranging from 85 to greater than or equal to 3,400; no recovery of Sr was observed in some experiments (Zavarin et al., 2007). This corresponds to K_d values ranging from 23 mL/g to greater than or equal to 917 mL/g.

Several Sr sorption experiments for the YMP were conducted with temperatures ranging from 20 to 80 °C. Figure 11-6 shows the relationship between Sr sorption and temperature for the three volcanic rock types. Although there may be an increase in Sr sorption with increasing temperature, the K_d values measured at higher temperatures were not outside the range of values measured at 20 °C. This result suggests that the variability in rock chemistry or aqueous chemistry creates as much uncertainty as temperature for this dataset.

11.5.2.4 Neptunium

Neptunium has been one the most studied radionuclides by the YMP. It is important due to its abundance in nuclear waste packages, its long half-life, and its relative low affinity for immobile minerals. Yet, the exact mechanisms controlling Np sorption are still only partially understood. Triay et al. (1997) and DOE/ORD (2001) describe in detail the history and results of Np sorption studies for YMP. The sorption behavior of Np on apparently similar rock types varies between samples, indicating that minor primary or secondary phases such as calcite, hematite, or trace quantities of ferrous iron may govern the exact sorption process. Thus, mechanistic predictions of Np adsorption would require detailed knowledge of the surface areas of these trace minerals in the various hydrologic units.

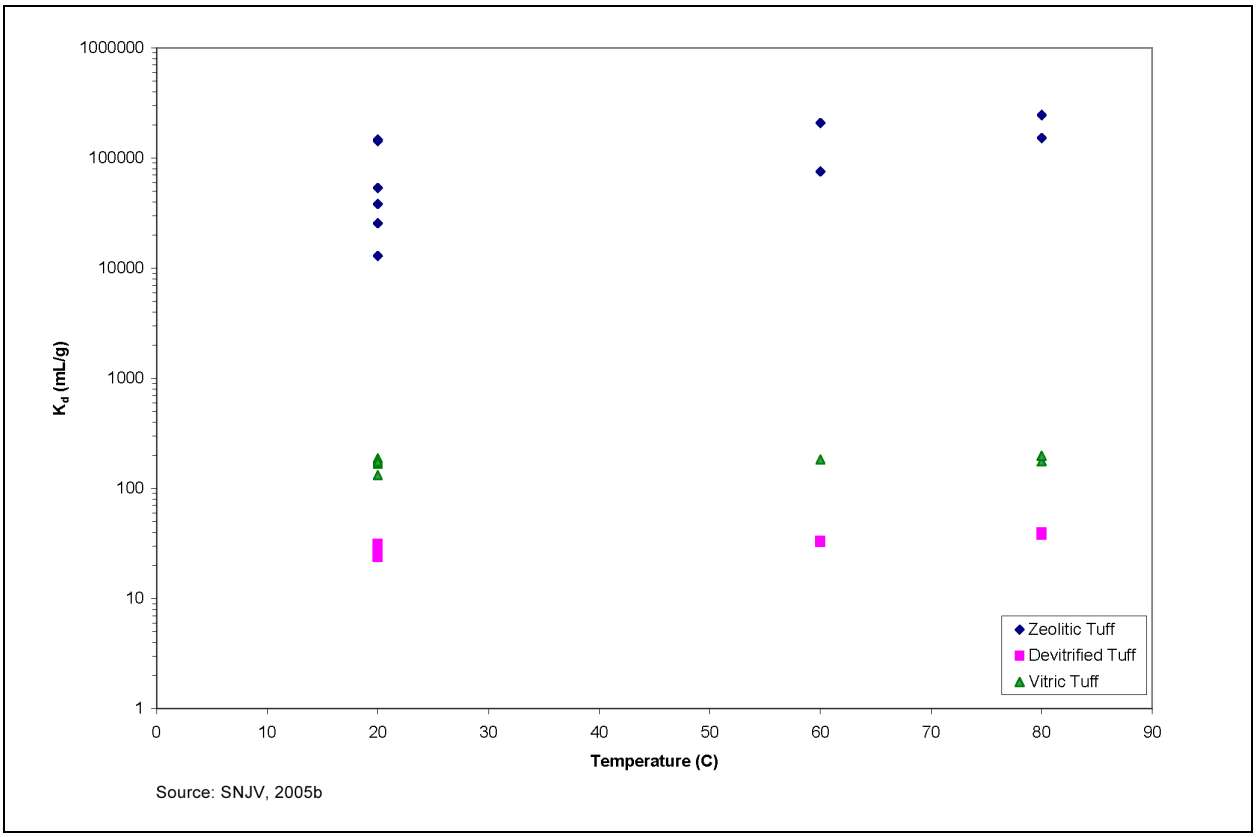

Figure 11-6
Strontium Sorption as a Function of Temperature (°C)
Measured During YMP Distribution Coefficient Experiments

An unexpected result of the YMP sorption studies involving Np is the relatively low K_d associated with zeolitic tuff. Whereas a strong cation exchange reaction was expected, the low values indicate that perhaps the neptunyl cation is too large relative to the zeolite cage sizes to come into contact with the exchange sites.

The complexities of Np sorption observations still present multiple challenges to decipher the precise governing mechanisms. The large number of K_d observations collected by YMP provides input to the present process of developing distributions of the parameter. It is expected that variability in K_d values represents variability in the processes controlling sorption (e.g., trace mineral quantities or reactive mineral surface area).

Vitric Tuff. Distribution coefficient experiments for Np using vitric-tuff samples in both J-13 and UE-25 p#1 water were reported in the YMP TDMS (YMP, 2004). Most experiments were conducted

in the presence of an ambient air atmosphere; however, several experiments were conducted in an N_2 atmosphere with less than 0.2 ppm O_2 and less than 20 ppm CO_2 to increase the pH during the experiments. Changes in pH between 7 and 9 appear to make no apparent difference in Np sorption to vitric tuff, nor do changes in water chemistry between J-13 and UE-25 p#1 water (see Appendix I). As stated previously, UE-25 p#1 water is not similar to the water composition of the volcanic-rock aquifers present at Yucca Flat; therefore, these data have been excluded from the dataset before the development of a K_d distribution. A total of 400 distribution coefficients have been measured using J-13 water and vitric-tuff rocks. The Np K_d values ranged from 0.1 to 2.5 mL/g; many outliers (ranging from 2.7 to 526 mL/g) are identified in the box and whisker plot (Figure 11-3).

Devitrified Tuff. As with vitric tuff, Np sorption to devitrified tuff is generally characterized with low K_d values. For the J-13 water experiments, pH and temperature do not appear to exert specific influence on the K_d values. The Np K_d values ranged from 0.1 to 4.3 mL/g; many outliers (ranging from 4.6 to 2,353 mL/g) are identified in the box and whisker plot (Figure 11-4).

Zeolitic Tuff. There were 578 Np sorption experiments onto zeolitic-tuff rocks reported in the YMP TDMS (YMP, 2004). Most experiments were conducted in the presence of an ambient air atmosphere; however, several experiments were conducted in an N_2 atmosphere with less than 0.2 ppm O_2 and less than 20 ppm CO_2 to increase the pH during the experiments. Changes in pH between 7 and 9 appear to make no apparent difference in Np sorption to zeolitic tuff. However, the presence of high Ca content in UE-25 p#1 causes a decrease in the total sorption to the zeolitic rocks (see Appendix I). As stated previously, UE-25 p#1 water is not similar to the water composition of the volcanic-rock aquifers present at Yucca Flat; therefore, these data have been excluded from the dataset. The Np K_d values ranged from 0.1 to 7.1 mL/g; several outliers (ranging from 7.8 to 3,661 mL/g) are identified in the box and whisker plot (Figure 11-5). Retardation factors were reported for Np (TCU study) as ranging from 4 to 95 (Zavarin et al., 2007). This corresponds to K_d values ranging from 0.8 to 25.9 mL/g.

11.5.2.5 Uranium

This section provides a summary of the evaluation of YMP U sorption data (Triay et al., 1997; DOE/ORD, 2001 and 2004) followed by results of the current analyses of the same dataset. Triay et al. (1997) summarize U sorption analyses, indicating that it will likely be affected by pH, carbonate

content, and concentrations of Ca and Mg. Complexation with carbonate species in solution will likely reduce the sorption coefficients for U. Thus, if pH decreases with carbonate concentration, one would expect reduced distribution coefficients. However, in the presence of zeolite minerals, decreasing pH would lead to an increase in uranyl ion concentrations and an increase in distribution coefficients. Data supporting this conclusion are cited in DOE/ORD (2001), in which sorption to zeolites in pH 9 water is near zero but increases to approximately 25 mL/g at pH of 6 in J-13 water. In UE-25 p#1 water, K_d values are generally smaller than in J-13 water due to increased complexes with carbonate and will not be used in this analysis because they are not representative of the water in the volcanic aquifers of Yucca Flat.

Vitric Tuff. Distribution coefficient experiments using vitric tuff samples in both J-13 and UE-25 p#1 water were reported in the YMP TDMS (YMP, 2004). Most experiments were conducted in the presence of an ambient air atmosphere; however, several experiments were conducted in an N_2 atmosphere with less than 0.2 ppm O_2 and less than 20 ppm CO_2 to increase the pH during the experiments. Changes in pH between 7 and 9 appear to make no apparent difference in U sorption to vitric tuff in the presence of J-13 water (see Appendix I). A total of 59 K_d values have been measured using J-13 water and vitric tuff rocks. The U K_d values ranged from 0.1 to 5.8 mL/g; two outliers (ranging from 11.2 to 12 mL/g) are identified in the box and whisker plot (Figure 11-3).

Devitrified Tuff. As with vitric tuff, U sorption to devitrified tuff is generally characterized with low K_d values. For the J-13 water experiments, pH and temperature do not appear to exert specific influence on the K_d values. The U K_d values ranged from 0.1 to 5.4 mL/g; several outliers (10 and 14.5 mL/g) are identified in the box and whisker plot (Figure 11-4).

Zeolitic Tuff. There were 176 U sorption experiments onto zeolitic-tuff rocks reported in the YMP TDMS (YMP, 2004). Most experiments were conducted in the presence of an ambient air atmosphere; however, several experiments were conducted in an N_2 atmosphere with less than 0.2 ppm O_2 and less than 20 ppm CO_2 to increase the pH during the experiments. Changes in pH between 7 and 9 appear to make no apparent difference in U sorption to zeolitic tuff. The presence of high Ca content present in UE-25 p#1, however, causes a decrease in the total sorption to the zeolitic rocks (see Appendix I). The U K_d values ranged from 0.1 to 108 mL/g; several outliers (ranging from 118 to 9,423 mL/g) are identified in the box and whisker plot (Figure 11-5). Retardation factors were

reported for Np (TCU study) as ranging from 6 to 55 (Zavarin et al., 2007). This corresponds to K_d values ranging from 0.9 to 9.6 mL/g.

Refinement of the distributions by pH was not specifically conducted for U sorption. Both Triay et al. (1997) and DOE/ORD (2001) indicate that pH may play an important role in controlling uranyl species formation. However, for the specific groundwater types used in these experiments, a clear trend in pH dependence was not observed.

11.5.2.6 Plutonium

Triay et al. (1997) provide a detailed discussion of the physiochemical processes affecting Pu speciation and sorption. The exact nature of Pu sorption is not well understood. Most importantly, sorption and desorption of Pu on the volcanic rocks is a redox-sensitive process. A possible explanation provided by DOE/ORD (2001) is that Pu^{+5} must undergo reduction before sorbing as Pu^{+4}. A result of this conclusion is that laboratory experiments conducted under oxidizing conditions may lead to smaller K_d values than exist in less oxidizing field conditions. This may not always be the case, however, because the use of a particular oxidation state during laboratory experiments may bias the results. The oxidation state of Pu in the field may vary within the same water, resulting in sorption of Pu in several other oxidation states that may be more or less sorbing than Pu^{+5}. It should be noted that regardless of what oxidation state is "used" in lab experiments, Pu redox changes with time. Kersting et al. (2002) have recently addressed the question of Pu^{+5} reduction to Pu^{+4} during sorption. Further, DOE/ORD (2001) concludes that K_d values derived from laboratory batch experiments would likely lead to conservative transport predictions (due to the short time scales associated with the laboratory Pu K_d measurements – longer contact with minerals leads to increased sorption).

Thomas (1987) found that sorption of Pu onto zeolitic rock samples had lower K_d values than vitric and devitrified tuffs due possibly to the lack of reduction sites. In that study, the largest K_d values were measured for samples with calcite and clays. Thomas (1987) also observed the strong dependence of K_d values on water composition, but not on pH. It was observed that the high bicarbonate concentration in UE-25 p#1 water might actually lead to coprecipitation of Pu rather than surface complexation or ion exchange.

For Pu sorption on various rock and mineral types, DOE/ORD (2001) discusses results for both J-13 and UE-25 p#1 water. Modifying the conclusions of Thomas (1987) and Wilson et al. (1994), DOE/ORD (2001) analysis indicates that the most important factors controlling Pu sorption in oxidizing water are the abundance of montmorillonite clays, zeolite minerals, and possibly calcite. Comparison of Figures 11-5 and 11-3 for Pu indicates that zeolitic tuffs sorb Pu similarly to vitric tuffs. Figure 11-4 shows that devitrified tuffs sorb Pu less strongly for both types of water, but the values are non-negligible. The data discussion provided by DOE/ORD (2001, Section 6.4.4) is not consistent with the distribution of K_d values provided in DOE/ORD (2004). A likely explanation for this discrepancy is that the ion radius of Pu is too large to enter the sorption sites on zeolitic materials, thus decreasing the total possible sorption of Pu onto zeolitic rocks. Additionally, the higher sorption of Pu on some volcanic rocks may be driven by the presence of secondary metal-oxide minerals; however, neither DOE/ORD (2001) nor (2004) addresses this issue.

Thomas (1987) and DOE/ORD (2001) note that water composition has a significant impact on Pu K_d distributions. That conclusion was used to support the decision to eliminate experiments in the presence of UE-25 p#1 in the following analyses because UE-25 p#1 is not similar to groundwater chemistries observed in Yucca Flat volcanic aquifers. Atmospheric conditions affecting pH in the experiments are included in this analysis. DOE/ORD (2001) points out that the pH of J-13 and UE-25 p#1 groundwater in contact with atmospheric CO_2 levels is generally in the range of 8.2 to 8.5. Therefore, in some experiments, the pH was adjusted down to near 7.0 by imposing an overpressure of CO_2 to address lower pH values observed among some saturated zone waters in the Yucca Mountain flow system.

Vitric Tuff. Seventy-one YMP sorption experiments were conducted with Pu, J-13 water, and vitric-tuff material. The Pu K_d values ranged from 21.5 to 1,174 mL/g; several outliers (ranging from 1,293 to 1,810 mL/g) are identified in the box and whisker plot (Figure 11-3).

Shaw (2003a) demonstrated a clear relationship between pH and K_d from data from a series of experiments that have been subsequently archived and removed from the current YMP database. The three values reported for the lower pH conditions were associated three lowest K_d values in the distribution. However, the next set of K_d values in the distribution were only a factor of two larger and they were obtained with pH values of 8.4 (Shaw, 2003a). The current dataset has a limited

number of samples with reported pH values and a more narrow range of pH values, between 8.28 and 9.26, and no obvious trend in K_d as a function of pH (see Appendix I).

Devitrified Tuff. Most experiments were conducted in the presence of an ambient air atmosphere; however, several experiments were conducted in an N_2 atmosphere with less than 0.2 ppm O_2 and less than 20 ppm CO_2 to increase the pH from approximately 8.5 to 9.5 during the experiments. However, there is an overlap between the air and N_2 experiments, and the values are weakly correlated to the duration of the experiments, so separate distributions are not established. Figure 11-7 shows the relationship between the experiment duration and K_d for air atmosphere experiments. This disequilibrium behavior for Pu sorption highlights the need for special care in parameter assignment and interpretation of results. If more data are collected for small duration experiments, the distribution is skewed to lower K_d values, which will lead to conservative Pu mobility estimates.

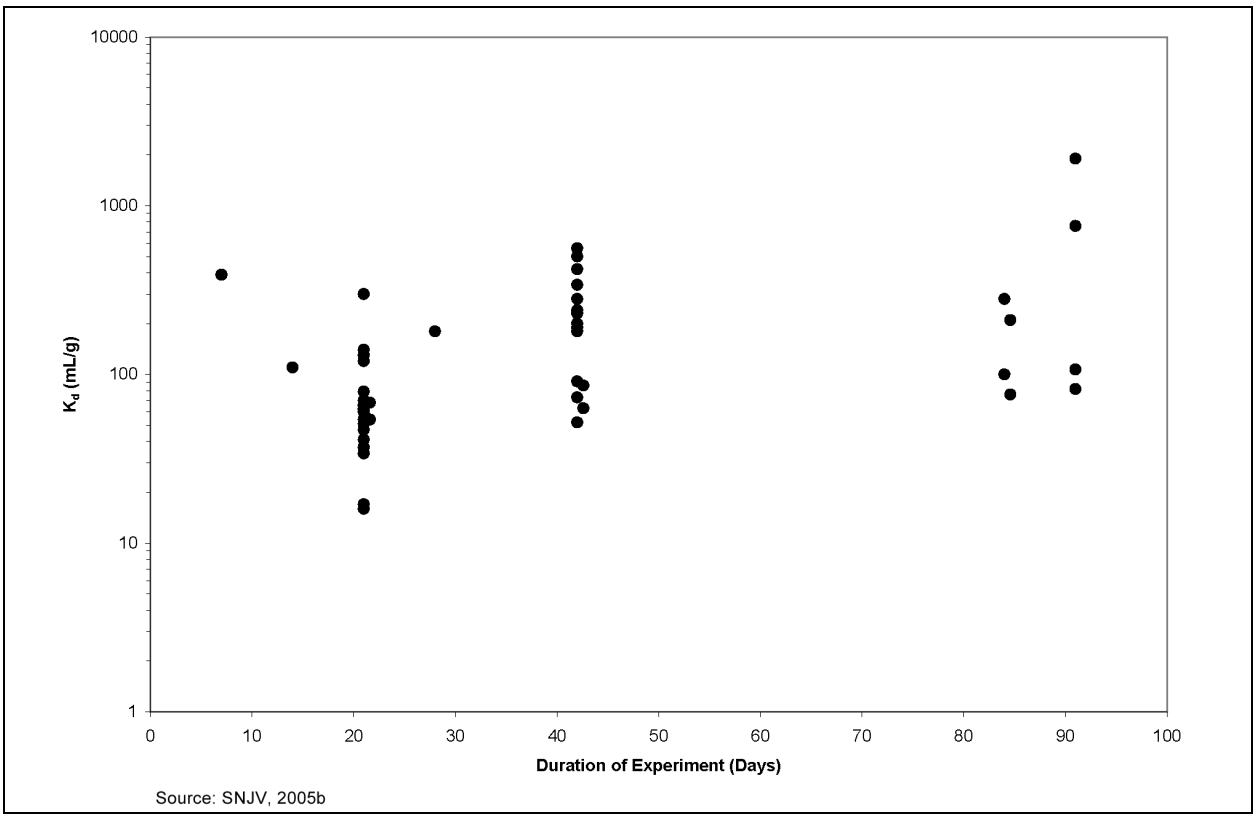

Figure 11-7
Distribution Coefficient (mL/g) for Plutonium Sorption onto Devitrified Tuff as a Function of Experiment Duration

There were 118 YMP sorption experiments conducted with Pu, J-13 water, and devitrified tuff material. The Pu K_d values ranged from 6 to 200 mL/g; several outliers (ranging from 210 to 1,900 mL/g) are identified in the box and whisker plot (Figure 11-4).

Zeolitic Tuff. The relative affinities for Pu on specific minerals are, in decreasing order, hematite > montmorillonite > clinoptilolite > calcite > gibbsite > albite ≥ quartz (DOE/ORD, 2001). Although this generalization does not take into account water chemistry, it is expected that rocks containing large abundances of secondary metal-oxide minerals should also show relatively strong affinities for Pu. The Pu K_d values ranged from 4.9 to 760 mL/g; several outliers (ranging from 1,000 to 2,000 mL/g) are identified in the box and whisker plot (Figure 11-5). Retardation factors were reported for Pu (TCU study) as ranging from greater than or equal to 600 to greater than or equal to 15,000; no recovery of Pu was observed in the experiments (Zavarin et al., 2005). This corresponds to K_d values ranging from greater than or equal to 240 mL/g to greater than or equal to 7,300 mL/g.

The large values in the data range are not as large as those for Pu sorption to vitric tuff, indicating that such sorption reactions may be dominated by the presence or absence of a few key minerals such as clay, which may determine the overall sorption capacity of a particular rock. There does not appear to be a strong correlation between pH and K_d values for Pu sorption to zeolitic tuffs.

11.5.3 Carbonate Rocks

Zavarin et al. (2007) summarize two studies that investigated radionuclide transport in fractures of the carbonate core performed in support of the UGTA Project (Zavarin et al., 2005; Ware et al., 2005). These experiments, also performed for the TCU, were described earlier. Retardation factors are related to K_d using Equation (11-2), and a bulk density for carbonate [$\rho_b = 2.85*(1-\phi)$] calculated using the rock porosity (ϕ) and mineral densities of dolomite. Porosity values are reported in Zavarin et al. (2007) and summarized in Section 7.0 of this report. Conclusions, regarding matrix sorption, from these studies are described below.

11.5.3.1 Carbon-14

Migration of ^{14}C was nearly unretarded through the fractured carbonate experiments. However, the retardation of ^{14}C as a result of isotope exchange on calcite surfaces may play a role over longer time and larger scales (i.e., field scales).

11.5.3.2 Strontium and Cesium

Essentially no matrix retardation of Sr and Cs was observed when only the carbonate matrix is present. It is apparent from the natural fracture experiments conducted by LANL that retardation associated with fracture lining minerals occurred. Because both Sr and Cs have high affinities for clays and zeolites, these minerals are expected to represent a significant fraction of the fracture lining mineralogy. Thus, Cs and Sr retardation in the LCA will be controlled primarily by fracture lining mineralogy.

11.5.3.3 Uranium

Transport of U in LCA is nearly unretarded. Fracture retardation factors from all experiments ranged from 1 to 3.8 (matrix retardation factors were set to 1). The highest fracture retardation factor was found in the synthetic induced fracture experiment conducted by LLNL. Because this fracture experiment is devoid of fracture lining minerals, the retardation may be interpreted as matrix retardation. Zavarin et al. (2005) reported fracture matrix retardation factors ranging from 6 to 20. The difference in modeling results underscores the problem of distinguishing between fracture and matrix retardation. In many cases, the difference between fracture retardation and matrix retardation was subtle and could not be clearly distinguished.

11.5.3.4 Neptunium

In general, Np transport is similar to that of U. However, higher retardation factors were observed on occasion. Np transport was interpreted as fracture retardation only. It appears that the high fracture retardation factors may be the result of fracture lining minerals; very low retardation was observed in fracture experiments that were free of fracture lining minerals.

11.5.3.5 Plutonium

From the fracture transport experiments, it appears that Pu can migrate for at least some time and distance in fractured carbonate as an aqueous phase. Matrix retardation factors of approximately 100 and 50 are reported in Zavarin et al. (2005). However, neither modeling exercise could accurately reproduce the Pu breakthrough profile. Thus, it is apparent that relevant processes controlling Pu transport were not included in the modeling exercises. The processes are likely to be a combination of colloid facilitated transport, rate-limited sorption/desorption, rate limited redox transformation, and possibly non-linear sorption.

Sorption data for radionuclides on carbonate material developed elsewhere, primarily in support of the WIPP Project, have been reported and summarized by Dosch and Lynch (1980), Stout and Carroll (1992), and Perkins et al. (1998). These studies provide primarily qualitative insight into the affinity of radionuclides for carbonate material; they do not represent specific NTS material or water chemistry. Dosch and Lynch (1980) report dolomite K_d values for Cs, Sr, Eu, Pu, and Am, examining differences in initial solute concentration and groundwater composition. Stout and Carroll (1992) summarize several studies from the literature up to 1992, and Perkins et al. (1998) provide K_d estimates for Pu and Am determined from a flowing column experiment. Table 11-5 summarizes the measured carbonate K_d values from these studies. (With regard to these studies, note that carbonate rock tends to have very low porosity and, as a result, very low reactive surface area. Crushed carbonate is likely to result in much higher K_ds than would be observed in the field.)

Table 11-5
Carbonate Sorption K_d (mL/g) Ranges

Radionuclide	Dosch and Lynch (1980)	Stout and Carroll (1992)	Perkins et al. (1998)	Total Range
Cs	4 - 101	-	-	4 - 101
Sr	5 - 16	-	-	5 - 16
Eu	$1x10^4$ - $4x10^5$	-	-	$1x10^4$ - $4x10^5$
Pu	$2x10^3$ - $7x10^3$	$1x10^2$ - $1x10^4$	275	$1x10^2$ - $1x10^4$
Am	$2x10^3$ - $2x10^4$	$2x10^3$ - $3x10^5$	150 - 350	150 - $3x10^5$
U	2 - 132	$1x10^{-5}$ - 0.3	-	0 - 132
Np	-	<$1x10^2$ - $5x10^3$	-	<$1x10^2$ - $5x10^3$

Source: Modified from SNJV, 2005b

11.5.4 K_d Derived from Upscaled Mechanistic Sorption Models

Reactions of solutes with immobile minerals involve a host of processes. Triay et al. (1997) and Zavarin and Bruton (2004a and b) provide descriptions of the reactive processes and controls affecting solute sorption to immobile minerals associated with the groundwater systems of the NTS. Mechanistic modeling approaches seek to represent the fundamental reactions between the solutes and the specific surfaces with which they come into contact. Using thermodynamic reaction-constant databases, mechanistic approaches represent processes including surface complexation, ion exchange, and precipitation. Additionally, the mechanistic modeling approach seeks to incorporate all aqueous-aqueous and aqueous-solid reactions. These include speciation reactions such as those involving carbonate complexes, oxidation/reduction reactions, and rock-water reactions that may control the concentration of surface sites with which radionuclides come into contact. Values of K_d can be developed from mechanistic models by simulating the effective distribution of a solute between its aqueous phase and sorbed phase by considering all relevant reactions, listed above, for a sample of aquifer material and specified geochemical conditions.

A benefit of the mechanistic modeling approach is its ability to specifically represent the reactions that control and affect radionuclide mobility. Due to the representation of all expected reactions, the mechanistic modeling approach describes how groundwater chemistry changes (e.g., pH), affect sorption reactions, as well as how sorption reactions may affect groundwater chemistry.

A limitation of the mechanistic modeling approach is that, although a detailed set of reactions may be simulated, parameters for those reactions may not be available, particularly at the CAU scale. For example, a mechanistic transport model requires the concentration of available reactive surface sites (often represented as percent mass of various minerals for which total reactive surface sites are known) be specified. Characterization of surfaces that a solute may come in contact with is generally not known and must be inferred. Further, coatings of reactive mineral sites with other compounds may serve to modify the available reactive surface sites for a given mineral. Another limitation of mechanistic models is that they require large amounts of computer resources due to the complexity and nonlinearity of the processes that they attempt to capture when used in a fully coupled flow and transport model. Although mechanistic models are faced with some limitations in their application for large-scale systems, they remain attractive due to their ability to capture heterogeneity. By doing so, they provide technical credibility to scaled or abstracted methods.

Until recently, mechanistic sorption modeling has been primarily focused on small-scale systems where detailed characterization of mineral composition is available. Recognizing the need to extend such models to CAU-scale problems, Zavarin et al. (2004) developed a methodology that upscales mechanistic sorption models to prescribe K_d values. This approach formalizes concepts for Pahute Mesa presented by Pawloski et al. (2001) and Wolfsberg et al. (2002, Appendix B), as well as by Davis et al. (1998) and others too numerous to fully review for other hydrogeologic systems. Only a brief summary of the method, results, and limitations of the mechanistic scaling approach are presented here. Further detail on the methods and results is provided in Zavarin et al. (2004).

Upscaled mechanistic sorption accounts for aqueous speciation, surface complexation, ion exchange, and precipitation reactions. Such processes for one radionuclide may be codependent upon the similar reactions associated with other radionuclides, thus leading to a large set of coupled reactions that must be considered simultaneously. The methods for solving such systems of equations are well documented. Zavarin et al. (2004) recognized that such methods are well suited for small or well-constrained problems, but that simplification is necessary for applicability at larger scales (e.g., CAU scale). Thus, following a set of assumptions, K_d values are developed based upon the mechanistic modeling approach. The assumptions include time-invariant solution groundwater chemistry and sorbing mineral abundances, far greater abundance of available sorption sites than sorbing radionuclides in solution, and conditions in which precipitation of minerals with the radionuclides can be neglected. Wolfsberg et al. (2002) made similar assumptions to justify simplifications in mechanistic models of fracture sorption K_d values (see Section 12.0).

Following the assumptions listed above, a set of numerical experiments can be performed to compute K_d values for a material. The information needed for such calculations include the initial radionuclide concentrations in solution, groundwater chemistry; thermodynamic reactions for all aqueous speciation and sorption reactions (e.g., Zavarin and Bruton, 2004a and b); and, most importantly, concentrations or available reactive surface sites (surface complexation and ion-exchange) at which sorption reactions occur.

Zavarin et al. (2004) calculated matrix K_d values for Ca, Sr, Cs, Am, Eu, Sm, Np, Pu, and U for Frenchman Flat alluvium in the presence of water consistent with groundwater ion concentrations near the CAMBRIC test. In addition, the K_d values for several regional HSUs were reported. The

K_d values estimated by Zavarin et al. (2004) for alluvium match measured values much better than the tuff estimates for Pahute Mesa because the speciation-reaction database used to calculate the alluvium K_d values was validated against direct K_d measurements (Zavarin et al., 2002). Further details about the validation procedure can be found in Zavarin et al. (2004).

The mechanistic scaling study of Zavarin et al. (2004) is dependent upon multiple other data sources. The modeling is conducted in accordance with LLNL procedures. The information used as model input to predict the K_d values are available in LLNL reports.

11.6 K_d Derived from Scaled Mechanistic Models

Using component additivity, Zavarin et al. (2004) computed K_d for a radionuclide for given bulk material as follows:

$$K_d = \sum_{i=1}^{n} K_{d,i}\phi_{m,i} \qquad (11\text{-}3)$$

where:

$K_{d,i}$ = is the specific K_d for individual mineral *i*

$\phi_{m,i}$ = mass fraction of mineral *i* with respect to the total bulk medium

Using mineralogic characterizations by several authors on multiple samples from core from five Frenchman Flat alluvial wells, Zavarin et al. (2004) predicted bulk K_d values for each rock chemistry sample using one aqueous chemistry. Table 11-6 reports the calculated mean and SD based on a log-normal distribution from each dataset for nine different radionuclides. The mean K_d predicted using the datasets is similar considering that there were differences among the mineralogic analyses with respect to detection limit, sampling method, sample interval, and sample area (Zavarin et al., 2004). Zavarin et al. (2004) report that the datasets suggest that heterogeneous distributions of sorbing mineral phases give rise to a large range in K_d variability for Frenchman Flat alluvium.

Table 11-7 lists the matrix K_d value reported in Zavarin et al. (2004) for vitric tuff HSUs from the regional NTS model (DOE/NV, 1997a). These HSUs include several CAU-specific HSUs in the Yucca Flat model area (Table 4-3). The minimum and maximum values represent variations due to differences in mineral composition. Water chemistry (consistent with samples from the CHESHIRE

Table 11-6
Predicted Average Radionuclide Distribution Coefficients (Log K_d, mL/g) for Frenchman Flat Alluvium Using Reported Radionuclide Sorbing Mineral Abundances

Drill Hole	Ramspott and McArthur (1977) and Beiriger (1977)	Warren et al. (2002)	Jones (1982)	Warren et al. (2002)	Daniels and Thompson (1984)	Warren et al. (2002)	Warren et al. (2002)	Sum of All Data
	Log K_d (mL/g)[a]							
	UE-5n	UE-5n	U-11g-1	U-11g-1	RNM-1	ER-5-3	ER-5-4	All Drill Holes
Ca	2.74±0.57	2.28±0.28	2.93±0.24	2.94±0.05	2.18±0.47	2.79±0.26	2.28±0.31	2.54±0.45
Cs	3.93±0.12	3.91±0.12	2.91±0.22	3.86±0.04	3.56±0.22	3.80±0.27	4.03±0.21	3.82±0.39
Sr	2.52±0.58	2.01±0.30	2.70±0.25	2.71±0.06	1.93±0.48	2.56±0.28	2.00±0.34	2.29±0.47
Am	3.39±0.22	3.84±0.09	4.02±0.18	3.79±0.04	3.45±0.35	3.79±0.23	3.91±0.22	3.78±0.30
Eu	2.83±0.23	2.23±0.09	3.52±0.19	3.24±0.07	2.88±0.34	3.27±0.23	3.32±0.23	3.22±0.30
Sm	3.14±0.25	3.45±0.09	3.89±0.21	3.54±0.15	3.16±0.33	3.62±0.25	3.56±0.26	3.50±0.33
Np	0.18±0.30	0.51±0.08	0.90±0.22	0.61±0.13	0.21±0.36	0.65±0.23	0.61±0.24	0.54±0.32
U	-0.52±0.39	0.06±0.07	-0.07±0.19	0.03±0.12	-0.42±0.48	-0.14±0.21	0.09±0.16	-0.11±0.33
Pu ($O_2 = 10^{-5}$)	0.44±0.25	0.91±0.08	1.02±0.18	0.86±0.06	0.52±0.37	0.82±0.22	0.97±0.20	0.83±0.30
Pu ($O_2 = 10^{-10}$)	0.84±0.26	1.30±0.08	1.43±0.18	1.26±0.06	0.92±0.37	1.23±0.21	1.37±0.20	1.23±0.30
Pu ($O_2 = 10^{-15}$)	1.33±0.27	1.77±0.08	1.93±0.18	1.76±0.06	1.40±0.38	1.73±0.20	1.84±0.20	1.71±0.30

Source: SNJV, 2005b

[a] Log K_d values reported are mean ± one standard deviation.

Table 11-7
Predicted Average Log K_d (mL/g) for Selected Regional Hydrostratigraphic Units from Zavarin et al. (2004) [a, b]

	TMA			TC			TCB			TBA			BCU			BAQ		
	E(x)	Min	Max	E(x)	Min	Max	E(x)	Min	Max	E(x)	Min	Max	E(x)	Min	Max	E(x)	Min	Max
Ca	3.44			3.37			3.57			2.99			2.94			3.74		
Cs	4.15	3.24		4.28	3.34		4.38	3.46		4.43	3.44		4.24	3.25		4.70	3.74	
Sr	3.22			3.14			3.35			2.73			2.67			3.50		
Am	4.05	3.77	4.40	4.19	3.90	4.54	3.47	3.18	3.81	4.62	4.35	4.96	4.62	4.35	4.97	5.08	4.81	5.42
Eu	3.60	3.14	4.06	3.73	3.27	4.20	3.04	2.56	3.52	4.18	3.72	4.65	4.18	3.72	4.65	4.65	4.19	5.12
Sm	3.79	3.32	4.26	3.92	3.46	4.39	3.23	2.76	3.72	4.41	3.94	4.89	4.41	3.94	4.88	4.90	4.43	5.38
Np	0.77	0.57	1.07	0.83	0.62	1.14	0.64	0.48	0.93	1.21	0.91	1.58	1.18	0.89	1.54	1.69	1.37	2.08
U	1.20	0.87	1.59	1.26	0.93	1.65	1.17	0.84	1.56	1.45	1.11	1.85	1.37	1.05	1.77	1.85	1.51	2.25
Pu (O_2=10^{-5})	1.16	0.77	1.62	1.27	0.85	1.74	0.89	0.59	1.31	1.64	1.17	2.12	1.62	1.16	2.11	2.09	1.62	2.58
Pu (O_2=10^{-10})	1.50	1.06	1.98	1.61	1.16	2.09	1.24	0.84	1.70	1.98	1.51	2.47	1.97	1.49	2.45	2.44	1.96	2.93
Pu (O_2=10^{-15})	2.21	1.73	2.69	2.31	1.84	2.79	1.96	1.49	2.44	2.68	2.21	3.16	2.66	2.19	3.14	3.14	2.66	3.62

Source: SNJV, 2005b

[a] Min and Max based on variations in mineral abundances.
[b] See Table 4-3 for descriptions of the regional HSUs.

test site conducted on Pahute Mesa), surface site density on individual minerals, and mineral densities are assumed constant.

11.6.1 Calculation of Distribution Coefficients Using Yucca Flat/Climax Mine Mineralogy and Water Chemistry Data

To obtain K_d values representative of the HSUs (see Table 4-2 for a description) and RMCs (see Tables 4-4 and 4-5 for descriptions) of the Yucca Flat/Climax Mine CAU, the mechanistic model was applied to mineralogy and water chemistry data specific to this CAU. The groundwater chemistry data are provided in Appendix E and discussed in Section 5.0. The extensive set of mineralogy (XRD) data is described in Appendix D. Distribution coefficients were modeled using the CRUNCH code (an updated version of the GIMRT code [Steefel and Yabusaki, 1995]) combined with the LLNL surface complexation and ion exchange sorption database (Zavarin and Bruton, 2004a and b).

As described in Table 4-4, the mineralogy of the Yucca Flat/Climax Mine is classified into nine RMCs. Estimation of K_d values for five of these (DMP, DMR, VMP, VMR, ZEOL) are presented within this section. The RMCs were assigned to each XRD (see Appendix D) and water chemistry (see Appendix E) sample. Groundwater chemistry data from ER-2-1, TW-B, and UE-14b were assigned to the DMP category and were used in the estimation of K_d values for both DMR and DMP RMCs because no water chemistry data are presently available for the DMR RMC. Similarly, no water chemistry data are presently available for the VMR category, so water chemistry data associated with the VMP (UE-1a, UE-6d, WW-3, and WW-A) were used for the calculations of K_d values for both the VMR and VMP RMCs. The resulting K_d values and histograms of these K_d values are presented in Appendix I. In addition, K_d values were also estimated based on the Yucca Flat/Climax Mine HSU. The resulting K_d values along with the associated histograms are presented in Appendix I. The CCUs were not considered in this analysis because they constitute very low permeability rocks through which there is little or no flow.

11.7 Summary of K_d Data

The K_d data described in this section are from both direct laboratory measurements and mechanistic model predictions. A comparison between these two types of data, labeled “Mechanistic Model

(Laboratory Studies)" and "Laboratory Studies," is shown in Figures 11-8 through 11-11. The alluvium data for these two datasets are from the Frenchman Flat alluvium dataset, and the volcanic datasets are primarily YMP data. To compare the direct measurements of radionuclide sorption with the mechanistic model of Zavarin et al. (2004), the mineralogy of the laboratory samples was substituted for the mineralogies reported in Zavarin et al. (2004), and the K_d values were calculated for each rock sample for which a mineralogy was reported. Although the mechanistic model conditions are similar to those of the laboratory experiments, they are not identical. The mechanistic model calculations are dependent on the quality of the rock mineralogical analysis because many trace minerals are important for radionuclide sorption. Therefore, poor quality mineralogical analyses may result in poor agreement between the laboratory K_d values and those calculated using the mechanistic model. Additionally, better comparison between the laboratory values and mechanistic model would be accomplished if the exact chemistry of the aqueous solution used during the experiment were used for the mechanistic model calculations; however, the aqueous chemistry often is not reported with the K_d. These comparisons show that the mechanistic model predictions (mean and 95 percent CI) are similar to the laboratory data, providing confidence that the mechanistic model values can be appropriately incorporated into the CAU transport model.

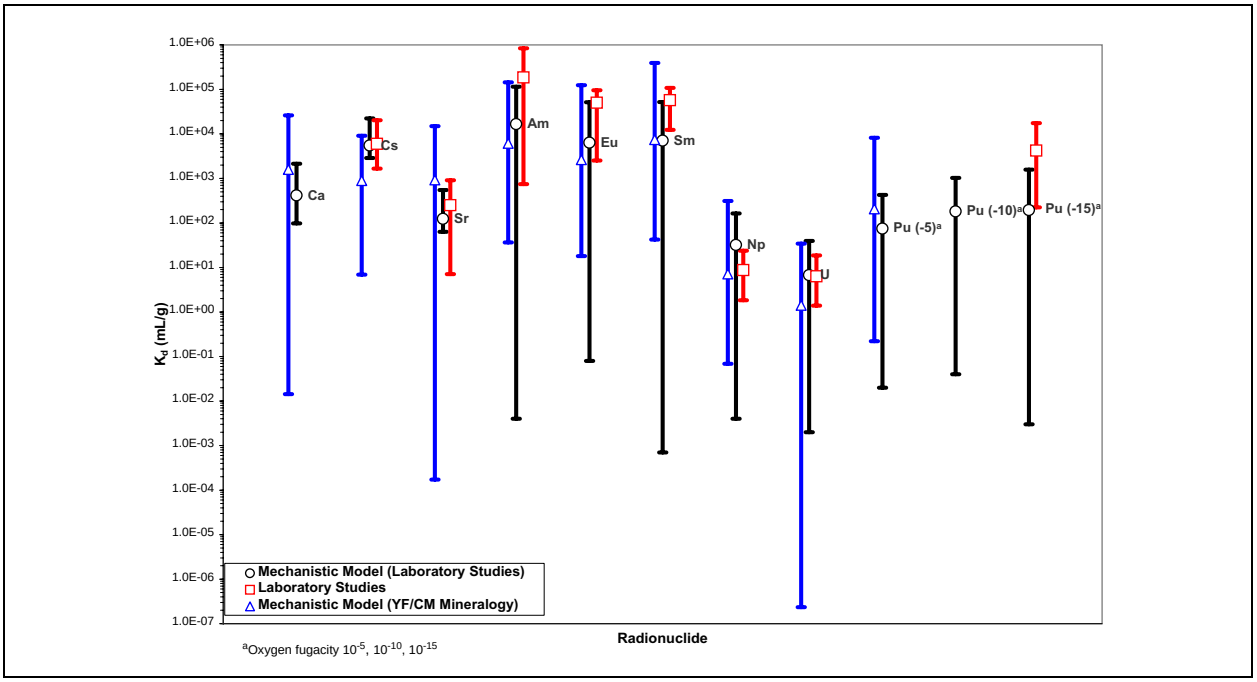

Figure 11-8
Comparison of Distribution Coefficients for Laboratory Studies and Mechanistic Model Calculations for the Alluvium

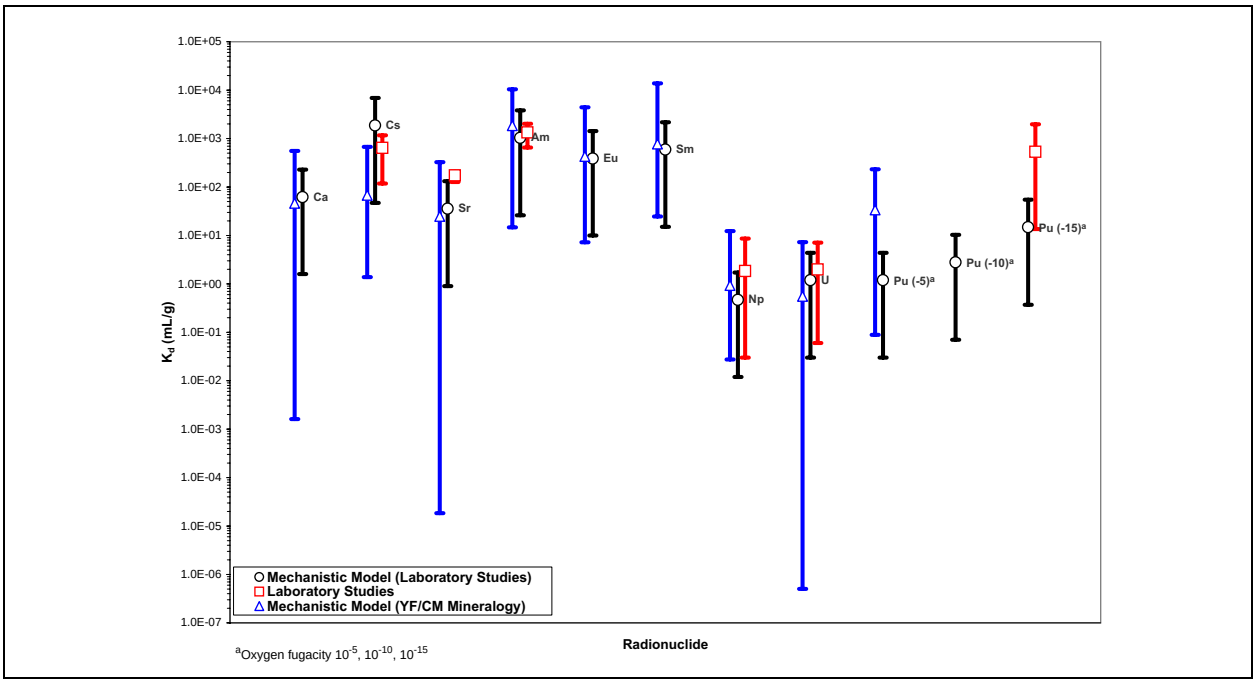

Figure 11-9
Comparison of Distribution Coefficients for Laboratory Studies and Mechanistic Model Calculations for Vitric Tuffs

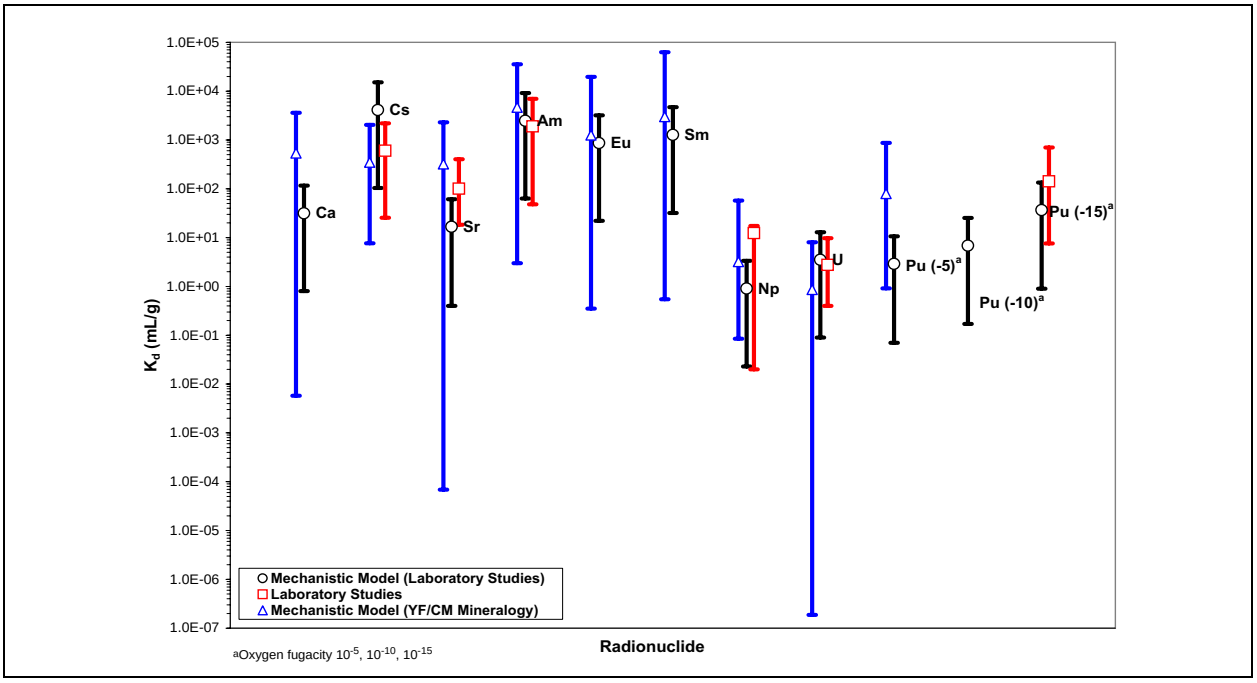

Figure 11-10
Comparison of Distribution Coefficients for Laboratory Studies and Mechanistic Model Calculations for Devitrified Tuffs

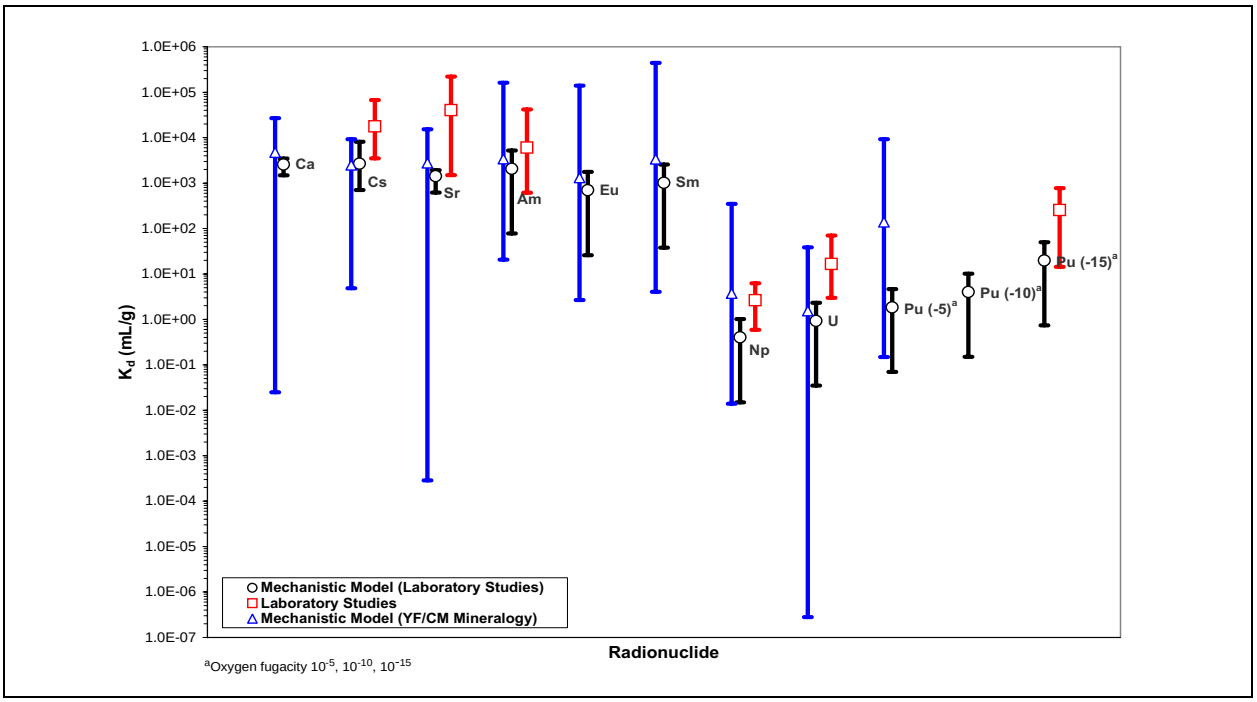

Figure 11-11
Comparison of Distribution Coefficients for Laboratory Studies and Mechanistic Model Calculations for Zeolitic Tuffs

The comparison for the alluvium includes laboratory measurements from U-1a samples that have an identical water chemistry to the one used in the mechanistic model. For Cs, Sr, Am, Eu, Sm, Np, and U, the mechanistic model provides values for K_d that generally encompass the entire distribution calculated for the direct measurements; however, the mechanistic model tends to overpredict the uncertainty in these values. This is likely because the number of experiments for which complete mineralogies were reported is relatively small compared to the entire set of laboratory measurements. For Pu, the mechanistic model tends to underpredict the K_d; this will result in conservative transport simulations, but may need to be further examined during transport model sensitivity analyses.
A likely interpretation is that Pu in the mechanistic model is being simulated at an oxygen fugacity that is too oxidizing (mechanistic model oxygen fugacity ranged from 10^{-5} to 10^{-15}); adjusting this fugacity to be more reducing may result in improved agreement between the mechanistic model and laboratory experiments.

The K_d values determined from the mechanistic model using the Yucca Flat/Climax Mine mineralogy (alluvium, vitric tuff [VMP and VMR RMCs], devitrified tuff [DMP and DMR RMCs], and zeolitic

tuffs [ZEOL RMC]) and water chemistry data are also presented in Figures 11-8 through 11-11 for comparison. The mechanistic model K_d ranges (95 percent CI) are calculated for the range of rock mineralogy found in Yucca Flat as well as the range of water chemistry. Note that the Yucca Flat mechanistic model was computed at an oxygen fugacity of 10^{-20}. Consequently the resulting K_d ranges may be different from the previous results due to differences in mineralogy and water chemistry between the sources of the samples for the Frenchman Flat alluvium and YMP volcanic datasets and for Yucca Flat. Also, the data available for Yucca Flat characterize the variability of the mineralogy and water chemistry more completely, accounting for the larger ranges. This comparison emphasizes the importance of the specific mineralogy and water chemistry, which vary spatially. These calculations of K_d for Yucca Flat are at the reconnaissance level for evaluating application of the mechanistic model to characterization of K_d for Yucca Flat, and do not constitute final input to transport modeling.

11.8 Scaling Considerations

Yucca Flat CAU transport simulations for contaminant boundary assessment will be conducted over various spatial scales. Volumes in the computational model represented with a single set of transport parameters will be much larger than sample volumes used for laboratory measurements. Scaling considerations for K_ds must address how well measurements conducted at the laboratory-scale represents the integrated sorptive behavior of a much larger volume in the CAU-scale model. Factors include representativeness of the samples used for laboratory measurements relative to variability of the formation characterized, and larger-scale longer-term processes that may not be well-characterized in the laboratory. One method for addressing this would be to use the data presented in this documentation report as representative of the small-scale system behavior. Scaling simulations could be designed to identify the effective K_d of a CAU-scale model grid block using multiple realizations of spatially distributed values from this study.

12.0 FRACTURE SORPTION PARAMETER

This section describes the fracture sorption process and possible methods for parameterizing it in the CAU models.

12.1 The Role of Fracture Sorption in Contaminant Transport

As with matrix sorption, fracture sorption is the physiochemical process at mineral-water interfaces that controls solute retardation on the surface of fractures, and hence solute mobility within flowing groundwater systems. Fracture sorption is treated separately from matrix sorption because it strictly involves the sorption of radionuclides to fracture surfaces, before diffusion into the matrix material or the fracture coating minerals, where matrix sorption may occur.

12.2 Data Types and Sources for Fracture Sorption

The simplest method to represent fracture sorption is to use retardation factors for solutes in fractures. Although easily derived from each other, the retardation factor is preferable to K_d because the K_d is based upon a volumetric sample of material, as appropriate for matrix material. In the fracture, all of the reactive processes leading to solute retardation are represented per unit length of fracture, rather than per unit volume of rock. As with the K_d, the retardation factor is straightforward to apply in transport models.

The use of a fracture retardation factor requires the assumption of local equilibrium. Reactions that are kinetic in nature must be assumed to occur fast enough that the retardation factor captures the process either adequately or conservatively in CAU-scale simulations. Further, the use of a fixed retardation factor does not allow for changing sorption behavior due to changes in water chemistry or mineral surfaces. It can vary spatially but is not capable of representing dynamic system changes during the course of a simulation.

12.2.1 Data Types

The modeling studies seeking to upscale mechanistic processes to larger-scale retardation factors are based upon the same processes as those described for mechanistic models of matrix K_d (see Section 11.0). The key components to estimating reactions with fracture coatings are as follows:

- The effective reactive surface area of fracture-coating minerals available to solutes flowing in the fracture
- The mineralogic composition of the fracture coatings
- The distribution (existence) of fracture-coating minerals in fractures

Once estimated, these three factors can be used to parameterize mechanistic models, which ultimately provide effective fracture retardation factors.

A benefit of the mechanistic modeling approach is that it specifically represents reactions that control and affect sorption to fracture-coating minerals. Due to the complete representation of all reactions, the mechanistic modeling approach can also describe how groundwater chemistry changes such as pH affect sorption reactions, as well as how sorption reactions may affect groundwater chemistry.

A limitation of the mechanistic modeling approach is that, although a detailed set of reactions may be simulated, parameters for those reactions may not be available, particularly at the CAU scale. This is important for estimating fracture retardation factors where spatial variation of fracture-coating materials will have first-order effects on the estimated parameters.

12.2.2 Data Sources

Three recent approaches within the UGTA Project have been used to assess fracture retardation. Wolfsberg et al. (2002, Chapter 7 and Appendix F) used estimates of fracture-coating thickness, distribution, mineral content, and availability in conjunction with surface complexation thermodynamic data reported by Pawloski et al. (2001) to predict fracture retardation factors. They found that the primary factor controlling fracture retardation is how much of the fracture coating is accessible to solutes migrating in the fracture. Zavarin et al. (2004) expand on developments made by Pawloski et al. (2001) with estimates of fracture retardation using mechanistic process models.

Wolfsberg et al. (2002) and Zavarin et al. (2004) have provided estimates of fracture retardation factors for various rock types on Pahute Mesa. Pahute Mesa volcanic aquifers have reasonably similar water composition to those observed in Yucca Flat volcanic aquifers; therefore, when HSUs from Pahute Mesa crosswalk to Yucca Flat HSUs, these data can be used directly (see Table 4-3 for the crosswalk). Fracture transport experiments were conducted by LLNL and LANL and the results summarized in Zavarin et al. (2007). The laboratory fracture transport experiments consisted of passing sorption solutions through TCU and LCA core as well as synthetic slotted fractures and measuring the breakthrough curves for specific radionuclides. Once the radionuclide breakthrough curves were determined, the models RELAP or RETRAN (a transient version of RELAP) were used to simulate the breakthroughs. Zavarin et al. (2007) summarized the rationale, methods, and results of both experiments as well as presented a summary interpretation of the data using mathematical models. Additional information regarding these experiments is provided in the original reports by Zavarin et al. (2005) (LLNL), and Ware et al. (2005) (LANL).

12.2.3 Data Transfer

Data from the Yucca Flat/Climax Mine HFM area and data from another NTS CAU, Central and Western Pahute Mesa, were used for this analysis due to the unavailability of comprehensive data from the Yucca Flat/Climax Mine HFM area for all HGUs. Specific discussion of the applicability of the transferred data is provided. A quantitative assessment of the sensitivity of transport modeling to the uncertainty in this parameter cannot be provided before the transport model development. The parameter description discusses the importance of this parameter.

12.3 Data Evaluation

The Wolfsberg et al. (2002) and Zavarin et al. (2004) modeling studies seek to incorporate information regarding specific reactions and estimates of fracture-coating properties. Coupled with other processes of matrix diffusion, matrix reaction, and colloid-facilitated transport, the expected values of fracture retardation factors were used by Wolfsberg et al. (2002) in predicting radionuclide concentrations in wells ER-20-5 #1 and ER-20-5 #3. In those simulations, the radionuclides with large retardation factors in fractures were shown to have minimal mobility in the absence of colloids. Zavarin et al. (2004) also demonstrate the increased predicted mobility when colloids are present and compete with immobile reactive minerals for radionuclide sorption.

12.3.1 Derivation by Wolfsberg et al. (2002)

Wolfsberg et al. (2002, Chapter 7 and Appendix F) apply a semi-mechanistic approach for estimating fracture retardation factors. They assume invariant water chemistry representative of Pahute Mesa groundwater and group radionuclides into the classes shown in Table 12-1. The derivation shows dependence of the fracture retardation factor on the uncertain fracture-coating properties listed in Section 12.2.1. The approach is based on three major assumptions: (1) a fixed percent coverage of fractures with coatings, (2) a fixed coating thickness where they exist, and (3) a fixed availability of reactive minerals within the coatings. Wolfsberg et al. (2002) ignored ion exchange reactions with fracture coatings, which are significant contributors to fracture sorption for Sr^{2+} and Cs^{+}. Variability in fracture retardation factors associated with variability in mineral content in the coatings calculated using this method are presented in Table 12-1 as the low, base, and high cases. Wolfsberg et al. (2002, Appendix F) noted that uncertainty in percent fracture-coating coverage and the percent of the coatings available for reactions can add up to three orders of magnitude of uncertainty on these values.

Table 12-1
Fracture Retardation Factors from Wolfsberg et al. (2002)

Radionuclide Class [a]	Range	Rock Type [b]			
		Welded	Lava	Altered [c]	Fractured Non-welded
Class II (^{151}Sm, ^{241}Am, ^{152}Eu, ^{154}Eu)	low	63	163	22	192
	base	195	207	25	223
	high	837	231	129	265
Class III (^{90}Sr, ^{137}Cs)	low	1.01	1.04	1	1.04
	base	1.07	1.05	1	1.05
	high	1.23	1.06	1.01	1.07
Class IV (^{234}U, ^{238}U, ^{237}Np)	low	1.13	1.35	1.03	1.43
	base	3.5	2.7	1.43	2.7
	high	13.5	4.9	2.5	5.5
Class V (^{239}Pu, ^{240}Pu)	low	2.7	9.2	1	8.4
	base	13.6	10.3	3.9	9.6
	high	39	13	6.8	15

[a] The fracture retardation factor is one for Class I radionuclides (^{3}H, ^{14}C, ^{36}Cl, ^{85}Kr, ^{99}Tc, ^{129}I).
[b] Fracture porosity is not applicable for the bedded, altered, and bedded-altered rock zones described in Wolfsberg et al. (2002).
[c] Alteration of vitric rocks at the NTS has produced zeolites, cristobalite, quartz, K-feldspars, and various clay minerals.

12.3.2 Derivation by Zavarin et al. (2004)

Zavarin et al. (2004) apply a mechanistic model using the thermodynamic reaction databases of Zavarin et al. (2002) to predict fracture retardation factors for several regional model HSUs. The potential link among effective porosity, fracture density, and aperture measurements with a mechanistic conceptual model is evaluated by requiring a relationship between the effective porosity and the volume of reactive minerals in contact with the flowing fluid. Thus, if the effective porosity is 1 percent and the porosity associated with open fractures in less than 1 percent, some of the flowing fluid was required to be associated with flow within the matrix. Diffusion between fractures and matrix material is not explicitly modeled. Rather, this method seeks to capture the effect of some diffusion into the matrix near the fracture wall with the increased effective porosity. Thus, the method also combines the effects of sorption to matrix material and fracture minerals with a single set of parameters. If matrix sorption and fracture retardation need to be separated for the CAU-scale flow and transport model, this method can be modified. Additional diffusion into the matrix beyond the matrix reactive zone can be simulated, understanding that the first portion of reactive matrix minerals is wrapped up in the fracture effective porosity abstraction with this method. Table 12-2 provides the estimated retardation factors from that study under the assumption that the primary metal oxide present in the rocks is an iron oxide. The reported range of uncertainty is only related to uncertainty in mineralogic composition of the fracture coatings, not of abundance or accessibility of those minerals to solutes in the fracture water.

12.3.3 Reactive Transport Experiments by Zavarin et al. (2007)

The simplest LLNL experiments included radionuclide transport through synthetic parallel-plate fractured tuff and carbonate cores (Zavarin et al., 2007). Because of the complex nature of reactive transport in fractures, a stepwise approach to identifying mechanisms controlling radionuclide transport was used. These simplified fracture transport experiments isolated matrix diffusion and sorption effects from all other fracture transport processes (e.g., fracture lining mineral sorption, heterogeneous flow). Additional fracture transport complexity was added by performing induced fractured LCA flowthrough experiments (effect of aperture heterogeneity) or iron-oxide-coated parallel-plate TCU flowthrough experiments (effect of fracture lining minerals.) Finally, naturally fractured tuff and carbonate cores were examined at LLNL and LANL. All tuff and carbonate core used in the experiments were obtained from the USGS Core Library, Mercury, Nevada.

Table 12-2
Fracture Retardation Factors, Log (R), from Zavarin et al. (2004)

Regional HSU [a]	Timber Mountain Aquifer (TMA)			Tuff Cone (TC)			Belted Range Aquifer (TBA)			Basal Aquifer (BAQ)		
Nuclide	**E(x) [b]**	**Min [c]**	**Max**	**E(x)**	**Min**	**Max**	**E(x)**	**Min**	**Max**	**E(x)**	**Min**	**Max**
Ca	3.34			2.95			3.24			3.36		
Cs	4.04	3.13		3.19	2.4		4.30	3.34		3.27	2.66	
Sr	3.12			2.72			2.99			3.14		
Am	2.03	1.99	2.06	1.92	1.88	1.94	2.64	2.61	2.65	2.26	1.94	2.50
Eu	2.06	1.98	2.08	1.98	2.03	1.89	2.69	2.59	2.73	2.60	2.49	2.65
Sm	2.14	2.11	2.16	2.06	2.02	2.11	2.74	2.70	2.78	2.98	2.92	3.02
Np	0.80	0.57	1.13	1.08	0.74	1.49	1.72	1.35	2.15	1.61	1.15	2.09
U	1.18	0.85	1.54	1.77	1.37	2.17	2.46	2.05	2.86	0.19	0.19	0.20
Pu (O_2=10^{-5})	1.12	0.74	1.51	1.36	0.93	1.77	2.04	1.57	2.46	1.46	1.03	1.87
Pu (O_2=10^{-10})	1.43	1.03	1.79	1.74	1.31	2.11	2.43	1.98	2.80	1.81	1.37	2.18
Pu (O_2=10^{-15})	1.94	1.62	2.12	2.31	1.97	2.50	3.00	2.66	3.20	2.34	2.00	2.54

Note: Assumes fracture coating iron-manganese oxides dominated by iron.
[a] Fracture retardation factors were categorized by regional HSUs.
[b] E(x) is the mean Log (R) for each HSU-radionuclide pair.
[c] Min and Max values incorporate the uncertainty associated with the mechanistic model reaction constants.

Once the radionuclide breakthrough curves were determined, the models RELAP or RETRAN (a transient version of RELAP) were used to simulate the breakthroughs. RELAP provides a simultaneous least-squares fit of up to four species (sorbing and/or non-sorbing) by automatically adjusting the following model parameters:

- Mean fluid residence time in the fractures
- Peclet number
- Matrix diffusion mass-transfer coefficient
- Characteristic fracture spacing
- Fracture retardation factor
- Matrix retardation factor
- Fracture and matrix sorption rate constants

Although RELAP was the computer model used for the majority of the interpretations, RETRAN was used for the LANL experiments in which there were significant flow rate changes early enough in an experiment to affect the shape of the breakthrough curves. The results of the analyses are estimates of the parameters listed above with the advantage of matching empirical rather than theoretical data. Table 12-3 provides the estimated retardation factors from this work.

Table 12-3
Summary of Fracture Retardation Factors Developed Through LLNL and LANL Fracture Retardation Experiments
(Page 1 of 2)

LLNL Fracture Experiments [a]	HGU	Sr	Cs	U	^{237}Np	$^{238/242}$Pu	^{14}C
UE-7az 1799, Synthetic slot	TCU	No rec (1)	No rec (1)	2.2 (2)	1 (1)	ND (1)	NA
UE-7az 1679, Natural	TCU	No rec (1)	No rec (1)	1.4 (2)	1 (1)	ND (1)	NA
UE-7az 1780, Natural	TCU	No rec (1)	No rec (1)	2.2 (2)	1.4 (1)	ND (1)	NA
UE-7ba 1627, Synthetic slot with colloids	TCU	NA	NA	3.5 (1)	1 (1)	60, 0.4† (1)	NA
UE-7az 1679, Synthetic slot with FeOH coating	TCU	No rec (1)	No rec (1)	12 (5)	1 (1) 1	ND (1)	NA
ER-6-1 2605, Synthetic slot	LCA	1 (1)	1 (1)	2.3 (1)	2.1 (1)	ND (1)	NA
ER-6-1 2733, Synthetic slot	LCA	1.1 (1)	1 (1)	1.5 (1)	2.6 (1)	3.5 (1)	NA
ER-6-1 2553, Synthetic included	LCA	No rec (1)	No rec (1)	3.5 (2)	3.5 (2)	2.5 (1)	NA
LANL Fracture Experiments [a]	**HGU**	**^{90}Sr**	**^{137}Cs**	**^{233}U**	**^{237}Np**	**^{239}Pu**	**^{14}C**
UE-4a 2029, High flow	TCU	1	0-0.5†	1	1	0-0.75†	1
UE-4a 2029, Low flow	TCU	1	0-0.24†	1	1	0-0.2†	1
UE-7az 1770, High flow	TCU	1	0-3.0†	1	1	0-2.3†	1
UE-7az 1770, Low flow	TCU	1	0-1.6†	1	1	0-0.5†	1
UE-7ba 1823, High flow	TCU	1	0-0.58†	1	1	0-0.75†	1
UE-7ba 1823, Low flow	TCU	1	0-0.3†	1	1	0-0.12†	1
UE-7ba 1863, High flow	TCU	1	0-0.39†	1	1	0-1.2†	1
UE-7ba 1863, Low flow	TCU	1	0-0.35†	1	1	0-0.3†	1
ER-6-1 2400, High flow	LCA	2	68	1.2	5.7	0-0.28†	1.5
ER-6-1 2400, Low flow	LCA	4.25	≥100	1.4	6	0-0.36†	1
ER-6-1 2400, Low flow #2	LCA	NA	≥100	NA [a]	7	NA	NA
ER-6-1 2512, High flow	LCA	20	58	1.5	5	0-0.18†	1.2
ER-6-1 2512, Low flow	LCA	≥30	50	1.6	3	40, 0-0.14†	1
ER-6-1 2512, Low flow #2	LCA	NA	≥50	NA	2.6	NA	NA
ER-6-1 2675, High flow	LCA	1	2.8	1.3	3.5	19, 0-0.64†	2.5

Table 12-3
Summary of Fracture Retardation Factors Developed Through LLNL and LANL Fracture Retardation Experiments
(Page 2 of 2)

LANL Fracture Experiments	HGU	^{90}Sr	^{137}Cs	^{233}U	^{237}Np	^{239}Pu	^{14}C
ER-6-1 2675, Low flow	LCA	2.5	3.5	1.3	8	33, 0-0.24†	1.5
ER-6-1 2675, Low flow #2	LCA	NA	4	NA	8	NA	NA
ER-6-1 2847, High flow	LCA	1	2.2	1	4	2.4	1.5
ER-6-1 2847, Low flow	LCA	1.5	2.8	1.3	5.2	42, 0.2†	1
ER-6-1 2847, Low flow #2	LCA	NA	3	NA	4.8	NA	NA
ER-6-1 2915, High flow	LCA	1.4	1.8	1.2	≥50	0-0.17†	1.5
ER-6-1 2915, Low flow	LCA	2	2	1.2	5	0-0.08†	1.1
ER-6-1 2915, Low flow #2	LCA	NA	2.3	NA	5	NA	NA
ER-6-1 3028, High flow	LCA	1.5	280	1.5	5	16	1.5
ER-6-1 3028, Low flow	LCA	NA	≥140	1.6	8	NA	1
ER-6-1 3028, Low flow #2	LCA	NA	≥100	NA	9	NA	NA
ER-6-2 2730, High flow	LCA	33	320	1.6	22	50	5
ER-6-2 2730, Low flow	LCA	NA	280	2.7	32	NA	1
ER-6-2 2730, Low flow #2	LCA	NA	160	NA	28	NA	NA
ER-6-2 2750, High flow	LCA	2	33	1.5	8.5	18	1.8
ER-6-2 2750, Low flow	LCA	NA	42	1.5	5	NA	1
ER-6-2 2750, Low flow #2	LCA	NA	40	NA	6	NA	NA

Source: Tang et al., 1981; Zavarin et al., 2005

Note: Data in parentheses indicate previous LLNL model fit parameters.
[a] Fracture experiment name reflects the source of the core used, the depth from which the core was extracted (ft), and the type of slot or flow rate.

≥ - Indicates that the value is a minimum.
Colloid - Colloid-facilitated transport strongly suspected; matrix retardation factors not applicable.
† - Colloid filtration rate constant range; breakthrough fitted assuming rate-limited and irreversible colloid filtration in fracture.
NA - Not available - element not in sorption solution.
ND - Not determined (very low, but early recovery; suspected of being colloid-facilitated).
No rec - No recovery of radionuclide; matrix retardation factors not estimated.

12.3.4 Fracture Retardation Factor Summary and Integration

Wolfsberg et al. (2002) and Zavarin et al. (2004) present approaches for estimating retardation in fractures due to reactions with fracture-coating minerals. Although methodologies to account for processes that may affect migration rates and groundwater concentration of reactive radionuclides are highlighted, these approaches are theoretical. The two approaches yield different results, in some cases, because of differences in the conceptual model and the assumptions about processes that lead to fracture retardation.

One of the largest differences is that Zavarin et al. (2004) include reactions with matrix minerals as well as with fracture-coating minerals, which leads to increased estimated retardation factors. Wolfsberg et al. (2002) only consider reactions with the minerals coating the fracture; reactions with matrix minerals are considered in conjunction with the matrix diffusion component of their model. The Zavarin et al. (2004) results may require modification to be implemented in the Yucca Flat/Climax Mine CAU transport model because fracture and matrix sorption may be treated independently in the model. Another difference between the two approaches is that Wolfsberg et al. (2002) do not consider ion exchange reactions, which are the primary reaction responsible for retardation of Sr^{2+} and Cs^{+}.

Zavarin et al. (2007) present estimates of retardation in fractures based on the analysis and matching of empirical data. In general, matrix sorption accounted for the observed retardation of radionuclides in the TCU (unless a radionuclide was transported as a colloid). Fracture sorption accounted for most of the observed retardation in the LCA. Fracture sorption was shown to play a significant role in the TCU for both U and Np, and was not significant for ^{14}C, Sr, Pu, and Cs. In the LCA, fracture sorption was shown to play a significant role for Sr, Cs, Np, and Pu and was not significant for either ^{14}C or U.

The results from the two mechanistic modeling approaches (Wolfsberg et al., 2002; Zavarin et al., 2004) as well as the empirical approach (Zavarin et al., 2007) for determining fraction sorption parameters are summarized in Table 12-4. Only the data for the HGUs that are considered to have fracture porosity (LFA, WTA, and CA) are shown (see Section 8.0 for further discussion). The results are correlated with HSUs in the Yucca Flat/Climax Mine CAU groundwater flow and transport model domain. Considering the mechanistic modeling approaches, the range of uncertainty is large due to the strictly theoretical nature of the estimation methods. With the exception of Sr^{2+} and Cs^{+}, the

retardation factors from Zavarin et al. (2007) are generally similar to those developed through the mechanistic modeling approach of Wolfsberg et al. (2002). However, the results from Zavarin et al. (2007) offer the advantage of empirical testing and provide results for the LCA.

Table 12-4
Summary of Fracture Retardation Factors for Yucca Flat HSUs

HGUs	HSUs	Alteration	Ca	Cs	Sr	Am	Eu	Sm	Np	U	Pu(10^{-5})	Pu(10^{-10}) [a] Pu(10^{-15})	Pu [b]	^{14}C
LFA [c]	BLFA PRETBG PRETBG1	Lava	NA (2,188) NA	(1.04, 1.06) [d] (1,349, 10,965) [e] NA [f, g]	(1.04, 1.06) (1,318) NA	(163, 231) (98, 115) NA	(163, 231) (95, 120) NA	(163, 231) (129, 145) NA	(1.35, 4.9) (3.7, 13) NA	(1.35, 4.9) (7.1, 35) NA	(9.2, 13) (5.5, 32) NA	(11, 62) (42, 132) NA	NA	NA
WTA [c]	TM-WTA TSA BRA TUBA	Welded, vitric to devitrified	NA (2,188) NA	(1.01, 1.23) (1,349, 10,965) NA	(1.01, 1.23) (1,318) NA	(63, 837) (98, 115) NA	(63, 837) (95, 120) NA	(63, 837) (129, 145) NA	(1.13, 13.5) (3.7, 13) NA	(1.13, 13.5) (7.1, 35) NA	(2.7, 39) (5.5, 32) NA	(11, 62) (42, 132) NA	NA	NA
CA	LCA	Fractured	NA NA NA	NA NA (1.0, 320.0)	NA NA (1.0, 33.0)	NA NA NA	NA NA NA	NA NA NA	NA NA (2.1, $\geq$ 50)	NA NA (1.0, 3.5)	NA NA NA	NA NA NA	0.00, 50	1.0, 5.0

[a] Retardation factors Pu for oxygen fugacities of 10^{-10} and 10^{-15} are reported in Zavarin et al., 2004.
[b] Retardation factors for Pu and ^{14}C are measured from laboratory experiments reported in Zavarin et al., 2007.
[c] The LFA and WTA HGUs are associated with the TMA regional HSU reported in Zavarin et al., 2004.
[d] Upper range in each cell represents retardation to fracture minerals only from Table 12-1 (Wolfsberg et al., 2002).
[e] Middle range in each cell represents retardation due to sorption to fracture minerals and matrix minerals from Table 12-2 (Zavarin et al., 2004)
[f] Lower range in each cell represents fracture retardation factors from Table 12-3 (Zavarin et al., 2007).
[g] Radionuclides shown include analysis of multiple isotopes in some cases.

NA - Not available

13.0 COLLOID-FACILITATED TRANSPORT PARAMETERS

This section presents a brief description of the current understanding of the role of colloid particles in the transport of radionuclides in groundwater and identifies parameters for colloid occurrence, movement in groundwater, and interaction with radionuclides for context. Documents characterizing colloids in groundwater, colloid-facilitated transport experiments, and radionuclide associations with colloids at the NTS are reviewed. Available data for the parameters are summarized and evaluated to assess the state of knowledge for each parameter, and the datasets are characterized as parameter value distributions. The objective of this compilation and analysis is to provide an overview of available information to support contaminant transport modeling regarding colloid-facilitated transport.

Data compilation and analysis builds directly upon the analysis presented in SNJV (2005b) and includes all colloid data available (through January 2007) for the NTS and vicinity. The focus is on available data relevant to the Yucca Flat/Climax Mine CAU. However, because colloid data specific to this CAU are limited, transfer of data from other UGTA CAUs (Frenchman Flat, Pahute Mesa, and Rainier Mesa/Shoshone Mountain) and from the YMP was necessary for the analysis. Colloid studies for UGTA CAUs provide data for the alluvium in Frenchman Flat; fractured volcanic rocks in Yucca Flat, Pahute Mesa, and Rainier Mesa; and fractured carbonate rocks in Yucca Flat. Studies performed in support of the YMP focused on colloids in the alluvium and volcanic tuffs.

Colloid data have been organized into five major categories: (1) colloid mineralogy, (2) colloid concentration and size data, (3) colloid transport parameters (colloid filtration [attachment and detachment] rate constants and the resultant retardation factors), (4) radionuclide distribution coefficients and sorption rates, and (5) radionuclide associations with colloids at source locations near cavities. These types of data are used for modeling colloid-facilitated transport.

Note that the distributions for colloid transport parameters presented here may not be appropriate for input distributions to colloid-facilitated transport modeling. Distributions are calculated in this

analysis for the purpose of characterizing the data. Lognormal distribution of parameters is common in physical systems and is used where it provides reasonable fit to the data distribution. The required form for modeling colloid-facilitated transport may be dependent upon model assumptions, and reinterpretation of the data within the context of the transport model may be required. The specific format for the transport model has not yet been determined, and the input parameter values and distributions would be dependent upon the model and assumptions. This section also does not address the subject of source term embodied in colloid form (i.e., how much of any radionuclide in a source region can become associated with the colloidal form and how that might occur). This would include estimates of colloid formation during glass dissolution in which Pu, for example, could either become an intrinsic colloid through hydrolysis, sorbed onto other colloids present in the source region, or embedded physically within a clay or glass colloid. Such data are not available.

13.1 Data Compilation and Data Transfer

Data from the Yucca Flat/Climax Mine HFM area and data from other NTS CAUs, YMP, and from another location (specifically data for alluvium, for which these data provided an expanded time scale) were used for this analysis due to the unavailability of comprehensive data from the Yucca Flat/Climax Mine HFM area for all HGUs. All data locations used in quantitative analyses are identified in Appendix J and the associated dataset referenced in Section J.7.0. Individual discussions of the applicability of the transferred data are provided for each HGU. A quantitative assessment of the sensitivity of transport modeling to the uncertainty in this parameter cannot be provided before the transport model development. The parameter description discusses the importance of this parameter.

13.2 Role of Colloids in Contaminant Transport

Colloids are small particles (less than 1 μm) that can facilitate the migration of contaminants in groundwater flow systems. Colloids are composed of either organic matter or inorganic mineral material from the host rock, herein referred to as “types,” associated with the mineralogic composition. Oxides and hydroxides of actinide elements (e.g., Pu) can also form colloids (Kersting et al., 1998). Dissolved solids may be removed from solution by attachment to colloids through ion exchange or adsorption.

Colloids facilitate the transport of strongly sorbing contaminants by providing mobile particles onto which the contaminants can sorb and be transported by the groundwater. It is generally accepted that one of the two following conditions must be met for colloid-facilitated transport to be significant:

- Colloids remain mobile over relatively long distance and time scales AND radionuclides are irreversibly or nearly irreversibly sorbed to the colloids, OR
- The product of the surface-area-based radionuclide partition coefficient onto colloids and the mobile colloid surface area is comparable to or greater than the product of the surface-area-based radionuclide partition coefficient onto immobile surfaces and the immobile surface area.

Regarding the types of data for colloids presented in this section, colloid filtration rate constants, colloid retardation factors, and radionuclide desorption rate constants from colloids are important for the factors listed in the first bullet. The mobile colloid surface area (dictated by colloid concentrations, sizes, and shapes) and radionuclide partition coefficients onto both colloids and immobile surfaces are important for the factors listed in the second bullet. Colloid mineralogy and size distributions are important because they affect the mobility (i.e., filtration, retardation) of colloids and the affinity of radionuclides for colloids.

Further discussions on the role of colloid-facilitated transport with regard to contaminant transport modeling are provided in DOE/NV (2000a) and NNSA/NSO (2004a).

13.3 Summary of Colloid Studies

Concern regarding the increased mobility of radionuclides through colloid-facilitated transport at the NTS was raised when Pu, Eu, Co, and Cs, associated with colloids, were detected in groundwater samples from the ER-20-5 site. These radionuclides apparently had been transported from the BENHAM site 1.3 km to the north (Kersting et al., 1998). This finding initiated a considerable number of studies regarding colloids at the NTS.

An investigation of colloids in the Rainier Mesa tunnels was performed by LLNL, and the results were published in Kersting et al. (2002). Reporting of this work was included and updated in Kersting and Reimus (2003). Unsaturated zone water from fractured volcanic tuffs in the Rainier Mesa E-, N-, and T-Tunnels was sampled in 1998 by LLNL and the Defense Threat Reduction

Agency (DTRA). In these tunnels, groundwater moving in the unsaturated zone can be accessed without the use of pumps. This is desirable because pumping can increase the mobilization of colloids. Samples were analyzed for colloid mineralogy as well as for groundwater composition, gamma-emitting radionuclides, Pu, Am, and ^{90}Sr. It was found that low-solubility radionuclides detected in the unsaturated zone water strongly sorbed to the colloidal fraction of the groundwater, and the majority of the radioactivity was associated with the colloidal fraction of the groundwater. The results of the mineralogy analysis are presented in Section 13.4

Kersting and Reimus (2003) comprehensively reviewed the literature and state of knowledge about colloid-facilitated transport at the NTS. The primary conclusions of this study are as follow:

- Colloids exist and are stable in groundwater at the NTS.
- Plutonium and Am are overwhelmingly associated with the colloidal fraction of groundwater in both the unsaturated and saturated fracture flow environments at the NTS.
- Plutonium has a high sorption affinity and concomitant low desorption rate for mineral colloids (zeolites, clays, manganese oxides, iron oxides, and silica) found in groundwater at the NTS.
- Plutonium-doped mineral colloids were transported through saturated fractured rock cores from Pahute Mesa.
- It is reasonable to expect a small fraction of radionuclide mass from a discrete source to move essentially at the rate of water flow through fractures over significant distances while sorbed onto colloids.
- Colloids can facilitate the transport of low levels of low-solubility radionuclides, and this is the dominant mechanism for the rapid transport of these radionuclides in groundwater.

The Bechtel SAIC (2004b) document, which was published for the YMP, contains analyses of data regarding colloid retardation factors representing reversible chemical and physical filtration of colloids in the saturated zone. Distributions of retardation factors for alluvium and fractured volcanics, and data on the fraction of colloid mass that transports unretarded in the natural system are presented. The document also discusses the validity of using microspheres as a surrogate for colloids in laboratory and field experiments.

Ware et al. (2005) report results of sorption, desorption, and fracture transport experiments conducted at LANL using six radionuclides (^{14}C, ^{137}Cs, ^{237}Np, ^{239}Pu, ^{90}Sr, ^{233}U) and numerous geologic samples from both the TCU and LCA. Although the experiments did not intentionally involve colloids as a transport mechanism, colloids were thought to have formed by silica or calcite precipitation in the synthetic groundwater used for the experiment. In this study, colloid-facilitated transport was implicated for the rapid transport of a fraction of the ^{137}Cs and ^{239}Pu in the TCU fracture experiments. The results indicated that the potential for colloid-facilitated transport of ^{137}Cs and ^{239}Pu is far greater than the potential for ^{90}Sr, ^{233}U, and ^{237}Np; the latter three radionuclides showed no evidence of colloid-facilitated transport in the TCU fractures. The results also indicated that ^{137}Cs and ^{239}Pu probably sorbed very strongly (and preferentially compared to the other radionuclides) to these colloids before being introduced to the fractures.

Zavarin et al. (2005) report on laboratory experiments designed to pursue understanding of how radionuclides migrate or are retarded in TCU fractures, and the migration behavior of radionuclides once they reach the fractured LCA. For one of the TCU cores used for the experiment, clinoptilolite colloids were included both in the radionuclide cocktail and background solution to examine the potential role of colloids in facilitating transport of strongly sorbing radionuclides, such as Pu. Zavarin et al. (2005) demonstrate that colloid-facilitated transport was not a significant mechanism for the transport of Cs, Np, and U. In contrast, breakthrough of Sm and Pu was significant only in the presence of colloids. The results indicate that Pu migration is likely to occur in the TCU only as a result of colloid-facilitated transport, and that any significant transport of Sm in the TCU fractures will likely be the result of colloid-facilitated transport. However, whether the colloid-facilitated transport is significant at the field scale will require further examination. As suggested by the TCU experiments, the introduction of colloids in the LCA may significantly enhance transport behavior of the strongly sorbing radionuclides.

Abdel-Fattah et al. (2005) report that LANL has been measuring colloid concentrations and size distributions in groundwater samples collected from monitoring wells at the NTS for several years, and this report presents the results of their analyses. These data are updated in Reimus et al. (2006a), where recent LANL results for measured colloid concentrations and size distributions are presented. In addition, new information is introduced regarding the associations of Cs, U, Np, and Pu with colloids in groundwater samples collected from eight near-field monitoring wells with very low

concentrations of radionuclides in the groundwater. This information has the practical importance of evaluating whether radionuclides are associated with colloids for transport. Further discussion is provided in Section 13.7.

Reimus et al. (2006c) report on laboratory experiments conducted to determine transport properties of tracers used in the ER-6-1 MWAT-TT within fractured core of the LCA, which included CML microspheres. Microsphere filtration and detachment rate constants are reported (see Section 13.6 for further discussion). The fracture transport experiments indicated that significant filtration of the microspheres can be expected in LCA fractures, possibly because of the relatively high ionic strength and high divalent cation concentrations in the LCA groundwater. Higher flow velocities and hydraulic conductivities in the LCA (compared to fractured volcanics at the NTS) may offset the greater tendency for colloid attachment to surfaces in the LCA and make the LCA just as susceptible to colloid-facilitated transport as the fractured volcanics. Further laboratory and field studies over a wide range of time scales, flow rates, and flow geometries are needed to fully address these questions.

Zavarin et al. (2006) summarize experiments that evaluated the role of colloids in radionuclide transport in fractured carbonate rocks. These studies indicate that ^{3}H and rhenium behave as conservative tracers, and Sm migration in carbonate fractures was only observed as a result of colloid-facilitated transport. Thus, in the absence of colloids, Sm transport is unlikely. Zavarin et al. (2006) state that based on their analogous reaction chemistry, it is likely that the transport of any of the trivalent rare earth radionuclides (as well as the Am[III] and Cm[III] actinides) will be attributable to colloid-facilitated transport. Although transport of Pu in carbonate fractures occurred in the absence of colloids, it is likely that this transport is attributable to Pu^{+5}. In the presence of mineral surfaces, Pu will tend to reduce to Pu^{+4} over time. Migration of Pu^{+4} as a free aqueous species in carbonate fractures is unlikely, although migration by colloid-facilitated transport may occur.

Zavarin et al. (2007) summarize results of laboratory experiments reported in Zavarin et al. (2005) and Ware et al. (2005) that examined radionuclide transport in tuff and carbonate fractures. In some of the LANL and LLNL experiments in volcanic tuff, it was apparent that ^{137}Cs, ^{239}Pu, and Sm did not migrate as free solutes, but rather as solutes sorbed to colloids, as a combination of free solutes and solutes sorbed to colloids, or as colloidal precipitates (Zavarin et al., 2007). This behavior was also evident for ^{14}C in a few of the tuff experiments, and for ^{239}Pu and Sm in the carbonate fracture

experiments. In LANL experiments, either silicate or calcite colloids (the latter would explain the colloidal behavior of ^{14}C) appear to have formed in the synthetic ER-2-1 water unintentionally, and to sorb ^{137}Cs and ^{239}Pu quite strongly. The ^{239}Pu concentrations used in LANL experiments were also high enough to have potentially created Pu colloids over time. The fact that ^{137}Cs and ^{239}Pu were two of the more strongly sorbing solutes in the LANL tuff batch sorption and desorption experiments (Ware et al., 2005) also suggests that the unretarded transport of these radionuclides is associated with colloid-facilitated transport.

Reimus (2007c) presents an evaluation of the CML microspheres used as a surrogate for colloids in the MWAT-TT conducted within the LCA at the ER-6-1 well site in southeastern Yucca Flat. Significant filtering of the CML microspheres in the LCA was observed during the ER-6-1 MWAT-TT, and filtration rate constants ranging from 0.002 to 0.004 hr^{-1} were calculated. Interpretations assuming reversible and irreversible filtration yielded equally good matches to the data. The results of this study are further discussed in Section 13.6.2.1.

13.4 Colloid Mineralogy

Kersting et al. (1998) report that groundwater samples from the ER-20-5 site contain Pu, Eu, Co, and Cs associated with colloids. Filtered colloids and particulates from the groundwater samples were analyzed by XRD and scanning electron microscopy, and were found to be composed of clays (illite and smectite), zeolites (mordenite and clinoptilolite/heulandite), and cristobalite (polymorphous silicon dioxide). These are common secondary minerals in altered rhyolitic tuff and are specifically identified in the local rocks.

Groundwater samples collected from pipes through the portals within U-12e, U-12t, and U-12n tunnels on Rainier Mesa contained colloids composed of calcite, clinoptilite, and illite, similar to the minerals identified in groundwater from ER-20-5 (Kersting et al., 2002). These samples represent groundwater from the unsaturated zone collected in the sealed tunnels. A sample was also collected from surface discharge on the wall of the U-12t tunnel.

Kersting and Reimus (2003, Chapter 2) report on the mineralogical analysis of colloid samples collected from ER-20-5 #1 and #3, and from U20n PS1 DDH (collected in and near the CHESHIRE

cavity) in Area 20 of the NTS, both completed in volcanic tuffs. Conclusions regarding colloid mineralogy were:

- The colloids in the NTS groundwater samples are mineralogically similar, although the actual abundance of each mineral may vary from aquifer to aquifer.
- The colloidal material is composed primarily of clays and zeolites. This suggests that the potentially important Pu-sorbing minerals are clays and zeolites for groundwater hosted in silicic volcanic units. This does not rule out the importance of minor colloidal minerals, those present at less than 10 percent (by mass).
- The same clays and zeolites identified in the groundwater samples are also present in the host rock aquifers at ER-20-5. The colloid minerals mimic the minor, host rock minerals from which they originated, and most likely represent the fracture lining minerals.

Refractory colloids generated at the time of nuclear test detonations or resulting from alteration of the resulting melt glass (probably mostly clays) cannot be ruled out as a potentially significant contributor to colloid-facilitated transport at the NTS. Kersting et al. (1998) specifically mentions smectite as an alteration product of melt glass from nuclear test cavities.

13.5 Colloid Concentrations and Size Distributions

Colloid concentrations and size distributions have been measured in groundwater samples from wells within the Yucca Flat/Climax Mine CAU, within other UGTA CAUs, and near Yucca Mountain. Samples from wells just to the south-southwest of the NTS (NC-EWDP wells) have also been analyzed for colloids; however, the results of those analyses are not included in this data compilation because the data have not yet been formally reported. These samples are primarily from alluvium. Because there are substantial colloid concentration and size distribution data available for the alluvium from NTS wells in Frenchman Flat, the lack of these data is not a critical problem. These data are compiled in the UGTA GEOCHEM06 database (SNJV, 2006a). Colloid data, included in the analysis, that were obtained following the release of GEOCHEM06 will be included in the next release of the database, GEOCHEM07. All data used for the analyses in this section are presented in Appendix J.

The colloid concentration and size data reported in this section have been measured at LANL using high-sensitivity liquid *in situ* particle spectrometry as described in Kung (2000). Initially, a Particle

Measuring Systems HSLIS-50 instrument, with a size-range measurement capability from 50 to 200 nanometers (nm) diameter and greater than 200 nm, was used to measure concentrations and size distributions of colloids. The system was later upgraded to include an HSLIS-100 spectrometer, with a size-range measurement capability from 100 to 1,000 nm and greater than 1,000 nm, to extend the analyzed size range up to 1,000 nm diameter. The reported colloid sizes are for an equivalent spherical particle diameter. This instrumentation provides a count of the total number of colloid particles for a standard sample volume within specified size-range bins, and the data for a bin were reported under the heading specifying the lower size of the bin range. For samples only analyzed on the HSLIS-50, only data for the 50- to 200-nm range and greater than 200 nm are available. For other samples also analyzed with the HSLIS-100, data for the 50- to 1,000-nm range and greater than 1,000 nm are available.

Colloids less than 50 nm diameter may also be significant but could not be characterized with the available instrumentation. There are a few incidental measurements of colloid mass for samples that differentiate mass between greater than 10 nm and some larger size, but colloids less than 50 nm have not been systematically characterized. The following analyses do not account for colloids less than 50 nm.

13.5.1 Colloid Concentration and Size Data

Colloid concentration and size distribution data are available from 131 unfiltered samples collected from 45 different wells/completion intervals. Although the GEOCHEM06 database (SNJV, 2006a) contains additional results for filtered samples, filtered samples are not considered representative of the natural colloids in groundwater and were not included in the analysis. Multiple analyses of groundwater samples from the same completion interval of the well reflecting various stages of well development, amounts of purging, or sampling pumping rates are reported. The most representative sample for concentration and size distribution for each well was selected as the sample having the lowest total colloid concentration (50- to 1,000-nm size range). This criterion was based on the general dependence of the colloid content of a sample upon cleanout and purging of the well before sampling. Colloid content decreases with development and purging as colloidal materials left from well construction and present from corrosion products of well materials are removed. It is also recognized that purging using higher pumping rates (resulting in high *in situ* groundwater flow

velocities) may mobilize colloids that are not mobile at natural groundwater flow velocities, but it is thought that extended purging may diminish this effect and the colloid content would become more representative. In one case, results for two duplicate samples were averaged.

Table 13-1 lists the wells for which there are colloid concentration and size data. The table lists the well name, the Master ID (National Water Information System [NWIS ID]), the sample ID for the selected representative sample, the CAU in which the well is located, the HSU(s) that the completion interval of the well accesses, the HGU group to which the sample was assigned for colloid concentration and size distribution analysis, and the total colloid concentration in the sample. Complete colloid concentration and size data for the all samples for wells listed in Table 13-1 are provided in Appendix J. Figure 13-1 shows the locations of these wells with different symbols for each CAU and with color codes for the HGU group to which the sample is assigned.

The samples represent a wide variety of HSUs from all UGTA CAUs as well as the Yucca Mountain area. The samples were assigned to seven functional HGU data groups (AA, VA, TCU, LCA3, UCCU, LCA, and GCU) for analysis. This was accomplished by determining the HSUs within the completion interval (assumed sampled formation) for each well, and then cross-referencing the HSUs to HGUs for grouping (see Tables 4-2 and 4-3 for the HSU/HGU crosswalk). The three volcanic aquifer HGUs (WTA, VTA, LFA) were combined into a single volcanic aquifer group (referred to as VA in Table 13-1). This was done because many completion intervals contained proportions of more than one of the volcanic aquifer HGUs, and there was no basis for specific HGU assignment. Also, there were insufficient data for analysis of each volcanic aquifer HGU separately. The LCA and LCA3 were separated due to substantial hydrologic differences between these two HSUs that may affect the colloid content as well as the hydrology of transport. Samples from nine wells within Yucca Flat were available, representing five of the seven HGU groups, although only two of the groups were represented by more than one sample.

13.5.2 Colloid Concentration Distribution

Table 13-1 presented the colloid concentration data (50- to 1,000-nm range) for all selected samples on a CAU and HGU-group basis. An empirical cumulative distribution function (ECDF) was calculated for the colloid concentration data and evaluated to fit a distribution. A lognormal distribution, shown in Figure 13-2, was optimal. The K-S statistic, measuring the goodness-of-fit

Table 13-1
Representative Colloid Samples and Concentrations
(Page 1 of 2)

SITE_ID	MASTER_ID	Sample_ID	CAU	Sampled HSU [a]	HGU Group	Colloids/mL (log_{10})
U-3cn PS #2	370338116011901	14377.71	YFCM	LTCU	TCU	9.78
U-4u PS #2A	370513116025101	14384.7	YFCM	LTCU	TCU	11.74
ER-12-2	371019116072101	14231.7	YFCM	UCCU	UCCU	6.58
ER-6-1 #2	365901115593501	14250.7	YFCM	LCA	LCA	7.05
ER-7-1	370424115594301	14251.7	YFCM	LCA	LCA	6.57
UE-7nS	370556116000900	14391.7	YFCM	LCA	LCA	7.42
Water Well 2 (USGS HTH #2) (3,422 ft)	370958116051512	14399.72	YFCM	LCA	LCA	8.40
Water Well 5A	364635115572901	7445.74	FF	AA	AA	8.04
Water Well 5C	364708115574401	7447.73	FF	AA	AA	6.11
Water Well 5B	364805115580801	7446.72	FF	AA	AA	6.97
UE-5n	364915115574101	14396.7	FF	AA	AA	6.91
RNM-2S	364922115580101	14395.7	FF	AA	AA	5.45
RNM-1	364928115580101	14394.7	FF	AA	AA	5.92
UE-5c Water Well	365011115584702	7443.74	FF	AA/LTCU	AA	8.20
UE-5 PW-3	365201115581601	7442.73	FF	TM-WTA	VA	5.93
Water Well 4A	365412116013901	7444.74	FF	TM-WTA	VA	5.20
ER-5-4 #2	364927115574801	14247.7	FF	LTCU	TCU	8.61
UE-2ce	370831116080701	14390.71	RMSM	LCA3	LCA3	8.06
ER-12-3	371142116125102	14236.71	RMSM	LCA3	LCA3	8.11
ER-12-4	371311116105902	14240.7	RMSM	LCA3	LCA3	7.59
U-12s Well	371342116125102	14402.7	RMSM	MGCU	GCU	8.13
ER-EC-7	365910116284401	7435.7	PMOV	FCCM	VA	6.66
ER-EC-5	370504116335201	7433.7	PMOV	TMCM	VA	6.30
ER-EC-8	370610116375301	7465.72	PMOV	FCCM/TMCM	VA	7.61
ER-18-2	370615116222401	7430.7	PMOV	TMCM	VA	7.68
UE-18r	370806116264001	6629.7	PMOV	TMCM	VA	8.44
ER-EC-2A (1,635-4,973 ft)	370852116340501	7466.7	PMOV	FCCM/TMCM	VA	6.57
ER-EC-4	370935116375301	7432.72	PMOV	TMA/FCCM/TCVA	VA	6.14

Table 13-1
Representative Colloid Samples and Concentrations
(Page 2 of 2)

SITE_ID	MASTER_ID	Sample_ID	CAU	Sampled HSU [a]	HGU Group	Colloids/mL (log_{10})
ER-EC-6 (1,581-5,000 ft)	371120116294801	7468.7	PMOV	BA/UPCU/TCA/LPCU/TSA/CHCU/CFCM	VA	7.53
ER-EC-1	371223116314701	7469.7	PMOV	BA/UPCU/TCA/LPCU/TSA/CHCU/CFCM	VA	7.61
ER-20-5 #3	371311116283801	14246.71	PMOV	CHZCM	VA	11.08
ER-20-5 #1	371312116283801	5164.7	PMOV	TSA/CHZCM	VA	10.10
U-20n PS#1 DD-H (3,025 ft)	371425116252401	5187.7	PMOV	CHZCM	VA	8.41
UE-20bh #1	371442116243301	6627.7	PMOV	CHZCM	VA	8.72
U-19ad PS 1A	371613116211701	14361.7	PMOV	PLFA	VA	10.57
UE-19h	372034116222501	7470.7	PMOV	BRA	VA	8.49
U-19v PS #1D	371453116205700	14366.71, 14366.72 [b]	PMOV	BFCU	TCU	8.72
U-19q PS#1d	371649116215401	5246.7	PMOV	BFCU	TCU	10.43
UE-25 WT #3	364757116245801	7453.7	YMP	TM-LVTA/TM-WTA/UTCU/TSA/LVTA	VA	6.87
UE-25 WT #17	364822116262601	7455.7	YMP	TM-LVTA/TM-WTA/UTCU/TSA/LVTA	VA	9.16
J-13 Water Well	364828116234001	7459.7	YMP	TSA	VA	6.01
UE-25c #2	364947116254401	7471.71	YMP	CHVTA/YMCFCM	VA	6.66
UE-29a #1 HTH	365629116222601	4922.7	YMP	PCM	VA	6.86
UE-29a #2 HTH	365629116222602	4925.7	YMP	YMCFCM	VA	7.56
USW SD-6 ST1	365040116275901	7461.7	YMP	Unknown	VA	8.02

[a] HSU for respective geologic model; see geologic model documentation for key
[b] Duplicate samples

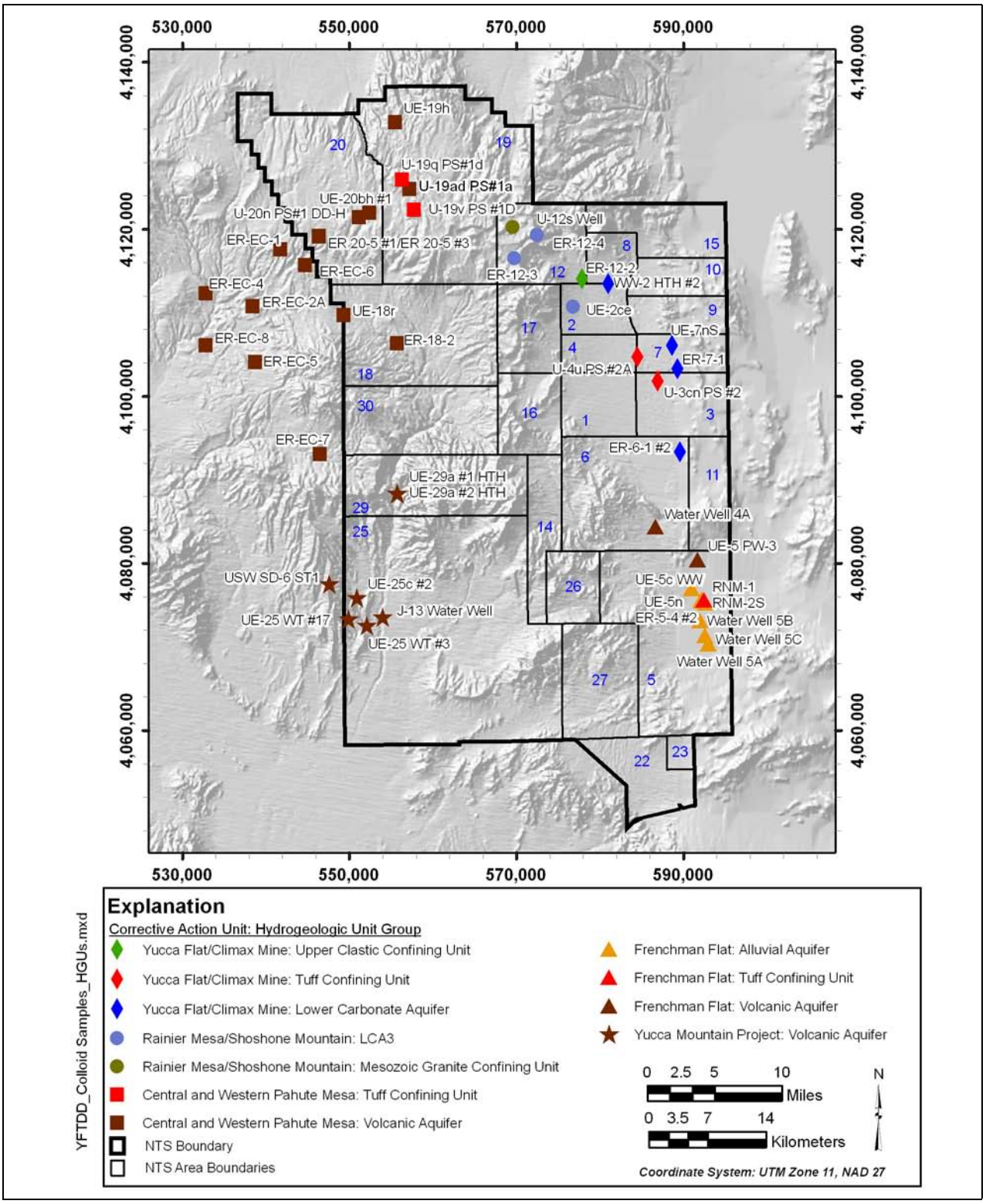

Figure 13-1
Location Map for Colloid Samples

across the entire scale of observations, indicates that the ECDF conforms to a lognormal distribution at the 95 percent confidence level. The data points in this figure are coded to indicate the HSU and the CAU for each. Table 13-2 presents a summary of the colloid concentration data (50- to 1,000-nm range) available for Yucca Flat and the NTS area on an HGU-group basis. Table 13-3 provides information on the lognormal CDF distribution fitted to the ECDF of the colloid concentrations.

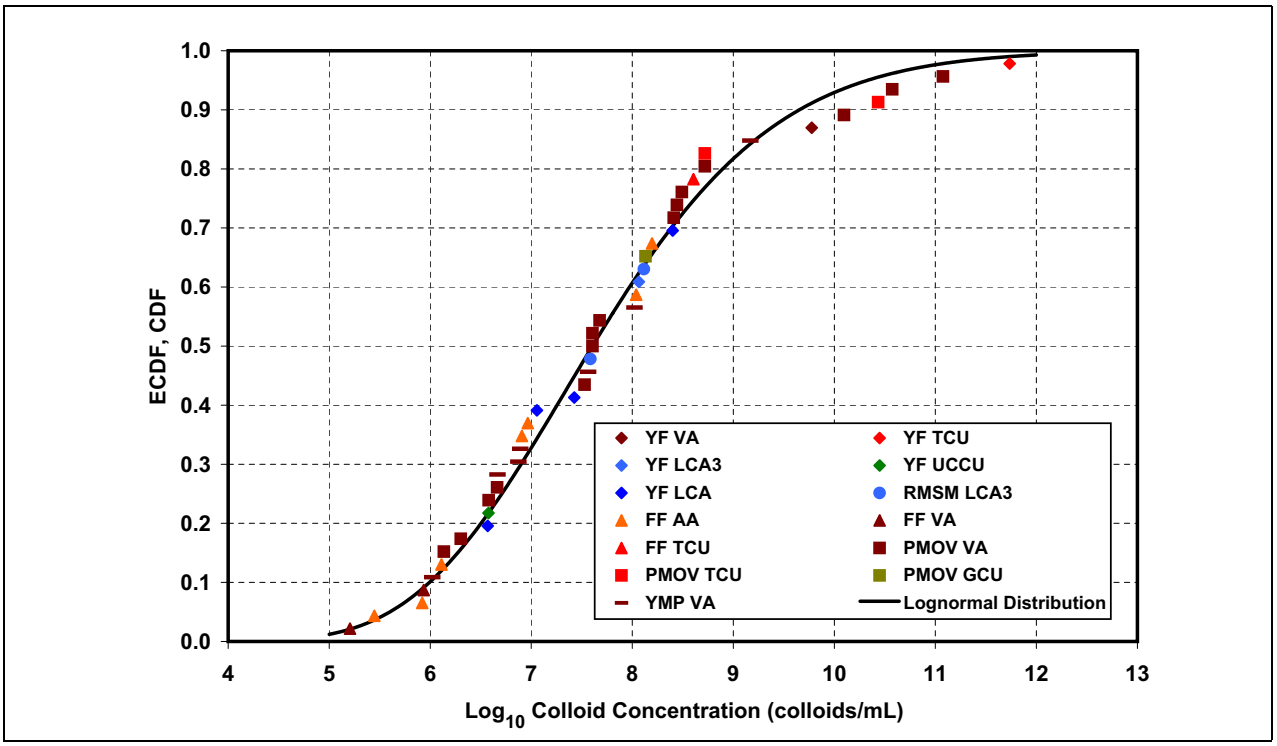

Figure 13-2
Cumulative Distribution Function of Log_{10} Colloid Concentrations for All NTS Data

As shown in Tables 13-1 and 13-2, there is great variability in colloid concentrations for the groundwaters of the NTS. For example, concentrations in the volcanic aquifers range almost six orders of magnitude (from $10^{5.20}$ to $10^{11.08}$ colloids per milliliter). Concentrations for HGU groups appear to vary between CAUs where there are data for an HGU group from more than one CAU. This variability was also reported and discussed in Abdel-Fattah et al. (2005) and Reimus et al. (2006a). Groundwaters were sampled by LANL in FY 2004 from a single well completed in the alluvial aquifer (RNM-1), two wells completed in a volcanic aquifer (U-20n PS#1 DD-H and U4u PS #2A), and one in a tuff confining unit (U-19ad PS 1A). Additional sampling took place in FY 2005 representing groundwaters associated with volcanic tuffs (ER-20-5 #3 and U-3cn PS#2) and the LCA3 (UE-2ce). Colloid concentrations in the well waters sampled in FY 2005 spanned a range

Table 13-2
Summary of Colloid Concentrations (Log_{10}) for HGU Groups

HGU Group	Yucca Flat/Climax Mine Colloid Samples				NTS Area Samples			
	Number of Observations	Min	Max	Mean [a]	Number of Observations	Min	Max	Mean [a]
		Log_{10} colloids/mL				Log_{10} colloids/mL		
AA	NA	N/A	N/A	N/A	7	5.45	8.20	6.80
VA	NA	N/A	N/A	N/A	24	5.20	11.08	7.67
TCU	2	9.78	11.74	10.76	5	8.61	11.74	9.85
LCA3	1	N/A	N/A	8.06	3	7.59	8.11	7.92
UCCU	1	N/A	N/A	6.58	1	N/A	N/A	6.58
LCA	4	6.57	8.40	7.36	4	6.57	8.40	7.36
GCU	NA	N/A	N/A	N/A	1	N/A	N/A	8.13
All HGUs	8	6.57	11.74	8.20	45	5.21	11.74	7.76

[a] Mean of the Log_{10} concentration (geometric mean)

N/A - Not applicable
NA - Not available

Table 13-3
Lognormal CDF Shape Parameters for Colloid Concentration

Parameter	Value (Log_{10} #colloids/mL)
Mean	7.73
SD	1.45
Lower 95% CI	5.3
Upper 95% CI	11.0

of about three orders of magnitude, and the range in colloid concentrations for the FY 2004 wells was even larger, spanning approximately five orders of magnitude. Abdel-Fattah et al. (2005) stated that the lower concentrations for the FY 2004 samples were measured in wells that had been more extensively pumped, more frequently sampled, or both (RNM-1 and U-20n PS#1 DD-H), and higher concentrations were measured in wells that had been pumped or developed to a lesser extent (U4u PS #2A and U-19ad PS 1A). Reimus et al. (2006a) reported that although well conditions and pumping history undoubtedly have a significant influence on colloid concentrations in the wells,

lower colloid concentrations tended to be observed in groundwater that had higher concentrations of dissolved multivalent cations.

13.5.3 Colloid Concentration Relationship to Water Chemistry

The chemistry of the water plays a major role in determining the stability of colloids (Kersting and Reimus, 2003, Chapter 1). The stability of colloids in a given aquifer setting is a function of pH, redox potential, water chemistry, and status of the hydrogeochemical system. Most field and laboratory experimental studies have demonstrated that lowering the ionic strength of groundwater results in the generation and stability of existing colloids, whereas increasing the ionic strength tends to decrease colloid concentration by promoting coagulation. In addition, the presence of organic material has a strong stabilizing effect on the inorganic colloids.

Alkaline element (Na^+, K^+) concentrations below 10^{-2} M and alkaline earth element (Mg^{2+}, Ca^{2+}) concentrations below 10^{-4} M increase colloid stability. Work on the YMP by Reimus and Kung, summarized in Kersting and Reimus (2003, Chapter 1), demonstrates such dependence of colloid concentration on cation concentration in groundwater. Colloid concentrations in wells completed in saturated alluvium south and southwest of Yucca Mountain are shown to vary as a function of divalent cation concentrations in the groundwater. There is significant variability in the divalent cation concentrations, and colloid concentrations from these wells were best correlated with divalent cation concentrations represented as Log([Ca^{2+}] + [Mg^{2+}]). A similar relationship of decreased colloid concentrations with higher concentrations of divalent cations was observed by Reimus et al. (2006a) for samples collected and analyzed from the AA, LCA3, TCU, and VA HGU groups, as described earlier. This result is consistent with colloid stability theory and the Shulze-Hardy rule (Hiemenz, 1986).

This relationship may be applicable to groundwater in the Yucca Flat HSUs to the extent that the colloid concentrations may be estimated based on concentrations observed for groundwater within the same HSU or an HSU with similar mineralogy and with similar total concentrations of the divalent cations, [Ca^{2+}] + [Mg^{2+}]. Additional studies are needed to determine whether a relationship similar to that reported for the alluvium near Yucca Mountain (i.e., Log {[Ca^{2+}] + [Mg^{2+}]} versus colloid concentrations) is observed for the Yucca Flat HSUs.

13.5.4 Colloid Size Distributions

The distribution of colloid sizes in groundwaters of the Yucca Flat/Climax Mine CAU is important because it impacts the mobility of colloids. Reimus et al. (2006a) report that most of the colloid surface area and mass is associated with smaller colloids (less than 200 nm diameter) that are probably more likely to transport over significant distances than larger colloids.

Normalized colloid size distributions were determined for the 45 samples taken from wells both in Yucca Flat and wells completed in units comparable to Yucca Flat HSUs. The size distributions were normalized by dividing the number of colloids in each size "bin" by the total number of colloids in all bins, allowing the shapes of the distributions to be compared. The proportion of colloids in each size bin is determined by "C," the number of colloids per milliliter measured within the "bin," divided by "C_T" the total number of colloids (per milliliter) for all size bins. The data have been placed on the graph according to the upper size for the bin range, which conforms to subsequent graphs of cumulative density. For the entire sample set, 99.9 percent of the colloids (by number) were less than 200 nm in diameter; however, only 97 percent of the normalized size distribution is below 200 nm.

Figure 13-3 shows the individual distributions for all 45 selected samples over the measured size range of 50 to 1,000 nm. There are, in fact, only 35 datasets for the entire range. For 10 datasets, the measured range is only 50 to 200 nm, and greater than 200 nm. Most of the size distributions are qualitatively similar in shape. As indicated by the two colored reference lines (the average normalized size distribution and the normalized average size distribution, which is weighted by the concentration distribution), samples with higher concentrations of colloids tend to have concentration distributions with greater proportion of smaller sizes. Figure 13-4 shows the size distributions for the 50- to 200-nm size range in greater detail. Because colloids were defined as particles up to 1,000 nm, the distributions were defined as 100 percent at 1,000 nm, and measured particles greater than 1,000 nm, which were 0.01 percent of the total, were excluded. For datasets of up to 200 nm and greater than 200 nm, the data greater than 200 nm were considered to be less than 1,000 nm.

For parameterization of the size distributions, all of the normalized colloid size distributions for an HGU group were averaged and an ECDF was calculated. CDFs were fitted using BestFit 4.5 distribution-fitting software (Palisade Corporation, 2002). Exponential or lognormal CDFs provided the best fits for all of the HGU groups, as identified in Table 13-4. Lognormal distributions provided fits almost as good as the exponential function in the cases where an exponential function provided

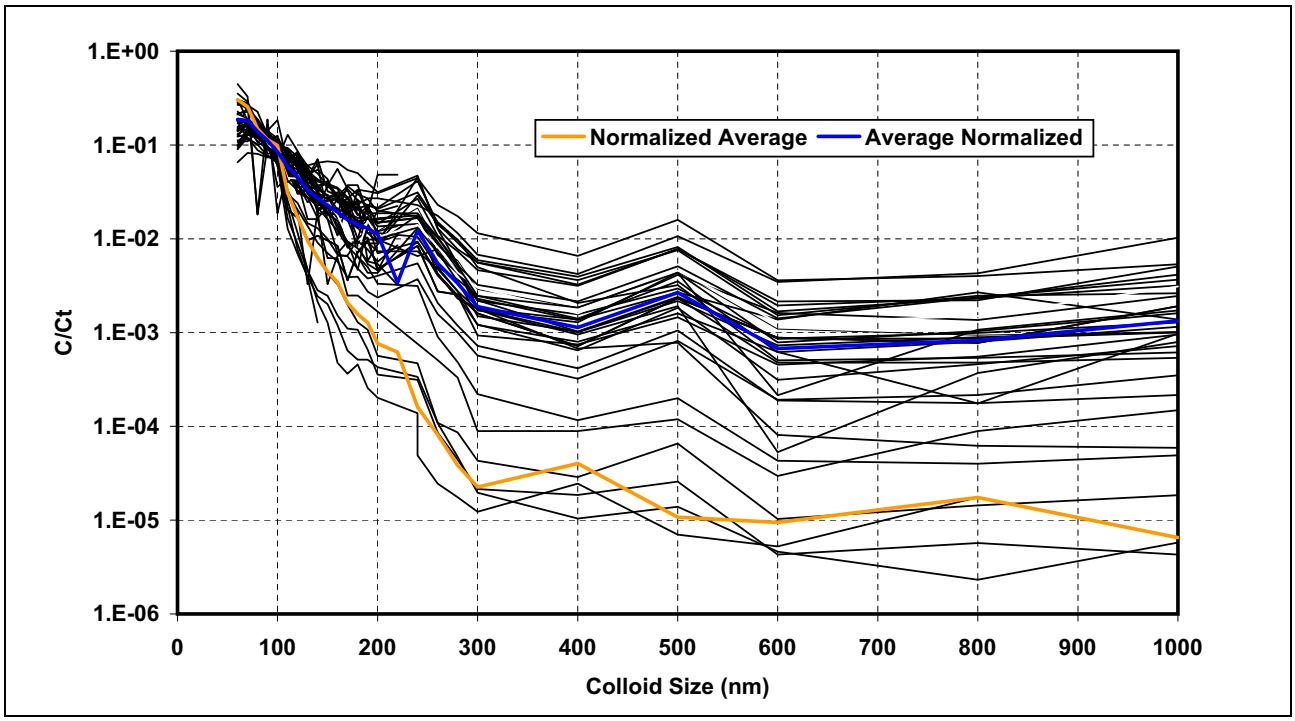

Figure 13-3
Normalized Size Distributions of Colloids for Samples Selected for Each Well

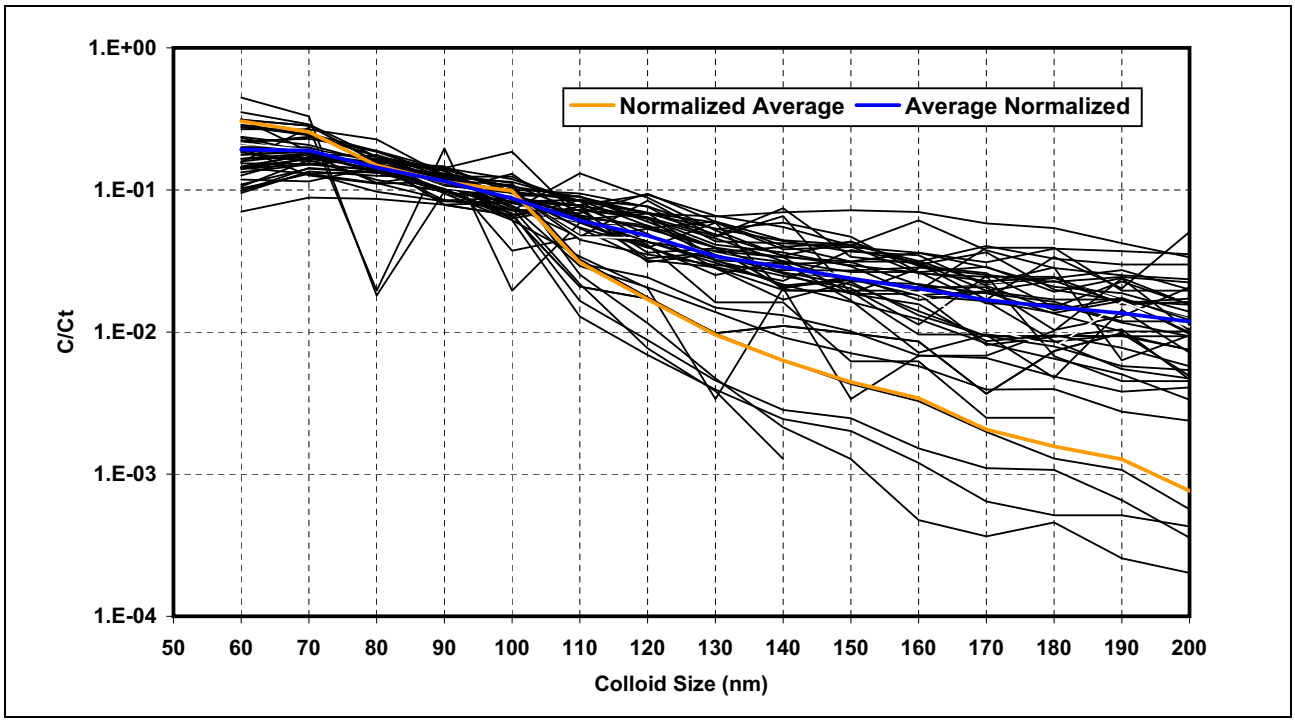

Figure 13-4
Normalized Size Distributions of Colloids in the 50- to 200-nm Range

the best fit. For consistency, the fitted lognormal CDFs are shown in Figure 13-5. The fitted distributions have a nominal shift of 50 nm to account for the lack of data less than 50 nm, and do not provide any information on the amount of colloids smaller than the lowest measured size of 50 nm. Colloids less than 50 nm represent an uncertainty for determining the total colloid sorption capacity. Note that sorption capacity is related to the colloid surface area, which varies as the square of the colloid particle radius (characterized as spherical), and that the proportion of smaller sizes would represent less uncertainty than the proportion by size.

Table 13-4
Shape Parameters for Colloid Size Lognormal Distributions

HGU Groups	AveNorm [a]	AA	VA	TCU	LCA	LCA3	UCCU	GCU
Mean (nm)	98	100	97	79	120	89	85	110
SD (nm)	65	68	61	31	87	42	55	92
+shift (nm) [b]	50	50	50	50	50	50	50	50
2.5% CI (nm)	54	54	54	53	57	55	52	54
97.5% CI (nm)	260	269	251	160	341	197	218	333

[a] Average normalized size distribution for all HGU groups.
[b] A more general 3-parameter form of the lognormal distribution includes an additional location parameter, +shift, which specifies a minimum value other than 0.

Also shown on Figure 13-5 are the average normalized size distribution and the normalized average size distributions. The average normalized distribution includes all samples for all HGU groups, averaged after normalization. The normalized average distribution is a normalized distribution of the average concentration for each size bin. The latter reflects weighting by the concentration of colloids, and is consistent with the earlier statement that the samples with higher concentrations had proportionally more colloids of smaller sizes.

Table 13-4 contains the lognormal fit statistics describing the CDF distributions for each HGU group.

13.5.5 Data Limitations

The first limitation is the quality of the samples used to determine colloid concentrations and size distributions. As previously mentioned, samples obtained from pumped wells for colloid analysis are potentially impacted by the necessary stressing of the aquifer to obtain the samples. Colloids in the

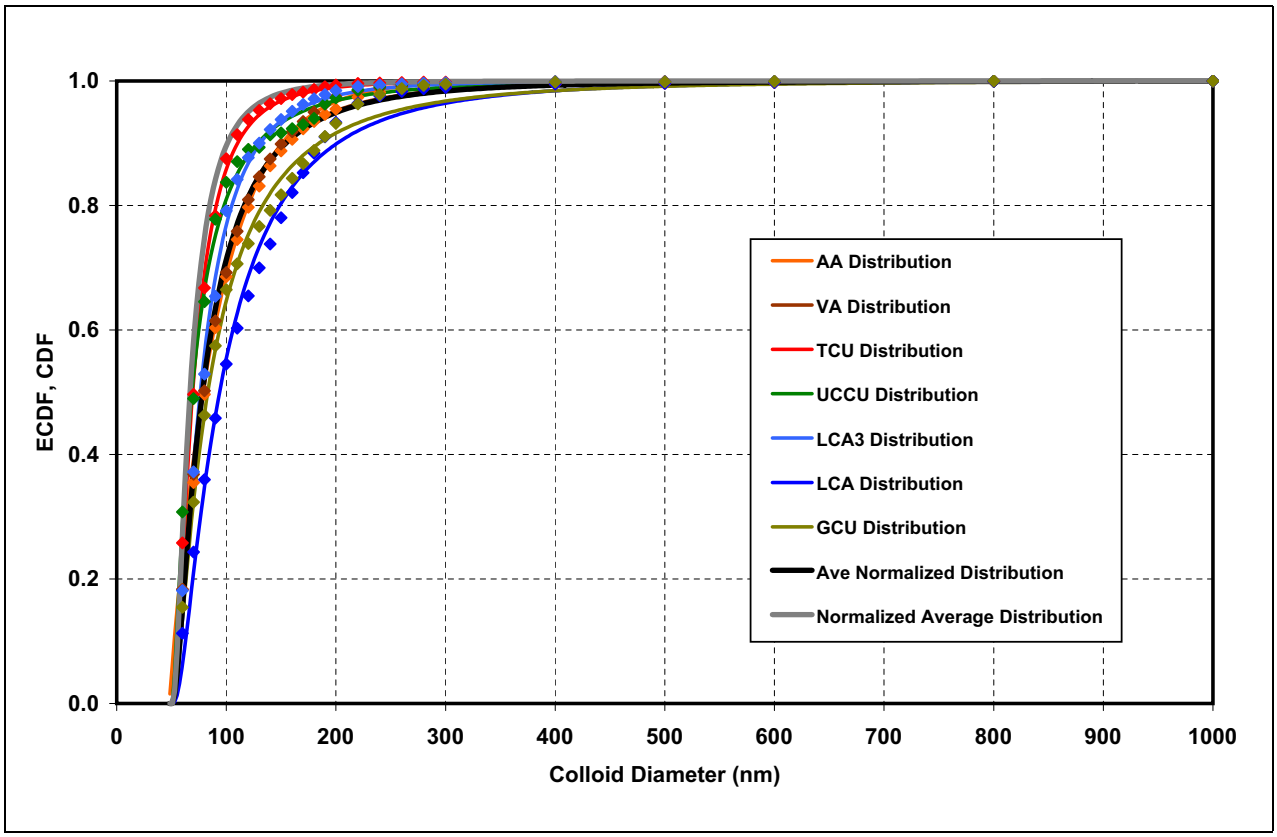

Figure 13-5
Cumulative Distribution Function of Colloid Diameter
for All NTS Data and HGU Groups

formation that are mobilized under pumping conditions may not necessarily be mobile under nonpumping, natural flow conditions. Also, the samples may contain residual foreign materials that were introduced during drilling (e.g., drilling muds, polymer additives) or result from corrosion of well construction materials (e.g., metallic casing, concrete) mobilized by the increased groundwater velocity around the well resulting from pumping.

It is considered best practice to purge a borehole before sampling for colloids. Unfortunately, well purging was not done in a consistent manner for the samples used for this analysis. Some of the samples came from wells that had produced large volumes of water at high flow rates for years before they were sampled (e.g., J-13 Water Well); others were pumped at medium to high rates for short periods of time; and some could only be pumped minimally or bailed before sampling. When sampling for colloids, it is best to pump the well at low flow rates to minimize the perturbations to the ambient flow system. High flow rates during sampling may lead to concentrations that are higher in

the samples than in the formation under ambient conditions. Pumped samples from the ER wells were collected at pumping rates that are considered high for representative colloid sampling. Consequently, colloid concentrations reported for the ER well samples may be greater than ambient concentrations in the groundwater. The impact of these sampling inconsistencies on the colloid data cannot be quantified and has not been incorporated in the data analysis.

Another significant data limitation is the lack of information on colloids less than 50 nm. There is only some miscellaneous measurements for colloid mass less than 50 nm, and no counting measurements of colloid concentrations (by number). It is not known how significant colloids in this size range may be. It has been observed that Pu forms colloids in this size range, as mentioned in Sections 13.3 and 13.7.

Further, it has been observed that there is significant variation in the colloid concentrations between CAUs, but there are insufficient data for most HGU groups within any one CAU to characterize the variability. Because it appears that samples with overall higher concentrations have proportionally more colloids of lower sizes, mixing data from different CAUs may result in size distributions for HGU groups that are not accurate for any particular CAU.

13.5.6 Representativeness and Scaling Considerations

With respect to colloid concentrations and size distributions, scaling considerations (measurement of values at a scale different from the application of the value) equate to the representativeness of the samples relative to the colloids moving through the CAU-scale system. As previously discussed, collection of representative samples from wells for colloid analysis has inherent problems due to effects of pumping on the colloid content of the sample and possible contributions of colloid-like material from the well. There has not been definitive investigation of such effects for NTS samples. Colloid concentrations and size distributions appropriate to CAU-scale transport modeling would not be expected to vary appreciably from those measured in representative groundwater samples that characterize the variability in the groundwater well, but the data for individual HGUs are limited. The data reported here are believed to be generally representative. Scaling of colloid transport parameters from measurement scales ranging from laboratory to approximately 100 m transport experiments to the CAU scale is probably much more uncertain.

13.6 Colloid Transport Parameters

Colloid-facilitated transport is subject to retardation resulting from reversible attachment and detachment of colloids from immobile surfaces by physical and/or chemical processes and irreversible removal as a result of size exclusion in pore throats, physical attachment to rough surfaces, and coagulation and settling. These processes are referred to in aggregate as filtration. Filtration rate constants (attachment and detachment rate constants) have been determined from analyses of tracer transport experiments conducted at both the laboratory and field scales using inorganic colloids and surrogates for colloids. These rate constants determine the retardation factor. Retardation factors represent the effect of reversible chemical and physical filtration of colloids. Within transport models, large retardation factors effectively result in irreversible or permanent filtration over the times scales of interest. The basis for determining transport parameter values is discussed in Section 13.6.1.

Bechtel SAIC (2004b) describes the determination of the colloid transport parameter values upon which the following data are based. In application to YMP performance assessment models, several shortcomings have been identified with the present YMP approach to determining the parameter distributions used for transport modeling, and revisions are being developed (see Section 13.6.3.3 for discussion concerning limitations of the data analysis). This does not affect the raw data, but rather affects the use of the data in transport modeling.

This section describes the data for attachment and detachment rate constants for colloids and the associated retardation factors. The data are presented and analyzed within three categories: alluvium, fractured volcanic rocks, and fractured carbonate rocks. The alluvium data are entirely from YMP (YMP-specific data and the outside field experiment data they have included), while the fractured volcanic rocks data include results from both YMP and UGTA experiments. The data for fractured carbonate rocks are entirely from the UGTA ER-6-1 MWAT-TT and associated laboratory experiments. A limited number of both field and laboratory tracer experiments have been conducted, producing a limited amount of data.

13.6.1 Basis for Transport Parameter Values

Colloid filtration (attachment and detachment) rate constants have been derived from colloid responses in tracer tests using the advection-dispersion equation with appropriate terms for a single

reversible first-order reaction to account for mass transfer between mobile water and immobile surfaces (attachment and detachment) to fit the data. Note that the attachment parameter is herein referred to as the filtration rate constant (k_{fil}) and the detachment parameter referred to as the detachment rate constant (k_{det}) to maintain consistency with the source YMP document (Bechtel SAIC, 2004b). In one-dimensional form, the transport equation for colloids may be written as:

$$\frac{\partial C}{\partial t} + V\frac{\partial C}{\partial x} - D\frac{\partial^2 C}{\partial x^2} + k_{fil}C - k_{det}S = 0 \qquad (13\text{-}1)$$

$$\frac{1}{b}\frac{\partial S}{\partial t} - k_{fil}C + k_{det}S = 0 \qquad (13\text{-}2)$$

Where:

C = Colloid concentration in solution, number of colloids/L^3
S = Colloid concentration on rock or fracture surfaces, number of colloids/L^2
V = Flow velocity in pores or fractures, L/T
D = Dispersion coefficient, L^2/T
k_{fil} = Filtration rate constant (1/T) = λV, where λ = filtration coefficient (1/L)
k_{det} = Detachment rate constant, 1/L-T
x, t = Independent variables for distance and time, respectively.
b = Water volume to rock surface area ratio (L) in the flow domain. For a parallel plate fracture model, b is equivalent to the fracture half-aperture

Values for V and D in Equation (13-1) and Equation (13-2) are obtained from interpretations of nonsorbing solute tracer responses included in the tests. Therefore, the filtration and detachment rate constants are the only parameters used to match the colloid responses. The filtration rate constant (k_{fil}) reflects the fraction of colloids that were not filtered during the tests (i.e., the filtration rate constant is constrained by the peak normalized concentration of the breakthrough curve representing colloids that arrive without any apparent retardation). The detachment rate constant (k_{det}) is constrained primarily by the tail of the response. Note that bk_{det} is the actual fitted value during analyses of colloid tracer tests, and k_{det} values implicitly include b.

The colloid retardation factor, R_{col}, is calculated from colloid filtration and detachment rate constants using the following expression:

$$R_{col} = 1 + \frac{k_{fil}}{bk_{det}} \qquad (13\text{-}3)$$

Symbols for Equation (13-3) are the same as those described in Equation (13-2).

In application, the tail of the response is fit with a retardation factor, and the detachment rate constant is calculated using Equation (13-2). This approach does not explicitly account for any permanent filtration. However, the associated retardation factors effectively embody permanent filtration over the time scales of the experiments. There is no practical approach to determining permanent filtration independently. Details of the interpretation procedure are provided in Bechtel SAIC (2004b).

13.6.2 Data Evaluation

Colloid filtration parameter values and retardation factors for NTS formations have been determined from a number of laboratory and field experiments conducted for YMP and the UGTA Project. To bolster the dataset, data from an outside field experiment in alluvium judged applicable have also been included. The data presented here are the same as the YMP data (Bechtel SAIC, 2004b) with the addition of more recently available data. However, the data are presented here without the manipulations incorporated in the YMP analysis for determining input distributions to the YMP performance assessment models, such as weighting of certain data and truncation of distributions.

Laboratory column experiments with alluvium and fractured volcanic and carbonates cores have been conducted using silica, montmorillonite, and clinoptilolite colloids in addition to CML microspheres. All field measurements used CML microspheres ranging in sizes from approximately 200 to 640 nm diameter as colloid analog. The use of CML microspheres as a surrogate for inorganic colloids is discussed in detail in Bechtel SAIC (2004b). Results of comparisons of transport in laboratory studies indicate that CML microspheres behaved as conservative surrogates for natural colloids in fractured volcanic rock, but that CML microspheres transported with somewhat greater attenuation than natural colloids in alluvium.

13.6.2.1 Colloid Filtration Rate Constants

Alluvium. Colloid filtration and detachment rate constants and retardation factors for NTS-area alluvium have been estimated in a number of laboratory experiments for the YMP. Only one field test of colloid transport in alluvium in the NTS area has been conducted, yielding field-scale filtration rate and detachment rates. This test was conducted at NC-EWDP Site 22 (see Figure 9-1 for location), and the test analysis is reported in Reimus (2007b). The analysis of this tracer test indicated two flow

pathways; colloid filtration and detachment rate constants were estimated for both pathways (Table 13-5).

Table 13-5
Results of the Field-Scale Alluvial Tracer Test

Parameter	Pathway 1	Pathway 2
Mass fraction, *f*	0.05	0.58-0.68
k_{fil} (hr^{-1})	0.16	0.048
k_{det} (1/cm-hr)	0.0011	0.00034

Source: Reimus, 2007b

Data taken from Schijven et al. (1999) for a field experiment investigating virus removal conducted in a dune area in Castricum, Netherlands, were also used to estimate colloid filtration and detachment rates at the field scale (Bechtel SAIC, 2004b). Filtration (referred to as attachment in Schijven et al., 1999) and detachment rates for bacteriophages were measured in alluvial material under natural gradient conditions. Two bacteriophages, denoted as MS-2 and PRD-1, were used in the field-scale test. These bacteriophages were chosen because they attach less than most pathogenic viruses and are relatively persistent during transport through the subsurface (Schijven et al., 1999). The size of these bacteriophages, 26 and 62 nm respectively, is near the lower end of the size range characterized for colloids.

The groundwater at the site studied by Schijven et al. (1999) had somewhat higher divalent cation concentrations than the alluvium in Yucca Flat (90 to 100 mg/L Ca^{2+} and 10 to 15 mg/L Mg^{2+} compared to 20.2 to 41.1 mg/L Ca^{2+} and 6.6 to 32.4 mg/L Mg^{2+} in Yucca Flat). Based on these data, colloids would be expected to be less stable at their site (see Section 13.5.3 for further discussion). The alluvium material at their study site was a bit coarser, with more sand, less clay, and more organic carbon than the alluvium of Yucca Flat, all of which would tend to result in enhanced transport relative to Yucca Flat conditions. Thus, the combination of colloid surrogate, groundwater chemistry, and alluvium characteristics at the site studied by Schijven et al. (1999) is judged sufficiently similar to natural colloids moving through Yucca Flat alluvium that there are no obvious reasons why their reported filtration and detachment rate constants would not be conservative (i.e., not reflecting greater retardation) when applied to Yucca Flat alluvium, recognizing there are uncertainties associated with

using these data. The two filtration rate constants determined for the NC-EWDP Site 22 field test are near the endpoints of the range of values determined from Schijven data (see Figure 13-6), suggesting that the datasets are consistent.

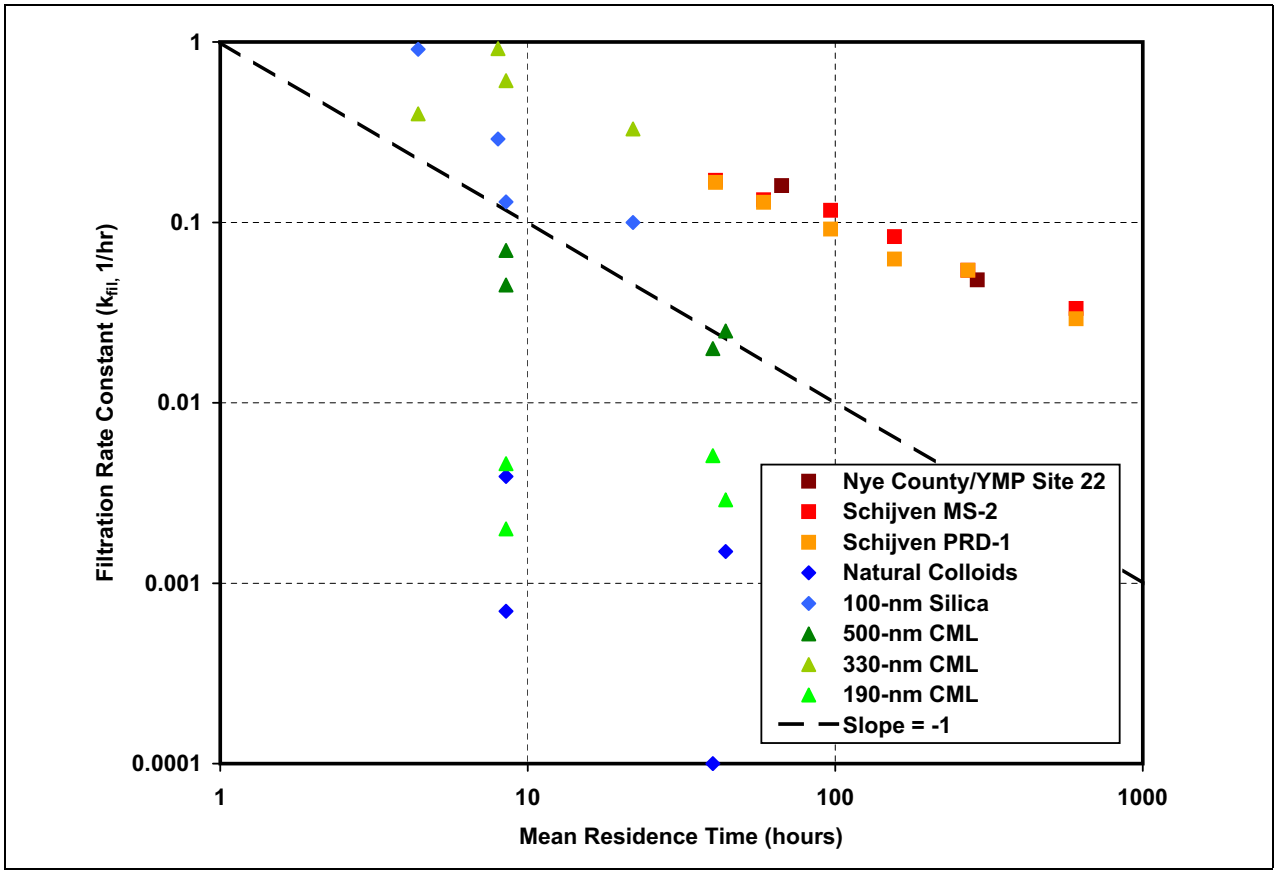

Figure 13-6
Colloid Filtration Rate Constants as a Function of Mean Residence Time in Alluvium

Filtration rate constants in the alluvium dataset are plotted in Figure 13-6 as a function of the mean residence time for the corresponding test. Natural colloids had the smallest filtration rate constants of any of the colloids in this figure. These natural colloids were approximately 96 percent by weight smectite clay. For all data, there is an apparent trend of decreasing filtration rate constant with residence time even though different sizes and types of colloids were used in the different tests. In particular, the field data (both from Schijven and NC-EWDP Site 22) support the time dependence trend. A reference line (not a distribution fit) with a slope of -1 is provided.

As previously stated, filtration rate constants reflect the fraction of colloids that were not filtered during the tests. The trend shown in Figure 13-6 suggests that some fraction of colloids may always transport through a fracture flow system regardless of the time or length scale of the observations. While this graph can be interpreted to indicate that filtration rate constants will continually decrease with increasing time scales, it also suggests that while the majority of colloids would be filtered quickly, a small fraction would be resistant to filtration and capable of traveling large distances over long time periods. This small fraction of unretarded colloids is referred to as the "fast fraction" in YMP documents (Bechtel SAIC, 2004b). This statement implies that there may be a distribution of colloid filtration rate constants rather than a fixed rate constant that applies to all colloids. The appearance of a small fraction of colloids at about the same time as nonsorbing solutes in tracer tests, regardless of the overall time scale of the test, forces filtration rate constants to decrease with time when a single-rate constant is assumed to apply to all colloids.

Figure 13-7 shows the ECDF of colloid filtration rate constants for alluvium determined from both laboratory and field-scale transport experiments. The ECDF is plotted with a logarithmic scale for the filtration rate constants to show the range of values clearly. Values from field-scale experiments are indicated, and in particular, the values for the NTS-area field experiment previously mentioned. Values from field-scale experiments only range across about one order of magnitude versus the four orders of magnitude range for all values.

Fractured Volcanic Rocks. Data were obtained from several field and laboratory tracer tests conducted in saturated, fractured volcanic rocks. These tracer tests include:

- The BULLION FGE (Reimus and Haga, 1999), referred to as "ER-20-6" in Figure 13-8
- Tracer tests in the Bullfrog Tuff (members of the Crater Flat Group) at the C-holes Complex near Yucca Mountain (Reimus et al., 1999), referred to as "C-Wells Bullfrog" in Figure 13-8
- Tracer tests in the Prow Pass Tuff (members of the Crater Flat Group) at the C-holes Complex near Yucca Mountain (Reimus et al., 1999), referred to as "C-Wells, Prow Pass" in Figure 13-8
- Laboratory experiments conducted at LANL using fractured cores from Pahute Mesa on the NTS (Kersting and Reimus, 2003, Chapter 5)

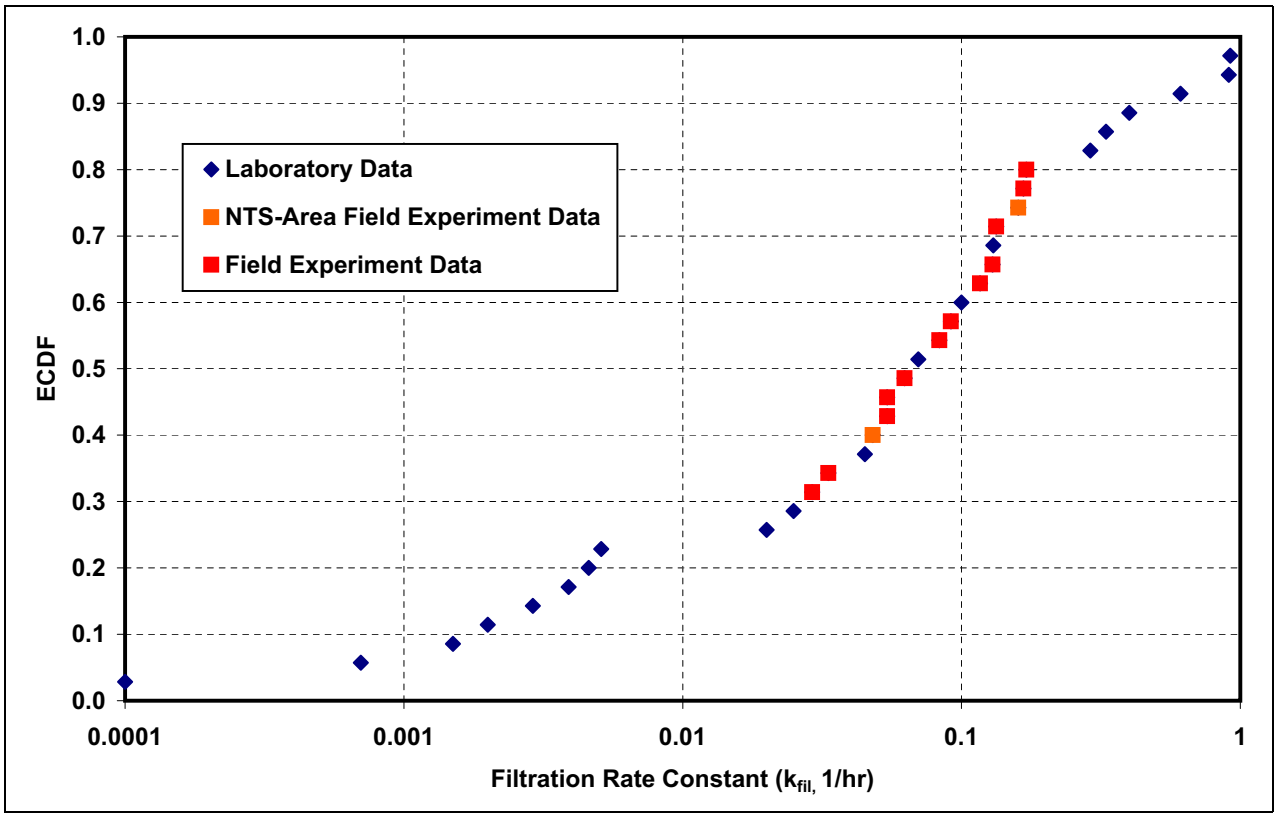

Figure 13-7
Cumulative Probability Distribution of Colloid Filtration Rate Constants for Alluvium

It is important to recognize that different CML microspheres were used in different field tests, and also that groundwater chemistry varied slightly from site to site and test to test.

Figure 13-8 shows a plot of filtration rate constants obtained from interpretations of the field and laboratory tracer tests conducted in saturated fractured volcanic rocks as a function of the time to reach peak nonsorbing tracer concentrations in the tests. This plot shows an apparent trend of decreasing filtration rate constant with residence time even though different sizes and types of colloids were used in the different tests. A reference line with a slope of -1 (not a fit) is provided, the same as for the alluvium data. Similar to the discussion for alluvium filtration, the trend shown in Figure 13-8 suggests that some small fraction of colloids transporting through a fracture flow system would be resistant to filtration and capable of traveling large distances over long time periods. This statement implies that there may be a distribution of colloid filtration rate constants rather than a fixed rate constant that applies to all colloids.

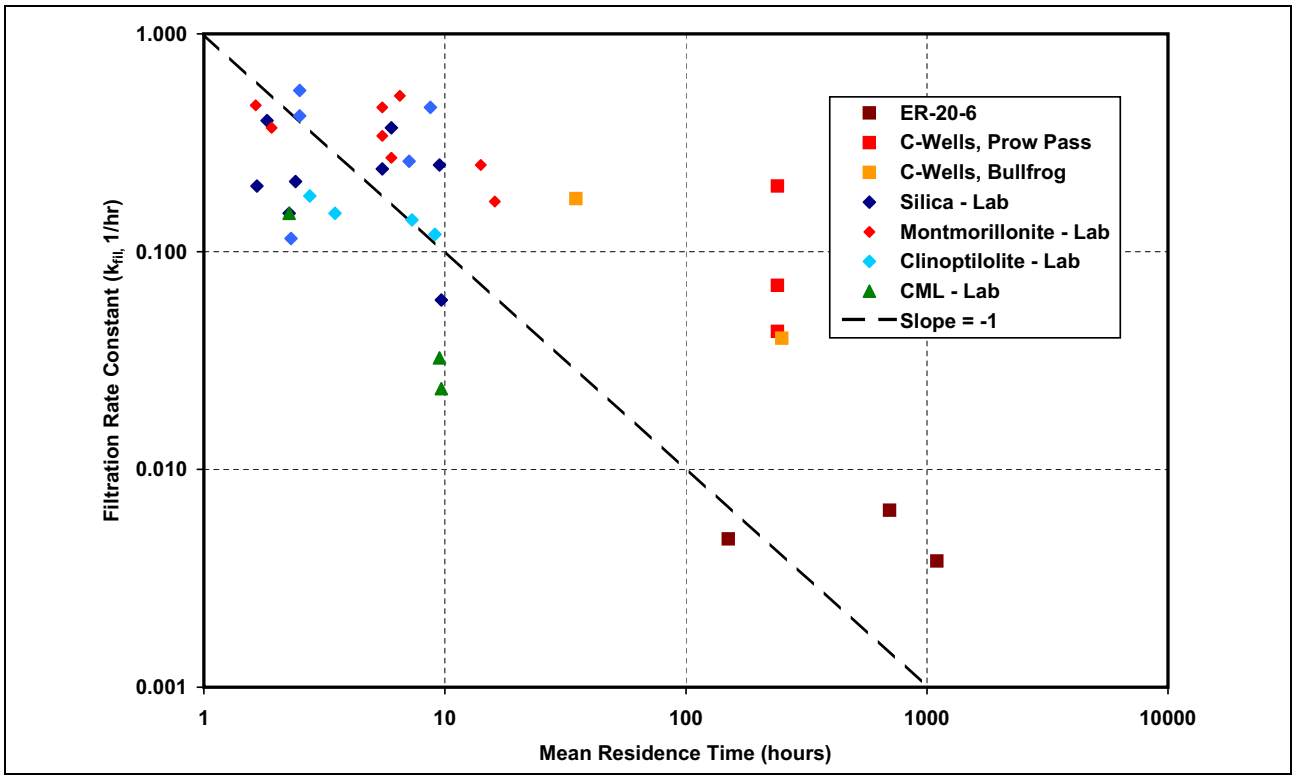

Figure 13-8
CML Microsphere and Colloid Filtration Rate Constants as a Function of Mean Residence Time in Fractured Volcanics

An ECDF for the volcanic rocks filtration rate constants, shown in Figure 13-9, was constructed from the data presented in Figure 13-8 without any adjustment for the possible scale effect, with the filtration rate constant values plotted on a logarithmic scale. Also included is an estimate of the filtration rate constant determined for observed radionuclide transport from the BENHAM nuclear test to ER-20-5, discussed below. There is no other information available for characterizing the apparent scale effect at the CAU scale. Values from field-scale experiments are indicated. The values for field-scale experiments only range across about two orders of magnitude versus the almost five orders of magnitude range for all values, and the estimated value from the BENHAM observation is almost two orders of magnitude lower than the next higher values (from field-scale experiments).

An additional data point was added to the dataset that did not come from a tracer test, but rather from the observation of colloid-facilitated Pu transport to the ER-20-5 wells that originated from the BENHAM nuclear test cavity (Kersting et al., 1998). The method used to estimate a filtration rate constant for the observed transport is outlined here and discussed in Bechtel SAIC (2004b). To

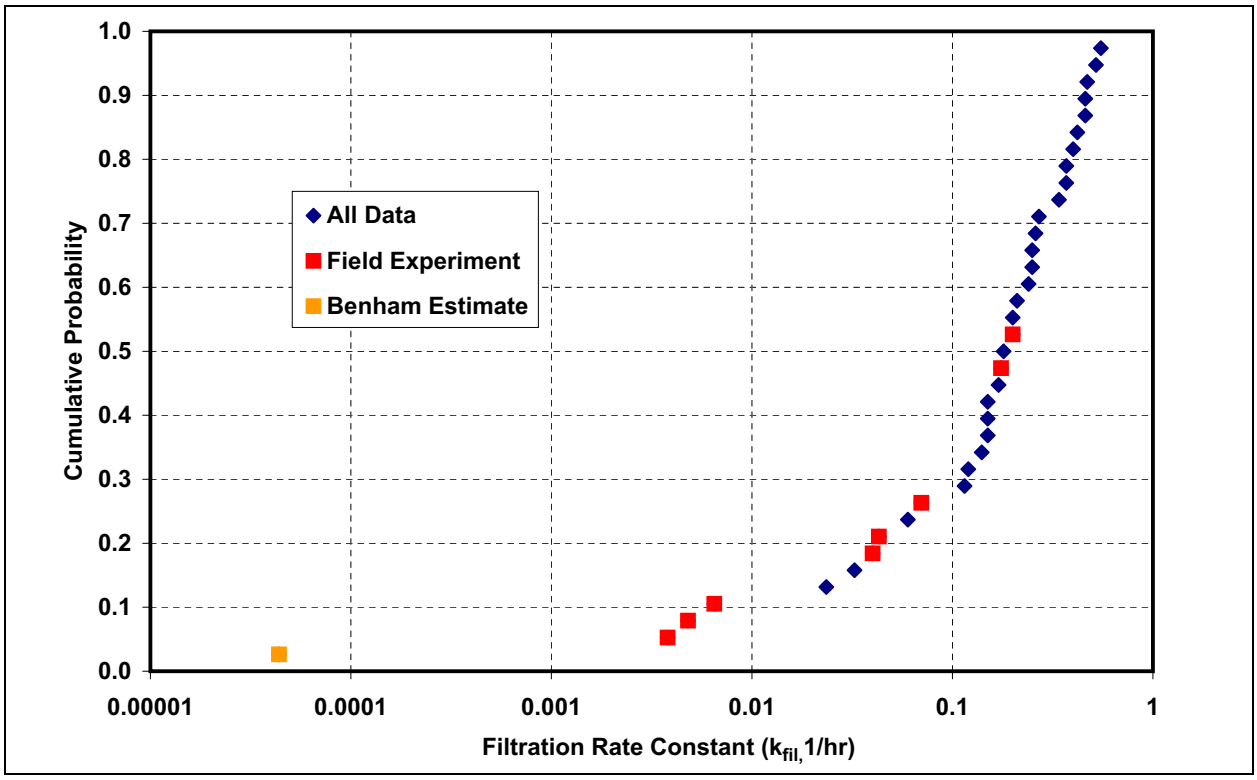

Figure 13-9
Cumulative Probability Distribution of Colloid Filtration Rate Constants for Fractured Volcanics

estimate a filtration rate constant for this observation, several assumptions were made. First, it was assumed that the Pu in the ER-20-5 wells was irreversibly sorbed to colloids, which means that Pu concentrations in the wells reflect colloid transport parameters reasonably well. Second, it was assumed that the concentrations measured in ER-20-5 #1 (on the order of 10^{-13} M Pu) represent a five orders of magnitude decrease from concentrations at the source. Thus, colloid filtration is assumed to result in a five orders of magnitude decrease in colloid concentrations. Third, it was assumed that any colloids that were filtered would never make it to the observation wells (i.e., effectively irreversibly filtered). Finally, the time from the BENHAM test until the measurement of Pu at the ER-20-5 well site was approximately 30 years, which represents an upper bound estimate for travel time. These assumptions result in a filtration rate constant estimate of 4.4×10^{-5} hr^{-1}. This estimate is not very sensitive to the assumed fraction of Pu-bearing colloids that travel from the source to the ER-20-5 wells; when this fraction is decreased from 1×10^{-5} to 1×10^{-8}, the estimated rate constant becomes 7×10^{-5} hr^{-1}. The filtration rate constant is inversely proportional to the assumed travel time, so if the

travel time is decreased by a factor of 3 (to 10) years, the filtration rate constant increases by a factor of 3 (to 1.3 x 10^{-4} hr^{-1}).

Detachment rates were also estimated from analyses of the C-Hole tracer tests in the Bullfrog and Prow Pass Formations. The colloid detachment rate constants reported in Bechtel SAIC (2004b) are 0.00015 (lower bound) and 0.00025 1/cm-hr (upper bound) for the Prow Pass Tuff, and 0.0002 and 1.08 1/cm-hr respectively for the Bullfrog Tuff, with this large range reflecting the different colloid transport behavior observed in the different transport pathways in this test.

Fractured Carbonate Rocks. Information on colloid filtration in fractured carbonate rocks at the field scale was obtained from the analysis of the ER-6-1 MWAT-TT conducted in FY 2004, which included CML microspheres as a colloid surrogate. Laboratory experiments on fractured carbonate core were also conducted in association with the tracer test to evaluate transport parameters for the LCA.

A semi-analytical analysis of the ER-6-1 MWAT-TT is presented in Reimus (2007c). The microsphere tracers were filtered significantly in the LCA, yielding filtration rate constants ranging from 0.002 to 0.004 hr^{-1}. Interpretations assuming reversible and irreversible filtration yielded equally good matches to the data. The results of the semi-analytical analysis of the CML microsphere transport were reported in Table 7 of Reimus (2007c), and the relevant results are shown in Table 13-6.

Table 13-6
ER-6-1 MWAT-TT Transport Analysis Results (Reimus, 2007c) for the LCA

Transport Parameter	Pathway 1	Pathway 2
Irreversible Filtration Rate Constant (hr^{-1})	0.004	0.002
Reversible Filtration Rate Constant (hr^{-1})	0.0035	0.0035
Reversible Detachment Rate Constant Times Fracture Half-Aperture (hr^{-1})	0.00027	0.00027

Reimus et al. (2006b) reports CML microsphere transport parameter estimates for laboratory experiments in five different LCA fractures in ER-6-1 core. The results reported in Table 17 of Reimus et al. (2006b) are excerpted in Table 13-7. The results of the laboratory experiments were consistent with the results of the ER-6-1 field tracer test in that the microsphere recoveries in the field

test were at least an order of magnitude lower than the nonsorbing solute tracers. In addition, very little difference in the breakthrough curves of the two different-sized microspheres was observed in both the field and laboratory experiments. The microsphere filtration rate constants in the field tracer test were an average of 0.0035 hr^{-1} for both microspheres (Reimus, 2007c), which is about an order of magnitude lower than the filtration rate constants in the laboratory fractures. This apparent trend of a decreasing filtration rate constant as a function of time or distance is consistent with that described previously for volcanic tuffs and the alluvium.

Table 13-7
Results of LCA Core Fracture Experiments (Reimus et al., 2006b)

Parameter	Fracture				
	2,400 ft	2,512 ft	2,675 ft	2,847 ft bgs	2,915 ft
Average Fracture Aperture (mm)	1.26	1.26	0.92	0.62	1.58
Microsphere Filtration Rate Constant (hr^{-1})	0.16/0.18	0.045/0.06	0.2/0.24	0.05/0.055	0.055/0.07
Fracture Half-Aperture Times Microsphere Detachment Rate Constant (hr^{-1})	0.0033/0.0026	<0.0001	0.0059/0.013	<0.0001	<0.0001

Note: Where two numbers are provided, the first is for the 500-nm microspheres, and the second is for the 200-nm microspheres.

13.6.2.2 Colloid Retardation Factors

Alluvium. Colloid retardation factors, R_{col}, were calculated using Equation (13-3) using the filtration rate values reported in Figure 13-6. An ECDF for the alluvium retardation factors was determined, shown in Figure 13-10. Note that the retardation factors are plotted on a logarithmic scale. The values for field-scale experiments, the NC-EWDP Site 22 field test and Schijven et al., 1999, are indicated. These values occupy the middle two orders of magnitude of the total range of four orders of magnitude.

Fractured Volcanic Rocks. An ECDF for R_{col} for volcanic rocks, shown in Figure 13-11, was generated using the interpretive results from all of the tests represented in Figure 13-8. Retardation factors are plotted on a logarithmic scale. The values for field-scale experiments are indicated and range across the full range of the data.

Note that values determined for two of the three microsphere responses from the BULLION FGE were excluded. The ER-20-5 observations were included by assigning a probability of 0.00001 to a

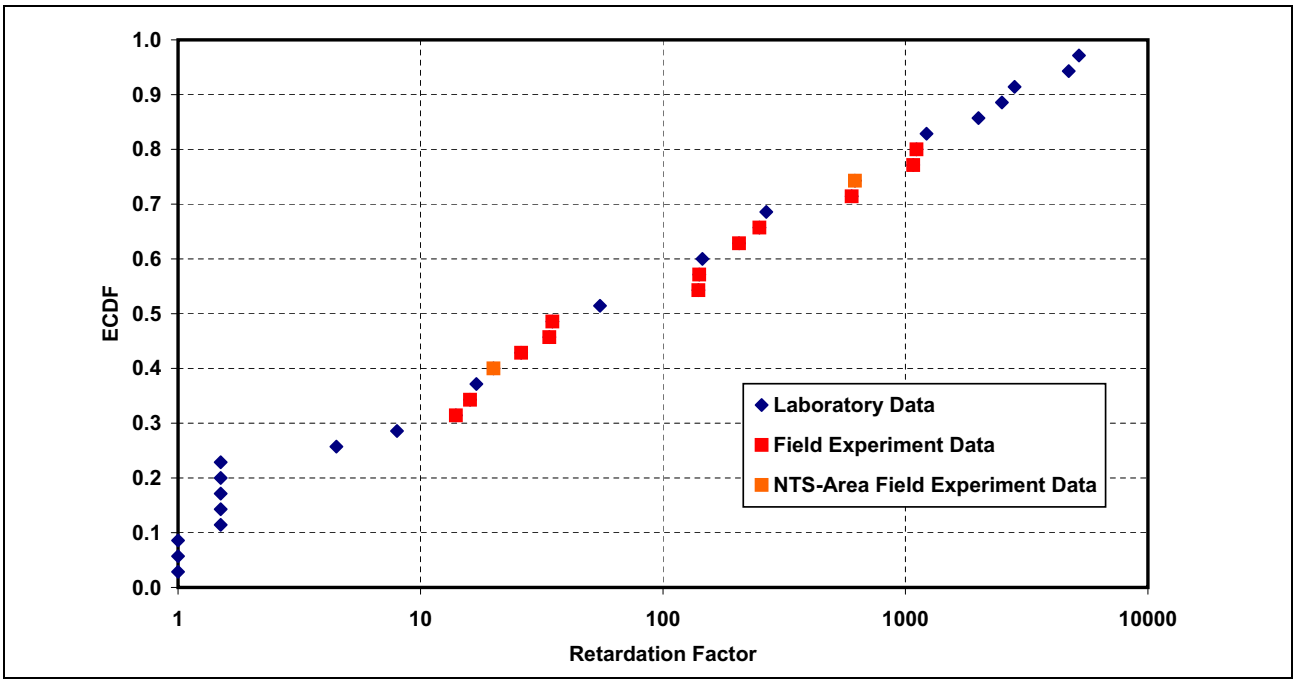

Figure 13-10
Cumulative Probability Distribution of Colloid Retardation Factors for Alluvium

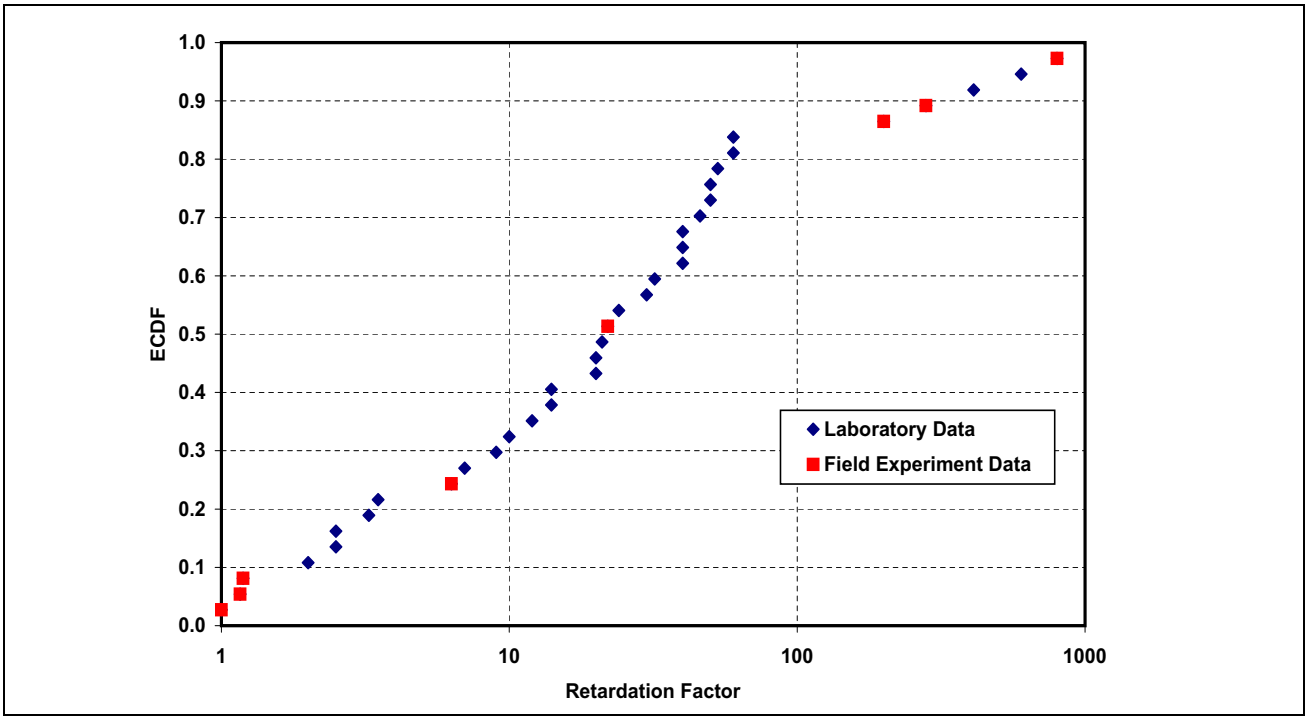

Figure 13-11
Cumulative Probability Distribution of Colloid Retardation Factors for Fractured Volcanic Rocks

R_{col} of 1.0, which assumes that 0.001 percent of the colloids from the source cavity moved unretarded to the ER-20-5 wells (consistent with the analysis of k_{fil}). The results from two of the microsphere responses in the BULLION FGE production well were omitted because there was a significant increase in microsphere concentrations in the tails of the responses that apparently resulted from a transient flow in the production well (this increase prevented an unbiased estimate of bk_{det}). The maximum R_{col} assumed for any of the colloid datasets was 1,001, which could not effectively be distinguished from an infinite retardation factor (because the colloid responses could be fitted equally well assuming no detachment at all). Thus, the distribution shown in Figure 13-11 is probably conservative at the upper end because of this somewhat arbitrary maximum value.

13.6.2.3 Additional Filtration and Retardation Analyses

Laboratory experiments to quantify reactive transport of radionuclides in fractured tuff and carbonate rocks were conducted by LANL and LLNL (Zavarin et al., 2007). As stated in Zavarin et al. (2007):

> In some of the LANL and LLNL TCU fracture experiments, it was apparent that ^{137}Cs, ^{239}Pu, and Sm did not migrate as free solutes, but rather as solutes sorbed to colloids, as a combination of free solutes and solutes sorbed to colloids, or as colloidal precipitates. This behavior was also evident for ^{14}C in a few of the TCU experiments and for ^{239}Pu and Sm in the LCA fracture experiments. One of LLNL's experiments was designed to include zeolite colloids and evaluate the role of colloid-facilitated transport. In LANL experiments, either silicate or calcite colloids (the latter would explain the colloidal behavior of ^{14}C) appear to have formed in the synthetic ER-2-1 water unintentionally and to sorb ^{137}Cs and ^{239}Pu quite strongly. The ^{239}Pu concentrations used in LANL experiments were also high enough to have potentially created Pu colloids over time. . . .
>
> The RELAP/RETRAN interpretive approach for ^{137}Cs and ^{239}Pu in the TCU fractures was modified to account for the fact that they appeared to be transported by colloids. . . . The rate-limited colloid filtration constant (or fracture sorption constant) was fitted while diffusion or sorption in the matrix was not allowed. Colloid filtration was assumed to be irreversible (i.e., an infinite sink), and the colloid desorption rate was set to zero.
>
> A combination of fracture retardation and sorption/colloid filtration rates constants was used for modeling ^{239}Pu in carbonates when it appeared that colloid-facilitated transport may better describe the breakthrough results. . . .

The results of experiments interpreted as colloid-facilitated transport are reported in Table 13-8, which identifies each experiment by rock type, well that the core came from, depth of the fracture, and experiment flow rate.

Table 13-8
Retardation Factors and Transport Parameters for Fracture Flowthrough Experiments

Tuff Confining Unit									
Experiment Identifier	UE-7ba, 1627, Synthetic slot with colloids	UE-4a, 2029, high flow	UE-4a, 2029, low flow	UE-7az, 1770, high flow	UE-7az, 1770, low flow	UE-7b, 1823, high flow	UE-7ba, 1823, low flow	UE-7ba, 1863, high flow	UE-7ba, 1863, low flow
k_{fil} ^{137}Cs (hr^{-1})	NA	0.5 [b]	0.24 [b]	3.0 [b]	1.6 [b]	0.58 [b]	0.3 [b]	0.39 [b]	0.35 [b]
R_{col} $^{238/242}$Pu	60	NA	NA	NA	NA	NA	NA	NA	NA
k_{fil} $^{238/242}$Pu	0.4 [a]	0.75 [b]	0.2 [b]	2.3 [b]	0.5 [b]	0.75 [b]	0.12 [b]	1.2 [b]	0.3 [b]
Aperture, cm	0.05	0.058	0.062	0.048, 0.086	0.048	0.102, 0.132	0.096, 0.112	0.06	0.06, 0.08
Lower Carbonate Aquifer									
Experiment Identifier	ER-6-1,2400, high flow	ER-6-1, 2400, low flow	ER-6-1, 2512, high flow	ER-6-1, 2512, low flow	ER-6-1, 2675, high flow	ER-6-1, 2675, low flow	ER-6-1, 2847, low flow	ER-6-1, 2915, high flow	ER-6-1, 2915, low flow
R_{col} $^{238/242}$Pu	NA	NA	NA	40	19	33	42	NA	NA
k_{fil} $^{238/242}$Pu (hr^{-1})	0.28 [b]	0.36 [b]	0.18 [b]	0.14 [b]	0.64 [b]	0.24 [b]	0.2 [a]	0.17 [a, b]	0.08 [b]
Aperture, cm	0.198	0.128, 0.154	0.158	0.140, 0.156	0.122, 0.162	0.092	0.072, 0.086	0.37, 0.404	0.192, 0.362

Data table excerpted from Zavarin et al. (2007); format modified per Reimus (original source of data).
Estimates assume that ALL of the radionuclide mass entering the fractures was associated with colloids and that none of the radionuclide mass desorbed from the colloids while in the fractures.

[a] Breakthrough fitted assuming rate-limited sorption/colloid filtration in fracture; modeled as reversible, one value is reported.
[b] Breakthrough fitted assuming rate-limited sorption/colloid filtration in fracture; modeled as irreversible, reported value is upper bound.

k_{fil} - Filtration Rate constant
NA - Not available
R_{col} - Retardation factor

These filtration rate constants were not included in the distribution analysis of Figure 13-9 because they were not estimated directly from colloid breakthrough curves, but rather were estimated from radionuclide breakthrough curves assuming that all the radionuclide mass entering the fractures was associated with colloids. If the radionuclide mass entering the fractures was only partially associated with colloids, the filtration rate constants would be smaller than the estimates of Table 13-8.

13.6.3 Limitations of the Colloid Transport Parameter Data and Analysis

There are several types of limitations for the colloid transport parameter analysis. These include data quality limitations, scaling considerations, and matching the available data to the parameters required for colloid-facilitated transport modeling. The analysis may require revision as more data become available and as colloid-facilitated transport understanding, theory, and modeling evolves.

13.6.3.1 Data Quality Limitations

There are few field-scale transport experiments for the HSUs in the NTS CAUs, and none of these actually involve colloid-facilitated radionuclide transport; rather, they involve surrogates for colloids. Much of the data are laboratory scale, and laboratory tests have been conducted on formation samples from only a few locations. Colloid transport parameters determined for transport media with different lithology and chemistry, as well as those derived from transport of colloid surrogates (bacteriophage and CML microspheres), must be used with caution and qualified. There may be important unidentified physical and chemical factors when compared to site-specific conditions and radionuclide transport.

Secondly, the transport parameter data are derived from interpretation of transport experiments rather than direct measurement, and the parameter values are determined within the context of evolving experimental and analysis methodology. There is also an inherent uncertainty associated with the colloid retardation factors because of the high degree of uncertainty associated with estimating detachment rate constants based on fitting the truncated tails of colloid breakthrough curves. In many cases, the detachment rate constants are poorly constrained by the breakthrough curves, and they could change significantly if the tests had been conducted longer so that the tails were longer.

The quality of the data varies and is difficult to assess. No weighting scheme has been used for the analysis because the basis for such weighting is so poorly known.

13.6.3.2 Scaling Considerations

The results of field and laboratory studies suggest that there may be important scale dependence (for time or distance) of colloid filtration rate constants and retardation factors. However, the available data are mostly from small-scale laboratory experiments and a few relatively small-scale field experiments. Filtration rates have been shown to be time-dependent. Determining the scale-dependency for CAU-scale modeling requires determining time scales for the predictions of colloid-facilitated transport at the CAU scale. There is no information at the CAU scale for colloid-facilitated transport other than the estimate for transport from the BENHAM test based on incidental data, which required several assumptions unsupported by data.

Rather than an explicit scale dependence, it is possible that there may be a wide distribution of colloid filtration rate constants associated with any colloid population and fracture flow system. As a result of this distribution, there may always be a small percentage of colloids that are resistant to filtration and capable of traveling over large distances at essentially the rate of water flow in any given groundwater flow system.

13.6.3.3 Colloid Retardation Transport Modeling Approach

There are several concerns with the current approach to parameter distributions to be used for colloid transport modeling as described in Bechtel SAIC (2004b). First, it does not account for scale dependence of filtration rate constants or retardation factors. Second, modeling of colloid-facilitated transport using their current approach results in a double-humped breakthrough that is inconsistent with observations in most colloid transport experiments. The double hump is produced as a result of a small fraction of unretarded colloids (fast fraction) based on the filtration rate constant distribution, and a second pulse of retarded colloids at a later time based on a single retardation factor for all non-fast-fraction colloids. Also, the use of a single retardation factor results in complete colloid recovery, also inconsistent with experimental observations.

A revised approach to colloid retardation is being developed for the YMP to more explicitly account for scale effects and address the modeling problem. The present data for filtration parameters and retardation factors would be used with a new approach to develop filtration and retardation factor distributions for use in modeling that incorporate scale dependence. The colloid-facilitated transport model would use the retardation factor distribution. It is recommended that the revision of the YMP approach be reviewed, and that the transport parameter analysis be updated before use of the transport parameters for contaminant transport modeling.

13.7 Radionuclide Associations with Colloids

Radionuclide associations with colloids have been evaluated in samples collected from near-field wells on the NTS known to contain radionuclides. Groundwaters are generally analyzed for radionuclide content without specific regard to whether the radionuclides are dissolved or associated with colloids. Two documents (Kersting et al., 1998; Kersting and Reimus, 2003) discuss the association of radionuclides with colloids in groundwater samples from the NTS.

The source of Pu in groundwater samples at the ER-20-5 (TYBO) site was traced to the BENHAM test 1.3 km to the north. In analyses performed by Kersting et al. (1998), it was found that greater than 99 percent of the Pu and Eu isotopes, approximately 91 percent of the Co, and 95 percent of the Cs were associated with the colloidal and particulate fractions filtered from the groundwater. This implies, but does not prove, that the radionuclides migrated associated with colloids.

Groundwater samples were collected from Rainier Mesa Tunnels (U12E, U12N, and U12T) from waters impounded in the tunnels behind portal seals, representing radionuclide transport in the unsaturated zone. The samples were analyzed for Pu concentration and isotopic composition, with separate analyses of the dissolved and the filterable solids fractions. The overwhelming majority of the Pu, Am, and ^{90}Sr was detected on the filterable, or colloidal fraction. For example, greater than 95 percent of the Pu was found in the colloidal, not the dissolved fraction (Kersting and Reimus, 2003).

The FY 2004 and FY 2005 near-field well (filtered and unfiltered) samples were analyzed to distinguish the fraction of each radionuclide (^{137}Cs, total U, ^{237}Np, and ^{239}Pu) associated with colloids in the sample (Reimus et al., 2006a). In the FY 2005 samples, ^{137}Cs was below the detection limit in

the unfiltered sample. For the FY 2004 samples, the fractional associations of ^{137}Cs with colloids correlated well with colloid mass loadings in the waters. Calculated K_d values of ^{137}Cs onto colloids were similar in all the wells, despite the large differences in colloid mass loadings in the waters. This result suggests that ^{137}Cs, when present in sufficient concentrations to measure, sorbs rather indiscriminately to colloid surfaces in the well waters based on available colloid mass and surface area. It also suggests that some sort of equilibrium or steady-state exists between the ^{137}Cs on the colloids and in solution. It is well known the Cs sorbs primarily to illite >> clay > zeolite via ion exchange, which is independent of surface area.

A significant fraction of total U was associated with colloids in groundwaters of three wells, but the colloid-associated U was naturally occurring. Samples from the remaining wells had little apparent partitioning, suggesting that U does not selectively partition to colloids to any significant degree. Both ^{237}Np, and ^{239}Pu were found in both solution and with colloids. Partitioning of ^{237}Np between solution and colloids is highly variable, with a maximum of about 30 percent associated with colloids. The variability is likely related to differences in colloid mineralogy. Greater than 80 percent of Pu was associated with colloids in all near-field samples (except RNM-1, which did not yield definitive results because of very low colloid and Pu concentrations), and is higher at higher concentrations of Pu, with greater than 90 percent above a threshold of 10^9 colloids per milliliter. In some cases colloid-bound Pu is found on the 10- to 50-nm colloids, which could affect the analysis because this size range is not always included in the analyses. The results suggest there is a high degree of variability in Pu associations with colloids, probably the result of variability in colloid mineralogy or groundwater redox conditions.

13.8 Actinide Distribution Coefficients and Sorption Rates onto Colloids

Actinide K_d values, sorption (forward) rates, and desorption (reverse) rates onto colloids were obtained from batch sorption and desorption experiments as well as fracture transport experiments conducted at both LANL and LLNL. Batch experiments have been conducted for both the UGTA Project (Pu) and the YMP (Pu, Am, Np, and U), and fracture-transport experiments have been conducted for the UGTA Project (Pu). The dataset for actinide K_d values onto colloids are presented in Appendix J; values of k_f and k_b are presented in Table 13-9.

Table 13-9
Ranges of Rate Constants for Sorption and Desorption of Actinides onto Colloids (Assuming Only a Single Type of Sorption Site) from UGTA and YMP Experiments

Colloids/Actinides	Batch k_f (hr^{-1})	Batch k_b (hr^{-1})	Fracture k_f (hr^{-1})	Fracture k_b (hr^{-1})
Montmorillonite				
Pu^{+4}	0.2-0.5	0.0001-0.01		
Pu^{+5}	0.005-0.04	0.0001-0.01	0.005-0.04	0.1-2
Np^{+5}	0.02-0.1	ND		
Am^{+3}	0.04-0.1	ND		
U^{+6}	0.02-0.1	ND		
Silica				
Pu^{+4}	0.2-0.5	0.01-0.2		
Pu^{+5}	0.01-0.06	0.01-0.2	0.01-0.06	0.5-1.5
Np^{+5}	0.02-0.1	ND		
Am^{+3}	0.04-0.1	ND		
U^{+6}	0.02-0.1	ND		
Hematite				
Pu^{+4}	1-50	0.00001-0.0001		
Pu^{+5}	0.04-0.1	0.00001-0.0001		
Np^{+5}	0.02-0.1	ND		
Am^{+3}	1-5	ND		
U^{+6}	0.02-0.1	ND		
Goethite				
Pu^{+4}	1-50	0.00001-0.001		
Pu^{+5}	0.06-0.1	0.00001-0.001		
Clinoptilolite				
Pu^{+4}	1-50	0.001-0.03	1-50	0.001-0.03
Pu^{+5}	0.001-0.01	ND		
Birnessite				
Pu^{+5}	1-50	ND		

k_f - Sorption rate constant
k_b - Desorption rate constant
ND - Not determined

Table 13-9 provides ranges of actinide sorption and desorption rate constants onto colloids from batch experiments and fracture transport experiments (Pu only) conducted for the UGTA Project and the YMP. It is apparent that the Pu desorption rate constants for montmorillonite and silica colloids are significantly greater in the fracture experiments than in the batch experiments, as discussed in the previous section.

Data for Pu^{+5} sorption and desorption onto "natural" smectite colloids have recently been collected from NC-EWDP-19D and are reported in the YMP TDMS (YMP, 2004). These data show that Pu sorption was very strong, and desorption was essentially negligible in batch experiments. Note that Pu^{+5} is typically reduced to Pu^{+4} during sorption. Column experiments using saturated alluvium from the same location were also conducted using Pu-tagged smectite colloids, and there was low but measurable desorption of the Pu from the colloids. However, while the significant facilitation of Pu transport in alluvium by "natural" colloids is noteworthy, the results should have negligible impact on the broad ranges of sorption parameters presented in this section (Reimus, 2007a).

13.8.1 Development of Parameter Distributions

The available data were assessed to derive K_d values and radionuclide desorption rates from colloids.

13.8.1.1 Distribution Coefficients

Between 1997 and 2000, Lu et al. (1998a and b, 2000) conducted several batch sorption and desorption experiments to measure the sorption of Pu^{+4}, Pu^{+5}, Am^{+3}, Np^{+5}, and U^{+6} onto hematite, goethite, montmorillonite, and silica colloids using filtered waters from Well J-13 located in Area 25 at the NTS (near Yucca Mountain) and synthetic J-13 water. The Pu^{+4} was always introduced as a polymeric colloid (less than or equal to 10 nm diameter) because Pu^{+4} is not stable as a solute at near-neutral pH, except at very low concentrations. The solubility of Pu^{+4} at near-neutral pH is less than 10^{-8} M. The measurements of Pu^{+4} polymeric colloid sorption are, therefore, likely to be valid because the concentrations of Pu in solution were very low after equilibration, even though the kinetics of precipitation, colloid formation, and oxidation are not well known. The hematite and goethite were selected to represent colloids that could form as a result of the corrosion of iron-containing waste package materials in the potential Yucca Mountain repository. Experiments

were conducted at different colloid concentrations, temperatures, and ionic strengths. The reader is referred to the Lu et al. (1998a and b, 2000) for details of the experiments.

Figure 13-12 depicts the ranges of radionuclide K_d values measured for the various radionuclide-colloid combinations at colloid concentrations of 200 mg/L at 20 °C in natural J-13 water under an ambient laboratory temperature of about 20 °C (Lu et al., 1998a and b, 2000; Reimus et al., 2002a; Kersting and Reimus, 2003). The results for Pu^{+5} K_d values onto silica and montmorillonite colloids in well water from U-20WW (Reimus et al., 2002a) and for Pu^{+5} K_d values onto goethite colloids in a synthetic J-13 well water (Kersting and Reimus, 2003) are shown as extensions of the bars for the J-13 K_d values in Figure 13-12. Again, note that Pu^{+5} is typically reduced to Pu^{+4} during sorption. Some of the key observations in the J-13 experiments, including the effects of changing the temperature, ionic strength, and colloid concentrations, are listed in brief summary fashion for each radionuclide and each colloid below.

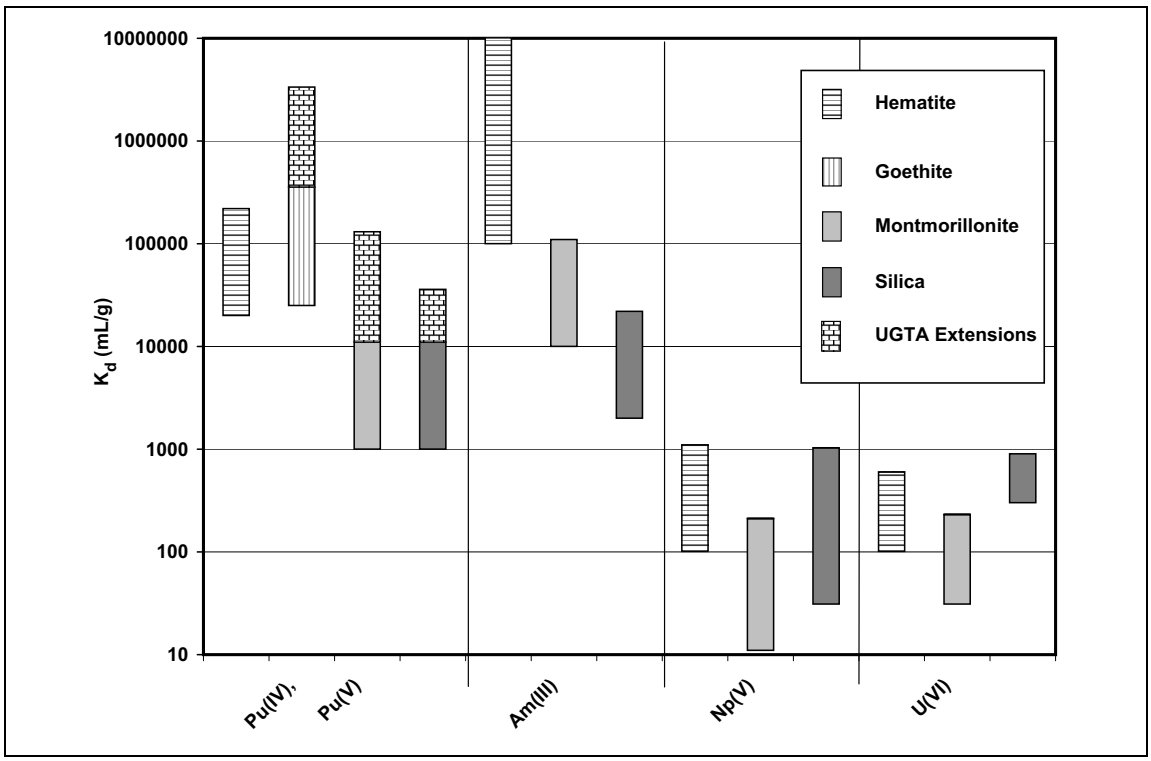

Figure 13-12
Ranges of K_d Values Measured for Actinide Sorption onto Colloids (Kersting and Reimus, 2003)

Pu^{+4} and Pu^{+5} Sorption to Hematite Colloids:

- Pu^{+4} sorption is much faster than Pu^{+5} sorption, although final K_d values were quite similar. (Note that Pu^{+5} is typically reduced to Pu^{+4} during sorption.)
- K_d ranges from 2 x 10^4 to 2 x 10^5 mL/g at 20 °C, J-13 water, 200 mg/L colloid concentration.
- K_d increases to 5 x 10^6 mL/g as temperature increases to 80 °C.
- K_d increases to 1 x 10^7 mL/g as ionic strength increases to 0.07 M or greater.
- K_d increases slightly (about a factor of 2) at low colloid concentrations (down to 10 mg/L).
- Desorption K_d is comparable to sorption K_d, so tests appear to indicate reversibility.

Pu^{+4} and Pu^{+5} Sorption to Goethite Colloids:

- Pu^{+4} sorption is much faster than Pu^{+5} sorption, although final K_d values were quite similar.
- No significant effect of ionic strength on K_d values; K_d increases to 3 x 10^4 mL/g at low colloid concentrations.
- Desorption K_d is comparable to sorption K_d, so tests appear to indicate reversibility.

Pu^{+4} and Pu^{+5} Sorption to Silica Colloids:

- Pu^{+4} sorption is much faster than Pu^{+5} sorption, although final K_d values were quite similar.
- K_d ranges from 10^3 to 10^4 mL/g at 20 °C, J-13 water, 200 mg/L colloid concentration.
- K_d upper limit of 10^4 mL/g as temperature increases to 80 °C.
- K_d lower limit of 10^3 mL/g as ionic strength increases to 0.1 M.
- K_d increases to 3 x 10^4 mL/g at low colloid concentrations.
- Desorption K_d is comparable to sorption K_d, so tests appear to indicate reversibility.

Am^{+3} Sorption to Hematite Colloids:

- K_d ranges from 10^5 to 10^7 mL/g at 20 °C, J-13 water, 200 mg/L colloid concentration.
- No significant effect of temperature, although slightly higher K_d values at higher temperatures.
- K_d approaches the lower end of the K_d range as ionic strength increases to 0.1 M.
- Upper end of K_d range is approached at low colloid concentrations.
- Desorption K_d is at lower end of range of sorption K_d, so tests appear to indicate reversibility.

Am^{+3} Sorption to Montmorillonite Colloids:

- K_d ranges from 10^4 to 10^5 mL/g at 20 °C, J-13 water, 200 mg/L colloid concentration.
- K_d increases to 3 x 10^5 mL/g as temperature increases to 80 °C.
- K_d values approach lower end of K_d range as ionic strength increases to 0.1 M.
- K_d increases to 10^6 mL/g at low colloid concentrations (10 mg/L).
- Desorption K_d is within range of sorption K_d, so tests appear to indicate reversibility.

Am^{+3} Sorption to Silica Colloids:

- K_d range from 2 x 10^3 to 2 x 10^4 mL/g at 20 °C, J-13 water, 200 mg/L colloid concentration.
- K_d increases to 6 x 10^4 mL/g as temperature increases to 80 °C.
- K_d values approach lower end of K_d range as ionic strength increases to 0.1 M.

- K_d increases to 10^5 mL/g at low colloid concentrations (10 mg/L).
- Desorption K_d is comparable to sorption K_d, so tests appear to indicate reversibility.

Np^{+5} Sorption to Hematite Colloids:

- K_d ranges from 10^2 to 10^3 mL/g at 20 °C, J-13 water, 200 mg/L colloid concentration.
- K_d increases to 4 x 10^3 mL/g as temperature increases to 80 °C.
- K_d values approach upper end of K_d range as ionic strength increases to 0.1 M.
- Desorption was not measurable, but this is not conclusive because of low amount of sorption.

Np^{+5} Sorption to Montmorillonite Colloids:

- K_d ranges from 10 to 200 mL/g at 20 °C, J-13 water, 200 mg/L colloid concentration.
- K_d increases to 3 x 10^3 mL/g as temperature increases to 80 °C.
- No significant effect of ionic strength on K_d values.
- Desorption was not measurable, but this is not conclusive because of low amount of sorption.

Np^{+5} Sorption to Silica Colloids:

- K_d ranges from 30 to 1,000 mL/g at 20 °C, J-13 water, 200 mg/L colloid concentration.
- K_d increases to 2 x 10^3 mL/g as temperature increases to 80 °C.
- K_d values approach lower end of K_d range as ionic strength increases to 0.1 M.
- Desorption was not measurable, but this is not conclusive because of low amount of sorption.

U^{+6} Sorption to Hematite Colloids:

- K_d ranges from 100 to 500 mL/g at 20 °C, J-13 water, 200 mg/L colloid concentration.
- K_d increases to upper end of K_d range as temperature increases to 80 °C.
- U precipitated at higher ionic strengths.
- Desorption was not measurable, but this is not conclusive because of low amount of sorption.

U^{+6} Sorption to Montmorillonite Colloids:

- K_d ranges from 30 to 200 mL/g at 20 °C, J-13 water, 200 mg/L colloid concentration.
- K_d increases to 700 mL/g as temperature increases to 80 °C.
- U precipitated at higher ionic strengths.
- Desorption was not measurable, but this is not conclusive because of low amount of sorption.

U^{+6} Sorption to Silica Colloids:

- K_d ranges from 300 to 600 mL/g at 20 °C, J-13 water, 200 mg/L colloid concentration.
- K_d increases to 2 x 10^3 mL/g as temperature increases to 80 °C.
- U precipitated at higher ionic strengths.
- Desorption was not measurable, but this is not conclusive because of low amount of sorption.

The results of the Pu^{+4} and Pu^{+5} experiments are consistent with at least partial reversibility of sorption, but the results would also be consistent with very slow desorption kinetics or irreversible

sorption of only a fraction of the Pu. Definitive results cannot be observed in the time frame of the experiments.

Separate Pu^{+4} and Pu^{+5} sorption experiments onto colloids were recently conducted at LLNL (Kersting and Reimus, 2003). The Pu^{+4} sorption onto clinoptilolite colloids was very fast and exhibited K_d values of 15,000 to 25,000 mL/g at 20 °C over a pH range of 7 to 9.5 (Kersting and Reimus, 2003). The Pu^{+5} experiments were conducted using seven different colloids. Note that Pu^{+5} is typically reduced to Pu^{+4} during sorption. The resulting K_d values for manganese oxide, birnessite and pyrolusite; calcite; zeolite, clinoptilolite; iron oxide and goethite; clay, montmorillonite; and silica are depicted in Figure 13-13 (Kersting and Reimus, 2003). The data in Figure 13-13 are in

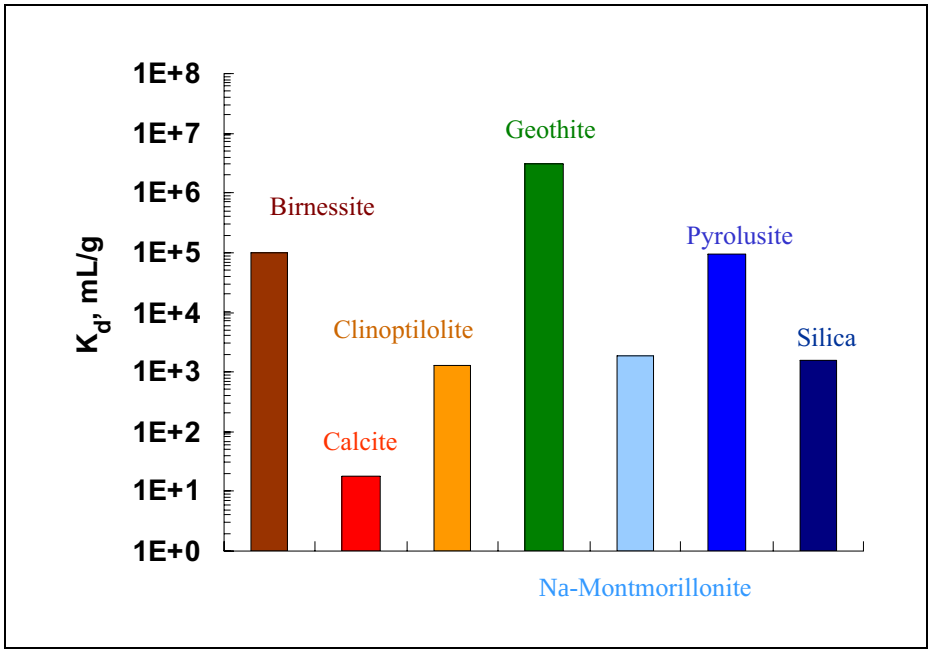

Figure 13-13
Distribution Coefficient Calculated for Pu^{+5} Sorbed onto Various Mineral Colloids (Kersting and Reimus, 2003)

good agreement with the Pu K_d values from LANL experiments shown in Figure 13-12. The K_d values for goethite are slightly higher in the LLNL experiments compared to the range in LANL experiments, although both datasets indicate very strong sorption of Pu^{+5} to goethite. These are the only types of mineral colloids for which comparisons are possible.

13.8.1.2 Radionuclide Sorption Rates onto Colloids

Sorption rates of Pu^{+4} and Pu^{+5} onto colloids have been measured in experiments at both LANL and LLNL. Colloid sorption rates for polymeric Pu^{+4} onto colloids are typically very rapid, with maximum (or equilibrium) sorption levels being attained within a few hours to at most a day. In experiments conducted at LANL for the UGTA Project, Pu^{+5} sorption rates onto silica colloids were initially faster than rates onto montmorillonite colloids, although final sorption K_d values tended to be somewhat higher on montmorillonite colloids. Maximum sorption levels were attained within a day or so on silica colloids, while they took 5 to 10 days on montmorillonite colloids. In sorption experiments conducted at LLNL, the sorption rates of Pu^{+5} onto birnessite and goethite colloids were very rapid (on the order of hours), but rates of Pu^{+5} sorption onto clinoptilolite colloids were extremely slow. In the latter case, it did not appear that equilibrium sorption levels were attained even after 50 days (Kersting and Reimus, 2003). These experiments were conducted in a synthetic water mimicking J-13 well water from near Yucca Mountain. The results were attributed to the ability of the birnessite and goethite surfaces to reduce Pu^{+5} to Pu^{+4}, followed by rapid subsequent sorption of the Pu^{+4} onto the colloids. In contrast, Pu^{+5} reduction to Pu^{+4} in the presence of clinoptilolite colloids was interpreted to occur only in the solution phase, a much slower process that was considered to be a necessary precursor to sorption onto the colloids. An alternative interpretation is that surface reduction was occurring, but at a much slower rate due to less effective reductants on the surfaces of the colloids. Spectroscopic methods confirmed that Pu^{+4}, not Pu^{+5}, was sorbed to the surfaces of all the colloids studied (Kersting and Reimus, 2003).

Sorption rates of U^{+6}, Np^{+5}, Pu^{+4}, Pu^{+5}, and Am^{+3} onto various types of inorganic colloids have been measured in experiments conducted at LANL for the YMP (Lu et al., 1998a and b, 2000). The results are summarized as follows (all at approximately 20 °C, 200 mg/L colloids, and ambient LANL atmosphere):

- The Pu^{+4} (colloidal) sorbed very quickly (hours) to hematite, goethite, montmorillonite, and silica colloids in J-13 well water.
- The Pu^{+5} sorbed more slowly to all of these colloids, taking one to three days to reach maximum sorption levels in J-13 water. Sorption tended to be somewhat faster (just a few hours) onto hematite and goethite colloids in a synthetic J-13 water that consisted of only sodium bicarbonate in solution.

- The Am^{+3} sorbed rapidly (within a few hours) and quite strongly onto hematite, montmorillonite, and silica colloids.
- The Np^{+5} sorbed relatively slowly onto hematite, montmorillonite, and silica colloids, taking a day or two to reach maximum sorption levels. Sorption of Np^{+5} onto these colloids was also much lower (lower K_d values) than for Pu and Am.
- The U^{+6} sorbed relatively weakly to hematite, montmorillonite, and silica colloids, although maximum sorption levels were reached within a day or so.

The Pu^{+5} sorption rates onto montmorillonite colloids in Well U-20WW water were significantly slower (5 to 10 days) than sorption rates onto these same types of colloids in Well J-13 water (one to three days). This was not explained; the two well waters are quite similar in composition. There may be a significant influence of a minor constituent present in one of the waters that is not present in the other, or there could be some differences in the montmorillonite colloids used in the different experiments.

From a practical standpoint, radionuclide sorption rates onto colloids are probably less important for CAU-scale modeling than distribution coefficients (K_d values) and desorption rates. Transport predictions will be relatively insensitive to whether sorption occurs over a matter of hours or a matter of weeks when time scales of interest are many years. However, relative sorption rates onto different colloids may be important from the standpoint of determining which types of colloids radionuclides tend to be associated with. If several different types of colloids are present, radionuclides will, for a while, tend to be preferentially sorbed onto the colloids that they sorb onto fastest, even if there are other colloids present that ultimately have larger distribution coefficients (because of slower desorption rates).

13.8.1.3 Radionuclide Desorption Rates from Colloids

Fewer studies have been conducted to determine radionuclide desorption rates from colloids than sorption rates onto colloids. There have been discrepancies in results of various experiments concerning the reversibility of sorption and desorption rates, and the reason(s) for the discrepancies are controversial. Results are reported according to the source document.

Studies conducted for the UGTA Project and the YMP exist only for Pu starting as either Pu^{+4} or Pu^{+5}. Kersting and Reimus (2003) report very slow desorption rates of Pu^{+4} from clinoptilolite colloids at

pHs ranging from 4 to 10. Total desorption over a seven-month period was 2 to 8 percent of the Pu that had sorbed.

In UGTA experiments at LANL, desorption rates were measured for Pu^{+5} sorbed onto montmorillonite and silica colloids, and also for Pu^{+4} sorbed onto clinoptilolite colloids (obtained from LLNL). These experiments were conducted at approximately 20 °C in water from U-20WW. In all cases, desorption rates were slow, although the results were mixed as to exactly how slow for the montmorillonite colloids (Reimus et al., 2002a). In some experiments, approximately 25 percent of the sorbed Pu desorbed in 7 to 11 months, and in other experiments only approximately 1 to 2 percent desorbed in 1 to 4 months. Desorption of Pu from silica colloids ranged from 20 to 30 percent in 7 to 11 months. Desorption of Pu^{+4} from clinoptilolite was slow, consistent with the LLNL results, with only 3 to 4 percent of the Pu desorbing in approximately 4 months. The inconsistencies in the montmorillonite results may be the result of using several different batches of montmorillonite colloids that were prepared from two different sources. Some of the differences might also be the result of starting desorption after different time periods of sorption in different experiments. Montmorillonite desorption experiments started after longer sorption time periods tended to have lower amounts and rates of desorption.

Montmorillonite, silica, and clinoptilolite colloids with Pu sorbed onto them were injected into naturally fractured cores from Pahute Mesa in experiments at LANL between 1999 and 2001 (Reimus et al., 2002a). Apparent Pu desorption rates from both montmorillonite and silica colloids were one to two orders of magnitude faster in the fractures than in the batch experiments described in the previous paragraph (the same Pu-colloid solutions were used in both experiments) (Reimus et al., 2002a). The Pu desorption from the clinoptilolite colloids, on the other hand, was essentially undetectable, consistent with the batch experimental results. The enhanced desorption rates for the montmorillonite and silica colloids were interpreted as the result of collisions between the colloids and the fracture surfaces, which offered opportunities for direct transfer of Pu from the colloids to the fracture surfaces, a process that was absent in the batch experiments (Reimus et al., 2002a). The fracture surfaces, which were coated with manganese oxides in two of the four fractures and had other mineral coatings in the other two, apparently had a greater affinity for the Pu than the montmorillonite and silica colloids. However, in the case of the clinoptilolite colloids, the Pu apparently had a greater affinity for the colloids than the fracture surfaces. These results indicate that

results from batch sorption and desorption experiments may not necessarily be directly transferable to modeling of colloid-facilitated transport in real fracture systems.

In YMP experiments, desorption rates have been measured for Pu^{+5} and Pu^{+4} (colloidal) from hematite, goethite, montmorillonite, and silica colloids over a 268-day period (Lu et al., 1998a). These experiments were conducted at approximately 20 °C, with 200 mg/L colloids in J-13 well water, and in ambient LANL atmosphere. The experiments were also conducted with sequential additions of fresh Pu-free water to the colloids at 2, 15, 50, 86, 107, 128, 150, 212, and 268 days (with removal and analyses of the solutions that had been in contact with the colloids at each of these times). This experimental method is in contrast to the methods used for the UGTA batch experiments where fresh solution was never added to the colloids after extracting water for a desorption measurement (i.e., only one desorption step, although measurements were made for several different contact periods). Figure 13-14 presents the results of YMP Pu desorption experiments in which Pu^{+5} was sorbed onto smectite and silica colloids for six days, the Pu was then desorbed in multiple batch steps in which Pu-free water was placed in contact with the colloids. The experiments were conducted at room temperature in J-13 well water (Lu et al., 1998b), and Pu was initially introduced as Pu^{+5} in solution.

The YMP results are summarized as follows:

- Less than 0.02 percent of the sorbed Pu^{+5} and Pu^{+4} desorbed from the hematite colloids.
- Less than 1 percent of the sorbed Pu^{+5} and Pu^{+4} desorbed from the goethite colloids.
- The Pu^{+5} desorption from montmorillonite colloids was less than 1 percent after 268 days, but Pu^{+4} desorption from these colloids exceeded 10 percent after 150 days.
- Much of the desorption of Pu^{+5} and Pu^{+4} from silica and smectite colloids occurred early in the experiments, with a tendency to reach a desorption plateau later in the experiments (Figure 13-14). Extrapolation of the results could lead one to conclude that some of the Pu sorption may be irreversible, even onto silica colloids that have relatively low measured K_d values.

The last bullet suggests that a multiple sorption site model may be appropriate for Pu sorption onto colloids. Some of the sites appear to be associated with relatively rapid desorption, while others may essentially behave as irreversible or very slowly reversible sites. The time-scale of transport should

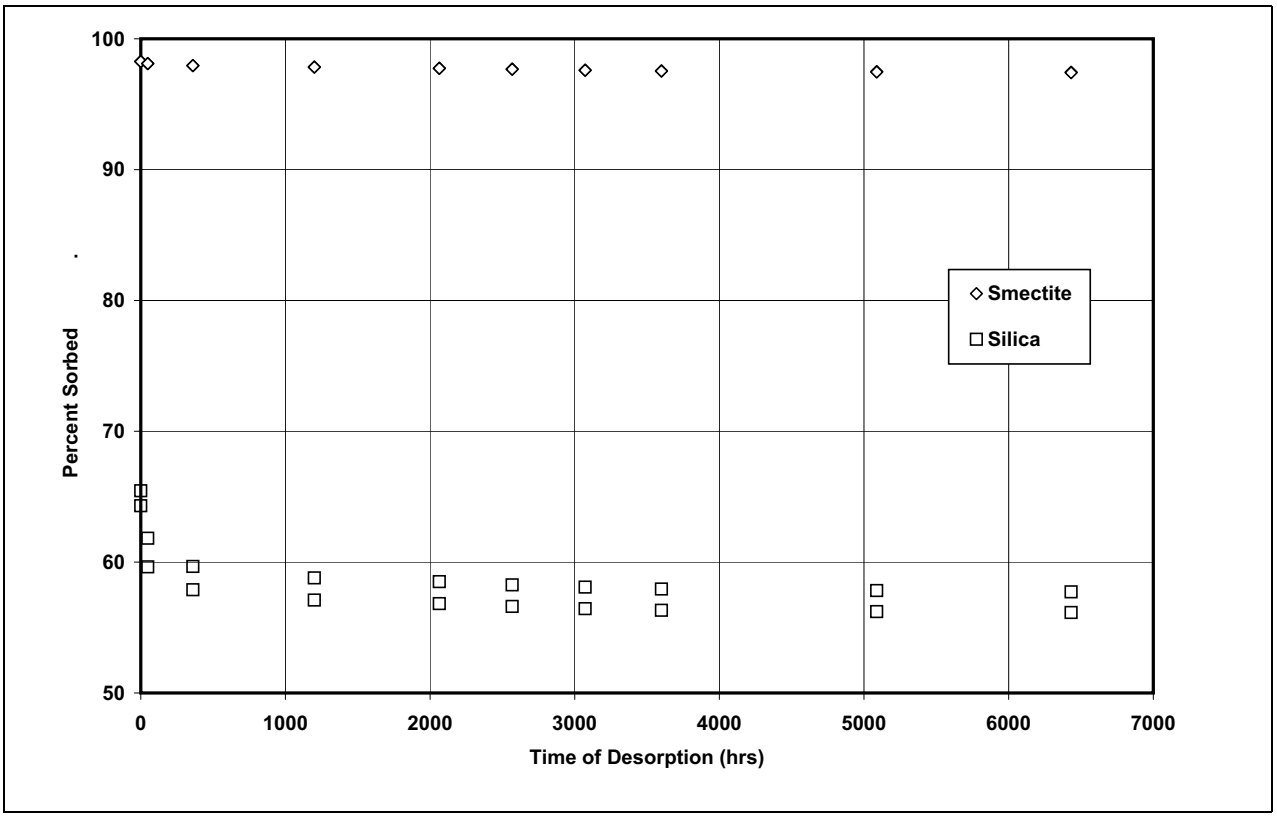

Figure 13-14
Yucca Mountain Project Pu Desorption Experiments Using Smectite and Silica Colloids (Lu et al., 1998b)

dictate whether the reverse rate is treated as effectively irreversible or slowly reversible. A two-site sorption model resulted in significantly improved model fits to the sorption and desorption data from the UGTA batch experiments, particularly in the case of the montmorillonite and silica colloids (Reimus et al., 2002b). Desorption experiments reported by Lu and Reimus (2003) indicate that long-term desorption rates of 0.35 yr^{-1} for smectite colloids and 0.12 yr^{-1} for silica colloids would be appropriate for systems with relatively long transport time scales.

The data of Lu et al. (1998a and b) are consistent with at least partial reversibility of actinide sorption onto colloids. However, the data of Figure 13-14 suggest that much of the sorbed Pu may either be irreversibly sorbed or have very slow desorption kinetics. The fracture data are probably more applicable than the batch data because of the presence of minerals that can compete with the colloids for sorption, which is consistent with the real system.

13.8.2 Data Limitations

It is important to recognize that the data in Figure 13-12 and Table 13-9 reflect only general trends observed in sorption and transport experiments; they do not account for the possibility of multiple types of sorption sites with different sorption strengths on colloids. The desorption rate constants in Table 13-9 should be considered upper bounds because some sites may behave as essentially irreversible sites with very low or zero desorption rates. The majority of batch experiments conducted to date have not been designed to explicitly investigate this possibility, although the desorption results shown in Figure 13-14 clearly suggest it. A small amount of desorption occurring early in a batch test will tend to skew estimates of desorption rate constants to large values that may apply to only a small percentage of sorption sites.

Also, batch experiments conducted to date also do not account for potential desorption that may occur when other natural mineral surfaces are present to compete with the colloid surfaces for actinides (as in the fracture transport experiments or a real fracture system). Sensitivity studies conducted with CAU-scale models using desorption rate constants that extend well beyond the ranges in Table 13-9 would be important to evaluate the potential impact of the situation.

13.8.3 Scaling Considerations

One important scaling consideration for actinide distribution coefficients and sorption/desorption rates onto colloids is how the desorption rate constants scale with time (or, alternatively, how reversible is the actinide sorbtion onto colloids). The experimental results shown in Figure 13-14 suggest that there may be a significant fraction of Pu that desorbs much more slowly from colloids than the initial desorbing mass fraction. In effect, the Pu desorption rates appear to decrease with time, although the observed behavior could also be explained by multiple sorption sites with different sorption strengths or degrees of reversibility. Such desorption behavior could have a profound impact on predictions of colloid-facilitated transport at CAU scales.

Another important “scaling” consideration is actinide sorption and desorption behavior on colloids in the presence of sorbing fracture surfaces (as opposed to being in the presence of only non-reactive test tube walls in batch sorption/ desorption experiments). The significant differences between the batch and fracture transport experimental results indicated in Table 13-9 clearly suggest that batch

sorption/desorption test results should be cautiously applied in field-scale fracture transport modeling exercises.

13.9 Summary

This section presents a summary of the available data for colloid-facilitated transport specifically applied to NTS CAUs. The data have been analyzed to the extent possible to provide parameter values and distribution parameter values that can be used for modeling colloid-facilitated transport. However, the data are not comprehensive or even complete for all rock types, much less individual HSUs. The data are most complete for alluvium and fractured volcanic rocks (in general), and there is a limited dataset for fractured carbonate rocks. There are only miscellaneous data for other rock types. As was discussed in Section 13.6, the approach used to determine colloid transport parameters has some problems that will be resolved with a revised approach currently in development by YMP. The analyst should review the current YMP approach to colloid-facilitated transport and update the transport parameter analysis before using the parameter values presented in this section for contaminant transport modeling. In general, it is recommended to conduct sensitivity studies with the CAU-scale transport model to determine what uncertainties regarding colloid-facilitated transport may be significant.

14.0 REFERENCES

Abdel-Fattah, A., D. Smith, M. Murrell, S. Goldstein, A. Nunn, R. Gritzo, B. Martinez, and P.W. Reimus. 2005. *Colloid Characteristics and Radionuclide Associations with Colloids in Source-Term Waters at the Nevada Test Site*, LA-UR05-5312. Los Alamos, NM: Los Alamos National Laboratory.

App, F.N., and N.L. Marusak. 1997. *Tuff Pile I - A Justification for the Projection of Material Properties within a Portion of Los Alamos Test Areas 1, 3, 4, and 7, Nevada Test Site*, LA-UR-97-1024. Los Alamos, NM: Los Alamos National Laboratory.

Archie, G.E. 1942. "The Electrical Resistivity Log as an Aid in Determining Some Reservoir Characteristics." In *Transactions of the American Institute of Mining and Metallurgical Engineers*, Vol. 146: 54 - 62.

Avon, L., and J.D. Bredehoeft. 1989. "An Analysis of Trichloroethylene Movement in Groundwater at Castle Air Force Base, California." In *Journal of Hydrology*, Vol. 110: 23-50.

BN, see Bechtel Nevada.

Barnes, H., R.L. Christiansen, and F.M. Byers, Jr. 1965. *Geologic Map of the Jangle Ridge Quadrangle, Nye and Lincoln Counties, Nevada*, Map GQ-363, scale 1:24,000. Washington, DC: U.S. Geological Survey.

Bear, J. 1972. *Dynamics of Fluids in Porous Media*. New York, NY: Elsevier Publishing Co.

Bear, J., and A. Verruijt. 1990. *Modeling Groundwater Flow and Pollution*. Reidel (Dordrecht).

Bechtel Nevada. 1997a. *Processing and Geologic Analysis of Conventional Cores from Well ER-20-6#1, Nevada Test Site*, DOE/NV/11718-162, UC-703. Las Vegas, NV.

Bechtel Nevada. 1997b. Written communication. Subject: *Draft of the Completion Report for Well ER-6-2*, DOE/NV--UC-700. Las Vegas, NV.

Bechtel Nevada. 2002. *A Hydrostratigraphic Model and Alternatives for the Groundwater Flow and Contaminant Transport Model of Corrective Action Units 101 and 102: Central and Western Pahute Mesa, Nye County, Nevada*, DOE/NV/11718--706. Las Vegas, NV.

Bechtel Nevada. 2003. *Completion Report for Well ER-18-2*, DOE/NV/11718--388. Las Vegas, NV.

Bechtel Nevada. 2004. *Completion Report for Well Cluster ER-6-1*, DOE/NV/11718--862. Las Vegas, NV.

Bechtel Nevada. 2005. *A Hydrostratigraphic Framework Model and Alternatives for the Groundwater Flow and Contaminant Transport Model of Corrective Action Unit 98: Frenchman Flat, Clark, Lincoln, and Nye Counties, Nevada*, DOE/11718--1064. Las Vegas, NV.

Bechtel Nevada. 2006. *A Hydrostratigraphic Model and Alternatives for the Groundwater Flow and Contaminant Transport Model of Corrective Action Unit 97: Yucca Flat-Climax Mine, Lincoln and Nye Counties, Nevada*, DOE/NV/11718--1119. Las Vegas, NV.

Bechtel SAIC. 2004a. *In Situ Field Testing of Processes*, ANL-NBS-HS-000005, Rev. 03. Las Vegas, NV.

Bechtel SAIC. 2004b. *Saturated Zone Colloid Transport*, Rev. 2, ANL-NBS-HS-000031. Los Alamos, NM: Los Alamos National Laboratory.

Bechtel SAIC. 2004c. *Saturated Zone In-Situ Testing*, ANL-NBS-HS-000039, Rev. 01, Yucca Mountain Project Analysis Report. Las Vegas, NV.

Bedinger, M.S., K.A. Sargent, W.H. Langer, F.B. Sherman, J.E. Reed, and B.T. Brady. 1989. *Studies of Geology and Hydrology in the Basin and Range Province, Southwestern United States, for Isolation of High-Level Radioactive Waste – Basis of Characterization Evaluation*, Professional Paper 1370-A. U.S. Geological Survey.

Beiriger, W. 1977. *X-ray Analysis of 36 Samples from Ue5n.* L.D. Ramspott, ed.

Belcher, W.R., J.B. Blainey, F.A. D'Agnese, C.C. Faunt, M.C. Hill, R.J. Laczniak, G.M. O'Brien, C.J. Potter, H.M. Putnam, C.A. San Juan, and D.S. Sweetkind. 2004. *Death Valley Regional Model Ground-Water Flow System, Nevada and California - Hydrogeologic Framework and Transient Ground-Water Flow Model*, Scientific Investigations Report 2004-5205. U.S. Geological Survey.

Benedict, Jr. F.C., T.P. Rose, J.M. Thomas, R. Waddell, and R. Jacobson. 2003. *Geochemistry Technical Basis Document*, DOE/NV/13609-34; Publication No. 45205. Las Vegas, NV: Desert Research Institute.

Berger, D.L. 1992. *Lithologic Properties of Carbonate-Rock Aquifers at Five Test Wells in the Coyote Spring Valley Area, Southern Nevada, as Determined from Geophysical Logs*, Water-Resources Investigations Report 91-4167. Carson City, NV: U.S. Geological Survey.

Blankennagel, R.K., and J.E. Weir, Jr. 1973. *Geohydrology of the Eastern Part of Pahute Mesa, Nevada Test Site, Nye County, Nevada*, Professional Paper 712-B. Washington, DC: U.S. Geological Survey.

Boardman, C.R. 1965. *A Measurement of the Void Volume and Fracture Permeability Resulting from the HARDHAT Event*, UCID-4893. Livermore, CA: University of California, Lawrence Radiation Laboratory.

Boardman, C.R. 1966. *Some Characteristics of the HARDHAT Chimney and Surrounding Wall Rock*, UCRL-50177. Livermore, CA: University of California, Lawrence Radiation Laboratory.

Boardman, C.R. 1967. *Results of an Exploration into the Top of the PILEDRIVER Chimney*, UCRL-50385. Livermore, CA: University of California, Lawrence Radiation Laboratory.

Boardman, C.R., and L. Meyer. 1970. "Postshot Environment." In *The HANDCAR Nuclear Explosion in Dolomite*, G.C. Werth (ed.), UCRL-50951. Livermore, CA: Lawrence Livermore National Laboratory.

Boardman, C.R., and J. Skrove. 1966. "Distribution in Fracture Permeability of a Granitic Rock Mass Following a Contained Nuclear Explosion." In *Journal of Petroleum Technology*, May; 619-623.

Borg, I.Y. 1970. *Survey of PILEDRIVER Results and Preliminary Interpretation of Three Postshot Cores In and Near the Cavity*, UCRL-50865. Livermore, CA: Lawrence Livermore National Laboratory.

Borg, I.Y. 1971. *Some Shock Effects in Granodiorite to 270 kbar at the PILEDRIVER Site*, UCRL-73377, Rev. 1. Livermore, CA: Lawrence Livermore National Laboratory.

Borg, I.Y. 1973. *Comparison of Shock Effects in Granitic Rock Recovered From the Monique Event, Algeria, and the PILEDRIVER Event, Nevada Test Site*, UCRL-51349. Livermore, CA: Lawrence Livermore Laboratory.

Borg, I.Y. 1974. "Radioactivity Trapped in Melt Produce by a Nuclear Explosion." In *Nuclear Technology*, Vol. 26: 88-100.

Borg, I.Y., R. Stone, H.B. Levy, and L.D. Ramspott. 1976. *Information Pertinent to the Migration of Radionuclides in Groundwater at the Nevada Test Site, Part 1: Review and Analysis of Existing Information*, UCRL-52078, Pt. 1. Livermore, CA: Lawrence Livermore National Laboratory.

Boving, T.B., and P. Grathwohl. 2001. "Tracer Diffusion Coefficients in Sedimentary Rocks: Correlation to Porosity and Hydraulic Conductivity." In *Journal of Contaminant Hydrology*, Vol. 53: 85-100. New York, NY: Elsevier Publishing Co.

Bowen, S.M., D.L. Finnegan, J.L. Thompson, C.M. Miller, P.L. Baca, L.F. Olivas, C.G. Geoffrion, D.K. Smith, W. Goishi, B.K. Esser, J.W. Meadows, N. Namboodiri, and J.F. Wild. 2001. *Nevada Test Site Radionuclide Inventory, 1951-1992*, LA-13959-MS. Los Alamos, NM: Los Alamos National Laboratory.

Bradley, H.B., Ed. 1992. *Petroleum Engineering Handbook*. Richardson, TX: Society of Petroleum Engineers.

Bryant, N.A. 2005. *Letter Report: Analysis of Hydraulic Conductivity and Fracture Porosity in ER-5-3 #2 and ER-5-4 #2 Based on Fracture Data from Borehole Image Logs with Implications for the Tuff Confining Unit Flow Framework, Nevada Test Site, Nevada*. Las Vegas, NV: Stoller-Navarro Joint Venture.

Buddemeier, R.W., and D. Isherwood. 1985. *Radionuclide Migration Project 1984 Progress Report*, UCRL-53628. Livermore, CA: Lawrence Livermore National Laboratory.

Burbey, T.J., and S.W. Wheatcraft. 1986. *Tritium and Chlorine-36 Migration from a Nuclear Explosion Cavity,* Publication No. 45050. Las Vegas, NV: Desert Research Institute.

Burkhard, N.R. 1989. *Physical Properties in LLNL Yucca Flat Areas: The ROCK PILE Concept*, UCRL-100837. Livermore, CA: Lawrence Livermore National Laboratory.

Byers, Jr., F.M., and H. Barnes. 1967. *Geologic Map of the Paiute Ridge Quadrangle, Nye and Lincoln Counties, Nevada*, Geologic Quadrangle Map GQ-577, scale 1:24,000. Washington, DC: U.S. Geological Survey.

CRWMS M&O, see Civilian Radioactive Waste Management System Management and Operating Contractor.

Carle, S.F., R.M. Maxwell, G.A. Pawloski, D.E. Shumaker, A.F.B. Tompson, and M. Zavarin. 2007. *Evaluation of the Transient Hydrologic Source Term for the Cambric Underground Nuclear Test at Frenchman Flat, Nevada Test Site*, UCRL-TR-226916. Livermore, CA: Lawrence Livermore National Laboratory.

Callahan, T.J., P.W. Reimus, R.S. Bowman, and M.J. Haga. 2000. "Using Multiple Experimental Methods to Determine Fracture/Matrix Interactions and Dispersion of Nonreactive Solutes in Saturated Volcanic Rock." In *Water Resources Research*, Vol. 36(12): 3547-3558. Washington, DC: American Geophysical Union.

Cashman, P.H., and J.H. Trexler, Jr. 1991. "The Mississippian Antler Foreland and Continental Margin in Southern Nevada: The Eleana Formation Reinterpreted." In J.D. Cooper and C.H. Stevens, eds., *Paleozoic Paleogeography of the Western United States - II: Pacific Section SEPM;* Vol. 67: 271-280.

Castany, G. 1967. *Traité Pratique des Eaux Souterraines*. Paris, France: Dunod.

Cavazos, A.P., S.L. Drellack, Jr., W.T. Huges, and P.H. Thompson. 1987. *Lithology and Stratigraphy of Drill Holes Completed During 1986 in LANL Use Areas of Yucca Flat, Nevada Test Site*, DOE/NV/10322-22. Las Vegas, NV: Fenix & Scisson, Inc.

Chapelle, F.H. 1986. "A Solute-Transport Simulation of Brackish-Water Intrusion Near Baltimore, Maryland." In *Ground Water*, Vol. 24(3): 304-311.

Chiang, C.Y., J.P. Salanitro, E.Y. Chai, J.D. Colthart, and C.L. Klein. 1989. "Aerobic Biodegradation of Benzene, Toluene, and Xylene in a Sandy Aquifer - Data Analysis and Computer Modeling." In *Ground Water*, Vol. 27(6): 823-834.

Civilian Radioactive Waste Management System Management and Operating Contractor. 2004. *UZ Flow Models and Submodels*, MDL-NBS-HS-000006, Rev. 02. Civilian Radioactive Waste Management System Management and Operating Contractor. Las Vegas, NV.

Claassen, H.C., and E.H. Cordes. 1975. "Two-Well Recirculation Tracer Test in Fractured Carbonate Rock, Nevada." In *Hydrological Sciences Bulletin*, Vol. 20 (3): 367 - 382. Oxford: Blackwell Scientific Publications.

Cole, J.C., U.S. Geological Survey. 1992. Written communication to S.L. Drellack regarding thickness of Paleozoic units at the NTS. Denver, CO: U.S. Geological Survey.

Cole, J.C. 1997. *Major Structural Controls on the Distribution of Pre-Tertiary Rocks, Nevada Test Site Vicinity, Southern Nevada*, Open-File Report 97-533. Denver, CO: U.S. Geological Survey.

Conca, J.L., and J. Wright. 1992. "Diffusion and Flow in Gravel, Soil, and Whole Rock." In *Applied Hydrogeology*, Vol. 5: 24.

Crank, J. 1975. *The Mathematics of Diffusion*. Oxford: Clarendon Press.

DOE/NV, see U.S. Department of Energy, Nevada Operations Office.

DOE/ORD, see U.S. Department of Energy, Office of Civilian Radioactive Waste Management, Office of Repository Development.

DOE/WIPP, see U.S. Department of Energy, Waste Isolation Pilot Plant.

Dynamic Graphics, see Dynamic Graphics, Inc.

D'Alessandro, M., F. Mousty, G. Bidoglio, J. Guimera, I. Benet, X. Sanchez-Vila, M.G. Gutierrez, and A.Y. De Llano. 1997. "Field Tracer Experiment in a Low Permeability Fractured Medium: Results from El Berrocal Site." In *Journal of Contaminant Hydrology*, Vol. 26: 189-201.

Daniels, W.R., and J.L. Thompson, compilers and editors. 1984. *Laboratory and Field Studies Related to the Hydrology/Radionuclide Migration Project: October 1, 1982 - September 30, 1983*, LA-10121-PR. Los Alamos, NM: Los Alamos National Laboratory.

Daniels, W.R., B.R. Erdal, and D.T. Vaniman, eds. 1983. *Research and Development Related to the Nevada Nuclear Waste Storage Investigations: July 1 - September 30, 1982,* LA-9577-PR. Los Alamos, NM: Los Alamos National Laboratory.

Davies, W.J., J.L. Gonzales, and S.L. Drellack, Jr. 1982. *Lithologic and Geophysical Logs of Selected Drill Holes in Eastern Area 4 and Western Area 7, Nevada Test Site,* DOE/NV/10322-3. Las Vegas, NV: Fenix & Scisson, Inc.

Davis, J.A., J.A. Coston, D.B. Kent, and C.C. Fuller. 1998. "Application of the Surface Complexation Concept to Complex Mineral Assemblages." In *Environmental Science & Technology,* Vol. 32 (19): 2820-2828. Washington, DC: American Chemical Society.

Decker, D.L, C. Papelis, R.L. Hershey, R. Harris, and G. Schmett. 2003. *Temperature Dependence of Sorption Behavior of Lead and Cesium Metal Ions on Western Pahute Mesa and Rainier Mesa Aquifer Rocks,* DOE/NV/13609-21. Reno, NV: Desert Research Institute, Division of Hydrologic Sciences.

de Marsily, G. 1986. *Quantitative Hydrogeology.* Orlando, FL: Academic Press Inc.

Dickerson, R.P., T.P. Rose, and G.F. Eaton. 2004. *Letter Report: Underground Test Area Project, Mineralogic and Isotopic Analysis of Fracture-Coating and Alteration Minerals in the Yucca Flat Tuff Confining Unit, Nevada Test Site,* 1 April. Livermore, CA: Lawrence Livermore National Laboratory.

Domenico, P.A., and G.A. Robbins. 1985. "The Displacement of Connate Water from Aquifers." In *Geol. Soc. Am. Bull.*, Vol. 96: 328-335.

Domenico, P.A., and F.W. Schwartz. 1990. *Physical and Chemical Hydrogeology 2nd ed.* New York, NY: John Wiley & Sons.

Dosch, R.G., and A.W. Lynch. 1980. "Radionuclide Transport in a Dolomite Aquifer, Scientific Basis for Nuclear Waste Management." In *Proceedings of the International Symposium*, held in Boston, Massachusetts, on November 27-30, 1979. New York, NY: Plenum Press.

Doty, G.C., and F. Rush. 1985. *Infow to a Crack in Playa Deposits of Yucca Lake, Nevada Test Site, Nye County, Nevada.* Water-Resources Investigations Report 84-4296. Denver, CO: U.S. Geological Survey.

Drellack, Jr., S.L., and P.H. Thompson. 1990. *Selected Stratigraphic Data for Drill Holes in LANL Use Areas of Yucca Flat, NTS,* DOE/NV/10322--39. Las Vegas, NV: Fenix & Scisson, Inc.

Drellack, Jr., S.L., L.B. Prothro, K.E. Roberson, B.A. Schier, and E.H. Price. 1997. *Analysis of Fractures in Volcanic Cores from Pahute Mesa, Nevada Test Site,* DOE/NV/11718-160. Las Vegas, NV: Bechtel Nevada.

Drever, J.I. 1988. *The Geochemistry of Natural Waters*. Englewood Cliffs, NJ: Prentice Hall, Inc.

Dullien, F.A.L. 1979. *Porous Media: Fluid Transport and Pore Structure*. Academic Press, Inc.

Dynamic Graphics, Inc. 2002. *EarthVision 7: Software for 3-D Modeling and Visualization*. Alameda, CA.

EPA, see U.S. Environmental Protection Agency.

Engesgaard, P., K.H. Jensen, J. Molson, E.O. Frind, and H. Olsen. 1996. "Large-Scale Dispersion in a Sand Aquifer: Simulation of Subsurface Transport of Environmental Tritium." In *Water Resources Research*, Vol. 32(11): 3253-3266.

Erickson, J.R., and R.K. Waddell. 1985. *Identification and Characterization of Hydrologic Properties of Fractured Tuff Using Hydraulic and Tracer Tests -- Test Well USW H-4, Yucca Mountain, Nye County, Nevada*, Water-Resources Investigations Report 85-4066. U.S. Geological Survey.

FFACO, see *Federal Facility Agreement and Consent Order.*

Federal Facility Agreement and Consent Order. 1996 (as amended). Agreed to by the State of Nevada; U.S. Department of Energy, Environmental Management; U.S. Department of Defense; and U.S. Department of Energy, Legacy Management. Appendix VI, which contains the Underground Test Area strategy, was last amended December 7, 2000, Revision No. 1.

Fenelon, J.M. 2005. *Analysis of Ground-Water Levels and Associated Trends in Yucca Flat, Nevada Test Site, Nye County, Nevada, 1951-200*3, Scientific Investigations Report 2005-5175. Carson City, NV: U.S. Geological Survey.

Ferguson, J.F., A.H. Cogbill, and R.G. Warren. 1994. "A Geophysical- Geological Transect of the Silent Canyon Caldera Complex, Pahute Mesa, Nevada." In *Journal of Geophysical Research*, Vol. 99(B3): 4323-4339. Columbus, OH: Groundwater Publishing Company.

Fernald, A.T., F.M. Byers, and J.P. Ohl. 1975. *Lithologic Logs and Stratigraphic Units of Drill Holes and Mined Shafts in Areas 1 and 6, Nevada Test Site*, Open-File Report 474-206. Denver, CO: U.S. Geological Survey.

Finnegan, D.L., and J.L. Thompson. 2002. *Laboratory and Field Studies Related to Radionuclide Migration at the Nevada Test Site in Support of the Underground Test Area and Hydrologic Resources Management Projects*, LA-13919-MS. Los Alamos, NM: Los Alamos National Laboratory.

Finnegan, D.L., and J.L. Thompson. 2003. *Laboratory and Field Studies Related to Radionuclide Migration at the Nevada Test Site in Support of the Underground Test Area and Hydrologic Resources Management Projects October 1, 2001-September 30, 2002*, LA-14042-PR. Los Alamos, NM: Los Alamos National Laboratory.

Finnegan, D.L., J.L. Thompson, and B.A. Martinez. 2004. *Laboratory and Field Studies Related to Radionuclide Migration at the Nevada Test Site in Support of the Underground Test Area and Hydrologic Resources Management Projects October 1, 2002-September 30, 2003*, LA-14151-PR. Los Alamos, NM: Los Alamos National Laboratory.

Finnegan, D.L., J.L. Thompson, and B.A. Martinez. 2005. *Laboratory and Field Studies Related to Radionuclide Migration in the Nevada Test Site in Support of the Underground Test Area Project and Hydrologic Resources Management Project, October 1, 2003-September 30, 2004*, LA-14238-PR. Los Alamos, NM: Los Alamos National Laboratory.

Fisher, R.A. 1922. *On the Mathematical Foundations of Theoretical Statistics*. Philos. Trans. Roy. Soc. London Ser. A.

Flint, L.E., A.L. Flint, C.A. Rautman, and J.D. Istok. 1996. *Physical and Hydrologic Properties of Rock Outcrop Samples at Yucca Mountain, Nevada*, Open-File Report 95-280. Denver, CO: U.S. Geological Survey.

Freeze, R.A., and J.A. Cherry. 1979. *Groundwater*. Englewood Cliffs, NJ: Prentice Hall.

Freeze, R.A., J. Massmann, L. Smith, T. Sperling, and B. James. 1990. "Hydrogeological Decision Analysis: I.A Framework." In *Groundwater*, Vol. 28: (5) 738-766. Columbus, OH: Groundwater Publishing Company.

Freifeld, B.M. 2001. *Estimation of Fracture Porosity in an Unsaturated Fractured Welded Tuff Using Gas Tracer Testing*. Department of Civil and Environmental Engineering, University of California, Berkeley, Ph. D. dissertation.

Geldon, A.L., A.M.A. Umari, J.D. Earle, M.F. Fahy, J.M. Gemmell, and J. Darnell. 1998. *Analysis of a Multiple-Well Interference Test in Miocene Tuffaceous Rocks at the C-Hole Complex, May-June 1995, Yucca Mountain, Nevada*, Water-Resources Investigations Report 97-4166. U.S. Geological Survey.

Gelhar, L.W. 1982. *Analysis of Two-Well Tracer Tests with a Pulse Input*, RHO-BW-CR-131 P. Richland, WA: Rockwell International, Rockwell Hanford Operations.

Gelhar, L.W., C. Welty, and K.R. Rehfeldt. 1992. "A Critical Review of Data on Field-Scale Dispersion in Aquifers." In *Water Resources Research*, 28: 1955-1972. Washington, DC.

Gonzales, J.L., S.L. Drellack, Jr., and W.J. Davies. 1982. *Lithologic and Geophysical Logs of Selected Drill Holes in Eastern Area 7, Nevada Test Site*, DOE/NV/10322-2. Las Vegas, NV: Fenix & Scisson, Inc.

Grisak, G.E., and J.F. Pickens. 1980. "Solute Transport Through Fractured Media: 1. The Effect of Matrix Diffusion." In *Water Resources Research*, Vol. 16(4): 719 730.

Grisak, G.E., and J.F. Pickens. 1981. "An Analytical Solution for Solute Transport Through Fractured Media with Matrix Diffusion." In *Journal of Hydrology*, Vol. 52: 47-52. Elsevier Scientific Publishing Company.

Grisak, G.E., J.F. Pickens, and J.A. Cherry. 1980. "Solute Transport Through Fractured Media: 2. Column Study of Fractured Till." In *Water Resources Research*, Vol. 16(4): 731 739.

Grove, D.B. 1971. *U.S. Geological Survey Tracer Study, Amargosa Desert, Nye County, Nevada Part II: An Analysis of the Flow Field of a Discharging Recharging Pair of Wells*, USGS-474-99 U.S. Geological Survey.

Grove, D.B. 1977. *The Use of Galerkin Finite-Element Methods to Solve Mass-Transport Equations*, Water-Resources Investigations 77-49. U.S. Geological Survey.

Grove, D.B., and W.A. Beetem. 1971. "Porosity and Dispersion Constant Calculations for a Fractured Carbonate Aquifer using the Two Well Tracer Method." In *Water Resources Research*, Vol. 7(1): 128-134. Washington, DC: American Geophysical Union.

Gustavsson, E., and M. Gunnarsson. 2005. *Oskarshamm Site Investigation. Laboratory Data from the Site Investigation Programme for the Transport Properties of the Rock. Boreholes KSH01A, KSH02A, and KLX02A, P-05-18*. Stockholm, Sweden: Svensk Karnbranslehantering AB, Swedish Nuclear Fuel and Waste Management Co.

Halevy, E., and A. Nir. 1962. "The determination of aquifer parameters with the aid of radioactive tracers." In *Journal of Geophysical Research*, Vol. 67, No. 6, pp. 2403 – 2409.

Halford, K.J., R.J. Laczniak, and D.L. Galloway. 2005. *Hydraulic Characterization of Overpressured Tuffs in Central Yucca Flat, Nevada Test Site, Nye County, Nevada*, Scientific Investigations Report 2005-5211. U.S. Geological Survey.

Hansen, D.J., P.D., Greger, C.A. Wills, and W.K. Ostler. 1997. *Nevada Test Site Wetlands Assessment*, Report DOE/NV/11718-124. Prepared for the U.S. Department of Energy, Nevada Operations Office. Las Vegas, NV: Bechtel Nevada.

Hershey, R.L., W. Howcroft, and P.W. Reimus. 2003. *Laboratory Experiments to Evaluate Diffusion of ^{14}C into Nevada Test Site Carbonate Aquifer Matrix*, Publication No. 45180. Las Vegas, NV: Desert Research Institute.

Hiemenz, P.C. 1986. *Principles of Colloid and Surface Chemistry,* Second edition. New York, NY: Marcel Dekker.

Himmelsbach, T., H. Hotzl, and P. Maloszewski. 1998. "Solute Transport Processes in a Highly Permeable Fault Zone of Lindau Fractured Rock Test Site (Germany)." In *Ground Water*, Vol. 36(5): 792-800.

Hodson, J.N., and D.L. Hoover. 1978. *Geologic and Lithologic Log for Drill Hole UE17a, Nevada Test Site*, Open-File Report USGS-1543-1. U.S. Geological Survey.

Hoover, D.L. 1968. "Genesis of Zeolites, Nevada Test Site." In *The Geological Society of America, Inc.*, Memoir 110. Boulder, CO.

Houser, F.N., and F.G. Poole. 1959. *"Granite" Exploration Hole, Area 15, Nevada Test Site, Nye County, Nevada–Interim Report, Part A, Structural Petrographic and Chemical Data,* TEM-836, 58p. Washington, DC: U.S. Geological Survey.

Houser, F.N., and F.G. Poole. 1961. "Age Relations of the Climax Composite Stock, Nevada Test Site, Nye County, Nevada." In *Short Papers in the Geologic and Hydrologic Sciences:* Prof. Paper 424-B, p. B176-177. Washington, DC: U.S. Geological Survey.

Hu, Q., D.K. Smith, T. Rose, L. Glascoe, C. Steefel, and M. Zavarin. 2003. *Radionuclide Mobility at the Nevada Test Site,* UCRL-TR-200953. Livermore, CA: Lawrence Livermore National Laboratory. Available at http://www.llnl.gov/tid/lof/documents/pdf/302632.pdf.

Hu, Q., T.P. Rose, D.L. Finnegan, and A.B. Kersting. 2006. "Interpretation of NTS Hot Well Actinide Data." In *Hydrologic Resources Management Program and Underground Test Area FY 2004 Progress Report*, UCRL-TR-216032, pp. 21-59, T.P. Rose, G.F. Eaton, and A.B. Kersting, eds. Livermore, CA: Lawrence Livermore National Laboratory.

Hudak, P.F. 1994. "Effective Porosity of Unconsolidated Sand; Estimation and Impact on Capture Zone Geometry." In *Environmental Geology,* Vol. 24(2): 140-143.

Hudson, B., and T. Stubbs. 1990. *INGOT Containment Data Report*, MISC-4804. Livermore, CA: Lawrence Livermore National Laboratory.

Huyakorn, P.S., B.H. Lester, and J.W. Mercer. 1983a. "An Efficient Finite Element Technique for Modeling Transport in Fractured Porous Media: 1. Single Species Transport." In *Water Resources Research*, Vol. 19(3): 841-854.

Huyakorn, P.S., B.H. Lester, and J.W. Mercer. 1983b. "An Efficient Finite Element Technique for Modeling Transport in Fractured Porous Media: 2. Nuclide Decay Chain Transport." In *Water Resources Research*, Vol. 19(5): 1286-1296.

IT, see IT Corporation.

Isherwood, D., J. Harrar, and E. Raber. 1982. *Characterization of Climax Granite Ground Water,* UCRL-53309. Livermore, CA: Lawrence Livermore National Laboratory.

IT Corporation. 1995. Written communication. Subject: *Pre-Completion Hydrologic Testing Documentation Package for Well UE-10j*. Prepared for the U.S. Department of Energy, Nevada Operations Office. Las Vegas, NV.

IT Corporation. 1996a. *Hydrologic Parameter Data Documentation Package (Phase 1 Data Analysis Documentation, Volume IV)*, ITLV/10972-181. Las Vegas, NV.

IT Corporation. 1996b. *Regional Geologic Model Data Documentation Package (Phase 1 Data Analysis Documentation, Volume I, Parts 1 and 2)*, ITLV/10972-181. Las Vegas, NV.

IT Corporation. 1996c. *Wells ER-6-1 and ER-6-2 Core Fracture Analyses and Geophysical Log Comparisons*, ITLV/10972-171. Las Vegas, NV.

IT Corporation. 1998. *Report and Analysis of the BULLION Forced-Gradient Experiment,* ITLV/13052-042. Las Vegas, NV.

IT Corporation. 1999. *Value of Information Analysis for Corrective Action Unit 97: Yucca Flat, Nevada Test Site, Nevada*, DOE/NV/13052--079; ITLV/13052--079. Las Vegas, NV.

IT Corporation. 2001. *Underground Test Area Fracture Analysis Report: Analysis of Fractures in Volcanic Rocks of Western Pahute Mesa – Oasis Valley*, ITLV/13052-150. Las Vegas, NV.

IT Corporation. 2002a. *Analysis of Well ER-18-2 Testing, Western Pahute Mesa-Oasis Valley FY 2000 Testing Program*, DOE/NV/13052--845; ITLV/13052--172. Las Vegas, NV.

IT Corporation. 2002b. *Analysis of Well ER-EC-1 Testing, Western Pahute Mesa-Oasis Valley FY 2000 Testing Program*, DOE/NV/13052--846; ITLV/13052--173. Las Vegas, NV.

IT Corporation. 2002c. *Analysis of Well ER-EC-4 Testing, Western Pahute Mesa-Oasis Valley FY 2000 Testing Program*, DOE/NV/13052--850; ITLV/13052--175. Las Vegas, NV.

IT Corporation. 2002d. *Analysis of Well ER-EC-5 Testing, Western Pahute Mesa-Oasis Valley FY 2000 Testing Program*, DOE/NV/13052--848; ITLV/13052--176. Las Vegas, NV.

IT Corporation. 2002e. *Analysis of Well ER-EC-6 Testing, Western Pahute Mesa-Oasis Valley FY 2000 Testing Program*, DOE/NV/13052--849; ITLV/13052--177. Las Vegas, NV.

IT Corporation. 2002f. *Analysis of Well ER-EC-7 Testing, Western Pahute Mesa-Oasis Valley FY 2000 Testing Program*, DOE/NV/13052--852; ITLV/13052--178. Las Vegas, NV.

IT Corporation. 2002g. *Analysis of Well ER-EC-8 Testing, Western Pahute Mesa-Oasis Valley FY 2000 Testing Program*, DOE/NV/13052--847; ITLV/13052--179. Las Vegas, NV.

Jakob, A. 2004. *Matrix Diffusion for Performance Assessment - Experimental Evidence, Modelling Assumptions and Open Issues*, PSI Bericht Nr. 04-08. Nuclear Energy and Safety Research Department Laboratory for Waste Management.

Johnston, R.H. 1968. *U.S. Geological Survey Tracer Study, Amargosa Desert, Nye County, Nevada. Part I: Exploratory Drilling, Tracer Well Construction and Testing, and Preliminary Findings*, Open-File Report 68-152. Washington, DC: U.S. Geological Survey.

Jones, B.F. 1982. *Mineralogy of Fine Grained Alluvium from Borehole U11G, Expl. 1, Northern Frenchman Flat Area, Nevada Test Site*, USGS-OFR-82-765. Denver, CO: U.S. Geological Survey, U.S. Department of Energy, Nevada Operations Office.

Jones, T.L., V.A. Kelley, J.F. Pickens, D.T. Upton, R.L. Beauheim, and P.B. Davies. 1992. *Integration of Interpretation Results of Tracer Tests Performed in the Culebra Dolomite at the Waste Isolation Pilot Plant Site*, SAND92-1579-UC-721. Albuquerque, NM: Sandia National Laboratories.

Journel, A.G., and C.J. Huijbregts. 1978. *Mining Geostatistics*. New York, NY: Academic Press.

Keller, G.V., and A.W. Ibrahim. 1982. *Research of the Physical Properties of Geothermal Reservoir Rocks*. Golden, CO: The Department of Geophysics, Colorado School of Mines.

Kersting, A.B. 1996. *The State of the Hydrologic Source Term*, UCRL-ID-126557. Livermore, CA: Lawrence Livermore National Laboratory.

Kersting, A.B., and P.W. Reimus, eds. 2003. *Colloid-Facilitated Transport of Low-Solubility Radionuclides: A Field, Experimental, and Modeling Investigation*, UCRL-ID-149688. Livermore, CA: Lawrence Livermore National Laboratory.

Kersting, A.B., D.W. Efurd, D.L. Finnegan, D.J. Rokop, D.K. Smith, and J.L. Thompson. 1998. "Migration of Plutonium in Groundwater at the Nevada Test Site." In *Hydrologic Resources Management Program and Underground Test Area Operable Unit FY 1997 Progress Report*, UCRL-ID-130792. Livermore, CA: Lawrence Livermore National Laboratory.

Kersting, A.B., P. Zhao, M. Zavarin, E.R. Sylvester, P.G. Allen, L. Wang, E.J. Nelson, and R.W. Williams, eds., T.P. Rose, G.G. Eaton, and R.I. Yamamoto. 2002. "Chapter 5 – Report on Field, Laboratory and Modeling Results on Mineral Colloids." In *Hydrologic Resources Management Program and Underground Test Area Project Fy2000 Progress Report*, UCRL-ID-145167: 37-59. Livermore, CA: Lawrence Livermore National Laboratory.

Klinkenberg, L.J. 1951a. "Analogy Between Diffusion and Electrical Conductivity in Porous Rocks." In *Bulletin of the Geological Society of America*, Vol. 62: 559-564.

Klinkenberg, L.J. 1951b. *The Permeability of Porous Media to Liquids and Gases*: Amer. Petro. Inst. Drilling Prod. Pract. 200-231.

Knox, J.B., D.E. Rawson, and J.A. Korve. 1965. "Analysis of a Groundwater Anomaly Created by an Underground Nuclear Explosion." In *Journal of Geophysical Research*, Vol. 70(4): 823-835.

Krupka, K.M., and R.J. Serne. 2002. *Geochemical Factors Affecting the Behavior of Antimony, Cobalt, Europium, Technetium, and Uranium in Vadose Sediments*, PNNL-14126. Richland, WA: Pacific Northwest National Laboratory.

Kung, K.S. 2000. *Colloid Characterization and Quantification in Groundwater Samples*, LAS-13727-MS. Los Alamos, NM: Los Alamos National Laboratory.

Laczniak, R.J., J. Cole, D.A. Sawyer, and D.A. Trudeau. 1996. *Summary of Hydrogeologic Controls on Ground-Water Flow at the Nevada Test Site, Nye County, Nevada*, Water-Resources Investigations Report 96-4109. Carson City, NV: U.S. Geological Survey.

Lallemand-Barres, P., and P. Peaudecerf. 1978. *Recherche des relations entre la valeur de la dispersivite macroscopique d'un milieu aquifere, ses autres caracteristiques et les conditions de mesure, etude bibligraphique:* Buleetin, Bureau de Recherches Geologiques et Minieres, Sec. 3/4:227-87.

Langmuir, D. 1997. S*olutions Manual - Aquous Environmental Geochemistry.* Upper Saddle River, NJ: Prentice Hall, Inc.

Lavenue, A.M., and P.A. Domenico. 1986. "A Preliminary Assessment of the Regional Dispersivity of Selected Basalt Flows at the Hanford Site, Washington, U.S.A." In *Journal of Hydrology,* Vol. 85: 151-167.

Leap, D.I., and P.M. Belmonte. 1992. "Influence of Pore Pressure on Apparent Dispersivity of a Fissured Mitic Dolomitic Aquifer." In *Groundwater,* Vol. 30(1): 87-95. Columbus, OH: Groundwater Publishing Company.

Lenda, A., and A. Zuber. 1970. "Tracer dispersion in groundwater experiments." In *Proceedings: Isotope Hydrology 1970*, p. 619 – 641. IAEA, Vienna, Austria.

Lerman, A. 1979. *Geochemical Processes: Water and Sediment Environments*. New York, NY: John Wiley & Sons.

Lindberg, R.E., and D.D. Runnells. 1984. "Ground water redox reactions: An analysis of equilibrium state applied to Eh measurements and geochemical modeling." In *Science* 225: 925-27.

Liu, H.-H., C.B. Haukawa, C.F. Ahlers, G.S. Bodvarsson, A.L. Flint, and W.B. Guertal. 2003. "Modeling flow and transport in usaturated fractured rock? An evaluation of the continuum approach." In *Journal of Contaminant Hydrology,* Vol. 62-63: 173-188.

Liu, H.-H., G.S. Bodvarsson, and G. Zhang. 2006. "Scale Dependency of the Effective Matrix Diffusion Coefficient." In *Vadose Zone Journal*, Vol. 3: 312-315.

Lu, N., and P.W. Reimus. 2003. "Summary of Radionuclide-Colloid Batch Sorption and Desorption Measurements for the Yucca Mountain Project." In *Colloid-Facilitated Transport of Low-Solubility Radionuclides: A Field, Experimental, and Modeling Investigation*, UCRL-ID-149688. Livermore, CA: Lawrence Livermore National Laboratory.

Lu, N., C.R. Cotter, H.D. Kitten, and J. Bentley. 1998a. "Reversibility of Sorption of Plutonium-239 onto Colloids of Hematite and Goethite." In *Radiochimica Acta*, Vol. 83: 167-173. Munich, Germany: R.Oldenburg.

Lu, N., I.R. Triay, C.R. Cotter, H.D. Kitten, and J. Bentley. 1998b. *Reversibility of Sorption of Plutonium-239 onto Colloids of Hematite, Goethite, Smectite and Silica*, LA-UR-98-3057. Los Alamos, NM: Los Alamos National Laboratory.

Lu, N., J. Conca, G.R. Parker, P.A. Leonard, B. Moore, E.A. Strietelmeier, and I.R. Triay. 2000. *Adsorption of Actinides onto Colloids as a Function of Time, Temperature, Ionic Strength and Colloid Concentration*, LA-UR-00-5121. Los Alamos, NM: Los Alamos National Laboratory.

Lyles, B.F., J. Edkins, R.L. Jacobson, and J.W. Hess. 1990. *Time-Series Analysis of Ion and Isotope Geochemistry of Selected Springs of the Nevada Test Site, Nye County, Nevada*, Water Resources Center, Report Publication, No. 45068, DOE/NV/10384-27. Prepared for the U.S. Department of Energy, Nevada Operations Office. Las Vegas, NV: Desert Research Institute.

Maldonado, F. 1977. *Summary of the Geology and Physical Properties of the Climax Stock, Nevada Test Site*, Open-File Report 77-356. Denver, CO: U.S. Geological Survey.

Maldonado, F., S.G. Steel, and D.R. Townsend. 1979. *Supplementary Lithologic Logs of Selected Vertical Drill Holes in Area 12, Nevada Test Site*, USGS-474-261. Denver, CO: U.S. Geological Survey.

Mas-Pla, J., T.-C.J. Yeh, J.F. McCarthy, and T.M. Williams. 1992. "A Forced Gradient Tracer Experiment in a Coastal Sandy Aquifer, Georgetown Site, South Carolina." In *Ground Water*, Vol. 30(6): 958-964.

Mathews, M., K. Hahn, J. Thompson, L. Gedeken, and W. Madigen. 1994. "Subsurface Radionuclide Investigation of a Nuclear Test." In *Journal of Applied Geophysics*, Vol. 32: 279-291.

Mazurek, M., and A. Jakob. 2002. "Evidence for Matrix Diffusion in the TRUE-1 Block at Aspo Based on Fracture Characterization and Modelling of Tracer Tests." In *Radionuclide Retention in Geologic Media*, Workshop Proceedings, Oskarshamn, Sweden, 7-9 May 2001, Nuclear Energy Agency, Paris, France OECD 2002, 137-154 (2002).

McArthur, R.D. 1962. *Preliminary Geologic Data From Drill Hole U15a 28S, HARDHAT Event, NTS*, GN 4-62. Livermore, CA: University of California, Lawrence Radiation Laboratory.

McArthur, R.D. 1963. *Geologic and Engineering Effects The HARDHAT Event, (Preliminary)*, UCID-4580. Livermore, CA: University of California, Lawrence Radiation Laboratory.

McKenna, S.A., and C.A. Rautman. 1996. *Scaling of Material Properties for Yucca Mountain: Literature Review and Numerical Experiments on Saturated Hydraulic Conductivity*, SAND95-1338. Albuquerque, NM: Sandia National Laboratories.

Mehta, M.M., V.S. Gupta, and W.H. Somerton. 1964. *Changes in Physical Properties of Rocks in the Vicinity of an Underground Nuclear Explosion*, UCRL-13105. Livermore, CA: Lawrence Livermore National Laboratory.

Meijer, A. 1990. *Yucca Mountain Project Far-Field Sorption Studies and Data Needs*, LA-11671-MS. Los Alamos, NM: Los Alamos National Laboratory.

Meijer, A. 1992. "A Strategy for the Derivation and Use of Sorption Coefficients in Performance Assessment Calculations for the Yucca Mountain Site." In *Proceedings of the DOE/Yucca Mountain Site Characterization Project Radionuclide Adsorption Workshop*, held at Los Alamos National Laboratory on September 11-12, 1990, LA-12325-C. Los Alamos, NM: Los Alamos National Laboratory.

Metcalf, J.G., H.E. Huckins-Gang, B.M. Allen, and M.J. Townsend. 1999. Written communication. Subject: *Geology and Rock Mass Character of U16b Tunnel and Vicinity, Nevada Test Site, Nye County, Nevada*. Las Vegas, NV: Bechtel Nevada.

Miller, C. 1989. *Modeling Molecular Diffusion in No-Migration Demonstration, Proceedings of the International Symposium on Class I and II Well Technology.* Dallas, TX: US EPA and the Underground Injection Practices Council Research Foundation.

Mills, R. 1973. "Self-Diffusion in Normal and Heavy Water in the Range 1-45°." In *The Journal of Physical Chemistry*, Vol. 77(5): 685-688.

Mills, R., and V.M.M. Lobo. 1989. *Self-Diffusion in Electrolyte Solutions, a Critical Examination of Data Compiled from the Literature*. New York, NY: Elsevier Science Publishing Company, Inc.

Moench, A.F. 1989. "Convergent Radial Dispersion: A Laplace Transform Solution for Aquifer Tracer Testing." In *Water Resources Research*, Vol. 25 (3): 439-447. Washington, DC: American Geophysical Union.

Moench, A.F. 1995. "Convergent Radial Dispersion in a Double-Porosity Aquifer with Fracture Skin: Analytical Solution and Application to a Field Experiment in Fractured Chalk." In *Water Resources Research*, Vol. 31(8): 1823-1835.

Moncure, G.K., R.C. Surdam, and H.L. McKague. 1981. "Zeolite Diagenesis Below Pahute Mesa, Nevada Test Site." In *Clays and Clay Minerals*, Vol. 29(5): 385-396. Washington, DC: The Clay Minerals Society.

Moreno, L., I. Neretnieks, and T. Eriksen. 1985. "Analysis of Some Laboratory Tracer Runs in Natural Fissures." In *Water Resources Research*, Vol. 21(7): 951-958.

Murray, W.A. 1981. *Geohydrology of the Climax Stock Granite and Surrounding Rock Formations, NTS*, UCRL-53138. Livermore, CA: Lawrence Livermore National Laboratory.

NNSA/NSO, see U.S. Department of Energy, National Nuclear Security Administration Nevada Site Office.

NSTec, see National Security Technologies, LLC.

National Security Technologies, LLC. 2007. *A Hydrostratigraphic Model and Alternatives for the Groundwater Flow and Contaminant Transport Model of Corrective Action Unit 99: Rainier Mesa-Shoshone Mountain, Nye County, Nevada*. DOE/NV/29546--146. Las Vegas, NV.

Neretnieks, I. 1980. "Diffusion in the Rock Matrix: An Important Factor in Radionuclide Retardation?" In *Journal of Geophysical Research*, Vol. 85(B8): 4379-4397. Washington, DC: American Geophysical Union.

Neretnieks, I., T. Eriksen, and P. Tahtinen. 1982. "Tracer Movement in a Single Fissure in Granitic Rock: Some Experimental Results and Their Interpretation." In *Water Resources Research*, Vol. 18(4): 849-858.

Nervik, W.E. 1970. "Radioactivity." In *The Handcar Nuclear Explosion in Dolomite*, UCRL-50951, Werth, G.C. (ed.). Livermore, CA: Lawrence Livermore National Laboratory.

Neuman, S.P. 1990. "Universal Scaling of Hydraulic Conductivities and Dispersivities in Geologic Media." In *Water Resources Research*, Vol. 26(8): 1749-1758. Washington, DC: American Geophysical Union.

Neuman, S.P. 1995. "On Advective Transport in Fractal Permeability and Velocity Fields." In *Water Resources Research*, Vol. 31(6): 1455-1460.

Neuman, S.P., and V. Di Federico. 2003. "Multifaceted Nature of Hydrogeologic Scaling and Its Interpretation." In *Reviews of Geophysics*, Vol. 41(3): 1014.

Nevada Bureau of Mines and Geology. 1996. *County Digital Geologic Mapping Project-Final Report*, Open-File Report 97-1, Scale 1:250,000. U.S. Geological Survey.

Newman, J.S. 1991. *Electrochemical Systems*. Englewood Cliffs, NJ: Prentice Hall.

Noorishad, J., and M. Mehran. 1982. "An Upstream Finite Element Method for Solution of Transient Transport Equation in Fractured Porous Media." In *Water Resources Research*, Vol. 18(3): 588-596.

Novakowski, K.S., and P.A. Lapcevic. 1994. "Field Measurement of Radial Solute Transport in Fractured Rock." In *Water Resources Research*, Vol. 30(1): 37-44.

Ogard, A.E., and J.F. Kerrisk. 1984. *Groundwater Chemistry Along Flow Paths Between a Proposed Repository Site and the Accessible Environment*. Los Alamos, NM: Los Alamos National Laboratory.

Ogard, A.E., J.L. Thompson, R.S. Rundberg, K. Wolfsberg, P.W. Kubic, D. Eklmore, and H.W. Bentley. 1988. "Migration of Chlorine-36 and Tritium from an Underground Nuclear Test." In *Radiochim. Acta*, Vol. 44/45: 213-217. Munich, Germany: R. Oldenburg.

Orkild, P.P., D.R. Townsend, M.J. Baldwin, D.L. Healey, G.D. Bath, C.E. Jahren, and J.G. Rosenbaum. 1983. *Geologic and Geophysical Investigations of Climax Stock Intrusive, Nevada*, Open-File Report 83-377, 82 pp. Denver, CO: U.S. Geological Survey

Palisade Corporation. 2002. "A Concise Summary of @Risk Probability Distribution Functions." Supplemental Document to Guide to Using BestFit; Distribution Fitting for Windows, Version 4.5 (included on the CD as part of the software package). Newfield, NY.

Papelis, C., and W. Um. 2003a. *Evaluation of Cesium, Strontium, and Lead Sorption, Desorption, and Diffusion in Volcanic Tuffs from Frenchman Flat, Nevada Test Site: Macroscopic and Spectroscopic Investigations*, DOE/NV/13609-18; Publication No. 45189. Las Vegas, NV: Desert Research Institute.

Papelis, C., and W. Um. 2003b. *Evaluation of Cesium, Strontium, and Lead Sorption, Desorption, and Diffusion in Volcanic Tuffs from Western Pahute Mesa, Nevada Test Site, Based on Macroscopic and Spectroscopic Investigations*, DOE/NV/13609-16; Publication No. 45187. Las Vegas, NV: Desert Research Institute.

Pawloski, G.A., A.F.B. Tompson, and S.F. Carle. 2001. *Evaluation of the Hydrologic Source Term from Underground Nuclear Tests on Pahute Mesa at the Nevada Test Site: CHESHIRE Test*, UCRL-ID-147023. Livermore, CA: Lawrence Livermore National Laboratory.

Perkins, W.G., D.A. Lucero, and G.O. Brown. 1998. *Column Experiments for Radionuclide Adsorption Studies of Culebra Dolomite: Retardation Parameter Estimation for Non-Eluted Actinide Species*, SAND98-1005. Albuquerque, NM: Sandia National Laboratories.

Phelps, G. A., V.E. Langenheim, and R.C. Jachens. 1999. *Thickness of Cenozoic Deposits of Yucca Flat Inferred from Gravity Data, Nevada Test Site, Nevada*, Open-File Report OF 99-310. U.S. Geological Survey.

Phelps, G.A., E.H. McKee, D.S. Sweetkind, and V.E. Langenheim. 2000. *Preliminary Model of the Pre-Tertiary Basement Rocks Beneath Yucca Flat, Nevada Test Site, Nevada, Based on Analysis of Gravity and Magnetic Data*, Open-File Report OF 00-134. U.S. Geological Survey.

Phelps, G.A., A.L. Justet, B.C. Moring, and C.W. Roberts. 2005. *A Preliminary Investigation of the Structure of Southern Yucca Flat, Massachusetts Mountain, and CP Basin, Nevada Test Site, Nevada, Based on Geophysical Modeling*, Open-File Report-2005-1367. U.S. Geological Survey.

Pickens, J.F., and G.E. Grisak. 1981a. "Scale-Dependent Dispersion in a Stratified Granular Aquifer." In *Water Resources Research*, Vol. 17(4): 1191-1211.

Pickens, J.F., and G.E. Grisak. 1981b. "Modeling of Scale-Dependent Dispersion in Hydrogeologic Systems." In *Water Resources Research*, Vol. 17(6): 1701-1711.

Poole, F.G., F.N. Houser, and P.P. Orkild. 1961. *Eleana Formation of Nevada Test Site and Vicinity, Nye County, Nevada*, Professional Paper 424-D: D-104-D-111. U.S. Geological Survey.

Prothro, L.B. 1998. Written communication. Subject: *Analysis of Fractures in Cores from the Tuff Confining Unit Beneath Yucca Flat, Nevada Test Site*. Las Vegas, NV: Bechtel Nevada.

Prothro, L.B. 2005. *Mineralogic Zonation Within the Tuff Confining Unit, Yucca Flat, Nevada Test Site*, DOE/NV/11718--995. Las Vegas, NV: Bechtel Nevada.

Prothro, L.B., and S.L. Drellack, Jr. 1997a. *Nature and Extent of Lava-Flow Aquifers Beneath Pahute Mesa, Nevada Test Site*, DOE/NV-11718--156. Las Vegas, NV: Bechtel Nevada.

Prothro, L.B., and S.L. Drellack, Jr. 1997b. *Review and Reconnaissance of the Hydrogeology of Tertiary Sedimentary Rocks in the Vicinity of Frenchman Flat, Nevada Test Site*, DOE/NV/11718--155. Las Vegas, NV: Bechtel Nevada.

Prothro, L.B., S.L. Drellack, Jr., and B.M. Allen. 1999. *Lithology and Stratigraphy of Holes Drilled in LANL-Use Areas of the Nevada Test Site, Volume XIII, 1991-1998*, DOE/NV/11718--254. Las Vegas, NV: Bechtel Nevada.

Ptak, T., and G. Teutsch. 1994. "Forced and Natural Gradient Tracer Tests in a Highly Heterogeneous Porous Aquifer: Instrumentation and Measurements." In *Journal of Hydrology*, Vol. 159: 79-104.

Quade, J., and J.V. Tingley. 1983. *A Mineral Inventory of the Nevada Test Site, and Portions of Nellis Bombing and Gunnery Range, Southern Nye County, Nevada*, DOE/NV/10295-1. Reno, NV: Nevada Bureau of Mines and Geology.

Quong, R. 1969. *Permeability Increases in Hardhat Ganodiorite Samples Fractured by Exploding Foils*, UCRL-50783. Livermore, CA: University of California, Lawrence Radiation Laboratory.

Rabb, D.D. 1968. *Size-Distribution Study of Piledriver Particles*, UCRL-50489. Livermore, CA: University of California, Lawrence Radiation Laboratory.

Ramspott, L.D., and R.D. McArthur. 1977. *Results of the Exploratory Drill Hole Ue5n, Frenchman Flat, Nevada Test Site*, UCID-17392. Livermore, CA: Lawrence Livermore Laboratory.

Rayburn, C.J., S.L. Drellack, Jr., and P.H. Thompson. 1989. "Occurrence, Distribution, and Measurement of Carbonate in the Alluvium of Southern Yucca Flat, Nevada Test Site." In *Proceedings of the Fifth Symposium on the Containment of Underground Nuclear Explosions*, CONF-8909163, Vol. 2: 186-205. Santa Barbara, CA: Lawrence Livermore National Laboratory.

Rehfeldt, K, W. Drici, D. Sloop, J. Watrus, T. Beard, M. Sully, C. Benedict, A. Wolfsberg, and P. Reimus. 2003. *Contaminant Transport Parameters for the Groundwater Flow and Contaminant Transport Model of Correction Action Units 101 and 102: Central and Western Pahute Mesa, Nye County, Nevada*, Shaw/13052-201. Las Vegas, NV: Shaw Environmental, Inc.

Reimus, P.W. 2003. "A Refined Approach to Estimating Effective Flow Porosity from Cross-Hole Tracer Tests in Fractured Media." In *Proceedings of the 10th International High-Level Radioactive Waste Management Conference*, American Nuclear Society, March 30-April 2, Las Vegas, NV, pp. 159-170.

Reimus, P.W., Los Alamos National Laboratory. 2006. Personal communication to P. Montazer and I. Farnham (SNJV) regarding dispersion data, 6 June.

Reimus, P.W., Los Alamos National Laboratory. 2007a. Personal communication to W. Fryer (SNJV) regarding comments on colloid-facilitated transport, 11 March.

Reimus, P.W. 2007b. *Saturated Zone In-Situ Testing*, Yucca Mountain Project Analysis Report, ANL-NBS-HS-0 00039, Rev. 02 (Appendix G). Las Vegas, NV.

Reimus, P.W. 2007c. *Semi-Analytical Interpretations of ER-6-1 Multiple-Well Tracer Test Results*, LA-UR-07-1410. Los Alamos, NM: Los Alamos National Laboratory.

Reimus, P.W., and T.J. Callahan. 2006. *Matrix Diffusion Rates in Fractured Volcanic Rock at the Nevada Test Site: Evidence for a Dominant Influence of Effective Fracture Apertures*, LA-UR-06-7126. Los Alamos, NM: Los Alamos National Laboratory.

Reimus, P.W., and M.J. Haga. 1999. *Analysis of Tracer Responses in the BULLION Forced-Gradient Experiment at Pahute Mesa, Nevada*, LA-13615-MS. Los Alamos, NM: Los Alamos National Laboratory.

Reimus, P.W., A. Adams, M.J. Haga, A. Humphrey, T. Callahan, I. Anghel, and D. Counce. 1999. *Results and Interpretation of Hydraulic and Tracer Testing in the Prow Pass Tuff at the C-Holes,* Yucca Mountain Site Characterization Project Milestone Report SP32E7M4. Los Alamos, NM: Los Alamos National Laboratory.

Reimus, P.W., S.D. Ware, N. Lu, K.S. Kung, A.I. Abdel-Fattah, I. Anghel, M.P. Neu, and S.D. Reilly. 2002a. "Chapter 7 - Colloid-Facilitated Plutonium Fracture Transport Experiments." In *Colloid-Facilitated Transport of Low-Solubility Radionuclides: A Field, Experimental, and Modeling Investigation,* UCRL-ID-149688. Livermore, CA: Lawrence Livermore National Laboratory and Los Alamos, NM: Los Alamos National Laboratory.

Reimus, P.W., M.J. Haga, A.R. Humphrey, D.A. Counce, T.J. Callahan, S.D. Ware, A. Adams, B. Wilson, and D. Gonzales. 2002b. *Diffusion Cell and Fracture Experiments to Support Interpretations of the BULLION Forced-Gradient Experiment,* LA-UR-02-6884. Los Alamos, NM: Los Alamos National Laboratory.

Reimus, P.W., S.D. Ware, F.C. Benedict, R.G. Warren, A. Humphrey, A. Adams, B. Wilson, and D. Gonzales. 2002c. *Diffusive and Advective Transport of ^{3}H, ^{14}C, and ^{99}Tc in Saturated, Fractured Volcanic Rocks from Pahute Mesa, Nevada,* LA-13891-MS. Los Alamos, NM: Los Alamos National Laboratory.

Reimus, P.W., M.J. Umari, R. Roback, J. Earle, J. Darnell, and I. Farnham. 2003a. *Estimates of Ambient Groundwater Velocity in the Alluvium South of Yucca Mountain, from Single-Well Tracer Tests,* LA-UR-02-5778. Los Alamos, NM: Los Alamos National Laboratory.

Reimus, P., G. Pohll, T. Miheve, J. Chapman, M. Haga, B. Lyles, S. Kosinski, R. Niswonger, and P. Sanders. 2003b. "Testing and Parameterizing A Conceptual Model for Solute Transport in A Fractured Granite Using Multiple Tracers in A Forced-Gradient Test." In *Water Resources Research,* Vol. 39(12): 1356, doi: 10.1029/2002WR001597. Washington, DC: American Geophysical Union.

Reimus, P.W., M. Murrell, A. Abdel-Fattah, E. Garcia, D. Norman, S. Goldstein, A. Nunn, R. Gritzo, and B. Martinez. 2006a. *Colloid Characteristics and Radionuclide Associations with Colloids in Near-Field Waters at the Nevada Test Site (FY 2005),* LA-UR-05-8612. Los Alamos, NM: Los Alamos National Laboratory.

Reimus, P.W., T.J. Callahan, S.D. Ware, M.J. Haga, and D.A. Counce. 2006b. *Matrix Diffusion Coefficients in Volcanic Rocks at the Nevada Test Site: Influence of Matrix Porosity, Matrix Permeability, and Fracture Coating Minerals,* LA-UR-06-7127. Los Alamos, NM: Los Alamos National Laboratory.

Reimus, P.W., R.L. Hershey, D.L. Decker, S.D. Ware, C. Papelis, S. Earman, A. Abdel-Fattah, M. Haga, D. Counce, S. Chipera, and C. Sedlacek. 2006c. *Tracer Transport Properties in the Lower Carbonate Aquifer of Yucca Flat,* LA-UR-06-0486. Los Alamos, NM: Los Alamos National Laboratory.

Rivett, M.O., S. Feenstra, and J.A. Cherry. 1994. "Transport of a Dissolved-Phase Plume from a Residual Solvent Source in a Sand Aquifer." In *Journal of Hydrology*, Vol. 159: 27-41.

Russell, C.E., D. Gillespie, J.C. Cole, S.L. Drellack, L.B. Prothro, P.H. Thompson, R.L. McCall, G.A. Pawloski, and R. Carlson. 1996. *Completion Report for Well ER-12-1*, DOE/NV/10845-36. Las Vegas, NV.

Shaw, see Shaw Environmental, Inc.

SNJV, see Stoller-Navarro Joint Venture.

Sauty, J.P. 1980. "An Analysis of Hydrodispersive Transfer in Aquifers." In *Water Resources Research*, Vol. 16 (1): 145-158. Washington, DC: American Geophysical Union.

Schijven, J.F., W. Hoogenboezem, S.M., Hassanizadeh, and J.H. Peters. 1999. "Modeling Removal of Bacteriophages MS2 and PRD1 by Dune Recharge at Castricum, Netherlands." In *Water Resources Research*, Vol. 35 (4): 1101-1111. Washington, DC: American Geophysical Union.

Schoff, S.L., and J.E. Moore. 1964. *Chemistry and Movement of Ground Water, Nevada Test Site*, Report TEI-838, p. 75. Denver, CO: U.S. Geological Survey.

Schulze-Makuch, D. 2005. "Longitudinal Dispersivity Data and Implications for Scaling Behavior." In *Ground Water*, Vol. 43(3): 443-456.

Shaw Environmental, Inc. 2003a. *Contaminant Transport Parameters for the Groundwater Flow and Transport Model of Corrective Actions Units 101 and 102: Central and Western Pahute Mesa, Nye County, Nevada*, Shaw/13052--201-CD Rev. 0. Las Vegas, NV.

Shaw Environmental, Inc. 2003b. *Modeling Approach/Strategy for Corrective Action Unit 97, Yucca Flat and Climax Mine*, Shaw/13052-305. Las Vegas, NV.

Short, N.M. 1964. *Memorandum: Variations in Physical Properties of the HARDHAT Medium*, UCID-4775. Livermore, CA: Lawrence Livermore National Laboratory.

Skagius, K., and I. Neretnieks. 1986. "Porosities and Diffusivities of Some Nonsorbing Species in Crystalline Rocks." In *Water Resources Research*, Vol. 22(3): 389-398. Washington, DC: American Geophysical Union.

Slate, J.L., M.E. Berry, P.D. Rowley, C.J. Fridrich, K.S. Morgan, J.B. Workman, O.D. Young, G.L. Dixon, V.S. Williams, E.H. McKee, D.A. Ponce, T.G. Hildenbrand, W.C. Swadley, S.C. Lundstrom, E.B. Ekren, R.G. Warren, J.C. Cole, R.J. Fleck, M.A. Lanphere, D.A. Sawyer, S.A. Minor, D.J. Grunwald, R.J. Laczniak, C.M. Menges, J.C. Yount, and A.S. Jayko. 1999. *Part A. Digital Geologic Map of the Nevada Test Site and Vicinity, Nye, Lincoln, and Clark Counties, Nevada, and Inyo County, California, Revision 4*, Open-File Report 99-554-A, scale 1:120,000. Denver, CO: U.S. Geological Survey.

Smith, D.K. 1997. *A Recent Drilling Program to Investigate Radionuclide Migration at the Nevada Test Site, Fourth International Conference on Methods and Applications of Radioanalytical Chemistry*, April 6-11, Kona, HI, UCRL-JC-127013. Livermore, CA: Lawrence Livermore National Laboratory.

Smith, D.K. 1998. "A Recent Drilling Program to Investigate Radionuclide Migration at the Nevada Test Site." In *Journal of Radioanalytical Nuclear Chemistry*, Vol. 235: 159-166.

Smith, D.K. 2002. *Evaluation of the Radiochemistry of Near-Field Water Samples at the Nevada Test Site Applied to the Definition of a Hydrologic Source Term*, UCRL-ID-149049. Livermore, CA: Lawrence Livermore National Laboratory.

Smith, D.K., B.K. Esser, J.M. Kenneally, R.J. Nagle, J.H. Rego, and J.L. Royval. 1996a. *Hydrologic Resources Management Program and Underground Test Area Project FY1995 Progress Report*, UCRL-ID-123486. Livermore, CA: Lawrence Livermore National Laboratory.

Smith, D.K., R.J. Nagle, and J.M. Kenneally. 1996b. "Transport of Gaseous Fission Products Adjacent to an Underground Nuclear Test Cavity." In *Radiochimica Acta*, Vol. 73: 177-183.

Smith, D.K., A.B. Kersting, T.P. Rose, J.M. Kenneally, G.B. Hudson, G. Eaton, and M.L. Davisson. 1998. *Hydrologic Resources Management Program and Underground Test Area Project Operable Unit FY1997 Progress Report*, UCRL-ID-130792. Livermore, CA: Lawrence Livermore National Laboratory.

Smith, D.K., D.L. Finnegan, and S.M. Bowen. 2003. "An Inventory of Long-Lived Radionuclides Residual from Underground Nuclear Testing at the Nevada Test Site, 1951-1992." In *Journal of Environ. Radioactivity*, Vol. 67: 35-51.

Steefel, C.I., and S.B. Yabusaki. 1995. *Software for Modeling Multicomponent-Multidimensional Reactive Transport, User Manual and Programmer's Guide*, OS3D/GIMRT. Richland, WA: Pacific Northwest National Laboratory.

Sterrett, T.S. 1969. *Drilling Investigation of the Lower Part of the Piledriver Cavity*, UCRL-50765. Livermore, CA: Lawrence Livermore National Laboratory.

Stoller-Navarro Joint Venture. 2004a. *Analysis of Well ER-7-1 Testing, Yucca Flat FY 2003 Testing Program, Nevada Test Site, Nevada*, S-N/99205--021. Las Vegas, NV.

Stoller-Navarro Joint Venture. 2004b. *Hydrologic Data for the Groundwater Flow and Contaminant Transport Model of Corrective Action Units 101 and 102: Central and Western Pahute Mesa, Nye County, Nevada*, S-N/99205-002, Shaw/13052-204. Las Vegas, NV.

Stoller-Navarro Joint Venture. 2004c. *Letter Report: Analysis of Well ER-2-1 Hydraulic Testing, Yucca Flat FY 2003, Nevada Test Site, Nevada*, DOE/NV--992. Las Vegas, NV.

Stoller-Navarro Joint Venture. 2004d. *The Role of Dispersion in Radionuclide Transport-Data and Modeling Requirements*, S-N/99205-003, Shaw/13052-200. Las Vegas, NV.

Stoller-Navarro Joint Venture. 2004e. *Transferability of Data Related to the Underground Test Area Project, Nevada Test Site, Nye County, Nevada*, S-N/99205-020. Las Vegas, NV.

Stoller-Navarro Joint Venture. 2005a. *Analysis of Hydraulic Responses from the ER-6-1 Multiple-Well Aquifer Test, Yucca Flat FY 2004 Testing Program, Nevada Test Site, Nye County, Nevada*, S-N/99205--051. Las Vegas, NV.

Stoller-Navarro Joint Venture. 2005b. *Phase II Contaminant Transport Parameters for the Groundwater Flow and Contaminant Transport Model of Corrective Action Unit 98: Frenchman Flat, Nye County, Nevada*, S-N/99205--043. Las Vegas, NV.

Stoller-Navarro Joint Venture. 2005c. *Underground Test Area Fracture Analysis Report for Frenchman Flat Well Clusters ER-5-3 and ER-5-4 Nevada Test Site, Nevada*, S-N/99205--060. Las Vegas, NV.

Stoller-Navarro Joint Venture. 2005d. *Underground Test Area Fracture Analysis Report for Yucca Flat Wells ER-2-1, ER-6-1#2, ER-7-1, and ER-12-2 Nevada Test Site, Nevada*, S-N/99205--040. Las Vegas, NV.

Stoller-Navarro Joint Venture. 2005e. Written communication. Subject: *ER-6-1 Well Cluster Multiple Well Aquifer Test – Tracer Test Data Report: Volume I – Overview,* Rev. 0. Las Vegas, NV.

Stoller-Navarro Joint Venture. 2005f. Written communication. Subject: *ER-6-1 Well Cluster Multiple Well Aquifer Test – Tracer Test Data Report: Volume III – MWAT-TT*, Rev. 0. Las Vegas, NV.

Stoller-Navarro Joint Venture. 2006a. *Comprehensive Water Quality Database for Groundwater in the Vicinity of the Nevada Test Site, Geochem06.mdb,* S-N/99205--059-Rev. 1. Las Vegas, NV.

Stoller-Navarro Joint Venture. 2006b. *Geochemical and Isotopic Evaluation of Groundwater Movement in Corrective Action Unit 97: Yucca Flat/Climax Mine, Nevada Test Site, Nevada,* Rev. 0, S-N/99205--070. Las Vegas, NV.

Stoller-Navarro Joint Venture. 2006c. *Phase I Hydrologic Data for the Groundwater Flow and Contaminant Transport Model of Corrective Action Unit 97: Yucca Flat/Climax Mine, Nevada Test Site, Nye County, Nevada,* Rev. 0, S-N/99205--077. Las Vegas, NV.

Stoller-Navarro Joint Venture. 2006d. *Well ER-6-1 Tracer Test Analysis: Yucca Flat, Nevada Test Site, Nye County, Nevada*, S-N/99205-084. Las Vegas, NV.

Stout, D.L., and S.A. Carroll. 1992. *A Literature Review of Actinide-Carbonate Mineral Interaction*, SAND92-7328. Albuquerque, NM: Sandia National Laboratories.

Tang, D.H., E.O. Frind, and E.A. Sudicky. 1981. "Contaminant Transport in Fractured Porous Media: Analytical Solution for a Single Fracture." In *Water Resources Research*, Vol. 17(3): 555-564.

Thomas, K.W. 1987. *Summary of Sorption Measurements Performed with Yucca Mountain, Nevada, Tuff Samples and Water from Well J-13*, LA-10960-MS. Los Alamos, NM: Los Alamos National Laboratory.

Thompson, J.L. 1988. *Laboratory and Field Studies Related to the Radionuclide Migration Project: October 1, 1986 - September 30, 1987*, LA-11223-PR. Los Alamos, NM: Los Alamos National Laboratory.

Thompson, J.L. 1991. *Laboratory and Field Studies Related to the Hydrology/Radionuclide Migration Project: October 1, 1989 - September 30, 1990*, LA-12100-PR. Los Alamos, NM: Los Alamos National Laboratory.

Thompson, J.L. 1992a. *Laboratory and Field Studies Related to the Hydrologic Resources Management Program: October 1, 1990 - September 30, 1991*, LA-12338-PR. Los Alamos, NM: Los Alamos National Laboratory.

Thompson, J.L. 1992b. "Studies of Fission Product Movement in Tuffaceous Media." In *Radiochim. Acta*, Vol. 58/59: 273-276.

Thompson, J.L. 1994. L*aboratory and Field Studies Related to the Hydrologic Resources Management Program: October 1, 1992 - September 30, 1993*, LA-12721-PR. Los Alamos, NM: Los Alamos National Laboratory.

Thompson, J.L. 1995. *Laboratory and Field Studies Related to the Hydrologic Resources Management Program: October 1, 1993 - September 30, 1994*, LA-12917-PR. Los Alamos, NM: Los Alamos National Laboratory.

Thompson, J.L. 1996a. *Laboratory and Field Studies Associated with the Hydrologic Resources Management Program*, LA-12917-PR. Los Alamos, NM: Los Alamos National Laboratory.

Thompson, J.L. 1996b. "Radionuclide Distribution in a Nuclear Test Cavity: The Baseball Event." In *Radiochim. Acta*, Vol. 72: 157-162.

Thompson, J.L. 1997. *Laboratory and Field Studies Related to the Hydrologic Resources Management Program: October 1, 1995-September 30, 1996*, LA-13270-PR. Los Alamos, NM: Los Alamos National Laboratory.

Thompson, J.L. 1999. *Laboratory and Field Studies Related to Radionuclide Migration at the Nevada Test Site: October 1, 1997-September 30, 1998*, LA-13576-PR. Los Alamos, NM: Los Alamos National Laboratory.

Tomasko, D., M. Reeves, V.A. Kelley, and J.F. Pickens. 1989. "Parameter Sensitivity and Importance for Radionuclide Transport in Double-Porosity Systems." In *Proceedings of the Conference on Geostatistical Sensitivity, and Uncertainty Methods for Ground-Water Flow and Radionuclide Transport Modeling*, p. 279-321, September 15-17, 1987, B.E. Bufton, ed. Battell Press. San Francisco, CA.

Tompson, A.F.B., C.J. Bruton, and G.A. Pawloski. 1999. *Evaluation of the Hydrologic Source Term from the Underground Nuclear Tests in Frenchman Flat and the Nevada Test Site: The CAMBRIC Test*, UCRL-ID-132300. Livermore, CA: Lawrence Livermore National Laboratory.

Tompson, A.F.B., A.B. Kersting, D.L. Finnegan, B.K. Esser, D.K. Smith, M. Zavarin, C.J. Bruton, G.A. Pawloski. 2003. *Radionuclide Decay and In-Growth Technical Basis Document*, UCRL-ID-153798. Livermore, CA: Lawrence Livermore National Laboratory.

Tompson, A.F.B., M. Zavarin, C.J. Bruton, and G.A. Pawloski. 2004. *Methods for Calculating a Simplified Hydrologic Source Term for Frenchman Flat Sensitivity Studies of Radionuclide Transport Away from Underground Nuclear Tests*, UCRL-TR-201817. Livermore, CA: Lawrence Livermore National Laboratory.

Travis, B.J., H.E. Nuttall, S.W. Hodson, and R.S. Rundberg. 1983. "Section B: Transport of Tritium the Cambric Cavity Region to RNM-2S: Modeling." In *Laboratory and Field Studies Related to the Hydrology/Radionuclide Migration Project: October 1, 1981 - September 30, 1982*, LA-9691-PR. Los Alamos, NM: Los Alamos National Laboratory.

Trexler, Jr., J.H., J.C. Cole, and P.H. Cashman. 1996. "Middle Devonian-Mississippian Stratigraphy On and Near the Nevada Test Site: Implications for Hydrocarbon Potential." In *American Association of Petroleum Geologists Bulletin*, Vol. 80(1): 1736-1762.

Triay, I.R., A. Meijer, J.L. Conca, K.S. Kung, R.S. Rundberg, E.A. Strietelmeier, C.D. Tait, D.L. Clark, M.P. Neu, and D.E. Hobart. 1997. *Summary and Synthesis Report on Radionuclide Retardation for the Yucca Mountain Site Characterization Project: Yucca Mountain Site Characterization Program Milestone 3784M*, LA-13262-MS, UC-903 and UC-940. Los Alamos, NM: Los Alamos National Laboratory.

Tsang, Y.W. 1984. "The Effect of Tortuosity on Fluid Flow Through a Single Fracture." In *Water Resources Research*, Vol. 20(9): 1209-1215.

Tsang, Y.W. 1992. "Usage of "Equivalent Apertures" for Rock Fractures as Derived From Hydraulic and Tracer Tests." In *Water Resources Research*, Vol. 28(5): 1451-1455.

USGS, see U.S. Geological Survey.

Umari, A., J.D. Earle, and M.F. Fahy. 2006. "Analysis of Single-Hole and Cross-Hole Tracer Tests Conducted at the Nye County Early Warning Drilling Program Well Complex, Nye County, Nevada." In *International High-Level Waste Management*, 20 April - 4 May. Las Vegas, NV.

U.S. Department of Energy, National Nuclear Security Administration Nevada Site Office. 2003. *Underground Test Area Quality Assurance Project Plan Nevada Test Site, Nevada*, DOE/NV--341-REV. 4. Las Vegas, NV.

U.S. Department of Energy, National Nuclear Security Administration Nevada Site Office. 2004a. *Corrective Action Investigation Plan for Corrective Action Unit 99: Rainier Mesa/Shoshone Mountain, Nevada Test Site, Nevada*, DOE/NV--1031. Las Vegas, NV.

U.S. Department of Energy, National Nuclear Security Administration Nevada Site Office. 2004b. *Well Completion Report for Well ER-2-1*, DOE/NV/11718--893. Las Vegas, NV: Bechtel Nevada.

U.S. Department of Energy, National Nuclear Security Administration Nevada Site Office. 2004c. *Well Completion Report for Well Cluster ER-6-1*, DOE/NV/11718--862. Las Vegas, NV: Bechtel Nevada.

U.S. Department of Energy, National Nuclear Security Administration Nevada Site Office. 2004d. *Well Completion Report for Well ER-7-1*, DOE/NV/11718--865. Las Vegas, NV: Bechtel Nevada.

U.S. Department of Energy, National Nuclear Security Administration Nevada Site Office. 2004e. *Well Completion Report for Well ER-8-1*, DOE/NV/11718--845. Las Vegas, NV: Bechtel Nevada.

U.S. Department of Energy, National Nuclear Security Administration Nevada Site Office. 2004f. *Well Completion Report for Well ER-12-2*, DOE/NV/11718--846. Las Vegas, NV: Bechtel Nevada.

U.S. Department of Energy, Nevada Operations Office. 1992. *Underground Radionuclide Migration at the Nevada Test Site*, DOE/NV-346, UC-703. Livermore, CA: Lawrence Livermore National Laboratory. Los Alamos, NM: Los Alamos National Laboratory.

U.S. Department of Energy, Nevada Operations Office. 1995a. *Completion Report for Well ER-3-1*, DOE/NV--396. Las Vegas, NV.

U.S. Department of Energy, Nevada Operations Office. 1995b. *Completion Report for Well ER-3-2*, DOE/NV--408. Las Vegas, NV.

U.S. Department of Energy, Nevada Operations Office. 1996. *Recompletion Report and Summary of Well History for Well UE-1q*, DOE/NV-444; UC-700. Las Vegas, NV.

U.S. Department of Energy, Nevada Operations Office. 1997a. *Regional Groundwater Flow and Tritium Transport Modeling and Risk Assessment of the Underground Test Area, Nevada Test Site, Nevada,* DOE/NV--477. Las Vegas, NV.

U.S. Department of Energy, Nevada Operations Office. 1997b. *Shaft and Tunnel Nuclear Detonations at the Nevada Test Site: Development of a Primary Database for the Estimation of Potential Interactions with the Regional Groundwater System*, DOE/NV-464, UC-700. Las Vegas, Nevada.

U.S. Department of Energy, Nevada Operations Office. 1998. *Completion Report for Well Cluster ER-20-6*, DOE/NV-467, UC-700. Las Vegas, NV.

U.S. Department of Energy, Nevada Operations Office. 2000a. *Corrective Action Investigation Plan for Corrective Action Unit 97: Yucca Flat/Climax Mine, Nevada Test Site, Nevada,* DOE/NV--659. Las Vegas, NV.

U.S. Department of Energy, Nevada Operations Office. 2000b. *United States Nuclear Tests, July 1945 through September 1992,* DOE/NV--209, Rev. 15. Las Vegas, NV.

U.S. Department of Energy, Office of Civilian Radioactive Waste Management, Office of Repository Development. 2001. *Unsaturated Zone and Saturated Zone Transport Properties (U0100)*, ANL-NBS-HS-000019, Rev. 0, ICN 02. Las Vegas, NV.

U.S. Department of Energy, Office of Civilian Radioactive Waste Management, Office of Repository Development. 2004. *Site-Scale Saturated Zone Transport*, MDL-NBS-HS-000010, Rev 01, ICN 00. Las Vegas, NV.

U.S. Department of Energy, Waste Isolation Pilot Plant. 2004. *Title 40 CFR Part 191 Compliance Certification Application for the Waste Isolation Pilot Plant*, DOE/WIPP 2004-3231. March. Carlsbad, NM: Carlsbad Field Office.

U.S. Environmental Protection Agency. 2000. *Rules and Regulations; Part II Environmental Protection Agency 40 CFR Parts 9, 141, and 142; National Primary Drinking Water Regulations; Radionuclides; Final Rule*. Federal Register, Vol. 65, No. 236.

U.S. Geological Survey. 2006. *Mercury Core Library & Data Center Rock-Property Information Rock-Property Database*. As accessed at http://nevada.usgs.gov/mercury/rock.html on 30 October. Mercury, NV.

van der Kamp, G., D.R. Van Stempvoort, and L.I. Wassenaar. 1996. "The Radial Diffusion Method 1. Using Intact Cores to Determine Isotopic Composition, Chemistry, and Effective Porosities for Groundwater in Aquitards." In *Water Resources Research*, Vol. 32 (6): 1815-1822.

Van Golf-Racht, T.D. 1982. *Developments in Petroleum Science 12: Fundamentals of Fractured Reservoir Engineering*. Elsevier, New York, NY.

Vanmarcke, E. 1983. *Random Fields: Analysis and Synthesis.* Cambridge, MA: The MIT Press.

Wagoner, J.L., and H.L. McKague. 1984. *Variation of Physical Properties of Alluvium in an Arid Basin*, UCRL-90672. Livermore, CA: Lawrence Livermore National Laboratory.

Wagoner, J.L., and W. Richardson. 1986. *Stratigraphic Contacts from Drillholes at the Nevada Test Site,* UCID-20790. Livermore, CA: Lawrence Livermore National Laboratory.

Walter, G.R. 1982. *Theoretical and Experimental Determination of Matrix Diffusion and Related Solute Transport Properties of Fractured Tuffs from the Nevada Test Site,* LA-9471-MS, UC-70. Los Alamos, NM: Los Alamos National Laboratory.

Ware, S.D., A. Abdel-Fattah, M. Ding, P.W. Reimus, C. Sedlacek, M. Haga, E. Garcia, and S. Chipera. 2005. *Radionuclide Sorption and Transport in Fractured Rocks of Yucca Flat, Nevada Test Site,* LA-UR-05-9279. Los Alamos, NM: Los Alamos National Laboratory.

Warren, R.G., F.C. Benedict, Jr., T.P. Rose, D.K. Smith, S.J. Chipera, E.C. Kluk, and K.M. Raven. 2002. *Alluvial Layering and Distribution of Reactive Phases within Drill Holes ER-5-4 and UE-5n of Frenchman Flat,* LA-UR-02-6206. Los Alamos, NM: Los Alamos National Laboratory.

Warren, R.G., D.A. Sawyer, F.M. Byers, Jr., and J.C. Cole. 2003. *A Petrographical, Geochemical and Geophysical Database and Framework for the Southwestern Nevada Volcanic Field,* LA-UR-03-1503. Los Alamos, NM: Los Alamos National Laboratory.

Welty, C., and L.W. Gelhar. 1989. *Evaluating of Longitudinal Dispersivity from Tracer Test Data,* R89-05, Ralph M. Parsons Laboratory Report. Cambridge, MA: Massachusetts Institute of Technology.

Werth, G.C. 1970. *The HANDCAR Nuclear Explosion in Dolomite*, UCRL-50951. Livermore, CA: University of California, Lawrence Radiation Laboratory.

Wilder, D.G. 1987. *Influence of Stress-Induced Deformations on Observed Water Flow in Fractures at the Climax Granitic Stock*, Rev.1, UCRL-95539. Livermore, CA: Lawrence Livermore National Laboratory.

Wilson, M.L., J.G. Gauthier, R.W. Barnard, G.E. Barr, H.A. Dockery, E. Dunn, R.R. Eaton, D.C. Guerin, N. Lu, M.J. Martinez, R. Nilson, C.A. Rautman, T.H. Robey, B. Ross, E.E. Ryder, A.R. Schenker, S.A. Shannon, L.H. Skinner, W.G. Halsey, J.D. Gansemer, L.C. Lewis, A.D. Lamont, I.R. Triay, A. Meijer, and D.E. Morris. 1994. *Total-System Performance Assessment for Yucca Mountain-SNL Second Iteration (TSPA-1993),* SAND93-2675. Albuquerque, NM: Sandia National Laboratories.

Winograd, I.J. 1971. "Hydrogeology of Ash Flow Tuff: A Preliminary Statement." In *Water Resources Research*, Vol. 7(4): 994-1006.

Winograd, I.J., and W. Thordarson. 1975. *Hydrogeologic and Hydrochemical Framework, South-Central Great Basin, Nevada-California, with Special Reference to the Nevada Test Site,* USGS-PP-712-C. Denver, CO: U.S. Geological Survey.

Winograd, I.J., and L.R. West. 1962. *Preliminary Tracer Experiment to Demonstrate Hydraulic Continuity Between Water Wells C and C-1, Yucca Flat, Nevada Test Site,* Technical Letter NTS-20. Denver, CO: U.S. Geological Survey.

Wohletz, K., A. Wolfsberg, A. Olson, and C. Gable. 1999. *Evaluating the Effects of Underground Nuclear Testing Below the Water Table on Groundwater and Radionuclide Migration in the Tuff Pile I Region of Yucca Flat–Numerical Simulations*: EES UGTA FY99 Report, 31 p. Los Alamos, NM: Los Alamos National Laboratory.

Wolfsberg, K. 1978a. *Sorption-Desorption Studies of Nevada Test Site Alluvium and Leaching Studies of Nuclear Test Debris,* LA-7216-MS. Los Alamos, NM: Los Alamos National Laboratory.

Wolfsberg, K. 1978b. *Sorptive Properties of Alluvium*, Office Memorandum dated October 24, 1978. Los Alamos, NM: Los Alamos National Laboratory.

Wolfsberg, K., B.P. Bayhurst, S.S. Levy, F.O. Lawrence, S.D. Knight, A.J. Mitchell, A.E. Ogard, and P.L. Wanek. 1983. *Research and Development Related to Sorption of Radionuclides on Soils*, LA-UR-83-800. Los Alamos, NM: Los Alamos National Laboratory.

Wolfsberg, A., L. Glascoe, G. Lu, A. Olson, P. Lichtner, M. McGraw, T. Cherry, and G. Roemer. 2002. *TYBO/BENHAM Model Analysis of Groundwater Flow and Radionuclide Migration from Underground Nuclear Tests in Southwestern Pahute Mesa, NTS,* LA-13977. Los Alamos, NM: Los Alamos National Laboratory.

Xu, M., and Y. Eckstein. 1995. *Use of Weighted Least-Squares Method in Evaluation of the Relationship between Dispersivity and Field Scale.* In *Ground Water,* Vol. 33, No. 6, pp. 905-908.

YMP, see Yucca Mountain Project.

Yucca Mountain Project. 1997. DTN:LAIT831361AQ95.003. "Transport Data of H3, Np, and Tc-95m Collected To Calculate Retardation Coefficients Using J-13 and Ue-25 P#1 Waters," 20 August. Las Vegas, NV.

Yucca Mountain Project. 2004. *Technical Data Management Service.* As accessed at http://connect.ymp.gov on 13 May.

Zavarin, M. 2002. *Matrix Diffusion and Colloid-Facilitated Transport in Fractured Rocks: Model and Parameter Validation*, UCRL-ID-149817. Livermore, CA: Lawrence Livermore National Laboratory.

Zavarin, M., and C.J. Bruton. 2004a. *A Non-Electrostatic Surface Complexation Approach to Modeling Radionuclide Migration at the Nevada Test Site: II. Aluminosilicates,* UCRL-TR-208672. June 6. Livermore, CA: Lawrence Livermore National Laboratory.

Zavarin, M., and C.J. Bruton. 2004b. *A Non-Electrostatic Surface Complexation Approach to Modeling Radionuclide Migration at the Nevada Test Site: I. Iron Oxides and Calcite,* UCRL-TR-208673, 6 June. Livermore, CA: Lawrence Livermore National Laboratory.

Zavarin, M., S.K. Roberts, T.P. Rose, and D.L. Phinney. 2002. *Validating Mechanistic Sorption Model Parameters and Process for Reactive Transport in Alluvium,* UCRL-ID-149728. Livermore, CA: Lawrence Livermore National Laboratory.

Zavarin, M., S.F. Carle, and R.M. Maxwell. 2004. *Upscaling Radionuclide Retardation - Linking the Surface Complexation and Ion Exchange Mechanistic Approach to a Linear K_d Approach,* UCRL-TR-204713. Livermore, CA: Lawrence Livermore National Laboratory.

Zavarin, M., M.R. Johnson, S.K. Roberts, R. Pletcher, T.P. Rose, A.B. Kersting, G. Eaton, Q. Hu, E. Ramon, J. Walensky, and P. Zhao. 2005. *Radionuclide Transport in Tuff and Carbonate Fractures from Yucca Flat, Nevada Test Site,* UCRL-TR-219836. Livermore, CA: Lawrence Livermore National Laboratory.

Zavarin, M., S.K. Roberts, M.R. Johnson, Q. Hu, B. Powell, P. Zhao, A.B. Kersting, R. Lindvall, and R. Pletcher. 2006. Written communication: *Colloid-Facilitated Radionuclide Transport in Fractured Carbonate Rocks from Yucca Flat, Nevada Test Site*. Lawrence Livermore National Laboratory Livermore, CA.

Zavarin, M., S. Roberts, P. Reimus, and M. Johnson. 2007. *Summary of Radionuclide Reactive Transport Experiments in Fractured Tuff and Carbonate Rocks from Yucca Flat, Nevada Test Site,* UCRL-TR-225271. Livermore, CA: Lawrence Livermore National Laboratory.

Zuber, A., 1974. "Theoretical possibilities of the two-well pulse method." In *Proceedings: Isotope Techniques in Groundwater Hydrology,* Vol. II, p. 277 – 294. IAEA, Vienna, Austria.

Zyvoloski, G.A., B.A. Robinson, Z.V. Dash, and L.L. Trease. 1997a. *Summary of Models and Methods for the FEHM Application - A Finite-Element Heat- and Mass-Transfer Code,* LA-13307-MS. Los Alamos, NM: Los Alamos National Laboratory.

Zyvoloski, G.A., B.A. Robinson, Z.V. Dash, and L.L. Trease. 1997b. *User's Manual for the FEHM Application - A Finite-Element Heat- and Mass-Transfer Code,* LA-13306-M. Los Alamos, NM: Los Alamos National Laboratory.

Appendix A

Underground Nuclear Tests in the Yucca Flat/Climax Mine Corrective Action Unit

A.1.0 UNDERGROUND NUCLEAR TESTS IN THE YUCCA FLAT/CLIMAX MINE CORRECTIVE ACTION UNIT

A total of 747 underground nuclear detonations were conducted in shafts and tunnels in the Yucca Flat/Climax Mine CAU. This included 744 detonations in Yucca Flat proper and three detonations in the Climax Mine tunnel complex (DOE/NV, 2000). Underground nuclear tests are designated (either individually or as groups) as CASs in the FFACO (1996; as amended, August 2006). In some cases, multiple detonations were conducted simultaneously in the same emplacement hole and therefore comprise a single CAS (FFACO, 1996; as amended, August 2006). Plate 1 shows the locations of the CASs. A variety of test-related surface effects — including collapse craters and associated radial and circumferential surface fractures, along with normal faults within the area (e.g., Yucca, Topgallant, and Carpetbag faults) — are also shown in Plate 1.

Yucca Flat is unique among the NTS CAUs in that it hosted nuclear tests with simultaneous detonations. A test is defined in the Threshold Test Ban Treaty as either a single underground nuclear explosion conducted at a test site, or two or more underground nuclear explosions conducted within an area delineated by a circle having a diameter of 2 km and conducted within a total period of time not to exceed 0.1 seconds. A total of 62 tests with simultaneous detonations took place on the NTS between 1963 and 1992 (DOE/NV, 2000). Sixty of these tests took place within the Yucca Flat area. From 1963 to 1988, 40 tests comprising 103 detonations are considered simultaneous, separate hole; and from 1964 to 1992, 20 tests comprising 45 detonations are considered simultaneous, same hole.

Unclassified information related to the underground nuclear tests conducted within the Yucca Flat/Climax Mine CAU is compiled primarily in two reports, *United States Nuclear Tests, July 1945 through September 1992* (DOE/NV, 2000) and *Shaft and Tunnel Nuclear Detonations at the Nevada Test Site: Development of a Primary Database for the Estimation of Potential Interactions with the Regional Groundwater System* (DOE/NV, 1997). These data — including the name and date of each detonation, name and location of the emplacement holes, announced yields, depths of burial,

estimated depths to the water table, and the HSU associated with the working point — are summarized in Table A.1-1.

The term "yield" refers to the total effective energy released in a nuclear explosion and is usually expressed in terms of equivalent tonnage of TNT required to produce the same energy release in an explosion. Announced yield ranges are reported in DOE/NV (2000); the specific yields for many tests remain classified. The announced yields for some Yucca Flat tests were termed low, intermediate, or slight (Table A.1-1). Between 1945 and 1963, a less-than-20-kt yield was defined as "low," while a 20-to-200-kt-yield range was referred to as "intermediate." In a few cases, the term "slight" was used without amplification (DOE/NV, 2000). The maximum upper limit of the announced yield range for Yucca Flat is 500 kt, whereas that of the Climax Mine tests is 62 kt. A zero yield was reported for three tests, SAN JUAN (Operation Hardtack II), COURSER (Operation Whetstone), and TRANSOM (Operation Cresset). The TRANSOM nuclear device did not detonate and was later destroyed, as planned, by the HEARTS detonation (Operation Quicksilver) approximately 16 months later (DOE/NV, 2000).

Nuclear devices were emplaced in one of four types of geologic medium in Yucca Flat and Climax Mine: alluvial deposits, Tertiary volcanics, carbonate rocks, or intrusives. The location of their emplacement is called the working point and the vertical depth to the device primary center line is referred to as the depth of burial (Table A.1-1). An estimate of the depth to the water table is also provided in Table A.1-1. These estimates were determined by interpolating regional and local (Yucca Flat and Pahute Mesa) water table surfaces and were selected as being the most representative estimate of the regional water table based on the data available at the time (DOE/NV, 1997). These data represent the only published compilation of water table data for the emplacement holes within the Yucca Flat/Climax Mine CAU and is all that is available until the groundwater flow modeling efforts have been completed. A detonation is considered as potentially interacting with the regional groundwater system if the elevation of the working point is 100 m above the water table or deeper (DOE/NV, 1997). Based on the data in Table A.1-1, less than 25 percent of the detonations (170) are considered to have impacted the water table. The HSUs associated with each working point are also presented in Table A.1-1. Hydrostratigraphic units are described in Section 4.1 and BN (2006).

Table A.1-1
Shaft and Tunnel Nuclear Detonations in the Yucca Flat/Climax Mine Corrective Action Unit
(Page 1 of 24)

Detonation Name	CAS Number	Date Expended	Emplacement Hole Name	UTM Easting	UTM Northing	Land Surface Elevation [a] (m amsl)	Announced Yield(kt)	Hole Depth (m)	Estimated Depth to Water (m)	Depth of Burial (m)	Working Point HSU
AARDVARK	03-57-013	05/12/1962	U-3am(s)	586202.6	4102340.7	1,240.8	40	494	503	434	LTCU
ABEYTAS	03-57-162	11/05/1970	U-3gx	587894.0	4098394.1	1,215.2	20 to 200	407	481	393	TM-LVTA
ABILENE	03-57-270	04/07/1988	U-3mn	585020.7	4096555.6	1,214.6	< 20	290	481	244	TM-WTA
ABO	03-57-263	10/30/1985	U-3mc	585707.0	4100717.6	1,229.0	< 20	213	495	198	AA
ABSINTHE	03-57-110	05/26/1967	U-3ep	587232.8	4100113.5	1,225.9	< 20	244	492	119	AA
ACE	02-57-145	06/11/1964	U-2n	582057.1	4111553.6	1,326.8	3	271	579	263	AA
ACUSHI	03-57-033	02/08/1963	U-3bg	587049.5	4100234.7	1,225.9	Low	329	492	261	AA
ADZE	03-57-137	05/28/1968	U-3fw	589379.6	4096098.6	1,215.2	< 20	253	475	240	TSA
AGILE	02-57-151	02/23/1967	U-2v	582934.9	4109148.8	1,297.2	20 to 200	771	543	733	TM-LVTA
AGOUTI	03-57-015	01/18/1962	U-3ao	585868.6	4100346.4	1,227.4	6.4	269	494	261	AA
AGRINI	02-57-122	03/31/1984	U-2ev	581343.1	4111306.7	1,330.8	< 20	429	584	320	AA
AHTANUM	02-57-143	09/13/1963	U-2l	581628.7	4113187.9	1,346.9	Low	233	604	226	AA
AJAX	09-57-035	11/11/1966	U-9al	584394.3	4110007.1	1,280.8	< 20	245	537	239	AA
AJO	03-57-144	01/30/1970	U-3gd	585851.5	4098524.0	1,218.6	< 20	320	486	304	AA
AKAVI	02-57-119	12/03/1981	U-2es	582515.1	4111539.4	1,320.4	20 to 150	518	576	494	TM-LVTA
AKBAR	10-57-028	11/09/1972	U-10ax	585846.5	4113082.3	1,321.9	< 20	305	588	267	TM-LVTA
ALEMAN	03-57-240	09/11/1986	U-3kz	584481.3	4102754.6	1,245.1	< 20	686	475	503	TM-LVTA
ALGODONES	03-57-208	08/18/1971	U-3jn	585682.5	4101447.6	1,233.2	20 to 200	549	497	528	TM-UVTA
ALIGOTE	07-57-028	05/29/1981	U-7bg	588499.6	4106431.8	1,337.5	< 20	396	606	320	LTCU
ALIMENT	03-57-150	05/15/1969	U-3gj	590293.1	4096467.7	1,234.1	< 20	254	503	241	OSBCU
ALLEGHENY	09-57-113	09/29/1962	U-9x	585931.2	4108050.1	1,297.8	Low	264	564	211	TM-WTA
ALPACA	02-57-001	02/12/1965	U-2a	581991.1	4113320.2	1,341.7	0.33	232	604	225	AA
ALUMROOT	09-57-081	02/14/1973	U-9cj	584359.2	4111408.7	1,291.4	< 20	206	546	183	AA
ALVA	02-57-142	08/19/1964	U-2j	581415.3	4112702.6	1,347.2	4.4	168	602	166	AA
ALVISO	02-57-099	06/11/1975	U-2du	582300.9	4107470.5	1,287.8	< 20	221	523	183	AA
ANACOSTIA	09-57-098	11/27/1962	U-9i	586258.2	4108733.8	1,300.9	5.2	296	569	227	TM-LVTA
ANCHOVY	03-57-042	11/14/1963	U-3bq	587295.9	4099504.2	1,221.3	Low	272	488	260	AA
ANGUS	03-57-201	04/25/1973	U-3jg	586440.9	4095646.4	1,207.6	< 20	503	472	453	AA
APODACA	03-57-158	07/21/1971	U-3gs	589680.9	4096739.6	1,221.9	< 20	253	487	241	LTCU
APSHAPA	09-57-031	06/06/1963	U-9ai	585282.1	4108928.5	1,281.4	Low	96	544	89	AA
ARABIS-BLUE	09-57-018	03/06/1970	U-9itsz26	586037.8	4110591.9	1,303.0	< 20	116	571	101	TM-LVTA

Table A.1-1
Shaft and Tunnel Nuclear Detonations in the Yucca Flat/Climax Mine Corrective Action Unit
(Page 2 of 24)

Detonation Name	CAS Number	Date Expended	Emplacement Hole Name	UTM Easting	UTM Northing	Land Surface Elevation [a] (m amsl)	Announced Yield(kt)	Hole Depth (m)	Estimated Depth to Water (m)	Depth of Burial (m)	Working Point HSU
ARABIS-GREEN	09-57-011	03/06/1970	U-9itsx28	585793.4	4110834.8	1,297.2	< 20	264	565	259	TM-LVTA
ARABIS-RED	09-57-003	03/06/1970	U-9itsv26	585550.2	4110590.2	1,291.7	< 20	265	558	250	TM-LVTA
ARIKAREE	09-57-108	05/10/1962	U-9r	584540.2	4109246.4	1,281.4	Low	181	538	166	AA
ARMADA	09-57-089	04/22/1983	U-9cs	586856.5	4107486.5	1,322.5	< 20	366	590	265	LTCU
ARMADILLO	03-57-018	02/09/1962	U-3ar	585464.2	4099935.1	1,225.0	7.1	309	492	240	AA
ARNICA-VIOLET	02-57-081	06/26/1970	U-2dd3	581366.4	4108055.4	1,298.8	< 20	279	558	264	AA
ARNICA-YELLOW	02-57-080	06/26/1970	U-2dd2	581193.9	4107698.2	1,296.9	< 20	325	554	309	TM-LVTA
ARSENATE	09-57-080	11/09/1972	U-9ci	585965.9	4108579.5	1,295.1	< 20	259	562	250	TM-LVTA
ARTESIA	07-57-060	12/16/1970	U-7x	588155.6	4106241.4	1,328.9	20 to 200	533	595	485	LTCU
ASCO	10-57-033	04/25/1978	U-10bc	585712.3	4112251.5	1,312.2	< 20	292	579	183	TM-LVTA
ASIAGO	02-57-016	12/21/1976	U-2ar	582842.2	4108821.8	1,292.0	< 20	701	545	331	AA
ATARQUE	03-57-188	07/25/1972	U-3ht	587626.0	4096508.4	1,209.1	< 20	309	474	294	AA
ATRISCO	07-57-035	08/05/1982	U-7bp	588299.3	4104471.7	1,294.8	138	686	538	640	OSBCU
AUGER	03-57-138	11/15/1968	U-3fx	588938.2	4100424.2	1,248.8	< 20	253	507	241	TM-LVTA
AUK	07-57-024	10/02/1964	U-7b	588134.1	4103773.3	1,281.1	< 20	471	529	452	LTCU
AUSTIN	06-57-003	06/21/1990	U-6e	588587.7	4094337.5	1,201.5	< 20	457	458	351	TM-LVTA
AVENS-ALKERMES	09-57-002	12/16/1970	U-9itsu24	585429.5	4110346.3	1,288.4	< 20	326	554	306	TM-LVTA
AVENS-ANDORRE	09-57-001	12/16/1970	U-9itst28	585305.9	4110833.1	1,291.1	< 20	395	555	379	LTCU
AVENS-ASAMLTE	09-57-006	12/16/1970	U-9itsw21	585674.2	4109981.4	1,290.5	< 20	319	557	306	LTCU
AVENS-CREAM	09-57-012	12/16/1970	U-9itsx29	585793.3	4110956.4	1,298.4	< 20	310	566	294	LTCU
AZUL	02-57-113	12/14/1979	U-2em	583216.9	4110319.0	1,302.4	< 20	221	556	205	AA
BACCARAT	07-57-022	01/24/1979	U-7ax	587818.7	4106819.5	1,337.8	< 20	381	606	326	OSBCU
BACKGAMMON	03-57-202	11/29/1979	U-3jh	586841.3	4094444.2	1,203.4	< 20	434	466	229	AA
BACKSWING	09-57-043	05/14/1964	U-9aw	585382.4	4108119.5	1,284.1	< 20	235	547	160	AA
BALTIC	09-57-099	08/06/1971	U-9itss25	585185.3	4110467.0	1,286.9	< 20	504	547	411	TM-LVTA
BANDICOOT	03-57-035	10/19/1962	U-3bj	587052.7	4099503.4	1,221.6	12.5	247	489	241	AA
BANEBERRY	08-57-010	12/18/1970	U-8d	580000.4	4114255.1	1,394.2	10	299	649	278	TM-LVTA
BANON	02-57-103	08/26/1976	U-2dz	581549.5	4108930.9	1,302.4	20 to 150	579	544	536	AA
BARBEL	03-57-049	10/16/1964	U-3bx	587539.6	4099505.1	1,221.3	< 20	282	488	259	AA
BARRACUDA	03-57-061	12/04/1963	U-3cr	587842.7	4099993.7	1,228.6	Low	282	495	263	AA
BARRANCA	03-57-168	08/04/1971	U-3he	587209.7	4098010.8	1,214.3	< 20	290	481	271	AA
BARSAC	03-57-143	03/20/1969	U-3gc	586266.6	4097550.4	1,213.7	< 20	314	480	304	AA

Table A.1-1
Shaft and Tunnel Nuclear Detonations in the Yucca Flat/Climax Mine Corrective Action Unit
(Page 3 of 24)

Detonation Name	CAS Number	Date Expended	Emplacement Hole Name	UTM Easting	UTM Northing	Land Surface Elevation [a] (m amsl)	Announced Yield(kt)	Hole Depth (m)	Estimated Depth to Water (m)	Depth of Burial (m)	Working Point HSU
BASEBALL	07-57-025	01/15/1981	U-7ba	584900.6	4104756.9	1,258.5	20 to 150	610	458	564	LTCU
BAY LEAF	03-57-156	12/12/1968	U-3gq	586238.9	4100326.6	1,226.2	< 20	139	493	130	AA
BEEBALM	03-57-131	05/01/1970	U-3fn	586404.5	4101679.9	1,235.7	< 20	411	503	390	TM-WTA
BELEN	03-57-043	02/04/1970	U-3br	585461.5	4101204.6	1,232.9	20 to 200	438	497	421	AA
BELLOW	04-57-004	05/16/1984	U-4ac	580586.7	4105316.2	1,292.7	< 20	244	418	207	TM-LVTA
BERNAL	03-57-218	11/28/1973	U-3jy	586788.9	4096333.3	1,209.8	< 20	308	475	283	AA
BERNALILLO	03-57-272	09/17/1958	U-3n	585974.7	4100603.9	1,227.7	0.015	160	495	140	AA
BEVEL	03-57-135	04/04/1968	U-3fu	587062.4	4100920.4	1,232.3	< 20	253	498	241	AA
BIGGIN	09-57-072	01/30/1969	U-9bz	585248.2	4109887.9	1,283.8	< 20	251	545	244	TM-LVTA
BILBY	03-57-058	09/13/1963	U-3cn	586983.0	4101819.0	1,241.8	249	785	509	714	OSBCU
BILGE	03-57-221	02/19/1975	U-3kc	586791.4	4095358.2	1,206.1	< 20	339	470	319	AA
BILLET	07-57-015	07/27/1976	U-7an	584996.6	4103457.6	1,249.7	20 to 150	963	487	636	LTCU
BIT-A	03-57-159	10/31/1968	U-3gt	586304.5	4100326.9	1,225.9	< 20	158	493	148	AA
BIT-B	03-57-159	10/31/1968	U-3gt	586304.5	4100326.9	1,225.9	< 20	158	493	118	AA
BITTERLING	03-57-063	06/12/1964	U-3cu	587844.3	4099445.5	1,231.1	< 20	320	497	193	AA
BLACK	09-57-106	04/27/1962	U-9p	585485.6	4108243.2	1,285.3	Low	224	549	218	AA
BLENTON	07-57-053	04/30/1969	U-7p	587645.2	4104167.5	1,281.7	20 to 200	579	536	558	LTCU
BOBAC	03-57-037	08/24/1962	U-3bl	586805.8	4100233.5	1,225.6	Low	211	492	206	AA
BOBSTAY	03-57-196	10/26/1977	U-3jb	587484.4	4095964.3	1,207.3	< 20	415	471	381	TM-WTA
BOGEY	09-57-041	04/17/1964	U-9au	585828.9	4108360.5	1,291.7	< 20	131	557	119	AA
BONARDA	03-57-161	09/25/1980	U-3gv	584638.4	4101323.3	1,236.6	20 to 150	450	490	381	TM-WTA
BONEFISH	03-57-045	02/18/1964	U-3bt	585947.4	4101693.8	1,234.4	< 20	483	498	301	AA
BOOMER	03-57-001	10/01/1961	U-3aa	585854.2	4100467.6	1,227.7	Low	164	495	101	AA
BORATE	02-57-137	10/23/1987	U-2ge	581824.2	4110807.4	1,321.3	20 to 150	585	573	543	AA
BORDEAUX	03-57-086	08/18/1967	U-3dr	585721.7	4096451.4	1,210.1	< 20	344	477	332	AA
BORREGO	07-57-036	09/29/1982	U-7br	584883.7	4105224.3	1,261.0	< 150	610	493	564	LTCU
BOURBON	07-57-051	01/20/1967	U-7n	588521.7	4106212.5	1,333.2	20 to 200	578	601	560	LCA
BOUSCHET	03-57-241	05/07/1982	U-3la	584857.3	4102756.2	1,244.5	20 to 150	686	479	564	LTCU
BOWIE	03-57-268	04/06/1990	U-3mk	589600.8	4102651.0	1,297.5	< 20	381	568	213	TM-LVTA
BOWL-1	02-57-041	06/26/1969	U-2bo1	581808.8	4113091.3	1,343.3	< 20	206	603	198	AA
BOWL-2	02-57-154	06/26/1969	U-2bo2	581763.8	4112901.9	1,341.7	< 20	236	600	229	AA

Table A.1-1
Shaft and Tunnel Nuclear Detonations in the Yucca Flat/Climax Mine Corrective Action Unit
(Page 4 of 24)

Detonation Name	CAS Number	Date Expended	Emplacement Hole Name	UTM Easting	UTM Northing	Land Surface Elevation [a] (m amsl)	Announced Yield(kt)	Hole Depth (m)	Estimated Depth to Water (m)	Depth of Burial (m)	Working Point HSU
BRACKEN	10-57-022	07/09/1971	U-10aq	585881.2	4113350.0	1,323.4	< 20	336	585	305	LTCU
BRANCO	02-57-123	09/21/1983	U-2ew	583900.0	4108548.8	1,282.9	< 20	457	520	293	AA
BRANCO-HERKIMER	02-57-123	09/21/1983	U-2ew	583900.0	4108548.8	1,282.9	< 20	457	520	427	TM-WTA
BRAZOS	09-57-092	03/08/1962	U-9d	584494.4	4108644.4	1,280.5	8.4	340	535	256	AA
BRETON	04-57-013	09/13/1984	U-4ar	582552.3	4104689.0	1,264.6	20 to 150	503	503	483	TM-LVTA
BRIE	10-57-042	06/18/1987	U-10cc	585645.9	4116576.5	1,345.1	< 20	230	326	203	LTCU
BRISTOL	04-57-017	11/26/1991	U-4av	582680.7	4105777.6	1,273.1	< 20	518	482	457	LTCU
BRONZE	07-57-044	07/23/1965	U-7f	585932.4	4105959.3	1,284.1	20 to 200	576	548	531	LTCU
BRUSH	03-57-111	01/24/1968	U-3eq	587690.7	4099871.0	1,225.6	< 20	221	492	118	AA
BUFF	03-57-077	12/16/1965	U-3dh	586307.9	4103157.5	1,250.3	20 to 200	507	515	500	LTCU
BULKHEAD	07-57-014	04/27/1977	U-7am	586391.0	4105626.1	1,286.0	20 to 150	625	551	594	OSBCU
BULLFROG	04-57-016	08/30/1988	U-4au	582789.3	4104607.5	1,263.4	< 150	533	500	489	TM-WTA
BUNKER	09-57-050	02/13/1964	U-9bb	585952.6	4109752.0	1,296.6	< 20	237	564	227	TM-LVTA
BURZET	04-57-007	08/03/1979	U-4ai	582669.8	4104386.5	1,262.5	20 to 150	489	501	450	AA
BYE	10-57-048	07/16/1964	U-10i	584741.3	4115308.7	1,321.3	20 to 200	532	566	391	LTCU
CABOC	02-57-067	12/16/1981	U-2cp	577928.4	4107733.7	1,374.6	< 20	381	522	335	TM-LVTA
CABRESTO	07-57-046	05/24/1973	U-7h	586153.4	4103766.4	1,255.2	< 20	470	519	198	AA
CABRILLO	02-57-096	03/07/1975	U-2dr	581340.0	4109927.8	1,314.6	20 to 200	616	566	601	AA
CALABASH	02-57-020	10/29/1969	U-2av	583141.8	4110977.8	1,310.0	110	668	569	625	LTCU
CAMPOS	09-57-086	02/13/1978	U-9cp	586012.8	4109098.3	1,296.3	< 20	335	564	320	TM-LVTA
CANFIELD	03-57-238	05/02/1980	U-3kx	587228.5	4101332.3	1,237.5	< 20	442	504	351	TM-LVTA
CAN-GREEN	03-57-072	04/21/1970	U-2dd1	581554.1	4107528.9	1,293.3	20 to 200	290	554	274	AA
CANJILON	03-57-132	12/16/1970	U-3fq	586673.3	4103158.8	1,254.6	< 20	411	522	302	TM-LVTA
CANNA-LIMOGES	09-57-100	11/17/1972	U-9itsyz26	585942.1	4110591.5	1,300.0	< 20	221	568	213	TM-LVTA
CANNA-UMBRINUS	09-57-100	11/17/1972	U-9itsyz26	585942.1	4110591.5	1,300.0	< 20	221	568	183	TM-LVTA
CAN-RED	03-57-073	04/21/1970	U-2dd4	581725.0	4107886.6	1,295.1	20 to 200	464	554	399	LTCU
CANVASBACK	03-57-060	08/22/1964	U-3cp	587529.6	4102369.5	1,253.6	< 20	454	515	448	LTCU
CAPITAN	03-57-204	06/28/1972	U-3jj	587017.0	4094295.5	1,202.7	< 20	175	465	134	AA
CAPROCK	04-57-031	05/31/1984	U-4q	584589.6	4106533.9	1,263.7	20 to 150	637	493	600	LTCU
CARMEL	02-57-141	02/21/1963	U-2h	581705.2	4112238.6	1,338.1	Low	171	599	164	AA
CARNELIAN	04-57-005	07/28/1977	U-4af	580782.8	4105880.6	1,291.7	< 20	305	492	208	AA
CARP	03-57-052	09/27/1963	U-3cb	587540.2	4099261.3	1,219.8	Low	344	486	330	AA

Table A.1-1
Shaft and Tunnel Nuclear Detonations in the Yucca Flat/Climax Mine Corrective Action Unit
(Page 5 of 24)

Detonation Name	CAS Number	Date Expended	Emplacement Hole Name	UTM Easting	UTM Northing	Land Surface Elevation [a] (m amsl)	Announced Yield(kt)	Hole Depth (m)	Estimated Depth to Water (m)	Depth of Burial (m)	Working Point HSU
CARPETBAG	02-57-084	12/17/1970	U-2dg	581456.2	4109387.3	1,311.2	220	692	552	662	TM-LVTA
CARRIZOZO	03-57-186	12/03/1970	U-3hr	585419.6	4095780.0	1,210.1	< 20	287	477	279	TM-WTA
CASHMERE	02-57-004	02/04/1965	U-2ad	583355.4	4109585.1	1,297.2	< 20	268	550	233	AA
CASSELMAN	10-57-047	02/08/1963	U-10g	584198.8	4111604.7	1,294.5	Low	309	549	303	AA
CASSOWARY	03-57-039	12/16/1964	U-3bn	586808.3	4099502.8	1,220.7	< 20	161	488	150	AA
CATHAY	09-57-079	10/08/1971	U-9ch	585530.1	4107725.7	1,288.1	< 20	421	552	378	TM-LVTA
CEBOLLA	03-57-197	08/09/1972	U-3jc	587278.0	4095916.3	1,207.6	< 20	309	472	287	AA
CEBRERO	09-57-091	08/14/1985	U-9cw	587572.4	4107446.1	1,342.6	< 20	213	611	183	TM-LVTA
CENTAUR	02-57-009	08/27/1965	U-2ak	582595.3	4110305.5	1,310.3	< 20	192	561	173	AA
CERISE	03-57-115	11/18/1966	U-3eu	588010.7	4099872.1	1,228.6	< 20	223	494	211	AA
CERNADA	03-57-227	09/24/1981	U-3kk	586852.1	4096059.6	1,208.2	< 20	442	473	213	AA
CERRO	03-57-245	09/02/1982	U-3lf	587562.6	4097311.1	1,211.6	< 20	341	478	229	AA
CHAENACTIS	02-57-090	12/14/1971	U-2dl	580879.2	4108806.6	1,307.9	20 to 200	347	565	331	AA
CHAMITA	03-57-261	08/17/1985	U-3lz	585146.9	4095352.4	1,208.2	< 20	457	475	335	TM-UVTA
CHANTILLY	02-57-087	09/29/1971	U-2di	581107.5	4108868.1	1,307.0	< 20	366	562	331	AA
CHARCOAL	07-57-045	09/10/1965	U-7g	587402.8	4103770.5	1,271.6	20 to 200	471	533	455	LTCU
CHATTY	02-57-040	03/18/1969	U-2bn	582052.4	4113070.5	1,339.3	< 20	212	601	195	AA
CHEEDAM	02-57-120	02/17/1983	U-2et	583164.7	4113141.5	1,320.4	< 20	427	585	343	TM-LVTA
CHENILLE	09-57-055	04/22/1965	U-9bg	586140.4	4107469.1	1,303.3	< 20	229	569	141	TM-WTA
CHESS	07-57-019	06/20/1979	U-7at	587513.1	4107062.2	1,336.2	< 20	460	604	335	LTCU
CHEVRE	10-57-029	11/23/1976	U-10ay	584102.8	4114137.0	1,304.8	< 20	335	572	317	AA
CHIBERTA	02-57-111	12/20/1975	U-2ek	583361.2	4109241.7	1,291.4	20 to 200	761	540	716	LTCU
CHINCHILLA	03-57-007	02/19/1962	U-3ag	586296.4	4100551.1	1,228.3	1.9	166	495	150	AA
CHINCHILLA II	03-57-019	03/31/1962	U-3as	585643.3	4100306.6	1,227.1	Low	172	494	137	AA
CHIPMUNK	03-57-025	02/15/1963	U-3ay	586098.9	4100544.6	1,227.7	Low	64	495	59	AA
CHOCOLATE	03-57-113	04/21/1967	U-3es	585627.5	4097243.7	1,21,2.8	< 20	253	480	240	AA
CIMARRON	09-57-096	02/23/1962	U-9h	584537.9	4109387.2	1,282.6	11.9	370	539	305	AA
CINNAMON	03-57-082	03/07/1966	U-3dm	586200.5	4098951.9	1,219.2	< 20	191	487	120	AA
CLAIRETTE	03-57-232	02/05/1981	U-3kr	586103.7	4096315.6	1,209.4	< 20	445	475	354	AA
CLARKSMOBILE	02-57-017	05/17/1968	U-2as	583612.8	4108400.9	1,285.6	20 to 200	518	515	472	TM-LVTA
CLUB	02-57-002	01/30/1964	U-2aa	582544.6	4110183.5	1,309.4	< 20	190	559	181	AA

Table A.1-1
Shaft and Tunnel Nuclear Detonations in the Yucca Flat/Climax Mine Corrective Action Unit
(Page 6 of 24)

Detonation Name	CAS Number	Date Expended	Emplacement Hole Name	UTM Easting	UTM Northing	Land Surface Elevation [a] (m amsl)	Announced Yield(kt)	Hole Depth (m)	Estimated Depth to Water (m)	Depth of Burial (m)	Working Point HSU
CLYMER	09-57-076	03/12/1966	U-9ce	584147.2	4111027.4	1,293.0	< 20	684	546	398	AA
COALORA	03-57-253	02/11/1983	U-3lo	584882.1	4101324.1	1,236.9	< 20	305	492	274	TM-UVTA
COBBLER	07-57-057	11/08/1967	U-7u	585690.7	4105288.4	1,269.2	< 20	686	531	667	LTCU
CODSAW	09-57-095	02/19/1962	U-9g	585533.3	4109241.7	1,285.3	Low	218	550	212	TM-WTA
COFFER	02-57-082	03/21/1969	U-2de	581126.4	4109837.8	1,317.7	< 100	479	569	465	AA
COGNAC	03-57-130	10/25/1967	U-3fm	585402.3	4100624.5	1,229.6	< 20	253	495	240	AA
COLFAX	03-57-219	10/05/1958	U-3k	585883.8	4100523.5	1,228.0	0.0055	168	495	107	AA
COLMOR	03-57-190	04/26/1973	U-3hv	587188.9	4096465.7	1,209.4	< 20	260	475	246	AA
COMMODORE	02-57-011	05/20/1967	U-2am	583146.8	4109545.6	1,297.8	250	779	549	745	LTCU
CONCENTRATION	03-57-229	12/01/1978	U-3kn	586798.4	4098405.5	1,216.5	< 20	274	483	243	AA
CORAZON	03-57-164	12/03/1970	U-3ha	585604.0	4095323.5	1,207.3	< 20	253	474	241	AA
CORDUROY	10-57-049	12/03/1965	U-10k	584139.0	4113364.3	1,302.4	20 to 200	729	568	679	OSBCU
CORMORANT	03-57-075	07/17/1964	U-3df	586329.3	4097063.0	1,211.6	< 20	279	478	272	AA
CORNICE-GREEN	10-57-021	05/15/1970	U-10ap3	585340.7	4113063.8	1,31,2.5	20 to 200	457	580	443	LTCU
CORNICE-YELLOW	10-57-020	05/15/1970	U-10ap1	585634.7	4113511.3	1,319.5	20 to 200	402	584	390	OSBCU
CORNUCOPIA	02-57-135	07/24/1986	U-2ga(s)	582496.6	4110908.2	1,314.3	< 20	548	566	381	AA
CORREO	03-57-260	08/02/1984	U-3lw	588279.8	4096993.7	1,209.1	< 20	427	475	335	TM-LVTA
COSO-BRONZE	04-57-012	03/08/1991	U-4an	582279.4	4106647.7	1,281.4	< 20	488	500	333	TM-WTA
COSO-GRAY	04-57-012	03/08/1991	U-4an	582279.4	4106647.7	1,281.4	< 20	488	500	442	LTCU
COSO-SILVER	04-57-012	03/08/1991	U-4an	582279.4	4106647.7	1,281.4	< 20	488	500	475	LTCU
COTTAGE	08-57-005	03/23/1985	U-8j	580872.6	4115022.7	1,388.7	20 to 150	610	627	515	OSBCU
COULOMMIERS	02-57-110	09/27/1977	U-2ei	582803.6	4111845.1	1,318.9	20 to 150	640	579	530	TM-LVTA
COURSER	03-57-084	09/25/1964	U-3do	587526.8	4103161.8	1,264.3	0	370	523	359	LTCU
COVE	03-57-225	02/16/1977	U-3ki	586180.9	4095843.9	1,207.9	< 20	351	474	335	AA
COWLES	03-57-191	02/03/1972	U-3hx	587249.9	4095237.9	1,205.5	< 20	321	468	302	AA
COYPU	03-57-006	04/10/1963	U-3af	586227.0	4100523.4	1,227.7	Low	81	495	75	AA
CREMINO	08-57-004	09/27/1978	U-8e	581041.3	4114029.9	1,367.9	< 20	610	588	210	AA
CREMINO-CAERPHILLY	08-57-004	09/27/1978	U-8e	581041.3	4114029.9	1,367.9	< 20	610	588	420	TM-LVTA
CREPE	02-57-147	12/05/1964	U-2q	584097.7	4107781.6	1,278.6	20 to 200	415	498	404	TM-LVTA
CRESTLAKE-BRIAR	02-57-101	07/18/1974	U-2dw	581277.2	4108289.7	1,301.2	< 20	381	560	374	AA
CRESTLAKE-TANSAN	02-57-101	07/18/1974	U-2dw	581277.2	4108289.7	1,301.2	< 20	381	560	272	AA
CREW	02-57-073	11/04/1968	U-2db	581142.7	4109533.4	1,314.3	20 to 200	632	561	359	AA

Table A.1-1
Shaft and Tunnel Nuclear Detonations in the Yucca Flat/Climax Mine Corrective Action Unit
(Page 7 of 24)

Detonation Name	CAS Number	Date Expended	Emplacement Hole Name	UTM Easting	UTM Northing	Land Surface Elevation [a] (m amsl)	Announced Yield(kt)	Hole Depth (m)	Estimated Depth to Water (m)	Depth of Burial (m)	Working Point HSU
CREW-2ND	02-57-073	11/04/1968	U-2db	581142.7	4109533.4	1,314.3	< 20	632	561	360	AA
CREW-3RD	02-57-073	11/04/1968	U-2db	581142.7	4109533.4	1,314.3	< 20	632	561	604	TM-LVTA
CREWLINE	07-57-017	05/25/1977	U-7ap	584882.5	4105559.8	1,264.3	20 to 150	625	498	564	LTCU
CROCK	10-57-014	05/08/1968	U-10ak	585695.3	4112557.4	1,315.8	< 20	207	583	182	AA
CROWDIE	02-57-132	05/05/1983	U-2fe	580886.0	4111213.7	1,335.9	< 20	450	590	390	AA
CRUET	02-57-065	10/29/1969	U-2cn	577488.7	4108504.9	1,398.7	11	472	523	264	TM-WTA
CUCHILLO	03-57-213	08/09/1972	U-3jt	587279.6	4095535.1	1,206.1	< 20	223	469	198	AA
CULANTRO-A	03-57-172	12/10/1969	U-3hia	588707.2	4096766.6	1,208.2	< 20	143	472	134	AA
CULANTRO-B	03-57-173	12/10/1969	U-3hib	588859.5	4096789.7	1,209.1	< 20	158	473	149	AA
CUMARIN	03-57-163	02/25/1970	U-3gz	588972.9	4099205.4	1,232.9	20 to 200	422	498	409	LTCU
CUMBERLAND	02-57-104	04/11/1963	U-2e	582495.2	4112453.8	1,326.5	Low	248	588	226	AA
CUP	09-57-074	03/26/1965	U-9cb	584998.0	4111471.6	1,293.9	20 to 200	558	554	538	LTCU
CYATHUS	08-57-002	03/06/1970	U-8b	580631.5	4114259.8	1,379.8	8.7	314	611	294	TM-LVTA
CYCLAMEN	03-57-065	05/05/1966	U-3cx	585554.7	4100717.3	1,230.2	12	343	496	305	AA
DAIQUIRI	07-57-052	09/23/1966	U-7o	585686.5	4106568.5	1,287.2	< 20	579	550	561	LTCU
DALHART	04-57-035	10/13/1988	U-4u	584497.3	4104964.6	1,255.8	< 150	671	477	640	LTCU
DAMAN I	03-57-031	06/21/1962	U-3be	586238.7	4099886.0	1,224.1	Low	268	491	260	AA
DANABLU	02-57-121	06/09/1983	U-2eu	580872.2	4112542.3	1,353.6	< 20	432	607	320	AA
DAUPHIN	09-57-087	11/14/1980	U-9cq	587191.7	4107487.7	1,332.6	< 20	336	600	320	LTCU
DEAD	09-57-102	04/21/1962	U-9k	586040.0	4108309.5	1,298.8	Low	238	566	194	AA
DECK	03-57-222	11/18/1975	U-3kd	587120.5	4097370.5	1,206.4	< 20	399	472	326	AA
DELPHINIUM	02-57-094	09/26/1972	U-2dp	581221.5	4108524.1	1,303.3	15	335	562	296	AA
DEXTER	03-57-187	06/23/1971	U-3hs	587503.6	4096587.2	1,209.4	< 20	130	475	120	AA
DIANTHUS	10-57-025	02/17/1972	U-10at	583792.8	4113467.9	1,306.1	< 20	335	572	305	AA
DISCUS THROWER	08-57-001	05/27/1966	U-8a	580092.9	4114839.3	1,406.7	22	360	661	337	TM-LVTA
DIVIDER	03-57-269	09/23/1992	U-3ml	590030.7	4097442.0	1,234.7	< 20	396	503	340	LTCU
DOFINO	10-57-031	03/08/1977	U-10ba	584072.7	4114634.8	1,309.4	< 20	290	575	183	AA
DOFINO-LAWTON	10-57-031	03/08/1977	U-10ba	584072.7	4114634.8	1,309.4	< 20	290	575	282	AA
DOLCETTO	07-57-030	08/30/1984	U-7bi	588930.9	4105098.7	1,318.0	< 20	457	568	366	LTCU
DORMOUSE	03-57-017	01/30/1962	U-3aq	585413.8	4100297.2	1,227.1	Low	370	493	363	AA
DORMOUSE PRIME	03-57-026	04/05/1962	U-3az	586834.7	4100052.0	1,224.1	10.6	269	490	261	AA

Table A.1-1
Shaft and Tunnel Nuclear Detonations in the Yucca Flat/Climax Mine Corrective Action Unit
(Page 8 of 24)

Detonation Name	CAS Number	Date Expended	Emplacement Hole Name	UTM Easting	UTM Northing	Land Surface Elevation [a] (m amsl)	Announced Yield(kt)	Hole Depth (m)	Estimated Depth to Water (m)	Depth of Burial (m)	Working Point HSU
DOVEKIE	03-57-053	01/21/1966	U-3cd	587542.6	4098651.5	1,216.5	< 20	345	483	333	AA
DRAUGHTS	07-57-013	09/27/1978	U-7al	587130.2	4103312.7	1,261.6	20 to 150	460	526	442	OSBCU
DRILL (SOURCE-LOWER)	02-57-008	12/05/1964	U-2ai	582627.0	4109970.4	1,306.4	3.4	226	557	219	AA
DRILL (TARGET-UPPER)	02-57-008	12/05/1964	U-2ai	582627.0	4109970.4	1,306.4	< 20	226	557	188	AA
DRIVER	09-57-039	05/07/1964	U-9ar	585259.1	4108440.8	1,280.2	< 20	160	543	150	AA
DUB	10-57-001	06/30/1964	U-10a	583769.3	4114435.6	1,308.5	11.7	430	575	259	AA
DUFFER	10-57-043	06/18/1964	U-10ds	585375.1	4113516.1	1,314.3	< 20	455	580	447	LTCU
DUMONT	02-57-149	05/19/1966	U-2t	583702.8	4107414.5	1,278.6	20 to 200	696	486	671	LTCU
DUORO	03-57-259	06/20/1984	U-3lv	585147.6	4095139.1	1,207.3	20 to 150	457	474	381	TM-UVTA
DUTCHESS	07-57-033	10/24/1980	U-7bm	588957.9	4103410.3	1,291.7	< 20	472	534	427	LTCU
EAGLE	09-57-042	12/12/1963	U-9av	584928.9	4109631.1	1,281.1	5.3	174	541	165	AA
EBBTIDE	03-57-234	09/15/1977	U-3kt	585104.5	4098734.7	1,220.7	< 20	460	487	381	AA
EDAM	02-57-102	04/24/1975	U-2dy	581080.2	4107892.3	1,299.4	20 to 200	427	556	412	TM-LVTA
EEL	09-57-104	05/19/1962	U-9m	584642.4	4108698.3	1,280.2	4.5	224	536	218	AA
EFFENDI	02-57-015	04/27/1967	U-2ap	583203.9	4110475.3	1,305.8	< 20	235	560	221	AA
ELIDA	03-57-192	12/19/1973	U-3hy	586183.3	4095234.1	1,205.5	< 20	399	471	381	AA
ELKHART	09-57-066	09/17/1965	U-9bs	585774.9	4107421.8	1,293.9	< 20	340	558	220	TM-WTA
EMBUDO	03-57-167	06/16/1971	U-3hd	587724.9	4098804.8	1,218.0	< 20	312	484	303	AA
EMERSON	02-57-010	12/16/1965	U-2al	583203.7	4110703.5	1,307.3	< 20	294	564	261	AA
ERMINE	03-57-002	03/06/1962	U-3ab	585930.0	4100474.6	1,227.7	Low	81	495	73	AA
ESCABOSA	07-57-004	07/10/1974	U-7ac	586063.2	4103430.9	1,250.3	20 to 200	675	513	640	LTCU
ESROM	07-57-012	02/04/1976	U-7ak	585529.5	4106927.3	1,285.0	20 to 200	686	548	655	LTCU
ESTACA	03-57-195	10/17/1974	U-3ja	587650.3	4095832.9	1,206.7	< 20	341	470	320	TM-UVTA
FADE	09-57-053	06/25/1964	U-9be	586292.9	4107438.8	1,307.0	< 20	235	574	205	TM-LVTA
FAHADA	07-57-029	05/26/1983	U-7bh	588352.9	4106547.1	1,338.7	< 20	396	606	384	OSBCU
FAJY	02-57-130	06/28/1979	U-2fc	581039.6	4110940.3	1,330.1	20 to 150	571	584	536	AA
FALLON	02-57-100	05/23/1974	U-2dv	581826.7	4108876.7	1,302.7	20 to 200	488	548	466	AA
FARALLONES	02-57-128	12/14/1977	U-2fa	581179.6	4110132.3	1,317.3	20 to 150	732	570	668	AA
FAWN	03-57-109	04/07/1967	U-3eo	586939.7	4101148.2	1,233.5	< 20	282	500	271	AA
FENTON	02-57-144	04/23/1966	U-2m1	581433.6	4112871.8	1,348.1	1.4	169	601	167	AA
FERRET	03-57-032	02/08/1963	U-3bf	586309.5	4101581.4	1,235.0	Low	370	502	326	TM-UVTA
FERRET PRIME	03-57-050	04/05/1963	U-3by	586809.2	4099258.7	1,219.8	Low	256	487	242	AA

Table A.1-1
Shaft and Tunnel Nuclear Detonations in the Yucca Flat/Climax Mine Corrective Action Unit
(Page 9 of 24)

Detonation Name	CAS Number	Date Expended	Emplacement Hole Name	UTM Easting	UTM Northing	Land Surface Elevation [a] (m amsl)	Announced Yield(kt)	Hole Depth (m)	Estimated Depth to Water (m)	Depth of Burial (m)	Working Point HSU
FILE	03-57-142	10/31/1968	U-3gb	585781.0	4097000.1	1,212.2	< 20	253	479	229	AA
FINFOOT	03-57-089	03/07/1966	U-3du	586321.6	4099257.0	1,220.4	< 20	221	488	196	AA
FISHER	03-57-008	12/03/1961	U-3ah	586464.9	4100198.2	1,225.3	13.4	370	492	364	AA
FIZZ	03-57-133	03/10/1967	U-3fr	586277.2	4100363.0	1,225.9	< 20	130	493	118	AA
FLASK-GREEN	02-57-026	05/26/1970	U-2az1	583308.9	4107656.6	1,277.7	105	555	497	529	TM-UVTA
FLASK-RED	02-57-028	05/26/1970	U-2az3	582917.7	4107966.4	1,286.3	0.035	168	518	152	AA
FLASK-YELLOW	02-57-027	05/26/1970	U-2az2	583194.3	4108184.0	1,286.3	0.09	351	516	335	AA
FLAX-BACKUP	02-57-088	12/21/1972	U-2dj	581421.8	4110588.1	1,323.1	< 20	723	577	445	AA
FLAX-SOURCE	02-57-088	12/21/1972	U-2dj	581421.8	4110588.1	1,323.1	< 20	723	577	688	TM-LVTA
FLAX-TEST	02-57-088	12/21/1972	U-2dj	581421.8	4110588.1	1,323.1	20 to 200	723	577	436	AA
FLORA	03-57-246	05/22/1980	U-3lg	586182.6	4095447.4	1,206.4	< 20	396	472	335	AA
FLOTOST	02-57-014	08/16/1977	U-2ao	583203.2	4111355.9	1,310.9	< 20	290	569	275	AA
FLOYDADA	07-57-042	08/15/1991	U-7cb	588718.6	4104823.3	1,306.7	< 20	564	545	503	OSBCU
FOB-BLUE	09-57-013	01/23/1970	U-9itsy27	585916.0	4110713.0	1,299.7	< 20	112	567	101	TM-LVTA
FOB-GREEN	09-57-005	01/23/1970	U-9iv27	585549.8	4110712.0	1,293.0	< 20	264	560	244	TM-LVTA
FOB-RED	09-57-004	01/23/1970	U-9iv24	585551.0	4110346.7	1,289.9	< 20	282	556	266	TM-LVTA
FORE	09-57-036	01/16/1964	U-9ao	584452.2	4110875.8	1,289.6	20 to 200	504	545	491	TM-LVTA
FOREFOOT	03-57-223	06/02/1977	U-3kf	586695.7	4101208.6	1,233.5	< 20	201	500	194	AA
FOREST	07-57-001	10/31/1964	U-7a	585989.4	4107000.2	1,296.9	< 20	823	562	387	LTCU
FREEZEOUT	03-57-237	05/11/1979	U-3kw	587403.4	4094918.5	1,204.3	< 20	415	466	335	AA
FRIJOLES-DEMING	03-57-216	09/22/1971	U-3jw	587513.1	4097518.2	1,212.2	< 20	169	478	150	AA
FRIJOLES-ESPUELA	03-57-214	09/22/1971	U-3ju	587500.5	4097640.0	1,212.8	< 20	169	479	149	AA
FRIJOLES-GUAJE	03-57-169	09/22/1971	U-3hf	587591.2	4097829.3	1,213.1	< 20	274	479	257	AA
FRIJOLES-PETACA	03-57-193	09/22/1971	U-3hz	587272.2	4097553.9	1,213.1	< 20	396	479	229	AA
FRISCO	08-57-008	09/23/1982	U-8m	580981.3	4114444.1	1,373.7	20 to 150	518	583	451	OSBCU
FUNNEL	03-57-141	06/25/1968	U-3ga	586239.2	4100250.4	1,226.2	< 20	131	493	119	AA
FUTTOCK	03-57-102	06/18/1975	U-3eh	586950.5	4102397.9	1,247.9	< 20	472	514	186	AA
GALENA-GREEN	09-57-090	06/23/1992	U-9cv	586059.4	4108855.0	1,295.7	< 20	457	563	401	OSBCU
GALENA-ORANGE	09-57-090	06/23/1992	U-9cv	586059.4	4108855.0	1,295.7	< 20	457	563	381	OSBCU
GALENA-YELLOW	09-57-090	06/23/1992	U-9cv	586059.4	4108855.0	1,295.7	< 20	457	563	290	LTCU
GARDEN	09-57-032	10/23/1964	U-9aj	586075.5	4108091.1	1,301.2	< 20	158	568	150	TM-LVTA

Table A.1-1
Shaft and Tunnel Nuclear Detonations in the Yucca Flat/Climax Mine Corrective Action Unit
(Page 10 of 24)

Detonation Name	CAS Number	Date Expended	Emplacement Hole Name	UTM Easting	UTM Northing	Land Surface Elevation [a] (m amsl)	Announced Yield(kt)	Hole Depth (m)	Estimated Depth to Water (m)	Depth of Burial (m)	Working Point HSU
GASCON	04-57-034	11/14/1986	U-4t	584590.7	4106233.8	1,263.1	20 to 150	616	490	593	LTCU
GAZOOK	02-57-093	03/23/1973	U-2do	581110.4	4108068.2	1,300.9	< 20	343	558	326	AA
GERBIL	03-57-041	03/29/1963	U-3bp	587294.7	4099748.0	1,222.9	Low	291	489	280	AA
GIBSON	03-57-117	08/04/1967	U-3ew	587850.6	4097830.2	1,213.1	< 20	253	479	241	AA
GILROY	03-57-118	09/15/1967	U-3ex	587084.7	4098985.4	1,218.6	< 20	253	485	241	AA
GLENCOE	04-57-025	03/22/1986	U-4i	583012.9	4104285.0	1,260.7	29	671	493	610	OSBCU
GORBEA	02-57-068	01/31/1984	U-2cq	578034.8	4107531.7	1,371.3	20 to 150	442	521	388	TM-LVTA
GOUDA	02-57-107	10/06/1976	U-2ef	583290.9	4110007.8	1,298.4	< 20	335	552	200	AA
GOURD-AMBER	02-57-033	04/24/1969	U-2bf	581716.8	4113255.2	1,346.6	< 20	187	606	181	AA
GOURD-BROWN	02-57-038	04/24/1969	U-2bl	581611.7	4112809.7	1,343.9	< 20	238	600	227	AA
GRAPE A	07-57-055	12/17/1969	U-7s	588741.4	4104384.9	1,300.9	20 to 200	579	539	551	OSBCU
GRAPE B	07-57-058	02/04/1970	U-7v	586511.3	4105992.2	1,296.3	20 to 200	579	563	554	LTCU
GREYS	09-57-044	11/22/1963	U-9ax	584827.1	4108332.3	1,274.7	Intermediate	328	533	301	AA
GROVE	02-57-097	05/22/1974	U-2ds	582208.3	4107805.4	1,291.1	< 20	379	537	314	TM-LVTA
GRUNION	03-57-051	10/11/1963	U-3bz	587052.9	4099259.6	1,219.8	Low	284	487	261	AA
GRUYERE	09-57-078	08/16/1977	U-9cg	584451.4	4111195.7	1,289.9	< 20	335	545	207	AA
GRUYERE-GRADINO	09-57-078	08/16/1977	U-9cg	584451.4	4111195.7	1,289.9	< 20	335	545	320	AA
GUANAY	03-57-078	09/04/1964	U-3di	586939.0	4097065.2	1,211.6	< 20	268	478	261	AA
GUNDI	03-57-038	11/15/1962	U-3bm	586807.8	4099746.3	1,222.2	Low	248	489	241	AA
GUNDI PRIME	03-57-070	05/09/1963	U-3db	587535.8	4100602.1	1,232.3	Low	282	498	272	AA
HADDOCK	03-57-081	08/28/1964	U-3dl	586920.1	4102550.5	1,248.8	< 20	370	515	364	LTCU
HANDCAR	10-57-030	11/05/1964	U-10b	582825.0	4114420.1	1,333.5	12	458	598	403	LCA
HANDICAP	09-57-049	03/12/1964	U-9ba	585600.0	4109517.7	1,287.8	< 20	189	554	144	AA
HAPLOPAPPUS	09-57-021	06/28/1972	U-9itsw22	585689.3	4110103.1	1,291.4	< 20	223	558	184	TM-LVTA
HARD HAT	15-57-001	02/15/1962	U-15a	583452.9	4120183.5	1,558.7	5.7	294	222	287	MGCU
HAREBELL	02-57-046	06/24/1971	U-2br	582872.3	4111349.9	1,314.3	20 to 200	557	572	519	TM-LVTA
HARKEE	03-57-047	05/17/1963	U-3bv	587537.9	4099992.9	1,225.9	Low	256	492	241	AA
HARLINGEN-A	06-57-004	08/23/1988	U-6g	587387.5	4094141.3	1,202.4	< 20	320	463	290	AA
HARLINGEN-B	06-57-005	08/23/1988	U-6h	587388.8	4093867.1	1,201.8	< 20	320	462	290	AA
HATCHET	03-57-140	05/03/1968	U-3fz	587178.3	4098284.9	1,215.2	< 20	253	482	241	AA
HATCHIE	09-57-093	02/08/1963	U-9e	585399.2	4109074.5	1,282.6	Low	66	546	61	AA
HAVARTI	10-57-037	08/05/1981	U-10bg	585685.2	4112160.0	1,310.0	< 20	221	578	200	TM-LVTA

Table A.1-1
Shaft and Tunnel Nuclear Detonations in the Yucca Flat/Climax Mine Corrective Action Unit
(Page 11 of 24)

Detonation Name	CAS Number	Date Expended	Emplacement Hole Name	UTM Easting	UTM Northing	Land Surface Elevation [a] (m amsl)	Announced Yield(kt)	Hole Depth (m)	Estimated Depth to Water (m)	Depth of Burial (m)	Working Point HSU
HAYMAKER	03-57-021	06/27/1962	U-3au(s)	586022.4	4099759.4	1,223.5	67	463	491	408	AA
HAZEBROOK-APRICOT	10-57-038	02/03/1987	U-10bh	584467.8	4115187.7	1,317.3	< 20	297	571	262	AA
HAZEBROOK-CHECKERBERRY	10-57-038	02/03/1987	U-10bh	584467.8	4115187.7	1,317.3	< 20	297	571	226	AA
HAZEBROOK-EMERALD	10-57-038	02/03/1987	U-10bh	584467.8	4115187.7	1,317.3	< 20	297	571	186	AA
HEARTS	04-57-028	09/06/1979	U-4n	584185.3	4104863.2	1,258.8	140	671	473	640	LTCU
HEILMAN	02-57-059	04/06/1967	U-2cg	577034.6	4110254.9	1432.3	< 20	190	531	153	AA
HERMOSA	07-57-037	04/02/1985	U-7bs	585994.6	4105624.7	1,277.7	20 to 150	677	541	640	LTCU
HOD-A (GREEN)	09-57-008	05/01/1970	U-9itsx23	585795.6	4110225.6	1,294.8	< 20	256	562	241	TM-LVTA
HOD-B (RED)	09-57-007	05/01/1970	U-9itsx20	585797.2	4109859.7	1,293.0	< 20	280	560	265	TM-LVTA
HOD-C (BLUE)	09-57-017	05/01/1970	U-9iz25	586038.5	4110470.0	1,302.4	< 20	116	570	101	TM-LVTA
HOGNOSE	03-57-009	03/15/1962	U-3ai	586168.2	4099984.8	1,225.0	Low	370	492	240	AA
HOOK	09-57-051	04/14/1964	U-9bc	586179.3	4109411.5	1,302.7	< 20	233	571	204	TM-LVTA
HOOPOE	03-57-054	12/16/1964	U-3cf	585968.1	4100478.0	1,227.1	< 20	81	494	70	AA
HOOSIC	09-57-101	03/28/1962	U-9j	585824.9	4108896.8	1,290.8	3.4	202	557	187	TM-LVTA
HOREHOUND	03-57-153	08/27/1969	U-3gm	589385.8	4094331.2	1,201.5	< 20	351	460	332	LTCU
HOSPAH	03-57-199	12/14/1971	U-3je	586356.6	4097977.3	1,215.2	< 20	321	482	302	AA
HUDSON	09-57-105	04/12/1962	U-9n	584845.4	4109204.2	1,280.2	Low	181	539	151	AA
HULA	09-57-068	10/29/1968	U-9bu	585210.3	4107663.6	1,280.8	< 20	375	543	200	AA
HULSEA	02-57-051	03/14/1974	U-2bx	583106.7	4112288.0	1,316.4	< 20	229	577	195	AA
HUPMOBILE	02-57-153	01/18/1968	U-2y	582976.7	4111227.4	1,313.7	7.4	280	573	247	AA
HURON KING	03-57-239	06/24/1980	U-3ky	585915.7	4097689.3	1,214.6	< 20	354	481	320	AA
HUTCH	02-57-083	07/16/1969	U-2df	581050.2	4110535.3	1,327.1	20 to 200	568	581	549	AA
HUTIA	03-57-029	06/06/1963	U-3bc	585694.3	4100015.7	1,225.0	Low	142	492	135	AA
HYRAX	03-57-034	09/14/1962	U-3bh	587050.7	4099990.9	1,224.4	Low	329	491	217	AA
ICEBERG	04-57-023	03/23/1978	U-4g	584315.6	4106380.6	1,265.5	20 to 150	744	485	640	LTCU
ILDRIM	02-57-019	07/16/1969	U-2au	583943.4	4108335.6	1,282.9	20 to 200	428	514	410	TM-WTA
IMP	02-57-037	08/09/1968	U-2bj	581937.1	4113015.3	1,340.8	< 20	187	602	182	AA
INGOT	02-57-139	03/09/1989	U-2gg	582867.7	4110922.0	1,307.3	20 to 150	555	564	500	TM-WTA
IPECAC-A	03-57-175	05/27/1969	U-3hka	588768.4	4096797.3	1,208.5	< 20	134	472	124	AA
IPECAC-B	03-57-176	05/27/1969	U-3hkb	588950.9	4096782.7	1,209.4	< 20	134	473	124	AA
ISLAY	02-57-118	08/27/1981	U-2er	582885.3	4112872.3	1,323.4	< 20	335	587	294	TM-LVTA

Table A.1-1
Shaft and Tunnel Nuclear Detonations in the Yucca Flat/Climax Mine Corrective Action Unit
(Page 12 of 24)

Detonation Name	CAS Number	Date Expended	Emplacement Hole Name	UTM Easting	UTM Northing	Land Surface Elevation [a] (m amsl)	Announced Yield(kt)	Hole Depth (m)	Estimated Depth to Water (m)	Depth of Burial (m)	Working Point HSU
IZZER	09-57-064	07/16/1965	U-9bp	585682.0	4107863.3	1,299.7	< 20	239	565	164	AA
JACKPOTS	03-57-226	06/01/1978	U-3kj	586113.6	4097397.5	1,212.8	< 20	351	479	305	AA
JAL	03-57-171	03/19/1970	U-3hh	586945.1	4095236.8	1,205.5	< 20	311	469	301	AA
JARA	03-57-099	06/06/1974	U-3hp	586883.1	4095541.3	1,207.0	< 20	396	471	378	AA
JARLSBERG	10-57-040	08/27/1983	U-10ca	585732.9	4116509.2	1,344.5	< 20	265	325	200	TM--LVTA
JERBOA	03-57-020	03/01/1963	U-3at	586571.4	4100049.9	1,224.1	Low	309	491	301	AA
JIB	03-57-165	05/08/1974	U-3hb	588834.1	4095243.7	1,204.3	< 20	253	463	180	TM-UVTA
JICARILLA	03-57-207	04/19/1972	U-3jm	587494.2	4095854.9	1,207.0	< 20	168	470	148	AA
JORNADA	04-57-026	01/28/1982	U-4j	584319.7	4105223.0	1,260.0	139	686	477	640	LTCU
KANKAKEE	10-57-052	06/15/1966	U-10p	584440.2	4114121.4	1,308.2	20 to 200	462	575	455	LCA
KARA	02-57-086	05/11/1972	U-2dh3	581340.7	4107540.3	1,294.5	< 20	290	554	259	AA
KARAB	04-57-006	03/16/1978	U-4ah	581625.6	4104512.0	1,274.7	< 20	351	525	331	LTCU
KASHAN	10-57-026	05/24/1973	U-10av	583820.0	4113082.8	1,303.9	< 20	320	567	265	AA
KAWEAH	09-57-025	02/21/1963	U-9ab	584777.9	4108442.2	1,276.2	3	233	534	227	AA
KAWICH A-BLUE	08-57-009	12/09/1988	U-8n	580630.7	4114503.8	1,384.4	< 20	577	540	384	OSBCU
KAWICH A-WHITE	08-57-009	12/09/1988	U-8n	580630.7	4114503.8	1,384.4	< 20	577	540	369	LTCU
KAWICH-BLACK	02-57-072	02/24/1989	U-2cu	577996.1	4109283.8	1,379.5	< 20	462	551	431	TM-LVTA
KAWICH-RED	02-57-072	02/24/1989	U-2cu	577996.1	4109283.8	1,379.5	< 20	462	551	370	TM-LVTA
KEEL	03-57-189	12/16/1974	U-3hu	587398.0	4096373.8	1,208.8	< 20	329	473	305	AA
KEELSON	07-57-010	02/04/1976	U-7ai	586217.5	4102791.8	1,244.8	20 to 200	664	508	640	LTCU
KENNEBEC	02-57-005	06/25/1963	U-2af	582780.2	4109651.9	1,303.0	Low	238	554	226	AA
KERMET	02-57-054	11/23/1965	U-2c	582493.4	4113032.5	1,331.4	< 20	233	594	196	AA
KESTI	09-57-085	06/16/1982	U-9cn	587373.1	4107793.1	1,338.4	< 20	336	606	289	LTCU
KESTREL	03-57-071	04/05/1965	U-3dd	586935.2	4097979.3	1,214.6	< 20	454	481	447	AA
KHAKI	03-57-114	10/15/1966	U-3et	587414.8	4100342.9	1,228.6	< 20	244	495	233	AA
KINIBITO	03-57-264	12/05/1985	U-3me	584883.3	4101004.2	1,235.0	20 to 150	686	496	579	LTCU
KLICKITAT	10-57-045	02/20/1964	U-10e	585241.1	4111838.4	1,300.3	70	511	568	493	LTCU
KLOSTER	02-57-115	02/15/1979	U-2eo	582422.6	4111935.2	1,324.1	20 to 150	558	584	536	TM-LVTA
KNIFE A	03-57-122	09/12/1968	U-3fb	587908.0	4098653.1	1,217.4	< 20	344	483	332	TM-LVTA
KNIFE B	03-57-093	11/15/1968	U-3dz	585990.5	4098006.5	1,215.2	< 20	375	482	363	AA
KNIFE C	03-57-112	10/03/1968	U-3er	589586.5	4098019.1	1,228.3	< 20	314	495	301	LTCU
KNOX	02-57-018	02/21/1968	U-2at	584072.8	4108017.9	1,279.9	20 to 200	669	504	645	LTCU

Table A.1-1
Shaft and Tunnel Nuclear Detonations in the Yucca Flat/Climax Mine Corrective Action Unit
(Page 13 of 24)

Detonation Name	CAS Number	Date Expended	Emplacement Hole Name	UTM Easting	UTM Northing	Land Surface Elevation [a] (m amsl)	Announced Yield(kt)	Hole Depth (m)	Estimated Depth to Water (m)	Depth of Burial (m)	Working Point HSU
KOHOCTON	09-57-034	08/23/1963	U-9ak	585690.0	4108966.8	1,300.6	Low	262	566	255	TM-LVTA
KOOTANAI	09-57-111	04/24/1963	U-9w	585615.8	4108481.7	1,287.8	Low	186	552	182	AA
KRYDDOST	02-57-066	05/06/1982	U-2co	577568.2	4107987.2	1,390.5	< 20	357	516	335	TM-LVTA
KYACK-A	02-57-044	09/20/1969	U-2bq1	582780.2	4112686.1	1,323.4	< 20	199	586	185	AA
KYACK-B	02-57-045	09/20/1969	U-2bq2	582920.0	4112540.3	1,320.1	< 20	206	582	192	AA
LABAN	02-57-133	08/03/1983	U-2ff	580942.1	4108258.1	1,303.0	< 20	366	561	326	AA
LABIS	10-57-019	02/05/1970	U-10an	585340.2	4113290.2	1,313.1	25	480	580	442	LTCU
LAGOON	10-57-023	10/14/1971	U-10ar	584056.7	4115032.4	1,312.8	< 20	369	575	305	AA
LAGUNA	03-57-124	06/23/1971	U-3fd	586937.0	4097552.4	1,213.4	20 to 200	469	480	455	TM-WTA
LAMPBLACK	07-57-049	01/18/1966	U-7i	587212.2	4105292.2	1,294.2	20 to 200	579	560	561	OSBCU
LANPHER	02-57-152	10/18/1967	U-2x	583723.9	4107906.7	1,282.0	20 to 200	782	498	715	LTCU
LAREDO	03-57-267	05/21/1988	U-3mh	590070.9	4098752.1	1,247.2	< 150	531	515	351	LTCU
LATIR	04-57-020	02/27/1974	U-4d	584162.6	4106654.3	1,270.1	20 to 200	686	486	641	LTCU
LEDOUX	01-57-001	09/27/1990	U-1a.01	583791.1	4095876.4	1,217.7	< 20	NA	479	291	AA
LEXINGTON	02-57-039	08/24/1967	U-2bm	582204.5	4113122.6	1,336.9	< 20	233	599	226	AA
LEYDEN	09-57-084	11/26/1975	U-9cm	587165.1	4108127.5	1,329.8	< 20	355	597	326	LTCU
LIME	07-57-047	04/01/1966	U-7j	587088.1	4106511.9	1,318.6	< 20	578	585	561	OSBCU
LINKS	09-57-054	07/23/1964	U-9bf	586002.4	4107727.0	1,300.0	< 20	127	566	120	AA
LIPTAUER	02-57-109	04/03/1980	U-2eh	581499.3	4111689.4	1,331.4	20 to 150	686	585	417	AA
LONGCHAMPS	02-57-091	04/19/1972	U-2dm	581388.9	4108588.7	1,303.0	< 20	344	560	326	AA
LOVAGE	03-57-125	12/17/1969	U-3fe	586942.7	4095846.3	1,207.9	< 20	396	472	378	AA
LOWBALL	07-57-021	07/12/1978	U-7av	584995.6	4103823.6	1,252.4	20 to 150	591	490	564	LTCU
LUBBOCK	03-57-271	10/18/1991	U-3mt	584879.0	4102131.9	1,239.6	20 to 150	472	468	457	LTCU
LUNA	03-57-262	09/21/1958	U-3m	585925.1	4100568.1	1,227.7	0.0015	160	495	148	AA
MACKEREL	04-57-018	02/18/1964	U-4b	584360.3	4105698.8	1,263.4	< 20	500	484	334	TM-LVTA
MAD	09-57-023	12/13/1961	U-9a	584500.3	4109136.9	1,281.4	0.5	187	537	182	AA
MALLET	03-57-136	01/31/1968	U-3fv	588164.0	4095241.4	1,204.3	< 20	253	465	240	AA
MANATEE	09-57-029	12/14/1962	U-9af	585284.7	4108882.8	1,280.8	Low	67	543	60	AA
MANTECA	04-57-010	12/10/1982	U-4al	582496.0	4103966.9	1,263.1	20 to 150	488	505	413	AA
MANZANAS	03-57-157	05/21/1970	U-3gr	589681.8	4096496.1	1,221.6	< 20	253	485	241	TSA
MARIBO	02-57-070	06/26/1985	U-2cs	577997.8	4108796.2	1,379.5	< 20	457	547	381	TM-LVTA

Table A.1-1
Shaft and Tunnel Nuclear Detonations in the Yucca Flat/Climax Mine Corrective Action Unit
(Page 14 of 24)

Detonation Name	CAS Number	Date Expended	Emplacement Hole Name	UTM Easting	UTM Northing	Land Surface Elevation [a] (m amsl)	Announced Yield(kt)	Hole Depth (m)	Estimated Depth to Water (m)	Depth of Burial (m)	Working Point HSU
MARSH	03-57-220	09/06/1975	U-3kb	586433.6	4097734.1	1,214.0	< 20	460	480	427	AA
MARSILLY	02-57-112	04/05/1977	U-2el	583306.2	4108418.4	1,286.3	20 to 150	732	520	690	LTCU
MARVEL	10-57-044	09/21/1967	U-10ds1	585381.5	4113496.4	1,314.3	2.2	626	580	176	AA
MATACO	03-57-036	06/14/1963	U-3bk	587293.9	4100235.9	1,227.1	Low	201	493	196	AA
MAUVE	03-57-085	08/06/1965	U-3dp	585415.1	4097059.5	1,21,2.5	< 20	348	479	321	AA
MAXWELL	09-57-065	01/13/1966	U-9br	586397.6	4108003.3	1,310.0	< 20	308	578	183	TM-LVTA
MEMORY	03-57-231	03/14/1979	U-3kq	585411.2	4098187.3	1,217.7	< 20	443	485	366	AA
MERIDA	02-57-092	06/07/1972	U-2dn	581263.2	4107916.4	1,297.8	< 20	232	556	204	AA
MERLIN	03-57-062	02/16/1965	U-3ct	586803.3	4100843.3	1,230.8	10.1	317	497	296	AA
MERRIMAC	03-57-030	07/13/1962	U-3bd	585946.0	4101214.5	1,231.7	Intermediate	422	498	413	AA
MESCALERO	03-57-160	01/05/1972	U-3gu	586298.9	4100174.2	1,225.3	< 20	128	492	120	AA
MESITA	03-57-198	05/09/1973	U-3jd	587541.9	4095817.0	1,207.0	< 20	162	470	149	AA
METROPOLIS	02-57-140	03/10/1990	U-2gh	583945.8	4107567.1	1,273.1	20 to 150	549	479	469	TM-LVTA
MICKEY	07-57-050	05/10/1967	U-7m	589307.3	4103777.5	1,304.5	20 to 200	518	573	500	LTCU
MIDLAND	07-57-040	07/16/1987	U-7by	586783.4	4106602.6	1,310.6	20 to 150	549	577	488	OSBCU
MIERA	07-57-005	03/08/1973	U-7ad	586483.2	4106603.9	1,306.1	20 to 200	599	573	569	OSBCU
MINERO	03-57-257	12/20/1984	U-3lt	584988.3	4096420.8	1,214.6	< 20	274	481	244	TM-UVTA
MINIATA	02-57-048	07/08/1971	U-2bu	584282.2	4107306.5	1,273.8	83	564	494	529	LTCU
MINK	03-57-005	10/29/1961	U-3ae	586157.6	4100495.8	1,227.7	Low	210	495	192	AA
MINNOW	03-57-064	05/15/1964	U-3cv	587843.5	4099749.6	1,225.9	< 20	274	492	241	AA
MISSISSIPPI	09-57-027	10/05/1962	U-9ad	584347.0	4110555.5	1,290.5	115	553	546	494	TM-LVTA
MIZZEN	07-57-009	06/03/1975	U-7ah	585660.0	4105623.5	1,274.1	20 to 200	978	536	637	LTCU
MOA	03-57-097	09/01/1965	U-3ed	587692.9	4099261.8	1,220.7	< 20	206	487	194	AA
MOGOLLON	03-57-248	04/20/1986	U-3li	584869.0	4096387.5	1,214.6	< 20	274	481	259	TM-UVTA
MONAHANS-A	03-57-250	11/09/1988	U-3lk	587113.8	4094139.8	1,202.1	< 20	396	463	290	AA
MONAHANS-B	06-57-006	11/09/1988	U-6i	587114.5	4093866.1	1,201.5	< 20	320	462	290	AA
MONERO	03-57-210	05/19/1972	U-3jq	588748.7	4102312.8	1,272.5	< 20	580	522	537	OSBCU
MONTEREY	04-57-008	07/29/1982	U-4aj	582197.9	4106418.6	1,280.2	20 to 150	488	495	400	TM-LVTA
MORRONES	03-57-103	05/21/1970	U-3ei	587740.8	4102979.7	1,264.3	20 to 200	533	518	483	LTCU
MUDPACK	10-57-051	12/16/1964	U-10n	582823.3	4114801.0	1,336.9	2.7	160	602	152	TM-LVTA
MUGGINS	03-57-256	12/09/1983	U-3ls	584899.0	4096509.5	1,215.2	< 20	305	482	244	TM-UVTA
MULESHOE	07-57-031	11/15/1989	U-7bk	587666.5	4106940.6	1,338.4	< 20	376	606	244	LTCU

Table A.1-1
Shaft and Tunnel Nuclear Detonations in the Yucca Flat/Climax Mine Corrective Action Unit
(Page 15 of 24)

Detonation Name	CAS Number	Date Expended	Emplacement Hole Name	UTM Easting	UTM Northing	Land Surface Elevation [a] (m amsl)	Announced Yield(kt)	Hole Depth (m)	Estimated Depth to Water (m)	Depth of Burial (m)	Working Point HSU
MULLET	02-57-006	10/17/1963	U-2ag	582878.8	4109587.4	1,301.5	Low	63	552	60	AA
MUNDO	07-57-034	05/01/1984	U-7bo	586866.8	4106899.7	1,319.2	20 to 150	610	586	567	OSBCU
MUSCOVY	03-57-091	04/23/1965	U-3dx	589376.5	4097073.4	1,216.5	< 20	191	482	180	TM-WTA
MUSHROOM	03-57-100	03/03/1967	U-3ef	588026.9	4099506.8	1,225.0	< 20	191	491	180	AA
MUSTANG	09-57-040	11/15/1963	U-9at	584660.2	4109770.1	1,283.8	Low	174	542	166	AA
NAMA-AMARYLIS	09-57-020	08/05/1971	U-9itsxy31	585853.1	4111200.7	1,300.3	< 20	305	568	273	LTCU
NAMA-MEPHISTO	09-57-019	08/05/1971	U-9itsz27	586037.6	4110713.8	1,303.0	< 20	264	571	244	TM-LVTA
NARRAGUAGUS	02-57-127	09/27/1963	U-2f	582284.4	4112241.0	1,328.9	Low	156	589	150	AA
NASH	02-57-058	01/19/1967	U-2ce	576803.9	4110955.3	1,452.1	39	370	527	365	LCA3
NATCHES	09-57-033	08/23/1963	U-9ak1	585702.2	4108966.8	1,288.4	Low	64	554	59	AA
NATOMA	10-57-027	04/05/1973	U-10aw	583987.3	4114820.4	1,309.7	< 20	416	574	244	AA
NAVATA	03-57-242	09/29/1983	U-3lb	587107.3	4101042.4	1,233.8	< 20	244	500	183	AA
NESSEL	02-57-116	08/29/1979	U-2ep	582922.5	4108524.0	1,286.6	20 to 150	543	532	464	AA
NEWARK	10-57-057	09/29/1966	U-10u	584694.2	4113804.8	1,306.1	< 20	233	573	229	AA
NIGHTINGALE	02-57-125	06/22/1988	U-2ey	582371.1	4113504.4	1,336.2	< 150	279	600	238	AA
NIPPER	03-57-152	02/04/1969	U-3gl	588163.4	4095423.9	1,204.9	< 20	253	466	241	AA
NIZA	09-57-088	07/10/1981	U-9cr	585829.0	4109372.2	1,293.0	< 20	369	560	341	LTCU
NOGGIN	09-57-070	09/06/1968	U-9bx	584631.9	4110188.0	1,286.3	20 to 200	640	543	582	TM-LVTA
NOOR	02-57-032	04/10/1968	U-2be	581797.0	4112191.7	1,336.5	20 to 200	399	596	381	AA
NORBO	08-57-003	03/08/1980	U-8c	581390.6	4115024.5	1,376.2	< 20	279	639	271	OSBCU
NORMANNA	10-57-041	07/12/1984	U-10cb	585704.1	4116403.1	1,342.3	< 20	230	350	200	LTCU
NUMBAT	03-57-046	12/12/1962	U-3bu	587537.7	4100236.7	1,228.3	Low	256	494	232	AA
OAKLAND	02-57-036	04/04/1967	U-2bi	581489.4	4113032.0	1,348.1	< 20	171	601	166	AA
OARLOCK	03-57-228	02/16/1977	U-3km	586422.3	4096606.3	1,210.1	< 20	343	476	320	AA
OBAR	07-57-008	04/30/1975	U-7ag	586293.8	4107185.6	1,306.4	20 to 200	602	573	569	OSBCU
OCATE	03-57-209	03/30/1972	U-3jp	587651.1	4095621.1	1,206.4	< 20	229	469	210	AA
OCHRE	03-57-096	04/29/1966	U-3ec	586928.6	4099960.0	1,223.2	< 20	136	490	126	AA
OCONTO	09-57-045	01/23/1964	U-9ay	585607.7	4109127.7	1,286.6	10.5	277	552	265	TM-LVTA
OFFSHORE	03-57-233	08/08/1979	U-3ks	588250.1	4096765.0	1,208.8	20 to 150	492	472	396	LTCU
ONAJA	03-57-212	03/30/1972	U-3js	587187.2	4095725.2	1,207.0	< 20	321	471	279	AA
ORGANDY	09-57-063	06/11/1965	U-9bo	586778.3	4107958.6	1,320.4	< 20	191	588	168	TM-LVTA

Table A.1-1
Shaft and Tunnel Nuclear Detonations in the Yucca Flat/Climax Mine Corrective Action Unit
(Page 16 of 24)

Detonation Name	CAS Number	Date Expended	Emplacement Hole Name	UTM Easting	UTM Northing	Land Surface Elevation [a] (m amsl)	Announced Yield(kt)	Hole Depth (m)	Estimated Depth to Water (m)	Depth of Burial (m)	Working Point HSU
ORKNEY	10-57-035	05/02/1984	U-10be	583958.3	4117105.7	1,378.3	< 20	229	606	210	AA
OSCURO	07-57-062	09/21/1972	U-7z	585633.6	4104206.1	1,252.1	20 to 200	581	513	560	LTCU
OTERO	03-57-274	09/12/1958	U-3q	586089.4	4100642.4	1,229.0	0.038	157	496	146	AA
PACA	03-57-024	05/07/1962	U-3ax	586701.4	4100279.2	1,225.6	Low	267	492	258	AA
PACKARD	02-57-150	01/15/1969	U-2u	582975.8	4111486.5	1,315.2	10	311	575	247	AA
PACKRAT	03-57-023	06/06/1962	U-3aw	585432.6	4100172.0	1,225.9	Low	270	492	262	AA
PAISANO	09-57-112	04/24/1963	U-9w1	585625.0	4108474.1	1,287.8	Low	62	553	57	AA
PAJARA	03-57-203	12/12/1973	U-3ji	586842.2	4094169.9	1,202.4	< 20	297	465	278	AA
PALISADE-1	04-57-015	05/15/1989	U-4at	578112.7	4106968.3	1,365.2	< 20	464	490	335	TM-LVTA
PALISADE-2	04-57-015	05/15/1989	U-4at	578112.7	4106968.3	1,365.2	< 20	464	490	390	TM-LVTA
PALISADE-3	04-57-015	05/15/1989	U-4at	578112.7	4106968.3	1,365.2	< 20	464	490	404	TM-LVTA
PALIZA	07-57-026	10/01/1981	U-7bd	588106.2	4104182.8	1,287.5	20 to 150	610	533	472	LTCU
PAMPAS	03-57-012	03/01/1962	U-3al	586380.7	4099687.8	1,222.9	9.5	370	490	363	AA
PANAMINT	02-57-136	05/21/1986	U-2gb	583468.9	4108952.6	1,286.0	< 20	573	529	480	TM-WTA
PANCHUELA	03-57-266	06/30/1987	U-3mg	585148.3	4094941.0	1,206.1	< 20	457	473	320	AA
PAR	02-57-146	10/09/1964	U-2p	581965.5	4111857.4	1,331.4	38	416	586	406	AA
PARNASSIA	02-57-030	11/30/1971	U-2bc	582555.9	4112872.7	1,328.9	< 20	346	592	331	TM-LVTA
PARROT	03-57-080	12/16/1964	U-3dk	587846.5	4098988.1	1,219.5	1.3	187	486	180	AA
PASCAL-A	03-57-194	07/26/1957	U-3j	585947.3	4100848.8	1,229.3	Slight	152	496	152	AA
PASCAL-B	03-57-068	08/27/1957	U-3d	585902.7	4100547.6	1,227.7	Slight	152	495	152	AA
PASCAL-C	03-57-094	12/06/1957	U-3e	586176.6	4100648.5	1,228.6	Slight	158	496	76	AA
PASSAIC	09-57-103	04/06/1962	U-9l	584931.9	4108150.8	1,275.0	Low	270	536	233	AA
PEBA	03-57-028	09/20/1962	U-3bb	586311.4	4101215.8	1,232.3	Low	283	499	241	AA
PEDERNAL	03-57-170	09/29/1971	U-3hg	588312.5	4096353.9	1,207.3	< 20	396	470	379	TM-LVTA
PEKAN	03-57-048	08/12/1963	U-3bw	587539.1	4099748.9	1,223.8	Low	311	490	302	AA
PENASCO	03-57-181	11/19/1970	U-3hl	587549.3	4096762.6	1,209.8	< 20	282	475	271	AA
PERA	10-57-034	09/08/1979	U-10bd	585407.4	4112296.1	1,307.3	< 20	335	575	200	TM-LVTA
PERSIMMON	03-57-083	02/23/1967	U-3dn	587548.2	4097067.6	1,210.7	< 20	309	476	299	AA
PETREL	03-57-092	06/11/1965	U-3dy	587416.2	4099870.0	1,224.1	1.3	192	490	181	AA
PICCALILLI	03-57-123	11/21/1969	U-3fc	588761.4	4098595.2	1,222.2	20 to 200	407	489	394	LTCU
PIKE	03-57-066	03/13/1964	U-3cy	587901.4	4100724.6	1,237.5	< 20	289	501	115	AA
PILE DRIVER	15-57-002	06/02/1966	U-15.01	583511.6	4119950.0	1,551.4	62	NA	185	463	MGCU

Table A.1-1
Shaft and Tunnel Nuclear Detonations in the Yucca Flat/Climax Mine Corrective Action Unit
(Page 17 of 24)

Detonation Name	CAS Number	Date Expended	Emplacement Hole Name	UTM Easting	UTM Northing	Land Surface Elevation [a] (m amsl)	Announced Yield(kt)	Hole Depth (m)	Estimated Depth to Water (m)	Depth of Burial (m)	Working Point HSU
PINEAU	07-57-016	07/16/1981	U-7ao	587154.5	4104958.3	1,286.3	< 20	460	552	204	TM-UVTA
PINEDROPS-BAYOU	10-57-024	01/10/1974	U-10as	584266.4	4114406.9	1,310.0	< 20	366	576	343	TM-LVTA
PINEDROPS-SLOAT	10-57-024	01/10/1974	U-10as	584266.4	4114406.9	1,310.0	< 20	366	576	213	AA
PINEDROPS-TAWNY	10-57-024	01/10/1974	U-10as	584266.4	4114406.9	1,310.0	< 20	366	576	282	TM-LVTA
PIPEFISH	03-57-059	04/29/1964	U-3co	586564.5	4099501.4	1,221.0	< 20	274	488	262	AA
PIRANHA	07-57-043	05/13/1966	U-7e	585905.9	4104740.6	1,263.7	20 to 200	587	526	549	LTCU
PITON-A	09-57-014	05/28/1970	U-9itsy30	585914.5	4111079.0	1,300.9	< 20	251	568	236	TM-LVTA
PITON-B	09-57-010	05/28/1970	U-9itsx27	585794.5	4110712.6	1,296.9	< 20	244	564	229	TM-LVTA
PITON-C	09-57-116	05/28/1970	U-9itsaa25	586160.7	4110470.4	1,305.8	< 20	122	573	101	TM-LVTA
PLAID II	02-57-148	02/03/1966	U-2r	582660.9	4109086.8	1,298.4	< 20	500	546	269	AA
PLANER	03-57-106	11/21/1969	U-3el	586939.8	4096760.4	1,210.4	< 20	396	476	378	AA
PLATYPUS	03-57-004	02/24/1962	U-3ad	586086.1	4100469.3	1,227.1	Low	66	494	58	AA
PLAYER	09-57-075	08/27/1964	U-9cc	585230.1	4108118.6	1,280.5	< 20	94	543	90	AA
PLEASANT	09-57-030	05/29/1963	U-9ah	584973.0	4109304.9	1,279.6	Low	219	540	211	AA
PLIERS	03-57-154	08/27/1969	U-3gn	585566.0	4097487.0	1,214.3	< 20	253	481	239	AA
PLOMO	03-57-126	05/01/1974	U-3ff	590224.1	4098600.6	1,253.9	< 20	283	522	149	TM-LVTA
POD-A	02-57-063	10/29/1969	U-2ch	577225.1	4110576.5	1,424.0	16.7 (total)	285	540	267	TM-LVTA
POD-B	02-57-060	10/29/1969	U-2ci	576218.3	4110593.9	1,491.7		267	444	249	TM-LVTA
POD-C	02-57-061	10/29/1969	U-2cj	576388.4	4110138.7	1,474.9		265	466	171	AA
POD-D	02-57-062	10/29/1969	U-2ck	576745.9	4110032.1	1,451.2		334	512	312	TM-LVTA
POLKA	10-57-008	12/06/1967	U-10ai	584091.8	4112756.8	1,299.4	< 20	207	558	190	AA
POLYGONUM	02-57-052	10/02/1973	U-2by	582313.0	4112686.0	1,330.8	< 20	244	592	213	AA
POMMARD	03-57-098	03/14/1968	U-3ee	587962.8	4100420.7	1,235.4	1.5	223	501	209	AA
PONGEE	02-57-007	07/22/1965	U-2ah	582887.3	4109696.8	1,301.5	< 20	142	553	135	AA
PONIL	07-57-039	09/27/1985	U-7bv	588717.6	4105097.9	1,310.6	< 20	396	556	366	LTCU
PORTMANTEAU	02-57-022	08/30/1974	U-2ax	581401.3	4111977.3	1,340.2	20 to 200	701	600	655	TM-LVTA
PORTOLA	10-57-032	02/06/1975	U-10bb	584194.6	4114881.4	1,31,2.2	< 20	290	575	198	AA
PORTOLA-LARKIN	10-57-032	02/06/1975	U-10bb	584194.6	4114881.4	1,312.2	< 20	290	575	274	AA
PORTULACA	02-57-049	06/28/1973	U-2bv	581181.7	4111525.2	1,337.5	20 to 200	518	591	466	AA
POTRERO	02-57-106	04/23/1974	U-2eb	582007.9	4112814.4	1,337.2	< 20	274	597	210	AA
POTRILLO	07-57-007	06/21/1973	U-7af	586452.7	4105321.5	1,282.3	20 to 200	606	548	568	OSBCU

Table A.1-1
Shaft and Tunnel Nuclear Detonations in the Yucca Flat/Climax Mine Corrective Action Unit
(Page 18 of 24)

Detonation Name	CAS Number	Date Expended	Emplacement Hole Name	UTM Easting	UTM Northing	Land Surface Elevation [a] (m amsl)	Announced Yield(kt)	Hole Depth (m)	Estimated Depth to Water (m)	Depth of Burial (m)	Working Point HSU
PRATT	03-57-185	09/25/1974	U-3hq	586270.5	4096453.4	1,210.1	< 20	335	476	313	AA
PRESIDIO	06-57-002	04/22/1987	U-6d	588591.5	4093261.8	1,198.5	< 20	396	458	320	TM-LVTA
PUCE	03-57-044	06/10/1966	U-3bs	585459.2	4101692.1	1,235.4	< 20	492	493	486	AA
PUDDLE	03-57-224	11/26/1974	U-3kg	587981.2	4095240.4	1,219.8	< 20	203	481	183	AA
PURPLE	03-57-087	03/18/1966	U-3ds	588160.5	4096154.9	1,206.7	< 20	346	469	333	TM-WTA
PUYE	03-57-206	08/14/1974	U-3jl	585717.6	4097700.5	1,215.2	< 20	460	482	430	AA
PYRAMID	07-57-027	04/16/1980	U-7be	586148.4	4106326.1	1,292.7	20 to 150	610	557	579	OSBCU
QUARGEL	02-57-129	11/18/1978	U-2fb	581380.9	4109135.7	1,301.8	20 to 150	567	539	542	TM-LVTA
QUESO	10-57-036	08/11/1982	U-10bf	584525.4	4116147.8	1,337.2	< 20	555	571	216	AA
QUINELLA	04-57-027	02/08/1979	U-4l	583986.5	4106455.6	1,267.7	20 to 150	710	484	579	LTCU
RACCOON	03-57-010	06/01/1962	U-3ajs	585861.6	4100165.0	1,225.6	Low	172	493	164	AA
RACK	09-57-037	08/15/1968	U-9ap	584551.1	4108818.9	1,280.5	< 20	236	536	200	AA
RARITAN	09-57-109	09/06/1962	U-9u	584853.6	4109551.9	1,281.4	Low	181	540	157	AA
REBLOCHON	02-57-114	02/23/1978	U-2en	583164.7	4108799.1	1,288.1	20 to 150	747	534	658	LTCU
REDMUD	07-57-003	12/08/1976	U-7ab	588743.0	4103928.1	1,295.7	< 20	519	533	427	LTCU
REO	10-57-050	01/22/1966	U-10m	585360.5	4112541.0	1,309.4	< 20	328	577	208	AA
RHYOLITE	02-57-126	06/22/1988	U-2ey	582371.1	4113504.4	1,336.2	< 150	279	600	207	AA
RIB	03-57-215	12/14/1977	U-3jv	587365.7	4097067.0	1,211.0	< 20	232	477	213	AA
RINGTAIL	03-57-011	12/17/1961	U-3ak	586678.0	4099901.2	1,223.5	Low	370	490	363	AA
RIOLA	02-57-117	09/25/1980	U-2eq	583107.7	4107931.4	1,281.1	1.07	520	508	424	AA
RIVET I	10-57-002	01/18/1967	U-10aa	584653.8	4113411.8	1,302.4	< 20	206	567	152	AA
RIVET II	10-57-061	01/26/1967	U-10z	584519.9	4113374.8	1,300.6	< 20	223	563	198	AA
RIVET III	10-57-060	03/02/1967	U-10y	584461.9	4113493.1	1,301.5	< 20	308	567	274	AA
RIVOLI	02-57-108	05/20/1976	U-2eg	582905.9	4110296.9	1,305.8	< 20	297	559	200	AA
ROANOKE	09-57-107	10/12/1962	U-9q	584322.4	4108706.0	1,279.6	Low	218	530	177	AA
ROMANO	02-57-124	12/16/1983	U-2ex	582414.6	4110652.3	1,314.0	20 to 150	612	561	515	TM-UVTA
ROQUEFORT	04-57-014	10/16/1985	U-4as	578066.1	4107227.1	1,367.9	20 to 150	442	508	415	TM-LVTA
ROUSANNE	04-57-030	11/12/1981	U-4p	584501.4	4107089.7	1,269.8	20 to 150	564	499	518	LTCU
ROVENA	10-57-055	08/10/1966	U-10s	584541.8	4113804.2	1,304.8	< 20	198	572	195	AA
RUDDER	07-57-011	12/28/1976	U-7aj(s)	585622.1	4106251.4	1,281.7	20 to 150	698	544	640	OSBCU
RUMMY	07-57-020	09/27/1978	U-7au	584324.5	4103942.8	1,253.0	20 to 150	744	489	640	LTCU
RUSSET	06-57-001	03/05/1968	U-6a	584046.3	4091762.8	1,197.9	< 20	130	459	120	PCUT

Table A.1-1
Shaft and Tunnel Nuclear Detonations in the Yucca Flat/Climax Mine Corrective Action Unit
(Page 19 of 24)

Detonation Name	CAS Number	Date Expended	Emplacement Hole Name	UTM Easting	UTM Northing	Land Surface Elevation [a] (m amsl)	Announced Yield(kt)	Hole Depth (m)	Estimated Depth to Water (m)	Depth of Burial (m)	Working Point HSU
SABADO	03-57-243	08/11/1983	U-3lc	588744.6	4094877.4	1,202.7	< 20	335	461	320	UTCU
SACRAMENTO	09-57-110	06/30/1962	U-9v	584629.8	4108118.6	1,273.1	Low	267	527	149	AA
SAN JUAN	03-57-273	10/20/1958	U-3p	586030.1	4100629.1	1,228.0	Zero	160	495	71	AA
SANDREEF	07-57-018	11/09/1977	U-7aq	584449.6	4103090.0	1,247.9	20 to 150	1103	479	701	LTCU
SANTEE	10-57-046	10/27/1962	U-10f	584053.6	4111651.4	1,296.6	Low	323	551	319	AA
SAPELLO	03-57-145	04/12/1974	U-3ge	585035.3	4096753.8	1,215.8	< 20	283	482	181	AA
SAPPHO	02-57-085	03/23/1972	U-2dh2	581666.9	4107605.1	1,292.7	< 20	282	552	198	AA
SARDINE	03-57-056	12/04/1963	U-3ch	586320.5	4099500.8	1,221.3	Low	273	489	262	AA
SATSOP	02-57-134	08/15/1963	U-2g	581994.9	4112161.9	1,332.9	Low	232	590	226	AA
SATZ	02-57-095	07/07/1978	U-2dq	581995.9	4107469.5	1,289.9	< 20	404	536	315	TM-LVTA
SAXON	02-57-056	07/28/1966	U-2cc	576988.3	4110605.5	1,438.4	1.2	189	536	154	TM-LVTA
SAZERAC	03-57-121	10/25/1967	U-3fa	586598.4	4098618.4	1,217.7	< 20	314	485	301	AA
SCANTLING	04-57-024	08/19/1977	U-4h	584008.0	4107293.7	1,272.5	20 to 150	732	482	701	OSBCU
SCAUP	03-57-069	05/14/1965	U-3da(s)	587973.7	4101654.6	1,249.1	< 20	454	507	427	LTCU
SCHELLBOURNE	02-57-138	05/13/1988	U-2gf	582427.0	4108875.8	1,295.1	< 150	552	541	463	AA
SCISSORS	03-57-148	12/12/1968	U-3gh	585481.1	4095536.4	1,208.5	< 20	253	475	241	AA
SCREAMER	03-57-076	09/01/1965	U-3dg	588155.5	4097678.9	1,211.6	< 20	309	478	302	TM-WTA
SCREE-ACAJOU	09-57-009	10/13/1970	U-9itsx24	585795.1	4110353.3	1,296.0	< 20	268	563	250	TM-LVTA
SCREE-ALHAMBRA	09-57-015	10/13/1970	U-9itsz21	586040.2	4109982.7	1,300.0	< 20	211	568	192	TM-LVTA
SCREE-CHAMOIS	09-57-016	10/13/1970	U-9itsz24	586038.9	4110344.7	1,301.8	< 20	207	569	101	TM-LVTA
SCUPPER	03-57-174	08/19/1977	U-3hj	586146.5	4097062.4	1,211.9	< 20	477	478	450	AA
SCUTTLE	02-57-035	11/13/1969	U-2bh	582143.2	4113332.6	1,339.3	1.7	183	602	165	AA
SEAFOAM	02-57-105	12/13/1973	U-2ea	582304.4	4112975.4	1,333.2	< 20	229	595	198	AA
SEAMOUNT	03-57-230	11/17/1977	U-3kp	586724.9	4097399.0	1,212.8	< 20	430	479	371	AA
SEAWEED B	03-57-177	10/16/1969	U-3hkd	589119.4	4096533.4	1,211.9	< 20	128	474	119	AA
SEAWEED-C	03-57-179	10/01/1969	U-3hke	589089.1	4096405.3	1,211.6	< 20	128	473	119	AA
SEAWEED-D	03-57-180	10/01/1969	U-3hkf	589005.6	4096302.6	1,210.4	< 20	128	472	118	AA
SEAWEED-E	03-57-178	10/01/1969	U-3hkc	589088.2	4096661.3	1,211.3	< 20	134	474	124	AA
SECO	08-57-007	02/25/1981	U-8l	581288.4	4115240.2	1,383.2	< 20	233	646	200	OSBCU
SEERSUCKER	09-57-061	02/19/1965	U-9bm	586089.7	4108118.3	1,301.2	< 20	152	568	144	TM-LVTA
SEPIA	03-57-108	11/12/1965	U-3en	586956.6	4100661.0	1,229.3	< 20	253	496	241	AA

Table A.1-1
Shaft and Tunnel Nuclear Detonations in the Yucca Flat/Climax Mine Corrective Action Unit
(Page 20 of 24)

Detonation Name	CAS Number	Date Expended	Emplacement Hole Name	UTM Easting	UTM Northing	Land Surface Elevation [a] (m amsl)	Announced Yield(kt)	Hole Depth (m)	Estimated Depth to Water (m)	Depth of Burial (m)	Working Point HSU
SEVILLA	03-57-129	06/25/1968	U-3fk	589611.2	4099756.1	1,253.0	< 20	411	516	359	TM-LVTA
SEYVAL	03-57-252	11/12/1982	U-3lm	586098.4	4097732.6	1,214.3	< 20	427	481	366	AA
SHALLOWS	03-57-200	02/26/1976	U-3jf	587543.9	4098286.2	1,215.2	< 20	260	481	244	AA
SHAPER	07-57-054	03/23/1970	U-7r	587003.8	4104683.3	1,278.6	20 to 200	579	545	560	OSBCU
SHAVE	03-57-151	01/22/1969	U-3gk	589468.7	4096860.4	1,218.0	< 20	254	483	241	UTCU
SHREW	03-57-003	09/16/1961	U-3ac	586005.9	4100481.8	1,227.4	Low	162	494	98	AA
SHUFFLE	10-57-056	04/18/1968	U-10t	585514.7	4112021.9	1,306.1	20 to 200	543	574	493	ATCU
SIDECAR	03-57-120	12/13/1966	U-3ez	588334.1	4098989.5	1,222.2	< 20	253	489	240	TM-WTA
SIENNA	03-57-057	01/18/1966	U-3cj	587296.4	4099260.1	1,220.1	< 20	310	487	275	AA
SILENE	09-57-082	06/28/1973	U-9ck	585209.7	4107846.4	1,280.8	< 20	336	543	198	AA
SIMMS	10-57-058	11/05/1966	U-10w	584589.5	4113947.6	1,306.4	2.3	201	573	199	AA
SNUBBER	03-57-116	04/21/1970	U-3ev2s	589971.4	4101236.8	1,279.9	12.7	358	551	344	LTCU
SOLANO	03-57-217	08/09/1972	U-3jx	587489.8	4095476.1	1,206.1	< 20	153	468	134	AA
SOLANUM	09-57-022	12/14/1972	U-9itsw24.5	585733.9	4110423.2	1,294.2	< 20	221	561	201	TM-LVTA
SOLENDON	03-57-067	02/12/1964	U-3cz	586313.5	4101389.8	1,233.2	< 20	161	500	150	AA
SPAR	03-57-211	12/19/1973	U-3jr	587291.6	4095759.1	1,207.0	< 20	163	471	149	AA
SPIDER-A	02-57-042	08/14/1969	U-2bp1	583144.6	4112855.9	1,318.6	< 20	221	582	213	AA
SPIDER-B	02-57-043	08/14/1969	U-2bp2	583130.8	4112627.6	1,318.3	< 20	236	581	228	AA
SPOON	09-57-052	09/11/1964	U-9bd	586581.4	4107729.0	1,315.5	< 20	189	583	180	TM-LVTA
SPRIT	03-57-166	11/10/1976	U-3hc	587388.7	4099108.4	1,219.2	< 20	202	486	183	AA
SPUD	03-57-139	07/17/1968	U-3fy	589078.2	4095244.0	1,205.8	< 20	253	464	240	TM-LVTA
ST. LAWRENCE	02-57-029	11/09/1962	U-2b	582280.6	4113243.5	1,336.2	Low	171	599	167	AA
STACCATO	10-57-007	01/19/1968	U-10ah	584012.5	4112436.3	1,298.8	20 to 200	462	559	443	AA
STANLEY	10-57-053	07/27/1967	U-10q	584495.7	4111592.0	1,291.4	20 to 200	512	547	484	TM-LVTA
STANYAN	02-57-021	09/26/1974	U-2aw	582749.8	4109788.0	1,301.8	20 to 200	660	554	573	TM-WTA
STARWORT	02-57-047	04/26/1973	U-2bs	583637.5	4108733.7	1,288.1	90	610	525	564	LTCU
STILLWATER	09-57-073	02/08/1962	U-9c	584153.6	4109205.1	1,282.9	3.07	194	537	181	AA
STILT	03-57-127	12/15/1967	U-3fh	588759.6	4099204.6	1,230.8	< 20	344	497	333	TM-LVTA
STOAT	03-57-016	01/09/1962	U-3ap	585809.3	4100056.4	1,225.6	5.1	309	493	302	AA
STODDARD	02-57-064	09/17/1968	U-2cms	577514.9	4108322.2	1,396.9	31	480	522	468	TM-LVTA
STONES	09-57-028	05/22/1963	U-9ae	585378.8	4107420.1	1,284.1	Intermediate	403	547	393	TM-LVTA
STRAIT	04-57-001	03/17/1976	U-4a	584191.6	4106990.5	1,270.7	200 to 500	961	484	780	OSBCU

Table A.1-1
Shaft and Tunnel Nuclear Detonations in the Yucca Flat/Climax Mine Corrective Action Unit
(Page 21 of 24)

Detonation Name	CAS Number	Date Expended	Emplacement Hole Name	UTM Easting	UTM Northing	Land Surface Elevation [a] (m amsl)	Announced Yield(kt)	Hole Depth (m)	Estimated Depth to Water (m)	Depth of Burial (m)	Working Point HSU
STRAKE	07-57-006	08/04/1977	U-7ae	588267.9	4104733.7	1,300.3	20 to 150	870	546	518	LTCU
STURGEON	03-57-040	04/15/1964	U-3bo	587294.8	4099991.8	1,225.0	< 20	156	491	150	AA
STUTZ	02-57-055	04/06/1966	U-2ca	576304.6	4110491.9	1,485.0	< 20	233	466	226	TM-LVTA
SUEDE	09-57-060	03/20/1965	U-9bk	586490.8	4107916.7	1,312.8	< 20	152	581	143	TM-LVTA
SUNDOWN-A	01-57-003	09/20/1990	U-1d	583883.6	4099324.7	1,233.5	< 20	457	495	270	AA
SUNDOWN-B	01-57-003	09/20/1990	U-1d	583883.6	4099324.7	1,233.5	< 20	457	495	256	AA
SUTTER	02-57-050	12/21/1976	U-2bw	583168.9	4111930.2	1,314.3	< 20	229	573	200	AA
SWITCH	09-57-069	06/22/1967	U-9bv	586287.3	4109038.6	1,303.6	3.1	312	572	302	LTCU
TAHOKA	03-57-265	08/13/1987	U-3mf	584880.3	4101857.7	1,239.6	20 to 150	671	487	640	LTCU
TAJIQUE	07-57-002	06/28/1972	U-7aa	589600.0	4102864.3	1,300.6	< 20	587	571	332	LTCU
TAJO	07-57-032	06/05/1986	U-7bl	587486.3	4106026.0	1,315.8	20 to 150	552	582	518	LTCU
TAN	07-57-048	06/03/1966	U-7k	585761.0	4102698.5	1,240.5	20 to 200	579	499	561	TM-LVTA
TANGERINE	03-57-095	08/12/1966	U-3eb	586318.1	4100247.1	1,225.6	< 20	95	492	88	AA
TANYA	02-57-098	07/30/1968	U-2dt	581536.8	4108016.4	1,297.5	20 to 200	559	558	381	AA
TAPESTRY	02-57-013	05/12/1966	U-2an	582505.7	4109969.7	1,307.9	< 20	279	557	249	AA
TAPPER	03-57-155	06/12/1969	U-3go	586271.8	4096087.7	1,208.5	< 20	319	475	303	AA
TARKO	02-57-131	02/28/1980	U-2fd	580969.6	4109096.1	1,306.7	< 20	465	561	369	AA
TAUNTON	09-57-024	12/04/1962	U-9aa	584387.9	4109300.1	1,282.9	Low	232	539	227	AA
TECHADO	04-57-029	09/22/1983	U-4o	584466.8	4106807.4	1,267.7	< 150	579	493	533	LTCU
TEE	02-57-003	05/07/1965	U-2ab	582895.8	4110647.9	1,309.7	7	233	564	184	AA
TEJON	03-57-055	05/17/1963	U-3cg	586045.8	4100469.2	1,227.1	Low	79	494	75	AA
TELEME	09-57-083	02/06/1975	U-9cl	586977.4	4107776.4	1,327.1	< 20	355	594	305	LTCU
TEMESCAL	04-57-003	11/02/1974	U-4ab	580723.6	4105392.9	1,290.5	< 20	299	445	263	AA
TEMPLAR	09-57-067	03/24/1966	U-9bt	586061.7	4107680.9	1,301.8	0.37	233	568	150	TM-WTA
TENAJA	03-57-247	04/17/1982	U-3lh	588082.0	4096993.0	1,204.6	< 20	427	470	357	TM-LVTA
TENDRAC	03-57-027	12/07/1962	U-3ba	586313.0	4100849.8	1,229.3	Low	337	496	303	AA
TERN	03-57-090	01/29/1965	U-3dw	587750.8	4100115.3	1,229.0	< 20	225	495	211	AA
TERRINE-WHITE	09-57-057	12/18/1969	U-9bi1	585749.6	4108470.0	1,290.8	20 to 200	480	556	457	TM-LVTA
TERRINE-YELLOW	09-57-058	12/18/1969	U-9bi2	586297.1	4108498.7	1,303.9	20 to 200	442	572	418	LTCU
TEXARKANA	07-57-041	02/10/1989	U-7ca	588835.4	4103653.9	1,293.6	20 to 150	549	519	503	OSBCU
THISTLE	07-57-056	04/30/1969	U-7t	588372.8	4105145.1	1,307.9	20 to 200	579	556	560	OSBCU

Table A.1-1
Shaft and Tunnel Nuclear Detonations in the Yucca Flat/Climax Mine Corrective Action Unit
(Page 22 of 24)

Detonation Name	CAS Number	Date Expended	Emplacement Hole Name	UTM Easting	UTM Northing	Land Surface Elevation [a] (m amsl)	Announced Yield(kt)	Hole Depth (m)	Estimated Depth to Water (m)	Depth of Burial (m)	Working Point HSU
THROW	02-57-034	04/10/1968	U-2bg	581491.1	4112444.2	1,343.6	< 20	236	601	228	AA
TICKING	09-57-059	08/21/1965	U-9bj	586536.1	4107607.3	1,314.9	< 20	236	582	208	TM-LVTA
TIJERAS	07-57-061	10/14/1970	U-7y	588441.4	4102969.9	1,276.2	20 to 200	579	523	561	OSBCU
TILCI	04-57-009	11/11/1981	U-4ak	582802.2	4103541.3	1,259.1	20 to 150	497	492	445	AA
TINDERBOX	09-57-046	11/22/1968	U-9az	585062.8	4110618.9	1,287.8	< 20	472	547	442	LTCU
TINY TOT	15-57-003	06/17/1965	U-15e	583635.8	4119815.4	1,530.7	< 20	NA	228	111	MGCU
TIOGA	09-57-094	10/18/1962	U-9f	585254.4	4109360.5	1,281.1	Low	66	543	59	AA
TOMATO	03-57-105	04/07/1966	U-3ek	589650.8	4097075.0	1,222.2	< 20	236	489	226	TM-LVTA
TOPGALLANT	04-57-021	02/28/1975	U-4e	583857.1	4106866.9	1,271.9	20 to 200	1022	483	713	LTCU
TOPMAST	07-57-023	03/23/1978	U-7ay	587120.4	4106085.7	1,309.4	< 20	488	576	457	OSBCU
TORCH	03-57-128	02/21/1968	U-3fj	588757.4	4099753.1	1,237.2	< 20	253	501	241	TM-WTA
TORNERO	03-57-251	02/11/1987	U-3ll	584991.2	4096281.3	1,213.4	< 20	396	480	298	TM-WTA
TORNILLO	09-57-038	10/11/1963	U-9aq	585832.6	4108278.0	1,293.6	0.38	157	559	150	AA
TORRIDO	07-57-059	05/27/1969	U-7w	589308.4	4103472.4	1,297.2	20 to 200	533	566	515	OSBCU
TORTUGAS	03-57-147	03/01/1984	U-3gg	584787.0	4102390.0	1,243.3	20 to 150	686	474	640	LTCU
TOYAH	09-57-026	03/15/1963	U-9ac	584855.0	4109054.6	1,279.2	Low	137	538	130	AA
TRANSOM	04-57-022	05/10/1978	U-4f	584199.5	4104826.1	1,258.5	Zero	713	472	640	LTCU
TRAVELER	02-57-057	05/04/1966	U-2cd	576639.2	4110223.7	1,457.2	< 20	233	497	198	AA
TREBBIANO	03-57-249	09/04/1981	U-3lj	584637.3	4101536.6	1,238.1	< 20	335	486	305	TM-UVTA
TROGON	03-57-079	07/24/1964	U-3dj	587842.1	4100237.5	1,231.1	< 20	200	497	193	AA
TRUCHAS-CHACON	03-57-184	10/28/1970	U-3hn	587366.7	4096674.8	1,209.4	< 20	128	475	118	AA
TRUCHAS-CHAMISAL	03-57-182	10/28/1970	U-3ho	587427.7	4096675.3	1,209.4	< 20	130	475	118	AA
TRUCHAS-RODARTE	03-57-183	10/28/1970	U-3hm	587244.5	4096761.5	1,210.1	< 20	282	476	266	AA
TRUMBULL	04-57-002	09/26/1974	U-4aa	580449.3	4105391.9	1,295.7	< 20	299	400	263	TM-LVTA
TUB-A	10-57-011	06/06/1968	U-10ajc	585011.6	4113677.3	1,308.8	< 20	207	575	189	AA
TUB-B	10-57-010	06/06/1968	U-10ajb	584929.5	4113446.3	1,306.1	< 20	200	573	189	AA
TUB-C	10-57-013	06/06/1968	U-10ajf	585174.5	4113447.5	1,310.0	< 20	198	577	189	AA
TUB-D	10-57-012	06/06/1968	U-10ajd	584806.4	4113620.2	1,305.2	< 20	286	572	273	TM-LVTA
TUB-F	10-57-009	06/06/1968	U-10aja	585051.1	4113621.3	1,308.8	< 20	209	575	189	AA
TULIA	04-57-033	05/26/1989	U-4s	583979.3	4104612.0	1,257.3	< 20	610	471	396	TM-UVTA
TULOSO	03-57-149	12/12/1972	U-3gi	587055.0	4098589.2	1,216.5	< 20	285	483	271	AA
TUNA	03-57-074	12/20/1963	U-3de	585950.0	4100962.2	1,229.9	Low	427	497	414	AA

Table A.1-1
Shaft and Tunnel Nuclear Detonations in the Yucca Flat/Climax Mine Corrective Action Unit
(Page 23 of 24)

Detonation Name	CAS Number	Date Expended	Emplacement Hole Name	UTM Easting	UTM Northing	Land Surface Elevation [a] (m amsl)	Announced Yield(kt)	Hole Depth (m)	Estimated Depth to Water (m)	Depth of Burial (m)	Working Point HSU
TUN-A	10-57-015	12/10/1969	U-10am1	581745.5	4113669.8	1,350.0	< 20	213	611	200	AA
TUN-B	10-57-016	12/10/1969	U-10am2	581744.8	4113867.8	1,351.5	< 20	206	613	194	AA
TUN-C	10-57-017	12/10/1969	U-10am3	581943.6	4113670.1	1,345.7	< 20	214	608	194	TM-LVTA
TUN-D	10-57-018	12/10/1969	U-10am4	581943.5	4113868.2	1,347.2	< 20	275	610	256	OSBCU
TURF	10-57-039	04/24/1964	U-10c	583885.9	4111681.3	1,298.4	20 to 200	588	553	506	TM-LVTA
TURNSTONE	03-57-088	10/16/1964	U-3dt	586734.5	4098831.9	1,218.0	< 20	136	485	126	AA
TURQUOISE	07-57-038	04/14/1983	U-7bu	584809.2	4103174.8	1,246.0	< 150	610	480	533	LTCU
TWEED	09-57-062	05/21/1965	U-9bn	586381.4	4108261.9	1,308.2	< 20	322	576	284	TM-LVTA
TYG-A	02-57-074	12/12/1968	U-2dc1e	581681.5	4108467.9	1,300.0	< 20	244	556	228	AA
TYG-B	02-57-075	12/12/1968	U-2dc2d	581773.6	4108110.1	1,296.6	< 20	270	555	251	AA
TYG-C	02-57-076	12/12/1968	U-2dc3c	581980.0	4108163.0	1,295.1	< 20	244	551	228	AA
TYG-D	02-57-077	12/12/1968	U-2dc4a	581887.9	4108520.7	1,298.8	< 20	223	553	207	AA
TYG-E	02-57-078	12/12/1968	U-2dc5b	582037.2	4108368.6	1,296.6	< 20	213	551	198	AA
TYG-F	02-57-079	12/12/1968	U-2dc6f	581579.9	4108250.8	1,299.7	< 20	282	559	265	AA
UMBER	03-57-107	06/29/1967	U-3em	586934.2	4098284.7	1,215.5	10	344	482	310	AA
VALENCIA	03-57-275	09/26/1958	U-3r	586269.3	4100609.8	1,228.0	0.002	160	495	148	AA
VALISE	09-57-071	03/18/1969	U-9by	585189.3	4110534.6	1,287.8	< 20	107	548	91	AA
VAT	09-57-077	10/10/1968	U-9cf	585065.4	4109887.0	1,282.6	< 20	213	543	192	AA
VAUGHN	03-57-255	03/15/1985	U-3lr	584881.4	4101537.4	1,238.1	20 to 150	457	489	427	TM-LVTA
VELARDE	03-57-205	04/25/1973	U-3jk	587114.1	4094413.1	1,203.4	< 20	297	465	277	AA
VERDELLO	03-57-235	07/31/1980	U-3ku	586940.5	4096562.4	1,210.1	< 20	411	476	366	AA
VERMEJO	04-57-032	10/02/1984	U-4r	584186.7	4104543.2	1,255.5	< 20	686	467	351	TM-UVTA
VICTORIA	03-57-236	06/19/1992	U-3kv	588070.9	4095728.3	1,205.8	< 20	488	468	244	AA
VIDE	08-57-006	04/30/1981	U-8k	581247.8	4114733.3	1,373.4	< 20	367	635	323	OSBCU
VIGIL	10-57-004	11/22/1966	U-10ad	584492.2	4113883.3	1,304.8	< 20	96	572	91	AA
VILLE	04-57-011	06/12/1985	U-4am	581416.3	4104858.4	1,276.8	< 20	335	520	293	TM-LVTA
VILLITA	03-57-244	11/10/1984	U-3ld	587433.1	4095131.9	1,204.6	< 20	457	467	373	AA
VISE	03-57-104	01/30/1969	U-3ej	586315.4	4101024.4	1,230.8	20 to 200	472	498	454	TM-LVTA
VITO	10-57-003	07/14/1967	U-10ab	584797.3	4113427.6	1,304.5	< 20	98	571	97	AA
VULCAN	02-57-031	06/25/1966	U-2bd	582390.6	4112300.5	1,327.1	25	370	588	323	AA
WACO	03-57-258	12/01/1987	U-3lu	588586.3	4094734.0	1,202.7	< 20	335	461	183	AA

Table A.1-1
Shaft and Tunnel Nuclear Detonations in the Yucca Flat/Climax Mine Corrective Action Unit
(Page 24 of 24)

Detonation Name	CAS Number	Date Expended	Emplacement Hole Name	UTM Easting	UTM Northing	Land Surface Elevation [a] (m amsl)	Announced Yield(kt)	Hole Depth (m)	Estimated Depth to Water (m)	Depth of Burial (m)	Working Point HSU
WAGTAIL	03-57-014	03/03/1965	U-3an	585598.6	4102259.1	1,237.5	20 to 200	767	492	750	LTCU
WALLER	02-57-053	10/02/1973	U-2bz	582787.2	4112149.8	1,320.7	< 20	408	582	311	AA
WARD	10-57-059	02/08/1967	U-10x	584599.3	4113678.0	1,303.9	< 20	265	571	260	AA
WASHER	10-57-054	08/10/1967	U-10r	584598.9	4112476.1	1,297.5	< 20	509	553	466	LTCU
WELDER	03-57-134	10/03/1968	U-3fs	586280.6	4100270.4	1,225.9	< 20	131	493	118	AA
WEMBLEY	03-57-119	06/05/1968	U-3ey	587511.0	4098986.9	1,218.6	< 20	253	485	238	AA
WEXFORD	02-57-069	08/30/1984	U-2cr	577687.2	4110989.1	1,403.3	< 20	417	558	314	TM-LVTA
WHITE	09-57-048	05/25/1962	U-9b	584215.2	4108940.6	1,280.5	Low	200	534	193	AA
WHITEFACE-A	03-57-254	12/20/1989	U-3lp	586173.7	4097976.7	1,214.6	< 20	411	481	197	AA
WHITEFACE-B	03-57-254	12/20/1989	U-3lp	586173.7	4097976.7	1,214.6	< 20	411	481	183	AA
WICHITA	09-57-114	07/27/1962	U-9y	583810.8	4109475.1	1,292.0	Low	224	547	150	AA
WINCH	03-57-146	02/04/1969	U-3gf	585205.0	4096144.9	1,212.2	< 20	254	479	241	TM-WTA
WOLVERINE	03-57-022	10/12/1962	U-3av	586027.4	4100518.2	1,227.4	Low	81	494	73	AA
WOOL	09-57-056	01/14/1965	U-9bh	586640.0	4108317.7	1,313.7	< 20	304	582	216	TM-LVTA
WORTH	10-57-006	10/25/1967	U-10ag	584481.7	4112435.8	1,295.7	< 20	206	548	187	AA
YANNIGAN-BLUE	02-57-025	02/26/1970	U-2ay3	583000.6	4107701.8	1,284.4	20 to 200	366	510	364	AA
YANNIGAN-RED	02-57-023	02/26/1970	U-2ay1	583384.8	4107989.6	1,284.4	20 to 200	402	508	392	AA
YANNIGAN-WHITE	02-57-024	02/26/1970	U-2ay2	582938.3	4108172.4	1,288.4	20 to 200	397	523	395	AA
YARD	10-57-005	09/07/1967	U-10af	584113.4	4112079.2	1,297.5	20 to 200	533	555	521	TM-LVTA
YERBA	01-57-002	12/14/1971	U-1c	583737.0	4097663.4	1,228.6	< 20	335	490	332	AA
YORK	09-57-115	08/24/1962	U-9z	585333.2	4108261.3	1,282.6	Low	233	546	226	AA
ZAZA	04-57-019	09/27/1967	U-4c	584134.2	4106044.8	1,267.4	20 to 200	686	488	667	LTCU
ZINNIA	02-57-089	05/17/1972	U-2dk	581030.2	4108432.1	1,304.2	< 20	366	563	323	AA

Source: DOE/NV, 1997 and 2000; FFACO, 1996, as amended, August 2006; BN, 2006
[a] Modified from information in DOE/NV, 2000

AA - Alluvial aquifer
amsl - Above mean sea level
ATCU - Argillic tuff confining unit
HSU - Hydrostratigraphic unit
kt - Kiloton
LCA - Lower carbonate aquifer
LCA3 - Lower carbonate aquifer - Yucca Flat upper plate
LCCU - Lower clastic confining unit
LTCU - Lower tuff confining unit
m - Meter
MGCU - Mesozoic granite confining unit
NA - Not available
OSBCU - Oak Spring Butte confining unit
PBRCM - Pre-Belted Range composite unit
PCUT - Playa confining unit
TM-WTA - Timber Mountain welded-tuff aquifer
TSA - Topopah Spring aquifer
TUBA - Tub Spring aquifer
UCCU - Upper clastic confining unit
UTCU - Upper tuff confining unit
UTM - Universal Transverse Mercator

A.2.0 REFERENCES

BN, see Bechtel Nevada.

Bechtel Nevada. 2006. *A Hydrostratigraphic Model and Alternatives for the Groundwater Flow and Contaminant Transport Model of Corrective Action Unit 97: Yucca Flat-Climax Mine, Lincoln and Nye Counties, Nevada*, Report DOE/NV/11718-1119. Las Vegas, NV.

DOE/NV, see U.S. Department of Energy, Nevada Operations Office.

FFACO, see *Federal Facility Agreement and Consent Order.*

Federal Facility Agreement and Consent Order. 1996 (as amended). Agreed to by the State of Nevada; U.S. Department of Energy, Environmental Management; U.S. Department of Defense; and U.S. Department of Energy, Legacy Management. Appendix III, which contains the Corrective Action Investigations/Corrective Actions, was last amended in January 2007, Revision No. 21.

Grasso, D.N. 2001. *GIS Surface Effects Archive of Underground Nuclear Detonations Conducted at Yucca Flat and Pahute Mesa, Nevada Test Site, Nevada*, Open-File Report 01-272. Denver, CO: U.S. Geological Survey.

U.S. Department of Energy, Nevada Operations Office. 1997. *Shaft and Tunnel Nuclear Detonations at the Nevada Test Site: Development of a Primary Database for the Estimation of Potential Interactions with the Regional Groundwater System*, DOE/NV--464, UC-700. Las Vegas, NV.

U.S. Department of Energy, Nevada Operations Office. 2000. *United States Nuclear Tests, July 1945 through September 1992*, DOE/NV--209, Rev. 15. Las Vegas, NV.

Appendix B

Data Collection Activities

B.1.0 SUMMARY OF DATA COLLECTION FOR THE YUCCA FLAT/CLIMAX MINE CORRECTIVE ACTION UNIT

Data collection is defined to encompass all activities conducted to characterize groundwater contamination that may have resulted from underground nuclear testing and support groundwater flow and transport modeling of radionuclide transport. At its inception in 1992, the characterization program was initially known as the Groundwater Characterization Project (GCP); it became the UGTA Project in 1992. The Yucca Flat/Climax Mine CAIP (DOE/NV, 2000a) discussed in detail the notable data collection developed during the GCP and the UGTA Project before calendar year 2000 and specified Yucca Flat/Climax Mine CAU-specific Phase I data collection and analysis activities to address identified data gaps. This appendix identifies and summarizes key UGTA Project data collection activities and documentation to date for the Yucca Flat/Climax Mine CAU. This compilation was originally developed for the *Phase I Hydrologic Data for the Groundwater Flow and Contaminant Transport Model of Corrective Action Unit 97: Yucca Flat/Climax Mine, Nevada Test Site, Nye County, Nevada* (SNJV, 2006b). The compilation has been updated with newly published work and relevant information on transport parameter data, and includes activities that have been conducted in or for other CAUs that provide information that supports analyses for the Yucca Flat/Climax Mine CAU.

B.2.0 YUCCA FLAT/CLIMAX MINE CAU-SPECIFIC WELL DRILLING AND TESTING

A total of 10 UGTA Project wells have been drilled, completed, and tested within the Yucca Flat/Climax Mine CAU for geologic and hydrologic characterization. Table B.2-1 lists the wells and their coordinates, and identifies the data documentation associated with these wells. The locations for these wells are shown in Figure B.2-1. Several other wells have been recompleted to use for groundwater sampling and testing. These are listed in Table B.2-2, and the limited available documentation is identified.

In addition, UGTA has supported joint work with other NTS programs (specifically, the HRMP, the RNM Program, and Defense Programs) on several wells that were installed as drillbacks and/or are sampled for the HRMP Hot Well Program. This work provides information on radionuclides in the groundwater associated with nuclear tests, which is used for determining locations of contaminated groundwater, for evaluating transport of radionuclides *in situ*, and for use in developing source term models. These wells are listed in Table B.2-3. Information gained from these wells specifically for Yucca Flat is discussed at greater length in Section 6.0. Data from the Hot Well sampling program for all of the CAUs support a variety of data collection and analyses tasks that generally support Yucca Flat data analysis, in particular radionuclide transport data for NTS formations and source term evaluation. Sampling of groundwater impounded behind tunnel portals in Rainier Mesa tunnels (U-12n and U-12t) has also been performed. Reports on tunnel sampling are listed in Table B.2-4.

Table B.2-1
Yucca Flat/Climax Mine Phase I Well Drilling and Testing
(Page 1 of 2)

Well Name	Criteria Document	Location UTM, NAD 27, Zone 11 (m)		Completion Date	Completion Report	Testing/Analysis Report
		Easting	Northing			
ER-2-1	*Yucca Flat Hydrogeologic Investigation Wells Drilling and Completion Criteria* (IT, 2002)	583,334.49	4,108,978.33	03/07/2003	*Completion Report for Well ER-2-1* (NNSA/NSO, 2004b)	*Letter Report: Analysis of Well ER-2-1 Hydraulic Testing, Yucca Flat FY 2003, Nevada Test Site, Nevada* (SNJV, 2004d)
ER-3-1	*Drilling/Completion Criteria for Underground Test Area Operable Unit Well ER-3-1* (DOE/NV, 1994)	594,658.28	4,097,338.98	05/20/1994	*Completion Report for Well ER-3-1* (DOE/NV, 1995a)	N/A
ER-3-2	*Drilling/Completion Criteria for Underground Test Area Remedial Investigation and Feasibility Study Well ER-3-2* (DOE/NV, 1993)	585,716.38	4,099,227.75	02/18/1994	*Completion Report for Well ER-3-2* (DOE/NV, 1995b)	N/A
ER-6-1	N/A	589,632.69	4,093,418.70	05/25/1995	*Completion Report for Well Cluster ER-6-1* (NNSA/NSO, 2004a)	*Analysis of Hydraulic Responses from the ER-6-1 Multiple-Well Aquifer Test, Yucca Flat FY 2004 Testing Program, Nevada Test Site, Nye County, Nevada* (SNJV, 2005a)
ER-6-1#1	N/A	589,635.80	4,093,403.75	07/16/1993		
ER-6-1#2	*Underground Test Area Project, ER-6-1 Multi-Well Aquifer Test - Tracer Test Plan*, Rev. 0 (SNJV, 2004f)	589,616.49	4,093,356.86	10/05/2002		

Table B.2-1
Yucca Flat/Climax Mine Phase I Well Drilling and Testing
(Page 2 of 2)

Well Name	Criteria Document	Location UTM, NAD 27, Zone 11 (m)		Completion Date	Completion Report	Testing/Analysis Report
		Easting	Northing			
ER-6-2	N/A	582,235.73	4,090,745,00	07/21/1994	*Completion Report for Well ER-6-2,* (DOE/NV, 1997)	*Analysis of Well ER-6-2 Testing, Yucca Flat FY 2004 Testing Program, Nevada Test Site, Nye County, Nevada* (SNJV, 2005b)
ER-7-1	*Yucca Flat Hydrogeologic Investigation Wells Drilling and Completion Criteria* (IT, 2002)	589,315.09	4,103,275.35	02/09/2003	*Completion Report for Well ER-7-1* (NNSA/NSO 2004c)	*Analysis of Well ER-7-1 Testing, Yucca Flat FY 2003 Testing Program, Nevada Test Site, Nevada* (SNJV, 2004a)
ER-8-1	*Yucca Flat Hydrogeologic Investigation Wells Drilling and Completion Criteria* (IT, 2002)	583,790.62	4,118,738.19	11/17/2002	*Completion Report for Well ER-8-1* (NNSA/NSO, 2004d)	N/A
ER-12-2	*Yucca Flat Hydrogeologic Investigation Wells Drilling and Completion Criteria* (IT, 2002)	577,902.59	4,114,057.67	04/17/2003	*Completion Report for Well ER-12-2* (NNSA/NSO, 2004e)	*Analysis of Well ER-12-2 Testing, Yucca Flat FY 2003 Testing Program, Nevada Test Site, Nevada* (SNJV, 2004b)

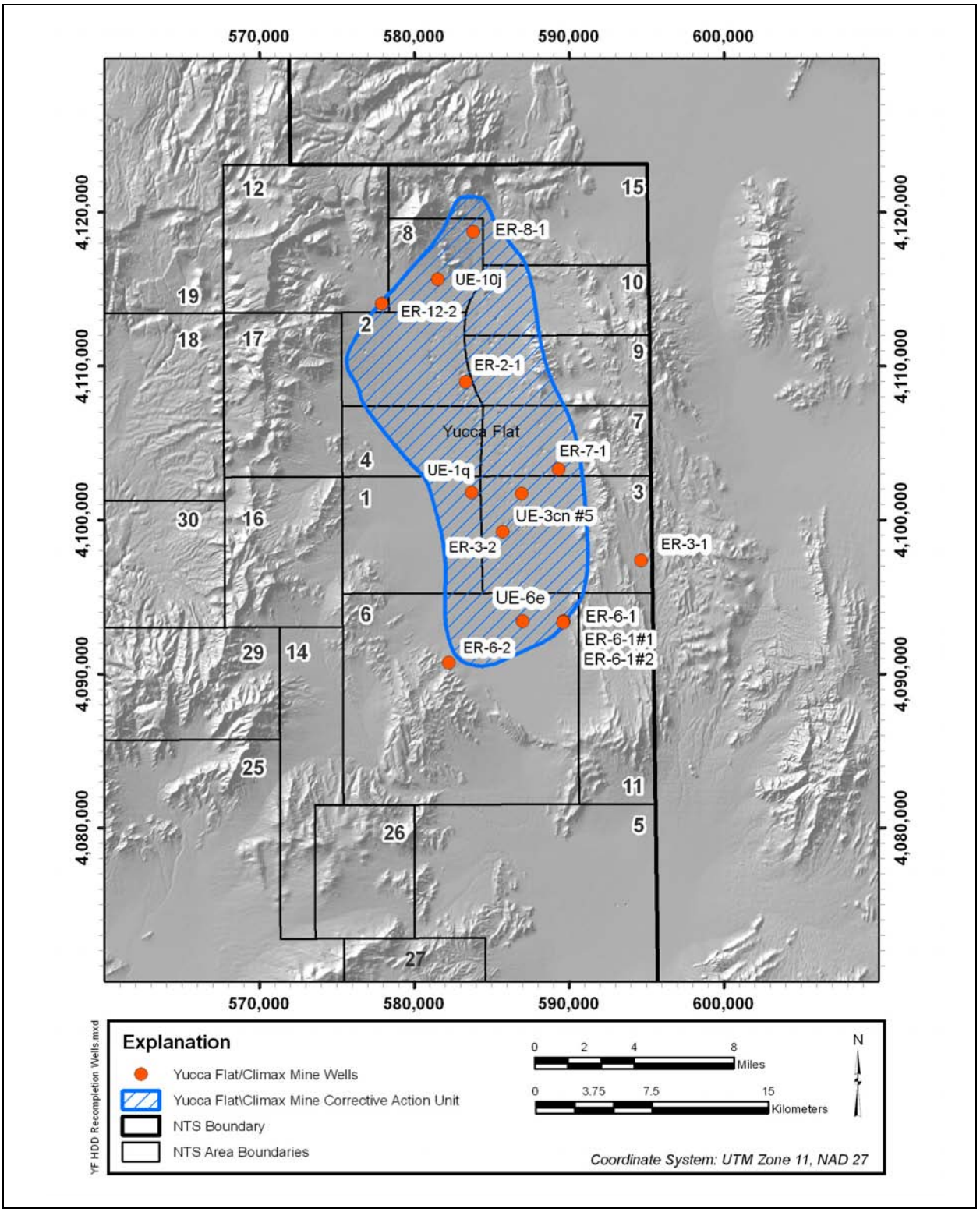

Figure B.2-1
Yucca Flat/Climax Mine CAU-Specific Investigation and Recompletion Well Locations

Table B.2-2
Yucca Flat/Climax Mine Phase I Well Recompletions and Testing

Well Name	Location UTM, NAD 27, Zone 11 (m)		Recompletion Date	Recompletion Report	Testing/Analysis Report
	Easting	Northing			
UE-10j	581,526.63	4,115,644.86	02/24/1993	*Recompletion Report for Well UE-10j* (DOE/NV, 1995c)	*Pre-Completion Hydrologic Testing Documentation Package for Well UE-10j* (IT, 1995)
UE-1q	583,722.73	4,101,777.68	05/22/1992	*Recompletion Report and Summary of Well History for Well UE-1q* (IT, 1996b)	*Data Report, UE-1q Aquifer Test* (DRI, 1992)
UE-6e	587,012.48	4,093,408.77	11/11/1992	*Recompletion Report and Summary of Well History for Well UE-6e* (IT, 1996c)	N/A
U-3cn #5	586,921.72	4,101,714.46	N/A	*Recompletion Report for BILBY* (BN, 1998)	*Environmental Restoration Program Underground Test Area Project Data Analysis, Hydrologic Testing Documentation Package for Bilby (U-3cn) Hydrologic Test Hole U-3cn #5 and Postshot Hole U-3cn PS #2* (IT, 1997)

Table B.2-3
Near-field Well Activities UGTA Has Supported

Well Name(s)	Associated Test Name	Activity	Recompletion Date
UE-2ce	NASH	Near-field well sampling	periodic
U-2gg PSE #3A	INGOT	Near-field well sampling	periodic
U-3cn PS #2	BILBY	Replace pump, pumping, and near-field well sampling	01/1997, periodic
U-3cn #5	BILBY	Pumping and sampling	01/1997, periodic
UE-3e #4	ALEMAN	Near-field well sampling	periodic
U-4t PS (#2A) 3A	GASCON	Near-field well sampling	periodic
U-4u PS #2A	DALHART	Near-field well sampling	periodic
RNM-2s, RNM-1,UE-5n	CAMBRIC	Pumping, sampling	04/26 - 07/10/2003
RNM-2s	CAMBRIC	Near-field well sampling	periodic
U-7ba PS #1AS	BASEBALL	Install pump and attempt pumping, near-field well sampling	periodic
UE-7ns	BOURBON	Near-field well sampling	periodic
U-19q PS1 D	CAMEMBERT	Re-entry, pump installation	1998
U-19ab PS#1A	CHANCELLOR	Drilling	2004, periodic
U-20n PS1 DD-H	CHESHIRE	Recompletion, pump installation, near-field well sampling	07/1998, periodic

Table B.2-4
Reports of Rainier Mesa Tunnel Sampling

Document Title	Reference
Hydrologic Resources Management Program and Underground Test Area Project FY2000 Progress Report	Rose et al., 2002
Letter Report: *Evaluation of Monitoring Data From Impounded Water Within U12n and U12t Tunnels*	DRI, 2003
Written Communication: *U12n and U12t Tunnels Preliminary Data Report Groundwater Sampling*	SNJV, 2007

B.3.0 YUCCA FLAT/CLIMAX MINE CAIP-IDENTIFIED CHARACTERIZATION ACTIVITIES

Nine specific characterization activities were identified in the Yucca Flat/Climax Mine CAIP (DOE/NV, 2000a). These characterization activities were:

- Mineralogy studies of the TCU
- Geophysical interpretation of the Paleozoic framework
- Analysis of existing seismic data
- Hydrologic investigation of ER-6-1 and ER-6-2
- Isotope/geochemistry mass-balance studies
- Analysis of existing tracer test data
- Laboratory radionuclide transport studies
- Rainier Mesa colloid transport studies
- Analysis of data for phenomenological models

The following subsections discuss data collection and studies that have been conducted under these categories of CAIP-specified data collection activities. A statement of the scope of the investigation area and the studies perceived to be needed is provided in the Yucca Flat/Climax Mine CAIP (DOE/NV, 2000a).

Additional activities and studies have been conducted that are related to these specific categories but more broadly support transport parameter data and analysis. These are described in Section B.4.0.

B.3.1 Tuff Confining Unit Mineralogical Studies

The TCU may partition the LCA from the overlying contaminated volcanic tuff aquifers because of its position between the underground nuclear tests and the LCA. Therefore, knowledge of the lateral continuity and hydraulic characteristics of the TCU is important in modeling groundwater movement from underground nuclear tests through the TCU to the LCA. Also of importance are the type and distribution of alteration minerals in the TCU. The alteration minerals, which can retard contaminant

transport within the TCU, possess a significant range in sorption capacity for radionuclides, which will be important to transport modeling.

The study of the TCU has been in progress for several years, embodied in a number of tasks for BN and NSTec (NTS M&O Contractors), SNJV (NTS Environmental Restoration Contractor), LANL, and LLNL. Table B.3-1 contains a list of major reports that have been published reporting on these studies. The most recent document, *Mineralogic Zonation Within the Tuff Confining Unit, Yucca Flat, Nevada Test Site* (Prothro, 2005), reports the analysis of the variation of alteration mineral assemblages in the TCU based on mineralogic data from 17 holes and stratigraphic data, lithologic descriptions, and geophysical logs from approximately 500 drill holes in Yucca Flat. A three-layer mineralogic model was developed to aid in the development of the HFM for the Yucca Flat/Climax Mine CAU. This model will further support transport modeling for the Yucca Flat/Climax Mine CAU.

Table B.3-1
Reports of TCU Studies

Document Title	Reference
"Examples of Textural and Mineralogical Alteration at the Interface of Vitric and Zeolitic Tuff, Yucca Flat, Nevada Test Site," in *Proceedings of the Sixth Symposium on Containment of Underground Nuclear Explosions*	Krier, 1991
Analysis of Fractures in Cores from the Tuff Confining Unit beneath Yucca Flat, Nevada Test Site	Prothro, 1998
Letter Report: Underground Test Area Project, Mineralogical and Isotopic Analysis of Fracture-Coating and Alteration Minerals in the Yucca Flat Tuff Confining Unit, Nevada Test Site	Dickerson et al., 2004
Mineralogical and Isotopic Analysis of Fracture-Coating and Alteration Minerals in the Climax Stock	Dickerson and Rose, 2004
Mineralogic Zonation Within the Tuff Confining Unit, Yucca Flat, Nevada Test Site	Prothro, 2005

A compilation of additional mineralogic data, XRD data, acquired during the weapons testing program has been completed. This compilation process is described in Appendix D. Geostatistical analysis of the mineralogic data for the TCU is presently being performed by LLNL and will be published in a future LLNL report.

B.3.2 Geophysical Interpretation of the Paleozoic Framework

A variety of geophysical data-based investigations have been conducted in Yucca Flat to determine the geologic structure of the basin. These activities are identified in the following subsections and reports. The results of these investigations were used for development of the Yucca Flat/Climax Mine HFM and are discussed in *A Hydrostratigraphic Model and Alternatives for the Groundwater Flow and Contaminant Transport Model of Corrective Action Unit 97: Yucca Flat-Climax Mine, Lincoln and Nye Counties, Nevada* (BN, 2006).

B.3.2.1 Natural-Source Magnetotelluric Survey

An MT survey was conducted by the USGS in Yucca Flat in 2003 to provide data on the pre-Tertiary stratigraphy and structure for use in developing the HFM. The survey included 51 stations variably spaced 2 to 3 km apart along seven east-west oriented lines across the basin. The results of the MT survey are published in *Deep Resistivity Structures of Yucca Flat, Nevada Test Site, Nevada* (Asch et al., 2005) and discussed in Appendix D of BN (2006). The MT method was very successful in providing constraints on the thickness and lateral extent of the CCU in the western portion of the Yucca Flat basin (BN, 2006).

B.3.2.2 Gravity and Aeromagnetic Data Interpretation

A variety of work supporting the development of the Yucca Flat/Climax Mine HFM has been based on many aeromagnetic surveys in support of the weapons testing program, and additional data collected by the USGS in 2003 (Phelps et al., 2005). Reports of geophysical interpretation studies related to the Yucca Flat/Climax Mine CAU area are listed in Table B.3-2.

Table B.3-2
Reports of Gravity and Aeromagnetic Studies
(Page 1 of 2)

Document Title	Reference
Thickness of Cenozoic Deposits of Yucca Flat Inferred from Gravity Data, Nevada Test Site, Nevada	Phelps et al., 1999
High-Angle Faults in the Basement of Yucca Flat, Nevada Test Site, Nevada, Based on the Analysis of a Constrained Gravity Inversion Surface	Phelps and McKee, 1999
Preliminary Model of the Pre-Tertiary Basement Rocks Beneath Yucca Flat, Nevada Test Site, Nevada, Based on Analysis of Gravity and Magnetic Data	Phelps et al., 2000

Table B.3-2
Reports of Gravity and Aeromagnetic Studies
(Page 2 of 2)

Document Title	Reference
Modeling of the Climax Stock and Related Plutons Based on the Inversion of Magnetic Data, Southwest Nevada	Phelps et al., 2004
A Preliminary Investigation of the Structure of Southern Yucca Flat, Massachusetts Mountain, and CP Basin, Nevada Test Site, Nevada, Based on Geophysical Modeling	Phelps et al., 2005

B.3.2.3 Analysis of Existing Seismic Data

Extensive seismic reflection and refraction investigations previously have been conducted in Yucca Flat by LLNL and LANL in support of weapons testing and site-characterization activities. The existing seismic data were evaluated for possible contribution to the interpretation of the geologic structure and stratigraphy of Yucca Flat. The object of this activity was to conduct a comprehensive reinterpretation of existing 2-D seismic data incorporating current structural understanding to provide, at basin-wide scale, an investigation of key features such as fault locations and HSU pinchouts or juxtapositions that may influence flow and transport. Analysis also allows for imaging to depths below those previously considered. In addition, the use of seismic data obtained from local arrays, and from regional seismological stations during underground nuclear tests, was evaluated for its contribution to the understanding of geologic structure in Yucca Flat. This work is documented in *Evaluation of Seismic Data Acquired in Yucca Flat, NTS, by the Lawrence Livermore National Laboratory* (Pawloski and Wagoner, 2003).

B.3.3 Hydrologic Investigation of Wells ER-6-1 and ER-6-2

In FY 2004, a large-scale multiple-well aquifer test-tracer test (MWAT-TT) was conducted at the ER-6-1 Well Cluster located in southwestern Yucca Flat to characterize the hydraulic and transport properties of the LCA in Yucca Flat. The plan for this test was documented in *Underground Test Area Project, ER-6-1 Multi-Well Aquifer Test - Tracer Test Plan* (SNJV, 2004f). Included in the program were extensive hydraulic testing in and between the pumping well and the primary tracer-injection well.

The test involved pumping of ER-6-1 #2 for a period of 90 days. Water level response was continuously monitored in all three ER-6-1 wells, in three other wells completed in the LCA located

up to 11.7 km from the ER-6-1 Well Cluster, and in two nearby wells completed in the overlying volcanics. A suite of tracers were injected into two other wells at the ER-6-1 Well Cluster, ER-6-1 and ER-6-1 #1, shortly after pumping began. Tracer breakthrough curves for ER-6-1 #2 were determined from analysis of water samples collected from the pump discharge and from downhole discrete sampling. The hydraulic analysis of the test data is documented in *Analysis of Hydraulic Responses from the ER-6-1 Multiple-Well Aquifer Test, Yucca Flat FY 2004 Testing Program, Nevada Test Site, Nye County, Nevada* (SNJV, 2005a). See Section B.3.5 for information on analysis of the tracer test.

B.3.4 Isotope/Geochemistry Mass-Balance Studies

The isotope/geochemistry mass-balance studies include field and laboratory activities, compilation of existing geochemistry data, and data interpretation including geochemical modeling. The purpose of these studies is to independently verify the origin and groundwater flow paths through the Yucca Flat/Climax Mine groundwater flow system, and to provide estimates of the age and travel time for groundwater flow. These studies are published in the report *Geochemical and Isotopic Evaluation of Groundwater Movement in Corrective Action Unit 97: Yucca Flat/Climax Mine, Nevada Test Site, Nevada* (SNJV, 2006a) and summarized in Section 5.0 of this report.

B.3.5 Analysis of Existing Tracer Test Data

Three two-well recirculating tracer tests were previously conducted in the Bonanza King Dolomite, which is one member of the group of formations included in the LCA HSU, at the Amargosa tracer calibration site in the Amargosa Desert, approximately 24 km southwest of Mercury, Nevada. This site was initially developed to study the velocity of groundwater movement through carbonate rocks underlying the NTS and the Amargosa Desert (Johnston, 1968). Further tests were run to determine the effective porosity and apparent longitudinal dispersivity in the carbonate aquifer (Leap and Belmonte, 1992). During the development of the Yucca Flat/Climax Mine CAIP (DOE/NV, 2000a), data from these tracer tests were identified for reanalyses using newer techniques to estimate transport parameters.

However, in lieu of reanalysis of the old tracer test data, the analysis effort was focused on results from a newly conducted MWAT-TT at the ER-6-1 Well Cluster in Yucca Flat (Section B.3.3). These

data were deemed to be more appropriate for use in transport modeling for the Yucca Flat/Climax Mine CAU. Analysis of the tracer test breakthroughs has been documented in the reports *Well ER-6-1 Tracer Test Analysis: Yucca Flat, Nevada Test Site, Nye County, Nevada* (SNJV, 2006c), and *Semi-Analytical Interpretations of ER-6-1 Multiple-Well Tracer Test Results* (Reimus, 2007). These analyses provide field-scale information on the transport properties of the LCA in Yucca Flat.

B.3.6 Laboratory Radionuclide Transport Studies

Laboratory transport studies (e.g., diffusion cell experiments, fractured-core column experiments, and colloid transport experiments) will help estimate parameters describing solute transport, including colloid and colloid-facilitated transport. Results will be laboratory estimates of radionuclide transport parameters (e.g., matrix diffusion, dispersion, and sorption) and the uncertainty associated with these parameters. This information will provide experimental insight into colloid transport processes and the parameters describing those processes, and will be used in the CAU-scale transport model.

Laboratory radionuclide transport studies conducted since the review presented in the Yucca Flat CAIP (DOE/NV, 2000a) have been reported in the documents listed in Table B.3-3.

Table B.3-3
Reports of Laboratory Radionuclide Transport Studies
(Page 1 of 2)

Document Title	Reference
Reversibility of Sorption of Plutonium-239 onto Colloids of Hematite, Goethite, Smectite, and Silica (LA-UR-98-3057)	Lu et al., 1998
Adsorption of Actinides onto Colloids as a Function of Time, Temperature, Ionic Strength and Colloid Concentration (LA-UR-00-5121)	Lu et al., 2000
Diffusive and Advective Transport of ^{3}H, ^{14}C, and ^{99}Tc in Saturated, Fractured Volcanic Rocks from Pahute Mesa, Nevada	Reimus et al., 2000a
Progress Report on Colloid-Facilitated Plutonium Transport in Fractured Rocks from Pahute Mesa, Nevada Test Site	Reimus et al., 2000b
Matrix Diffusion and Colloid-Facilitated Transport in Fractured Rocks: Model and Parameter Validation (UCRL-ID-149817)	Zavarin, 2002
Laboratory Experiments to Evaluate Diffusion of ^{14}C into Nevada Test Site Carbonate Aquifer Matrix (DOE/NV/11508-55)	Hershey et al., 2003
Plutonium Colloid-Facilitated Transport in the Environment - Experimental and Transport Modeling Evidence for Plutonium Migration Mechanisms (UCRL-JC-151924)	Zavarin et al., 2003
Colloid-Facilitated Transport of Low-Solubility Radionuclides: A Field, Experimental, and Modeling Investigation (UCRL-ID-149688)	Kersting and Reimus, 2003

Table B.3-3
Reports of Laboratory Radionuclide Transport Studies
(Page 2 of 2)

Document Title	Reference
Radionuclide Transport in Tuff and Carbonate Fractures from Yucca Flat, Nevada Test Site, Final Report (UCRL-TR-219836)	Zavarin et al., 2005
Colloid Characteristics and Radionuclide Associations with Colloids in Source-Term Waters at the Nevada Test Site (LA-UR-05-5312)	Abdel-Fattah et al., 2005
"Errata for Table 1," in *Radionuclide Sorption and Transport in Fractured Rocks of Yucca Flat, Nevada Test Site* (LA-UR-05-9279)	Ware et al., 2005a
Radionuclide Sorption and Transport in Fractured Rocks of Yucca Flat, Nevada Test Site (LA-UR-05-9279)	Ware et al., 2005b
Np and Pu Sorption to Manganese Oxide Minerals (UCRL-TR-214984)	Zhao et al., 2005
Colloid Characteristics and Radionuclide Associations with Colloids in Near-Field Waters at the Nevada Test Site (FY 2005 Progress Report) (LA-UR-05-8612)	Reimus et al., 2006a
"Errata for Table 10," in *Tracer Transport Properties in the Lower Carbonate Aquifer of Yucca Flat* (LA-UR-06-0486)	Reimus et al., 2006b
Tracer Transport Properties in the Lower Carbonate Aquifer of Yucca Flat (LA-UR-06-0486)	Reimus et al., 2006c
Written communication: *Colloid-Facilitated Radionuclide Transport in Fractured Carbonate Rocks from Yucca Flat, Nevada Test Site*	Zavarin et al., 2006
Summary of Radionuclide Reactive Transport Experiments in Fractured Tuff and Carbonate Rocks from Yucca Flat, Nevada Test Site (UCRL-TR-225271)	Zavarin et al., 2007

B.3.7 Rainier Mesa Colloid Transport Studies

From 1957 to 1992, 61 underground nuclear tests were conducted at Rainier Mesa, 59 in tunnels and 2 in shafts (DOE/NV, 2000b). These tunnel tests were conducted above the water table in tuffs variably fractured by inelastic failure adjacent to the tests. The resulting fracture system allows groundwater recharge from the surface of Rainier Mesa to infiltrate and interact with residual radionuclides from the tests. The tunnels provide access to an evolved hydrologic source term of radionuclides transported by groundwater through volcanic tuffs under variably saturated flow conditions. Data from Rainier Mesa tuffs should be applicable to tuff units in Yucca Flat because of the similarities with regards to stratigraphy, lithology, and alteration. Results may also be extrapolated to younger tuffs that overlie the older tuffs at Yucca Flat. The objective of this activity is to investigate the geochemical and radiochemical controls on the movement of actinides introduced from underground nuclear testing under ambient flow conditions such as those found in the tunnel complexes. This study will provide information on transport of radionuclides under variably

saturated conditions and will help to define the range of colloid-facilitated transport that may be expected under various groundwater conditions. The Rainier Mesa colloid transport studies have been discussed in the reports listed in Table B.3-4.

Table B.3-4
Reports of Rainier Mesa Colloid Transport Studies

Document Title	Reference
Hydrologic Resources Management Program and Underground Test Area Project FY2000 Progress Report (UCRL-ID-145167)	Rose et al., 2002
Colloid-Facilitated Transport of Low-Solubility Radionuclides: A Field, Experimental, and Modeling Investigation (UCRL-ID-149688)	Kersting and Reimus, 2003

B.3.8 Analysis of Data for Phenomenological Models

Phenomenology describes the effects of the nuclear explosion on the surrounding medium during and immediately following the explosion of an underground nuclear test. Phenomenological models that are representative of reality are essential to understanding the sources of groundwater contamination present at the underground nuclear test locations. Therefore, they are essential to the modeling of groundwater flow and contaminant transport away from underground nuclear test locations. Under this CAI activity, existing data from drillbacks and minebacks, pre-test, post-test, and calculational data will be analyzed to develop phenomenological models of the near-field environment of underground nuclear tests in the Yucca Flat/Climax Mine CAU. A general summary of the available for nuclear tests, phenomenologic, and source term data is presented in Section 6.0. The phenomenologic analyses and source term evaluation for the Yucca Flat/Climax Mine CAU will be presented in future report(s).

B.4.0 OTHER STUDIES

Other studies have been conducted that support the Yucca Flat/Climax Mine CAU characterization. Major reports on these studies are summarized in Table B.4-1.

Table B.4-1
Reports of Other Studies Conducted for the Yucca Flat/Climax Mine Phase I Characterization
(Page 1 of 2)

Document Title	Synopsis
Potential for Infiltration Through Fractured Alluvium in Yucca Flat of the Nevada Test Site: Preliminary Field Investigation (McKinnis and Kao, 1993)	This report evaluates recharge through alluvium and volcanics in Yucca Flat.
New Observations of Infiltration through Fractured Alluvium in Yucca Flat, Nevada Test Site: A Preliminary Field Investigation (Kao et al., 1994)	This report evaluates recharge through alluvium and volcanics in Yucca Flat.
ER-6-1 and ER-6-2 Core Fracture Analyses and Geophysical Log Comparisons (IT, 1996a)	This report characterizes fracturing of core samples obtained in wells ER-6-1 and ER-6-2.
Estimation of Groundwater Velocities from Yucca Flat to the Amargosa Desert Using Geochemistry and Environmental Isotopes (Hershey and Acheampong, 1997)	This report presents the evaluation of groundwater mixing models and geochemical evolution models to potential flow from Yucca Flat to Amargosa Desert. The results provide perspective for large-scale flow patterns and travel times from Yucca Flat.
Evaluation of Recharge Potential at Subsidence Crater U10i, Northern Yucca Flat, Nevada Test Site (Hokett et al., 2000)	This report evaluates recharge in a crater area in Yucca Flat.
Temperature Data Evaluation (Gillespie, 2003)	This report evaluates thermal gradient and associated heat flow for 13 wells on the NTS, 8 of which are in the Yucca Flat/Climax Mine data compilation area. These wells were selected after evaluation of 145 temperature logs for 63 wells.
Final Report: Depth-Specific Hydraulic Testing of Yucca Flat and Frenchman Flat Environmental Restoration Wells, FY 2003 (Oberlander and Russell, 2003)	This report evaluates flow logging data for wells in Yucca Flat and Frenchman Flat.

Table B.4-1
Reports of Other Studies Conducted for the Yucca Flat/Climax Mine Phase I Characterization
(Page 2 of 2)

Document Title	Synopsis
Hydrologic Data for the Groundwater Flow and Contaminant Transport Model of Corrective Action Units 101 and 102: Central and Western Pahute Mesa, Nye County, Nevada (SNJV, 2004c)	This report documents Pahute Mesa hydrologic data and provides peripheral information related to the Yucca Flat/Climax Mine CAU.
Phase II Hydrologic Data for the Groundwater Flow and Contaminant Transport Model of Corrective Action Unit 98: Frenchman Flat, Nye County, Nevada (SNJV, 2004e)	This report documents the Frenchman Flat hydrologic data and provides peripheral information related to the Yucca Flat/Climax Mine CAU.
Letter Report: Horizontal Hydraulic Conductivity Profile with Depth at Wells ER-6-1 and ER-6-1#2 (Oberlander and Russell, 2004)	This report documents the flow, temperature, and tracer conductivity logging and interpretation specific to the ER-6-1 MWAT-TT for ER-6-1 and ER-6-1#2.
Phase II Contaminant Transport Parameters for the Groundwater Flow and Contaminant Transport Model of Corrective Action Unit 98: Frenchman Flat, Nye County, Nevada (SNJV, 2005c)	This report documents the Frenchman Flat transport parameter data compilation and analysis, which includes information on many topics for the entire NTS, and provided the basis for the Yucca Flat/Climax Mine CAU contaminant transport parameter compilation.
Analysis of Ground-Water Levels and Associated Trends in Yucca Flat, Nevada Test Site, Nye County, Nevada, 1951-2003 (Fenelon, 2005)	This report provides a broad overview of water level information for Yucca Flat, a compilation of historic records, and an analysis of trends in water levels over the historic time period.
Hydraulic Characterization of Overpressured Tuffs in Central Yucca Flat, Nevada Test Site, Nye County, Nevada (Halford et al., 2005)	Water levels within bedded tuffs in central Yucca Flat were elevated hundreds of meters in response to nuclear testing in the tuffs. This report documents the USGS analysis of anomalous high pore pressures in the Yucca Flat Tuff Pile area. Calibration of cross-sections and 3-D groundwater flow models to land subsidence rates yields hydraulic conductivity estimates for the tuff units.
Temperature Profiles and Hydrologic Implications from the Nevada Test Site Area (Gillespie, 2005)	This report follows the Gillespie (2003) study determining the thermal gradient and associated heat flow for an additional 39 wells on the NTS, of which 20 are in the Yucca Flat/Climax Mine data compilation area.
Underground Test Area Fracture Analysis Report for Yucca Flat Wells ER-2-1, ER-6-1#2, ER-7-1, and ER-12-2, Nevada Test Site, Nevada (SNJV, 2005d)	This report provides fracture characterization analyses from borehole logs obtained in Yucca Flat Wells ER-2-1, ER-6-1 #2, ER-7-1, and ER-12-2.
Phase I Hydrologic Data for the Groundwater Flow and Contaminant Transport Model of Corrective Action Unit 97: Yucca Flat/Climax Mine, Nevada Test Site, Nye County, Nevada (SNJV 2006b)	This report documents the hydrologic data available for the Yucca Flat/Climax Mine CAU.

B.5.0 REFERENCES

Abdel-Fattah, A., D. Smith, M. Murrell, S. Goldstein, A. Nunn, R. Gritzo, B. Martinez, and P.W. Reimus. 2005. *Colloid Characteristics and Radionuclide Associations with Colloids in Source-Term Waters at the Nevada Test Site*, LA-UR-05-5312. Los Alamos, NM: Los Alamos National Laboratory.

Asch, T.A., B.D. Rodriguez, J.A. Sampson, E. Walling, and J.M. Williams. 2005. *Deep Resistivity Structures of Yucca Flat, Nevada Test Site, Nevada*. U.S. Geological Survey Open-File Report (in press). U.S. Geological Survey.

BN, see Bechtel Nevada.

Bechtel Nevada. 1998. *Recompletion Report for BILBY.* Prepared for the U.S. Department of Energy, Nevada Operations Office, DOE/NV-500. Las Vegas, NV.

Bechtel Nevada. 2006. *A Hydrostratigraphic Model and Alternatives for the Groundwater Flow and Contaminant Transport Model of Corrective Action Unit 97: Yucca Flat-Climax Mine, Lincoln and Nye Counties, Nevada*, DOE/NV/11718-210. Las Vegas, NV.

DOE/NV, see U.S. Department of Energy, Nevada Operations Office.

DRI, see Desert Research Institute.

Desert Research Institute. 1992. *Data Report, UE-1q Aquifer Test*. Las Vegas, NV: Water Resources Center.

Desert Research Institute. 2003. Letter Report: *Evaluation of Monitoring Data From Impounded Water Within U12n and U12t Tunnels*. June. Las Vegas, NV.

Dickerson, R., and T. Rose. 2004. *Mineralogical and Isotopic Analysis of Fracture-Coating and Alteration Minerals in the Climax Stock*. Lafayette, CO: Stoller-Navarro Joint Venture. Livermore, CA: Lawrence Livermore National Laboratory.

Dickerson, R., T.P. Rose, and G. Eaton. 2004. Written communication. Subject: *Letter Report: Underground Test Area Project, Mineralogical and Isotopic Analysis of Fracture-Coating and Alteration Minerals in the Yucca Flat Tuff Confining Unit, Nevada Test Site*. Lafayette, CO: Stoller-Navarro Joint Venture. Livermore, CA: Lawrence Livermore National Laboratory.

Fenelon, J.M. 2005. *Analysis of Ground-Water Levels and Associated Trends in Yucca Flat, Nevada Test Site, Nye County, Nevada, 1951-2003*, Scientific Investigations Report 2005-5175: 87. Carson City, NV: U.S. Geological Survey.

Gillespie, D. 2003. *Temperature Data Evaluation*, DOE/NV/13609-22; Publication No. 45194. Prepared for the U.S. Department of Energy, National Nuclear Security Administration Nevada Site Office. Reno, NV: Desert Research Institute.

Gillespie, D. 2005. *Temperature Profiles and Hydrologic Implications from the Nevada Test Site Area*, DOE/NV--3609-40; Publication No. 45211. Las Vegas, NV: Desert Research Institute.

Halford, K.J., R.J. Laczniak, and D.L. Galloway. 2005. *Hydraulic Characterization of Overpressured Tuffs in Central Yucca Flat, Nevada Test Site, Nye County, Nevada*, Scientific-Investigations Report 2005-5211. U.S. Geological Survey.

Hershey, R.L., and S.Y. Acheampong. 1997. *Estimation of Groundwater Velocities from Yucca Flat to the Amargosa Desert Using Geochemistry and Environmental Isotopes*, DOE/NV/11508-26; Publication No. 45157. Desert Research Institute.

Hershey, R.L., W. Howcroft, and P.W. Reimus. 2003. *Laboratory Experiments to Evaluate Diffusion of ^{14}C into Nevada Test Site Carbonate Aquifer Matrix*, DOE/NV/11508-55. DRI Publication No. 45180. Las Vegas, NV.

Hokett, S.L., D.R. Gillespie, G.V. Wilson, and R.H. French. 2000. *Evaluation of Recharge Potential at Subsidence Crater U10i, Northern Yucca Flat, Nevada Test Site*, DOE/NV/11508-53; Publication No. 45174. Reno, NV: Desert Research Institute.

IT, see IT Corporation.

IT Corporation. 1995. *Pre-Completion Hydrologic Testing Documentation Package for Well UE-10j*. Las Vegas, NV.

IT Corporation. 1996a. *ER-6-1 and ER-6-2 Core Fracture Analyses and Geophysical Log Comparisons*. Las Vegas, NV.

IT Corporation. 1996b. *Recompletion Report and Summary of Well History for Well UE-1q*, DOE/NV--444. Las Vegas, NV.

IT Corporation. 1996c. *Recompletion Report and Summary of Well History for Well UE-6e*, DOE/NV--434. Las Vegas, NV.

IT Corporation. 1997. *Environmental Restoration Program Underground Test Area Project Data Analysis, Hydrologic Testing Documentation Package for Bilby (U-3cn) Hydrologic Test Hole U-3cn #5 and Postshot Hole U-3cn PS #2*. Las Vegas, NV.

IT Corporation. 2002. *Yucca Flat Hydrogeologic Investigation Wells Drilling and Completion Criteria*, Rev. 0, ITLV/13052-164. Las Vegas, NV.

Johnston, R.H. 1968. *U.S. Geological Survey Tracer Study Amargosa Desert, Nye County, Nevada - Part 1: Exploratory Drilling, Tracer Well Construction and Testing, and Preliminary Findings*, Open File Report-474-98. Denver, CO: U.S. Geological Survey.

Kao, C.S., D.K. Smith, and W.B. McKinnis. 1994. *New Observations of Infiltration through Fractured Alluvium in Yucca Flat, Nevada Test Site: A Preliminary Field Investigation*, U.S. Department of Energy, UCRL-ID-116129. Livermore, CA: Lawrence Livermore National Laboratory.

Kersting, A.B., and P.W. Reimus, eds. 2003. *Colloid-Facilitated Transport of Low-Solubility Radionuclides: A Field, Experimental, and Modeling Investigation*, UCRL-ID-149688. Livermore, CA: Lawrence Livermore National Laboratory.

Krier, D.J. 1991. "Examples of Textural and Mineralogical Alteration at the Interface of Vitric and Zeolitic Tuff, Yucca, Flat, Nevada Test Site." In *Proceedings of the Sixth Symposium on Containment of Underground Nuclear Explosions*, Reno, NV. Livermore, CA: Lawrence Livermore National Laboratory.

Leap, D.I., and P.M. Belmonte. 1992. "Influence of Pore Pressure on Apparent Dispersivity of a Fissured MITIC Dolomitic Aquifer." In *Groundwater*, v. 30(1): 87-95. Washington, DC: American Geophysical Union.

Lu, N., I.R. Triay, C.R. Cotter, H.D. Kitten, and J. Bentley. 1998. *Reversibility of Sorption of Plutonium-239 onto Colloids of Hematite, Goethite, Smectite, and Silica*, LA-UR- 98-3057. Los Alamos National Laboratory Unrestricted Report, Los Alamos, NM.

Lu, N., J. Conca, G.R. Parker, P.A. Leonard, B. Moore, E.A. Strietelmeier, and I.R. Triay. 2000. *Adsorption of Actinides onto Colloids as a Function of Time, Temperature, Ionic Strength and Colloid Concentration*, LA-UR-00-5121. Los Alamos National Laboratory Unrestricted Report, Los Alamos, NM.

McKinnis, W.B., and C.S. Kao. 1993. *Potential for Infiltration Through Fractured Alluvium in Yucca Flat of the Nevada Test Site: Preliminary Field Investigation.* Lawrence Livermore National Laboratory and University of California at Berkeley.

NNSA/NSO, see U.S. Department of Energy, National Nuclear Security Administration Nevada Site Office.

Oberlander, P.L., and C.E. Russell. 2003. *Final Report: Depth-Specific Hydraulic Testing of Yucca Flat and Frenchman Flat Environmental Restoration Wells, FY 2003*, DOE/NV/13609-28; Publication No. 45199. Reno, NV: Desert Research Institute.

Oberlander, P.L., and C.E. Russell. 2004. *Letter Report: Horizontal Hydraulic Conductivity Profile with Depth at Wells ER-6-1 and ER-6-1#2*, DOE/NV/13609-LTR2004-02. Reno, NV: Desert Research Institute.

Pawloski, G.A., and J.L. Wagoner. 2003. *Evaluation of Seismic Data Acquired in Yucca Flat, NTS, by the Lawrence Livermore National Laboratory.* Livermore, CA: Lawrence Livermore National Laboratory.

Phelps, G.A., and E.H. McKee. 1999. *High-Angle Faults in the Basement of Yucca Flat, Nevada Test Site, Nevada, Based on the Analysis of a Constrained Gravity Inversion Surface*, Open-File Report-99-383. U.S. Geological Survey.

Phelps, G.A., V.E. Langenheim, and R.C. Jachens. 1999. *Thickness of Cenozoic Deposits of Yucca Flat Inferred from Gravity Data, Nevada Test Site, Nevada*, Open-File Report-99-310. U.S. Geological Survey.

Phelps, G.A., E.H. McKee, D.S. Sweetkind, and V.E. Langenheim. 2000. *Preliminary Model of the Pre-Tertiary Basement Rocks Beneath Yucca Flat, Nevada Test Site, Nevada, Based on Analysis of Gravity and Magnetic Data*, Open-File Report-2000-134. U.S. Geological Survey.

Phelps, G.A., R.C. Jachens, B.C. Moring, and C.W. Roberts. 2004. *Modeling of the Climax Stock and Related Plutons Based on the Inversion of Magnetic Data, Southwest Nevada*, Open-File Report-2004-1345.

Phelps, G.A., A.L. Justet, B.C. Moring, and C.W. Roberts. 2005. *A Preliminary Investigation of the Structure of Southern Yucca Flat, Massachusetts Mountain, and CP Basin, Nevada Test Site, Nevada, Based on Geophysical Modeling*, Open-File Report-2005-1367. U.S. Geological Survey.

Prothro, L.B. 1998. *Analysis of Fractures in Cores from the Tuff Confining Unit Beneath Yucca Flat, Nevada Test Site*. Las Vegas, NV: Bechtel Nevada.

Prothro, L.B. 2005. *Mineralogic Zonation Within the Tuff Confining Unit, Yucca Flat, Nevada Test Site*, DOE/NV/11718--995. Las Vegas, NV: Bechtel Nevada.

Reimus, P.W., S.D. Ware, A. Humphrey, A. Adams, B. Wilson, D. Gonzales, R.G. Warren, and F.C. Benedict. 2000a. *Diffusive and Advective Transport of ^{3}H, ^{14}C, and ^{99}Tc in Saturated, Fractured Volcanic Rocks from Pahute Mesa, Nevada*. Prepared for U.S. DOE, UGTA Project, Los Alamos, NM.

Reimus, P.W., S.D. Ware, N. Lu, S. Kung, A. Abdel-Fattah, A. Kersting, N. Hakem, P. Zhao, and G. Eaton. 2000b. *Progress Report on Colloid-Facilitated Plutonium Transport in Fractured Rocks from Pahute Mesa, Nevada Test Site*. Prepared for U.S. DOE, UGTA Project, Los Alamos, NM.

Reimus, P.W., M. Murrell, A. Abdel-Fattah, E. Garcia, D. Norman, S. Goldstein, A. Nunn, R. Gritzo, and B. Martinez. 2006a. *Colloid Characteristics and Radionuclide Associations with Colloids in Near-Field Waters at the Nevada Test Site* (FY 2005 Progress Report), LA-UR-05-8612. Los Alamos, NM: Los Alamos National Laboratory.

Reimus, P.W., R.L. Hershey, D.L. Decker, S.D. Ware, C. Papelis, S. Earman, A. Abdel-Fattah, M. Haga, D. Counce, S. Chipera, and C. Sedlacek. 2006b. "Errata for Table 10." In *Tracer Transport Properties in the Lower Carbonate Aquifer of Yucca Flat*, LA-UR-06-0486. Los Alamos, NM: Los Alamos National Laboratory.

Reimus, P.W., R.L. Hershey, D.L. Decker, S.D. Ware, C. Papelis, S. Earman, A. Abdel-Fattah, M. Haga, D. Counce, S. Chipera, and C. Sedlacek. 2006c. *Tracer Transport Properties in the Lower Carbonate Aquifer of Yucca Flat*, LA-UR-06-0486. Los Alamos, NM: Los Alamos National Laboratory.

Reimus, P.W. 2007. *Semi-Analytical Interpretations of ER-6-1 Multiple-Well Tracer Test Results*, LA-UR-07-1410. Los Alamos, NM: Los Alamos National Laboratory.

Rose, T.P., G.F. Eaton, and R.I. Yamamoto, eds. 2002. *Hydrologic Resources Management Program and Underground Test Area Project FY2000 Progress Report*, UCRL-ID-145167. July. Livermore, CA: Lawrence Livermore National Laboratory.

SNJV, see Stoller-Navarro Joint Venture.

Stoller-Navarro Joint Venture. 2004a. *Analysis of Well ER-7-1 Testing, Yucca Flat FY 2003 Testing Program, Nevada Test Site, Nevada*, S-N/99205--021. Las Vegas, NV.

Stoller-Navarro Joint Venture. 2004b. *Analysis of Well ER-12-2 Testing, Yucca Flat FY 2003 Testing Program, Nevada Test Site, Nevada*, Rev. 0, S-N/99205--015. Las Vegas, NV.

Stoller-Navarro Joint Venture. 2004c. *Hydrologic Data for the Groundwater Flow and Contaminant Transport Model of Corrective Action Units 101 and 102: Central and Western Pahute Mesa, Nye County, Nevada*, S-N/99205--002; Shaw/13052-204. Las Vegas, NV.

Stoller-Navarro Joint Venture. 2004d. *Letter Report: Analysis of Well ER-2-1 Hydraulic Testing, Yucca Flat FY 2003, Nevada Test Site, Nevada*, DOE/NV--992. Las Vegas, NV.

Stoller-Navarro Joint Venture. 2004e. *Phase II Hydrologic Data for the Groundwater Flow and Contaminant Transport Model of Corrective Action Unit 98: Frenchman Flat, Nye County, Nevada*, S-N/99205--032. Las Vegas, NV.

Stoller-Navarro Joint Venture. 2004f. *Underground Test Area Project, ER-6-1 Multi-Well Aquifer Test - Tracer Test Plan*, Rev. 0, S-N/99205--013. Las Vegas, NV.

Stoller-Navarro Joint Venture. 2005a. *Analysis of Hydraulic Responses from the ER-6-1 Multiple-Well Aquifer Test, Yucca Flat FY 2004 Testing Program, Nevada Test Site, Nye County, Nevada,* S-N/99205--051. Las Vegas, NV.

Stoller-Navarro Joint Venture. 2005b. *Analysis of Well ER-6-2 Testing, Yucca Flat FY 2004 Testing Program, Nevada Test Site, Nevada*, S-N/99205--053. Las Vegas, NV.

Stoller-Navarro Joint Venture. 2005c. *Phase II Contaminant Transport Parameters for the Groundwater Flow and Contaminant Transport Model of Corrective Action Unit 98: Frenchman Flat, Nye County, Nevada, Rev. 0,* S-N/99205--043. Las Vegas, NV.

Stoller-Navarro Joint Venture. 2005d. *Underground Test Area Fracture Analysis Report for Yucca Flat Wells ER-2-1, ER-6-1#2, ER-7-1, and ER-12-2, Nevada Test Site, Nevada,* S-N/99205--040. Las Vegas, NV.

Stoller-Navarro Joint Venture. 2006a. *Geochemical and Isotopic Evaluation of Groundwater Movement in Corrective Action Unit 97: Yucca Flat/Climax Mine, Nevada Test Site, Nevada* S-N/99205--070. Las Vegas, NV.

Stoller-Navarro Joint Venture. 2006b. *Phase I Hydrologic Data for the Groundwater Flow and Contaminant Transport Model of Corrective Action Unit 97: Yucca Flat/Climax Mine, Nevada Test Site, Nye County, Nevada*, Rev. 0, S-N/99205--077. Las Vegas, NV.

Stoller-Navarro Joint Venture. 2006c. *Well ER-6-1 Tracer Test Analysis: Yucca Flat, Nevada Test Site, Nye County, Nevada*, Rev. 0, S-N/99205--084. Las Vegas, NV.

Stoller-Navarro Joint Venture. 2007. Written Communication: *U12n and U12t Tunnels Preliminary Data Report Groundwater Sampling*. Las Vegas, NV.

U.S. Department of Energy, National Nuclear Security Administration Nevada Site Office. 2004a. *Completion Report for Well Cluster ER-6-1,* DOE/NV/11718-862. Las Vegas, NV.

U.S. Department of Energy, National Nuclear Security Administration Nevada Site Office. 2004b. *Completion Report for Well ER-2-1,* DOE/NV/11718-893. Las Vegas, NV.

U.S. Department of Energy, National Nuclear Security Administration Nevada Site Office. 2004c. *Completion Report for Well ER-7-1,* DOE/NV/11718-865. Las Vegas, NV.

U.S. Department of Energy, National Nuclear Security Administration Nevada Site Office. 2004d. *Completion Report for Well ER-8-1,* DOE/NV/11718-854. Las Vegas, NV.

U.S. Department of Energy, National Nuclear Security Administration Nevada Site Office. 2004e. *Completion Report for Well ER-12-2,* DOE/NV/11718-846. Las Vegas, NV.

U.S. Department of Energy, Nevada Operations Office. 1993. *Drilling/Completion Criteria For Underground Test Area Remedial Investigation and Feasibility Study Well ER-3-2*, DOE/NV/10972-80. Las Vegas, NV

U.S. Department of Energy, Nevada Operations Office. 1994. *Drilling/Completion Criteria for Underground Test Area Operable Unit Well ER-3-1*, DOE/NV/10972-76. Las Vegas, NV.

U.S. Department of Energy, Nevada Operations Office. 1995a. *Completion Report for Well ER-3-1,* DOE/NV-396, UC-700. Las Vegas, NV.

U.S. Department of Energy, Nevada Operations Office. 1995b. *Completion Report for Well ER-3-2,* DOE/NV-408, UC-700. Las Vegas, NV.

U.S. Department of Energy, Nevada Operations Office. 1995c. Written communication. Subject: *Recompletion Report for Well UE-10j*. Las Vegas, NV.

U.S. Department of Energy, Nevada Operations Office. 1997. Written communication. Subject: *Completion Report for Well ER-6-2*. Las Vegas, NV.

U.S. Department of Energy, Nevada Operations Office. 2000a. *Corrective Action Investigation Plan for Corrective Action Unit 97: Yucca Flat/Climax Mine, Nevada Test Site, Nevada,* DOE/NV--659. Las Vegas, NV.

U.S. Department of Energy, Nevada Operations Office. 2000b. *United States Nuclear Tests, July 1945 through September 1992*, DOE/NV--209, Rev. 15. Las Vegas, NV.

Ware, S.D., A. Abdel-Fattah, M. Ding, P.W. Reimus, C. Sedlacek, M. Haga, E. Garcia, and S. Chipera. 2005a. "Errata for Table 1." In *Radionuclide Sorption and Transport in Fractured Rocks of Yucca Flat, Nevada Test Site*, LA-UR-05-9279. Los Alamos NM: Los Alamos National Laboratory.

Ware, S.D., A. Abdel-Fattah, M. Ding, P.W. Reimus, C. Sedlacek, M. Haga, E. Garcia, and S. Chipera. 2005b. *Radionuclide Sorption and Transport in Fractured Rocks of Yucca Flat, Nevada Test Site*, LA-UR-05-9279. Los Alamos NM: Los Alamos National Laboratory.

Zavarin, M. 2002. *Matrix Diffusion and Colloid-Facilitated Transport in Fractured Rocks: Model and Parameter Validation*, UCRL-ID-149817. Livermore, CA: Lawrence Livermore National Laboratory.

Zavarin, M., R.M. Maxwell, A.B. Kersting, P. Zhao, E.R. Sylwester, P.G. Allen, and R.W. Williams. 2003. *Plutonium Colloid- Facilitated Transport in the Environment - Experimental and Transport Modeling Evidence for Plutonium Migration Mechanisms*, UCRL-JC-151924. Livermore, CA: Lawrence Livermore National Laboratory.

Zavarin, M., M.R. Johnson, S.K. Roberts, R. Pletcher, T.P. Rose, A.B. Kersting, G. Eaton, Q. Hu, E. Ramon, J. Walensky, and P. Zhao. 2005. *Radionuclide Transport in Tuff and Carbonate Fractures from Yucca Flat, Nevada Test Site, Final Report,* UCRL-TR-219836. Livermore, CA: Lawrence Livermore National Laboratory.

Zavarin, M., S.K. Roberts, M.R. Johnson, Q. Hu, B. Powell, P. Zhao, A.B. Kersting, R. Lindvall, and R. Pletcher. 2006. Written communication: *Colloid-Facilitated Radionuclide Transport in Fractured Carbonate Rocks from Yucca Flat, Nevada Test Site*. Livermore, CA: Lawrence Livermore National Laboratory.

Zavarin, M., S. Roberts, P. Reimus, and M. Johnson. 2007. *Summary of Radionuclide Reactive Transport Experiments in Fractured Tuff and Carbonate Rocks from Yucca Flat, Nevada Test Site,* UCRL-TR-225271. Livermore, CA: Lawrence Livermore National Laboratory.

Zhao, P., M.R. Johnson, S.K. Roberts, and M. Zavarin. 2005. *Np and Pu Sorption to Manganese Oxide Minerals,* UCRL-TR-214984. Livermore, CA: Lawrence Livermore National Laboratory.

Appendix C

Yucca Flat/Climax Mine Alternative Hydrostratigraphic Framework Models

C.1.0 INTRODUCTION

The geologic complexity of the Yucca Flat/Climax Mine model area and the non-uniqueness of some of the interpretations incorporated into the base HFM made it necessary to formulate alternative interpretations for some of the major geologic features in the model. Each of these alternative HFMs honors the data, with differences between the models representing differences in interpretations of various features described by the data. Thus, each alternative HFM is a permissible and viable hydrogeologic representation. These alternatives can be used to explore the sensitivity of the flow and transport models to different geologic interpretations.

C.2.0 Process of Addressing Alternatives to the Base Model

Twenty-seven ideas for alternative interpretations to the Phase I Base HFM were identified, in collaboration with the UGTA TWG preemptive review committee, during its construction phase (see Table 5-1 in BN, 2006). Each alternative idea was evaluated and categorized, with the main criterion being whether the proposed change or alternative interpretation had the potential to significantly affect groundwater flow and transport. The geological likelihood and amount of constraining data were also considered. Alternative ideas were grouped into four priority categories:

- Group A alternatives were judged to be significant and viable enough to be included in the base model. Two alternatives were identified as Group A and incorporated directly into the base model.
- Group B alternatives were judged to be significant enough to develop as separate models. Five alternative ideas were identified and inserted into separate copies of the base model.
- Group C alternatives were judged to be potentially significant. If identified as significant during hydrologic modeling, these alternatives would be addressed by varying the assignment of model parameters within the base HFM to address the alternative feature(s) of interest.
- Group D alternatives were deemed not significant or viable enough to warrant development as alternative models and were not considered further.

Following this evaluation of the alternative ideas, the base HFM model was updated using the Group A alternatives, and the alternative ideas categorized as Group B were developed into HFMs. The alternative models were constructed after the base model was completed, generally using the same model construction techniques. Each alternative model is equally bound by all the data and interpretation methods used for development of the base model. However, each alternative scenario is of limited geographic extent and thus affects only a portion of the base HFM. The alternative HFMs are fully functional replicas of the base model that can be used to test whether the alternative interpretations affect flow and transport.

C.3.0 ALTERNATIVE MODELS

Brief descriptions of the five alternative HFMs developed for the Yucca Flat/Climax Mine model area are provided below. All figures cited in the following sections are from BN (2006). Additional details can be found in the framework model documentation report: *A Hydrostratigraphic Model and Alternatives for the Groundwater Flow and Contaminant Transport Model of Corrective Action Unit 97: Yucca Flat-Climax Mine, Lincoln and Nye Counties, Nevada* (BN, 2006).

C.3.1 CP Thrust Alternative

Based on magnetotellutic (MT) data and regional structural analysis, Mississippian siliciclastic rocks that compose the UCCU were shown to occur within the footwall of the CP thrust fault. This thrust fault is modeled as steepening rapidly eastward and forming a ramp structure beneath central Yucca Flat coincident with the Carpetbag-Topgallant normal fault system. As a result, the base model limits the UCCU to the western portion of the model area west of the Carpetbag-Topgallant fault system. However, MT data are sparse in northern Yucca Flat east of the Carpetbag fault due to the presence of power lines that interfere with MT recordings. The eastern limit of the UCCU is therefore poorly constrained east of the Carpetbag fault in northern Yucca Flat.

The CP thrust alternative scenario models the CP thrust ramp coinciding with the Carpetbag-Topgallant fault system in the southern and central portions of Yucca Flat, but shifting to the east in northern Yucca Flat to become coincident with the Yucca fault (Figures C.3-1 and C.3-2). In this scenario, the UCCU within the footwall rocks of the CP thrust fault extends eastward to the Yucca fault, and thus underlies northern Yucca Flat between the Carpetbag and Yucca faults (Figure C.3-1). More extensive UCCU in the subsurface of northern Yucca Flat could have significant hydrologic effects, particularly with regard to influx of groundwater into Yucca Flat from the north.

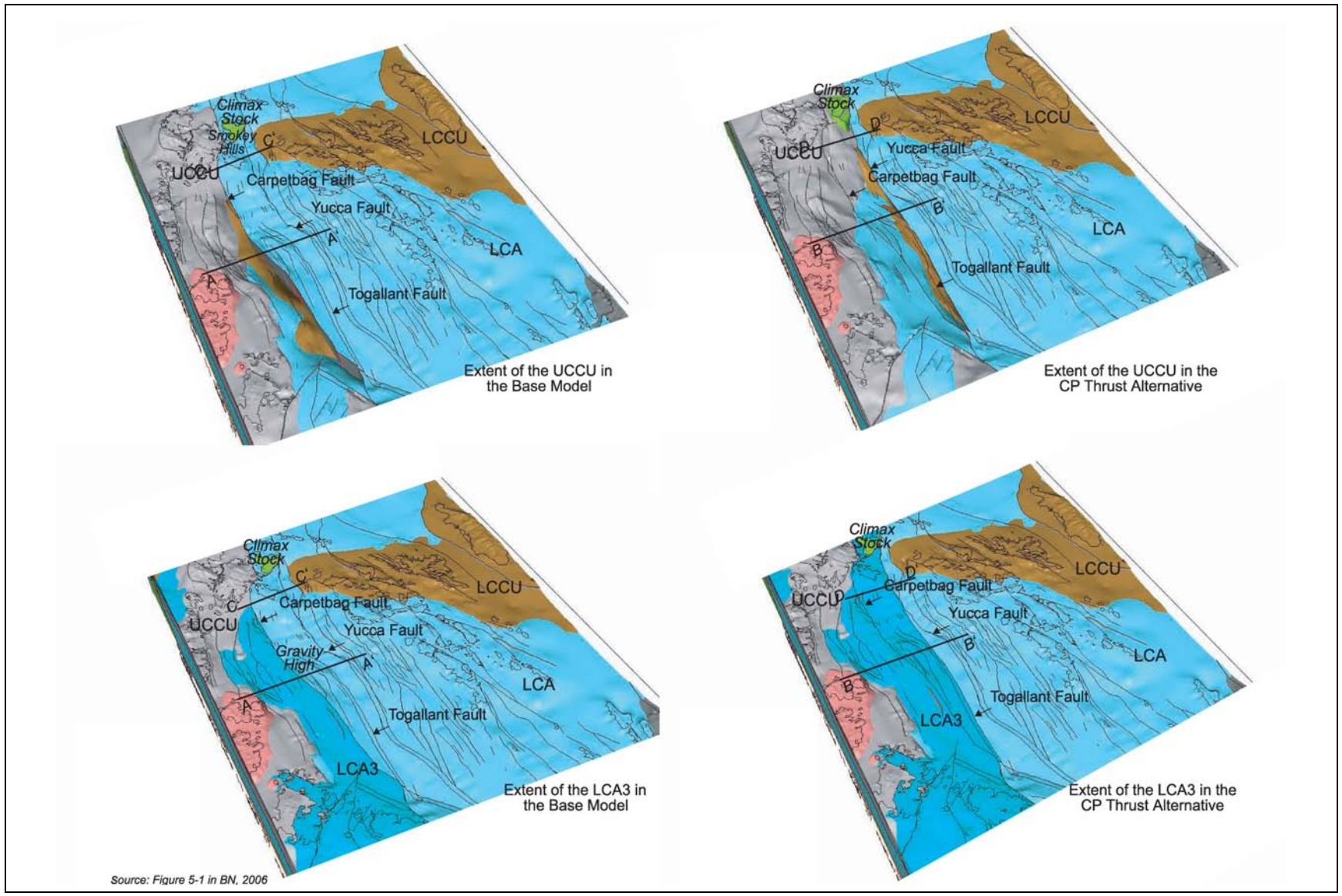

Figure C.3-1
Comparison of the UCCU Extent and CP Thrust Location in the Base Model with the CP Thrust Alternative (Tertiary HSUs Removed for These Views)
(Profiles shown on Figure C.3-2)

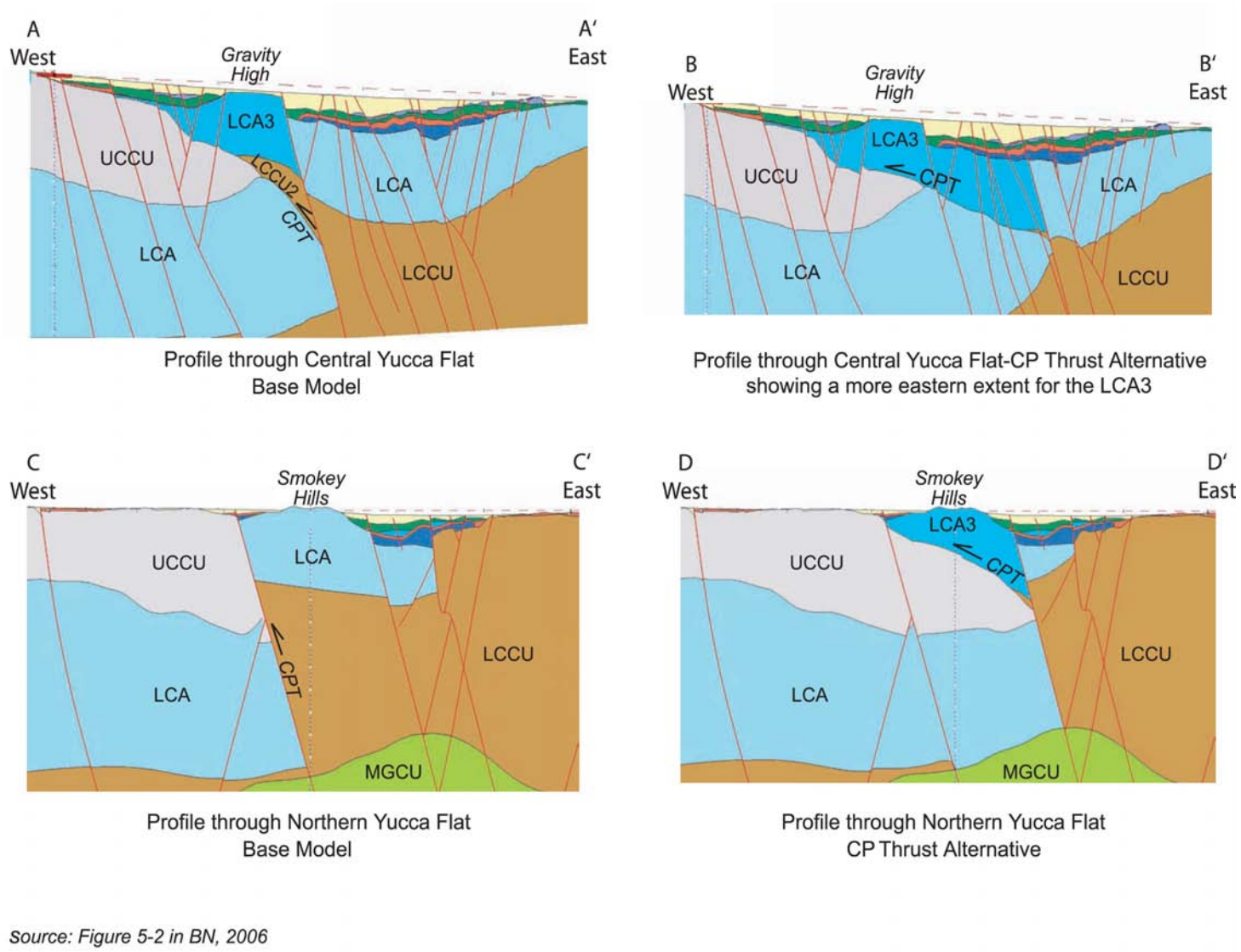

Source: Figure 5-2 in BN, 2006

Figure C.3-2
West-East Profiles Through Central and Northern Yucca Flat Comparing the Base Model with the CP Thrust (CPT) Alternative

C.3.2 Hydrologic Barrier in Northern Yucca Flat

The intent of this alternative is to limit inter-basin groundwater flow into Yucca Flat from the north. The LCCU, UCCU, and MGCU form a hydrologic barrier immediately north of Yucca Flat. If this barrier is too low, the model may allow too much water to flow into Yucca Flat; if it is too high, the model will not allow enough lateral flow to occur. This alternative restricts inflow, while the base model allows for some flow on the east side over the LCCU at the northwestern end of the Halfpint Range anticline. To restrict flow on the east side of the Climax Stock, the alternative HFM raises the LCCU up to the water table at the northwestern end of the Halfpint Range anticline (Figures C.3-3 and C.3-4). Flow on the west side of Climax is limited to deeper flow under the UCCU in both cases.

C.3.3 Contiguous UCCU in Southwestern Yucca Flat

Magnetotellutic data suggest that the UCCU is not continuous within the southwest portion of the model area, such as beneath the CP Hills and Mid Valley. The data seem to indicate that much of the area is underlain by thick, highly resistive carbonate rocks, and that the more electrically conductive Mississippian siliciclastic rocks that compose the UCCU are structurally broken up in this area and thus do not form a thick continuous sheet of clastic confining unit. This interpretation was incorporated into the base model. However, interpretation of the MT data in this area is difficult due to sparse drill-hole data in the area and the possible presence of abundant higher-resistance, quartzite-rich units within the UCCU that may make it difficult to distinguish Mississippian siliciclastic rocks (i.e., UCCU) from older carbonate rocks (i.e., LCA and LCA3). In addition, foreland imbrication related to the Belted Range thrust fault likely results in complex structural geometries in the area, further complicating interpretation of the MT data.

Because of the uncertainty with regard to the occurrence of the UCCU beneath the southwest portion of the HFM area and the potential significance to groundwater flow, particularly flow out of the basin to the southwest, an alternative model was created that modeled the UCCU as a continuous sheet within the subsurface in the southwest portion of the model area (Figures C.3-5 and C.3-6).

C.3.4 Fault Juxtaposition

Because basin-forming faults typically have large vertical displacements, the juxtaposition of shallow aquifers against deeper aquifers could occur, and may be significant with regard to flow and transport

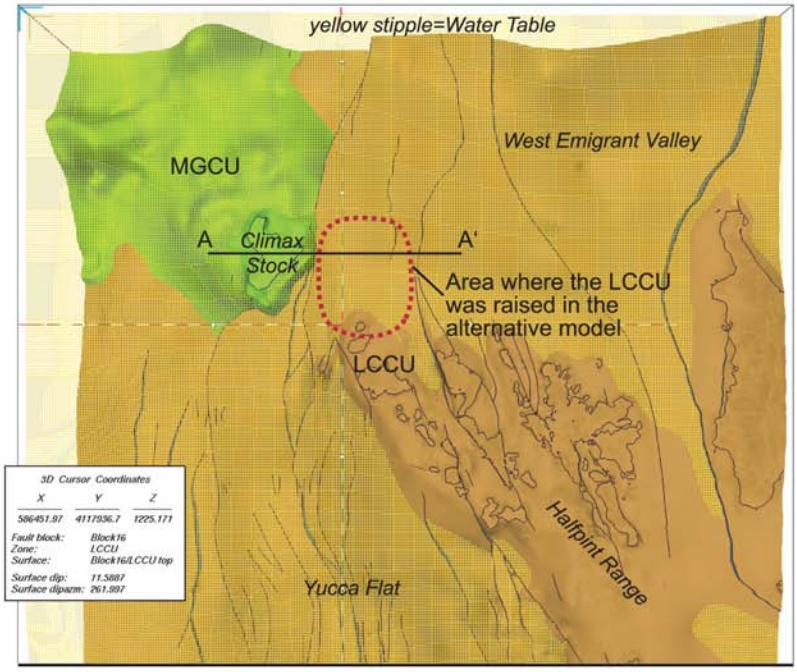

View of the LCCU and MGCU in the Base Model
(all other HSUs removed)

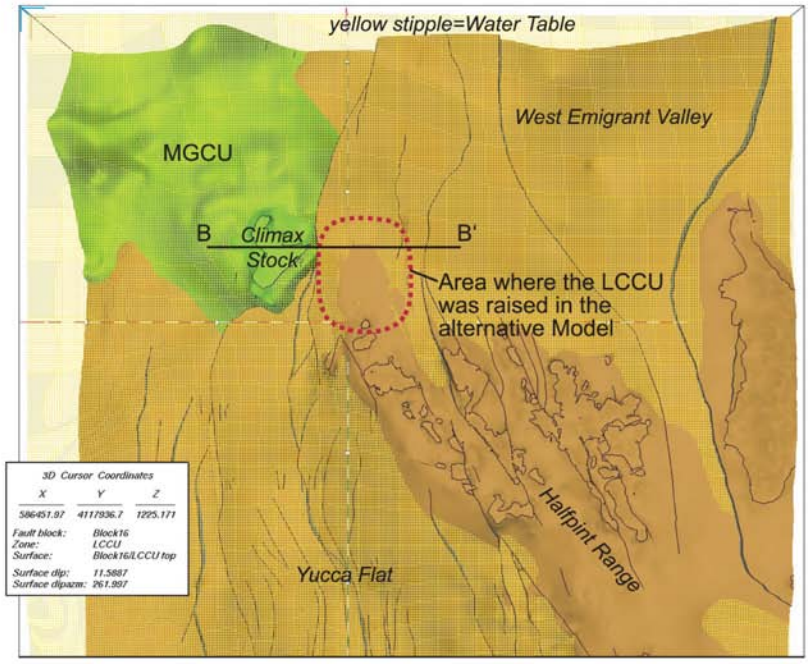

View of the LCCU and MGCU in the Alternative Model
(all other HSUs removed)

Source: Figure 5-3 in BN, 2006

Figure C.3-3
Comparison of the LCCU Geometry in the Base Model with the Hydrologic Barrier Alternative
(Profiles shown in Figure C.3-4)

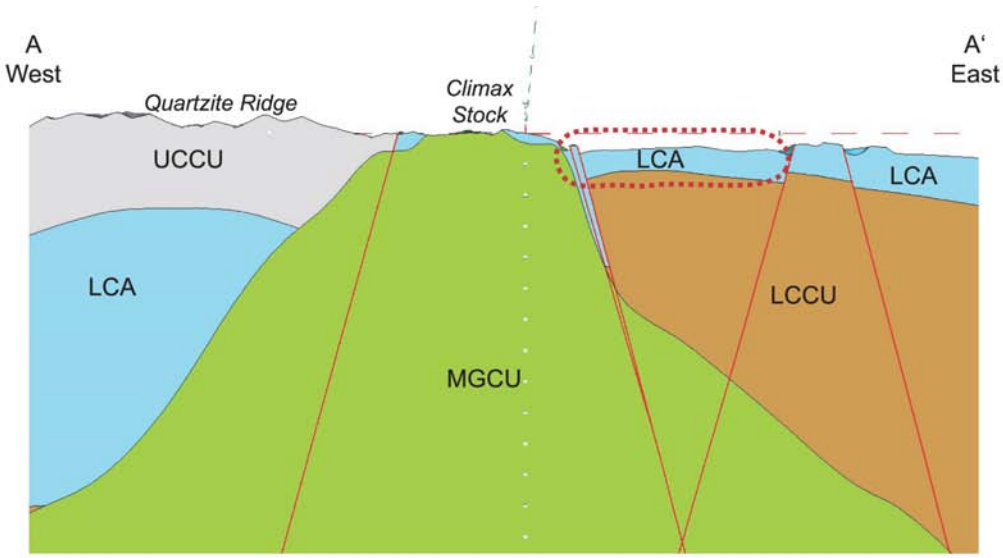

Profile through Climax Stock
Base Model
(alluvium and volcanic HSUs removed)

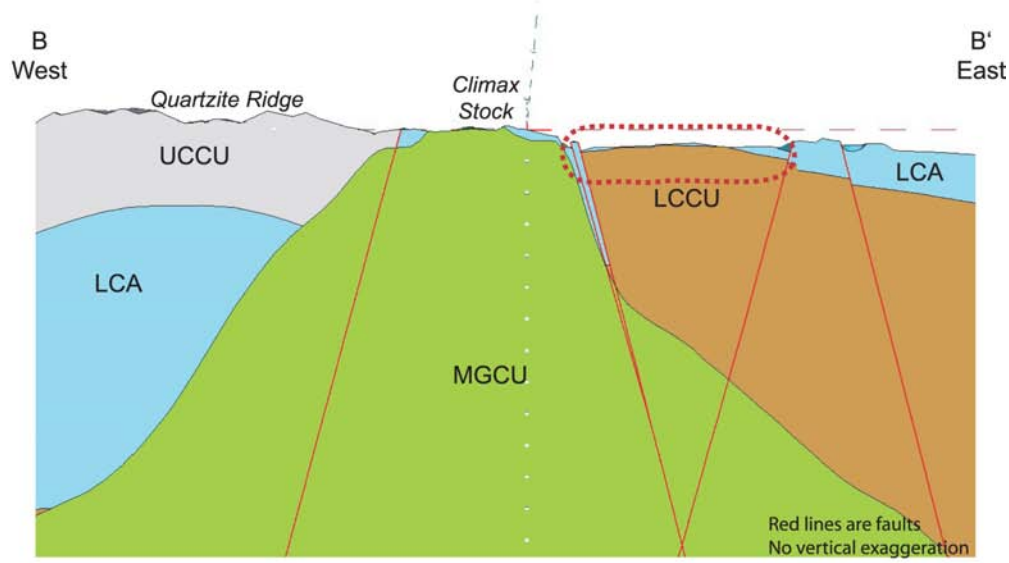

Profile through Climax Stock
Hydrologic Barrier Alternative showing the LCCU raised to the water table
(alluvium and volcanic HSUs removed)

Source: Figure 5-4 in BN, 2006

Figure C.3-4
West-East Profiles Through Climax Stock Comparing the Base Model with the Hydrologic Barrier Alternative

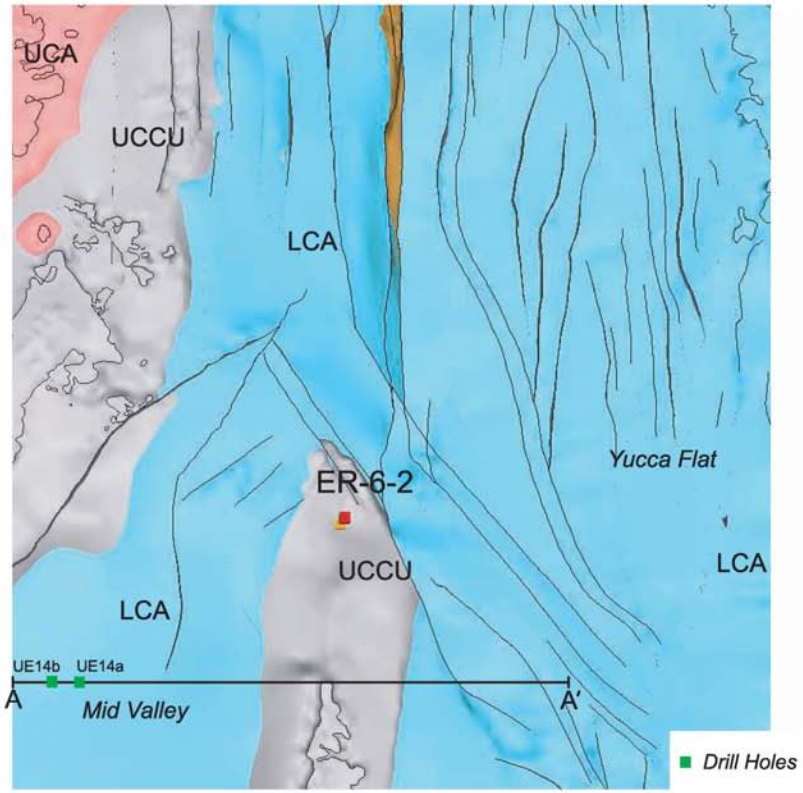

Extent of the UCCU in the Southwestern Corner of the Yucca Flat/Climax Mine Base Model

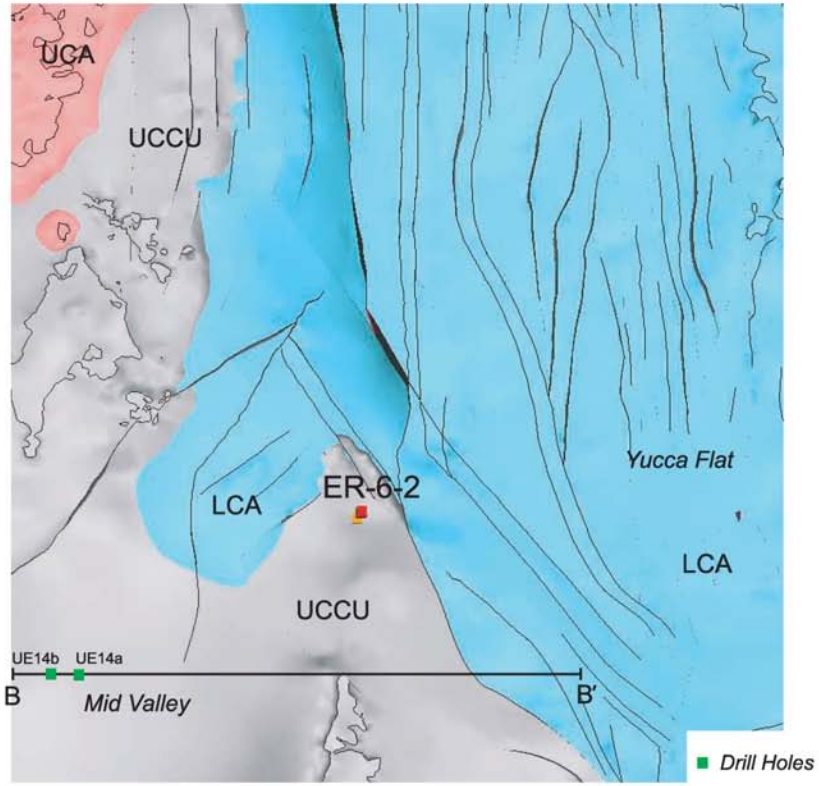

Extent of the UCCU in the Southwestern Corner of the Contiguous UCCU Alternative

Source: Figure 5-5 in BN, 2006

Figure C.3-5
Comparison of the UCCU Extent in the Base Model with the Contiguous UCCU Alternative (Tertiary HSUs Removed)
(Profiles shown on Figure C.3-6)

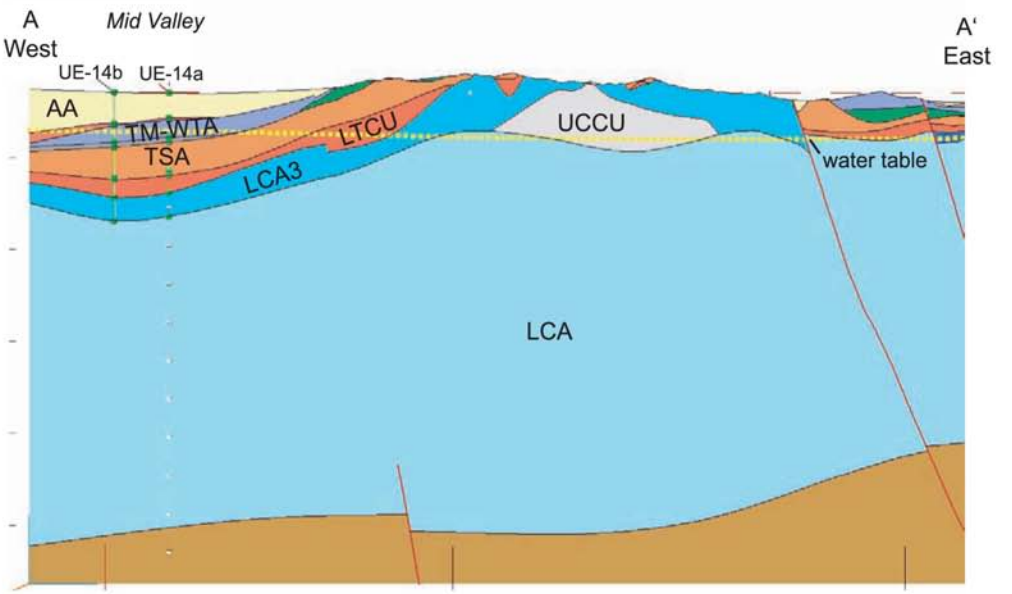

Profile through southwest corner of the Base Model showing limited extent of the UCCU

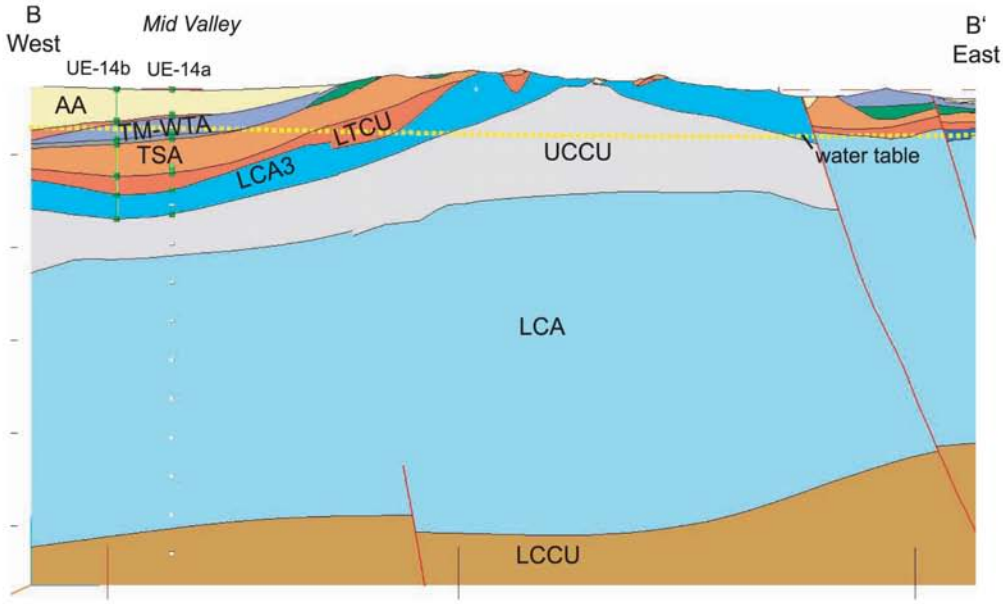

Profile through Contiguous UCCU Alternative Model showing extension of UCCU beneath Mid Valley

Source: Figure 5-6 in BN, 2006

Figure C.3-6
West-East Profile Through the Southwestern Corner of the Yucca Flat/Climax Mine HFM Comparing the Base Model with Contiguous UCCU Alternative

modeling in the Yucca Flat area. In the base HFM, aquifers may be juxtaposed slightly in some places due to faulting along the main basin-forming faults. However, the locations, orientations and amounts of displacement associated with these faults are not precisely constrained. Therefore, an alternative model was developed that juxtaposes shallow volcanic aquifer HSUs with the LCA along the major basin-forming faults (Figure C.3-7).

For this alternative, volcanic aquifers, typically the TM-WTA or TM-LVTA, are positioned against the LCA. This is accomplished by either increasing fault displacements or thinning underlying confining units, while still conforming to any existing nearby data. The target areas for this manipulation were the testing areas in central Yucca Flat that are below the water table. Most commonly the larger basin-forming faults are involved (e.g., the Carpetbag, Topgallant, and Yucca faults). The base model does contain such geometries, but this alternative provides more such situations, particularly in the testing areas.

C.3.5 Partial Zeolitization

Geologists at NTS have recognized a zone of partial zeolitization above the level of pervasive zeolitization in Areas 2 and 9 of north-central Yucca Flat. The zone of partial zeolitization is defined as areas of partial (less than 30 percent) zeolitization as well as areas of sporadic zeolitization where beds of zeolitized tuff (more than 30 percent zeolitization) alternate with weakly to nonzeolitized rocks. This has consequences for vertical and horizontal conductivity and transport of radionuclides.

It is difficult to define an exact boundary for the zone of partial zeolitization because it was not consistently identified on older lithologic logs, and because of its sporadic occurrence. The zone is modeled as a separate HSU that includes all partially zeolitized strata below the water table down to the top of the LTCU (i.e., top of pervasive zeolitization) in Area 2, Area 9, and the very northeast corner of Area 4 (Figure C.3-8). This zone may exist above the water table.

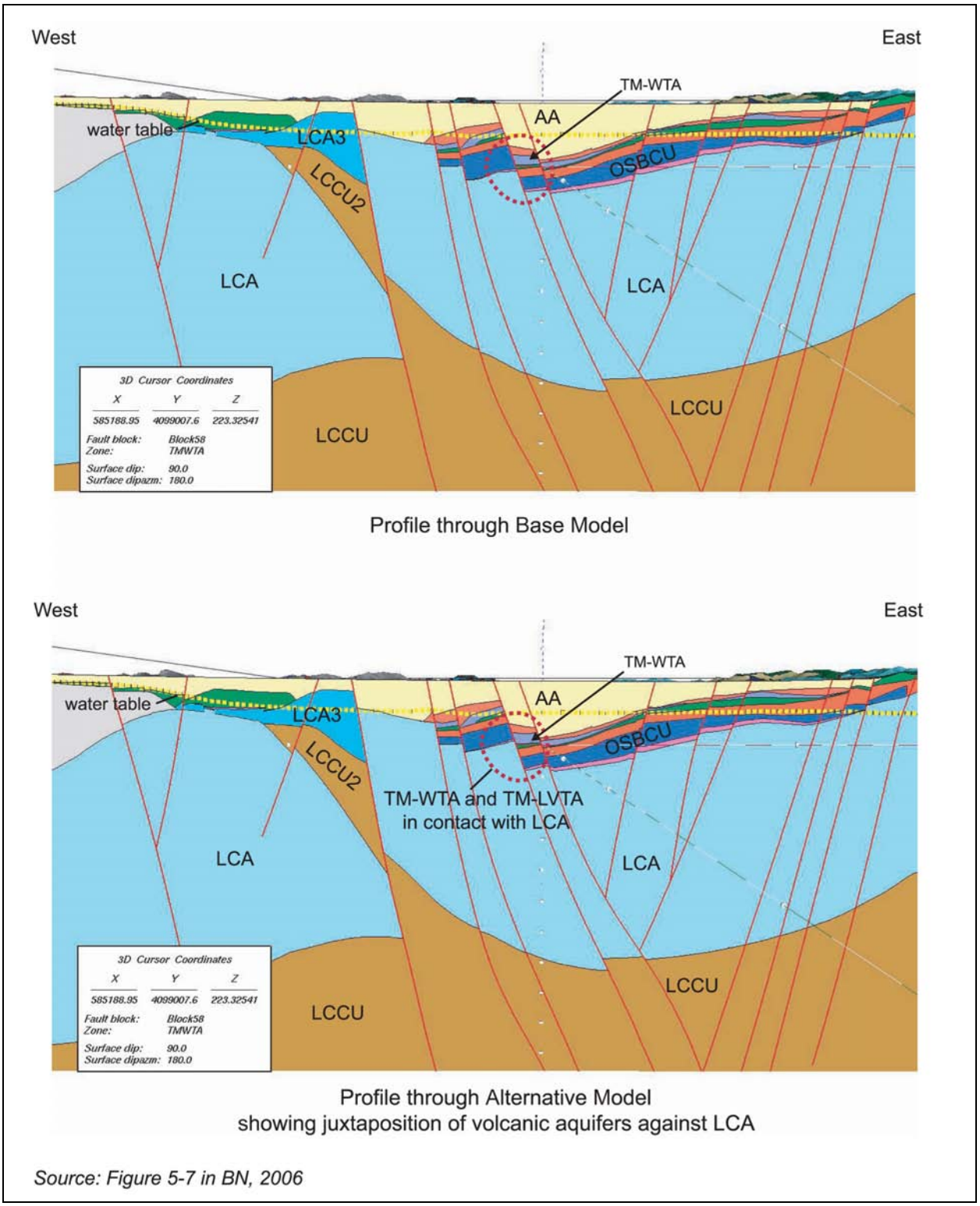

Source: Figure 5-7 in BN, 2006

Figure C.3-7
West-East Profiles Through Central Yucca Flat Comparing the Base Model with Fault Juxtaposition Alternative

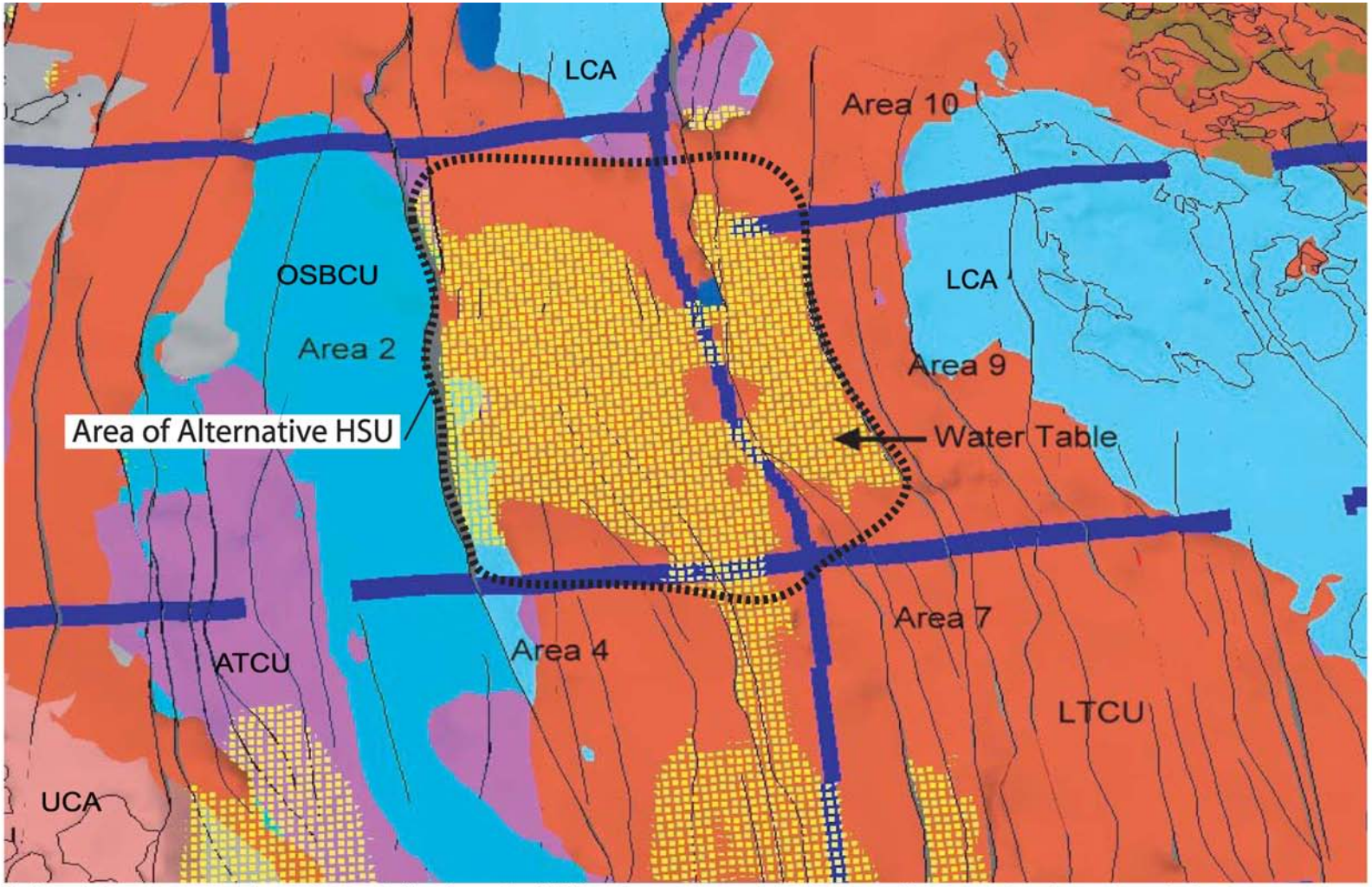

Yellow dots represent surface of water table above the HSU surfaces shown; blue lines are NTS operational area boundaries.

Source: Figure 5-8 in BN, 2006

Figure C.3-8
View of the Base Model Showing Area Affected in the Partial Zeolitization Alternative (Alluvium and Volcanic Aquifer HSUs Removed)

C.4.0 REFERENCES

BN, see Bechtel Nevada.

Bechtel Nevada. 2006. *A Hydrostratigraphic Model and Alternatives for the Groundwater Flow and Contaminant Transport Model of Corrective Action Unit 97: Yucca Flat-Climax Mine, Lincoln and Nye Counties, Nevada*, DOE/NV/11718--1119. Las Vegas, NV.

Appendix D

Compilation of Mineralogy Data

D.1.0 Compilation of X-ray Diffraction Analyses and Formal Definitions for Alteration

The results of XRD analysis were compiled in FY 2006 for samples collected primarily from the Yucca Flat/Climax Mine CAU within the SWNVF. The compilation focused specifically on drill holes of Yucca Flat to provide a sound basis to model the subsurface mineralogy of this basin. The XRD data include results documented in (1) historical LANL and LLNL files generated for the weapons testing program, (2) a BN report describing a study of the tuff confining units of Yucca Flat (Prothro, 2005), and (3) an LANL report describing the geologic characterization of the newly drilled ER wells (WoldeGabriel et al., 2004). The latter two studies were performed in support of the UGTA Project. These analyses, along with additional supporting information, are also available within the Petrographic, Geochemical, and Geophysical (PGG) database for the SWNVF (Warren et al., 2003) or will become available within the next update of this online database. Further details regarding this compilation are provided in Warren (2007).

Included in this compilation are XRD analysis results from Schroeder and Williams (1962) through the year 2003, a period spanning 42 years. During this period, analysts from different organizations applied techniques that evolved through four major stages, significantly improving the analytical methodology. Particularly from the year 2000, quantitative methods have greatly improved the sensitivity and precision, which has markedly affected results for certain minerals. In addition, different sampling procedures and collection of a variety of sample types have been employed by geologists from different organizations.

The goal of this compilation was to obtain a dataset that is representative of the relative mineral abundances present within drill holes of Yucca Flat. Compilation of XRD analyses favored volcanic units, which includes underlying paleocolluvium but excludes tephra intercalated with alluvium. A larger number of analyses were compiled for the northern Yucca Flat holes (LLNL drill holes) than

those in the southern NTS areas of Yucca Flat (LANL drill holes) as described in Warren (2007). The drill holes represented within the dataset are shown in Figures D.2-1 and D.2-2 for the northern and southern NTS areas, respectively.

Geologic information (e.g., stratigraphic unit, stratigraphic bounds, lithology, and alteration, together with depth and elevation) is also provided to establish the geologic context for the subsurface mineralogy. Alteration relates directly to mineralogy of volcanic rocks and alluvium within the SWNVF. Definitions for alteration are provided to help recognize and understand lateral variations in mineralogy, and to substantially improve accuracy in alteration assignments based on examination of hand samples using binocular microscope.

D.2.0 DATASET SUMMARY

Location Id - The unique symbol for Location Id represents a specific, usually unique location on the surface, or a specific, usually unique location within a tunnel. Drill-hole locations for testing of weapons use "U" ("underground") as the initial character within the Location Id, followed by "E" for exploratory holes, followed by the area within the NTS. Thus, U4A designates an emplacement hole within Area 4, and U7AV designates an exploratory hole within Area 7. Holes drilled for the Environmental Restoration Project use "ER" (e.g., ER7/1). The only exceptions for this system of nomenclature are Water Well C (WWC), located in Area 6 and select holes in NTS Area 6 that are identified as U-3 holes (Figure D.2-2). The dash character (-) is reserved for Sample Ids, and therefore dashes in published locations are converted to a foreslash (/). Location Ids for drill holes are matched as closely as possible to those commonly used, but unnecessary characters such as "#" are always eliminated, and short, recognizable character strings substitute for extremely long location names. For instance, U3GS2 and ER6/1/2 are the Location Ids for U-3gs Ex. 2/Inst and ER-6-1#2, respectively. All location Ids are converted to capital letters, which is inconsistent with the conventional nomenclature. Conventional nomenclature is presented in Figures D.2-1 and D.2-2.

Sample Id - This unique symbol represents up to a few kilograms of contiguous material from the surface or subsurface. The dash special character (-) is reserved to designate multiple samples from a single location. Sample Ids for vertical drill holes always contain the Location Id followed by a dash (-) and the sample depth (or sample depth interval) in feet. Often an extension is added that identifies the sample type.

Split_Id - This unique symbol represents a split of a sample for analysis. A split represents analysis for one or more element or component that is performed by a single laboratory. Usually, a few grams are split from the sample and specially prepared for the analytical procedure, such as a glass-covered thin section for petrographic analysis or pulverized rock for chemical or XRD analysis. A left parenthesis designates each split from a single sample. Multiple chemical or XRD analyses of the same sample by the same laboratory and multiple analyses of the same thin section are considered to

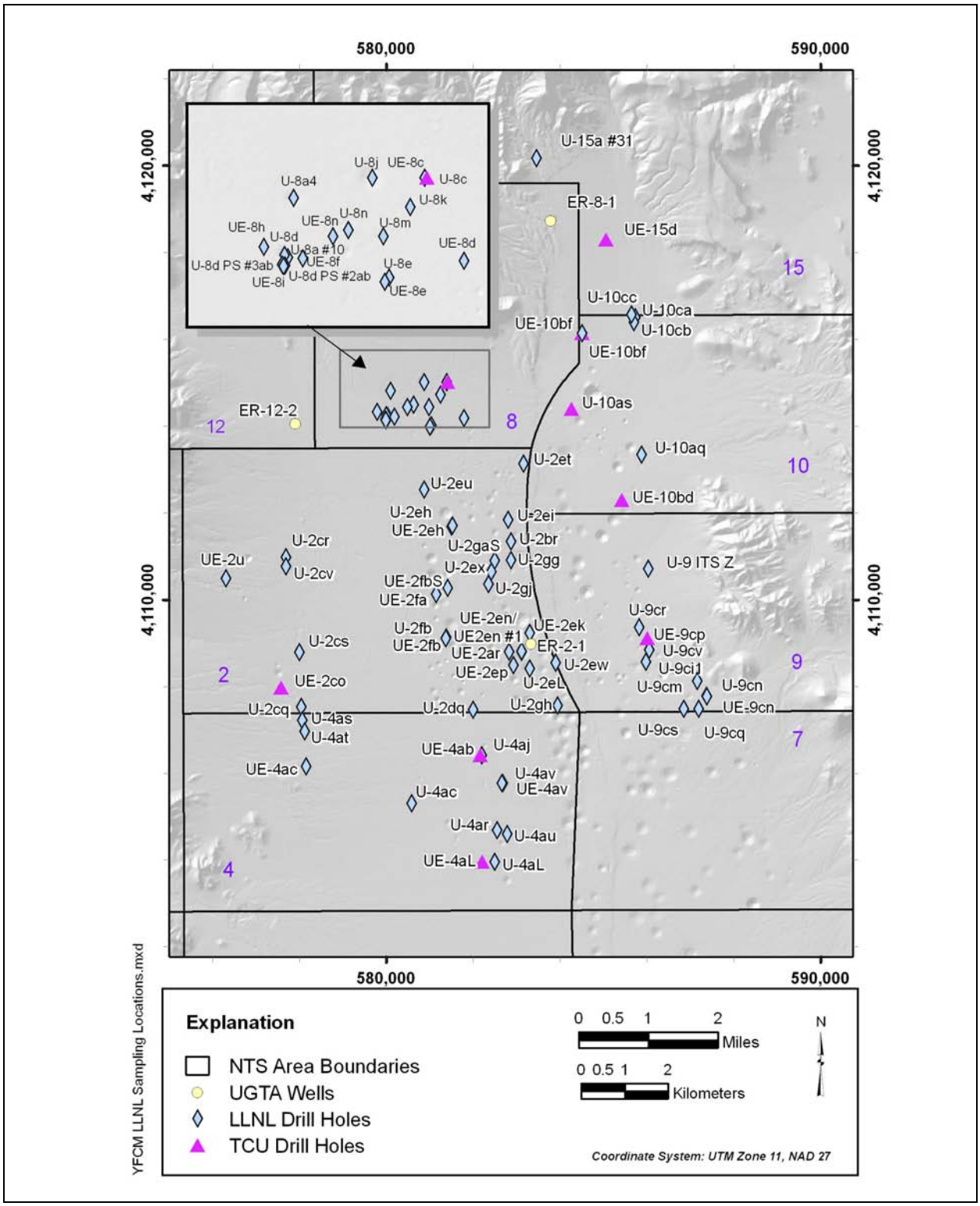

Figure D.2-1
Sampling Locations in the Northern Areas of Yucca Flat Formally Used for Testing by Lawrence Livermore National Laboratory

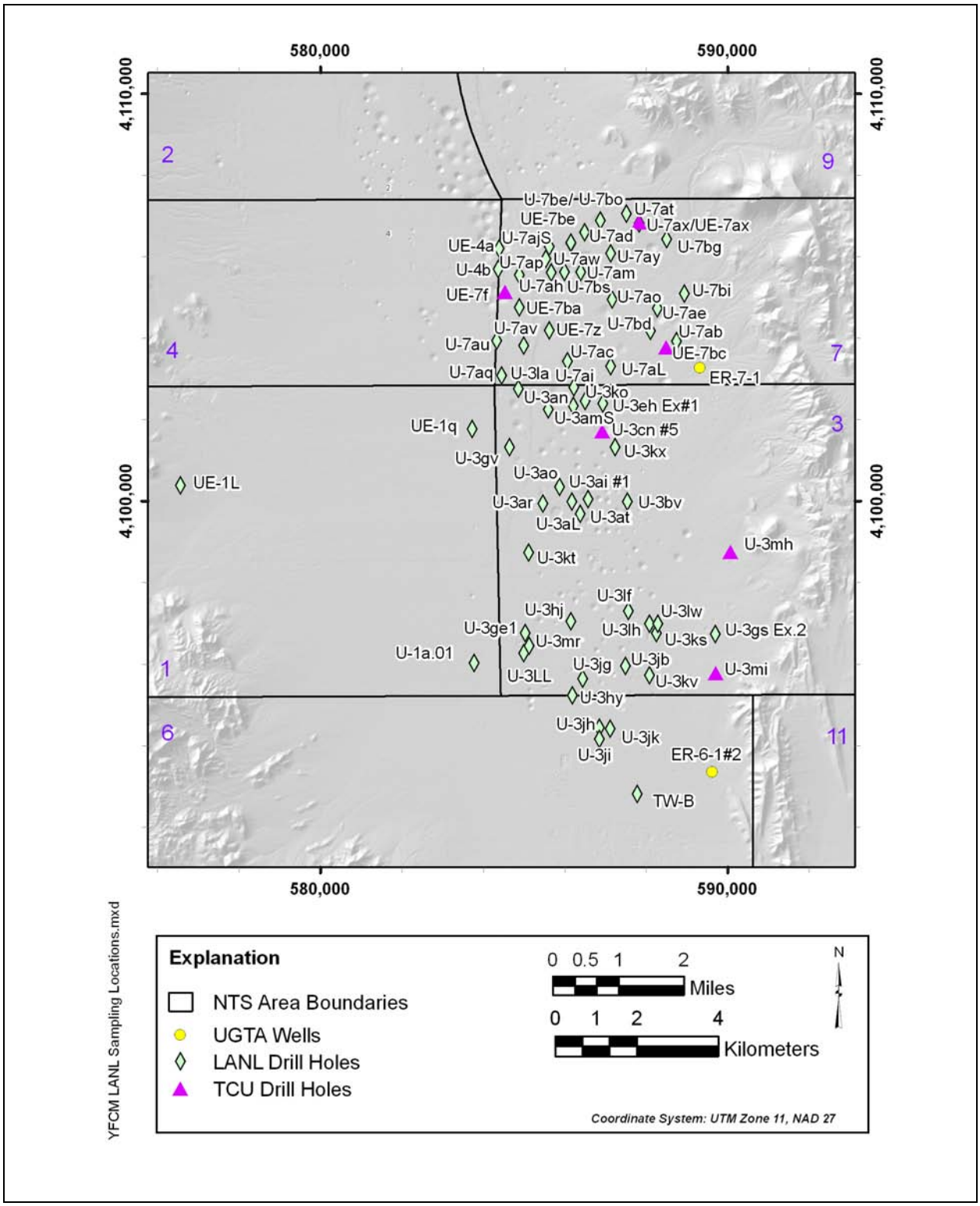

Figure D.2-2
Sampling Locations in the Southern Areas of Yucca Flat Formally Used for Testing by Los Alamos National Laboratory

represent replicate analyses. Individual replicate analyses are not stored within the PGG database, nor are they provided within the Yucca Flat/Climax Mine XRD dataset. Three splits from drill-hole UE5N of Frenchman Flat (each analyzed in triplicate) and nine splits from U12E tunnel (each analyzed in duplicate) provide the only replicate XRD analyses presently known for the SWNVF. The published sources for these analyses are provided in the PGG database table, PGG_SPLIT_REF. Note that the "PGG" prefix is used to identify tables within the PGG database and is not included in the table name within the database.

UTM_e - This value, in meters, is the Easting for location in Zone 11 of Universal Transverse Mercator (UTM) projection, 1927 North American Datum (NAD).

UTM_n - This value, in meters, is the Northing for location in Zone 11 of UTM projection, 1927 NAD.

Sample_Depth_U - This value provides the uppermost bound for the sample depth in meters beneath the ground surface, and is applicable only to samples from vertical drill holes, trenches, or pits. For samples that represent rock caved from uphole, sample types DB2 and DB3, this depth represents the upper bound for the source of the material.

Sample_Depth_L - This value provides the lowermost bound for the sample depth in meters beneath the surface.

Sample_Elev_Av - This value provides the sample elevation in meters above mean sea level, or the average from uppermost and lowermost bounding depths if available from drill hole.

Alteration and Minor Alteration - Virtually all volcanic rocks of the SWNVF are tuff or lava erupted as magma that either crystallized to form devitrified rock or quenched to glass that initially comprises an average abundance of 80 percent for vitric rocks (Figure D.2-3). Devitrified rocks are resistant to subsequent alteration, but glass within vitric rocks is often progressively transformed into characteristic secondary mineral assemblages with increasing temperature by circulating fluids. Alteration, simply viewed, attaches ranges in temperature, Eh, and pH that form the observed secondary mineral assemblages. Several types of alteration frequently affect a single sample; for example, a rock can be partly vitric and partly devitrified, and minor zeolitic.

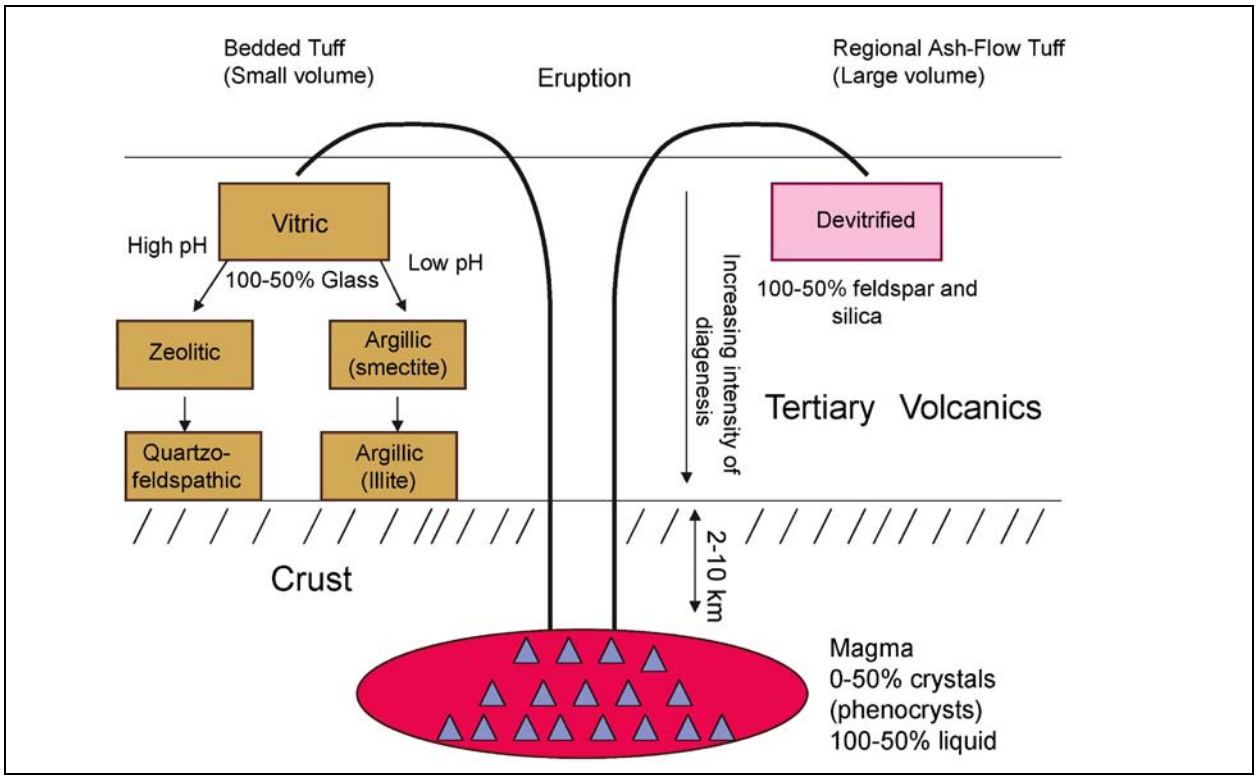

Figure D.2-3
Schematic Diagram Illustrating Eruption and Subsequent Alteration of Volcanic Rocks Within SWNVF
Graphics image by Clayton S. Painter (Warren, 2005)

Precise definitions for alteration are based on abundances for secondary phases (and glass) within assemblages that reflect distinctively different conditions controlled by temperature, Eh, and pH (Table D.2-1). Devitrified rocks can be overprinted by quartzofeldspathic or propylitic alteration, but cannot be transformed to less highly altered assemblages. However, devitrified rocks occasionally contain veins that lead to co-assignment of minor alteration for less highly altered assemblages.

Alteration is initially assigned by examination of samples using binocular microscope for depth intervals within each drill hole. Uncertainties in alteration assigned by binocular microscope are resolved using petrographic and XRD analyses, which are typically complementary. Modern XRD analysis always quantifies mineral assemblages. All assignments for the alteration and minor alteration columns within the dataset consider available petrographic and XRD analyses, as well as assignments from binocular microscope. In a few cases where the sample is considered nonrepresentative, alteration is assigned from the lithologic description for the appropriate depth interval (Warren, 2007).

Table D.2-1
Definitions for Alteration

Assemblage	Member	Name	Phases	Requirement
GL		Vitric	Glass (GL)	GL≥20%
CB		Carbonaceous	Carbonate (CB)	CB≥5%
	CC	Calcareous	Calcite (CC)	CC≥5%
	DM	Dolomitic	Dolomite (DM), Ankerite (AK), Siderite (ST)	DM+AK+ST≥5%
OP		Opaline	Opal-CT and Opal-A (OP)	OP≥20%
AR		Argillic	Smectite (SM), Mica, and Illite (MI)	SM+MI≥20%
	KA	Kaolinitic	Kaolinite (KA)	KA≥5%
	SC	Sericitic	Mica and Illite (MI), Albite (AB)	MI+AB≥20%
ZE		Zeolitic	Zeolite (ZE)	ZE≥20%
	ZC	Clinoptilolite	Clinoptilolite (ZC)	ZC≥20%
	ZM	Mordenite	Mordenite (ZM)	ZM≥20%
	ZA	Analcime	Analcime (ZA)	ZA≥20%
QF		Quartzofeldspathic	Chalcedony (QC), Adularia (AA), Albite (AB)	QC+AA+AB≥20%
	QZ	Silicic	Chalcedony (QC), Granophyric Quartz (GQ)	QC+GQ ≥20%
	KF	Potassic	Adularia (AA)	AA≥20%
	AB	Albitic	Albite (AB)	AB≥20%
PR		Propylitic	Chlorite (CH), Albite, (AB), Epidote (EP), Carbonate (CB)	CH+AB+EP+CB≥20%
	PY	Pyritic	Pyrite (PY)	PY≥1%
	CH	Chloritic	Chlorite (CH)	CH≥1%
	AE	Albite/epidote	Albite, (AB), Epidote (EP)	AB+EP≥20%
DV		Devitrified	Chalcedony (QC), Granophyric Quartz (GQ), Groundmass K-spar (GK), Groundmass Plagioclase (GP)	QC+GQ+GK+GP≥20%
	VP	Vapor phase	Tridymite (TR)	TR≥5%
	GR	Granophyric	Granophyric Quartz (GQ)	GQ≥5%
	SR	Spherulitic	Chalcedony (QC), Groundmass K-spar (GK), Groundmass plagioclase (GP)	Spherulitic (QC+GK+GP)≥20%

Alterations are progressively intense as listed, although minerals from any assemblage extend into adjacent assemblages and a few, such as carbonates, can associate with most or all assemblages. Multiple alterations frequently occur within a single split (e.g., partly devitrified, partly zeolitic is represented by DV/ZE). Minor alterations are assigned when the abundance of the appropriate phase occurs below the required value, except that minor argillic alteration also requires SM+MI>10%. Abundances apply only to sample matrix (groundmass), excluding lithics and phenocrysts.

Translation of the codes used in the alteration (Altn) and minor alteration (mAlt) fields are also provided in the worksheet titled “Strat_Alt_Lith” within the “YF_CM_XRD_Dataset.xls” spreadsheet. A series of tables, providing additional information regarding the assignment of alteration, are provided in the PGG database. These include the tables PGG_ALT_FK (provides a complete list of abbreviations for alteration), PGG_ALT_INT (provides the depth intervals for alteration assignments of individual sample locations), PGG_SAMPLE_WORKER (identifies the

worker responsible for the alteration assignment), PGG_SAMPLE_REF (provides documentation for alteration assignments for samples unrepresentative of sampled depth intervals), and PGG_GEOL_INT_REF (provides the appropriate source of the assignment documented in PGG_SAMPLE_REF).

Strat_Unit - This symbol identifies the stratigraphic unit associated with the sample split. Assignments for the Strat Unit column are from petrographic analyses, if available. Chemical analysis is also very useful for the assignment of stratigraphic unit, especially paired together with petrographic analysis. Otherwise, assignments are from binocular microscope (Warren, 2007). Except for a few analyses of XRD splits that demonstrate a low phenocryst content or show a distinctive content of a characteristic primary mineral, XRD analyses provide no information for stratigraphic assignment. Translation of the codes used in this field are provided in the worksheet titled "Strat_Alt_Lith" within the "YF_CM_XRD_Dataset.xls" spreadsheet. Additional supporting data are provided within the PGG database. For instance, the table PGG_STRAT lists about 300 volcanic stratigraphic units for the SWNVF. All of those that erupted within the volcanic field are associated within 16 volcanic assemblages (Warren, 2005). Additional tables include PGG_SAMPLE_WORKER (identifies worker responsible for the stratigraphic unit assignment), PGG_STRAT_INT (provides the depth interval for each stratigraphic unit for each borehole), PGG_SAMPLE_REF (cites the published source for the stratigraphic assignment), and PGG_ GEOL_INT_REF (cites the published source of the stratigraphic assignments within drill holes).

Strat_T Elev - This value represents the elevation in meters for the top of the stratigraphic unit assigned in the Strat Unit column.

Strat_B Elev - This value represents the elevation in meters for base of stratigraphic unit assigned in the Strat Unit column.

Strat_Above - This symbol identifies the stratigraphic unit above the sampled unit and provides an upper stratigraphic bound for XRD splits where the Strat Unit column is unassigned or unknown.

Strat_Below - This symbol identifies the stratigraphic unit below the sampled unit. This column provides a lower stratigraphic bound for XRD splits where the Strat Unit column is unassigned or unknown.

Lith - This field represents the lithology associated with the XRD split. Assignments for the Lithology column are from petrographic analyses if available. Otherwise, assignments are from binocular microscope. No information for lithology in provided by XRD analyses. Translation of the codes used in this field are provided in the worksheet titled "Strat_Alt_Lith" within the "YF_CM_XRD_Dataset.xls" spreadsheet. Additional data are provided in the PGG database tables: PGG_LITH_INT (provides lithology depth intervals for all sample locations), PGG_LITH_LIST (provides a list of all lithologies), PGG_SAMPLE_WORKER (identifies the worker responsible for assignment of lithology), PGG_SAMPLE_REF (cites published source of lithology), and PGG_GEOL_INT_REF (cites published source of lithology within drill holes).

HSU - This field represents the hydrostratigraphic unit as defined in Table 4-2 of Section 4.0. In most cases, the HSU was assigned using a database developed in support of the development of the EV® HFM (Dynamic Graphics, 2002). When data were not available for a particular well, the data were assigned using the EV® HFM.

RMC - This field represents the reactive mineral category as defined in Table 4-4 of Section 4.0.

RMU - This field represents the reactive mineral unit, which is a preliminary assignment of spatial units associated with various reactive mineral categories within select HSUs.

Sample type - This code translates into the type of sample analyzed by XRD (Table D.2-2). As described in Warren (2007), there are some limitations associated with various sample types. For instance, samples of cuttings are routinely collected within 10-ft intervals throughout a drill hole and have frequently lost fine matrix to provide a concentrate of hard components, typically lithic fragments and occasionally felsic phenocrysts from vitric rock**.** In addition, cuttings are almost always contaminated by generally soft rock caved from uphole that must be excluded from the analysis. Contamination is best eliminated by selection of fragments considered to represent the borehole wall (hand picking). Because hand picking is extremely laborious, especially when the diameter of fragments are less than 10 mm as is typical, LLNL routinely analyzed unprepared

cuttings. To minimize loss of fine matrix, LLNL collected large buckets of "whole cuttings," which were later dried without the standard practice of washing, better preserving the fine fraction. Cuttings collected in this way are termed "unwashed cuttings," as noted in the comments column. Due to their fine particle size, unwashed cuttings are not amenable to petrographic analysis, so contamination levels cannot be determined for individual samples of unwashed cuttings. Warren (2007) demonstrates that although unwashed cuttings are the most likely sample type to suffer contamination, the lowest percentage for glass in zeolitic rock is observed for these samples, indicating that contamination of unwashed cuttings is typically insignificant. Pawloski (1989) concluded that unwashed cuttings provide reliable averages for grain densities from a comparison with samples by percussion sidewall. However, as Pawloski (1989) noted, individual examples of cuttings that do not represent the borehole wall are well known

Table D.2-2
Description of Sample Type Codes

Sample Type Codes	Sample Type Description
C	Core
D	Drill cuttings
DA	Drill cuttings that represent petrographic character of interval
DB1	Drill cuttings enriched in hard components
DB3	Drill cuttings with combined characters of db1
HS	Hunt sidewall that represents petrographic character of interval
HSS	Particle size fraction separated from Hunt sidewall
O	Outcrop
PS	Percussion sidewall
SC	Sidewall core
T	Tunnel wall

With the exception of vitric alluvium of Frenchman Flat, which contains clasts that are invariably vapor phase altered (Warren et al., 2002), the presence of the vapor phase index mineral tridymite and glass together were not observed during petrographic analysis of several thousand samples in Warren et al. (2003). Given the unique association of tridymite and glass observed within several samples within the dataset, it seems likely that the glass represents fragments caved into the cuttings, which

were not entirely removed by hand picking. Samples obtained by ineffective handpicking are identified as such within the dataset and were not used for further analyses.

Before XRD analysis, mudcake from the borehole wall must be removed from sidewall samples. Analysis of two mudcake samples report 45 to 50 percent glass and 15 to 20 percent zeolite. Petrographic analyses, a method that is far more sensitive than XRD analyses for glass, demonstrate that minor relict glass does not commonly occur within zeolitic rocks of the SWNVF (Warren, 2007). An analysis of the zeolitic Hunt sidewall samples represented within the dataset shows a relatively large percentage of minor glass (26 percent) when compared to other sample types analyzed by XRD (0 to 12 percent) and to petrographic analyses (6.3 percent). This suggests that mudcake may contaminate samples of Hunt sidewall for XRD analyses (Warren, 2007).

Analysis Date - The split was reported as analyzed on this date. This date generally represents the date that reflection intensities were transformed into abundances, with the reflection intensities usually collected at an earlier date.

XRD_Meth - The methodology of XRD analysis has evolved during the span of 42 years when splits in this report were analyzed. Table D.2-3 lists methods encoded in the XRD Meth column that reflects increasing refinement of analyses**.** Semiquantitative analyses are often represented by values in non-numerical form, or in parts per 10. Quantitative estimates are typically presented for the reactive minerals zeolite and smectite when present in relatively high concentrations. At low concentrations, symbols typically proxied for analyte abundances, accompanied by a key to translate the symbols into numerical values. Symbols were translated only when a key was available. Table D.2-4 provides such a key used for a series of analyses performed at LLNL, along with the corresponding values reported in the XRD dataset. A slightly different set of symbols were employed during a later period at LLNL that referenced no key; these symbols have not been translated (see discussion in Warren, 2007) but are provided in the comments column. An attempt to translate the symbols used for these subsequent analyses substituted “very weak” XRD intensities with less than 5 and “very very weak” treated the same as “trace” (Table D.2-4). However, attempts to employ such a translation invariably provide totals for all analytes far below 100 percent, typically 60 to 70 percent, demonstrating that the analyses cannot be reduced to trustworthy numerical values for the minerals present at relatively low levels. Because quantifying the amount of clays (particularly

smectite) and zeolite was often the goal of the XRD analyses, these minerals were often estimated numerically for semiquantitative analyses; other minerals were simply reported using symbols such as those reported in Table D.2-4.

Table D.2-3
Methods of XRD Analysis for Splits from the SWNVF

Code	Type	Description	Reference
S	Semiquantitative		
E	Quantitative	External standard	Pawloski, 1983
I	Quantitative	Internal standard	Bish and Chipera, 1989
F	Quantitative	Full pattern fitting	Chipera and Bish, 2002

Note: Analytical totals are a valid test of analytical quality only for methods I and F because totals are normalized to 100% for method E.

Table D.2-4
Translation of Symbols Used During the Early 1970s by LLNL To Represent Semiquantitative XRD Analyses

Term	Symbol	Definition	Database Value
Strong	S	>50	75 ± 25
Moderate	M	10-50	30 ± 20
Weak	W	<10	5 ± 5
Trace	Tr or T	~1	0.5 ± 0.5
	----	Not observed	0

Note: All values are weight percent.

Analytical sensitivity is lowest for the external standard method (Pawloski, 1983), resulting in a very low percentage of splits detecting kaolinite, and none in which analcime or tridymite were reported (Warren, 2007). A detection limit as high as 40 percent is reported for glass using this method.

Comments - Comments amplify information from an XRD analysis and provide additional information not otherwise represented in the database. Three types of comments are of particular value:

1. Description of clay mineralogy such as interlayering between smectite and illite and polymorphism between kaolinite and halloysite

2. Terms describing reflection intensities when numerical values are not provided

3. Definition of unusual minerals

Qualifier Code - Code assigned to a specific sample split. A code of R is primarily used in this field and designates that the sample should be rejected and not included in further analyses.

Qualifier - Qualifiers are used to provide supporting information associated with the qualifier code.

Remarks - This field contains text describing possible anomalies within the dataset. This field is used to describe sample splits that were collected near an HSU contact or had an unusually high abundance of a particular mineral. Many of these sample splits were included in the analyses because they often represent the high variability of the minerals within an HSU or RMC.

Analyst Code - This code represents the analyst that performed the XRD analysis. Each XRD analyst applied individual criteria for analyses, resulting in different assignments and different nomenclature for some minerals (Warren, 2007). Reconciling these assignments is described for the individual minerals below.

ZE - This code represents the mineral group zeolite. Most zeolite within the SWNVF is clinoptilolite, but mordenite and analcime are prevalent. From inception of work for Yucca Mountain during the late 1970s, LANL XRD analysts have reported values for all three zeolites (Waters et al., 1981), emphasizing their individual associations with depth and alteration intensity (Broxton et al., 1987). The USGS reported zeolite almost entirely as clinoptilolite, rarely reporting mordenite or analcime, so USGS analyses represented as clinoptilolite should be assumed to represent clinoptilolite plus mordenite. Until the latest reports in 1991, LLNL reported zeolite entirely as clinoptilolite, neglecting mordenite, which occurs in one-third of the splits analyzed by LANL. Therefore, analysis for clinoptilolite by LLNL has been properly translated to represent total zeolite, including clinoptilolite, mordenite, and analcime. Because of the inconsistent assignments of the zeolite minerals, only total zeolite is reported within the dataset. More detailed presentation of specific zeolite minerals, as stated above, are provided within the PGG database or within Warren (2007).

It is worth noting that mineral abundances are typically reported only for minerals observed above the minimum detection limit; therefore, it is not always clear whether a null value in the dataset indicates a mineral that was analyzed for but not detected, or the mineral was simply not analyzed. Because

historical analyses often focused on the reactive minerals, zeolite and smectite, null values can be assumed to indicate zeolite was analyzed for but was not detected, or was detected but was reported using a symbol as described earlier for the semiquantitative analyses. The exception to this assumption is for those splits for which only smectite was analyzed.

SM - This code represents the mineral smectite. A high percentage of argillic and highly argillic XRD splits is expected for Area 8 of the NTS, where the BANEBERRY test was located in drill hole U8D. Post-test drilling demonstrated that intense argillic alteration was a primary cause for the prompt release of radiation following the test (USGS, 1974), and thereafter determination of clay mineral abundance by XRD analysis became routine. A summary of the percentage of splits with high smectite abundances within each of the NTS areas of the Yucca Flat/Climax Mine CAU is presented in Table D.2-5. Area 6 shows a similar percentage of argillic and highly argillic XRD splits for a relatively small dataset, but differs from Area 8 by including very few splits with argillic minor alteration. The high argillic content is associated with playa deposits in the extreme southern Yucca Flat. Areas 2, 4, and 20 show the lowest percentages of argillic splits, each showing about 20 percent of the XRD splits to contain at least 10 percent smectite.

Table D.2-5
Percentages of XRD Splits Within NTS Areas in Yucca Flat that Contain Moderate to High Abundances of Clay Minerals

Area	n	High AR	AR	mAR
2	619	0.3	8.2	15
3	199	5.5	15	14
4	274	0.7	8.8	18
6	70	10	23	1.4
7	438	0.2	9.1	26
8	335	9.3	30	21
9	240	0.4	10	27
10	148	0.0	25	29
12	14	8	8	8

AR - Argillic (>20% smectite plus mica/illite).
High AR - Highly argillic (>45% smectite).
mAR - Minor argillic (10-20% smectite plus mica/illite).
n - The number of splits analyzed by XRD within each area.

CC - This code represents calcite. Note that in some cases, only total carbonate was reported; these values were assigned to calcite.

DM - This code represents dolomite.

MI - This code represents the mineral group mica. Individual micas can be distinguished by XRD analysis and were reported separately for muscovite, biotite, and illite by LLNL (Pawloski, 1983). Recent analyses by LANL report mica mostly or entirely as biotite, sharply higher compared to petrographic analyses for biotite. The recent XRD results require that secondary mica within groundmass of zeolitic rock occur mostly or entirely as biotite, which is inconsistent with its optical character unless the secondary mica were highly iron-poor. Considering their apparent discrepancy with petrographic analyses, recent XRD values for biotite are included specifically for biotite only in the comments column. These values for biotite are included within the value for mica/illite. Because of the inconsistencies in determining individual micas (biotite, illite, and muscovite), only total mica is reported within the dataset. More detailed presentation of mica minerals, as stated above, are provided within the PGG database or within Warren (2007).

HM - This code represents the mineral hematite and hydrated iron oxides such as goethite.

GL - This code represents glass. Some XRD analyses report amorphous rather than glass, as noted in the comments column within the dataset. Two entirely amorphous phases, glass and opal-A, are known to occur within the SWNVF. Glass is widespread, identified optically by petrographic analyses and chemically by microprobe analysis for countless splits (Warren et al., 2003), but opal-A is uncommon, presently identified by petrographic analysis only within a single sample within the PGG database (Warren, 2007). Due to the known rarity of opal-A, most XRD analysts assume that the broad reflection from amorphous material is due entirely to glass, a convention followed during this compilation process.

In some cases, petrographic analyses are available to identify amorphous material as opal-A for some XRD splits. However, petrographic analyses accompany very few XRD splits from Yucca Flat. Some XRD splits reveal amorphous material within a mineral assemblage that suggests severe alteration, and may well contain opal-A, erroneously assigned as glass. Examples of such splits are sample U7BD-1385S and those deeper within U7BD.

OP - This code represents the mineral opal. For this dataset, and the PGG database, opal-CT and opal-A are combined, but individual amounts are provided in the comments column.

CR - This code represents the mineral cristobalite. Most opal within the SWNVF has short-range ordering of cristobalite, and so although amorphous, it exhibits weak and diffuse reflections with angles identical to cristobalite. Until the recent application of the full pattern fitting method, reflections for cristobalite were analyzed either as opal-CT or as cristobalite (Warren, 2007). In some cases, XRD results were reported as "cristobalite-opaline silica," which has been arbitrarily translated as opal-CT. During compilation, a choice between phases was followed, almost always made as cristobalite. The most recent XRD analyses indicate that both phases are prevalent and frequently occur together, so earlier "one or the other" analyses for opal-CT and cristobalite should be used with caution.

TR - This code represents the mineral tridymite. Tridymite, found only in devitrified rocks, has only been reported by one analyst (Warren, 2007).

QZ - This code represents the mineral quartz.

HN - This code represents the mineral hornblende. Individual amphiboles can be distinguished by XRD analysis, but their abundances within the SWNVF are typically far too low to accomplish this. Furthermore, only a single petrographic analysis among several thousands reveals an amphibole other than hornblende in amounts detectable by XRD (Warren, 2007). Both actinolite and anthophyllite occur within four petrographic splits, with a maximum abundance of 0.02 percent for anthophyllite. Based on the rarity of amphiboles other than hornblende within the SWNVF, all amphibole is assumed to represent hornblende within the PGG database and for this dataset; no other amphibole was specifically reported.

FS - This code represents the total of the felsic minerals. The daughters of feldspar, alkali feldspar (KF) and plagioclase (PL), are analyzed only in a few cases (Warren, 2007). The daughters of the individual feldspars from XRD analyses are adularia (AA), sanidine (SD), and orthoclase (OR) for KF; and albite (AB), bytownite (BY), and anorthite (AN) for PL. More detailed presentation of the feldspar minerals, as stated above, are provided within the PGG database or within Warren (2007).

KA - This code represents the mineral kaolinite.

CH - This code represents the mineral chlorite.

MT - This code represents the mineral magnetite.

PY - This code represents the mineral pyrite.

O1 - This code indicates other minerals that are either uncommon or unspecified in the XRD results. Comments associated with values reported within this field are reported in the comments field.

WW - This code represents the total of all mineral abundances.

Total - This field contains the summed total of the abundances of all minerals reported for the particular split. These totals are a valid test of analytical quality only for methods I and F because totals are normalized to 100 percent for method E, and abundances estimated using method S often do not incorporate the non-reactive minerals.

Note: An additional set of 10 minerals and mineral constituents were analyzed for in a number of splits within Yucca Flat, but were uniformly undetectable and therefore were not included in the dataset. These minerals are clinopyroxene (CX), ilmenite (IL), olivine (OL), pyroxene (PX), anorthite content of plagioclase (AN), apatite (AP), fluorite (FL), gypsum (GY), halite (HL), and garnet (GT).

D.3.0 HISTOGRAMS OF REACTIVE MINERALS FOR HYDROSTRATIGRAPHIC UNITS

Histograms of the five reactive minerals used for calculating matrix distribution coefficients are presented in Figures D.4-1 through D.4-5. The reactive minerals are presented for each of the HSUs and specific areas within HSUs as presented in Section 4.0 and summarized in Table 4-6. These include the AA (typical and altered), PCU, IDP, TM-UVTA, TM-WTA (typical and altered), TM-LVTA (typical and argillic), UTCU, TSA (typical and zeolitic), TUBA, LTCU, OSBCU (total, zeolitic, and ash-flow tuffs), ATCU, MGCU, UCCU (Eleana Formation and Chainman Shale), and LCA HSUs.

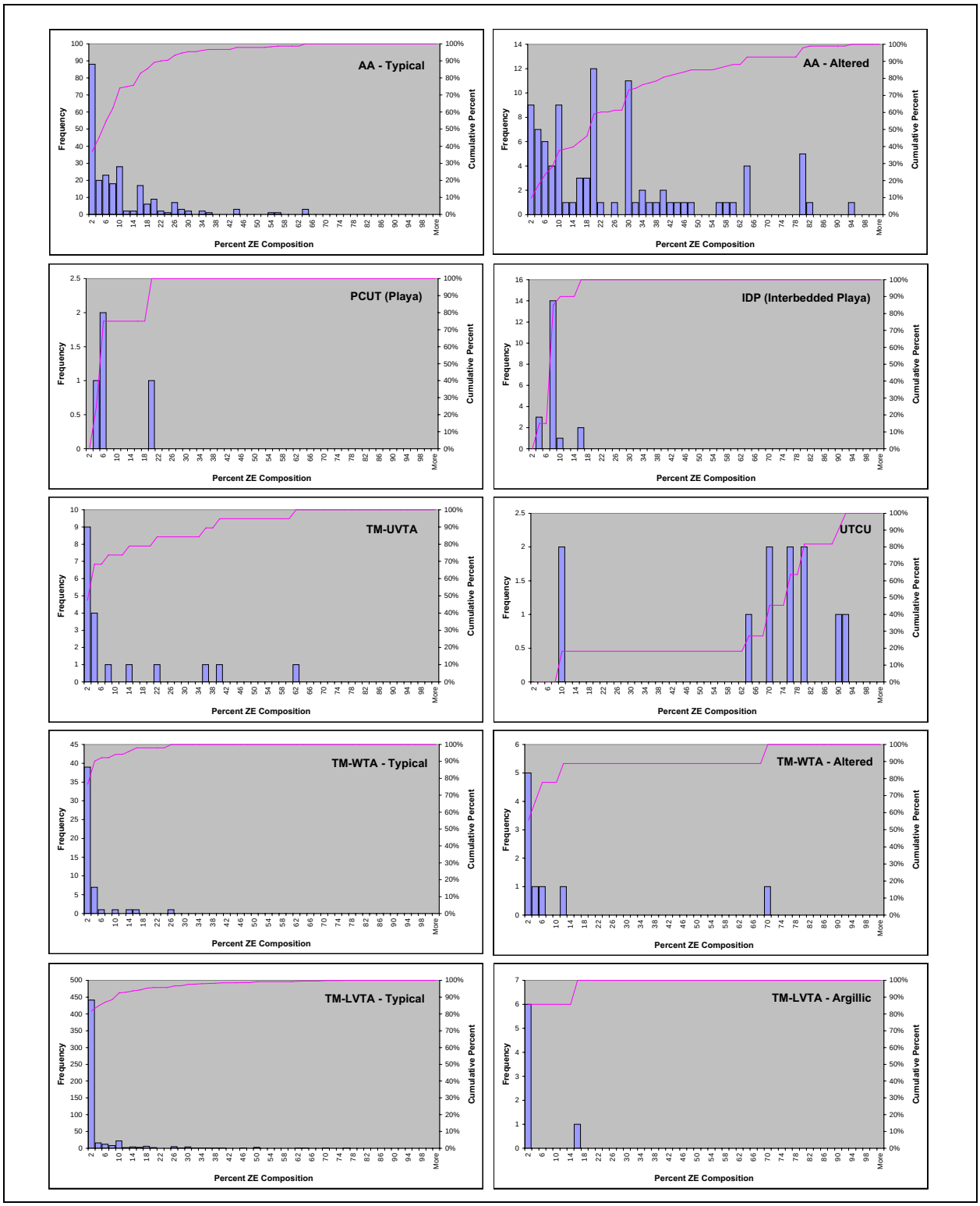

Figure D.4-1
Histograms and Percent Cumulative Probability Distributions for Zeolite Abundances in Yucca Flat/Climax Mine HSUs (Part 1 of 3)

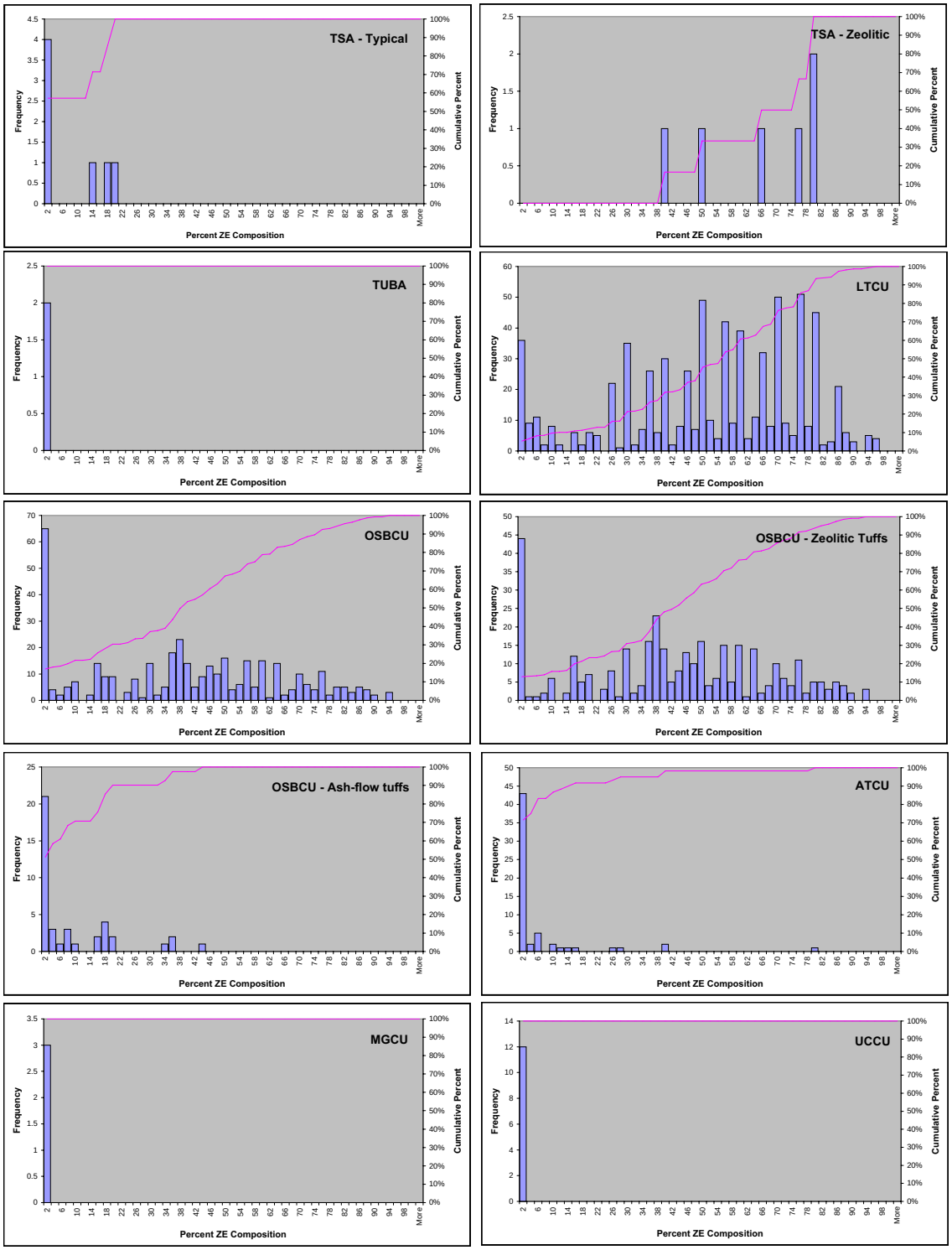

Figure D.4-1
Histograms and Percent Cumulative Probability Distributions for Zeolite Abundances in Yucca Flat/Climax Mine HSUs (Part 2 of 3)

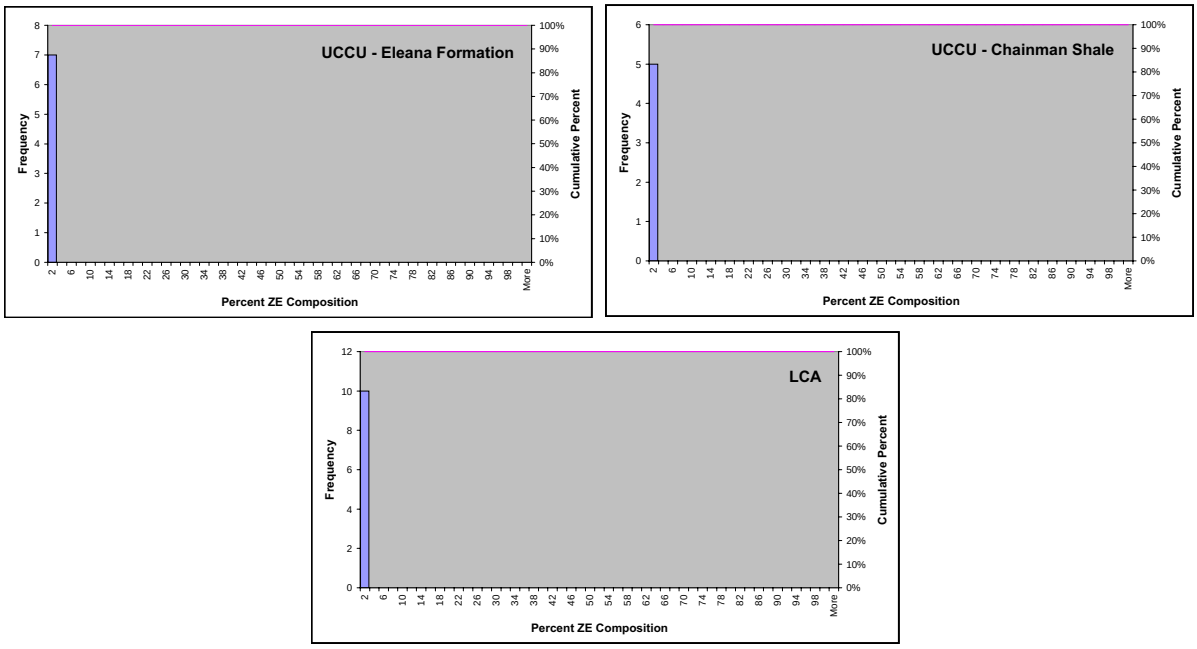

Figure D.4-1
Histograms and Percent Cumulative Probability Distributions for Zeolite Abundances in Yucca Flat/Climax Mine HSUs (Part 3 of 3)

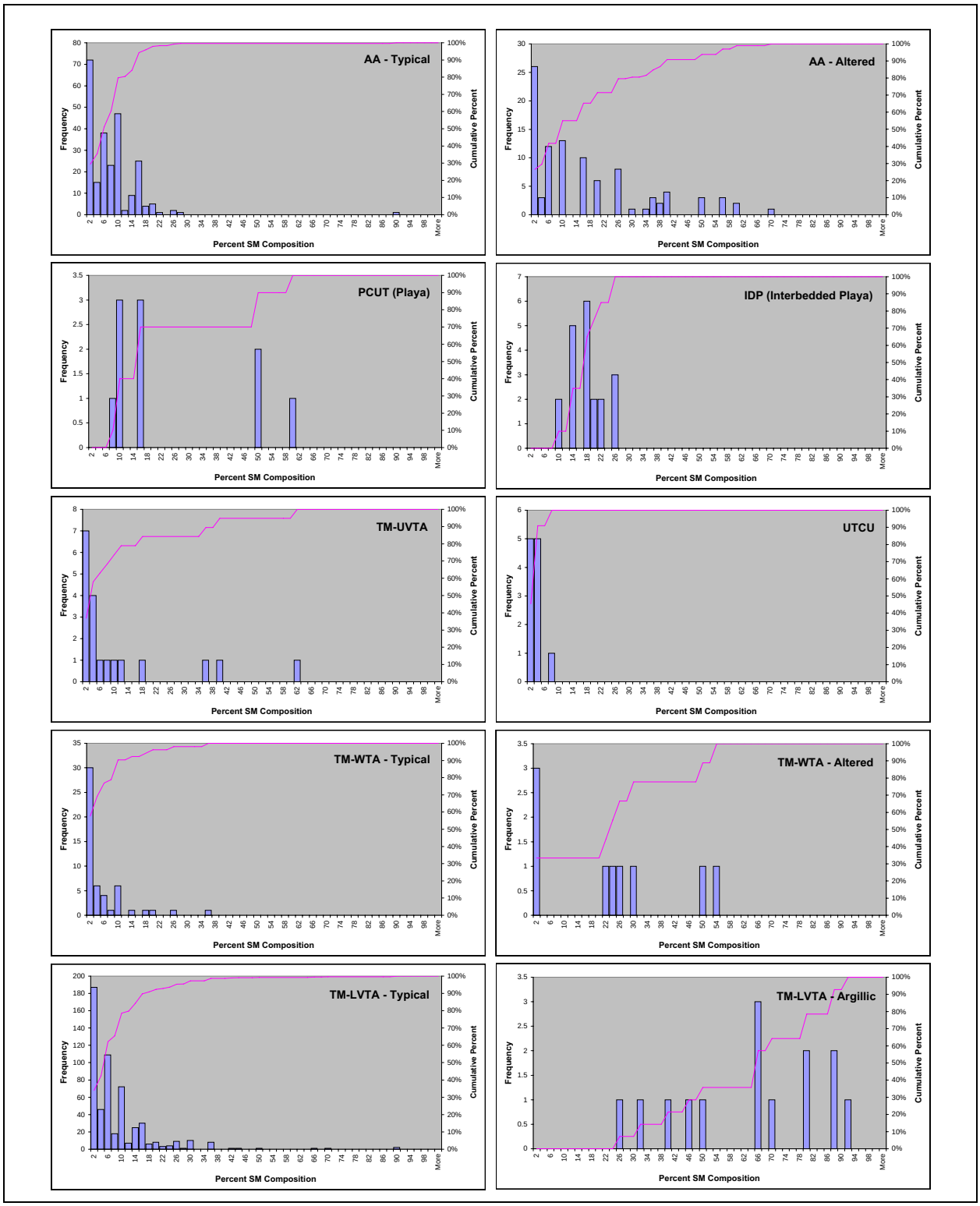

Figure D.4-2
Histograms and Percent Cumulative Probability Distributions for Smectite Abundances in Yucca Flat/Climax Mine HSUs (Part 1 of 3)

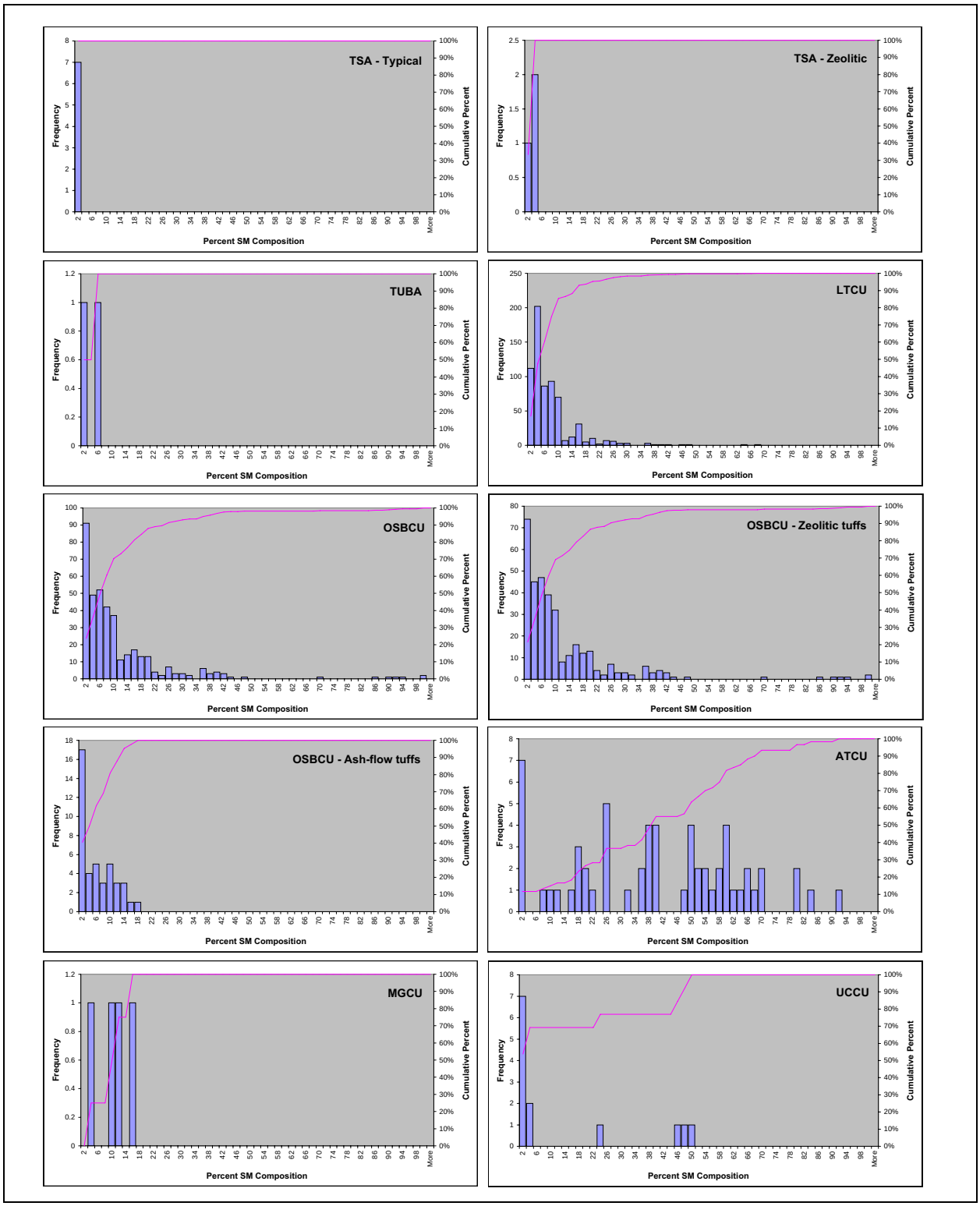

Figure D.4-2
Histograms and Percent Cumulative Probability Distributions for Smectite Abundances in Yucca Flat/Climax Mine HSUs (Part 2 of 3)

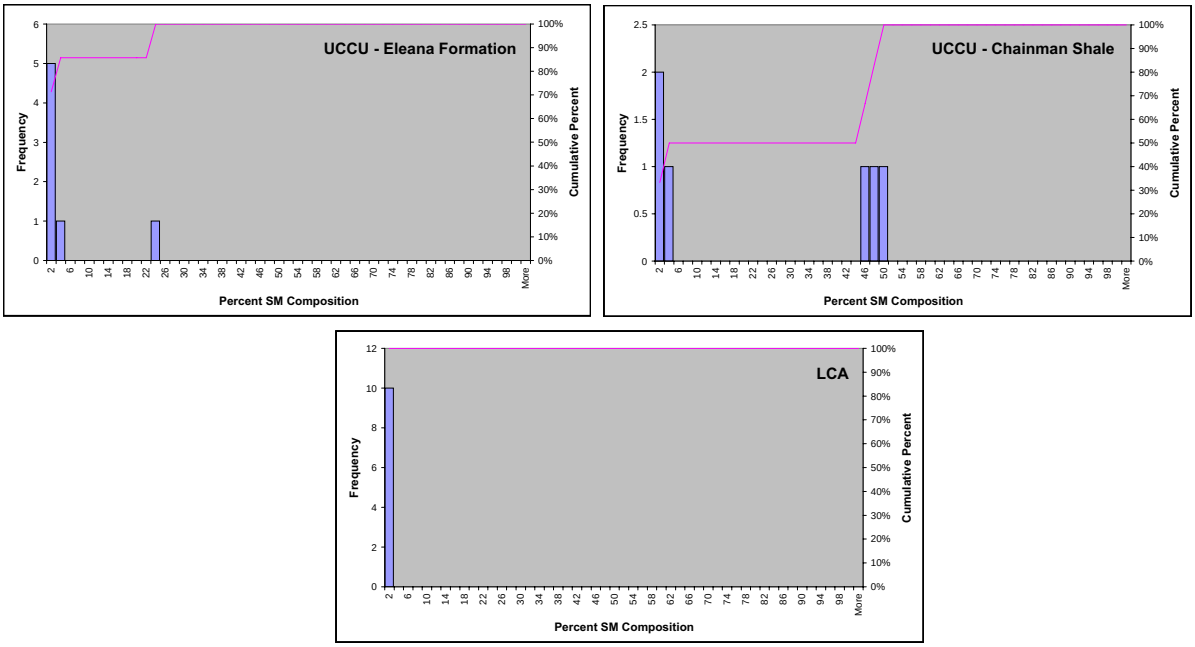

Figure D.4-2
Histograms and Percent Cumulative Probability Distributions for Smectite Abundances in Yucca Flat/Climax Mine HSUs (Part 3 of 3)

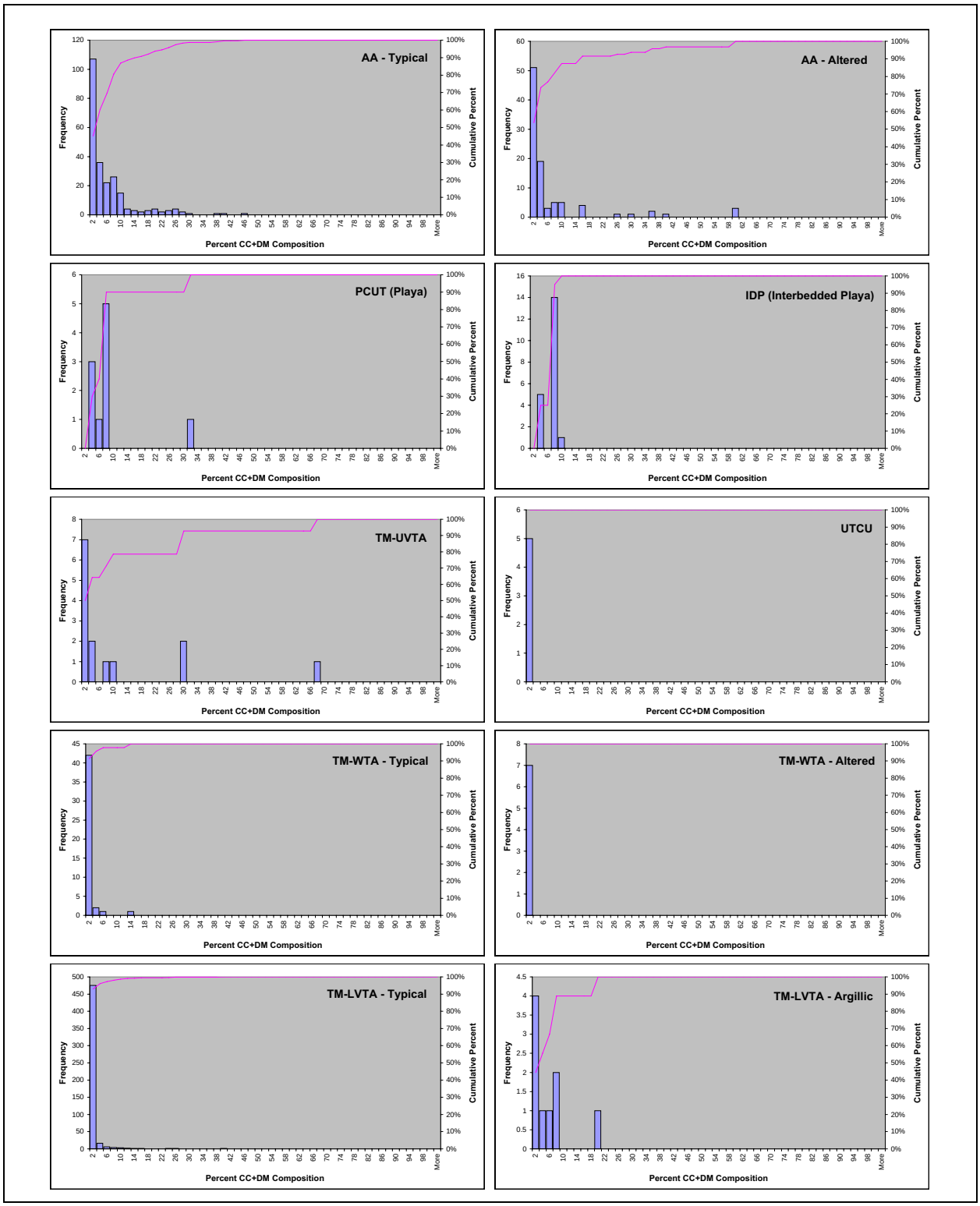

Figure D.4-3
Histograms and Percent Cumulative Probability Distributions for Carbonate (Calcite plus Dolomite) Abundances in Yucca Flat/Climax Mine HSUs (Part 1 of 3)

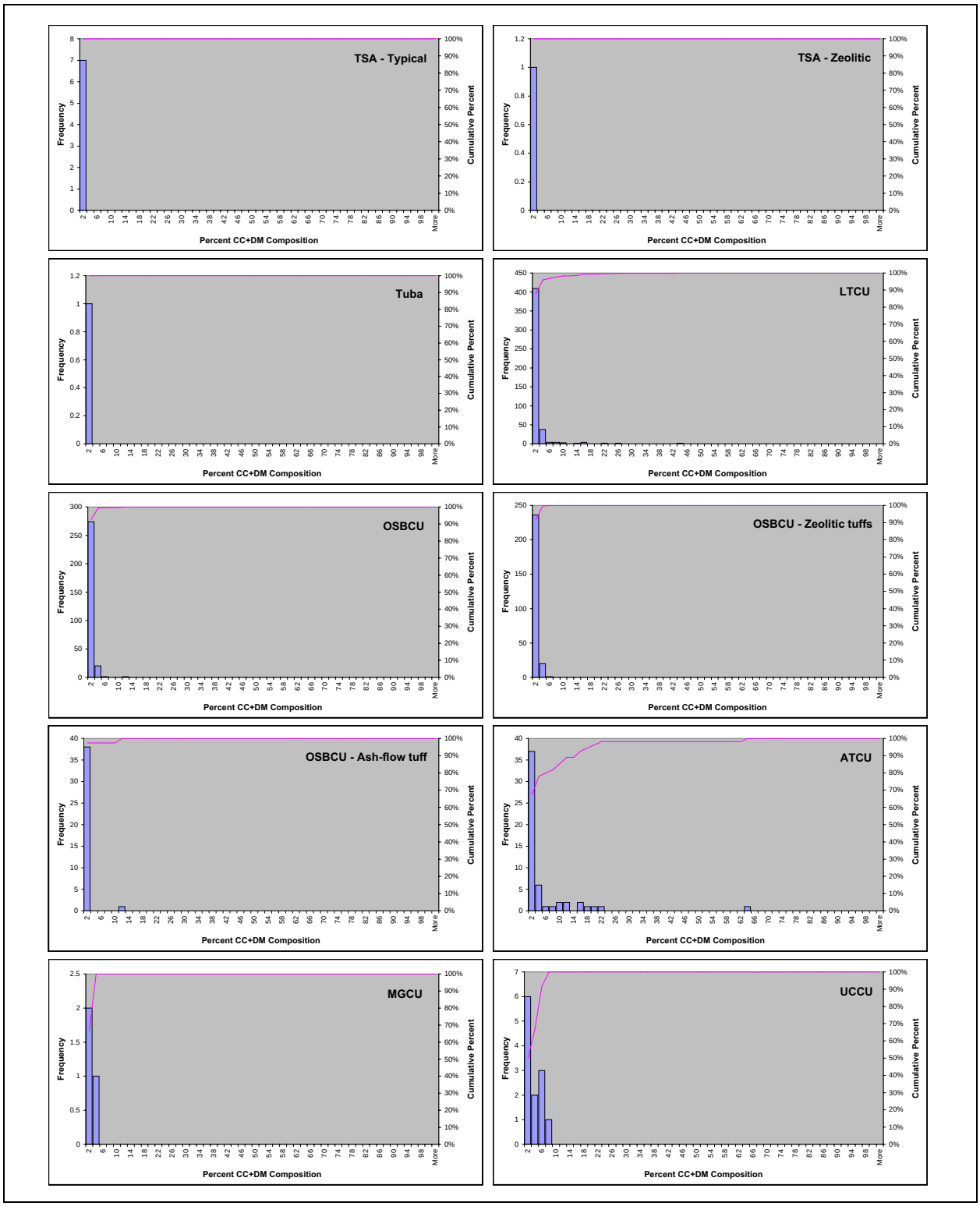

Figure D.4-3
Histograms and Percent Cumulative Probability Distributions for Carbonate (Calcite plus Dolomite) Abundances in Yucca Flat/Climax Mine HSUs (Part 2 of 3)

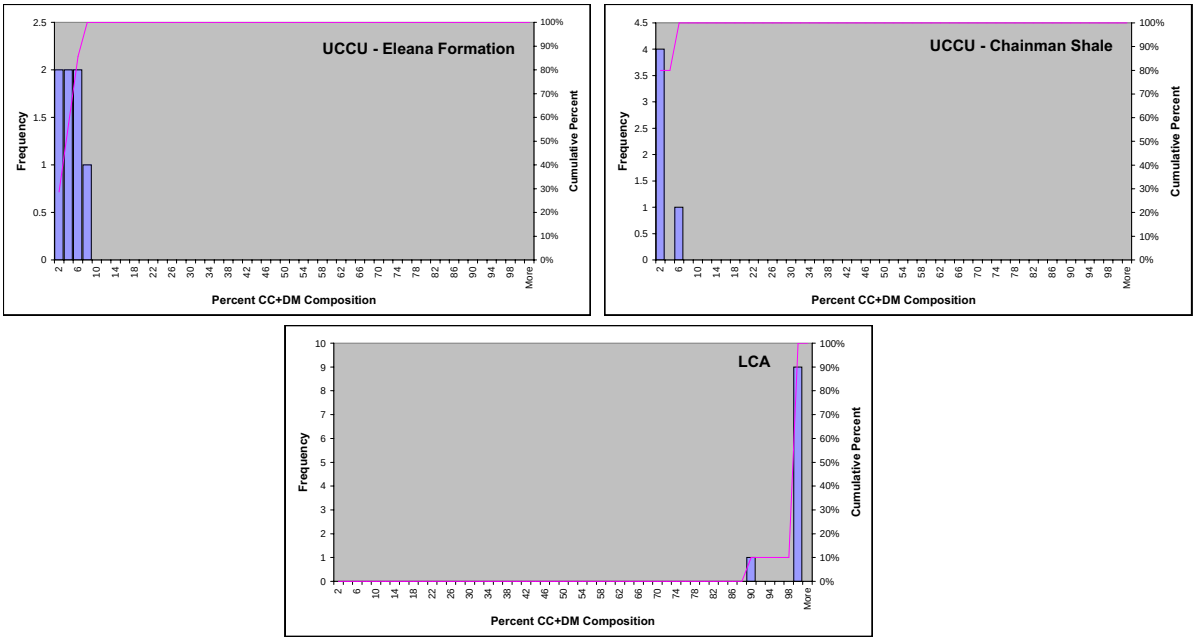

Figure D.4-3
Histograms and Percent Cumulative Probability Distributions for Carbonate (Calcite plus Dolomite) Abundances in Yucca Flat/Climax Mine HSUs (Part 3 of 3)

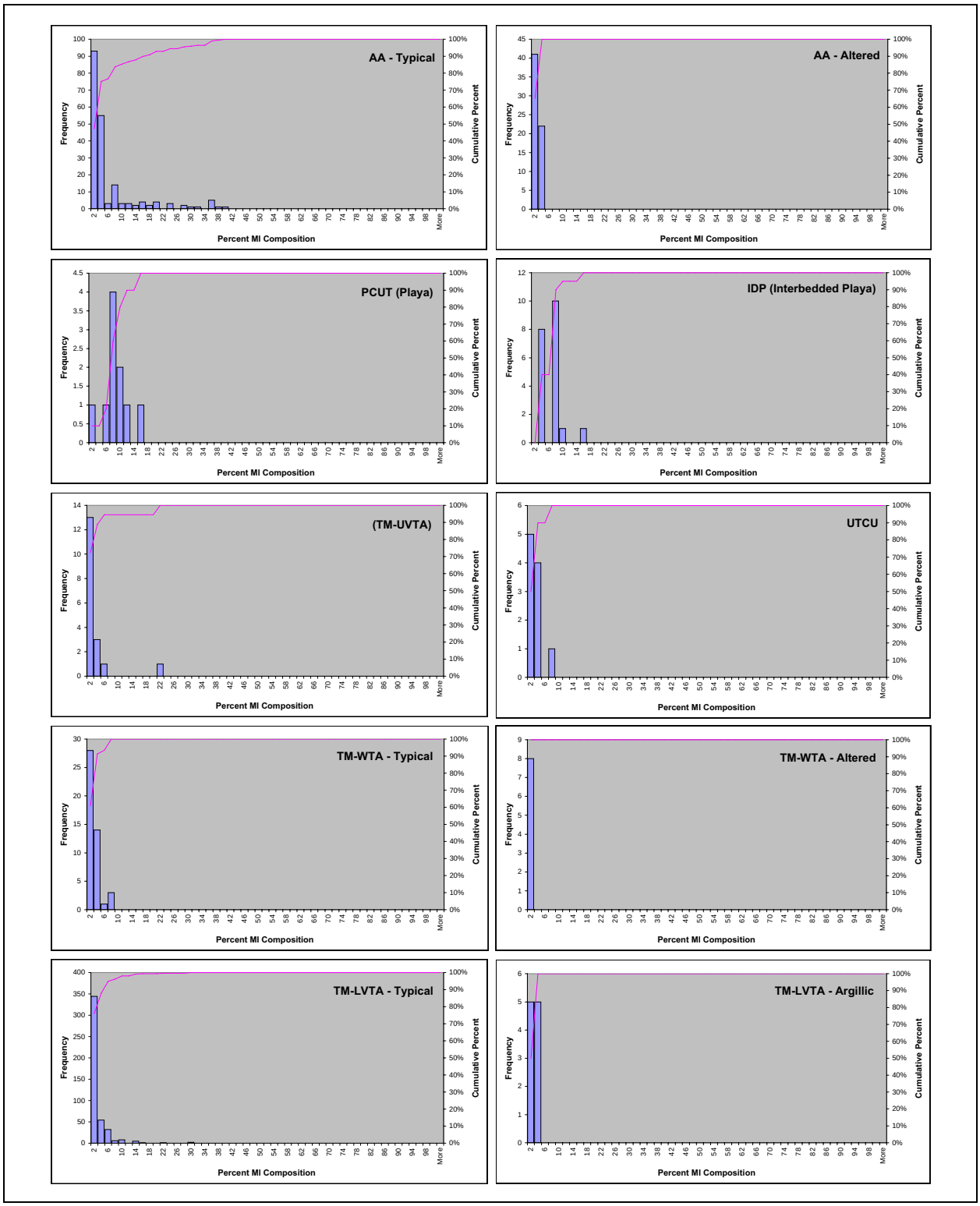

Figure D.4-4
Histograms and Percent Cumulative Probability Distributions for Mica Abundances in Yucca Flat/Climax Mine HSUs (Part 1 of 3)

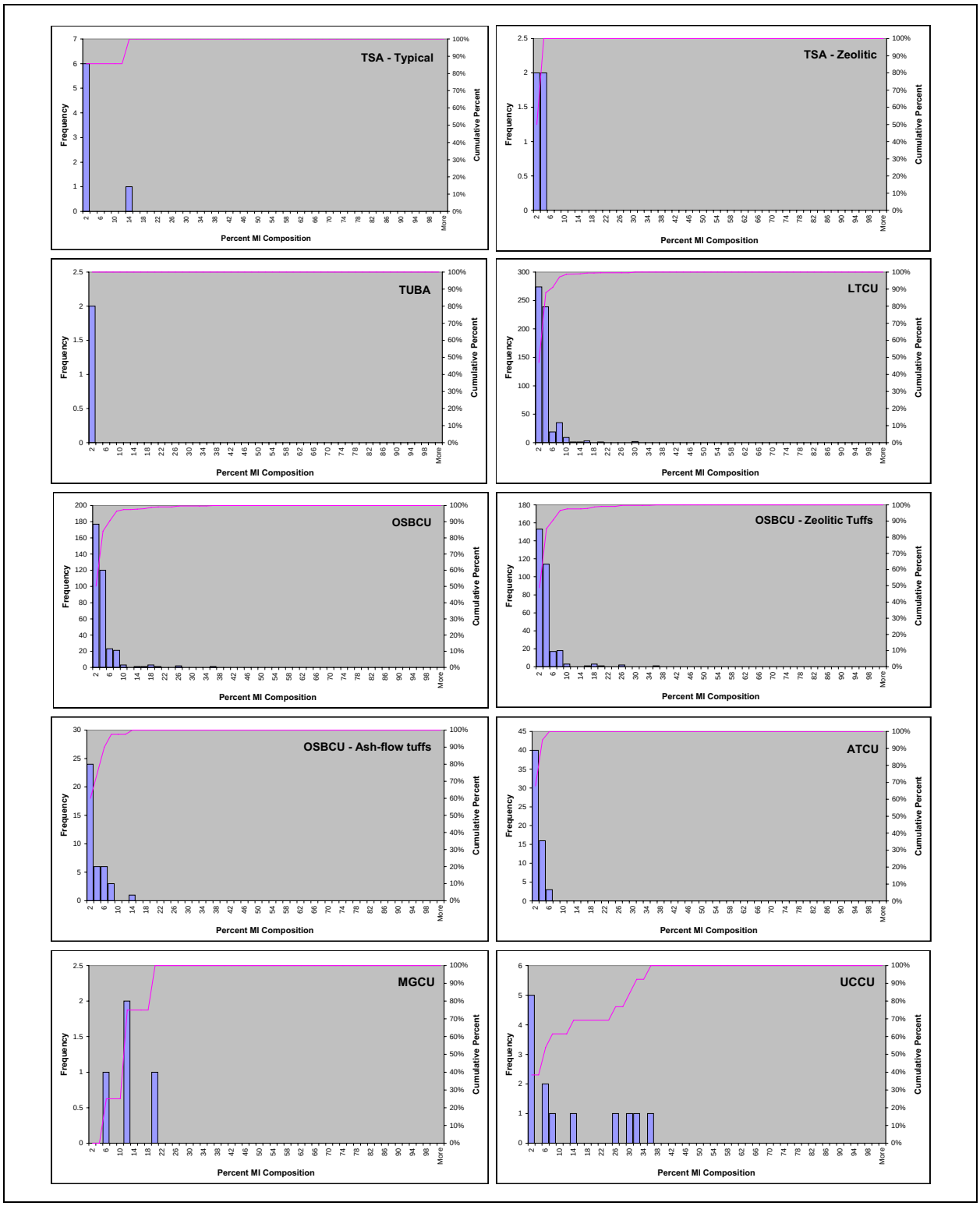

Figure D.4-4
Histograms and Percent Cumulative Probability Distributions for Mica Abundances in Yucca Flat/Climax Mine HSUs (Part 2 of 3)

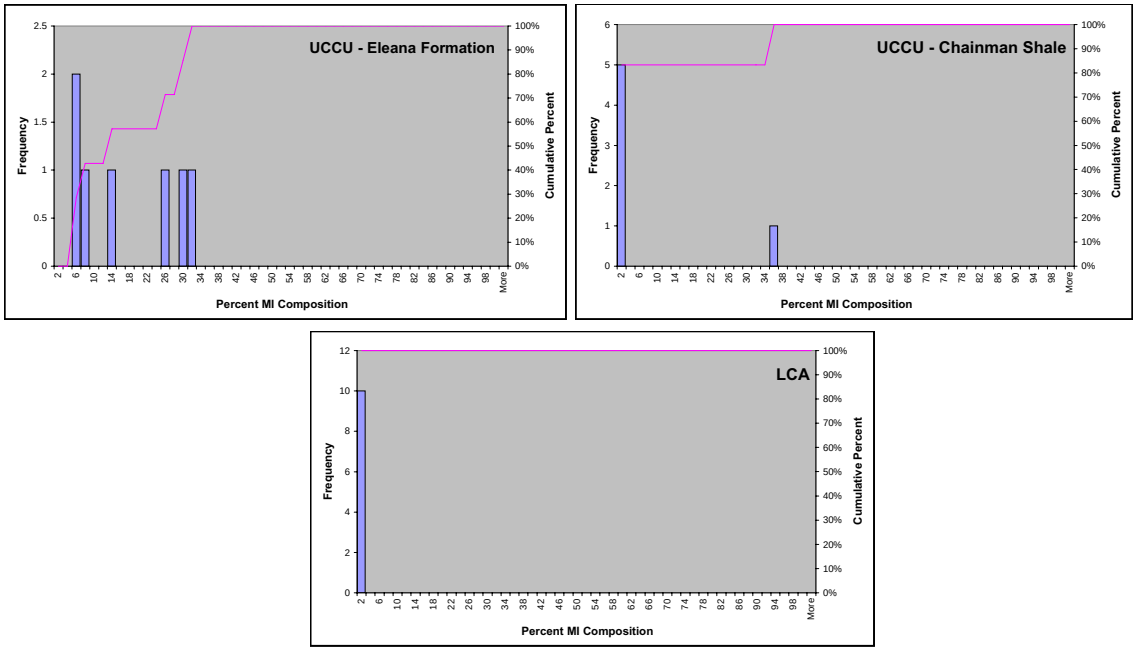

Figure D.4-4
Histograms and Percent Cumulative Probability Distributions for Mica Abundances in Yucca Flat/Climax Mine HSUs (Part 3 of 3)

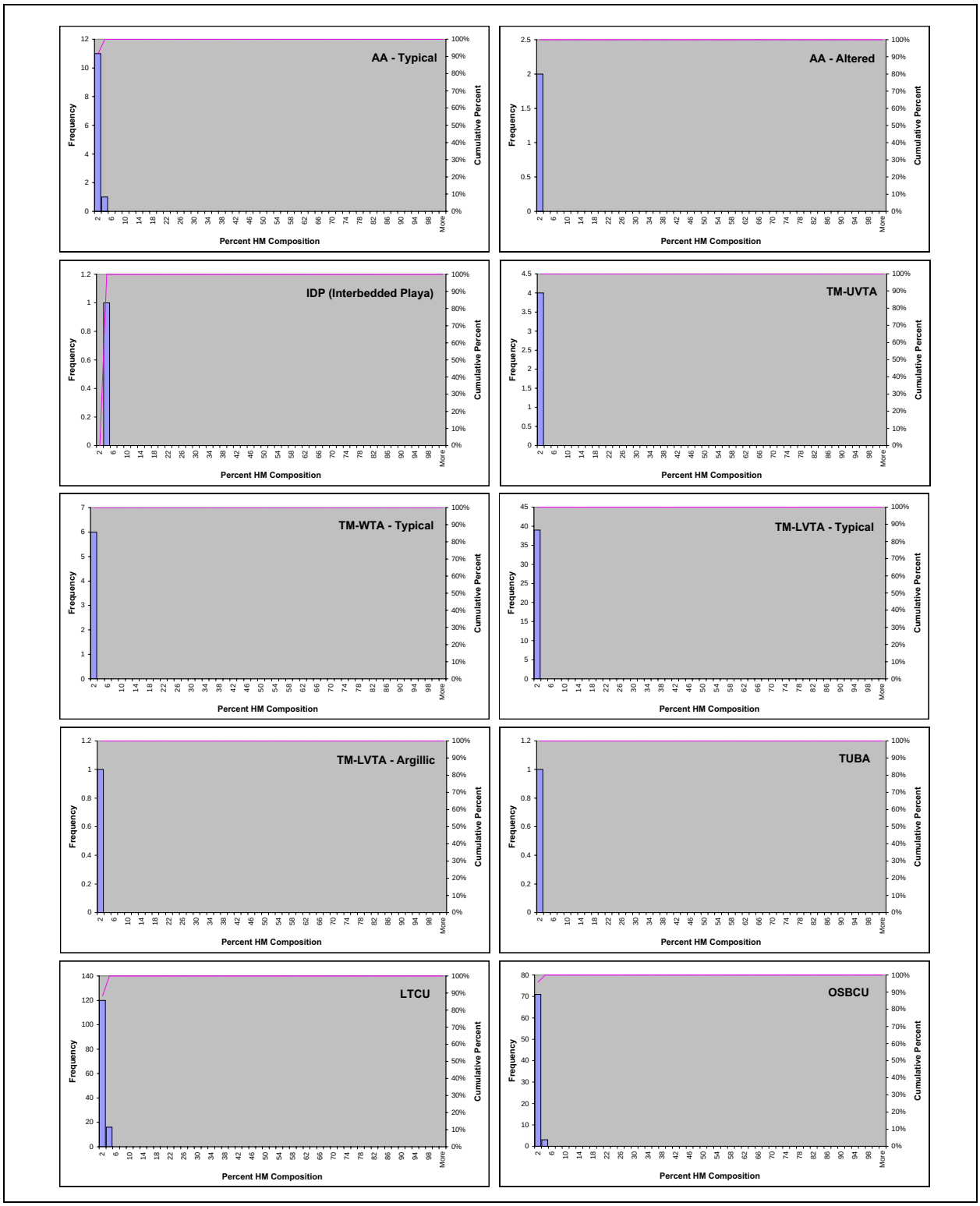

Figure D.4-5
Histograms and Percent Cumulative Probability Distributions for Hematite Abundances in Yucca Flat/Climax Mine HSUs (Part 1 of 2)

Note: No data for hematite are available for PCUT, UTCU, TM-WTA (altered), TSA, TSA (zeolitic), and LCA HSUs.

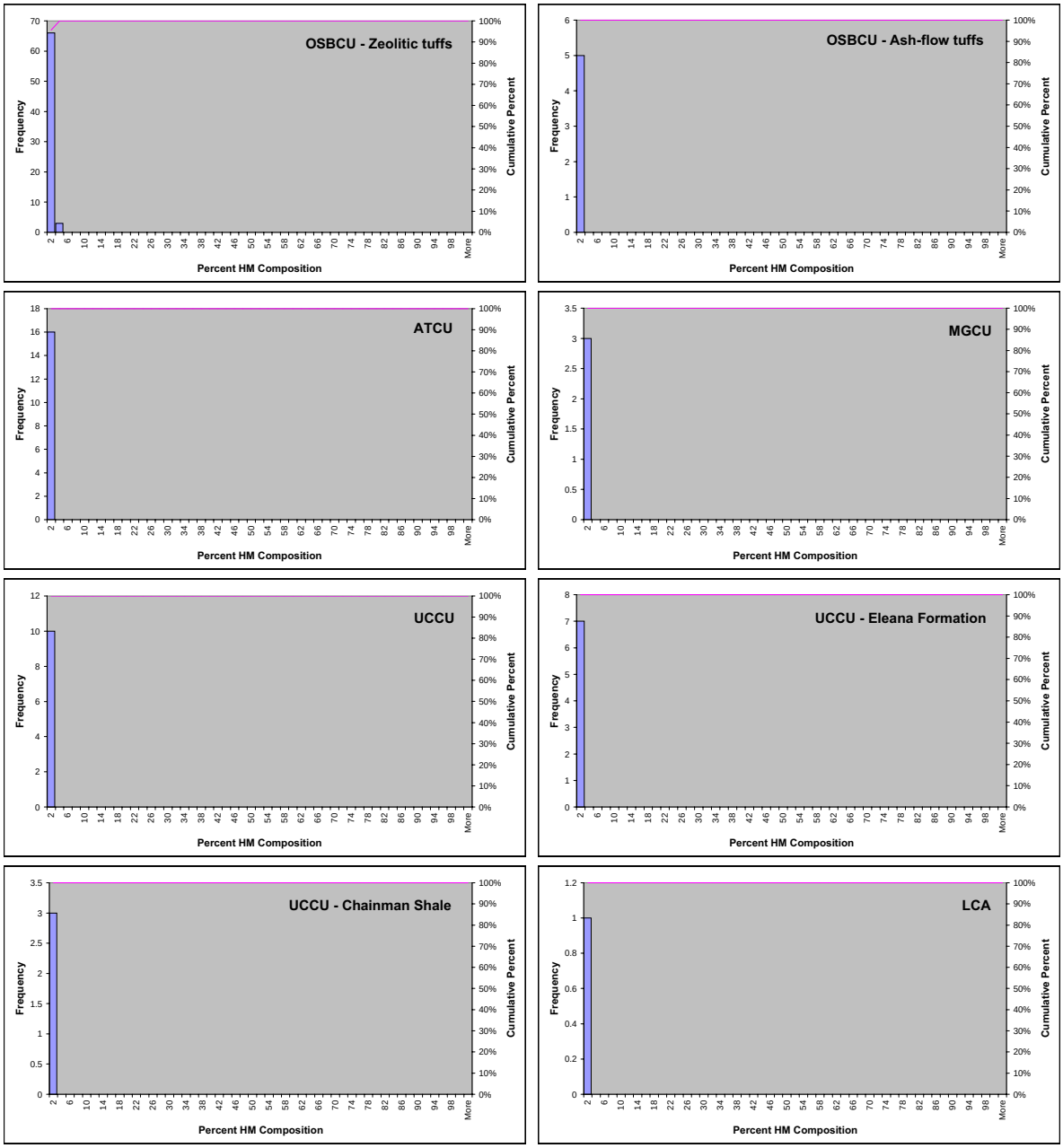

Figure D.4-5
Histograms and Percent Cumulative Probability Distributions for Hematite Abundances in Yucca Flat/Climax Mine HSUs (Part 2 of 2)

Note: No data for hematite are available for PCUT, UTCU, TM-WTA (altered), TSA, TSA (zeolitic), and LCA HSUs.

D.4.0 ACCESS TO DATASET

The full XRD mineralogy dataset is provided in an Excel spreadsheet (YF_CM_XRD_Dataset.xls) on the compact disc-read-only memory (CD-ROM) accompanying this report.

D.5.0 REFERENCES

Bish, D.L., and S.J. Chipera. 1989. *Revised Mineralogic Summary of Yucca Mountain, Nevada*, LA-11497-MS, 68 pp. March. Los Alamos National Laboratory Report. Los Alamos, NM.

Broxton, D.E., D.L. Bish, and R.G. Warren. 1987. "Distribution and chemistry of diagenetic minerals at Yucca Mountain, Nye County, Nevada." In *Clays and Clay Minerals*, Vol. 35, No. 2, p. 89-110.

Chipera, S.J., and D.L. Bish. 2002. *FULLPAT: A Full-Pattern Quantitative Analysis Program for X-ray Powder Diffraction Using Measured and Calculated Patterns*, J. Appl. Cryst., Vol. 35, p. 744-749.

Dynamic Graphics, see Dynamic Graphics, Inc.

Dynamic Graphics, Inc. 2002. *EarthVision 7: Software for 3-D Modeling and Visualization*. Alameda, CA.

Pawloski, G.A. 1983. "Quantitative Determination of Minerals in Nevada Test Site Samples by X-ray Diffraction." In *Proceedings of the Second Symposium on Containment of Underground Nuclear Explosions*, CONF-830882, Vol. 1, p. 75-96. Lawrence Livermore National Laboratory.

Pawloski, G.A. 1989. "A Statistical Analysis of Grain Density Measurements from Cuttings and Percussion Gun Samples." In *5th Symposium on Containment of Underground Nuclear Explosions*, CONF-8909163-Vol. 2, p. 372-384. September. Lawrence Livermore National Laboratory.

Prothro, L.B. 2005. *Mineralogic Zonation Within the Tuff Confining Unit, Yucca Flat, Nevada Test Site*, DOE/NV/11718--995. Las Vegas, NV: Bechtel Nevada.

Schroeder, M.L., and W.P. Williams. 1962. *Chemical, Spectrographic, and X-ray Data from Rock Samples from Drill Hole Ue4a, Nevada Test Site*, U.S. Geological Survey Technical Letter: Yucca-2, Supplement 5, 17 pp. 29 January.

USGS, see U.S. Geological Survey.

U.S. Geological Survey. 1974. *Results of Exploration of Baneberry Site, Early 1971*, U.S. Geological Survey NTS-235 (USGS-474-145), 94 pp. July.

Warren, R.G. 2005. *Field Trip to Nevada Test Site 17 March 2004, Los Alamos National Laboratory, New Mexico*, LA-UR-05-2439. Los Alamos National Laboratory Unlimited Release. Los Alamos, NM.

Warren, R.G. 2007. Written communication. Subject: *A Compilation of X-ray Diffraction Analyses and Formal Definitions for Alteration within the Southwestern Nevada Volcanic Field.* Comprehensive Volcanic Petrographics, LLC.

Warren, R.G., F.C. Benedict, T.P. Rose, D.K. Smith, S.J. Chipera, E.C. Kluk, and K.M. Raven. 2002. *Alluvial Layering and Distribution of Reactive Phases within Drill Holes ER5/4 and UE5N of Frenchman Flat*, LA-UR-02-6206, 86 pp. September. Los Alamos National Laboratory Unlimited Release. Los Alamos, NM.

Warren, R.G., D.A. Sawyer, F.M. Byers, Jr., and G.L. Cole. 2003. *A Petrographic, Geochemical, and Geophysical Database and Stratigraphic Framework for the Southwestern Nevada Volcanic Field*, LA-UR-03-1503, 54 pp. March. Los Alamos National Laboratory Unlimited Release. Los Alamos, NM.

Waters, A.C., P.R. Carroll, D.L. Bish, F.A. Caporuscio, J.F. Copp, B.M. Crowe, J.D. Purson, J.R. Smyth, and R.G. Warren. 1981. *Preliminary Stratigraphic and Petrologic Characterization of Core Samples from USW-G1, Yucca Mountain, Nevada*, LA-8840-MS, 66 pp. November. Los Alamos National Laboratory Report. Los Alamos, NM.

WoldeGabriel, G., S.J. Chipera, G.N. Keating, E.C. Kluk, S.S. Levy, and M.G. Snow. 2004. *Geological Characterization of Wells ER 2-1, ER 6-1#2, ER 7-1, ER 8-1, and ER 12-2, Nevada Test Site*, LA-UR-04-1831. Los Alamos National Laboratory Unlimited Release. Los Alamos, NM.

Appendix E

Description of Geochemistry Dataset

E.1.0 INTRODUCTION

The GEOCHEM06.mdb database (SNJV, 2006) contains data for a wide variety of geochemical parameters for groundwater of the NTS and the vicinity. The datasets included in this appendix contain a subset of parameters for groundwaters of wells and springs within the Yucca Flat/Climax Mine HFM boundaries compiled from this database. The goal of the data compilation was to acquire a dataset that contains representative major (Ca^{2+}, Na^{+}, Mg^{2+}, K^{+}, Cl^{-}, SO_4^{2-}, HCO_3^{-}, and SiO_2) and minor (CO_3^{2-}, NO_3^{-}, Br^{-}, PO_4^{3-}, and F^{-}) solute data for groundwaters of the HSUs of the Yucca Flat/Climax Mine HSUs. Also of interest are the results of ORP, pH, and water temperature measurements. The SI for both calcite and dolomite are also presented. Representative samples were selected if a full suite of the above parameters were available and if the charge balance was within ±5 percent. Samples were removed if multiple outliers (outliers for multiple parameters) were present.

E.2.0 SUMMARY OF DATASETS

The first dataset is presented in Table E.3-1, parts a and b, and reports the mean and SD for the parameters described above. The number of samples for each sampling location is also presented, along with the top and bottom of the formation access interval (FAI) of each well, and the reactive mineral category (RMC) assigned to the sample. In some cases, the top of the FAI is described as the top of the water table.

The second dataset is provided electronically as a spreadsheet. A description of this datasets includes the following items:

- MASTER_ID - Location ID, indicating the completion status of the well at the time of sampling, as reported in the GEOCHEM06.mdb database (SNJV, 2006); this ID generally is the NWIS ID
- BI_ID - Location ID assigned from the UGTA Borehole Index
- SITE_ID - Sample location name as reported in the GEOCHEM06.mdb database (SNJV, 2006)
- HSU - Primary hydrostratigraphic unit associated with the groundwater sample (see Table 4-2 for a description of HSUs)
- RMC - Reactive Mineral Unit associated with the groundwater sample
- SAMPLE_ID - Unique identifier for the sample in the GEOCHEM06.mdb database (SNJV, 2006) or subsequent version of the database
- S_Date - Sample collection date
- S_Time - Sample collection time
- S_Depth (m) - Sample collection depth, m
- HCO3 (mg/L) - Concentration of bicarbonate, mg/L
- CO3 (mg/L) - Concentration of carbonate, mg/L
- SO4 (mg/L) - Concentration of sulfate, mg/L
- Cl (mg/L) - Concentration of chloride, mg/L
- Mg (mg/L) - Concentration of magnesium, mg/L

- Na (mg/L) - Concentration of sodium, mg/LK (mg/L) - Concentration of potassium, mg/L
- Ca (mg/L) - Concentration of calcium, mg/L
- SiO2 (mg/L) - Concentration of silica, mg/L
- pH - pH
- Charge Balance - Charge balance calculated from the major and minor ions
- T (ºC) - Water temperature
- NO3 (mg/L) - Concentration of nitrate, mg/L
- Br (mg/L) - Concentration of bromide, mg/L
- PO4 (mg/L) - Concentration of phosphate, mg/L
- F (mg/L) - Concentration of fluoride, mg/L
- DDF - Data documentation flag indicating level of documentation associated with the sample
- Reference - Laboratory associated with the sample analysis; additional information is provided for each sample in the GEOCHEM06.mdb database (SNJV, 2006)
- Comments - Comments related to any of the parameters associated with a given sample

E.3.0 ACCESS TO DATASET

The chemistry dataset is provided in an Excel spreadsheet (YF_CM_chemistry_Data.xls) on the CD-ROM accompanying this report.

Table E.3-1
Groundwater Chemistry Related Parameters for the Yucca Flat/Climax Mine CAU (Part a)
(Page 1 of 3)

SITE_ID	Common Name	Number of Samples	FAI (m)		RMC	SI [a]		pH		T (°C)		NO_3 (mg/L)		Br (mg/L)		PO_4 (mg/L)		F mg/L	
			Top Depth	Bottom Depth		Dolomite	Calcite	Mean	SD	Mean	SD	Mean	SD	Mean	SD	Mean	SD	Mean	SD
Alluvial Aquifer (AA)																			
USGS Water Well A	WW-A	14	488.3 [b]	570.0	VMP	0.15	0.13	7.8	0.2	25.2	2.4	5.8	2.2	NA	N/A	0.1	N/A	0.5	0.1
Well 3 Water Well	WW-3	8	466.9 [b]	548.6	VMP	0.14	0.02	7.9	0.1	22.4	1.1	7.1	2.1	NA	N/A	0.1	0.1	0.9	0.1
UE-1a	UE-1a	1	166.2 [b]	291.7	VMP	NA	NA	8.01	N/A	25.4	N/A	0.04	N/A	NA	N/A	NA	N/A	NA	N/A
UE-6d	UE-6d	1	647.7	1,187.5	VMP	2.79	1.43	8.30	N/A	NA	N/A	7.6	N/A	NA	N/A	NA	N/A	NA	N/A
Lower Carbonate Aquifer (LCA)																			
ER-3-1 #1, deep	ER-3-1	1	772.3	793.1	CC	0.00	-0.03	6.7	N/A	37.8	N/A	NA	N/A	NA	N/A	NA	N/A	1.38	N/A
ER-6-1	ER-6-1	5	554.4	683.7	CC	0.84	-0.06	7.3	0.1	38.1	4.2	0.5	0.2	0.7	0.1	NA	N/A	0.72	0.03
ER-6-1 #2	ER-6-1 #2	4	540.9	975.4	CC	-0.31	-0.20	7.6	0.1	36.9	5.4	1.1	N/A	0.4	0.3	NA	N/A	0.8	N/A
ER-7-1	ER-7-1	4	564.9 [b]	762.0	CC	1.03	0.11	7.6	0.04	49.0	1.1	0.1	N/A	0.2	0.1	NA	N/A	0.8	N/A
U-3cn #5	U-3cn #5	8	863.2	923.5	CC	0.30	0.01	7.5	0.6	44.7	N/A	0.3	0.1	NA	N/A	0.2	N/A	0.7	0.3
UE-10j, Zone #1	UE-10j-1	1	759.9 [b]	796.4	CC	-0.53	-0.29	6.4	N/A	32.7	N/A	NA	N/A	NA	N/A	NA	N/A	0.33	N/A
UE-10j, Zone #2	UE-10j-2	1	721.5 [b]	741.3	CC	-0.49	-0.28	6.7	N/A	32.3	N/A	NA	N/A	NA	N/A	NA	N/A	0.33	N/A
UE-10j, Zone #3	UE-10j-3	2	680.3 [b]	700.1	CC	0.04	-0.02	7.1	0.2	32.1	N/A	NA	N/A	0.1	N/A	NA	N/A	0.3	N/A
UE-1q	UE-1q	4	749.5	792.5	CC	1.06	NA	NA	0.2	28.1	3.8	NA	N/A	NA	N/A	NA	N/A	0.4	0.1
USGS Test Well D	TW-D	7	525.2 [b]	594.4	CC	-0.26	-0.08	8.2	0.2	23.3	0.7	0.2	N/A	NA	N/A	NA	N/A	1.3	0.1
USGS Test Well E	TW-E	1	769.0	798.6	CC	-1.21	-0.16	8.4	N/A	NA	N/A	0.1	N/A	NA	N/A	NA	N/A	NA	N/A
USGS Water Well C	WW-C	15	470.0 [b]	519.5	CC	0.57	0.24	7.4	0.3	36.7	0.3	0.3	0.2	NA	N/A	NA	N/A	1.1	0.1
Water Well C-1	WW-C1	18	469.2 [b]	503.8	CC	0.28	0.10	7.4	0.4	36.2	1.3	0.4	0.1	0.2	N/A	NA	N/A	1.1	0.1
UE-7ns	UE-7ns	3	600.2 [b]	672.1	CC	-0.46	-0.08	7.6	0.1	34.6	1.6	NA	N/A	NA	N/A	NA	N/A	0.9	0.1
WW-2	WW-2	11	781.2	1,043.0	CC	0.05	-0.04	7.8	0.3	33.7	1.2	5.1	0.7	0.06	0.01	NA	N/A	0.37	0.03
UE-1h	UE-1h	1	650.4	1,023.5	CC	0.72	0.29	8.2	N/A	25.3	N/A	NA	N/A	NA	N/A	NA	N/A	NA	N/A
Lower Carbonate Aquifer-Thrust Plate (LCA3)																			
ER-12-1	ER-12-1	2	500.2	562.7	CC	0.97	0.40	7.7	0.3	25.0	N/A	0.1	N/A	0.4	N/A	NA	N/A	0.3	0.1
ER-6-2	ER-6-2	3	544.1 [b]	1,038.8	CC	1.08	-0.18	7.3	0.2	35.2	0.5	0.8	0.8	0.4	0.4	NA	N/A	1.4	0.1
UE-1c [c]	UE-1c	2	395.4 [b]	573.0	CC	-0.39	-0.17	7.5	0.6	NA	N/A	2.4	N/A	NA	N/A	0.002	N/A	0.5	N/A
UE-2ce [d]	UE-2ce	1	419.6	502.8	CC	-0.15	0.06	7.3	N/A	32.4	N/A	1.6	N/A	NA	N/A	NA	N/A	0.7	N/A

Table E.3-1
Groundwater Chemistry Related Parameters for the Yucca Flat/Climax Mine CAU (Part a)
(Page 2 of 3)

SITE_ID	Common Name	Number of Samples	FAI (m)		RMC	SI [a]		pH		T (°C)		NO_3 (mg/L)		Br (mg/L)		PO_4 (mg/L)		F mg/L	
			Top Depth	Bottom Depth		Dolomite	Calcite	Mean	SD	Mean	SD	Mean	SD	Mean	SD	Mean	SD	Mean	SD
Upper Carbonate Aquifer (UCA)																			
UE-16d (Eleana)	UE-16d	11	349.0	592.5	CC	0.29	0.15	7.6	0.2	23.1	1.8	0.2	0.1	NA	N/A	NA	N/A	0.54	0.04
Lower Clastic Confining Unit (LCCU)																			
UE-15d Water Well	UE-15d WW	8	528.8	1,645.9	SC	0.88	0.46	7.4	0.5	35.0	0.4	0.8	N/A	NA	N/A	0.002	N/A	1.5	0.5
UE-15j	UE-15j	1	4.2	380.1	SC	-0.37	-0.14	6.6	N/A	45.0	N/A	NA	N/A	NA	N/A	NA	N/A	3.3	N/A
UE-15j A-5	UE-15j A-5	2	2.5	227.1	SC	0.21	0.15	6.7	N/A	44.3	N/A	1.6	2.1	NA	N/A	NA	N/A	3.2	N/A
Upper Clastic Confining Unit (UCCU)																			
ER-12-2	ER-12-2	4	903.4	2,097.9	ARG	-1.08	-0.52	8.3	0.2	35.0	0.9	NA	N/A	0.4	0.2	NA	N/A	2.3	0.3
UE-16f	UE-16f	1	394.1	441.4	ARG	0.46	0.28	9.4	N/A	NA	N/A	0.01	N/A	NA	N/A	NA	N/A	NA	N/A
UE-17a (Eleana) [e]	UE-17a	1	368.8	370.0	ARG	0.54	0.18	NA	N/A	17.5	N/A	NA	N/A	NA	N/A	NA	N/A	1.00	N/A
UE-1b	UE-1b	1	196.5 [b]	382.2	ARG	0.44	0.25	8.1	N/A	NA	N/A	2.7	N/A	NA	N/A	NA	N/A	NA	N/A
Lower Tuff Confining Unit (LTCU)																			
ER-2-1	ER-2-1	4	525.8 [b]	663.5	ZEOL/DMP	-0.13	0.26	9.1	0.2	23.3	2.4	2.4	N/A	0.19	0.04	NA	N/A	1.9	0.2
Test Well #7 (HTH)	TW-7	1	613.9	692.5	ZEOL	-2.46	-1.13	7.3	N/A	20.6	N/A	NA	N/A	NA	N/A	NA	N/A	2.4	N/A
U-2bs	U-2bs	2	525.2 [b]	585.2	ZEOL	-3.47	-1.52	7.1	0.4	25.8	0.4	0.6	0.3	NA	N/A	0.1	0.0	1.3	0.0
U-3cn PS #2	U-3cn PS #2	4	472.4 [b]	793.4	ZEOL	-0.45	-0.13	7.9	0.2	24.6	0.9	5.9	1.0	0.4	0.2	NA	N/A	0.9	0.3
U-4u PS #2A	U-4u PS #2A	2	472.0	501.0	ZEOL	NA	NA	7.4	0.2	28.0	N/A	19.3	N/A	NA	N/A	NA	N/A	0.5	N/A
UE-10 ITS #3	UE-10 ITS #3	1	563.8 [b]	587.0	ZEOL	-0.17	0.38	8.3	N/A	NA	N/A	5.5	N/A	NA	N/A	NA	N/A	NA	N/A
Topopah Spring Aquifer (TSA)																			
UE-14b	UE-14b	3	625.1	1,121.7	DMP	-0.56	0.15	8.4	0.1	NA	N/A	9.6	0.5	NA	N/A	NA	N/A	NA	N/A
USGS Test Well B	TW-B	5	469.1	510.5	DMP	-1.32	-0.43	8.1	0.4	NA	N/A	0.12	0.13	NA	N/A	NA	N/A	NA	N/A
Mesozoic Granite Confining Unit (MGCU)																			
U-15.01 Shaft, C-30	C-30	1	N/A	N/A	DMR	NA	NA	8.1	N/A	NA	N/A	NA	N/A	NA	N/A	1.90	N/A	NA	N/A
U-15.01 Shaft, C-36	C-36	1	N/A	N/A	DMR	NA	NA	7.8	N/A	NA	N/A	NA	N/A	NA	N/A	1.20	N/A	NA	N/A
U-15.01 Shaft, CGW-1	CGW-1	1	N/A	N/A	DMR	NA	NA	7.3	N/A	NA	N/A	NA	N/A	NA	N/A	NA	N/A	0.9	N/A
U-15.01 Shaft, NH-01	NH-01	1	N/A	N/A	DMR	NA	NA	8.2	N/A	NA	N/A	NA	N/A	NA	N/A	0.50	N/A	NA	N/A
U-15.01 Shaft, UG-02	UG-02	1	N/A	N/A	DMR	NA	NA	7.5	N/A	NA	N/A	NA	N/A	NA	N/A	NA	N/A	1.4	N/A

Table E.3-1
Groundwater Chemistry Related Parameters for the Yucca Flat/Climax Mine CAU (Part a)
(Page 3 of 3)

SITE_ID	Common Name	Number of Samples	FAI (m)		RMC	SI [a]		pH		T (°C)		NO_3 (mg/L)		Br (mg/L)		PO_4 (mg/L)		F mg/L	
			Top Depth	Bottom Depth		Dolomite	Calcite	Mean	SD	Mean	SD	Mean	SD	Mean	SD	Mean	SD	Mean	SD
Springs																			
Captain Jack Spring	Captain Jack Spring	7	N/A	N/A	ZEOL	-4.12	-1.82	7.3	0.2	NA	N/A	1.8	1.4	NA	N/A	NA	N/A	NA	N/A
Oak Spring	Oak Spring	5	N/A	N/A	ZEOL	-2.92	-1.25	7.0	0.6	NA	N/A	2.4	2.7	NA	N/A	NA	N/A	NA	N/A
Whiterock Spring	Whiterock Spring	49	N/A	N/A	ZEOL	-3.81	-2.05	6.5	1.5	13.9	2.7	NA	N/A	NA	N/A	NA	N/A	NA	N/A

[a] Saturation Index - Positive SI indicates oversaturation and negative indicates undersaturation.
[b] Top of formation access interval corresponds to the average water level
[c] Bailed sample was collected from the LCA3
[d] The groundwater chemistry for this well has been highly variable over the 30-year sampling period. Therefore, only data for the most recent sample, collected on July 12, 2005, are reported.
[e] The groundwater chemistry for this well is highly variable; mean concentration represents composite samples collected from different zones that appear to have different water chemistries.

N/A - Not applicable
NA - Not available
SD - Standard deviation

Table E.3-1
Groundwater Chemistry Related Parameters for the Yucca Flat/Climax Mine CAU (Part b)
(Page 1 of 3)

SITE_ID	*In situ* ORP (mV) [a]	HCO_3 (mg/L)		CO_3 (mg/L)		SO_4 (mg/L)		Cl (mg/L)		Mg (mg/L)		Na (mg/L)		K (mg/L)		Ca (mg/L)		SiO_2 (mg/L)		Charge Balance
		Mean	SD	Mean	SD	Mean	SD	Mean	SD	Mean	SD	Mean	SD	Mean	SD	Mean	SD	Mean	SD	
Alluvial Aquifer (AA)																				
USGS Water Well A	NA	203	16	NA	N/A	17.4	5.2	9.4	7.6	6.6	0.8	50.5	1.9	8.4	0.8	21.7	2.5	63.9	23.1	0.5
Well 3 Water Well	52 to 169 (472-533)	194	3	NA	N/A	21.1	1.5	5.8	1.2	12.3	1.0	38.9	1.1	7.6	0.4	20.2	1.3	64.5	16.3	0.6
UE-1a	NA	448	N/A	NA	N/A	1.00	N/A	30.7	N/A	32.4	N/A	59	N/A	12.3	N/A	41.1	N/A	19	N/A	4.0
UE-6d	NA	245	N/A	0.50	N/A	18.5	N/A	8.20	N/A	9.6	N/A	58	N/A	11.6	N/A	21.2	N/A	53	N/A	1.0
Lower Carbonate Aquifer (LCA)																				
ER-3-1 #1, deep	NA	741	N/A	0.21	N/A	68.1	N/A	43.40	N/A	35.1	N/A	143	N/A	19.00	N/A	94.9	N/A	37.0	N/A	1.8
ER-6-1	134 to 276 (472-503)	248	8	NA	N/A	33.3	0.8	10.9	1.0	12.7	0.5	46.2	2.7	7.7	0.5	33.0	0.8	32.9	1.9	2.2
ER-6-1 #2	NA	244	0.2	0.6	N/A	34.3	0.5	11.0	0.8	13.3	0.5	43.8	2.5	7.5	0.8	32.9	0.7	32.3	2.1	2.7
ER-7-1	NA	241	6	0.6	N/A	34.1	0.2	11.4	1.3	13.6	0.5	46.6	4.1	7.4	1.2	33.8	4.7	37.1	1.4	0.2
U-3cn #5	NA	257	17	NA	N/A	36.2	2.4	23.3	2.3	18.4	2.1	55.2	2.1	9.2	0.7	32.6	7.4	54.6	24.3	0.5
UE-10j, Zone #1	NA	504	N/A	0.07	N/A	83.0	N/A	24.00	N/A	42.3	N/A	64	N/A	12.30	N/A	101.0	N/A	42.8	N/A	4.2
UE-10j, Zone #2	NA	403	NA	0.11	N/A	67.0	N/A	16.00	N/A	30.0	N/A	43	N/A	8.30	N/A	68.0	N/A	36.4	N/A	3.2
UE-10j, Zone #3	-439 to -342 (661-710)	322	38	0.2	N/A	58.5	3.3	12.8	0.4	26.8	1.9	36.8	2.5	7.3	0.6	60.0	5.7	32.0	3.2	0.7
UE-1q (2600 ft)	NA	206	19	NA	N/A	24.5	1.7	10.5	6.0	14.3	0.9	40.7	13.5	7.2	3.0	24.8	5.3	34	23	1.9
USGS Test Well D	NA	234	10	2.0	1.1	29.9	8.6	6.6	0.4	5.1	0.5	84.5	2.7	8.5	0.6	12.0	1.4	47.6	2.9	1.3
USGS Test Well E	NA	58	N/A	1.80	N/A	1.10	N/A	8.20	N/A	0.6	N/A	17	N/A	1.71	N/A	10.2	N/A	3	N/A	2.1
USGS Water Well C	NA	580	9	NA	N/A	66.9	3.1	32.8	2.8	28.1	2.8	125	6	14.0	1.0	73.6	3.2	30.6	2.0	0.4
Water Well C-1	NA	573	29	NA	N/A	66.1	1.6	33.5	1.9	29.2	1.4	123	3	14.0	0.7	73.1	5.3	30.4	1.9	0.1
UE-7nS	NA	193	4	2.4	N/A	4.8	7.5	22.1	3.7	3.2	0.3	55.1	0.4	5.2	1.1	18.9	0.9	21.2	0.1	3.6
WW-2	-149 to -97 (634-732)	205	18	NA	N/A	22.8	1.6	6.8	1.0	14.6	1.8	27.3	2.5	6.6	0.6	31.9	4.4	48.9	3.6	1.0
UE-1h	NA	270	N/A	1.97	N/A	2.5	N/A	43.6	N/A	7.5	N/A	102	N/A	25.0	N/A	15.3	N/A	12	N/A	5.6
Lower Carbonate Aquifer-Thrust Plate (LCA3)																				
ER-12-1	-113 to13 (469-762)	224	22	0.3	0.4	355.7	0.4	17.5	0.4	60.0	1.6	37.4	1.3	3.1	0.2	94.0	7.8	23.3	N/A	1.2
ER-6-2	NA	377	25	0.7	N/A	55.6	2.7	19.5	3.8	20.4	1.7	67.4	5.1	10.6	0.4	59.4	7.0	30.8	4.2	1.0
UE-1c [b]	179 to 183 (399-518)	241	4	NA	N/A	33.0	1.5	7.1	0.6	13.6	0.6	34.9	1.6	12.8	0.2	36.5	3.5	91.8	8.8	1.2
UE-2ce [c]	NA	305	N/A	0.3	N/A	16.6	N/A	14.2	N/A	24.9	N/A	38.0	N/A	17.6	N/A	46.0	N/A	27.3	N/A	0.0

Table E.3-1
Groundwater Chemistry Related Parameters for the Yucca Flat/Climax Mine CAU (Part b)
(Page 2 of 3)

SITE_ID	*In situ* ORP (mV) [a]	HCO_3 (mg/L)		CO_3 (mg/L)		SO_4 (mg/L)		Cl (mg/L)		Mg (mg/L)		Na (mg/L)		K (mg/L)		Ca (mg/L)		SiO_2 (mg/L)		Charge Balance
		Mean	SD	Mean	SD	Mean	SD	Mean	SD	Mean	SD	Mean	SD	Mean	SD	Mean	SD	Mean	SD	
Upper Carbonate Aquifer (UCA)																				
UE-16d (Eleana)	NA	355	15	NA	N/A	58.1	1.1	10.9	1.6	24.0	1.1	30.7	3.1	6.7	0.4	77.9	3.1	31.1	2.3	0.0
Lower Clastic Confining Unit (LCCU)																				
UE-15d Water Well	NA	382	29	NA	N/A	46.4	5.2	14.8	2.9	15.6	1.5	86.0	7.2	15.3	1.1	45.2	7.7	28.4	13.4	0.4
UE-15j	NA	908	N/A	NA	N/A	123	N/A	39.0	N/A	12.0	N/A	310	N/A	56.0	N/A	46.0	N/A	36	N/A	1.4
UE-15j A-5	NA	870	2	NA	N/A	112	2	38.0	N/A	12.0	N/A	286	1	51.5	3.5	46.5	0.7	33.5	0.7	2.2
Upper Clastic Confining Unit (UCCU)																				
ER-12-2	NA	298	13	3.3	3.1	27.3	0.5	6.8	0.2	1.8	0.3	114	5	3.1	0.7	5.5	0.9	20.3	3.8	3.6
UE-16f	NA	799	N/A	132	N/A	1.7	N/A	19.70	N/A	0.4	N/A	412	N/A	1.4	N/A	1.52	N/A	6.0	N/A	0.1
UE-17a (Eleana) [d]	-349 to -159 (195-358)	295	N/A	NA	N/A	160	N/A	23.00	N/A	21.0	N/A	130	N/A	8.0	N/A	29.0	N/A	NA	N/A	0.9
UE-1b	NA	248	N/A	NA	N/A	20.3	N/A	7.70	N/A	13.5	N/A	32	N/A	11.5	N/A	37.9	N/A	85	N/A	0.8
Lower Tuff Confining Unit (LTCU)																				
ER-2-1	NA	130	13	27.2	7.8	16.5	0.6	5.4	0.6	0.3	0.2	75.3	2.6	4.9	0.7	2.8	0.7	76	32	1.9
Test Well #7 (HTH)	-59 to 206 (503-671)	286	N/A	NA	N/A	2.1	N/A	8.00	N/A	0.2	N/A	113	N/A	4.6	N/A	1.0	N/A	1.4	N/A	0.2
U-2bs	NA	198	13	NA	N/A	24.5	4.9	7.5	1.6	0.5	0.3	79.0	0.0	6.0	0.6	3.1	0.9	53.0	1.4	3.2
U-3cn PS #2	NA	275	15	1.40	0.70	20.4	1.8	10.50	4.60	3.4	0.1	92.8	5.3	18.1	2.3	13.9	1.4	67.7	22.2	0.4
U-4u PS #2A	NA	284	202	0.1	N/A	10.4	1.3	7.5	2.2	2.2	1.1	83	31	17.9	9.5	20	19	50.5	6.4	1.7
UE-10 ITS #3, 1926 ft	NA	543	N/A	1.60	N/A	42.8	N/A	10.20	N/A	0.4	N/A	209	N/A	21.5	N/A	7.79	N/A	62	N/A	0.8
Topopah Spring Aquifer (TSA)																				
UE-14b	NA	115	3	3.0	2.0	85.9	6.2	7.3	0.2	0.22	0.04	81.4	1.3	1.1	0.1	11.5	3.4	43.7	0.2	0.2
USGS Test Well B	NA	164	15	NA	N/A	23.0	3.6	17.0	4.1	0.5	0.2	74.9	3.5	3.3	0.4	5.5	1.0	18.6	2.9	0.3
Mesozoic Granite Confining Unit (MGCU)																				
U-15.01 Shaft, C-30	NA	167	N/A	NA	N/A	750.00	N/A	77	N/A	118	N/A	72	N/A	5.5	N/A	161	N/A	29.3	N/A	1.0
U-15.01 Shaft, C-36	NA	316	N/A	NA	N/A	325.00	N/A	52	N/A	63	N/A	56	N/A	4.8	N/A	126	N/A	33.8	N/A	2.1
U-15.01 Shaft, CGW-1	NA	163	N/A	NA	N/A	1,060.00	N/A	77	N/A	0.9	N/A	250	N/A	3.4	N/A	283	N/A	15.8	N/A	3.5
U-15.01 Shaft, NH-01	NA	65	N/A	NA	N/A	850.00	N/A	160	N/A	4.8	N/A	229	N/A	3.8	N/A	240	N/A	22.5	N/A	1.9
U-15.01 Shaft, UG-02	NA	165	N/A	NA	N/A	480.00	N/A	70	N/A	1.5	N/A	214	N/A	4.7	N/A	114	N/A	23.9	N/A	1.7

Table E.3-1
Groundwater Chemistry Related Parameters for the Yucca Flat/Climax Mine CAU (Part b)
(Page 3 of 3)

SITE_ID	*In situ* ORP (mV) [a]	HCO_3 (mg/L)		CO_3 (mg/L)		SO_4 (mg/L)		Cl (mg/L)		Mg (mg/L)		Na (mg/L)		K (mg/L)		Ca (mg/L)		SiO_2 (mg/L)		Charge Balance
		Mean	SD	Mean	SD	Mean	SD	Mean	SD	Mean	SD	Mean	SD	Mean	SD	Mean	SD	Mean	SD	
Springs																				
Captain Jack Spring	NA	78	30	NA	N/A	11.7	4.2	6.1	0.9	0.9	0.5	32.4	9.4	2.5	0.9	3.6	1.1	34.6	8.2	0.4
Oak Spring	NA	113	2	NA	N/A	10.5	1.2	9.2	0.7	4.4	0.2	20.6	0.8	6.2	0.1	17.8	0.6	56.6	0.9	1.4
Whiterock Spring	NA	81	4	NA	N/A	32.5	4.2	10.9	1.6	0.7	0.4	44.0	3.5	6.4	0.7	5.8	1.2	46.2	2.0	2.3

[a] Range of depths (m) associated with the *in situ* ORP measurements are presented in parentheses. Sources for these measurements are Finnegan et al., 2004 and 2005; and Finnegan and Thompson, 2002 and 2003.
[b] Bailed sample was collected from the LCA3.
[c] The groundwater chemistry for this well has been highly variable over the 30-year sampling period. Therefore, only data for the most recent sample, collected on July 12, 2005, are reported.
[d] The groundwater chemistry for this well is highly variable; mean concentration represents composite samples collected from different zones that appear to have different water chemistries.

N/A - Not applicable
NA - Not available
SD - Standard deviation

E.4.0 REFERENCES

Finnegan, D.L., and J.L. Thompson. 2002. *Laboratory and Field Studies Related to Radionuclide Migration at the Nevada Test Site in Support of the Underground Test Area and Hydrologic Resources Management Projects*, LA-13919-MS. Los Alamos, NM: Los Alamos National Laboratory.

Finnegan, D.L., and J.L. Thompson. 2003. *Laboratory and Field Studies Related to Radionuclide Migration at the Nevada Test Site in Support of the Underground Test Area and Hydrologic Resources Management Projects October 1, 2001-September 30, 2002*, LA-14042-PR. Los Alamos, NM: Los Alamos National Laboratory.

Finnegan, D.L., J.L. Thompson, and B.A. Martinez. 2004. *Laboratory and Field Studies Related to Radionuclide Migration at the Nevada Test Site in Support of the Underground Test Area and Hydrologic Resources Management Projects October 1, 2002-September 30, 2003*, LA-14151-PR. Los Alamos, NM: Los Alamos National Laboratory.

Finnegan, D.L., J.L. Thompson, and B.A. Martinez. 2005. *Laboratory and Field Studies Related to Radionuclide Migration in the Nevada Test Site in Support of the Underground Test Area Project and Hydrologic Resources Management Project, October 1, 2003-September 30, 2004*, LA-14238-PR. Los Alamos, NM: Los Alamos National Laboratory.

SNJV, see Stoller-Navarro Joint Venture.

Stoller-Navarro Joint Venture. 2006. *Comprehensive Water Quality Database for Groundwater in the Vicinity of the Nevada Test Site, Geochem06.mdb*, S-N/99205--059-Rev. 1. Las Vegas, NV.

Appendix F

Description of Matrix Porosity Data

F.1.0 INTRODUCTION

Matrix porosity data are derived from laboratory measurements of borehole core samples and from the interpretation of borehole geophysical logs (Epithermal Neutron Porosity [ENP] and Sonic Porosity). This section presents the matrix porosity data developed from the geophysical logs performed on the ER Wells within Yucca Flat and additional supporting data analyses from the USGS Rock-Property Database (USGS, 2006). In addition, average porosity values measured using ENP and Sonic Porosity are contained in Tables F.3-1 through F.3-3. Figures F.3-1 through F.3-10 show histograms and CDFs of HGU matrix porosity from the ER Wells geophysical log data

Section F.2.0 describes the matrix porosity dataset and includes the following items:

- A summary of the contents of the dataset
- The structure and fields description of the table containing the dataset
- Directions on how to access the full dataset

Section F.3.0 presents statistical fits to the geophysical log data and summary data tables.

Section F.4.0 provides the reference list for this appendix.

F.2.0 DATASET SUMMARY

There are five datasets. The first holds matrix porosity values, measured for wells within Yucca Flat, that were extracted from the USGS Rock-Property Database (USGS, 2006). The second and third datasets present a summary of the average matrix porosities (obtained from the USGS Rock-Property Database) for each well in Yucca Flat; average porosities for each well and for each HGU (and each HSU) are presented. The fourth and fifth datasets contain the ENP and Sonic Porosity geophysical log data. Descriptions of the fields within each of these datasets are provided in Section F.2.1.

F.2.1 Table Structures

The Yucca Flat matrix porosity table has the following fields:

- BIN - UGTA Borehole Index Number
- Well Name - Name of the borehole/well
- Top (m) - The top depth of the sample in units of m bgs
- Base (m) - The bottom depth of the sample in units of m bgs
- HGU - Hydrogeologic unit assignment from the HSU
- HSU - Hydrostratigraphic unit assignment from the EV® HFM (Dynamic Graphics, 2002)
- Porosity - Porosity derived from a core sample(s)

The table providing the average matrix porosities from the USGS Rock-Property Database (USGS, 2006) for each Yucca Flat well has the following fields (categorized by HGU):

- BIN - UGTA Borehole Index Number
- Well Name - Name of the borehole/well
- N - Total number of samples for the respective well
- Max - Maximum reported porosity value for the respective well
- Min - Minimum reported porosity value for the respective well
- SD - Standard deviation for all reported porosity values for the respective well

- HGU fields - Mean porosity for each HGU (AA, CA, CCU, GCU, LFA, PCU, TCU, VTA, WTA,) for each well
- None - Porosity value for samples that were not assigned to a specific HGU

The table providing the average matrix porosities from the USGS Rock-Property Database (USGS, 2006) for each Yucca Flat well has the following fields (categorized by HSU):

- BIN - UGTA Borehole Index Number
- Well Name - Name of the borehole/well
- N - Total number of samples for the respective well
- Max - Maximum reported porosity value for the respective well
- Min - Minimum reported porosity value for the respective well
- SD - Standard deviation for all reported porosity values for the respective well
- HSU fields - Mean porosity for each HSU (AA2, AA3, ATCU, BLFA, BRCU, LCA, LCA3, LCCU, LTCU, MGCU, OSBCU, PCUT, TM-LVTA, TM-UVTA, TM-WTA, TSA, TUBA, UCCU, UTCU) for each well
- None - Porosity value for samples that were not assigned to a specific HSU

The ENP and Sonic Porosity geophysical log data tables have the following fields:

- BIN - UGTA Borehole Index Number
- Well Name - Name of the borehole/well
- Elev (m) - The elevation of the measurement in units of meters above mean seal level
- HGU - Hydrogeologic unit assignment from the HSU
- HSU - Hydrostratigraphic unit assignment from the EV® HFM (Dynamic Graphics, 2002)

F.2.2 Access to Datasets

The Yucca Flat datasets are provided in Microsoft Excel Spreadsheet (YF_Matrix_Porosity_Data.xls) on the CD-ROM accompanying this report.

F.3.0 GEOPHYSICALLY DERIVED MATRIX POROSITY DATA ANALYSIS

This section presents the HGU matrix porosity histograms and CDFs for the ENP and Sonic Porosity geophysical data in graphical and tabular format. Geophysical log data were selected using industry standard geophysical interpretation techniques. Average porosities obtained using ENP and Sonic Porosity geophysical logs categorized by HGU and HSU are provided in Tables F.3-1 through F.3-3. Figures F.3-1 through F.3-10 show histograms and CDFs of HGU matrix porosity from the ER Wells geophysical log data.

Table F.3-1
Average HGU ENP Porosity by Well

HGU	N	Max	Min	SD	ER-12-2	ER-2-1	ER-6-1	ER-7-1	ER-8-1
AA	6,191	0.65	0.10	0.08	NA	0.33	NA	0.28	0.50
CA	8,042	1.40	-0.03	0.12	NA	NA	0.05	0.06	0.10
CCU	24,277	1.10	-0.05	0.12	0.07	NA	NA	NA	NA
TCU	9,254	1.04	0.08	0.10	NA	0.45	NA	0.31	0.29
VTA	4,325	0.53	0.18	0.07	NA	0.38	NA	0.25	0.27
WTA	580	0.48	0.14	0.06	NA	0.27	NA	NA	NA

NA - Not available

Table F.3-2
Average HSU ENP Porosity by Well

HSU	N	Max	Min	SD	ER-12-2	ER-2-1	ER-6-1	ER-7-1	ER-8-1
AA	6,191	0.65	0.10	0.08	NA	0.33	NA	0.28	0.50
LCA	8,042	1.40	-0.03	0.12	NA	NA	0.05	0.06	0.10
LTCU	4,350	0.77	0.23	0.10	NA	0.45	NA	0.31	NA
OSBCU	4,904	1.04	0.08	0.07	NA	NA	NA	0.30	0.29
TMLVTA	3,524	0.53	0.18	0.05	NA	0.35	NA	0.25	0.27
TMUVTA	801	0.48	0.29	0.03	NA	0.40	NA	NA	NA
TMWTA	580	0.48	0.14	0.06	NA	0.27	NA	NA	NA
UCCU	24,277	1.10	-0.05	0.12	0.07	NA	NA	NA	NA

NA - Not available

Table F.3-3
Average HGU Sonic Porosity by Well

HGU	N	Max	Min	SD	ER-12-2	ER-2-1	ER-7-1
CA	758	0.16	-0.03	0.04	NA	NA	0.04
CCU	24,261	0.60	-0.10	0.11	0.28	NA	NA
TCU	2,278	0.53	0.33	0.03	NA	0.40	NA

NA - Not available

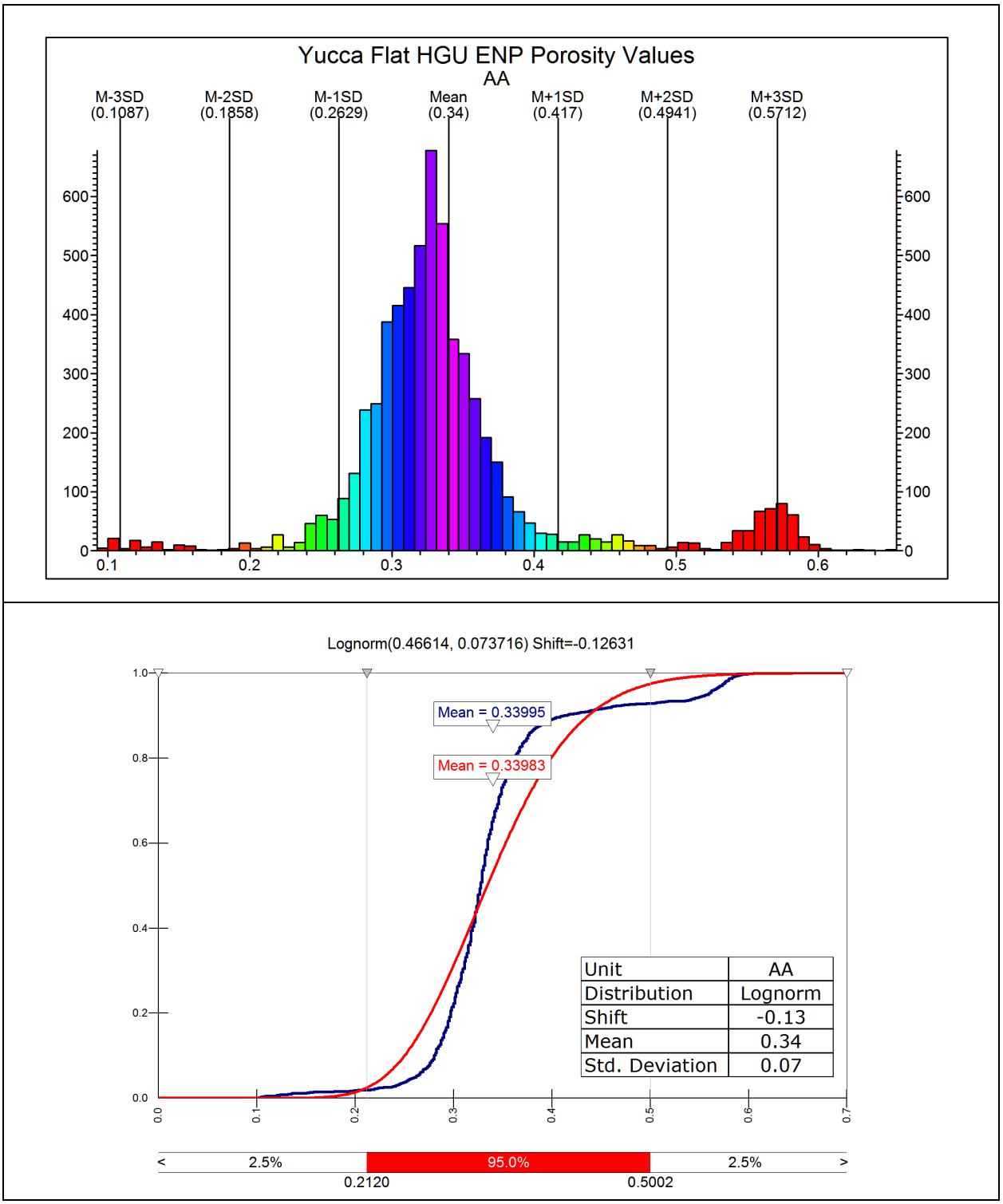

Figure F.3-1
AA HGU ENP Matrix Porosity Histogram and CDF

Note: M + 2SD – Mean plus two standard deviations; Blue curve (darker line) and annotations – Sample data CDF; Red curve (lighter line) and annotations – Fitted PDF

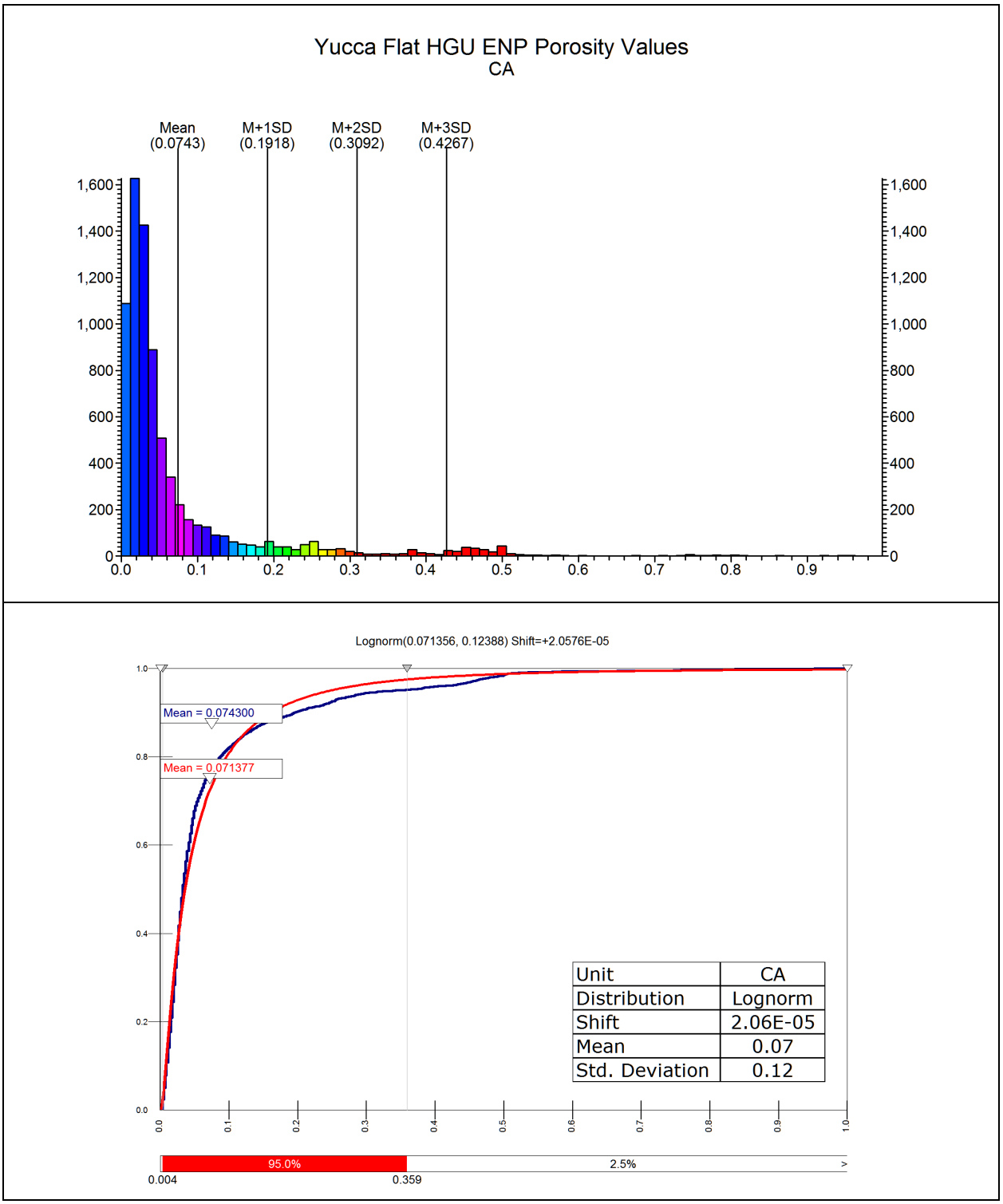

Figure F.3-2
CA HGU ENP Matrix Porosity Histogram and CDF

Note: M + 2SD – Mean plus two standard deviations; Blue curve (darker line) and annotations – Sample data CDF; Red curve (lighter line) and annotations – Fitted PDF

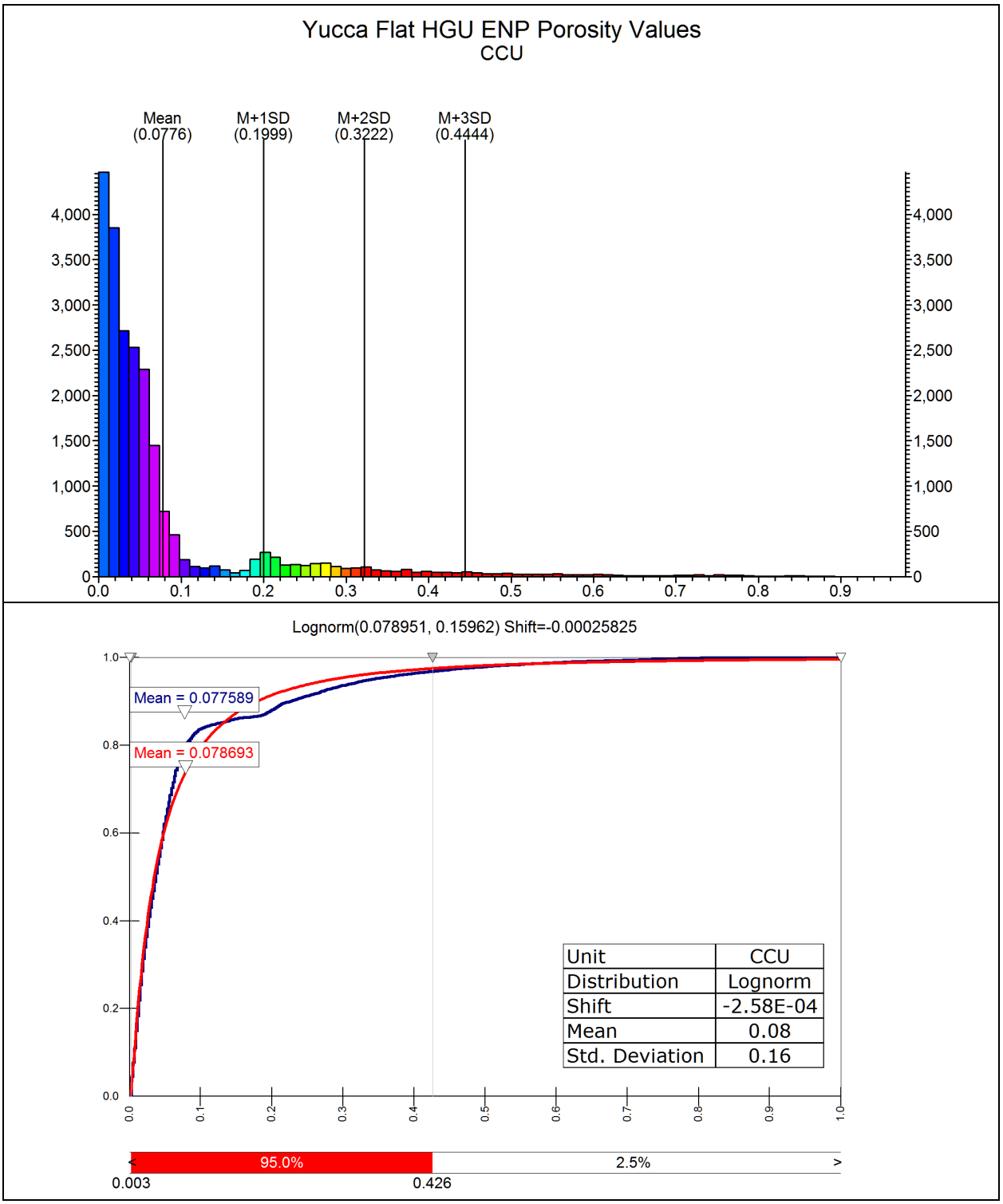

Figure F.3-3
CCU HGU ENP Matrix Porosity Histogram and CDF

Note: M + 2SD – Mean plus two standard deviations; Blue curve (darker line) and annotations – Sample data CDF; Red curve (lighter line) and annotations – Fitted PDF

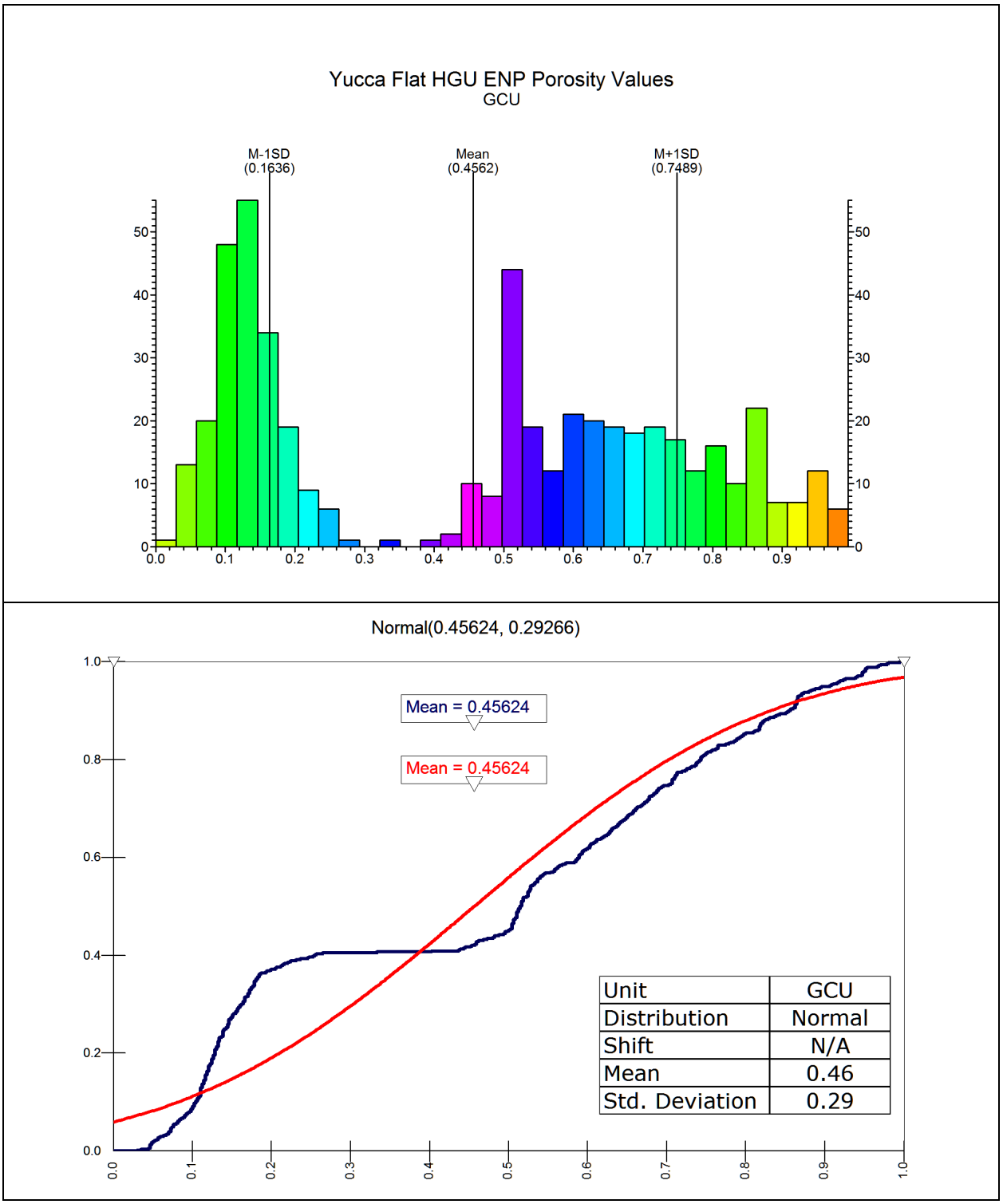

Figure F.3-4
GCU HGU ENP Matrix Porosity Histogram and CDF

Note: M + 2SD – Mean plus two standard deviations; Blue curve (darker line) and annotations – Sample data CDF; Red curve (lighter line) and annotations – Fitted PDF

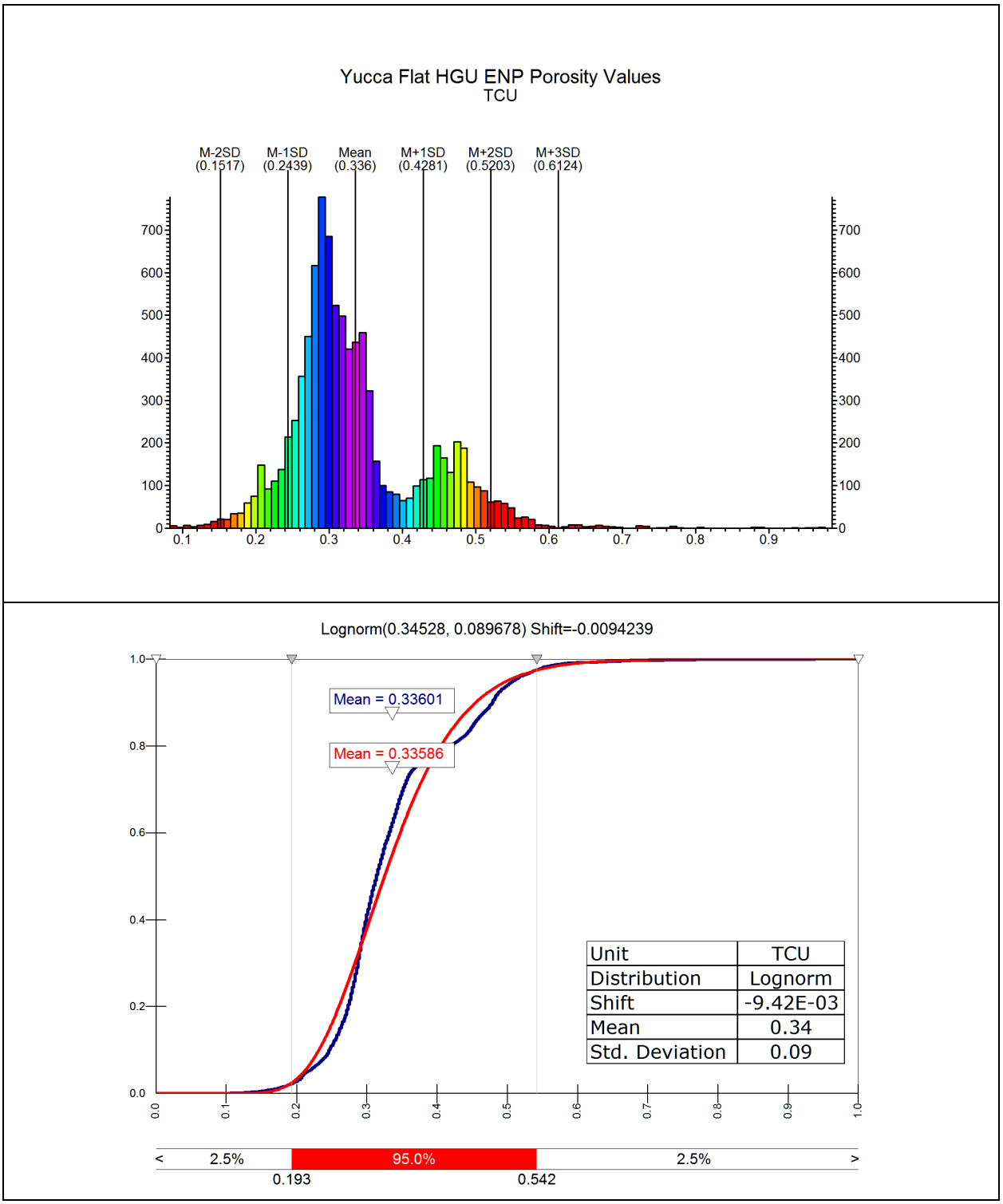

Figure F.3-5
TCU HGU ENP Matrix Porosity Histogram and CDF

Note: M + 2SD – Mean plus two standard deviations; Blue curve (darker line) and annotations – Sample data CDF; Red curve (lighter line) and annotations – Fitted PDF

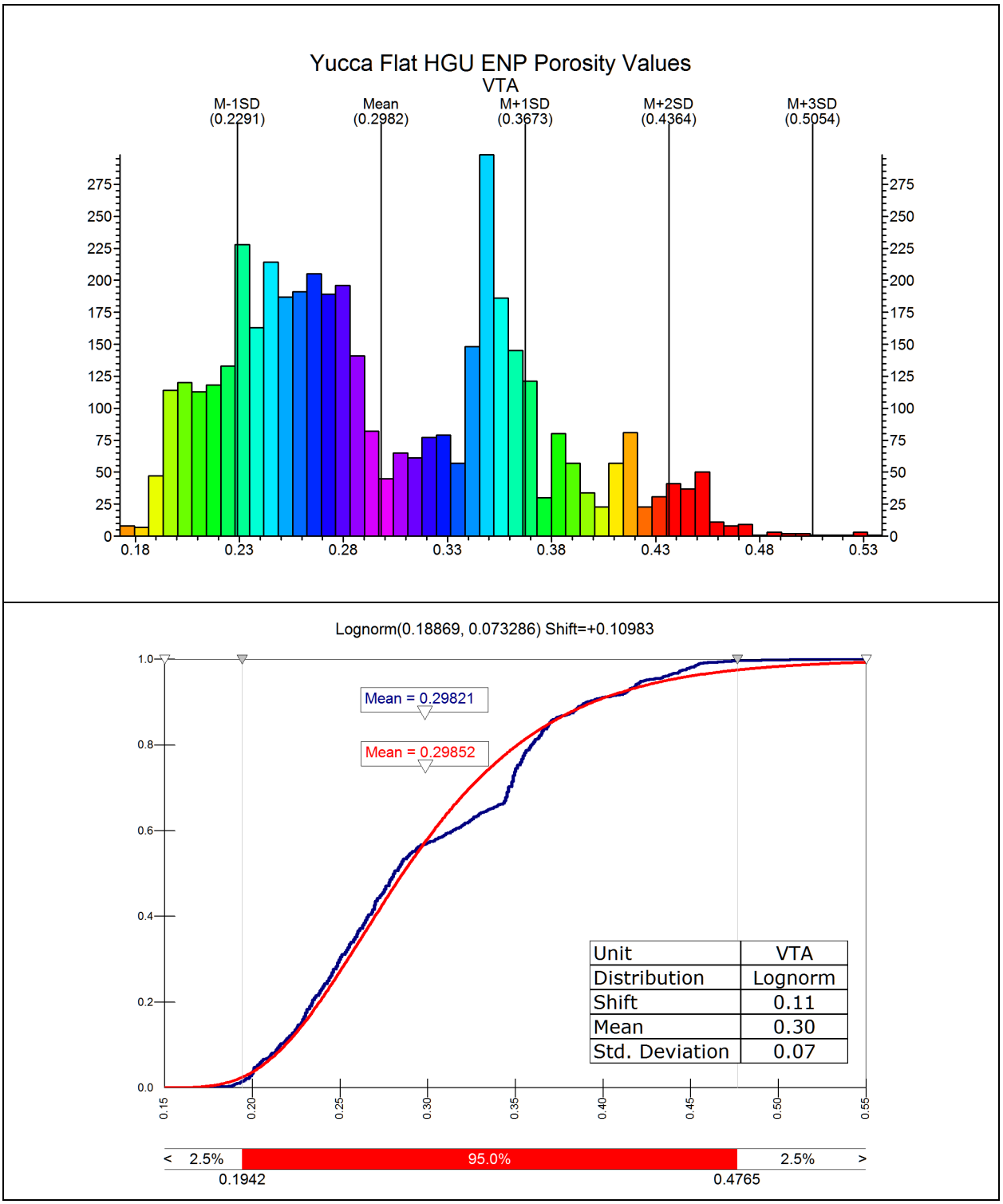

Figure F.3-6
VTA HGU ENP Matrix Porosity Histogram and CDF

Note: M + 2SD – Mean plus two standard deviations; Blue curve (darker line) and annotations – Sample data CDF; Red curve (lighter line) and annotations – Fitted PDF

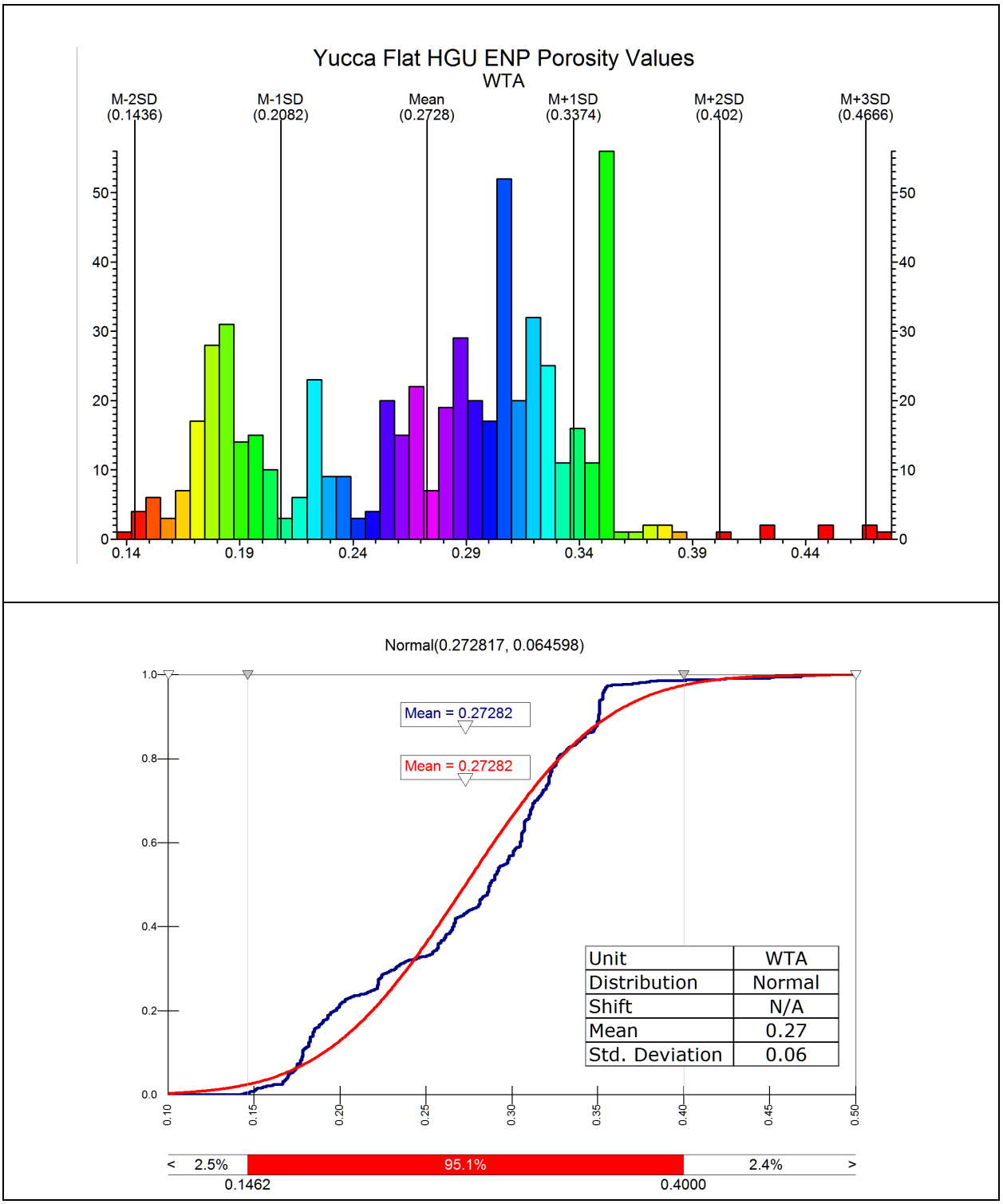

Figure F.3-7
WTA HGU ENP Matrix Porosity Histogram and CDF

Note: M + 2SD – Mean plus two standard deviations; Blue curve (darker line) and annotations – Sample data CDF; Red curve (lighter line) and annotations – Fitted PDF

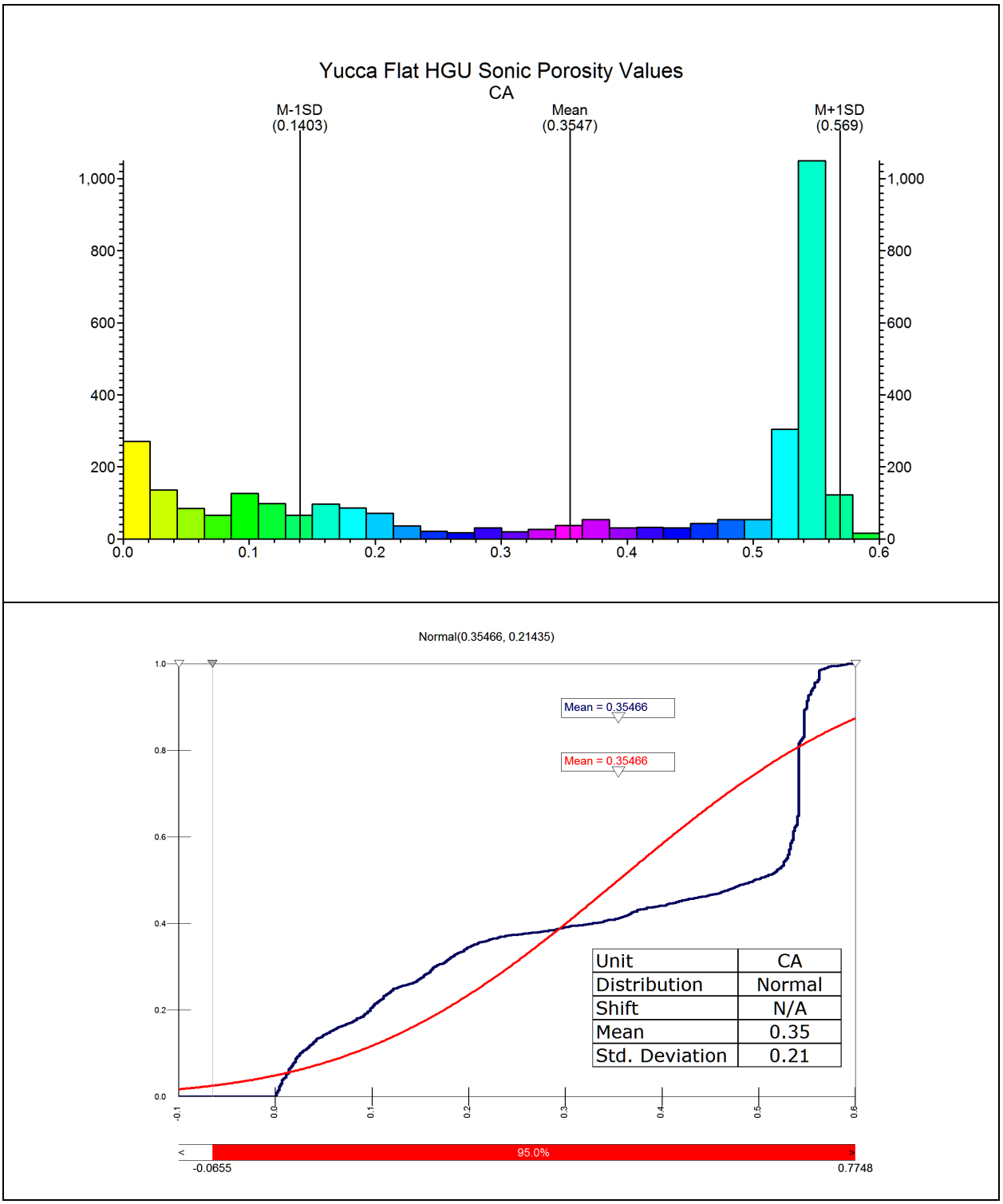

Figure F.3-8
CA HGU Sonic Matrix Porosity Histogram and CDF

Note: M + 2SD – Mean plus two standard deviations; Blue curve (darker line) and annotations – Sample data CDF; Red curve (lighter line) and annotations – Fitted PDF

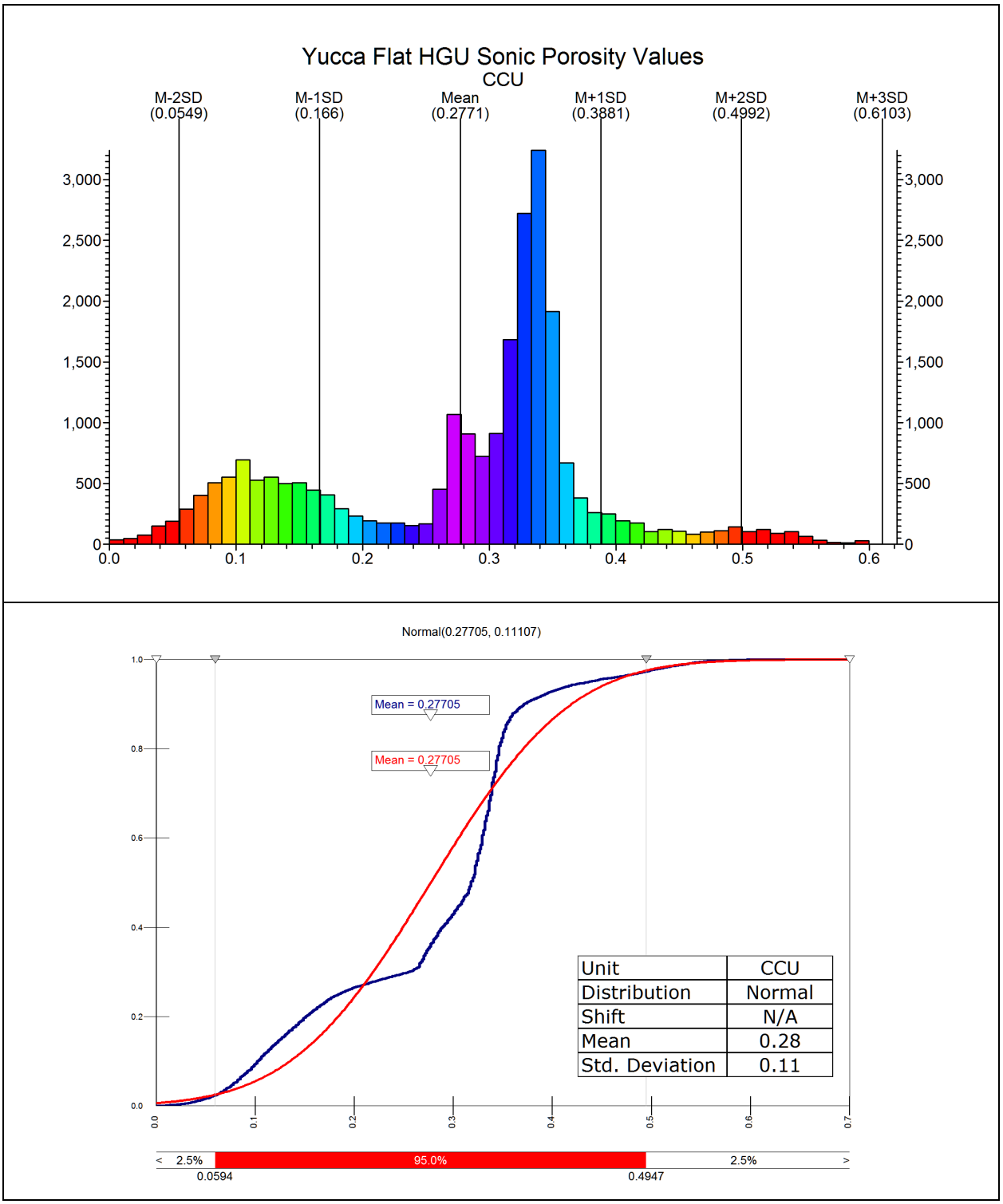

Figure F.3-9
CCU HGU Sonic Matrix Porosity Histogram and CDF

Note: M + 2SD – Mean plus two standard deviations; Blue curve (darker line) and annotations – Sample data CDF; Red curve (lighter line) and annotations – Fitted PDF

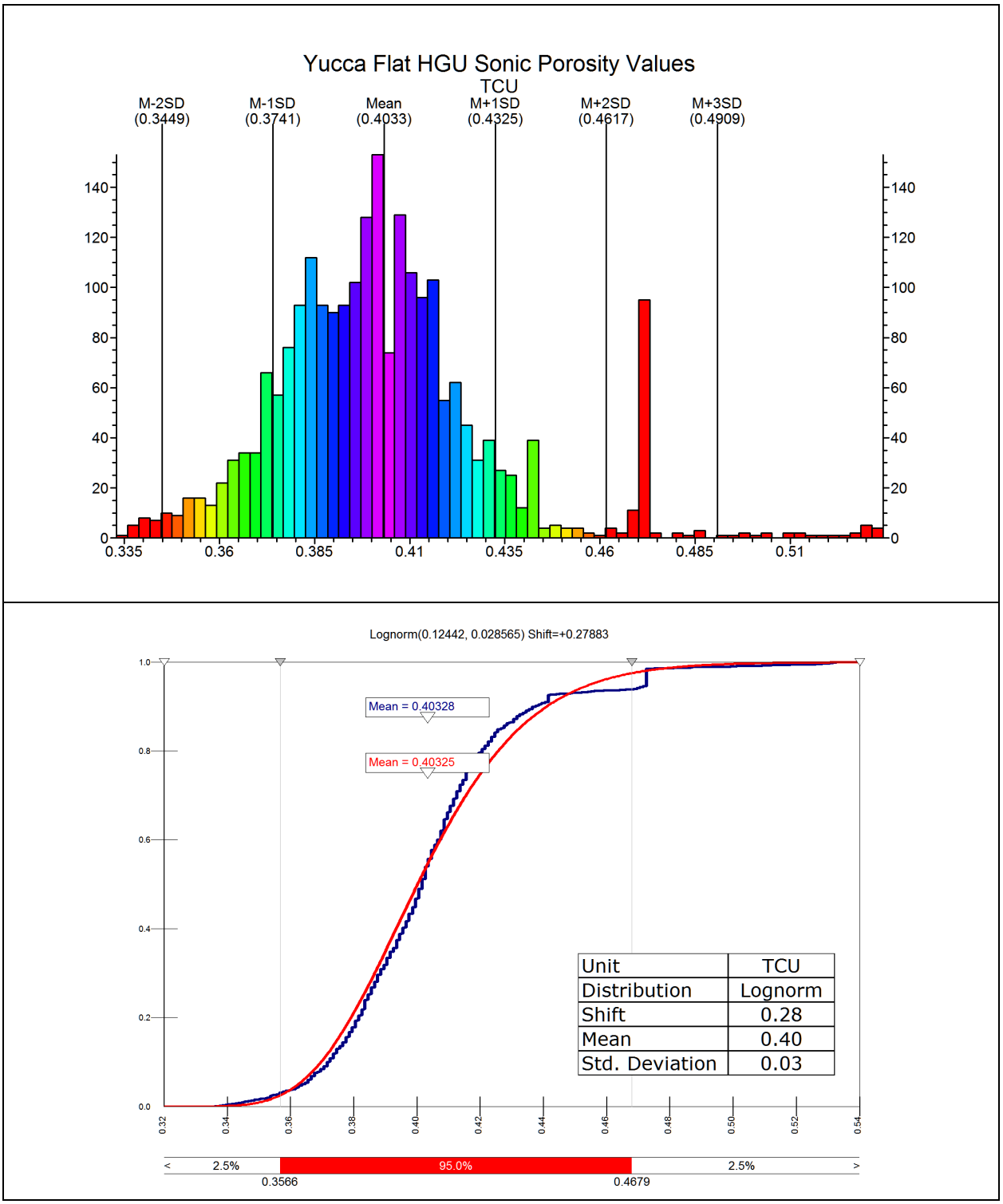

Figure F.3-10
TCU HGU Sonic Matrix Porosity Histogram and CDF

Note: M + 2SD – Mean plus two standard deviations; Blue curve (darker line) and annotations – Sample data CDF; Red curve (lighter line) and annotations – Fitted PDF

F.4.0 REFERENCES

Dynamic Graphics, see Dynamic Graphics, Inc.

Dynamic Graphics, Inc. 2002. *EarthVision 7: Software for 3-D Modeling and Visualization*. Alameda, CA.

USGS, see U.S. Geological Survey.

U.S. Geological Survey. 2006. *Mercury Core Library & Data Center Rock-Property Information Rock-Property Database*. As accessed at http://nevada.usgs.gov/mercury/rock.html on 30 October. Mercury, NV.

Appendix G

Description of Dispersivity Dataset

G.1.0 INTRODUCTION

This section provides a road map to the data required to develop the uncertainty model of longitudinal dispersivity as a function scale and the original datasets compiled from tracer test sites worldwide.

This description of the dispersivity dataset includes the following items:

- A summary of the contents of the dataset
- The structure of the table containing the dataset
- Directions on how to access the dataset

G.2.0 DATASET SUMMARY

Each record of the dispersivity dataset contains information about a given tracer test and the results of the data analysis following a specific method of analysis. The dataset is, therefore, organized primarily by the tracer test location and secondarily by the data analysis method. The dispersivity dataset contains data from different sites throughout the world. The dataset contains information about the data source, the method of analysis, the various dispersivity types, and an indication of the quality of the data by author reliability.

G.3.0 TABLE STRUCTURE

The dispersivity dataset contains the following fields:

- site_name - Name of test, if any, and generalized location of the test
- Rock Types - A uniform naming convention for aquifer material for categorization.
- aquifer_material - Geologic material in which the test was conducted
- min_scale_of_test (m) - The minimum distance of the test in meters; if only one distance is given, it is placed in this field
- max_scale_of_test (m) - The maximum distance of the test in meters
- Average_scale_of_test (m) - Average of min_scale_of_test and max_scale_of_test
- dispersivity_longitudinal_min (m) - The minimum longitudinal dispersivity in meters for the given test material; if only one value is given, it is placed in this field
- dispersivity_longitudinal_intermediate (m) - The intermediate longitudinal dispersivity in meters for the given test material
- dispersivity_longitudinal_max (m) - The maximum longitudinal dispersivity in meters for the given test material
- dispersivity_longitudinal_Geometric_Mean (m) - Geometric mean of dispersivity_longitudinal_min, dispersivity_longitudinal_intermediate, and dispersivity_longitudinal_max
- Percent of Scale (fraction) - Ratio of dispersivity_longitudinal_Geometric_Mean to Average_scale_of_test
- dispersivity_transverse - The transverse dispersivity in meters for the given test material
- dispersivity_vertical - The vertical dispersivity in meters for the given test material
- author_reliability - Categorization of reliability assigned by various authors in the original numerical form, if available
- author_reliability_Unified - Roman numerals assigned to unify reliability for statistical analysis purposes
- data_source - The original source of the data

G.4.0 ACCESS TO DATASET

The full dispersivity dataset is provided in an Excel spreadsheet (Dispersivity_ Data.xls) on the CD-ROM accompanying this report.

Appendix H

Description of Matrix Diffusion Dataset

H.1.0 INTRODUCTION

Data relating to matrix diffusion include diffusion values that were obtained from diffusion cell experiments and fracture transport experiments.

This description of the matrix diffusion datasets includes the following items:

- A summary of the contents of the dataset
- The structure of the tables containing the dataset
- Directions on how to access the full dataset
- References cited in this appendix

H.2.0 DATASET SUMMARY

Each record of the dataset for the diffusion cell experiments contains information about a given measurement for a porous media sample. Of the 309 matrix diffusion measurements in the dataset, 73 measurements are for samples located in Yucca Mountain, 198 measurements are for samples located in Pahute Mesa, 24 measurements are for samples in Yucca Flat, 3 measurements are for samples in Rainier Mesa, and 11 measurements are obtained in miscellaneous regions. The matrix diffusion dataset includes information on the interval tested for each site, the porosity in the tested interval, the various diffusion parameter values and multiplier factors that indicate each measurement's quality and transferability to HSUs, comments on the experimental techniques and quality, and information on geology and mineralogy of the samples.

H.3.0 TABLE STRUCTURE

The matrix diffusion table from the diffusion cell experiments contain the following fields:

- SampleID - The number of data entry
- Sample number - The name of the well, unique sample numbers, and typically the depth in feet
- Location - Yucca Flat (YF), Yucca Mountain (YM), Rainier Mesa (RM), or Pahute Mesa (PM)
- Porosity - The fraction of void space within the rock, the void volume divided by the bulk volume
- Effective porosity - The fraction of void space within the rock that is interconnected and available for fluid flow (only two references reported effective porosity: Hershey et al., 2003; Walter, 1982)
- HSU - Hydrostratigraphic unit for this sample
- Lithology - The type of rock: quartz, carbonate, tuff, zeolitic tuff, or granite/crystalline
- Depth (m) - The depth below ground surface of the well core from which the rock sample was obtained
- Entry date - The date that the matrix diffusion data were added to this dataset (or substantially modified or updated)
- Diffusion coef (m^2/s) - Experimentally derived diffusion coefficient, in m^2/s
- Derived diffusion - Matrix diffusion coefficient that is not reported directly in the reference source, but rather calculated or derived from the reported tortuosity and the free water diffusion coefficient using Equation (10-2)
- Chemical species - Tracer chemical used in the diffusion cell experiment
- Species adj diffusion coefficient (to tritiated water) - Experimentally derived diffusion coefficient, in m^2/s, adjusted from the actual tracer species used in the measurement to a tritiated water basis, to achieve a consistent tracer basis for the entire dataset of measurements

- Original source - Reference source reporting the diffusion coefficient measurement
- Source page #, Table # - Page and table number, where available, from original source reporting diffusion coefficient measurement and other raw data
- Tortuosity - The bulk measure of the constrictivity and tortuous nature of the interconnected pore space through which diffusion is occurring; in the form presented in Equation (10-2), tortuosity should always have a magnitude greater than zero and less than one
- Derived tortuosity - Tortuosity that is not reported directly in the reference source, but rather calculated or derived from the reported matrix diffusion coefficient and the free water diffusion coefficient using Equation (10-2)
- Permeability m^2 - A measure of the ability of a porous material to transmit fluids; related to the constrictivity or tortuosity of the rock
- Temp. ºC - Temperature at which matrix diffusion was measured (rarely reported)
- M2b test series meth - Indicates the quality of the test series experimental method and calibration

H.4.0 ACCESS TO DATASET

The matrix diffusion dataset is provided in an Excel spreadsheet (Matrix_Diffusion_Dataset.xls) on the CD-ROM accompanying this report.

H.5.0 REFERENCES

Hershey, R.L., W. Howcroft, and P.W. Reimus. 2003. *Laboratory Experiments to Evaluate Diffusion of ^{14}C into Nevada Test Site Carbonate Aquifer Matrix*, Publication No. 45180. Las Vegas, NV: Desert Research Institute.

Walter, G.R. 1982. *Theoretical and Experimental Determination of Matrix Diffusion and Related Solute Transport Properties of Fractured Tuffs from the Nevada Test Site*, LA-9471-MS, UC-70. Los Alamos, NM: Los Alamos National Laboratory.

Appendix I

Description of Matrix Sorption Dataset

I.1.0 INTRODUCTION

This section presents data relating to matrix sorption parameters, including matrix sorption parameters calculated from laboratory studies and the Yucca Flat/Climax Mine mineralogy and water chemistry data. The laboratory studies were performed at a variety of experimental conditions, including different lithologies, groundwater types, temperature, pH, and atmospheric conditions. A description of the data transferability process for developing probability distributions for the data derived from the laboratory studies is also presented.

I.2.0 DATASET SUMMARY

I.2.1 Matrix Distribution Coefficients from Yucca Flat/Climax Mine Mineralogy and Water Chemistry Data

The matrix distribution coefficient dataset, developed from the mechanistic model and mineralogy and groundwater chemistry data from the Yucca Flat/Climax Mine CAU, contains K_d data as well as histograms generated from the K_ds. Two spreadsheets, Mechanistic_Kd_by_RMC.xls and Mechanistic_Kd_by_HSU.xls, contain data calculated specifically for RMCs and HSUs, respectively. Each spreadsheet contains a series of worksheets that describe the K_d data and the corresponding histograms for each RMC or HSU. These spreadsheets are on the CD-ROM included with this document.

The spreadsheet Mechanistic_Kd_by_RMC.xls contains a total of 948 K_d estimates for the DMP, 699 K_d estimates for the DMR, 1,484 K_d estimates for the VMP, and 448 K_d estimates for the VMR RMCs for a total of 10 radionuclides (Am, Ca, Cs, Eu, Ni, Np, Pu, Sm, Sr, and U). Histograms for each RMC are presented in separate worksheets; histograms for all 10 radionuclides for a given RMC are presented in the same worksheet.

The spreadsheet Mechanistic_Kd_by_HSU.xls contains a total of 1,417 K_d estimates for the AA, 322 K_d estimates for the ATCU, 3,873 K_d estimates for the LTCU, 2,268 K_d estimates for the TM-LVTA, 76 K_d estimates for the TM-UVTA, 223 K_d estimates for the TM-WTA, 57 K_d estimates for the TSA, and 54 K_d estimates for the PCUT.

I.2.1.1 Table Structure

The matrix K_d table contains the following fields:

- XRD_SAMPLE_ID - Unique sample identification number that links the K_d value to a specific XRD sample split
- HSU - Hydrostratigraphic unit assigned to the XRD sample split, and thus to the K_d

- RMC - Reactive mineral category assigned to the XRD sample split, and thus to the K_d
- RMU - Reactive mineral unit assigned to the XRD sample split, and thus to the K_d
- Water_Chemistry - Groundwater chemistry sample used for the K_d calculation
- Am_kd_mL_g - Am K_d for the specified water chemistry and mineralogy sample, mL/g
- Ca41_kd_mL_g - ^{41}Ca K_d for the specified water chemistry and mineralogy sample, mL/g
- Cs_kd_mL_g - Cs K_d for the specified water chemistry and mineralogy sample, mL/g
- Eu_kd_mL_g - Eu K_d for the specified water chemistry and mineralogy sample, mL/g
- Ni_kd_mL_g - Ni K_d for the specified water chemistry and mineralogy sample, mL/g
- Np_kd_mL_g - Np K_d for the specified water chemistry and mineralogy sample, mL/g
- Pu_kd_mL_g - Pu K_d for the specified water chemistry and mineralogy sample, mL/g
- Sm_kd_mL_g - Sm K_d for the specified water chemistry and mineralogy sample, mL/g
- Sr_kd_mL_g - Sr K_d for the specified water chemistry and mineralogy sample, mL/g
- U_kd_mL_g - U K_d for the specified water chemistry and mineralogy sample, mL/g

I.2.2 Matrix Sorption Parameters from Laboratory Studies

The matrix sorption parameter dataset from laboratory studies is provided as one table containing the experimental results for every rock type and species. There are 7,211 records in the dataset, comprising 380 records for alluvial samples; 1,070 records for vitric tuffs; 1,936 records for devitrified tuffs; 1,667 records for zeolitic tuffs; and 2,158 records for other tuffs and pure mineral samples. The dataset is included in an Excel spreadsheet (Matrix_Sorption_Lab.xls) on the CD-ROM included with this document. The data are sorted first on the basis of whether the experiment is a sorption or desorption experiment, then by the rock type, and finally by the ionic species for which the sorption coefficient was measured.

I.2.2.1 Table Structure

The matrix sorption parameter table contains the following fields:

- Chemical_Species - The ionic species for which the distribution coefficient was determined
- Site_Location - General location where the rock sample was acquired
- Sample well - Name of the well from which the rock sample was taken

- Sample Depth - Depth below ground surface in meters from which the sample was taken
- Rock_type - General rock type of the sample; includes alluvium, vitric tuff, devitrified tuff, zeolitic tuff, and various mineral names (for experiments using pure mineral phases)
- Lithostratigraphic Unit - Stratigraphic unit from which the rock sample was taken
- Mass % Calcite - Weight percent calcite of the rock sample, generally from XRD analysis
- Mass % zeolite - Weight percent zeolite of the rock sample, generally from XRD analysis
- Mass % smectite - Weight percent smectite of the rock sample, generally from XRD analysis
- Mass % hematite - Weight percent hematite of the rock sample, generally from XRD analysis
- Mass % mica - Weight percent mica of the rock sample, generally from XRD analysis
- Sorption/Desorption - Denotes whether the K_d is a sorption or desorption coefficient
- K_d or R_d (mL/g) - Experimentally determined sorption/desorption coefficient for the ionic species
- Recommended sorption coefficient - Alternate sorption coefficient recommended by the data source to account for experimental limitations
- stnd_dev (+/-) - Standard deviation of the sorption/desorption coefficient
- Water_type - Type of water used in the sorption experiment
- Water - Water sample ID of water used by the lab in the sorption experiment
- Initial pH - pH of water before equilibration
- Final pH - pH of water after equilibration (if available)
- Eh (mV) - The final Eh of the water in millivolts
- Temp (deg C) - The temperature at which the sorption experiment was performed
- aq Cl- (mg/L) - Concentration of Cl^- in the water used for the experiment
- aq NO3- (mg/L) - Concentration of NO_3^- in the water used for the experiment
- aq SO42- (mg/L) - Concentration of SO_4^{2-} in the water used for the experiment
- aq Na+ (mg/L) - Concentration of Na^+ in the water used for the experiment
- aq Mg2+ (mg/L) - Concentration of Mg^{2+} in the water used for the experiment
- aq K+ (mg/L) - Concentration of K^+ in the water used for the experiment
- aq Ca2+ (mg/L) - Concentration of Ca^{2+} in the water used for the experiment
- aq F- (mg/L) - Concentration of F^- in the water used for the experiment
- aq Sr2+ (mg/L) - Concentration of Sr^{2+} in the water used for the experiment

- Test_Duration (days) - Length of time in days that the ionic solution was left in contact with the rock sample
- Atmosphere - Type of atmosphere in which the sorption experiment was conducted
- Sample_number - Sample number of the rock on which the sorption experiment was performed
- Sample_description - Lab designated description of the rock sample. Generally includes water type for experiment, well name and depth of rock sample, and some temperature designation
- Experiment - Designator for the experiment
- Initial Species Concentration - Concentration of the sorbed ionic species at the beginning of the experiment
- Initial Species Concentration Units - Units of the initial species concentration measurement
- Remarks - Any other pertinent information relating to the experiment or the measurement
- ref_id - Reference number for the source of measurements in the UGTA library
- Source - Reference number of source used by originator of the data
- YMP_ID - Yucca Mountain Data Tracking number containing the data

I.3.0 DATA TRANSFER AND DATA QUALITY PROTOCOL FOR LABORATORY DISTRIBUTION COEFFICIENTS

Data quality flags and transferability weights must be assigned to the laboratory K_d data before developing probability distributions for use in the contaminant transport model. The transferability approach is consistent with the general methodology suggested in SNJV (2004), and integrates data transfer weights and multipliers during the development of probability functions for the sorption data. The following is a detailed description of the data transferability protocol for distribution coefficients.

I.3.1 Weights

Data weights are applied to describe the geologic context of the data in question. For K_d data, information about the rock type and alteration is not sufficient to categorize the relevance of a data point to the appropriate CAU. To account for this situation, the generalized weighting scheme suggested by SNJV (2004) was modified to account for the aqueous chemistry and the mineralogy of the rock used during the sorption experiments.

I.3.2 Rock Type

If the rock type is different from the rocks observed in the CAU, the data should be rejected. The following classification criteria are used provide a weight for rock type definitions.

I.3.2.1 Alluvium

Generally, alluvium is considered the detrital deposits made by streams, flood plains, and alluvial fans. Alluvium at the NTS is almost exclusively the result of alluvial fan deposition. The upland areas around the alluvial basin should contain similar rocks/rock mineralogy to the CAU of interest. Alluvium tends to be highly heterogeneous; therefore, site-specific alluvial mineralogy is necessary to evaluate the transferability of other alluvium data.

I.3.2.2 Volcanic Rocks

Generally, volcanic rocks are classified by mineralogy and texture. The HSUs developed for CAU geologic models tend to emphasize the physical hydrologic significance of a unit, as opposed to the mineralogy. To account for this, the CAU transport model may require refinement to specifically identify volcanic rocks based on mineralogy. Class definitions for the volcanic rocks were selected to be consistent with the class definitions used for the YMP so that YMP data can be readily incorporated into the analysis, where appropriate. These classes are defined as:

Vitric Tuff

Greater than 40 percent glass
Less than 10 percent clay
Less than 10 percent zeolite

Devitrified Tuff

Less than 10 percent clay
Less than 10 percent zeolite

Zeolitic Tuff

Greater than 20 percent zeolite
Less than 10 percent clay
Less than 10 percent glass

I.3.2.3 Scores

1.0 - If the rock classification is the same and all reported minerals are within the 95 percent CI of the rock classification.

0.9 - If the rock is the same type and the reported mineral content is within the 95 percent CI of the rock classification, but not from the same CAU. This slightly lower score accounts for the unmeasured differences in the rock deposition, pore structure, etc.

0.8 - If the rock type is the same, but the mineral chemistry is within the bounds of the 99 percent mineral CI or meets the definition of the typical rock classification.

0.5 - If the rock classification is the same but outside the 99 percent CI for the rock chemistry at the CAU, or if the rock mineralogy does not fit within the rock classification scheme above.

I.3.3 Deposition and Alteration History

Distribution coefficients are dependent on the deposition and alteration history of the rock; therefore, they should be the same for all transferred distribution coefficients. For this analysis, a uniform weight of 0.7 is assigned.

I.3.4 Water Chemistry, Especially pH and Major Cation Concentrations

0.3 - pH within 95 percent CI of observed variability within an HSU and major cation chemistry within 50 percent of reported values for the CAU.

0.2 - pH within 95 percent CI of observed variability within an HSU, but major cation concentrations in experiments appear to be outside 50 percent bounds of cation concentrations observed at the CAU (at this point, there are no data to support an evaluation of minor cation effects on K_d measurements).

0.1 - pH outside 95 percent CI or suspect cation concentrations that may lead to underestimation or overestimation of distribution coefficients.

I.3.5 Multipliers

These values are used to reflect both the quality and uncertainty of the method and scale of the measurement. Ultimately, the use of these parameters allows for the appropriate use of data that are highly uncertain or poorly documented without allowing these data to unduly skew a dataset.

I.3.6 Measurement Method Considerations

The measurement method considerations include the quality and uncertainty of the method as well as the scale of the measurement.

- Reported distribution coefficients less than 0 should be rejected because they reflect an unquantifiable level of uncertainty in the measurement and potentially poor data collection techniques.
- High-quality measurements that contain multiple concentration values, water-to-solid ratios of less than 4, and low detection limits for radionuclides in solution received a 1.2.
- Average-quality values that contain, at minimum, duplicate concentration values and detection limits at least an order of magnitude lower than observed concentration changes were scored 1.0.

- Low-quality values that have only one sample or poor detection limits relative to concentration changes were scored 0.5.

I.3.7 Data Reduction and Analysis Method

Data reduction and analysis methods are evaluated independently of the type of measurement being evaluated. However, the analyst must be familiar with state-of-the-art methods in order to make an evaluation. The following multipliers applied:

- Current and widely accepted data reduction and analysis method with reputable and traceable calibration information - 1.0
- Good method, but calibration information is suspect or missing - 0.5
- Based on older or less widely accepted methods, but calibration information is good - 0.5
- Both methods and calibration information are suspect or missing - 0.2

I.3.8 Quality Documentation

Documentation quality is also evaluated independently of the type of measurement being evaluated as follows:

- Good (thorough, easy to follow, traceable) - 1.0
- Appearing in a reputable journal or peer-reviewed report, but otherwise lacking in thoroughness - 0.6
- Poor - 0.3

Note that poor documentation often results in the inability to evaluate the data reduction and analysis method (including the calibration information) for a given dataset. Thus, poorly documented estimates can, in effect, be doubly penalized as a result of both poor documentation scores and poor data reduction and analysis scores.

I.3.9 Overall Scores

The overall score for a given dataset is taken to be the sum of the weights multiplied by the product of the multipliers. This overall score is then able to be used in downstream analyses to calculate probability distribution functions for model sensitivity analyses.

I.4.0 REFERENCES

SNJV, see Stoller-Navarro Joint Venture.

Stoller-Navarro Joint Venture. 2004. *Transferability of Data Related to the Underground Test Area Project, Nevada Test Site, Nye County, Nevada*, S-N/99205-020. Las Vegas, NV.

Appendix J

Description of Colloid Parameter Datasets

J.1.0 INTRODUCTION

The data on colloids discussed in Section 13.0 is contained in five datasets:

- Colloid Size, Concentration Data
- Alluvium Transport Parameter Data
- Volcanics, Carbonates Transport Parameter Data
- Colloid K_d Range Data
- Colloid Sorption, Desorption Data

Following is a description of the datasets including the following items:

- A summary of the contents of each dataset
- The structure of the table containing each dataset
- Directions for accessing each dataset

J.2.0 COLLOID SIZE, CONCENTRATION DATA

Each record in the colloid concentrations and size distribution dataset contains information about a given measurement of colloid concentrations for a given borehole. The dataset is organized by the borehole name. The dataset contains colloid concentrations by size range for 45 different boreholes. The entire colloid database dataset from the GEOCHEM06 database (SNJV, 2006) is also included.

The colloid concentration and size distribution table contains the following fields:

- Master_ID - NWIS ID for well
- Site_ID - Name of the well sampled
- Sample_ID - GEOCHEM06 database sample ID
- 50-60 nm - Number of colloids in the 50-60 nm size bin
- 60-70 nm - Number of colloids in the 60-70 nm size bin
- 70-80 nm - Number of colloids in the 70-80 nm size bin
- 80-90 nm - Number of colloids in the 80-90 nm size bin
- 90-100 nm - Number of colloids in the 90-100 nm size bin
- 100-110 nm - Number of colloids in the 100-110 nm size bin
- 110-120 nm - Number of colloids in the 110-120 nm size bin
- 120-130 nm - Number of colloids in the 120-130 nm size bin
- 130-140 nm - Number of colloids in the 130-140 nm size bin
- 140-150 nm - Number of colloids in the 140-150 nm size bin
- 150-160 nm - Number of colloids in the 150-160 nm size bin
- 160-170 nm - Number of colloids in the 160-170 nm size bin
- 170-180 nm - Number of colloids in the 170-180 nm size bin
- 180-190 nm - Number of colloids in the 180-190 nm size bin
- 190-200 nm - Number of colloids in the 190-200 nm size bin
- >200 nm - Number of colloids greater than 200 nm size
- 200-220 nm - Number of colloids in the 200-220 nm size bin
- 220-240 (nm) - Number of colloids in the 220-240 nm size bin
- 240-260 (nm) - Number of colloids in the 240-260 nm size bin
- 260-280 (nm) - Number of colloids in the 260-280 nm size bin
- 280-300 (nm) - Number of colloids in the 280-300 nm size bin
- 300-400 (nm) - Number of colloids in the 300-400 nm size bin
- 400-500 (nm) - Number of colloids in the 400-500 nm size bin
- 500-600 (nm) - Number of colloids in the 500-600 nm size bin
- 600-800 (nm) - Number of colloids in the 600-800 nm size bin
- 800-1000 (nm) - Number of colloids in the 800-1000 nm size bin
- >1000 (nm) - Number of colloids greater than 1000 nm size bin
- Total, Particle Size Range 50 - 200 nm
- Total, Particle Size Range 50 - 1000 nm
- Total, Particle Size Range 50 - >1000 nm

J.3.0 ALLUVIUM TRANSPORT PARAMETER DATA

The alluvium transport parameter dataset contains information about filtration rate constants, detachment rate constants, and retardation factors for various wells. The data are presented in two tables. The first table contains data for laboratory tracer responses, and the second table contains data for field tracer responses. Both datasets are organized primarily by an experiment/well name.

The alluvium transport parameter data table for laboratory tracer test responses contains the following fields:

- Experiment/Well Name
- Residence Time (hours)
- Filtration Rate Constant (k_{fil}, 1/hour)
- Retardation Factor (R_{col})
- Colloid (or Analog) - Type of colloid used in the experiment
- Source - Source of the information

J.4.0 VOLCANICS, CARBONATES TRANSPORT PARAMETER DATA

The volcanics, carbonates transport parameter dataset contains information about filtration rate constants, detachment rate constants, and retardation factors for various wells/tests. The data are presented in two tables. The first table contains data for field tracer responses, and the second table contains data for laboratory tracer responses. Both datasets are organized primarily by well name.

The volcanics, carbonates transport parameter data table for field tracer test responses contains the following fields:

- Site Name (of record)
- Mean Residence Time (hour)
- Filtration Rate Constant (k_{fil}, 1/hour)
- Detachment Rate Constant (k_{det}, 1/cm-hour)
- Retardation Factor (R_{col})

J.5.0 COLLOID K_d RANGE DATA

Each record in the colloid distribution coefficients table contains distribution coefficient data for a specific actinide and colloid combination. As a result, the table is organized primarily by the sorbing actinide and secondarily by the composition of the colloid. The dataset contains 13 distribution coefficient ranges for 4 different actinides. The dataset contains information about the colloid type, the distribution coefficient range, and the source of the data.

The colloid distribution coefficients table contains the following fields:

- actinide - Actinide
- colloid_type - Type of colloid
- lower_K_d_bound (mL/g) - Lower K_d bound in milliliters per gram
- upper_K_d_bound (mL/g) - Upper K_d bound in milliliters per gram
- UGTA_extension (mL/g) - Extensions to the bounds determined from U-20WW experiments
- comments - Comments on the record
- source - Source of the information
- ref_id - Reference for the record

J.6.0 COLLOID SORPTION, DESORPTION DATA

Each record in the actinide sorption and desorption rate constants table contains forward- and reverse-rate constants for a given colloid and actinide combination. As a result, the table is organized primarily by the colloid type and secondarily by the sorbing actinide. The dataset contains 20 records of information that document rate constant ranges for both sorption and desorption of actinides onto various colloid types.

The actinide sorption and desorption rate constants table contains the following fields:

- Colloids/Actinides - Colloid and actinide combination
- batch_kf (hr-1) - Batch sorption rate constant per hour
- batch_kb (hr-1) - Batch desorption rate constant per hour
- fracture_kf (hr-1) - Fracture sorption rate constant per hour
- fracture_kb (hr-1) - Fracture desorption rate constant per hour
- comments - Comments regarding the values
- source - Source of the information
- ref_id - Reference for the record

J.7.0 ACCESS TO DATASETS

The CD-ROM accompanying this document contains electronic files of the datasets in PDF format with the following file names:

- Colloid Size, Concentration Data.xls
- Alluvium Transport Parameter Data.pdf
- Volcanics, Carbonates Transport Parameter Data.pdf
- Colloid Kd Range Data.pdf
- Colloid Sorption, Desorption Data.pdf

J.8.0 REFERENCES

SNJV, see Stoller-Navarro Joint Venture.

Stoller-Navarro Joint Venture. 2006. *Comprehensive Water Quality Database for Groundwater in the Vicinity of the Nevada Test Site, Geochem06.mdb,* S-N/99205--059-Rev. 1. Las Vegas, NV.

Appendix K

Nevada Division of Environmental Protection Comment Responses

(16 Pages)

NEVADA ENVIRONMENTAL RESTORATION PROJECT
DOCUMENT REVIEW SHEET

1. Document Title/Number: Phase I Contaminant Transport Parameters for the Groundwater Flow and Contaminant Transport Model of Corrective Action Unit 97; Yucca Flat/Climax Mine, Nye County, Nevada (Draft Rev. 1)	2. Document Due Date: June, 2007
3. Revision Number: Rev. 0	4. Originator/Organization:
5. Responsible DOE NNSA/NSO Subproject Mgr.: Bill Wilborn	6. Date Comments Due: July, 18, 2007
7. Review Criteria: Complete Document	
8. Reviewer/Organization Phone No.: State of Nevada; Mr. John J. Jones (702-486-2850)	9. Reviewer's Signature:
10. Initial Responses to NDEP review comments in their letter to NNSA/NSO dated 7-31-07	**11. Comment Response Date : August 16, 2007**

12. Comment Number/Location	13. Type[a]	14. Comment	15. Comment Response	16. Accept
1) General		There are large amounts of data being transferred from other areas for the transport model for this CAU. The UGTA Transferability of Data document suggests that for transferred data an estimated sensitivity of the CAU model be included (Data Transfer Protocol Outline item B.3) and the disqualification criteria be explained (Data Transfer Protocol Outline item B.6). For this CAU/ document, and in particular porosity and geochemistry, the items are unclear regarding the transferred data (except for the uncertainty for dispersivity and the uncertainty and disqualification criteria for laboratory distribution coefficients). NDEP requests a statement clarifying the uncertainty and disqualification criteria connected to the use and transfer of data into this CAU.	(Note corrected citations for the Data Transfer Protocol Outline items.) Sec. 5, Bullet 2 of the Data Transferability document states: Consider the sensitivity of predictions of the contaminant boundary to variation in the parameter value. Although the use of modeling simulations would be ideal for determining the parameter sensitivity, informed professional judgment is appropriate, especially during the early phases... No quantitative sensitivity estimate was included, nor can be provided, since the transport model has not been developed for use in computation. Consideration was given to basic transport processes and factors, e.g. zeolites increase sorption, lower matrix porosity decreases matrix diffusion, etc., with the focus on data representativeness and data quality. Sec. 5, Bullet 5 of the Data Transferability document states: Discuss the important considerations for using data from another source, and develop disqualification criteria. The criteria should reflect the importance of the parameter to the determination of the Contaminant Boundary and the reduction of uncertainty that might result from more stringent criteria. A general guideline is that the criteria should be established to eliminate data of poor quality and to eliminate inappropriate use of data.	See comment response.

[a]Comment Types: M = Mandatory, S = Suggested.

12. Comment Number/Location	13. Type[a]	14. Comment	15. Comment Response	16. Accept
1) General (continued)		Continuation of response to Comment 1.	Given the variable nature of data and data transfer considerations, judgments of uncertainty and disqualification were made using informed professional judgment suitable to each situation, and the basis for judgments are stated, as illustrated in the response to comment #4. General criteria are addressed by reference to the UGTA Data transferability document. No geochemistry or porosity data was transferred from outside of the YF/CM CAU boundary.	
2) Page 2-5, Section 2.2.2.4, 1st paragraph, 1st sentence		Explain why the actual groundwater chemistry data are not used as input into the Transport Model?	Page 2-5, Section 2.2.2.4, 1st paragraph, 1st sentence states "Groundwater chemistry data are not directly used as input in the transport model; rather, interpretations of groundwater chemistry data are used to evaluate and verify calibration of the groundwater flow and transport models. As with most parameters used in the transport model, discrete values for parameters for specific locations are not used in modeling, but rather, values representative of spatial scales over which the model operates. Such values are derived from discrete information, which is one objective of this document. Chemistry is simulated by the model, and as such is not a direct input. Chemistry could be an output state variable of the model. However, to date this information has been used to help test the goodness of the models.	See comment response.

[a]Comment Types: M = Mandatory, S = Suggested.

12. Comment Number/Location	13. Type[a]	14. Comment	15. Comment Response	16. Accept
3) Page 3-7, Section 3.2.1, 1st bullet point, 3rd sentence		This statement contradicts the UGTA data transferability document and can not be justified. Data transferred under this condition should not be used.	Page 3-7, Section 3.2.1, 1st bullet point, 3rd sentence states: "Under less desirable conditions, data may have to be transferred from locations that have no similarities to the original study area, other than data collected for the specific parameter of interest." The UGTA data transferability document recommends the "Accept unless Rejected" approach (Sec. 3) for data transfer. The cited statement refers to situations in which many criteria for judging the suitability of transferred data are unavailable. However, the statement does not disregard judgment of suitability, and statements justifying data transfer are required. There may be concomitant uncertainty requiring careful sensitivity analysis during modeling.	See comment response.
4) Page 4-40, Section 4.2.5, 4th paragraph, 4th sentence		Explain how, if the sample population is small that the anomalous samples are anomalous and not representative samples.	The referenced sentence discusses average mineralogical composition of the Timber Mountain Welded Tuff Aquifer (TM-WTA). The samples identified as anomalous are altered, often related to faults or near formation contacts. Thus, the argillic or zeolitic character of the samples is derived from cataclasis along faults or other alteration and is not representative of average TM-WTA mineralogy. Fracture-coating minerals are characterized separately. The discussion in the surrounding sentences states that sampling this hard, welded unit via sidewall sampling is difficult, and that the dataset is consequently small. For small datasets, the average is sensitive to outliers. Identification of samples judged anomalous provides a more accurate characterization of the average mineralogy of the unit. The argument is based on informed professional judgment. Note that omission of these minerals from the TM-WTA assemblage will reduce their ability to sorb reactive radionuclides, which is considered conservative with respect to transport.	See comment response.
5) Page 6-6. Section 6.2. 2nd Paragraph. 1st sentence		"... collected at only 15 locations, shown on Figure 6-2 .~ Figure 6-2 has more than 15 wells shown. Please indicate the appropriate well locations.	The text refers to 'test' locations rather than well locations. There is more than one well on some test locations. The text will be clarified to state 'test' locations.	Accept, see comment response.

[a]Comment Types: M = Mandatory, S = Suggested.

12. Comment Number/Location	13. Type[a]	14. Comment	15. Comment Response	16. Accept
6) Page 7-12, Table 7-3		For the AA and AA3 minimum porosity values in the table, negative values are given. Please correct these values.	An erroneous data value (-8.38) was mistakenly included in the matrix porosity summary statistics for the AA HGU and AA3 HSU. This value will be removed and the summary statistics corrected. This value was not used in any figure.	Accept, see comment response.
7) Page 8-13. Section 8.4.2.1 , 2nd paragraph, 1st sentence		'Fracture porosity can also be calculated using Equation (8-3) ...", however, Equation (B-3) assumes homogeneous isotropic volume and plug flow. How can this equation be used for flow in fractures?	Equation (8-3) assumes a homogeneous isotropic volume. Actual field conditions, whether in fractured or porous media, will generally be more complex than the homogeneous isotropic case. However, initial estimates of fracture porosity using Equation (8-3) have been demonstrated to be consistent with final calibrated values from the calibration of field tracer tests (e.g., Jones et al., 1992).	See comment response.
8) Page 8-23, Section 8.4.2.6, Equations (8-7) and (8-8)		Both equations are missing a minus sign. Please correct these equations.	Page 8-23, Section 8.4.2.6, Equations (8-7) and (8-8): These equations do not require a minus sign. They are consistent with Domenico and Schwartz (1990, p. 87) for Equation (8-7) and Domenico and Schwartz (1990, p. 75) for Equation (8-8). To address this comment, the text will be clarified as follows to indicate that volumetric flow rates are being discussed: Page 8-22: "The cubic law describing <u>the volumetric</u> flow <u>rate</u> between parallel, smooth plates is given by Domenico and Schwartz (1990):" Page 8-23: "Darcy's law, which calculates the water discharge <u>or flow rate</u> through a porous medium, is given by <u>Domenico and Schwartz (1990)</u>:" The underlined phrases above are additions to the original text.	See comment response.
9) Page 8-70, Figure 8-5		The indicator for the range of effective porosity on the Current Report-Yucca Flat is not located at the appropriate upper value as given in Table 8-21. Please correct this figure.	Page 8-70, Figure 8-5: The range for the Current Report-Yucca Flat case, lowest bar on the graph, will be revised to conform to the last entry on Table 8-21. That is, the high end of the bar will be extended to $2X10^{-2}$.	Accept, see comment response.

[a]Comment Types: M = Mandatory, S = Suggested.

12. Comment Number/Location	13. Type[a]	14. Comment	15. Comment Response	16. Accept
10) Page 9-11, Section 9.3.1, 2nd paragraph, 1st sentence		Please explain why a geometric average of dispersivities is used.	Either an arithmetic or a geometric mean of dispersivities could have been chosen. We chose to use a geometric mean. For the data analysis reported by Schulze-Makuck (2005), he states "If a range in longitudinal dispersivity was provided, the geometric mean was used (Table 1). The geometric mean was thought to represent a more suitable mean for dispersivity because the values varied commonly by an order of magnitude." His rationale is reasonable.	See comment response.
11) Page 10-36, Section 10.5, 3rd paragraph, 1st sentence		How will the scaling issue be addressed?	The text will be modified by removing this sentence/paragraph. This sentence discusses a modeling issue which is not appropriate to this data document. This issue is an active research area that will be addressed during transport analysis.	Accept, see comment response.

[a]Comment Types: M = Mandatory, S = Suggested.

NEVADA ENVIRONMENTAL RESTORATION PROJECT
DOCUMENT REVIEW SHEET

1. Document Title/Number: Phase I Contaminant Transport Parameters for the Groundwater Flow and Contaminant Transport Model of Corrective Action Unit 97; Yucca Flat/Climax Mine, Nye County, Nevada (Draft Rev. 1)	2. Document Date: June, 2007
3. Revision Number: Rev. 0	4. Originator/Organization:
5. Responsible DOE NNSA/NSO Subproject Mgr.: Bill Wilborn	6. Date Comments Due: July, 18, 2007
7. Review Criteria: Complete Document	
8. Reviewer/Organization Phone No.: State of Nevada; Mr. John J. Jones (702-486-2850)	9. Reviewer's Signature:
10. Final Comment Responses as discussed in telecom with NDEP and NNSA/NSO on 9/13/07.	**11. Comment Response Date: September 21, 2007**

12. Comment Number/Location	13. Type[a]	14. Comment	15. Comment Response	16. Accept
1) General		There are large amounts of data being transferred from other areas for the transport model for this CAU. The UGTA Transferability of Data document suggests that for transferred data an estimated sensitivity of the CAU model be included (Data Transfer Protocol Outline item B.3) and the disqualification criteria be explained (Data Transfer Protocol Outline item B.6). For this CAU/ document, and in particular porosity and geochemistry, the items are unclear regarding the transferred data (except for the uncertainty for dispersivity and the uncertainty and disqualification criteria for laboratory distribution coefficients). NDEP requests a statement clarifying the uncertainty and disqualification criteria connected to the use and transfer of data into this CAU.	(Note that citations for the Data Transfer Protocol Outline items are revised.) Re: estimated sensitivity Sec. 5, Bullet 2 of the Data Transferability document states (underline added): Consider the sensitivity of predictions of the contaminant boundary to variation in the parameter value. Although the use of modeling simulations would be ideal for determining the parameter sensitivity, <u>informed professional judgment is appropriate, especially during the early phases</u>... No quantitative sensitivity estimate was included, nor can be provided, since the transport model has not been developed for use in computation. Since model sensitivity cannot be quantitatively evaluated, professional judgment was used to comment on the importance of the parameter in general relative to the effect on modeling predictions. Consideration was given to basic transport processes and factors, with the focus on data representativeness and data quality. Re: disqualification criteria Sec. 5, Bullet 5 of the Data Transferability document states (underline added): Discuss the important considerations for using data from another source, and develop disqualification	Accept, see comment response.

[a]Comment Types: M = Mandatory, S = Suggested.

12. Comment Number/Location	13. Type[a]	14. Comment	15. Comment Response	16. Accept
1) General (continued)		Continuation of response to Comment 1.	criteria. The criteria should reflect the importance of the parameter to the determination of the Contaminant Boundary and the reduction of uncertainty that might result from more stringent criteria. A general guideline is that the criteria should be established to eliminate data of poor quality and to eliminate inappropriate use of data. Regarding the first underlined passage, the response is the same as for estimated uncertainty. Regarding the second underlined passage, these are the primary, general criteria discussed for each data type. Given the variable nature of data for transport parameters, qualification and disqualification criteria vary by data type and are based on informed professional judgment concerning specific criteria. The basis for such judgments is provided in the text, as illustrated in the response to comment #4. Specific criteria are developed based on technical considerations. The Data Transferability document primarily addresses the transfer of material property value data with specific prescriptions. However, a number of data types addressed in this document deal with functional parameters that are not measured directly but are interpreted from tests or experiments according to transport theory. The actual original data are not transferred, but the derived parameter values are the data transferred. For these parameter values, data transfer must be handled somewhat differently. The derived parameter values are judged for consistency with a theory or theoretical distribution that can be applied to the CAU, and HGU or HSU in question. Typically few parameter values are available, and the theory determining the parameter values is generalized. The data transfer process considers application of the derived distribution or parameter values through technical arguments and professional judgment. This contrasts with material properties values, for which acceptance is based on criteria relating to specific similarities of the material measured to the CAU, HGU or HSU material and quality of measurement, and disqualification is specific to detail problems. For functional parameter values, disqualification must be for functional parameter values, disqualification	

[a]Comment Types: M = Mandatory, S = Suggested.

12. Comment Number/Location	13. Type[a]	14. Comment	15. Comment Response	16. Accept
1) General (continued)		Continuation of response to Comment 1.	must be judged within the context of consistency with theory and appropriate application of the theory to modeling in the CAU, HGU or HSU. Regarding data transfer, subsections discussing data sources and data transfer will be added to each data-type section. The text that will be added and location of the addition for each section is listed below, with changes in quotes. Sec. 4 Yucca Flat/Climax Mine Hydrostratigraphic Framework Sec 4.2 Mineralogy of Hydrostratigraphic Units in the Yucca Flat/Climax Mine HFM "Sec. 4.2.1 Data Compilation and Data Transfer" "All data used in the quantitative analyses are from the Yucca Flat/Climax Mine HFM area; see Appendix D and the associated dataset referenced in Section D.4.0." Sec. 5 Yucca Flat/Cllimx Mine Geochemistry Sec. 5.2 "Data Compilation and Data Transfer" "Sec. 5.2.2 Data Transfer" "All data used in the quantitative analyses in this section are from the Yucca Flat/Climax Mine HFM area and surrounding springs; see Figure 5-2, Appendix E and the associated dataset referenced in Section E.3.0." Sec. 6 Contamination Sources and Extent "Sec. 6.1 Data Compilation and Data Transfer" "All data used in the quantitative analyses in this section are from the Yucca Flat/Climax Mine HFM area; see Appendix A." Sec. 7 Matrix Porosity Sec. 7.2. Data Compilation "and Data Transfer" "All data used in the quantitative analyses are from the Yucca Flat/Climax Mine HFM area; see Appendix F and associated dataset referenced in Section F.2.2."	

[a]Comment Types: M = Mandatory, S = Suggested.

12. Comment Number/Location	13. Type[a]	14. Comment	15. Comment Response	16. Accept
1) General (continued)		Continuation of response to Comment 1.	Sec. 8 Effective Porosity "Sec. 8.2 Data Compilation and Data Transfer" "Data from the Yucca Flat/Climax Mine HFM area and data from other NTS CAUs and YMP were used for this analysis due to the unavailability of comprehensive data from the Yucca Flat/Climax Mine HFM area for all HGUs. Figure 8-1 shows the source locations for the data used in the analysis. Individual discussions of the applicability of the transferred data are provided for each HGU. The data were used to determine a distribution appropriate for the Yucca Flat/Climax Mine CAU based on professional judgment. A quantitative assessment of the sensitivity of transport modeling to the uncertainty in this parameter cannot be provided before the transport model development. The parameter description discusses the importance of this parameter." Sec. 9 Dispersivity Sec. 9.2 Data Compilation "and Data Transfer" The dispersivity data types, data sources, and data documentation evaluation process are described in this section. "Data from the Yucca Flat/Climax Mine HFM area and data from other NTS CAUs, YMP, and Nye County were used for this analysis due to the unavailability of comprehensive data from the Yucca Flat/Climax Mine HFM area for all HGUs. Figure 9-1 shows the source locations for the NTS-area data used in the analysis. All data locations used in quantitative analyses are identified in Appendix G and the associated dataset referenced in Section G.4.0. Individual discussions of the applicability of the transferred data are provided for each HGU. There are limited data from the NTS area to determine a Yucca Flat/Climax Mine specific distribution for the parameter values. Data from literature for locations worldwide were used to evaluate the NTS area data with respect to the general distribution of dispersivity and scale dependence. A quantitative assessment of the sensitivity of transport modeling to the uncertainty in this parameter cannot be provided before the transport model development. The parameter description discusses the importance of this parameter."	

[a]Comment Types: M = Mandatory, S = Suggested.

12. Comment Number/Location	13. Type[a]	14. Comment	15. Comment Response	16. Accept
1) General (continued)		Continuation of response to Comment 1.	Sec. 10 Matrix Diffusion (change the present Sec. 10.2 to Sec. 10.1.1) "Sec. 10.2 Data Compilation and Data Transfer " "Data from the Yucca Flat/Climax Mine HFM area and data from other NTS CAUs, YMP, and some literature values from other locations (specifically for granites, for which there were no NTS area data) were used for this analysis due to the unavailability of comprehensive data from the Yucca Flat/Climax Mine HFM area for all HGUs. All data locations used in quantitative analyses are identified in Appendix H and the associated dataset referenced in Section H.4.0. Individual discussions of the applicability of the transferred data are provided for each HGU. There are limited data for the NTS area to determine a distribution for matrix diffusion values directly. The data were used to determine functional relationships with other parameters (see Section 10.4.6), for which there are more comprehensive data. A quantitative assessment of the sensitivity of transport modeling to the uncertainty in this parameter cannot be provided before the transport model development. The parameter description discusses the importance of this parameter." Sec. 11 Matrix Sorption "Sec. 11.2 Data Compilation and Data Transfer " "Data from the Yucca Flat/Climax Mine HFM area and data from other NTS CAUs, YMP, and a nearby location (see note) were used for this analysis due to the unavailability of comprehensive data from the Yucca Flat/Climax Mine HFM area for all HGUs. (Note: The nearby location was the low-level radioactive waste disposal facility in Beatty, Nevada. There were no NTS area data for some radionuclides for alluvium). All data locations used in quantitative analyses are identified in Appendix I and the associated dataset referenced in Section I.2.0. Individual discussions of the applicability of the transferred data are provided for each HGU. A quantitative assessment of the sensitivity of transport modeling to the uncertainty in this parameter cannot be provided before the transport model development. The parameter description discusses the importance of this parameter."	

[a]Comment Types: M = Mandatory, S = Suggested.

12. Comment Number/Location	13. Type[a]	14. Comment	15. Comment Response	16. Accept
1) General (continued)		Continuation of response to Comment 1.	Sec. 12 Fracture Sorption "Sec. 12.2.3 Data Transfer" "Data from the Yucca Flat/Climax Mine HFM area and data from another NTS CAU, Central and Western Pahute Mesa, were used for this analysis due to the unavailability of comprehensive data from the Yucca Flat/Climax Mine HFM area for all HGUs. Specific discussion of the applicability of the transferred data is provided. A quantitative assessment of the sensitivity of transport modeling to the uncertainty in this parameter cannot be provided before the transport model development. The parameter description discusses the importance of this parameter." Sec. 13 Colloid Facilitated Transport "Sec. 13.1 Data Compilation and Data Transfer " "Data from the Yucca Flat/Climax Mine HFM area and data from other NTS CAUs, YMP, and from another location (specifically data for alluvium, for which these data provided an expanded time scale) were used for this analysis due to the unavailability of comprehensive data from the Yucca Flat/Climax Mine HFM area for all HGUs. All data locations used in quantitative analyses are identified in Appendix J and the associated dataset referenced in Section J.7.0. Individual discussions of the applicability of the transferred data are provided for each HGU. A quantitative assessment of the sensitivity of transport modeling to the uncertainty in this parameter cannot be provided before the transport model development. The parameter description discusses the importance of this parameter."	

[a]Comment Types: M = Mandatory, S = Suggested.

12. Comment Number/Location	13. Type[a]	14. Comment	15. Comment Response	16. Accept
2) Page 2-5, Section 2.2.2.4, 1st paragraph, 1st sentence		Explain why the actual groundwater chemistry data are not used as input into the Transport Model?	As with most parameters used in the transport model, discrete values for parameters for specific locations are not used in modeling, but rather, parameter values representative of spatial scales over which the model operates. Such values are derived from discrete information, which is the objective of this document. Chemistry is simulated by the model, and as such is not a direct input. Groundwater chemistry is used for a variety of purposes in development of the transport model. In particular, groundwater chemistry analyses provide information used to help test the goodness of the models. Page 2-5, Section 2.2.2.4, will be revised to read: "Groundwater chemistry data are not directly used as input in the transport model; rather, representative groundwater chemistries are determined from the data and are used for a variety of analyses. Interpretations of groundwater flow paths and consequent geochemical mixing of characteristic groundwater chemistries are used to evaluate and verify groundwater flow and transport models. These interpretations provide independent information on potential groundwater flow paths and travel times that may be used in developing and calibrating the groundwater flow model for the Yucca Flat/Climax Mine CAU."	Accept, see comment response.

[a]Comment Types: M = Mandatory, S = Suggested.

12. Comment Number/Location	13. Type[a]	14. Comment	15. Comment Response	16. Accept
3) Page 3-7, Section 3.2.1, 1st bullet point, 3rd sentence		This statement contradicts the UGTA data transferability document and can not be justified. Data transferred under this condition should not be used.	The UGTA data transferability document recommends the "Accept unless Rejected" approach (Sec. 3) for data transfer. The cited statement refers to situations in which many criteria for judging the suitability of transferred data are unavailable. However, the statement does not disregard judgment of suitability, and statements justifying data transfer are required. There may be concomitant uncertainty requiring careful sensitivity analysis during modeling. Page 3-7, Section 3.2.1, 1st bullet will be revised to read: "For each parameter of interest, sites are identified that contain data of the same type. In an ideal situation, sites could be found in the same general area that have roughly the same geologic setting. More likely, sites will be identified that are located farther away but have similar rock types. In the least desirable situation, data may be transferred from locations that are less similar to the original study area but otherwise can be justified as appropriate."	Accept, see comment response.

[a]Comment Types: M = Mandatory, S = Suggested.

12. Comment Number/Location	13. Type[a]	14. Comment	15. Comment Response	16. Accept
4) Page 4-40, Section 4.2.5, 4th paragraph, 4th sentence		Explain how, if the sample population is small that the anomalous samples are anomalous and not representative samples.	The referenced sentence discusses average mineralogical composition of the Timber Mountain Welded Tuff Aquifer (TM-WTA). The samples identified as anomalous are altered, often related to faults or near formation contacts. Thus, the argillic or zeolitic character of the samples is derived from cataclasis along faults or other alteration and is not representative of average TM-WTA mineralogy. Fracture-coating minerals are characterized separately. The discussion in the surrounding sentences states that sampling this hard, welded unit via sidewall sampling is difficult, and that the dataset is consequently small. For small datasets, the average is sensitive to outliers. Identification of samples judged anomalous provides a more accurate characterization of the average mineralogy of the unit. The argument is based on informed professional judgment. Note that omission of these minerals from the TM-WTA assemblage will reduce their ability to sorb reactive radionuclides, which is considered conservative with respect to transport. Page 4-40, Now Section 4.2.6, 4th paragraph, 4th sentence will be revised to read: “The samples identified as anomalous are typically from altered zones (ZEOL or ARG) often related to faults or near formation contacts (TM WTA-Altered in Table 4-6) as determined from cuttings, boring and geophysical logs, and display mineralogic characteristics related to alteration not representative of welded tuffs in general. Sampling bias in the database was discussed in Section 4.2.”	Accept, see comment response.
5) Page 6-6. Section 6.2. 2nd Paragraph. 1st sentence		"... collected at only 15 locations, shown on Figure 6-2 .~ Figure 6-2 has more than 15 wells shown. Please indicate the appropriate well locations.	Page 6-6, now Section 6.3, 2nd paragraph: The text refers to ‘test’ locations rather than well locations. There is more than one well on some test locations. The text will be clarified to state ‘test’ locations.	Accept, see comment response.
6) Page 7-12, Table 7-3		For the AA and AA3 minimum porosity values in the table, negative values are given. Please correct these values.	Page 7-12, Table 7-3: An erroneous data value (-8.38) was mistakenly included in the matrix porosity summary statistics for the AA HGU and AA3 HSU. This value will be removed and the summary statistics corrected. This value was not used in any figure.	Accept, see comment response.

[a]Comment Types: M = Mandatory, S = Suggested.

12. Comment Number/Location	13. Type[a]	14. Comment	15. Comment Response	16. Accept
7) Page 8-13. Section 8.4.2.1 , 2nd paragraph, 1st sentence		"Fracture porosity can also be calculated using Equation (8-3) ...", however, Equation (B-3) assumes homogeneous isotropic volume and plug flow. How can this equation be used for flow in fractures?	Page 8-13. Now Section 8.5.2.1 , 3rd paragraph will be revised to read: "Fracture porosity can also be calculated using Equation (8-3) and the peak-concentration arrival time. Equation (8-3) assumes a homogeneous, isotropic volume and plug flow. In application, the total fracture volume is treated as homogeneous and isotropic, with no flow in the matrix. While actual field conditions, whether in fractured or porous media, are generally more complex, initial estimates of fracture porosity using this equation have been demonstrated to be consistent with final calibrated values from calibration of numeric transport models to field tracer tests (Jones et al., 1992). This time is considered to be representative of the time for tracer to travel through the fractures from the tracer-injection well to the pumping well. Because the mean residence times determined by Bechtel SAIC (2004c) are relatively similar to the peak-concentration arrival times (see above), fracture porosity was not calculated using the peak-concentration arrival times."	Accept, see comment response.
8) Page 8-23, Section 8.4.2.6, Equations (8-7) and (8-8)		Both equations are missing a minus sign. Please correct these equations.	Now Section 8.5.2.6, Page 8-23 and 8-24: These equations are consistent with Domenico and Schwartz (1990, p. 87) for Equation (8-7) and Domenico and Schwartz (1990, p. 75) for Equation (8-8). To address this comment, the text will be clarified as follows to indicate that equation gives the volumetric flow rates in the direction of flow. Page 8-23, Equation 8-7: "The cubic law describing the volumetric flow rate in the direction of flow between parallel, smooth plates is given by Domenico and Schwartz (1990) as:" Page 8-24, Equation 8-8: "Darcy's law, which calculates the water discharge or flow rate through a porous medium in the direction of flow, is given by Domenico and Schwartz (1990) as:"	Accept, see comment response.
9) Page 8-70, Figure 8-5		The indicator for the range of effective porosity on the Current Report-Yucca Flat is not located at the appropriate upper value as given in Table 8-21. Please correct this figure.	Now Page 8-71, Figure 8-5: The range for the Current Report-Yucca Flat case, lowest bar on the graph, will be revised to conform to the last entry on Table 8-21. That is, the high end of the bar will be extended to $2X10^{-2}$.	Accept, see comment response.

[a]Comment Types: M = Mandatory, S = Suggested.

12. Comment Number/Location	13. Type[a]	14. Comment	15. Comment Response	16. Accept
10) Page 9-11, Section 9.3.1, 2nd paragraph, 1st sentence		Please explain why a geometric average of dispersivities is used.	Either an arithmetic or a geometric mean of dispersivities could have been chosen. We chose to use a geometric mean. For the data analysis reported by Schulze-Makuch (2005), he states "If a range in longitudinal dispersivity was provided, the geometric mean was used (Table 1). The geometric mean was thought to represent a more suitable mean for dispersivity because the values varied commonly by an order of magnitude." His rationale is reasonable. Page 9-11, Section 9.3.1, 2nd paragraph will be revised to include the following sentences: "For the data analysis reported by Schulze-Makuch (2005), he states: "If a range in longitudinal dispersivity was provided, the geometric mean was used (Table 1). The geometric mean was thought to represent a more suitable mean for dispersivity because the values varied commonly by an order of magnitude."	Accept, see comment response.
11) Page 10-36, Section 10.5, 3rd paragraph, 1st sentence		How will the scaling issue be addressed?	Page 10-36, Section 10-5, 3rd paragraph: The text will be modified by removing this sentence/paragraph. This sentence discusses a modeling issue which is not appropriate to this data document. This issue is an active research area that will be addressed during transport analysis.	Accept, see comment response.

[a]Comment Types: M = Mandatory, S = Suggested.

Plates

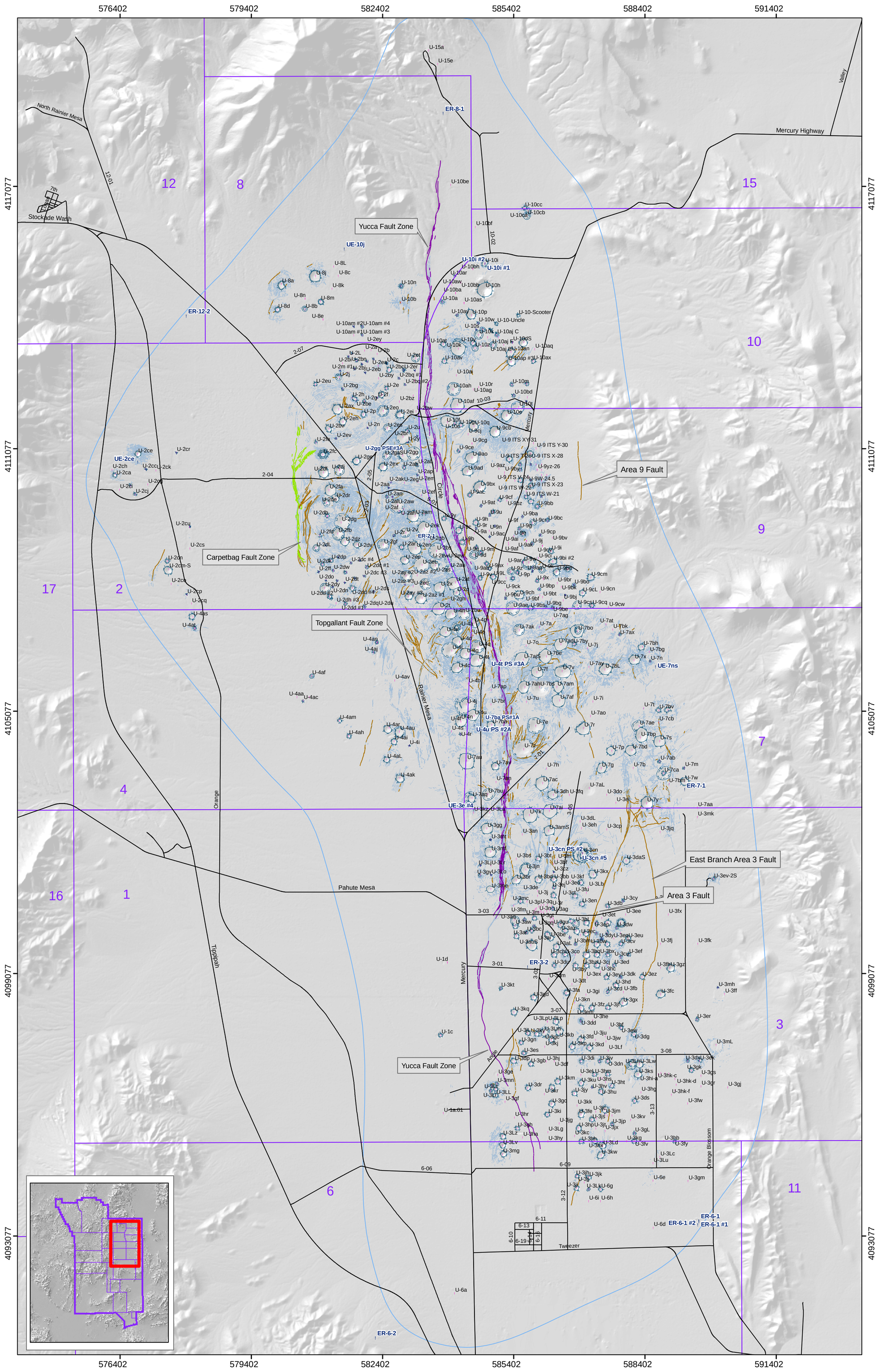

Explanation

- NTS Area Boundaries
- Corrective Action Unit Boundary
- UGTA Corrective Action Sites
- UGTA Well Locations
- Surface Crack
- Collapse Crater
- Major Roads

Source: modified from Grasso, 2001

Plate 1

MAP OF YUCCA FLAT/CLIMAX MINE AREA SHOWING UGTA CORRECTIVE ACTION SITES, UGTA WELL LOCATIONS, TEST-RELATED SURFACE EFFECTS, AND SELECTED BASIN-FORMING FAULTS

P:\Ugta\Ugta_Common\YF_HDD\GISFiles\Crack.mxd

North-South Model Profile (A-A') through Western Yucca Flat

Scale: 1:48,000

No Vertical Exaggeration

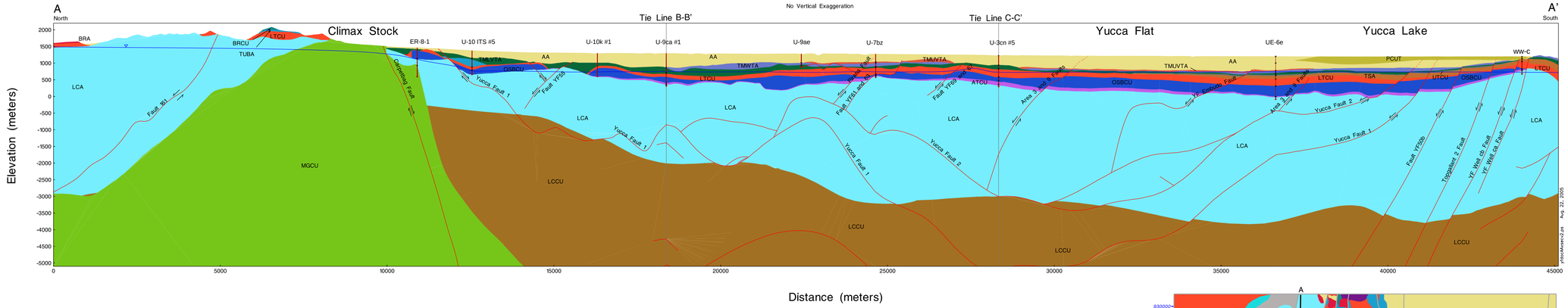

LEGEND FOR PROFILES

WW-C — Drill-hole in the line of profile. Black tick marks represent tops of hydrostratigraphic units determined from drill-hole data. Red tick mark indicates total depth of hole.

Fault with sense of displacement shown.

Water-table elecation (m)

Tie Line B-B' — Tie line indicates location where another profile intersects this profile.

Note: See report for definitions of hydrostratigraphic units.

West-East Model Profile (B-B') through Well Gravity High #1

Scale: 1:48,000

No Vertical Exaggeration

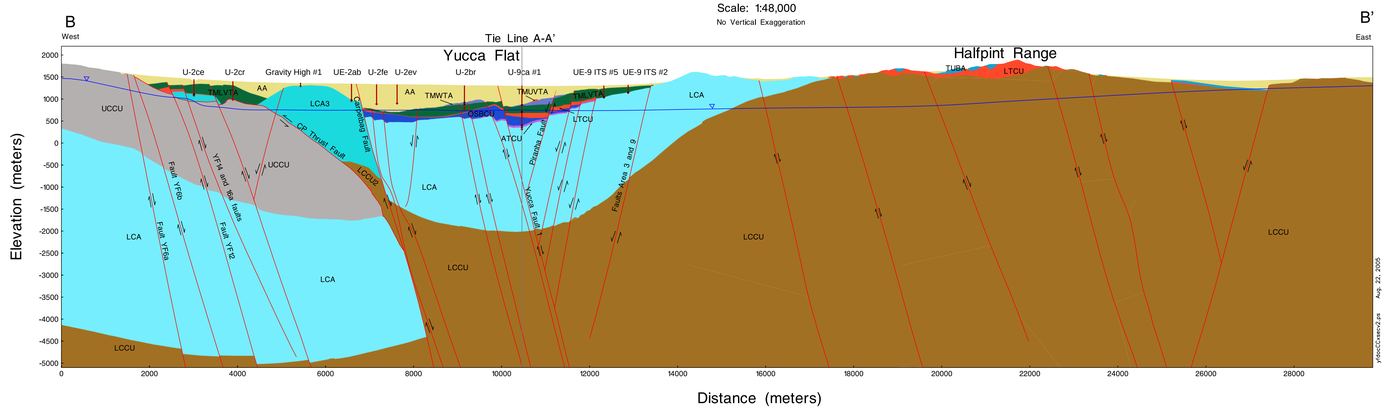

West-East Model Profile (C-C') through Central Yucca Flat at Well U-3cn #5

Scale: 1:48,000

No Vertical Exaggeration

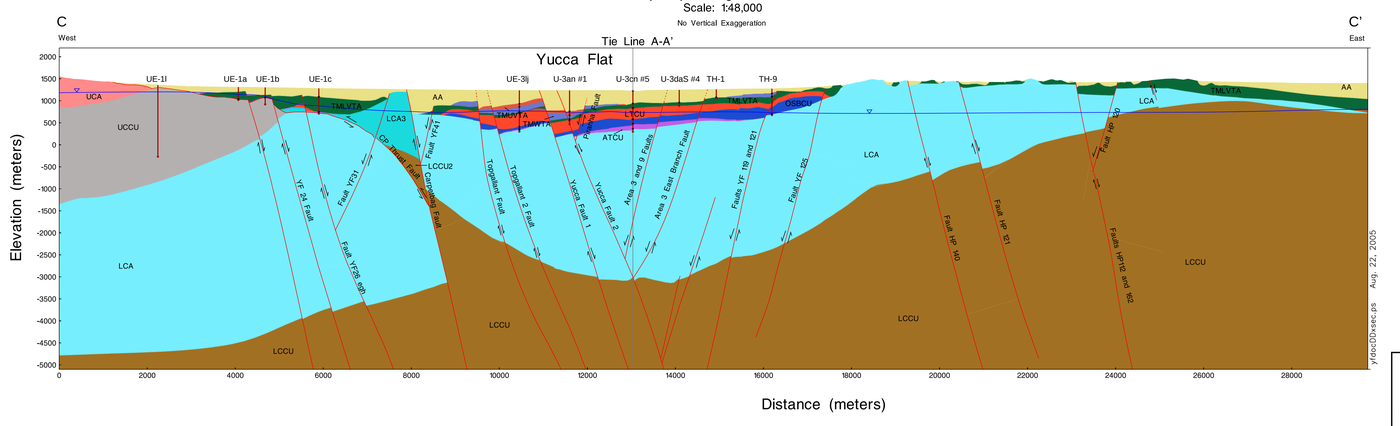

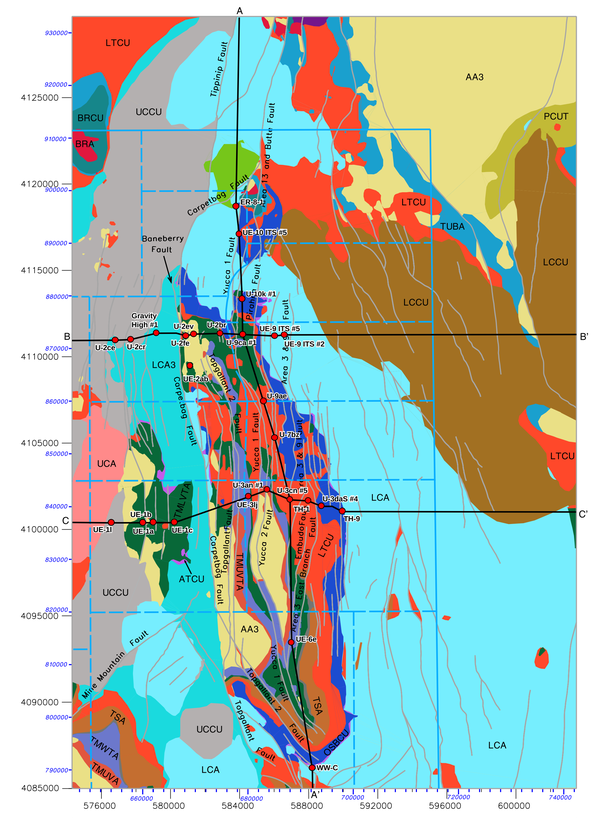

Hydrostratigraphic Units+

- AA3
- PCUT
- AA2
- BLFA
- AA1
- TMUVTA
- TMWTA
- TMLVTA
- UTCU
- TSA
- LVTA
- BRA
- BRCU
- PRETBG
- TUBA
- LTCU
- PRETBG_1
- OSBCU
- ATCU
- LCCU1
- LCA3
- LCCU2
- UCA
- UCCU
- VCU
- LCA
- LCCU
- MGCU

+See report for definitions for hydrostratigraphic units

Plate 2
Select Profiles of Hydrostratigraphic Units for the Yucca Flat/Climax Mine Model Area

DISTRIBUTION

Tim Murphy State of Nevada Division of Environmental Protection 1771 E. Flamingo Road, Suite 121A Las Vegas, NV 89119	2 HC/2CD
Bill R. Wilborn Environmental Restoration Project U.S. Department of Energy National Nuclear Security Administration Nevada Site Office P.O. Box 98518, MS/505 Las Vegas, NV 89193-8518	2 HC/2CD
Alicia Tauber Environmental Management Records U.S. Department of Energy National Nuclear Security Administration Nevada Site Office P.O. Box 98518, MS/505 Las Vegas, NV 89193-8518	1 CD
U.S. Department of Energy National Nuclear Security Administration Nevada Site Office Technical Library P.O. Box 98518, M/S 505 Las Vegas, NV 89193-8518	1 HC
U.S. Department of Energy Office of Scientific and Technical Information P.O. Box 62 Oak Ridge, TN 37831-0062	1 CD
Southern Nevada Public Reading Facility c/o Nuclear Testing Archive P.O. Box 98521, M/S 400 Las Vegas, NV 89193-8521	1 HC

Manager, Northern Nevada FFACO Public Reading Facility c/o Nevada State Library & Archives 100 N Stewart Street Carson City, NV 89701-4285	1 HC
Celeste Sandoval Nye County Nuclear Waste Repository Project Office 1210 E. Basin Road, Suite #6 Pahrump, Nevada 89060	1 HC/1 CD
Naomi Becker Los Alamos National Laboratory, M/S F665 Bikini Atoll Rd., SM30 Los Alamos, NM 87545	1 CD
Gayle Pawloski Lawrence Livermore National Laboratory 7000 East Avenue, L-221 Livermore, CA 94550-9234	1 CD
Mavrik Zavarin Lawrence Livermore National Laboratory 7000 East Avenue, L-221 Livermore, CA 94550-9234	1 CD
Bonnie Thompson USGS WRD 160 North Stephanie Street Henderson, NV 89074	1 CD
Chuck E. Russell Desert Research Institute 755 E. Flamingo Las Vegas, NV 89119	1 CD
Ken Ortego National Security Technologies, LLC P.O. Box 98521, M/S NLV 082 Las Vegas, NV 89193-8521	1 CD

John P. McCord Stoller-Navarro Joint Venture 7710 W. Cheyenne, Bldg. 3 Las Vegas, NV 89129	1 CD
Greg Ruskauff Stoller-Navarro Joint Venture 7710 W. Cheyenne, Bldg. 3 Las Vegas, NV 89129	1 CD
William Fryer Stoller-Navarro Joint Venture 105 Technology Drive, Suite 190 Broomfield, CO 80021	1 CD
Stoller-Navarro Joint Venture FFACO Support Office 7710 W. Cheyenne Ave., Bldg. 3 Las Vegas, NV 89129	1 HC/1 CD
Stoller-Navarro Joint Venture Central Files 7710 W. Cheyenne, Bldg. 3 Las Vegas, NV 89129	1 HC/1 CD